Springer Geochemistry

Daniel E. Harlov
Leonid Aranovich *Editors*

The Role of Halogens in Terrestrial and Extraterrestrial Geochemical Processes

Surface, Crust, and Mantle

Springer

Springer Geochemistry

More information about this series at http://www.springer.com/series/13486

Daniel E. Harlov · Leonid Aranovich
Editors

The Role of Halogens in Terrestrial and Extraterrestrial Geochemical Processes

Surface, Crust, and Mantle

Springer

Editors
Daniel E. Harlov
Deutsches GeoForschungsZentrum
Potsdam
Germany

Leonid Aranovich
Institute of Ore Geology, Petrography,
Mineralogy, and Geochemistry
Russian Academy of Sciences
Moscow
Russian Federation

ISSN 2366-6293 ISSN 2366-6285 (electronic)
Springer Geochemistry
ISBN 978-3-319-61665-0 ISBN 978-3-319-61667-4 (eBook)
https://doi.org/10.1007/978-3-319-61667-4

Library of Congress Control Number: 2017943837

Printed on acid-free paper

This Springer imprint is published by Springer Nature
The registered company is Springer International Publishing AG
The registered company address is: Gewerbestrasse 11, 6330 Cham, Switzerland

Contents

Chapter 1
The Role of Halogens in Terrestrial and Extraterrestrial Geochemical Processes: Surface, Crust, and Mantle

Daniel E. Harlov and Leonid Aranovich

Abstract Terrestrial worlds on which H_2O-bearing fluids are stable tend to show a higher degree of chemical differentiation than similar worlds on which such fluids are not present or stable. Other than CO_2 and S, important components of these H_2O-bearing fluids are the halogens, specifically the more common F and Cl and, to a lesser degree, the less common Br and I. When taken together in combination with H_2O, F and Cl are potentially powerful ligands with respect to solution-enabled mass transport of most metal cations. This characteristic has indirect implications with respect to the reactivity of halogen-bearing fluids with many mineral species from among the silicates, oxides, sulfides, and orthophosphates and with melts. The low wetting angle of Cl-bearing solutions along grain boundaries, coupled with a high reactivity, allow them to flow easily along and through grain boundaries under mid-crustal to lower crustal/lithospheric mantle P-T conditions, thus aiding both mineral re-equilibration and mass transfer on a local (cm's) as well as on a large (km's) scale during metamorphism. The low H_2O activity of these brines under high-grade conditions enables them to co-exist with nominally anhydrous Fe-Mg silicate minerals characteristic of the lower crust and the lithospheric mantle, such as orthopyroxene, clinopyroxene, and olivine. Evidence for the presence of these brines is seen in the fluid and melt inclusions found in the minerals from igneous rocks, ore deposits, sedimentary rocks, lower crustal rocks, and the lithospheric mantle. In magmas, halogens play an important role with regard to the solubility of various metal cations as well as affecting crystallization temperatures. During crystallization

D.E. Harlov (✉)
Deutsches GeoForschungsZentrum, Telegrafenberg, 14473 Potsdam, Germany
e-mail: dharlov@gfz-potsdam.de

and

Department of Geology, University of Johannesburg, P.O. Box 524,
Auckland Park 2006, South Africa

L. Aranovich
Institute of Ore Geology, Petrography, Mineralogy, and Geochemistry,
Russian Academy of Sciences, Staromonetnyi Per. 35, 119017 Moscow, Russian Federation
e-mail: lyaranov@igem.ru; chivonara47@yandex.ru

D.E. Harlov and L. Aranovich (eds.), *The Role of Halogens in Terrestrial and Extraterrestrial Geochemical Processes*, Springer Geochemistry,
https://doi.org/10.1007/978-3-319-61667-4_1

of plutonic magma bodies, while F tends to be retained in felsic melts, fluorapatite, and micas, Cl is expelled as a NaCl-KCl-$CaCl_2$-bearing fluid into the surrounding country rock taking with it a large variety of other metal cations. These are subsequently deposited in associated fissures, veins, and pegmatites as ore minerals/deposits during crystallization of the main magma body. The presence of such fluids has been confirmed by extensive fluid inclusion and experimental studies. Beyond the Earth, halogens play an important role in the geochemistry of other terrestrial worlds in the solar system on which H_2O can exist as a fluid whether on or beneath the surface. These include Mars, volatile-rich asteroids, and those ice moons of Jupiter and Saturn believed to contain subsurface oceans. In each of these cases both direct observation and terrestrial analogues allow for a more complete understanding of the role that halogens play in the various H_2O-aided geochemical processes present on these worlds. The goal of this volume is to bring together a diverse group of geoscientists with long-range interests, knowledge, and experience concerning the role that halogens play in or during a variety of geochemical and hydrothermal processes in the crust and mantle of the Earth as well as on volatile-rich asteroids, Mars, and the ice moons of Jupiter and Saturn in a series of review chapters. The range and depth of knowledge contained within these chapters regarding the role of halogens in geochemical processes, both terrestrial and extraterrestrial, outline and provide a firm foundation on which to base our current understanding of how halogens contribute to the geochemical/geophysical evolution and stability of liquid H_2O-bearing terrestrial worlds in the solar system overall.

1.1 Introduction

The term halogen is derived from the Greek words halas (‘αλας) or ‘salt’ and genos (γενος) or ‘derived from’. It was first coined by the Swedish chemist Baron Jöns Jakob Berzelius in 1842 as a general term describing the first four elements in this group as laid out in the periodic table. These include the stable elements fluorine (F), chlorine (Cl), bromine (Br), and iodine (I). A fifth highly unstable, halogen, radioactive astatine (At), whose most stable isotope has an approximate half-life of 8.1 h, was first synthesized and characterized in 1940.

The halogens are characterized by a very high electronegativity due to a one electron deficiency in their outer p shell, which means that they have a strong tendency to form anionic species. Disregarding At, which, due to its short half life, is one of the rarest elements in the Earth’s crust, and subsequently has little importance geologically, the four remaining halogens, F, Cl, Br, and I are highly reactive with practically all metals, with which they form halides, and most nonmetals in the periodic table. The chemical bonds formed by halogens range from purely ionic to nearly completely covalent with the degree of the covalent character of the bond tending to increase with atomic mass, i.e. chemical bonds formed with Br and especially I tend to exhibit a considerable degree of covalent character as opposed to ionic. They also will bond with oxygen to form oxyhalogen compounds such as

fluorates (FO_3^-), chlorates (ClO_3^-), bromates (BrO_3^-), and iodates (IO_3^-) in addition to a number of other oxygen derivatives. Of these the fluorates and chlorates are powerful oxidizers. The Group I elements or the alkali metals (Li, Na, K, Rb, Cs) and the Group II elements or alkaline earth metals (Be, Mg, Ca, Sr, Ba, and Ra) tend to form chlorides with Cl that are soluble in a strong polar solvent such as H_2O. In contrast, most fluorides, with some exceptions (e.g., NaF and KF), are relatively insoluble in H_2O. This is due to the fact that the fluoride ion is the least polarizable of the halides and accordingly is presumed to form the most perfectly ionic derivatives. This can also be seen in the melting temperatures of the fluorides, which tend to be higher than the melting temperature for the corresponding chloride, bromide, or iodide for the same metal cation. In general, a decrease in melting temperature is seen going from fluoride to chloride to bromide to iodide. Lastly, from a geochemical perspective, the relatively small size of the F^- anion and its relatively high electronegativity, compared to Cl, Br, and I, allows it to fit into many mineral lattice sites where it forms strong chemical bonds. Subsequently, in most geochemical systems, F^- is a minor anion component in H_2O-based solutions compared to Cl^-, Br^-, and I^-. Of the halides, the most abundant (and most important) components in terrestrial fluid environments include NaCl, KCl, and $CaCl_2$.

Over the last 20–30 years, much progress has been made in better understanding the role of halogens in both metamorphic/metasomatic processes (Newton and Manning 2010; Harlov 2012; Manning and Aranovich 2014) and igneous processes, specifically granitoid melts (Aranovich et al. 2013, 2014; Makhluf et al. 2016; Dolejs and Zajacz 2018) and mafic melts (Signorelli and Carroll 2002; Webster et al. 2018). This exploration has also included a relatively large amount of experimental work involving phase equilibria in the presence of aqueous salt solutions (Aranovich and Newton 1996, 1997, 1998; Shmulovich and Graham 1996) and the solubility of various common minerals in high-grade halogen-bearing fluids including quartz (Newton and Manning 2000, 2006, 2008; Shmulovich et al. 2001, 2006; Akinfiev and Diamond 2009; Cruz and Manning 2015); albite (Shmulovich et al. 2001); diopside (Shmulovich et al. 2001); albite + K-feldspar + andalusite + quartz (Hauzenberger et al. 2001; Pak et al. 2003); wollastonite (Newton and Manning 2006); grossular garnet (Newton and Manning 2007); andradite (Wykes et al. 2008); corundum (Walther 2001, 2002; Newton and Manning 2006); calcite (Newton and Manning 2002a); anhydrite (Newton and Manning 2005); fluorite (Tropper and Manning 2007); fluorapatite (Antignano and Manning 2008a); monazite (Tropper et al. 2011, 2013; Zhou et al. 2016); xenotime (Tropper et al. 2011, 2013; Zhou et al. 2016); rutile (Audetat and Keppler 2005; Rapp et al. 2010; Tanis et al. 2016); and zircon (Newton et al. 2010; Ayers et al. 2012; Wilke et al. 2012). These experiments contrast with similar solubility experiments on these and other minerals using only pure H_2O. These include quartz (Manning 1994); wollastonite (Fockenberg et al. 2006); corundum (Tropper and Manning 2007); corundum + kyanite (Manning 2007); zircon (Newton et al. 2005); rutile (Tropper and Manning 2005); enstatite + forsterite (Newton and Manning 2002b); and albite + quartz + paragonite and jadeite + paragonite + quartz (Manning et al. 2010; Wohlers et al. 2011). Other types of solubility experiments include alkaline aqueous fluids (zircon—Ayers et al. (2012)); acids ($NdPO_4$—Poitrasson et al. (2004)); and melts such as carbonatitic

melts (apatite—Hammouda et al. (2010)); albitic melts (rutile—Antignano and Manning (2008b); Manning et al. (2008); Hayden and Manning (2011)), or granitic melts (corundum and andalusite—Acosta-Vigil et al. (2002); monazite and xenotime—Skora and Blundy (2012); Duc-Tin and Keppler (2015)). The albitic melt experiments build on the work of Paillat et al. (1992). The basic gist of these experiments is that, with the exception of quartz (Newton and Manning 2000), the other minerals so far investigated are considerably more soluble in Na-bearing brines (NaCl or NaF) or albitic melts under high-grade conditions than they are in pure H_2O.

The increased solubility of these minerals in brines enhances mass transfer during high-grade metamorphism. Transport of the dissolved mineral species is further aided by the low wetting angle of brines along mineral grain boundaries (Watson and Brenan 1987; Brenan and Watson 1988; Gibert et al. 1998). This is in contrast to the high wetting angle shown by CO_2, which would explain its being preferentially trapped as fluid inclusions during metamorphic processes as opposed to brines, which are not (Gibert et al. 1998). Evidence for this stark difference in wetting angles is seen in the large abundance of dense CO_2-rich fluid inclusions in high-grade metamorphic rocks as opposed to the paucity of brine-rich fluid inclusions (van den Kerkhof et al. 2014). It is also conceivable that the specific CO_2-rich composition of these inclusions may have originated due to the unmixing of complex H_2O-CO_2-(± other non-polar gases)-halide-bearing fluids with a much lower initial CO_2 content (e.g., Johnson 1991; Heinrich 2007; Shmulovich and Graham 2008; Aranovich et al. 2010). The unmixing also serves as an efficient mechanism to concentrate halogens in the brine phase (Manning and Aranovich 2014). The low wetting angle of brines potentially allows them to flow on the scale of kilometers compared to CO_2-rich fluids, which due to their high wetting angle, can only flow along grain boundaries a few meters at most under similar high grade conditions (Harlov and Förster 2002a, b; Harlov et al. 2006; also see discussion in Harlov 2012). In addition, the fact that the H_2O activity in NaCl and KCl brines approaches $X^2_{H_2O}$ at pressures above 500 MPa (Aranovich and Newton 1996, 1997) allows for such brines to be relatively H_2O-rich and yet co-exist with the H_2O-absent silicate mineral assemblages normally present in the lower crust and lithospheric mantle (Newton and Manning 2010; Manning and Aranovich 2014). All of this work builds on the pioneering work of Korzhinskii (1959, 1962) who treated the chemical potentials of Na and K as inherent thermodynamic parameters (like pressure and temperature) within any metamorphic geochemical system (undergoing metasomatically induced re-equilibration) in which these elements were found (Safonov and Aranovich 2014).

The F and Cl abundances in both biotite and apatite are very useful indicators of the presence of halogen bearing fluids during metamorphism (cf., Harlov and Förster 2002a, b; Harlov et al. 2006; Hansen and Harlov 2007) and during magmatic-hydrothermal processes (Munoz 1984, 1992; Webster and Piccoli 2015). For example, biotite can be used to estimate the relative fugacities of F and Cl relative to OH or rather the relative fugacities of HF and HCl relative to H_2O (Munoz 1984, 1992; see also Harlov and Förster 2002a). Taken together and assuming equilibrium, the F and Cl contents in co-existing apatite and biotite can be used to estimate a temperature based on the biotite-apatite F-Cl exchange (Zhu and Sverjensky 1992; Sallet 2000; see discussion in Harlov and Förster 2002a).

The 16 chapters, following this one, attempt to cover as completely as possible the role of halogens in geochemical processes on terrestrial worlds where liquid H_2O is found. In addition to the Earth, these worlds include Earth-like worlds such as volatile-rich asteroids, Mars, and the various ice moons of the outer gas giants for which there is good evidence of them possessing subterranean oceans of H_2O (Hand 2018). The H_2O on all these worlds makes up one component in both fluids and melts that also contain varying amounts of mostly Cl^- and CO_3^{2-} and lesser amounts of S (in a variety of oxidation states), F^-, Br^-, and I^- along with a whole range of metal cations of which the majority are Na^+, K^+, and Ca^{2+}. The Moon, Mercury, and Venus are not included in this survey simply because they are completely free of H_2O as a free fluid. In the case of the Moon, whatever halogens are present in lunar igneous rocks and breccia (principally F and Cl) will be found chemically bound in minerals, such as apatite (McCubbin et al. 2011). In the case of Mercury or Venus, a lack of any sort of realistic sampling precludes, at this time, making reasonable speculations regarding the role of halogens in magmatic processes on either world except by analogy with terrestrial processes.

1.2 Halogens in Terrestrial and Cosmic Geochemical Systems: Abundances, Geochemical Behaviors, and Analytical Methods: Chap. 2

Chapter 2 (Hanley and Koga 2018) provides a complete chemical background on halogens in geochemical and cosmochemical systems. These include (i) summarizing the halogen distribution in different fluids (surficial, formation, and crystalline shield waters, metamorphic, magmatic-hydrothermal-geothermal) and in different domains (oceanic and continental crust, mantle and core) of the Earth, and various extra-terrestrial materials and bodies (meteorites, planets and moons, and the Sun); (ii) to briefly discuss characteristic fractionation processes; (iii) to provide an estimate of the total halogen abundance for the Earth and in its dominant reservoirs contributing to the Earth's halogen endowment; and (iv) to discuss some missing observations that could further improve our understanding of halogen abundances and geochemical systematics. The chapter discusses the most recent advances in techniques for analyzing usually very minor concentrations of halogens and their isotope composition in geologic and cosmic materials. A key motivation for this method stems from an increased awareness of the value in halogen characterization for studying specific processes in the Earth's hydrosphere, crust, mantle, and core (e.g., crustal and mantle metasomatism; ore metal transfer; magmatic differentiation and volatile exsolution; fluid reservoir contamination and fluid mixing; mineral-melt-fluid partitioning; and basinal fluid evolution) in which the chemical and isotopic properties of the halogens provide significant advantages over other element groups. Building upon the most reliable bulk abundances, and specific halogen element and isotope ratios, the authors provide an outlook for halogen storage in various terrestrial reservoirs.

1.3 Halogen-Rich Minerals: Crystal Chemistry and Geological Significances: Chap. 3

Chapter 3 (Mi and Pan 2018) provides the crystal chemistry and mineralogy background to the behavior of halogens in geological processes. Halogen-rich minerals containing at least one halogen (F, Cl, Br, or I) on a dominant crystallographic site can be divided into three broad groups: (1) halides, (2) halogenates, and (3) native halogens. Approximately 700 halogen-rich minerals in the 09/2014 list of species have been approved by the International Mineralogical Association (IMA), accounting for ~15% of the mineral species known to date. Still scores of other minerals contain significant amounts of F and/or Cl, especially in many hydrous minerals via the common substitution of $(F, Cl)^-$ for OH^- on the hydroxyl site. Amphiboles, micas, and apatites are the dominant carriers of halogens in most rocks, whereas scapolites and sodalites serve as important hosts of these elements in more exotic lithologies. These minerals not only play important roles in controlling halogen geochemical cycles but also are useful for calculating the halogen composition and evolution of the fluids/melts from which they crystallized.

1.4 Halogen Elements in Sedimentary Systems and Their Evolution During Diagenesis: Chap. 4

Chapter 4 (Worden 2018; see also Kendrick 2018 and Yardley 2013) covers the full range of processes capable of influencing halogen concentrations in sediments, sedimentary rocks, and formation waters and other fluids involved in diagenetic reactions. Chlorides and bromides are focused on with respect to their conservative behavior in sedimentary and diagenetic systems, though there are circumstances when Br may not be conservative compared to Cl. These include hydration reactions, evaporative concentration, incongruent dissolution of Br-poor halite, dissolution of Br-enriched potash facies evaporates, breakdown of Br-bearing organic matter (see also Kendrick 2018), or retarded membrane filtration of Br compared to Cl. In addition, chloride and bromide concentrations in formation waters can be enormously variable. Fluoride is treated as being non-conservative in formation waters due to its preferential incorporation into minerals whereas iodide is treated as non-conservative in formation waters due to the breakdown of I-enriched, organic-bearing sedimentary rocks. After summarizing the current understanding about where the halogen elements exist in sediments and sedimentary rocks, this chapter deals with the key processes (weathering, dissolution, atmospheric processes, evaporation, mineral precipitation, burial, and diagenesis) that change the concentration of halogens, and their element and isotope ratios at various stages in the diagenetic cycle. In that regard, the patterns of halogen concentration in sedimentary formation waters can be of great significance since they reveal much about the fluid flow history of the basin in general, and oil or gas fields in particular.

1.5 Halogen Geochemistry of Ore Deposits: Contributions Towards Understanding Sources and Processes: Chap. 5

Chapter 5 (Lecumberri-Sanchez and Bodnar 2018; see also Pirajno 2013, 2018) considers the role of halogens in the origin of hydrothermal ore deposits. Due to the incompatible nature of halogens in most mineral phases, geofluid reservoirs commonly have distinct halogen geochemistry signatures. Through comparison of the halogen geochemistry of ore-related fluids with that of geofluid reservoirs, this chapter provides insights into the sources of halogens and, by extension, of the fluids associated with ore formation. It also discusses the modifications of the Pressure-Volume-Temperature-Composition (PVTX) properties of hydrothermal fluids that result from the addition of halides to H_2O. These modifications impose major control over the regions of the Earth's crust in which metal partitioning and depositional mechanisms, such as fluid immiscibility (boiling), may occur. Furthermore, addition of chloride salts to H_2O significantly increases metal solubilities, compared to solubilities in pure H_2O, thus enhancing the metal carrying capability of ore forming fluids. Halogens also influence the partitioning behavior of metals between different fluid phases. As a result, some types of ore deposits show a systematic variation in time and space of halogen abundances and geochemistry, which may be used in the exploration for these deposits.

1.6 Halogens in Mafic and Intermediate-Silica Content Magmas: Chap. 6

Webster et al. (2018) in Chap. 6 review halogen abundances in basaltic to andesitic magmas and in their alkaline equivalents (basanites to phonolites). They examine and apply the results of hydrothermal experiments and thermodynamic modeling to the impact of halogens on melting and crystallization behavior; exsolution of vapor and/or hydrosaline liquids from these magmas; thermal stability of hydrous minerals; viscosity and diffusion in these melts; and the partitioning between fluids and these melts, which have direct bearing on volcanic degassing and the generation of halogen-bearing mineralizing fluids. Data on halogen behavior in basaltic and andesitic magmatic systems are applied to processes of assimilation and partial melting in magmatic seafloor environments in order to interpret observed glass compositions, and the processes responsible for halogens being erupted via volcanic plumes into the atmosphere. While rather extensive data sets for F and Cl in these magma systems are available, data sets for Br and I in the same magma systems are insufficient and much more is needed. It is also apparent that additional experiments on halogen-bearing mafic to intermediate-silica content melts and fluids are required and that thermodynamic models of magmatic and hydrothermal processes should include the role of Cl in melt-vapor-hydrosaline equilibria. Lastly,

the chapter covers the effect of volcanic emission of halogens into the atmosphere and its long- and short-term impact on atmospheric chemistry. These can range from global perturbation of the stratospheric O_3 budget to more localized life-threatening contamination of soils and fresh water.

1.7 Halogens in Silicic Magmas and Their Hydrothermal Systems: Chap. 7

Chapter 7 (Dolejs and Zajacz 2018) focuses on the role of halogens in silicic magmas and the hydrothermal systems associated with them. Crystal chemical considerations are invoked to explain differences in the solubility of halogens, mainly F and Cl, in silicate melts and aqueous fluids. The similarity in the ionic radii of O, OH, and F, coupled with the much greater size of Cl, are responsible for (i) higher solubility, hence compatibility of F in silicate melts, (ii) the greater lattice energies of fluorides, therefore their more refractory character and lower solubilities in fluids, and (iii) the higher hardness of F as a ligand for complexing, leading to a distinct spectrum of metal-fluoride vs. metal-chloride complexes. Chlorine is dominantly present as NaCl, KCl, $FeCl_2$, and HCl species in aqueous magmatic fluids; The relative proportions of which are strongly influenced by silicate melt composition, pressure, and total dissolved chloride concentration. Based on the thermodynamic representation of F and Cl solubilities in felsic melts, some major phase relations along the differentiation paths for the F and Cl-bearing silicic magmas are presented, including fluoride-silicate liquid immiscibility in the F-rich systems and silicic melt-brine-vapor relations in the Cl- bearing systems. Differences in the ore-forming potential of F- and Cl-bearing magmas are also discussed (see also Chap. 5, Lecumberri-Sanchez and Bodnar 2018). The fluoride ligand is responsible for the effective sequestration of hard cations, (mainly REE, Th, U, and Zr), into hydrothermal fluids, whereas the chloride ions are dominant, or at least significant complex forming ligands, for a broad range of economically important elements found in Cu-, Au-, Mo-, Pb-, Zn-, Sn-, and W-bearing magmatic-hydrothermal ore deposits.

1.8 The Behavior of Halogens During Subduction-Zone Processes: Chap. 8

The behavior of halogens during subduction-zone processes is reviewed by Barnes et al. (2018) in Chap. 8 (see also Bebout 2013; Klemd 2013; Kendrick 2018). Halogens (Cl, F, I, and Br) are enriched in surface reservoirs compared to the mantle. The subduction of these reservoirs in the form of sedimentary pore fluids, sediments, altered oceanic crust, and serpentinized mantle lithosphere return halogens to the mantle and to regions of arc magma genesis. It is proposed that serpentinites $\pm$ altered oceanic crust are responsible for subducting the largest amount of

halogens to those depths where magma genesis occurs. The addition of halogens, particularly Cl, increases the ability of subduction-zone fluids to transport metals and trace elements. The amount of Cl in solution is a function of the P-T conditions of the subduction zone, such that higher temperatures at a given depth and lower pressures at a given temperature favor ion pair formation ($NaCl_{aq}$, KCl_{aq}). Mass balance calculations and halogen concentrations in back-arc basalts and ocean island basalts show that more halogens are subducted than returned to the Earth's surface through volcanic arc fronts, implying the transport of halogens into the upper mantle. Chlorine is the halogen most efficiently recycled to the surface, and F the least. Loss of I and Br, early on through shallow fore-arc fluids that are not accounted for in mass balance calculations, likely explain the unbalance in these cycles.

1.9 Halogens in Seawater, Marine Sediments, and the Altered Oceanic Lithosphere: Chap. 9

Chapter 9 (Kendrick 2018; see also Bach et al. 2013) aims to provide a framework for understanding the distribution of halogens in the oceanic lithosphere. It reviews the concentration of F, Cl, Br, and I in seawater, marine sediment pore waters, hydrothermal vent fluids, fluid inclusions from deeper in the crust, and the complementary solid-phase reservoirs of organic matter and minerals present in sediments and crustal rocks from varying depths. Altered oceanic crust has F concentrations close to the initial value. In contrast, Cl is mobilized within layer 2 pillows and dykes and strongly enriched in layer 3 gabbros subjected to high temperature alteration. Amphibole is the dominant Cl host in the oceanic crust, with Cl concentrations of <500 ppm under greenschist-facies conditions and up to wt% levels under amphibolite-facies conditions. The increasing Cl content of amphibole as a function of metamorphic grade most likely reflects a decreasing water/rock ratio and a general increase in fluid salinity as a function of depth in the crust. Amphibole preferentially incorporates Cl relative to Br and I. However, it is possible that I is enriched in absolute terms, and relative to Cl, in clay-rich alteration and biogenic alteration of glassy rocks in the upper oceanic crust. Serpentinites, formed in the oceanic lithosphere, can contain thousands of ppm Cl and some serpentinites preserve Br/Cl and I/Cl signatures very similar to sedimentary pore waters, indicating that all the halogens have high compatibilities in serpentine. Fluorine is slightly enriched in serpentinites compared to peridotites, which may indicate mobilization of F from igneous lithologies in the crust. Overall, the altered oceanic lithosphere reaching subduction zones is estimated to have a maximum median Cl content of $\sim$400 ppm, and it is estimated to have an F/Cl ratio of $\sim$0.25 compared to $\sim$2 in pristine crust. It is therefore estimated that approximately 90% of the Cl present in altered oceanic lithosphere is introduced during seawater alteration. By employing bulk halogen content and indicator ratios, Chap. 9 traces

the routes followed by the four major halogens from seawater to sediments to serpentinite to the altered ocean crust to subduction zones.

1.10 The Role of Halogens During Regional and Contact Metamorphism: Chap. 10

The role of halogens during regional and contact metamorphism is thoroughly covered by Hammerli and Rubenach (2018) in Chap. 10 (see also Rubenach 2013 and Aranovich and Safanov 2018). Minerals useful for understanding halogen behavior during metamorphism include scapolite, apatite, titanite, biotite, and amphibole. However, their ability to incorporate halogens depends on parameters such as bulk rock composition, fluid properties, and fluid-rock ratios. Recent analytical advancements allow for the more routine analyses of halogen contents in minerals and fluid inclusions. For instance, in situ LA-ICP-MS analyses of Cl and Br allow for the reconstruction of the interaction of halogen-bearing fluids with crustal rocks in complex geological settings that have undergone multiple fluids events. In such cases, scapolite can be used as an archive for fluid properties during metamorphism. Research on F and Cl in apatite in siliceous marbles from five classic aureoles highlights the use of this mineral regarding rock or fluid buffering, and in establishing fluid sources. Chlorine enrichment in biotite and amphibole, associated with regional albitization, demonstrate that advection of saline fluids during albitization and K-feldspar metasomatism occurs in association with regional mineralization. Chlorine-bearing fluids are capable of mobilizing large amounts of metals during large-scale metamorphism on a regional, whole rock, and mineral scale. Consequently, Cl-bearing fluid flow could be an essential prerequisite to actively discharge metals from metamorphic rocks into neighboring rocks allowing for the potential formation of ore bodies (see also Lecumberri-Sanchez and Bodnar 2018).

1.11 Halogens in High-Grade Metamorphism: Chap. 11

Chapter 11 (Aranovich and Safonov 2018; see also Touret and Nijland 2013; Hammerli and Rubenach 2018) reviews the factors, which control the distribution of the two major halogens, F and Cl, in high-grade metamorphic rocks; their compositional correlations and partitioning between minerals; experimental data on the stability and phase equilibria of the halogen-bearing minerals; the influence of halogens on Fe-Mg exchange reactions; and the means of estimating the concentrations/activity of halogen species in the fluid phase ("chlorimetry and fluorimetry") via calculation of equilibrium conditions for mineral assemblages containing halogen-bearing phases. While natural biotite and amphibole obey the Fe-F avoidance rule, a scattering of points on the X_{Fe}-Cl and TiO_2-Cl diagrams indicate the possible involvement of an exotic Cl-rich phase (fluid or melt) during the

formation of Cl-bearing biotite and amphibole. Fluorine and Cl, substituting for OH-groups, substantially stabilize minerals relative to dehydration and melting. Calculations, based on recent thermodynamic systematics, show that a relatively Mg-rich, Cl-poor biotite may coexist with a fairly Cl-rich fluid under granulite facies P-T conditions. Alkali (and Ca) metasomatism, caused by interaction of high grade rocks with halogen-bearing fluids, may have a major impact on subsolidus phase transformation and melting processes during high-grade metamorphism and anatexis.

1.12 Halogens in Hydrothermal Fluids and Their Role in the Formation and Evolution of Hydrothermal Mineral Systems: Chap. 12

Chapter 12 (Pirajno 2018) discusses halogen complexes and ligands in hydrothermal solutions (see also Pirajno 2013; Lecumberri-Sanchez and Bodnar 2018). The progress of halogens during the differentiation of granitic magmas and their role in the development of granitoid-related mineral systems are considered. The exsolution and near surface venting of halogens in hot springs, geysers, and volcanic complexes in general are treated and examples provided. The function of F in greisen-type mineralization is elucidated, followed by specific examples of fluorite associated with continental porphyry deposits in eastern China and the giant Vergenoeg Fe and fluorite deposit in South Africa. Halogens in hydrothermal fluids, associated with the formation of skarn deposits, are also discussed. Finally, the presence and very important role of halogens in evaporite sequences during the creation of continental hydrothermal deposits is emphasized. It is important to note that evaporite sequences may have an active or passive role in supplying halogens to ore-making hydrothermal fluids. The former is exemplified by the sabkah evaporites, which form by direct interaction of basinal fluids with seawater leading to the formation of copper belt-type mineral systems. Whereas in the latter case, fluids passively leach and transport halogen-based complexing agents for the epigenetic precipitation of ores. Halogens responsible for the uptake and transport of metals in MVT (Mississippi Valley-type deposits), SEDEX (sedimentary exhalative deposits), IOCG (iron oxide-copper-gold deposits), and orogenic mineral systems conclude this chapter.

1.13 The Role of Halogens in the Lithospheric Mantle: Chap. 13

Chapter 13 (Frezzotti and Ferrando 2018) focuses on the still poorly known sources, distribution, and fractionation of halogens in the oceanic and continental lithospheric mantle in intraplate and extensional tectonic settings, and in the deep cratonic sub-continental mantle that hosts diamonds and kimberlites (see also

O'Reilly and Griffin 2013; Kendrick 2018; Barnes et al. 2018). In the lithospheric mantle, halogens can be stored not only in volatile-bearing metasomatic minerals, such as apatite, amphibole, and phlogopite, but also in the nominally anhydrous minerals, incorporating measurable amounts of water as hydroxyl. The halogen contents of these minerals influence their stability in the lithospheric mantle. Consequently, these minerals might be responsible for halogen enrichment and trace element signatures in some primitive basaltic melts. Based on fluid inclusion studies, the nature of halogen-bearing fluids in intraplate and extensional settings, including those related to diamond-forming processes, is discussed in detail. Fluid inclusion data, has confirmed that relatively high amounts of halogens can be dissolved in aqueous-carbonic fluids, which may be locally immiscible, and in hydrous carbonate melts which ascend through the lithospheric mantle in intraplate and extensional settings. Metasomatic halide-bearing fluids are important carriers of incompatible trace elements (e.g., LILE and LREE). Halogen enrichment in lithospheric mantle fluids, both in the vicinity of, and away from, subduction zones, suggests a dynamic balance in the halogen geochemical cycle, which is ruled by recycling of surface halogens and mantle fractionation processes.

1.14 Halogens in the Earth's Mantle: Chap. 14

Chapter 14 by Klemme and Stalder (2018) presents an overview of the currently available experimental, analytical, and theoretical data on halogen storage in mantle minerals, halogen concentrations in nominally halogen free mantle minerals, and halogen partitioning between mantle minerals and mantle magmatic processes (see also Frezzotti and Ferrando 2018).

1.15 Halogens in Chondritic Meteorites: Chap. 15

Chapter 15 (Brearley and Jones 2018) reviews the abundances, distributions, and isotopic compositions of halogens in chondritic meteorites (see also Brearley and Krot 2013). Chapter 15 also considers the formation of halogen-bearing minerals and possible fluids associated with these elements. Halogens can act as tracers for processes that occurred in circumstellar and interstellar environments, within the solar nebula, and after accretion within asteroidal meteorite parent bodies. Knowledge of the halogen abundances in chondrites is fundamental to understanding the halogen contents of the Earth and other terrestrial planets. Analytical challenges and uncertainties in halogen condensation temperatures hamper the application of halogens to constrain processes in the solar nebula and the chondrite parent bodies. However, although there are significant variations in the analytical data, even within individual chondrite groups, distinct, but complex differences between the main classes of chondrites, carbonaceous, ordinary, and enstatite meteorites, are still evident. The

origin of halogen-bearing phases in various chondrites is also discussed. The application of halogen stable isotope geochemistry for constraining the condensation and secondary alteration processes and radiogenic isotope geochemistry in the dating of early solar system processes is demonstrated. This chapter also provides a broad overview of future research for this very promising direction in the geochemical investigation of meteoritics and planetary science.

1.16 The Role of Halogens During Fluid and Magmatic Processes on Mars: Chap. 16

Chapter 16 (Rampe et al. 2018) covers halogens in the martian mantle, their role during igneous evolution of the martian crust and lithospheric mantle, their presence in the aqueous processes that have sculpted the surface of Mars, and their role in the potential habitability of Mars both for native life and terrestrial life. Fluorine, Cl, Br, and I abundances have been measured from martian meteorites, in situ by landers and rovers, and from orbital missions around Mars. All four halogens have been detected in silicate, phosphate, sulfate, oxide, and halide group minerals in martian meteorites. These halogen-bearing minerals are found in melt inclusions, as secondary hydrothermal or aqueous alteration products, or in the interstices between cumulus igneous silicates. The bulk rock abundances of halogens have been determined for many martian meteorite samples for all five types (nakhlites, chassignites, shergottites, orthopyroxenites, and regolith breccias). Measurements of basaltic martian meteorites (i.e., shergottites and regolith breccias) provide important insights into halogen abundances in mantle and crustal reservoirs. Measurements from both meteorites and from martian missions indicate that Cl is the most abundant halogen on and in Mars. Measurements of the martian surface from landed missions suggest that Cl is commonly present in oxychlorine compounds (e.g., perchlorate and chlorate salts), whereas measurements from orbit have identified both oxychlorine minerals and halite. Halite is constrained to local depressions in the ancient southern highlands, suggesting precipitation from the evaporation of water in closed basins $\sim$3.5–4 Ga. The presence of oxychlorine minerals on the martian surface has important implications for the habitability of the modern Mars because oxychlorine minerals may deliquesce to create seasonal deposits of liquid water. Furthermore, oxychlorine compounds are considered both a resource and potential hazard to the eventual human exploration of Mars.

1.17 Halogens on and Within the Ocean Worlds of the Outer Solar System: Chap. 17

Halogens on and within the ocean worlds of the outer solar system are covered by Chap. 17 (Hand 2018). A number of gas giant moons located in the outer solar system, including three of the Galilean satellites of Jupiter, i.e. Europa, Ganymede,

and Callisto, and three moons of Saturn, Enceladus, Mimas, and Titan, harbor oceans beneath icy crusts. Halogen salts serve as a key indicator of whether or not these liquid water environments could satisfy important requirements for life. The presence of salts within these oceans is, and can be, an indicator of water-rock interactions between liquid water and silicate, halogen-rich, seafloors. In some cases, seafloor cycling within these moons may be sufficient to drive low-, or possibly even high-temperature hydrothermal activity. In this Chapter, the current state of knowledge of these oceans beyond the Earth is reviewed and both empirical and modeling constraints on halogens within these environments are provided. Past, present, and future spacecraft missions to these worlds are described, and the implications for future discoveries of astrobiological importance are discussed.

References

Acosta-Vigil A, London D, Dewers TA, Morgan GB (2002) Dissolution of corundum and andalusite in H_2O-saturated haplogranitic melts at 800 °C and 200 MPa: constraints on diffusivities and the generation of peraluminous melts. J Petrol 43:1885–1908

Akinfiev NN, Diamond LW (2009) A simple predictive model of quartz solubility in water–salt–CO_2 systems at temperatures up to 1000 °C and pressures up to 1000 MPa. Geochim Cosmochim Acta 73:1597–1608

Antignano A, Manning CE (2008a) Fluorapatite solubility in H_2O and H_2O–NaCl at 700 to 900 °C and 0.7 to 2.0 GPa. Chem Geol 251:112–119

Antignano A, Manning CE (2008b) Rutile solubility in H_2O, H_2O–SiO_2, and H_2O–$NaAlSi_3O_8$ fluids at 0.7–2.0 GPa and 700–1000 °C: implications for mobility of nominally insoluble elements. Chem Geol 255:283–293

Aranovich LY, Newton RC (1996) H_2O activity in concentrated NaCl solutions at high pressures and temperatures measured by the brucite-periclase equilibrium. Contrib Mineral Petrol 125:200–212

Aranovich LY, Newton RC (1997) H_2O activity in concentrated KCl and KCl-NaCl solutions at high temperatures and pressures measured by the brucite-periclase equilibrium. Contrib Mineral Petrol 127:261–271

Aranovich LY, Newton RC (1998) Reversed determination of the reaction: phlogopite + quartz = enstatite + potassium feldspar + H_2O in the ranges 750–875 °C and 2–12 kbar at low H_2O activity with concentrated KCl solutions. Am Mineral 83:193–204

Aranovich L, Safonov O (2018) Halogens in high-grade metamorphism. In: Harlov DE, Aranovich L (eds) The role of halogens in terrestrial and extraterrestrial geochemical processes: surface, crust, and mantle. Springer, Berlin, pp 713–757

Aranovich LY, Zakirov IV, Sretenskaya NG, Gerya TV (2010) Ternary system H_2O-CO_2-NaCl at high T-P parameters: an empirical mixing model. Geochem Int 48:446–455

Aranovich LY, Newton RC, Manning CE (2013) Brine-assisted anatexis: experimental melting in the system haplogranite–H_2O–NaCl–KCl at deep-crustal conditions. Earth Planet Sci Lett 374:111–120

Aranovich LY, Makhluf AR, Manning CE, Newton RC (2014) Dehydration melting and the relationship between granites and granulites. Precambr Res 253:26–37

Audetat A, Keppler H (2005) Solubility of rutile in subduction zone fluids, as determined by experiments in the hydrothermal diamond anvil cell. Earth Planet Sci Lett 232:393–402

Ayers JC, Zhang L, Luo Y, Peters TJ (2012) Zircon solubility in alkaline aqueous fluids at upper crustal conditions. Geochim Cosmochim Acta 96:18–28

Bach W, Jöns N, Klein F (2013) Metasomatism within the ocean crust. In: Harlov DE, Austrheim H (eds) Metasomatism and the chemical transformation of rock: the role of fluids in terrestrial and extraterrestrial processes. Springer, Berlin, pp 253–288

Barnes J, Manning C, Scambelluri M, Selverstone J (2018) The behavior of halogens during subduction zone processes. In: Harlov DE, Aranovich L (eds) The role of halogens in terrestrial and extraterrestrial geochemical processes: surface, crust, and mantle. Springer, Berlin, pp 545–590

Bebout GE (2013) Metasomatism in subduction zones of subducted oceanic slabs, mantle wedges, and the slab-mantle interface. In: Harlov DE, Austrheim H (eds) Metasomatism and the chemical transformation of rock: the role of fluids in terrestrial and extraterrestrial processes. Springer, Berlin, pp 289–349

Brearley A, Jones R (2018) Halogens in chondritic meteorites. In: Harlov DE, Aranovich L (eds) The role of halogens in terrestrial and extraterrestrial geochemical processes: surface, crust, and mantle. Springer, Berlin, pp 871–958

Brearley AJ, Krot AN (2013) Metasomatism in the early solar system: the record from chondritic meteorites. In: Harlov DE, Austrheim H (eds) Metasomatism and the chemical transformation of rock: the role of fluids in terrestrial and extraterrestrial processes. Springer, Berlin, pp 659–789

Brenan JM, Watson EB (1988) Fluids in the lithosphere, 2. Experimental constraints on CO_2 transport in dunite and quartzite at elevated P-T conditions with implications for mantle and crustal decarbonation processes. Earth Planet Sci Lett 91:141–158

Cruz MF, Manning CE (2015) Experimental determination of quartz solubility and melting in the system SiO_2–H_2O–NaCl at 15–20 kbar and 900–1100 °C: implications for silica polymerization and the formation of supercritical fluids. Contrib Mineral Petrol 170:35

Dolejs D, Zajacz Z (2018) Halogens in silicic magmas and their hydrothermal systems. In: Harlov DE, Aranovich L (eds) The role of halogens in terrestrial and extraterrestrial geochemical processes: surface, crust, and mantle. Springer, Berlin, pp 431–543

Duc-Tin Q, Keppler H (2015) Monazite and xenotime solubility in granitic melts and the origin of the lanthanide tetrad effect. Contrib Mineral Petrol 169:168. https://doi.org/10.1007/s00410-014-1100-9

Fockenberg T, Burchard M, Maresch WV (2006) Experimental determination of the solubility of natural wollastonite in pure water up to pressures of 5 GPa and at temperatures of 400–800 °C. Geochim Cosmochim Acta 70:1796–1806

Frezzotti M-L, Ferrando S (2018) The role of halogens in the lithospheric mantle. In: Harlov DE, Aranovich L (eds) The role of halogens in terrestrial and extraterrestrial geochemical processes: surface, crust, and mantle. Springer, Berlin, pp 805–845

Gibert F, Guillaume D, Laporte D (1998) Importance of fluid immiscibility in the H_2O-NaCl-CO_2 system and selective CO_2 entrapment in granulites: experimental phase diagram at 5–7 kbar, 900 °C and wetting textures. Eur J Mineral 10:1109–1123

Hand KP (2018) Halogens on and within the ocean worlds of the outer solar system. In: Harlov DE, Aranovich L (eds) The role of halogens in terrestrial and extraterrestrial geochemical processes: surface, crust, and mantle. Springer, Berlin, pp 997–1016

Hanley JJ, Koga K (2018) Halogens in terrestrial and cosmic geochemical systems: abundances, geochemical behaviors, and analytical methods. In: Harlov DE, Aranovich L (eds) The role of halogens in terrestrial and extraterrestrial geochemical processes: surface, crust, and mantle. Springer, Berlin, pp 21–121

Hansen EC, Harlov DE (2007) Whole-rock, phosphate, and silicate compositional trends across an amphibolite- to granulite-facies transition, Tamil Nadu, India. J Petrol 48:1641–1680

Hammerli J, Rubenach M (2018) The role of halogens during regional and contact metamorphism. In: Harlov DE, Aranovich L (eds) The role of halogens in terrestrial and extraterrestrial geochemical processes: surface, crust, and mantle. Springer, Berlin, pp 649–712

Hammouda T, Chantel J, Devidal J-L (2010) Apatite solubility in carbonatitic liquids and trace element partitioning between apatite and carbonatite at high pressure. Geochim Cosmochim Acta 74:7220–7235

Harlov DE (2012) The potential role of fluids during regional granulite-facies dehydration in the lower crust. Geosci Front 3:813–827

Harlov DE, Förster H-J (2002a) High-grade fluid metasomatism on both a local and a regional scale: the Seward Peninsula, Alaska, and the Val Strona di Omegna, Ivrea-Verbano Zone, northern Italy. Part I: petrography and silicate mineral chemistry. J Petrol 43:769–799

Harlov DE, Förster H-J (2002b) High-grade fluid metasomatism on both a local and a regional scale: the Seward Peninsula, Alaska, and the Val Strona di Omegna, Ivrea-Verbano Zone, northern Italy. Part II: phosphate mineral chemistry. J Petrol 43:801–824

Harlov DE, Johansson L, Van den Kerkhof A, Förster H-J (2006) The role of advective fluid flow and diffusion during localized, solid-state dehydration: Söndrum stenhuggeriet, Halmstad, SW Sweden. J Petrol 47:3–33

Hauzenberger CA, Baumgartner LP, Pak TM (2001) Experimental study on the solubility of the "model"-pelite mineral assemblage albite + K-feldspar + andalusite + quartz in supercritical chloride-rich aqueous solutions at 0.2 GPa and 600 °C. Geochim Cosmochim Acta 65:4493–4507

Hayden LA, Manning CE (2011) Rutile solubility in supercritical $NaAlSi_3O_8$–H_2O fluids. Chem Geol 284:74–81

Heinrich W (2007) Fluid immiscibility in metamorphic rocks. Rev Mineral Geochem 65:389–430

Johnson EL (1991) Experimentally determined limits for H_2O-CO_2-NaCI immiscibility in granulites. Geology 19:925–928

Kendrick M (2018) Halogens in seawater, marine sediments, and the altered oceanic lithosphere. In: Harlov DE, Aranovich L (eds) The role of halogens in terrestrial and extraterrestrial geochemical processes: surface, crust, and mantle. Springer, Berlin, pp 591–648

Kerkhof A van den, Kronz A, Simon K (2014) Deciphering fluid inclusions in high-grade rocks. Geosci Front 5:683–695

Klemd R (2013) Metasomatism during high-pressure metamorphism: eclogites and blueschist-facies rocks. In: Harlov DE, Austrheim H (eds) Metasomatism and the chemical transformation of rock: the role of fluids in terrestrial and extraterrestrial processes. Springer, Berlin, pp 351–413

Klemme S, Stalder R (2018) Halogens in the Earth's mantle: what we know and what we don't. In: Harlov DE, Aranovich L (eds) The role of halogens in terrestrial and extraterrestrial geochemical processes: surface, crust, and mantle. Springer, Berlin, pp 847–869

Korzhinskii DS (1959) Physicochemical basis of the analysis of the paragenesis of minerals. Chapman and Hall, New York, p 142

Korzhinskii, DS (1962) The role of alkalinity in the formation of charnockitic gneisses. In: Precambrian geology and petrology: general and regional problems. Trudy Vostochono-Sibirskogo Geologicheskogo Institute, Geological Series 5:50–61 (In Russian)

Lecumberri-Sanchez P, Bodnar R (2018) Halogen geochemistry of ore deposits: contributions towards understanding sources and processes. In: Harlov DE, Aranovich L (eds) The role of halogens in terrestrial and extraterrestrial geochemical processes: surface, crust, and mantle. Springer, Berlin, pp 261–305

Makhluf AR, Newton RC, Manning CE (2016) Hydrous albite magmas at lower crustal pressure: new results on liquidus H_2O content, solubility, and H_2O activity in the system $NaAlSi_3O_8$–H_2O–NaCl at 1.0 GPa. Contrib Mineral Petrol 171:75

Manning CE (1994) The solubility of quartz in H_2O in the lower crust and upper mantle. Geochim Cosmochim Acta 58:4831–4839

Manning CE (2007) Solubility of corundum + kyanite in H_2O at 700 °C and 10 kbar: evidence for Al-Si complexing at high pressure and temperature. Geofluids 7:258–269

Manning CE, Aranovich LY (2014) Brines at high pressure and temperature: thermodynamic, petrologic and geochemical effects. Precambr Res 253:6–16

Manning CE, Wilke M, Schmidt C, Cauzid J (2008) Rutile solubility in albite-H_2O and $Na_2Si_3O_7$ –H_2O at high temperatures and pressures by in-situ synchrotron radiation micro-XRF. Earth Planet Sci Lett 272:730–737

Manning CE, Antignano A, Lin HA (2010) Premelting polymerization of crustal and mantle fluids, as indicated by the solubility of albite + paragonite + quartz in H_2O at 1 GPa and 350–620 °C. Earth Planet Sci Lett 292:325–336

McCubbin FM, Jolliff BL, Nekvasil H, Carpenter PK, Zeigler RA, Steele A, Elardo SM, Lindsley DH (2011) Fluorine and chlorine abundances in lunar apatite: implications for heterogeneous distributions of magmatic volatiles in the lunar interior. Geochim Cosmochim Acta 75:5073–5093

Mi J-X, Pan Y (2018) Halogen-rich minerals: crystal chemistry and geological significances. In: Harlov DE, Aranovich L (eds) The role of halogens in terrestrial and extraterrestrial geochemical processes: surface, crust, and mantle. Springer, Berlin, pp 123–184

Munoz JL (1984) F-OH and Cl-OH exchange in micas with applications to hydrothermal ore deposits. In: Bailey SW (ed) Micas. Mineralogical Society of America, Reviews in Mineralogy 13:469–494

Munoz JL (1992) Calculation of HF and HCl fugacities from biotite compositions: revised equations. Geological Society of America, Abstracts with Programs 26:221

Newton RC, Manning CE (2000) Quartz solubility in H_2O-NaCl and H_2O-CO_2 solutions at deep crust-upper mantle pressures and temperatures: 2–15 kbar and 500–900 °C. Geochim Cosmochim Acta 64:2993–3005

Newton RC, Manning CE (2002a) Experimental determination of calcite solubility in H_2O-NaCl solutions at deep crust/upper mantle pressures and temperatures: implications for metasomatic processes in shear zones. Am Mineral 87:1401–1409

Newton RC, Manning CE (2002b) Solubility of enstatite + forsterite in H_2O at deep crust/upper mantle conditions: 4 to 15 kbar and 700 to 900 °C. Geochim Cosmochim Acta 66:4165–4176

Newton RC, Manning CE (2005) Solubility of anhydrite, $CaSO_4$, in NaCl–H_2O solutions at high pressures and temperatures: applications to fluid–rock interaction. J Petrol 46:701–716

Newton RC, Manning CE (2006) Solubilities of corundum, wollastonite and quartz in H_2O–NaCl solutions at 800 °C and 10 kbar: interaction of simple minerals with brines at high pressure and temperature. Geochim Cosmochim Acta 70:5571–5582

Newton RC, Manning CE (2007) Solubility of grossular, $Ca_3Al_2Si_3O_{12}$, in H_2O–NaCl solutions at 800 °C and 10 kbar, and the stability of garnet in the system $CaSiO_3$–Al_2O_3–H_2O–NaCl. Geochim Cosmochim Acta 71:5191–5202

Newton RC, Manning CE (2008) Thermodynamics of SiO_2–H_2O fluid near the upper critical end point from quartz solubility measurements at 10 kbar. Earth Planet Sci Lett 274:241–249

Newton RC, Manning CE (2010) Role of saline fluids in deep-crustal and upper-mantle metasomatism: insights from experimental studies. Geofluids 10:58–72

Newton RC, Manning CE, Hanchar JM, Finch RJ (2005) Gibbs free energy of formation of zircon from measurements of solubility in H_2O. J Am Ceram Soc 88:1854–1858

Newton RC, Manning CE, Hanchar JM, Colasanti CV (2010) Free energy of formation of zircon based on solubility measurements at high temperature and pressure. Am Mineral 95:52–58

O'Reilly SY, Griffin WL (2013) Mantle metasomatism. In: Harlov DE, Austrheim H (eds) Metasomatism and the chemical transformation of rock: the role of fluids in terrestrial and extraterrestrial processes. Springer, Berlin, pp 471–533

Paillat O, Elphick SC, Brown WL (1992) The solubility of water in $NaAlSi_3O_8$ melts: a re-examination of Ab-H_2O phase relationships and critical behaviour at high pressures. Contrib Mineral Petrol 112:490–500

Pak TM, Hauzenberger CA, Baumgartner LP (2003) Solubility of the assemblage albite + K-feldspar + andalusite + quartz in supercritical aqueous chloride solutions at 650 °C and 2 kbar. Chem Geol 200:377–393

Pirajno F (2013) Effects of metasomatism on mineral systems and their host rocks: alkali metasomatism, skarns, greisens, tourmalinites, rodingites, black-wall alteration and listevenites. In: Harlov DE, Austrheim H (eds) Metasomatism and the chemical transformation of rock: the role of fluids in terrestrial and extraterrestrial processes. Springer, Berlin, pp 203–251

Pirajno F (2018) Halogens in hydrothermal fluids and their role in the formation and evolution of hydrothermal mineral systems. In: Harlov DE, Aranovich L (eds) The role of halogens in terrestrial and extraterrestrial geochemical processes: surface, crust, and mantle. Springer-Verlag, Berlin, pp 759–804

Poitrasson F, Oelkers E, Schott J, Montel J-M (2004) Experimental determination of synthetic $NdPO_4$ monazite end-member solubility in water from 2 °C to 300 °C: implications for rare earth element mobility in crustal fluids. Geochim Cosmochim Acta 68:2207–2221

Rampe EB, Cartwright JA, McCubbin FM, Osterloo MM (2018) The role of halogens during fluid and magmatic processes on Mars. In: The role of halogens in terrestrial and extraterrestrial geochemical processes: surface, crust, and mantle. Springer, Berlin, pp 959–995

Rapp JF, Klemme S, Butler IB, Harley SL (2010) Extremely high solubility of rutile in chloride and fluoride-bearing metamorphic fluids; an experimental investigation. Geology 38:323–326

Rubenach M (2013) Structural controls of metasomatism on a regional scale. In: Harlov DE, Austrheim H (eds) Metasomatism and the chemical transformation of rock: the role of fluids in terrestrial and extraterrestrial processes. Springer, Berlin, pp 93–140

Safanov OG, Aranovich LY (2014) Alkali control of high-grade metamorphism and granitization. Geosci Front 5:711–727

Sallet R (2000) Fluorine as a tool in the petrogenesis of quartz-bearing magmatic associations: applications of an improved F-OH biotite-apatite thermometer grid. Lithos 50:241–253

Shmulovich KI, Graham CM (1996) Melting of albite and dehydration of brucite in H_2O-NaCl fluids to 9 kbars and 700–900 °C: implications for partial melting and water activities during high pressure metamorphism. Contrib Mineral Petrol 124:370–382

Shmulovich KI, Graham CM (2008) Plagioclase–aqueous solution equilibrium (NaCl-$CaCl_2$): concentration dependence. Petrology 16:191–206

Shmulovich K, Graham C, Yardley B (2001) Quartz, albite, and diopside solubilities in H_2O-NaCl and H_2O-CO_2 fluids at 0.5–0.9 GPa. Contrib Mineral Petrol 141:95–108

Shmulovich KI, Yardley BWD, Graham CM (2006) Solubility of quartz in crustal fluids: experiments and general equations for salt solutions and H_2O–CO_2 mixtures at 400–800 °C and 0.1–0.9 GPa. Geofluids 6:154–167

Signorelli S, Carroll MR (2002) Experimental study of Cl solubility in hydrous alkaline melts: constraints on the theoretical maximum amount of Cl in trachytic and phonolitic melts. Contrib Mineral Petrol 143:209–218

Skora S, Blundy J (2012) Monazite solubility in hydrous silicic melts at high pressure conditions relevant to subduction zone metamorphism. Earth Planet Sci Lett 321–322:104–114

Tanis EA, Simon AC, Zhang Y, Chow P, Xiao Y (2016) Rutile solubility in NaF-NaCl-KCl-bearing aqueous fluids at 0.5–2.79 GPa and 250–650 °C. Geochim Cosmochim Acta 177:170–181

Tropper P, Manning CE (2005) Very low solubility of rutile in H_2O at high pressure and temperature, and its implications for Ti mobility in subduction zones. Am Mineral 90:502–505

Tropper P, Manning CE (2007) The solubility of fluorite in H_2O and H_2O–NaCl at high pressure and temperature. Chem Geol 242:299–306

Tropper P, Manning CE, Harlov DE (2011) Solubility of $CePO_4$ monazite and YPO_4 xenotime in H_2O and H_2O–NaCl at 800 °C and 1 GPa: implications for REE and Y transport during high-grade metamorphism. Chem Geol 282:58–66

Tropper P, Manning CE, Harlov DE (2013) Experimental determination of $CePO_4$ and YPO_4 solubilities in H_2O–NaF at 800 °C and 1 GPa: implications for rare earth element transport in high-grade metamorphic fluids. Geofluids 13:372–380

Touret JLR, Nijland TG (2013) Prograde, peak and retrograde metamorphic fluids and associated metasomatism in upper amphibolite to granulite facies transition zones. In: Harlov DE, Austrheim H (eds) Metasomatism and the chemical transformation of rock: the role of fluids in terrestrial and extraterrestrial processes. Springer, Berlin, pp 415–469

Walther JV (2001) Experimental determination and analysis of the solubility of corundum in 0.1 and 0.5 m NaCl solutions between 400 and 600 °C from 0.5 to 2.0 kbar. Geochim Cosmochim Acta 65:2843–2851

Walther JV (2002) Experimental determination and analysis of the solubility of corundum in 0.1 molal $CaCl_2$ solutions between 400 and 600 °C at 0.6 to 2.0 kbar. Geochim Cosmochim Acta 66:1621–1626

Watson EB, Brenan JM (1987) Fluids in the lithosphere, 1. Experimentally-determined wetting characteristics of CO_2-H_2O fluids and their implications for fluid transport, host-rock physical properties, and fluid inclusion formation. Earth Planet Sci Lett 85:497–515

Webster JD, Piccoli PM (2015) Magmatic apatite: a powerful, yet deceptive, mineral. Elements 11:177–182

Webster J, Baker DR, Aiuppa A (2018) Halogens in mafic and intermediate-silica content magmas. In: Harlov DE, Aranovich L (eds) The role of halogens in terrestrial and extraterrestrial geochemical processes: surface, crust, and mantle. Springer, Berlin, pp 307–430

Wilke M, Schmidt C, Dubrail J, Appel K, Borchert M (2012) Zircon solubility and zirconium complexation in H_2O + Na_2O + SiO_2 + Al_2O_3 fluids at high pressure and temperature. Earth Planet Sci Lett 349–350:15–25

Wohlers A, Manning CE, Thompson AB (2011) Experimental investigation of the solubility of albite and jadeite in H_2O, with paragonite + quartz at 500 and 600 °C, and 1–2.25 GPa. Geochim Cosmochim Acta 75:2924–2939

Worden RH (2018) Halogen elements in sedimentary systems and their evolution during digenesis. In: Harlov DE, Aranovich L (eds) The role of halogens in terrestrial and extraterrestrial geochemical processes: surface, crust, and mantle. Springer, Berlin, pp 185–260

Wykes JL, Newton RC, Manning CE (2008) Solubility of andradite, $Ca_3Fe_2Si_3O1_2$ in a 10 mol% NaCl solution at 800 °C and 10 kbar; implications for the metasomatic origin of grandite garnet in calc-silicate granulites. Am Mineral 93:886–892

Yardley BWD (2013) The chemical composition of metasomatic fluids in the crust. In: Harlov DE, Austrheim H (eds) Metasomatism and the chemical transformation of rock: the role of fluids in terrestrial and extraterrestrial processes. Springer, Berlin, pp 17–51

Zhou L, Mavrogenes JA, Spandler C, Li H (2016) A synthetic fluid inclusion study of the solubility of monazite-(La) and xenotime-(Y) in H_2O-Na-K-Cl-F-CO_2 fluids at 800 °C and 0.5 GPa. Chem Geol 442:121–129

Zhu C, Sverjensky DA (1992) F-Cl-OH partitioning between biotite and apatite. Geochim Cosmochim Acta 56:3435–3467

Chapter 2
Halogens in Terrestrial and Cosmic Geochemical Systems: Abundances, Geochemical Behaviors, and Analytical Methods

Jacob J. Hanley and Kenneth T. Koga

Abstract The aims of this review chapter are to (i) summarize the distribution of halogens in different fluid (surficial, formation and crystalline shield waters, metamorphic, magmatic-hydrothermal-geothermal) and solid (oceanic and continental crust, mantle and core) domains of the Earth, and various extra-terrestrial materials and bodies (meteorites, planets and moons, and the Sun); (ii) briefly discuss characteristic fractionation processes; and direct the reader to other chapters in this volume; (iii) provide an estimate of the total halogen abundance for the Earth and in its dominant reservoirs contributing to the Earth's halogen endowment; and (iv) discuss some missing observations that could further improve our understanding of halogen abundances and geochemical systematics. Determination of the distribution of the non-radioactive halogen elements (fluorine, F; chlorine, Cl; bromine, Br; and iodine, I) in, and the geochemical processes controlling their mass transfer between, solid and fluid repositories on Earth and in extraterrestrial environments has seen increasing attention in recent years. In part, this has been enabled by the development of dedicated analytical methodologies (e.g., in situ beam methods, secondary ion mass-spectrometer [SIMS], laser ablation-inductively coupled mass-spectrometer [LA-ICPMS], combined noble gas-halogen methods) that can provide a low detection level, accurate and precise determinations of halogen concentrations, and their isotope systematics in complex matrices (e.g., fluid inclusions, glasses, and minerals). However, a key motivation for this method development stems from an increased awareness of the value in halogen characterization for studying specific processes in Earth's hydrosphere, crust, mantle, and

J.J. Hanley (✉)
Mineral Exploration Laboratory, Department of Geology, Saint Mary's University, 923 Robie Street, B3H3C3 Halifax, Nova Scotia, Canada
e-mail: jacob.hanley@smu.ca

K.T. Koga
Laboratoire Magmas et Volcans, Université Clermont Auvergne, TSA 60026 - CS 60026 6 Avenue Blaise Pascal, 63178 AUBIERE Cedex, France
e-mail: Ken.Koga@uca.fr

D.E. Harlov and L. Aranovich (eds.), *The Role of Halogens in Terrestrial and Extraterrestrial Geochemical Processes*, Springer Geochemistry,
https://doi.org/10.1007/978-3-319-61667-4_2

core (e.g., crustal and mantle metasomatism; ore metal transfer; magmatic differentiation and volatile exsolution; fluid reservoir contamination and fluid mixing; mineral-melt-fluid partitioning; and basinal fluid evolution) in which the chemical and isotopic properties of the halogens provide significant advantages over other element groups. These properties include their (i) differential (i.e., temperature- and melt composition-dependent) incompatibility during fluid-melt and mineral-melt partitioning; (ii) collectively highly mobile and volatile nature but with only a few processes capable of fractionating the halogens from one another or leading to significant halogen mass transfer from one repository to another (e.g., the formation of evaporites, fluid phase separation [immiscibility, boiling], crystallization and degassing of magmas, subduction devolatilization and metamorphism); and (iii) strong systematic covariance of Cl and Br, but commonly differential behaviors of F and I (in response to organic processes) in most fluids in the hydrosphere, sediments, crustal rocks in general, the mantle, and mantle-derived lavas. Mass balance calculations show that F is dominantly hosted by mantle and crust, while Cl and Br show nearly identical distribution patterns in which a total of the seawater, formation waters, and evaporites comprise more than half of the Earth's halogen budget. Experimentally determined metal-silicate partition coefficients suggest that a significant quantity of I is potentially hosted by the Earth's core.

2.1 Introduction

The stable halogen elements (F, Cl, Br and I) play an important role in geochemical and biogeochemical systems, despite their relatively low overall abundance on the Earth and in the Cosmos. For example, F and Cl can exert a significant control on the behavior and composition of magmas (e.g., Manning 1981; Rabinovich 1983; Mysen and Virgo 1985; Webster et al. 1989; Webster and Holloway 1990; Holtz et al. 1993; Mysen et al. 2004; Aranovich et al. 2013; Webster et al. 2018; Dolejš and Zajacz 2018), the composition of hydrothermal fluids, and the transportation of ore metals in the crust (Shinohara et al. 1989; Carroll and Webster 1994; Yardley 2005; Aiuppa et al. 2009; Baker and Balcone-Boissard 2009; Webster et al. 2009; Vigneresse 2009; Lecumberri-Sanchez and Bodnar 2018). Bromine and I are present in abundances many orders of magnitude less than those of F and Cl. They play key roles in many biochemical reaction pathways, which influences their distribution in geochemical systems (e.g., Fuge and Johnson 1986; Fuge 1988, 2005 and authors therein). Knowledge of the key repositories of the halogens, and the factors controlling their bulk and isotope distribution, can be used to address many ongoing areas of research for geochemists. For example, these include tracing the evolution and source of hydrothermal fluids and how they play a role in ore deposit formation; metamorphism and subsolidus alteration; reconstruction of marine sedimentary paleo-environments; tracking mantle to crust mass transfer associated with subduction; and the modeling marine-land biogeochemical cycling. Beginning with the first comprehensive work to characterize the halogen contents of meteorites in

the mid-20th Century (Correns 1956 and references therein), considerable effort has been put into the advancement of analytical techniques to accurately determine the halogen contents of minerals, rocks, and magmas, as well as aqueous and non-aqueous volatiles (fluids, gases) associated with all geological environments.

In this chapter, we present an overview of the chemical behavior of the halogens and an introduction to the analytical techniques that are relevant to evaluating halogens in some geochemical systems. This is followed by a review of the distribution of halogens in various terrestrial and cosmic rocks, fluids, and reservoirs. A presentation of some representative data sets from these media, and some key processes responsible for the variability in the halogen abundance and ratios in those media are discussed. A short discussion is also presented on the Earth's halogen mass balance, and the challenges associated with utilizing data from various reservoirs in light of the paucity of data.

2.2 Chemical Properties of the Halogens Relevant to Geological Systems

The stable halogens (F, Cl, Br, I; Table 2.1) are non-metallic, highly volatile, lithophile elements occurring within Group VIIA (Group 17) of the periodic table. Iodine also exhibits some metallic properties and chalcophile behavior in some sulfide-bearing hydrothermal and magmatic systems (Goles and Anders 1962; Dawson and Fuge 1980; Fuge and Johnson 1986; Swindle et al. 1991; Mungall and Brenan 2003). Both I and Br are also considered biophile in surficial and low-temperature hydrothermal settings where they concentrate in organic matter and derived sedimentary rock types (Worden 2018). With decreasing ionic size (from I^- to F^-), the stable halogen anions show increasing energy of formation for NaX-like compounds, increasingly stronger short-range order (in minerals) with low charge "modifier" cations Ca, Na, and K (Luth 1988; Zeng and Stebbins 2000), and increasing volatility and solubility. These variable physical properties are partly predictive of the differential behavior and abundance of the halogens in minerals, rocks, melts, and fluids/volatile phases (Table 2.1).

In the geochemical systems discussed here, none of the halogens occur naturally in their elemental form. Rather, they occur as monovalent anions (F^-, Cl^-, Br^-, I^-) bound to metal ions in salts (halides, oxyhalides), silicate minerals, and non-silicate minerals grown from/equilibrated with hydrosaline aqueous fluids or having grown from silicate melt and possibly immiscible halide melts (Klemme 2004; Dolejš and Baker 2004; Renno et al. 2004; Hanley et al. 2005, 2008; Veksler et al. 2005, 2012; Teague et al. 2011; Vasyukova and Williams-Jones 2014, 2016). In aqueous fluids, and in a variety of melts (silicate, halide, sulfide), these elements exist as dissolved monovalent anions, except I, which also occurs as the oxyanionic species iodate (IO_3^-) in some aqueous repositories (e.g., meteoric water and seawater) where the

Table 2.1 Properties of the stable halogens relevant to geochemistry

Halogen (Ion)	M.P./B.P. (°C)	NaX energy of formation (kcal/g mol)	Ionic radius (Å)	CTR (Å)	First ionization energy (kJ/mol)	Electro-negativity	Electron affinity (kJ/mol)	[1]Stable Isotopes
F (F^{-1})	−219.7/−188.1	136	1.33	0.71	1681	4.0	−328	^{19}F (100%)
Cl (Cl^{-1})	−101/−34.6	98	1.81	0.99	1251	3.0	−349	^{35}Cl (75.78%) ^{37}Cl (24.22%)
Br (Br^{-1})	−7.2/58.8	91	1.96	1.14	1140	2.8	−324.6	^{79}Br (50.69%) ^{81}Br (49.31%)
[2]I (I^{-1})	113.7/184.4	77	2.20	1.33	1008	2.5	−295.2	^{127}I (100%)

Data are from Goldschmidt (1926); Pauling and Huggins (1934); Pauling (1960); Lide (2016)

[1]isotope mass and % natural abundance

[2]not included here are data for iodate (IO_3^-) which is the thermodynamically stable form of I in oxygenated, alkaline seawater and a major proportion of total I in meteoric waters (Fuge 2005)

proportions of I^- and IO_3^- are dependent on pH, oxidation potential, and biological activity (Fuge 2005). Whereas many minerals contain F and Cl as a major (10 s of wt%) to minor (wt% or sub wt%) constituents (e.g., halides, oxyhalides, borates, phosphates, carbonates, silicates and hydroxysilicates), Br and I occur as trace (ppm) constituents in various minerals and are uncommon as major to minor constituents (e.g., in rare halides and oxyhalides). Table 2.2 provides an inventory of IMA-recognized, naturally-occurring, halogen-bearing minerals, and lists representative phases from various groups and subgroups. Further discussion of halogen-bearing minerals can be found in Chap. 3 (Mi and Pan 2018). The relatively large ionic radii and low binding energies of Br^- and I^- reduce the stability of Br and I minerals, and limit their structural replacement of F^-, Cl^-, or OH^- in minerals. Fluorine and Cl data are particularly abundant for common rock-forming hydroxysilicate minerals (i.e., di- and tri-octahedral micas, amphiboles, serpentine-group minerals) from a wide variety of rock types, allowing confirmation of the major contribution that these minerals make to the F and Cl balance in the crust and mantle. With the exception of halide salts containing Br and I, data on their abundance are rare, limiting an assessment of the variability of Br and I in common rock-forming minerals. In magmatic-hydrothermal systems, the F and Cl content of hydroxysilicate minerals is influenced by the temperature at which crystallization or later hydroxyl-halogen exchange occurs, the halogen concentration in the fluids from which phases are crystallizing or equilibrating, the associated cation structural controls, and post-crystallization leaching (Munoz 1984; Morrison 1991). For example, the cation composition (Fe-F, Ni-Cl, and Mg–Cl avoidance; Si content; alkali site occupancy; and edenite substitution) exerts a dominant control on the halogen content in amphiboles and some trioctahedral micas (Ramberg 1952; Volfinger et al. 1985; Kamineni 1986; Morrison 1991; Enami et al. 1992; Oberti and Ghose 1993; Aranovich and Safonov 2018).

Chloride and Br^- usually show strong systematic covariation in almost all terrestrial fluid types, and F^- shows covariation with Cl^- and Br^- in some environments (e.g., sedimentary formation waters; cf., Worden 2018). Iodide, however, rarely correlates to these, indicating that unique controlling mechanisms are at work. The highly mobile and volatile nature of the halogens in most geological environments makes an accurate determination of the distribution and concentration of these elements in parental (unmodified) magmas or fluid end-members difficult. In particular, Cl^-, Br^-, and I^-, are incompatible elements whose ratios are highly conservative and characteristic of specific geological reservoirs (fluids in environments with high fluid-rock ratios, sediment, rock, and magma), which vary by up to many orders of magnitude between them. Furthermore, with the exception of I^-, halogen ions do not play a role in oxidation or reduction reactions in geochemical systems and do not strongly adsorb to mineral surfaces. Thus, the use of halogens and halogen abundance ratios, in combination with other types of data (recently, noble gas chemistry, Pb isotope chemistry, and abundances of other volatiles) has been widely established to (i) delineate the origin of fluid salinity; (ii) to model mixing, dilution, and evaporation in aqueous and hydrocarbon fluid systems,

Table 2.2 Inventory of IMA-approved natural halogen-bearing minerals, and representative examples

Class	Mineral	Formula	Mineral	Formula
Halides (F, 43)				
	Griceite	LiF	Barberiite	$(NH_4)BF_4$
	Cryptohalite	$(NH_4)_2SiF_6$	Cryolithionite	$Na_3Li_3Al_2F_{12}$
	Sellaite	MgF_2	Weberite	Na_2MgAlF_7
	Cryolite	Na_3AlF_6	Avogadrite	$(K,Cs)BF_4$
	Fluorite	CaF_2	Villiaumite	NaF
	Carobbiite	KF	IMA2009-014	SrF_2
	Fluocerite-(Ce)	$(Ce,La)F_3$	Frankdicksonite	BaF_2
Oxyhalides (F, 4)				
	Haleniusite-(La)	(La,Ce)OF	Zavaritskite	BiOF
	Murataite	$(Y,Na)_6(Zn,Fe^{3+})_5(Ti,Nb)_{12}O_{29}(O,F)_{14}$	Fluornatromicrolite	$(Na,Ca,Bi)_2Ta_2O_6F$
[2]*Silicates (F, 193)*				
	Norbergite	$Mg_3(SiO_4)(F,OH)_2$	Topaz	$Al_2SiO_4(F,OH)_2$
	Zinnwaldite	$KLiFe^{++}Al(AlSi_3O_{10})(F,OH)_2$	Siderophyllite	$KFe_2^{++}Al(Al_2Si_2O_{10})(F,OH)_2$
	Leucophanite	$(Na,Ca)_2BeSi_2(O,OH,F)_7$	Humite	$(Mg,Fe^{++})_7(SiO_4)_3(F,OH)_2$
	Narsarsukite	$Na_2(Ti,Fe^{+++})Si_4(O,F)_{11}$	Lepidolite	$K(Li,Al)_3(Si,Al)_4O_{10}(F,OH)_2$
	Polylithionite	$KLi_2AlSi_4O_{10}(F,OH)_2$	Phlogopite	$KMg_3(Si_3Al)O_{10}(F,OH)_2$
	Zunyite	$Al_{13}Si_5O_{20}(OH,F)_{18}Cl$	Boromuscovite	$KAl_2(Si_3B)O_{10}(OH,F)_2$
	Fluorbritholite-(Ce)	$(Ca,Ce,La,Na)_5(SiO_4,PO_4)_3(OH,F)$	Annite	$KFe_3^{++}AlSi_3O_{10}(OH,F)_2$
	Muscovite	$KAl_2(AlSi_3O_{10})(OH,F)_2$	Britholite-(Y)	$(Y,Ca)_5(SiO_4,PO_4)_3(OH,F)$
[3]*Other*	*(F, 187)*			
	Hephaistosite	$TlPb_2Cl_5$	Calciobetafite	$Ca_2(Ti,Nb)_2(O,OH)_7$
	Fersmite	$(Ca,Ce,Na)(Nb,Ta,Ti)_2(O,OH,F)_6$	Microlite	$(Na,Ca)_2Ta_2O_6(O,OH,F)$

(continued)

Table 2.2 (continued)

Class	Mineral	Formula	Mineral	Formula
	Ceriopyrochlore-(Ce)	$(Ce,Ca,Y)_2(Nb,Ta)_2O_6(OH,F)$	Pyrochlore	$(Na,Ca)_2Nb_2O_6(OH,F)$
	Fluoborite	$Mg_3(BO_3)(F,OH)_3$	Bastnasite-(Y)	$Y(CO_3)F$
	Isokite	$CaMg(PO_4)F$	Amblygonite	$(Li,Na)Al(PO_4)(F,OH)$
	Bastnasite-(La)	$La(CO_3)F$	Bastnasite-(Ce)	$Ce(CO_3)F$
	Synchysite-(Ce)	$CaCe(CO_3)_2F$	Apatite-(F)	$Ca_5(PO_4)_3F$
	Wilcoxite	$MgAl(SO_4)_2F•_{18}(H_2O)$	Nefedovite	$Na_5Ca_4(PO_4)_4F$
	Natrophosphate	$Na_7(PO_4)_2F•_{19}(H_2O)$	Wavellite	$Al_3(PO_4)_2(OH,F)_3•_5(H_2O)$
	Rostite	$AlSO_4(OH,F)•_5(H_2O)$		
Halides (Cl, 62)				
	Salammoniac	NH_4Cl	Molysite	$Fe^{+++}Cl_3$
	Halite	$NaCl$	Chlorocalcite	$KCaCl_3$
	Scacchite	$MnCl_2$	Lawrencite	$(Fe^{++},Ni)Cl_2$
	Tolbachite	$CuCl_2$	Sylvite	KCl
	Mitscherlichite	$K_2CuCl_4•_2(H_2O)$	Hydrohalite	$NaCl•_2(H_2O)$
	Bischofite	$MgCl_2•_6(H_2O)$	Antarcticite	$CaCl_2•_6(H_2O)$
	Cotunnite	$PbCl_2$	Chlorargyrite	$AgCl$
	Boleite	$KPb_{26}Ag_9Cu_{24}Cl_{62}(OH)_{48}$	Calomel	Hg_2Cl_2
	Matlockite	$PbFCl$	Kuzminite	$Hg_2(Br,Cl)_2$
Oxyhalides (Cl, 27)				
	Bismoclite	$BiOCl$	Ecdemite	$Pb_6As_2^{+++}O_7Cl_4$
[2]*Silicates (Cl, 76)*				
	Pyrosmalite(Mn)	$(Mn,Fe^{++})_8Si_6O_{15}(OH,Cl)_{10}$	Quadridavyne	$(Na,K)_6Ca_2Al_6Si_6O_{24}Cl_4$
	Rustumite	$Ca_{10}(Si_2O_7)_2(SiO_4)Cl_2(OH)_2$	Sodalite	$Na_8Al_6Si_6O_{24}Cl_2$

(continued)

Table 2.2 (continued)

Class	Mineral	Formula	Mineral	Formula
	Ferrochloropargasite	$NaCa_2(Fe_4^{++}Al)Si_6Al_2O_{22}Cl_2$	Davyne	$Na_4K_2Ca_2Si_6Al_6O_{24}(SO_4)Cl_2$
	Marialite(Cl-scapolite)	$Na_4Al_3Si_9O_{24}Cl$	Kalborsite	$K_6Al_4Si_6BO_20(OH)_4Cl$
	Nasonite	$Pb_6Ca_4Si_6O_{21}Cl_2$	Eudialyte	$Na_4(Ca,Ce)_2(Fe^{++},Mn,Y)ZrSi_8O_{22}(OH,Cl)_2$
	Hauyne	$(Na,Ca)_{48}Al_6Si_6(O,S)_{24}(SO_4,Cl)_{12}$		
[3]*Other (Cl, 175)*				
	Jarandolite	$Ca[B_3O_4(OH)_3]$	Marrucciite	$Hg_3Pb_{16}Sb_{18}S_{46}$
	Boracite	$Mg_3B_7O_{13}Cl$	Iowaite	$Mg_4Fe^{+++}(OH)_8OCl•_{24}(H_2O)$
	Pyromorphite	$Pb_5(PO_4)_3Cl$	Vanadinite	$Pb_5(VO_4)_3Cl$
	Mimetite	$Pb_5(AsO_4)_3Cl$	Dadsonite	$Pb_{21}Sb_{23}S_{55}Cl$
	Phosgenite	$Pb_2(CO_3)Cl_2$	Apatite-(Cl)	$Ca_5(PO_4)_3Cl$
	Atacamite	$Cu_2Cl(OH)_3$	Paratacamite	$(Cu,Zn)_2(OH)_3Cl$
Halides (Br, 12)				
	Bromargyrite	AgBr	Kuzminite	$Hg_2(Br,Cl)_2$
	Arzakite	$Hg_3S_2(Br,Cl)_2$	Grechishchevite	$Hg_3S_2(Br,Cl,I)_2$
	Iltisite	HgSAg(Cl,Br)		
Oxyhalides (Br 4)				
	Murdochite	$PbCu_6O_8 - x(Cl,Br)_2 - x$	Comancheite	$Hg_{13}(Cl,Br)_8O_9$
[3]*Other (Br 8)*				
	[a]Steropesite	Tl_3BiCl_6	[a]Hephaistosite	$TlPb_2Cl_5$
Halides (I 11)				
	Marshite	CuI	Miersite	(Ag,Cu)I
	Iodargyrite	AgI	Moschelite	$Hg_2^+I_2$
	Perroudite	$Hg_5 - xAg_4 + xS_5 - x(Cl,I,Br)_4 + x$	Capgaronnite	HgAg(Cl,Br,I)S

(continued)

Table 2.2 (continued)

Class	Mineral	Formula	Mineral	Formula
Oxyhalides (I 13)				
	Lautarite	$Ca(IO_3)_2$	Bruggenite	$Ca(IO_3)_2 \cdot (H_2O)$
	Salesite	$Cu(IO_3)(OH)$	Hectorfloresite	$Na_9(IO_3)(SO_4)_4$
[3]*Other (I 1)*				
	Demicheleite-(Br)	BiSBr		

[1]Number in parenthesis of phases that are IMA-recognized, and are listed for each halogen, and in four broad classes (halides, oxyhalides, silicates, and "other")
[2]Also some silicate-phosphate minerals
[3]Halogens present as minor or trace elements in phosphates, carbonates, borates, vanadates, arsenates, chloro-hydroxides, silicates, sulf-halides, sulfosalts, oxides and hydroxides, and also in other [a]halides

notably in ore-forming environments; and (iii) to evaluate the physical and chemical processes involved in the assimilation, redistribution, inheritance, and tectonic recycling of solid earth materials in the crust and mantle where the interpretation of conventional trace element data may be ambiguous (e.g., Böhlke and Irwin 1992a, b, c; Yardley et al. 1993; Graupner et al. 2006; Fairmaid et al. 2011; Kendrick et al. 2001a, b, 2002a, b, 2006a, b, 2008, 2011, 2012a, b, 2014; Fu et al. 2012; Le Voyer et al. 2010; Rose-Koga et al. 2012, 2014; Debret et al. 2014; Cabral et al. 2014; Debret et al. 2015). Halogen-bearing minerals can provide constraints on the abundance of halogens in melts and fluids where partition coefficients between coexisting mineral, melt, and fluid phases are known (e.g., Piccoli and Candela 1993). Experimental studies (e.g., Mungall and Brenan 2003; Liebscher et al. 2006; Fabbrizio et al. 2013) have shown that fluid phase separation (immiscibility, boiling), silicate melt-sulfide melt interaction, and fluid-silicate mineral interaction can strongly fractionate the halogens from one another. This is in agreement with the observed distribution of the halogens in various magmatic-hydrothermal systems, demonstrating the applicability of the halogens in evaluating such processes. Fractionation of halogens from one another is not restricted to magmatic-hydrothermal systems. For example, the differential leaching of Cl^- and I^- relative to Br^- from minerals and fluid inclusions during chemical weathering in low temperature surficial environments results in a decrease in the whole-rock Cl/Br and I/Br with decreasing distance from the surface, whereas Br and F appear to behave conservatively during weathering (Behne 1953; Kronberg et al. 1987).

In silicate melts, halogens dissolve through interaction with cations of the alkali metal, alkali earth metal, transition metals, and Al and Si (Wyllie and Tuttle 1964; van Groos and Wyllie 1969; Mysen and Virgo 1985; Foley et al. 1986; Luth 1988; Luth and Muncill 1989; Kohn et al. 1991; Schaller et al. 1992; Zeng and Stebbins 2000; Liu and Tossell 2003; Mysen et al. 2004; Mysen and Richet 2005; Dolejš and Baker 2007a, b; Evans et al. 2008; Baasner et al. 2013; Dalou et al. 2015a, b; Webster et al. 2018; Dolejš and Zajacz 2018). Previously, it was considered that the contrasting solubility behavior of Cl and F in silicate melts resulted from Cl interacting only with metal cations such as alkalis and alkaline earths, whereas F can bond with all cations in melts. This difference accounts for the large differences in their solubility and also for their different influences on the properties of silicate melts. Furthermore, because F can bond with Si and break the silicate network, F exhibits a stronger depolymerization tendency than Cl (Baasner et al. 2013; Dalou et al. 2015a, b). Fluorine and Cl solubility show a strong, although distinct, dependence on melt composition, in particular the Mg, Ca, Fe, and Si contents, as well as Al/(Al + Si) (e.g., Dalou et al. 2015a). The differences between the F and Cl incorporation mechanisms are also reflected in contrasting diffusivities, where F diffuses faster than Cl in phonolitic melts (Balcone-Boissard et al. 2009; Böhm and Schmidt 2013), and F diffuses slower than Cl in basaltic melts (Alleti et al. 2007). In general, the halogens behave as volatile elements in igneous systems below 100 MPa. However they tend to remain in the melt fraction during crystallization,

especially under crustal conditions, where F shows the least incompatible behavior of the stable halogens in most igneous systems.

A limited number of experimental mineral-melt partition coefficients for the halogens exists. At mantle conditions, F and Cl partition into silicate melt rather than anhydrous silicate minerals (i.e. olivine, pyroxene, and garnet) as shown by some recent studies (Hauri et al. 2006; Bromiley and Kohn 2007; Beyer et al. 2012; Dalou et al. 2012, 2014; Rosenthal et al. 2015; Joachim et al. 2015; Adam et al. 2016). A similar behavior for Br and I relative to Cl is also implied from geochemical systematics. Fluorine, in contrast, may partition into amphibole relative to fluid and hydrous silicate melt when present (Bernini et al. 2013; Wu and Koga 2013; Van den Bleeken and Koga 2015). Fluorine can also occur in nominally-anhydrous minerals such as olivine at concentrations much higher than the other halogens (100 s ppm; Beyer et al. 2012; Bernini et al. 2013) making olivine, due to its abundance, an important F carrier in the mantle. At crustal depths, mineral-melt partition coefficients (reported as $D_i^{C/L} = C_i^C/C_i^L$) are reported for biotite and are higher for granitic melts ($D_F \sim 7$; $D_{Cl} \sim 6$) than for basalts and basanites ($D_F \sim D_{Cl} < 2$) (Latourrette et al. 1995; Bindeman et al. 1998; Icenhower and London 1997). With increasing fractionation, F will partition into certain mineral phases (notably amphiboles, micas, apatite, and topaz) whereas Cl, Br, and I are largely excluded from these phases and tend to concentrate in residual melts and exsolved magmatic volatiles. However, as halogen concentrations reach high levels in residual melts, mineral-melt and fluid-melt partition coefficients increase, and result in, for example, Cl enrichment in apatites and coexisting aqueous fluids in layered mafic-ultramafic intrusions (Mathez and Webster 2005) and felsic peraluminous, peralkaline and hyperagpaitic magmas (Webster et al. 1989; Webster and Holloway 1990). Mineral-melt partitioning data for Br and I are especially rare. For example, Dong (2005) reported partition coefficients for Br between phosphate-carbonate-halide melts and coexisting apatite, scapolite, and sodalite, and demonstrated greater compatibility of Br with chlorapatite than with fluorapatite, as well as partition coefficients between melt and marialitic scapolite and sodalite near unity. Thus the Cl/Br values for these minerals might closely reflect the halogen proportions in coexisting melts and fluids. Halogen behavior in silicic anhydrous and hydrous melts, as well as partitioning behavior, are discussed in Chap. 6 (Webster et al. 2018), Chap. 7 (Dolejš and Zajacz 2018) and Chap. 14 (Klemme and Stalder 2018).

While F and I are both monoisotopic, the stable isotopes of Cl (^{35}Cl, ^{37}Cl) and Br (^{79}Br, ^{81}Br) have been investigated through studies of experimental and natural halogen-bearing systems. Natural isotope variations for Cl and Br are small and not impacted by the redox state. This, combined with analytical challenges (e.g., difficulties in Br extraction from high Cl samples), and the low concentrations of Br in most samples, has led to a paucity of Br isotope data (Eggenkamp and Coleman 2000; Eggenkamp 2014). Estimations of the Cl isotope fractionation, based on the first principal (ab initio) model, suggest that silicate minerals will be preferentially enriched in ^{37}Cl by 2–3‰ relative to a coexisting saline fluid at standard conditions (Schauble et al. 2003). There are, however, limited data at magmatic-hydrothermal

temperatures and pressures. Experimental studies have noted negligible (<0.2‰) Cl isotope fractionation associated with vapour-liquid phase separation at 400–450 °C and <0.5 kbar (Liebscher et al. 2006). This is not surprising as coexisting liquid and vapour would have similar densities and bulk compositions at such conditions. More importantly, the ratio of partition functions, which is equivalent to a chemical exchange constant expressed by quantum mechanics states of chemical bonds, approaches unity at high temperature conditions (e.g., Urey 1947). This is due to cancellation of a mass-effect term by a vibration-energy term and leads to no fractionation at high temperature. The effects of increasing temperature on Cl isotope fractionation between silicate minerals and single-phase fluids are also not well known. Experimental and theoretical studies of silicate mineral-fluid partitioning (Eggenkamp 1995; Schauble et al. 2003) suggest a decrease in the partition coefficient for ^{37}Cl-^{35}Cl exchange by a factor of $\sim$5 at 300 °C and by an order of magnitude or more at 500 °C, relative to 22 °C, confirming limited Cl isotope fractionation at magmatic-hydrothermal conditions. Discussion of the historical and current state of knowledge for halogen stable isotope studies in geological systems is examined by Barnes et al. (2018).

Analysis of the halogens poses considerable challenges, such that these elements are not conventionally measured during whole rock analysis. Instead, the majority of labs offer bulk or total soluble halide quantification as an add-on. In situ and isotope methods are far from being routinely commercially available. A variety of methods suitable for bulk and in situ elemental analysis (glasses, minerals, fluid inclusions), as well as Cl and Br stable isotope methods, have been developed with applications to delineating halogen abundance and tracking halogen behavior. These methods are summarized in Table 2.3 along with representative references and applications. This list is not exhaustive but highlights advances, in particular, in isotope and in situ methods, that have developed markedly in only the last $\sim$15 years with a few exceptions (e.g., SIMS; see Method abbreviations at the bottom of Table 2.3).

Overall, there has been a general shift of the focus of analytical development. These range from bulk analytical methods to in situ techniques affording high spatial resolution analysis (on the order of tens of μm) of texturally complex samples. Such applications include halogen content measurements of individual mineral grains, glassy matrices or silicate melt inclusions, or fluid inclusions. Bulk halogen determination by methods such as RNAA, RPAA and PGA (e.g., Nakamoto et al. 2007; Sekimoto and Ebihara 2013), XRF (e.g., Wang et al. 2004 and references therein), and bulk extraction and analysis techniques (e.g., pyrohydrolysis followed by IC; Hall et al. 1986; Schnetger and Muramatsu 1996; Michel and Villemant 2003; Köhler et al. 2009; Marks et al. 2012) are useful in compositionally-simple matrices in which the halogen content of the sample (soluble and residue) was fixed by a single hydrothermal or magmatic event (e.g., Mangler et al. 2014). However, these methods require relatively large sample masses, and in some instances are increasingly impractical. For example, NAA has the potential problem of a lack of appropriate high neutron flux reactor facilities for

Table 2.3 Analytical methods for quantification of halogen abundances and isotope ratios in Earth and cosmic materials

Method	Analyte/s	Materials analyzed	Representative references
LA-ICP-MS	Cl, Br	Fluid inclusions/minerals (in-situ)	Seo et al. (2011), Leisen et al. (2012), Hammerli et al. (2013), Sekimoto and Ebihara (2013)
EMPA	F, Cl	Minerals (in-situ)	Stromer et al. (1993), Kendrick et al. (2014)
SIMS	F, Cl, Br	Minerals/silicate glasses (in-situ)	Hervig et al. (1989), Stix et al. (1995), Hauri et al. (2002), Straub and Layne (2003), Rose-Koga et al. (2008, 2012), Boyce et al. (2012), Marks et al. (2012), Beyer et al. (2012), Dalou et al. (2012), Kendrick et al. (2014)
TOF-SIMS	F, Cl	Minerals/silicate glasses (in-situ)	Joachim et al. (2015)
PIXE	Cl, Br	Fluid inclusions/ silicate glasses (in-situ)	Heinrich et al. (1992), Ryan et al. (1993), Bureau and Métrich (2003)
TXRF	Cl, Br	Mineral (powder)	Klockenkämper (1996), Marks et al. (2012)
INAA	F, Cl, Br	Mineral (powder)	Marks et al. (2012)
INAA	Cl, Br	Fluid inclusions (bulk)	Heinrich et al. (2003)
Leachate GC/IC	Cl, Br, I	Mineral (powder)	Channer and Spooner (1992), Channer et al. (1999)
Pyrohydrolysis IC	F, Cl, Br	Mineral (powder)/ bulk rock	Hall et al. (1986), Schnetger and Muramatsu (1996), Michel and Villemant (2003), Köhler et al. (2009), Marks et al. (2012)
XRF	F, Cl, Br, I	Mineral (powder)/ bulk rock	Wang et al. (2004)
XRF microprobe	F,Cl,Br,I	Minerals (in-situ)	Pan and Dong (2003)
RNAA	Cl, Br, I	Bulk rock	Nakamoto et al. (2007), Sekimoto and Ebihara (2013)
RPAA	F,Cl,Br,I	Bulk rock	Nakamoto et al. (2007)
LA-ICP-IDMS	Cl, Br, I	Bulk rock	Boulyga and Heumann (2005)
In vacuo, laser microprobe, and step heating NG-MS after irradiation	F,Cl,Br,I	Bulk rock, mineral separates, fluid inclusions	Böhlke and Irwin (1992a, b, c), Johnson et al. (2000), Kendrick et al. (2001a, b, 2006a, b)
PGA	Cl	Bulk rock	Nakamoto et al. (2007)

(continued)

Table 2.3 (continued)

Method	Analyte/s	Materials analyzed	Representative references
SIMS	$^{37}Cl/^{35}Cl$	Silicate glasses (in situ)	Layne et al. (2004), John et al. (2010)
TIMS	$^{37}Cl/^{35}Cl$	Bulk rock/mineral separates	Xiao and Zhang (1992), Magenheim et al. 1994), Rosenbaum et al. (2000)
IRMS	$^{37}Cl/^{35}Cl$	Bulk rock/mineral separates	Long et al. (1993), Musashi et al. (1998), Rosenbaum et al. (2000), Barnes and Sharp (2006)
GC-IRMS	$^{81}Br/^{79}Br$	Solution	Eggenkamp and Coleman (2000)
CF-IRMS	$^{81}Br/^{79}Br$	Solution	Shouakar-Stash et al. (2005)
CF-MC-ICP-MS	$^{81}Br/^{79}Br$	Solution	Gelman and Halicz (2011)
GasBench II-IRMS	$^{81}Br/^{79}Br$	Solution	Du et al. (2013)

Method abbreviations: *LA-ICP-MS* laser ablation inductively coupled mass spectrometry; *EMPA* electron microprobe analyzer; *PIXE* proton induced X-ray emission; *SIMS* secondary ion mass spectrometry; *TOF* time-of-flight; *TXRF* total reflection X-ray fluorescence analysis; *INAA* instrumental neutron activation analysis; *RNAA* radiochemical neutron activation analysis; *RPAA* radiochemical photon activation analysis; *NG-MS* noble gas mass spectrometry; *PGA* prompt gamma-ray analysis; *LA-ICP-IDMS* laser ablation inductively coupled plasma isotope dilution mass spectrometry; *IC* ion chromatography; *GC* gas chromatography; *TIMS* thermal ionization mass spectrometry; *IRMS* isotope ratio mass spectrometry; *CF* continuous flow

the general scientific community, and stricter guidelines concerning the handling and storage of radioactive samples after counting. The advantage of many in situ methods is that they offer the opportunity to determine, together with the halogens, complementary or simultaneous measurements of element abundances, other than the halogens, for single crystals, matrices, or inclusions. These include PIXE for major elements or cations and Cl and Br in glasses and glassy melt inclusions, and fluid inclusions (e.g., Heinrich et al. 1992; Ryan et al. 1993; Bureau and Metrich 2003) and SIMS (negative secondary ion mode) for F and Cl, + and C, OH, P, and S abundances as well as C, O, Cl, and S isotope ratios in glasses and glassy melt inclusions (e.g., Hervig et al. 1989; Stix et al. 1995; Hauri et al. 2002; Layne et al. 2004; John et al. 2010; Rose-Koga et al. 2008, 2012). The measurements by these in situ techniques require calibration with external standards. Therefore, continuing efforts in developing shared, inter-laboratory tested and certified standards are need for an establishment of a routine in situ technique in the future. Alternatively, electron microprobes are used for in situ F and Cl measurements. However, the technique is limited to solid substrates with relatively high abundances (detection limits of 100 s ppm for F and 50 to 100 ppm for Cl). Furthermore, due to an interference with a tail of a Fe L-line, low concentration analysis of F is a challenge in natural Fe-bearing samples (e.g., Witter and Kuehner 2004).

Historically, the most comprehensive (total fluid) analytical approach for quantification of halogens and halogen ratios in fluid inclusions involved integrated GC-IC analysis of volatiles (including water) and cations-anions leached from

crushed bulk mineral samples (e.g., Channer and Spooner 1992; Channer et al. 1999; Nahnybida et al. 2009). While bulk sample analysis averages multiple fluid inclusions (recording different hydrothermal events), which severely limits interpretations of geochemical data, this method remains the only approach that allows simultaneous cation and anion analysis including F^- and I^-, and offers very low detection limits for the halogens (ppm to sub-ppm). Recently, development and application of complementary (from single samples) laser microprobe, and step-heating NG-MS analysis of bulk, extracted, naturally-occurring, noble gas isotopes and irradiation-produced, noble gas proxy isotopes (i.e., ^{38}Ar[Cl], ^{80}Kr[Br], and ^{128}Xe[I]) has provided remarkable insight into the origin of magmatic-hydrothermal fluids in mineral deposits, and new constraints on the alteration of oceanic crust, and subduction-related cycling of halogens and noble gases (e.g., Fairmaid et al. 2011; Fu et al. 2012; Kendrick 2001a, b, 2002a, b, 2011, 2012b, 2013d, 2015b; Marschik and Kendrick 2015). In situ analysis of Cl^- and Br^- in fluid inclusions has been achieved by LA-ICPMS (Seo et al. 2011; Marks et al. 2012; Leisen et al. 2012; Hammerli et al. 2013) and PIXE (Heinrich et al. 1992; Ryan et al. 1993), which enables analysis of single inclusions in texturally complex samples, providing refined geochemical data that was irresolvable with bulk methods. While LA-ICPMS has shown some success in determining halogen contents in some minerals (e.g., sodalite, scapolite), the method is ideal for fluid inclusions due to the necessity to sample inclusions buried at depth. Calibration of Cl and Br sensitivities has been achieved in the studies mentioned here through the application of mineral standards, and synthetic inclusions or capillary tubes containing trapped standard solutions. Detection limits are typically $\sim$250 ppm for Cl (comparable to, or higher than, detection limits achieved by EMPA and TXRF for halogen-bearing minerals (Stromer et al. 1993; Klockenkämper 1996; Marks et al. 2012; Kendrick et al. 2014) and $\sim$15 ppm for Br. Of particular concern are (i) the relatively low sensitivities for the halogens by LA-ICPMS, resulting from the first ionization potential of Cl^+ and Br^+ being close to that for Ar^+ in the plasma source; (ii) polyatomic interferences (e.g., $(^{40}Ar^{39}K)^+$ and $(^{40}Ar^{41}K)^+$ on $^{79}Br^+$ and $^{81}Br^+$, respectively), which precludes the analysis of K-rich minerals or K-rich fluid inclusions; and (iii) halogen fractionation impacting the absolute abundances of Cl^- and Br^- (but not Cl/Br ratios) measured in minerals and fluid inclusions, which can be reduced by avoiding deep ablation.

2.3 Terrestrial Abundances

Relevant terrestrial fluid reservoirs for the halogens are seawater (the dominant repository of all halogens in the hydrosphere), meteoric water, formation waters in sedimentary basins (e.g., oil field brines), crystalline shield environments, metamorphic fluids produced by the devolatilization of halogen-bearing hydrous minerals, and fluids associated with magmatic environments (e.g., exsolved magmatic volatiles, fumarolic, volcanic and geothermal fluids). The latter may have a mixed

parentage depending on the original source and proportions of fluid end-members contributing H_2O and dissolved halogens.

2.3.1 The Hydrosphere

2.3.1.1 Surficial Waters

Seawater, representing only 0.02% of Earth's mass, is a major reservoir of Cl (~24% by mass of the Earth's budget) and Br (~31%), but is a negligible host for F and I containing less than 1% of the bulk Earth budget for these elements. When considering only the hydrosphere, seawater overwhelmingly dominates the mass balance for all four halogens. The preferred mean seawater values for the halogens are F = 1.3 ppm, Cl = 18800 ppm, Br = 67 ppm, I = 0.06 ppm; and Cl/Br = 280 (Li 1991; Whitfield and Turner 1972; Table 2.4). In rain water, rivers, and other

Table 2.4 Halide abundances in selected seawater, precipitation and other freshwater, and associated particulates

Material	F^- [ppm]	Cl^- [ppm]	Br^- [ppm]	I^- [ppm]	$Br^-/Cl^- \times 100$	$I^-/Cl^- \times 10000$	References
Seawater	1.3	18800	67	0.06	0.36	0.0319	1, 2, 3, 4
River/stream water							
Europe (median)		8.8	0.01	0.00033		0.375	5
River particulate			2–54				6
Marine clay	1300	21000	70	0.05–28	0.25–2.86	0.119–1.36	4, 7
Rain waters							
Japan		0.2–6.1	0.0025–0.015		0.84		8
[a]Netherlands		2.5	0.021		0.48		9
[b]Netherlands		8.9	0.043		0.42		9
UK (Wales)		4.6	0.019				10
[c]UK (by county)							
Nottingham		7.93	0.059				11
Oxfordshire		6.27	0.029				11
Cumbria		4.11	0.022				11
Sweden			0.004–0.012				12

[a]Continental; [b]marine; [c]weighted mean rainfalls (1972–1981)
Sources [1]Wong and Brewer (1974); [2]Wilson (1975); [3]Whitfield and Turner (1972); [4]Li (1991); [5]median values from FOREGS database: Buccianti (2015) and references therein; [6]Martin and Meybeck (1979); [7]Baturin (1988); [8]Yuita (1984); [9]Asman et al. (1981); [10]Neal et al. (1990); [11]Cawse (1987); [12]Lundström et al. (1984)

surface run-off, the median and standard deviations for the mean halide ion abundances are very low but show 3–4 orders of magnitude variation in absolute concentration. For example, analyses of more than 800 surface water samples in Europe (FOREGS database; Buccianti 2015) yielded median values of Cl^-, Br^-, and I^- of 8.81 ppm, 0.01 ppm, 0.00033 ppm, but ranges of 0.14–4560 ppm, 0.03–2.97 ppm, and 0.00001–0.104 ppm, respectively. Of the halogens, Cl^- is transported most conservatively through catchment areas and represents the dominant anion responsible for the leaching of cations from soils and bedrock (Neal et al. 1990; Peters et al. 1998; Smart et al. 2001), whereas the Cl^-/Br^- and Cl^-/I^- ratios of surface waters, as well as shallow groundwaters, can be modified by the release of Br^- and I^- from decomposing and rock-bound organic matter (organic-rich shales, muds and clays, peat, coal-bearing formations; e.g., Gerritse and George 1988; Biester et al. 2006), through dilution by high rainfall, and through the release of halogens from the weathering of halogen-bearing minerals, fluid inclusions, and halide- or fluid-filled pore spaces in rocks, especially marine sedimentary formations and evaporites (Edmunds 1996 and references therein). Volatilization of inorganic Cl, Br, and I from the marine environment to generate sea-salt aerosol leads to the enrichment of these elements in surface waters and soils relative to F in coastal areas, where F is controlled dominantly by its content in the parental material (Keene et al. 1999; Sander et al. 2003; Keene et al. 2007). It also leads to a correlation between river water Cl^- and distance from the coast (Smart et al. 2001). Further modification by the addition of anthropogenic halides (e.g., road salt, agricultural fertilizers) has also been demonstrated widely. Halide ions present in volcanic plume emissions are reported to significantly increase the F^- and Cl^- contents of local surface waters (Cuoco et al. 2013). It should be noted that data for I in rain water, seawater, and other surficial waters rarely report IO_3^{1-}, despite it representing a significant proportion of the total I analysis. Therefore, where I^- is reported for seawater and meteoric waters, it represents only a portion of the total I.

2.3.1.2 Formation Waters and Crystalline Shield Brines

For sedimentary basins, formation waters show a wide range in Cl^- and Br^- concentrations ($\sim$4 orders of magnitude globally) and a variable Br^-/Cl^- ratio (from 0.00075 to 0.018) that increases with increasing halogen ion concentrations above the seawater composition, reflecting the evaporation trend (Table 2.5; Fig. 2.1a). Whereas Cl^- and Br^- show a strong positive covariance in formation waters, I^- and F^- are decoupled from Cl^- and Br^-, and from each other (Fig. 2.1b–d; see also Worden 2018). These systematics reflect a few dominant processes controlling the salinity and halogen ratios in formation waters, namely sub-aerial seawater evaporation and later interactions between formation waters and evaporite sequences (leading to salt dissolution) as well as the presence of halogenated organic matter (e.g., Worden 1996; Kendrick and Bernard 2013a and references therein). The age of the reservoir, and specific kerogen-types associated with the dominant hydrocarbon source units in the basin, also demonstrate a control on specific

Table 2.5 Mean halogen abundances in some formation (i.e., basinal or oil field brines) waters

Location	F^- [ppm]	Cl^- [ppm]	Br^- [ppm]	I^- [ppm]	$Br^-/Cl^- \times 100$	$I^-/Cl^- \times 100$	Source
Michigan Basin	–	188,000	2310	–	1.23	–	1
Centennial mine	–	128,000	997	–	0.78	–	1
Greenwood mine	–	3,030	–	–	–	–	1
Michigan Basin	–	253,800	8475	–	1.33	–	2
New York [salt]	–	21,200	–	–	–	–	1
New Mexico [Salado]	–	16,800	–	–	–	–	1
Utah [Great Salt Lake]	–	86,600	10	–	0.01	–	1
Deep-basin brines, Texas	–	136,810	313	23.5	0.15	0.0172	3
Frio Formation [Oligocene], Texas	–	36,015	117	19.8	0.24	0.0550	4
Frio Formation, Texas	–	47,027	206	12.8	0.34	0.0272	5
Mississippi Salt Dome basin	3.6	131,696	1083	26.7	0.80	0.0203	6
Mississippi	–	155,667	1376	–	0.79	–	7
Kettleman North Dome, California	3.3	14,132	131	32.6	0.94	0.2305	8
Illinois Basin	–	98,100	278	–	0.28	–	1
Illinois Basin	–	58,957	202	–	0.34	–	9
Illinois Basin	–	67,897	15160	–	0.20	–	10
Clinton Formation, Ohio	–	157,698	1858	–	1.13	–	11
Smackover formation, Arkansas	13.1	169,054	4467	12.8	2.43	0.0076	12
Alberta Basin		48,190	294.4	–	0.45	–	13
Alberta formation water		112,700	763		0.61		1
Tunisia	–	148,458	1126	–	0.76	–	14
Norwegian shelf	–	1,231	2.9	–	0.23	–	15
Pattani Basin, Gulf of Thailand	1.9	708	4.5	–	0.64	–	16

Sources [1]Frape and Fritz (1982); [2]Wilson and Long (1993a, b); [3]Fisher and Kreitler (1987); [4]Land (1995a, b); [5]Macpherson (1992); [6]Kharaka et al. (1987); [7]Carpenter et al. (1974); [8]Merino (1975); [9]Stueber and Walter (1991); [10]Stueber et al. (1993); [11]Sanders (1991); [12]Moldovanyi (1992); [13]Connolly et al. (1990); [14]Morad et al. (1994); [15]Egeberg (1989); [16]Lundegard and Trevena (1990)

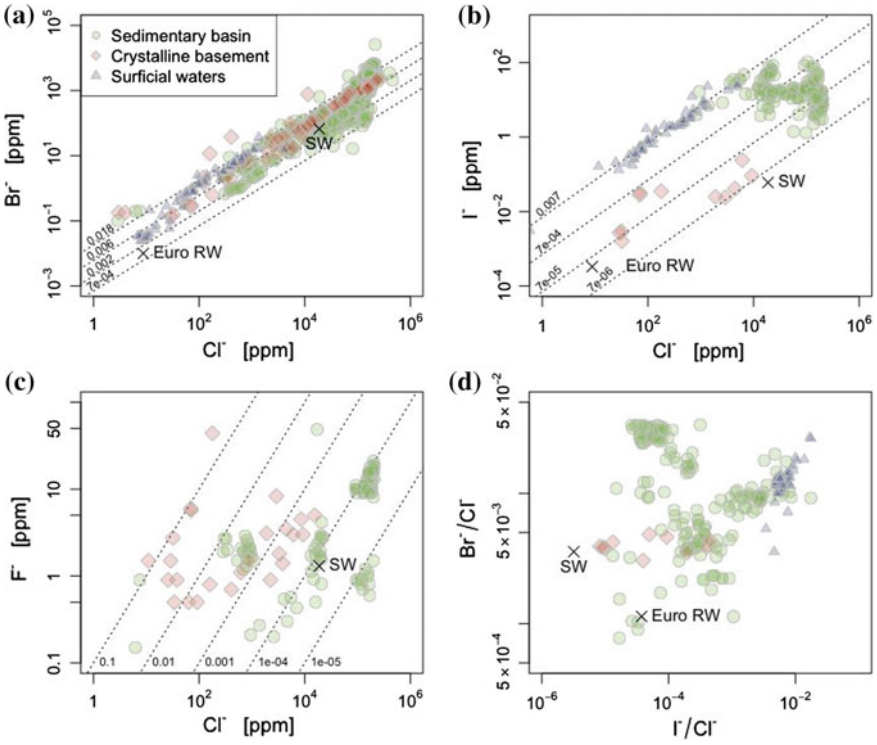

Fig. 2.1 Plots summarizing abundance and ratios of halogen ions in some terrestrial fluid types (formation waters from sedimentary basins; shallow, brackish, saline, and briny waters from crystalline shield environments and granites, and surficial waters/sediments including rainwater [EuroRW], seawater [SW], rivers and fluvial particulates) showing (**a**) Br^- and Cl^-, (**b**) I^- and Cl^-, (**c**) F^- and Cl^-, and (**d**) Br^-/Cl^- vs. I^-/Cl^-. This is a graphical representation of the data summarized in Tables 2.4, 2.5 and 2.6. Diagonal lines in (**a**)–(**c**) represent constant Br^-/Cl^-, I^-/Cl^-, and F^-/Cl^- ratios. Note the increase in Br^-/Cl^- ratio with increasing Cl^- for sedimentary basin fluids above seawater value, reflecting the evaporation trend

halogen abundances. Halogen abundances, however, are independent of the maximum depth and temperature reached during burial, basin architecture, and structural deformation, as well as lithostratigraphy other than the presence of evaporites and organics (Worden 1996, 2018). Evaporitic brines preserve seawater Br/Cl and I/Cl ratios, but once halite saturates, the relative incompatibility of Br and I in halite leads to an increase in the Br and I content of the residual "bittern" or "primary" brines leaving evaporitic sequences with progressively lower Br and I concentrations (e.g., McCaffrey et al. 1987; Yardley et al. 2000; Leisen et al. 2012 and references therein). This is in contrast to evaporite deposits and fluids formed via meteoric or seawater dissolution of those deposits, which leads to "secondary" brines enriched in Na and Cl and depleted in Br and I relative to seawater (see also

Worden 2018). Ratios of Br/Cl and I/Cl in these brines will be variable, depending partly on differential halide-brine partitioning behavior associated with the various stages of evaporite mineralogical evolution at the time of brine extraction, and post-depositional recrystallization of evaporite minerals, a process that preferentially remobilizes Br and I (Fontes and Matray 1993). The formation of evaporites removes vast quantities of halogens from seawater, and evaporite deposits represent a large proportion of the Earth's crustal Cl, Br, and I mass balance, contributing the same order of magnitude to this halogen budget as ocean water. Formation waters comprising bitterns, and fluids modified through interaction (dissolution) of evaporites and organic matter, supply large quantities of halogens to deeper crustal metamorphic and magmatic environments following burial, or introduce high salinity pore fluids and halide salts to sub-surface hydrological processes and mineral reactions through the infiltration of saline brines into the sedimentary veneer.

Aqueous solutions present in pore spaces, fracture networks, and isolated pockets within crystalline shield environments (Edmunds et al. 1987; Lahermo and Lampen 1987; Vovk 1987; Frape et al. 1984; Frape and Fritz 1982; Möller et al. 1997; Grawinkel and Stöckhert 1997; Bottomley et al. 1999; Shouakar-Stash et al. 2007) show systematic variations in salinity with depth (brines, saline waters, brackish waters, fresh waters), with the deepest samples approaching halite saturation (Pearson 1985). In contrast to this behavior, halogen ratios vary non-systematically with depth (Table 2.6). Whereas shallower shield waters have been modified by infiltration of meteoric water, deep brines and saline waters are considered to have initially formed from the evaporation or freezing of seawater, or represent formation waters, or waters that had previously interacted with high salinity, high density fluid-infiltrated basement rocks. These fluids were subsequently trapped in fractures and faults, and within the limited porosity of the crystalline rocks (Carpenter et al. 1974; Starinsky 1974; Carpenter 1978; Wilson and Long 1993a, b; Herut et al. 1990; Bottomley et al. 1994, 1999 and references therein). Some researchers have proposed that the brines were subsequently modified through long term, low temperature water-rock interaction with Ca-rich, crystalline basement rocks (e.g., fluid-rock Ca–Na exchange; Yardley and Bodnar 2014), in order to explain the high Ca^{2+}/Na^{+} ratios reported for shield brines (Frape et al. 1984; Frape and Fritz 1987; McNutt et al. 1990; Kamineni et al. 1992). In general, cation abundances and ratios in deep crystalline shield aqueous solutions may be influenced by prolonged water-rock interaction. However this process cannot modify halogen concentrations and ratios since halogen-bearing minerals are relatively stable at the low temperatures at which the fluids circulate. Furthermore, halogens in fluid inclusions cannot diffuse out of the inclusions or be efficiently accessed through changes in rock permeability in crystalline rocks. Mixing (for example with magmatic fluids of suspected high Cl^{-}/Br^{-} ratio; Hanley et al. 2004), and halide saturation are other viable mechanisms for modifying halogen ratios in these shield brines.

Table 2.6 Representative halogen abundances in shallow, saline, brackish and briny fluids from crystalline shield rocks and granites

Location	Reservoir	Depth [m]	F^- [ppm]	Cl^- [ppm]	Br^- [ppm]	I^- [ppm]	$Br^-/Cl^- \times 100$	$I^-/Cl^- \times 100$	Source
Cornwall, U.K.	South Crofty Mine	580	3.1	1900	8.02	0.025	0.422	0.0013	1
	Wheal Jane	150	44	179	0.63	0.035	0.352	0.0196	1
	Wheal Jane	400	3	6090	18.6	0.24	0.305	0.0039	1
	Wheal Pendarves	130	1.5	29	0.134	0.003	0.462	0.0093	1
	Wheal Pendarves	40	2.75	32.2	0.156	0.002	0.484	0.0050	1
Fennoscandian Shield	Lavia, Finland	907	–	14	0.1	–	0.714	–	2
	Jurmo, Finland	–	–	880	–	–	–	–	2
	Hiittinen, Finland	–	–	3250	–	–	–	–	2
	Olkiluoto, Finland	188	–	980	–	–	–	–	2
	Hastholmen, Finland	193	–	5040	18	–	0.357	–	2
	Ylistaro, Finland	600	–	8940	–	–	–	–	2
	Pori, Finland	600	–	1078	–	–	–	–	2
	Eurajoki, Finland	32	–	5390	–	–	–	–	2
	Eura, Finland	232	–	3124	–	–	–	–	2
	Urjala, Finland	76	–	2120	–	–	–	–	2
	Polvijarvi, Finland	–	–	1875	–	–	–	–	2
	Outokumpu, Finland	1250	–	16800	–	–	–	–	2
	Kotalahti mine, Finland	136	–	18000	–	–	–	–	2
	Stripa, Sweden	–	–	700	6.2	–	0.886	–	2
Ukrainian Crystalline Massif	Lenin Mine	975	–	19732	–	–	–	–	3
	Rodina Mine	1090	–	62050	–	–	–	–	3
	Drenazhnaya Mine	427	–	13963	–	–	–	–	3

(continued)

Table 2.6 (continued)

Location	Reservoir	Depth [m]	F^- [ppm]	Cl^- [ppm]	Br^- [ppm]	I^- [ppm]	$Br^-/Cl^- \times 100$	$I^-/Cl^- \times 100$	Source
	Communar Mine	540	–	11559	–	–	–	–	3
	Commintern Mine	1123	–	56675	–	–	–	–	3
	East-European Platform	700	–	59260	31	–	0.052	–	3
	East-European Platform	5099	–	209450	1870	–	0.893	–	3
Canadian Shield	Yellowknife	1372	–	115000	1010	–	0.878	–	4
	Yellowknife	1372	–	35900	324	–	0.903	–	4
	Yellowknife	457	–	5250	96.8	–	1.844	–	4
	Yellowknife	130	–	51	0.4	–	0.784	–	4
	Thompson	1220	–	115000	1110	–	0.965	–	4
	Thompson	1220	–	41400	405	–	0.978	–	4
	Thompson	305	–	3120	34.4	–	1.103	–	4
	Thompson	100	–	123	1.4	–	1.138	–	4
	Sudbury	1600	–	166200	1200	–	0.722	–	4
	Sudbury	1006	–	11300	78.7	–	0.696	–	4
	Sudbury	488	–	97	–	–	–	–	4
	Sudbury	152	–	63	–	–	–	–	4
	Yellowknife Con Mine	–	–	119000	1190	–	1.000	–	4
	Sudbury North Mine	1097	1.4	3820	37.4	–	0.979	–	5
	Sudbury Fraser Mine	1006	–	13900	87.5	–	0.630	–	5
	Sudbury Lockerby Mine	1219	5	15500	117	–	0.755	–	5
	Sudbury Lockerby Mine	792	1.5	870	7.4	–	0.851	–	5
	Sudbury Copper Cliff South Mine	152	0.9	26	–	–	–	–	5

(continued)

Table 2.6 (continued)

Location	Reservoir	Depth [m]	F^- [ppm]	Cl^- [ppm]	Br^- [ppm]	I^- [ppm]	$Br^-/Cl^- \times 100$	$I^-/Cl^- \times 100$	Source
	Sudbury Copper Cliff South Mine	625	–	1280	–	–	–	–	5
	Sudbury Copper Cliff South Mine	975	–	55200	570	–	1.033	–	5
	Sudbury Garrison Mine	488	–	97	–	–	–	–	5
	Sudbury Dowling Wells	152	0.5	63	–	–	–	–	5
	Nipigon, Ontario	–	–	5680	14.9	–	0.262	–	2
	Yellowknife Con mine	70	–	309	2	–	0.647	–	6
	Yellowknife Con mine	701	–	2015	14	–	0.695	–	6
	Yellowknife Con mine	1372	–	49429	445	–	0.900	–	6
	Yellowknife Con mine	1616	–	174134	1544	–	0.887	–	6
Siberia	East Siberian brine	–	–	252000	3785	–	1.502	–	5

Sources: [1]Edmunds et al. (1987); [2]Lahermo and Lampen (1987); [3]Vovk (1987); [4]Frape et al. (1984); [5]Frape and Fritz (1982); [6]Bottomley et al. (1999)

2.3.1.3 Magmatic-Hydrothermal Fluids, Metamorphic Fluids, Geothermal Waters, and Volcanic Emissions

With the exception of near surface or surficial sources such as geothermal springs, fumaroles, and some oil field brines, most hydrothermal fluids cannot be directly sampled. Useful information about the halogen composition of hydrothermal (magmatic, and metamorphic) volatiles can be obtained directly from fluid inclusion studies, or indirectly through the analysis of halogen-bearing minerals and glasses (former melts) that equilibrated with volatiles. These analyses serve as conservative proxies for halogen abundances in related fluids (e.g., Pan and Dong 2003; Kendrick and Phillips 2009; Aranovich et al. 2015). Building upon earlier bulk analytical approaches for halogens in fluid inclusions (e.g., Channer et al. 1999 and references therein), significant advances in our understanding of fluid sources and the physicochemical pathways of fluid evolution in barren and ore-forming hydrothermal systems have been made in the last 15 years through the development of in situ methods for halogen analysis in fluid inclusions, as well as the integration of data for halogen abundances in such fluids with noble gas and halogen isotope data (e.g., Böhlke and Irwin 1992a, b; Banks and Yardley 1992; Banks et al. 2000a, b; Kendrick et al. 2001a; Baker et al. 2008; Nahnybida et al. 2009; Gleeson and Smith 2009; Seo et al. 2011; Fairmaid et al. 2011; Leisen et al. 2012; Fu et al. 2012; Hammerli et al. 2013; Marschik and Kendrick 2015). In addition, these fluid inclusion analytical methods have been extended to geological fluid environments where robust halogen data were totally lacking in the past (e.g., metamorphic fluids; Yardley et al. 1993; McCaig et al. 2000; Svensen et al. 2001a, b). Table 2.7 summarizes halogen abundance and ratio data from some of the above studies and Fig. 2.2 summarizes the key compositional summary fields represented in this database.

Halogen abundances determined from fluid inclusions, that are interpreted to have trapped relatively unmodified magmatic fluids, have consistently low I^-/Cl^- and Br^-/Cl^- ratios that are close to mantle values, and show significant variation in Br^-/Cl^- and I^-/Cl^- due to the inheritance of halogens from the country rocks hosting intrusive systems (Fig. 2.2; e.g., Böhlke and Irwin 1992a, Irwin and Roedder 1995; Jambon et al. 1995; Banks et al. 2000; Johnson et al. 2000; Kendrick et al. 2001a, 2012b, 2013b; German and Von Damm 2003; Layne et al. 2009; Nahnybida et al. 2009). Primary magmatic halogen ratios in such fluids can also be potentially modified by halide degassing (e.g., in volcanic eruptions; Symonds et al. 1994), and by igneous fractionation involving the formation of halogen-bearing minerals, although the systematics of how these processes influence halogen ratios are poorly constrained. With the exception of some MOR vent fluids, fumarole vapours, and condensates, as well as geothermal waters, are typically modified with respect to their primary halogen ratios. This occurs during the migration of primary magmatic volatiles through the crust from their source (Pyle and Mather 2009 and references therein).

Table 2.7 Halogen abundances in some hydrothermal (ore-forming, geothermal), magmatic and metamorphic fluids, indicated as minimum–maximum (average)

Setting (reference)	F [ppm]	Cl [‰]	Br [ppm]	I [ppm]	Br/Cl × 10^3	I/Cl × 10^4
Metamorphic						
Regional, Cloncurry District, Australia[(1)]	–	25.3–418 (177)	47–2097 (620)	–	0.75–30.6 (4.79)	–
Talc deposit, Trimouns, French Pyrenees[(2)]	–	4.28–4.55 (4.44)	8–32 (18)	–	1.77–7.14 (3.95)	–
Alpine quartz, Mont Blanc Granite, France[(2)]	–	0.9–1.05 (1.00)	1–4 (1)	–	0.9–4.0 (1.46)	–
Nautanen Deform. Zone, Norrbotten, Sweden[(6)]	–	12–33 (20) × 10^{-3}	0.009–0.05 (0.030)	–	0.73–2.51 (1.51)	–
Metamorphic (orogenic gold)						
Stawell–Magdala, Victoria, Australia[(10)]	–	–	–	–	0.88–1.6 (1.30)	0.11–0.91 (0.65)
Bendigo, Victoria, Australia[(10)]	–	–	–	–	0.96–3 (1.80)	0.93–4.8 (2.30)
Wattle Gully, Victoria, Australia[(10)]	–	–	–	–	0.04–1.7 (1.00)	0.19–6.1 (2.00)
Fosterville, Victoria, Australia[(10)]	–	–	–	–	0.5–4.3 (2.10)	0.21–5.6 (2.80)
Maldon, Victoria, Australia[(10)]	–	–	–	–	0.32–1.3 (1.70)	0.3–32 (3.30)
Mount Piper, Victoria, Australia[(10)]	–	–	–	–	0.55–1.5 (0.82)	0.18–8.1 (3.70)
Woods Point, Victoria, Australia[(10)]	–	–	–	–	1–2.6 (1.70)	3.8–21 (9.30)
Walhalla, Victoria, Australia[(10)]	–	–	–	–	1.5–3.6 (2.70)	4–52 (28)
Magmatic-hydrothermal						
Granitoid, Cloncurry District, Australia[(1)]	–	153–513 (299)	82–161 (123)	–	0.24–0.68 (0.43)	–

(continued)

Table 2.7 (continued)

Setting (reference)	F [ppm]	Cl [‰]	Br [ppm]	I [ppm]	Br/Cl × 10^3	I/Cl × 10^4
IOCG deposit, Cloncurry District, Australia[1]	–	34.2–719 (260)	48–1220 (429)	–	0.11–7.32 (1.99)	–
Capitan Pluton, New Mexico, USA[4]	–	–	–	–	0.28–0.66 (0.49)	–
Cornubian batholith, SW England[4]	–	–	–	–	1.1–1.5 (1.3)	–
Fe-oxide/apatite deposit Norrbotten, Sweden[6]	–	8–87 (28) $\times 10^{-3}$	0.01–0.06 (0.023)	–	0.48–2.47 (1.09)	–
Magmatic-hydrothermal (porphyry-epithermal)						
Greenstone belt, Norrbotten, Sweden[6]	–	19–40 (25) $\times 10^{-3}$	0.009–0.02 (0.014)	–	0.37–1.05 (0.57)	–
Cu-Mo-Au, Butte, Montana, USA[7]	–	–	–	–	1.35–4.24 (2.20)	–
Cu-Mo-Au, Bingham Canyon, Utah, USA[7]	–	–	–	–	0.41–8.29 (2.38)	–
Cu-Mo-Au, Bingham Canyon, Utah, USA[8]	–	–	–	–	3.5–4.4 (3.89)	–
Cu-Mo-Au, Bingham Canyon, Utah, USA[11]	–	–	–	–	1.05–1.87 (1.37)	0.16–0.28 (0.21)
Cu-Mo-Au, El Teniente, Chile[8]	–	–	–	–	3.7–4.3 (4.09)	–
Sn-W, Mole Granite, Australia[8]	–	–	–	–	1.9–2.1 (1.99)	–
Cu, Ray, Arizona, USA[11]	–	–	–	–	0.87–0.91 (0.89)	0.09–0.18 (0.14)
Cu, Globe-Miami, Arizona, USA[11]	–	–	–	–	1–1.1 (1.05)	0.16–0.36 (0.26)
Cu, Pinto Valley, Arizona, USA[11]	–	–	–	–	1.06–1.37 (1.22)	0.24–0.28 (0.26)
Cu, Silver Bell, Arizona, USA[11]	–	–	–	–	1.23–1.58 (1.38)	0.69–1.21 (0.95)
Cu, Mission, Arizona, USA[11]	–	–	–	–	0.94	0.42

(continued)

Table 2.7 (continued)

Setting (reference)	F [ppm]	Cl [‰]	Br [ppm]	I [ppm]	Br/Cl × 10^3	I/Cl × 10^4
Geothermal and volcanic fumarole						
Mahanagdong, Leyte, Phillipines[3]	1.3–3.0 (2.2)	0.61–7.46 (4.60)	4–38 (22)	–	4.5–5.88 (4.93)	–
Hot springs, Cascade Range, Oregon[5]	0.4–9 (2.6)	0.39–19.1 (3.24)	1.1–48 (7.8)	0.02–7 (0.8)	2.52–2.8 (2.42)	0.51–3.67 (1.41)
Fumarole, Oldoinyo Lengai, Tanzania[9]	3.4–7 (5.2)	3.7–4 (3.85)	7–20 (13)	–	1.65–5.41 (3.53)	–

Sources: [1]Baker et al. (2008); [2]Leisen et al. (2012); [3]Angcoy and Arnórsson (2015); [4]Banks et al. (2000a); [5]Hurwitz et al. (2005); [6]Gleeson and Smith (2009); [7]Nahnybida et al. (2009); [8]Seo et al. (2011); [9]Mangler et al. (2014); [10]Fu et al. (2012); [11]Kendrick et al. (2001)

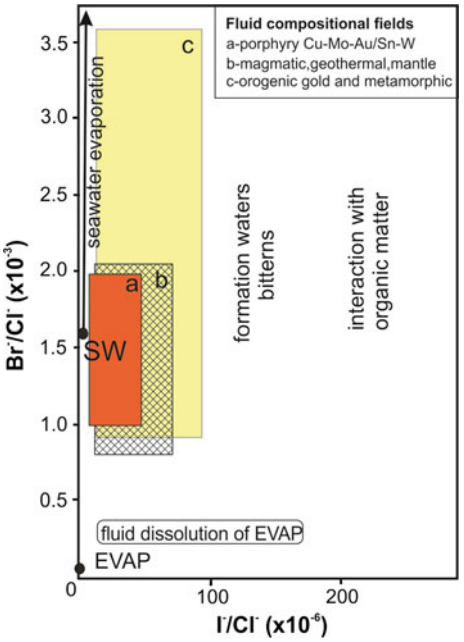

Fig. 2.2 Plot of Br^-/Cl^- (× 10^{-3}) vs. I^-/Cl^- (× 10^{-6}) for fluids summarized in Table 2.7 and in text for various geothermal-volcanic-fumarolic fluids (directly sampled), mantle fluids (inferred or measured from diamonds and other mantle mineral phase and rock compositions, and ridge vent fluids (Jambon et al. 1995; Johnson et al. 2000; German and Von Damm 2003; Layne et al. 2009; Kendrick et al. 2013b)), barren and mineralizing magmatic-hydrothermal (from fluid inclusions), and metamorphic fluids (from fluid inclusions). Generalized field for formation waters and fluids that have interacted with organic matter (i.e., pore fluids) are from Table 2.5. Values for evaporites (EVAP) and seawater (SW) are from Tables 2.13 and 2.2. The seawater evaporation trend is modified from Zherebtsova and Volkova (1966)

Metamorphic fluids can have a highly variable halogen composition and salinity reflecting the source protolith composition but can also be significantly modified (fractionated) by subsequent fluid-rock interaction at the typically low water-rock ratios of metamorphic systems (e.g., Kendrick et al. 2015). For example, the halogen ratios and salinity of metamorphic fluids in metasedimentary belts may be associated with the original halogen contents of sedimentary rocks (e.g., evaporitic, organic-rich). The interaction of externally-derived metamorphic fluids with these rock types can modify the fluid Cl-Br-I ratios (e.g., McCaig et al. 2000; Boiron et al. 2003, 2007; Leisen et al. 2012). The involvement of organic matter remains a dominant control on the I^-/Cl^- ratio in metamorphic fluids (Fairmaid et al. 2011). In contrast, fluids produced by devolatilization of hydrous silicate minerals usually have low salinities and high Cl^-/Br^- and Cl^-/I^- ratios owing to the low halogen and I-Br abundance of these minerals (e.g., Svensen et al. 2001a, b; Kendrick et al. 2006a). Water loss via dehydration and hydration reactions during prograde and retrograde metamorphism, respectively, may also modify the primary metamorphic fluid salinity to some extent (Markl and Bucher 1998a, b; Kullerud and Erambert 1999; Yardley et al. 2000; Yardley and Graham 2002; Yardley 2009, 2013). In the lower crust, this process can significantly increase the salinity of initially low Cl crustal metamorphic fluids to the point of halite saturation, as well as stabalize Cl-rich, hydrous silicate minerals such as biotite and amphibole from initially anhydrous, olivine- and pyroxene-rich granulites and eclogites. These processes can lead to changes in halogen abundances and ratios in such rocks, and in the corresponding fluids (Markl and Bucher 1998a, b; Svensen et al. 2001a; Yardley and Graham 2002; Yardley 2009, 2013).

2.3.2 The Crust

2.3.2.1 Continental Crust

Including evaporites, the bulk of the halogens in the crust reside in the continental crust (CC; McDonough and Sun 1995) but are distributed differently in various rock types, with the upper continental crust (UCC) enriched in halogens on an average of 1.4 to 2.3 times (for F, Cl, Br) and 10 times (for I) relative to the lower continental crust (LCC). Difficulty arises in accurately evaluating the relative contributions of rock types in the CC, since reported halogen abundances are not tied exclusively to the mineral constituents of the great diversity of rock types, but also to the proportion of Cl, Br, and I trapped in fluid inclusions of variable salinity. Such rock diversity and compositional variability likely contribute significantly to the overall sample mass balance, in particular for Br and I, which are highly incompatible in all common rock-forming minerals. Negligible distinction has been made between the soluble and insoluble fractions of halogens associated with whole-rock analyses reported for crustal rocks, and a very large proportion of bulk halogens (i.e., up to 70–80% of Br and Cl; mean 25–40%), even in

non-sedimentary rock samples, may be water-soluble and leachable from fluid inclusions (Hanley et al. 2004). Further modification of the crust during hydrothermal alteration, mineralization, and weathering, and the overall high mobility of halogens have led to an order of magnitude variations in halogen abundances locally.

Estimations of bulk halogen abundances in the CC are sparse, especially with respect to what are called "fresh" rock types. Halogen abundances in the CC, as a whole and in its various parts, are reported by Gao et al. (1998) and Rudnick and Gao (2003), based on calculated or estimated abundances from Wedepohl (1995). Halogens in the bulk CC are reported to be F = 553 ppm, Cl = 244 ppm, Br = 0.88 ppm, and I = 0.7 ppm. These values are an average of upper crust (F = 611 ppm; Cl = 640 ppm; Br = 1.6 ppm; and I = 1.4 ppm) and lower crust (F = 429 ppm; Cl = 278 ppm; Br = 1 ppm; and I = 0.14 ppm). For Cl and F, the estimate of Wedepohl (1995) was based on a mixture of various average UCC lithologies, as compiled by Wedepohl (1987). For the lower crust, only an average of granulites and gabbros was used. For I and Br, calculations and estimates for UCC and LCC (Wedepohl 1995) were made from a mixture of lithologies compiled by Fuge (1974) and Becker et al. (1972), which took into account organic matter contributions modeled by the correlation between Cl and I (Price and Calvert 1970). The estimate of I for the LCC should be used with caution, as the details of how this estimate was obtained are not clear (Wedepohl 1995).

With the exception of some phosphatic shales (with very high I and F contents; Gulbrandsen 1966; Becker et al. 1972; Manheim et al. 1980; Wang et al. 2004; Álvarez et al. 2015), caliche (nitrate) deposits (up to ~4000 ppm I; Salminen et al. 2005) and evaporites, there is no systematic variation in the halogen abundance and relative abundance, which can vary by several orders of magnitude in sedimentary rocks of both clastic and chemical types (Table 2.8; Fig. 2.3). The volumes of halide salts formed throughout various periods of the Earth's history have been comparable to, or an order of magnitude less than, the mass of sediments. As a current estimate, evaporites constitute a large mass proportion of the Cl (~13%) and Br (~16%) on Earth (estimated with data from Land 1995a; McDonough 2003; details are given in Sect. 2.5). Marine and freshwater sediments, including suspended particulates, muds, and pelagic sediments, and their clay-rich rock derivatives are typically highly enriched in Br and I, to ppm levels (Fuge and Johnson 1986; Martin et al. 1993; Muramatsu et al. 2007). The accumulation of high concentrations of Br and I in the tissues of organisms, in particular in the marine environment (Bowen 1979), is a primary contributor to this. Variability in Br and I within sedimentary rocks can be linked partly to contained organic matter, to the halogen content of detrital and authigenic minerals (e.g., formed during diagenesis), and contained pore fluids. Consequently, Br/Cl and I/Cl ratios for the majority of sedimentary rocks are higher than for formation waters and seawater (Fig. 2.4). The majority (~70%) of crustal I and a significant proportion of Br are

Table 2.8 Halogen abundances in some continental crustal rock types and sedimentary particulates; means and ranges

Example	F [ppm]	Cl [ppm]	Br [ppm]	I [ppm]	Source
Metamorphic					
Amphibolites	659	296	–	–	1
Amphibolites	–	250 [100–400]	–	0.023 [0.020–0.026]	2,3
Felsic granulites	413	–	–	0.013 [0.009–0.017]	1,3
Intermediate granulites	582	–	–	–	1
Mafic granulites	845	341	–	–	1
Gneisses	–	570 [140–1000]	–	0.031 [0.007–0.055]	2,3
Metapelite	–	431.154 [8–3085]	0.123 [0.014–0.191]	0.144 [0.012–.355]	4
Sedimentary					
Carbonates	459 [454–465]	169 [99–305]	6.4 [6.2–6.6]	1.4 [1.2–1.6]	1,5,6
Carbonates (limestones)	–	16.433 [14.6–17.6]	0.104 [0.0889–0.118]	7.275 [0.279–29]	7,8
Dolomites	–	35.867 [31.2–42.8]	0.622 [0.576–0.692]	0.789 [0.739–0.832]	8
Sandstones	485.5 [482–489]	124 [68–180]	–	–	1
Sandstones (graywacke, argillaceous)	–	12.5 [10–15]	1	6.36 [0.068–37.6]	5,6,7
Phosphorites	10115.5 [8796–11435]	–	–	–	9
Phosphatic shale	16301.5 [2.99– 32600]	–	–	–	10
River particulates	–	–	15.2 [2–54]	–	11
Shales	–	175 [170–180]	4.15 [4–4.3]	10.49 [2.2–38]	5,6,7
Marine shales	740	180	20	19	6
Oceanic sediment (carbonate & clay)	–	20500 [20000–21000]	200.5 [70–331]	18.28 [0.025–49]	5,6,7
Oceanic sediment (non-carbonate)	826 [393–1259]	1018.4 [44.8–1992]	45 [20–70]	14.025 [0.05–28]	12
Marine pelagic clay	1300	21000	70	14.025 [0.05–28]	6,13
Manganese nodules	200	–	21	400	14
Pelites	860 [780–940]	74.5 [57–92]	–	–	1

(continued)

Table 2.8 (continued)

Example	F [ppm]	Cl [ppm]	Br [ppm]	I [ppm]	Source
Greywackes	–	147 [68–243]	0.74 [0.255–1.292]	0.22 [0.091–0.54]	4
Fresh water lake sediment	–	59 [57–61]	7.82 [7.22–8.5]	9.05 [8.19–9.52]	8
Slate	–	11.03 [6.96–14.7]	0.096 [0.052–0.136]	0.10 [0.090–0.119]	8
Stream sediments	–	40.15 [20.7–74.9]	2.25 [1.1–3.98]	1.91 [0.587–4.69]	8
Chert	–	4.76 [4.52–5.08]	0.027 [0.023–0.032]	0.12 [0.101–0.131]	8
Igneous, ultramafic intrusive					
Spinel lherzolites	5.5 [5–6]	5	–	–	15
Spinel peridotites	88	53	0.01	–	16
Igneous, mafic intrusive					
Mafic intrusions	660	154	–	–	1
Norite	13	307.5 [215–400]	0.235 [0.08–0.39]	–	17–21
Gabbro	13	307.5 [215–400]	0.235 [0.08–0.39]	–	17–21
Igneous, mafic extrusive	681	78	–	–	1
MORB	267 [100–600]	38.33 [20–50]	–	–	22–24
OIB	35	90	–	–	22,23
Igneous, intermediate intrusive/extrusive					
Andesites	500	3250 [1500–5000]	–	–	22,23
Diorite	631	144	–	–	1
TTG	539 [514–564]	90 [69–111]	–	–	1
Igneous, felsic intrusive/extrusive					
Felsic volcanics	846	93	–	–	1
Felsic intrusives (granites, granodiorites, tonalites)	–	358 [283–433]	0.25 [0.2–0.3]	0.0433 [0.0016–0.085]	2,3,16,19,25,26
Granites	613 [533–692]	104 [34–174]	–	–	1
Felsic volcanics	441	30	–	–	1

(continued)

Table 2.8 (continued)

Example	F [ppm]	Cl [ppm]	Br [ppm]	I [ppm]	Source
Silica-oversaturated felsic rocks	5567 [200–15000]	4020 [600–9000]	–	–	21,22
Rhyolite	–	662.46 [119–1080]	1.52 [0.545–2.15]	0.18 [0.074–0.519]	8

[a]Including some river particulates

Sources—[1]Gao et al. (1998); [2]Muramatsu and Wedepohl (1998); [3]Johns and Huang (1967); [4]Boneß et al. (1991); [5]Horn and Adams (1966); [6]Turekian and Wedpohl (1961); [7]Becker et al. (1972); [8]Sekimoto and Ebihara (2013); [9]Manheim et al. (1980); [10]Gulbrandsen (1966); [11]Martin and Meybeck (1979); [12]John et al. (2011); [13]Li (1982); [14]Baturin (1988); [15]Wedepohl and Hartman (1994); [16]McDonough (1990); [17]Sugiura (1968); [18]Lieberman (1966); [19]Ganapathy et al. (1970); [20]Cattermole and Fuge (1969); [21]Jambon and Zimmermann (1990); [22]Johnson et al. (1993); [23]Wallace and Anderson (2000); [24]Edmond et al. (1979); [25]Fuge et al. (1978); [26]Vinogradov (1961)

hosted in organic-rich marine sedimentary rocks (Elderfield and Truesdale 1980). Iodine and Br values for oxidized sediments (outer-shelf) are typically higher than for reduced sediments (inner-shelf), due to the preferential sorption of I and Br by suspended living and non-living organic matter. Consequently, organic matter abundance in *some* sedimentary marine settings may be correlated to the abundance of Br and I (e.g., Price and Calvert 1977; Leri et al. 2014). Coal and surficial organic matter also accumulate I and Br, which also leads to a correlation of these halogens with organic carbon in terrestrial sediments and soils (e.g., Kabata-Pendias 2001). Although the abundance of Br and I in clastic rock types is low relative to marine sediments (Salminen et al. 2005), elevated levels of these elements in argillaceous sandstones can be significant as a result of adsorption onto clay surfaces (Becker et al. 1972).

The halogen content of different igneous rock types in the CC (Table 2.8; Fig. 2.3) is also highly variable. This reflects the range in corresponding halogen abundances in silicate glasses and halogen-bearing silicate and phosphate minerals (predominantly) derived from igneous liquids in which magmatic differentiation and differential partitioning behavior control the ultimate distribution of the halogens. This variation may also reflect the influence of the original halogen budget of protoliths that have been melted such as orogenic granites. The abundance would be diminished by magmatic degassing, which also raises the F/Cl and F/Br ratio of magmas through the loss of more volatile-compatible Cl and Br (e.g., Miller et al. 1990). For F and Cl, halogen contents typically are in the 100 s to 1000 s of ppm range, with highly fractionated peraluminous and peralkaline granitoids, and some basaltic rocks, showing the highest values as crystal fractionation increased the halogen concentration. During the weathering of volcanic products, glass devitrification results in mobilization of Cl and F, with F being more mobile (e.g., Stix et al. 1995). Generally, glassy volcanic rocks contain higher concentrations of the halogens than their crystallized equivalents (Sugiura 1968). A limited amount of data for Br and I in fresh oceanic basaltic crust are available (see Sect. 2.3.2.2), and

data for Br and I in both volcanic and plutonic igneous rocks in the continental crust are rarely reported (Table 2.8), and, when reported, generally do not exceed ~2 ppm (Fuge and Johnson 1986; Sekimoto and Ebihara 2013).

Data for the halogens in metamorphic rocks are rarely reported (Table 2.8), such that estimates for bulk mass balance purposes are derived largely from the composition of the protoliths. Data for granulites, amphibolites, gneisses, and metapelitic rocks have been reported, in which F abundances are always higher than Cl. The relationship between metamorphic grade or reaction type, and changes in the halogen abundance and ratio are unclear. The halogens do not show a concomitant change in abundance with changes in H_2O and CO_2 associated with devolatilization reactions (Boneß et al. 1991). Metamorphosed sedimentary rocks preserve primary halogen ratios related to the original pore fluids and primary clay or mica phases (e.g., Boneß et al. 1991). Whereas some fluid inclusion data suggests that prograde metamorphism can lead to lower halogen abundances in metamorphic fluids (Yardley and Bodnar 2014), retrograde reactions in the lower crust can lead to enrichment in bulk rock Cl for metamorphic rocks as fluid phases become progressively "dehydrated" via the formation of OH-bearing hydrous silicates from olivine-pyroxene-bearing granulites, leading to less H_2O while maintaining Cl abundances. It should be noted that fluid volumes associated with these reactions are very small and are likely to be consumed entirely through such reactions. This implies that halogen-bearing free fluid phases do not have long residence times in the lower crust once they infiltrate (Markl and Bucher 1998a, b; Yardley et al. 2000; Yardley 2013).

2.3.2.2 Oceanic Crust

The oceanic crust comprises igneous rocks overlain by variable amounts of sediment. The proposed Penrose ophiolite model (1972) describes that an oceanic crust consists of a stratigraphic sequence of sediments, extrusive basaltic lavas, sheeted dikes, and plutonic gabbros, underlain by peridotite, in which igneous rocks originate from mantle-derived basalt. It should be noted that some oceanic crusts show poor lava coverage as well as a lack of sheeted dikes, and instead, are dominantly composed of serpentinized peridotites with some sediment cover (e.g., Cannat 1993). Acknowledging that variable magmatic activity occurs along mid-ocean ridges, it is unlikely that the Penrose ophiolite model represents the bulk composition of oceanic crust comprising the entire ocean floor. Specifically, for magma-poor oceanic crust, serpentinite is tectonically mixed with plutonic gabbros, decreasing the contribution of igneous material in the crust. Here, in an attempt to provide an estimate of halogen abundance in the oceanic crust, the representative concentrations were assessed for each lithology. These included fresh magmatic crust, altered oceanic crust, sediments, and serpentinite (Table 2.9). A combination of these lithologies in varying proportions should represent the oceanic crust, once these proportions are known.

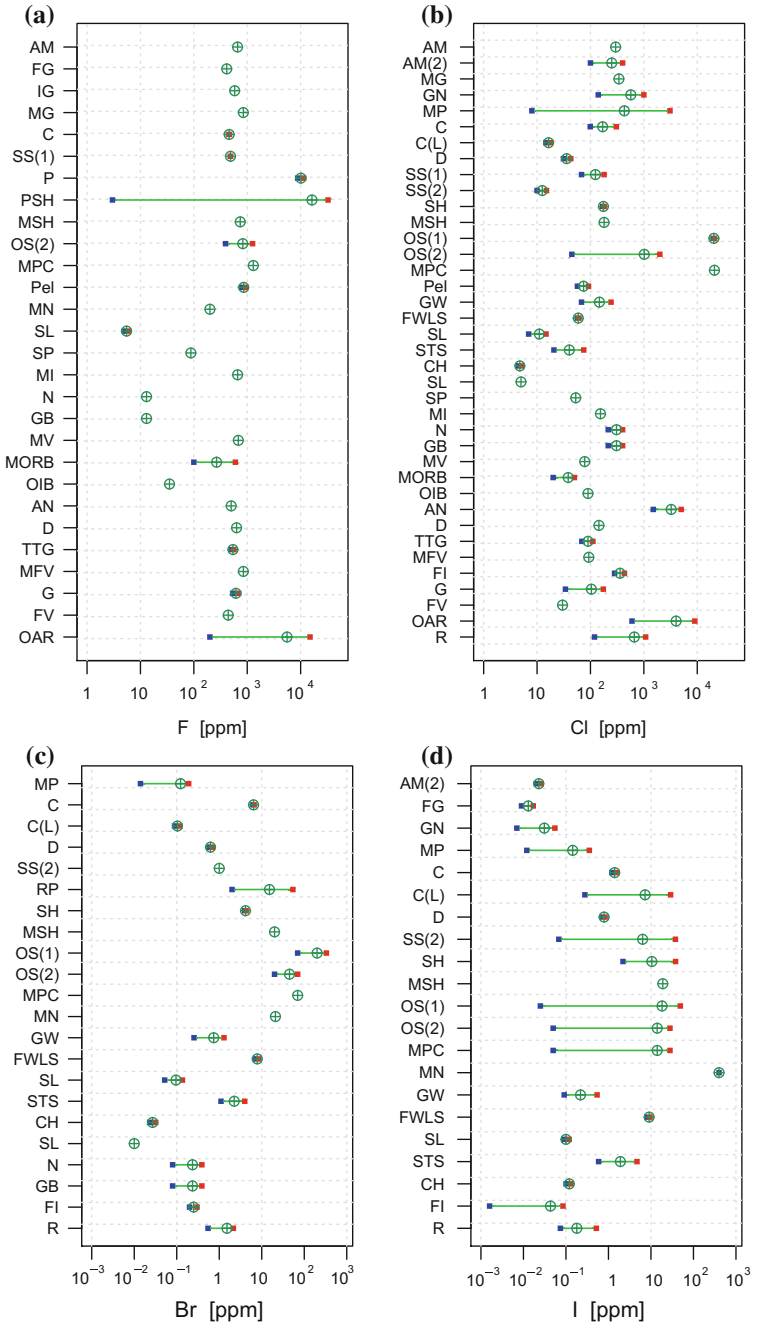
(a)
AM
FG
IG
MG
C
SS(1)
P
PSH
MSH
OS(2)
MPC
Pel
MN
SL
SP
MI
N
GB
MV
MORB
OIB
AN
D
TTG
MFV
G
FV
OAR
1
10
10 2
10 3
10 4
F [ppm]
(b)
AM
AM(2)
MG
GN
MP
C
C(L)
D
SS(1)
SS(2)
SH
MSH
OS(1)
OS(2)
MPC
Pel
GW
FWLS
SL
STS
CH
SL
SP
MI
N
GB
MV
MORB
OIB
AN
D
TTG
MFV
FI
G
FV
OAR
R
1
10
10 2
10 3
10 4
Cl [ppm]
(c)
MP
C
C(L)
D
SS(2)
RP
SH
MSH
OS(1)
OS(2)
MPC
MN
GW
FWLS
SL
STS
CH
SL
N
GB
FI
R
10 −3
10 −2
10 −1
1
10
10 2
10 3
Br [ppm]
(d)
AM(2)
FG
GN
MP
C
C(L)
D
SS(2)
SH
MSH
OS(1)
OS(2)
MPC
MN
GW
FWLS
SL
STS
CH
FI
R
10 −3
10 −2
10 −1
1
10
10 2
10 3
I [ppm]

◂**Fig. 2.3** Abundances of the halogens **a** F, **b** Cl, **c** Br, and **d** I in some continental and oceanic crustal rock types showing mean and ranges. A graphical representation of the data summarized in Table 2.8 (references for data listed at the bottom of Table 2.8). Rock type abbreviations: *AM (1)* amphibolites(1), *AM(2)* amphibolites(2), *AN* andesites, *C* carbonates, *C(L)* carbonates (limestones), *CH* chert, *DI* diorite, *D* dolomites, *FG* felsic granulites, *FI* felsic intrusive (granites, granodiorites, tonalites), *FV* felsic volcanics, *FWLS* fresh water lake sediment, *G* granites, *GB* gabbro, *GN* gneisses, *GW* greywackes, *IG* intermediate granulites, *MFV* metafelsic volcanics, *MG* mafic granulites, *MI* mafic intrusions, *MN* manganese nodules, *MORB* mid ocean ridge basalt, *MP* metapelites, *MPC* marine pelagic clay, *MSH* marine shales, *MV* mafic volcanics, *N* norite, *OAR* oversaturated acid rocks, *OIB* ocean island basalt, *OS(1)* oceanic sediment (carbonate & clay), *OS (2)* oceanic sediment (non-carbonate), *P* phosphorites, *Pel* pelites, *PSH* phosphatic shale, *R* rhyolite, *RP* river particulates, *SH* shales, *SLH* spinel lherzolites, *SL* slate, *SP* spinel peridotites, *SS(1)* sandstones, *SS(2)* sandstones (white, graywacke, red, argillaceous), *STS* stream sediment, and *TTG* tonalites-trondhjemites-granodiorites

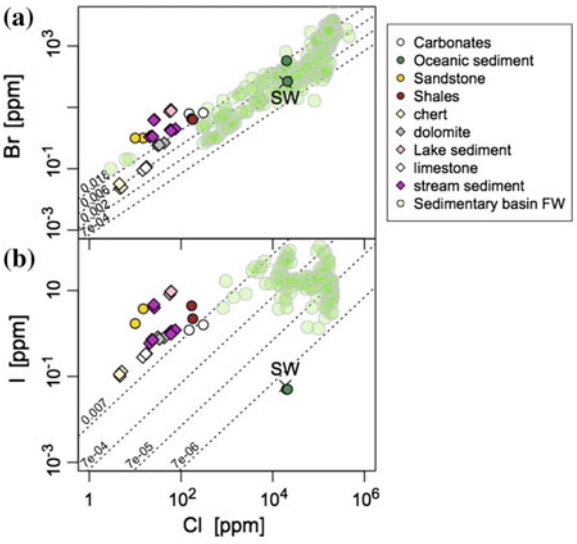

Fig. 2.4 Concentration of **a** Br and Cl, and **b** I and Cl, in various sedimentary rock types (from Table 2.6) compared to halogen ion concentrations in sedimentary formation waters (from Table 2.5)

The average composition of a fresh magmatic section of oceanic crust can be approximated by the composition of primitive basalts, as all of a single batch of a mantle-derived magma would crystallize to form oceanic crust, with no magma lost to mantle, nor to the ocean. Table 2.9 reports the average halogen content of reported primitive basalts. The bulk halogen content of altered oceanic crust (AOC) is difficult to assess. It has been frequently demonstrated that all halogens increase with increasing alteration of basaltic igneous rocks (e.g., Ito et al. 1983; Gillis et al. 2001; Debret et al. 2014). Furthermore, because the degree of alteration of oceanic crust is highly variable (e.g., Ito and Anderson 1983), a single value representing the composition of the altered ocean crust is probably only accurate to an order of magnitude at best. Nevertheless, several attempts have been made to assess the composition of altered oceanic crust. For example, in terms of halogens, Straub and Layne (2003), incorporating previously published data, modeled the increase in F and Cl content with respect to the amount of metamorphic amphibole produced during

Table 2.9 Compositions of oceanic crust lithologies (ppm = $\mu g.g^{-1}$)

	Primitive MORB	AOC	Sediments	Serpentinite
F	130 (40)	400	393–1259	51–320
Cl	48 (26)	250	44.8–1992	144–1200
Br	0.8 (1.6)	0.8	20–70	0.32–2.60
I	0.021 (20)	0.027	0.05–28	0.06–0.70

Primitive MORB composition is derived from averages of melt inclusion data: Saal et al. (2002); Shaw et al. (2010); Wanless and Shaw (2012) for F and Cl. Br and I concentrations are from Schilling et al. (1980); Déruelle et al. (1992); Jambon et al. (1995); Kendrick et al. (2011, 2013b). AOC is a model concentration used in Van den Bleeken and Koga (2015), and Br and I values are derived from Br/Cl and I/Cl reported for oceanic amphiboles (Kendrick et al. 2015a). Sediment data from John et al. (2011). Serpentinites data are from John et al. (2011); Kendrick et al. (2013c); Debret et al. (2014)

hydrothermal alteration in the crust. This approach is expanded in a recent study by Debret et al. (2015), accounting for the compositional variations of metamorphic amphiboles. Several bulk measurements of marine sediments were reported as ranges in halogen content. Altered mantle, a part of the subducting lithosphere, also experiences a significant increase in halogens through serpentinization, as the halogen content in serpentine is significantly higher than olivine or pyroxenes by a factor of 20 to 1000 (Debret et al. 2014). The bulk measurements show a smaller extent in halogen enrichment compared to the gain in halogens observed in individual minerals comprising the bulk rock, and these gains are correlated to the degree of serpentinization (John et al. 2011; Kendrick et al. 2013c). Bulk analyses of oceanic sediments have also recently been reported (John et al. 2011). Considering this recent work, there are sufficient data to model the bulk halogen abundance of altered ocean crust as a function of the degree of alteration and the proportions of sedimentary, mafic, and ultramafic lithologies (see examples in Straub and Layne 2003; Van den Bleeken and Koga 2015). An in-depth discussion of the issue surrounding altered oceanic crust is covered by Kendrick (2018).

Owing to their high fluid-mineral and fluid-silicate melt partition coefficients, the halogens are useful in tracing the fate of minerals and melts, and the fate of associated water in subduction zones where metamorphic dehydration and fluid-induced partial melting are inferred from erupted arc lavas (Bureau et al. 2000; Pyle and Mather 2009), and the distinct ratios of halogens in seawater, sediment pore fluids, sediments, and oceanic crust could help identify the provenance of fluids (Kastner et al. 1990; Martin et al. 1993; Muramatsu and Wedepohl 1998; Philippot et al. 1998; Bureau et al. 2000; Fehn et al. 2006; Muramatsu et al. 2007; Sumino et al. 2010; Kendrick et al. 2012, 2014; Debret et al. 2015). Noble gas and bulk halogen concentrations in, and halogen isotope studies of, exhumed peridotites and serpentinites show that, whereas large quantities of halogens are released from hydroxysilicate minerals in subducting oceanic crust during slab devolatilization (Sumino et al. 2010; Kendrick et al. 2013c; Debret et al. 2015), altered and metamorphosed oceanic lithosphere preserves the original seawater Cl isotope composition, even up to greenschist facies conditions during subduction zone

metamorphism (e.g., Barnes et al. 2013). Thus, the compositional evolution of subducting oceanic crust cannot be treated as a simplified geochemical transfer process. An in-depth discussion of the issues surrounding subduction and consequent metamorphism is covered in Chaps. 8, 9, and 11 (Barnes et al. 2018; Kendrick 2018; Aranovich and Safonov 2018).

2.3.3 Mantle and Core

2.3.3.1 Halogen Elements in the Mantle

Fluorine

The abundance of trace elements in the mantle is commonly assessed through compositional correlations and systematics among primitive basalt, peridotite xenoliths, and chondritic meteorites (Hart and Zindler 1986; Allègre et al. 1995; McDonough and Sun 1995). The model halogen content of the mantle has been assessed by the same methods (Table 2.10), and there is only a limited number of direct measurements of mantle xenoliths have been reported so far. Because measurements of bulk halogen concentrations often require specific extractions of the soluble and insoluble fractions, long counting times, and low method sensitivity, and because of a lack of certified and robust standards for instrument calibration, the number of reported F measurements remains small compared to other lithophile elements. Some subcontinental xenoliths have been measured (e.g., Table 2.10, Jagoutz et al. 1979), and a bulk mantle F content has been modeled from F abundances in olivine and orthopyroxene from various subcontinental xenoliths (12 ppm, Beyer et al. 2012). It should be cautioned that metasomatized subcontinental mantle could be significantly different from the mantle source for Mid-Ocean Ridge Basalt (MORB) and Ocean Island Basalt (OIB). In fact, reported xenolith values are within the range of depleted mantle (DM), while they differ from that of the model bulk silicate earth (BSE).

The modeled F content of BSE ranges from 18 to 25 ppm, with different estimates agreeing within reported uncertainty. Slight differences in the estimated F abundances are due to the models used to determine the depletion factors for incompatible trace elements. All BSE models tied F abundance to canonical ratios of either $F/P = 0.3 \pm 0.1$, $F/K = 0.09 \pm 0.04$, and/or $F/Sr = 2$ (Schilling et al. 1980; F/P, F/Sr used in McDonough and Sun 1995; F/P, F/K used in Palme and O'Neil 2003; Lyubetskaya and Korenaga 2007; F/P used by Slaters and Stracke 2004). A canonical ratio is a trace element ratio that appears to be constant among mantle-derived magmas that have experienced little modification through interaction with the crust, (i.e. primitive MORB, OIB). Therefore, the ratio found in such magmas is considered independent of various degrees of partial melting, and thus the ratio should represent the value of the source. Here, BSE is commonly considered as being equivalent to primitive mantle that did not record any depletion as a result of permanent extraction of melts that ultimately formed the continental

Table 2.10 Halogen abundance in mantle

	Xenolith [J79]	BSE [MS95]	BSE [PO03]	BSE [LK07]	DM [SS04]
F [$\mu g.g^{-1}$]	10.5 (3.5)	25[a]	25 (10)	18 (8)	11 (5)
Cl [$\mu g.g^{-1}$]	1.33 (0.61)	17[a]	30 (12)	1.4 (0.5)	0.51 (9)
Br [$ng.g^{-1}$]	11.2 (5.4)	50[a]	75 (38)	3.6 (0.4)	
I [$ng.g^{-1}$]		10[a]	7 (>3.5)	10[a]	

Number inside parenthesis indicates one standard deviation of least significant digits, in where 25 (10) should read as 25 ± 10, and 0.51(9) as 0.51 ± 0.09. [a]Standard deviation is not reported. References are Jagoutz et al. 1979 [J79]; McDonough and Sun 1995 [MS95]; Palme and O'Neil 2003 [PO03]; Lyubetskaya and Korenaga 2007 [LK07]; Salters and Stracke 2004 [SS04]. "Xenolith" is the 6 peridotite xenoliths reported in the paper. "BSE" is a model bulk silicate Earth. "DM" is depleted mantle which is the source of mid-ocean ridge basalts

crust. BSE is also synonymous with the term "pyrolite" (Ringwood 1962a, b), while they are modeled by different methods.

MORB are derived from a mantle that is depleted (DM) relative to BSE. There are two studies that assessed the composition of DM (Salters and Stracke 2004; Workman and Hart 2005). While the method and data selection differ slightly, these studies tied absolute concentrations of the depleted mantle to the constraints given by parent-daughter ratios of radiogenic isotope systems (e.g., Sm/Nd, Lu/Hf, Rb/Sr) and melting depletion trends for the mantle. Once some element abundances are fixed, other element abundances are determined by canonical element ratios that are influenced negligibly by melting. From a compilation of primitive MORB melt inclusions, Salters and Stracke (2004) report a F abundance (11 ± 5 ppm), that is based on an F/P = 0.27 ± 0.11, The application of the ratio to P abundance by Workman and Hart (2005) gives F = 22 ± 9 ppm. However, Workman et al. (2006) advocate another canonical ratio, F/Nd = 20.1 ± 5.8, for MORB. Use of this ratio would result in a F abundance of 12 ± 3 ppm using DM values from Workman and Hart (2005). It should be noted that DM that has been influenced by early differentiation processes from an initial non-chondritic Sm/Nd ratio, which would result in F abundances of 6 to 12 ppm, depending on the choice of canonical ratio used (K = 68.4 ppm, Nd = 0.81 ppm, Boyet and Carlson 2006). Given the uncertainty (F = 6–22 ppm), we conclude that F = 11 ± 5 ppm (Salters and Strecke 2004) is possibly the closest estimate of the median value of F abundances from current DM models. However, it should also be noted that Shimizu et al. (2016) report enriched and depleted DM compositions, deconvolved from an extensive submarine glass data set (F = 31 and 8 ppm, respectively).

Data for the bulk F content in mantle xenoliths are quite limited. For the few data available, variability appears to be significant, ranging from 7 ppm (Potrillo xenolith, Jagoutz 1976) to 400 ppm (spinel lherzolite from Khibiny massif, Arzamastsev and Glaznev 2008). In addition to the paucity of data, the composition of the subcontinental xenoliths has commonly been modified by metasomatism. Therefore, an independent, current assessment of F abundances in the mantle, using only peridotite xenoliths, is not possible. A significant increase in the size of the whole rock xenolith database in the future could lead to independent constraints on the F abundance in the mantle.

Chlorine

The Cl content of the mantle (BSE) is modeled by the same method as for F, using canonical ratios of Cl/Ba, Cl/Rb, and Cl/K (McDonough and Sun 1995; Palme and O'Neil 2003; Lyubetskaya and Korenaga 2007). Furthermore, Cl/Nb is also reported as relatively constant for MORB-OIB (i.e. a canonical ratio). In contrast to F, the model BSE abundance of Cl differs significantly more than that of F, from 1.4 to 30 ppm (Table 2.10). These variations suggest that secondary processes (i.e., sample alteration and weathering) complicate the interpretation of Cl abundance measurements. For example, MORB glass data systematically show large variations in Cl compared to F (Fig. 2.5), suggesting that even carefully selected submarine MORB glasses might have interacted with seawater (the same conclusions are usually derived from examination of the Cl/K ratio). Furthermore, Cl is more incompatible than F during mantle partial melting, such that variations in the degree of melting would influence the Cl abundance more than that of F. The variability among reported BSE halogen abundance models reflects the choices of canonical ratios. For example, Cl/Ba = 2.5 and Cl/Rb = 28 are used by McDonough and Sun (1995). A sum of the total Cl found in oceanic crust and present-day mantle (which contains twice more Cl than a total of the Earth's surface reservoirs) was used in the BSE estimate of Palme and O'Neil (2003). Finally, Lyubetskaya and Korenaga (2007) used Cl/K = 0.0075 ± 0.0025 (Saal et al. 2002), which is a canonical ratio measured from what is considered to be the most depleted MORB sample suite available. This suite unambiguously shows strong depletion, but it is not clear if the reported Cl value represents the entire mantle. For example, the mantle value for Cl/K reported by Michael and Cornell (1998) varies from 0.01 to 0.08, depending on the degree of depletion. Also, it should be noted that the K abundance in the model of Lyubetskaya and Korenaga (2007) is approximately 25% less than that of Palme and O'Neil (2003) (i.e., 190 and 260 ppm respectively). This contributes to a disparity in Cl abundances, i.e., 1.4 and 30 ppm for Lyubetskaya and Korenaga (2007) and Palme and O'Neil (2003), respectively (Table 2.10).

Chlorine is also significantly depleted in the DM relative to the BSE. The DM of Salters and Stracke (2004) is also constrained by Cl/K (0.01 to 0.007). Similarly, application of Cl/K = 0.01 to the K content of Workman and Hart (2005) and Boyet and Carlson (2006) gives 0.50 and 0.68 ppm K, respectively. With these model K values, Salters and Stracke (2004) calculated a Cl value of 0.51 ± 0.09 ppm. These model DM values are comparable to the estimate of Saal et al. (2002) of 1.0 ± 0.5 ppm. In addition, the recent report by Shimizu et al. (2016) determines Cl abundances in enriched and depleted DM to be 22 and 0.4 ppm, respectively.

Bromine

The Br content of the mantle can also be modeled from canonical ratios, such as Br/Cl or its reciprocal (Schilling et al. 1978, 1980; Jambon et al. 1995; Kendrick 2012; Kendrick et al. 2012). The most recent compilation gives Br/Cl = $(2.8 \pm 0.6) \times 10^{-3}$ (Kendrick et al. 2013b). As noted by these authors, Br correlates well with Cl, and the relative variability of Br/Cl among typical mantle-derived basalts is approximately 20% (Kendrick et al. 2013b, also see Fig. 2.6). It is inferred

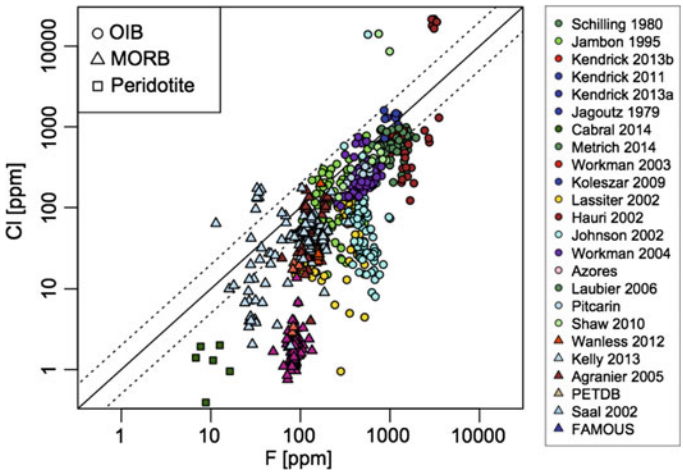

Fig. 2.5 Concentration of F and Cl in basalt and peridotite. The *circles* are basalts, in which OIB samples are indicated by *open symbols*. *Squares* are subcontinental mantle xenoliths. OIB data are taken from, Schilling et al. (1980), Jambon et al. (1995), Kendrick et al. (2011, 2013a, b, c), Cabral et al. (2014), Metrich et al. (2014), Workman et al. (2004), Koleszar et al. (2009), Lassiter et al. (2002), Hauri (2002), Johnson et al. (2002). MORB data are from Wanless and Shaw (2012), Shaw et al. (2010), Kelley et al. (2013), Agranier et al. (2005), Saal et al. (2002). Peridotite data is Jagoutz et al. (1979)

that the variability of Br in the mantle should be similar to that of Cl. Furthermore, Br concentrations in the mantle can be determined once its Cl content is known. For example, if one adopts the Cl content of the depleted mantle as 1 ± 0.5 ppm, as determined by Saal et al. (2002), the calculated Br content would be 2.8 ± 1.5 ppb.

It should be noted that recently there have been significant improvements in Br concentration measurements. Some of the scatter seen in Fig. 2.6 is most likely contributed by various uncertainties in analytical methods. Bromine concentrations in bulk silicate rocks, mineral separates, and glasses have been determined by several methods. Neutron activation analysis with various Br separation methods has been used widely (Unni and Schilling 1977; Jambon et al. 1995). For example, epithermal neutron activation analysis (ENAA) reports precision better than 10% (2σ) for concentrations above 0.1 ppm (Unni and Schilling 1977). The method of irradiation-produced noble gas proxy isotopes reports high-precision Br measurements with 2–4% (2σ) internal precision for various geological materials (Johnson et al. 2000; Kendrick et al. 2001; Kendrick 2012). An additional strength of this method is that a combination of a laser and gas-extraction line permits in situ analysis of solid material.

Only a limited number of studies have focused on Br analysis of basalt samples. This is likely due to the strong correlation of Br with Cl, in which concentration measurements of two perfectly correlating elements would imply redundant information. This must have discouraged geochemists from investing time on the difficult measurement of Br. Glassy, submarine basalts from normal ridge segments

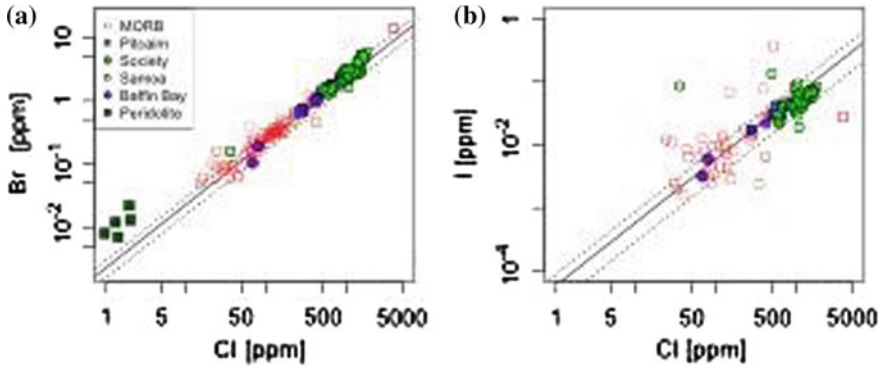

Fig. 2.6 **a** Concentration of Cl and Br in mantle-related materials. **b** Concentration of Cl and I. Symbols are the same in the previous figure. Note the excellent correlation between Br and Cl, which indicates a lack of fractionation of these elements in magmatic systems. MORB: Schilling et al. (1980); Jambon et al. (1995); Kendrick et al. (2011, 2013c); Pitcairn, Society: Kendrick et al. (2013b); Samoa and Baffin Bay: Kendrick et al. (2015b); Peridotite: Jagoutz et al. (1979)

have Br contents of 0.08 ± 0.02 ppm (n = 16), whereas those from the Azores hotspot have contents of 0.79 ± 0.53 ppm (n = 20) (Schilling et al. 1978, 1980; Unni and Schilling 1978). Jambon et al. (1995) reports a range of Br abundances from 62 to 1320 ppb, and Cl/Br of 430 ± 130 (Br/Cl = (2.3 ± 0.7) × 10^{-3}). Kendrick et al. (2013b) report an updated compilation with values from 100 to 5900 ppb, and Br/Cl = (2.8 ± 0.6) × 10^{-3}.

On the basis of these Br and Br/Cl data, primitive mantle Br contents (i.e., bulk silicate earth, pyrolite mantle) have been modeled as 50 ppb (McDonough and Sun 1995); 75 ± 38 ppb (Palme and O'Neill 2003, uncertainty is 1σ); and 3.6 ± 0.8 ppb (Lyubetskaya and Korenaga 2007). Each estimate is tied to a Br/Cl value of Jambon et al. (1995). The significant differences among different models are tied to assessments of the Cl concentration in the primitive mantle (see discussion above in Chlorine section). It should be noted that an estimate of the Br abundance in depleted MORB-source mantle is lower than BSE (1.4 ± 0.4 ppb; using 0.51 $\mu g.g^{-1}$ Cl from Salters and Stracke 2004). An average Br concentration in mantle xenoliths, derived from the subcontinental lithosphere, is 11.2 ± 5.4 ppb (n = 6, Jagoutz et al. 1979).

Iodine

The ratio I/Cl is considered as a canonical ratio, and has been used to model mantle composition from MORB and OIB basalts. The most recent compilation gives I/Cl = (60 ± 30) × 10^{-6} (Kendrick et al. 2013b). The correlation between I and Cl is poorer than between Br and Cl (Fig. 2.6), suggesting some fractionation processes during partial melting, crystal fractionation, and/or degassing. Using the canonical ratio, the I concentration in the mantle is determined from an assumed Cl content. For example, if the Cl content for depleted mantle is 1 ± 0.5 ppm (Saal et al. 2002), the I content in the mantle would be 0.06 ± 0.04 ppb (Table 2.10).

A small number of I measurements have been reported for basalts. Déruelle et al. (1992) report measurements of 31 MORB samples. The concentrations fall into three groups: E-type MORB 63 ± 96 ppb (n = 13, range 7–363 ppb), N-type MORB 7.7 ± 3.2 ppb (n = 11), and T-type MORB 7.4 ± 1.8 ppb (n = 7). The I content of BSE is estimated as 9–24 ppb, with 10 ppb as a recommended value. Recent MORB data shows similar variations in I, ranging from 1.6 to 82 ppb (n = 40, Kendrick et al. 2011, 2013b; note that 2011 data is corrected following Kendrick et al. 2013b), and I/Cl = (60 ± 30) × 10^{-6}. Ocean island basalts from the Pitcairn and Society seamounts show similar ranges (21–77 ppb; n = 20, Kendrick et al. 2013a). This leads to a range in the I/Cl ratio of (50–90) × 10^{-6} and (40–80) × 10^{-6} for Pitcairn (EM1), Hart et al. (1992) and Society (EM2), respectively. So far, a discernable mantle I/Cl heterogeneity tied to isotopically defined mantle components has not been found.

Wänke and Dreibus (1988) modeled the I abundance of the mantle as 6.2 × 10^{13} atoms.g^{-1} (13 ppb). McDonough and Sun (1995) and Lyubetskaya and Korenaga (2007) adopted the value estimated by Déruelle et al. (1992), which is 10 ppb. Palme and O'Neill (2003) estimated 7 ppb I, noting that the reported error exceeds 50% relative. Lastly, an estimate of I abundance in depleted MORB-source mantle is 0.031 ± 0.016 ppb (using 0.51 ppm Cl from Salters and Stracke 2004).

Subcontinental lithosphere, kimberlites, and carbonatites

The halogen abundances discussed above represent values for the convecting upper mantle, which is the source of basaltic magmas, specifically MORB and OIB. Thus they represent the composition of the DM, the primitive mantle, as well as other mantle compositional heterogeneities recorded in erupted oceanic basalts. In contrast, the mantle below the continents (i.e., the subcontinental lithosphere) is known to produce a wide range of magma types, including alkali basalts, kimberlites, and carbonatites. Some of these magmas and associated phases are very enriched in the halogen elements. For example, a fresh, Cl-rich kimberlite from Udachnaya-East (Yakutia, Russia) is reported to contain 2.8 wt% Cl in its groundmass and 18.5 wt% Cl in associated melt inclusions (Kamenetsky et al. 2004). Carbonatites from Ol Doinyo Lengai, Tanzania contain between 1.2 to 3.5 wt% F and 1.2 to 4.5 wt% Cl (Keller and Zaitsev 2012), which takes the form of an immiscible halide melt (now halide glass; Teague et al. 2011). Halide melt inclusions are also found in magmatic minerals from an intrusive carbonatite (St.-Honoré, Quebec, Canada, Kamenetsky et al. 2015). Similarly, F-rich micas and amphiboles are reported from various mantle nodules. For example, up to 8 wt% F is reported for phlogopite found in peridotite nodules from ultra-potassic lavas (Liu et al. 2011). Fluorine contents of 0.05 to 0.4 wt% have been reported in amphibole and mica in xenoliths from Kerguelen Island (Moine et al. 2000). Furthermore, fluoride melt has been reported in peridotite xenoliths (Klemme 2004).

From these examples, it is clear that significant enrichment of halogen occurs within the mantle, however high-halogen content magmas are volumetrically insignificant compared to basaltic magmas. Because these magmas are enriched in volatile and alkali elements, metasomatism of the source mantle is probably

required for their generation. Metasomatic processes recorded in mantle xenoliths have been extensively discussed elsewhere: see the reviews by Pearson et al. (2003) and O'Reilly and Griffin (2012) for an overview of the compositional variability of mantle xenoliths and the processes that cause the variation. However, the exact chemical reactions that can enrich halogens in the mantle are unknown. Additional high-quality data, in combination with experimental partitioning data on the corresponding chemical systems, is required for the development of a definitive model for halogen transfer and accumulation in the subcontinental lithosphere. Further discussion of halogens in the lithospheric mantle is found in Chap. 13 (Frezzotti and Ferrando 2017).

2.3.3.2 Halogen Elements in Core

There is little direct information regarding the presence of halogen elements in the Earth's core. Even if the halogen content of the core is lower than that of mantle by 1/30th, given that the weight fraction of the core is 32% of the Earth, the core could contribute 1% of halogen budget of the Earth. Further research efforts will hopefully provide better constraints on this uncertainty.

There are several laboratory experiments demonstrating halogen incorporation, or lack of, in metals, metal alloys, and sulfides. The interaction of halogens with Fe metal under atmospheric conditions commonly results in corrosion reactions, which form new phases. In general, the halogens are not expected to form extensive solid solutions with metal alloys or Fe sulfides. A consequence of such observations is the common assumption that most of the Earth's halogen budget is found outside of the core. In addition, we are not aware of any measurements of halogen concentrations in iron meteorites. However, based on the difference between chondritic bulk measurements (Déruelle et al. 1992) and bulk silicate Earth compositions (McDonough and Sun 1995), McDonough (2003) proposed the following halogen abundances in the core: F = 0, Cl = 200, Br = 0.7, and I = 0.13 [ppm]. Based on this model, 85% of the Cl, Br, and I on the Earth should reside in the core. It should be noted that heavy halogens are found to form metallic bonds at very high pressures: around 20 GPa for I (e.g., Balchan and Drickamer 1961; Sakai et al. 1982) and around 80 GPa for Br (e.g., Shimizu et al. 1994). Significant incorporation of the heavier halogen elements in the core is therefore plausible. Alternatively, the difference between chondritic and BSE abundances of Cl (and perhaps Br) can be reconciled with the loss of these elements in Earth's early atmosphere through collisional erosion (Sharp and Draper 2013).

There have been experimental efforts to constrain the abundance of halogens in the core using high-pressure, liquid metal-silicate melt partition coefficient measurements. Notably, $D_{\mathrm{I}}^{(\text{liquid metal})/(\text{silicate melt})}$ has been determined to be between 1 and 4, depending on the metal composition (Armytage et al. 2013). Such results confirm the presence of significant I in the core (I = 3.3 to ~24.3 [ppb], corresponding up to 83% of the I budget). On the other hand, an earlier study of

$D_{\mathrm{I}}^{(\text{sulfide melt})/(\text{silicate melt})}$ showed a value of less than 1 at 10 kb, suggesting much lower abundances of I in the core (Peters et al. 1995). A study of metal-silicate melt partitioning showed that $D_{\mathrm{Cl}}^{(\text{metal})/(\text{silicate melt})}$ is less that 0.01, up to 15 GPa (Sharp and Draper 2013). Given that the metal silicate partitioning showed little pressure-dependence, only a negligible quantity of Cl is expected in the core. It should also be noted that low pressure (below 1.8 GPa) experiments showed $D_{\text{halogen}}^{(\text{sulfide})/(\text{silicate melt})} < 1$ (Mungall and Brenan 2003), in which $D_{Cl} \sim 0.038$, $D_{Br} \sim 0.026$, and $D_I \sim 0.15$. In conclusion, I is likely to be incorporated into the core as a dissolved element in metallic alloy, while F and Cl are unlikely to be found in any significant concentration in the core. The constraint on Br is determined only for a sulfide-silicate melt pair. Bromine affinity to metal alloy at high-pressure conditions is unknown. Subsequently, the presence (or absence) of Br in the core is an unconstrained question for now.

2.4 Cosmic Abundances

2.4.1 Solar Abundances

The halogen group elements ($_9$F, $_{17}$Cl, $_{35}$Br, $_{53}$I) are produced via a variety of nucleosynthesis processes in stars, predating the solar system (Cameron 1973). Fluorine, with a single mass $^{19}_{9}$F is produced through neutrino spallation of ^{20}Ne and hydrogen-helium burning involving ^{14}N ^{18}F, ^{18}O, and ^{15}N (Woosley and Haxton 1988; Forestini et al. 1992). There are two isotopes of Cl, $^{35}_{17}$Cl and $^{37}_{17}$Cl, which are produced by explosive nucleosynthesis (Anders and Grevesse 1989), or explosive oxygen and silicon burning (Cameron 1973). Additional $^{37}_{17}$Cl can be produced by carbon burning and the stellar s-process (Anders and Grevesse 1989). Both isotopes of Br, $^{79}_{35}$Br and $^{81}_{35}$Br, are produced by the stellar r-process, with minor contribution from the s-process. The single mass of I ($^{127}_{53}$I) is produced by the stellar r-process (Cameron 1973; Anders and Grevesse 1989).

The halogens are usually classified as highly volatile elements with a condensation temperature below 640 K at 10^{-4} bars, except for F, which is a moderately volatile element (Lodders and Fegley 1998). The solar abundance of these elements has been assessed by several methods, including spectrometry of the Sun's photosphere and corona, and measurements of volatile element-rich meteorites such as CI chondrites. However, solar energetic particles data reflect fractionation to lower abundances for high first ionization potential atoms (Anders and Grevesse 1989; note first ionization potentials are F:17.4228, Cl:12.9676, Br:11.8138, and I:10.4513 eV; CRC Handbook). Furthermore, no spectroscopic determination of Br and I are available because the absorption lines are blended or inaccessible (Lodders 2010). Absorption signals from sunspots are used for photosphere abundances of F and Cl, but the data have significant uncertainty (Hall and Noyes 1969, 1972).

Recommended solar abundance values for halogen elements are therefore tied to assessment of CI chondrite composition. It should be noted that despite the challenges faced by different methods, abundance data agree within the data uncertainties, and furthermore the data agreement for F, Br, and I are within 10% (Table 2.11).

There is a systematic decrease in abundance from Cl, to Br, to I. Fluorine is notably less abundant than the heavier element Cl. In addition, compared to neighboring elements, namely C, N, O, and Ne, F abundance is lower by 3 to 4 orders of magnitude.

There are several assessments of halogen abundances in CI chondrites, and reported values differ to some degree (Table 2.12). These variations reflect an increased number of measurements and improved quality of measurements in recent years. This is combined with the choices of the average Si content for CI chondrites, and the choices of how the data from Orgueil (France) are statistically represented, which is the largest CI chondrite meteorite with an observed fall. Nevertheless, variations among the halogen elements are comparable to other relatively well-characterized lithophile elements.

It should be noted that the reported halogen values for meteorites, and precision in their determinations, have not changed significantly since the work of Anders and Ebihara (1982). While there have been significant improvements to the analytical precision of many elements that can be measured by ICPMS, the data quality for the halogen elements has remained the same since the 1970s. Also, Anders and Ebihara (1982) pointed out significant disparity between F data obtained by RNAA in combination with pyrolysis, and the nuclear reaction method, $^{19}F(p, \alpha\gamma)^{16}O$. Similarly, the Cl data show inter-laboratory disparity. Bromine abundances show considerable variation, from 2.3 to 5.1 ppm for the Orgueil CI chondrite. It should be noted that Br abundances were determined by examining the Br/Cd and Br/In values of volatile element-rich chondrites (C4 and E4), and then correcting for volatile depletion. After these corrections, the average Br concentration is found to be 3.59 ± 0.68 ppm, ranging from 3.02 to 4.59 ppm (Anders and Ebihara 1982). Iodine was also determined by correcting for volatile element fractionation, using In, Cd, F, and Br determinations for CI, CM, and EH chondrites.

Table 2.11 Solar system abundance of halogen group elements (Si = 10^6)

	Solar photosphere	CI [AE, AG]	CI [PJ]	CI [LPG]
F	812 (617)	843 (126)	806 (121)	804 (121)
Cl	7100 (6500)	5240 (786)	5180 (777)	5170 (780)
Br		11.8 (2.2)	11.5 (1.2)	10.7 (1.6)
I		0.90 (0.19)	0.897 (0.179)	1.10 (0.22)

Normalized to Si = 10^6. Data of solar photosphere is from Ross and Aller (1976), and the values are convered by $10^{(\log A - 1.65)}$, where "logA" is reported in the paper. *AE* Anders and Ebihara (1982); *AG* Anders and Grevesse (1989); *PJ* Palme and Jones (2003); *LPG* Lodders et al. (2009). The values in parenthesis are one sigma standard deviation

Table 2.12 Abundance of halogen group elements in CI chondrite (ppm = $\mu g.g^{-1}$)

	Orgueil [AE]	CI [AG]	CI [PJ]	CI [LPG]
F	58.2 (8.7)	60.7 (9.1)	58.2 (8.7)	58.2 (8.7)
Cl	698 (105)	704 (106)	698 (105)	698 (105)
Br	3.56 (0.68)	3.57 (0.68)	3.50 (0.35)	3.26 (0.49)
I	0.430 (0.090)	0.433 (0.082)	0.433 (0.087)	0.530 (0.106)

Concentration is reported as ppm (i.e. $\mu g.g^{-1}$). *AE* Anders and Ebihara (1982); *AG* Anders and Grevesse (1989); *PJ* Palme and Jones (2003); *LPG* Lodders et al. (2009). The values in parenthesis are one sigma standard deviation

2.4.2 *Halogen Elements in Meteorites*

Halogen element abundances in meteorites vary by factors of 20 to 100 (F, Cl ~ 20 and Br, I ~ 100). Typically, CI and EH chondrites show higher halogen abundances among the different chondrite classes (Fig. 2.7). Wasson and Kallemeyn (1988) provide a compilation of chondrite compositions by their classes (Fig. 2.7, red circles). In comparison with individual data (shown by plus signs,

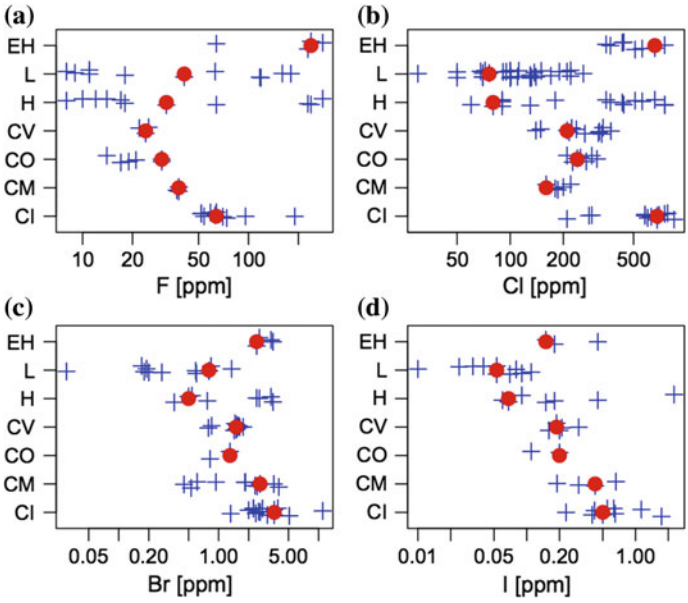

Fig. 2.7 Abundance of halogen elements found in different classes of meteorites are plotted here. Note the concentration axis (horizontal) is on the log scale. The *filled red circles* are published compilation values (Wasson and Kellemeyn 1988). *Blue crosses* are individual values found in various studies (Dreibus et al. 1979; Goldberg et al. 1974; Goles et al. 1967; Reed 1964, 1966; Krahenbürhl et al. 1973; Greenland and Lovering,1965; Mittlefehldt 2002; Noll et al. 2003; Kato et al. 2000; Jarosewich et al. 2010; Wänke et al. 1974; Sharp et al. 2013)

Fig. 2.7), the Wasson and Kellemeyn (1988) compilation globally occurs at the mode (the most probably value of the distribution). However, there are some notable offsets. For example, the Cl content of the L chondrites and the Br content in CI chondrites show slight offsets between the compilation (Wasson and Kellemeyn 1988) and the data distribution.

Variations in halogen abundances for each meteorite class, notably for CI, H, and L chondrites, can be attributed to a series of factors. (i) Analytical method: Bulk halogen abundances have been measured by several methods such as selective electrode, neutron activation analysis (NAA), photon activation analysis (PAA), and ICPMS (notably I and Br). Nakamoto et al. (2007) compared several analytical techniques that were applied to natural samples and concluded that NAA provides measurements that are less influenced by sample preparation than the other method. They cautioned that there is an issue of potentially incomplete extraction for the pyrohydrolysis procedure as indicated by an offset between NAA data with and without the pyrohydrolysis step (Nakamoto et al. 2007). Measurement of F cannot be achieved by NAA, but PAA can be used. However, the same study cautions the large uncertainty contributed by Na. Alternatively, extracted F in solution can be determined by ISE. (ii) Sample volume and heterogeneity: Meteorite samples are notoriously limited in their availability and are known to be heterogeneous. Besides the well-analyzed meteorites that are widely available (e.g., Orguile, Allende), it is impossible to assess the true representation of bulk meteorite compositions. (iii) Alteration: Some meteorite classes are known to have experienced alteration (low temperature metamorphism) (cf., Brearley and Krot 2012; Brearley and Jones 2018). These processes are often identified by variations in the abundances of the mobile (or volatile) elements. For example, changes in In, Cd, and Br are often used as an indicator of alteration. Our data compilation only focuses on the bulk data that are available in the literature. We did not attempt to separate alteration processes.

Given the strong affinity of halogen elements for apatite, the data from the compilation of Wasson and Kallemeyn (1988) is plotted by normalizing to P, because of its refractory character; an Si-normalized plot is also presented (Fig. 2.8). Figure 2.8 shows a clear depletion of the halogen-group elements in non-CI chondrites compared to CI chondrites. However, significant fractionation of F, compared to other halogen elements, is evident among H, L, and EH chondrites. On the other hand, Cl is significantly depleted compared to I, Br, and F in CM chondrites. The cause of this fractionation trend is not clear. Processes associated with variations of halogen abundances in meteorites are discussed in Chap. 15 (Brearley and Jones 2018).

2.5 Moon, Mars, and Vesta

There is significantly less information available for the halogen content of planetary bodies other than Earth. However, there are recent reports on the volatile contents of Moon rocks that can be used to infer the bulk composition of the Moon. While

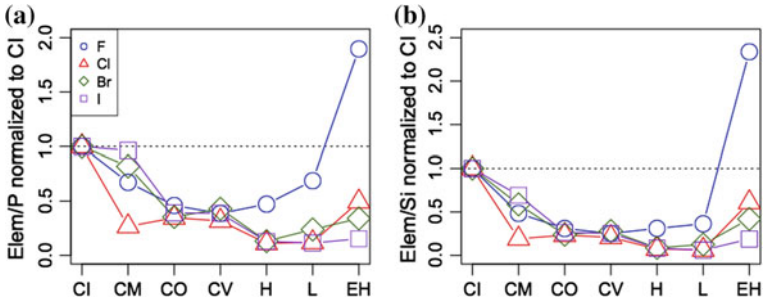

Fig. 2.8 Normalized abundance plot of halogen elements. Each halogen is normalized to the P (**a**) and Si (**b**) concentration in the rock, then the ratios (Elem/P and Elem/Si) are renormalized to CI chondrite. This allows for comparison of halogen depletion with respect to refractory components of meteorites. This plot also illustrates contrasting element behavior of the halogen group. Data are taken from the compilation of Wasson and Kellemeyn (1988)

these studies focused on the abundance of water, F and Cl concentrations were also reported for various magmatic glasses and melt inclusions (Saal et al. 2008; Hauri et al. 2011, 2015; Chen et al. 2015). As for the most recent assessment of F and Cl abundance in the Moon's mantle, Chen et al. (2015) estimate 5.3 ppm F and Hauri et al. (2015) give 0.142 and 0.205 ppm Cl depending on a canonical ratio. This value compares well with the estimates of Swindle et al. (1986): 4.5 to 5.4 ppm F, 0.142 to 0.205 ppm Cl, 0.026 ppm Br, and 0.0003 ppm I. Here, F and Cl contents of the Moon's mantle are based on magmatic glass measurements (e.g., Swindle et al. 1986), whereas Br estimates are based on moderately volatile element ratios determined by Krahenbühl et al. (1973). Iodine is determined by Xe isotope measurement in lunar rocks (Swindle et al. 1986). It should be noted that the volatile content of the bulk lunar mantle is lower than that of the Earth, where the ratios of halogen abundances in the Moon mantle over the Earth mantle are approximately 0.3.

Estimated halogen abundances for Mars have been determined using several key observations, such as orbital gamma-ray radiation measurements, Martian meteorite data, and surface measurements by unmanned probes. These led to bulk Mars estimates of 19.1 ppm F, 0.7 ppm Cl, 3.83 ppb Br, and 0.48 ppb I (Morgan et al. 1979). Dreibus et al. (1990, 1987) provided estimates of 38 ppm Cl, 145 ppb Br, and 32 ppb I for the Martian mantle. From the oxygen isotope data, a Martian bulk composition was modeled by mixing different classes of meteorites, resulting in 41 ppm F; 150 ppm Cl; 0.94 ppm Br; and 120 ppb I (Lodder et al. 1997). Alternatively, a recent report on bulk Mars halogen contents gives new estimates of 21 ppm F, 32 ppm Cl, 0.191 ppm Br, and 0.036 I (Taylor 2013). The eucrite parent body, Vesta, probably contains some volatile elements, because F-rich apatites have been found in this class of meteorites (e.g., Sarafian et al. 2013). The role of halogens in various solar system objects are discussed in Chaps. 15, 16, and 17 (Brearley and Jones 2018; Rampe et al. 2018; Hand 2018).

2.6 Earth's Halogen Distribution

Given the available estimates of average halogen concentrations in different domains of the Earth, it is possible to assess their mass distributions in the Earth. Our estimates are summarized in Table 2.13. We caution that this is an approximation because (1) estimates of average concentrations of each domain can vary by a factor of two, and (2) total terrestrial halogen abundances are not adapted as a constraint. Based on the discussion above, we have selected our preferred values judiciously. However, most of these values are in agreement with previous estimates (e.g., Sharp and Draper 2013).

Concentrations of halogens in the atmosphere, ocean, continental crust, and bulk earth are taken directly from the references cited above (cf., footnotes Table 2.13). For other reservoirs, we have chosen values from a variety of existing estimates. For example, the oceanic crust composition was determined by setting F and Cl concentrations slightly higher than typical MORB compositions using reasoning similar to that used by Straub and Layne (2003). Then, with constant Br/Cl and I/Cl, concentrations of Br and I were determined. Mantle F and Cl abundances were set using averages of various published data, and Br and I were determined using canonical ratios. The core composition was set as zero (or negligible) for F and Cl. Iodine content in the core was based on the model estimate of Armytage et al. (2013), approximately 20 ppb I. For saline formation waters, we adapted the value used in Sharp and Draper (2013). Then, we calculated the total mass of the formation water by assuming the Cl concentration as 10 wt%. The abundances of F, Br, and I in the formation water were derived from Fig. 2.1.

This exercise illustrates some intriguing key issues surrounding the Earth's halogen budget. For example, the core is likely to be a significant reservoir of I (Fig. 2.9), while the continental crust also hosts a quarter of the I budget. Furthermore, despite their small volume, evaporites and saline formation waters contribute significant amounts of Cl, Br, and I. Fluorine shows a strong lithophile character as nearly 100% of this element occurs in silicates. The distributions of Cl and Br in the Earth are similar.

2.7 Future Directions for Halogen Characterization in Earth and Extraterrestrial Materials

Long-standing uncertainties limit our ability to accurately constrain halogen mass balance with respect to numerous key reservoirs. In addition, a general lack of data for specific halogen sources and a lack of understanding of halogen behavior in most geological environments, other than under the surface conditions, persists. For example, in the core, I (and to a lesser extent Br) estimates are lacking, and so continued efforts are needed to determine the halogen abundance in iron meteorites (Goles and Anders 1960, 1961), perform experiments (cf., Armytage et al. 2013), and make thermodynamic predictions (cf., such as ab initio models). These efforts

Table 2.13 Distribution of halogen elements in the Earth

	Mass [Yg]	F [Zg]	Cl [Zg]	Br [Eg]	I [Eg]
Atmosphere[1]	5.2×10^{-3}		7.1×10^{-6}	2.2×10^{-3}	5.3×10^{-4}
Ocean[2]	1.35	1.8×10^{-3}	25	90	7.8×10^{-2}
Crust					
Oceanic crust[a]	4.80	1.2	0.72	2.0	4.3×10^{-2}
Continental crust[3]	21.7	12	5.3	19	15
Evaporite[5]		1.0×10^{-4}	14	51	4.3×10^{-2}
Saline formation water[a]	0.15	7.5×10^{-4}	15	30	1.5
Mantle[a]	4019	80	44	124	2.7
Core[a]	1932	0	0	0^{+}	39
Total sum		94	105	316	58
Bulk Earth estimate[4]	5974	90	102	299	60

Units are following the SI unit convention Y = 10^{24}, Z = 10^{21}, and E = 10^{18}
[a]Explanations about the choices of these values are given in the body text
[+]Br abundance in the core is completely unknown
[1]Simpson et al. (2015) added polar air values
[2]Li (1991)
[3]Rudnick and Gao (2003)
[4]McDonough (2003)
[5]The quantity of Cl is based on the estimates of halide volume (e.g., 9.6×10^{6} km^3 NaCl, Land 1995a modified by Sharp and Draper 2013; F, Br, and I are derived from seawater abundance ratio)

should be aimed at reconciling the uncertainty in the partitioning behavior of I in the core that stems from the different alloy compositions that have been used in models to date. Characterization of halogen abundances in deep crustal formation waters (below 2 km in cratonic crystalline shields), in the lower crust, and in the mantle is nearly totally lacking. Recent studies of fluid inclusions and metasomatized UHP/UHT rocks show evidence of extensive re-equilibration with halide melt-brine-CO_2 mixtures (e.g., Frezzotti and Touret 2014). Thus, although deep crustal fluids are considered to be volumetrically insignificant, non-pervasive, and short-lived (consumed through hydration reactions; Markl and Bucher 1998a, b; Yardley and Graham 2002; Yardley 2009; Yardley and Bodnar 2014) they appear to be powerful metasomatic agents. The importance of halogen-rich volatiles in the mantle and crust as contributors to the Earth's halogen budget is not known. Specifically, there are two issues: (1) their phase relations with silicate melts, and (2) the extent to which interaction with these volatiles has modified the halogen budgets of the crust and shallower fluid reservoirs (e.g., formation waters, metamorphic fluids). Constraints on the estimated amount of seawater-derived halogens that are stored in oceanic crust, and better definition of the marine-solid earth boundary in terms of the halogen

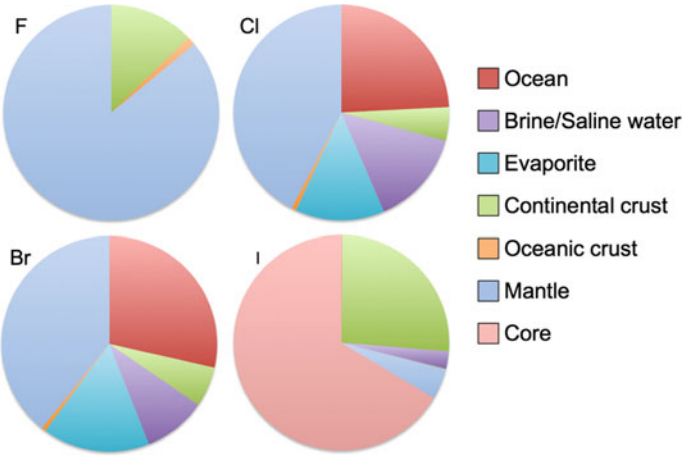

Fig. 2.9 Pie charts of the halogen element budget, which represents a graphic illustration of the data in Table 2.13. Note the different dominant reservoirs for different halogen elements

budget and exchange, are also lacking. For example, what is the net flux of halogens through mid-ocean ridge volcanic systems and what mass of halogens are lost through degassing, versus those gained through hydrothermal exchange with heated seawater? Basic data collection must focus on those halogens and halogen-bearing systems and reservoirs for which data are lacking. For example, continued efforts to analyze Br and I (cf., Bureau and Métrich 2003; Kendrick et al. 2014, 2015) by in situ techniques with application to minerals, melt inclusions, and fluid inclusions would encourage improved constraints on partitioning relationships between coexisting phases, and would confirm the exact proportions of end-member fluids in proposed mixing scenarios. Halogen in situ analyses of magmatic Br and I are also needed because, like Cl and F, their abundances are modified by degassing and post-crystallization changes, rendering bulk rock data useless for determining source compositions by themselves. Alternatively, it should be noted that rapidly quenched magmatic glasses can provide high precision data with minimum influence of degassing. Given the advances in high precision whole rock analysis and microanalysis for F and Cl to sub-ppm levels, re-measurement of these elements in rocks that represent different reservoirs, especially crustal rocks, and in nominally-anhydrous minerals (e.g., in the mantle; Bromiley and Kohn 2007; Beyer et al. 2012; Bernini et al. 2013; Fabbrizio et al. 2013) would provide critical information on halogen exchange among different reservoirs with different sizes from small (mineral) to large (rocks and lithology) scale.

Glossary of acronyms

BSE	Bulk silicate earth
CC	Continental crust
CF	Continuous flow
DM	Depleted mantle
EMPA	Electron microprobe analyzer
ENAA	Epithermal neutron activation analysis
GC	Gas chromatography
IC	Ion chromatography
ICPMS	Inductively coupled mass spectrometry
IMA	International mineralogical association
INAA	Instrumental neutron activation analysis
IRMS	Isotope ratio mass spectrometry
LA-ICP-IDMS	Laser ablation inductively coupled plasma isotope dilution mass spectrometry
LA-ICPMS	Laser ablation inductively coupled mass spectrometry
LCC	Lower continental crust
MORB	Mid-ocean ridge basalt
NAA	Instrumental neutron activation
NG-MS	Noble gas mass spectrometry
PAA	Photon activation analysis
PGA	Prompt gamma-ray analysis
PIXE	Proton induced X-ray emission
RNAA	Radiochemical neutron activation analysis
RPAA	Radiochemical photon activation analysis
SE	Ion-selective electrode
SIMS	Secondary ion mass spectrometry
STP	Standard temperature and pressure
TIMS	Thermal ionization mass spectrometry
TOF	Time-of-flight
TXRF	Total reflection X-ray fluorescence analysis
UCC	Upper continental crust
UHP/UHT	Ultra high pressure/Ultra high temperature
XRF	X-ray fluorescence

Appendix

Schilling et al. (1980)

Sample name	F [ppm]	Cl [ppm]	Br [ppm]	I [ppm]
AII0073-1-005-002	314	112	0.25	
N-1	326	21	0.1	
TRI0089-021-001	560	632	1.39	
TRI0089-030-002-5	388	166	0.31	
TRI0119-004-SG	375	213	0.46	
TRI0119-006-010	270	74	0.16	
TRI0119-007-SG	550	403	0.9	
TRI0122-003-SG	175	70	0.24	
TRI0123-001-005A	210	67	0.16	
TRI0123-004-007	522	64	0.24	
TRI0123-005-003	225	57	0.11	
TRI0138-001-002	394	218	0.5	
TRI0138-002-003	225	61	0.18	
TRI0138-005-SG	245	37	0.09	
TRI0138-006-001	280	24	0.09	
TRI0138-007-001	150	16	0.06	
TRI0138-008-001	180	34	0.06	
TRI0138-009-002	200	15	0.05	
TRI0138-011-001	289	23	0.06	
TRI0154-007-002	215	122	0.29	
TRI0154-008-001	495	387	0.94	
TRI0154-010-003	547	774	1.76	
TRI0154-012-001	339	267	0.64	
TRI0154-013-002	199	106	0.25	
TRI0154-014-004	295	223	0.66	
TRI0154-017-002	260	104	0.28	
TRI0154-018-002	149	53	0.14	
TRI0154-019-002	266	67	0.17	
TRI0154-020-003	335	295	0.79	
TRI0154-021-003	520	384	0.93	
TRI0164-016-003	239	159	0.36	

Jambon et al. (1995); Deruelle et al. (1992)

Sample name	F [ppm]	Cl [ppm]	Br [ppm]	I [ppm]
ALV0981-R026		30	0.082	0.0025
CHR0097-002		413	0.46	0.0065

(continued)

(continued)

Sample name	F [ppm]	Cl [ppm]	Br [ppm]	I [ppm]
CHR0097-005		519	1.32	0.363
CHR0098-010		24	0.159	0.012
CHR0098-011		28	0.09	0.011
CHR0098-012		45	0.064	0.0063
CHR0098-015		43	0.062	0.0084
CHR0098-017		89	0.196	0.0051
CHRCLIP-001-005V		62	0.392	0.0066
CYA1982-009-003		91	0.208	0.0094
CYA1982-018-001		130	0.3	0.0081
CYA1982-027-001		142	0.378	0.0044
CYA1982-031-002		67	0.158	0.013

Kendrick et al. (2013c)

Sample name	F [ppm]	Cl [ppm]	Br [ppb]	I [ppb]
Alv-529-4		111	300	4.5
Alv-523-1		135	350	7.2
Alv-526-5		167	446	8.2
Alv-525-5-2		81	215	3.2
Alv-527-1-1		39	95	1.6
CH98-DR08g3		630	1900	20
CH98-DR11		32	97	2
2pD43-1		282	730	14
2pD43-2		285	740	15
2pD43-3		265	689	12
2pD43-4		290	757	15
Alv-2262-8		86	256	2.5
Alv-2269-2		154	488	2.9
Alv-1652-3		3790	13600	27
Alv-1652-10		340	1230	2.4
Alv-1652-5		3870	13900	28
CL-DR01		92	309	3.7

Kendrick et al. (2011)

Sample name	F [ppm]	Cl [ppm]	Br [ppb]	I [ppb]
47979-a		114	400	12
47979-b		121	382	17
47979-c		146	499	86
47979-dd		131	436	14

(continued)

(continued)

Sample name	F [ppm]	Cl [ppm]	Br [ppb]	I [ppb]
GG256-a		681	2142	50
GG256-be		658	2101	52
60701		435	1375	33
G882b		955	3124	76
GG53a-a		512	1645	39
GG53a-b		440	1512	36
47963		1356	4565	109
G465		225	764	22
G452a		71	262	10
G929a-a		498	1671	44
G929a-be		537	1703	44
G499a		392	1313	98
G860a		517	1825	33
25603		799	2640	60
MQ650		375	1277	31
40428		494	1580	36
25601		845	2853	65
38287		504	1632	37
LB197a		842	2970	56

Kendrick et al. (2013b)

Dredge name	F [ppm]	Cl [ppm]	Br [ppb]	I [ppb]
490_610		860	3000	53
760_770		630	2100	33
1290_1420		500	1700	38
1970_2080		420	1300	27
1610_1860		280	870	22
1610_1860		860	2500	58
1610_1860		270	840	21
2800_2850		670	2100	51
410		660	2100	37
2500_2820		550	1900	53
2500_2700a		610	1900	28
2500_2700		1000	2800	46
2500_3000a		1340	3600	70
2500_3000a		1450	3700	71
2500_3000a		1380	3500	67
2100_2600		960	3700	42
2360_2800		590	1700	38

(continued)

(continued)

Dredge name	F [ppm]	Cl [ppm]	Br [ppb]	I [ppb]
3000_3500		1030	2900	77
2200_2660		1180	3500	49
2100_2600		1210	3600	59

Kendrick et al. (2015)

Sample name	F [ppm]	Cl [ppm]	Br [ppb]	I [ppb]
68-03	930	1565	6288	59
70-01	840	1006	3832	47
71-02	900	1793	7229	82
71-11	920	1605	5478	56
71-13	880	1524	6512	74
71-22	1030	1529	6580	71
73-03	1000	1595	6603	75
73-12	980	1360	5415	59
74-02	1870	869	2478	41
75-02	1370	717	2116	46
75-10	1230	653	1893	40
76-03	1180	1611	5625	72
76-08-a	1240	1372	4892	69
76-11	1230	1616	6218	67
77-09	1600	1071	3554	70
78-01-a	1250	955	3470	83
104-04	1030	1088	3809	18.7
128-21	1270	1046	3001	93

Jagoutz et al. (1979)

Sample name	F [ppm]	Cl [ppm]	Br [ppm]
Ka168	7.7	1.93	0.022
D1	12.6	2	0.013
Fr1	10.6	1.3	0.012
SC1	16.3	0.95	0.008
KH1	8.8	0.39	0.0051
Po1	6.8	1.4	0.007

Cabral et al. (2014)

Sample Name	F [ppm]	Cl [ppm]
MGA-B-25-1	1469	718
MGA-B-25-2	1406	948
MGA-B-25-4	1518	983
MGA-B-47-AES6	1583	890
MGA-B-47-AES7	1509	277
MGA-B-47-AES8	1498	666
MGA-B-47-RAC2	1188	512
MGA-B-47-RAC3	1370	714
MGA-B-47-RAC4	1357	626
MGA-B-47-RAC7	1305	502
MGA-B-47-RAC10	1426	467
MGA-B-47-RAC11	1328	552
MGA-B-47-RAC16	1356	806
MG1001-1	1416	723
MG1001-2Bc	1478	753
MG1001-3b	1742	761
MG1001-5	1352	249
MG1001-6c	1476	641
MG1001-7c	1402	698
MG1001-9	1515	620
MG1001-10	1509	779
MG1001-14c	1390	528
MG1001-17c	1406	523
MG1001A1	1300	700
MG1001A3A	1359	583
MG1001A3B	1260	505
MG1001A5	1463	598
MG1001A6	1420	585
MG1001A9	1123	505
MG1001A10	1468	685
MG1001A11	1588	589
MG1001A12	1438	377
MG1001A14	1073	526
MG1001A15	1480	689
MG1001A16	1481	768
MG1001A17	1503	713
MG1001A18A	1573	733
MG1001A19A	1578	513
MG1001A20A	1549	778

(continued)

(continued)

Sample Name	F [ppm]	Cl [ppm]
MG1001A20B	1449	514
MG1006-7c	1950	732

Metrich et al. (2014)

Sample name	F [ppm]	Cl [ppm]
D-C	899.667	655.667
D-E	955.667	602
D-F	940.667	698.667
D-G	992	778.333
D-H	1018.667	772
E-9	1027.333	611.333
E-52	861	488
E-23	842.333	677.333
E-51	1116	772.667
C-1a	742	382.333
C-1b	837.333	375
C-28a	754	608.667
C-32a	901.667	678
C-32b	908.333	596.667
C-38	863.333	354.333
C-40	1179.667	523
C-47	779.333	330.667
C-49 emb	1000.667	613.333
C-20	1250.333	788.667
C-26	872	679.333
C-29a	1324.667	748.667
C-29b emb	1442.333	900
C-41 emb	1002	465.333
C-39	1099.333	775.667

Workman et al. (2004, 2006)

Sample name	F [ppm]	Cl [ppm]
68-34	935	1296
71-03	860	1598
71-03	879	1256
71-06	874	719
72-12	1107	541
72-12	1022	517

(continued)

(continued)

Sample name	F [ppm]	Cl [ppm]
76-07	1129	1403
76-08	1233	1411
76-10	1182	1279
76-13	1150	1295
76-14	1170	1470
77-06	1239	1051
Glass	903	1490
Glass	980	1752
Glass	937	1651
Glass	865	1558
Glass	972	1718
Glass	1064	1478
Glass	947	1656
Glass	966	1744
Glass	1026	1610
Glass	915	1522
Glass	878	1366
Glass	967	1267
Glass	949	1708
Glass	918	1545
Glass	944	1775
Glass	957	1715
Glass	1110	1670
Glass	960	1726
Glass	983	1818
Glass	962	1711
Glass	973	1754
Glass	990	1400
Glass	1056	1377
Glass	1077	1570
Glass	1188	670
Glass	1060	623
Glass	1148	598
Glass	867	547
Glass	1050	596
Glass	1109	628
Glass	921	567
Glass	801	651
Glass	1872	982
Glass	802	451

(continued)

(continued)

Sample name	F [ppm]	Cl [ppm]
Glass	1871	975
Glass	1866	990
Glass	1856	928
Glass	818	469
Glass	1854	971
Glass	1887	1023
Glass	1339	689
Glass	1371	734
Glass	1235	657
Glass	1338	692
Glass	1262	674
Glass	1291	551
Glass	1240	534
Glass	1234	526
Glass	1245	531
Glass	1448	629
Glass	1299	536
Glass	1216	519
Glass	1311	574
Glass	1219	520
Glass	1294	541
Glass	1175	514
Glass	1222	1283
Glass	1220	1361
Glass	1180	1074
Glass	1237	1348
Glass	1182	925
Glass	1236	1195
Glass	1300	1725
Glass	1236	1403
Glass	1409	1541
Glass	1228	1615
Glass	1245	1396
Glass	1221	1436
Glass	1211	1562
Glass	1173	1055
Glass	1254	1004
Glass	1226	968
Glass	1310	1021
Glass	1206	886

Koleszar et al. (2009)

Sample name	F [ppm]	Cl [ppm]
D25C-2-02	301	74
D25C-2-06	304	135
D25C-2-09	387	115
D25C-2-12	462	47
D25C-2-16A	419	142
D25C-2-19A	387	154
D25C-2-19B	372	109
D25C-2-21A	389	96
D25C-2-21B	380	111
D25C-2-21C	420	129
D25C-2-24D	330	13
D25C-2-25A	340	119
D25C-2-26	332	113
D25C-2-27	437	155
D25C-2-29D	515	15
D25C-2-30v	377	113
D25C-2-34	412	117
D25C-2-35D	409	46
D25C-2-37	406	105
D25C-2-38B	408	102
D25C-2-38C	379	91
D25C-2-39AD	243	6
D25C-2-39B	263	105
D25C-2-40A	457	90
D25C-2-40B	398	76
D25C-2-44vD	520	20
D25C-2-46vD	522	4
D25C-2-48	395	125
D25C-2-51v	397	159
D25C-2-52A	376	110
D25C-2-52BD	351	22
D25C-2-53A	288	99
D25C-2-53B	267	100
D25C-2-54	389	148
D25C-2-55	297	106
D25C-2-56v	317	74
D25C-2-57D	283	1
D25C-2-58	378	134
D25C-2-59	424	138

(continued)

(continued)

Sample name	F [ppm]	Cl [ppm]
D25C-2-62v	440	138
D25C-3-02	419	131
D25C-3-07v	394	138
D25C-3-08	399	136
D25C-3-10	404	92
D25C-3-12	350	129
D25C-3-14v	508	156
D25C-3-18	307	86
D25C-3-20	452	98
D25C-3-21D	364	31
D25C-3-23D	432	26
D25C-3-28	390	131
D25C-3-29	452	147
D25C-3-30v	315	112
D25C-3-31	414	123
D25C-3-33	442	144
D25C-3-34vD	337	62
D25C-3-35	292	140
D25C-3-37v	421	127
D25C-3-38v	477	170
D25C-3-41A	387	108
D25C-3-41B	398	119
D25C-3-42	372	138
D25C-3-43	293	118
D25C-3-44	394	185
D25C-3-46	469	152
D25C-3-47D	355	5
D25C-3-48	462	145
D25C-3-49	324	80
D25C-3-50	465	137
D25C-3-52	318	106
D25C-3-55D	428	84
D25C-3-56	343	104
D25C-3-58	347	113
D25C-3-62	299	116
STG06-29-02B	140	21
STG06-29-03	140	25
STG06-29-04	135	14
STG06-29-06	176	35
STG06-29-07	136	25

(continued)

(continued)

Sample name	F [ppm]	Cl [ppm]
STG06-29-08	129	18
STG06-29-09v	115	19
STG06-29-10E	337	133
STG06-29-11Av	149	30
STG06-29-12	137	29
STG06-29-13	150	26
STG06-29-14v	145	16
STG06-29-15	141	26
STG06-29-16A	157	27
STG06-29-16B	155	26
STG06-29-16C	133	22
STG06-29-16D	135	23
STG06-29-17	141	22
STG06-29-19D	94	7
STG06-29-20	138	24
STG06-29-21	148	28
STG06-29-23A	113	19
STG06-29-23B	101	16
STG06-29-24	138	26
STG06-29-25A	165	28
STG06-29-27	163	26
STG06-29-29	155	27
STG06-29-32	146	23
STG06-29-34A	128	23
STG06-29-34B	134	27
STG06-29-35A	173	13
STG06-29-35B	184	15
STG06-29-37A	120	21
STG06-29-39	141	27
STG06-29-40	145	26
STG06-29-42A	88	15
STG06-29-42B	130	24
STG06-29-43	131	22
STG06-29-44	151	25
STG06-29-47	138	24

Lassiter et al. (2002)

Sample name	F [ppm]	Cl [ppm]
RVV310m5	1680	122
RVV310m15	1849	200
RVV310m21	1347	204
AVE RVV310	1576	241
RVV370m13	1369	222
RVV370m20	1386	305
RVV370m34	1735	311
AVE RVV370	1514	314
RPA502m8b	1472	467
RPA502m26	1605	606
RPA502m37	1468	478
AVE RPA502	1478	413
RVV318m20	2751	645
RVV318m25	2438	900
RVV318m28	3525	1296
AVE RVV318	2706	723
RVV318m22	3107	21689
RVV318m45	2956	17912
RVV318m47	2925	21497
RVV318m48	3338	19943
RVV318m49	3109	16520

Hauri et al. (2002)

Sample name	F [ppm]	Cl [ppm]
KK31-12	446	162
KK31-12	675	358
KK31-12	683	392
KK31-12	629	375
KK31-12	494	435
KK31-12	535	300
KK31-12	704	201
KK31-12	659	209
KK31-12	567	13940
KK31-12	559	315
MK91-6	316	66
MK91-6	453	67
MK91-6	498	93
MK91-6	469	112

(continued)

(continued)

Sample name	F [ppm]	Cl [ppm]
MK91-6	457	95
MK91-6	487	87
MK91-6	466	84
MK91-6	468	96
MK91-6	476	93
MK91-6	488	122
MK91-6	444	164
MK91-6	494	83
MK91-6	446	114
MK91-6	515	108
MK91-6	483	105
MK91-6	522	129
MK91-6	503	117
MK91-6	345	89
MK91-6	512	94
MK91-6	559	84
MK91-6	567	76
MK91-6	549	85
MK91-6	490	57
MK91-6	471	84
MK91-6	444	95
MK91-6	439	90
MK91-6	449	142
MK91-6	535	224
MK91-6	553	344
MK91-6	490	91
KS87-24	446	99
KS87-24	460	68
KS87-24	377	64
KS87-24	420	76
KS87-24	371	78
KS87-24	397	72
KS87-24	388	70
KS87-24	481	67
KS87-24	356	66
KS87-24	365	64
KS87-24	361	74
KS87-24	417	75
KS87-24	413	72
KS87-24	465	85

(continued)

(continued)

Sample name	F [ppm]	Cl [ppm]
KS87-24	360	74
KS87-24	442	73
KS87-24	395	74
KS87-24	448	73
KS87-24	1002	73
KS87-24	975	76
KS87-24	429	67
KS87-24	434	68
KS87-24	446	85
KS87-24	384	68
KS87-24	460	64
KS87-24	435	61
KS87-24	433	73
KOO-17A	669	22
KOO-17A	476	160
KOO-17A	380	229
KOO-17A	344	142
KOO-17A	843	20
KOO-17A	670	25
KOO-17A	662	17
KOO-17A	510	93
KOO-17A	308	577
KOO-17A	665	32
KOO-17A	722	28
KOO-17A	680	13
KOO-17A	620	16
KOO-17A	478	30
KOO-17A	516	38
KOO-17A	384	20
KOO-17A	548	15
KOO-49	461	27
KOO-49	460	25
KOO-49	451	35
KOO-49	437	33
KOO-49	540	51
KOO-49	515	34
KOO-49	676	29
KOO-49	611	54
KOO-49	453	16
KOO-49	575	28

(continued)

(continued)

Sample name	F [ppm]	Cl [ppm]
KOO-49	657	27
KOO-49	469	24
KOO-49	514	37
KOO-49	457	38
KOO-49	552	28
KOO-49	629	9
KOO-49	766	15
KOO-49	686	8
KOO-49	609	25
KOO-49	492	23
KOO-49	646	43
KOO-49	400	38

Johnson et al. (2002)

Sample name	F [ppm]	Cl [ppm]
PRD1-3	448	714
PRD1-4	481	627
PRD1-5	414	619
PRD3-1	472	197
PRD4-3	532	325
PRD4-6	614	240
PRD5-1	547	660
PRD5-2	443	748
PRD6-1	534	241
PRD6-2	316	452
PRD7-1	520	233
PRD7-2	503	279
PRD8-1	458	185
PRD9-3	462	187
PRD10-1	366	187
PRD12-1	474	175
PRD13-1	394	155
PRD14-1	457	201.5
PRD14-2	498	211
PRD14-3	463	185
PRD15-1	495	201
PRD17-1	451	263
PRD17-2	572	243
PRD17-4	520	217

(continued)

(continued)

Sample name	F [ppm]	Cl [ppm]
PRD19-2	428	181
PRD20-1	554	179
PRD21-1	441	186
PRD22-3	343	131
PRC1GL1	359	134
PRC1LIMU	326.5	142.5
PRC1DKPUM	676	309
PRC1LTSPIND	670	209
PRC1DKSPIND	302	135.5
PRC1LTPUM	597	176
PRC8SPIND	591	195
PRC8PUM	643.5	188
PRC11	716	297
PRC12	704	301
PRC16PUM	599	220
PRC16SPIND	494.5	169.5
PRC17SPIND	522	178
PRC18	538	222
PRC18LIMU	614	264
PRC18PUM	646	215
PRC18SPIND	598	243
PRC18TEAR	444	132
PRC23SPAT	451	310
PRC23PUM1	261	113
PRC23PUM2	282	104
PRC24GL1	612	251.5
PRC24GL2	473	177
PRC24LIMU	606	268
PRC24SPAT	571	378
PRC26	451	243
PRC27	601	249
PRC28	685	274
PRC28SPIND	699	256
PRC29SPIND	472	252
PRC30	470	203
PRC30LIMU	494	159
PRC30SPIND	429.5	278
PRC31GL1	515	263
PRC32SPAT	443	234
PRC34GL1	407	200

(continued)

(continued)

Sample name	F [ppm]	Cl [ppm]
PRC34GL2	555	238
PRC35	479	208
PRC35SPAT	444	242
PRC35FROTH	397	422
PRC36	473	211
PRC39	466	191
PRC41	476	189
PRC45GL	495	189
PRC45SPIND	405	276
PRC46GL	498	177
PRC46TEAR	649	232
PRC47GL1	515.5	231
PRC47GL2	591	215
PRC47DPUM	805	247
PRC47SPIND	632	192
PRC47LIMU	354	225
PRC47TEAR1	456	305
PRC47TEAR2	601	194
PRC48GL	594	199
PRC48SPIND	548	199
PRC49GL1	505	155
PRC49GL2	472	178
PRC51SPIND	664	204
PRC53SPIND	617	195
PRC53TEAR	346	137
PRC54LIMU	545	186
PRC55GL1	706	262
PRC55GL2	674.5	282.5
PRC55TEAR	451	138
PRC56GL1	710	239
PRC56TEAR	552	206
S492-R1	458	187
S492-R6	481	209
S495-R1	800	322

São Miguel (Rose-Koga et al. 2017)

Sample name	F [ppm]	Cl [ppm]
ACO95-03a	1017	551
ACO95-03a-2	1000	625

(continued)

(continued)

Sample name	F [ppm]	Cl [ppm]
ACO95-03b	893	585
ACO95-03b-2	893	585
ACO95-56a	637	592
ACO95-56c	785	909
ACO95-56e	773	601
ACO95-56e-2	773	601
ACO95-56f	1399	860
ACO95-56f-2	1046	920
ACO95-56g	1185	732
ACO95-56g-2	1185	732
ACO95-62b	782	582
ACO95-62c	808	940
ACO95-62d	918	863
ACO95-62d-2	918	863
ACO95-62i	997	335
ACO95-62i-2	1016	388
ACO95-62h	860	481
ACO95-68a	1023	618
ACO95-68b	896	479
a4-2-00	1199	574
a4-2-00-2	1199	574
a4-4-00	1252	966
a4-5-00	1261	682
a4-6-00	1088	205
a9-1-00	990	540
a9-2-00	1073	539
a9-4-00	1198	493

Laubier (2006)

Sample name	F [ppm]	Cl [ppm]
CAI5-A6	341	219
CAI5-A'6	369	235
NEI1-2-A1	463	273
NEI1-2-F1	507	339
NEI1-2-B5	518	271
MAU2-F3	595	269
MAU3-E1	595	303
MAU3-D7	568	335
MAU4-F3	500	260

(continued)

(continued)

Sample name	F [ppm]	Cl [ppm]
MAU4-A6	529	323
MAU4-F8	330	200

Shaw et al. (2010)

Sample name	F [ppm]	Cl [ppm]
12-1_1	157	27
12-1_2	155	27
12-1_4	140	24
12-1_5	141	24
12-1_6	159	28
12-1_7a	171	22
12-1_7b	158	26
12-1_7b	153	25
12-1_8	158	27
12-1_9	149	26
12-1_10	156	24
12-1_12	152	27
12-1_14	156	27
13-1_3	157	30
13-1_5	168	198
13-1_6	150	21
13-1_8	160	26
13-1_9	156	28
13-1_10	153	27
13-1_15	159	24
13-1_16a	157	24
13-1_16a	157	24
13-1_16b	158	28
13-1_17	157	22
13-1_18	157	30
13-1_19	162	27
13-1_21	160	25
13-1_22	158	27

Wanless and Shaw (2012)

Sample name	F [ppm]	Cl [ppm]
4203-6-1-21	118	51
4203-6-1-22	112	49

(continued)

(continued)

Sample name	F [ppm]	Cl [ppm]
4203-6-2-24	109	51
4203-6-3-25	101	48
4203-6-6-30	96	46
4203-6-10-32	99	49
4203-6-11-35	102	48
4203-6-12-36	97	47
4203-6-13a-38	101	48
4203-6-13b-39	93	46
4203-6-14-41	94	48
4203-6-15-42	151	67
4203-6-16a-43	94	46
4203-6-16b-44	97	48
4203-6-16c-45	89	46
4203-6-17a-47	122	47
4203-6-17b-50	107	44
4203-6-20a-51	96	48
4203-6-20b-52	136	54
4203-6-21-54	123	54
4203-6-24a-55	97	45
4203-6-25a-56	98	49
4203-6-25b-59	136	46
4204-6-33-61	175	49
4204-6-34-62	101	37
4204-6-35-63	158	49
4204-6-37b-65	125	45
4204-6-39-66	148	66
4204-6-43a-67	111	55
4204-6-43b-68	123	61
4204-6-44-72	124	54
4204-6-45-73	106	45
4204-6-46a-74	168	60
4204-9-49-79	145	43
4204-9-50-80	100	50
4204-9-55-83	97	35
4204-9-56-87	112	51
4204-9-57a-88	96	50
4204-9-57b-89	100	47
4204-9-58-90	102	49
4204-9-60-91	105	48
4204-9-61-93	101	46

(continued)

(continued)

Sample name	F [ppm]	Cl [ppm]
4204-9-62-94	105	49
4204-9-65-95	103	48
4204-9-66-98	102	50
4204-9-73-99	100	51
4204-9-74-100	108	48
4204-9-75b-102	102	52
4204-9-75a-101	108	50
4204-9-81-104a	97	47
4204-9-81-104b	108	53
4204-9-81-104c	108	52
4203-2-2a-122	77	44
4203-2-2b-123	79	43
4203-2-3-124	96	42
4203-2-4-125	89	45
4203-2-5-126	97	48
4203-2-6-127	87	43
4203-2-8-128	81	45
4203-2-10a-129	90	45
4203-2-13a-130	85	42
4203-2-13b-131	88	43
4203-2-16a-133	16	10
4203-2-17-134	85	45
4203-2-18-135	18	11
4203-2-21a-136	77	40
4203-2-29a-138	103	49
4203-2-30-139	91	46
4203-2-33a-140	85	44
4203-2-33b-141	78	45
4203-2-39-142	92	44
4203-2-44-143	86	43
2737-3x_97	106	48
2737-3x_99	120	47
2737-3x_100	134	21
2737-3x_101	127	40
2737-3x_103	109	48
2737-3x_104	131	29
2737-3x_109	119	25
2737-3x_112	130	32
2737-3x_113	125	31
2737-3x_117	116	35

(continued)

(continued)

Sample name	F [ppm]	Cl [ppm]
2737-3x_125	126	35
2737-3x_123	115	24
2737-3x_128	111	25
2737-3x_129	133	35
2737-3x_131	128	34
2737-3x_132	118	39
2737-3x_122	101	25
2737-3x_120	109	34
1248N_1	189	49
1248N_2	176	39
1248N_3r	342	65
1248N_5	171	41
1248N_7	180	43
1248N_9	197	58
1248N_10	170	38
1248N_11	177	48
1248N_12	183	41
1248N_14	173	38
1248N_15	179	44
1248N_17	185	9
1248N_19	175	37
1248N_24	184	37
1248N_25	178	43
1248N_26	149	69
1248N_29	179	46
1248N_30a	173	42
1248N_30b	177	40
1248N_36	187	34
1248N_37	195	30
1248N_39	202	51
1248N_40	181	40
1248N_41	189	42
1248N_43a	177	47
1248N_43b	178	39
1248N_44	175	45
1248N_45	179	44
sample	F	Cl
DR12A_3_1	127	75
DR12A_3_2	114	53
DR12A_3_5	129	48

(continued)

(continued)

Sample name	F [ppm]	Cl [ppm]
DR12A_3_6	125	135
DR12A_3_7	131	74
DR12A_3_10	127	52
DR12A_3_12	121	24
DR12A_3_15	123	94
DR12A_3_20	123	62
DR12A_1_21	123	17
DR12A_1_22	115	58
DR12A_1_23	109	103
DR12A_1_30	119	86
DR12A_1_35	114	95
DR12A_1_36	115	103
DR12A_1_38	62	24
DR12A_1_34	113	15
DR12A_2_39	94	28
DR12A_2_49a	118	59
DR12A_2_49b	122	63
DR12A_2_50	111	51
DR12A_7_54	126	37
DR12A_7_57	127	58
DR12A_7_58	124	38
DR12A_2_60	126	60
DR12A_7_62a	103	32
DR12A_7_62b	103	28
DR12A_7_65	122	62
DR12A_7_66	120	64
DR12A_7_72	112	56
DR12A_7_76b	120	67
DR12A_7_76a	125	73
DR12A_7_81	116	163
DR12A_7_83	130	4
DR12A_7_84a	122	66
DR12A_7_84b	118	64
DR12A_7_90	117	56
ATV181_2	186	133
ATV181_10	174	81
ATV181_11	186	95
ATV181_13	185	113
ATV181_14a	204	128
ATV181_14b	201	135

(continued)

(continued)

Sample name	F [ppm]	Cl [ppm]
ATV181_16	192	103
ATV181_19	192	103

Glass data from PETDB

Sample name	F [ppm]	Cl [ppm]
AII0073-1-005-002	314	112
AII0073-1-005-002	314	112
AII0073-1-005-002	314	112
AII0107-6-056-027	110	14
AII0107-6-057-008	370	170
AII0107-6-057-019	240	40
AII0125-11-010	212	901
AII0125-11-011	160	315
AII0125-11-012-A	133	217
AII0125-11-012-B	129	998
AII0125-11-013	312	823
AII0125-11-017	146	756
AII0125-11-018	157	896
AII1991-020-001	83.6	3.4
AII1991-020-005	82.4	17.5
ALV0906-R001	30	20
ALV0906-R003	50	10
ALV0907-R001	60	130
ALV0907-R003	80	10
ALV0910-R003	40	70
ALV0910-R004	30	60
ALV0911-R005	80	140
ALV0912-R006	60	30
ALV0916-R008	120	140
ALV0918-R001	50	10
ALV0994-005B	100	400
ALV1002-004B	200	3400
ALV1181-005	140	790
ALV1181-006	70	610
ALV2077-003	138	154
ALV2078-004	124	254
ALV2079-006b	141	151
ALV2080-001a	140	213
ALV2092-002	137	151

(continued)

(continued)

Sample name	F [ppm]	Cl [ppm]
ALV2261-003	112	1014
ALV2262-004	134	1571
ALV2262-007	132	911
ALV2262-009	141	616
ALV2263-001	151	529
ALV2263-006B	202	795
ALV2263-007	198	2046
ALV2263-008	204	911
ALV2264-001a	155	321
ALV2264-002	135	1529
ALV2266-001	130	1407
ALV2266-002	133	1513
ALV2268-002	198	1690
ALV2268-003	191	2580
ALV2268-004	194	1358
ALV2269-001	139	2283
ALV2269-002	155	2987
ALV2269-003	132	219
ALV2355-008	206	54
ALV2356-007	213	53
ALV2358-003	239	59
ALV2365-003	241	82
ALV2384-001	84.7	20.9
ALV2384-002	89.1	16.9
ALV2384-003	104.3	18.3
ALV2384-006	94	2.92
ALV2384-009	96.4	19.4
ALV2390-005	630	241
ALV2430-001	163	969
ALV2430-002	198	292
ALV2432-001	165	433
ALV2432-002	180	560
ALV2489-002	422	799
ALV2489-005	434	425
ALV2489-009	355	522
ALV2490-003	189	42
ALV2490-010	193	44
ALV2497-001B	201	42
ALV2697-001	197	30
ALV2759-005	268	62

(continued)

(continued)

Sample name	F [ppm]	Cl [ppm]
ALV2768-004	321	702
ALV2768-006	222	119
CHN0115-4-003	150	42
CHN0115-4-008	430	170
END0112-002-001	120	46
END0112-004-001	250	400
END0112-005-005	150	40
END0112-005-010	180	50
END0112-005-011	210	50
END0112-006-001	150	60
END0112-007-002	40	24
END0112-007-004	310	650
END0112-007-013	390	1090
END0113-003-001	320	190
ENV7115-077-006	250	220
ENV7714-033-A	260	150
ENV7714-036-002	90	460
ENV7906-032-001	250	130
ENV7906-032-039	380	280
ENVCSM5-003-002	470	330
ENVCSM5-005-001	212	420
ENVCSM5-008-001	360	370
ENVCSM5-010-001	310	230
GIL7202-076-004	140	140
GIL7202-081-005	250	530
GIL7202-082-002	220	720
GIL7202-084-002	190	280
GIL7202-087-001	280	620
GIL7202-087-012	140	210
GIL7202-089-008	350	570
GIL7202-090-002	200	180
GIL7202-090-004	260	170
GIL7202-094-004	180	220
GIL7202-094-006	100	30
KAK1979-012-040	100	300
KAK1979-012-057	200	900
KAK1979-018-021	100	600
MELVULC-5-024-017	370	120
MELVULC-5-027-019	190	54
MELVULC-5-027-034	480	200

(continued)

(continued)

Sample name	F [ppm]	Cl [ppm]
MELVULC-5-030-060	350	120
MELVULC-5-042-010	370	440
N-1	326	21
NHOCHEP-003-003	218	131
NHOCHEP-006-001	338	163
NHOCHEP-015-006	235	42
NHOCHEP-024-007	287	45
NHOCHEP-031-004	312	222
NHOCHEP-116-002	428	214
NHOCHEP-116-003	140	71
NHOCHEP-121-002	277	369
PS4CSM4-1501-001	460	670
PS4CSM4-1502-009	580	800
PS4CSM4-1506-002	230	120
TRI0041-018-002	93	62
TRI0041-022-001	142	64
TRI0101-003-006	80	60
TRI0101-011-002	458	173
TRI0101-027-001	172	140
TRI0101-030-012G	232	65
TRI0101-035-003G	236	185
TRI0139-016-001	100	210
TRI0139-030-002	590	600
TRI0139-031-002	200	110
TRI0139-032-002	230	140
TRI0139-033-001	250	140
WASVNTR-006	292	99
WASVNTR-007-A	272	82
WASVNTR-010	119	44
WASVNTR-024-A	280	122
WASVNTR-026	260	355
WASVNTR-027-C	191	39
WASVNTR-029-B	237	229
WASVNTR-029-C	101	13.5

Saal et al. (2002)

Sample name	F [ppm]	Cl [ppm]
Siq1-1	98	1.5
Siq1-2	90	2.0

(continued)

(continued)

Sample name	F [ppm]	Cl [ppm]
Siq1-3	85	1.7
Siq1-4	80	2.3
Siq1-5	84	1.5
Siq1-6	84	1.6
Siq1-7	80	2.3
Siq1-8	85	1.1
Siq1-9-1	86	1.7
Siq1-9-2*	97	1.7
Siq2-1	107	2.0
Siq2-2	83	2.6
Siq2-3-1	90	1.2
Siq2-3-2	84	1.4
Siq2-4	81	2.6
Siq2-5	91	3.2
Siq3-9	135	1.7
Siq3-10-1	95	1.6
Siq3-11	96	1.8
Siq6-1	79	2.4
Siq6-2-1	92	2.2
Siq6-2-2	105	1.8
Siq6-3	87	1.9
Siq6-4	85	4.0
Siq6-4A	81	4.1
Siq6-5	85	1.5
Siq6-6-1	87	1.5
Siq6-6-2	89	1.3
Siq6-7-1	93	1.5
Siq6-7-2	92	1.5
Siq6-7-3	87	1.7
Siq9-1-2-3	77	1.0
Siq9-1-3	78	1.6
Siq9-1-4	79	1.3
Siq9-1-5	79	1.1
Siq9-1-6	77	1.3
A-1	81	1.5
A-2	88	1.1
A-3	81	1.9
A-4	79	1.9
A-5	84	1.6
A-7	82	2.0

(continued)

(continued)

Sample name	F [ppm]	Cl [ppm]
A-8-1	74	2.3
A-8-2*	71	2.1
A-10	50	1.7
A-11	74	1.9
D-6-1	83	1.5
D-6-2*	85	1.3
D-6-3*	81	1.3
D-7	86	2.3
D-8	80	2.6
D-9	80	2.0
D-10-1	82	1.9
Siq2-6	90	2.5
Siq2-7-1	90	1.7
Siq2-7-2	91	1.6
Siq2-7-3	88	1.5
Siq2-8-1.	90	1.6
Siq2-8-2.	97	1.5
Siq2-9.	92	2.0
Siq2-10.	83	1.9
Siq3-1.	125	2.4
Siq3-2.	89	1.8
Siq3-3.	89	2.0
Siq3-4.	90	2.1
Siq3-5	88	1.2
Siq3-6	97	2.4
Siq3-7	107	3.3
Siq3-8	102	1.6
Siq6-8	82	1.9
Siq6-9	88	2.8
Siq9-1	77	1.9
Siq9-2	89	1.0
Siq9-3-1	91	13.7
Siq9-3-2	86	1.2
Siq9-4	79	2.4
Siq9-5	81	2.3
Siq9-6-1	87	1.4
Siq9-6-2	88	1.4
Siq9-7	83	2.3
Siq9-8-1	85	1.1
Siq9-8-2	83	1.1

(continued)

(continued)

Sample name	F [ppm]	Cl [ppm]
Siq9-1-1	94	6.8
Siq9-1-2-1	80	1.1
Siq9-1-2-2	78	1.0
A-12-2	85	1.3
A-14-1	65	1.1
A-15	89	2.5
A-16-1	73	3.0
A-16-2*	72	0.8
A-17	77	1.9
D-1-1	93	2.1
D-1-2	84	1.7
D-2	87	2.2
D-3-2	70	2.4
D-4	71	0.8
D-5	79	2.0
D-11	86	2.0
D-12-1	85	1.4
D-12-2	80	1.1
2384-1	85	20.9
2384-2	89	16.9
2384-3	104	18.3
2384-6	81	2.9
2384-9	96	19.4
A25-D20-5	82	17.5
A25-D20-1	84	3.4

References

Adam J, Turner M, Hauri EH, Turner S (2016) Crystal/melt partitioning of water and other volatiles during the near-solidus melting of mantle peridotite: Comparisons with non-volatile incompatible elements and implications for the generation of intraplate magmatism. Am Mineral 101(4):876–888

Agranier A, Blichert-Toft J, Graham D, Debaille V, Schiano P, Albarède F (2005) The spectra of isotopic heterogeneities along the Mid-Atlantic Ridge. Earth Planet Sci Lett 238:96–109

Aiuppa A, Baker DR, Webster JD (2009) Halogens in volcanic systems. Chem Geol 263(1):1–8

Allègre CJ, Poirier JP, Humler E (1995) The chemical composition of the Earth. Earth Planet Sci Lett 134:515–526

Alletti M, Baker DR, Freda C (2007) Halogen diffusion in a basaltic melt. Geochim Cosmochim Acta 71:3570–3580

Álvarez F, Reich M, Pérez-Fodich A, Snyder G, Muramatsu Y, Vargas G, Fehn U (2015) Sources, sinks and long-term cycling of iodine in the hyperarid Atacama continental margin. Geochim Cosmochim Acta 161:50–70

Anders E, Ebihara M (1982) Solar-system abundances of the elements. Geochim Cosmochim Acta 46:2363–2380

Anders E, Grevesse N (1989) Abundances of the elements: meteoritic and solar. Geochim Cosmochim Acta 53:197–214

Angcoy EC Jr, Arnórsson S (2015) Systematics of rare alkalis and Halogens in the high-temperature mahanagdong geothermal field, Leyte, Philippines. In: Proceedings World Geothermal Congress 2015

Aranovich L, Safonov OG (2018) Halogens in high-grade metamorphism. In: Harlov DE, Aranovich L (eds) The role of halogens in terrestrial and extraterrestrial geochemical processes: surface, crust, and mantle. Springer, Berlin, pp 713–757

Aranovich LY, Newton RC, Manning CE (2013) Brine-assisted anatexis: experimental melting in the system haplogranite–H_2O–NaCl–KCl at deep-crustal conditions. Earth Planet Sci Lett 374:111–120

Aranovich L, Prokofiev VY, Pertsev AN, Bortnikov NS, Ageeva OA (2015) Composition and origin of a K_2O-rich granite melt in the Mid-Atlantic Ridge, 13°34′N: evidence from the analysis of melt inclusions and minerals of the gabbro-plagiogranite association. Dokl Earth Sci 460(2):174–179

Armytage RM, Jephcoat AP, Bouhifd MA, Porcelli D (2013) Metal–silicate partitioning of iodine at high pressures and temperatures: implications for the Earth's core and ^{129}Xe budgets. Earth Planet Sci Lett 373:140–149

Arzamastsev AA, Glaznev VN (2008) Plume-lithosphere interaction in the presence of an ancient sublithospheric mantle keel: an example from the Kola alkaline province. Dokl Earth Sci 419:384–387

Asman WA, Slanina J, Baard JH (1981) Meteorological interpretation of the chemical composition of rain-water at one measuring site. Water Air Soil Pollut 16(2):159–175

Baasner A, Schmidt BC, Webb SL (2013) Compositional dependence of the rheology of halogen (F, Cl) bearing aluminosilicate melts. Chem Geol 346:172–183

Baker DR, Balcone-Boissard H (2009) Halogen diffusion in magmatic systems: Our current state of knowledge. Chem Geol 263(1):82–88

Baker T, Mustard R, Fu B, Williams PJ, Dong G, Fisher L, Ryan CG (2008) Mixed messages in iron oxide–copper–gold systems of the Cloncurry district, Australia: insights from PIXE analysis of halogens and copper in fluid inclusions. Mineral Deposita 43(6):599–608

Balchan AS, Drickamer HG (1961) Effect of pressure on the resistance of iodine and selenium. J Chem Phys 34(6):1948–1949

Balcone-Boissard H, Baker DR, Villemant B, Boudon G (2009) F and Cl diffusion in phonolitic melts: influence of the Na/K ratio. Chem Geol 263:89–98

Banks DA, Yardley BW (1992) Crush-leach analysis of fluid inclusions in small natural and synthetic samples. Geochim Cosmochim Acta 56(1):245–248

Banks DA, Giuliani G, Yardley BW, Cheilletz A (2000a) Emerald mineralisation in Colombia: fluid chemistry and the role of brine mixing. Mineral Deposita 35(8):699–713

Banks DA, Green R, Cliff RA, Yardley BWD (2000b) Chlorine isotopes in fluid inclusions: determination of the origins of salinity in magmatic fluids. Geochim Cosmochim Acta 64 (10):1785–1789

Barnes JD, Sharp ZD (2006) A chlorine isotope study of DSDP/ODP serpentinized ultramafic rocks: insights into the serpentinization process. Chem Geol 228:246–265

Barnes JD, Eldam R, Lee C-TA, Errico JC, Loewy S, Cisneros M (2013) Petrogenesis of serpentinites from the Franciscan Complex, Western California, USA. Lithos 178:143–157

Barnes JD, Manning C, Scambelluri M, Selverstone J (2018) The behavior of halogens during subduction-zone processes. In: Harlov DE, Aranovich L (eds) The role of halogens in terrestrial and extraterrestrial geochemical processes: surface, crust, and mantle. Springer, Berlin, pp 549–590

Baturin GN (1988) The geochemistry of manganese and manganese nodules in the ocean. D. Reidel, Dordrecht, p 356

Becker VJ, Manuel OK (1972) Chlorine, bromine, iodine, and uranium in tektites, obsidians, and impact glasses. J Geophys Res 77(32):6353–6359

Behne W (1953) Untersuchungen zur Geochemie des Chlor und Brom. Geochim Cosmochim Acta 3(4):186–215

Bernini D, Audétat A, Dolejš D, Keppler H (2013) Zircon solubility in aqueous fluids at high temperatures and pressures. Geochim Cosmochim Acta 119:178–187

Beyer C, Klemme S, Wiedenbeck M, Stracke A, Vollmer C (2012) Fluorine in nominally fluorine-free mantle minerals: experimental partitioning of F between olivine, orthopyroxene and silicate melts with implications for magmatic processes. Earth Planet Sci Lett 337:1–9

Biester H, Cortizas AM, Keppler F (2006) Peatlands: evolution and records of environmental and climate changes occurrence and fate of halogens in mires. Elsevier, Boston, pp 465–478

Bindeman IN, Davis AM, Drake MJ (1998) Ion microprobe study of plagioclase-basalt partition experiments at natural concentration levels of trace elements. Geochim Cosmochim Acta 62 (7):1175–1193

Böhlke JK, Irwin JJ (1992a) Brine history indicated by argon, krypton, chlorine, bromine, and iodine analyses of fluid inclusions from the Mississippi valley type lead-fluorite-barite deposits at Hansonburg, New Mexico. Earth Planet Sci Lett 110(1):51–66

Böhlke JK, Irwin JJ (1992b) Laser microprobe analyses of Cl, Br, I, and K in fluid inclusions: implications for sources of salinity in some ancient hydrothermal fluids. Geochim Cosmochim Acta 56:203–225

Böhlke JK, Irwin JJ (1992c) Laser microprobe analyses of noble gas isotopes and halogens in fluid inclusions: analyses of microstandards and synthetic inclusions in quartz. Geochim Cosmochim Acta 56(1):187–201

Böhm A, Schmidt BC (2013) Fluorine and chlorine diffusion in phonolitic melt. Chem Geol 346:162–171

Boiron MC, Cathelineau M, Banks DA, Fourcade S, Vallance J (2003) Mixing of metamorphic and surficial fluids during the uplift of the Hercynian upper crust: consequences for gold deposition. Chem Geol 194(1):119–141

Boiron MC, Cathelineau M, Ruggieri G, Jeanningros A, Gianelli G, Banks DA (2007) Active contact metamorphism and CO_2–CH_4 fluid production in the Larderello geothermal field (Italy) at depths between 2.3 and 4 km. Chem Geol 237(3):303–328

Boneß M, Heumann KG, Haack U (1991) Cl, Br and I analyses of metamorphic and sedimentary rocks by isotope dilution mass spectrometry. Contrib Mineral Petrol 107(1):94–99

Bottomley DJ, Gregoire DC, Raven KG (1994) Saline ground waters and brines in the Canadian Shield: geochemical and isotopic evidence for a residual evaporite brine component. Geochim Cosmochim Acta 58(5):1483–1498

Bottomley DJ, Katz A, Chan LH, Starinksy A, Douglas M, Clark ID, Raven KG (1999) The origin and evolution of Canadian Shield brines: evaporation or freezing of seawater? New lithium isotope and geochemical evidence from the Slave craton. Chem Geol 155:295–320

Boulyga SF, Heumann KG (2005) Direct determination of halogens in powdered geological and environmental samples using isotope dilution laser ablation ICP-MS. Int J Mass Spectrom 242:291–296

Bowen HJM (1979) Environmental chemistry of the elements. Academic, London, p 333

Boyce JW, Eiler JM, Channon MB (2012) An inversion-based self-calibration for SIMS measurements: application to H, F, and Cl in apatite. Am Mineral 97:1116–1128

Boyet M, Carlson RW (2006) A new geochemical model for the Earth's mantle inferred from 146Sm-142Nd systematics. Earth Planet Sci Lett 250:254–268

Brearley AJ, Jones RH (2018) Halogens in chondritic meteorites. In: Harlov DE, Aranovich L (eds) The role of halogens in terrestrial and extraterrestrial geochemical processes: surface, crust, and mantle. Springer, Berlin, pp 871–958

Brearley AJ, Krot AN (2012) Metasomatism in chondritic meteorites. In: Harlov DE, Austrheim H (eds) Metasomatism and the chemical transformation of rock: the role of fluids in terrestrial and extraterrestrial processes. Springer, Berlin, pp 653–782

Bromiley DW, Kohn SC (2007) Comparisons between fluoride and hydroxide incorporation in nominally anhydrous and fluorine-free mantle minerals. Geochim Cosmochim Acta, 71

Buccianti A (2015) The FOREGS repository: modelling variability in stream water on a continental scale revising classical diagrams from CoDA (compositional data analysis) perspective. J Geochem Explor 154:94–104

Bureau H, Métrich N (2003) An experimental study of bromine behaviour in water-saturated silic melts. Geochim Cosmochim Acta 67:1689–1697

Bureau H, Kepler H, Metrich N (2000) Volcanic degassing of bromine and iodine: experimental fluid/melt partitioning data and applications to stratospheric chemistry. Earth Planet Sci Lett 183:51–60

Cabral RA, Jackson MG, Koga KT, Rose-Koga EF, Hauri EH, Whitehouse MJ, Price AA, Day JMD, Shimizu N, Kelley KA (2014) Volatile cycling of H_2O, CO_2, F, and Cl in the HIMU mantle: a new window provided by melt inclusions from oceanic hot spot lavas at Mangaia, Cook Islands. Geochem Geophys Geosys 15:4445–4467

Cameron AGW (1973) Abundances of the elements in the solar system. Space Sci Rev 15:121–146

Cannat M (1993) Emplacement of mantle rocks in the seafloor at mid-ocean ridges. J Geophys Research-Solid Earth 98:4163–4172

Carpenter AB (1978) Origin and chemical evolution of brines in sedimentary basins. SPE annual fall technical conference and exhibition, Society of Petroleum Engineers

Carpenter AB, Trout ML, Pickett EE (1974) Preliminary report on the origin and chemical evolution of lead-and zinc-rich oil field brines in central Mississippi. Econ Geol 69 (8):1191–1206

Carroll MR, Webster JD (1994) Solubilities of sulfur, noble gases, nitrogen, chlorine, and fluorine in magmas. Rev Mineral Geochem 30(1):231–279

Cattermole PJ, Fuge R (1969) The abundances and distribution of fluorine and chlorine in a layered intrusion at Rhiw. North Wales. Geochim Cosmochim Acta 33(10):1295–1298

Cawse PA (1987) Trace and major elements in the atmosphere at rural locations in Great Britain, 1972–1981. Spec Publ Br Ecol Soc 1987

Channer DMD, Spooner ETC (1992) Analysis of fluid inclusion leachates from quartz by ion chromatography. Geochim Cosmochim Acta 56:249–259

Channer DMD, Bray CJ, Spooner ETC (1999) Intergrated cation-anion/volatile fluid inclusion analysis by gas and ion chromatography; methodology and examples. Chem Geol 154:59–82

Chen Y, Zhang Y, Liu Y, Guan Y, Eiler J, Stolper EM (2015) Water, fluorine, and sulfur concentrations in the lunar mantle. Earth Planet Sci Lett 427:37–46

Connolly CA, Walter LM, Baadsgaard H, Longstaffe FJ (1990) Origin and evolution of formation waters, Alberta basin, western Canada sedimentary basin. I. Chemistry. Appl Geochem 5 (4):375–395

Correns CW (1956) The geochemistry of the halogens. Phys Chem Earth 1:181–233

Cuoco E, Tedesco D, Poreda RJ, Williams JC, De Francesco S, Balagizi C, Darrah TH (2013) Impact of volcanic plume emissions on rain water chemistry during the January 2010 Nyamuragira eruptive event: implications for essential potable water resources. J Hazard Mater 244:570–581

Dalou C, Koga KT, Shimizu N, Boulon J, Devidal JL (2012) Experimental determination of F and Cl partitioning between lherzolite and basaltic melt. Contrib Mineral Petrol 163(4):591–609

Dalou C, Koga KT, Le Voyer M, Shimizu N (2014) Contrasting partition behavior of F and Cl during hydrous mantle melting: implications for Cl/F signature in arc magmas. Prog Earth Planet Sci 1(1):1–7

Dalou C, Le Losq C, Mysen BO, Cody GD (2015a) Solubility and solution mechanisms of chlorine and fluorine in aluminosilicate melts at high pressure and high temperature. Am Mineral 100(10):2272–2283

Dalou C, Mysen BO, Foustoukos D (2015b) In-situ measurements of fluorine and chlorine speciation and partitioning between melts and aqueous fluids in the Na_2O-Al_2O_3-SiO_2-H_2O system. Am Mineral 100(1):47–58

Dawson JB, Fuge R (1980) Halogen content of some African primary carbonatites. Lithos 13 (2):139–143

Debret B, Koga KT, Nicollet C, Andreani M, Schwartz S (2014) F, Cl and S input via serpentinite in subduction zones: implications for the nature of the fluid released at depth. Terra Nova 26:96–101

Debret B, Koga KT, Cattani F, Nicollet C (2015) Volatile (Li, B, F and Cl) mobility during amphibole breakdown in subduction zones. Lithos 244:165–181

Déruelle B, Dreibus G, Jambon A (1992) Iodine abundances in oceanic basalts: implications for Earth dynamics. Earth Planet Sci Lett 108:217–227

Dolejš D, Baker DR (2004) Thermodynamic analysis of the system Na_2O-K_2O-CaO-Al_2O_3-SiO_2-H_2O-F_2O^{-1}: stability of fluorine-bearing minerals in felsic igneous suites. Contrib Mineral Petrol 146(6):762–778

Dolejš D, Baker DR (2007a) Liquidus equilibria in the system K_2O-Na_2O-Al_2O_3-SiO_2-F_2O^{-1}-H_2O to 100 MPa: I. Silicate-fluoride liquid immiscibility in anhydrous systems. J Petrol 48:785–806

Dolejš D, Baker DR (2007b) Liquidus equilibria in the system K_2O-Na_2O-Al_2O_3-SiO_2-F_2O^{-1}-H_2O to 100 MPa: II. Differentiation paths of fluorosilicic magmas in hydrous systems. J Petrol 48:807–828

Dolejš D, Zajacz Z (2018) Halogens in silicic magmas and their hydrothermal systems. In: Harlov DE, Aranovich L (eds) The role of halogens in terrestrial and extraterrestrial geochemical processes: surface, crust, and mantle. Springer, Berlin, pp 431–543

Dong P (2005) Halogen-element (F, Cl, and Br) behaviour in apatites, scapolite and sodalite: an experimental investigation with field applications. Ph.D. thesis, University of Saskatchewan, Saskatoon, pp 1–222

Dreibus G, Wänke H (1987) Volatiles on Earth and Mars: a comparison. Icarus 71:225–240

Dreibus G, Wänke H (1990) Comparison of the chemistry of Moon and Mars. Adv Space Res 10:7–16

Dreibus G, Jagoutz E, Palme H, Spettel B, Wänke H (1979) Volatile and other trace element abundances in the eucrite parent body and in the Earth's mantle: A comparison. Meteoritics 14:385

Du Y, Ma T, Yang J, Liu L, Shan H, Cai H, Liu C, Chen L (2013) A precise analytical method for bromine stable isotopes in natural waters by GasBench II-IRMS. J Mass Spectrom 338:50–56

Edmond JM, Measures C, McDuff RE, Chan LH, Collier R, Grant B (1979) Ridge crest hydrothermal activity and the balances of the major and minor elements in the ocean; the Galapagos data. Earth Planet Sci Lett 46(1):1–18

Edmunds W (1996) Bromine geochemistry of British groundwaters. Mineral Mag 60 (399):275–284

Edmunds WM, Kay RLF, Miles DL, Cook JM (1987) The origin of saline groundwaters in the Carnmenellis Granite, Cornwall (UK): Further evidence from minor and trace elements. In: Fritz P, Frape SK (eds) Saline water and gases in crystalline rocks. Geological Association of Canada Special Paper 33, pp 127–143

Egeberg PK, Aagaard P (1989) Origin and evolution of formation waters from oil fields on the Norwegian shelf. Appl Geochem 4(2):131–142

Eggenkamp H (2014) The geochemistry of stable chlorine and bromine isotopes. Springer, Berlin

Eggenkamp HGM, Coleman ML (2000) Rediscovery of classical methods and their application to the measurement of stable bromine isotopes in natural samples. Chem Geol 167:393–402

Eggenkamp HGM, Kreulen R, Koster van Groos AF (1995) Chlorine stable isotope fractionation in evaporites. Geochim Cosmochim Acta 59:5169–5175

Elderfield H, Truesdale VW (1980) On the biophilic nature of iodine in seawater. Earth Planet Sci Lett 50(1):105–114

Enami M, Liou JG, Bird DK (1992) Cl-bearing amphibole in the Salton Sea geothermal system, California. Can Mineral 30(4):1077–1092

Evans KA, Mavrogenes JA, O'Neill HSC et al (2008) A preliminary investigation of chlorine XANES in silicate glasses. Geochem Geophys Geosys 9:Q10003

Fabbrizio A, Stalder R, Hametner K, Günther D, Marquardt K (2013) Experimental partitioning of halogens and other trace elements between olivine, pyroxenes, amphibole and aqueous fluid at 2 GPa and 900–1,300 C. Contrib Mineral Petrol 166(2):639–653

Fairmaid AM, Kendrick MA, Phillips D, Fu B (2011) The origin and evolution of mineralizing fluids in a sediment-hosted orogenic-gold deposit, Ballarat East, Southeastern Australia. Econ Geol 106(4):653–666

Fehn U, Lu Z, Tomaru H (2006) Data report: ^{129}I/I ratios and halogen concentrations in pore water of Hydrate Ridge and their relevance for the origin of gas hydrates: a progress report. In: Trehu AM, Bohrmann G, Torres ME, Colwell FS (eds) Proceedings of the ocean drilling program, Scientific results 204, pp 1–25

Fisher RS, Kreitler CW (1987) Geochemistry and hydrodynamics of deep-basin brines, Palo Duro Basin, Texas, USA. Appl Geochem 2(5):459–476

Foley SF, Taylor WR, Green DH (1986) The effect of fluorine on phase relationships in the system $KAlSiO_4$-Mg_2SiO_4-SiO_2 at 28 kbar and the solution mechanism of fluorine in silicate melts. Contrib Mineral Petrol 93:46–55

Fontes JC, Matray JM (1993) Geochemistry and origin of formation brines from the Paris Basin, France: 1. Brines associated with Triassic salts. Chem Geol 109(1):149–175

Forestini M, Goriely S, Jorissen A (1992) Fluorine production in thermal pulses on the asymptotic giant branch. Astron Astrophys 261:157–163

Frape SK, Fritz P (1982) The chemistry and isotopic compositions of saline groundwaters from the Sudbury Basin, Ontario. Can J Earth Sci 19:645–661

Frape SK, Fritz P (1987) Geochemical trends for groundwaters from the Canadian Shield. In: Saline water and gases in crystalline rocks. Geological Association of Canada, Ottawa, vol 33, pp 19–38

Frape SK, Fritz P, McNutt RH (1984) Water-rock interaction and chemistry of groundwaters from the Canadian Shield. Geochim Cosmochim Acta 48:1617–1627

Frezzotti ML, Touret JL (2014) CO_2, carbonate-rich melts, and brines in the mantle. Geosci Front 5(5):697–710

Fu B, Kendrick MA, Fairmaid AM, Phillips D, Wilson CJL, Mernagh TP (2012) New constraints on fluid sources in orogenic gold deposits, Victoria Australia. Mineral Petrol 163:427–447

Fuge R (1974) Bromine. Handbook of geochemistry 100:3

Fuge R (1988) Sources of halogens in the environment, influences on human and animal health. Environ Geochem Health 10(2):51–61

Fuge R (2005) Soils and iodine deficiency. In: Selinus O (ed) Essentials of medical geology. Springer, Heidelberg, p 417

Fuge R, Johnson CC (1986) The geochemistry of iodine—a review. Environ Geochem Health 8 (2):31–54

Fuge R, Johnson CC, Phillips WJ (1978) Iodine in granitic and associated rocks. Chem Geol 22:347–352

Ganapathy R, Keays RR, Laul J, Anders E (1970) Trace elements in Apollo 11 lunar rocks: implications for meteorite influx and origin of moon. Geochim Cosmochim Acta Suppl 1:1117

Gao S, Luo T-C, Zhang B-R, Zhang H-F, Han Y-W, Zhao Z-D, Hu Y-K (1998) Chemical composition of the continental crust as revealed by studies in East China. Geochim Cosmochim Acta 62:1959–1975

Gelman F, Halicz L (2011) High-precision isotope ratio analysis of inorganic bromide by continuous flow MC-ICPMS. Int J Mass Spectrom 307:211–213

German CR, Von Damm KL (2003) Hydrothermal processes. In Holland HD, Turrekian KK (eds) Treatise on geochemistry, vol 6. Elsevier, Amsterdam, The Netherlands, pp 181–222

Gerritse RG, George RJ (1988) The role of soil organic matter in the geochemical cycling of chloride and bromide. J Hydrol 101(1):83–95

Gillis KM, Meyer PS (2001) Metasomatism of oceanic gabbros by late stage melts and hydrothermal fluids: evidence from the rare earth element composition of amphiboles. Geochem Geophys Geosys 2:1012

Gleeson SA, Smith MP (2009) The sources and evolution of mineralising fluids in iron oxide–copper–gold systems, Norrbotten, Sweden: constraints from Br/Cl ratios and stable Cl isotopes of fluid inclusion leachates. Geochim Cosmochim Acta 73(19):5658–5672

Goldberg RH, Burnett DS, Furst MJ, Tombrello TA (1974) Fluorine concentrations in carbonaceous chondrites. Meteoritics 9:347

Goldschmidt VM (1926) The laws of crystal chemistry. Naturwissenschaften 14(21):477–485

Goles GG, Anders E (1960) Iodine content of meteorites and their ^{129}I–^{129}Xe ages. J Geophys Res 65(12):4181–4184

Goles GG, Anders E (1961) Theories on the origin of meteorites. J Chem Educ 38(2):586

Goles GG, Anders E (1962) Abundances of iodine tellurium and uranium in meteorites. Geochim Cosmochim Acta 26(7):723–737

Goles GG, Greenland LP, Jérome DY (1967) Abundances of chlorine, bromine and iodine in meteorites. Geochim Cosmochim Acta 31:1771–1787

Graupner T, Niedermann S, Kempe U, Klemd R, Bechtel A (2006) Origin of ore fluids in the Muruntau gold system: constraints from noble gas, carbon isotope and halogen data. Geochim Cosmochim Acta 70(21):5356–5370

Grawinkel A, Stöckhert B (1997) Hydrostatic pore fluid pressure to 9 km depth-Fluid inclusion evidence from the KTB deep drill hole. Geophys Res Lett 24(24):3273–3276

Greenland L, Lovering JF (1965) Minor and trace element abundances in chondritic meteorites. Geochim Cosmochim Acta 29(8):821–858

Groos AF van, Wyllie PJ (1969) Melting relationships in the system $NaAlSi_3O_8$-NaCl-H_2O at 1 kilobar pressure, with petrological applications. J Geol 77:581–605

Gulbrandsen RA (1966) Chemical composition of phosphorites of the phosphoria formation. Geochim Cosmochim Acta 30(8):769–778

Hall DNB, Noyes RW (1969) Observation of hydrogen fluoride in sunspots and the determination of the solar fluorine abundance. Astrophys Lett 4:143

Hall DNB, Noyes RW (1972) The identification of the 1-0 and 2-1 Bands of HCI in the infrared sunspot spectrum. Astrophys J 175:L95–L97

Hall GEM, MacLaurin AI, Vaive J (1986) The analysis of geological materials for fluorine, chlorine and sulfur using pyrohydrolysis and ion chromatrography. J Geochem Explor 26 (2):177–186

Hammerli J, Rusk B, Spandler C, Emsbo P, Oliver NHS (2013) In situ quantification of Br and Cl in minerals and fluid inclusions by LA-ICP-MS: a powerful tool to identify fluid sources. Chem Geol 337–338:75–87

Hand KP (2018) Halogens on and within the ocean worlds of the outer solar system. In: Harlov DE, Aranovich L (eds) The role of halogens in terrestrial and extraterrestrial geochemical processes: surface, crust, and mantle, Springer, Berlin, pp 997–1016

Hanley JJ, Mungall JE, Bray CJ, Gorton MP (2004) The origin of bulk and water-soluble Cl and Br enrichments in ore-hosting Sudbury Breccia in the Fraser Copper Zone, Strathcona Embayment, Sudbury, Ontario, Canada. Can Mineral 42(6):1777–1798

Hanley JJ, Pettke T, Mungall JE, Spooner ET (2005) The solubility of platinum and gold in NaCl brines at 1.5 kbar, 600 to 800 C: a laser ablation ICP-MS pilot study of synthetic fluid inclusions. Geochim Cosmochim Acta 69(10):2593–2611

Hanley JJ, Mungall JE, Pettke T, Spooner ET, Bray CJ (2008) Fluid and halide melt inclusions of magmatic origin in the ultramafic and lower banded series, stillwater complex, Montana, USA. J Petrol 49(6):1133–1160

Hart SR, Zindler A (1986) In search of a bulk-Earth composition. Chem Geol 57:247–267

Hart SR, Hauri EH, Oschmann LA, Whitehead JA (1992) Mantle plumes and Entrainment: isotopic evidence. Science 256:517–520

Hauri E, Wang J, Dixon J, King PL, Mandeville C, Newman S (2002) SIMS analysis of volatiles in silicate glasses 1. Calibration, matrix effects and comparisons with FTIR. Chem Geol 182:99–114

Hauri EH (2002) SIMS analysis of volatiles in silicate glasses, 2: isotopes and abundances in Hawaiian melt inclusions. Chem Geol 183:115–141

Hauri EH, Gaetani GA, Green TH (2006) Partitioning of water during melting of the Earth's upper mantle at H2O-undersaturated conditions. Earth Planet Sci Lett 248:715–734

Hauri EH, Saal AE, Rutherford MJ, Van Orman JA (2015) Water in the Moon's interior: truth and consequences. Earth Planet Sci Lett 409:252–264

Hauri EH, Weinreich T, Saal AE, Rutherford M, Van Orman JA (2011) High pre-eruptive water contents preserved in lunar melt inclusions. Science 333:213

Heinrich CA, Ryan CG, Mernagh TP, Eadington PJ (1992) Segregation of ore metals between magmatic brine and vapor: a fluid inclusion study using PIXE microanalysis. Econ Geol 87:1566–1583

Heinrich CA, Pettke T, Halter WE, Aigner-Torres M, Audétat A, Günther D, Hattendorf B, Bleiner D, Guillong M, Horn I (2003) Quantitative multi-element analysis of minerals, fluid and melt inclusions by laser-ablation inductively-coupled-plasma mass-spectrometry. Geochim Cosmochim Acta 67(18):3473–3497

Herut B, Starinsky A, Katz A, Bein A (1990) The role of seawater freezing in the formation of subsurface brines. Geochim Cosmochim Acta 54(1):13–21

Hervig RL, Dunbar NW, Westrich HR, Kyle PR (1989) Pre-eruptive water content of rhyolitic magmas as determined by ion microprobe analyses of melt inclusions in phenocrysts. J Volcanol Geotherm Res 36:293–302

Holtz F, Dingwell DB, Behrens H (1993) Effects of F, B_2O_3 and P_2O_5 on the solubility of water in haplogranite melts compared to natural silicate melts. Contrib Mineral Petrol 113(4):492–501

Horn MK, Adams JA (1966) Computer-derived geochemical balances and element abundances. Geochim Cosmochim Acta 30(3):279–297

Hurwitz S, Mariner RH, Fehn U, Snyder GT (2005) Systematics of halogen elements and their radioisotopes in thermal springs of the cascade range, Central Oregon, Western USA. Earth Planet Sci Lett 235(3):700–714

Icenhower JP, London K (1997) Partitioning of fluorine and chlorine between biotite and granitic melt: experimental calibration at 200 Mpa H_2O. Contrib Mineral Petrol 127:17–29

Irwin JJ, Roedder E (1995) Diverse origins of fluid in magmatic inclusions at Bingham (Utah, USA), Butte (Montana, USA), St. Austell (Cornwall, UK), and Ascension Island (mid-Atlantic, UK), indicated by laser microprobe analysis of Cl, K, Br, I, Ba + Te, U, Ar, Kr, and Xe. Geochim Cosmochim Acta 59(2):295–312

Ito E, Anderson AT Jr (1983) Submarine metamorphism of gabbros from the Mid-Cayman Rise: petrographic and mineralogic constraints on hydrothermal processes at slow-spreading ridges. Contrib Miner Petrol 82(4):371–388

Ito E, Harris DM, Anderson AT (1983) Alteration of oceanic crust and geologic cycling of chlorine and water. Geochim Cosmochim Acta 47(9):1613–1624

Jagoutz E, Palme H, Baddenhausen H, Blum K, Cendales M, Dreibus G, Spettel B, Lorenz V, Waenke H (1979) The abundances of major, minor and trace elements in the Earth's mantle as derived from primitive ultramafic nodules. In: Merrill RB, Bogard DD, Hoerz F, McKay DS, Robertson PC (eds) Proceedings of the lunar and planetary science conference, vol 2. Pergamon, New York, pp 2031–2050

Jambon A, Zimmermann JL (1990) Water in oceanic basalts: evidence for dehydration of recycled crust. Earth Planet Sci Lett 101(2):323–331

Jambon A, Déruelle B, Dreibus G, Pineau F (1995) Chlorine and bromine abundance in MORB: the contrasting behaviour of the Mid-Atlantic Ridge and East Pacific Rise and implications for chlorine geodynamic cycle. Chem Geol 126:101–117

Jarosewich E (2010) Chemical analyses of meteorites at the Smithsonian Institution: an update. Meteorit Planet Sci 41:1381–1382

Joachim B, Pawley A, Lyon IC, Marquardt K, Henkel T, Clay PL, Ruzié L, Burgess R, Ballentine CJ (2015) Experimental partitioning of F and Cl between olivine, orthopyroxene and silicate melt at Earth's mantle conditions. Chem Geol 416:65–78

John T, Layne GD, Haase KM, Barnes JD (2010) Chlorine isotope evidence for crustal recycling into the Earth's mantle. Earth Planet Sci Lett 298:175–182

John T, Scambelluri M, Frische M, Barnes JD, Bach W (2011) Dehydration of subducting serpentinite: implications for halogen mobility in subduction zones and the deep halogen cycle. Earth Planet Sci Lett 308:65–76

Johns WD, Huang WH (1967) Distribution of chlorine in terrestrial rocks. Geochim Cosmochim Acta 31(1):35–49

Johnson MC, Anderson AT, Rutherford MJ (1993) Pre-eruptive volatile contents of magmas. In: Carroll MR, Holloway JR (eds) Volatiles in magmas. Mineralogical Society of America, Washington, DC, pp 281–330

Johnson LH, Burgess R, Turner G, Milledge HJ, Harris JW (2000) Noble gas and halogen geochemistry of mantle fluids: comparison of African and Canadian diamonds. Geochim Cosmochim Acta 64(4):717–732

Johnson KTM, Reynolds JR, Vonderhaar DL, Smith DK, Kong LSL (2002) Petrological systematics of submarine basalt glasses fromt Puna Ridge, Hawaii: implications for rift zone plumbing and magmatic processes. In: Takahashi E et al (eds) Hawaiian volcanoes: deep underwater perspectives, geophysical monograph, vol 128. American Geophysical Union, Washington, DC, pp 143–159

Kabata-Pendias A, Pendias H (2001) Trace elements in soils and plants. CRC, Boca Raton

Kamenetsky MB, Sobolev AV, Kamenetsky VS, Maas R, Danyushevsky LV, Thomas R, Pokhilenko NP, Sobolev NV (2004) Kimberlite melts rich in alkali chlorides and carbonates: a potent metasomatic agent in the mantle. Geology 32:845

Kamenetsky VS, Mitchell RH, Maas R, Giuliani A, Gaboury D, Zhitova L (2015) Chlorine in mantle-derived carbonatite melts revealed by halite in the St.-Honoré intrusion (Québec, Canada). Geology 43(8):687–690

Kamineni DC (1986) A petrochemical study of calcic amphiboles from the East Bull Lake anorthosite-gabbro layered complex, District of Algoma, Ontario. Contrib Mineral Petrol 93 (4):471–481

Kamineni DC, Gascoyne M, Melnyk TW, Frape SK, Blomqvist R (1992) Cl and Br in mafic and ultramafic rocks: significance for the origin of salinity in groundwater. In: Water–rock interaction. Proceedings of the 7th international symposium on water–rock interaction, Park City, UT 1: 801–804

Kastner M, Elderfield H, Martin JB, Suess E, Kvenvolden KA, Garrison RE (1990) Diagenesis and interstitial-water chemistry at the Peruvian continental margin—major constituents and strontium isotopes. In: Suess E, von Huene R (eds) Proceedings of the ocean drilling program, Scientific results. 112:413–440

Kato F, Ozaki H, Ebihara M (2000) Distribution of halogens in an Antarctic ordinary chondrite, Y-74014 (H6). Antarct Meteor Res 13:121–134

Keene W, Khalil MA, Erickson D, McCulloch A, Graedel TE, Lobert JM, Aucott ML, Gong SL, Harper DB, Kleiman G, Midgley P (1999) Composite global emissions of reactive chlorine from anthropogenic and natural sources: reactive chlorine emissions inventory. J Geophys Res: Atmos 104(7):8429–8440

Keene WC, Stutz J, Pszenny AA, Maben JR, Fischer EV, Smith AM, von Glasow R, Pechtl S, Sive BC, Varner RK (2007) Inorganic chlorine and bromine in coastal New England air during summer. J Geophy Res: Atmos. 112(D10). https://doi.org/10.1029/2006JD007689

Keller J, Zaitsev AN (2012) Geochemistry and petrogenetic significance of natrocarbonatites at Oldoinyo Lengai, Tanzania: composition of lavas from 1988 to 2007. Lithos 148:45–53

Kelley KA, Kingsley R, Schilling J-G (2013) Composition of plume-influenced mid-ocean ridge lavas and glasses from the Mid-Atlantic Ridge, East Pacific Rise, Galápagos Spreading Center, and Gulf of Aden. Geochem Geophys Geosys 14:223–242

Kendrick MA (2012) High precision Cl, Br and I determinations in mineral standards using the noble gas method. Chem Geol 292–293:116–126

Kendrick MA (2018) Halogens in seawater, marine sediments and the altered oceanic lithosphere. In: Harlov DE, Aranovich L (eds) The role of halogens in terrestrial and extraterrestrial geochemical processes: surface, crust, and mantle. Springer, Berlin, pp 591–648

Kendrick MA, Burnard P (2013) Noble gases and halogens in fluid inclusions: a journey through the Earth's crust. The noble gases as geochemical tracers. Springer, Berlin, pp 319–369

Kendrick MA, Phillips D (2009) New constraints on the release of noble gases during in vacuo crushing and application to scapolite Br–Cl–I and $^{40}Ar/^{39}Ar$ age determinations. Geochim Cosmochim Acta 73(19):5673–5692

Kendrick MA, Burgess R, Pattrick RAD, Turner G (2001a) Fluid inclusion noble gas and halogen evidence on the origin of Cu-Porphyry mineralising fluids. Geochim Cosmochim Acta 65:2651–2668

Kendrick MA, Burgess R, Pattrick RA, Turner G (2001b) Halogen and Ar–Ar age determinations of inclusions within quartz veins from porphyry copper deposits using complementary noble gas extraction techniques. Chem Geol 177(3):351–370

Kendrick MA, Burgess R, Leach D, Pattrick RA (2002a) Hydrothermal fluid origins in Mississippi valley-type ore districts: combined noble gas (He, Ar, Kr) and halogen (Cl, Br, I) analysis of fluid inclusions from the Illinois-Kentucky fluorspar district, Viburnum Trend, and Tri-State districts, midcontinent United States. Econ Geol 97(3):453–469

Kendrick MA, Burgess R, Pattrick RA, Turner G (2002b) Hydrothermal fluid origins in a fluorite-rich Mississippi Valley-type district: combined noble gas (He, Ar, Kr) and halogen (Cl, Br, I) analysis of fluid inclusions from the South Pennine ore field United Kingdom. Econ Geol 97(3):435–451

Kendrick MA, Duncan R, Phillips D (2006a) Noble gas and halogen constraints on mineralizing fluids of metamorphic versus surficial origin: Mt Isa. Aust Chem Geol 235(3):325–351

Kendrick MA, Phillips D, Miller JM (2006b) Part I. Decrepitation and degassing behaviour of quartz up to 1560 C: analysis of noble gases and halogens in complex fluid inclusion assemblages. Geochim Cosmochim Acta 70(10):2540–2561

Kendrick MA, Baker T, Fu B, Phillips D, Williams PJ (2008) Noble gas and halogen constraints on regionally extensive mid-crustal Na–Ca metasomatism, the Proterozoic Eastern Mount Isa Block, Australia. Precambr Res 163(1):131–150

Kendrick MA, Scambelluri M, Honda M, Phillips D (2011) High abundances of noble gas and chlorine delivered to the mantle by serpentinite subduction. Nat Geosci 4:807–812

Kendrick MA, Kamenetsky VS, Phillips D, Honda M (2012) Halogen systematics (Cl, Br, I) in mid-ocean ridge basalts: a Macquarie Island case study. Geochim Cosmochim Acta 81:82–93

Kendrick MA, Jackson MG, Kent AJR, Hauri EH, Wallace PJ, Woodhead JD (2013a) Contrasting behaviours of CO_2, S, H_2O and halogens (F, Cl, Br, and I) in enriched-mantle melts from Pitcairn and Society seamounts. Chem Geol 370:69–81

Kendrick MA, Arculus RJ, Burnard P, Honda M (2013b) Quantifying brine assimilation by submarine magmas: examples from the Galápagos Spreading Centre and Lau Basin. Geochim Cosmochim Acta 123:150–165

Kendrick MA, Honda M, Pettke T, Scambelluri M, Phillips D, Giuliani A (2013c) Subduction zone fluxes of halogens and noble gases in seafloor and forearc serpentinites. Earth Planet Sci Lett 365:86–96

Kendrick MA, Jackson MG, Kent AJ, Hauri EH, Wallace PJ, Woodhead J (2014) Contrasting behaviours of CO_2, S, H_2O and halogens (F, Cl, Br, and I) in enriched-mantle melts from Pitcairn and Society seamounts. Chem Geol 370:69–81

Kendrick MA, Honda M, Vanko DA (2015a) Halogens and noble gases in Mathematician Ridge metagabbros, NE Pacific: implications for oceanic hydrothermal root zones and global volatile cycles. Contrib Mineral Petrol 170(43):1–20

Kendrick MA, Jackson MG, Hauri EH, Phillips D (2015b) The halogen (F, Cl, Br, I) and H_2O systematics of Samoan lavas: Assimilated-seawater, EM2 and high-$^3He/^4He$ components. Earth Planet Sci Lett 410:197–209

Kharaka YK, Maest AS, Carothers WW, Law LM, Lamothe PJ, Fries TL (1987) Geochemistry of metal-rich brines from central Mississippi Salt Dome basin, USA. Appl Geochem 2 (5):543–561

Klemme S (2004) Evidence for fluoride melts in Earth's mantle formed by liquid immiscibility. Geology 32:441

Klemme S, Stalder R (2018) Halogens in the Earth's mantle: what we know and what we don't. In: Harlov DE, Aranovich L (eds) The role of halogens in terrestrial and extraterrestrial geochemical processes: surface, crust, and mantle. Springer, Berlin, pp 847–869

Klockenkämper R (1996) Total-reflection X-ray fluorescence analysis. Wiley, Hoboken, p 245

Köhler J, Schönenberger J, Upton B, Markl G (2009) Halogen and trace-element chemistry in the Gardar Province, South Greenland: subduction-related mantle metasomatism and fluid exsolution from alkali melts. Lithos 113:731–747

Kohn SC, Dupree R, Mortuza M, Henderson C (1991) NMR evidence for five-and six-coordinated aluminum fluoride complexes in F-bearing aluminosilicate glasses. Am Mineral 76:309–312

Koleszar AM, Saal AE, Hauri EH, Nagle AN, Liang Y, Kurz MD (2009) The volatile contents of the Galapagos plume; evidence for H_2O and F open system behavior in melt inclusions. Earth Planet Sci Lett 287:442–452

Krahenbühl U, Ganapathy R, Morgan JW, Anders E (1973) Volatile elements in Apollo 16 samples: implications for highland volcanism and accretion history of the moon. Lunar Planet Sci Conf 4:1325–1348

Kronberg BI, Nesbitt HW, Fyfe WS (1987) Mobilities of alkalis, alkaline earths and halogens during weathering. Chem Geol 60(1):41–49

Kullerud K, Erambert M (1999) Cl-scapolite, Cl-amphibole, and plagioclase equilibria in ductile shear zones at Nusfjord, Lofoten, Norway: implications for fluid compositional evolution during fluid-mineral interaction in the deep crust. Geochim Cosmochim Acta 63 (22):3829–3844

Lahermo PW, Lampén PH (1987) Brackish and Saline groundwaters in Finland. In: Fritz P, Frape SK (eds) Saline water and gases in crystalline rocks. Geological Association of Canada, Newfoundland, pp 103–109 (Special Paper 33)

Land LS (1995a) The role of saline formation water in crustal cycling. Aquat Geochem 1:137–145

Land LS (1995b) Na–Ca–Cl saline formation waters, Frio Formation (Oligocene), south Texas, USA: products of diagenesis. Geochim Cosmochim Acta 59(11):2163–2174

Lassiter JC, Hauri EH, Nikogosian IK, Barsczus HG (2002) Chlorine–potassium variations in melt inclusions from Raivavae and Rapa, Austral Islands: constraints on chlorine recycling in the mantle and evidence for brine-induced melting of oceanic crust. Earth Planet Sci Lett 202:525–540

Latourrette T, Hervig RL, Holloway JR (1995) Trace-element partitioning between amphibole, phlogopite, and basanite melt. Earth Planet Sci Lett 135(1–4):13–30

Layne GD, Godon A, Webster JD, Bach W (2004) Secondary ion mass spectrometry for the determination of δ^{37}Cl Part I. Ion microprobe analysis of glasses and fluids. Chem Geol 207:277–289

Layne GD, Kent AJR, Bach W (2009) Delta Cl-37 systematics of a backarc spreading system: the Lau basin. Geology 37:42–430

Le Voyer M, Rose-Koga EF, Shimizu N, Grove TL, Schiano P (2010) Two contrasting H_2O-rich components in primary melt inclusions from Mount Shasta. J Petrol 51:1571–1595

Lecumberri-Sanchez P, Bodnar RJ (2018) Halogen geochemistry of ore deposits: contributions towards understanding sources and processes. In: Harlov DE, Aranovich L (eds) The role of halogens in terrestrial and extraterrestrial geochemical processes: surface, crust, and mantle. Springer, Berlin, pp 261–305

Leisen M, Boiron M-C, Richard A, Dubessy J (2012) Determination of Cl and Br concentrations in individual fluid inclusions by combining microthermometry and LA-ICPMS analysis: implications for the origin of salinity in crustal fluids. Chem Geol 330–331:197–206

Leri AC, Mayer LM, Thornton KR, Ravel B (2014) Bromination of marine particulate organic matter through oxidative mechanisms. Geochim Cosmochim Acta 142:53–63

Li Y-H (1982) A brief discussion on the mean oceanic residence time of elements. Geochim Cosmochim Acta 46:2671–2675
Li Y-H (1991) Distribution patterns of the elements in the ocean: a synthesis. Geochim Cosmochim Acta 55:3223–3240
Lide DR (ed) (2016) CRC Handbook of chemistry and physics, 96th edn. CRC, Boca Raton
Lieberman KW (1966) The determination of bromine in terrestrial and extraterrestrial materials by neutron activation analysis. Dept. of Chemistry, Kentucky Univ., Lexington
Liebscher A, Barnes J, Sharp Z (2006) Chlorine isotope vapor–liquid fractionation during experimental fluid-phase separation at 400 C/23 MPa to 450 C/42 MPa. Chem Geol 234 (3):340–345
Liu Y, Tossell J (2003) Possible Al-F bonding environment in fluorine-bearing sodium aluminosilicate glasses: from calculation of ^{19}F NMR shifts. J Phys Chem B 107 (41):11280–11289
Liu CZ, Wu FY, Chung SL, Zhao ZD (2011) Fragments of hot and metasomatized mantle lithosphere in Middle Miocene ultrapotassic lavas, southern Tibet. Geology 39:923–926
Lodders K (2010) Solar system abundances of the elements. Principles and perspectives in cosmochemistry. Springer, Berlin, pp 379–417
Lodders K, Fegley B (1997) An oxygen isotope model for the composition of Mars. Icarus 126:373–394
Lodders K, Fegley B (1998) The planetary scientist's companion. Oxford University Press, New York
Lodders K, Palme H, Gail HP (2009) Abundances of the elements in the solar system. Astronomy and astrophysics. Springer, Berlin, pp 560–630
Long A, Eastoe CJ, Kaufmann RS, Martin JG, Wirt L, Finley JB (1993) High-precision measurements of chlorine stable isotope ratios. Geochim Cosmochim Acta 57:2907–2912
Lundegard PD, Trevena AS (1990) Sandstone diagenesis in the Pattani Basin (Gulf of Thailand): history of water-rock interaction and comparison with the Gulf of Mexico. Appl Geochem 5 (5):669–685
Lundström U, Olin Å, Nydahl F (1984) Determination of low levels of bromide in fresh water after chromatographic enrichment. Talanta 31(1):45–48
Luth RW (1988) Raman spectroscopic study of the solubility mechanisms of F in glasses in the system CaO-CaF_2-SiO_2. Am Mineral 73(3–4):297–305
Luth RW, Muncill GE (1989) Fluorine in aluminosilicate systems: phase relations in the system $NaAlSi_3O_8$-$CaAl_2Si_2O_8$-F_2O^{-1}. Geochim Cosmochim Acta 53(8):1937–1942
Lyubetskaya T, Korenaga J (2007) Chemical composition of Earth's primitive mantle and its variance: 1 method and results. J Geophys Res 112:B03211
Macpherson GL (1992) Regional variations in formation water chemistry: major and minor elements, Frio formation fluids, Texas. AAPG Bullet 76(5):740–757
Magenheim AJ, Spivack AJ, Volpe C, Ransom B (1994) Precise determination of stable chlorine isotopic ratios in low-concentration natural samples. Geochim Cosmochim Acta 58:3117–3121
Mangler MF, Marks MA, Zaitzev AN, Eby GN, Markl G (2014) Halogens (F, Cl and Br) at Oldoinyo Lengai volcano (Tanzania): effects of magmatic differentiation, silicate–natrocarbonatite melt separation and surface alteration of natrocarbonatite. Chem Geol 365:43–53
Manheim FT, Pratt RM, McFarlin PF (1980) Composition and origin of phosphorite deposits of the Blake Plateau. Soc Econ Paleontol Mineral 29:117–137
Manning DA (1981) The effect of fluorine on liquidus phase relationships in the system Qz-Ab-Or with excess water at 1 kb. Contrib Mineral Petrol 76(2):206–215
Markl G, Bucher K (1998a) Composition of fluids in the lower crust inferred from metamorphic salt in lower crustal rocks. Nature 391(6669):781–783
Markl G, Bucher K (1998b) Metamorphic salt in granulites: implications for the presence and composition of fluid in the lower crust. Nature 391:781–783
Marks MAW, Wenzel T, Whitehouse MJ, Loose M, Zack T, Barth M, Worgard L, Krasz V, Eby GN, Stosnach H, Markl G (2012) The volatile inventory (F, Cl, Br, S, C) of magmatic apatite: an integrated analytical approach. Chem Geol 291:241–255

Marschik R, Kendrick MA (2015) Noble gas and halogen constraints on fluid sources in iron oxide-copper-gold mineralization: Mantoverde and La Candelaria, Northern Chile. Mineral Deposita 50(3):357–371

Martin JB, Gieskes JM, Torres M, Kastner M (1993) Bromine and iodine in Peru margin sediments and pore fluids: implications for fluid origins. Geochim Cosmochim Acta 57:4377–4389

Martin JM, Meybeck M (1979) Elemental mass-balance of material carried by major World rivers. Mar Chem 7(3):173–206

Mathez ED, Webster JD (2005) Partitioning behavior of chlorine and fluorine in the system apatite-silicate melt-fluid. Geochim Cosmochim Acta 69(5):1275–1286

McCaffrey MA, Lazar B, Holland HD (1987) The evaporation path of seawater and the coprecipitation of $Br^{(-)}$ and $K^{(+)}$ with halite. J Sediment Res 57(5):928–937

McCaig AM, Tritlla J, Banks DA (2000) Fluid mixing and recycling during Pyrenean thrusting: evidence from fluid inclusion halogen ratios. Geochim Cosmochim Acta 64(19):3395–3412

McDonough WF (1990) Constraints on the composition of the continental lithospheric mantle. Earth Planet Sci Lett 101(36):909

McDonough WF (2003) Compositional model for the Earth's core. In: Holland HD, Turrekian KK (eds) Treatise on geochemistry, vol 2. Elsevier, Amsterdam, pp 547–568

McDonough WF, Sun S-S (1995) Composition of the Earth. Chem Geol 120:223–253

McNutt RH, Frape SK, Fritz P, Jones MG, MacDonald IM (1990) The $^{87}Sr^{86}Sr$ values of Canadian shield brines and fracture minerals with applications to groundwater mixing, fracture history, and geochronology. Geochim Cosmochim Acta 54(1):205–215

Merino E (1975) Diagenesis in tertiary sandstones from Kettleman North Dome, California. I diagenetic mineralogy. J Sed Res 45(1):320–336

Metrich N, Zanon V, Creon L, Hildenbrand A, Moreira M, Marques FO (2014) Is the "Azores Hotspot" a Wetspot? Insights from the geochemistry of fluid and melt inclusions in olivine of pico Basalts. J Petrol 55:377–393

Mi J-X, Pan Y (2018) Halogen-rich minerals: crystal chemistry and geological significances. In: Harlov DE, Aranovich L (eds) The role of halogens in terrestrial and extraterrestrial geochemical processes: surface, crust, and mantle. Springer, Berlin, pp 123–184

Michael PJ, Cornell WC (1998) Influence of spreading rate and magma supply on crystallization and assimilation beneath mid-ocean ridges: evidence from chlorine and major element chemistry of mid-ocean ridge basalts. J Geophys Res 103:18325–18356

Michel A, Villemant B (2003) Determination of halogens (F, Cl, Br, I), sulfur and water in seventeen geological reference materials. Geostand Newsl 27(2):163–171

Miller TL, Zoller WH, Crowe BM, Finnegan DL (1990) Variations in trace metal and halogen ratios in magmatic gases through an eruptive cycle of the Pu'u O'o vent, Kilauea, Hawaii: July–August 1985. J Geophys Res 95(B8):12607–12615

Mittlefehldt DW (2002) Geochemistry of the ungrouped carbonaceous chondrite Tagish Lake, the anomalous CM chondrite bells, and comparison with CI and CM chondrites. Meteorit Planet Sci 37:703–712

Moine BN, Cottin J-Y, Shepard SMF, Grégoire M, O'Reilly SY, Giret A (2000) Incompatible trace element and isotopic (D/H) characteristics of amphibole-and phlogopite-bearing ultramafic to mafic xenoliths from Kerguelen Islands (TAAF, South Indian Ocean). Eur J Mineral 12:761–777

Moldovanyi EP, Walter LM (1992) Regional trends in water chemistry, smackover formation, Southwest Arkansas: geochemical and physical controls (1). AAPG Bullet 76(6):864–894

Möller P, Weise SM, Althaus E, Bach W, Behr HJ, Borchardt R, Bräuer K, Drescher J, Erzinger J, Faber E, Hansen BT (1997) Paleofluids and recent fluids in the upper continental crust: results from the German Continental deep drilling program (KTB). J Geophys Res: Solid Earth 102 (8):18233–18254

Morad S, Ismail HB, Ros LD, Al-Aasm IS, Serrhini NE (1994) Diagenesis and formation water chemistry of Triassic reservoir sandstones from southern Tunisia. Sedimentology 41 (6):1253–1272

Morgan JW, Anders E (1979) Chemical composition of Mars. Geochim Cosmochim Acta 43:1601–1610
Morrison JA (1991) Chemistry of the polyhedral boron halides and the diboron tetrahalides. Chem Rev 91(1):35–48
Mungall JE, Brenan JM (2003) Experimental evidence for the chalcophile behavior of the halogens. Can Mineral 41:207–220
Munoz JL (1984) F-OH and Cl-OH exchange in micas with applications to hydrothermal ore deposits. Rev Mineral Geochem 13(1):469–493
Muramatsu Y, Wedepohl KH (1998) The distribution of iodine in the Earth's crust. Chem Geol 147:201–216
Muramatsu Y, Doi T, Tomaru H, Fehn U, Takeuchi R (2007) Halogen concentrations in pore waters and sediments of the Nankai Trough, Japan: implications for the origin of gas hydrates. Appl Geochem 22:534–556
Musashi M, Markl G, Kreulen R (1998) Stable chlorine-isotope analysis of rock samples: new aspects of chlorine extraction. Anal Chim Acta 362:261–269
Mysen BO, Richet P (2005) Silicate glasses and melts. Elsevier, Amsterdam
Mysen BO, Virgo D (1985) Structure and properties of fluorine-bearing aluminosilicate melts: the system Na_2O-Al_2O_3-SiO_2-F at 1 atm. Contrib Mineral Petrol 91(3):205–220
Mysen BO, Cody GD, Smith A (2004) Solubility mechanisms of fluorine in peralkaline and meta-aluminous silicate glasses and in melts to magmatic temperatures. Geochim Cosmochim Acta 68(12):2745–2769
Nahnybida T, Gleeson SA, Rusk BG, Wassenaar LI (2009) Cl/Br ratios and stable chlorine isotope analysis of magmatic–hydrothermal fluid inclusions from Butte, Montana and Bingham Canyon, Utah. Mineral Deposita 44(8):837–848
Nakamoto T, Oura Y, Ebihara M (2007) Comparative study of activation analyses for the determination of trace halogens in geological and cosmochemical samples. Anal Sci 23:1113–1119
Neal C, Smith CJ, Walls J, Billingham P, Hill S, Neal M (1990) Hydrogeochemical variations in Hafren forest stream waters, mid-Wales. J Hydrol 116(1):185–200
Noll K, Dobeli M, Krahenbühl U, Grambole D, Herrmann F, Koeberl C (2003) Detection of terrestrial fluorine by proton induced gamma emission (PIGE). A rapid quantification for Antarctic meteorites. Meteorit Planet Sci 38:759–765
O'Reilly SY, Griffin WL (2012) Mantle Metasomatism. In: Harlov DE, Austrheim H (eds) Metasomatism and the chemical transformation of rock (Lecture notes in Earth System Sciences). Springer, Berlin, pp 471–533
Oberti R, Ghose S (1993) Crystal-chemistry of a complex Mn-bearing alkali amphibole (tirodite') on the verge of exsolution. Eur J Mineral 5(6):1153–1160
Palme H, Jones A (2003) Solar system abundances of the elements. In: Holland HD, Turrekian KK (eds) Treatise on geochemistry, vol 1. Elsevier, Amsterdam, pp 41–61
Palme H, O'Neill H St C (2003) Cosmochemical estimates of mantle composition. In: Holland HD, Turrekia KK (eds) Treatise on geochemistry, vol 2. Elsevier, Amsterdam, pp 1–38
Pan Y, Dong P (2003) Bromine in scapolite-group minerals and sodalite: XRF microprobe analysis, exchange experiments, and application to skarn deposits. Can Mineral 41(2):529–540
Pauling L (1960) The nature of the chemical bond and the structure of molecules and crystals: an introduction to modern structural chemistry. Cornell University Press, Ithaca
Pauling L, Huggins ML (1934) Covalent radii of atoms and interatomic distances in crystals containing electron-pair bonds. Z Kristallogr-Cryst Mater 87(1):205–238
Pearson FJ (1985) Sondierbohrung Boettstein-results of hydrochemical investigations: analysis and interpretation. Nationale Genossenschaft fuer die Lagerung Radioaktiver Abfaelle NAGRA, Switzerland
Pearson DG, Canil D, Shirey S, Holland H, Turrekian KK (2003) Mantle samples included in volcanic rocks: xenoliths and diamond. In: Holland HD, Turrekian KK (eds) Treatise on geochemistry, vol 2. Elsevier, Amsterdam, pp 171–275

Peters MT, Baker MB, Burnett DS (1995) The partitioning of iodine between sulfide liquid and silicate liquid: implications for the cosmochemistry of iodine. Lunar Planet Sci Conf 26:1115–1116

Peters NE, Ratcliffe ER, Tranter M (1998) Tracing solute mobility at the Panola Mountain Research Watershed, Georgia, USA. In: Kovar K, Tappeiner U, Peters NE, Craig RG (eds) Hydrology, water resources and ecology in headwaters, vol 248. IAHS, Wallingford

Philippot P, Agrinier P, Scambelluri M (1998) Chlorine cycling during subduction of altered oceanic crust. Earth Planet Sci Lett 161(1):33–44

Piccoli PM, Candela PA (1993) Magmatic-Hydrothermal volatile history of the Billy Lake-Rush Creek volcano-plutonic complex, ritter range, Sierra Nevada Batholith, California. EOS Trans Am Geophys Union 74:333

Price NB, Calvert SE (1970) Compositional variation in Pacific Ocean ferromanganese nodules and its relationship to sediment accumulation rates. Mar Geol 9(3):145–171

Price NB, Calvert SE (1977) The contrasting geochemical behaviours of iodine and bromine in recent sediments from the Namibian shelf. Geochim Cosmochim Acta 41(12):1769–1775

Pyle DM, Mather T (2009) Halogens in igneous processes and their fluxes to the atmosphere and oceans from volcanic activity: a review. Chem Geol 263:110–121

Rabinovich EM (1983) Structural role of fluorine in silicate glasses. Phys Chem Glasses 24 (2):54–56

Ramberg H (1952) Chemical bonds and distribution of cations in silicates. J Geol 1:331–355

Rampe EB, Ming DW, Blake DF et al (2017) Mineralogy of an ancient lacustrine mudstone succession from the Murray formation, Gale crater, Mars. Earth Planet Sci Lett 471:172–185. https://doi.org/10.1016/j.epsl.2017.04.021

Rampe EB, Cartwright JA, McCubbin FM, Osterloo MM (2018) The role of halogens during fluid and magmatic processes on Mars. In: Harlov DE, Aranovich L (eds) The role of halogens in terrestrial and extraterrestrial geochemical processes: surface, crust, and mantle. Springer, Berlin, pp 959–995

Reed GW Jr (1964) Fluorine in stone meteorites. Geochim Cosmochim Acta 28:1729–1743

Reed GW Jr, Ralph OA Jr (1966) Halogens in chondrites. Geochim Cosmochim Acta 30:779–800

Renno AD, Franz L, Witzke T, Herzig PM (2004) The coexistence of melts of hydrous copper chloride, sulfide and silicate compositions in a magnesiohastingsite cumulate, TUBAF seamount, Papua New Guinea. Can Mineral 42:1–16

Ringwood AE (1962a) A model for the upper mantle. J Geophys Res: Solid Earth 67:857–867

Ringwood AE (1962b) A model for the upper mantle: 2. J Geophys Res: Solid Earth 67:4473–4478

Rose-Koga EF, Shimizu N, Devidal J, Koga KT, Le Voyer M (2008) Investigation of F, S, and Cl standards by ion probe and electron microprobe. EOS Trans Am Geophys Union 89(53), Fall Meet Suppl, Abstract V31B-2145

Rose-Koga EF, Koga KT, Schiano P, Le Voyer M, Shimizu N, Whitehouse MJ, Clocchiatti R (2012) Mantle source heterogeneity for South Tyrrhenian magmas revealed by Pb isotopes and halogen contents of olivine-hosted melt inclusions. Chem Geol 334:266–279

Rose-Koga EF, Koga KT, Hamada M, Helouis T, Whitehouse MJ, Shimizu N (2014) Volatile (F and Cl) concentrations in Iwate olivine-hosted melt inclusions indicating low-temperature subduction. Earth Planet Space 66:81

Rose-Koga EF, Koga KT, Moreira M, Vlastelic I, Jackson MG, Whitehouse MJ, Shizimu N, Habib N (2017) Geochemical systematics of Pb isotopes, fluorine and sulfur in melt inclusions from São Miguel, Azores. Chem Geol 458:22–37

Rosenbaum JM, Cliff RA, Coleman ML (2000) Chlorine stable isotopes: a comparison of dual inlet and thermal ionization mass spectrometric measurements. Anal Chem 72:2261–2264

Rosenthal A, Hauri EH, Hirschmann MM (2015) Experimental determination of C, F, and H partitioning between mantle minerals and carbonated basalt, CO_2/Ba and CO_2/Nb systematics of partial melting, and the CO_2 contents of basaltic source regions. Earth Planet Sci Lett 412:77–87

Ross JE, Aller LH (1976) The chemical composition of the Sun. Science 191:1223–1229

Rudnick RL, Gao S (2003) Composition of the continental crust. In: Holland HD, Turekian KK (eds) Treatise on geochemistry, vol 3. Elsevier, Amsterdam, pp 1–64

Ryan CG, Heinrich CA, Mernagh TP (1993) PIXE Microanalysis of fluid inclusions and its application to study ore metal segregation between magmatic brine and vapor. Nucl Instrum Methods Phys Res Sect B: Beam Interact Mat Atom 77:463–471

Saal AE, Hauri EH, Langmuir CH, Perfit MR (2002) Vapour undersaturation in primitive mid-ocean-ridge basalt and the volatile content of Earth's upper mantle. Nature 419:451–455

Saal AE, Hauri EH, Cascio ML, Van Orman JA, Rutherford MJ, Cooper RF (2008) Volatile content of lunar volcanic glasses and the presence of water in the Moon's interior. Nature 454:192–195

Sakai N, Takemura K, Tsuji K (1982) Electrical properties of high-pressure metallic modification of iodine. J Phys Soc Jpn 516:1811–1816

Salminen R (ed), Batista MJ, Bidovec M, Demetriades A, De Vivo B, De Vos W, Duris M, Gilucis A, Gregorauskiene V, Halamic J, Heitzmann P, Lima A, Jordan G, Klaver G, Klein P, Lis J, Locutura J, Marsina K, Mazreku A, O'Connor PJ, Olsson SÅ, Ottesen R-T, Petersell V, Plant, JA, Reeder S, Salpeteur I, Sandström H, Siewers U, Steenfelt A, Tarvainen T (2005) Geochemical atlas of Europe. Part 1: background information, methodology and maps. Geological Survey of Finland, Espoo

Salters VJM, Stracke A (2004) Composition of the depleted mantle. Geochem Geophys Geosyst 5:1525–2027

Sander R, Keene WC, Pszenny AA, Arimoto R, Ayers GP, Baboukas E, Cainey JM, Crutzen PJ, Duce RA, Hönninger G, Huebert BJ (2003) Inorganic bromine in the marine boundary layer: a critical review. Atmos Chem Phys 3(5):1301–1336

Sanders LL (1991) Geochemistry of formation waters from the Lower Silurian Clinton formation (Albion Sandstone), Eastern Ohio. AAPG Bullet 75(10):1593–1608

Sarafian AR, Roden MF, Patiño-Douce AE (2013) The volatile content of Vesta: clues from apatite in eucrites. Meteorit Planet Sci 48:2135–2154

Schaller T, Dingwell DB, Keppler H, Knöller W, Merwin L, Sebald A (1992) Fluorine in silicate glasses: a multinuclear nuclear magnetic resonance study. Geochim Cosmochim Acta 56:701–707

Schauble EA, Rossman GR, Taylor HP (2003) Theoretical estimates of equilibrium chlorine-isotope fractionations. Geochim Cosmochim Acta 67(17):3267–3281

Schilling JG, Unni CK, Bender ML (1978) Origin of chlorine and bromine in the oceans. Nature 273:631–636

Schilling J, Bergeron M, Evans R (1980) Halogens in the mantle beneath the North Atlantic. Philos Trans R Soc A297:147–178

Schnetger B, Muramatsu Y (1996) Determination of halogens, with special reference to iodine, in geological and biological samples using pyrohydrolysis for preparation and inductively coupled plasma mass spectrometry and ion chromatography for measurement. Analyst 121 (11):1627–1631

Sekimoto S, Ebihara M (2013) Accurate determination of chlorine, bromine, and iodine in sedimentary rock reference samples by radiochemical neutron activation analysis and a detailed comparison with inductively coupled plasma mass spectrometry literature data. Anal Chem 85:6336–6341

Seo JH, Guillong M, Aerts M, Zajacz Z, Heinrich CA (2011) Microanalysis of S, Cl, and Br in fluid inclusions by LA-ICP-MS. Chem Geol 284:35–44

Sharp ZD, Draper DS (2013) The chlorine abundance of Earth: implications for a habitable Planet. Earth Planet Sci Lett 369–370:71–77

Sharp ZD, Mercer JA, Jones RH, Brearley AJ, Selverstone J, Bekker A, Stachel T (2013) The chlorine isotope composition of chondrites and Earth. Geochim Cosmochim Acta 107:189–204

Shaw AM, Behn MD, Humphris SE, Sohn RA, Gregg PM (2010) Deep pooling of low degree melts and volatile fluxes at the 85°E segment of the Gakkel Ridge: evidence from olivine-hosted melt inclusions and glasses. Earth Planet Sci Lett 289:311–322

Shimizu K, Yamauchi T, Tamitani N, Takeshita N, Ishizuka M, Amaya K, Endo S (1994) The pressure-induced superconductivity of iodine. J Supercond 7(6):921–924
Shimizu K, Alberto ES, Corinne EM, Ashley NN, Erik HH, Donald WF, Vadim SK, Yaoling N (2016) Two-component mantle melting-mixing model for the generation of mid-ocean ridge basalts: implications for the volatile content of the Pacific upper mantle. Geochim Cosmochim Acta 176:44–80
Shinohara H, Iiyama JT, Matsuo S (1989) Partition of chlorine compounds between silicate melt and hydrothermal solutions: I. partition of NaCl-KCl. Geochim Cosmochim Acta 53 (10):2617–2630
Shouakar-Stash O, Frape SK, Drimmie RJ (2005) Determination of bromine stable isotopes using continuous-flow isotope ratio mass spectrometry. Anal Chem 77:4027–4033
Shouakar-Stash O, Alexeev SV, Frape SK, Alexeeva LP, Drimmie RJ (2007) Geochemistry and stable isotopic signatures, including chlorine and bromine isotopes, of the deep groundwaters of the Siberian Platform, Russia. Appl Geochem 22(3):589–605
Simpson WR, Brown SS, Saiz-Lopez A, Thornton JA, Glasow RV (2015) Tropospheric Halogen Chemistry: sources, cycling, and impacts. Chem Rev 115:4035–4062
Smart RP, Soulsby C, Cresser MS, Wade A, Townend J, Billett MF, Langan SJ (2001) Riparian zone influence on stream water chemistry at different spatial scales: a GIS based modelling approach, an example for the Dee, NE Scotland. Sci Total Environ 280:173–193
Starinsky A (1974) Relationship between Ca-chloride brines and sedimentary rocks in Israel. Doctoral dissertation
Stix J, Layne GD, Spell TL (1995) The behavior of light lithophile and halogen elements in felsic magma: geochemistry of the post-caldera Valles Rhyolites, Jemez Mountains Volcanic Field, New Mexico. J Volcanol Gertherm Res 67:61–77
Straub SM, Layne GD (2003) The systematics of chlorine, fluorine, and water in Izu arc front volcanic rocks: implications for volatile recycling in subduction zones. Geochim Cosmochim Acta 67:4179–4203
Stromer JC, Pierson ML, Tacker RC (1993) Variation of F and Cl X-ray intensity due to anisotropic diffusion in apatite during electron microprobe analysis. Am Mineral 78:641–648
Stueber AM, Walter LM (1991) Origin and chemical evolution of formation waters from Silurian-Devonian strata in the Illinois basin, USA. Geochim Cosmochim Acta 55(1):309–325
Stueber AM, Walter LM, Huston TJ, Pushkar P (1993) Formation waters from Mississippian-Pennsylvanian reservoirs, Illinois basin, USA: chemical and isotopic constraints on evolution and migration. Geochim Cosmochim Acta 57(4):763–784
Sugiura T (1968) Bromine to chlorine ratios in igneous rocks. Bull Chem Soc Jpn 41 (5):1133–1139
Sumino H, Burgess R, Mizukami T, Wallis SR, Holland G, Ballentine CJ (2010) Seawater-derived noble gases and halogens preserved in exhumed mantle wedge peridotite. Earth Planet Sci Lett 294:163–172
Svensen H, Jamtveit B, Banks DA, Austrheim H (2001a) Halogen contents of eclogite facies fluid inclusions and minerals: Caledonides, Western Norway. J Metamorph Geol 19:165–178
Svensen H, Jamtveit B, Banks DA, Karlsen D (2001b) Fluids and halogens at the diagenetic-metamorphic boundary: evidence from veins in continental basins, Western Norway. Geofluids 1:53–70
Swindle TD, Caffee MW, Hohenberg CM, Taylor SR (1986) I-Pu-Xe dating and the relative ages of the earth and moon. In: Hartmann WK, Phillips RJ, Taylor GJ (eds) Origin of the moon. Lunar Planet Institute, Houston, pp 331–357
Swindle TD, Caffee MW, Hohenberg CM, Lindstrom MM, Taylor GJ (1991) Iodine-xenon studies of petrographically and chemically characterized Chainpur chondrules. Geochim Cosmochim Acta 55(3):861–880
Symonds RB, Rose WI, Bluth GJ, Gerlach TM (1994) Volcanic-gas studies; methods, results, and applications. Rev Mineral Geochem 30(1):1–66
Taylor GJ (2013) The bulk composition of Mars. Chem Erde-Geochem 73:401–420

Teague AJ, Hanley J, Seward TM, Reutten F (2011) Trace-element distribution between coexisting aqueous fumarole condensates and natrocarbonatite lavas at Oldoinyo Lengai volcano, Tanzania. Geol Soc Am Spec Pap 478:159–172
Turekian KK, Wedepohl KH (1961) Distribution of the elements in some major units of the Earth's crust. Geol Soc Am Bull 72:175–192
Unni CK, Schilling JG (1977) Determination of bromine in silicate rocks by epithermal neutron activation analysis. Anal Chem 49:1998–2000 (Washington, D.C.)
Unni CK, Schilling JG (1978) Cl and Br degassing by volcanism along the Reykjanes Ridge and Iceland. Nature 272:19–23
Urey HC (1947) The thermodynamic properties of isotopic substances. J Chem Soc 562–581. https://doi.org/10.1039/JR9470000562 (London)
Van den Bleeken G, Koga KT (2015) Experimentally determined distribution of fluorine and chlorine upon hydrous slab melting, and implications for F-Cl cycling through subduction zones. Geochim Cosmochim Acta 171:353–373
Vasyukova O, Williams-Jones AE (2014) Fluoride–silicate melt immiscibility and its role in REE ore formation: evidence from the Strange Lake rare metal deposit, Québec-Labrador, Canada. Geochim Cosmochim Acta 139:110–130
Vasyukova O, Williams-Jones AE (2016) The evolution of immiscible silicate and fluoride melts: implications for REE ore-genesis. Geochim Cosmochim Acta 172:205–224
Veksler IV, Dorfman AM, Kamanetsky M, Dulski P, Dingwell DB (2005) Partitioning of lanthanides and Y between immiscible silicate and fluoride melts, fluorite and cryolite and the origin of the lanthanide tetrad effect in igneous rocks. Geochim Cosmochim Acta 69:2847–2860
Veksler IV, Dorfman AM, Dulski P, Kamenetsky VS, Danyushevksy LV, Jeffries T, Dingwell DB (2012) Partitioning of elements between silicate melt and immiscible fluoride, chloride, carbonate, phosphate and sulfide melts, with implications to the origin of natrocarbonatite. Geochim Cosmochim Acta 79:20–40
Vigneresse JL (2009) Evaluation of the chemical reactivity of the fluid phase through hard–soft acid–base concepts in magmatic intrusions with applications to ore generation. Chem Geol 263 (1):69–81
Vinogradov AP (1961) The origin of the material of the Earth's crust. Communication 1(1):1–52
Volfinger M, Robert JL, Vielzeuf D, Neiva AM (1985) Structural control of the chlorine content of OH-bearing silicates (micas and amphiboles). Geochim Cosmochim Acta 49(1):37–48
Vovk IF (1987) Radiolytic salt enrichment and brines in the crystalline basement of the East European platform. In: Fritz P, Frape SK (eds) Saline water and gases in crystalline rocks. Geological Association of Canada (Special Paper 33). The Runge, Ottawa, pp 197–210
Wallace P, Anderson AT (2000) Volatiles in magmas. In: Sigurdsson H, Houghton BF, Mcnutt SR, Rymer H, Stix J (eds) Encyclopedia of volcanoes. Academic, San Diego, pp 149–170
Wang X, Li G, Zhang Q, Wang Y (2004) Determination of major, minor and trace elements in seamount phosphorite by XRF spectrometry. Geostand Geoanal Res 28:81–88
Wänke H, Dreibus G (1988) Chemical composition and accretion history of terrestrial planets. Philos Trans R Soc London Ser A 325:545–557
Wänke H, Baddenhausen H, Palme H (1974) On the chemistry of the Allende inclusions and their origin as high temperature condensates. Earth Planet Sci Lett 23:1–7
Wanless VD, Shaw AM (2012) Lower crustal crystallization and melt evolution at mid-ocean ridges. Nat Geosci 5:651–655
Wasson JT, Kallemeyn GW (1988) Compositions of chondrites. Philos Trans R Soc A: Math Phys Eng Sci 325:535–544
Webster JD, Holloway JR (1990) Partitioning of F and Cl between magmatic hydrothermal fluids and highly evolved granitic magmas. Geol Soc Am Spec Pap 246:21–34
Webster JD, Holloway JR, Hervig RL (1989) Partitioning of lithophile trace elements between H_2O and $H_2O + CO_2$ fluids and topaz rhyolite melt. Econ Geol 84(1):116–134

Webster JD, Tappen CM, Mandeville CW (2009) Partitioning behavior of chlorine and fluorine in the system apatite–melt–fluid. II: Felsic silicate systems at 200 MPa. Geochim Cosmochim Acta 73(3):559–581

Webster JD, Baker DR, Aiuppa A (2018) Halogens in mafic and intermediate-silica content magmas. In: Harlov DE, Aranovich L (eds) The role of halogens in terrestrial and extraterrestrial geochemical processes: surface, crust, and mantle. Springer, Berlin, pp 307–430

Wedepohl KH (1987) The chlorine and sulfur crustal cycle–abundance of evaporites. Geochemistry and mineral formation in the Earth surface, p 3–27

Wedepohl KH (1995) The composition of the continental crust. Geochim Cosmochim Acta 59:1217–1239

Wedepohl KH, Hartmann G (1994) The composition of the primitive upper Earth's mantle. In: Meyer HOA, Leonardos OH (eds) Kimberlites, related rocks and mantle xenoliths. Companhia de Pesquisa de Recursos Minerais, Rio de Janeiro, 1, pp 486–495

Whitfield M, Turner DR (1972) Water–rock partition coefficients and the composition of seawater and river water. Nature 278:132–137

Wilson TRS (1975) Salinity and the major elements of seawater. In: Riley JP, Skirrow G (eds) Chemical oceanography. Academic, New York, pp 365–413

Wilson TP, Long DT (1993a) Geochemistry and isotope chemistry of Michigan Basin brines: Devonian formations. Appl Geochem 8(1):81–100

Wilson TP, Long DT (1993b) Geochemistry and isotope chemistry of Ca Na Cl brines in Silurian strata, Michigan Basin, USA. Appl Geochem 8(1):81–100

Witter JB, Kuehner SM (2004) A simple empirical method for high-quality electron microprobe analysis of fluorine at trace levels in Fe-bearing minerals and glasses. Am Mineral 89:57–63

Wong GTF, Brewer PG (1974) The determination and distribution of iodate in South Atlantic waters. J Mar Res 32(1):25–36

Woosley SE, Haxton WC (1988) Supernova neutrinos, neutral currents and the origin of fluorine. Nature 334:45–47

Worden RH (1996) Controls on halogen concentrations in sedimentary formation waters. Mineral Mag 60(399):259–274

Worden RH (2018) Halogen elements in sedimentary systems and their evolution during diagenesis. In: Harlov DE, Aranovich L (eds) The role of halogens in terrestrial and extraterrestrial geo-chemical processes: surface, crust, and mantle. Springer, Berlin, pp 185–260

Workman RK, Hart SR (2005) Major and trace element composition of the depleted MORB mantle (DMM). Earth Planet Sci Lett 231:53–72

Workman RK, Hart SR, Jackson MG, Regelous M, Farley KA, Blusztajn J, Kurz MD, Staudigel H (2004) Recycled metasomatized lithosphere as the origin of the Enriched Mantle II (EM2) end-member: evidence from the Samoan Volcanic Chain. Geochem Geophys Geosys 5: Q04008

Workman RK, Hauri EH, Hart SR, Wang J, Blusztajn J (2006) Volatile and trace elements in basaltic glasses from Samoa: implications for water distribution in the mantle. Earth Planet Sci Lett 241:932–951

Wu J, Koga KT (2013) Fluorine partitioning between hydrous minerals and aqueous fluid at GPa and 770–947 °C: a new constraint on slab flux. Geochim Cosmochim Acta 119:77–92

Wyllie PJ, Tuttle OF (1964) Experimental investigation of silicate systems containing two volatile components. Part III. The effects of SO_3, P_2O_5, HCl, and Li_2O, in addition to H_2O, on the melting temperatures of albite and granite. Am J Sci 262:930–939

Xiao YK, Zhang CG (1992) High precision isotopic measurements of chlorine by thermal ionization mass spectrometry of the Cs_2Cl^+ ion. Int J Mass Spectrom Ion Process 116:183–192

Yardley BW (2005) 100th anniversary special paper: metal concentrations in crustal fluids and their relationship to ore formation. Econ Geol 100(4):613–632

Yardley BW (2009) The role of water in crustal evolution. J Geol Soc London 166:613–632

Yardley BW (2013) The chemical composition of metamorphic fluids in the crust. In: Harlov DE, Austrheim H (eds) Metasomatism and the chemical transformation of rock. Springer, Berlin, pp 17–51

Yardley BW, Bodnar RJ (2014) Fluids in the continental crust. Geochem Perspect 3(1):127
Yardley BW, Graham JT (2002) Origins of salinity in metamorphic fluids. Geofluids 2:249–256
Yardley BW, Banks DA, Bottrell SH, Diamond LW (1993) Post-metamorphic gold-quartz veins from NW Italy: the composition and origin of the ore fluid. Mineral Mag 57:407
Yardley BW, Banks DA, Barnicoat AC (2000) The chemistry of crustal brines: tracking their origins. In: Porter TM (ed) Hydrothermal iron oxide coper gold and related deposits: a global perspective. Australian Mineral Foundation, Adelaide, pp 61–70
Yuita K (1984) Iodine, bromine and chlorine content of soils and plants of Japan, 2: Iodine, bromine and chlorine content of the andosols and plants of central Honshu [Japan]. Jpn J Soil Sci Plant Nutr, Japan
Zeng Q, Stebbins JF (2000) Fluoride sites in aluminosilicate glasses: high-resolution 19F NMR results. Am Mineral 85(5–6):863–867
Zherebtsova IK, Volkova NN (1966) Experimental study of the behavior of trace elements in the process of natural solar evaporation of Black Sea water and Sasyk-Sivash brine. Geochem Int 3:656–670

Chapter 3
Halogen-Rich Minerals: Crystal Chemistry and Geological Significances

Jin-Xiao Mi and Yuanming Pan

Abstract Halogen-rich minerals containing at least one halogen (F, Cl, Br or I) on a dominant crystallographic site can be divided into three broad groups: (1) halides, (2) halogenates, and (3) native halogens. There are approximately 700 halogen-rich minerals in the 09/2014 list of species approved by the International Mineralogical Association (IMA), accounting for ~15% of the entire mineral kingdom known to date. Still scores of other minerals contain significant amounts of F and/or Cl, especially in many hydrous minerals via the copious substitution $(F,Cl)^- = OH^-$. Amphiboles, micas and apatites are the dominant carriers of halogens in most rocks, whereas scapolites and sodalites serve as important hosts of these elements in some exotic lithologies. These minerals not only play important roles in controlling the halogen geochemical cycles but also are useful for calcuating the halogen composition and evolution of fluids/melts from which they crystallized.

3.1 Introduction

Halogen-rich minerals are herein defined as species containing at least one halogen (F, Cl, Br or I) dominant site in the crystal lattices and occur in almost all rock types and some meteorites. Halogen-rich minerals are critical to many human activities and are the sources for some of the most important materials that form the cornerstones of modern agriculture and industries. For example, halite [NaCl] or the common salt is needed for the very survival of human bodies and has been mined from sedimentary deposits or extracted from brines since antiquity. Fluorite [CaF_2]

J.-X. Mi (✉)
Fujian Provincial Key Laboratory of Advanced Materials, Department of Materials Science and Engineering College of Materials, Xiamen University, 361005 Xiamen, People's Republic of China

Y. Pan
Department of Geological Sciences, University of Saskatchewan, 114 Science Place, SK S7N 5E2 Saskatoon, Canada
e-mail: yuanming.pan@usask.ca

D.E. Harlov and L. Aranovich (eds.), *The Role of Halogens in Terrestrial and Extraterrestrial Geochemical Processes*, Springer Geochemistry,
https://doi.org/10.1007/978-3-319-61667-4_3

or fluorspar deposits, that are usually associated with alkaline and acid igneous intrusions (Gagnon et al. 2003; González-Partida et al. 2003; Dill et al. 2012), are mined as the principal source of F for the chemical industry. Sylvite [KCl] and carnallite [$KMgCl_3 \cdot 6H_2O$], from giant evaporite basins such as the Middle Devonian Prairie Evaporite Formation in the Williston Basin of western Canada and the Permian Zeichstein evaporites of Europe, are mined mainly as potash fertilizers (Holter 1969; Lowenstein and Spencer 1990). Similarly, fluorapatite [$Ca_{10}(PO_4)_6(F, OH)_2$] is often the principal mineral of marine phosphorite and igneous phosphate deposits that are extracted for phosphate fertilizers and other industrial applications (Pan and Fleet 2002). In addition, halogen-rich minerals are occasionally the main carriers of metals in mineral deposits (e.g., bastnäsites [$(Ce,La,Nd,Y)(CO_3)F$] in the Bayan Obo REE deposit, Chao et al. 1997; Ling et al. 2012).

Other halogen-rich minerals, which may be less common or even rare in nature, possess attractive physical properties and often inspire the discovery and development of synthetic analogues for technological applications. For example, herbertsmithite [$Cu_3Zn(OH)_6Cl_2$] is a prototype compound for strongly correlated spin frustration and has attracted great interest in potential applications such as quantum spin liquids, high-temperature superconductors, and molecular magnets (Han et al. 2012; Welch et al. 2014; Zhu et al. 2014; Sun et al. 2016). Similarly, discoveries of unusual optical and magnetic properties in rare-earth fluoride minerals have given impetus to the research and development of similar materials for diverse industrial applications such as catalysts, lasers, permanent magnets, phosphors, and solid-oxide fuel-cell electrodes and electrolytes (Grice et al. 2007; Piilonen et al. 2010). This chapter starts with a section on the crystal chemistry of halogen-rich minerals and continues with a synthesis on halogens in rock-forming minerals, with emphasis on applications to the evaluation of the halogen chemistry and the evolution of the fluids/melts from which they crystallized.

3.2 Crystal Chemistry of Halogen-Rich Minerals

Halogen-rich minerals can first be divided into three broad groups: (1) halides, (2) halogenates, and (3) native halogens. Here, halide minerals are defined in the broadest sense and include all species containing at least one halide (F^-, Cl^-, Br^- or I^-) dominant site in the crystal lattices, whereas halogenate minerals are restricted to a small number of iodates. The existence of native halogens remain questionable (see below). Crystal-chemical syntheses of some halide minerals are available (e.g., aluminofluorides, Hawthorne 1984; fluorcarbonates, Grice et al. 2007). In this section we use selected examples to illustrate some of the most salient crystal-chemical features of halogen-rich minerals, rather than present a comprehensive description of all species. It should be pointed out that our definition of halogen-rich minerals, on the basis of at least one halogen-dominant crystallographic site, is not completely satisfactory, because it excludes some minerals containing significant but subordinate halogens at individual site(s). For example,

pyrosmalites [$(Fe,Mn)_8Si_6O_{15}(OH)_{10}$], containing up to 5.14 wt% Cl (Pan et al. 1993a), are excluded from halogen-rich minerals defined herein.

3.2.1 Native Halogens?

Of the four stable halogens, only iodine appears as a native element in the IMA list of approved minerals but carries the designation Q (i.e., questionable status). This mineral was grandfathered on the basis of its pre-IMA description as a sublimation product of fumaroles from the 1895 Mt. Vesuvius eruption (Matteucci 1897) but lacks adequate characterization. While halogen mineralogy and geochemistry of volcanic fumaroles, including those at Mt. Vesuvius, have been the subjects of much research over the last century, there have been no reports of native iodine or bromine (Pelloux 1927; Cruciani et al. 2005; Zalenski et al. 2006; Demartin et al. 2010). Synthetic solid halogens are isostructural with strongly covalent diatomic molecules (I_2, Br_2 and Cl_2) linked by characteristic halogen bonds of the type I-I…I, Br-Br…Br and Cl-Cl…Cl (Desiraju et al. 2013; Cavallo et al. 2016) in face-centered orthorhombic unit cells, do not exhibit any phase transitions from the lowest temperatures investigated to their respective melting points (Powell et al. 1984; Petrillo et al. 1992), but undergo complex phase transitions at high pressures (Mukose et al. 2002; Kenichi et al. 2003; Wu et al. 2016).

3.2.2 Halide Minerals

Table 3.1 is based on the IMA's 09/2014 list and subdivides fluorides and chlorides into simple and complex types, whereas the number of bromides and iodides is too small to warrant such subdivisions. Simple halides include those containing halides as the only anions as well as those with other simple anions such as O^{2-}, OH^- and S^{2-}. Complex halides are composed of a mixture of halide anions and various oxyanion group(s) such as CO_3^{2-}, $PO_4^{3-}$and SiO_4^{4-}. Also included in complex halides are those containing the rare fluorophosphate and fluorosulfate anion groups: e.g., bobdownsite [$(Ca_9Mg(PO_3F)(PO_4)_6]$ (Tait et al. 2011) and reederite-(Y) [$(Na,Mn,Fe)_{15}(Y,REE)_2(CO_3)_9(SO_3F)Cl$] (Grice et al. 1995).

Of the approximately 700 halide minerals, fluorides and chlorides predominate (Table 3.1). A few minerals contain two or three halogens as major constituents: e.g., kelyanite [$Hg_{12}SbO_6BrCl_2$] and vasilyevite [$(Hg_2)^{2+}_{10}O_6I_3Br_2Cl(CO_3)$]. The large number of fluoride minerals, including many rock-forming minerals (see below), is attributable to not only the relatively high crustal abundance of F but also the unique chemistry of the F^- anion (Hanley and Koga 2018). Indeed, the high electronegativity, strong reactivity and small ionic radius of the F^- anion make it possible to synthesize fluorides with almost all elements in the periodic table, including heavy rare-gas fluorides (e.g., [XeF_4] and [XeF_6]). Also, the similarity in

Table 3.1 Frequencies of major elements in halide minerals

Fluorides				Chlorides				Bromides		Iodides	
Simple		Complex		Simple		Complex					
#	71	#	260	#	127	#	192	#	9	#	12
Al	31	O	260	O	76	O	192	Hg	6	Hg	7
Na	23	Si	139	H	66	H	95	O	4	Cl	5
H	21	Ca	117	Cu	32	Na	60	Cl	3	S	5
O	21	Na	115	Pb	31	Ca	59	S	3	Ag	3
Ca	19	H	91	Hg	18	Si	59	H	2	O	3
Pb	9	Al	90	K	17	Pb	49	Ag	1	Br	2
REE	9	P	55	S	16	S	45	Bi	1	As	1
Cl	8	REE	54	Fe	14	Cu	38	C	1	Bi	1
K	8	Mg	53	Mg	13	Al	37	Cu	1	C	1
Mg	8	C	37	F	8	B	29	F	1	Cu	1
Si	7	K	38	Ca	7	K	27	I	1	Pb	1
Sr	7	Ba	32	N	7	Fe	26	Sb	1		
Ba	5	Ti	32	Ag	6	As	22				
B	4	Fe	30	Al	6	C	19				
Li	4	S	29	I	5	Mg	16				
Cu	3	Mn	24	Na	5	Ba	15				
N	3	Li	22	Bi	4	Mn	12				
Ag	1	B	16	Ni	4	F	11				
Bi	1	Cl	11	Mn	4	Se	11				
Br	1	Nb	10	Sb	4	Zr	11				
		Sr	10	Tl	4	Te	9				
		Be	9	Zn	3	N	6				
		As	8	Sn	2	Ti	6				
		Zr	8	Te	2	V	6				
		Pb	7	As	1	P	5				
		U	5	Ba	1	Sr	5				
		Cu	3	Br	1	Zn	5				
		Cs	3	Cd	1	Bi	4				
		V	3	Cr	1	Sb	4				
		Cr	2	Co	1	REE	4				
		Ta	2			Hg	3				
		Zn	2			W	3				
		Bi	1			Cd	2				
		Cd	1			Cr	2				
		Ge	1			I	2				
		N	1			Nb	2				
		Sb	1			Br	2				
		Sn	1			Ag	1				
		Rb	1			Be	1				
		Th	1			Mo	1				
						U	1				

refers the total number of minerals in each category; REE includes Ce, La, Nd and Y

ionic radii between F^- and OH^- makes them substitute for each other easily in minerals. In contrast, Cl^- is substantially larger than OH^-, severely restricting its uptake in hydroxyl minerals and giving rise to extremely distorted polyhedra (e.g., $[MgO_4Cl]$, $[MgO_4Cl_2]$ and $[MgO_4Br_2]$ in boracites; Zhou et al. 2016, 2017). Chloride minerals, albeit large in number (Table 3.1), are much less common than their fluoride counterparts in most rock types.

3.2.2.1 Simple Halides of the Closest Packing Structures

The structures of many simple halides can be described by anions or cations in the closest packing schemes. For example, the halite-, fluorite-, sphalerite-, and $CdCl_2$-type structures involving the cubic closest packing scheme are featured by many simple halides (Tables 3.2, 3.3, 3.4 and 3.5), whereas the hexagonal closest packing mode is represented by iodargyrite [AgI] and sellaite $[MgF_2]$.

The halite structure (space group $Fm\bar{3}m$) consists of the cubic closest packing of Cl anions (Cl^-) with Na cations (Na^+) occupying the octahedral voids (Fig. 3.1a). The ($NaCl_6$) octahedra are linked by sharing edges and each edge is common to two octahedra. At ambient conditions, many halide minerals (Table 3.2) adopt the

Table 3.2 Halide minerals with the halite-type structure

Minerals	Formula	Unit cell (Å)	Cation–Anion (Å)	Reference
Griceite	LiF	a = 4.0263(1)	2.013 (× 6)	Thewlis (1955)
Villiaumite	NaF	a = 4.6340(1)	2.317 (× 6)	Deshpande (1961)
Varobbiite	KF	a = 5.367(10)	2.683 (× 6)	Finch and Fordham (1936)
Chlorargyrite	AgCl	a = 5.5463(2)	2.773 (× 6)	Hull and Keen (1999)
Halite	NaCl	a = 5.6418(2)	2.821 (× 6)	Fontana et al. (2011)
Sylvite	KCl	a = 6.2879	3.143 (× 6)	Walker et al. (2004)
Bromargyrite	AgBr	a = 5.7721(2)	2.886 (× 6)	Hull and Keen (1999)

Table 3.3 Halide minerals with the fluorite-type and derivative structures

Minerals	Formula	Cation–Anion (Å)	Reference
Fluorite	CaF_2	2.366 (Ca–F)	Speziale and Duffy (2002)
Strontiofluorite	SrF_2	2.511 (Sr–F)	Yakovenchuk et al. (2010a)
Fluorocronite	PbF_2	2.572 (Pb–F)	Mills et al. (2011)
Frankdicksonite	BaF_2	2.683 (Ba–F)	Radtke and Brown (1974)
Hieratite	K_2SiF_6	1.683(Si–F), 2.900(K–F)	Hester et al. (1993)
Cryptohalite	$(NH_4)_2SiF_6$	1.688(Si–F), 2.996(NH_4–F)	Schlemper and Hamilton (1966)
Panichiite	$(NH_4)_2SnCl_6$	2.429(Sn–Cl), 3.559(NH_4–Cl)	Demartin et al. (2009)
Håleniusite-(La)	LaOF	2.437 (La–F)	Holtstam et al. (2004)

Table 3.4 Halide minerals with the sphalerite-type and derivative structures

Minerals	Formula	Cation–Anion (Å)	Reference
Nantokite	CuCl	2.347 (× 4)	Hull and Keen (1994)
Marshite	CuI	2.625 (× 4)	Cooper and Hawthorne (1997)
Miersite	AgI	2.814 (× 4)	Hull and Keen (1999)
Gananite	BiF_3	mean = 2.710	Hund and Frick (1949)

Table 3.5 Halide minerals with the $CdCl_2$-type structure

Minerals	Formula	Cation–Anion (Å)	Reference
Chloromagnesite	$MgCl_2$	2.487 (× 6)	Partin and OKeeffe (1991)
Lawrencite	$FeCl_2$	2.488 (× 6)	Vettier and Yelon (1975)
Scacchite	$MnCl_2$	2.552 (× 6)	Tornero and Fayos (1990)

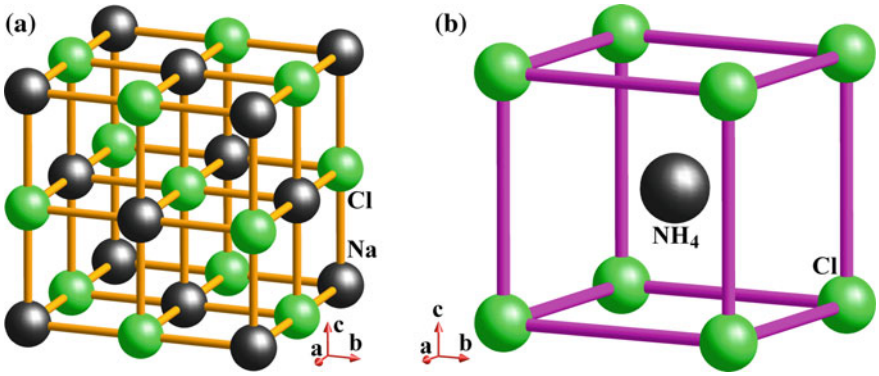

Fig. 3.1 Crystal structures of **a** halite and **b** salammoniac

halite-type structure. Halite and sylvite having high solubilities in H_2O are usually some of the last minerals to crystallize during the evaporation of seawater and other saline waters.

Salammoniac, [$(NH_4)Cl$], at ambient conditions adopts the α-CsCl-type structure, in which the Cl^- ions are located at the corners of the cube and the NH_4^+ ion occupies the centre (Fig. 3.1b). As such the NH_4^+ cations are coordinated by eight Cl^- anions to form [$(NH_4)Cl_8$] cubes (Fig. 3.1b). By analogy with [CsCl], salammoniac is expected to convert to the halite-type structure at elevated temperatures.

Fluorite (space group $Fm\bar{3}m$) has a crystal structure composed of cubic closest packed Ca^{2+} cations with F^- anions occupying all the tetrahedral interstices (Fig. 3.2a). Each Ca^{2+} is coordinated by 8 F^- anions. Strontiofluorite, fluorocronite, and frankdicksonite are isostructural with fluorite (Table 3.3). Hieratite, cryptohalite, and panichiite adopt the [K_2PtCl_6] structure type with the space group $Fm\bar{3}m$, which can be described in terms of either the fluorite type or the inverse

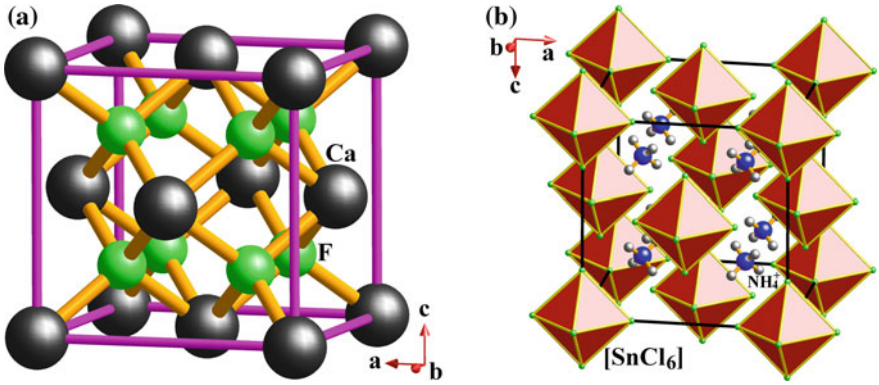

Fig. 3.2 Crystal structures of **a** fluorite and **b** panichiite

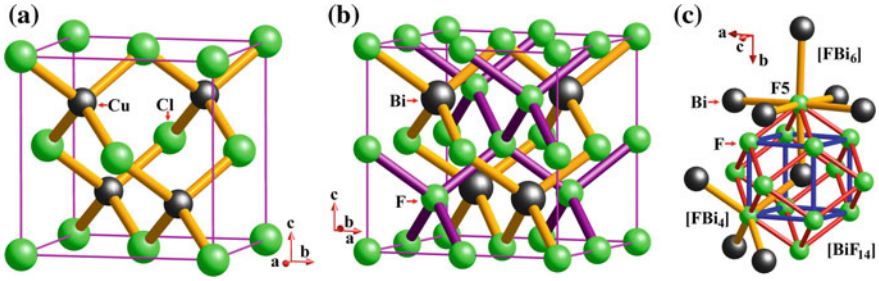

Fig. 3.3 Crystal structures of **a** nantokite and **b-c** gananite

fluorite (or anti-fluorite) structure (i.e., the coordinations of the cationic and anionic components are reversed relative to those in the fluorite structure). For example, the $[SiF_6]^{2-}$ octahedra in cryptohalite can be treated as spherical anions occupying the Ca^{2+} sites, whereas $[NH_4]^+$ is analogous to a spherical cation at the F^- position (Fig. 3.2b). In addition, håleniusite-(La) [LaOF] and tveitite-(Y) $[(Y,Na)_6(Ca,Na,REE)_{12}(Ca,Na)F_{42}]$, have the fluorite-type structures (Holtstam et al. 2004; Yakubovich et al. 2007). The crystal structure of tveitite-(Y) (space group $R\bar{3}$), which can be derived from the fluorite type by the presence of vacancies at both the cation and anion sites, is characterized by a mixed occupation of all four distinct cation positions but a disordered distribution of F atoms over the majority of the anion positions (Yakubovich et al. 2007).

Nantokite [CuCl], (space group $F\bar{4}3m$) adopts the sphalerite-type structure with Cl^- in a cubic closest packing mode and Cu^+ in half of the tetrahedral sites (Fig. 3.3a). In this configuration the cations are coordinated by 4 anions, forming $[CuCl_4]$ tetrahedra. The $[CuCl_4]$ tetrahedra are linked via shared corners, each corner is common to four tetrahedra. At ambient conditions, marshite and miersite are isostructural with nantokite (Table 3.4). In the crystal structure of gananite

(space group $P\bar{4}3m$), Bi is positioned at (0.737(5), 0.737(5), 0.737(5)), slightly deviating from the ideal atomic coordinates (0.75, 0.75, 0.75) for Zn in the sphalerite structure. The crystal structure of gananite can be derived from the sphalerite-type, where two sets of BiF and "F"F sphalerite-type networks are interleaved (Fig. 3.3b). There are five crystallographically distinct F positions: four of them (F1, F2, F3, F4) are each coordinated by four Bi atoms at the length of 2.672, 2.408, 2.499, 2.587 Å, respectively. The remaining F site (F5) is linked to six Bi atoms at 2.858 and 3.011 Å. Each Bi atom is coordinated by 14 F atoms to form a $[BiF_{14}]$ cage (Fig. 3.3c).

Chloromagnesite, lawrencite, and scacchite (Table 3.5) crystallize in the $CdCl_2$–type structure (space group $R\bar{3}m$; Fig. 3.4a). Here, the cubic closest packing sequence along the *c* axis is AcB□CbA□BaC□AcB□C, where the capital letters A, B, C denote the relative positions of anions, lower-case letters a, b, c represent the positions of the octahedral cations, and open squares □ indicate vacant octahedral interstices (Li et al. 2008). In a unit cell there are three repeated trioctahedral layers stacked along the *c* direction and held together by weak interlayer forces. The trioctahedral layer is formed by $[MgCl_6]$ octahedra sharing six edges with neighboring octahedra (Fig. 3.4b). Note that lawrencite also has a $P\bar{3}m$ modification with the CdI_2-type structure, which has only one repeated trioctahedral layer in the unit cell (Fig. 3.4c).

Iodargyrite (space group $P6_3mc$) adopts a wurtzite-type structure, in which I^- ions are arranged in a hexagonal closest packing mode with half of the tetrahedral interstices filled by Ag^+ cations (Hull and Keen 1999). The Ag atoms are each coordinated by four I atoms with one short and three long Ag-I bonds at 2.521 and 2.931 Å, respectively. Likewise each I atom is coordinated by four Ag atoms (Fig. 3.5a).

Sellaite (space group $P4_2/mnm$) adopts a rutile-type structure, which may be described as an approximately hexagonal closest packing of anions, with cations occupying half of the octahedral interstices (Vidal-Valat et al. 1979; Fig. 3.5b). Each Mg atom is coordinated by six F atoms, whereas each F atom is linked to three

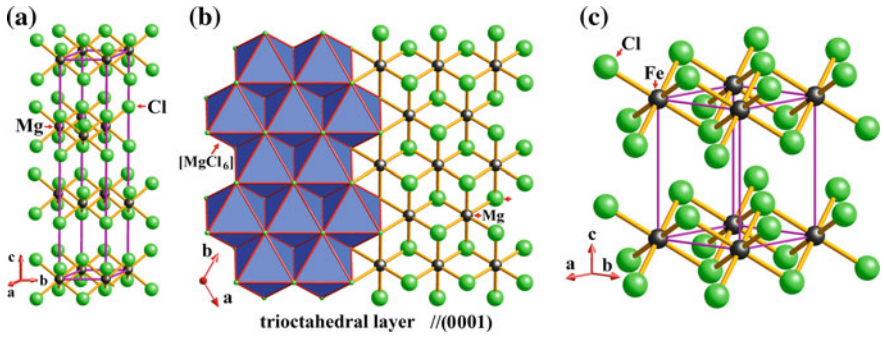

Fig. 3.4 The crystal structure of chloromagnesite showing **a** the unit cell and **b** the trioctahedral layer. The crystal structure of lawrencite is given in **c** for comparison

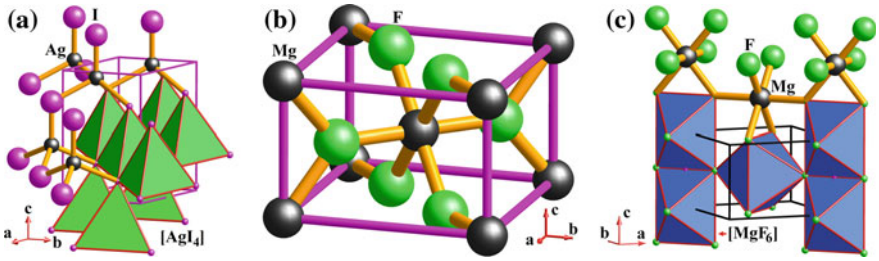

Fig. 3.5 Crystal structures of **a** iodargyrite and **b-c** sellaite

Table 3.6 Silicofluoride and borofluoride minerals

Mineral	Formula	Space group	Reference
Ferruccite	$NaBF_4$	*Cmcm*	Brunton (1968)
Avogadrite	KBF_4	*Pnma*	Brunton (1969)
Barberiite	NH_4BF_4	*Pnma*	Caron and Ragle (1971)
Malladrite	Na_2SiF_6	$P3_2$	Zalkin et al. (1964)
Bararite	$(NH_4)_2SiF_6$	$R\bar{3}m$	Schlemper and Hamilton (1966)
Cryptohalite	$(NH_4)_2SiF_6$	$Fm\bar{3}m$	Schlemper et al. (1966)
Hieratite	K_2SiF_6	$Fm\bar{3}m$	Hester et al. (1993)
Demartinite	K_2SiF_6	$P6_3mc$	Gramaccioli and Campostrini (2007)
Heklaite	KNa_2SiF_6	*Pnma*	Garavelli et al. (2010)
Knasibfite	$K_3Na_4[SiF_6]_3[BF_4]$	*Imm*2	Demartin et al. (2008)

Mg atoms. Each $[MgF_6]$ octahedron shares two *trans*-edges with neighboring ones to form a linear chain running along [001] (Fig. 3.5c). These chains share vertices with four neighboring chains to form a three-dimensional (3D) framework.

3.2.2.2 Silicofluoride $[SiF_6]^{2-}$ and Borofluoride $[BF_4]^-$ Minerals

The F^- anion without any *d* electron differs significantly from other halides but is closely comparable in both the electronic configuration and ionic radius to O^{2-}, resulting in the widespread $F^- \leftrightarrow O^{2-}$ substitutions in minerals (e.g., $F^- = (OH)^-$ in silicates and phosphates; see discussion below). Differences between F^- and O^{2-} are also well known, including the much smaller covalencies of the metal-F (*M*-F) bonds than their *M*-O counterparts. This difference in bond covalency is best illustrated by the higher coordination numbers of cations in fluorides than the corresponding oxides. For example, the coordination number of Si in silicofluorides is 6 (Table 3.6), higher than 4 in common silicates. Similarly, the coordination number of B in borofluorides is 4 (Table 3.6), but being 3 and 4 in borates. Silicofluorides and borofluorides are few in number (Table 3.6) and do not appear

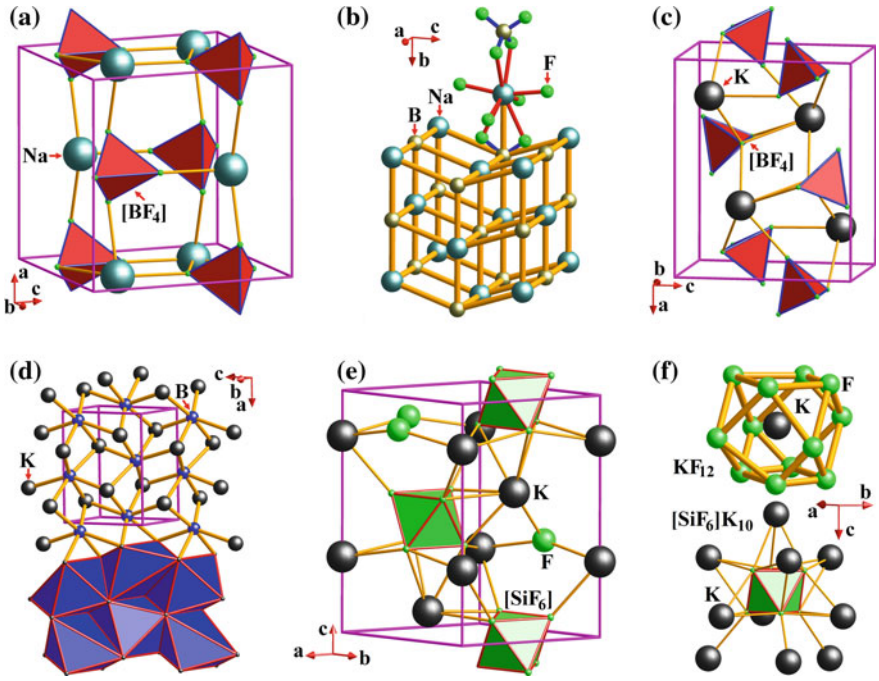

Fig. 3.6 Crystal structures of **a-b** ferruccite, **c-d** avogadrite, and **e-f** demartinite

to show the complex polymerization schemes exhibited by the $[AlF_6]^{3-}$ groups in aluminofluorides (Hawthorne 1984).

The structure of ferruccite consists of Na^+ ions and $[BF_4]$ tetrahedra in a distorted halite-type distribution, where the Cl positions are replaced by the $[BF_4]$ tetrahedra (Fig. 3.6a, b). Sodium is surrounded by eight F atoms from six $[BF_4]$ tetrahedra. Avogadrite and barberiite are isostructural and consist of K^+/NH_4^+ ions and $[BF_4]$ tetrahedra, which can be topologically described in terms of "$[KB_6]$" octahedra sharing edges to form a 3D structure. Potassium is surrounded by ten F atoms (<3.1 Å) from seven $[BF_4]$ tetrahedra (Fig. 3.6c, d).

It has been shown above that the structures of hieratite and cryptohalite with the $[SiF_6]^{2-}$ group can be considered as derivatives of the fluorite type (Table 3.3). Of the two $(NH_4)_2SiF_6$ polymorphs, cryptohalite is stable at room temperature, whereas bararite is stable below 5 °C but metastable at room temperature (Schlemper et al. 1966). By analogy, hieratite and demartininite may represent the high- and low-temperature polymorphs of K_2SiF_6, respectively (Table 3.6). The crystal structure of demartinite consists of $[SiF_6]$ octahedra and K^+ ions. Seven tridentate K^+ ions each link to a face of a horizontally lying $[SiF_6]$ octahedron, except for the basal face that bonds to three unidentate K^+ ions. Each K^+ is coordinated by 12 F anions to form a $[KF_{12}]$ cuboctahedron (Fig. 3.6e, f).

Knasibfite is the only example containing both the $[SiF_6]^{2-}$ and $[BF_4]^-$ anion groups (Demartin et al. 2008). In the asymmetrical unit, there is one

crystallographically distinct B atom along with two Si, K and Na atoms (Fig. 3.7). One of the Na atoms (Na1) is coordinated to five F atoms in a tetragonal pyramid if five weak bonds are not included. The second Na atom (Na2) is coordinated by six F atoms in an octahedral configuration. The [$Na2F_6$] octahedron shares three corners each with a [$Si2F_6$] octahedron, two corners each with a [$Si1F_6$] octahedron, and one corner with a [BF_4] tetrahedron. The [$Si1F_6$] octahedron shares four equatorial corners each with a [$Na2F_6$] octahedron, and a pair of *trans*-equatorial edges with two [$Na1F_5$] tetragonal pyramids. The [$Na1F_5$] tetragonal pyramid shares one edge with a [$Si1F_6$] octahedron, two corners each with a [$Na2F_6$] octahedron, and the other three corners each with a [$Si2F_6$] octahedron. The [$Si2F_6$] octahedron shares three corners each with a [$Na2F_6$] octahedron on one side and the other three corners each with a [$Na1F_5$] tetragonal pyramid on the opposite side. The [$Na2F_6$], [$Si1F_6$] and [$Si2F_6$] octahedra, together with [BF_4] tetrahedra share corners to form a 3D framework structure that contains a triangular channel consisting of 12 alternate [$Na2F_6$] and [SiF_6] octahedra. This gives rise to channels running along [100], where K atoms are located (Fig. 3.7a). The two crystallographically distinct K atoms (K1 and K2) are coordinated by 10 and 12 F atoms (<3.15 Å), respectively (Fig. 3.7c).

Silicofluoride and borofluoride minerals are restricted exclusively to volcanic fumaroles, which are characterized by high acidity (pH down to 2.5; Di Liberto et al. 2002; Madonia and Liotta 2010). The restricted occurrences of these minerals are readily attributable to the limited stabilities of the $[SiF_6]^{2-}$ and $[BF_4]^{-}$ anion groups in water. For example, the $[SiF_6]^{2-}$ anion in aqueous solutions readily hydrolyzes at neutral pH conditions via the following reaction:

$$[SiF_6]^{2-} + 2H_2O + 2H^+ = SiO_2 + 6HF.$$

Similarly, $[BF_4]^{-}$ is not stable in aqueous solutions, because it hydrolyzes to $[BF_3(OH)]^{-}$, $[BF_2(OH)_2]^{-}$, $[BF(OH)_3]^{-}$, and $[B(OH_4)]^{-}$ under all conditions investigated by Freire et al. (2010).

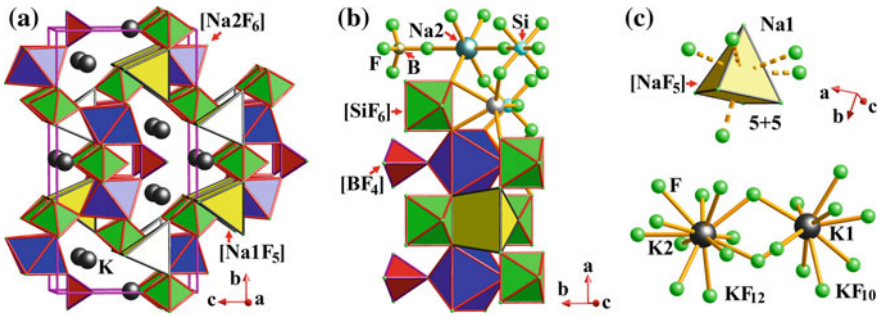

Fig. 3.7 The crystal structure of knasibfite showing **a** the unit-cell with the K atoms in channels along [100], **b** linkages of [BF_4], [SiF_6], [$Na1F_5$] and [$Na2F_6$] polyhedra, and **c** local environments of Na1, K1 and K2

3.2.2.3 Rare Earth Fluoride Minerals

One of the most salient features in Table 3.1 is the large number of rare earth fluoride minerals, in contrast with the scarcity of REE chlorides (see also Table 3.7). Table 3.7 also shows that REE are often coordinated directly by F atom(s), but the REE-Cl bond has not been documented in minerals. The marked difference in the number of REE fluorides and chlorides cannot be attributed entirely to the higher crustal abundance of F than Cl but may be partially influenced by the high stabilities of REE fluoride complexes relative to their chloride counterparts. For example, the stability constants of REE monofluoride complexes in aqueous solutions at 25 °C and atmospheric pressure are two orders of magnitude higher than those of the corresponding monochloride species (Wood 1990). Although both F^- and Cl^- are known to enhance the partitioning of REE into aqueous solutions and melts at elevated temperatures and pressures, experimental studies have shown that the partition coefficients for REE between fluoride-rich melts/fluids and silicate melts are orders of magnitude higher than those between chloride-rich fluids and silicate melts (Flynn and Burnham 1978; Reed et al. 2000; Veksler et al. 2005). This is consistent with the general consensus that F^- plays important roles in the transportation and enrichment of REE in fluids and melts and thus, the formation of REE deposits (Wood 1990; Pan and Fleet 1996; Pan et al. 2003; Veksler et al. 2005; Tropper et al. 2011, 2013; Vasyukova and Williams-Jones 2014).

The smaller covalency of *M*-F bonds relative to *M*-O bonds is also evident in the coordination of REE: i.e., the coordination numbers of 9 to 11 in simple REE fluorides (Table 3.7) *versus* 6 to 7 in the corresponding oxides. For example, the structures of fluocerites (Cheetham et al. 1976) are characterized by the presence of $[(Ce,La)F_{11}]$ polyhedra (Fig. 3.8). There are three crystallographically distinct F atoms (F1, F2 and F3) in the asymmetrical unit. F1 occupies a general position, whereas F2 and F3 occupy special positions (Fig. 3.8a). Each F1 is surrounded by four Ce atoms to form the $[F1Ce_4]$ tetrahedron (Fig. 3.8b). Two $[F1Ce_4]$ tetrahedra share one common face to form a trigonal dipyramial dimer of $[F1_2Ce_5]$. The crystal structure of fluocerite-(Ce) can be described in terms of three $[F1_2Ce_5]$ dimers sharing corners to form three-membered-ring channels parallel to the *c*-axis, with F2 and F3 atoms residing in the channels.

Gagarinite-(Y) and gagarinite-(Ce) are isostructural with neighborite $[NaMgF_3]$. Their crystal structures consist of face-sharing $[NaF_6]$ octahedral chains held together by Ca/Y/Ce atoms (Fig. 3.9). The latter are disordered over the same site that is coordinated by nine F atoms in a 3-3-3 pattern, and best described as a tricapped trigonal prism. The NaF_6 octahedra have equal Na-F lengths of 2.323 Å but very different bond angles with the two axial F atoms (73.62º and 106.38º). There is also a very short Na–Na distance at 1.770 Å, arising from the disordered distribution of Ca/Y/Ce and half or lesser occupancy of Na (Fig. 3.9c).

The coordination of REE in complex fluorides, as expected, shows a greater variability and ranges from 6 to 11 (Table 3.7). Figure 3.10 provides examples of this variability, including details regarding the bonding configurations. Also, the numbers of F atoms coordinated to REE are variable, but those with a single F atom

Table 3.7 Summary of rare-earth halide minerals

Mineral	Formula	REE polyhedra	Ref
Fluocerite-(Ce)	CeF_3	CeF_{11}	1
Fluocerite-(La)	LaF_3	LaF_{11}	1
Gagarinite-(Y)	$NaCaYF_6$	YF_9	2
Gagarinite-(Ce)	$NaCaCeF_6$	CeF_9	2
Polezhaevaite-(Ce)	$NaSrCeF_6$	CeF_9	3
Tveitite-(Y)	$(Y,Na)_6(Ca,Na,REE)_{12}(Ca,Na)F_{42}$	YF_9 (or $YF_{8.5}$)	4
Waimirite-(Y)	YF_3	YF_9	5
Håleniusite-(La)	LaOF	LaF_8	6
Murataite-(Y)	$Y_6ZnZn_4Ti_{12}O_{29}O_{10}F_4$	YO_6F_2	7
Arisite-(Ce)	$NaCe_2(CO_3)_2[F_{2x}(CO_3)_{1-x}]F$	CeO_9F	8
Arisite-(La)	$NaLa_2(CO_3)_2[F_{2x}(CO_3)_{1-x}]F$	LaO_9F	8
Bastnäsite-(Ce)	$Ce(CO_3)F$	CeO_6F_3	9
Bastnäsite-(La)	$La(CO_3)F$	LaO_6F_3	9
Bastnäsite-(Nd)	$Nd(CO_3)F$	NdO_6F_3	9
Bastnäsite-(Y)	$Y(CO_3)F$	YO_6F_3	9
Cebaite-(Ce)	$Ba_3Ce_2(CO_3)_5F_2$	CeO_9F	10
Cordylite-(Ce)	$NaBaCe_2(CO_3)_4F$	CeO_9F	11
Cordylite-(La)	$NaBaLa_2(CO_3)_4F$	LaO_9F	12
Horváthite-(Y)	$NaY(CO_3)F_2$	YO_4F_4	13
Huanghoite-(Ce)	$BaCe(CO_3)_2F$	CeO_9F	14
Kukharenkoite-(Ce)	$Ba_2Ce(CO_3)_3F$	CeO_9F	15
Kukharenkoite-(La)	$Ba_2La(CO_3)_3F$	LaO_9F	16
Lukechangite-(Ce)	$Na_3Ce_2(CO_3)_4F$	CeO_9F	17
Mineevite-(Y)	$Na_{25}BaY_2(CO_3)_{11}(HCO_3)_4(SO_4)_2F_2Cl$	YO_9	18
Parisite-(Ce)	$CaCe_2(CO_3)_3F_2$	CeO_6F_3	9
Peatite-(Y)	$Li_4Na_{12}Y_{12}(PO_4)_{12}(CO_3)_4F_8$	YO_8,YO_4F_4	19
Röntgenite-(Ce)	$Ca_2Ce_3(CO_3)_5F_3$	CeO_6F_3	9
Qaqarssukite-(Ce)	$BaCe(CO_3)_2F$	CeO_6F_3	20
Reederite-(Y)	$Na_{15}Y_2(CO_3)_9(SO_3F)Cl$	YO_9	21
Synchysite-(Ce)	$CaCe(CO_3)_2F$	CeO_6F_3	9
Synchysite-(Nd)	$CaNd(CO_3)_2F$	NdO_6F_3	9
Synchysite-(Y)	$CaY(CO_3)_2F$	YO_6F_3	9
Chukhrovite-(Y)	$Ca_3YAl_2(SO_4)F_{13}{\cdot}12H_2O$	$Y(H_2O)_3F_4$	22
Chukhrovite-(Nd)	$Ca_3NdAl_2(SO_4)F_{13}{\cdot}12H_2O$	$Nd(H_2O)_3F_4$	23
Chukhrovite-(Ce)	$Ca_3CeAl_2(SO_4)F_{13}{\cdot}12H_2O$	$Ce(H_2O)_3F_4$	22
Belovite-(Ce)	$Na_2Ce_2Sr_6(PO_4)_6F_2$	CeO_9	24

(continued)

Table 3.7 (continued)

Mineral	Formula	REE polyhedra	Ref
Belovite-(La)	$Na_2La_2Sr_6(PO_4)_6F_2$	LaO_9	24
Cappelenite-(Y)	$BaY_6B_6Si_3O_{24}F_2$	YO_7F	25
Carlgieseckeite-(Nd)	$Na_2Nd_2Ca_6(PO_4)_6F$	NdO_9	26
Kuannersuite-(Ce)	$Na_2Ce_2Ba_6(PO_4)_6FCl$	CeO_9	27
Bussyite-(Ce)	$Ce_3(Na,H_2O)_6MnSi_9Be_5(O,OH)_{30}F_4$	CeO_8	28
Byelorussite-(Ce)	$NaBa_2Ce_2MnTi_2Si_8O_{26}F{\cdot}H_2O$	CeO_8F	29
Cayalsite-(Y)	$CaY_6Al_2Si_4O_{18}F_6$		30
Dollaseite-(Ce)	$CaCe(Mg_2Al)[Si_2O_7][SiO_4]F(OH)$	CeO_{10}	31
Fluorbritholite-(Ce)	$(Ce,Ca)_5(SiO_4)_3F$	CeO_7F, CeO_9	32
Fluorbritholite-(Y)	$(Y,Ca)_5(SiO_4)_3F$	YO_7F, YO_9	32
Fluorthalénite-(Y)	$Y_3Si_3O_{10}F$	YO_6F, YO_7F	33
Hainite	$Na_2Ca_4YTi(Si_2O_7)_2OF_3$	CeO_6F	34
Kapitsaite-(Y)	$Ba_4Y_2Si_8B_4O_{28}F$	YO_7F	35
Khristovite-(Ce)	$CaCe(MgAlMn^{2+})[Si_2O_7][SiO_4]F(OH)$	CeO_{10}	36
Kuliokite-(Y)	$Y_4Al(SiO_4)_2(OH)_2F_5$	YO_4F_3, YO_4F_4	37
Laptevite-(Ce)	$NaFe^{2+}(REE_7Ca_5Y_3)(SiO_4)_4(Si_3B_2PO_{18})(BO_3)F_{11}$	CeO_8F, CeO_9F, CeO_7F_2, CeO_6F_3, CeO_3F_5	38
Magnesiorowlandite-(Y)	$Y_4(Mg,Fe)(Si_2O_7)_2F_2$	YO_7, YO_6F_2	39
Nacareniobsite-(Ce)	$NbNa_3Ca_3Ce(Si_2O_7)_2OF_3$	CeO_6F	40
Okanoganite-(Y)	$(Y,REE,Ca,Na,Th)_{16}(Fe^{3+},Ti)(Si,B,P)_{10}(O,OH)_{38}F_{10}$	CeO_8F, CeO_9F_2, YO_6F_3, YO_4F_4	41
Rowlandite-(Y)	$FeY_4(Si_2O_7)_2F_2$	YO_7, YO_6F_2	42
Schlüterite-(Y)	$Y_2AlSi_2O_7(OH)_2F$	YO_7F_2,YO_8	43
Västmanlandite-(Ce)	$Ce_3CaMg_2Al_2Si_5O_{19}(OH)_2F$	CeO_{10}, CeO_{11}	44
Proshchenkoite-(Y)	$(Y,REE,Ca,Na,Mn)_{15}(Fe^{2+},Mn)Ca(P,Si)Si_6B_3O_{34}F_{14}$	YO_5F_4, NdO_4F_5, NdO_7F_4, NdO_9F	45
Yftisite-(Y)	$Y_4Ti(SiO_4)_2OF_6$	YO_5F_3, YO_2F_5	46
Hiortdahlite	$(Na,Ca)_4Ca_8Zr_2(Y,Na)_2(Si_2O_7)_4O_3F_5$	YO_5F	47
Vicanite-(Ce)	$(Ca,REE,Th)_{15}Fe^{3+}(SiO_4)_3(Si_3B_3O_{18})(BO_3)(As^{5+}O_4)(AsO_3)_x(NaF_3)_{1-x}F_7{\cdot}0.2H_2O$	CeO_8F, LaO_9F_2	48
Semenovite-(Ce)	$Ce_2Fe_{0.5}Mn_{0.5}Na_{6.8}Ca_{2.6}(Be_6Si_{14}O_{39.32})O_{0.88}(OH)_{5.8}F_2$	CeO_8	49
Byzantievite	$Ba_5(Ca,Sr,Y)_{22}(Ti,Nb)_{18}(SiO_4)_4[(PO_4),SiO_4)]_4(BO_3)_9O_{21}[(OH),F]_{43}(H_2O)_{1.5}$	YO_{10}	50
Hundholmenite-(Y)	$(Y,REE,Ca,Na)_{15}(Al,Fe^{3+})Ca_xAs^{3+}_{1-x}(Si,As^{5+})Si_6B_3(O,F)_{48}$	YO_8F	51
Miserite	$(Ca,K)_{0.5}KCa_5(RE)[Si_8O_{22}](OH)F{\cdot}0.5H_2O$	YO_5F	52

(continued)

Table 3.7 (continued)

Mineral	Formula	REE polyhedra	Ref
Seidite-(Ce)	$Na_4(Ce,Sr)_2Ti[Si_8O_{22}]F{\cdot}5H_2O$	CeO_6	53
Decrespignyite-(Y)	$Y_4Cu(CO_3)_4Cl(OH)_5{\cdot}2H_2O$		54

Reference *1* Cheetham et al. (1976); *2* Hughes and Drexler (1994); *3* Yakovenchuk et al. (2010b); *4* Yakubovich et al. (2007); *5* Cheetham and Norman (1974); *6* Holtstam et al. (2004); *7* Ercit and Hawthorne (1995); *8* Piilonen et al. (2010); *9* Ni et al. (1993); *10* Yang (1995); *11* Giester et al. (1998); *12* Mills et al. (2012); *13* Grice and Chao (1997a); *14* Yang and Pertlik (1993); *15* Krivovichev et al. (1998); *16* Krivovichev et al. (2003); *17* Grice and Chao (1997b); *18* Yamonva et al. (1992); *19* McDonald et al. (2013); *20* Grice et al. (2006); *21* Grice et al. (1995); *22* Bokiy and Gorogotskaya (1965); *23* Pautov et al. (2005); *24* Rakovan and Hughes (2000); *25* Shen and Moore (1984); *26* Pekov et al. (2012); *27* Friis et al. (2004); *28* Grice et al. (2009); *29* Zubkova et al. (2004); *30* Malcherek et al. (2012); *31* Peacor and Dunn (1988); *32* Oberti et al. (2001); *33* Schleid and Müller-Bunz (1998); *34* Sokolova (2006); *35* Sokolova et al. (2000); *36* Ercit (2002); *37* Sokolova et al. (1986); *38* Uvarova et al. (2013); *39* Matsubara et al. (2014); *40* Sokolova and Hawthorne (2008a); *41* Boiocchi et al. (2004); *42* Shipovalov and Stepanov (1971); *43* Cooper et al. (2013); *44* Holtstam et al. (2005); *45* Raade et al. (2008); *46* Balko and Bakakin (1975); *47* Merlino and Perchiazzi (1987); *48* Ballirano et al. (2002); *49* Mazzi et al. (1979); *50* Sokolova et al. (2010); *51* Raade et al. (2007); *52* Scott (1976); *53* Ferraris et al. (2003); *54* Wallwork et al. (2002)

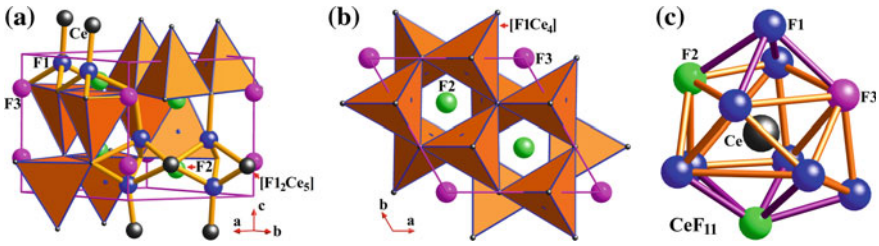

Fig. 3.8 The crystal structure of fluocerite-(Ce) showing **a** the [F1$_2$Ce$_5$] trigonal dipyramial dimer in the unit cell, **b** F2 and F3 atoms in the channels formed by the three-membered rings of the [F1$_2$Ce$_5$] dimers, and **c** the coordination polyhedron of CeF$_{11}$

are the most common (Table 3.7). Further research is needed to examine possible relationships that may exist between the coordination of REE polyhedra in minerals and those that occur in the fluids/melts from which they developed.

3.2.2.4 Copper Chloride Minerals

Also evident in Table 3.1 is the very large number of Pb and Cu chlorides, although the majority of which are restricted to surficial environments and are rare. The stabilities of the mixed Pb and Cu chlorides (e.g., boleite and pseudoboleite) in aqueous solutions at ambient conditions are controlled by aCl and pH (Abdul-Samad et al. 1981).

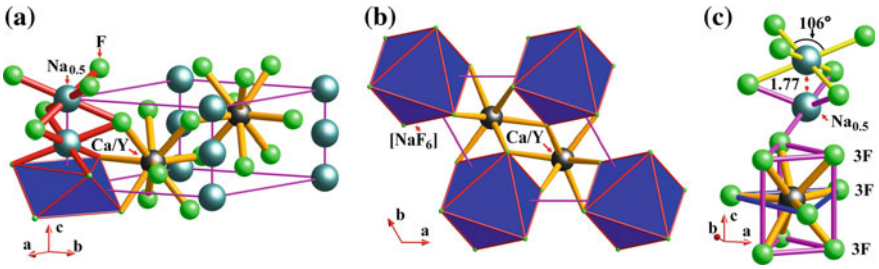

Fig. 3.9 Crystal structures of **a** gagarinite-(Y), **b** viewed down the *c*-axis, and **c** illustration for the coordination of the 3-3-3 tricapped trigonal prism and the deviations of the axial bond angles from 90°

One interesting feature of Cu chlorides is that they, with a few exceptions (e.g., nantokite and marshite; Table 3.4), are composed of $Cu^{2+}\phi_6$ (where ϕ = O, OH, H_2O and Cl) octahedra with strong distortions due to a marked Jahn-Teller effect. The $Cu^{2+}\phi_6$ octahedra in Cu chlorides polymerize to give rise to diverse geometrical configurations, including the 1D $\{CuO_3Cl\}_\infty$ chains. Figure 3.11 shows different linkages of the 1D $\{CuO_3Cl\}_\infty$ chains to form the Kagomé layers in several Cu oxychloride minerals (Table 3.8). These Cu oxychlorides with the Kagomé layers have attracted considerable recent research for their interesting magnetic properties (e.g., Colman et al. 2008, 2011; Welch et al. 2014; Zhu et al. 2014; Sun et al. 2016).

Atacamite, botallackite, clinoatacamite, and paratacamite are $[Cu_2(OH)_3Cl]$ polymorphs, although a minor amount of Zn is now known to be important in stabilizing the structure of paratacamite (Welch et al. 2014). Atacamite is isostructural with kempite $[Mn_2(OH)_3Cl]$. There are two crystallographically distinct Cu^{2+} ions in the asymmetric unit of atacamite: Cu1 is coordinated by four equatorial O and two axial Cl atoms in an elongated octahedral form and Cu2 is coordinated by one Cl and five O atoms in a distorted octahedral configuration (Fig. 3.12). The $[Cu1O_4Cl_2]$ octahedra are arranged in a *trans*-edge-sharing to form an octahedral chain along [010], whereas the $[Cu2O_5Cl]$ octahedra are arranged in a *trans*-edge-sharing to form another chain along [100]. These cross-over octahedral chains are further combined together via edge-sharing to form a 3D framework structure. These $Cu\phi_6$ octahedra also form a six-membered ring and a Kagomé layer parallel to $(10\bar{1})$ or $(01\bar{1})$, but neither the six-membered ring nor the Kagomé layer in atacamite has trigonal symmetry. Four $Cu\phi_6$ octahedra form a Cu tetramer. The Cu tetramers are alternately arranged such that they are pointing up or down; they share corners to form a Kagomé net parallel to $(01\bar{1})$ (Fig. 3.12). Successive Kagomé nets are further held together by sharing corners to form a 3D framework structure.

There are also two types of Cu^{2+} ions in the asymmetric unit of botallackite $[Cu_2(OH)_3Cl]$: Cu2 is coordinated by four equatorial O atoms and two axial Cl atoms, but Cu1 is coordinated by one Cl and five O atoms. Botallackite adopts a 2D

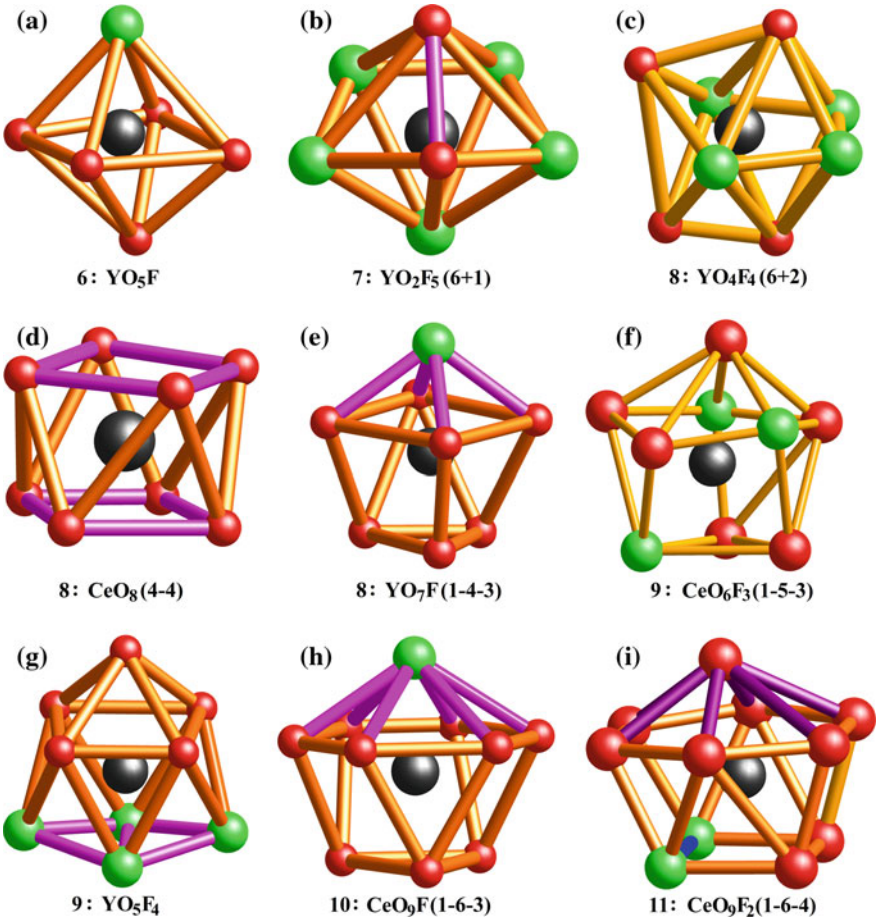

Fig. 3.10 Representative $REEO_xF_y$ polyhedra in rare earth fluorides: **a** $[YO_5F]$ octahedron in miserite; **b** $[YO_2F_5]$ in yftisite-(Y), derived from an octahedron with an additional vertex: i.e., (6 + 1); **c** $[YO_4F_4]$ in horvathite-(Y), derived from an octahedron with two additional vertices (6 + 2); **d** $[CeO_8]$ in semenovite-(Ce), tetragonal anti-prism (4 + 4); **e** $[YO_7F]$ in kapitsaite-(Y) having an 1-4-3 crown shape; **f** CeO_6F_3 in synchysite-(Ce) with an 1-5-3 crown shape; **g** $[YO_5F_4]$ in proshchenkoite-(Y), tetragonal anti-prism with an additional vertex (1 + 4 + 4); **h** $[CeO_9F]$ in huanghoite-(Ce) with an 1-6-3 crown shape; and **i** $[CeO_9F_2]$ in okanoganite-(Y) with an 1-6-4 crown shape

layer structure, which can be best described as a trioctahedral layer in which all the octahedral sites are occupied by the two types of Cu^{2+} ions. There is one trioctahedral layer per unit cell, this being stacked along [100]. Successive layers are only weakly coupled by O–H···Cl hydrogen bonds. Belloite, [Cu(OH)Cl], is isostructural with botallackite but has a single copper octahedral site in its asymmetric unit (Fig. 3.13d; Effenberger 1984). The crystal structure of bobkingite, $[Cu_5Cl_2(OH)_8(H_2O)_2]$, is also related to that of botallackite but contains three

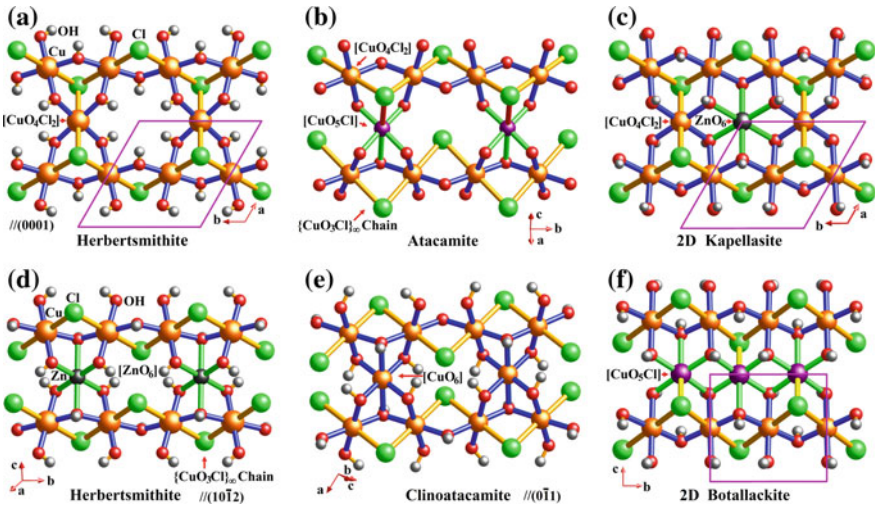

Fig. 3.11 Linkages of one-dimensional infinite octahedral $\{CuO_3Cl\}_\infty$ chains with zig-zag distributed Cl atoms, which are built from $[CuO_4Cl_2]$ octahedra sharing two [OH-Cl] *trans*-edges with neighboring ones: **a** two cross-over octahedral $\{CuO_3Cl\}_\infty$ chains in herbertsmithite linked by $[Cu(OH)_4Cl_2]$ octahedra to form a Kagomé layer // (0001); **b** neighboring octahedral $\{CuO_3Cl\}_\infty$ chains in atacamite held together by $[Cu(OH)_5Cl]$ octahedra; **c** neighboring octahedral $\{CuO_3Cl\}_\infty$ chains in kapellasite linked by both $[Cu(OH)_4Cl_2]$ and $[Zn(OH)_6]$ octahedra; **d** neighboring octahedral $\{CuO_3Cl\}_\infty$ chains in herbertsmithite held together by $[Zn(OH)_6]$ octahedra to form a layer // (10$\bar{1}$2); **e** neighboring octahedral $\{CuO_3Cl\}_\infty$ chains in clinoatacamite held together by $[Cu(OH)_6]$ octahedra; and **f** neighboring octahedral $\{CuO_3Cl\}_\infty$ chains in botallackite linked by $[Cu(OH)_5Cl]$ octahedral

distinct Cu^{2+} sites in the asymmetric unit (Fig. 3.13e; Hawthorne et al. 2002). Each $[Cu3(OH)_4Cl_2]$ octahedron shares two *trans*-edges to form an 1D octahedral $\{CuO_3Cl\}_\infty$ chain along [010], similar to those shown in Fig. 3.11. Two $[Cu2(OH)_2(H_2O)_2Cl]$ tetragonal monopyramids share a common edge to form a Cu2-dimer. The $\{CuO_3Cl\}_\infty$ chains are linked together by $[Cu1(OH)_6]$ octahedra to form a highly distorted Kagomé layer parallel to (001) (Fig. 3.13f). Successive Kagomé layers are held together by the Cu2-dimers and water molecules between them (Fig. 3.13e).

Clinoatacamite and paratacamite can be viewed as being isotypic with each other but have different crystal symmetries. There are three crystallographically distinct Cu sites in the asymmetrical unit of clinoatacamite (Fig. 3.14). Two of them are coordinated by four equatorial OH groups and two axial Cl atoms in an elongated octahedral form, whereas the third one is coordinated by six OH groups. The two types of the $[Cu(OH)_4Cl_2]$ octahedra each share Cl–OH edges with four neighboring octahedra to form a 2D Kagomé layer parallel to (504) (Fig. 3.14c). The Kagomé layers are further linked by the $[Cu(OH)_6]$ octahedra via edge-sharing to form a three dimensional framework structure. In comparison, there are four crystallographically distinct Cu sites in the asymmetrical unit of paracatamite

Table 3.8 Copper chloride minerals with Kagomé layers

Mineral	Formula	Space group	Reference
Atacamite	$Cu_2(OH)_3Cl$	*Pnma*	Zheng et al. (2005)
Botallackite	$Cu_2(OH)_3Cl$	$P2_1/m$	Hawthorne (1985)
Belloite	Cu(OH)Cl	$P2_1/a$	Effenberger (1984)
Bobkingite	$Cu_5C_{l2}(OH)_8H_2O_2$	*C*2/*m*	Hawthorne et al. (2002)
Clinoatacamite	$Cu_2(OH)_3Cl$	$P2_1/n$	Malcherek and Schlueter (2009)
Paratacamite	$(Cu,Zn)_2(OH)_3Cl$	$R\bar{3}$	Fleet (1975); Welch et al. (2014)
Paratacamite-(Mg)	$Cu_3Mg(OH)_6Cl_2$	$R\bar{3}$	Kampf et al. (2013b)
Paratacamite-(Ni)	$Cu_3Ni(OH)_6Cl_2$	$R\bar{3}$	Sciberras et al. (2014)
Leverettite	$Cu_3Co(OH)_6Cl_2$	$R\bar{3}$	Kampf et al. (2013a); Li and Zhang (2013)
Claringbullite	$Cu_3(OH)_6ClF$	$P6_3/mmc$	Burns et al. (1995); Rumsey et al. (2014)
Herbertsmithite	$Cu_3Zn(OH)_6Cl_2$	$R\bar{3}m$	Welch et al. (2014)
Gillardite	$Cu_3Ni(OH)_6Cl_2$	$R\bar{3}m$	Clissold et al. (2007)
Tondiite	$Cu_3Mg(OH)_6Cl_2$	$R\bar{3}m$	Malcherek et al. (2014)
Kapellasite	$Cu_3Zn(OH)_6Cl_2$	$P\bar{3}m$	Colman et al. (2008)
Haydeeite	$Cu_3Mg(OH)_6Cl_2$	$P\bar{3}m$	Colman et al. (2011)
Misakiite	$Cu_3Mn(OH)_6Cl_2$	$P\bar{3}m$	Nishio-Hamane et al. (2014b)
Centennialite	$Cu_3Ca(OH)_6Cl_2{\cdot}0.7H_2O$	$P\bar{3}m$	Crichton and Müller (2014)
Iyoite	$MnCu(OH)_3Cl$	$P2_1/m$	Nishio-Hamane et al. (2014a)
Anatacamite	$Cu_2(OH)_3Cl$	*P*1	Malcherek and Schlüter (2009)

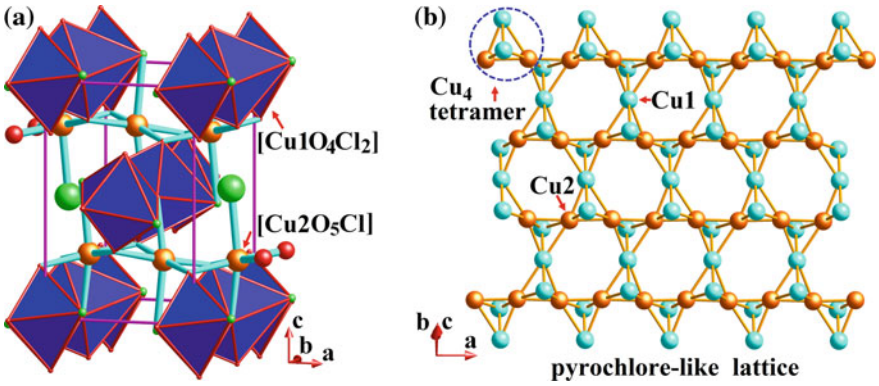

Fig. 3.12 The crystal structure of atacamite showing **a** the unit cell denoted by the *purple lines* and **b** the Kagomé net parallel to $(01\bar{1})$

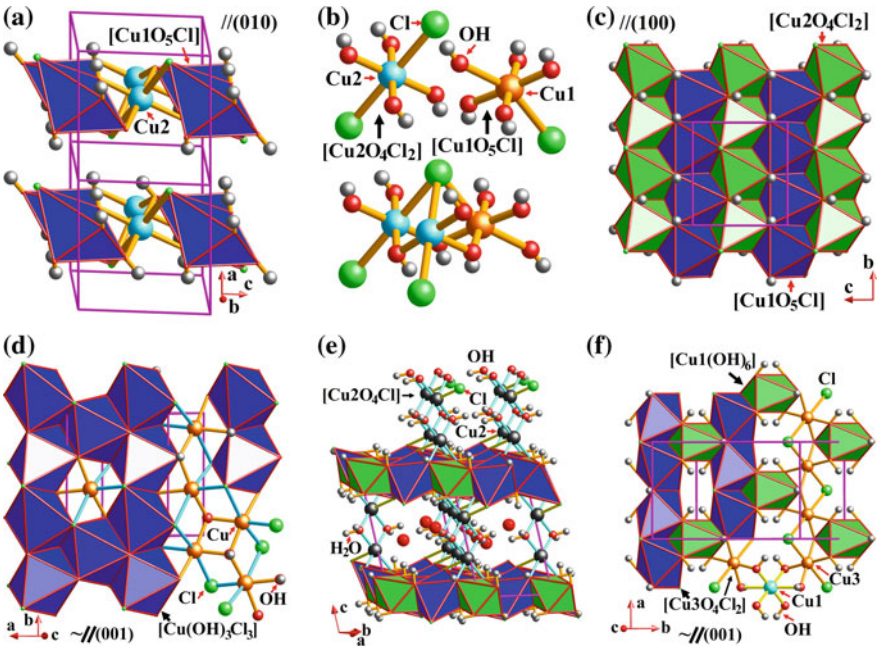

Fig. 3.13 The crystal structures of botallackite (**a-c**) and related minerals (**d-f**): **a** the unit cell marked by the *purple lines*, **b** the cyclic Cu trimer, **c** a closed packed trioctahedral layer of Cu^{2+} octahedra, **d** the trioctahedral layer in belloite, **e** the unit cell of bobkingite, and **f** the distorted Kagomé layer in bobkingite

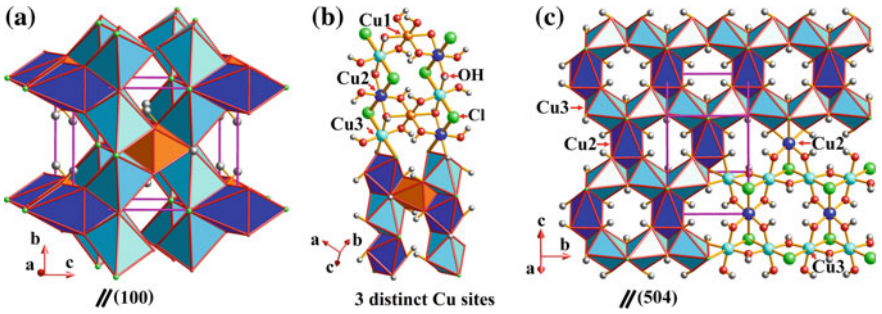

Fig. 3.14 The crystal structure of clinoatacamite showing **a** the unit cell marked by the *purple lines*, **b** three crystallographically distinct Cu sites, and **c** the Kagomé net parallel to (504)

(Fig. 3.15). Two of them are coordinated by four equatorial OH groups and two axial Cl atoms in an elongated octahedral form, whereas the other two are coordinated by six OH groups. The two types of $[Cu(OH)_4Cl_2]$ octahedra each share Cl–OH edges with four neighboring octahedra to form a 2D Kagomé layer parallel to

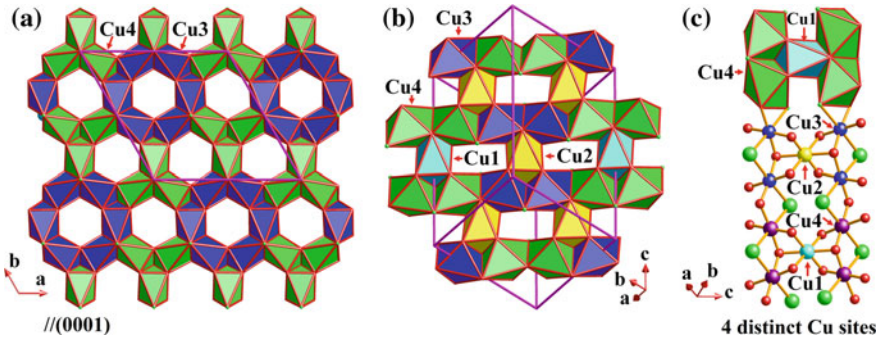

Fig. 3.15 The crystal structure of paratacamite: **a** the Kagomé layer parallel to (0001), **b** linkage between the Kagomé layers, and **c** four crystallographically distinct Cu sites

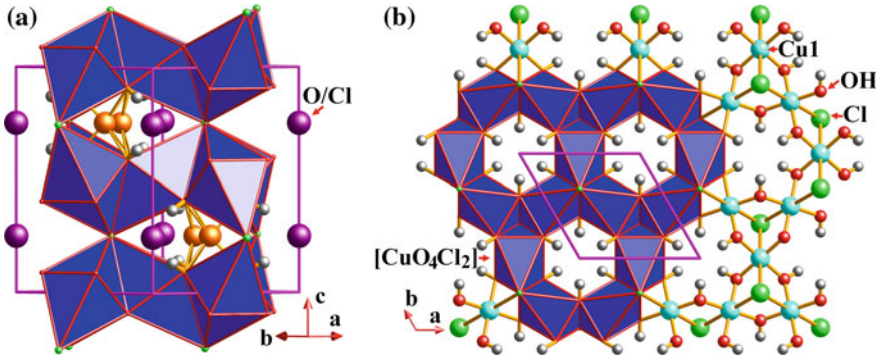

Fig. 3.16 The crystal structure of claringbullite showing **a** the unit cell marked by the *purple lines* and **b** the Kagomé layer

(0001) (Fig. 3.15a). The Kagomé layers are further linked by the two types of $[Cu(OH)_6]$ octahedra via edge-sharing to form a 3D framework structure.

The crystal structure of claringbullite, containing Cu^{2+} in trigonal-prismatic coordination (Burns et al. 1995), is also characterized by a 2D Kagomé layer parallel to (0001) (Fig. 3.16). Successive Kagomé layers are held together by sharing common Cl atoms to form a 3D framework structure. Disordered O/Cl and Cu atoms are positioned at the interstices between the layers (Fig. 3.16).

Herbertsmithite, gillardite and tondiite are isostructural and can all be considered as substituted members of the atacamite group, in which one-quarter of the octahedral sites in a pyrochlore-like lattice are occupied by Zn^{2+} (Mg^{2+}or Ni^{2+}) and the remaining octahedral sites are occupied by Cu^{2+} to form the Kagomé net (Fig. 3.17a, b). Each Cu atom is coordinated by four O atoms in a square-planar fashion with equal Cu–O distances at 1.982 Å, and by two Cl atoms at axial sites at 2.768 Å. Three elongated $[CuO_4Cl_2]$ octahedra are interconnected by sharing three

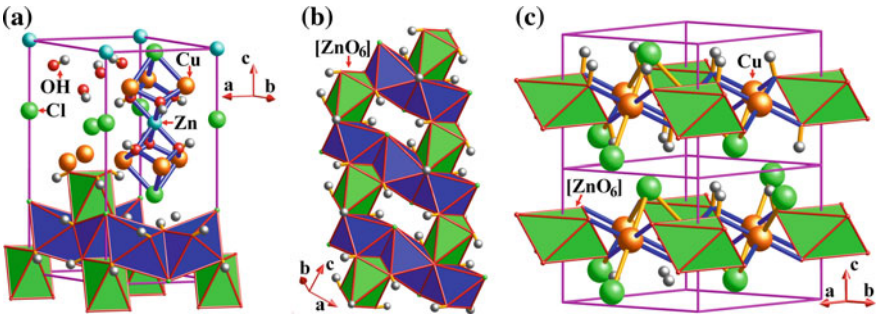

Fig. 3.17 Crystal structures of **a-b** herbertsmithite and **c** kapellasite

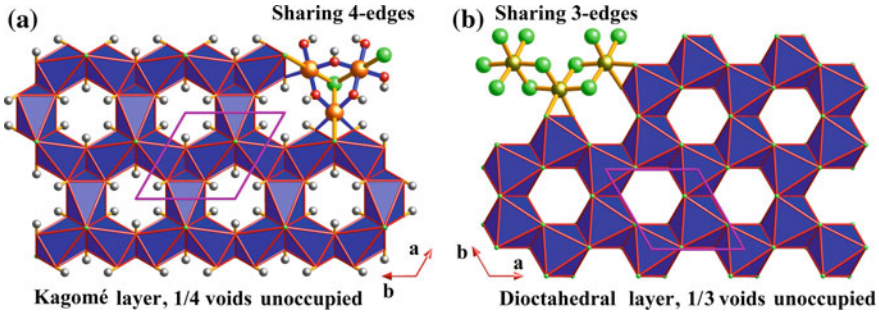

Fig. 3.18 Comparison of **a** the Kagomé layer in herbertsmithite and **b** the dioctahedral layer in gibbsite

cis-bridging-oxygen atoms and one common Cl atom to form the $[[Cu_3(\mu_3\text{-}Cl)(OH)_3](OH)_6Cl_3]$ cyclic trimer (Fig. 3.17a, b). Six neighboring $[CuO_4Cl_2]$ octahedra each share two skewed-edges to form a six-membered ring (in blue, Fig. 3.18a). Each cyclic trimer or the six-membered ring further links to the neighboring counterparts by the same mode to form the Kagomé net (Fig. 3.18a). Successive $[CuO_4Cl_2]$ octahedral layers are held together by $[Zn(OH)_6]$ octahedra to form a 3D structure (Fig. 3.17a). This 3D structure, therefore, consists of Zn^{2+} ions sandwiched between Kagomé layers, which are hexagonal sheets composed of corner-shared triangles of interconnected $[Cu(OH)_4Cl_2]$ octahedra.

The crystal structure of kapellasite can be viewed as a substituted variant of the botallackite type, wherein one-quarter of the octahedral interstices of the trioctahedral layer are occupied by Zn^{2+} and the remaining sites are occupied by Cu^{2+} to form the Kagomé net. Kapellasite also contains *cis*-corner-shared $[[Cu_3(\mu_3\text{-}Cl)(OH)_3](OH)_6Cl_3]$ cyclic trimers and skewed-edge-shared six-membered rings, as well as the Kagomé lattice of Cu atoms (Fig. 3.17c). The major difference between kapellasite and herbertsmithite is that the former has a 2D layer structure, whereas the latter has a 3D framework structure. The $[Zn(OH)_6]$ octahedra of kapellasite are located at the interstices of six-membered rings of $[CuO_4Cl_2]$ octahedra within the

2D Kagomé lattice layer, whereas those of herbertsmithite are sandwiched between the Kagomé layers. There is one trioctahedral layer per unit cell, being stacked along [001]. Successive Kagomé layers are only weakly coupled by O–H···Cl hydrogen bonds. Haydeeite and misakiite are isostructural with kapellasite. Also, centennialite (Crichton and Müller 2014) is isostructural with kapellasite but contains additional molecular H_2O between the Kagomé layers (Sun et al. 2016).

Chlorine-35 (^{35}Cl: 75.8% and nuclear spin I = 3/2) nuclear magnetic resonance (NMR) spectroscopic analyses of an oriented powder sample of synthetic kapellasite resolved four peaks (Kermarrec et al. 2014). This result contradicts the single line (i.e., the central $-1/2 \leftrightarrow +1/2$ transition) scheme expected for a perfect Kagomé layer with one unique Cl environment (i.e., linked to three Cu^{2+} ions or Cu_3; Fig. 3.17c), but provides a line of clear evidence for the Cu/Zn mixing disorder. Specifically, the observed NMR peaks arise from four distinct Cl environments with different Cu/Zn configurations: i.e., Cu_3, Cu_2Zn, $CuZn_2$ and Zn_3 (Kermarrec et al. 2014). Also, the amount of Cu/Zn mixing at 25(1)% in synthetic kapellasite, extracted from the ^{35}Cl NMR data, agrees with the value of 27% determined from neutron diffraction refinements (Colman et al. 2011).

The Kagomé layers can be described as octahedral sheets with 1/4 of the octahedral sites being unoccupied, analogous to the gibbsite layer with 1/3 octahedral vacancies (Fig. 3.18). However, the Kagomé layer is composed of $[Cu(OH)_4Cl_2]$ octahedra sharing two pairs of opposite OH-Cl edges with a neighboring counterpart (Fig. 3.18a), whereas only three edges are shared for each octahedron in the gibbsite layer (Fig. 3.18b). Successive Kagomé layers are held together by a $[M(OH)_6]$ octahedron (M = Zn, Mg or Ni) via sharing its six-edges from two top and basal faces to form a 3D trigonal herbertsmithite structure. When the interlayered $[Zn(OH)_6]$ octahedra are replaced by $[Cu(OH)_6]$ octahedra, the herbertsmithite structure is changed to those of trigonal paratacamite or monoclinic clinoatacamite. If the 1/4 octahedral vacancies in the Kagomé layers are occupied by $[Zn(OH)_6]$, the resulting structure is the trigonal kapellasite. If the octahedral vacancies in the Kagomé layers are occupied by $[Ca(OH)_6]$ and H_2O molecules are added between the Kagomé layers, the trigonal centennialite structure forms. If the neighboring 1D infinite octahedral $\{CuO_3Cl\}_\infty$ chains are held together by $[Cu(OH)_5Cl]$ octahedra rather than $[Cu(OH)_4Cl_2]$, the structure formed is that of atacamite. If the octahedral vacancies within the atacamite layers are occupied by $[Cu(OH)_5Cl]$, we have the monoclinic botallackite. When successive Kagomé layers are combined directly by sharing corners, the claringbullite structure results. The Kagomé networks and the Cu(II) trimers in orthorhombic, monoclinic, and triclinic members of the atacamite group deviate slightly from the perfect threefold symmetry (Malcherek and Schlüter 2009).

Antiferromagnetic solids, based on the Kagomé lattices, are of great interest because of their geometrically induced magnetic frustration. The Kagomé layers of herbertsmithite and kapellasite, in particular, retain the perfect threefold symmetry with equilateral triangular motifs, where competing interactions between neighboring Cu^{2+} ions (S = 1/2) cannot be satisfied simultaneously (i.e., the freeze of the spin is frustrated). However, intrinsic inter-site mixing (i.e. ~15–25%) between similar Zn^{2+} and Cu^{2+} occurs invariably in herbertsmithite and kapellaste, and

potentially breaks the magnetic two-dimensionality. In contrast, centennialite features Kagomé layers with the threefold symmetry but <5% substitution between Cu and Ca, hence representing a better model material than herbertsmithite and kapellasite for evaluating competing interactions between neighboring Cu^{2+} ions and their effects on magnetic properties (Sun et al. 2016).

3.2.2.5 Mercury Halide Minerals and the Halogen Bond

Table 3.1 shows that chloride, bromide and iodide minerals containing Hg figure prominently. Many mercury halides contain the Hg_2 dimer, which is characterized by a short Hg–Hg bond and is commonly referred to as a "van der Waals dimer" for the lack of covalent bonding in the ground state. Theoretical calculations have shown that the dimer ground-state potential, formed from two ^1S ground-state Hg atoms, is essentially repulsive but possesses a shallow van der Waals minimum due to correlation effects (Czuchaj et al. 1997). For example, each Hg atom in minerals having the calomel-type structure (*I*4/*mmm*) is coordinated to five halogen atoms forming a tetragonal pyramid, but this configuration includes an additional short Hg–Hg bond of 2.490 to 2.724 Å (Table 3.9).

Similarly, the crystal structure of aurivilliusite (Hg_2OI) is characterized by the short Hg–Hg bonds at 2.534 Å and can be best described in terms of tetrahedral [O_2Hg_6] dimers sharing corners to form a 2D tetrahedral layer parallel to (100), while I atoms are located in cavities formed by surrounding [OHg_4] tetrahedra (Fig. 3.19). Each I atom is linked to two Hg atoms at 3.051–3.136 Å, and to five additional Hg atoms with longer distances at 3.466–3.761 Å. Successive 2D tetrahedral layers are joined via the Hg–Hg bonds (Stalhandske et al. 1985).

One rare example of mercury halides without the Hg_2 dimer is coccinite (HgI_2), in which the Hg atoms are coordinated by four I atoms at a distance of 2.786 Å and each I atom bridges two Hg (Schwarzenbach et al. 2007; Fig. 3.20). Each [HgI_4] tetrahedron shares all I-corners with surrounding tetrahedra to form a layer parallel to (001). The layers are held together by weak interlayer forces. This crystal structure of coccinite, similar to those of many simple halides, can also be described in terms of a cubic closest packing of the I atoms with the Hg atoms occupying

Table 3.9 Mercury halides with the calomel-type structure

Minerals	Formula	Bond distances	Reference
Calomel	Hg_2Cl_2	2.551(Hg–Hg), 2.507, 3.181 (× 4) (Hg–Cl)	Dorm (1970)
Kuzminite	Hg_2Br_2	2.490(Hg–Hg), 2.707, 3.318 (× 4) (Hg–Br)	Dorm (1970)
Moschelite	Hg_2I_2	2.724(Hg–Hg), 2.747, 3.503 (× 4) (Hg–I)	Huggins and Magill (1927)

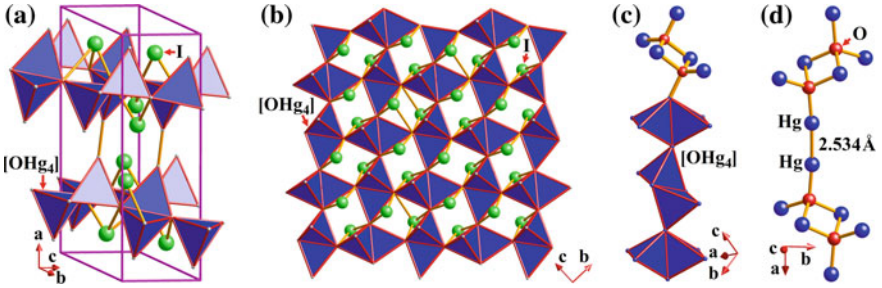

Fig. 3.19 The crystal structure of aurivilliusite: **a** the unit cell marked by the *purple lines*, **b** the tetrahedral layer, **c** linkage of the $[O_2Hg_6]$ dimers, and **d** the short Hg–Hg bonds at 2.534 Å

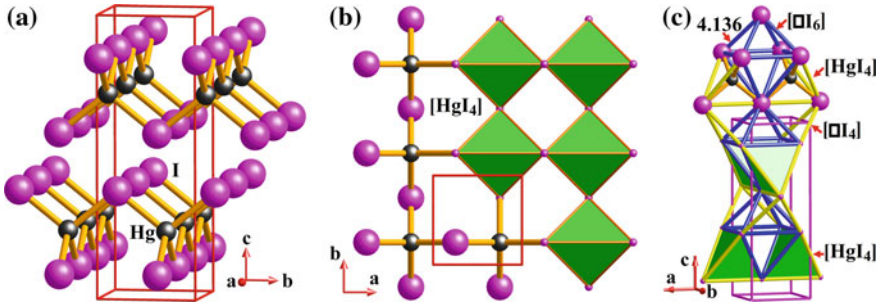

Fig. 3.20 The crystal structure of coccinite: **a** the unit cell marked by *purple lines*, **b** the tetrahedral layer, and **c** the $[HgI_4]$ tetrahedra, $[\square I_4]$ tetrahedral voids, and $[\square I_6]$ octahedral voids

one-quarter of the tetrahedral voids forming layers composed of corner-linked $[HgI_4]$ tetrahedra. Three quarters of the tetrahedral voids and all octahedral voids are unoccupied. The I atoms are coordinated by two Hg atoms. There exist weak I–I bonds (4.136 Å) between the $[HgI_4]$ tetrahedral layers (Fig. 3.20).

These mercury halides are excellent examples of the halogen bond in minerals, which "occurs when there is evidence of a net attractive interaction between an electrophilic region associated with a halogen atom in a molecular entity and a nucleophilic region in another, or the same, molecular entity" (Desiraju et al. 2013). The halogen bond (XB) is analogous to the well known hydrogen bond (HB), because halogens act as electrophiles in the former as the hydrogen atoms do in the latter (Cavallo et al. 2016). The Hg_2-X···X configurations in calomel, kuzminite and moschelite possess the characteristic geometries of the halogen bond (i.e., the R-X···Y angle of $\sim 180°$) and have the Cl···Cl, Br···Br and I···I distances of 3.335, 3.228 and 3.422 Å, respectively. These distances can be compared with the van de Waals radii of halogens (1.47, 1.75, 1.85 and 1.98 Å for F, Cl, Br and I, respectively), consistent with the order of the XB donor ability (I > Br > Cl > F; Cavallo et al. 2016).

3.2.3 Halogenate Minerals

Halogenates are these containing the oxyanions of Cl, Br and I, where they have the oxidation numbers of +1, +3, +5 or +7. For example, Cl is known to form various oxyanions such as hypochlorite (ClO^-), chlorite (ClO_2^-), chlorate (ClO_3^-), and perchlorate (ClO_4^-). Trace amounts of perchlorates have been known to occur in the nitrate deposits of the Atacama Desert of northern Chile since the 1880s (Ericksen 1981; Böhlke et al. 2009). It has been proposed that they are natural products, arising from the oxidation of atmospheric or aqueous Cl species (e.g., lighting, ultraviolet light, or thermal induced processes; Kounaves et al. 2010; Rao et al. 2010, 2012). Considerable interest in perchlorates has also come from their potential discovery on the Mars by the Phoenix lander in 2008 and the Curiosity rover in 2012 (Chevrier et al. 2009; Hecht et al. 2009; Kounaves et al. 2014; Rampe et al. 2017; Grotzinger et al. 2015). At the present time, however, no minerals containing essential perchlorate have been discovered on Earth. The scarcity of halogenate minerals is attributable to the high reactivity and solubility of such compounds in water. To date, all halogenate minerals known are iodates, with the exception of schwartzembergite (Table 3.10), and are found almost exclusively from the nitrate deposits of the Atacama Desert.

The stereochemistry of I^{5+} is characterized by the presence of the lone-pair electrons, similar to that of Pb^{2+} (Burns and Hawthorne 1993; Welch et al. 2001). The iodate group $[IO_3]^-$ has three O atoms located on the other side of the lone-pair electrons (Burns and Hawthorne 1993), with the average <I–O> bond distance of 1.8106(77) Å. The $[IO_3]^-$ group is also linked weakly to one or more additional

Table 3.10 Summary of iodate minerals

Mineral	Formula	Space group	Reference
Bruggenite	$Ca(IO_3)_2{\cdot}H_2O$	$P2_1/c$	Alici et al. (1992)
Lautarite	$Ca(IO_3)_2$	$P2_1/n$	Ghose et al. (1978)
Bellingerite	$Cu_3(IO_3)_6{\cdot}2H_2O$	$P\bar{1}$	Ghose and Wan (1974)
Salesite	$Cu(IO_3)(OH)$	*Pnma*	Ghose and Wan (1978)
Seeligerite	$Pb_3IO_4Cl_3$	*Cmm*2	Bindi et al. (2008)
Dietzeite	$Ca_2H_2O(IO_3)_2(CrO_4)$	$P2_1/c$	Burns and Hawthorne (1993)
Georgeericksenite	$Na_6CaMg(IO_3)_6(CrO_4)_2{\cdot}12H_2O$	*C*2/*c*	Cooper et al. (1998)
Hectorfloresite	$Na_9(IO_3)(SO_4)_4$	$P2_1/a$	Ericksen et al. (1989)
Fuenzalidaite	$K_6(Na,K)_4Na_6Mg_{10}(SO_4)_{12}(IO_3){\cdot}12H_2O$	$P\bar{3}c$	Konnert et al. (1994)
Carlosruizite	$K_6(Na,K)_4Na_6Mg_{10}(SeO_4)_{12}(IO_3){\cdot}12H_2O$	$P\bar{3}c$	Konnert et al. (1994)
Schwartzembergite	$Pb_5IO_6H_2Cl_3$	*I*4/*mmm*	Welch et al. (2001)

O atoms on the side of the lone-pair electrons to form a variety of fourfold to eightfold coordination polyhedra (e.g., distorted squares, distorted trigonal bipyramids, distorted octahedra, distorted pentagonal bipyramids or irregular sevenfold coordination polyhedra, and distorted square antiprisms). In salesite the I atom is bonded to the three nearest O atoms at 1.791 to 1.804 Å on one side as well as one OH group at 2.507 Å and two more O atoms at 2.702 Å on the other side (i.e., a distorted [IO_5(OH)], Ghose and Wan 1978). Iodate polymerization is well known in synthetic compounds (e.g., a bent molecule consisting of two [IO_3] pyramids sharing a corner in diiodine pentoxide; Selte and Kjekshus 1970), but has not been observed in iodate minerals.

The crystal structure of seeligerite (Bindi et al. 2008) consists of five distinct types of layers parallel to (001) (Fig. 3.21). In a tetragonal anti-prism layer (labelled as AL in Fig. 3.21), each Pb^{2+} ion is surrounded by four O atoms on one side and four Cl atoms on another side forming a tetragonal anti-prism, which is arranged in a chessboard mode. In a square layer (SL), each Pb^{2+} ion bonds to four Cl^- ions in a square where Pb^{2+} slightly deviates from the square plane of four Cl^- ions. Also present are two tetrahedral layers: TL1 and TL2. Each [OPb_4] tetrahedron shares its four edges and all corners with neighboring counterparts to form the [OPb_4] tetrahedral layer (TL1). In TL2 one quarter of the [OPb_4] tetrahedral corners is replaced by I to give rise to a chemically distinct layer of [OPb_3I] tetrahedra.

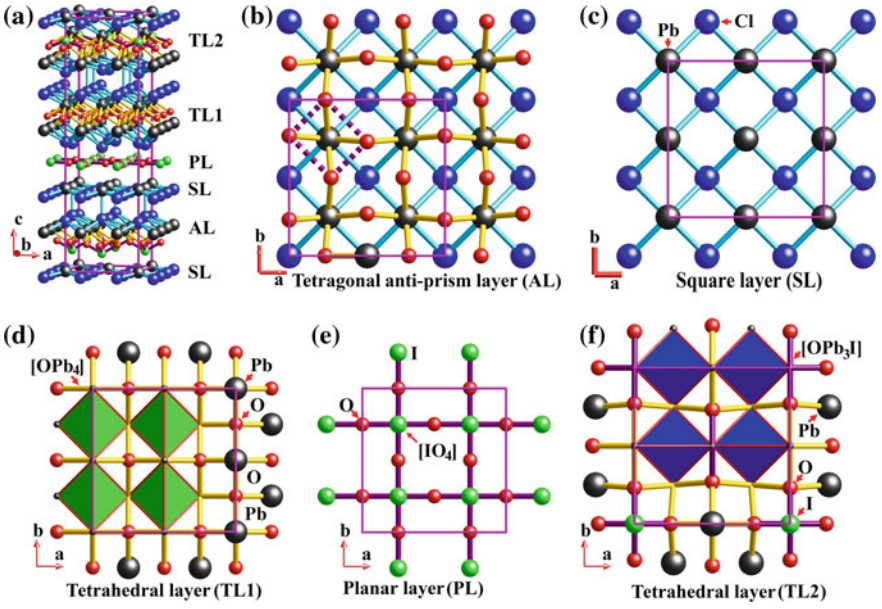

Fig. 3.21 The crystal structure of seeligerite: **a** the unit cell consisting of 5 distinct types of layers; **b** the anti-prism layer (AL); **c** the square layer (SL); **d** the tetrahedral layer 1 (TL1); **e** the planar layer (PL); and **f** the tetrahedral layer 2 (TL2). *Black, blue, red, and green spheres* represent Pb, Cl, O and I atoms, respectively

The crystal structure of seeligerite can thus be described in terms of these layers stacked along the *c*-axis. Each I atom (I2) in the planar plane (PL) bonds to four O atoms in a square planar configuration, vice versa. The other two I atoms (I1 and I3) are also coordinated by four oxygen atoms but feature a "one-sided" configuration. These $[IO_4]^{3-}$ groups in seeligerite have I-O bond distances from 1.92 to 2.00 Å, significantly longer than those of the classical iodate $[IO_3]^{-}$ groups. Welch et al. (2001) and Bindi et al. (2008) classified schwartzembergite containing I^{3+} and seeligerite as members of a family of "layered Pb-sheet oxychlorides", rather than iodates containing chlorine.

3.3 Halogens in Rock-Forming Minerals

Rock-forming minerals of the amphibole, apatite, epidote, mica, scapolite, sodalite, tourmaline and vesuvianite groups or supergroups often contain significant amounts of halogens (mainly F and less commonly Cl) and are usually the main carriers of these important elements in rocks (Petersen et al. 1982; Valley et al. 1983; Groat et al. 1992; Oen and Lustenhouwer 1992; Bernal et al. 2017; Zhang et al. 2017; Galuskin et al. 2003; Patino Douce et al. 2011; Zhang et al. 2012; Teiber et al. 2014). The incorporation of halogens in hydrous rock-forming minerals occur mainly via the isovalent substitution for the hydroxyl anion: $(F,Cl)^{-} = (OH)^{-}$ (Petersen et al. 1982; Pan and Fleet 1990, 1992a, b; Groat et al. 1992; Harlov and Melzer 2002; Henry et al. 2011; Hawthorne et al. 2012). Other substitutions such as $(Mg,Fe)^{2+} + F^{-} = Al^{3+} + O^{2-}$, may also be important in some hydrous minerals (e.g., dollaseite-(Ce); Peacor and Dunn 1988; Pan and Fleet 1990; Armbruster et al. 2006). In addition, complex substitutions such as $[BO_3F]^{4-} = [SiO_4]^{4-}$, $[F,OH]_4^{4-} = [SiO_4]^{4-}$ and $(Al,Fe)^{3+} + F^{-} = Ti^{4+} + O^{2-}$ have been proposed to explain the incorporation of F^{-} into nominally anhydrous minerals such as olivines, garnets and titanite (Valley et al. 1983; Manning and Bird 1990; Smyth et al. 1990; Pan et al. 1993b; Schreyer et al. 2003; Harlov et al. 2006; Sharova et al. 2012). Halogens in open framework silicates, such as scapolites and sodalities, are more diverse (i.e., mainly Cl but Br and I as well) and are generally accommodated in large structural cages (Fleet 1989; Pan and Dong 2003; Galuskin et al. 2015; Bernal et al. 2017; Zhang et al. 2017).

Nominally anhydrous rock-forming minerals, such as olivines and pyroxenes, are also known to contain trace amounts of halogens and are expected to play important roles in the halogen geochemical cycles in the mantle (Zhang et al. 2007; Beyer et al. 2012; Dalou et al. 2012; Fabbrizio et al. 2013a, b; Frezzotti and Ferrando 2018; Klemme et al. 2018). However, information about halogen speciation and local structural environments in nominally anhydrous minerals is generally lacking. Similarly, serpentine-group minerals probably contain only trace amounts of halogens but have been proposed to play critical roles in controlling halogen geochemical cycles during subduction processes (Scambelluri et al. 2004; Kendrick et al. 2011; Barnes et al. 2018; Kendrick 2018). Again, little is known about the distribution and structural environments of halogens in serpentinite-group

minerals (Labouriau et al. 1995). Natural and synthetic calcite has been desmonstrated to be capable of accommodating trace amounts of I and other halogens as well (Lu et al. 2010; Podder et al. 2017).

This section starts with a discussion on the mechanisms by which F and Cl are incorporated into amphiboles and micas. Amphiboles and micas are common minerals in diverse igneous and metamorphic rocks and their crystal-chemical features are widely useful for calculating the fluid/melt compositions in igneous, metamorphic, and hydrothermal systems. Understanding the halogen composition and evolution of fluids and melts is important, not only for elucidating igneous and metamorphic processes, but also for unravelling the transportation and deposition mechanisms responsible for the formation of mineral deposits (Aranovich and Safonov 2018; Lecumberri-Sanchez and Bodnar 2018; Hammerli and Rubenach 2018; Webster et al. 2018; Dolejs and Zajacz 2018). Also discussed in this section are scapolites and sodalities, which can serve as important hosts of halogens in some meteorites and exotic rocks (Pan 1998; Pan and Dong 2003; Brearley and Jones 2018). In addition, minerals of the apatite supergroup, which are stable over a wide range of physio-chemical conditions from surficial environments to the mantle, are included. While they typically occur as accessory phases, they can also serve as the dominant carriers of halogens in some geological environments (Pan and Breaks 1997; Harlov et al. 2002; Hansen and Harlov 2007). Also, apatites are useful for calculating the fluid/melt compositions in diagenetic, metamorphic, and igneous systems (Aranovich and Safonov 2018; Lecumberri-Sanchez and Bodnar 2018; Hammerli and Rubenach 2018; Webster et al. 2018; Worden 2018; Dolejs and Zajacz 2018).

3.3.1 Amphiboles

The latest classification scheme of Hawthorne et al. (2012) first divides the minerals of the amphibole supergroup, with the general formula $AB_2C_5T_8O_{22}W_2$, into two groups on the basis of the dominant W anions at the O3 site: (1) ^{W}(OH, F, Cl)-dominant amphiboles and (2) ^{W}O-dominant amphiboles or oxo-amphiboles. All F- and Cl-dominant amphiboles (F > OH,Cl and Cl > OH,F) in the first group are named by using the prefixes “fluoro” and “chloro”, respectively, to the root names (Table 3.11). There are several other F- (e.g., “fluoro-tremolite”, Petersen et al. 1982) and Cl-dominant (e.g., “potassic-ferro-chloro-edenite”, Pan and Fleet 1992a; “potassic-ferro-chloro-pargasite”, Castelli 1988; “ferro-chloro-sadanagaite”, Kullerud and Erambert 1999) compositions known in the literature, but they require further characterization before being considered as valid species.

The local structural environment of F^- at the O3 site in amphiboles is closely comparable but not identical to that of the OH^- anion (Fig. 3.22). Here, the O atom, that is part of the OH^- group, is bonded to two *M*1, one *M*3, and one H atom, whereas the coordination number of F, without a neighboring H atom, is reduced to 3. The substitution of F for OH in amphiboles also leads to reductions in the sizes of the octahedral sites (e.g., the *M*1-F and *M*3-F bonds at 2.057(3) and 2.011(4) Å in

Table 3.11 Summary of halogen-dominant amphiboles

Mineral	Formula	Reference
Fluoro-cannilloite	$CaCa_2(Mg_4Al)(Si_5Al_3)O_{22}F_2$	Hawthorne et al. (1996a)
Fluoro-edenite	$NaCa_2Mg_5(Si_7Al)O_{22}F_2$	Gianfagna and Oberti (2001)
Magnesio-fluoro-hastingsite	$NaCa_2(Mg_4Fe^{3+})(Si_6Al_2)O_{22}F_2$	Bojar and Walter (2006)
Potassic-fluoro-hastingsite	$KCa_2(Fe_4^{2+}Fe^{3+})(Si_6Al_2)O_{22}F_2$	Lupulescu et al. (2009)
Ferri-fluoro-leakeite	$NaNa_2(Mg_2Fe_2^{3+}Li)Si_8O_{22}F_2$	Cámara et al. (2010)
Ferro-ferri-fluoro-leakeite	$NaNa_2(Fe_2^{2+}Fe_2^{3+}Li)Si_2O_{22}F_2$	Hawthorne et al. (1996b)
Fluoro-leakeite	$NaNa_2(Mg_2Al_2Li)Si_8O_{22}F_2$	Oberti et al. (2009b)
Fluoro-nybøite	$NaNa_2(Mg_3Al_2)(Si_7Al)O_{22}F_2$	Oberti et al. (2003)
Fluoro-pargasite	$NaCa_2(Mg_4Al)(Si_6Al_2)O_{22}F_2$	Lupulescu et al. (2005)
Potassic-fluoro-pargasite	$KCa_2(Mg_4Al)Si_6Al_2O_{22}F_2$	Oberti et al. (2010)
Fluoro-pedrizite	$NaLi_2(Mg_2Al_2Li)Si_8O_{22}F_2$	Oberti et al. (2005)
Ferro-fluoro-pedrizite	$NaLi_2(Fe_2^{2+}Al_2Li)Si_8O_{22}F_2$	Oberti et al. (2009a)
Magnesio-fluoro-arfvedsonite	$NaNa_2(Mg_4Fe^{3+})Si_8O_{22}F_2$	Bazhenov et al. (2000)
Potassic-magnesio-fluoro-arfvedsonite	$KNa_2(Mg_4Fe^{3+})Si_8O_{22}F_2$	Hogarth (2006)
Ferri-fluoro-katophorite	$Na(NaCa)(Mg_4Fe^{3+})(Si_7Al)O_{22}F_2$	Hawthorne et al. (2006)
Fluoro-richterite	$Na(NaCa)Mg_5Si_8O_{22}F_2$	Cameron et al. (1983)
Potassic-fluoro-richterite	$K(NaCa)Mg_5Si_8O_{22}F_2$	Della Ventura et al. (1983)
Fluoro-riebeckite	$\square Na_2(Fe_3^{2+}Fe_2^{3+})Si_8O_{22}F_2$	Hawthorne (1978)
Fluoro-taramite	$Na(NaCa)(Mg_3Al_2)(Si_6Al_2)O_{22}F_2$	Oberti et al. (2007)
Potassic-chloro-hastingsite	$KCa_2(Fe_4^{2+}Fe^{3+})(Si_6Al_2)O_{22}Cl_2$	Pekov et al. (2005)
Potassic-chloro-pargasite	$KCa_2(Mg_4Al)(Si_6Al_2)O_{22}Cl_2$	Chukanov et al. (2002)

synthetic "fluoro-tremolite" in comparison with the corresponding *M*1-O3 and *M*3-O3 bonds at 2.083(2) and 2.057(3) Å in tremolite; Cameron and Gibbs 1973). Spectroscopic studies (e.g., FTIR and NMR) have shown that the substitution of F for OH in amphiboles have marked effects on the short-range order (Robert et al. 1999, 2000; Della Ventura et al. 2001, 2014). For example, FTIR spectra showed that Si and Al at the tetrahedral sites in the fluoro-edenite and fluoro-pargasite structures are ordered in such a way that Si-O7-Si linkages regularly alternate with Si–O7–Al linkages along the double chain (Della Ventura et al. 2014). The large

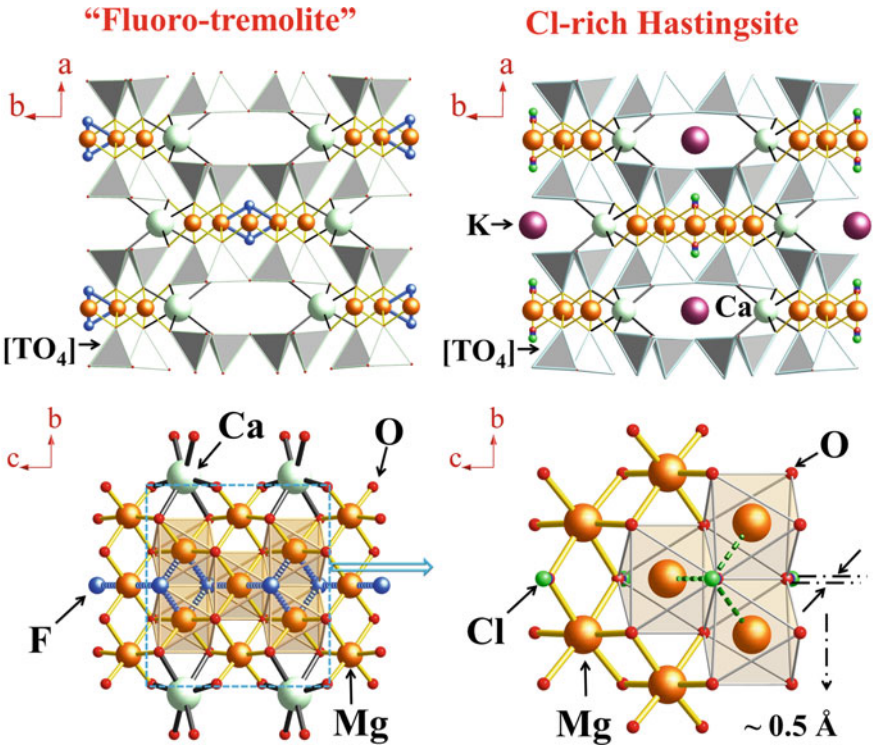

Fig. 3.22 Crystal structures of "fluoro-tremolite" (*left*) and Cl-rich hastingsite (*right*) with emphasis on the environments of F (*lower left*) and Cl (*lower right*). Note that Cl is displaced from the O3 site by ~0.5 Å along [100]. (Makino et al. 1993)

number of F-dominant species (Table 3.12) and the common occurrences of F-rich amphiboles in diverse geological environments have been interpreted that their formation is directly related to F-rich melt/fluid compositions with minimal structural restrictions. Nevertheless, F-rich amphiboles commonly have low Fe^{2+} contents (Petersen et al. 1982; Valley et al. 1983), giving rise to what is referred to as the "Fe^{2+}-F avoidance rule" in silicates (Ramberg 1952; Rosenberg and Foit 1977; Volfinger et al. 1985; Volfinger and Pascal 1989; Zhang et al. 2012).

Structural studies of Cl-rich amphiboles (Makino et al. 1993; Oberti et al. 1993; Rastvetaeva et al. 1996) have shown that the Cl atom at the O_3 site is markedly different from the F and hydroxyl O atoms in local structural environments (Fig. 3.22). For example, structure refinements by Oberti et al. (1993) showed that the monovalent anion site in amphiboles with intermediate Cl contents is split into two distinct sites: O3 and O3′. These two sites are separated by ~0.5 Å along [100] and are preferentially occupied by (OH,F) and Cl, respectively. The Cl atom at the O3′ site is not only coordinated to the cations at the two *M*1 and one *M*3 sites but also has a strong bonding interaction with K at the A site, resulting in a fourfold

Table 3.12 List of F-dominant micas

Mineral	Formula	Reference
Fluorannite	$KFe_3(AlSi_3O_{10})F_2$	Shen et al. (2000)
Fluorokinoshitalite	$BaMg_3(Al_2Si_2O_{10})F_2$	Miyawaki et al. (2011a)
Fluorophlogopite	$KMg_3(AlSi_3O_{10})F_2$	Gianfagna et al. (2007)
Fluorotetraferriphlogopite	$KMg_3(Fe^{3+}Si_3O_{10})F_2$	Miyawaki et al. (2011a)
Masutomilite	$K(Li,Mn^{3+},Al)_3(Al_2Si_2O_{10})F_2$	Mizota et al. (1986)
Montdorite	$K(Fe^{2+}_{1.5}Mn^{2+}_{0.5}Mg_{0.5})(Si_4O_{10})F_2$	Robert and Maury (1979)
Orlovite	$K(Li_2Ti(Si_4O_{10})OF$	Agakhanov et al. (2011)
Polylithionite	$KLi_2Al(Si_4O_{10})F_2$	Takeda and Burnham (1969)
Shirokshinite	$KNaMg_2(Si_4O_{10})F_2$	Pekov et al. (2003)
Sokolovaite	$CsLi_2Al(Si_4O_{10})F_2$	Pautov et al. (2006)
Tainiolite	$KLiMg_2(Si_4O_{10})F_2$	Toraya et al. (1977)
Trilithionite	$KLi_{1.5}Al_{1.5}(AlSi_3O_{10})F_2$	Brigatti et al. (2005)
Voloshinite	$KLiAl_{1.5}(Al_{0.5}Si_{3.5}O_{10})F_2$	Pekov et al. (2010)
Yangzhumingite	$KMg_{2.5}(Si_4O_{10})F_2$	Miyawaki et al. (2011b)

coordination. The structural data of Oberti et al. (1993) also provide compelling evidence for a Fe^{2+}-Cl short-range order and show that the expansion of the octahedral sheet caused by the incorporation of Cl involves a concomitant expansion of the tetrahedral chain mainly by an increased substitution of $^{[4]}Al$ for Si. These results provide the structural explanation for the common correlations of Cl-bearing amphiboles with (1) Fe^{2+}-rich (Mg-poor) compositions, (2) abundant K on the A site, and (3) elevated Al at the tetrahedral sites (Pan and Fleet 1992a; Oberti et al. 1993; Sato et al. 2005; Su et al. 2015).

The effects of the F for OH substitution in amphiboles on the expansion of the upper thermal stabilities of these minerals have long been proposed but not sufficiently demonstrated (Gilbert et al. 1982; Harlow 2002). The most spectacular example is that the upper stability limit of "fluoro-tremolite" at atmospheric pressure is 584 °C higher than that of tremolite, which is greatly reduced at elevated pressures (Gilbert et al. 1982). Similarly, Gilbert et al. (1982) noted that the low-pressure difference of ~300 °C in stability between potassic-richterite and potassic-fluoro-richterite is diminished with increasing pressure. However, Foley (1991) showed that the trend in stability differences between potassic-richterite and potassic-fluoro-richterite is reversed at still higher pressures between 35 and 50 kbar. Harlow (2002) reported that F in potassic-richterite from his experiments between 3 and 11 GPa decreases with increasing P but increases upon increasing T, different from the trends reported by Foley (1991).

The F and Cl contents in amphiboles have been shown to be useful for determining the compositions and evolution of coexisting melts and fluids in igneous systems and quantifying fluid-rock interactions in metamorphic rocks (Xiao et al. 2005; Zhang et al. 2012; Su et al. 2015). Fabbrizio et al. (2013b) reported a D_F value of 0.24 between aqueous fluid and tremolite at 2 GPa and 900 °C, where

D_F = concentration^{fluid}/concentration^{tremolite}. Wu and Koga (2013), in their experimental study of the fluid-hornblende-humite system at 1 GPa and 770–947 °C, showed that the D_F between fluid and hornblende (Mg# = 0.88–0.91) is not sensitive to temperature in the range investigated and can be represented by a single value of 0.13 ± 0.03. Anfilogov et al. (1977) reported a D_F = 6.1 between granitic melt and hornblende (Mg# = 0.61) at 780 °C and 1000 atmosphere. Edgar and Pizzolato (1995) reported the D_F values from 0.7 to 1.4 between potassic-richterite and melt at 2 GPa and 1000–1100 °C. The reported D_F values include 1.59–2.78 between basaltic melt and hornblende and ~1.4 between hastingsite and rhyolite (cited in Wu and Koga 2013). Zhang et al. (2012) proposed an empirical equation for the partitioning of F and OH between melt and amphibole,

$$\log\left[(F/OH)^{amphibole}/(F/OH)^{melt}\right] = -0.19 + 1.10Mg\# \tag{3.1}$$

Sato et al. (2005) determined the exchange coefficients for Cl and OH between hornblende and dacite melt at 2–3 kbar and 800–850 °C and showed them to depend on both the major-element composition (Mg#) of hornblende and the absolute temperature (T):

$$\ln\left[(Cl/OH)^{Hb}/(Cl/OH)^{melt}\right] = 8.62 - 3.46Mg\# - 0.0062T \tag{3.2}$$

Giesting and Filiberto (2014) re-evaluated the Sato et al. (2005) dataset and proposed the following model for igneous amphiboles in general:

$$\ln\left[(X_{Cl}/X_{OH})^{amphibole}/([Cl]/[OH])^{melt}\right] = 6.59K/\left(Na + {}^{[A]}\right) - 0.679Mg + 0.487{}^{[6]}Fe \tag{3.3}$$

where X_{Cl} and X_{OH} denote the molar fractions of Cl and OH at the W site, respectively; [Cl] and [OH] are the molar fractions of Cl and OH in the melt on the one-oxygen basis; K, Na, Mg and $^{[6]}$Fe represent the atomic proportion of each component per amphibole formula unit; and $^{[A]}$ denotes the number of vacancies at the A site. Fabbrizio et al. (2013b) reported a D_{Cl} value of ~0.005 between an aqueous fluid and tremolite at 2 GPa and 900 °C. Su et al. (2015) reported the diffusion coefficients of chlorine in pargasitic amphibole at 1.0 GPa and 625–800 °C.

3.3.2 *Micas*

Similar to the amphiboles, halogens in the micas are dominantly F and less commonly Cl, and are preferentially incorporated into the trioctahedral varieties over their dioctahedral counterparts (Munoz 1984; Robert et al. 1993; Boukili et al. 2001, 2002; Fechtelkord et al. 2003a, b). Fluorophlogopite was first synthesized

from laboratory experiments (Hazen and Burnham 1973) and has recently been established as a mineral species (Gianfagna et al. 2007). Other F-dominant minerals of the mica supergroup are listed in Table 3.12. Although a number of Cl-rich compositions in micas (up to 7.45 wt% or 1.08 *apfu*) have been reported in the literature (Tracy 1991; Oen and Lustenhouwer 1992; Nash and Connor 1993; Léger et al. 1996; Izraeli et al. 2004; Uher et al. 2014), there is no approved Cl-dominant mica yet (Rieder et al. 1998).

The environment of F in micas has been investigated by diverse structural techniques (e.g., Hazen and Burnham 1973; Mason 1992; Robert et al. 1993; Papin et al. 1997; Rancourt et al. 1996; Russell and Guggenheim 1999; Boukili et al. 2001, 2002; Fechtelkord et al. 2003a, b; Brigatti et al. 2007; Gianfagna et al. 2007; Scordari et al. 2013). Fluorine at the O4 site is located at the same level of the apical O atoms from the tetrahedral sheet and is bonded to 3 and 2 octahedral cations in trioctahedral and dioctahedral micas, respectively (Fig. 3.23; Hazen and Burnham 1973; Redhammer and Roth 2002; Brigatti et al. 2007; Gianfagna et al. 2007). The F–OH substitution in trioctahedral micas changes the H^+–K^+ columbic repulsion to

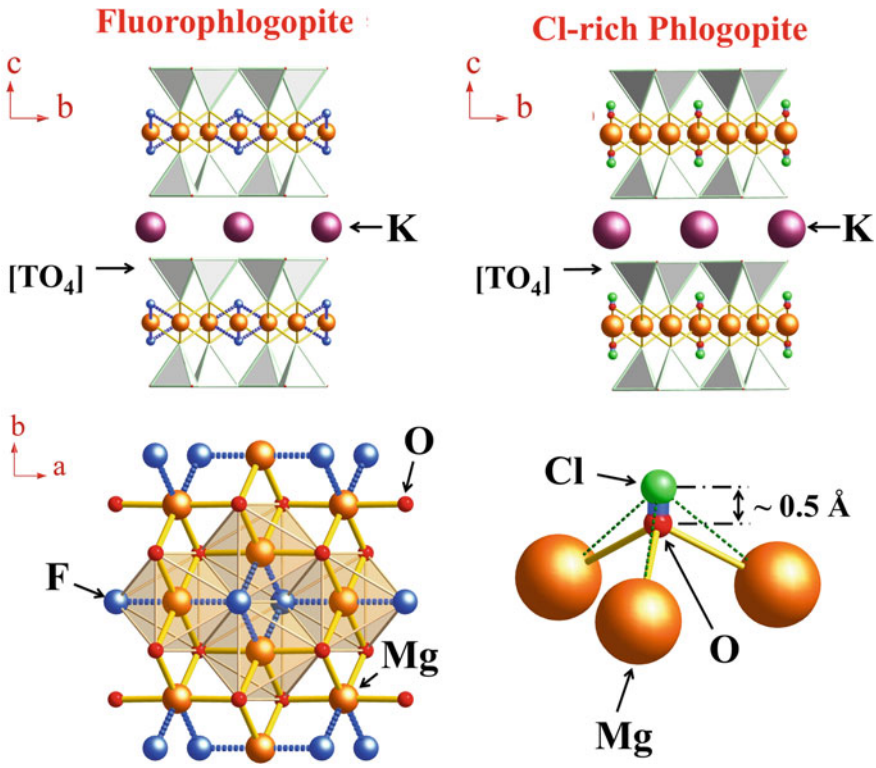

Fig. 3.23 Crystal structures of fluorophlogopite (*left*) and Cl-bearing phlogopite. Note that Cl is located at ~0.5 Å away from the O4 site. (Nazzareni et al. 2008)

F^-–K^+ attraction, resulting in a marked reduction in the interlayer separation from 3.487 Å in phlogopite (Redhammer and Roth 2002) to 3.322 Å in fluorophlogopite (Gianfagna et al. 2007) and from 3.375 Å in annite to 3.316 Å in fluorannite (Brigatti et al. 2007). This effect is less important in dioctahedral micas, where H^+ moves towards the vacant octahedral site and is repositioned in the octahedral layer, about 1 Å further away from the interlayer cation (Hazen and Burnham 1973). Therefore, the F–OH substitution in muscovite does not alter the columbic forces acting on the interlayer cations (Hazen and Burnham 1973). Other important structural effects arising from the F–OH substitution in micas include: (1) reducing the misfit between the tetrahedral and octahedral (T–O) sheets, (2) increasing the octahedral angle, and (3) shrinking the octahedral sheet due to the shortening of the octahedral cation-anion distances (Gianfagna et al. 2007; Brigatti et al. 2007). Gianfagna et al. (2007) attributed the effects of the F-OH substitution on the structural features of micas to the following two reasons: (1) the structure becomes more compact due to the substitution of the attractive K–F for the repulsive K–OH effect and (2) a decreased tetrahedral rotation angle (α) causes an effective coordination around K, enhancing the structural stabilities. Russell and Guggenheim (1999) noted that the *M*1 and *M*2 octahedra in phlogopite expand in volume without a significant change in shape at elevated temperatures, whereas these octahedra in fluorophlogopite become elongated approximately along [001] (Takeda and Morosin 1975).

The Fe^{2+}-F avoidance rule in micas has been attributed to the facts that Mg–F bonds are stronger than Fe–F bonds (Ramberg 1952), and that Fe^{2+} has smaller crystal field splitting parameters when coordinated by F^- *versus* OH^- (Rosenberg and Foit 1977). The observation of F-dominant, homogeneous domains in biotite from infrared (IR), nuclear magnetic resonance (NMR), Mossbauer, and synchrotron X-ray absorption spectroscopic (XAS) studies (Sanz and Stone 1983; Manceau et al. 1990) led Mason (1992) to propose a structural model with F only coordinated to groups of three Mg cations. Mason's (1992) model predicts that biotite may exhibit cation disorder on the octahedral sites only if the F content is below a maximum level (X_F^{max}), where $X_F^{max} = (X_{Mg})^3$, and that F in biotite, with F greater than X_F^{max}, must form clusters to comply with the Fe^{2+}-F avoidance rule. However, violations of the Fe^{2+}-F avoidance rule are not uncommon in natural micas and are attributable to the effects from other factors (e.g., P-T conditions and fluid/melt compositions, Mason 1992; Zhu and Sverjensky 1991, 1992; Webster et al. 2009).

The incorporation of the large Cl^- anion into micas is expected to have marked effects on the O4 site as well as on the neighboring octahedral and tetrahedral sites (Fig. 3.23). Single-crystal, X-ray structure refinement of a synthetic, Cl-bearing phlogopite (Nazzareni et al. 2008) showed that Cl is located at $\sim$0.5 Å away from the O4 site and has an appreciable bonding with K at 3.520(6) Å, similar to those found for Cl in amphiboles (Makino et al. 1993; Oberti et al. 1993; Rastvetaeva et al. 1996). The *M*1-Cl and *M*2-Cl bond distances at 2.319 and 2.337 Å are notably longer than their counterparts in phlogopite and fluorophlogopite (Hazen and Burnham 1973; Redhammer and Roth 2002; Gianfagna et al. 2007). However, the octahedral sheet thickness at 2.156 Å for Cl-bearing phlogopite (Nazzareni et al.

2008) is comparable with those of natural phlogopite (Brigatti and Guggenham 2002). Also, the tetrahedral rotation angle α of 2.58° (Nazzareni et al. 2008) is on the low side in comparison with those of phlogopite and fluorophlogopite (Gianfagna et al. 2007).

Many experimental studies have been made to investigate the partitioning of F and Cl between micas and fluids and have been synthesized in Munoz (1984, 1992) and Zhu and Sverjensky (1991, 1992). Using the partitioning coefficients for F and Cl between biotite and fluid, as determined by Zhu and Sverjensky (1991, 1992), Munoz (1992) formulated the following equations to calculate the fugacities of H_2O, HF, and HCl in the fluid (i.e., fH_2O, fHF, and $fHCl$) from the biotite compositions:

$$\log(fH_2O/fHF) = (1000/T) \times \left(2.37 + 1.1X_{Mg}\right) + 0.43 - \log(F/OH)_{Bt} \quad (3.4)$$

and

$$\log(fH_2O/fHCl) = (1000/T) \times \left(1.15 - 0.55X_{Mg}\right) + 0.68 - \log(Cl/OH)_{Bt} \quad (3.5)$$

where T is the absolute temperature in Kelvin, X_{Mg} = Mg/($^{[6]}$Al + Ti + Mn + Mg + Fe), $(F/OH)_{Bt}$ and $(Cl/OH)_{Bt}$ are the molar ratios in biotite.

The partitioning of F and Cl between biotite and melts has also been investigated for granitic, lamprophyric, basanitic, and phonolitic compositions (Anfilogov et al. 1977; Patino Douce and Johnston 1991; La Tourrette et al. 1995; Righter and Carmichael 1996; Icenhower and London 1997; Lukkari and Holtz 2007; Chevychelov et al. 2008). Icenhower and London (1997) showed that the partition coefficient of F between biotite and rhyolitic melt ($D_F^{Bt/melt}$), at 200 MPa H_2O, 640–680 °C, and fO_2 = the Ni–NiO (NNO) buffer varies from ~1.5 to 7.2 and has a strong dependence on the biotite composition over the range of Mg# [= Mg/(Mg + Mn + Fe)] from 0.21 to 0.76. Icenhower and London (1997) also reported that the $D_{Cl}^{Bt/melt}$ values of ~1 to 6 in the same experiments inversely correlate with the Mg# of biotite. Chevychelov et al. (2008) showed that that $D_F^{Bt/melt}$ with phonolitic melts at 200 MPa, ~850 °C and fO_2 = NNO decreases sharply from ~ 3.0 to 1.0 with an increasing total F content in the system, whereas $D_{Cl}^{Bt/melt}$ increases from 0.17 to 0.33 with an increasing total Cl content. Chevychelov et al. (2008) also noted that the apparent partition coefficients $D_F^{Bt/melt}$ in natural magmatic rocks are higher than their experimental values and interpreted this discrepancy to the influences of late oxidation reactions and re-equilibration of biotite.

3.3.3 Scapolites and Sodalites

The crystal structures of minerals belonging to the scapolite- and sodalite-groups are both characterized by large cages in the frameworks of AlO_4 and SiO_4

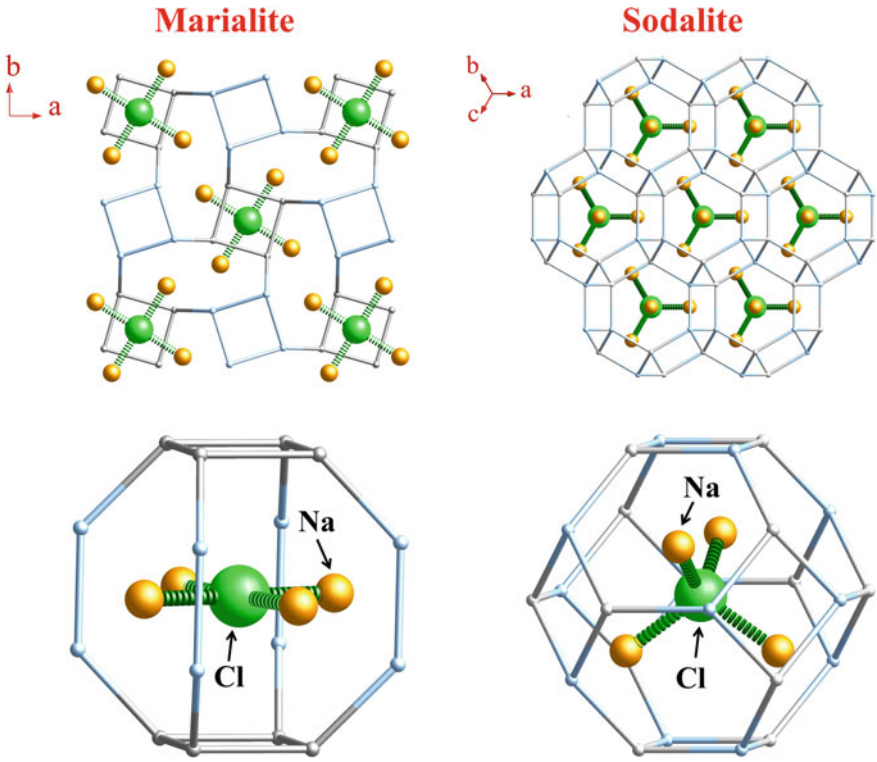

Fig. 3.24 Crystal structures of marialite (*left*) and sodalite (*right*). The *lower panels* showing the $[ClNa_4]^{3+}$ square-planar cluster and the $[ClNa_4]^{3+}$ tetrahedron in the marialite- and sodalite-type cages with an internal diameter of ~5.4 and ~6 Å, respectively

tetrahedra (Fig. 3.24). The cage in the scapolite-group member, marialite $[Na_4Al_3Si_9O_{24}Cl]$, is occupied by the Cl^- anion and is surrounded by four Na^+ cations residing in oval shaped channels parallel to the c-axis, forming the $[Cl{\cdot}Na_4]^{3+}$ square planar cluster (Fig. 3.24; Papike and Zoltai 1965; Sokolova and Hawthorne 2008b). Similarly, the so-called β-cage in sodalite, $[Na_8(Al_6Si_6O_{24})Cl_2]$ is bounded by eight six-membered rings parallel to the {111} planes and six four-membered rings parallel to the {001} planes (i.e., a truncated octahedron) (Fig. 3.24). The β-cage in sodalite encloses the $[Cl{\cdot}Na_4]^{3+}$ cluster in the tetrahedral configuration, which also occurs in the cage of the isotypic tugtupite $[Na_8(Al_2Be_2Si_8O_{24})Cl_2]$ (Hassan and Grundy 1991). In comparison, Cl in the ε-cages of the cancrinite-group minerals (e.g., davyne, microsommite and qudridavyne) is linearly coordinated by two Ca atoms to the ···Ca–Cl-Ca·· chains (Hassan and Grundy 1990; Ballirano et al. 1996).

Scapolites have been reported to occur as primary minerals in some igneous rocks (Boivin and Camus 1981; Goff et al. 1982; Vanko and Bishop 1982; Smith et al. 2008) and are particularly abundant in many metamorphic and metasomatic

rocks, some on a regional scale, representing a significant carrier of halogens (Mora and Valley 1989; Rebbert and Rice 1997; Teertstra and Sherriff 1997; Pan 1998; Hammerli et al. 2013, 2014; Kusebauch et al. 2015; Bernal et al. 2017; Zhang et al. 2017). X-ray fluorescence microprobe analyses of natural scapolites from various geological associations (Pan and Dong 2003) yielded up to 144(15) ppm Br and a wide range of Cl/Br values, from 80 to 1700, reflecting fluids from diverse sources (see also Hammerli et al. 2014).

Chlorine and Br exchange experiments between marialite and melt at 800 °C and atmospheric pressure yielded a distribution coefficient K_D at 0.97 ± 0.08 and a Br diffusion coefficient in marialite $D_{Br} = 1.7 \pm 0.3 \times 10^{-19}$ m^2/s (Pan and Dong 2003). These experimental results (i.e., lack of fractionation between Cl and Br and the low diffusivity of Br) led Pan and Dong (2003) to suggest that the Cl/Br values in scapolite are useful in constraining the sources and evolution of hydrothermal fluids. This suggestion has since been supported by LA-ICPMS analyses of Hammerli et al. (2014), which showed the Cl/Br values in scapolites from the Mary Kathleen Fold Belt (Australia) are comparable to those measured in fluid inclusions (Kendrick et al. 2008). The Cl/Br values of marialite in the Tieshan Fe skarn deposit (China) cluster around 650 ± 40, supporting an origin involving hydrothermal brines from associated evaporites (Pan and Dong 2003). The decrease in the Cl/Br values in scapolites from 560–570 in exoskarns to 130–180 in endoskarns and vuggy cavities, from the Nickel Plate Au skarn deposit (British Columbia), has been interpreted to record an increased involvement of magmatic water from distal to proximal zones (Pan et al. 1994). Similarly, the Cl/Br variation from 80 to 380 in scapolites from the Grenville U–Th–Mo– REE pegmatite–skarn–vein deposits has been interpreted to reflect mixed sources of hydrothermal fluids (Pan and Dong 2003). Kendrick and Phillips (2009) reported similar Cl/Br values for Grenville scapolites by INAA analyses and suggested a dominantly magmatic source.

Sodalites occur mainly in alkaline igneous rocks such as nepheline syenites but are also present in meteorites, metamorphic rocks, and hydrothermally altered igneous intrusions (Sharp et al. 1989, 2007). Natural sodalite contains up to 395(16) ppm Br (Pan and Dong 2003). Exchange experiments of Cl and Br between sodalite and melt at atmospheric pressure and 800–1000 °C yielded the distribution coefficient K_D at 0.9 ± 0.1 and a diffusion cofficient of Br in sodalite $D_{Br} = 6.5 \times 10^{-7}$ exp(–270 ± 10 kJ/mol/RT) m^2/s (Pan and Dong 2003). The significantly lower diffusion rates of Br in scapolites and sodalite, compared to its diffusion rate in apatite (see below), have been attributed to the locations of the $[Br{\cdot}Na_4]^{3+}$ clusters in cages surrounded by AlO_4 and SiO_4 tetrahedra (Pan and Dong 2003). The occurrences of the $[Br{\cdot}Na_4]^{3+}$ and $[I{\cdot}Na_4]^{3+}$ clusters in sodalites have been confirmed by the syntheses of $[Na_8(Al_6Si_6O_{24})Br_2]$ and $[Na_8(Al_6Si_6O_{24})I_2]$ (Henderson and Taylor 1978) and the structure refinements of $[Na_8(Al_6Ge_6O_{24})Br_2]$ and $[Na_8(Al_6Ge_6O_{24})I_2]$ (Fleet 1989). Trill et al. (2003) reported on the synthesis of mixed halide (Cl/Br, Cl/I, and Br/I) sodalite-like compounds at 450 K under autogenous pressures and showed that the incorporation of mixed halides into the cage depends on both the halide stoichiometry in the precursor gel and the halogen being incorporated. Trill et al. (2003) also noted that the Cl/Br and Br/I sodalite-like

compounds show close to ideal miscibility behavior, whereas in the Cl/I counterparts domain segregation effects prevail. Synthesis and characterization of other Br- and I-rich compounds, with the sodalite type structure, or Cl-, Br- and I-bearing zeolites with the sodalite-type cages, have also been reported (e.g., Stein et al. 1992; Jelinek et al. 1993; Maddrell et al. 2014).

In addition, sodalites are capable of accommodating the chlorate, perchlorate, and iodate anions in the cages (Veit et al. 1991; Buhl 1996; Borhade et al. 2010). Buhl (1996) used infrared (IR) analysis to confirm the presence of the iodate anion in synthetic sodalite and showed that iodate sodalite undergoes thermal decomposition in the temperature range of 450–730 °C to form iodide sodalite [$Na_8(Al_6Si_6O_{24})IO_{0.5}$]. Buhl (1996) determined the upper thermal stability of 857 °C for [$Na_8(Al_6Si_6O_{24})IO_{0.5}$], which is lower than that for the pure iodide sodalite (953 °C) (Henderson and Taylor 1978). Single-crystal XRD structure refinements of sodalite showed that the perchlorate anion, whose presence had been confirmed by IR and Raman spectra, occupies the centre of the cage and has a similar geometry to the free $[ClO_4]^-$ anion (Veit et al. 1991; Borhade et al. 2010). Sodalites, and related compounds with capacities for accommodating diverse I species, combined with their thermal stability and durability, have long been proposed as attractive matrices for encapsulating radionuclides such as ^{129}I and ^{131}I. In this context, the ^{129}I isotope is one of the most abundant long-lived volatile fission products of U and Pu and poses the most serious challenges to the long-term disposal of nuclear wastes. ^{131}I (half-life = 8 days) is one of the most important risk drivers immediately after nuclear accidents such as those that occurred at Chernobyl and Fukushima (Chino et al. 2011; Kaplan et al. 2014). Maddrell et al. (2014) measured a leach rate for iodide sodalitie at 0.005–0.01 $gm^{-2}d^{-1}$ and suggested a very slow dissolution in natural underground water saturated with the constituent elements.

Most industrial applications of sodalities and related materials are generally related to their catalytic properties. Another interesting property, related directly to the $[Cl{\cdot}Na_4]^{3+}$ cluster in the cages, is the antiferromagnetism observed in the so-called sodium-electro-sodalite (SES; Srdanov et al. 1998). Upon exposure to high energy irradiation or alkali vapor, the central Cl^- anion in the sodalite cage is replaced by an unpaired electron trapped by the four equivalent Na ions forming the $[Na_4]^{3+}$ ionic cluster (i.e., the F center), which at high concentrations in SES forms periodic arrays. The origin of the F center electron wave function in SES coincides with the center of the sodalite cage but a fraction of the electron density extends beyond the cage boundaries. This gives rise to a strong exchange coupling between neighboring unpaired electrons, which culminates in an antiferromagnetic transition at 48 K. The unpaired electrons in the $[Na_4]^{3+}$ clusters have predominantly an *s* character, therefore making SES the first example of an *s*-electron antiferromagnet (Srdanov et al. 1998).

Chlorine-rich minerals in terrestrial rocks and meteorites are excellent materials for Cl isotope analyses to understand geological and planetary processes (e.g., Eggenkamp and Schuiling 1995; Sharp et al. 2007, 2013; Kusebauch et al. 2015; Bernal et al. 2017). In this context, scapolites and sodalities are particularly attractive, because of their high thermal stabilities (Sharp et al. 1989; Pan 1998) and

the slow diffusion coefficients of halogens in these minerals (Pan and Dong 2003). Kusebauch et al. (2015) documented systematic increases in the $\delta^{37}Cl$ values of amphibole and scapolite separates from an unaltered gabbro towards a shear zone in the Bamble lower crustal rocks (SE Norway) and interpreted them to most likely record isotope fractionation that causes the evolution of a distinct infiltrating fluid by reactive flow. These authors also noted that the $\delta^{37}Cl$ values of amphiboles are 1‰ higher than those of the coexisting scapolites and interpreted this difference to isotopic fractionation during the formation or recrystallization of these minerals.

Other notable minerals with halogens in zeolite-like cages include those of the mayenite supergroup (Feng et al. 1988; Yu et al. 1997; Galuskin et al. 2015). Several minerals of the mayenite supergroup, such as adrianite $Ca_{12}(Al_4Mg_3Si_7)O_{32}Cl_6$, chlormayenite $Ca_{12}Al_{14}O_{32}Cl_2$ and wadalite $Ca_{12}(Al_{10}Si_4)O_{32}Cl_6$, have recently attracted particular attentions, because of their occurrences in alteration assemblages of chondrite meteorites (Ishii et al. 2010; Ma et al. 2010; Ma and Krot 2014; Brearley and Jones 2018). The crystal structure of the mayenite supergroup can be described as a derivative from that of grossular garnet, but with unoccupied octahedral sites and lower symmetry ($I\bar{4}3d$ *vs.* $Ia\bar{3}d$); Feng et al. 1988; Yu et al. 1997; Galuskin et al. 2015). The Cl atom located in the cage of chlormayenite, constructed from an $[Al_{14}O_{32}]$ tetrahedral framework, is linearly coordinated by two Ca atoms. In comparison with chlormayenite, the incorporation of additional Cl^- ions in adrianite and wadalite can be considered as charge compensation for the substitution of Si^{4+} for Al^{3+} (i.e., $Si^{4+} + Cl^- = Al^{3+} + \square$). However, Galuskin et al. (2015) cautioned that the formula of adrianite (Ma and Krot 2014) is not a proper endmember in their IMA-approved classification scheme. In terrestrial environments, chlormayenite and wadalite, along with other members of the mayenite supergroup (chlorkyuygenite $Ca_{12}Al_{14}O_{32}(H_2O)_4Cl_2$, fluorkyuygenite $Ca_{12}Al_{14}O_{32}(H_2O)_4F_2$, fluormayenite $Ca_{12}Al_{14}O_{32}F_2$, eltyubyuite $Ca_{12}Fe_{10}Si_4O_{32}Cl_6$), occur mainly in volcanic xenoliths and pyrometamorphic rocks (Galuskin et al. 2015).

3.3.4 Apatites

Apatites (mainly fluorapatite and less commonly chlorapatite and other members of this supergroup, Pan and Fleet 2002; Pasero et al. 2010) are the dominant phases in marine phosphorite and igneous phosphate deposits and occur as ubiquitous but usually minor minerals in almost all igneous, metamorphic and sedimentary rocks (Pan and Breaks 1997; Harlov et al. 2002; Hansen and Harlov 2007; McCubbin et al. 2011). As such, fluorapatite is one of the most important carriers of halogens in diverse rock types. However, accurate determination of the F contents in apatites by the commonly used electron microprobe technique is not routine and can be influenced by crystal orientation as well (Schettler et al. 2011; Goldoff et al. 2012).

Synthetic Br- and I-endmembers of the apatite supergroup such as $Ca_{10}(PO_4)_6Br_2$ and $Pb_{10}(VO_4)_6I_2$ have long been known (Elliott et al. 1981; Ono et al. 2001; Pan and Fleet 2002). O'Reilly and Griffin (2000) reported up to 54 ppm

Br in fluorapatite from mantle xenoliths by ICP-MS. Instrumental neutron activation analyses (INAA) and XRF microprobe analyses showed that chlorapatite, associated with diopside and tremolite from Bob's Lake, Ontario, has as much as 75 ppm Br (Pan and Dong 2003). Campayo et al. (2011) reported that hydroxylapatite, precipitated at 90 °C, incorporates up to ~7 wt% iodate in the *c*-axis column (see below) and demonstrated that iodate-doped hydroxylapatite does not release iodine below 550 °C and has a leaching rate of only $\sim 10^{-4}$ g/cm^2/day in deionized water, suggesting the potential for effective confinement of radioactive iodate in this material.

The crystal structures of fluorapatite, chlorapatite, and hydroxylapatite are composed of two types of Ca polyhedra: Ca1 is coordinated by nine O atoms in a tricapped trigonal prism and Ca2 is bonded to six O atoms and one X anion (X = F, Cl, OH) in an irregular 1-5-1 polyhedron (Fig. 3.25a). The F^- anions in fluorapatite sit on the 2a position ($\bar{6}$..) within the mirror planes at z = ¼ and z = ¾, lying in the center of the triangle formed by three Ca2 atoms (Fig. 3.25b). Because Cl^- and OH^- are too large to fit in the center of the Ca2 triangle, they are displaced from the mirror planes. Chlorine and the hydroxyl group are disordered at 4e (3..) (0, 0, *z*) positions with half-occupancies, and deviate from the mirror plane at 1.31 Å and 0.35 Å, respectively (Fig. 3.25c). The disordering successfully maintains the $P6_3/m$ symmetry, although monoclinic polymorphs have been found for pure

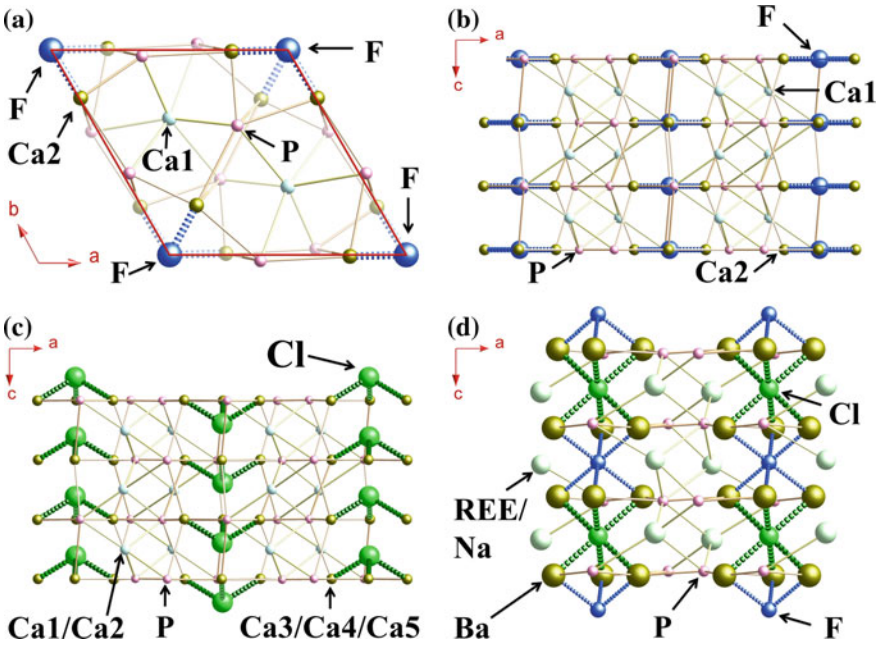

Fig. 3.25 Crystal structures of **a** fluorapatite, **b** F atoms in the c-axis column in fluorapatite, **c** Cl atoms in the c-axis columns in chlorapatite, and **d** F and Cl atoms in distinct octahedral voids in kuannersuite-(Ce)

chlorapatite (Hounslow and Chao 1970), pure hydroxylapatite (Elliott 1973), and a low-temperature ternary apatite (Hughes et al. 1990). These low crystal symmetries have been shown to arise from ordering in the anion column.

For example, Hughes et al. (1990) showed that in low-temperature ternary apatites, a monoclinic structure is created due to anion ordering that destroys the mirror plane. However, $P6_3/m$ ternary apatites can exist with a Markovian sequence of column anions and a second Cl site that allows column reversals to permit the mirror symmetry. Hughes et al. (1990) also suggested that the $P6_3/m$ apatite symmetry may not be maintained in binary F–Cl and OH–Cl apatites, and that there must be either symmetry breaking, immiscible compositional zones along the Cl–OH and Cl–F binaries, long-range ordering of immiscible regions, or stoichiometric and vacancies in the anion columns, although the latter includes an unknown method of charge balance (Nokhrin et al. 2005). In both natural and synthetic binary F–Cl apatites without any OH, Hughes et al. (2014a, b) have shown that Cl-rich fluorapatite is attained by the creation of a new off-mirror F site to accommodate the distances between F and Cl in the columns.

Further complication of F and Cl local structural environments in apatites arising from the effects of neighboring cations is evident in the $P\overline{3}$ structure of kuannersuite-(Ce) (Friis et al. 2004). The large Ba^{2+} ion, together with the coupled substitution of REE + Na, results in two types of octahedral voids for accommodating F^- and Cl^- anions in kuannersuite-(Ce). As such, the Cl^- anion resides in the larger octahedral voids formed by the Ba atoms and is situated at the same level (along the c-axis) as the REE atoms (Fig. 3.25d).

Experimental studies and thermodynamic modeling (Tacker and Stormer 1989; Zhu and Sverjensky 1991, 1992; Piccoli and Candela 1994; Piccoli et al. 1999; Mathez and Webster 2005; Patino Douce and Roden 2006; Webster et al. 2009; Patino Douce et al. 2011) have investigated the partitioning of F, Cl and OH in the apatite-melt/fluid systems. Piccoli and Candela (1994), assuming ideal mixing for apatites (Tacker and Stormer 1989) and using thermodyanic data of fluorapatite, chlorapatite, and hydroxylapatite from Zhu and Sverjensky (1991), formulated the following equations for calculating the concentrations of F and Cl in parts per million (ppm) in coexisting aqueous fluids (C_F^{fluid} and C_{Cl}^{fluid}) from apatite compositions:

$$C_F^{fluid} = \frac{X_{FAp}}{X_{HAp}} \cdot \frac{1.9 \times 10^7}{18} + \frac{1}{10^{\left[0.18219 + \frac{5301.1}{T} - \frac{0.00360\,(P-1)}{T}\right]}}$$

$$C_{Cl}^{fluid} = \frac{\frac{X_{ClAp}}{X_{HAp}} \cdot \frac{3.54 \times 10^7}{18} + \frac{1}{10^{\left[0.04661 + \frac{2535.8}{T} - \frac{0.0303(P-1)}{T}\right]}}}{10^{(-0.63-0.00035P)}}$$

The F and Cl concentrations of coexisting melts (C_F^{melt} and C_{Cl}^{melt}, in ppm) can then be determined from those of the aqueous fluids by applying the appropriate partition coefficients $D^{fluid/melt}$ (Piccoli and Candela 1994).

Hydrothermal experiments by Mathez and Webster (2005) and Webster et al. (2009), however, showed that the partitioning of F, Cl, and OH in the apatite-melt-fluid systems also depends on the melt composition, which was not included in the equations of Piccoli and Candela (1994). For example, Mathez and Webster (2005) reported that the weight-percent ratio between Cl in apatite and Cl in melt in an apatite-bearing basaltic melt aqueous fluid system at 1066–1150 °C and ~200 MPa is 0.8 for silicate melts containing less than ~3.8 wt% Cl but increases for higher melt Cl contents. The partitioning of F between apatite and melt in this system, in contrast to Cl, is constant over a wide range of melt composition. Similarly, Webster et al. (2009) demonstrated that the partitioning behavior of Cl between apatite and melt in the system of apatite, rhyolitic to rhyodacitic melts, and aqueous fluid (s) at 900–924 °C and ~200 MPa is a complex function of melt composition and the Cl concentration in the system. The Cl concentration in the apatite is a simple and linear function of the Cl content in the fluid, but the $D_{Cl}^{fluid/apatite}$ values of 9 to 43 in this system with felsic melts are an order of magnitude higher than those determined in the system with basaltic melts at 1066–1150 °C. Webster et al. (2009) also noted that many of the partitioning coefficients for F between apatite and melt in a felsic melt system are an order of magnitude greater than those from the basaltic melt system.

Brenan (1994) performed apatite-melt exchange experiments from 900–1200 °C at atmospheric pressure, and from 800–1100 °C at 1 GPa. He obtained similar diffusion coefficients for F, Cl and OH in natural fluorapatite, as expected by the requirement of charge neutrality:

$$D(1\,\text{atom}, //\text{c}) = 1.6 \times 10^{-4}\ \text{m}^2\text{s}^{-1}\exp[-284\,\text{kJmol}^{-1}/\text{RT}]$$
$$D(1\,\text{atom}, //\text{a}) = 1.3 \times 10^{-9}\ \text{m}^2\text{s}^{-1}\exp[-216\,\text{kJmol}^{-1}/\text{RT}]$$
$$D(1\,\text{GPa}, //\text{c}) = 8.1 \times 10^{-8}\ \text{m}^2\text{s}^{-1}\exp[-173\,\text{kJmol}^{-1}/\text{RT}].$$

These diffusion coefficients for F, Cl and OH in apatites, especially those along the c axis, are orders of magnitudes higher than those observed in scapolites and sodalities (Pan and Dong 2003) and are attributable to the connectivity of the anion column in the apatite structure (Hughes et al. 1990). These results led Brenan (1994) to suggest that apatite, in response to changes in P, T, or fluid/melt chemistry, may rapidly develop measurable F–Cl–OH zoning profiles via diffusion parallel to the c axis but little or no gradients expected parallel to the a axis. Brenan (1994) also cautioned about interpretation of apatite halogen chemistry in the absence of independent evidence for halogen retention.

Halogen partition coefficients between fluorapatite/chlorapatite and coexisting melts in the system of CaO-P_2O_5-CaF_2-$CaCl_2$-NaBr have been determined by experiments at 1120 °C to 1400 °C and atmospheric pressure (Dong 2005):

$$D_F^{ClAp/melt} = 3.59(64) \text{ at } 1120\,^{\circ}C \text{ to } 4.13(22) \text{ at } 1330\,^{\circ}C,$$
$$D_F^{FAp/melt} = 1.05(4) \text{ at } 1220\,^{\circ}C \text{ to } 1.07 \text{ at } 1400\,^{\circ}C,$$
$$D_{Cl}^{ClAp/melt} = 1.07(1) \text{ at } 1120\,^{\circ}C \text{ to } 0.83 \text{ at } 1330\,^{\circ}C,$$
$$D_{Cl}^{FAp/melt} = 0.127(2) \text{ at } 1250\,^{\circ}C \text{ to } 0.115 \text{ at } 1400\,^{\circ}C,$$
$$D_{Br}^{ClAp/melt} = 0.32(9) \text{ at } 1120\,^{\circ}C \text{ to } 0.42(5) \text{ at } 1330\,^{\circ}C,$$
$$D_{Br}^{FAp/melt} = 0.020(3) \text{ at } 1220\,^{\circ}C \text{ to } 0.016 \text{ at } 1400\,^{\circ}C.$$

The estimated uncertainties in 1σ, where available, are given in parentheses. These experimental results have been applied to fluorapatite from the Aoshan fluorapatite-magnetite deposit (Kiruna type) in the middle-lower Changjiang metallogenic belt (China) and the Oka carbonatite complex (Quecbec, Canada). The halogen compositions of fluorapatite in the Aoshan deposit are consistent with a magmatic crystallization, and the Br/Cl values (0.00–0.03) are compatible with a mantle source (Dong 2005). The anomalously high Br/Cl values (0.154–1.195) in the Oka fluorapatite, on the other hand, require Br-enriched sources (Dong 2005).

In summary, halogen-bearing, rock-forming minerals such as amphiboles, micas, and apatites have been widely used for calculating the fluid/melt compositions in igneous, metamorphic, and hydrothermal systems (see Chaps. 6, 7, 10, and 11). Existing thermodynamic models for these calculations assume ideal mixing for F, Cl, and OH in these minerals. Structural studies have demonstrated significant crystal chemical controls on the uptake of F and Cl into amphiboles, micas, and apatites, suggesting that non-ideal mixing behavior may be the rule rather than the exception in these minerals. Indeed, excess heat capacity and entropy of mixing along the chlorapatite-fluoapatite join have been confirmed by calorimetric measurements (Dachs et al. 2010). Therefore, the development of appropriate mixing models for these minerals would be highly desirable in their application for the accurate determination of the evolution of the halogen chemistry of fluids and melts in diverse geological and planetary processes.

Acknowledgements We thank Dr. Daniel Harlov for invitation to write this chapter and Drs. John M. Hughes and Andrew M. McDonald for constructive reviews and many helpful suggestions. YMP also thanks Dr. Wei Sun for assistance with drafting of four figures as well as CAS/SAFEA IPP for CRT project 20140491534 and NSERC for financial support.

References

Abdul-Samad FA, Humphries DA, Thomas JH, Williams PA (1981) Chemical studies on the stabilities of boleite and pseudoboleite. Mineral Mag 44:101–104

Agakhanov AA, Pautov LA, Karpenko VYu, Bekenova GK, Uvarova YA (2011) Orlovite, $KLi_2TiSi_4O_{11}F$, a new mineral of the mica group. New Data Mineral 46:13–19

Alici E, Schmidt T, Lutz HD (1992) Zur Kenntnis des Calciumbromats und -Iodats, Kristallstruktur, rontgenographische, IR- und Raman-spektroskopische und thermo-analytische Untersuchungen. Z Anorg Allgem Chem 608:135–144

Anfilogov VN, Bushlyakov IN, Villisov VA, Bragina GI (1977) Fluorine partition between biotite, amphibole, and granite melt at a temperature of 780 °C and a pressure of 1000 atm. Geokhimiya 3:471–475

Aranovich L, Safonov O (2018) Halogens in high-grade metamorphism. In: Harlov DE, Aranovich L (eds) The role of halogens in terrestrial and extraterrestrial geochemical processes: surface, crust, and mantle, Springer, Berlin, pp 713–757

Armbruster T, Bonazzi P, Akasaka M, Bermanec V, Chopin C, Giere R, Heuss-Assbichler S, Liebscher A, Menchetti S, Pan Y, Pasero P (2006) Recommended nomenclature of epidote-group minerals. Eur J Mineral 18:551–567

Balko VP, Bakakin VV (1975) The crystal structure of yftisite. Zh Strukt Khim 16:837–842

Ballirano P, Maras A, Buseck PR (1996) Crystal chemistry and IR spectroscopy of Cl- and SO_4-bearing cancrinite-like minerals. Am Mineral 81:1003–1012

Ballirano P, Callegari A, Caucia F, Maras A, Mazzi F, Ungaretti L (2002) The crystal structure of vicanite-(Ce), a borosilicate showing an unusual $(Si_3B_3O_{18})^{15-}$ polyanion. Am Mineral 87:1139–1143

Barnes JD, Manning C, Scambelluri M, Selverstone J (2018) The behaviour of halogens during subduction-zone processes. In: Harlov DE, Aranovich L (eds) The role of halogens in terrestrial and extraterrestrial geochemical processes: surface, crust, and mantle, Springer, Berlin, pp 545–590

Bazhenov AG, Nedosekova IL, Krinova TV, Mironov AB, Khvorov PV (2000) Fluormagnesioarfvedsonite $NaNa_2(Mg, Fe^{2+})_4Fe^{3+}$ $[Si_8O_{22}](F, H_2O)_2$—a new mineral species of the amphibole group. Zap Vser Mineral Obsh 129:28–35

Bernal NF, Gleeson SA, Smith MP, Barnes JD, Pan Y (2017) Evidence of multiple halogen sources in scapolites from iron oxide-copper-gold (IOCG) deposits and regional Na-Cl metasomatic alteration, Norrbotten County, Sweden. Chem Geol 451:90–103

Beyer C, Klemme S, Wiedenbeck M, Stracke A, Vollmer C (2012) Fluorine in nominally fluorine-free mantle minerals: experimental partitioning of F between olivine, orthopyroxene and silicate melts with implications for magmatic processes. Earth Planet Sci Lett 337–338:1–9

Bindi L, Welch MD, Bonazzi P, Pratesi G, Menchetti S (2008) The crystal structure of seeligerite, $Pb_3IO_4Cl_3$, a rare Pb-I-oxychloride from the San Rafael mine, Sierra Gorda, Chile. Mineral Mag 71:771–783

Böhlke JK, Hatzinger PB, Sturchio NC, Gu B, Abbene I, Mroczkowski SJ (2009) Atacama perchlorate as an agricultural contaminant in groundwater: Isotopic and chronologic evidence from Long Island, New York. Environ Sci Tech 43:5619–5625

Boiocchi M, Callegari A, Ottolini L, Maras A (2004) The chemistry and crystal structure of okanoganite-(Y) and comparison with vicanite-(Ce). Am Mineral 89:1540–1545

Boivin P, Camus G (1981) Igneous Scapolite-Bearing Associations in the Chaine-Des-Puys, Massif Central (France) and Atakor (Hoggar-Algeria). Contrib Mineral Petrol 77:365–375

Bojar H-P, Walter F (2006) Fluoro-magnesiohastingsite from Dealul Uroi (Hunedoara county, Romania): mineral structure of a new amphibole end-member. Eur J Mineral 18:503–508

Bokiy GB, Gorogotskaya LI (1965) The crystal structure of chukrovite. Dokl Akad Nauk SSSR 163:92–94

Borhade AV, Dholi AG, Wakchaure SG (2010) Synthesis, characterization and crystal structure of gallosilicate perchlorate sodalite. Int J Chem 2:3–13

Boukili B, Robert J-L, Beny J-M, Holtz F (2001) Structural effects of OH-F substitution in trioctahedral micas of the system: K_2O-FeO-Fe_2O_3-Al_2O_3-SiO_2-H_2O-HF. Schweiz Mineral Petrogr Mitt 81:55–67

Boukili B, Holtz F, Beny J-M, Robert J-L (2002) Fe–F and Al–F avoidance rule in ferrous aluminous (OH,F) biotites. Schweiz Mineral Petrogr Mitt 82:549–559

Brearley A, Jones R (2018) Halogens in chondritic meteorites. In: Harlov DE, Aranovich L (eds) The role of halogens in terrestrial and extraterrestrial geochemical processes: surface, crust, and mantle. Springer, Berlin, pp 871–958

Brenan J (1994) Kinetics of fluorine, chlorine and hydroxyl exchange in fluorapatite. Chem Geol 110:195–210

Brigatti MF, Guggenheim S (2002) Mica crystal chemistry and the influence of pressure, temperature, and solid solution on atomistic models. Rev Mineral Geochem 46:1–100

Brigatti MF, Caprilli E, Malferrari D, Medici L, Poppi L (2005) Crystal structure and chemistry of trilithionite-2M2 and polylithionite-2M2. Eur J Mineral 17:475–481

Brigatti MF, Caprilli E, Malferrari D, Mottana A (2007) Crystal structure and crystal chemistry of fluorannite and its relationships to annite. Mineral Mag 71:683–690

Brunton G (1968) Refinement of the structure of $NaBF_4$. Acta Cryst B 24:1703–1704

Brunton G (1969) The crystal structure of KBF_4. Acta Cryst B 25:2161–2162

Buhl J-C (1996) The properties of salt-filled sodalites. Part 4. Synthesis and heterogeneous reactions of iodate-enclathrated sodalite $Na_8[A1SiO_4]_6(IO_3)_{2-x}(OH.H_20)_x$; $0.7 < x < 1.3$. Thermochim Acta 286:251–262

Burns PC, Hawthorne FC (1993) The crystal structure of dietzeite, $Ca_2H_2O(IO_3)_2(CrO_4)$, a heteropolyhedral framework structure. Can Mineral 31:313–319

Burns PC, Cooper MA, Hawthorne FC (1995) Claringbullite—a Cu^{2+} oxysalt with Cu^{2+} in trigonal-prismatic coordination. Can Mineral 33:633–639

Cámara F, Hawthorne FC, Ball NA, Bekenova G, Stepanov AV, Kotel'nikov PE (2010) Fluoroleakeite, $NaNa_2(Mg_2Fe_2^{3+}Li)Si_8O_{22}F_2$, a new mineral of the amphibole group from the Verkhnee Espe deposit, Akjailyautas Mountains, Eastern Kazakhstan District, Kazakhstan: description and crystal structure. Mineral Mag 74:521–528

Cameron M, Gibbs GV (1973) The crystal structure of fluor-tremolite and a comparison with hydroxyl tremolite. Am Mineral 58:879–888

Cameron M, Sueno S, Papike JJ, Prewitt CT (1983) High temperature crystal chemistry of K and Na fluorrichterites. Am Mineral 68:924–943

Campayo L, Grandjean A, Coulon A, Delorme R, Vantelon D, Laurencin D (2011) Incorporation of iodates into hydroxyapatites: a new approach for the confinement of radioactive iodine. J Mater Chem 21:17609–17611

Caron AP, Ragle JL (1971) Refinement of the structure of orthorhombic ammonium tetrafluoroborate, NH_4BF_4. Acta Cryst B 27:1102–1107

Castelli D (1988) Chlorpotassium ferro-pargasite from Sesia-Lanzo marbles (Western Italian Alps): a record of highly saline fluids. Rend Soc Ital Mineral Petrol 43:129–13

Cavallo G, Metrangolo P, Milani R, Pilati T, Priimagi A, Resnati G, Terraneo G (2016) The halogen bond. Chem Rev 116:2478–2601

Chao ECT, Back JM, Minkin JA, Tatsumoto M, Wang J, Conrad JE, Mckee EH, Hou Z, Meng Q, Huang S (1997) The sedimentary carbonate-hosted giant Bayan Obo REE-Fe-Nb ore deposit of Inner Mongolia, China: a cornerstone example for giant polymetallic ore deposits of hydrothermal origin. US Geol Surv Bull No. 2143, p 65

Cheetham AK, Norman N (1974) The structures of yttrium and bismuth trifluorides by neutron diffraction. Acta Chem Scand A28:55–60

Cheetham AK, Fender BEF, Fuess H, Wright AF (1976) A powder neutron diffraction study of lanthanum and cerium trifluorides. Acta Crystall B32:94–97

Chevrier VC, Hanley J, Altheide TS (2009) Stability of perchlorate hydrates and their liquid solutions at the Phoenix landing site. Mars. Geophys Res Lett 36:L10202

Chevychelov VY, Botcharnikov RE, Holtz F (2008) Experimental study of fluorine and chlorine partitioning between fluid and subalkaline basaltic melt. Dokl Earth Sci 422:1089–1092

Chino M, Nakayama H, Naga H, Terada H, Katata G, Yamazawa H (2011) Preliminary estimation of release amounts of ^{131}I and ^{137}Cs accidentally discharged from the Fukushima Daiichi nuclear power plant into the atmosphere. J Nucl Sci Tech 48:1129–1134

Chukanov NV, Konilov AN, Zadov AE, Belakovsky DI, Pekov IV (2002) The new amphibole potassic chloropargasite (K, Na)Ca_2(Mg, Fe^{2+})$_4$Al($Si_6Al_2O_{22}$)(Cl, OH)$_2$ and conditions of its

formation in the granulite complex of Sal'nye Tundry Massif (Kola Pennisula). Zap Vser Mineral Obsh 131:58–62

Clissold ME, Leverett P, Williams PA, Hibbs DE, Nickel EH (2007) The structure of gillardite, the Ni-analogue of herbertsmithite, from Widgiemooltha, western Australia. Can Mineral 45:317–320

Colman RH, Ritter C, Wills AS (2008) Toward perfection: kapellasite, $Cu_3Zn(OH)_6Cl_2$, a new model S = 1/2 Kagome antiferromagnet. Chem Mater 20:6897–6899

Colman RH, Sinclair A, Wills AS (2011) Magnetic and crystallographic studies of Mg-herbertsmithite, gamma-$Cu_3Mg(OH)_6Cl_2$—a new S = 1/2 Kagome magnet and candidate spin liquid. Chem Mater 23:1811–1817

Cooper MA, Hawthorne FC (1997) A note on the crystal structure of marshite. Can Mineral 35:785–786

Cooper MA, Hawthorne FC, Roberts AC, Grice JD, Stirling JAR, Moffatt EA (1998) Georgeericksenite, $Na_6CaMg(IO_3)_6(CrO_4)_2(H_2O)_{12}$, a new mineral from Oficina Chacabuco, Chile: description and crystal structure. Am Mineral 83:390–399

Cooper M, Husdal TA, Ball NA, Abdu YA, Hawthorne FC (2013) Schlüterite-(Y), ideally (Y, REE)$_2$Al(Si_2O_7)$(OH)_2F$, a new mineral species from the Stetind pegmatite, Tysfjord, Nordland, Norway: description and crystal structure. Mineral Mag 77:353–366

Crichton WA, Müller H (2014) Cententiallite, IMA 2013-110. Mineral Mag 78:165–170

Cruciani G, Orlandi P, Pasero M, Russo M (2005) First Italian occurrence of cumengéite from Vesuvius: crystal-structure refinement and revision of the chemical formula. Mineral Mag 69:1037–1045

Czuchaj E, Rebentrost F, Stoll H, Preuss H (1997) Calculation of ground- and excited-state potential energy curves for the Hg_2 molecule in a pseudopotential approach. Chem Phys 214:277–289

Dachs E, Harlov D, Benisek A (2010) Excess heat capacity and entropy of mixing along the chlorapatite–fluorapatite binary join. Phys Chem Minerals 37:665–676

Dalou C, Koga KT, Shimizu N, Boulon J, Devidal J (2012) Experimental determination of F and Cl partitioning between lherzolite and basaltic melt. Contrib Mineral Petrol 163:591–609

Della Ventura G, Maras A, Parodi GC (1983) Potassium-fluorrichterite from Monte Somma (Campania) Italy. Period Mineral 52:617–630

Della Ventura G, Robert J-L, Sergent J, Hawthorne FC, Delbove F (2001) Constraints on F vs. OH incorporation in synthetic $^{[6]}$Al-bearing monoclinic amphiboles. Eur J Mineral 13:841–847

Della Ventura G, Bellatreccia F, Mara FCA, Oberti R (2014) Crystal-chemistry and short-range order of fluoro-edenite and fluoro-pargasite: a combined X-ray diffraction and FTIR spectroscopic approach. Mineral Mag 78:293–310

Demartin F, Gramaccioli CM, Campostrini I, Orlandi P (2008) Knasibfite, $K_3Na_4[SiF_6]_3[BF_4]$, a new hexafluorosilicate-tetrafluoroborate from La Fossa crater, volcano, Aeolian Islands, Italy. Can Mineral 46:447–453

Demartin F, Campostrini I, Gramaccioli CM (2009) Panichiite, natural ammonium hexachlorostannate (IV), $(NH_4)_2SnCl_6$, from La Fossa Crater, Vulcano, Aeolian Islands, Italy. Can Mineral 47:367–372

Demartin F, Gramaccioli CM, Campostrini I (2010) Demicheleite-(I), BiSI, a new mineral from La Fossa Crater, Vulcano, Aeolian Islands, Italy. Mineral Mag 74:141–145

Deshpande VP (1961) Thermal expansion of sodium fluoride and sodium bromide. Acta Crystallogr 14:794–794

Desiraju GR, Ho PS, Kloo L, Legon AC, Marquardt R, Metrangolo P, Politzer P, Resnati G, Rissanen K (2013) Definition of the halogen bond (IUPAC recommendations 2013). Pure Appl Chem 85:1711–1713

Di Liberto V, Nuccio PM, Paonita A (2002) Genesis of chlorine and sulphur in fumarolic emissions at Vulcano Island (Italy): assessment of pH and redox conditions in the hydrothermal system. J Volcanol Geotherm Res 116:137–150

Dill HG, Weber B, Eigler G, Kaufhold S (2012) The fluorite deposits NE of Regensburg, SE Germany-A mineralogical and chemical comparison of unconformity-related fluorite vein-type deposits. Chem Erde 72:261–278

Dolejs D, Zajacz Z (2018) Halogens in silicic magmas and their hydrothermal systems. In: Harlov DE, Aranovich L (eds) The role of halogens in terrestrial and extraterrestrial geochemical processes: surface, crust, and mantle, Springer, Berlin, pp 431–543

Dong P (2005) Halogen-element (F, Cl and Br) behaviour in apatites, scapolite and sodalite: An experimental investigation with field applications. Unpubl. PhD thesis, University of Saskatchewan, Saskatoon, Canada

Dorm E (1970) Studies on the crystal chemistry of the mercurous ion and of mercurous salts. University of Stockholm, Institute of Inorganic and Physical Chemistry, 48pp

Edgar AD, Pizzolato LA (1995) An experimental study of partitioning of fluorine between K-richterite, apatite, phlogopite, and melt at 20 kbar. Contrib Mineral Petrol 121:247–257

Effenberger H (1984) Verfeinerung der Kristallstruktur von Kupfer(II)-hydroxichlorid, Cu(OH)Cl. Monatsh Chem 115:725–730

Eggenkamp HGM, Schuiling RD (1995) δ^{37}Cl variations in selected minerals: a possible tool for exploration. J Geochem Explor 55:249–255

Elliott JC (1973) Monoclinic hydroxyapatite. Science 180:1055–1057

Elliott JC, Dykes E, Mackie PE (1981) Structure of bromapatite, $Ca_5(PO_4)_3Br$, and the radius of the bromide ion. Acta Crystallogr B 37:435–438

Ercit TS (2002) The mess that is "allanite". Can Mineral 40:1411–1419

Ercit TS, Hawthorne FC (1995) Murataite, a UB_{12} derivative structure with condensed Keggin molecules. Can Mineral 33:1223–1229

Ericksen GE (1981) Geology and origin of the Chilean nitrate deposits. US Geol Surv Prof Pap 1188, p 37

Ericksen GE, Evans HT Jr, Mrose ME, McGee JJ, Marinenko JW, Konnert JA (1989) Mineralogical studies of the nitrate deposits of Chile: VI. Hectorfloresite, $Na_9(IO_3)(SO_4)_4$, a new mineral. Am Mineral 74:1207–1214

Fabbrizio A, Stalder R, Hametner K, Günther D (2013a) Experimental chlorine partitioning between forsterite, enstatite and aqueous fluid at upper mantle conditions. Geochim Cosmochim Acta 121:684–700

Fabbrizio A, Stalder R, Hametner K, Günther D, Marquardt K (2013b) Experimental partitioning of halogens and other trace elements between olivine, pyroxenes, amphiboles and aqueous fluid at 2 GPa and 900 to 1300 °C. Contrib Mineral Petrol 166:639–653

Fechtelkord M, Behrens H, Holtz F, Bretherton JL, Fyfe CA, Groat LA, Raudsepp M (2003a) Influence of F content on the composition of Al-rich synthetic phlogopite: Part I. New information on structure and phase-formation from ^{29}Si, ^{1}H, and ^{19}F MAS NMR spectroscopies. Am Mineral 88:47–53

Fechtelkord M, Behrens H, Holtz F, Bretherton JL, Fyfe CA, Groat LA, Raudsepp M (2003b) Influence of F content on the composition of Al-rich syntheticphlogopite: Part II. Probing the structural arrangement of aluminum in tetrahedral and octahedral layers by ^{27}Al MQMAS and ^{1}H/^{19}F-^{27}Al HETCOR and REDOR experiments. Am Mineral 88:1046–1054

Feng QL, Glasser FP, Howie RA, Lachowski EE (1988) Chlorosilicate with the $12CaO{\cdot}7Al_2O_3$ structure and its relationship to garnet. Acta Crystallogr C 44:589–592

Ferraris G, Belluso E, Gula A, Soboleva SV, Khomyakov AP (2003) The crystal structure of the seidite-(Ce), $Na_4(Ce, Sr)_2\{Ti(OH)_2(Si_8O_{18})\}(O, OH, F)_4{\cdot}5H_2O$, a modular microporous titanosilicate of the rhodesite group. Can Mineral 41:1183–1192

Finch GJ, Fordham S (1936) The effect of crystal-size on lattice-dimensions. Proc Phys Soc 48:85–94

Fleet ME (1975) The crystal structure of paratacamite, $Cu_2(OH)_3Cl$. Acta Cryst B31:183–187

Fleet ME (1989) Structures of sodium alumino-germanate sodalities [$Na_8(Al_6Ge_6O_{24})A_2$, A = Cl, Br, I]. Acta Crystallogr C45:843–847

Flynn RT, Burnham CW (1978) An experimental determination of rare earth partition coffiecients between a chloride containing vapor phase and silicate melts. Geochim Cosmochim Acta 42:685–701

Foley S (1991) High-pressure stability of the fluor- and hydroxy-endmembers of pargasite and K-richterite. Geochim Cosmochim Acta 55:2689–2694

Fontana P, Schefer J, Pettit D (2011) Characterization of sodium chloride crystals grown in microgravity. J Cryst Growth 324:207–211

Freire MG, Neves CMSS, Marrucho IM, Coutinho JAP, Fernandes AM (2010) Hydrolysis of tetrafluoroborate and hexafluorophosphate counter ions in imidazolium-based ionic liquids. J Phys Chem A 114:3744–3749

Frezzotti ML, Ferrando S (2018) The role of halogens in the lithospheric mantle. In: Harlov DE, Aranovich L (eds) The role of halogens in terrestrial and extraterrestrial geochemical processes: surface, crust, and mantle. Springer, Berlin, pp 805–845

Friis H, Balic-Zunic T, Pekov IV, Petersen OV (2004) Kuannersuite-(Ce), $Ba_6Na_2REE_2(PO_4)_6FCl$, a new member of the apatite group, from the Ilimaussaq Alkaline Complex, South Greenland: description and crystal chemistry. Can Mineral 42:95–106

Gagnon JL, Samson IM, Fryer BJ, Williams-Jones AW (2003) Compositional heterogeneity in fluorite and the genesis of fluorite deposits: insights from LA-ICP-MS analysis. Can Mineral 41:365–382

Galuskin EV, Armbruster T, Malsy A, Galuskina IO (2003) Morphology, composition and structure of low-temperature P4/nnc high-fluorine vesuvianite whiskers from Polar Yakutia, Russia. Can Mineral 41:843–856

Galuskin EV, Gfeller F, Galuskina IO, Armbruster T, Bailau R, Sharygin VV (2015) Mayenite supergroup, Part I: recommended nomenclature. Eur J Mineral 27:99–111

Garavelli A, Balić-Žunić T, Mitolo D, Acquafredda P, Leonardsen E, Jakobson SP (2010) Heklaite, $KNaSiF_6$, a new fumarolic mineral from Hekla volcano, Iceland. Mineral Mag 74:147–157

Ghose S, Wan C (1974) Structural chemistry of copper and zinc minerals. II. Stereochemistry of copper(II) and iodine(V) in bellingerite, $3Cu(IO_3)_2.2H_2O$. Acta Crystallogr B30:965–974

Ghose S, Wan C (1978) Salesite, $CuIO_3(OH)$, and $Cu(IO_3)_2{\cdot}2H_2O$: a comparison of the crystal structures and their magnetic behavior. Am Mineral 63:172–179

Ghose S, Wan C, Wittke O (1978) The crystal structure of synthetic lautarite, $Ca(IO_3)_2$. Acta Crystallogr B34:84–88

Gianfagna A, Oberti R (2001) Fluoro-edenite from Biancavilla (Catania, Sicily, Italy): crystal chemistry of a new amphibole end-member. Am Mineral 86:1489–1493

Gianfagna A, Scordari F, Mazziotti-Tagliani S, Ventruti G, Ottolini L (2007) Fluorophlogopite from Biancavilla (Mt. Etna, Sicily, Italy): crystal structure and crystal chemistry of a new F-dominant analog of phlogopite. Am Mineral 92:1601–1609

Giester G, Ni Y, Jarosch D, Hughes JM, Ronsbo JG, Yang Z, Zemann J (1998) Cordylite-(Ce): a crystal chemical investigation of material from four localities, including type material. Am Mineral 83:178–184

Gilbert MC, Helz RT, Popp RK, Spear FS (1982) Experimental studies of amphibole stability. Amphiboles: petrology and Experimental Phase Relations (DR Veblen & PH Ribbe, eds) Rev Mineral 9B:229–353

Goff F, Arney BH, Eddy AC (1982) Scapolite Phenocrysts in a Latite Dome, Northwest Arizona, USA. Earth Planet Sci Lett 60:86–92

Goldoff B, Webster JD, Harlov D (2012) Characterization of fluo-chlorapatites by electron probe microanalysis with a focus on time-dependent intensity variation of halogens. Am Mineral 97:1103–1115

González-Partida E, Carrillo-Chávez A, Grimmer JOW, Pironon J, Mutterer J, Levresse G (2003) Fluorite deposits at Encantada-Buenavista, Mexico: products of Mississippi Valley type processes. Ore Geol Rev 23:107–124

Gramaccioli CM, Campostrini I (2007) Demartinite, a new polymorph of K_2SiF_6 from La Fossa Crater, Vulcano, Aeolian Islands, Italy. Can Mineral 45:1275–1280

Grice JD, Chao GY (1997a) Horváthite-(Y), rare-earth-fluorocarbonate, a new mineral species from Mont Saint-Hilaire, Quebec. Can Mineral 35:743–749
Grice JD, Chao GY (1997b) Lukechangite-(Ce), a new rare-earth-fluorocarbonate mineral from Mont Saint-Hilaire, Quebec. Am Mineral 82:1255–1260
Grice JD, Gault RA, Chao GY (1995) Reederite-(Y), a new sodium rare-earth mineral with a unique fluorosulfate anion. Am Mineral 80:1059–1064
Grice JD, Gault RA, Rowe R, Johnsen O (2006) Qaqarssukite-(Ce), a new barium-cerium fluorcarbonate mineral species from Qaqarssuk, Greenland. Can Mineral 44:1137–1146
Grice JD, Maisonneuve V, Lebalnc M (2007) Natural and synthetic fluoride carbonates. Chem Rev 107:114–132
Grice JD, Rowe R, Poirier G, Pratt A, Francis J (2009) Bussyite-(Ce), a new beryllium silicate mineral species from Mont Saint-Hilaire, Quebec. Can Mineral 47:193–204
Groat LA, Hawthorne FC, Ercit TS (1992) The role of fluorine in vesuvianite: a crystal structure study. Can Mineral 30:1065–1075
Grotzinger JP, Crisp JA, Vasavada AR, Sci Team MSL (2015) Curiosity's mission of exploration at Gale Crator, Mars. Elements 11:19–26
Hammerli J, Rubenach M (2018) The role of halogens during regional and contact metamorphism. In: Harlov DE, Aranovich L (eds) The role of halogens in terrestrial and extraterrestrial geochemical processes: surface, crust, and mantle. Springer, Berlin, pp 649–712
Hammerli J, Rusk B, Spandler C, Emsbo P, Oliver NHS (2013) In situ quantification of Br and Cl in minerals and fluid inclusions by LA-ICP-MS: a powerful tool to identify fluid sources. Chem Geol 337–338:75–87
Hammerli J, Spandler C, Oliver NHS, Rusk B (2014) Cl/Br of scapolite as a fluid tracer in the earth's crust: insights into fluid sources in the Mary Kathleen Fold Belt, Mt. Isa Inlier, Australia. J Metamorp Geol 32:93–112
Han TH, Helton JS, Chu SY, Nocera DG, Rodriguez-Rivera JA, Broholm C, Lee YS (2012) Fractionalized excitations in the spin-liquid state of a kagome-lattice antiferromagnet. Nature 492:406–410
Hanley JJ, Koga KT (2018) Halogens in terrestrial and cosmic geochemical systems: abundances, geochemical behaviors, and analytical methods. In: Harlov DE, Aranovich L (eds) The role of halogens in terrestrial and extraterrestrial geochemical processes: surface, crust, and mantle, Springer, Berlin, pp 21–121
Hansen EC, Harlov DE (2007) Whole rock, phosphate, and silicate compositional trends across an amphibolite- to granulite-facies transition, Tamil Nadu, India. J Petrol 48:1641–1680
Harlov DE, Melzer S (2002) Experimental partitioning of Rb and K between phlogopite and concentrated (K, Rb)Cl brine: implication for the role of concentrated KCl brines in the depletion of Rb in phlogopite and the stability of phlogopite during charnockite genesis. Lithos 64:15–28
Harlov DE, Förster HJ, Niland T (2002) Fluid-induced nucleation of (Y + REE)-phosphate minerals with apatite: nature and experiment. Part I. Chlorapatite. Am Mineral 87:245–261
Harlov D, Tropper P, Seifert W, Nijland T, Förster HJ (2006) Formation of Al-rich titanite ($CaTiSiO_4O$-$CaAlSiO_4OH$) reaction rims on ilmenite in metamorphic rocks as a function of fH_2O and fO_2. Lithos 88:72–84
Harlow GE (2002) Diopside + F-rich phlogopite at high P and T: systematics, crystal chemistry and the stability of $KMgF_3$, clinohumite and chondrodite. Geol Mater Res 4:1–28
Hassan I, Grundy HD (1990) Structure of davyne and implications for stacking faults. Can Mineral 28:341–349
Hassan I, Grundy HD (1991) The crystal structure and thermal expansion of tugtupite, $Na_8[Al_2Be_2Si_8O_{24}]Cl_2$. Can Mineral 29:385–390
Hawthorne FC (1978) The crystal structure of the amphiboles. VIII. The crystal structure and site chemistry of fluor-riebeckite. Can Mineral 16:187–194
Hawthorne FC (1984) The crystal structure of stenonite and the classification of the aluminofluoride minerals. Can Mineral 22:245–251

Hawthorne FC (1985) Description and crystal structure of bobkingite, $Cu_2{+}5Cl_2(OH)8(H_2O)2$, a new mineral from New Cliffe Hill Quarry, Stanton-under-Bardon, Leicestershire, UK. Mineral Mag 66:301–311

Hawthorne FC, Oberti R, Ungaretti L, Grice JD (1996a) A new hyper-calcic amphibole with Ca at the A site: fluor-cannilloite from Pargas, Finland. Am Mineral 81:995–1002

Hawthorne FC, Oberti R, Ungaretti L, Ottolini L, Grice JD, Czamanske GK (1996b) Fluor-ferro-leakeite, $NaNa_2(Fe_2^{2+}Fe_2^{3+}Li)Si_8O_{22}F_2$, a new alkali amphibole from the Canada Pinabete pluton, Questa, New Mexico, U.S.A. Am Mineral 81:226–228

Hawthorne FC, Cooper MA, Grice JD, Roberts AC, Hubbard N (2002) Description and crystal structure of bobkingite, $(Cu^{2+})_5Cl_2(OH)_8(H_2O)_2$. Mineral Mag 66:301–311

Hawthorne FC, Oberti R, Martin RF (2006) Short-range order in amphiboles from the Bear Lake Diggings, Ontario. Can Mineral 44:1171–1179

Hawthorne FC, Oberti R, Harlow GE, Maresch WV, Martin RF, Schumacer JC, Welch MD (2012) Nomenclature of the amphibole supergroup. Am Mineral 97:2031–2048

Hazen RM, Burnham CW (1973) The crystal structures of one-layer phlogopite and annite. Am Mineral 58:889–890

Hecht MH, Kounaves SP, Quinn R, West SJ, Young SMM, Ming DW, Catling DC, Clark BC, Boynton WV, Hoffman J, DeFlores LP, Gospodinova K, Kapit J, Smith PH (2009) Detection of perchlorate and the soluble chemistry of Martian soil at the Phoenix Mars Lander Site. Science 325:64–67

Henderson CMB, Taylor D (1978) The thermal expansion of synthetic aluminosilicate-sodalites, $M_8(Al_6Si_6O_{24})X_2$. Phys Chem Mineral 2:337–347

Henry DJ, Novak M, Hawthorne FC, Ertl A, Dutrow BL, Uher P, Pezzotta F (2011) Nomenclature of the tourmaline-supergroup minerals. Am Mineral 96:895–913

Hester JR, Maslen EN, Spadaccini N, Ishizawa N, Satow Y (1993) Accurate synchrotron radiation delta rho maps for K_2SiF_6 and K_2PdCl_6. Acta Crystall B49:967–973

Hogarth DD (2006) Fluoro-potassic-magnesio-arfvedsonite, $KNa_2Mg_5Si_8O_{22}F_2$, from the Outaouais region, Québec, Canada. Can Mineral 44:289

Holter ME (1969) The Middle Devonian Prairie Evaporite of Saskatchewan. Department of Mineral Resources, Geological Sciences Branch, Industrial Minerals Division, Province of Saskatchewan, Report No. 123, p 134

Holtstam D, Grins J, Nysten P (2004) Håleniusite-(La) from the Bastnäs deposit, Västmanland, Sweden: A new REE oxyfluoride mineral species. Can Mineral 42:1097–1103

Holtstam D, Kolitsch U, Andersson UB (2005) Västmanlandite-(Ce)—a new lanthanide- and F-bearing sorosilicate mineral from Västmanland, Sweden: description, crystal structure, and relation to gatelite-(Ce). Eur J Mineral 17:129–142

Hounslow AW, Chao GY (1970) Monoclinic chlorapatite from Ontario. Can Mineral 10:252–259

Huggins ML, Magill PL (1927) The crystal structures of mercuric and mercurous iodides. J Am Chem Soc 49:2357–2367

Hughes JM, Drexler JW (1994) Refinement of the structure of gagarinite-(Y), $Na_x(Ca_xREE_{2-x})F_6$. Can Mineral 32:563–565

Hughes JM, Cameron M, Crowley KD (1990) Crystal structures of natural ternary apatites: Solid solution in the $Ca_5(PO_4)_3X$ (X = F, OH, Cl) system. Am Mineral 75:295–304

Hughes JM, Heffernan KM, Goldoff B, Nekvasil H (2014a) Cr-rich fluorapatite, devoid of OH, from the Three Peaks area, Utah: the first reported structure of natural Cl-rich fluorapatite. Can Mineral 52:643–652

Hughes JM, Nekvasil H, Ustunisik G, Lindsley DH, Coraor AE, Vaugh J, Phillips BL, McCubbin FM, Woerner WR (2014b) Solid solution in the fluorapatite-chlorapatite binary system: high-precision crystal structure refinements of synthetic F-Cl apatite. Am Mineral 99:369–376

Hull S, Keen DA (1994) High-pressure polymorphism of the copper (I) halides—a neutron-diffraction study to similar-to-10 GPa. Phys Rev B 50:5868–5885

Hull S, Keen DA (1999) Pressure-induced phase transitions in AgCl, AgBr, and AgI. Phys Rev B 59:750–761

Hund F, Fricke R (1949) Der kristallbau von BiF_3-alpha. Zeit Anorg Allgem Chem 258:198–204
Icenhower J, London D (1997) Partitioning of fluorine and chlorine between biotite and granitic melt: experimental calibration at 200 MPa H_2O. Contrib Mineral Petrol 127:17–29
Ishii HA, Krot AN, Bradley JP, Keil K, Nagashima K, Teslich N, Jacobsen B, Yin Q-Z (2010) Discovery, mineral paragenesis, and origin of wadalite in a meteorite. Am Mineral 95:440–448
Izraeli ES, Harris IW, Navon O (2004) Fluid and mineral inclusions in cloudy diamonds from Koffiefontein, South Africa. Geochim Cosmochim Acta 68:2561–2575
Jelinek R, Stein A, Ozin GA (1993) ^{35}Cl and ^{81}Br NMR investigation of sodium, silver, halo-sodalite semiconductor supperlattices. J Am Chem Soc 115:2390–2396
Kampf AR, Sciberras MJ, Williams PA, Dini M, Molina Donoso AA (2013a) Leverettite from the Torrecillas mine, Iquique Provence, Chile: the Co-analogue of herbertsmithite. Mineral Mag 77:3047–3054
Kampf AR, Sciberras MJ, Leverett P, Williams PA, Malcherek T, Schlüter J, Welch MD, Dini M, Molina Donoso AA (2013b) Paratacamite-(Mg), $Cu_3(Mg, Cu)Cl_2(OH)_6$; a new substituted basic copper chloride mineral from Camerones, Chile. Mineral Mag 77:3113–3124
Kaplan DI, Denham ME, Zhang S, Yeager C, Xu C, Schwehr KA, Li HP, Ho YF, Wellman D, Santschi PH (2014) Radioiodine biogeochemistry and prevalence in ground water. Crit Rev Environ Sci Technol 44:2287–2335
Kendrick MA (2018) Halogens in seawater, marine sediments and the altered oceanic lithosphere. In: Harlov DE, Aranovich L (eds) The role of halogens in terrestrial and extraterrestrial geochemical processes: surface, crust, and mantle, Springer, Berlin, pp 591–648
Kendrick MA, Phillips D (2009) New constraints on the release of noble gases during in vacuo crushing and application to scapolite Br-Cl-I and $^{40}Ar^{39}Ar$ age determinations. Geochim Cosmochim Acta 73:5673–5692
Kendrick MA, Baker T, Fu B, Phillips D, Williams PJ (2008) Noble gas and halogen constraints on regionally extensive mid-crustal Na-Ca metasomatism, the Proterozoic Eastern Mount Isa Block, Australia. Precambr Res 163:131–150
Kendrick MA, Scambelluri M, Honda M, Phillips D (2011) High abundances of noble gas and chlorine delivered to the mantle by serpentinite subduction. Nat Geosci 4:807–812
Kenichi T, Kyoko S, Hiroshi F, Mitsuko O (2003) Modulated structure of solid iodine during its molecular dissociation under high pressure. Nature 423:971–974
Kermarrec E, Zorko A, Bert F, Colman RH, Koteswararao B, Bouquet F, Bonville P, Hillier A, Amato A, van Tol J, Ozarowski A, Wills AS, Mendels P (2014) Spin dynamics and disorder effects in the S = ½ kagome Heisenberg spin-liquid phase of kapellasite. Phys Rev B 90:205103
Klemme S, Stalder R (2018) Halogens in the Earth's mantle: what we know and what we don't. In: Harlov DE, Aranovich L (eds) The role of halogens in terrestrial and extraterrestrial geochemical processes: surface, crust, and mantle. Springer, Berlin, pp 845–867
Konnert JA, Evans HT Jr (1994) Mineralogical studies of the nitrate deposits of Chile: VII. Two new saline minerals with the composition $K_6(Na,K)_4Na_6Mg_{10}(XO_4)_{12}(IO_3)\cdot 12H_2O$: fuenzalidaite (X = S) and carlosruizite (X = Se). Am Mineral 79:1003–1008
Kounaves SP, Stroble ST, Anderson RM, Moore Q, Catling DC, Douglas S, McKay CP, Ming DW, Smith PH, Tamppari LK, Zent AP (2010) Natural perchlorate in the antarctic dry valleys and implications for its global distribution and history. Environ Sci Technol 44(7):2360–2364
Kounaves SP, Chaniotakis NA, Chevrier VF, Carrier BL, Folds KE, Hansen VM, McElhoney KM, O'Neil GD, Wieber AW (2014) Identification of the perchlorate parent salts at the Phoenix Mars landing site and possible implications. Icarus 232:226–231
Krivovichev SV, Filatov SK, Zaitsev AN (1998) The crystal structure of kukharenkoite-(Ce), $Ba_2REE(CO_3)_3F$, and an interpretation based on cation-coordinated F tetrahedra. Can Mineral 36:809–815
Krivovichev SV, Armbruster T, Pekov IV (2003) Cation frameworks in structure of natural fluocarbonates of barium and rare-earth elements: crystal structure of kukharenkoite-(La), $Ba_2(La, Ce)(CO_3)_3F$. Zap Vser Mineral Obsh 132:65–72

Kullerud K, Erambert M (1999) Cl-scapolite, Cl-amphibole, and plagioclase equilibria in ductile shear zones at Nusfjord, Lofoten, Norway: implications for fluid compositional evolution during fluid-mineral interaction in the deep crust. Geochim Cosmochim Acta 63:3829–3844

Kusebauch C, John T, Barnes J, Klügel A, Austrheim H (2015) Halogen element and stable chlorine isotope fractionation caused by fluid-rock interaction (Bamble sector, SE Norway). J Petrol 56:299–324

La Tourrette T, Hervig RL, Holloway JR (1995) Trace element partitioning between amphibole, phlogopite, and basanite melt. Earth Planet Sci Lett 135:13–30

Labouriau A, Kim Y-W, Chipera S, Bish DL, Earl WL (1995) A ^{19}F nuclear magnetic resonance study of natural clays. Clays Clay Mineral 43:697–704

Lecumberri-Sanchez P, Bodnar B (2018) Halogen geochemistry of ore deposits: contributions towards understanding sources and processes. In: Harlov DE, Aranovich L (eds) The role of halogens in terrestrial and extraterrestrial geochemical processes: surface, crust, and mantle. Springer, Berlin, pp 261–305

Lėger A, Rebbert C, Webster J (1996) Cl-rich biotite from Black Rock Forest, Cornwall, New York. Am Mineral 81:495–504

Li Y-S, Zhang Q-M (2013) Structure and magnetism of S = 1/2 kagome antiferromagnets $NiCu_3(OH)_6Cl_2$ and $CoCu_3(OH)_6Cl_2$. J Phys Condens Mater 25:026003

Li W-K, Zhou G-D, Mak TCW (2008) Advanced structural inorganic chemistry. Oxford University Press, Oxford

Ling M-X, Liu Y-L, Williams IS, Teng F-Z, Yang XY, Ding X, Wei GJ, Xie L-H, Deng W-F, Sun W-D (2012) Formation of the world's largest REE deposit through protracted fluxing of carbonatite by subduction-derived fluids. Sci Rep 3:1776

Lowenstein TK, Spencer RJ (1990) Syndepositional origin of potash evaporates: petrographic and fluid inclusion evidence. Am J Sci 290:1–42

Lu Z, Jenkyns HC, Rickaby REM (2010) Iodine to calcium ratios in marine carbonate as a paleo-redox proxy during oceanic anoxic events. Geology 38:1107–1110

Lukkari S, Holtz F (2007) Phase relations of a F-enriched peraluminous granite: an experimental study of the Kymi topaz granite stock, Southern Finland. Contrib Mineral Petrol 153:273–288

Lupulescu MV, Rakovan J, Robinson GW, Hughes JM (2005) Fluoropargasite, a new member of the Group 2, calcic amphiboles, from Edenville, Orange County, New York. Can Mineral 43:1423–1428

Lupulescu MV, Rakovan J, Dyar MD, Robinson GW, Hughes JM (2009) Fluoro-potassichastingsite from the Greenwood mine (Orange County, New York, USA): a new end member calcic amphibole. Can Mineral 47:909–916

Ma C, Krot AN (2014) Adrianite, IMA 2014-028. CNMNC Newsletter No. 21, August 2014. Mineral Mag 78:797–804

Ma C, Sweeney Smith SA, Connolly HC, Beckett JR, Rossman GR, Schrader DL (2010): discovery of Cl-bearing mayenite, $Ca_{12}Al_{14}O_{32}Cl_2$, a new mineral in a CV3 Meteorite. 73rd Annual Meteoritical Society Meeting, 2010, 5134

Maddrell E, Gandy A, Stennett M (2014) The durability of iodide sodalite. J Nucl Mater 449:168–172

Madonia P, Liotta M (2010) Chemical composition of precipitation at Mt. Vesuvius and Volcanoc Island, Italy: volcanological and environmental implications. Environ Earth Sci 61:159–171

Makino E, Tomita K, Suwa K (1993) Effect of chlorine on the crystal structure of a chlorine-rich hastingsite. Mineral Mag 57:677–685

Malcherek T, Schlueter J (2009) Structures of the pseudo-trigonal polymorphs of $Cu_2(OH)_3Cl$. Acta Crystallogr B 65:334–341

Malcherek T, Schlüter J (2010) Anatacamite from La Vendida mine, Sierra Gorda, Atacama desert, Chile: a triclinic polymorph of $Cu_2(OH)_3Cl$. Neues Jahrb Mineral Abh 187:307–312

Malcherek T, Schlüter J, Husdal TA, Cooper MA (2012) Cayalsite-(Y), IMA 2011-094. Mineral Mag 76:807–817

Malcherek T, Bindi L, Dini M, Ghiara MR, Donoso AM, Nestola F, Rossi M, Schlüter J (2014) Tondiite, $Cu_3Mg(OH)_6Cl_2$, the Mg-analogue of herbertsmithite. Mineral Mag 78:583–590

Manceau A, Bonnin D, Stone WEE, Sanz J (1990) Distribution of Fe in the octahedral sheet of trioctahedral micas by polarised EXAFS. Comparison with NMR results. Phys Chem Mineral 17:363–370

Manning CE, Bird DK (1990) Fluorian garnets from the host rocks of the Skaergaard intrusion: implications for metamorphic fluid composition. Am Mineral 75:859–873

Mason RA (1992) Models of order and iron-fluorine avoidance in biotite. Can Mineral 30:343–354

Mathez EA, Webster JD (2005) Partitioning behavior of chlorine and fluorine in the system apatite-silicate melt-fluid. Geochim Cosmochim Acta 69:1275–1286

Matsubara S, Miyawaki R, Yokoyama K, Shigeoka M, Momma K, Yamamoto S (2014) Magnesiorowlandite-(Y), $Y_4Mg(Si_2O_7)_2F_2$, a new mineral in a pegmatite at Souri Valley, Komono, Mie Prefecture, central Japan. J Mineral Petrol Sci 109:109–117

Matteucci RV (1897) Iodio e bromo nei prodotti delle fumarole dell'eruzione vesuviana del 1895 (Nota preliminare). Rendiconti dell'Accademia di Scienze Naturali e Matematiche di Napoli fasc 7

Mazzi F, Ungaretti L, Dal Negro A, Petersen OV, Ronsbo JG (1979) The crystal structure of semenovite. Am Mineral 64:202–210

McCubbin FM, Jolliff BL, Nekvasil H, Carpenter PK, Zeigler RA, Steele A, Elardo SM, Lindsley DH (2011) Fluorine and chlorine abundances in lunar apatite: Implications for heterogeneous distributions of magmatic volatiles in the lunar interior. Geochim Cosmochim Acta 75:5073–5093

McDonald AM, Back ME, Gault RA, Horváth L (2013) Peatite-(Y) and ramikite-(Y), two new Na-Li-Y ± Zr phosphate-carbonate minerals from the Poudrette pegmatite, Mont Saint-Hilaire, Québec. Can Mineral 51:569–596

Merlino S, Perchiazzi M (1987) The crystal structure of hiortdahlite II. Mineral Petrol 37:25–35

Mills SJ, Kartashov PM, Gamyanin GN, Whitfield PS, Kern A, Guerault H, Kampf AR, Raudsepp M (2011) Fluorocronite, the natural analogue of β-PbF_2, from the Sakha Republic, Russian Federation. Eur J Mineral 23:695–700

Mills SJ, Kartashov PM, Kampf AR, Konev AA, Konev AA, Raudsepp M (2012) Cordylite-(La), a new mineral species in fenite from the Biraya Fe-REE deposit, Irkutsk, Russia. Can Mineral 50:1281–1290

Miyawaki R, Shimazaki H, Shigeoka M, Yokoyama K, Matsubara S, Yurimoto H, Yang Z, Zhang P, Inoue A, Kogure T, Jige M (2011a) Fluorokinoshitalite and fluorotetraferriphlogopite; new species of fluoro-mica from Bayan Obo, Inner Mongolia, China. Clay Science 15:13–18

Miyawaki R, Shimazaki H, Shigeoka M, Yokoyama K, Matsubara S, Yurimoto H (2011b) Yangzhumingite, $KMg_{2.5}Si_4O_{10}F_2$, a new mineral in the mica group from Bayan Obo, Inner Mongolia, China. Eur J Mineral 23:467–473

Mizota T, Kato T, Harada K (1986) The crystal structure of masutomilite Mn analog of zinnwaldite. Mineral J (Japan) 13:13–21

Mora CI, Valley JW (1989) Halogen-rich scapolite and biotite: implications for metamorphic fluid-rock interaction. Am Mineral 74:721–737

Mukose K, Fukano R, Miyagi H, Yamaguchi K (2002) First-principles studies of solid halogens under pressure. Scaling rules of properties among I_2, Br_2 and Cl_2. J Phys Condens Matter 14:10441–10444

Munoz J (1992) Calculation of HF and HCl fugacities from biotite compositions: revised equations. Geol Soc Am Abst Programs 26:A221

Munoz JL (1984) F-OH and Cl-OH exchange in micas with applications to hydrothermal ore deposits. Rev Mineral 13:469–494

Nazzareni S, Comodi P, Bindi L, Safonov OG, Litvin YA, Perchuk LL (2008) Synthetic hypersilicic Cl-bearing mica in the phlogopite-celadonite join: a mulitmethodical characterization of the missing link between di- and tri-octahedral micas at high pressures. Am Mineral 93:1429–1436

Nash JT, Connor JJ (1993) Iron and chlorine as guides to stratiform Cu-Co- Au deposits, Idaho Cobalt Belt, USA. Mineral Deposita 28:99–106

Ni Y, Hughes JM, Mariano AN (1993) The atomic arrangement of bastnasite-(Ce), $Ce(CO_3)F$, and structural elements of synchysite-(Ce), rontgenite-(Ce) and parisite-(Ce). Am Mineral 78:415–418

Nishio-Hamane D, Momma K, Ohnishi M, Shimobayashi N, Miyawaki R, Tomita N, Minakawa T (2014a) Iyoite, IMA 2013-130. CNMNC Newsletter No. 20. Mineral Mag 78:549–558

Nishio-Hamane D, Momma K, Ohnishi M, Shimobayashi N, Miyawaki R, Tomita N, Minakawa T (2014b) Misakiite, IMA 2013-131. CNMNC Newsletter No. 20. Mineral Mag 78:549–558

Nokhrin S, Pan Y, Weil JA, Nilges MJ (2005) Multifre-quency EPR study of radiation-induced defects in chlorapatite. Can Mineral 43:1581–1588

Oberti R, Ungaretti L, Cannillo E, Hawthorne FC (1993) The mechanism of Cl incorporation into amphiboles. Am Mineral 78:746–752

Oberti R, Ottolini L, Della Ventura G, Parodi GC (2001) On the symmetry and crystal chemistry of britholite: new structural and microanalytical data. Am Mineral 86:1066–1075

Oberti R, Boiocchi M, Smith DC (2003) Fluoronyböite from Jianchang (Su-Lu, China) and nyböite from Nybö (Nordfjord, Norway): a petrological and crystal-chemical comparison of these two high-pressure amphiboles. Mineral Mag 67:769–782

Oberti R, Cámara F, Ottolini L (2005) Clinoholmquistite discredited: the new amphibole end-member fluoro-sodic-pedrizite. Am Mineral 90:732–736

Oberti R, Boiocchi M, Smith DC, Medenbach O (2007) Alumotaramite, alumino-magnesiotaramite, and fluoro-alumino-magnesiotaramite: mineral data and crystal chemistry. Am Mineral 92:1428–1435

Oberti R, Boiocchi M, Ball NA, Hawthorne FC (2009a) Fluoro-sodic-ferropedrizite, $NaLi_2(Fe^{2+}Al_2Li)Si_8O_{22}F_2$, a new mineral of the amphibole group from the Sutlug River, Tuva Republic, Russia: description and crystal structure. Mineral Mag 73:487–494

Oberti R, Cámara F, Hawthorne FC, Ball NA (2009b) Fluoro-aluminoleakeite, $NaNa_2(Mg_2Al_2Li)Si_8O_{22}F_2$, a new mineral of the amphibole group from Norra Kärr, Sweden: description and crystal structure. Mineral Mag 73:817–824

Oberti R, Boiocchi M, Hawthorne FC, Pagano R, Pagano A (2010) Fluoro-potassic-pargasite, $KCa_2(Mg_4Al)(Si_6Al_2)O_{22}F_2$ from the Tranomaro area, Madagascar: mineral description and crystal chemistry. Mineral Mag 74:961–967

Oen IS, Lustenhouwer WJ (1992) Cl-rich biotite, Cl-K hornblende, and Cl- rich scapolite in meta-exhalites: Nora, Bergslagen, Sweden. Econ Geol 87:1638–1648

Ono M, Shinohara M, Kurosaki K, Yamanaka S (2001) Some properties of a vanado-iodoapatite $Pb_{10}(VO_4)_6I_2$. J Nucl Mater 294:119–122

O'Reilly SY, Griffin WL (2000) Apatite in the mantle: implications for metasomatic processes and high heat production in Phanerozoic mantle. Lithos 53:217–232

Pan Y (1998) Scapolite in skarn deposits: petrological and geo-chemical significance. In: Mineralized intrusion-related skarn system, Mineralogical Association of Canada, Short Course Series 26:169–209

Pan Y, Breaks FW (1997) Rare-earth elements in fluorapatite, Separation Lake area, Ontario: evidence for S-type granite-rare-metal pegmatite linkage. Can Mineral 35:659–672

Pan Y, Dong P (2003) Bromine in scapolite and sodalite: X-ray microprobe analysis, exchange experiments and application to skarn deposits. Can Mineral 41:529–540

Pan Y, Fleet ME (1990) Halogen-bearing allanite from the White River gold occurrences, Hemlo area, Ontario. Can Mineral 28:67–75

Pan Y, Fleet ME (1992a) Mineralogy and genesis of calc-silicates associated with Archean volcanogenic massive sulphide deposits at the Manitouwadge mining camp, Ontario. Can J Earth Sci 29:1375–1388

Pan Y, Fleet ME (1992b) Calc-silicate alteration in the Hemlo gold deposit, Ontario: mineral assemblages, P-T-X constraints and significance. Econ Geol 87:1104–1120

Pan Y, Fleet ME (1996) Rare-earth element mobility during prograde granulite facies metamorphism: significance of fluorine. Contrib Mineral Petrol 123:251–262

Pan Y, Fleet ME (2002) Compositions of the apatite-group minerals: substitution mechanisms and controlling factors. Rev Mineral Geochem 49:13–49

Pan Y, Fleet ME, Barnett RL, Chen Y (1993a) Pyrosmalite in Canadian Precambrian sulfide deposits: mineral chemistry, petrogenesis and significance. Can Mineral 31:695–710

Pan Y, Fleet M, MacRae N (1993b) Late alteration in titanite ($CaTiSiO_5$): redistribution and remobilization of rare earth elements and implications for U/Pb and Th/Pb geochronology and. Geochim Cosmochim Acta 57:355–367

Pan Y, Fleet ME, Ray GE (1994) Scapolite in two Canadian gold deposits: Nickel Plate, British Columbia and Hemlo, Ontario. Can Mineral 32:825–837

Pan Y, Dong P, Chen N (2003) Non-Henry's Law behavior of REE partitioning between fluorapatite and CaF_2-rich melts: Controls of intrinsic vacancies and implications for natural apatites. Geochim Cosmochim Acta 67:1889–1900

Papike JJ, Zoltai T (1965) The crystal structure of a marialite scapolite. Am Mineral 50:641–655

Papin A, Sergent J, Robert J-L (1997) Intersite OH-F distribution in an Al-rich synthetic phlogopite. Eur J Mineral 9:501–508

Partin DE, OKeeffe M (1991) The structures and crystal-chemistry of magnesium-chloride and cadmium chloride. J Solid State Chem 95:176–183

Pasero M, Kampf AR, Ferraris C, Pekov IV, Rakovan J, White TJ (2010) Nomenclature of the apatite supergroup minerals. Eur J Mineral 22:163–179

Patino Douce AE, Johnston AD (1991) Phase equilibria and melt productivity in the pelitic system: Implications for the origin of peraluminous granitoids and aluminous granulites. Contrib Mineral Petrol 107:202–218

Patino Douce AE, Roden M (2006) Apatite as a probe of halogen and water fugacities in the terrestrial planets. Geochim Cosmochim Acta 70:3173–3196

Patino Douce AE, Roden MF, Chaumba J, Fleisher C, Yogodzinski G (2011) Compositional variability of terrestrial mantle apatites, thermodynamic modeling of apatite volatile contents, and the halogen and water budgets of planetary mantles. Chem Geol 288:14–31

Pautov LA, Bekenova GK, Karpenko VYu, Agakhanov AA (2005) Chukhrovite-(Nd), Ca_3(Nd, Y) $Al_2(SO_4)F_{13}{\cdot}12H_2O$, a new mineral. New Data Mineral 40:5–10

Pautov LA, Agakhanov AA, Bekenova GK (2006) Sokolovaite $CsLi_2AlSi_4O_{10}F_2$—a new minerals species of the mica group. New Data Mineral 41:5–13

Peacor DR, Dunn PJ (1988) Dollaseite-(Ce) (magnesium orthite redefined): structure refinement and implications for F + M^{2+} substitutions in epidote-group minerals. Am Mineral 73:838–842

Pekov IV, Chukanov NV, Ferraris G, Ivaldi G, Pushcharovsky DY, Zadov AE (2003) Shirokshinite, $K(NaMg_2)Si_4O_{10}F_2$, a new mica with octahedral Na from Khidiny massif, Kola Peninsula. Eur J Mineral 15:447–454

Pekov IV, Chukanov NV, Nefedova ME, Pushcharovsky DY, Rastvetaeva RK (2005) Chloro-potassichastingsite (K,Na)$Ca_2(Fe^{2+}$, $Mg)_4Fe^{3+}$ $(Si_6Al_2O_{22})(Cl,OH)_2$: revalidation and the new name of dashkesanite. Zap Vser Mineral Obsh 134:31–36

Pekov IV, Konokova NN, Agakhanov AA, Belakovsky DI, Kazantsev SS, Zubkova NV (2010) Voloshinite, a new rubidium mica from granitic pegmatite of Voron'I Tundras, Kola Peninsula, Russia. Geol Ore Deposits 52:591–698

Pekov IV, Zubkova NV, Husdal TA, Kononkova NN, Agakhanov AA, Zadov AE, Pushcharovsky DY (2012) Carlgieseckeite-(Nd), $NaNdCa_3(PO_4)_3F$, a new belovite-group mineral species from the Ilimaussaq alkaline complex, South Greenland. Can Mineral 50:571–580

Pelloux A (1927) The minerals of Vesuvius. Am Mineral 12:14–21

Petersen EU, Essene EJ, Peacor DR, Valley JW (1982) Fluorine end-member micas and amphiboles. Am Mineral 67:538–544

Petrillo C, Moze O, Ibberson RM (1992) High resolution neutron powder diffraction investigation of the low temperature crystal structure of molecular iodine (I_2). J Phys Condens Matter 180–181:639–641

Piccoli P, Candela P (1994) Apatite in felsic rocks: a model for the estimation of initial halogen concentrations in the Bishop Tuff (Long Valley) and Tuolumne intrusive suite (Sierra Nevada Batholith) magmas. Am J Sci 294:92–135

Piccoli P, Candela P, Williams T (1999) Estimation of aqueous HCl and Cl concentrations in felsic systems. Lithos 46:591–604

Piilonen PC, McDonald AM, Grice JD, Cooper MA, Kolitsch U, Rowe R, Gault RA, Poirier G (2010) Arisite-(La), a new REE-fluorcarbonate mineral from the Aris phonolite (Namibia), with descriptions of the crystal structures of arisite-(La) and arisite-(Ce). Mineral Mag 74:257–268

Podder J, Lin J, Sun W, Botis SM, Tse JS, Chen N, Hu Y, Li D, Seaman J, Pan Y (2017) Iodate in calcite and vaterite: Insights from synchrotron X-ray absorption spectroscopy and first-principles calculations. Geochim Cosmochim Acta 198:218–228

Powell BM, Heal KM, Torrie BH (1984) The temperature dependence of the crystal structures of the solid halogens, bromine and chlorine. Mol Phys 53:929–939

Raade G, Johnsen O, Erambert M, Petersen OV (2007) Hundholmenite-(Y) from Norway—a new mineral species in the vicanite group: descriptive data and crystal structure. Mineral Mag 71(2):179–192

Raade G, Grice JD, Erambert M, Kristiansson P, Witzke T (2008) Proshchenkoite-(Y) from Russia—a new mineral species in the vicanite group: descriptive data and crystal structure. Mineral Mag 72(5):1071–1082

Radtke AS, Brown GE (1974) Frankdicksonite, BaF_2, a new mineral from Nevada. Am Mineral 59:885–888

Rakovan JF, Hughes JM (2000) Strontium in the apatite structure: Strontian fluorapatite and belovite-(Ce). Can Mineral 38:839–845

Ramberg H (1952) Chemical bonds and the distribution of cations in silicates. J Geol 60:33l–355

Rampe EB, Ming DW, Blake DF et al (2017) Mineralogy of an ancient lacustrine mudstone succession from the Murray formation, Gale crater, Mars. Earth Planet Sci Lett (in press). https://doi.org/10.1016/j.epsl.2017.04.021

Rancourt DG, Ping LY, Boukili B, Robert J-L (1996) Octahedral-site Fe^{2+} quadripole splitting distributions from Mossbauer spectroscopy along the (OH,F)-annite join. Phys Chem Minerals 23:63–71

Rao B, Anderson TA, Redder A, Jackson WA (2010) Perchlorate formation by ozone oxidation of aqueous chlorine/oxy-chlorine species: Role of ClxOy radicals. Environ Sci Technol 44:2961–2967

Rao B, Estrada N, Mangold J, Shelly M, Gu B, Jackson WA (2012) Perchlorate production by photodecomposition of aqueous chlorine. Environ Sci Technol 46:11635–11643

Rastvetaeva RK, Pushcharovski DY, Vinogradova RA, Pekov IV (1996) Crystal Chemistry of dashkesanite. Crystallogr Rep 41:58–62

Rebbert CR, Rice JM (1997) Scapolite-plagioclase exchange: Cl-CO_3 scapolite solution chemistry and implications for peristerite plagioclase. Geochim Cosmochim Acta 61:555–567

Redhammer GJ, Roth G (2002) Single-crystal structure refinements and crystal chemistry of synthetic trioctahedral micas $KM_3(Al^{3+}, Si^{4+})_4O_{10}(OH)_2$, where $M = Ni^{2+}$, Mg^{2+}, Co^{2+}, Fe^{2+} or Al^{3+}. Am Mineral 87:1464–1476

Reed MJ, Candela PA, Piccoli PM (2000) The distribution of rare earth elements between monzogranitic melt and the aqueous volatile phase in experimental investigations at 800 °C and 200 MPa. Contrib Mineral Petrol 140:251–262

Rieder M, Cavazzini G, D'Yakonov YS, Frank-Kamenetskii VA, Gottardt G, Guggenheim S, Koval PV, Muller G, Neiva AMR, Radoslovich EW, Robert JL, Sassi FP, Takeda H, Weiss Z, Wones DR (1998) Nomenclature of the micas. Can Mineral 36:905–912

Righter K, Carmichael ISE (1996) Phase equilibria of phlogopite lamprophyres from Western Mexico: biotite–liquid equilibria and P-T estimates for biotite-bearing igneous rocks. Contrib Mineral Petrol 123:1–21

Robert J-L, Maury RC (1979) Natural occurrence of a (Fe, Mn, Mg) tetrasilicic potassium mica. Contrib Mineral Petrol 68:117–123

Robert J-L, Beny J-M, Della Ventura G, Hardy M (1993) Fluorine in micas: crystal-chemical control of the hydroxyl-fluorine distribution between trioctahedral and dioctahedral sites. Eur J Mineral 5:7–18

Robert J-L, Della Ventura G, Hawthorne FC (1999) Near-infrared study of short-range disorder of OH and F in monoclinic amphiboles. Am Mineral 84:86–91

Robert J-L, Della Ventura G, Welch M, Hawthorne FC (2000) OH-F substitution in synthetic pargasite at 1.5 kbar, 850°C. Am Mineral 85:926–931

Rosenberg PE, Foit FF (1977) Fe^{2+}-F avoidance in silicates. Geochim Cosmochim Acta 41:345–346

Rumsey M, Welch MD, Origlieri M, Cressey G, Kampf A, Burgio L, Spratt J, Humphreys-Williams E, Kirk C (2014) A redefinition of claringbullite to $Cu_4ClF(OH)_6$; the importance of type material and group/series based studies. 21st General Meeting of the International Mineralogical Association at South Africa, Abstract Volume:375

Russell R, Guggenheim S (1999) Crystal structures of near-end-member phlogopite at high temperatures and heat-treated Fe-rich phlogopite: the influence of the O, OH, F site. Can Mineral 37:711–720

Sanz J, Stone WE (1983) NMR applied to minerals: IV. Local order in the octahedral sheet of micas: Fe-F avoidance. Clay Mineral 18:187–192

Sato H, Holtz F, Behrens H, Botcharnikov R, Nakada S (2005) Experimental petrology of the 1991-1995 Unzen dacite, Japan. Part II: Cl/OH partitioning between hornblende and melt and its implications for the origin of oscillatory zoning of hornblende phenocrysts. J Petrol 46:339–354

Scambelluri M, Münthener O, Ottolini L, Pettke T, Vannucci R (2004) The fate of B, Cl and Li in the subducted oceanic mantle and in the antigorite breakdown fluids. Earth Planet Sci Lett 222:217–234

Schettler G, Gottschalk M, Harlov DE (2011) A new semi-micro wet chemical method for apataite analysis and its application to the crystal chemistry of fluorapatite-chlorapatite solid solutions. Am Mineral 96:138–152

Schleid T, Müller-Bunz H (1998) Single crystals of $Y_3F[Si_3O_{10}]$ with thalenite-type structure. Zeits Anorg Allgem Chem 624:1082–1084

Schlemper EO, Hamilton WC (1966) On the structure of trigonal ammonium fluorosilicate. J Chem Phys 45:408–409

Schlemper EO, Hamilton WC, Rush JJ (1966) Structure of cubic ammonium fluosilicate: neutron-diffraction and neutron-inelastic-scattering studies. J Chem Phys 44:2499–2505

Schreyer W, Armbruster T, Bernhardt H-J, Medenbach O (2003) Pertsevite, a new silicitian magnesioborate mineral with an end-member composition Mg_2BO_3F, in kotoite marble from east of Verkhoyansk, Sakha-Yakutia, Russia. Eur J Mineral 15:1007–1018

Schwarzenbach D, Birkedal H, Hostettler M, Fischer P (2007) Neutron diffraction investigation of the temperature dependence of crystal structure and thermal motions of red HgI_2. Acta Cryst B63:828–835

Sciberras MJ, Leverett P, Williams PA, Hibbs DE, Welch MD, Downes PJ, Kampf AR (2014) Paratacamite-(Ni), Cu_3(Ni, Cu)$Cl_2(OH)_6$, a new mineral from the Carr Boyd Rocks mine, Western Australia. Aust J Mineral 17:39–44

Scordari F, Schingaro E, Ventruti G, Nicotra E, Viccaro M, Tagliani SM (2013) Fluorophlogopite from Piano delle Concazze (Mt. Etna, Italy): crystal chemistry and implications for the crystallization conditions. Am Mineral 98:1017–1025

Scott JD (1976) Crystal structure of miserite, a Zoltai type 5 structure. Can Mineral 14:515–528

Selte K, Kjekshus A (1970) Iodine oxides. Part III. The crystal structure of I_2O_5. Acta Chem Scand 24:1912–1924

Sharova OI, Chudnenko KV, Avchenko OV, Badredinov ZG, Vakh AS (2012) Aluminum-fluorine sphene (titanite) as an indicator of fluorine fluid. Geochemistry 442:250–253

Sharp ZD, Helffrich GR, Bohlen SR, Essene EJ (1989) The stability of sodalite in the system $NaAlSiO_4$-NaCl. Geochim Cosmochim Acta 53:1943–1954

Sharp ZD, Barnes JD, Brearley AJ, Chaussidon M, Fischer TP, Kamenetsky VS (2007) Chlorine isotope homogeneity of the mantle, crust and carbonaceous chondrites. Nature 446:05748

Sharp ZD, Mercer JA, Jones RH, Brearley AJ, Selverstone J, Bekker A, Stachel T (2013) The chlorine isotope composition of chondrites and Earth. Geochim Cosmochim Acta 107:189–204

Shen J, Moore PB (1984) Crystal structure of cappelenite, $Ba(Y,RE)_6[Si_3B_6O_{24}]F_{2:}$ a silicoborate sheet structure. Am Mineral 69:190–195

Shen G, Lu Q, Xu J (2000) Fluorannite: a new mineral of the mica group from the western suburb of Suzhou, Zhejiang Province, China. Yanshi Kuangwuxue Zazhi 19:355–362

Shipovalov YV, Stepanov AV (1971) X-ray structural study of rowlandite. Issled Oblast Khim Fiz Metod Anal Min Syr'ya 189–192

Smith GC, Holness MB, Bunbury JM (2008) Interstitial magmatic scapolite in glass-bearing crystalline nodules from the Kula Volcanic Province, Western Turkey. Mineral Mag 72:1243–1259

Smyth JR, Madel RE, McCormick TC, Munoz JL, Rossman GR (1990) Crystal-structure refinement of a F-bearing spessartine garnet. Am Mineral 75:314–318

Sokolova E (2006) From structure topology to chemical composition. I. Structural hierarchy and stereochemistry in titanium disilicate minerals. Can Mineral 44:1273–1330

Sokolova E, Hawthorne FC (2008a) From structure topology to chemical composition. V. Titanium silicates: the crystal chemistry of nacareniobsite-(Ce). Can Mineral 46:1333–1342

Sokolova E, Hawthorne FC (2008b) The crystal chemistry of the scapolite-group minerals. 1. Crystal structure and long-range order. Can Mineral 46:1527–1554

Sokolova EV, Egorov-Tismenko YK, Voloshin AV, Pakhomovsky YA (1986) Crystal structure of the new Y-Al silicate kuliokite-(Y), $Y_4Al[SiO_4]_2(OH)_2F_5$. Sov Phys Doklady 31:601–603

Sokolova EV, Ferraris G, Ivaldi G, Pautov LA, Khvorov PV (2000) Crystal structure of kapitsaite-(Y), a new borosilicate isotypic with hyalotekite—Crystal chemistry of the related isomorphous series. Neues Jahrb Mineral Monat 2000:74–84

Sokolova E, Hawthorne FC, Pautov LA, Agakhanov AA (2010) Byzantievite, $Ba_5(Ca, Sr, Y)_{22}(Ti, Nb)_{18}(SiO_4)_4[(PO_4), SiO_4)]_4(BO_3)_9O_{21}[(OH), F]_{43}(H_2O)_{1.5}$, the crystal structure and crystal chemistry of the only known mineral with the oxyanions (BO_3), (SiO_4) and (PO_4). Mineral Mag 74(2):285–308

Speziale S, Duffy TS (2002) Single-crystal elastic constants of fluorite (CaF_2) to 9.3 GPa. Phys Chem Minerals 29:465–472

Srdanov VI, Stucky GD, Lippmaa E, Engelhardt G (1998) Evidence for an antiferromagnetic transition in a zeolite-supported cubic lattice of F centers. Phys Rev Lett 80:2449–2452

Stalhandske C, Aurivillius K, Bertinsson GI (1985) Structure of mercury (I, II) iodide oxide, Hg_2OI. Acta Cryst C41:167–168

Stein A, Ozin GA, Stucky GD (1992) Class B sodalities. Nonstoichiometric silver, sodium halosodalites. J Am Chem Soc 114:8119–8129

Su W, Baker DR, Pu L, Bai L, Liu X, Shaughnessy C (2015) Chlroine-hydroxyl diffusion in pargasitic amphibole. Am Mineral 100:138–147

Sun W, Huang Y-X, Pan Y, Mi J-X (2016) Synthesis and magnetic property of centennialite: a new S = ½ Kagomé antiferromagnet and comparison with herbertsmithite and kapellasite. Phys Chem Mineral 43:127–136

Tacker RC, Stormer JC Jr (1989) A thermodynamic model for apatite solid solutions, applicable to high-temperature geological problems. Am Mineral 74:877–888

Tait KT, Barkley MC, Thompson RM, Origlieri MJ, Evans SH, Prewitt CT, Yang H (2011) Bobdownsite, a new mineral species from big fish river, Yukon, Canada, and its structural relationship with whitlockite-type compounds. Can Mineral 49:1065–1078

Takeda H, Burnham CW (1969) Fluor-polylithionite: a lithium mica with nearly hexagonal $(Si_2O_5)^{2-}$ ring. Mineral J (Japan) 6:102–109

Takeda H, Morosin B (1975) Comparison of observed and predicted structural parameters of mica at high temperature. Acta Cryst B31:2444–2452

Teertstra DK, Sherriff BL (1997) Substitutional mechanisms, compositional trends and the end-member formulae of scapolite. Chem Geol 136:233–260

Teiber H, Marks MAW, Wenzel T, Siebel W, Altherr R, Markl G (2014) The distribution of halogens (F, Cl, Br) in granitic rocks. Chem Geol 374–375:92–109

Thewlis J (1955) Unit-cell dimensions of lithium fluoride made from ^{6}Li and ^{7}Li. Acta Crystallogr 8:36–38

Toraya H, Iwai S, Marumo F, Hirao M (1977) The crystal structure of taeniolite, $KLiMg_2Si_4O_{10}F_2$. Z Kristallogr 146:73–83

Tornero JD, Fayos J (1990) Single-crystal structure refinement of $MnCl_2$. Z Kristallogr 192:147–148

Tracy RJ (1991) Ba-rich micas from the Franklin Marble, lime crest and sterling hill, New Jersey. Am Mineral 76:1683–1693

Tropper P, Manning CE, Harlov DE (2011) Solubility of $CePO_4$ monazite and YPO_4 xenotime in H_2O and H_2O–NaCl at 800 °C and 1 GPa: implications for REE and Y transport during high-grade metamorphism. Chem Geol 282:58–66

Tropper P, Manning CE, Harlov DE (2013) Experimental determination of $CePO_4$ and YPO_4 solubilities in H_2O–NaF at 800 °C and 1 GPa: implications for rare earth element transport in high-grade metamorphic fluids. Geofluids 13:372–380

Trill H, Eckert H, Srdanov VI (2003) Mixed halide sodalite solid solution systems. Hydrothermal synthesis and structural characterization by solid state NMR. J Phys Chem B 107:8779–8788

Uher P, Kodera P, Lexa J, Bacik P (2014) Halogen-rich biotites from the Detva, Biely Vrch Au-porphyry deposit (Slovakia): compositional variations and genetic aspects. 4th Central European Mineralogical Conference, Skalsky Dvur, 2014, pp 146–14

Uvarova YA, Sokolova E, Hawthorne FC, Agakhanov AA, Karpenko VY, Pautov LA (2013) The crystal structure of laptevite-(Ce), $NaFe^{2+}(REE_7Ca_5Y_3)(SiO_4)_4(Si_3B_2PO_{18})(BO_3)F_{11}$, a new mineral species from the Darai-Pioz alkaline massif, Northern Tajikistan. Z Kristallogr Cryst Mater 228:550–557

Valley JW, Essene EJ, Peacor DR (1983) Fluorine-bearing garnets in Adirondack calc-silicates. Am Miner 68:444–448

Vanko DA, Bishop FC (1982) Occurrence and origin of marialitic scapolite in the Humboldt lopolith, NW Nevada. Contrib Mineral Petrol 81:877–888

Vasyukova O, Williams-Jones AE (2014) Fluoride-silicate melt immiscibility and its roles in REE ore formation: evidence from the Strang Lake rare metal deposit, Quebec-Labrador, Canada. Geochim Cosmochim Acta 139:110–130

Veit Th, Buhl J-Ch, Hoffmann W (1991) Hydrothermal synthesis, characterization and structure refinement of chlorate- and perchlorate-sodalite. Catal Today 8:405–413

Veksler IV, Dorfman AM, Kamenetsky M, Dulski P, Dingwell DB (2005) Partitioning of lanthanides and Y between immiscible silicate and fluorides melts, fluorite and cryolite and the origin of the lanthanide tetrad effect in igneous rocks. Geochim Cosmochim Acta 69:2847–2860

Vettier C, Yelon WB (1975) The structure of FeC_{l2} at high pressures. J Phys Chem Solids 36:401–405

Vidal-Valat G, Vidal JP, Zeyen CME, Kurki-Suonio K (1979) Neutron diffraction study of magnesium fluoride single crystals. Acta Cryst B 35:1584–1590

Volfinger M, Pascal ML (1989) Partitioning of chlorine between muscovite and HCl-buffered solutions from 400 to 600 °C at 2 kbar. Eur J Mineral 1:791–800

Volfinger M, Robert IL, Vielzeuf D, Neiva AMR (1985) Structural control of the chlorine content of OH-bearing silicates (micas and amphiboles). Geochim Cosmochim Acta 49:37–48

Walker D, Verma PK, Cranswick LMD, Jones RL, Clark SM, Buhre S (2004) Halite-sylvite thermoelasticity. Am Mineral 89:204–210

Wallwork K, Kolitsch U, Pring A, Nasdala L (2002) Decrespignyite-(Y), a new copper yttrium rare earth carbonate chloride hydrate from Paratoo, South Australia. Miner Mag 66:181–188

Webster JD, Tappen CM, Mandeville CW (2009) Partitioning behavior of chlorine and fluorine in the system apatite-melt-fluid. II: felsic silicate systems at 200 MPa. Geochim Cosmochim Acta 73:559–581

Webster JD, Baker DR, Aiuppa A (2018) Halogens in mafic and intermediate-silica content magmas. In: Harlov DE, Aranovich L (eds) The role of halogens in terrestrial and extraterrestrial geochemical processes: surface, crust, and mantle. Springer, Berlin, pp 307–430

Welch MD, Hawthorne FC, Cooper MA, Kyser TK (2001) Trivalent iodine in the crystal structure of schwartzembergite, $Pb_5IO_6H_2Cl_3$. Can Mineral 39:785–795

Welch MD, Sciberras MJ, Williams PA, Leverett P, Schlüter J, Malcherek T (2014) A temperature-induced reversible transformation between paratacamite and herbertsmithite. Phys Chem Mineral 41:33–48

Wood SA (1990) The aqueous geochemistry of the rare-earth elements and yttrium: 1. Review of low-temperature data for inorganic complexes and the inorganic REE speciation of natural water. Chem Geol 82:159–186

Worden RH (2018) Halogen elements in sedimentary systems and their evolution during digenesis. In: Harlov DE, Aranovich L (eds) The role of halogens in terrestrial and extraterrestrial geochemical processes: surface, crust, and mantle. Springer, Berlin, pp 185–260

Wu J, Koga KT (2013) Fluorine partitioning between hydrous minerals and aqueous fluid at 1 GPa and 770–947 °C: a new constraint on slab flux. Geochim Cosmochim Acta 119:77–92

Wu M, Tse JS, Pan Y (2016) Anomalous bond length behavior and a new solid phase of bromine under pressure. Sci Rep 6:25649

Xiao Y, Hoefs J, Kronz A (2005) Compositionally zoned Cl-rich amphiboles from North Dabie Shan, China: monitor of high-pressure metamorphic fluid/rock interaction processes. Lithos 81:279–295

Yakovenchuk VN, Ivanyuk GY, Pakhomovsky YA, Selivanova EA, Korchak JA, Nikolaev AP (2010a) Strontiofluorite, SrF_2, a new mineral species from the Khibiny massif, Kola peninsula, Russia. Can Mineral 48:1487–1492

Yakovenchuk VN, Selivanova EA, Ivanyuk GYu, YaA Pakhomovsky, Mikhailova JA, Nikolaev AP (2010b) Polezhaevaite-(Ce), $NaSrCeF_6$, a new mineral from the Khibiny massif (Kola Peninsula, Russia). Am Mineral 95:1080–1083

Yakubovich OV, Massa W, Pekov IV, Gavrilenko PG (2007) Crystal structure of tveitite-(Y): fractionation of rare-earth elements between positions and the variety of defects. Cryst Rep 52:71–79

Yamonva NA, Pushcharovskii DY, Vyatkin SV, Khomyakov AP (1992) Crystal structure of the new natural sulfate-carbonate $Na_{25}BaTR_2(CO_3)_{11}(HCO_3)_4(SO_4)_2F_2Cl$. Sov Phys Crystallogr 37:753–756

Yang Z (1995) Structure redetermination of natural cebaite-(Ce), $Ba_3Ce_2(CO_3)_5F_2$. Neues Jahrb Mineral Monat 1995:56–64

Yang ZM, Pertlik F (1993) Huanghoite-(Ce), $BaCe(CO_3)_2F$, from Khibina, Kola peninsula, Russia: redetermination of the crystal structure with a discussion on space group symmetry. Neues Jahbr Mineral Monat 1993:163–171

Yu Q, Suguta S, Feng X, Mi J (1997) On the preparation of single crystals of $11CaO{\cdot}7Al_2O_3{\cdot}CaF_2$ and the confirmation of its crystal structure. Cement Concret Res 27:1439–1449

Zalenski M, Balic-Žunic T, Bindi L, Garavelli A, Makovicky E, Pinto D, Vurro F (2006) First occurrence of iodine in natural sulfosalts: the case of mutnovskite, $Pb_3AsS_3(I,Cl,Br)$, a new mineral from the Mutnovsky volcano, Kamchatka Peninsula, Russian Federation. Am Mineral 91:21–28

Zalkin A, Forrester JD, Templeton DH (1964) The crystal structure of sodium fluorosilicate. Acta Crystallogr 17:1408–1412

Zhang RY, Li T, Rumble D, Yui T-F, Li L, Yang JS, Pan Y, Liou JG (2007) Multiple mantle metasomatism in the Sulu ultrahigh-P garnet peridotite constrained by petrological and geochemical investigation. J Metamorp Geol 25:149–164

Zhang C, Holtz F, Ma C, Wolff PE, Li Y (2012) Tracing the evolution and distribution of F and Cl in plutonic systems from volatile-bearing minerals: a case study from the Liujiawa pluton (Dabie orogen, China). Contrib Mineral Petrol 164:859–879

Zhang C, Lin J, Pan Y, Feng R, Almeev R, Holtz F (2017) Electron probe microanalysis of bromine in minerals and glasses with correction for spectral interference from aluminum, and

comparison with microbeam synchrotron X-Ray fluorescence spectrometry. Geostand Geoanal Res (in press)

Zheng XG, Mori T, Nishiyama K, Higemoto W, Yamada H, Nishikubo K, Xu CN (2005) Antiferromagnetic transitions in polymorphous minerals of the natural cuprates atacamite and botallackite $Cu_2Cl(OH)_3$. Phys Rev B 71:174404

Zhou B, Sun W, Zhao B-C, Mi J-X, Laskowski R, Terskikh V, Zhang X, Yang L, Botis S, Pan Sherriff BL, Pan Y (2016) ^{11}B MAS NMR and first principles study of the [OBO_3] pyramids in borates. Inorg Chem 55:1970–1977

Zhou B, Faucher A, Laskowski R, Terskikh VV, Kroeker S, Sun W, Lin J, Mi J-X, Michaelis VK, Pan Y (2017) Ultrahigh-field ^{25}Mg NMR and DFT study of magnesium borate minerals. ACS Earth Space Chem (in press)

Zhu C, Sverjensky DA (1991) Partitioning of F-CI-OH between minerals and hydrothermal fluids. Geochim Cosmochim Acta 55:1837–1858

Zhu C, Sverjensky DA (1992) F-Cl-OH partitioning between biotite and apatite. Geochim Cosmochim Acta 56:3435–3467

Zhu T-T, Sun W, Huang Y-X, Sun Z-M, Pan Y, Balents L, Mi JX (2014) Strong spin frustration from isolated triangular Cu(II) trimers in $SrCu(OH)_3Cl$ with a novel cuprate layer. J Mater Chem C 2:8170–8178

Zubkova NV, Pushcharovsky DY, Giester G, Tillmanns E, Pekov IV, Krotova OD (2004) Crystal structure of byelorussite-(Ce) $NaMnBa_2Ce_2(TiO)_2[Si_4O_{12}]_2(F, OH)\cdot H_2O$. Crystallogr Rep 49:964–968

Chapter 4
Halogen Elements in Sedimentary Systems and Their Evolution During Diagenesis

Richard H. Worden

Abstract The full range of processes capable of influencing halogen concentrations in sediments, sedimentary rocks, and formation waters and other fluids involved in diagenetic reactions have been investigated. Chloride and Br^- are typically assumed to be conservative in sedimentary and diagenetic systems since they are considered to be independent of silicate, carbonate, sulphate, sulphide, or oxide diagenetic processes. Chloride distribution in sedimentary systems is controlled by variable degrees of seawater evaporation; seawater dilution by meteoric water, freshwater evaporation in arid continental basins; seawater freezing; evaporite dissolution; seawater concentration by silicate diagenetic hydration reactions in the sediment column; seawater dilution by diagenetically-produced water associated with overpressure build-up; and membrane filtration through low permeability rocks. There are circumstances under which Br may not be a conservative element when compared to Cl. These include hydration reactions, which may lead to increasing Cl^- and Br^- concentrations but slightly higher Cl/Br ratios; evaporative concentration, which may lead to loss of Br^- by atmospheric ozonation processes; incongruent dissolution of Br-poor halite; dissolution of Br-enriched potash facies evaporites; breakdown of Br-bearing organic matter; or retarded membrane filtration of Br compared to Cl. Water geochemical data from oil and gas fields have been collated and compared with a range of likely controlling processes. Chloride and Br^- concentrations in formation water are enormously variable with the most important controls being dilution of seawater by meteoric water; evaporative concentration (of seawater or continental waters); dissolution of halite- and/or potash-bearing evaporites; diagenetic hydration reactions; and diagenetic dehydration reactions. Dissolution of mixed halite-potash facies evaporites by meteoric water can explain the huge range of Cl/Br ratios found in formation waters.

R.H. Worden (✉)
Department of Earth Ocean & Ecological Sciences, School of Environmental Science, University of Liverpool, L69 3GP Liverpool, UK
e-mail: r.worden@liv.ac.uk

D.E. Harlov and L. Aranovich (eds.), *The Role of Halogens in Terrestrial and Extraterrestrial Geochemical Processes*, Springer Geochemistry,
https://doi.org/10.1007/978-3-319-61667-4_4

High Br^- concentrations in deeply buried formation waters are typically assumed to represent the residue of extreme evaporation of seawater although here it is shown that they can also be the result of the dissolution of Br-enriched, potash-bearing evaporites. Fluoride is non-conservative in formation waters and its concentrations are typically low since this element is incorporated in minerals, following alteration and diagenesis, such as fluorite, apatite, and clay minerals. Iodide is also non-conservative and is found at relatively high concentrations in some formation waters due to the breakdown of I-enriched and organic-bearing sedimentary rocks. The patterns of halogen concentration in sedimentary formation waters can be of great significance since they reveal much about the fluid flow history of the basin in general and the oil or gas field in particular.

4.1 Introduction

The halogen elements play significant roles in surface sedimentary environments and during diagenesis in the sedimentary column. Fluorine, Cl, Br, and I have some fundamental geochemical similarities and yet display marked differences in behaviour in sediments, sedimentary rocks, and their fluids. Key technical definitions related to the presence of halogen elements in sedimentary and diagenetic systems are defined in Table 4.1. The wide variety of processes that lead to sedimentary rocks (weathering, dissolution, atmospheric processes, evaporation, mineral precipitation, burial, and diagenesis) result in discrete patterns of changing concentrations of F, Cl, Br, and I. After summarising current understanding about where the halogen elements exist in sediments and sedimentary rocks, this chapter will deal with the key processes that change the concentration of halogen elements at the various stages in the diagenetic cycle (Fig. 4.1). A collation of oil field formation water data is then compared to the effects of the main processes.

The study of halogen elements in sediments and sedimentary rocks is not simply an academic pursuit. The over- and undersupply of F and I from the natural environment have well-known implications for human health and well-being (Edmunds and Smedley 2013). Halite plays a crucial role in many petroleum systems with halokinesis leading to petroleum traps, halite-, and other evaporite-dominated lithologies behaving as nearly perfect caprocks, and the Cl- concentration of formation water having important effects on how mixed-phase oil and water flow through reservoirs during petroleum production. The specific composition of formation waters (notably the Cl-Br relationships) can be used to help reveal movement patterns of fluids in sedimentary basins.

Table 4.1 Definition of terms employed in studies of sediment diagenesis and evaporite sedimentology

Term	Definition
Authigenesis	In situ mineral growth
Bittern	Highly saline (>26 wt% salinity) solution remaining after the precipitation of halite from seawater or other brines
Brine	Formation water ranging in salinity from 3.5 wt% (seawater) to about 26 wt% salinity
Cementation	Growth or precipitation of minerals in pore spaces
Compaction	Suite of processes due to overburden resulting in loss of pore space in sedimentary rocks
Chemical compaction	Chemical processes that lead to reduced porosity: pressure-enhanced dissolution leading to stylolites and precipitation in pores
Closed system	All mineral-forming species in a sedimentary rock were present at the time of deposition
Connate water	Water that was trapped in the pores of sedimentary rocks as they were deposited (depositional water)
Decarboxylation	Loss of CO_2 from organic matter due to heating
Dehydration	Hydrous minerals, such as clays, breaking down to create anhydrous minerals (such as feldspars) and free water
Diagenesis	Combination of processes that lead to the conversion of friable sediment into sedimentary rock
Diagenetic water	Water of marine, meteoric or connate origin strongly influenced by diagenetic processes of water-rock interaction
Dissolution	Minerals destroyed by interaction with a fluid leaving behind a pore or cavity
Evaporite	Sedimentary rock formed by precipitation of a range of mineral salts due to evaporation of seawater or continental water
Formation water	Water found in deeply buried, porous and permeable sedimentary rocks
Halokinesis	Mobilization and upward flow of subsurface, deeply buried and ductile halite-dominated evaporites
Hydration (feldspar hydrolysis)	Water-induced breakdown of anhydrous feldspar, creating a range of neoformed clay minerals
Juvenile water	Water-rich volatile fluids that were originally derived from an igneous (magmatic) source
Lithification	The process of converting loose primary sediment into rock (incl. cementation and compaction)
Mechanical compaction	Physical processes that lead to reduced porosity due to overburden increase: grain repacking, ductile deformation, and grain fracturing
Meteoric water	Water in sediment that was originally derived from atmospheric precipitation (rain or snow)
Microporosity	Pores that are too small to see with an optical microscope that still contribute to total (i.e., helium) porosity
Neoformation	New growth of a mineral during diagenesis
Neomorphism	Transformation of a mineral during diagenesis (change may be in form (habit), crystallographic or chemical)

(continued)

Table 4.1 (continued)

Term	Definition
Open system	Some mineral-forming species in rock have fluxed in, or out, of the rock in question
Overpressure	Fluid pressure that is significantly greater than hydrostatic pressure (also known as geopressure)
Paragenetic sequence	The order in which diagenetic events occurred
Playa	Arid intracontinental (desert) basin, typically with very low relief
Pore water	Interstitial water occupying the space between sediment grains
Potash	K- and Mg-dominated, very late stage evaporitic sedimentary rocks representing the end of the evaporation series
Precipitation	Crystallisation of mineral from a fluid
Pressure solution	See chemical compaction
Recrystallisation	Dissolution followed by precipitation involving a change in crystal size or habit
Replacement	Growth of a chemically-different mineral within the body of an existing mineral
Salt	General term for rocks of evaporitic origin, typically dominated by halite but including all other evaporite minerals
Salt diapir (salt dome)	Structural dome formed when a thick, deeply buried bed of halite-dominated evaporites vertically intrudes overlying rock strata
Secondary porosity	Porosity in a rock resulting from dissolution of grains or pre-existing mineral cement

Adapted from Worden and Burley (2003)

The key questions that will be addressed in this paper are:

1. What are the absolute and relative halide concentrations of water relevant to sedimentary basins, including meteoric water, river water, and groundwater?
2. What are the absolute and relative halide concentrations in sediments and sedimentary rocks?
3. What are the main processes that influence the concentration and distribution of the halogen elements in sediments, sedimentary rocks, and related fluids?
4. What controls Cl and Br stable isotope values in sedimentary rocks and formation waters?
5. What controls the concentration of halide elements in formation waters deep in sedimentary basins?
6. What do halogen elements reveal about the origin and evolution of sedimentary rocks and their formation waters?

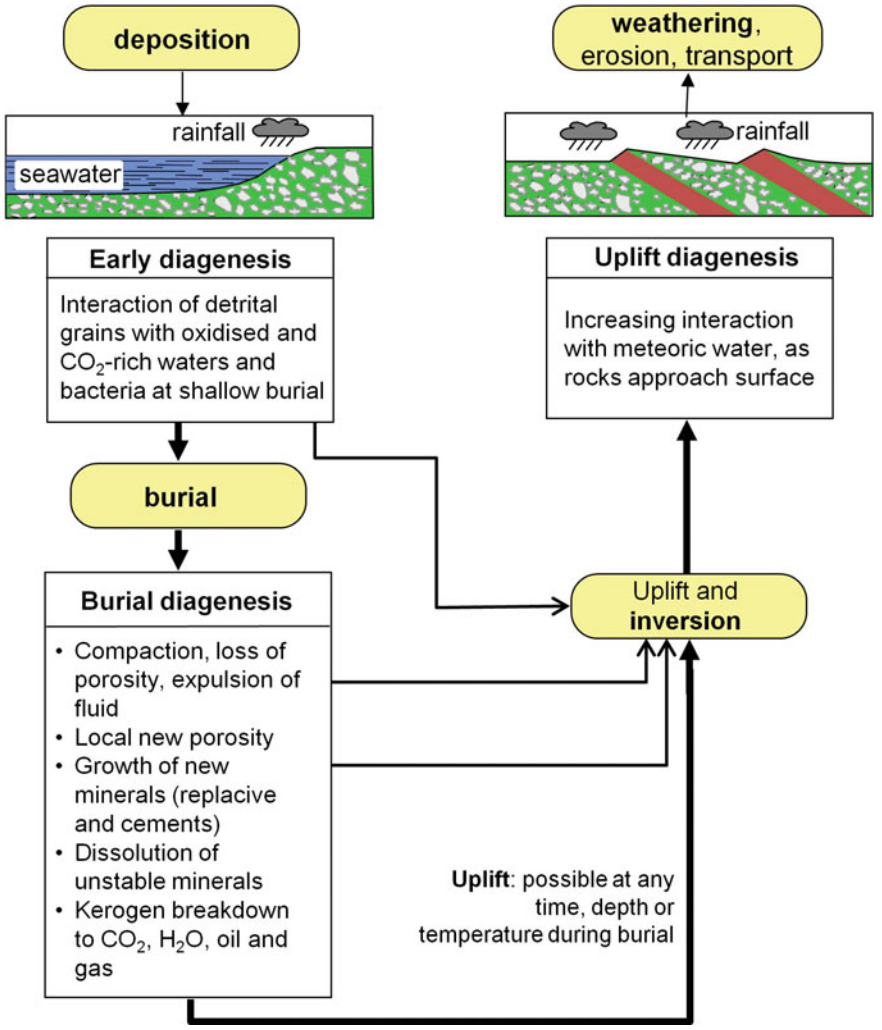

Fig. 4.1 Diagenetic perspective on the rock cycle including processes that can alter halogen element distribution. Modified from Worden and Burley (2003). See Table 4.1 for definitions of terms

4.2 Sediments, Diagenesis, Sedimentary Rocks, and Fluids, and the Rock Cycle

Sediment includes clastic material from eroded hinterlands, biogenic and chemical sediments, and evaporites. Clastic sediment is the eroded material that accumulates, permanently or transiently, in sedimentary basins. Sediment is composed of the weathered residue from the elevated perimeter of the basin, also known as the

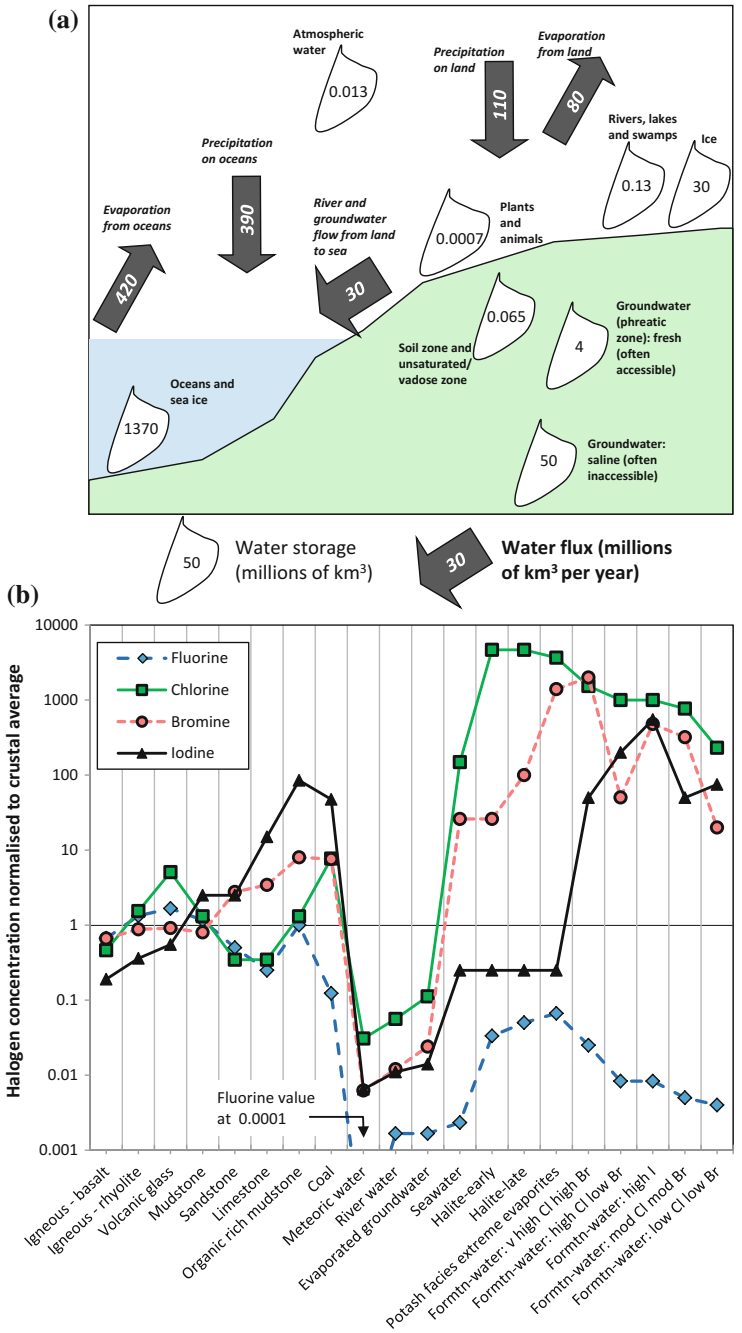
(a)
Atmospheric water
0.013
Precipitation on land
110
Evaporation from land
80
Rivers, lakes and swamps
0.13
Ice
30
Precipitation on oceans
390
Evaporation from oceans
420
River and groundwater flow from land to sea
30
0.0007
Plants and animals
0.065
Soil zone and unsaturated/ vadose zone
4
Groundwater (phreatic zone): fresh (often accessible)
Oceans and sea ice
1370
50
Groundwater: saline (often inaccessible)
50
Water storage (millions of km³)
30
Water flux (millions of km³ per year)
(b)
Halogen concentration normalised to crustal average
10000
1000
100
10
1
0.1
0.01
0.001
Fluorine
Chlorine
Bromine
Iodine
Fluorine value at 0.0001
Igneous - basalt
Igneous - rhyolite
Volcanic glass
Mudstone
Sandstone
Limestone
Organic rich mudstone
Coal
Meteoric water
River water
Evaporated groundwater
Seawater
Halite-early
Halite-late
Potash facies extreme evaporites
Formtn-water: v high Cl high Br
Formtn-water: high Cl low Br
Formtn-water: high I
Formtn-water: mod Cl mod Br
Formtn-water: low Cl low Br

◂**Fig. 4.2** (**a**) The hydrological cycle showing relative reservoir volumes and the annual net flux of water; Adapted from Price (1996). (**b**) Collation of halogen concentration data from igneous rocks, sedimentary rocks; surface waters and formation waters, normalised to average crustal abundances of the halogens: F, 600 ppm; Cl, 130 ppm; Br, 2.5 ppm; I, 0.2 ppm (Krauskopf 1979). Values >1 represent enrichment. Values <1 represent depletion relative to an average crustal value

hinterland (Fig. 4.1). Clastic sediment is predominantly transported by water (rivers and the sea), but very fine sediment (clay grade and finer) can also be transported long distances by wind. Water is a key medium for sediments and diagenesis (Table 4.1). Naturally, a large proportion of water at the surface and in sedimentary basins is found in the sea (Fig. 4.2a) (Price 1996) with much smaller volumes stored in land-ice and as deep groundwater (typically too deep and too saline for human use). The proportion of groundwater that is shallow and fresh enough for human use is relatively small but this is still greater than the amounts of water in rivers and lakes and in the atmosphere or stored within plants and animals (Fig. 4.2a). Water is not static on the Earth's surface. There is a huge annual flux of evaporation from the oceans with a smaller amount of evaporation from the land. There is also a substantial flux of meteoric water (defined in Table 4.1) onto the land and oceans with the main movement of water represented by river and groundwater flow from the land to the oceans (Fig. 4.2a). The reservoirs and flux of water are important considerations to help understand the locations and behaviour of the halogen elements in sedimentary and diagenetic systems.

Clastic sediments are predominantly composed of physically disaggregated rock fragments, or grains. Sediment typically has a rather different mineralogy compared to the mineralogy of the primary rocks undergoing weathering in the hinterland. This difference is due to chemical weathering as a result of rocks formed at high temperature (igneous and metamorphic rocks, and even diagenetically altered rocks) being out of equilibrium with the low temperature, water-, O_2-, and CO_2-rich conditions found at the Earth's surface. Chemical weathering tends to be enhanced in warm and wet climatic conditions and is inhibited in cold and dry conditions. Primary mineral alteration by chemical weathering is more advanced in sedimentary systems where there is more time for alteration to occur. Thus sediment in long and low relief river systems will be more chemically-altered that sediment in short and steep river systems. Clastic sediments have nearly identical mineralogy to the rocks in the hinterland in basins where chemical weathering is muted due to one or more factors including cold climatic conditions, arid climatic conditions, or insufficient time to allow weathering to occur. Chemical weathering of the sediment occurs from the moment the hinterland rock interacts with the atmosphere right through to the time at which sediment has been buried and isolated from atmospheric influences. In terms of the distribution of halogen elements in primary sediment, it is important to consider the composition and origin of the rocks and minerals in the hinterland relative to the basin and the degree of alteration in those rocks.

Some sediments, such as evaporites, are chemical precipitates formed due to extreme degrees of evaporative concentration. Such sediments, naturally, are an

important part of the sedimentary and diagenetic inventory of halogen elements. Other primary sediments (e.g., carbonates) are strongly influenced by the biological realm in the sedimentary basin. Those halogen elements, concentrated in organic-rich primary sediments, will be discussed further on in the text.

Diagenesis is the collection of processes that converts unconsolidated sediment into sedimentary rock (Fig. 4.1, Table 4.1). It includes early diagenesis, which is the alteration of sediment in the environment of deposition. Early diagenetic processes include bioturbation, reaction with the acidic products from organic decay, and the final stages of reaction with near surface (O_2- and CO_2-rich) groundwater leading to redox reactions.

Diagenesis incorporates a range of compaction processes involving the rearrangement of primary sedimentary grains when the sediment is progressively buried. Mechanical compaction processes will not much influence the phase distribution of halogen elements in sedimentary rocks. Mechanical compaction leads to significant loss of porosity and therefore loss of mobile water from rocks (Worden and Burley 2003). Since water plays a major role on halogen diagenesis, compactional processes can strongly influence halogen distribution patterns. Chemical compaction is the pressure- and -temperature assisted dissolution at grain-grain contacts and may lead to halogen release from minerals into formation water. Halite-rich evaporites are distinctly ductile when loaded so that burial of such low density and soluble rocks leads, on geological timescales, to major upward flow (halokinesis) of evaporites and rearrangement of beds at the basin-scale.

Burial diagenesis occurs when sediments are buried to significant depths of burial such that they are hotter than about 50–70 °C (Fig. 4.1, Table 4.1) (Worden and Burley 2003). The increasing temperature during burial accelerates the rate of chemical alteration of reactive materials. Minerals and rock fragments (lithic grains) that formed at high temperature are intrinsically more reactive than minerals that form at Earth surface temperatures. If lithic grains have survived weathering, transport, and the early stages of burial then they may finally undergo chemical breakdown to minerals that are more stable at the ambient conditions. Thus feldspar grains in primary sandy sediment are altered to clay minerals. Biotite and muscovite in sandstone and siltstone are replaced by lower temperature phyllosilicates. Semi-amorphous phosphate minerals are replaced by more crystalline diagenetic phosphates. Such reactions can have a strong influence on the distribution of halogen elements during diagenesis. Similarly, Br-rich primary halite can undergo incongruent dissolution in low salinity formation waters with concomitant loss of Br (Stoessell and Carpenter 1986).

Burial diagenesis also causes the progressive alteration of organic matter in sedimentary rocks with the conversion of biomolecules to kerogen, and then the cracking of kerogen to fluid phase molecules with increasingly C-rich and H-poor material left behind in the sediment (Fig. 4.1). The halogen content of the primary organic matter depends on the site of deposition, but halogens tend to be lost from the sedimentary organic material during burial and diagenesis.

Hydrothermal activity can be an important event in the life cycle of a sedimentary basin. The notable aspect of hydrothermal activity is the introduction of

fluids alien to, and thus out of equilibrium with, the host rock. Such fluids can lead to mineral dissolution or precipitation in the sedimentary rock and can have an impact on the distribution of the halogen elements.

4.3 The Location of Halogen Elements Within the Diagenetic Realm and Within the Rocks and Fluids that Contribute to Sedimentary Basins

The average concentrations of the halogen elements have been collated for igneous rocks (basalt, rhyolite, and volcanic glass), sedimentary rocks (mudstone, sandstone, limestone), organic-rich sedimentary rocks (petroleum source rock, coal), surface waters (meteoric, river, and ground water, evaporated groundwater and seawater), evaporites, and a range of types of oil and gas field formation water (see later text for details and references). Evaporites have here been split into early and late stage halite-dominated salt deposits and K- and Mg-dominated very late stage potash facies evaporites (defined in Table 4.1) representing the end of the seawater evaporation series (Warren 1999). These concentrations have been normalised to average crustal halogen abundances, i.e. F, 600 ppm; Cl, 130 ppm; Br, 2.5 ppm; and I, 0.2 ppm (Krauskopf 1979). Values of 1 represent concentrations equal to crustal abundance. Values less than 1 represent depletion relative to the crust. Values greater than 1 represent enrichment relative to the crust (Fig. 4.2b). This figure helps to visualise those parts of sedimentary systems that are enriched or depleted in halogens. Chlorine and Br tend to be most enriched in halite and potash-bearing evaporites and in Cl-rich formation waters. Iodine tends to be most enriched in organic rich sediments and sedimentary rocks and in formation water. Fluorine tends to be depleted in all sedimentary fluids and rocks, except for mudstones that appear to be the resting place of crustal fluorine in sedimentary systems.

4.3.1 Fluorine

The average F concentration in the Earth has been estimated to be 25 ppm (McDonough and Sun 1995). Fluorine tends to be enriched in more evolved igneous rocks such as rhyolite (Yoshida et al. 1971) and occurs in minerals that form at the final stages of magma crystallization such as apatite (fluorapatite) and topaz in acid igneous rocks (Fig. 4.2b, Table 4.2). Fluorine is the least incompatible of the halogen elements and, although it has a higher crustal average concentration than Cl (17 ppm, see later), its emission from volcanoes is between 5 and 25% that of Cl (Symonds et al. 1988). Fluorine is also found to be able to substitute for OH groups in hydroxyl-bearing igneous and metamorphic silicate minerals such as biotite, muscovite, or hornblende (Jagadeshan et al. 2015). Hinterlands enriched in

Table 4.2 Halide-containing minerals in sedimentary systems

Natural mineral	Formula	Roles in sedimentary systems	Major halide	Trace halide
Halite	NaCl	Evaporite	Cl	Br
Sylvite	KCl	Evaporite	Cl	Br
Carnallite	$KMgCl_3 \cdot 6H_2O$	Evaporite	Cl	Br
Bischofite	$MgCl_2 \cdot 6H_2O$	Evaporite	Cl	Br
Kainite	$KMg(SO_4)Cl \cdot 3H_2O$	Evaporite	Cl	Br
Hydrohalite	$NaCl \cdot 2H_2O$	Cryogenic evaporite	Cl	Br
Fluorite	CaF_2	Hydrothermal, diagenetic	F	
Topaz	$Al_2SiO_4(F,OH)_2$	Detrital	F	
Sodalite	$Na_8Al_6Si_6O_{24}Cl_2$	Detrital	Cl	
Scapolite	$(Na,Ca)_4[Al_3Si_9O_{24}]Cl$	Detrital	Cl	
Fluorapatite	$Ca_5(PO_4)_3(OH,F)$	Detrital, diagenetic	F	Cl
Chlorapatite	$Ca_5(PO_4)_3(OH,Cl)$	Detrital, diagenetic	Cl	F
Hornblende	$Ca_2(Mg,Fe,Al)_5(Si_6Al_2)O_{22}(OH)_2$	Detrital		F (Cl, Br)
Biotite	$K(Mg,Fe)_3AlSi_3O_{10}(OH)_2$	Detrital		F (Cl, Br)
Muscovite	$KAl_3Si_3O_{10}(OH)_2$	Detrital		F (Cl, Br)
Illite	$K_{0.7}Al_{2.5}Si_{3.5}O_{10}(OH)_2$	Diagenetic		F
Smectite	$(Ca,Na)_{0.7}(Al,Mg,Fe)_4(Si,Al)_8O_{10}(OH)_4 \cdot nH_2O$	Diagenetic		F
Kaolinite	$Al_2Si_2O_5(OH)_4$	Diagenetic		F
Lautarite	$Ca(IO_3)_2$	Diagenetic	I	
Fuenzalidite	$K_6(NaK)_4Na_6Mg_{10}(SO_4)_{12}(IO_3)_{12} \cdot 12H_2O$	Diagenetic	I	
Hectorfloresite	$Na_9(IO_3)(SO_4)_4$	Diagenetic	I	

these minerals will tend to supply sediment enriched in F to the final sedimentary basin. Fluorine is found in fluorite (CaF_2) which may be a detrital mineral but can also result from diagenetic processes, especially in carbonate host rocks (Jiang et al. 2014). Fluorine commonly occurs at trace concentrations replacing hydroxyls in clay minerals such as smectite or kaolinite (Chipera and Bish 2002). Illite and smectite group clay minerals are reported to be important sinks for F in marine sediments (Rude and Aller 1994; Matthies and Troll 1990). The most important F-bearing detrital and diagenetic minerals in sediments and sedimentary rocks are the apatite family of minerals. Detrital apatite can have a primary igneous origin but in Phanerozoic rocks, apatite may also have a biogenic origin since the apatite group of minerals has been an important part of bone construction since the evolutionary emergence of vertebrate animals in the Cambrian (Holland and Chen 2001). In sedimentary basins, fluorite is found at some of the highest concentrations

in veins hosted by limestones and dolomites (Neilson and Oxtoby 2008; Neal et al. 2003).

Fluoride is present in seawater at about 1.4 mg/L and is reported to have an approximately constant ratio with Cl^-, the dominant anion in seawater (Sverdrup et al. 1942; Chester and Jickells 2012).

Meteoric water typically has low but measurable concentrations of F^-. A mean F^- concentration of 34 µg/L (range from below detection to 230 µg/L with a mean of 100 µg/L) in meteoric water was reported for part of the UK (Neal et al. 1990). Fluoride concentrations in meteoric water tend to be highest at sites close to recent volcanic eruptions (and especially alkaline volcanoes) (Bellomo et al. 2003). Based on an average fluvial F^- concentration of 0.1 mg/L, an average marine F^- concentration of 1.4 mg/L, a river water flux to the ocean of 3.47×10^{17} kg/yr, and an estimated ocean water mass of 1.35×10^{21} kg, the ocean residence time for F^- is about 0.5 Myr (Table 4.3).

Fluoride concentration in river water and extractable groundwater is highly variable, ranging from below detection (typically <0.1 mg/L) to 250 mg/L (Edmunds and Smedley 2013). Fluoride concentration in groundwater and rivers tends to be controlled by the saturation state of fluorapatite (Neal et al. 2003). Fluoride concentrations tend to be elevated in alkaline Na-dominated river or groundwater, where there is limited dissolved Ca to allow for fluorite or fluorapatite growth. Fluoride concentrations also tend to be elevated in host aquifers that contain elevated whole rock F^- concentrations (Rao and Devadas 2003). Even at low concentrations, the precise F^- concentration of river and groundwater tends to be controlled by the presence or absence of F-bearing minerals in the river's hinterland. For example, elevated concentrations of F^- (and Ba) has been linked to upstream fluorite-barite vein mineralization in bedrock in river water (Neal et al. 2003).

Table 4.3 Marine residence times derived for halogen elements and major cations (for comparison) based on the methodology reported in Chester and Jickells (2012); an assumed flux of river water to the ocean of 3.47×10^{17} kg/yr; and an estimated ocean water mass of 1.35×10^{21} (Berner and Berner 2012; Chester and Jickells 2012)

Dissolved species	Symbol	Concentration in rivers (ppm)	Absolute amount added to rivers (Mt/yr)	Concentration in the ocean (ppm)	Absolute amount in the ocean (10^6 Mt)	Residence time in the ocean (Myr)
Fluorine	F	0.1	3740	1.4	1960	0.5
Chlorine	Cl	7.00	261,800	19,354	27,095,600	103.5
Bromine	Br	0.025	935	69	96,600	103.3
Iodine	I	0.002	74.8	0.05	70	0.9
Sodium	Na	5	187,000	10,770	15,078,000	80.6
Magnesium	Mg	3	112,200	1290	1,806,000	16.1
Calcium	Ca	13	486,200	412	576,800	1.2
Sulphate	SO_4	10	374,000	2712	3,796,800	10.2

ppm: parts per million, Mt: megatonnes, Myr: millions of years, yr: years

Fluoride is also present at low concentrations in sedimentary formation waters, typically at <5 mg/L, but is more rarely reported than any other halide (Worden 1996). Some formation waters have values up to 25 mg/L F^-. These typically are associated with very high salinity formation water (see later).

4.3.2 Chlorine

The average Cl concentration of the Earth has been estimated to be 17 ppm (McDonough and Sun 1995). Chlorine is present in most igneous rocks at low concentrations with little difference in concentration shown between granite and basic igneous rocks (both have a Cl^- concentration of about 0.02%). However, igneous glass typically has higher Cl concentrations (e.g., 0.08%) (Kuroda and Sandell 1953). Chlorine is concentrated within any residual vapour phase during volcanic eruptions (Bureau et al. 2000) so the contribution of volcanically erupted Cl to the atmosphere is considerable. For example, the estimated global volcanic emission of Cl is between 0.4 and 170 mt/year (Aiuppa et al. 2009) while individual eruptions can produce hundreds of kilotons of Cl. For example, in 1980, St Helens emitted 670 kt of Cl into the atmosphere (Bureau et al. 2000). Chlorine is an essential component in the mineral sodalite (Table 4.2), found in Na-enriched alkali igneous rocks, but this mineral occurrence is relatively rare. Serpentinized ultramafic rocks can be somewhat enriched in Cl due to metasomatic interaction with seawater (Kodolanyi et al. 2012). Chlorine is most commonly found substituting for -OH groups in hydrous silicates such as biotite, muscovite, or hornblende (Table 4.2). Chlorine also substitutes for hydroxyl groups in igneous apatite. The hinterlands of sedimentary basins that contain primary igneous rocks enriched in biotite, muscovite, hornblende, or apatite will contribute more Cl to the sediment supply than anhydrous igneous rocks. High-grade metamorphic terrains can contain Cl-rich mica and amphibole as well as scapolite due to the small quantities of available water during high pressure and temperature metamorphism (Johnson and Plank 1999; Visser et al. 1999; Kullerud and Erambert 1999). Chloride is routinely assumed to be a conservative element in fluids in the sedimentary and diagenetic environment since it is considered to be not involved in silicate, carbonate, sulphide, and oxide mineral reactions. Chloride remains as a solute unless halite saturation is reached. Conversely, if Cl^--undersaturated waters come into contact with halite-bearing evaporites, then the Cl^- concentration will increase. Chlorine is the main non-metal in sedimentary evaporite deposits, occurring predominantly as halite (NaCl; Table 4.2). Further extreme evaporation results in what is collectively known as potash, which includes halides such as sylvite (KCl), carnallite ($KMgCl_3{\cdot}6H_2O$), and bischofite ($MgCl_2{\cdot}6H_2O$) (Zherebtsova and Volkova 1966). Chlorine is found in trace amounts substituting for hydroxyl groups in diagenetic apatite and clays such as smectite and illite. Unusual and rare chlorate minerals are locally associated with nitrate deposits in arid intermontane basins (Dasgupta et al. 2005; Perez-Fodich et al. 2014).

Chloride is the dominant anion in seawater, being present at a global mean value 19 300 mg/L (Sverdrup et al. 1942; Chester and Jickells 2012). Chloride concentration in seawater can be somewhat lower than 19 300 mg/L as a function of near-shore freshwater input in semi-enclosed basins, typically in temperate regions. Chloride concentration in seawater can be somewhat higher than 19 300 mg/L as a function of seawater evaporation particularly in semi-enclosed basins, typically in arid tropical regions. Based on an average fluvial Cl^- concentration of 7 mg/L (see later), an average marine Cl^- concentration of 19 300 mg/L, and the same fluvial flux and ocean water mass values assumed for F^- residence times, then the ocean residence time of Cl^- is about 103 Myr (Table 4.3).

Meteoric water typically has low but measurable concentrations of Cl. A mean Cl^- concentration of 4.6 mg/L in meteoric water (range 0.3–44 mg/L) was reported for part of the UK (Neal et al. 1990). Chloride concentrations in meteoric water tend to be higher at maritime sites than at continental sites (Berner and Berner 2012).

Dissolved Cl^- is ubiquitous in groundwater and river water. River water concentrations of Cl^- are highly variable but they tend to increase down rivers going from upland regions to flood plains. They also tend to be higher in near-coastal regions and in areas where there is more net evaporation than net flow down the river channel. An estimated average fluvial Cl^- concentration is approximately 7 mg/L (Berner and Berner 2012). There are no systematic patterns of variation in groundwater Cl^- concentrations with depth due to the variability of competing processes of mineral weathering, dilution by infiltration and lateral flow, extent of evaporation, hydration reactions (defined in Table 4.1) in soil to say nothing of anthropogenic influences, the influences of modern or ancient seawater, or an influx of old and saline deeper groundwater (Barker et al. 1998; Tellam 1995, 1996; Mohamed and Worden 2006).

Chlorine is ubiquitously found as dissolved Cl^- in sedimentary formation waters. Chloride concentrations in deeper sedimentary formation water are highly variable ranging from 100 mg/L to >250 000 mg/L but typically Cl^- is present at much higher concentrations than in seawater (Worden 1996). There is no universal variation pattern of Cl^- concentration with depth in formation water; Cl^- concentrations do not simply increase with depth (Worden 1996). Since dissolved Cl^- is typically assumed to be a conservative element, it is routinely used to track water movement patterns in groundwater and formation waters (Alcala and Custodio 2008).

4.3.3 Bromine

In crystalline igneous rocks Br is found at low concentrations, typically <1 ppm in mid ocean ridge basalts (MORB) (Aiuppa et al. 2009). The average Br concentration of the Earth has been estimated to be 0.05 ppm (McDonough and Sun 1995). Chlorine/Bromine ratios are typically between 200 and 1000 in igneous rocks (Sugiura 1968). Bromine is, however, found at relatively high concentrations

(up to 300 ppm) in melt inclusions and matrix glass in acid igneous rocks since it is a highly incompatible element that does not easily sit within silicate, oxide or sulphide minerals (Bureau and Metrich 2003). Bromine is concentrated within any residual vapour phase during volcanic eruptions. Based on experimentally-derived fractionation factors for halogens in volcanic materials, crustal average halogen concentrations, and measured amounts of Cl emitted from volcanoes, it can be concluded that the contribution of volcanically-erupted Br to the atmosphere is considerable (Bureau et al. 2000). For example, the estimated global volcanic emission of Br is between 2.6 and 78 kt (Aiuppa et al. 2009) while individual eruptions (e.g., St Helens in 1980) can emit 2.4–5.6 kt (Bureau et al. 2000). High grade metamorphic terrains can contain Br-enriched mica and amphibole due to the small quantities of available water at ultra high pressure and temperature (Svensen et al. 1999) (Table 4.2). The hinterlands of sedimentary basins predominantly enriched in primary igneous rocks will provide only small quantities of Br into the sediment supply but rocks enriched in glass-bearing igneous rocks may supply relatively greater amounts of Br. Bromine is found in sedimentary basins as dissolved Br^-, in solid solution in halite ($NaCl_xBr_{1-x}$) (Table 4.2), or in less common salts resulting from potash-facies extreme evaporites, such as sylvite (Tables 4.1 and 4.2). Bromine is also associated with organic-rich sediments, especially in marine settings, including organic-rich mudstone (Cosgrove 1970) and coal (Vassilev et al. 2000).

At a concentration of 65 mg/L, Br^- is the second most abundant halogen in seawater (Sverdrup et al. 1942; Chester and Jickells 2012). Localised freshwater input tends to slightly decrease concentrations of Br^- (and Cl^-), while evaporation of semi-closed marine basins tends to increase Br^- and Cl^-. At the present day, the Cl/Br ratio in seawater is effectively constant in the world's oceans. Based on an average fluvial Br^- concentration of 0.025 mg/L (see below), an average marine Br^- concentration of 69 mg/L, and the same fluvial water flux and ocean water mass values assumed for F^- and Cl^-, then the ocean residence time of Br^- is about 103 Myr (Table 4.3). The ocean residence time of Br^- and Cl^- are thus effectively the same.

Meteoric water typically has low but measurable concentrations of Br^-. A mean Br^- concentration of 19 μg/L (range 3–102 μg/L) in rainfall was reported for part of the UK (Neal et al. 1990) but the value varies as a function of proximity to the sea and the season (Edmunds 1996).

Bromide is found in surface waters at low concentrations with median values of 20–30 μg/L in UK river water (Neal et al. 2007a) and similar values in groundwater (Edmunds 1996). Variations in Br^- concentration are typically closely related to variations in the Cl concentration although Cl/Br ratios can increase when the groundwater has percolated through organic rich sediment.

Bromide is found in sedimentary formation waters over a wide range of concentrations from <1 mg/L to >6000 mg/L. Bromine concentration does not have a simple variation pattern with depth of formation water; Br^- concentrations do not simply increase with depth (Worden 1996). Bromine has been routinely assumed to be a conservative element, since it does not form any discrete minerals

in sedimentary rocks. This assumption will be explored in the following sections. Cl/Br ratios have routinely been used to track water movement patterns and to interpret the specific sources of the saline load in formation waters (Rittenhouse 1967).

4.3.4 Iodine

The average I concentration of the Earth has been estimated to be 0.01 ppm (McDonough and Sun 1995). In crystalline igneous rocks I is found at low concentrations, for example typically <0.014 ppm in MORB (Aiuppa et al. 2009) and varying from 0.005 to 0.065 ppm in a range of igneous rocks (Muramatsu and Wedepohl 1998). Iodine is a highly incompatible element in magmas. Iodine is concentrated within any residual vapour phase during volcanic eruptions. Based on experimentally-derived fractionation factors for halogens in volcanic materials, crustal average halogen concentrations, and measured amounts of Cl emitted from volcanoes, it can be concluded that the contribution of volcanically-erupted I to the atmosphere is considerable (Bureau et al. 2000). For example, the estimated global volcanic emission of I is between 0.04 and 7.7 kt (Aiuppa et al. 2009) while individual eruptions (e.g., St Helens in 1980) can emit several kilotons (Bureau et al. 2000). Despite the lower crustal abundance of I compared to Br, the greater incompatibility of the former leads to broadly similar amounts in volcanic emissions (Aiuppa et al. 2009; Bureau et al. 2000). Primary igneous rocks provide very small quantities of I into the sediment supply but rocks enriched in glass-bearing igneous rocks may supply relatively greater amounts of I. In sedimentary basins, I is typically linked to fine-grained rocks with elevated total organic carbon (Cosgrove 1970). Rare iodate mineralisation in basins is locally associated with desert-controlled nitrate mineral deposits, such as those found in the Atacama region of Chile (Reich et al. 2009; Ericksen 1983; Perez-Fodich et al. 2014) (Table 4.2). Iodate minerals are also associated with supergene minerals and precious metal deposits (Cabral et al. 2011).

At a concentration of about 0.05 mg/L, I is the least abundant halogen in seawater (Sverdrup et al. 1942; Chester and Jickells 2012). Based on an average fluvial I^- concentration of 0.002 mg/L (see later), an average marine I^- concentration of 0.05 mg/L, and the same fluvial flux and ocean water mass values assumed for the other halides, then the ocean residence time of I^- is about 0.9 Myr (Table 4.3). Iodine is strongly associated with organic matter in marine sediments and sedimentary rocks. Organic rich algal mudstone were reported to contain a mean of 17 ppm I with a maximum of 34 ppm (Cosgrove 1970). Coals were reported to contain a mean of 1.27 ppm I, with values up to 39.5 ppm I. Iodine was reported to be more abundant in marine coals than fresh water coals, with the I concentration increasing with increasing coal rank (Wu et al. 2008). The marine residence time of I is presumably much shorter than Cl and Br because I is cycled out of the ocean as organo-iodine compounds. During sequential evaporation of seawater, I remains in

aqueous solution up to and beyond the point of extreme evaporation when carnallite precipitation has commenced. At this stage of evaporation, I reaches up to 4 mg/L in the bittern (Zherebtsova and Volkova 1966).

Meteoric water typically has very low but measurable concentrations of I. A mean I concentration of 1.48 μg/L (range 0.6–5.3 μg/L) in meteoric water has been reported for part of the UK (Neal et al. 1990).

Groundwater and river water I^- concentrations are highly variable (with an average value of 1–2 μg/L) but are either similar to, or slightly lower than the I^- concentration in the initial parent meteoric water (Neal et al. 1990).

Iodide concentrations in sedimentary formation waters range from <1 to >100 mg/L (Worden 1996). Iodide concentrations in formation waters do not simply increase with depth in sedimentary basins (Worden 1996). Some oil field formation waters have very high I^- concentrations; in these cases the element has been commercially extracted from the coincidentally produced oil field formation waters (Collins 1969).

4.4 Key Processes that Influence Halogen Elements in the Diagenetic and Sedimentary Realm

4.4.1 Alteration of Primary Igneous Rocks and Minerals and Sediment Diagenesis

Alteration of pristine high temperature rocks has two potential effects on halogens: (1) release of halogens from igneous minerals and (2) creation of new, hydrous diagenetic minerals that can contain trace halides substituted for hydroxyls. The halogens released during alteration will potentially become part of the hydrological cycle (Fig. 4.2a) and so are carried by streams until they reach the ocean. Igneous rock types and their minerals thus exert a primary control on the amounts of halogen elements fed into sedimentary systems. A typical order of abundance of halogen elements in primary igneous rocks is F (800 ppm) > Cl (200 ppm) > Br (0.5 ppm) > I (0.014 ppm) with the supply of F during the weathering far outweighing the supply of all the other halogens. Rocks enriched in apatite, amphibole, and mica minerals will be relatively enriched in F and, to a lesser extent, Cl (Table 4.2) (Jagadeshan et al. 2015). Precursor igneous rocks enriched in volcanic glass, resulting from the final stages of fractional crystallization, will be relatively enriched in all halogen elements compared to the earlier stages of crystallization. The host mineral for halogen elements is an important consideration since different minerals weather at different rates. For example, biotite weathers, and releases its F and Cl, comparatively quickly and is thus relatively unlikely to become an abundant mineral in a sedimentary rock (Zhang et al. 2007). In contrast detrital apatite resists weathering and can retain its original F and Cl intact, well into the zone of low-medium grade metamorphism (Smith and Yardley 1999). However, even when liberated during weathering, the relative concentrations of halogen

elements in fluvial run-off or percolating groundwater is controlled by the variable incorporation of halogen elements into new diagenetic minerals. Thus F^- concentrations in run-off are often limited by excess dissolved Ca and phosphate with concomitant growth of apatite. Secondary clay minerals also commonly have F^- substitution for hydroxyls (Chipera and Bish 2002). In contrast, I-, and possibly Br^-, concentrations in the water associated with igneous mineral alteration, may be limited by the incorporation of these elements into organic compounds, e.g., organic matter in soils and organic-rich sediments.

Analysis of pore waters from the Pliocene and younger volcaniclastic marine sediments in the Aoba Basin of the New Hebrides (south Pacific), from the seafloor to a depth 700 m, showed that hydration reactions (e.g., feldspar to clay or zeolite reactions) led to Cl^- concentrations broadly increasing with depth of burial (Fig. 4.3) from marine values (~20 000 mg/L) to >44 000 mg/L (Martin 1999). This shows that removal of H_2O from a relatively closed system can significantly affect Cl^- concentration. Bromide concentrations also increased with depth from marine values (~70 mg/L) to 125 mg/L. Comparison of Cl^- to Br^- concentrations from these altered igneous-derived sediments, relative to seawater evaporation and dilution trends (see later), shows that Br^- is depleted relative to Cl^- (Fig. 4.4a) since the water compositional data fall below the seawater concentration trend.

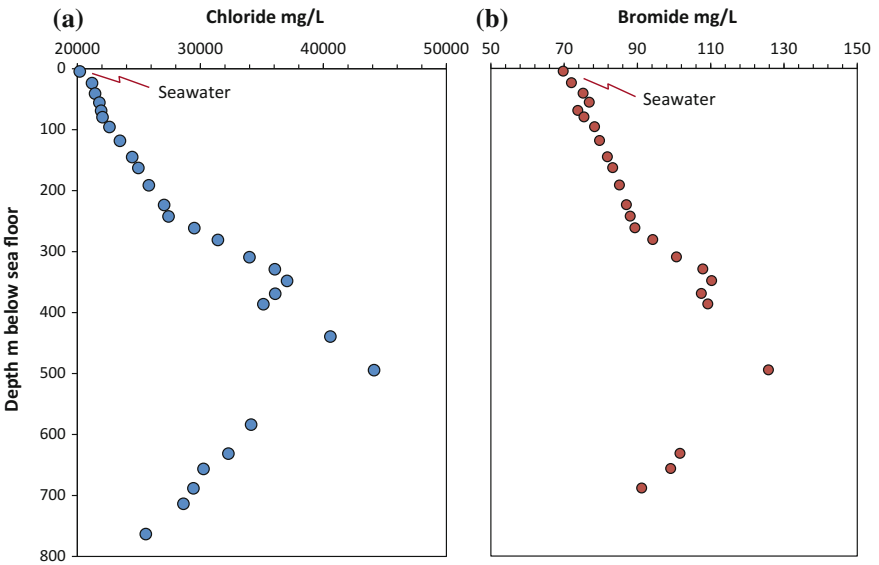

Fig. 4.3 Chloride and Br^- concentrations from pore waters in Pliocene marine volcaniclastic sediments from the New Hebrides in the South Pacific (Martin 1999). (**a**) Chloride concentration tends to increase from a marine value in the shallowest interval to a maximum that is more than twice the seawater concentration at 500 m. (**b**) Bromide concentration tends to increase from a marine value in the shallowest interval to a maximum, at 500 m, 80% greater than its mean concentration in seawater

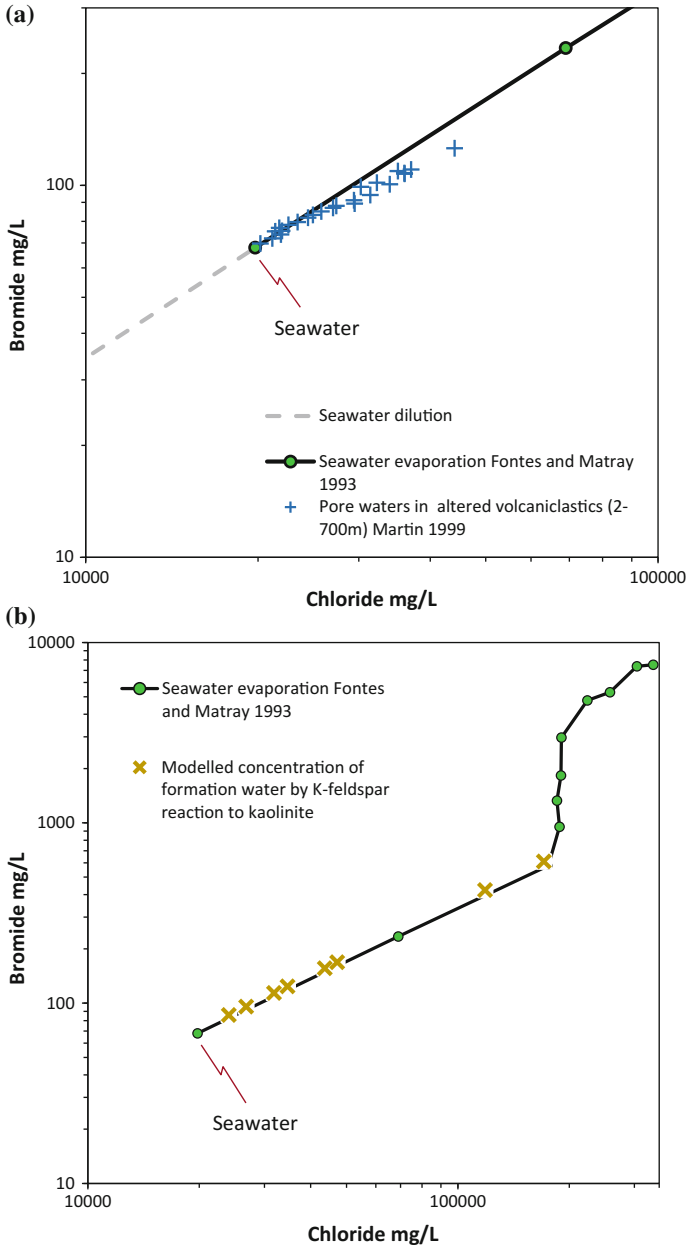
(a)
Bromide mg/L
100
10
10000
100000
Chloride mg/L
Seawater
Seawater dilution
Seawater evaporation Fontes and Matray 1993
Pore waters in altered volcaniclastics (2-700m) Martin 1999
(b)
10000
1000
100
10
Bromide mg/L
10000
100000
Chloride mg/L
Seawater evaporation Fontes and Matray 1993
Modelled concentration of formation water by K-feldspar reaction to kaolinite
Seawater

◂**Fig. 4.4** (**a**) Chloride and Br^- concentrations from volcaniclastic pore water (see Fig. 4.3) (Martin 1999) compared to a seawater evaporation trend (Fontes and Matray 1993a) and to a seawater dilution trend revealing the subtly non-conservative behaviour of Cl^- and Br^- during the alteration of volcaniclastic sediments. The increase in anion concentration is the result of hydration reactions removing liquid phase H_2O. The non-conservative behaviour (relative loss) of Br^- suggests that Br is preferentially absorbed by the rock. (**b**) Modelled effects of the diagenetic hydration of K-feldspar to kaolinite on Cl^- and Br^- concentrations (see Table 4.4)

Table 4.4 Modelled effect on Cl^- concentration of the K-feldspar to kaolinite hydration reaction for rocks with variable porosity, initially filled with seawater (Cl^- concentration of 19 300 mg/L), and variable K-feldspar proportions (see Fig. 4.4b)

Water-filled porosity %	Initial K-feldspar % proportion in sediment by volume	Proportion of initial water reacted	Proportion of initial water remaining	Final modelled Cl-concentration (mg/L)
10	15	0.443	0.557	34,650
10	30	0.887	0.113	170,796
10	45	0.950	0.050	386,000
15	15	0.279	0.721	26,768
15	30	0.558	0.442	43,665
15	45	0.837	0.163	118,405
20	15	0.197	0.803	24,035
20	30	0.394	0.606	31,848
20	45	0.591	0.409	47,188

This subtly non-conservative Cl/Br behaviour was explained by a combination of selective leaching of Cl from the volcaniclastic sediments and preferential absorption of Br onto mineral surfaces, especially those altered by organic matter (Martin 1999).

A typical clastic sedimentary rock has between 10% and 20% porosity and 15%–45% K-feldspar. The diagenetic hydration (hydrolysis, Table 4.1) of K-feldspar to kaolinite, a typical reaction in clastic rocks (Worden and Burley 2003), can have a considerable effect on overall salinity and thus the Cl^- and Br^- concentrations. Every mole of K-feldspar that reacts requires two moles of water. A range of initial porosities and K-feldspar proportions have been used to determine the modelled effects of K-feldspar hydration (to clay minerals) on Cl^- concentrations starting from an initial seawater composition, taking account of the molar weights of K-feldspar and water (Table 4.4). In the extreme, a K-feldspar-rich, low porosity sedimentary rock (typical of a fine, sand-silt, matrix-rich, mineralogically immature sediment) that undergoes reaction to kaolinite could lead to >100 000 mg/L Cl^-. The Br^- concentration should also increase since it has conservative behaviour and is not incorporated into diagenetic minerals. From this simple analysis it is possible to conclude that the effects of K-feldspar diagenetic hydration reactions may be indistinguishable from seawater evaporation (Fig. 4.4b).

While K-feldspar hydration reactions can lead to a net reduction in the quantity of water and so concentrate the solutes, there is a range of processes that are common in basins that liberate previously immobile connate water (Table 4.1) or even create new water. Compactional processes have the capacity to squeeze the immobile (typically marine) connate water out of low permeability, fine-grained rocks (mudstones, siltstones). The liberated water will then move down hydraulic gradients, along high permeability routes, and will mix with waters in more porous and permeable sandstones and limestones. Such compactional water, hard to sample and analyse, is likely to be indistinguishable in terms of its halide concentrations, from marine connate waters.

Low temperature, depositional, aluminous smectitic clay has more hydroxyls per mole than higher temperature, diagenetic kaolinite or illite (Table 4.2). Conversion of smectite to illite (a partial dehydration process) is known to lead to overpressure (defined in Table 4.1) due to the creation of new water from the liberated hydroxyls (O'Connor et al. 2011). This new water will have very low salinity and has the capacity to dilute all ions, including chloride and bromide. Halide concentrations should be diminished equally by the addition of smectite-derived water. The thermal maturation of source rock into oil and gas is preceded by the generation of large volumes of water as hydroxyl groups (and other oxygen-bearing functional groups such as ketones, acids and alcohol) are cleaved from the complex geo-molecules in the kerogen. This process too can lead to overpressure and will also result in the addition of low salinity water (O'Connor et al. 2011). Halide concentrations should be diminished equally by the addition of kerogen-derived water. Deeply buried overpressure zones in the Gulf of Mexico have been associated with vastly reduced chloride, and presumably bromide, concentrations (Hanor 1994), effectively disproving any assumption that formation water salinity increases with depth.

The reaction of sulphate minerals with petroleum (thermochemical sulphate reduction: TSR) is well known as the main cause of high concentrations of H_2S in sedimentary basins (Krouse et al. 1988). TSR creates new water following the oxidation of petroleum compounds. TSR has been reported to lead to major reductions in salinity, from 25 wt% to as low as 5 wt% (Jiang et al. 2015; Worden et al. 1996). TSR-derived water will decrease Cl^- and Br^- concentrations equally.

4.4.2 Meteoric Water, Atmospheric Processes, and Aerosols

Meteoric water is of huge relevance to the diagenesis of sedimentary rocks and the geochemistry of groundwater and formation water because practically all groundwater originates as meteoric water. The same is also generally true for formation waters deep in sedimentary basins since commonplace periods of relative sea level fall create a major driving force, which allows for meteoric water to be flushed through the sedimentary column, thus replacing any marine connate waters. Most diagenetic processes in porous and permeable rock units are the result of the

interaction of meteoric-derived water with sedimentary rock. Exceptions to this generalisation are those processes that occur in pelagic sediments deep in ocean basins and rapidly-deposited Miocene and Pliocene sediments (e.g., of the northern Gulf of Mexico) that have not yet had time to undergo meteoric water influx. The halide concentrations in meteoric water that falls on, and percolates into, sediments and sedimentary rocks are thus an important consideration.

Meteoric water results from the condensation of water vapour. It picks up its impurities, both soluble and insoluble, from the atmosphere (Berner and Berner 2012). These impurities are known as aerosols, which are defined as small particles of solids or liquids that range in size from nanometers to about 20 μm in radius. Natural aerosols include mineral dust (e.g., from weathered and eroded mountains or other land surfaces), volcanic particulates, biogenic particulates (e.g., from eroded soils), and sea salt picked up from wind-induced waves and sea spray. The dissolved load of meteoric water, typically present at very low concentrations, results from the relative contributions of these various sources. In marine and coastal regions, the dominant aerosol input is sea salt so that meteoric water is similar in composition to ultra-dilute seawater. In continental-interior regions, the dominant aerosol tends to be mineral dusts leading to variable meteoric water compositions dominated by dissolved sulphate and carbonate mineral particulates (Herut et al. 2000).

Chloride is the only halide that is routinely present in meteoric water at concentrations that are easily and routinely measured. Chloride in meteoric water is typically assumed to be derived mainly from sea salt aerosols. This is not surprising given the dominant contribution of sea salt to the global balance of aerosols (Berner and Berner 2012) and that Cl^- is present in seawater at vastly higher concentrations than the other halides. Furthermore, Cl^- is typically the dominant anion in marine and coastal meteoric water due to seawater being the dominant source of solutes. In contrast, continental meteoric water, being more isolated from the seawater source of sea salt aerosol, typically has a lower Cl^- concentration and is not always the dominant anion. Sulphate in meteoric water is derived partly from sea salt aerosols but the highest SO_4^{2-} concentrations, typically found in continental meteoric waters, are picked up from mineral dust derived from eroded evaporites, or weathered and oxidized pyrite-bearing surficial materials. The relative proportions of Cl^- to SO_4^{2-} depend on the specific source of mineral dust and proximity to coastal and marine zones (Herut et al. 2000). Sulphate concentration can be higher than Cl^- concentration in some continental meteoric water. Marine and coastal meteoric water has Cl^- concentrations between 1 and 10 mg/L with a typical near maritime value of about 4 mg/L (Neal et al. 1990). In contrast, typical continental meteoric water has between 0.2 and 2.0 mg/L Cl^- (Berner and Berner 2012).

Bromide and I^- concentrations have also been measured in meteoric water although rather less frequently than Cl^-. Bromide is the second most abundant halide in seawater, and Br^- in meteoric water is assumed to be derived from sea salt aerosols. It has been reported that Br^- preferentially concentrates in the finest (smallest diameter) aerosol fraction while Cl^- displays no such preference (Winchester and Duce 1967). The larger aerosol particles with relatively high Cl^-

concentrations are more effective in raindrop nucleation and are thus relatively rapidly removed from the atmosphere. This decreases the meteoric water Cl^- concentrations inland and so contributes to lower Cl/Br ratios in inland (continental) meteoric water. Bromide concentration in meteoric water at a maritime location has been reported to fluctuate between 10 and 35 μg/L with a mean of about 15.6 μg/L (Fig. 4.5) (Neal et al. 1990). Coastal meteoric water has Cl/Br ratios that tend to be broadly similar to seawater but continental meteoric water has lower Cl/Br ratios than seawater (Goni et al. 2001).

Iodide in meteoric water may also be partly derived from sea salt aerosols although the absolute contribution of I^- is necessarily far lower than Cl^-, or even Br^-, since the I^- concentration in seawater is low (Fig. 4.2b). Iodide concentration in meteoric water at a maritime location has been reported to fluctuate between 0.3 and 1.8 μg/L with a mean of about 1.3 μg/L (Neal et al. 1990). I/Br concentration ratios in meteoric water have been reported to be relatively constant at between 0.1 and 0.2 (Winchester and Duce 1967) suggesting that they are broadly subject to the same processes. This implies that I^- is also found preferentially in the finest aerosol fractions. However, the biological production of the gas phase methyl-iodide in seawater is now considered to be the dominant route for the relative enrichment of

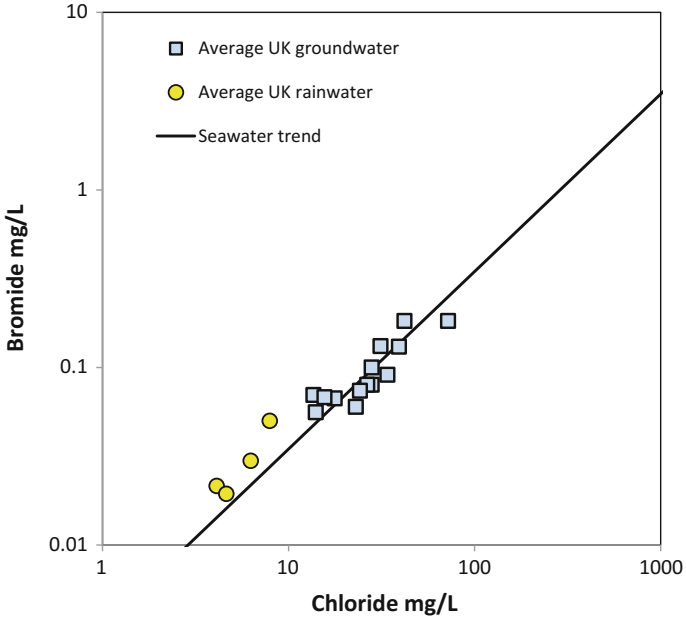

Fig. 4.5 Meteoric water and groundwater Cl^- and Br^- concentrations from the United Kingdom compared to the expected seawater dilution/meteoric water evaporation trend (Edmunds 1996). This confirms that, at least in maritime regions, meteoric water is ultra-dilute seawater in terms of the Cl-Br ratio. It also shows that groundwater is slightly more concentrated in Cl^- and Br^- than the primary meteoric water (presumably due to evapotranspiration, but also possibly by hydration reactions in the weathering zone)

I^- in meteoric water, instead of an aerosol-dominated source (Lovelock and Maggs 1973; Truesdale and Jones 1996). By reference to I^-, it seems at least possible that Br^- enrichment in meteoric water (Goni et al. 2001) is also partly controlled by biologically-produced, halogenated, hydrocarbon gases.

Fluoride concentration in meteoric water at a maritime location (UK) has been reported to fluctuate from below-detection (<1 μg/L) to 200 μg/L (Neal et al. 1990). The controls of F^- concentrations in meteoric water have been debated for many years with a consensus that F^- in modern meteoric water is predominantly not derived from sea salt aerosol since there is reportedly no correlation between F and Na concentrations (Barnard and Nordstrom 1982). They reported only minor differences between marine or coastal and inland meteoric water F^- concentrations with a mean of 8.1 μg/L (and a range from 2 to 20 μg/L). This, and other studies, have shown that much of the F^- concentration in modern meteoric water is the result of dissolution of particulates, with modern industrial activity accounting for most of the F^- load (Walna et al. 2013). It is also significant that meteoric water down-wind from degassing and erupting volcanoes has elevated F^- concentrations with values greater than 20 mg/L F^- in meteoric water and Cl/F ratios less than 40 (Bellomo et al. 2003; Madonia and Liotta 2010). However, it has been concluded that only a small fraction of the total emitted F is locally deposited via rainfall implying that the remainder adds to the global atmospheric-meteoric water F^- budget, resulting in it being independent of the sea salt aerosol (Bellomo et al. 2003).

Of minor but interesting relevance to the overall halide budget in sedimentary basins is the reported occurrence of perchlorate (ClO_4^-) in meteoric water. This compound is known as an industrial pollutant but it has been found in small quantities in unpolluted areas and is now considered to be the result of atmospheric processes such as electrical discharge (lightning) (Dasgupta et al. 2005). Perchlorate in meteoric water is also associated with elevated iodate (IO_3^-) concentrations, which may also be related to lightning, although iodate dominates over I^- in many groundwaters (Li et al. 2014). Perchlorate mineral deposits in the Atacama desert in Chile, found in conjunction with surficial nitrate mineral deposits, are an important industrial resource and have been linked to direct meteoric water-atmospheric input of dissolved perchlorate (Perez-Fodich et al. 2014). Interestingly, iodate (IO_3^-) minerals are also associated with the Chilean nitrate deposits but the bulk of the I has been interpreted to be derived from old marine shales, deep beneath the surficial deposits (Alvarez et al. 2015). Transiently elevated I^- concentrations in meteoric water have also been locally related to the passing of volcanic plumes that are more than a thousand kilometers away from the originating volcanic vent (Seda et al. 2012).

4.4.3 Halogen Elements in Rivers and Groundwater in Temperate Regions

Before meteoric water becomes groundwater, it must pass through, and potentially interact with, surface materials such as soil and regolith. While it is seldom possible to track an individual volume of meteoric water during its passage through such materials, a review of the composition of the surface water (e.g., river water) and groundwater, can reveal the general geochemical effects of meteoric water-soil and meteoric water-aquifer interaction. Given that meteoric water can be considered to be dilute seawater (especially in marine and coastal regions), comparing river and groundwater halide concentrations to their marine counterparts is a useful way of determining any net gain or loss of halides as meteoric water passes through soil, regolith, or groundwater (Fig. 4.5).

A key problem of studying modern river water and groundwater is anthropogenic contamination. Human activities, such as road-salting, application of agricultural fertilizers to farm land, tannery, coal and mineral extraction activities, passing wastewater (raw or treated human waste) into water courses, leakage from landfill sites, etc., all potentially have a marked effect on the overall composition of river water and groundwater. Although most studies of river water and groundwater are concerned with monitoring, understanding, and mitigating the worst effects of pollution, anthropogenic activities are not the focus of this review, which is, instead, focussed on natural processes.

Some studies have focussed on catchments that have relatively little anthropogenic influence, to try to understand the natural controls on halogen concentrations in river catchments. Chloride and Br^- concentrations in river and groundwater tend to be significantly higher than the original meteoric water (Fig. 4.5). For example a catchment in Wales, UK, showed that Cl^- concentrations in river water (7.3 mg/L) approach two times those of the incoming meteoric water (4.1 mg/L; a typical value for maritime environments) with Cl^- in groundwater (10.2 mg/L) being two and half times that of meteoric water (Neal et al. 2007a). This increase in Cl^- concentration was interpreted to be due to evapotranspiration. Bromide in incoming meteoric water, typical for the United Kingdom, is at 15.6 μg/L with the Cl/Br ratio staying broadly constant (Neal et al. 2007a, c). Fluctuations in Cl/Br ratios in river and groundwater were linked to dissolved organic carbon with the suggestion of the transient take up, and release of, Br^- by organic compounds.

In a relatively pristine basin, river water F^- concentrations display less variation than F^- concentrations in the meteoric water, but the overall pattern is similar. There was a mean fluvial F^- concentration of about 53 μg/L compared to a local meteoric water mean of 30 μg/L, suggesting the occurrence of evaporative concentration (Neal et al. 1990).

Iodine displayed a different pattern. The incoming meteoric water had a typical maritime I concentration of 1.55 μg/L (Neal et al. 2007b). Although the I concentration increased in absolute terms to 1.76 and 2.20 μg/L in river water and

groundwater, respectively, the I/Cl ratio decreased from 0.38 in meteoric water to 0.25 and 0.23 in river water and groundwater, respectively, relative to the incoming meteoric water. This was interpreted to reflect the same effects of evaporation as experienced by Cl^- and Br^- but with a net retention of I in the sediment and regolith within the hydrological basin. The uptake of I was interpreted to be related to the presence of organic matter (e.g., in humic materials in soil or in algae) and the creation of I-bearing organic compounds (Neal et al. 2007b).

Thus, in the case of a relatively pristine, small hydrological catchment, river water and groundwater experienced simple evaporative concentration of Cl^-, F^-, and Br^- to approximately double that of the meteoric water while I^- experienced a much lower increase in concentration due to I being held in organic matter in soils, rivers, and in aquifers.

Groundwaters are typically studied and geochemically analysed when they present a problem to human health. In terms of the halides, the biggest medical problem comes from elevated F^- in groundwater, leading to a disease known as fluorosis (Dissanayake and Chandrajith 1999). Elevated F^- concentrations in groundwater (>1.5 mg/L) are commonly associated with F-rich igneous rocks, such as alkaline granitoids (Dissanayake and Chandrajith 1999) or basalts (Moghaddam and Fijani 2008), and with clays that are enriched in F-bearing clays (Rao and Devadas 2003). Groundwater with high F^- concentrations seem only to occur in HCO_3-rich, Na-dominated water where there is a low Ca concentration thus limiting the role of fluorapatite and fluorite precipitation (Wen et al. 2013; Jacks et al. 2005; Guo et al. 2007). In these settings, F^- concentrations are independent of Cl^- concentrations (Tian et al. 2015).

4.4.4 Seawater Dilution and Evaporation in Sedimentary Basins

Seawater typically contains about 1.4 mg/L F^-, 19 300 mg/L Cl^-, 65 mg/L Br^- and 0.05 mg/L total I (Sverdrup et al. 1942). Global average seawater salinity has varied over time as a function of how much NaCl is locked up in rock salt; for example over the Mesozoic it has been proposed that salinity has fluctuated between 34 and 40 wt% (Warren 2010; Hay et al. 2006). At the present day, high volumes of river water influx into semi-enclosed marine basins can lead to lower halide concentrations. For example, the Black Sea has 10 200 mg/L Cl^- and 35 mg/L Br^- (Zherebtsova and Volkova 1966). While there have been controversial reports that marine major ion ratios have fluctuated markedly over the Phanerozoic (Lowenstein et al. 2003; Lowenstein and Timofeeff 2008; Timofeeff et al. 2001, 2006), there has been little attention paid to secular marine Cl/Br ratios. However it is possible to speculate that the long marine residence times for Cl^- and Br^- (Table 4.3) have probably helped to buffer their marine ratio. An assumption of uniform marine Cl/Br ratios over the Phanerozoic was made in an attempt to relate halite-Br concentrations to the controversial issue of secular variations in marine

Ca, Mg, and SO_4^{2-} concentrations (Siemann 2003). There has been some research comparing Cl/Br ratios from fluid inclusions in 3.3 Ga evaporitic rocks to the Cl/Br in the modern ocean but there is much uncertainty about the degree of evaporation and the degree of water-rock interaction (Pinti 2005).

In open marine basins, seawater evaporation is typically balanced by net river water input thus maintaining the absolute concentrations of dissolved halides. In contrast, in enclosed or semi-enclosed marine basins that are relatively isolated from fresh water inputs, evaporation will lead to elevated concentrations of halides and other anions and cations. Local variations in low latitude, low river water input, partially-enclosed marine basins can lead to slightly elevated halide concentrations; for example the Red Sea has 22 980 mg/L Cl^- and 74 mg/L Br^- (Kim et al. 2014).

Evaporated seawater is potentially important in sedimentary basins and deep formation waters since the resulting evaporated water has a relatively high density and potentially may sink through a column of porous sediment, displacing lower salinity water. The presence of diagenetically-altered, evaporated seawater in deeply buried, porous rock units has been interpreted in several sedimentary basins (Stueber and Walter 1991) (see Sect. 4.5.1).

Seawater evaporation has been studied experimentally and by collecting samples from variably evaporated natural marine brine pools (e.g., at low tide) (McCaffrey et al. 1987; Collins 1969; Fontes and Matray 1993a; Carpenter 1978) (Fig. 4.6). The results from all of these studies showed that Cl^- concentration increases during evaporation up to the point of halite precipitation after which other anions tend to increase more significantly. Bromide concentration increases proportionally to Cl^- concentration up to the point of halite saturation. The studies of seawater evaporation largely concurred with regard to matching changes in Br^- and Cl^- concentrations through to the extreme degrees of evaporation (Fig. 4.6a). From here, only the output from the most modern study of seawater evaporation will be referred to (Fontes and Matray 1993a), as a reference curve for other processes added to Cl-Br diagrams.

Seawater proportionally increases in Cl^- and Br^- concentrations during evaporation even when gypsum starts to precipitate (Fontes and Matray 1993a). Chloride and Br^- concentrations are 69 000 mg/L and 234 mg/L, respectively, when seawater is evaporated to the point of gypsum precipitation. This continues during evaporation until the start of halite precipitation when Cl^- and Br^- concentrations are 188 000 mg/L and 578 mg/L, respectively (Fontes and Matray 1993a). Once halite starts to precipitate, it preferentially takes Cl^- out of the residual water as evaporation proceeds and leaves most of the aqueous Br^- to simply increase its concentration in the residual brine. At advanced degrees of seawater evaporation, resulting in the growth of sylvite, Cl^-, and Br^- concentrations can reach 223 000 mg/L and 4770 mg/L, respectively (Fontes and Matray 1993a). At the most extreme degrees of evaporation, bischofite ($MgCl_2 \cdot 6H_2O$) grows in the presence of water with Cl^- and Br^- concentrations reaching 337 000 mg/L and 7530 mg/L. This represents extreme partitioning of the relatively incompatible Br^- into the tiny quantity of remaining bittern (defined in

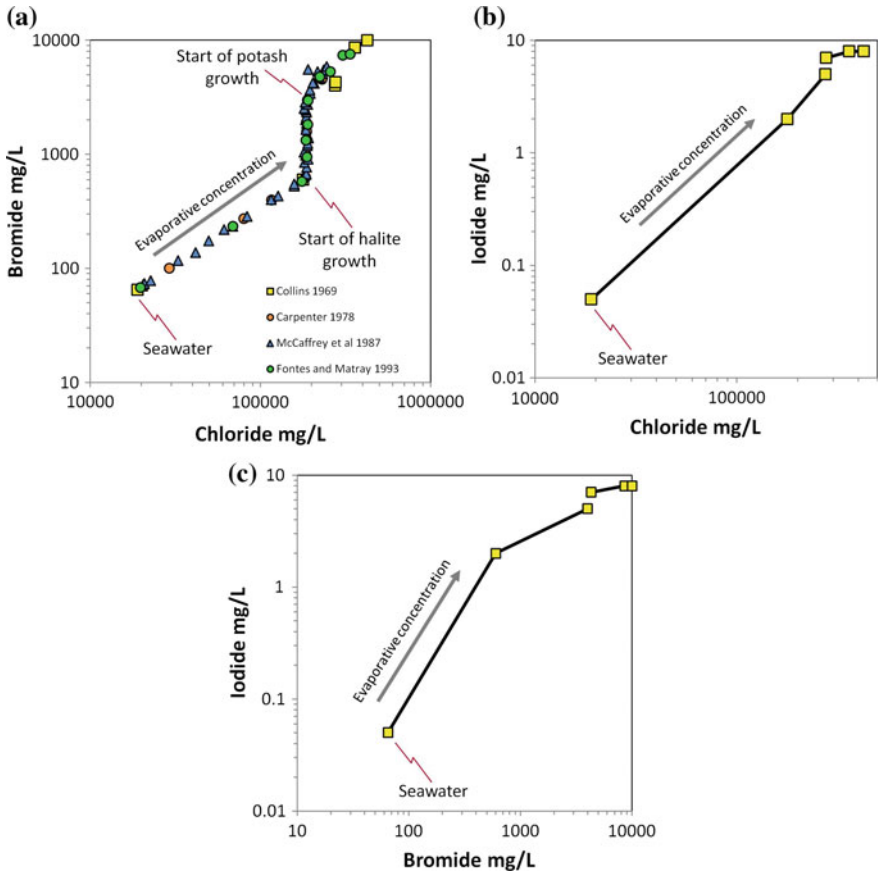

Fig. 4.6 (**a**) Effect of evaporation of seawater on Cl^- and Br^- concentrations (McCaffrey et al. 1987; Carpenter 1978; Fontes and Matray 1993a; Collins 1969). The four models of seawater Cl^- and Br^- evolution during progressive evaporation of seawater largely concur. The start of halite growth sees a relative increase in Br^- since NaCl partitions the remaining Br into the aqueous phase. (**b**) and (**c**) Effect of evaporation of seawater on Cl^--I^- and Br^--I^- concentrations (Collins 1969)

Table 4.1) and late stage potash facies minerals. Seawater evaporation is thus capable of creating some extremely Br-enriched waters and results in Br-bearing evaporite minerals in sedimentary basins.

Iodide concentrations also increase during seawater evaporation (Zherebtsova and Volkova 1966; Collins 1969) (Figs. 4.5c and 4.6b). Iodide concentrations up to 8 mg/L have been reported following extreme evaporation starting from seawater I^- concentration of 0.05 mg/L. No discrete I^- salts have been reported to form during seawater evaporation.

Fluoride concentrations must also increase during seawater evaporation, although these data have not thus far been reported from experimental or empirical

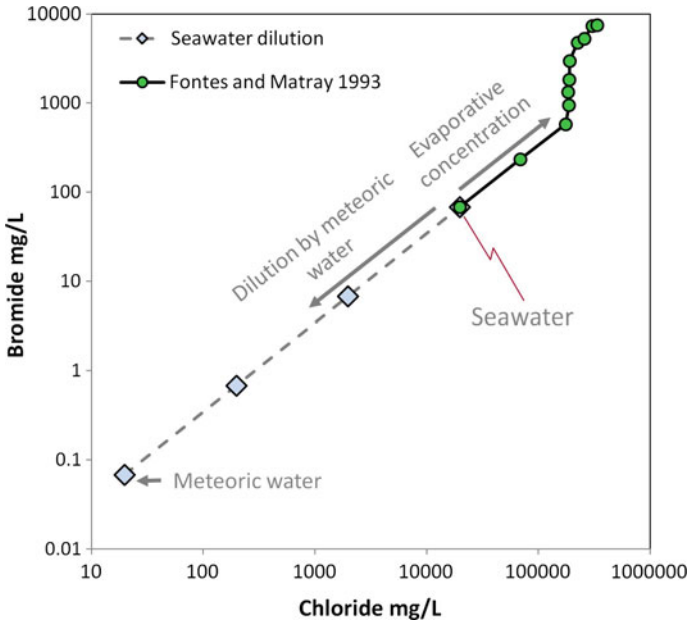

Fig. 4.7 Effect of the modelled dilution of seawater by low-salinity (i.e. meteoric) water on Cl^- and Br^- concentrations, compared to seawater evaporation (McCaffrey et al. 1987)

studies. Fluorite saturation may limit F^- concentration increase but with Ca concentration being limited and diminished by calcite and gypsum growth (Collins 1969), it is possible that evaporation may result in elevated F^- concentrations.

In buried sedimentary rocks that have connate seawater flushed by meteoric water, the resulting hybrid water will simply have the characteristics of dilute seawater, probably modified by variable degrees of water-rock interaction. In the absence of evaporites, the dilute seawater might be expected to lie between pristine seawater and meteoric water. Meteoric water has low Cl^- and Br^- concentrations with a Cl/Br ratio similar to seawater (Fig. 4.5) so that dilution of seawater by low salinity groundwater can be represented by proportional decreases in concentrations of Cl^- and Br^- (Fig. 4.7).

4.4.5 Halogen Elements in Marine Evaporites

At various stages during the evaporation of seawater, different minerals reach saturation and precipitate out of the fluid phase as mineral salts. As found in the thick Upper Permian Zechstein evaporites of NW Europe (Tucker 1991), a common series of mineral precipitates in progressively evaporated seawater is calcite ($CaCO_3$), gypsum ($CaSO_4 \cdot 2H_2O$) and then halite (NaCl) (Fig. 4.8). At extreme

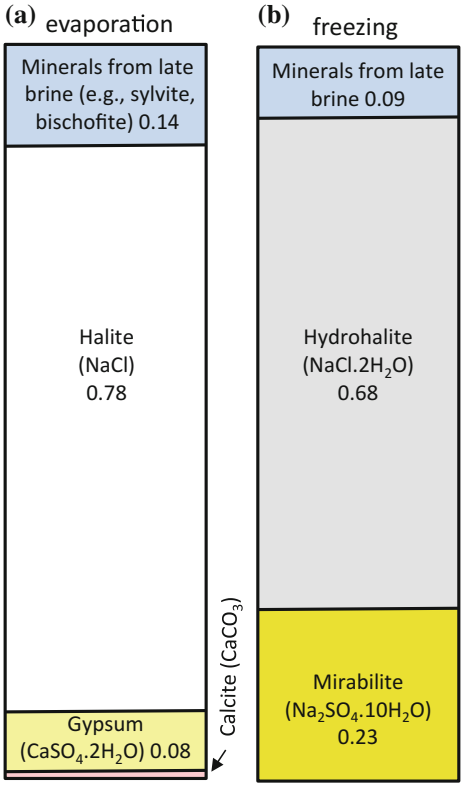

Fig. 4.8 Typical relative volumes of evaporite minerals after complete evaporation or freezing. (**a**) Salt mineral volumes due to evaporation (McCaffrey et al. 1987). (**b**) Salt mineral volumes due to freezing (Nelson and Thompson 1954)

evaporation, halite growth is then followed by a series of Mg- and K-bearing Cl- and sulphate minerals such as: sylvite, bischofite ($MgCl_2{\cdot}6H_2O$), Langbeinite ($K_2Mg(SO_4)_3$), polyhalite ($K_2Ca_2Mg(SO_4)_6$), kainite ($KMg(SO_4)Cl{\cdot}3H_2O$) and kieserite ($MgSO_4$), which are collectively known as potash, or bittern, minerals (Warren 1999; Bottrell et al. 1996; Wittrup and Kyser 1990). Simple models show that a 100 m column of sea water evaporated to dryness, assuming no subsequent reaction between the deposited salts and the evolving brine, would lead to 0.01 m of calcite, 0.06 m of gypsum, 1.33 m of halite and about 0.30 m of potash minerals.

As well as simple, one-stage evaporation, it is possible that previously-deposited gypsum beds, at the margins of enclosed evaporating basins, may experience back-reaction with residual K- and Mg-enriched brines that result from extreme evaporation of the original sea water. Thus, under some circumstances, evaporite deposits may undergo continuous diagenetic reaction with the evolving brine. The observed growth of polyhalite in gypsum beds from Baja, California has been explained by a K- and Mg-enriched brine reaction with gypsum in modern evaporites (Pierre and Fritz 1984). The growth of polyhalite in Permian Zechstein evaporites has also been explained by the same diagenetic back-reaction between basin margin gypsum and highly evaporated marine brines (Peryt et al. 2005).

As reported by Warren (2010), marine evaporites have been reported to commonly develop in epeiric seaways in times of greenhouse climate in tectonic settings where continental plates were in close proximity. Transient partial isolation from the open sea and a low base level, due to tectonic conditions, are considered to be typical preconditions for the development of such evaporites.

Where present, halite-rich evaporites are an important part of the stratigraphy since they can create exceptionally low permeability caprocks to oil and gas accumulations. Halite is also relatively mobile in basins due to its high degree of plasticity under moderately high lithostatic pressures. Halokinesis and salt diapirs (Table 4.1) are an important part of the story in all sedimentary basins that accumulated thick marine evaporites, such as the Gulf Coast of North America or the Southern North Sea Basin. Halokinesis leads to upwards, plastic, movement of relatively low density halite through the sedimentary succession creating diapiric salt intrusions and salt pillows. These diapirs slowly punch their way through overlying clastic and carbonate rocks creating ideal trapping conditions for petroleum in anticlines overlying the diapir, and in dipping structures marginal to the diapir, with halite forming a fault seal.

The role of halogen elements other than Cl in marine evaporite rocks is relatively muted and has been afforded relatively little attention. Bromide, the second most abundant halogen in seawater, partitions into the remaining brine when halite starts to grow (Fig. 4.6). This is because the Br partition coefficient between halite and brine, D_{Br} (equal to $(Br^-/Cl^-)_{halite}/(Br^-/Cl^-)_{brine}$), is approximately 0.032 (McCaffrey et al. 1987) with an effective partition coefficient d_{Br} (equal to $(Br^-_{halite}/Br^-_{brine})$) of 0.13 (Holser 1979). First-formed halite should have a Br^- concentration of 65–75 ppm at the initial stage of halite growth. As the remaining Br^- concentration increases, later formed halite can acquire up to ~200 ppm Br- (Land et al. 1988; Kuester et al. 2009) (Fig. 4.9). Bromine concentration profiles through halite have been determined from some well-known evaporites. It has been shown that Br increases from ~50 ppm at the base to ~150 ppm at the top of the Permian Zechstein evaporite succession in NW Europe (Holser 1979; Kuester et al. 2009; Siemann 2003). This was interpreted to reflect the enrichment of Br^- in the residual brine during progressive evaporation (Fig. 4.6a). Stratigraphically consistent Br^- profiles, in the Permian Zechstein in Europe, have been interpreted as evidence of negligible water rock interaction (i.e. incongruent dissolution) that would preferentially strip the evaporites of Br (Kuester et al. 2009). In contrast, unusually low Br concentrations in diapiric, Jurassic Louann salt in the Gulf Coast of America, together with elevated $^{87}Sr/^{86}Sr$ ratios, have been interpreted as consequences of prolonged halite-rock interaction during halokinesis (Land et al. 1988).

The growth of potash facies sylvite and Mg-salts occurs at extreme degrees of seawater evaporation (Table 4.1). Sylvite has a higher Br^- partition coefficient than halite with a D_{Br} (equal to $(Br^-/Cl^-)_{sylvite}/(Br^-/Cl^-)_{brine}$), of approximately 0.21 and an effective partition coefficient d_{Br} (equal to $(Br^-_{sylvite}/Br^-_{brine})$) of ~0.8 (Holser 1979). Thus, by the time sylvite starts to grow the remaining brines are extremely Br^- rich and, since sylvite preferentially partitions Br^- relative to halite, sylvite and

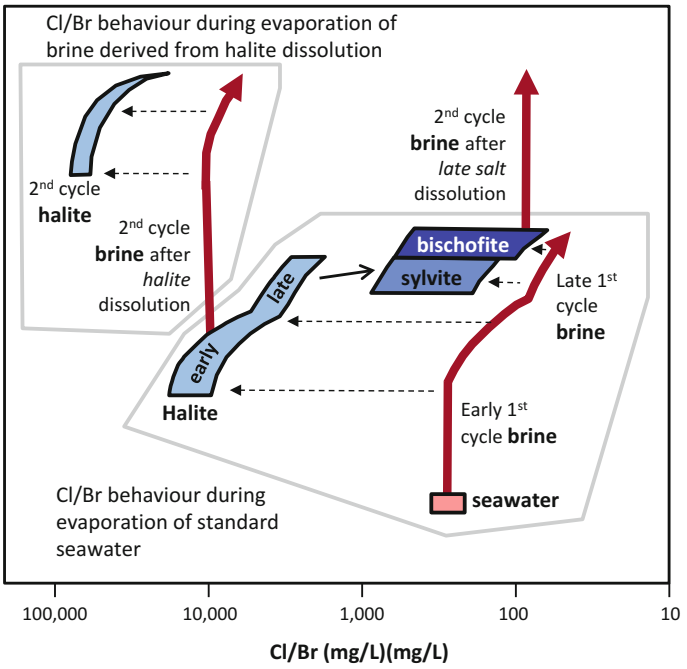

Fig. 4.9 Schematic diagram showing the relative Cl/Br ratios in primary seawater, and the effect of evaporation on residual water as well the resulting salt deposits. The effects of dissolution of halite-dominated salt and sylvite-dominated salt are also shown. Adapted from Holser (1979)

other late stage evaporite minerals, i.e. potash, tend to have very high Br^- concentrations, e.g., ~3500 ppm Br (Krupp 2005) compared to 50–200 ppm in halite (Kuester et al. 2009; Krupp 2005) (Fig. 4.9). Note that late stage potash deposits are commonly exploited for their high Br concentrations (Jensen et al. 2006; Warren 2010; Wittrup and Kyser 1990).

4.4.6 *Halogen Elements in Rivers and Groundwater in Arid Regions*

Groundwater and surface water typically have much lower salinity than seawater but extensive evaporation can still lead to salinities sufficient to result in some minerals reaching saturation. There can be major differences between the concentrations and ratios of the dominant ions in seawater and continental waters although it is not possible to come up with a typical surface or groundwater composition in the same way that is routinely reported for seawater. However, extreme evaporation of groundwater and surface water typically leads to a different suite of mineral precipitates than evaporated seawater. In arid to semi-arid continental interiors,

non-marine evaporites tend to have spatially-separated zones of precipitated calcite, dolomite, gypsum, and halite, each representing progressively greater degrees of evaporation (Schmid et al. 2003; Worden and Burley 2003). Calcretes are typically associated with relatively coarse sandstones while dolocretes, requiring greater evaporation and thus loss of mass of the flowing water, tend to be associated with fine sandstone and siltstone. A continental evaporite sequence tends to lead first to calcrete as water is lost and the groundwater salinity increases. An example of this is the calcrete-bearing Triassic Sherwood Sandstone of the south of England (Newell 2006). Further down the flow path, calcrete is replaced by dolocrete, as found in the finer grained Sherwood Sandstone in the northern part of England and Ireland (Schmid et al. 2004, 2006) and then gypcrete deposits in the later sediments (Armitage et al. 2013, 2016). Extreme evaporation in playa deposits (defined in Table 4.1) in continental basins leads to growth of halite, typically interlayered with mudstone. An example of such deposits are the finely interbedded evaporites and mudstones of the Mid-Upper Triassic Mercia Mudstone Group in various UK basins (Seedhouse and Racey 1997).

Given that most meteoric water can be considered to be extremely dilute seawater in terms of the relative proportions of Cl and Br, it is to be expected that both Cl^- and Br^- increase in concentration during river and groundwater evaporation in arid, non-marine basins. Studies of water the interior basins in Australia confirmed that high concentrations of Cl^- can be achieved in groundwater within arid continental basins (Arakel and Ridley 1986; Arakel and Moulton 1986; Arakel 1986; Jacobson et al. 1988; Jones et al. 1994). It was initially assumed that Cl/Br ratios of Australian playa-related surface waters and groundwaters were conservative (Ullman 1995). However, it was later revealed that Br^- displays non-conservative behaviour in some Australian intracontinental hydrological basins (Tweed et al. 2011). Loss of Br from water to the atmosphere was recognized during high rates of evaporation, possibly by reaction with ozone, leading to gas-phase bromate (BrO) formation (Tweed et al. 2011; Matveev et al. 2001; Platt and Honninger 2003). A study of water composition in the intracontinental Central Andes Basin (Chile and Bolivia) has detailed the concentration variation of Cl^- and Br^- (Risacher et al. 2006). These data have been compared to typical meteoric water and a simple evaporative concentration pattern (Fig. 4.10) showing that the Andean surface waters have lost a considerable amount of Br^-. These intracontinental waters reach high salinity values, with Cl^- concentrations of up to 200 000 mg/L, but have much lower Br^- concentrations than is compatible with simple evaporative processes. The low Br^- concentrations in surface water in the Andean Basin was explained by loss of Br, as bromate, to atmosphere (Risacher et al. 2006).

It is noteworthy that the halite associated with these Andean deposits has relatively low Br^- concentrations (5–20 ppm) (Risacher et al. 2006) suggesting that low Br^- concentrations, induced by loss of Br to the atmosphere, might be a general characteristic of playa-related, halite-bearing evaporites.

As well as Br loss in arid settings, Br^- concentrations in river and groundwater may also be affected by variable degrees of Br loss or gain by interaction with organic matter (Neal et al. 2007a). Thus Cl/Br patterns in marine and non-marine

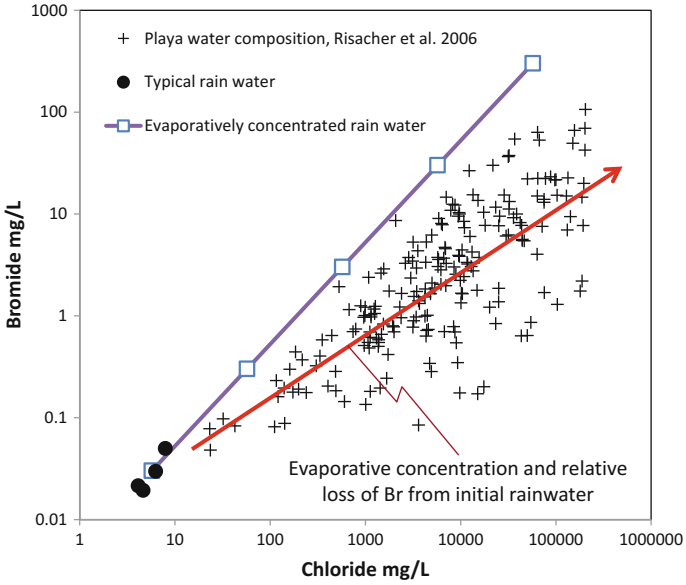

Fig. 4.10 Surface water Cl^- and Br^- concentrations from the Central Andean Basin (Risacher et al. 2006) compared to typical meteoric water and simple evaporative concentration of seawater. Surface waters in arid intracontinental basins display non-conservative Br behaviour due to bromate (BrO) loss to the atmosphere

evaporites may be broadly similar or they may be affected by increases or decreases in Br^- relative to Cl^-. This leads to the conclusion that a Cl/Br ratio in halite is not simply diagnostic of depositional environments (i.e. it cannot be simply used to differentiate between marine and non-marine evaporites). This problem is further compounded by post-depositional (diagenetic) water-evaporite interaction (see later).

4.4.7 Seawater Freezing

When saline water freezes, the quantity of available liquid-phase water decreases and so the salinity increases. Seawater freezing has been proposed as an important process in the creation of high salinity groundwaters in sub- and periglacial environments, for example in groundwaters in Antarctica, Scandinavia and Canada (Bottomley et al. 1999; Herut et al. 1990; Starinsky and Katz 2003; Takamatsu et al. 1998). These cryogenic brines penetrate aquifers via joints and fractures in the rocks. Thus, freezing needs to be considered in any study of brine-rock interaction in high latitude settings (at least during icehouse climatic times).

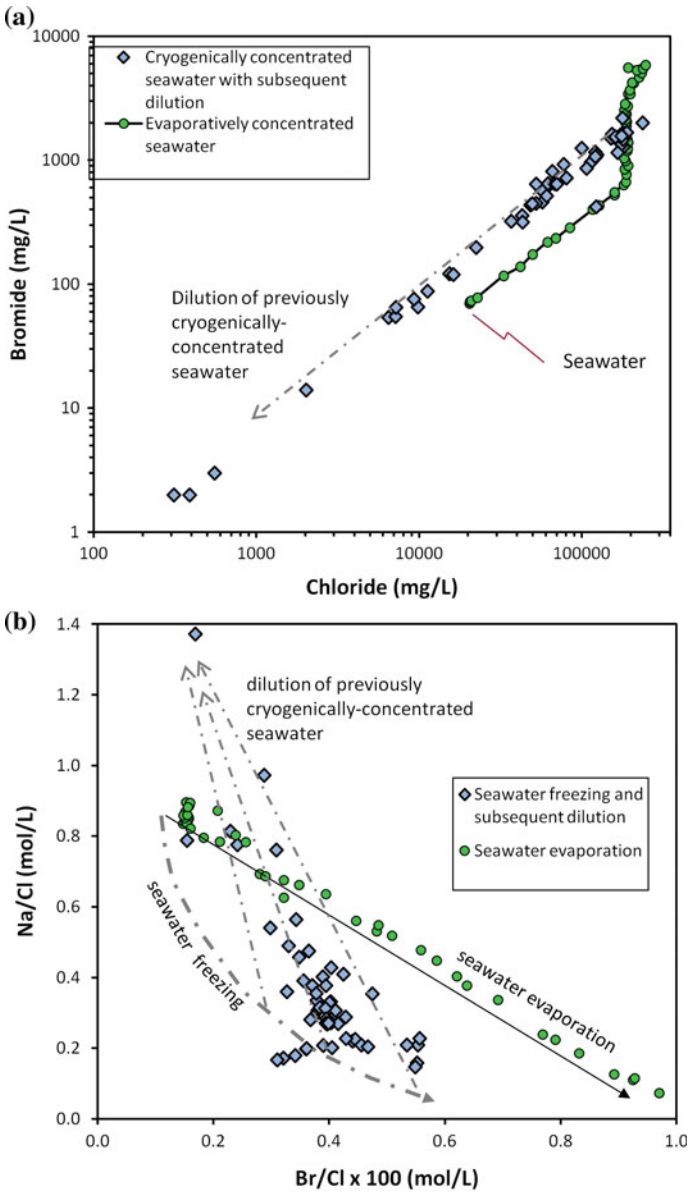
(a)
Cryogenically concentrated seawater with subsequent dilution
Evaporatively concentrated seawater
Dilution of previously cryogenically-concentrated seawater
Seawater
Bromide (mg/L)
Chloride (mg/L)
10000
1000
100
10
1
100
1000
10000
100000
(b)
dilution of previously cryogenically-concentrated seawater
Seawater freezing and subsequent dilution
Seawater evaporation
seawater freezing
seawater evaporation
Na/Cl (mol/L)
Br/Cl x 100 (mol/L)
1.4
1.2
1.0
0.8
0.6
0.4
0.2
0.0
0.0
0.2
0.4
0.6
0.8
1.0

◀**Fig. 4.11** (**a**) Seawater freezing and its effect on Cl^- and Br^- (Starinsky and Katz 2003; Bottomley et al. 1999; Herut et al. 1990; Stotler et al. 2010), compared to seawater evaporation (McCaffrey et al. 1987). Freezing can lead to cryogenically-concentrated seawater that precipitates hydrohalite and leads to relative enrichment of Br^- in the brine. Subsequent dilution by meteoric water (or melt water) then dilutes the brine and leads to saline waters enriched in Br^- relative to Cl^-. Based on halides alone, this pattern cannot be distinguished from water concentrated due to evaporation followed by meteoric dilution. (**b**) Seawater freezing can be discerned from evaporation by examining Na/Cl and Br/Cl ratios. Because Na is lost early from the frozen brine due to the growth of a Na-sulphate (mirabilite, Fig. 4.8), the Na/Cl ratio quickly decreases at roughly constant Br/Cl until hydrohalite reaches saturation when the Br/Cl ratio also increases (Herut et al. 1990; Bottomley et al. 1999; Starinsky and Katz 2003)

Freezing proportionally concentrates halide elements, at least up to the point of the precipitation of Cl^- salts. The effects of freezing can be differentiated (Fig. 4.11a) from those of evaporation only by examining Br-Cl and Na-Cl molar ratios since mirabilite ($Na_2SO_4{\cdot}10H_2O$) forms relatively early during freezing (in contrast to gypsum that forms early during evaporation) (Herut et al. 1990; Nelson and Thompson 1954) (Fig. 4.8). Hydrohalite ($NaCl{\cdot}2H_2O$) precipitates during cryogenic removal of water as salinity increases (in contrast to halite that forms due to evaporation). The sequence of mineral growth due to seawater freezing is therefore subtly different to the sequence of mineral growth due to seawater evaporation (Fig. 4.8). Freezing leads to lower Na-Cl ratios than evaporation for a given Br-Cl ratio due to mirabilite growth (Fig. 4.11a) (Herut et al. 1990; Bottomley et al. 1999; Starinsky and Katz 2003). Chloride and Br^- become proportionally more concentrated by cryogenic processes so that Br-Cl cross plots alone cannot be used to differentiate evaporation and freezing (Fig. 4.11b).

4.4.8 Dissolution of Halite and Other Evaporite Salts in Formation Waters and the Partitioning of Halogen Elements

The composition of formation water is strongly altered when it comes into contact with evaporites in the subsurface. Any water that is below saturation with halite will cause halite to dissolve, thus increasing the Cl^- concentration of the formation water. It is noteworthy that formation waters in parts of basins that are devoid of evaporites have much lower Cl^- concentrations than parts of basins that contain evaporites. An example of this phenomenon can be found in the Upper Jurassic and Lower Permian sandstones in the Zechstein (marine evaporite)-bearing Central and Southern North Sea Basins, which have formation waters at close to halite saturation with Cl^- concentrations of $\geq$200 000 mg/L. In contrast, the Mid Jurassic Brent Group reservoirs of the North Viking Graben, hundreds of kilometres north of the northern limit of Zechstein evaporites, have salinity values rather less than seawater, with typical Cl^- concentrations of $\sim$12 000 mg/L (Warren and Smalley 1994).

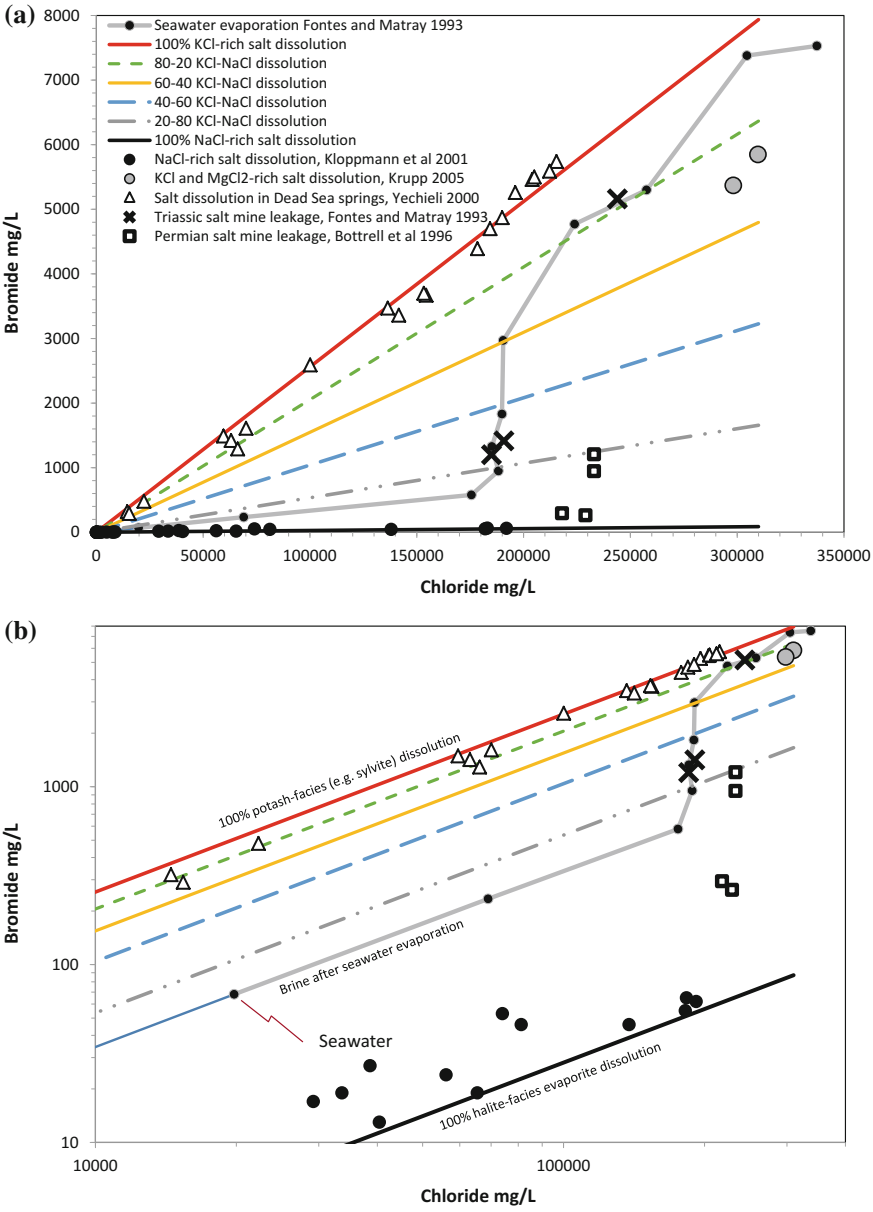
(a)
Seawater evaporation Fontes and Matray 1993
100% KCl-rich salt dissolution
80-20 KCl-NaCl dissolution
60-40 KCl-NaCl dissolution
40-60 KCl-NaCl dissolution
20-80 KCl-NaCl dissolution
100% NaCl-rich salt dissolution
NaCl-rich salt dissolution, Kloppmann et al 2001
KCl and MgCl2-rich salt dissolution, Krupp 2005
Salt dissolution in Dead Sea springs, Yechieli 2000
Triassic salt mine leakage, Fontes and Matray 1993
Permian salt mine leakage, Bottrell et al 1996
Bromide mg/L
Chloride mg/L
0
1000
2000
3000
4000
5000
6000
7000
8000
0
50000
100000
150000
200000
250000
300000
350000
(b)
100% potash-facies (e.g. sylvite) dissolution
Brine after seawater evaporation
Seawater
100% halite-facies evaporite dissolution
Bromide mg/L
Chloride mg/L
10
100
1000
10000
100000

◂**Fig. 4.12** (**a**) Modelled trends of (i) the dissolution of Br-rich, sylvite-rich evaporites by low salinity meteoric water (leading to water with 310 000 mg/L Cl^- and 6000 mg/L Br^- (Krupp 2005; Bottrell et al. 1996), and (ii) the dissolution of Br-poor halite-dominated evaporites by low salinity meteoric water (leading to water with 310 000 mg/L Cl^- and 87 mg/L Br^- (Kloppmann et al. 2001)). The dissolution of mixtures of sylvite- and halite-dominate evaporites by low salinity meteoric water is shown in 20% steps. (**b**) Same modelled trends as in part **a**, but on a log plot. The effects of evaporation of seawater on Br-Cl concentrations are also shown for comparison (McCaffrey et al. 1987). Brines that dissolved potash-bearing salts-bearing evaporites in the Dead Sea region have elevated Br concentrations (Carpenter and Trout 1978; Yechieli 2000). Water data collected from Triassic evaporites in the Paris Basin, which are ascribed to residual primary evaporated seawater, are also presented (Fontes and Matray 1993a). The type of salt undergoing dissolution has an important role in controlling the Cl-Br concentration ratios. High Br concentrations in waters sedimentary basins can be the result of dissolution of Br-rich evaporites as well as representing the highly concentrated bittern remainder of evaporated seawater

Thus, salt-rich sedimentary basins have formation water with higher Cl^- concentrations than salt-poor basins (Worden 1996). Where salt is present, the spatial distribution of formation water salinity, driven by halite dissolution, is a function of local and regional water flow patterns (Hanor 1994; Hanor and Mercer 2010). Formation water salinity has been mapped in three dimensions in the Gulf Coast region, USA, revealing that water in the immediate vicinity of halite-rich diapirs is highly saline with multi-kilometre tongues of high salinity water mapped along high permeability conduits away from the diapir (Hanor and McIntosh 2007).

If flowing water is undersaturated relative to halite then there will be mass dissolution of halite-dominated evaporites leading to Cl-rich, Br-poor waters since halite has low Br concentrations of 60–200 ppm (Fig. 4.9) (Kuester et al. 2009; Land et al. 1988; Krupp 2005). Groundwater in the vicinity of a near-surface Permian Zechstein salt dome in NW Europe has a maximum of 200 000 mg/L Cl^- due to halite dissolution but has a maximum of only 62 mg/L Br^- (Kloppmann et al. 2001) because the halite has relatively low concentrations of Br (Kuester et al. 2009) (Fig. 4.12). These Br-poor halite dissolution-related waters have Cl/Br ratios of ~3000. If water is at, or close to, saturation relative to halite, then it is conceivable that Br would be removed from the halite by preferential leaching (also known as incongruent dissolution); i.e. the NaBr dissolves preferentially relative to NaCl, thus leaving ever-more pure NaCl and increasing the Br/Cl ratio in the formation water (Moldovanyi and Walter 1992; Land et al. 1988; Eastoe et al. 2001). Such Br-leaching will be slow since the rate of halite dissolution will be slow given that the water must be at, or close to, halite saturation for this phenomenon to occur.

In contrast to halite, potash facies halide minerals, such as sylvite or bischofite ($MgCl_2 \cdot 6H_2O$), formed during the latest stages of seawater evaporation, tend to have relatively high Br concentrations (>3500 ppm) (Fig. 4.9). Dissolution of potash facies evaporites is thus likely to lead to waters with relatively high Br^- concentrations as well as high Cl^- concentrations. Water that seeped into a potash mine in Canada was reported to have up to 6520 mg/L Br^- and >200 000 mg/L Cl^- (Jensen et al. 2006). Water that seeped from a bischofite bed located in Permian

evaporites in Germany had up to 5850 mg/L Br^- and 309 000 mg/L Cl^- (Krupp 2005) (Fig. 4.12). Groundwater that interacted with potash deposits on the margins of the Dead Sea had a range of Br^- and Cl^- concentrations, with maximum values of 5740 and 215 400 mg/L respectively, all with a low Cl/Br ratio of about 45 (Yechieli 2000).

Water that results from variable dissolution of potash facies evaporites (e.g., bischofite or sylvite) by meteoric water thus has intermediate Cl^- concentrations between the water derived from potash dissolution (>300 000 mg/L) and the low Cl^- concentration of the meteoric water (19 mg/L). Meteoric water that dissolves potash facies evaporites also has Br^- concentrations intermediate between water derived from potash dissolution (>5000 mg/L) and the low Br^- concentration of the meteoric water (0.065 mg/L). Meteoric dissolution of potash facies evaporites has been modelled and added to Fig. 4.12. An analogous mixing model has also been produced for dissolved halite. The model broadly matches empirical analyses from natural examples of halite-dissolution by meteoric water (Fig. 4.12). Dissolution models of mixtures of potash facies evaporites and halite-dominated evaporites have been produced in 20% increments using the Dead Sea example as the low Cl/Br potash end-member and the Zechstein example as the high Cl/Br halite end-member (Yechieli 2000; Kloppmann et al. 2001; García-Veigas et al. 2009). Water from a potash mine, associated with the halite-rich Zechstein deposits in NE England, has high a Cl^- concentration due to groundwater-induced dissolution, but has a range of Br^- concentrations (Fig. 4.12) suggesting that a mixed potash-halite evaporite has dissolved (Bottrell et al. 1996).

The behaviour of I and F during evaporite dissolution has not been well reported. This is doubtless due to the relatively low I and F concentrations assumed to be in the evaporites, resulting in the tacit assumption that evaporite dissolution has little impact on I^- and F^- concentrations.

4.4.9 *Halogen Incorporation in Organic Matter in Sediments and Sedimentary Basins*

Natural organic matter in sediments and sedimentary rocks typically contains negligible quantities of F (Garcia and Borgnino 2015). Bromine and Cl have been studied in natural organic matter such as peat, coal, kerogen, and oil. In contrast to the other halogens, I has a strong affinity for organic matter (Muramatsu and Wedepohl 1998). Igneous rocks, seawater, evaporites, silicate rocks, and carbonate sedimentary rocks all have low I concentrations (Fig. 4.2b) but I can be relatively concentrated in organic matter, such that I is classed as a biophile element (Fuge 1988).

Chloride concentration in water from a peat bog from Chile was reported to be typical of the local groundwater (7–15 mg/L) although Br^- and I^- concentrations were rather higher than groundwater (56–123 and 10–20 μg/L respectively) (Biester et al. 2006). Chloride was found to be present as a simple anion in

peat-waters but Br^- and I^- were found to be present as dissolved organo-halide compounds. This suggests that organic activity in the peat concentrated the Br^- and I^- from the primary meteoric water but has not affected the Cl^- concentration.

Coastal peat and coal have higher Br concentrations than their inland equivalents. Inland peat was reported to contain up to 20 ppm Br whereas coastal peat has up to 200 ppm Br present in pore waters or as solid salts derived from seawater (Vainikka and Hupa 2012). The Cl and Br content of coal has been the focus of considerable work since they influence its value. A study of Cl and Br in British coal concluded that they were predominantly associated with moisture (as dissolved or salt-related Cl^- and Br^-) and there were negligible quantities of other forms of these elements (Spears 2005). However, detailed geochemical studies have shown that small quantities of organo-Cl and organo-Br compounds may be present in some coals, with Cl possibly linked to carboxyl groups and Br possibly linked to amine groups (Vassilev et al. 2000; Yudovich and Ketris 2006). Small quantities of organo-chloride and organo-bromide compounds have been identified in coals, mostly consisting of Cl and Br substitutions for hydrogen on benzene rings (Wei et al. 2004).

Iodine concentration has been shown to increase as peat ages and as it is diagenetically altered during burial, from lignite to bituminous coal, and finally anthracite. Iodine increases from a mean value of 0.49 ppm in lignite to 4.0 ppm in anthracite (Wu et al. 2008). The I concentration is higher in marine coals than freshwater coals suggesting that the specific depositional environment plays a major role.

In general, some of the highest concentrations of I are associated with marine sediments (Muramatsu and Wedepohl 1998). Marine algae are known to concentrate I (Fuge 1988) with a strong association reported between algae-rich shaley source rocks and relatively high bulk sedimentary rock I concentrations (Collins et al. 1971). Organic matter in sediments undergoes progressive changes during burial, resulting in kerogen and then generating oil followed by gas when heated to >80–90 °C and buried to 3000–4000 m. However, the earliest stages of conversion of biomolecules to geomolecules (kerogen) can lead to major effects on the halogen elements, especially I, in pore waters. Analysis of waters from sediments buried from 0 to 250 m in the Peru margin revealed approximately constant, marine concentrations of Cl^- ($\sim$20 000 mg/L) but showed aqueous I^- concentrations far greater than marine values of 0.05 mg/L. Iodide increased from just less than 1 mg/L–150 mg/L in the deepest samples at 250 m (Fig. 4.13) (Fehn et al. 2007). The excess I^- in these marine sediments was interpreted to be the result of alteration and breakdown of I-rich organic matter. The association between elevated Br^- and I^- for constant Cl^- concentration suggests that some excess Br^- (Fig. 4.13b), as well as I^-, in pore waters must also be the result of the diagenetic breakdown of organic matter, as proposed previously (Price and Calvert 1977). Elevated I- concentrations in much deep formation waters are typically interpreted to have resulted from the maturation of kerogen in marine source rocks (Collins 1969; Fehn et al. 2007; Moran 1996).

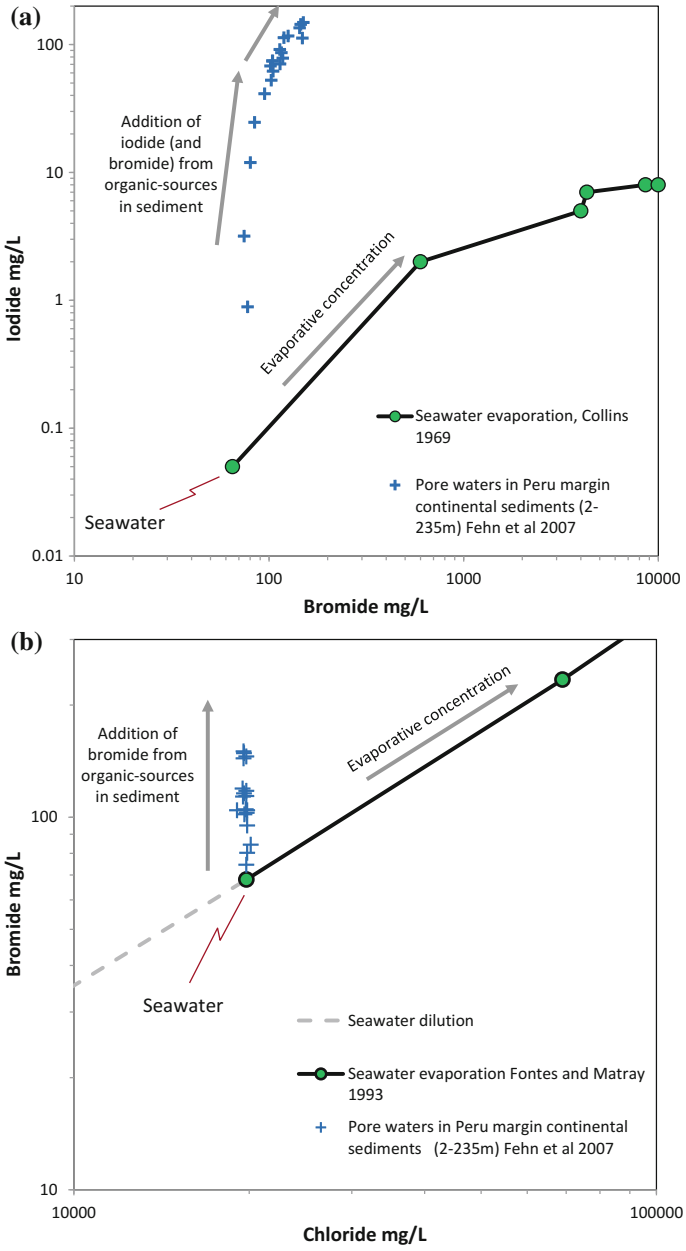
(a)
Addition of iodide (and bromide) from organic-sources in sediment
Evaporative concentration
Seawater
Seawater evaporation, Collins 1969
Pore waters in Peru margin continental sediments (2-235m) Fehn et al 2007
Iodide mg/L
Bromide mg/L
100
10
1
0.1
0.01
10
100
1000
10000
(b)
Addition of bromide from organic-sources in sediment
Evaporative concentration
Seawater
Seawater dilution
Seawater evaporation Fontes and Matray 1993
Pore waters in Peru margin continental sediments (2-235m) Fehn et al 2007
Bromide mg/L
Chloride mg/L
100
10
10000
100000

◂**Fig. 4.13** Chloride, Br^- and I^- concentrations in pore waters from sediments buried between 0 m and 250 m the Peru margin (Fehn et al. 2007). (**a**) Peru margin Cl^--Br^- concentration data compared to a seawater evaporation curve (Fontes and Matray 1993a). Chloride concentrations remain constant and resemble the seawater that the sediments were deposited in but Br^- increases progressively with depth of sample reaching a value 80% higher than the initial seawater-like concentration in the shallow samples. (**b**) Peru margin Br^--I^- concentration data compared to a seawater evaporation curve for reference (Collins 1969). Bromide concentrations increase slightly (80%) with depth (and see Fig. 4.14a) but I concentrations increase by more than two orders of magnitude. The excess I^- and Br^- were interpreted to be derived from altered I^- and Br-enriched organic matter in the sediment column

4.4.10 Membrane Filtration

Membrane filtration, by clay-rich, low permeability rocks, was proposed as a mechanism that could influence salinity and possibly lead to non-conservative halide concentration variations (Kharaka and Berry 1973). Aqueous solutions forced through compacted clay-rich materials under pressure gradients were found to preferentially retard various ions. For halides, the order of increasing retardation at 70 °C was I^-, followed by Cl^- and then Br^-, which is retarded the most of all (Kharaka and Berry 1973). The relevance of membrane filtration on water composition in general, and relative halide concentrations in particular, has remained somewhat uncertain but studies of natural diffusion under fluid pressure gradients have become increasingly important.

Mass movement of water through low permeability lithologies is limited by the diffusion coefficient of the rocks. Much attention has been recently given to diffusion through mudstones since they are being globally assessed for their effectiveness in the long term isolation of nuclear waste. Recent detailed studies of water compositional profiles through a series of aquifers and aquicludes have been employed to assess the diffusion rates of water and their solutes. A key conclusion from studies in Canada is that in very low permeability, Lower Palaeozoic rocks (effective diffusion coefficients as low as 10^{-14} m^2/s) pore water residence times approximate the depositional age of the rocks suggesting that diffusion rates are exceptionally slow (Al et al. 2015; Clark et al. 2013). In contrast, studies of low permeability Mesozoic rocks from France (effective diffusion coefficients greater than 10^{-12} m^2/s) suggested that diffusion played a major role in controlling water movement patterns and water compositions (Bensenouci et al. 2014).

Interestingly both the Canadian and French studies seemed to assume that any difference in Cl^- and Br^- diffusion rates was irrelevant (Bensenouci et al. 2014; Clark et al. 2013). Both studies revealed similar variation patterns for Cl^- and Br^- through their respective stratigraphic successions (Fig. 4.14a). However, it is significant that the Cl/Br ratio, for the waters in the low permeability units in the French succession, is lower than that which would result from a simple mixture between the high salinity (halite dissolution-derived) water deep in the succession and the lower salinity groundwater (Fig. 4.14b). This seems to imply that Br^- is being retained in the mudstones or that Cl^- has a faster rate of diffusion through the

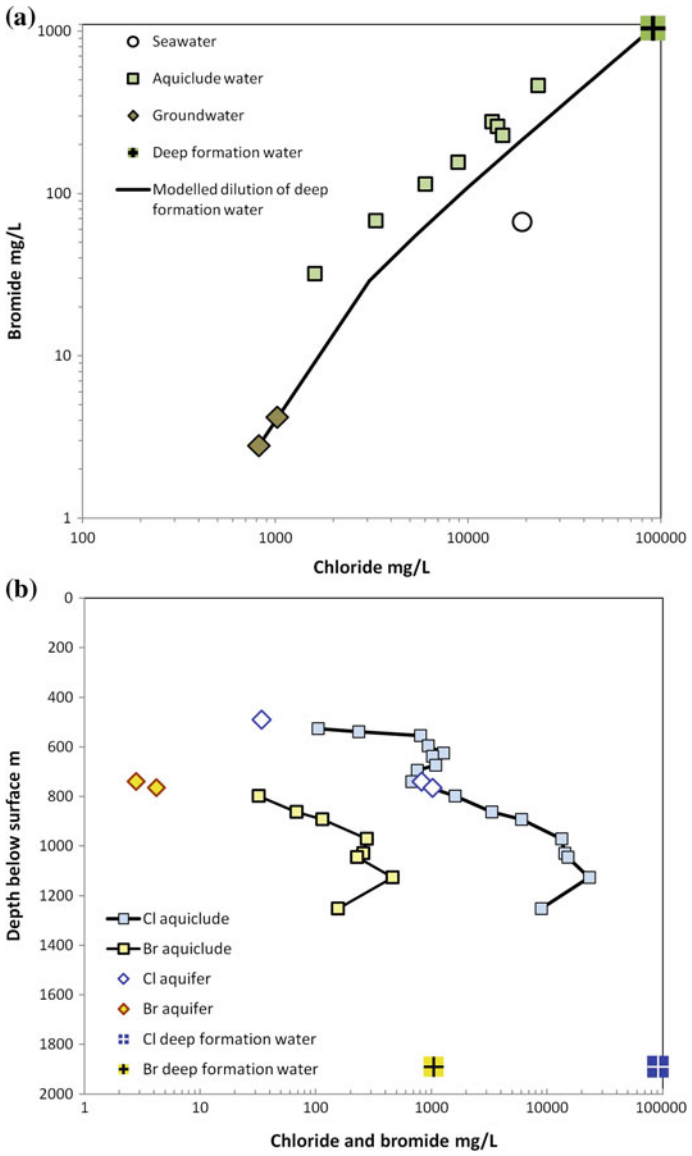

Fig. 4.14 (**a**) Chloride and Br^- concentration data versus depth from waters extracted from a succession of low permeability mudstones (aquicludes) from the Paris Basin (Bensenouci et al. 2014). Also shown are data from interbedded aquifers and deeper formation waters. (**b**) Comparison of Cl^- and Br^- concentration data with seawater, deep saline formation waters, and the modelled path of simple dilution of the deep saline water by low salinity groundwater. The waters from the low permeability successions seem to have excess Br^- suggesting either an additional source of Br^- or relatively greater loss, or flux, of Cl^-

mudstones, echoing back to the relative rates of membrane filtration of Cl^- and Br^- deduced experimentally (Kharaka and Berry 1973).

4.4.11 Summary of Processes that Influence Halide Concentrations in Formation Waters

Chloride and Br^- are routinely assumed to be conservative elements in sedimentary formation waters at least for Cl^- concentrations up to the point of halite precipitation. Chlorine/Bromine relationships are thus routinely used to interpret the origin of the water with the assumption that that there is little or no interaction between these halides and silicate, carbonate, sulphide, oxide, or any other common minerals. The analysis here has shown that this assumption is not necessarily correct. In comparison, I^- concentrations are known to be non-conservative with a major contribution coming from organic-rich sediments (Fig. 4.13). Fluoride concentrations are also known to be non-conservative since commonly there are F-bearing minerals in sedimentary rocks (fluorapatite and fluorite).

Processes that may control Cl^- concentrations in formation waters include: (i) seawater concentration by silicate diagenetic hydration reactions in the sediment column (Fig. 4.4), (ii) seawater dilution by diagenetically-produced water associated with overpressure build-up, (iii) seawater evaporation (Fig. 4.6), (iv) seawater dilution by meteoric water (Fig. 4.7), (v) freshwater evaporation in arid continental basins (Fig. 4.10), (vi) seawater freezing (Fig. 4.11), (vii) evaporite dissolution (Fig. 4.12), and (viii) membrane filtration (or diffusion) through low permeability rocks (Fig. 4.14).

Processes that control Br^- concentrations are similar to those that control Cl^- but there are circumstances under which Br^- may not be a conservative element. These include: (i) hydration reactions may preferentially remove Br^- from water leading to higher Cl/Br ratios than seawater (Fig. 4.4a); (ii) evaporative concentration may lead to loss of Br^- to the atmosphere by ozonation processes, thus leading to higher Cl/Br ratios than seawater (Fig. 4.10); (iii) congruent dissolution of Br-poor halite will lead to very low Br^- concentrations thus leading to very high Cl/Br ratios (Fig. 4.12); (iv) incongruent dissolution of Br-poor halite will lead to higher Br^- concentrations, and thus somewhat lower Cl/Br ratios, than congruent halite dissolution; (v) dissolution of Br-enriched potash facies evaporites will lead to high Br^- concentrations in solution thus leading to low Cl/Br ratios (Fig. 4.12); (vi) breakdown of Br-bearing organic matter in mudstones or coal may lead to elevated Br/Cl ratios (Fig. 4.13); and (vii) membrane filtration may lead to slightly lower Cl/Br ratios due to the easier movement of Cl^- than Br^- through low permeability, clay-rich rock units (Fig. 4.14).

4.5 Halogen Isotope Geochemistry in Sedimentary and Diagenetic Systems

4.5.1 Stable and Radioactive Isotopes of Halogens

Isotopes of a given element, by definition, have the same number of protons but they have different numbers of neutrons. Some isotopes are stable, meaning that they can last for all eternity. Different isotopes of an element undergo identical chemical and physical reactions but the different isotopes have different rates of reactions. Stable isotopes are thus used to probe the mechanisms and rates of various physical and geochemical processes and reactions.

Fluorine is monoisotopic; it has only one stable isotope (^{18}F). Chlorine has two stable isotopes: ^{35}Cl and ^{37}Cl. These are found in relative proportions (mole fraction) of: 0.7576 and 0.2424, respectively. Bromine has two stable isotopes: ^{79}Br and ^{81}Br. These are found in relative proportions of: 0.5069 and 0.4931 respectively. Iodine is monoisotopic: it has only one stable isotope (^{127}I).

In contrast to stable isotopes, other isotopes can be radioactive and are, by definition, unstable. Radioactive isotopes have a defined half-life and release various types of radiation as they breakdown to create new isotopes of other elements. Such isotope systems can be used to date geological materials if there is sufficient knowledge about the decay constant and the concentrations of parent and daughter isotopes are known.

Chlorine has one geologically-useful radioactive isotope, ^{36}Cl, which has a half-life of 0.301 Myrs. Iodine has one geologically-useful radioactive isotope, ^{129}I, which has a half-life of 15.7 Myrs.

4.5.2 Controls on Cl Stable Isotopes in Sedimentary Rocks

Chlorine isotopes are reported using the delta notation:

$$\delta^{37}\mathrm{Cl} = \left[\left({}^{37}\mathrm{Cl}/{}^{35}\mathrm{Cl} \right)_{\mathrm{sample}} / \left({}^{37}\mathrm{Cl}/{}^{35}\mathrm{Cl} \right)_{\mathrm{standard}} - 1 \right] \times 1000$$

The standard employed is standard mean ocean water Cl so that results are reported as δ^{37}Cl SMOC ‰. Chloride in seawater, by definition, has a δ^{37}Cl value of 0.0‰ SMOC.

Terrestrial and marine sedimentary rocks have a relatively wide range of δ^{37}Cl values and there is no unique Cl isotope value that denotes sedimentary rocks (Selverstone and Sharp 2015). However, the same authors concluded that there are no systematic changes in sedimentary δ^{37}Cl values during burial through to low grade metamorphism suggesting that primary sedimentary Cl isotope signals may be retained. The analysis of δ^{37}Cl has been undertaken using both isotope ratio

mass spectrometry and positive ion thermal ionization mass spectrometry. The two techniques have been shown to have rather different degrees of precision, with questions remaining about the precision and interpretation of some published $\delta^{37}Cl$ data (Eggenkamp 2015; Luo et al. 2014, 2015).

The processes that potentially have an important impact on Cl^- isotopes in sedimentary and diagenetic systems are: (i) halite and potash facies evaporite mineral precipitation from evaporating seawater; (ii) evaporite dissolution; (iii) release of isotopically distinct Cl from Cl-bearing silicates, such as biotite and amphibole, during weathering and diagenesis; (iv) wind-blown transport of halite dust; and (v) diffusion of Cl^- though low permeability rocks such as mudstone membranes.

The partitioning of Cl isotopes between mineral and residual brine is controlled by the fractionation factor, α, which is defined as:

$$\alpha = \left({}^{37}Cl/{}^{35}Cl\right)_{\text{mineral}} / \left({}^{37}Cl/{}^{35}Cl\right)_{\text{brine}}$$

Chloride bonded to monovalent ions such as K and Na tends to have lower fractionation factors than Cl^- bonded to divalent ions such as Fe or Mg (Stewart and Spivack 2004; Schauble et al. 2003). Thus Cl-bearing amphibole and biotite, formed during high temperature interaction between Cl^--rich water (e.g., seawater) and basic magma, tend to have positive $\delta^{37}Cl$ values of 2.0–3.5‰ SMOC (Magenheim et al. 1995; Stewart and Spivack 2004). In contrast, halite tends to have $\delta^{37}Cl$ values <1‰ SMOC. At sedimentary temperatures, the fractionation factor between water and halite has been defined as 1.00026 (±0.00007), for kainite ($KMg(SO_4)Cl{\cdot}3H_2O$) it is 1.00013 (±0.00008), for carnallite it is 1.00002 (±0.00009), while for bischofite it is 0.99994 (±0.00010) (Eggenkamp et al. 1995). These are small fractionation factors compared to lighter element isotopic systems, such as hydrogen or oxygen, whose stable isotopes have greater relative mass differences than ^{37}Cl and ^{35}Cl. The implication of this relatively small isotopic mass difference is that halide mineral growth and dissolution can only have a limited effect on $\delta^{37}Cl$.

The first precipitated halite growing from evaporating seawater ($\delta^{37}Cl$ of 0.0‰ SMOC) should have a $\delta^{37}Cl$ of between 0.18 and 0.33‰ SMOC (Eggenkamp et al. 1995) (Fig. 4.15). As halite continues to precipitate, the Cl^- in the remaining water becomes isotopically lighter as the heavier isotopes are taken out of the system. Up to the point of bischofite growth, the brine should have an ever-decreasing $\delta^{37}Cl$ of as low as −0.30 to −0.62‰ SMOC. Halite, kainite, and carnallite, growing from an increasingly isotopically light Cl^--rich brine can have $\delta^{37}Cl$ values between −0.23 and −0.55‰ SMOC. At the final stages of evaporation, bischofite, with its fractionation factor of <1, has a lower $\delta^{37}Cl$ than the brine and so reverses the isotope fractionation trend. As evaporation progresses, the theoretical $\delta^{37}Cl$ evaporite range, decreasing from a maximum of 0.33 to −0.55‰ SMOC, is largely supported by reported values from Phanerozoic evaporites around the world (Eastoe et al. 2007) (Fig. 4.16a). Most pure halite evaporites have a $\delta^{37}Cl$ slightly higher than the

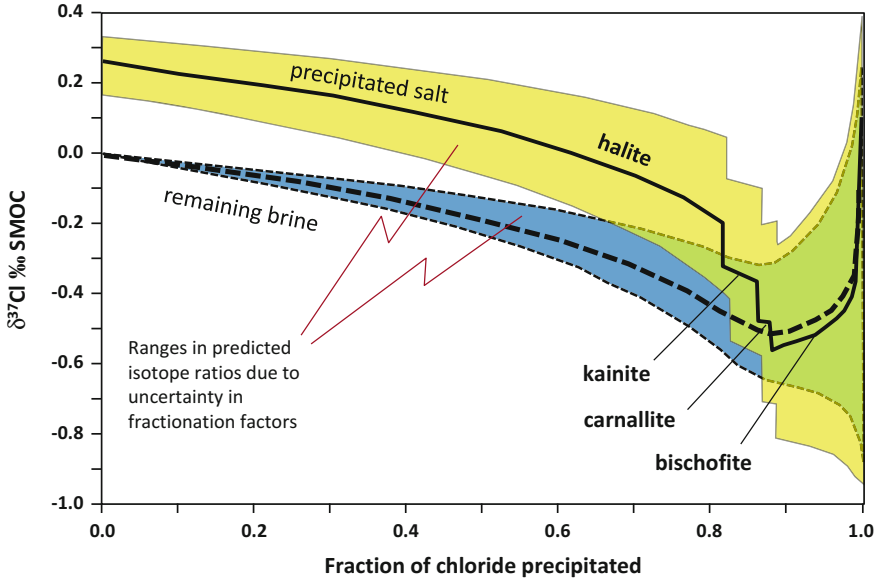

Fig. 4.15 Diagram illustrating the fractionation of ^{37}Cl between evaporated seawater and precipitating salts. Fraction factors taken from Eggenkamp et al. (1995). Salts tend to have a higher $\delta^{37}Cl$ than the brine so that first formed evaporites have $\delta^{37}Cl$ up to 0.33‰ SMOC, later formed salts get progressively lighter until bischofite growth, which then reverses the trend since it has a fractionation factor of <1. The areas of uncertainty result from uncertainty in the fractionation factors. Residual waters after extreme seawater evaporation have a narrow range of possible $\delta^{37}Cl$ values

more evolved potash-bearing evaporites, which supports the model described above (Fig. 4.16a).

In marine sabkhas that are undergoing evaporite precipitation, aqueous $\delta^{37}Cl$ values seem to be decoupled from O and H isotopes in shallow pore waters despite all three being influenced by the extent of evaporation. This was interpreted to be the result of local, wind-induced redistribution of dust-grade halite, which dissolves if it lands on wet surfaces, thus obscuring any primary $\delta^{37}Cl$ patterns in sabkha evaporites (Duane et al. 2004).

Evaporites with higher $\delta^{37}Cl$ values (up to 0.8‰ SMOC) have been interpreted to be non-marine with an addition of isotopically enriched Cl being derived from weathered Cl^--bearing silicate minerals, such as amphibole and biotite (Eastoe and Peryt 1999) (Fig. 4.16a). Groundwater and river water have also been reported to have slightly elevated $\delta^{37}Cl$ values due to the input of isotopically-enriched Cl from weathered minerals (Zhang et al. 2007; Liu et al. 1997).

It is possible that halite, or other evaporite minerals, in contact with under-saturated water will undergo bulk (congruent) dissolution with no influence on mineral $\delta^{37}Cl$ values and so will create formation water with same $\delta^{37}Cl$ as the parent salt. However, when halite interacts with under-saturated water, it is also

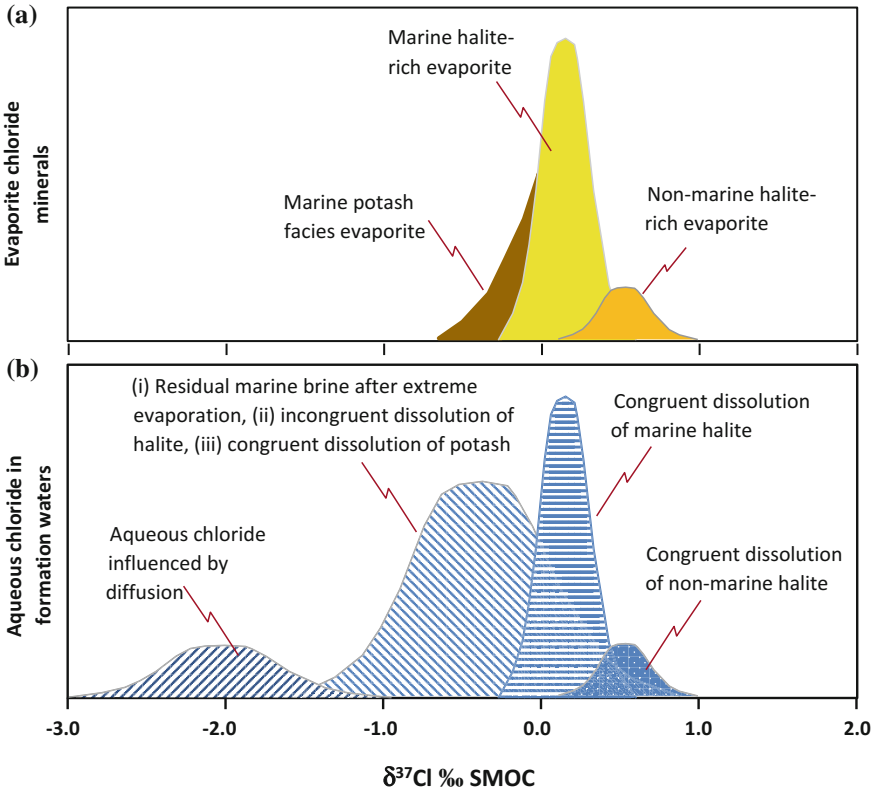

Fig. 4.16 Diagram summarising: (**a**) the typical range of $\delta^{37}Cl$ values for halite- and potash-bearing salts resulting from seawater evaporation and non-marine evaporites influenced by Cl input from weathered silicate minerals (Eastoe et al. 2007; Stewart and Spivack 2004). (**b**) the typical range of formation waters in oil fields with processes responsible for different ranges of formation water $\delta^{37}Cl$ outlined (Stewart and Spivack 2004). Three different processes may be responsible for water having $\delta^{37}Cl$ approximately 0.5‰ lighter than evaporites: (i) residual marine brine after extreme evaporation, (ii) incongruent dissolution of halite, and (iii) congruent dissolution of potash-bearing evaporites. This ambiguity hinders a unique interpretation of formation water $\delta^{37}Cl$ values. Some waters have distinctly low $\delta^{37}Cl$ values, which have been explained by the role of diffusional processes (Eggenkamp and Coleman 2009; Ziegler et al. 2001)

possible that it will undergo incongruent dissolution with isotopically light halite ($Na^{35}Cl$) dissolving faster than isotopically heavy halite ($Na^{37}Cl$). Bedded salt in the Gulf of Mexico has $\delta^{37}Cl$ values between −0.5 and 0.3‰ SMOC, while diagenetically-affected diapric salt has slightly higher $\delta^{37}Cl$ values between 0.0 and 0.5‰ SMOC. This has been interpreted to be the result of the preferential (incongruent) dissolution of the light Cl isotope in halite (Eastoe et al. 2001).

Overall, brines tend to have slightly lower $\delta^{37}Cl$ values than evaporites in the sedimentary succession (Stewart and Spivack 2004) although this may be due to

secondary processes that overwrite any fractionation factor controls related to Cl^- salt dissolution (Fig. 4.16b).

Chlorine isotopes are affected by aqueous diffusion with the lighter ^{35}Cl isotope diffusing faster than the heavier ^{37}Cl isotope (Eggenkamp and Coleman 2009; Desaulniers et al. 1986; Eastoe et al. 2001; Lavastre et al. 2005; Zhang et al. 2007). Diffusional redistribution is relatively unimportant in porous and permeable rocks but it may play a role in fractionating the stable isotopes of Cl, where these isotopes are forced, under a pressure gradient, through low permeability mudstones. Diffusion affects $\delta^{37}Cl$ with the heavier isotope left enriched nearer the source and the lighter isotope enriched down the diffusion gradient (Rebeix et al. 2014; Lavastre et al. 2005). Empirical data, supported by modelling, suggest that this can lead to up to 2‰ differences in $\delta^{37}Cl$ (Fig. 4.16b). Relatively low salinity formation waters in sandstones in the Gulf of Mexico were interpreted to have low $\delta^{37}Cl$ values (down to −1.6‰) due to the effects of diffusion (Eastoe et al. 2001).

As described, formation waters that result from extreme evaporation of seawater, can theoretically have $\delta^{37}Cl$ values ranging from 0.0 to −0.53‰ SMOC (Eggenkamp et al. 1995). Waters that dissolve evaporite can either have the same $\delta^{37}Cl$ value as the salt (congruent dissolution) or they may have $\delta^{37}Cl$ values very slightly lower than the original salt if there was fractionation (incongruent dissolution). It is therefore not easy to differentiate the Cl^- in residual sea water after extreme evaporation from the Cl^- in water following evaporite dissolution (Fig. 4.16).

4.5.3 Bromine Stable Isotopes in Sedimentary Rocks

The study of Br isotopes is in its infancy following recent improvements in analytical techniques (Eggenkamp and Coleman 2000). Bromine displays many geochemical similarities to Cl and it was initially expected that the two isotope systems may reveal similar sets of controls, (e.g., extent of precipitation, evaporite dissolution, differential diffusion, and/or release from silicate minerals during weathering).

Like ^{37}Cl (Magenheim et al. 1995; Stewart and Spivack 2004), ^{81}Br may be slightly enriched in silicate minerals, such as amphibole and biotite, which, after weathering, leads to groundwater with slightly positive $\delta^{81}Br$ values (approaching +1.0‰ SMOB) (Du et al. 2015; Chen et al. 2014). Thus groundwater-derived Br^-, influenced by weathering, can potentially be differentiated from marine-derived Br^- (close to 0.0‰ SMOB).

Some studies have shown a degree of correlation between $\delta^{37}Cl$ and $\delta^{81}Br$, hinting at common processes controlling these two stable isotope systems (Shouakar-Stash et al. 2007; Stotler et al. 2010; Chen et al. 2014; Alexeeva et al. 2015). In contrast, others have shown an inverse correlation between the two

isotope systems (Gwynne et al. 2013; Eggenkamp and Coleman 1998). Overall, there remain many questions about the value and interpretation of Br isotopes in sedimentary and diagenetic systems.

4.5.4 Dating in Sedimentary Systems Using Cl and I Radioactive Isotopes

Radioactive ^{36}Cl, with its geologically brief half-life (301 Kyrs), has limited application in most diagenetic systems but it has been used to place a Quaternary date to groundwater Cl^- in the Dead Sea area (Yechieli et al. 1996). It has also been used to date formation waters in Plio-Pleistocene-hosted gas accumulations, with the age broadly corroborated by ^4He data (Mahara et al. 2013). However, the young formation water ages were at odds with the much greater and inconsistent (17.4 and 25 Ma) ages derived from dissolved ^{129}I data. The I ages, which are much greater than the age of the host sediment, were interpreted to reflect the age of old I-bearing organic matter accumulated on the sea floor (Mahara et al. 2013), which were subsequently mobilised and incorporated into the fluid phase.

The addition of old I from organic-rich sediments was also reported in ^{129}I studies of gas hydrates and fore-arc fluids where the I is much older than the host sediment (Fehn et al. 2007). ^{129}I studies of the relatively I-rich formation waters of the Anadarko Basin have been used to constrain the timing of I expulsion from Palaeozoic source rocks to between 2 and 90 Ma (Moran 1996). A similar approach, using ^{129}I, was used to constrain the timing of water migration in coalbed methane reservoirs (Snyder et al. 2003).

4.6 The Halogen Elements in Sedimentary Oil and Gas Field Formation Waters: Relative Influences of Diagenetic and Other Processes in Sedimentary Basins

4.6.1 Oil and Gas Field Water Cl^--Br^- Concentrations

4.6.1.1 Chloride and Br^- Concentration Ranges

Analysis of the Cl^- concentration of formation water is routine during oil and gas field appraisal and development since it is usually the dominant anion, thus closely correlating with overall salinity. The salinity of formation water, in turn, controls its resistivity and is a key input into interpreting downhole resistivity logs in terms of the amount of oil or gas in place. Chloride concentration is also routinely monitored in produced waters from oil and gas wells since it can help reveal breakthrough

times of injected waters used for pressure support. There are probably millions of Cl^- analyses from oil and gas field formation waters that are unpublished and languishing in long-forgotten archives. Chloride concentrations in oil and gas field formation waters can vary from as low as 100 mg/L to in excess of 300 000 mg/L (Worden 1996). A study of Cl^- concentration on its own is, however, rather uninteresting. Chloride concentration data collections have revealed that there is no simple pattern of increasing Cl^- concentration with depth and that there is no relationship between host lithology or age and Cl^- concentration (Worden 1996). Simple conclusions from an analysis of published data are that Cl^- concentrations tend to be highest in sedimentary basins that contain halite-rich evaporites (Worden 1996); they are highest in the vicinity of salt bodies; and they tend to be high in the down gradient flow directions away from salt bodies (Hanor 1994; Hanor and McIntosh 2007; Hanor and Mercer 2010).

4.6.1.2 Chloride Versus Br^- Concentration Patterns

More interesting and revealing is an analysis of Cl^--Br^- relationships from deep sedimentary formation waters in oil and gas producing basins. Chloride-Br^- concentration data have been collated from 36 published studies representing ~1175 data points from oil- and gas-producing sedimentary basins in China, Europe, North America, the Middle East, and North Africa (Table 4.5). Iodide and F^- concentration data have also been collected from these sources, where available. These data can be studied on their own to see if there are any simple patterns. However it is more useful and interesting to compare the formation water Cl^--Br^- concentration data with the range of possible controls on Cl^--Br^- concentration relationships, discussed in the previous section (see Figs. 4.3, 4.4, 4.5, 4.6, 4.7, 4.8, 4.9, 4.10, 4.11, 4.12, 4.13 and 4.14).

There is an overall crude correlation between Cl^- and Br^- concentrations when the Br^- concentration exceeds 1000 mg/L and when the Cl^- concentration is greater than about 100 000 mg/L (Figs. 4.17 and 4.18). However, the pattern is not simple, with a wide range of Br^- concentrations in highly saline (high Cl^- concentration) formation waters. The collated Cl-Br data have been plotted on log and linear bivariate graphs (Figs. 4.14b and 4.17a). These display the enormous range of concentrations reported and help illustrate the dominant controls.

4.6.1.3 Early Comparisons of Cl^- and Br^- Concentrations to Evaporated Seawater

The systematic comparison of Br^- concentration to bulk salinity (which reflects Cl^- concentration) in oil field formation waters seems to have been first attempted in the 1960s (Rittenhouse 1967). In this paper, oilfield water Br concentration and salinity data were, for the first time, compared to published seawater evaporation curves. Different types of formation water were identified based on the relative

Table 4.5 Basins, reservoir units, and publication details utilised in the data analysis (Figs. 4.17, 4.18, 4.19, 4.20, 4.21, 4.22 and 4.23)

Basin and Country	Age of host reservoir	Reference
North German	Carboniferous to Permian	Lueders et al. (2010)
North Sea Norwegian sector	Triassic to Cretaceous	Egeberg and Aagaard (1989)
North Sea UK and Norway	Triassic to Palaeocene	Warren and Smalley (1994)
North Sea Norwegian sector	Mid Jurassic	Ziegler et al. (2001)
Wessex, UK	Triassic	Worden et al. (2006)
Wessex, UK	Triassic	Edmunds et al. (1982)
Paris Basin, France	Jurassic	Matray et al. (1994)
Paris Basin, France	Triassic to Jurassic	Fontes and Matray (1993b)
Paris Basin, France	Triassic	Millot et al. (2011)
Paris Basin, France	Triassic	Worden et al. (1994)
Tarim Basin, China	Ordovician	Cai et al. (2001)
Tarim Basin, China	Ordovician	Chen et al. (2013)
North Africa, Tunisia	Triassic	Morad et al. (1994)
Iran, Persian Gulf	Triassic	Bagheri et al. (2014)
Michigan, USA	Devonian	Wilson and Long (1993b)
Michigan, USA	Silurian	Wilson and Long (1993a)
Michigan, USA	Palaeozoic	Kaufmann et al. (1993)
Illinois, USA	Carboniferous	Demir and Seylor (1999)
Ohio, USA	Silurian	Sanders (1991)
Gulf of Mexico, USA	Tertiary	Land and Macpherson (1992)
Gulf of Mexico, USA	Oligocene Frio Fm	Macpherson (1992)
Arkansas, USA	Jurassic	Moldovanyi and Walter (1992)
Gulf Coast, Mexico	Jurassic to Cretaceous	Birkle et al. (2009)
Gulf Coast, Mexico	Jurassic to Tertiary	Birkle et al. (2002)
Texas Gulf Coast, USA	Jurassic to Tertiary	Kharaka et al. (1977)
Gulf of Mexico, USA	Jurassic to Miocene	Houston et al. (2011)
Gulf of Mexico, USA	Jurassic to Miocene	Eastoe et al. (2001)
Arkansas, USA	Jurassic	Carpenter and Trout (1978)
Palo Duro, USA	Permian	Eastoe et al. (1999)
Palo Duro, USA	Permian	Knauth (1988)
San Joaquin, USA	Tertiary	Fisher and Boles (1990)
Western Canada Basin	Devonian to Cretaceous	Connolly et al. (1990)
Western Canada Basin	Devonian to Cretaceous	Hitchon et al. (1971)
Mississippi, USA	Jurassic to Cretaceous	Carpenter et al. (1974)
Appalachian, USA	Devonian	Osborn et al. (2012)
North Slope Alaska, USA	Carboniferous to Triassic	Kharaka and Carothers (1988)

quantity of Br^- to (Cl^--dominated) salinity with emphasis placed on formation waters that have more Br^- than can be explained by simple seawater evaporation (i.e. low Cl/Br ratios). The anomalously elevated Br^- was explained by meteoric

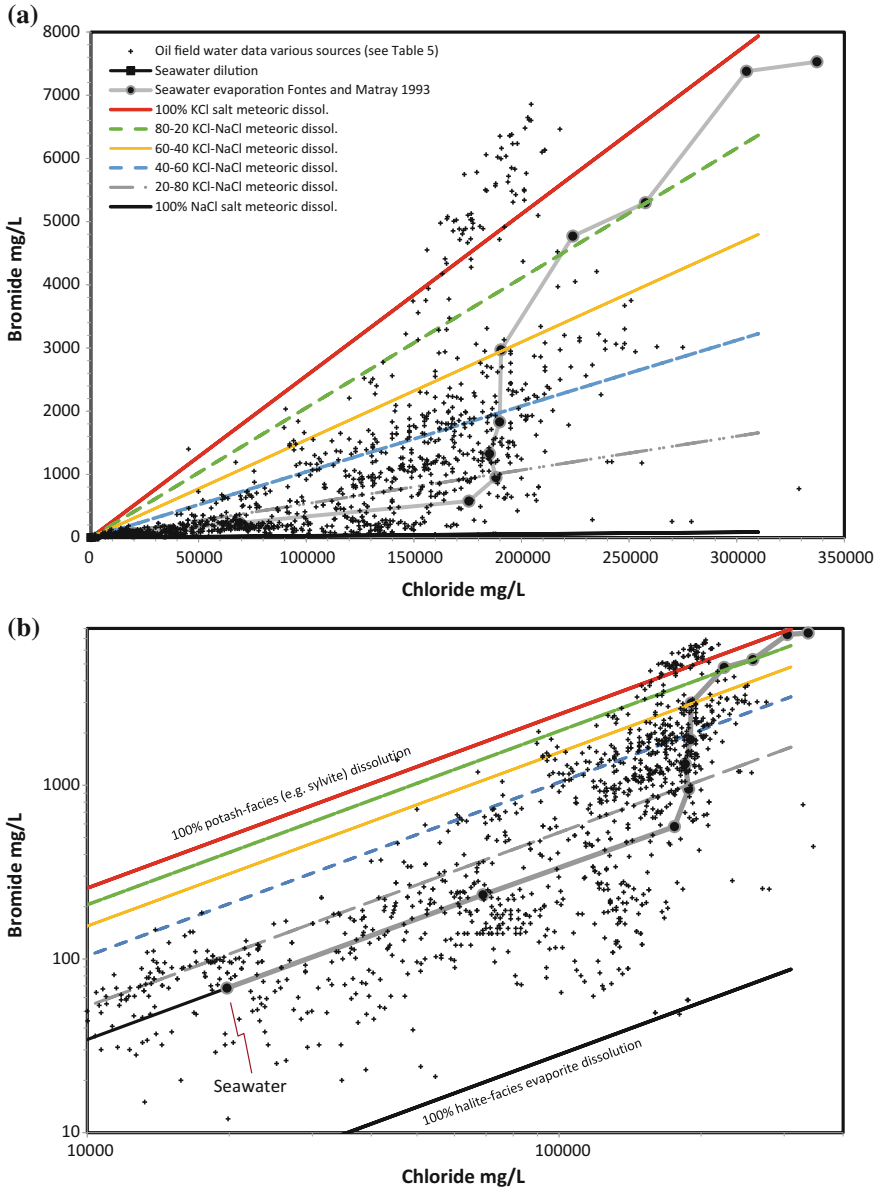

Fig. 4.17 (**a**) More than 1100 Cl^--Br^- concentration data points taken from 36 publications from various global basins (Table 4.5). These data have been overlaid with seawater evaporation and dilution trends and the trends for sylvite and halite dissolution by meteoric water (and various mixtures between pure sylvite and pure halite) (see Fig. 4.12 for details). (**b**) Same dataset and modelled trends as part a but plotted on a log plot

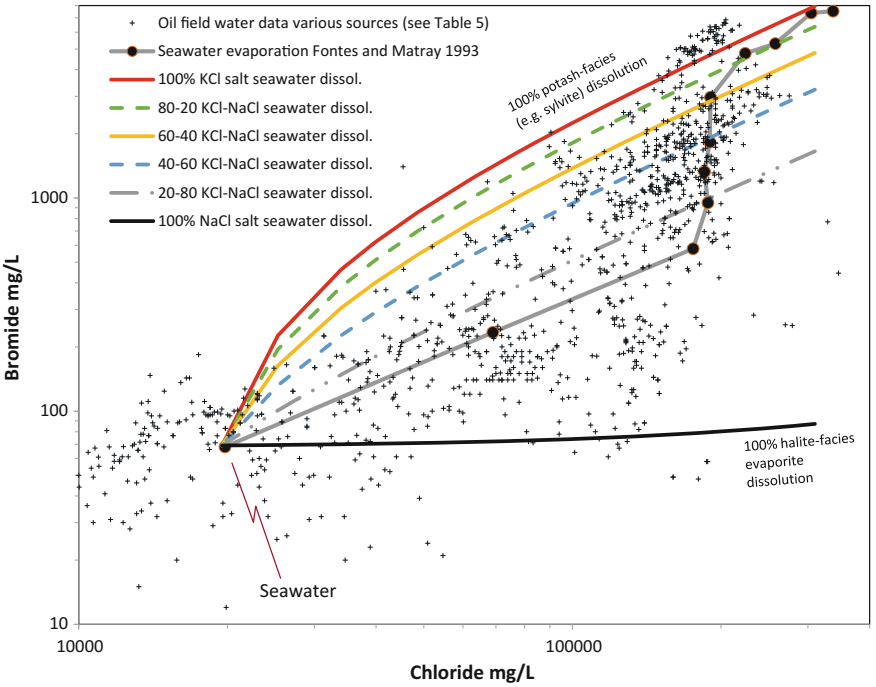

Fig. 4.18 Same dataset and plot as Fig. 4.17b but overlaid with seawater evaporation and dilution trends and trends representing the dissolution of sylvite and halite by seawater (as opposed to meteoric water in Fig. 4.17b). Mass dissolution of evaporites by seawater is less likely than by meteoric water given there are issues about allowing mass movement of seawater via downward percolation under a hydraulic potential

water dilution of seawater evaporated to well beyond the point of halite precipitation, which thus acquired reduced Cl/Br ratios at lower salinity than found in brines. Rittenhouse (1967) also assessed typical Br^--salinity relations for formation waters that had dissolved halite and concluded they would be Br^- poor. Notably, this study failed to assess the effect of the dissolution of Br-rich, potash-bearing evaporites, which could also lead to Br^--rich formation waters (Fig. 4.12). Subsequent studies of oil field waters typically followed the lead offered by Rittenhouse (1967) and interpreted water composition in terms of variable seawater evaporation and subsequent dilution of variably evaporated seawater by meteoric water (Collins 1969). Some early studies suggested that Br^- may be non-conservative and suggested addition from organic sources (Hitchon et al. 1971). Many studies of sedimentary formation waters have henceforth tended to use the approach adopted by Rittenhouse (1967). These compare Cl/Br formation water data to seawater evaporation patterns. They have tended to assume that higher salinity waters with low Cl/Br ratios must be due to dilution of highly evaporated residual seawater. Although formation waters in oil fields may be highly concentrated residual brines following extreme seawater evaporation, studies that ignore

the effects of potash-bearing salts on evaporite dissolution, and the range of potentially non-conservative influences on Br^- concentration in formation waters (see Sect. 4.4.11), run the risk of obtaining a misleading interpretation regarding both the origin of the water and fluid dynamics.

Following the early lead offered by Rittenhouse (1967), relatively saline formation water samples that sit on or near to the seawater evaporation curve have routinely been ascribed to evaporated seawater. The formation water in such reservoirs has been interpreted to be the remnants of the seawater from which the source evaporite was originally precipitated. This is the most common interpretation for high salinity formation waters with high Cl^- and high Br^- concentrations. Examples of this include the Palaeozoic reservoirs in the Illinois Basin (Walter et al. 1990), Jurassic reservoirs in the Gulf of Mexico Basin (Moldovanyi and Walter 1992), and Permian reservoirs from the Arabian Basin (Birkle et al. 2013). A seawater evaporation curve has been superimposed on the >1100 formation water data points (Table 4.5) to reveal the degree of coincidence (Fig. 4.17). The data have been plotted in linear and log format (Fig. 4.17a, b). There is little agreement in detail between the evaporation curve and the formation water data but high Br^- concentrations need to be explained.

4.6.1.4 Consideration of Other Processes that Can Influence Cl^- and Br^- Concentrations

Taking an overview of the wide range of processes capable of influencing halide concentrations in formation waters, it is reasonable to conclude that Cl^- and Br^- concentrations elevated beyond seawater values have a number of possible origins including: (1) influx of evaporated seawater (Fig. 4.6) (Fontes and Matray 1993a; Collins 1969; Carpenter 1978; McCaffrey et al. 1987); (2) hydration reactions leaving behind a more concentrated solution as the remaining formation water (Fig. 4.4) (Martin 1999); (3) influx of evaporated continental waters in arid environments (Fig. 4.10) (Risacher et al. 2006); (4) influx of water that has dissolved either Br-poor halite or Br-rich K salts (Fig. 4.12) (Krupp 2005; Kloppmann et al. 2001); and (5) diffusion or membrane filtration (Fig. 4.14) (Bensenouci et al. 2014; Kharaka and Berry 1973).

Formation water Cl^--Br^- concentration data have been compared here with patterns expected not only for seawater evaporation and seawater dilution by meteoric water, but also taking into account the results of the dissolution of Br-poor halite and Br-rich KCl (and other extreme evaporite minerals) by meteoric water. While most sedimentary rocks are deposited in marine basins, it is noteworthy that rather few oil or gas field formation waters lie at or near seawater Cl-Br concentrations (Fig. 4.17). Many formation waters have a meteoric water origin due to the influx of groundwater deep into sedimentary successions at times of low base level although the effect of meteoric invasion is muted in young (i.e. Pliocene or Miocene) basins where there is a lack of time for influx of water to occur.

4.6.1.5 Formation Waters that Are Residual Brines Following Seawater Evaporation Versus Brines that Result from Evaporite Dissolution

Pristine seawater has a density of 1.024 g/cm^3. Highly evaporated seawater has a relatively high density. For example at the start of halite growth, the brine has a density of about 1.204 g/cm^3. Later, at the start of sylvite growth, the brine has a density of 1.290 g/cm^3 (McCaffrey et al. 1987; Fontes and Matray 1993a). Such high density fluids may be liable to downward percolation through porous sediments. However, there are some abiding problems with using evaporated seawater residue to explain formation waters with high Cl^- and Br^- concentrations. (1) There is relatively little seawater remaining after evaporation. By the start of halite growth, more than 90% of the initial seawater volume has been lost, and towards the later stages of halite growth, 97% has been lost. By the time sylvite starts to grow, at the latest stages of evaporation of highly Br-enriched marine brines, there is less than 2% of the volume of the initial seawater remaining. (2) Evaporites have a very low porosity with the bulk densities of halite-dominated evaporitic rocks typically having the density of halite (i.e. there is negligible porosity). This means there can only ever be a trivial amount of water stored within evaporites. (3) Evaporites are low permeability lithologies in the subsurface; they make excellent caprocks to oil and gas accumulations. Their low permeability seems to make them rather unlikely to be effective at contributing large volumes of saline water into porous and permeability reservoir units. For example, the thick, low permeability evaporites in the Dead Sea have been reported to inhibit infiltration of the high density brines into the subsurface terrain (Klein BenDavid et al. 2004).

The Pliocene evaporites beneath the modern Dead Sea contain potash-bearing salts following periodic isolation of the Dead Sea rift from the Mediterranean and nearly total evaporation of seawater (García-Veigas et al. 2009). It is known that dissolution of potash-bearing salts results in Br^--enriched groundwater (Yechieli 2000) so it is possible that high salinity formation waters with high Cl^- and high Br^- concentrations may be the result of potash-bearing salt dissolution. The mixing lines modelled for KCl (a proxy for potash-bearing salts) dissolution by meteoric water and NaCl dissolution by meteoric water (and the dissolution of mixtures of NaCl and KCl; Fig. 4.12) have been superimposed on the oil and gas field formation water data (Fig. 4.17). Formation waters with low Cl/Br ratios and high Ca/(Ca + Na) indices have previously been reported to be the result of extreme seawater evaporation (Houston et al. 2011). However, it is significant that waters with elevated salinity, gained from the dissolution of potash-bearing salt evaporites, can also lead to high Cl/Br ratios and high Ca/(Ca + Na) ratios (Wittrup and Kyser 1990; García-Veigas et al. 2009). This suggests that cation ratios cannot necessarily be used to differentiate between residual evaporated seawater and waters from evaporite dissolution.

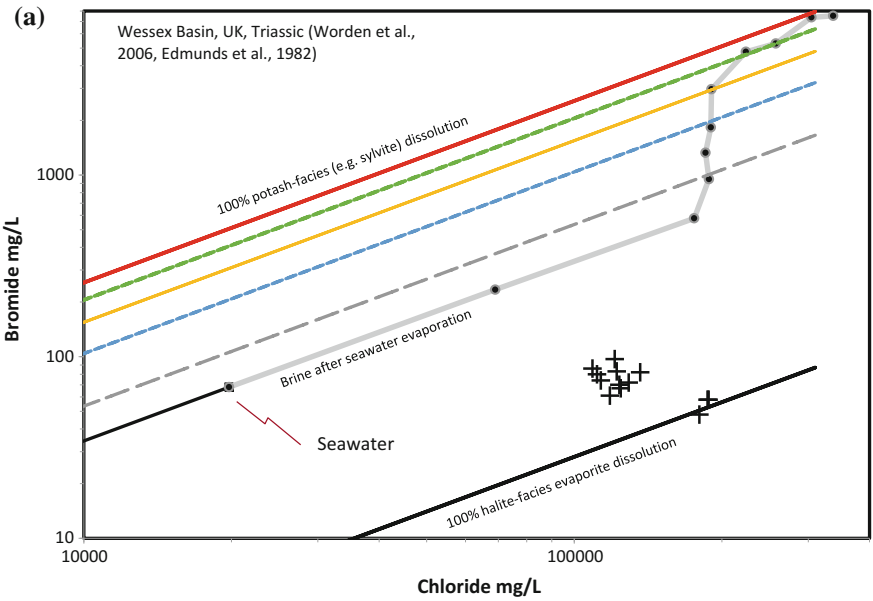
(a)
Wessex Basin, UK, Triassic (Worden et al., 2006, Edmunds et al., 1982)
100% potash-facies (e.g. sylvite) dissolution
Brine after seawater evaporation
Seawater
100% halite-facies evaporite dissolution
Bromide mg/L
Chloride mg/L
1000
100
10
10000
100000

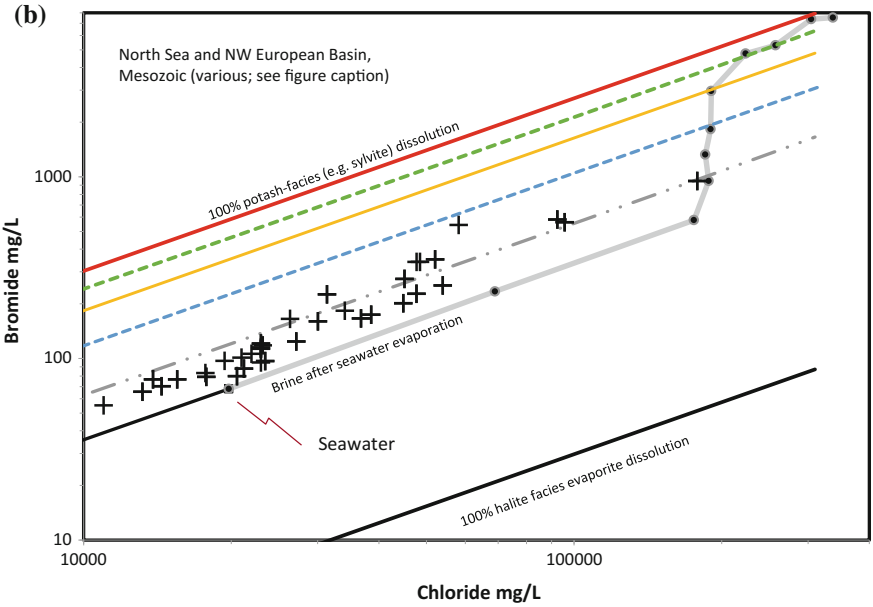
(b)
North Sea and NW European Basin, Mesozoic (various; see figure caption)
100% potash-facies (e.g. sylvite) dissolution
Brine after seawater evaporation
Seawater
100% halite facies evaporite dissolution
Bromide mg/L
Chloride mg/L
1000
100
10
10000
100000

◂**Fig. 4.19** (**a**) Water compositional data from the Wessex Basin, United Kingdom (Worden et al. 2006; Edmunds et al. 1982). The Triassic evaporites in the Wessex Basin are halite-rich, continental evaporites with no sylvite or other signs of extreme marine evaporation. (**b**) Water compositional data from the North Sea Basin with the main evaporite being the sylvite-bearing Permian Zechstein (Egeberg and Aagaard 1989; Ziegler et al. 2001; Warren and Smalley 1994). The North Sea data can be explained by a combination of seawater dilution by meteoric water and one or more of (i) meteoric dissolution of halite-dominated evaporites that contain 20% sylvite (or other Br-rich potash salts), (ii) the formation waters represent the remnants of evaporatively concentrated seawater, (iii) concentration by diagenetic hydration reactions (Fig. 4.4) with either addition of Br- from organic sources (Fig. 4.13) or preferential incorporation of Cl in neoformed clay minerals. See Figs. 4.12 and 4.17 for a definition of the modelled trends

4.6.1.6 Examples from NW European Sedimentary Basins

In NW Europe, there are two main evaporite deposits: the potash-bearing, halite-dominated Permian Zechstein and the potash-free, halite-dominated Triassic Mercia evaporites. Triassic formation waters in the Wessex Basin, UK, are saline with high Cl^- and low Br^- concentrations (Fig. 4.19a). These waters have their salinity derived from the dissolution of the continental Mercia evaporites, which contain no sylvite, bischofite, or other potash-facies evaporites characteristic of advanced seawater evaporation, thus explaining the low Br^- concentrations. The Mercia halite must have only 2–5 ppm Br to have resulted in such low Br^- concentrations in the resulting water (Stoessell and Carpenter 1986).

In contrast, the Permian and Mesozoic formation waters from the North Sea basin range in Cl^- concentration from 12 000 to 200 000 mg/L (Fig. 4.19b). The lowest Cl^- concentrations are found in parts of the basin where there is an absence of Zechstein evaporites and the Cl-Br relationship appears to be the result of seawater dilution by meteoric water. The higher Cl^- and Br^- concentrations sit above the seawater evaporation trend. This could be due to the non-conservative addition of Br, e.g., from the breakdown of organic matter (Fig. 4.13a) (Martin et al. 1993; Fehn et al. 2007), which alters the sea water evaporation trajectory. However, this pattern could also be interpreted in terms of the dissolution of potash-bearing evaporites by meteoric water or even by seawater (Figs. 4.12 and 4.18). The Zechstein evaporites would need to contain ~80% halite and ~20% potash-bearing halides. This is not unreasonable since the Zechstein evaporites are known to be potash-bearing (Bottrell et al. 1996; Krupp 2005). Note that it is also possible that hydration reactions (e.g., by anhydrous minerals, such as feldspar, undergoing alteration to clay minerals, Fig. 4.4) could account for some of the increase of Cl^- and Br^- concentrations in the North Sea formation waters.

4.6.1.7 Examples of Relatively Low Concentration Cl^- and Br^- Formation Waters

Two examples of high Cl^--low Br^- concentration formation waters come from the Gulf of Mexico Basin and the Illinois Basin, USA (Fig. 4.20a, b). These

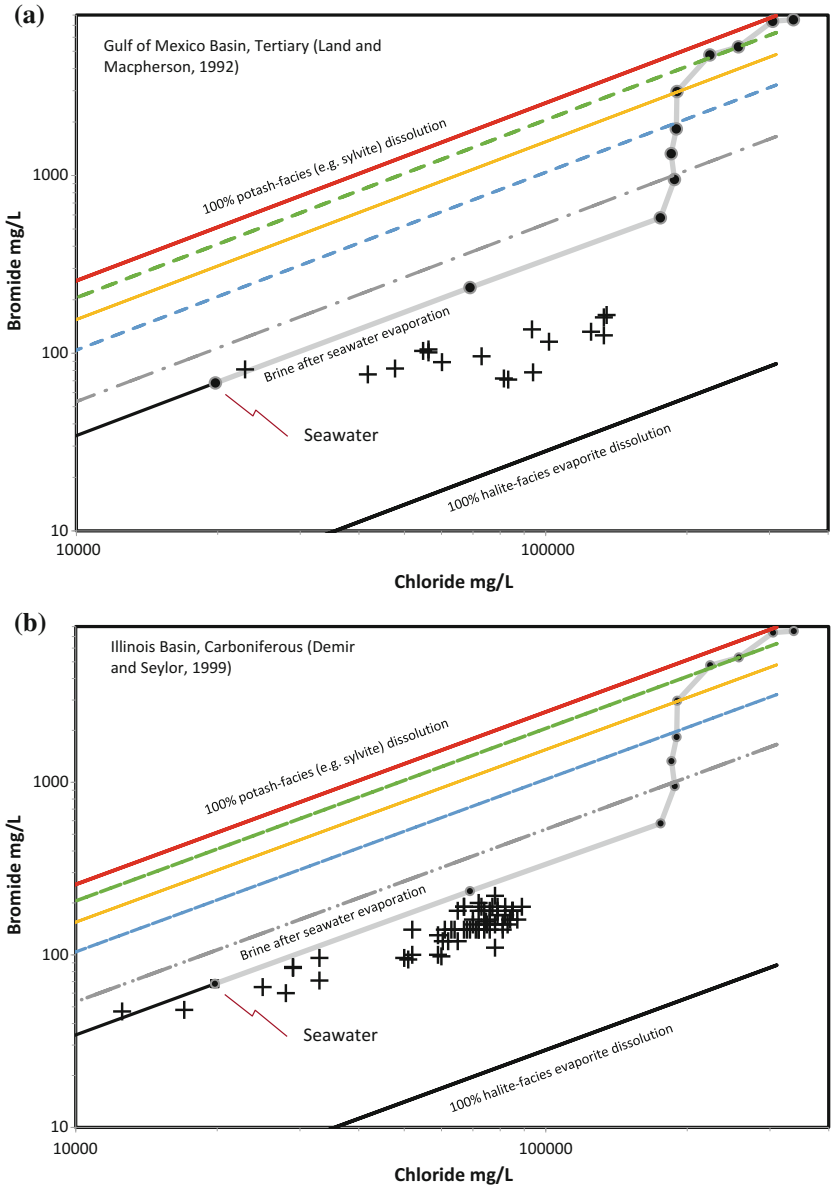

Fig. 4.20 (**a**) Water compositional data from the Tertiary of the Gulf of Mexico Basin, USA (Land and Macpherson 1992) with the Cl^-/Br^- ratio suggesting an evaporite-dissolution source (from evaporites with >90% halite and <10% Br-rich potash salts such as sylvite. (**b**) Water compositional data from the Carboniferous of the Illinois Basin, USA (Demir and Seylor 1999). The formation water track is below the seawater evaporation curve but seems more likely to be the result of dissolution of evaporites with ~90% halite and ~10% sylvite. See Figs. 4.12 and 4.17 for a definition of modelled trends

waters have a range of Cl^- concentrations approaching values as low as those characteristic of seawater but also extending to values in excess of 100 000 mg/L, all with relatively low Br^- concentrations. These waters can be explained by the progressive dissolution of halite-dominated evaporites. Halite dissolution patterns, resulting from regional groundwater flow in the Gulf Coast, have been mapped out in three dimensions (Hanor 1994), thus confirming that datasets, such as that displayed in Fig. 4.20a, are due to low potash-bearing salt dissolution.

4.6.1.8 Examples of Relatively High Concentration Br- Formation Waters

Two further examples of datasets with high Br^- concentrations come from the Mississippi and Michigan Basins, USA (Fig. 4.21a, b). These high-Br waters all have high Cl^- concentrations. The high Br^- and Cl^- concentrations in these oil field formation waters could be the result of (i) extreme seawater evaporation, especially since the Michigan Basin data lie roughly on the evaporative concentration trend, or (ii) dissolution of evaporites with roughly 50–50 potash-bearing salts and halite. It is also possible that the saline waters could be a mixture of both mechanisms, i.e. a combination of Br-enriched, potash-bearing salt dissolution and the liberation of residual, highly evaporated seawater with high Br-concentrations due to the exclusion of Br from halite. Mixed halite-potash-bearing salt dissolution in low salinity water (meteoric or even sea water) can produce a full spectrum of Cl^- and Br^- concentrations from oil and gas field formation waters (Fig. 4.17).

4.6.2 Oil and Gas Field Water Cl^--I^- and Br^--I^- Concentrations

The collation of 492 I^- concentration data points from oil and gas fields, compared with either Cl^- or Br^- concentration data, shows that oil and gas field formation waters are highly enriched in I^- relative to seawater evaporation (Fig. 4.22, Table 4.5). The lack of any correlation between I^- and either Cl^- or Br^- suggests that evaporites have little role in controlling the concentration of I^- in formation waters. There is no relationship between reservoir age and I^- concentration (Worden 1996).

Elevated I^- concentrations have long been associated with the release of I from organic rich rocks (Collins et al. 1971) and the obvious source of the extra I in

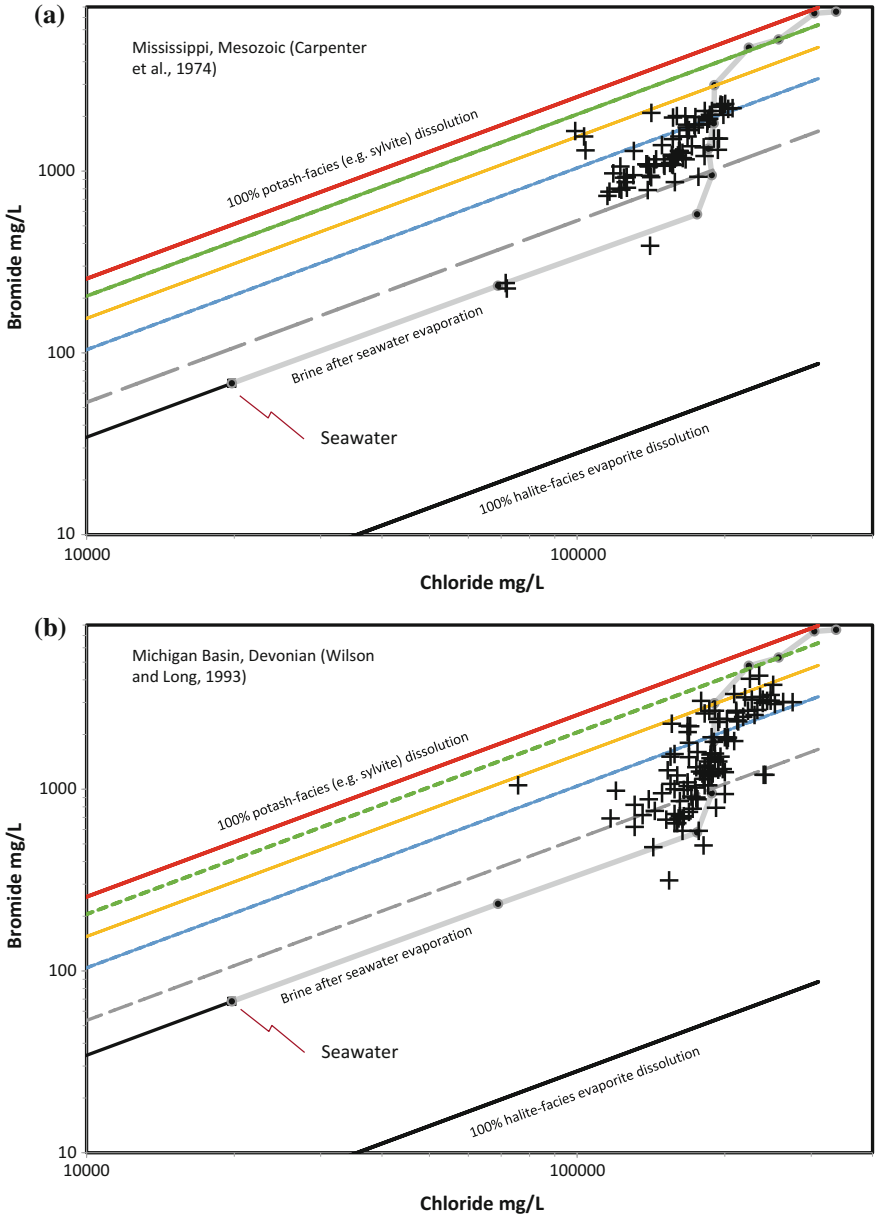

Fig. 4.21 (**a**) Water compositional data from Jurassic and Cretaceous reservoirs from the Mississippi Basin (Carpenter et al. 1974). These waters could be the brine residue of advanced evaporite formation, perhaps mixed with meteoric water, or they could be the result of meteoric dissolution of evaporites with roughly 50–50 sylvite and halite. (**b**) Water compositional data from the Devonian reservoirs of the Michigan Basin (Wilson and Long 1993b). These waters have extremely high Br^- concentrations that could be the bulk residue of extreme seawater evaporation (i.e. when <2% of the original water volume remained), or they could be the result of meteoric dissolution of sylvite-rich evaporites (or dissolution of other late stage, Br-rich evaporite minerals). See Figs. 4.12 and 4.17 for a definition of modelled trends

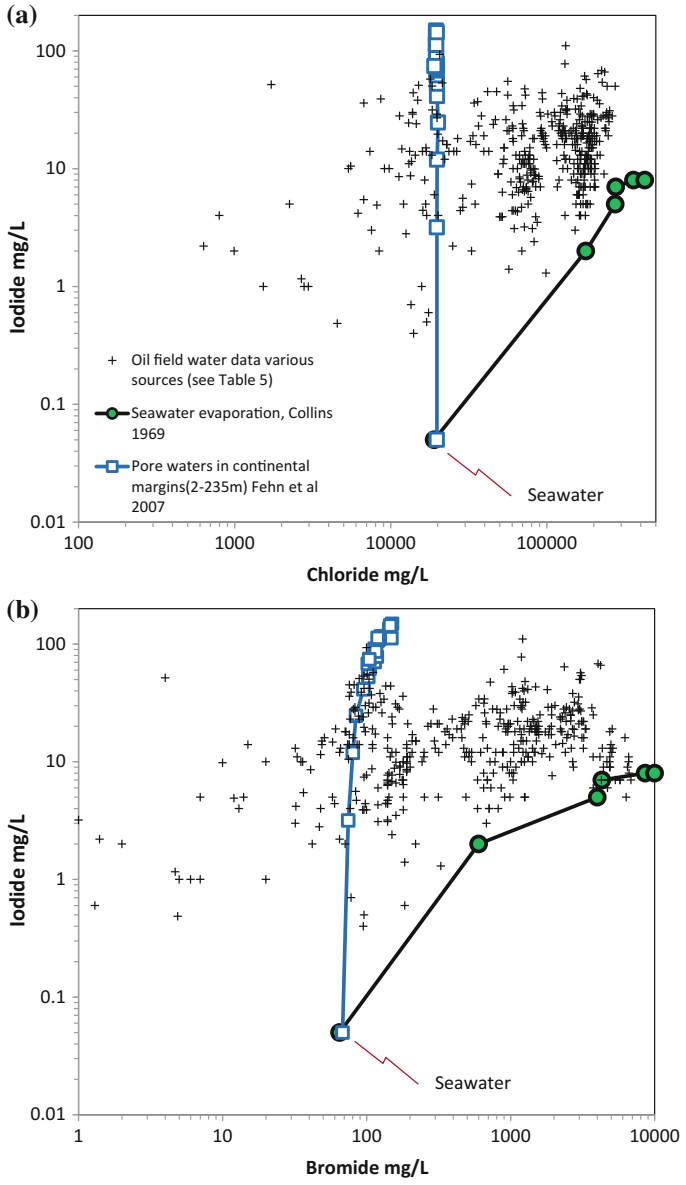

Fig. 4.22 (**a**) Chloride-I^- concentration data from oil and gas fields (492 data points) taken from 36 publications from various global basins (Table 4.5). These data have been overlaid with a seawater evaporation trend (Fig. 4.6) (Collins 1969). The plot also has pore water compositions from moderately buried organic-rich sediments showing I^- enrichment due to release of I from altered organic matter (Fehn et al. 2007). (**b**) Same data plotted as Br^--I^- concentrations. All oil and gas field formation waters contain higher I^- concentrations than can be accounted for by evaporation. Input of I from organic-rich sediment is normal showing that I is not a conservative element in formation waters associated with sedimentary basins

formation waters is the breakdown of organic matter (especially algae) in source rocks (Fehn et al. 2007). The maximum reported I^- concentration in oil field waters in this dataset is 110 mg/L with an average of 19 mg/L for the 480 reported analyses. It is noteworthy that formation waters, in general, represent some of the greatest accumulations of I on Earth. This is due to its initial fractionation into organic matter (coal, algae, bacteria) at the time of deposition and then its release from organic matter into the aqueous phase during burial and diagenetic alteration.

4.6.3 Oil and Gas Field Water Cl^--F^- Concentrations

Fluoride concentrations in oil field formation waters are rarely reported since they are never the dominant anion and are not typically found to be a problem for scale precipitation, produced water disposal, or toxicity. For >1100 paired Cl^- and Br^- analyses, there are only 88 F^- concentration values reported in the 36 datasets listed in Table 4.5. The maximum F^- concentration in the dataset is 22 mg/L. The derived average from these 32 datasets is 10 mg/L but that is probably skewed to an unrealistically high value by the exclusion of the majority of samples that have F^- below detection and are thus not reported.

Chloride-F^- concentration data from oil field formation waters seem to show that the highest F^- concentrations, those >10 mg/L, are only found in waters with Cl^- concentrations >100 000 mg/L (Fig. 4.23). However, F^- can approach 10 mg/L in shallow groundwaters that are alkaline, low salinity (at least relative to oil field formation waters), with low Ca concentrations, and that have interacted with F-rich bedrock such as gneiss or basalt (Yoshida et al. 1971). Fluoride concentrations seldom seem to exceed 10 mg/L in any natural waters, shallow or deep. Key questions are why F^- concentrations are so much lower than all other halides and why are elevated F^- concentrations found in high Cl^- concentration formation waters?

Unlike the other halogens, F^- concentrations are controlled by phosphate and silicate minerals and by the low solubility of fluorite (CaF_2). Apatite can have its hydroxyl groups replaced by F^- (creating fluorapatite, Table 4.2) since hydroxyl and F^- ions have a similar size and the same charge. Fluoride can also substitute for hydroxyl in clay minerals such as kaolinite or smectite (Table 4.2) (Chipera and Bish 2002). Phosphates and clay minerals are ubiquitous throughout sedimentary successions and so are the most likely causes of low F^- concentrations in formation waters. Growth of small quantities of fluorite at temperatures >80 °C is not uncommon during diagenesis, especially in carbonate host rocks (Neilson and Oxtoby 2008; Cai et al. 2008; Jiang et al. 2014; Videtich 1994). Fluorite is typically

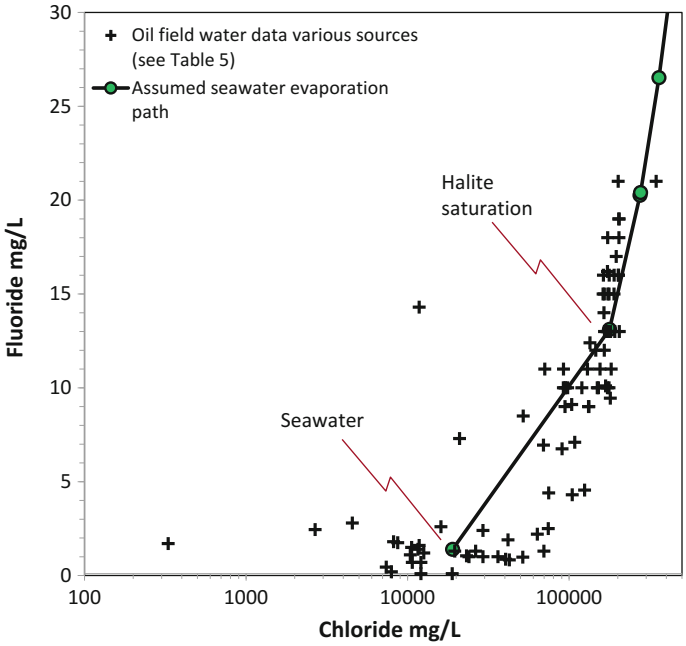

Fig. 4.23 The sum total of all Cl^{-}-F^{-} concentration data (88 data points) taken from 36 publications from various global basins (Table 4.5). These data have been overlaid with a speculative seawater evaporation trend based on assumed proportional increase of F^{-} and Cl^{-}. High F^{-} concentrations (>10 mg/L) are only found in formation waters with Cl^{-} concentration >100 000 mg/L

present as a trace mineral in faulted and fractured carbonate host rocks. Fluorite is typically associated with the common occurrence of minerals such as barite and metal sulphides (Neilson and Oxtoby 2008). This association suggests that there is a possible role for hydrothermal input of F^{-} from one or more of the following sources: basement rocks, cooling intrusions, or from hot deeper parts of the basin. However, large scale input of mineralizing fluids from basement or deep crustal sources into sedimentary formation waters seems to be unlikely given that metamorphism leads to relatively dry rocks. In general, fluid movement is more likely to be in the opposite direction, i.e. from sedimentary into crustal rocks (Yardley et al. 2000). The precise source of the F in diagenetic fluorite is unclear but it could be derived from the diagenetic alteration of fluorapatite (Neilson and Oxtoby 2008) or from clay minerals (Hitchon 1995) much deeper in the succession where diagenesis has led to clay mineral dehydration reactions.

4.7 Conclusions

1. Following weathering, F remains in sedimentary minerals, most likely in apatite or clay minerals, and is strongly depleted in all surface waters, evaporites, organic rich sediments, and oil and gas field formation water.
2. Chlorine and Br have broadly similar distributions following weathering. They are much depleted in all sedimentary minerals except in halite, sylvite and other K-Mg evaporite minerals where they tend to be enriched. Chlorine and Br are also strongly enriched in formation waters.
3. Iodine is moderately enriched in most sedimentary minerals and materials but is especially concentrated in organic-rich sediment. Iodine is also highly enriched in most sedimentary formation waters.
4. Chloride is broadly assumed to be a conservative element in sedimentary systems unless the water is saturated with halite or if low salinity water comes into contact with evaporites.
5. Processes that increase Cl^- concentration in formation waters include: feldspar hydration reactions in the sediment column, seawater and continental water evaporation, seawater freezing, evaporite dissolution, and membrane filtration (diffusion) through low permeability rocks.
6. Processes that decrease Cl^- concentration in formation waters include dehydration reactions, such as kerogen breakdown and smectite transformation to illite; seawater and formation water dilution by meteoric water; and saline water dilution by connate seawater expelled from compacting mudstones.
7. Bromide concentrations in formation waters have controls that are broadly similar to that of Cl^-, but there are circumstances under which Br^- may not be a wholly conservative element relative to Cl^-. This includes Br adsorption by clay minerals during hydration reactions; minor addition of Br derived from the breakdown of Br-bearing organic matter; loss of Br- in continental evaporites to the atmosphere; dissolution of Br-poor halite; dissolution of Br-enriched, potash-bearing salts; and membrane filtration.
8. Chlorine isotopes in evaporites are mostly at, or fractionally greater than, 0‰ although non-marine evaporites may have slightly higher $\delta^{37}Cl$ values due to the input of Cl from weathered silicate minerals. Formation waters tend to have very slightly more negative $\delta^{37}Cl$ values than evaporites. Formation water $\delta^{37}Cl$ values are influenced by: primary seawater evaporation; evaporite congruent versus incongruent dissolution; input of isotopically heavy Cl^- from altered silicates; and diffusional fractionation. The interpretation of formation water $\delta^{37}Cl$ values is not straightforward but can be used to help refine interpretations of the origin and evolution of formation water and solutes in some circumstances.
9. The study of Br isotopes is still in its infancy. The geochemical similarity between Br and Cl suggests that they should be subject to the same geochemical influences. This is supported by some studies showing positive

correlations between $\delta^{37}Cl$ and $\delta^{81}Br$. However, other studies have revealed inverse trends. More work is needed to be able to interpret $\delta^{81}Br$ in formation waters and evaporites.

10. Oil and gas field waters display a huge range of Cl^- and Br^- concentrations that can be explained largely by a combination of seawater evaporation, seawater dilution, halite-dissolution by meteoric water and dissolution of potash-bearing salts by meteoric water. The role of residual seawater after extreme evaporation has been emphasised in previous studies. The role of the dissolution of mixed halite-potash-bearing salts evaporites hitherto may not have been fully appreciated.
11. Oil and gas field waters have ubiquitously elevated I^- concentrations that are best explained by the mass input of I following the diagenetic decay of I-rich organic-rich sedimentary rocks.
12. Fluoride concentrations in oil and gas field waters are generally low (≤ 25 mg/L) with concentrations limited by F-uptake in minerals such as fluorapatite and F-bearing clays in which hydroxyl ions are replaced by F^-.

Acknowledgements I would like to thank reviewers Bruce Yardley, Jeff Hanor and Ross McCartney for their uniformly thoughtful and positive comments; they led to many significant improvements and additions to the paper. I would also like to thank Dan Harlov for his support, encouragement, constructive input, and the elastic timetable for preparation and revision of this paper.

References

Aiuppa A, Baker DR, Webster JD (2009) Halogens in volcanic systems. Chem Geol 263(1–4): 1–18. https://doi.org/10.1016/j.chemgeo.2008.10.005

Al TA, Clark ID, Kennell L, Jensen M, Raven KG (2015) Geochemical evolution and residence time of porewater in low-permeability rocks of the Michigan Basin, Southwest Ontario. Chem Geol 404:1–17. https://doi.org/10.1016/j.chemgeo.2015.03.005

Alcala FJ, Custodio E (2008) Using the Cl/Br ratio as a tracer to identify the origin of salinity in aquifers in Spain and Portugal. J Hydrol 359(1–2):189–207. https://doi.org/10.1016/j.jhydrol.2008.06.028

Alexeeva LP, Alexeev SV, Kononov AM, Teng M, Yunde L (2015) Halogen isotopes (Cl-37 and Br-81) in brines of the Siberian Platform. In: Millot R, Negrel P (eds) 11th Applied isotope geochemistry conference: AIG-11, vol 13. Procedia earth and planetary science. pp 47–51. https://doi.org/10.1016/j.proeps.2015.07.011

Alvarez F, Reich M, Perez-Fodich A, Snyder G, Muramatsu Y, Vargas G, Fehn U (2015) Sources, sinks and long-term cycling of iodine in the hyperarid Atacama continental margin. Geochim Cosmochim Acta 161:50–70. https://doi.org/10.1016/j.gca.2015.03.032

Arakel AV (1986) Evolution of calcrete in paleodrainages of the Lake Napperby area, central Australia. Palaeogeogr Palaeoclimatol Palaeoecol 54(1–4):283–303. https://doi.org/10.1016/0031-0182(86)90129-x

Arakel AV, Moulton T (1986) Hydrochemistry of surficial brines in Hutt Lagoon Western Australia. Palaeogeogr Palaeoclimatol Palaeoecol 54(1–4):261–282. https://doi.org/10.1016/0031-0182(86)90128-8

Arakel AV, Ridley WF (1986) Origin and geochemical evolution of saline groundwater in the Brisbane coastal plain, Australia. Catena 13(3):257–275. https://doi.org/10.1016/0341-8162(86)90002-0

Armitage PJ, Worden RH, Faulkner DR, Aplin AC, Butcher AR, Espie AA (2013) Mercia Mudstone Formation caprock to carbon capture and storage sites: petrology and petrophysical characteristics. J Geol Soc 170(1):119–132. https://doi.org/10.1144/jgs2012-049

Armitage PJ, Worden RH, Faulkner DR, Butcher AR, Espie AA (2016) Permeability of the Mercia Mudstone: suitability as caprock to carbon capture and storage sites. Geofluids 16(1):26–42. https://doi.org/10.1111/gfl.12134

Bagheri R, Nadri A, Raeisi E, Shariati A, Mirbagheri M, Bahadori F (2014) Chemical evolution of a gas-capped deep aquifer, southwest of Iran. Environ Earth Sci 71(7):3171–3180. https://doi.org/10.1007/s12665-013-2705-4

Barker AP, Newton RJ, Bottrell SH, Tellam JH (1998) Processes affecting groundwater chemistry in a zone of saline intrusion into an urban sandstone aquifer. Appl Geochem 13(6):735–749. https://doi.org/10.1016/s0883-2927(98)00006-7

Barnard WR, Nordstrom DK (1982) Fluoride in precipitation 2. implications for the geochemical cycling of fluorine. Atmos Environ 16(1):105–111. https://doi.org/10.1016/0004-6981(82)90317-1

Bellomo S, D'Alessandro W, Longo M (2003) Volcanogenic fluorine in rainwater around active degassing volcanoes: Mt. Etna and Stromboli Island, Italy. Sci Total Environ 301(1–3):175–185. https://doi.org/10.1016/s0048-9697(02)00284-x

Bensenouci F, Michelot JL, Matray JM, Savoye S, Massault M, Vinsot A (2014) Coupled study of water-stable isotopes and anions in porewater for characterizing aqueous transport through the Mesozoic sedimentary series in the eastern Paris Basin. Mar Petrol Geol 53:88–101. https://doi.org/10.1016/j.marpetgeo.2013.12.012

Berner EK, Berner RA (2012) Global environment: water, air and geochemical cycles, 2nd edn. Princeton University Press, Princeton

Biester H, Selimovic D, Hemmerich S, Petri M (2006) Halogens in pore water of peat bogs—the role of peat decomposition and dissolved organic matter. Biogeosciences 3(1):53–64

Birkle P, Aragon JJR, Portugal E, Aguilar JLF (2002) Evolution and origin of deep reservoir water at the Activo Luna oil field, Gulf of Mexico, Mexico. Am Assoc Petrol Geol Bull 86(3):457–484

Birkle P, Martinez Garcia B, Milland Padron CM (2009) Origin and evolution of formation water at the Jujo-Tecominoacan oil reservoir, Gulf of Mexico. Part 1: chemical evolution and water-rock interaction. Appl Geochem 24(4):543–554. https://doi.org/10.1016/j.apgeochem.2008.12.009

Birkle P, Jenden PD, Al-Dubaisi JM (2013) Origin of formation water from the Unayzah and Khuff petroleum reservoirs, Saudi Arabia. In: Hellmann R, Pitsch H (eds) Proceedings of the fourteenth international symposium on water-rock interaction: WRI 14, vol 7. Procedia earth and plantetary science, pp 77–80. https://doi.org/10.1016/j.proeps.2013.03.214

Bottomley DJ, Katz A, Chan LH, Starinsky A, Douglas M, Clark ID, Raven KG (1999) The origin and evolution of Canadian Shield brines: evaporation or freezing of seawater? New lithium isotope and geochemical evidence from the Slave craton. Chem Geol 155(3–4):295–320. https://doi.org/10.1016/s0009-2541(98)00166-1

Bottrell SH, Leosson MA, Newton RJ (1996) Origin of brine inflows at Boulby potash mine, Cleveland, England. Trans Inst Min Metall Sect B Appl Earth Sci 105:B159–B164

Bureau H, Metrich N (2003) An experimental study of bromine behaviour in water-saturated silicic melts. Geochim Cosmochim Acta 67(9):1689–1697. https://doi.org/10.1016/s0016-7037(02)01339-x

Bureau H, Keppler H, Metrich N (2000) Volcanic degassing of bromine and iodine: experimental fluid/melt partitioning data and applications to stratospheric chemistry. Earth Planet Sci Lett 183(1–2):51–60. https://doi.org/10.1016/s0012-821x(00)00258-2

Cabral AR, Radtke M, Munnik F, Lehmann B, Reinholz U, Riesemeier H, Tupinamba M, Kwitko-Ribeiro R (2011) Iodine in alluvial platinum-palladium nuggets: evidence for biogenic

precious-metal fixation. Chem Geol 281(1–2):125–132. https://doi.org/10.1016/j.chemgeo.2010.12.003
Cai CF, Franks SG, Aagaard P (2001) Origin and migration of brines from Paleozoic strata in Central Tarim, China: constraints from Sr-87/Sr-86, delta D, delta O-18 and water chemistry. Appl Geochem 16(9–10):1269–1284. https://doi.org/10.1016/s0883-2927(01)00006-3
Cai CF, Li KK, Li HT, Zhang BS (2008) Evidence for cross formational hot brine flow from integrated Sr-87/Sr-86, REE and fluid inclusions of the Ordovician veins in Central Tarim. China Appl Geochem 23(8):2226–2235. https://doi.org/10.1016/j.apgeochem.2008.03.009
Carpenter AB (1978) Origin and chemical evolution of brines in sedimentary basins. Oklahoma Geol Surv Circular 79:589–606
Carpenter AB, Trout ML (1978) Geochemistry of bromide-rich brines of the Dead Sea and Southern Arkansas. Oklahoma Geol Surv Circular 79:78–88
Carpenter AB, Trout ML, Pickett EE (1974) Preliminary report on origin and chemical evolution of lead-rich and zinc-rich oil field brines in Central Mississippi. Econ Geol 69(8):1191–1206
Chen J, Liu D, Peng P, Yu C, Zhang B, Xiao Z (2013) The sources and formation processes of brines from the Lunnan Ordovician paleokarst reservoir, Tarim Basin, northwest China. Geofluids 13(3):381–394. https://doi.org/10.1111/gfl.12033
Chen LZ, Ma T, Du Y, Yang J, Liu L, Shan HM, Liu CF, Cai HS (2014) Origin and evolution of formation water in North China Plain based on hydrochemistry and stable isotopes (H-2, O-18, Cl-37 and Br-81). J Geochem Explor 145:250–259. https://doi.org/10.1016/j.gexplo.2014.07.006
Chester R, Jickells TD (2012) Marine geochemistry, 3rd edn. Wiley-Blackwell, Oxford
Chipera SJ, Bish DL (2002) Thermal evolution of fluorine from smectite and kaolinite. Clays Clay Miner 50(1):38–46. https://doi.org/10.1346/000986002761002658
Clark ID, Al T, Jensen M, Kennell L, Mazurek M, Mohapatra R, Raven KG (2013) Paleozoic-aged brine and authigenic helium preserved in an Ordovician shale aquiclude. Geology 41(9):951–954. https://doi.org/10.1130/g34372.1
Collins AG (1969) Chemistry of some Anadarko Basin brines containing high concentrations of iodide. Chem Geol 4(1–2):169–187. https://doi.org/10.1016/0009-2541(69)90044-8
Collins AG, Bennett JH, Manuel OK (1971) Iodine and algae in sedimentary rocks associated with iodine-rich brines. Geol Soc Am Bull 82(9):2607. https://doi.org/10.1130/0016-7606(1971)82[2607:iaaisr]2.0.co;2
Connolly CA, Walter LM, Baadsgaard H, Longstaffe FJ (1990) Origin and evolution of formation waters, Alberta Basin, Western Canada Sedimentary Basin. 1. Chemistry. Appl Geochem 5(4):375–395. https://doi.org/10.1016/0883-2927(90)90016-x
Cosgrove ME (1970) Iodine in bituminous Kimmeridge shales of Dorset Coast, England. Geochim Cosmochim Acta 34(7):830–836. https://doi.org/10.1016/0016-7037(70)90033-5
Dasgupta PK, Martinelango PK, Jackson WA, Anderson TA, Tian K, Tock RW, Rajagopalan S (2005) The origin of naturally occurring perchlorate: the role of atmospheric processes. Environ Sci Technol 39(6):1569–1575. https://doi.org/10.1021/es048612x
Demir I, Seylor S (1999) Chemical composition and geologic history of saline waters in Aux Vases and Cypress Formations, Illinois Basin. Aquat Geochem 5:281–311
Desaulniers DE, Kaufmann RS, Cherry JA, Bentley HW (1986) 37Cl-35Cl variations in a diffusion-controlled groundwater system. Geochim Cosmochim Acta 50(8):1757–1764. https://doi.org/10.1016/0016-7037(86)90137-7
Dissanayake CB, Chandrajith R (1999) Medical geochemistry of tropical environments. Earth Sci Rev 47(3–4):219–258. https://doi.org/10.1016/s0012-8252(99)00033-1
Du Y, Ma T, Chen LZ, Shan HM, Xiao C, Lu Y, Liu CF, Cai HS (2015) Genesis of salinized groundwater in quaternary aquifer system of coastal plain, Laizhou Bay, China: geochemical evidences, especially from bromine stable isotope. Appl Geochem 59:155–165. https://doi.org/10.1016/j.apgeochem.2015.04.017
Duane MJ, Al-Zamel A, Eastoe CJ (2004) Stable isotope (chlorine, hydrogen and oxygen), geochemical and field evidence for continental fluid flow vectors in the Al-Khiran sabkha (Kuwait). J Afr Earth Sc 40(1–2):49–60. https://doi.org/10.1016/j.jafrearsci.2004.07.004

Eastoe CJ, Peryt T (1999) Stable chlorine isotope evidence for non-marine chloride in Badenian evaporites, Carpathian mountain region. Terra Nova 11(2–3):118–123. https://doi.org/10.1046/j.1365-3121.1999.00235.x

Eastoe CJ, Long A, Knauth LP (1999) Stable chlorine isotopes in the Palo Duro Basin, Texas: evidence for preservation of Permian evaporite brines. Geochim Cosmochim Acta 63(9):1375–1382. https://doi.org/10.1016/s0016-7037(99)00186-6

Eastoe CJ, Long A, Land LS, Kyle JR (2001) Stable chlorine isotopes in halite and brine from the Gulf Coast Basin: brine genesis and evolution. Chem Geol 176(1–4):343–360. https://doi.org/10.1016/s0009-2541(00)00374-0

Eastoe CJ, Peryt TM, Petrychenko OY, Geisler-Cussey D (2007) Stable chlorine isotopes in Phanerozoic evaporites. Appl Geochem 22(3):575–588. https://doi.org/10.1016/j.apgeochem.2006.12.012

Edmunds WM (1996) Bromine geochemistry of British groundwaters. Mineral Mag 60(399):275–284. https://doi.org/10.1180/minmag.1996.060.399.03

Edmunds WM, Smedley PL (2013) Fluoride in natural waters. In: Selinius O, Alloway B, Ceneno JA et al (eds) Essentials of medical geology, Revised edn. Springer, Dordrecht, pp 311–336

Edmunds WM, Bath AH, Miles DL (1982) Pore fluid geochemistry of the Bridport Sands (Lower Jurassic) and the Sherwood Sandstone (Triassic) intervals of the Winterborne Kingston borehole, Dorset. In: Rhys GH, Lott G, Calver MA (eds) The Winterborne Kingston borehole, Dorset, England, vol 81/3. Institute of Geological Sciences, pp 149–163

Egeberg PK, Aagaard P (1989) Origin and evolution of formation waters from oil fields on the Norwegian Shelf. Appl Geochem 4:131–142

Eggenkamp HGM (2015) Comment on "Stable isotope fractionation of chlorine during the precipitation of single chloride minerals" by Luo, C.-g., Xiao, Y.-k., Wen, H.-j., Ma, H.-z., Ma, Y.-q., Zhang, Y.-l., Zhang, Y.-x. and He, M.-y. [Applied Geochemistry 47 (2014) 141–149]. Appl Geochem 54:111–116. https://doi.org/10.1016/j.apgeochem.2014.11.018

Eggenkamp HGM, Coleman ML (1998) Heterogeneity of formation waters within and between oil fields by halogen isotopes. Water-Rock Interact 9:309–312

Eggenkamp HGM, Coleman ML (2000) Rediscovery of classical methods and their application to the measurement of stable bromine isotopes in natural samples. Chem Geol 167(3–4):393–402. https://doi.org/10.1016/s0009-2541(99)00234-x

Eggenkamp HGM, Coleman ML (2009) The effect of aqueous diffusion on the fractionation of chlorine and bromine stable isotopes. Geochim Cosmochim Acta 73(12):3539–3548. https://doi.org/10.1016/j.gca.2009.03.036

Eggenkamp HGM, Kreulen R, Groos AFK van (1995) Chlorine stable isotope fractionation in evaporites. Geochim Cosmochim Acta 59(24):5169–5175. https://doi.org/10.1016/0016-7037(95)00353-3

Ericksen GE (1983) The Chilean nitrate deposits. Am Sci 71(4):366–374

Fehn U, Snyder GT, Muramatsu Y (2007) Iodine as a tracer of organic material: I-129 results from gas hydrate systems and fore arc fluids. J Geochem Explor 95(1–3):66–80. https://doi.org/10.1016/j.gexplo.2007.05.005

Fisher JB, Boles JR (1990) Water rock interaction in Tertiary sandstones, San Joaquin Basin, california, USA—diagenetic controls on water composition. Chem Geol 82(1–2):83–101. https://doi.org/10.1016/0009-2541(90)90076-j

Fontes JC, Matray JM (1993a) Geochemistry and origin of formation brines from the Paris Basin, France. 1. Brines associated with Triassic salts. Chem Geol 109(1–4):149–175. https://doi.org/10.1016/0009-2541(93)90068-t

Fontes JC, Matray JM (1993b) Geochemistry and origin of formation brines from the Paris Basin, France. 2. Saline solutions associated with oil fields. Chem Geol 109(1–4):177–200. https://doi.org/10.1016/0009-2541(93)90069-u

Fuge R (1988) Sources of halogens in the environment, influences on human and animal health. Environ Geochem Health 10(2):51–61. https://doi.org/10.1007/bf01758592

Garcia MG, Borgnino L (2015) Chapter 1: Fluoride in the context of the environment. In: Preedy VR (ed) Fluorine: Chemistry, analysis, function and effects. The Royal Society of Chemistry, London, pp 3–21. https://doi.org/10.1039/9781782628507-00003

García-Veigas J, Rosell L, Zak I, Playà E, Ayora C, Starinsky A (2009) Evidence of potash salt formation in the Pliocene Sedom Lagoon (Dead Sea Rift, Israel). Chem Geol 265(3–4):499–511. https://doi.org/10.1016/j.chemgeo.2009.05.013

Goni IB, Fellman E, Edmunds WM (2001) Rainfall geochemistry in the Sahel region of northern Nigeria. Atmos Environ 35(25):4331–4339. https://doi.org/10.1016/s1352-2310(01)00099-1

Guo Q, Wang Y, Ma T, Ma R (2007) Geochemical processes controlling the elevated fluoride concentrations in groundwaters of the Taiyuan basin, Northern China. J Geochem Explor 93 (1):1–12. https://doi.org/10.1016/j.gexplo.2006.07.001

Gwynne R, Frape S, Shouakar-Stash O, Love A (2013) Br-81, Cl-37, and Sr-87 studies to assess groundwater flow and solute sources in the southwestern Great Artesian Basin, Australia. In: Hellmann R, Pitsch H (eds) Proceedings of the fourteenth international symposium on water-rock interaction: WRI 14, vol 7. Procedia earth and planetary science. pp 330–333. https://doi.org/10.1016/j.proeps.2013.03.084

Hanor JS (1994) Physical and chemical control on the composition of waters in sedimentary basins. Mar Pet Geol 11(1):31–45. https://doi.org/10.1016/0264-8172(94)90007-8

Hanor JS, McIntosh JC (2007) Diverse origins and timing of formation of basinal brines in the Gulf of Mexico sedimentary basin. Geofluids 7:227–237

Hanor JS, Mercer JA (2010) Spatial variations in the salinity of pore waters in northern deep water Gulf of Mexico sediments: implications for pathways and mechanisms of solute transport. Geofluids 10(1–2):83–93. https://doi.org/10.1111/j.1468-8123.2009.00271.x

Hay WW, Migdisov A, Balukhovsky AN, Wold CN, Flogel S, Soding E (2006) Evaporites and the salinity of the ocean during the Phanerozoic: implications for climate, ocean circulation and life. Palaeogeogr Palaeoclimatol Palaeoecol 240(1–2):3–46. https://doi.org/10.1016/j.palaeo.2006.03.044

Herut B, Starinsky A, Katz A, Bein A (1990) The role of seawater freezing in the formation of subsurface brines. Geochim Cosmochim Acta 54(1):13–21. https://doi.org/10.1016/0016-7037(90)90190-v

Herut B, Starinsky A, Katz A, Rosenfeld D (2000) Relationship between the acidity and chemical composition of rainwater and climatological conditions along a transition zone between large deserts and Mediterranean climate, Israel. Atmos Environ 34(8):1281–1292. https://doi.org/10.1016/s1352-2310(99)00291-5

Hitchon B (1995) Fluorine in formation waters, Alberta Basin, Canada. Appl Geochem 10(3):357–367. https://doi.org/10.1016/0883-2927(95)00004-4

Hitchon B, Billings GK, Klovan JE (1971) Geochemistry and origin of formation waters in Western Canada Sedimentary Basin 3. Factors controlling chemical composition. Geochim Cosmochim Acta 35(6):567–598. https://doi.org/10.1016/0016-7037(71)90088-3

Holland ND, Chen JY (2001) Origin and early evolution of the vertebrates: new insights from advances in molecular biology, anatomy, and palaeontology. BioEssays 23(2):142–151. https://doi.org/10.1002/1521-1878(200102)23:2<142:aid-bies1021>3.0.co;2-5

Holser WT (1979) Trace elements and isotopes in evaporites. In: Burns RG (ed) Marine minerals; Reviews in mineralogy, 6th edn. Mineralogical Society of America, Washington, pp 295–346

Houston SJ, Smalley PC, Laycock A, Yardley BWD (2011) The relative importance of buffering and brine inputs in controlling the abundance of Na and Ca in sedimentary formation waters. Mar Petrol Geol 28(6):1242–1251. https://doi.org/10.1016/j.marpetgeo.2011.03.002

Jacks G, Bhattacharya P, Chaudhary V, Singh KP (2005) Controls on the genesis of some high-fluoride groundwaters in India. Appl Geochem 20(2):221–228. https://doi.org/10.1016/j.apgeochem.2004.07.002

Jacobson G, Arakel AV, Chen YJ (1988) The central Australian groundwater discharge zone—evolution of associated calcrete and gypcrete deposits. Aust J Earth Sci 35(4):549–565. https://doi.org/10.1080/08120098808729469

Jagadeshan G, Kalpana L, Elango L (2015) Major ion signatures for identification of geochemical reactions responsible for release of fluoride from geogenic sources to groundwater and associated risk in Vaniyar River basin, Dharmapuri district, Tamil Nadu, India. Environ Earth Sci 74(3):2439–2450. https://doi.org/10.1007/s12665-015-4250-9

Jensen GKS, Rostron BJ, Duke MJM, Holmden C (2006) Bromine and stable isotopic profiles of formation waters from potash mine-shafts, Saskatchewan, Canada. J Geochem Explor 89(1–3):170–173. https://doi.org/10.1016/j.gexplo.2005.11.071

Jiang L, Worden RH, Cai CF (2014) Thermochemical sulfate reduction and fluid evolution of the Lower Triassic Feixianguan Formation sour gas reservoirs, northeast Sichuan Basin, China. Am Assoc Petrol Geol Bull 98(5):947–973. https://doi.org/10.1306/10171312220

Jiang L, Worden RH, Cai CF (2015) Generation of isotopically and compositionally distinct water during thermochemical sulfate reduction (TSR) in carbonate reservoirs: Triassic Feixianguan Formation, Sichuan Basin, China. Geochim Cosmochim Acta 165:249–262. https://doi.org/10.1016/j.gca.2015.05.033

Johnson MC, Plank T (1999) Dehydration and melting experiments constrain the fate of subducted sediments. Geochem Geophys Geosyst 1:1007. https://doi.org/10.1029/1999gc000014

Jones BF, Hanor JS, Evans WR (1994) Sources of dissolved salts in the Central Murray Basin. Aust Chem Geol 111(1–4):135–154. https://doi.org/10.1016/0009-2541(94)90087-6

Kaufmann RS, Frape SK, McNutt R, Eastoe C (1993) Chlorine stable isotope distribution of Michegan Basin formation waters. Appl Geochem 8(4):403–407. https://doi.org/10.1016/0883-2927(93)90008-5

Kharaka YK, Berry FAF (1973) Simultaneous flow of water and solutes through geological membranes 1. experimental investigation. Geochim Cosmochim Acta 37(12):2577–2603. https://doi.org/10.1016/0016-7037(73)90267-6

Kharaka YK, Carothers WW (1988) Geochemistry of oil field waters from the North Slope. In: Gryc G (ed) Geology and exploration of the National Petroleum Reserve in Alaska, 1974 to 1982: USGS professional paper, vol 1399. U.S. Geological Survey, Washington, pp 551–561

Kharaka YK, Callender E, Carothers WW (1977) Geochemistry of geopressured geothermal waters from the Texas Gulf Coast. Paper presented at the Geopressured-geothermal energy conference, Lafayette, Loiusiana

Kim Y-D, Thu K, Masry ME, Ng KC (2014) Water quality assessment of solar-assisted adsorption desalination cycle. Desalination 344:144–151. https://doi.org/10.1016/j.desal.2014.03.021

Klein BenDavid O, Sass E, Katz A (2004) The evolution of marine evaporitic brines in inland basins: the Jordan-Dead Sea Rift valley. Geochim Cosmochim Acta 68(8):1763–1775. https://doi.org/10.1016/j.gca.2003.08.002

Kloppmann W, Négrel P, Casanova J, Klinge H, Schelkes K, Guerrot C (2001) Halite dissolution derived brines in the vicinity of a Permian salt dome (N German Basin). Evidence from boron, strontium, oxygen, and hydrogen isotopes. Geochim Cosmochim Acta 65(22):4087–4101. https://doi.org/10.1016/S0016-7037(01)00640-8

Knauth LP (1988) Origin and mixing history of brines, Palo Duro Basin, Texas, U.S.A. Appl Geochem 3:455–474

Kodolanyi J, Pettke T, Spandler C, Kamber BS, Gmeling K (2012) Geochemistry of ocean floor and forearc serpentinites. Pangaea 53(2):235–270. https://doi.org/10.1594/PANGAEA.779555

Krauskopf KB (1979) Introduction to geochemisty, 2nd edn. McGraw-Hill, Tokyo

Krouse HR, Viau CA, Eliuk LS, Ueda A, Halas S (1988) Chemical and isotopic evidence of thermochemical sulfate reduction by light hydrocarbon gases in deep carbonate reservoirs. Nature 333(6172):415–419

Krupp RE (2005) Formation and chemical evolution of magnesium chloride brines by evaporite dissolution processes—Implications for evaporite geochemistry. Geochim Cosmochim Acta 69(17):4283–4299. https://doi.org/10.1016/j.gca.2004.11.018

Kuester Y, Schramm M, Bornemann O, Leiss B (2009) Bromide distribution characteristics of different Zechstein 2 rock salt sequences of the Southern Permian Basin: a comparison between bedded and domal salts. Sedimentology 56(5):1368–1391. https://doi.org/10.1111/j.1365-3091.2008.01038.x

Kullerud K, Erambert M (1999) Cl-scapolite, Cl-amphibole, and plagioclase equilibria in ductile shear zones at Nusfjord, Lofoten, Norway: implications for fluid compositional evolution during fluid-mineral interaction in the deep crust. Geochim Cosmochim Acta 63(22):3829–3844. https://doi.org/10.1016/s0016-7037(99)00150-7

Kuroda PK, Sandell EB (1953) Chlorine in igneous rocks—–some aspects of the geochemistry of chlorine. Geol Soc Am Bull 64(8):879–896. https://doi.org/10.1130/0016-7606(1953)64[879:ciir]2.0.co;2

Land LS, Macpherson GL (1992) Origin of saline formation waters, Cenozoic section, Gulf of Mexico sedimentary basin. Am Assoc Petrol Geol Bull 76(9):1344–1362

Land LS, Kupecz JA, Mack LE (1988) Louann Salt geochemistry (Gulf of Mexico sedimentary basin, USA)—a preliminary synthesis. Chem Geol 74(1–2):25–35. https://doi.org/10.1016/0009-2541(88)90144-1

Lavastre W, Jendrzejewski N, Agrinier P, Javoy M, Evrard M (2005) Chlorine transfer out of a very low permeability clay sequence (Paris Basin, France): Cl-35 and C-37 evidence. Geochim Cosmochim Acta 69(21):4949–4961. https://doi.org/10.1016/j.gca.2005.04.025

Li J, Wang Y, Guo W, Xie X, Zhang L, Liu Y, Kong S (2014) Iodine mobilization in groundwater system at Datong basin, China: evidence from hydrochemistry and fluorescence characteristics. Sci Total Environ 468:738–745. https://doi.org/10.1016/j.scitotenv.2013.08.092

Liu WG, Xiao YK, Wang QZ, Qi HP, Wang YH, Zhou YM, Shirodkar PV (1997) Chlorine isotopic geochemistry of salt lakes in the Qaidam Basin, China. Chem Geol 136(3–4):271–279. https://doi.org/10.1016/s0009-2541(96)00134-9

Lovelock JE, Maggs RJ (1973) Halogenated hydrocarbons in and over the Atlantic. Nature 241(5386):194–196. https://doi.org/10.1038/241194a0

Lowenstein TK, Timofeeff MN (2008) Secular variations in seawater chemistry as a control on the chemistry of basinal brines: test of the hypothesis. Geofluids 8(2):77–92. https://doi.org/10.1111/j.1468-8123.2007.00206.x

Lowenstein TK, Hardie LA, Timofeeff MN, Demicco RV (2003) Secular variation in seawater chemistry and the origin of calcium chloride basinal brines. Geology 31(10):857–860. https://doi.org/10.1130/g19728r.1

Lueders V, Plessen B, Romer RL, Weise SM, Banks DA, Hoth P, Dulski P, Schettler G (2010) Chemistry and isotopic composition of Rotliegend and Upper Carboniferous formation waters from the North German Basin. Chem Geol 276(3–4):198–208. https://doi.org/10.1016/j.chemgeo.2010.06.006

Luo CG, Xiao YK, Wen HJ, Ma HZ, Ma YQ, Zhang YL, Zhang YX, He MY (2014) Stable isotope fractionation of chlorine during the precipitation of single chloride minerals. Appl Geochem 47:141–149. https://doi.org/10.1016/j.apgeochem.2014.06.005

Luo CG, Xiao YK, Wen HJ, Ma HZ, Ma YQ, Zhang YL, Zhang YX, He MY (2015) Reply to the comment on the paper "Stable isotope fractionation of chlorine during the precipitation of single chloride minerals". Appl Geochem 54:117–118. https://doi.org/10.1016/j.apgeochem.2014.11.026

Macpherson GL (1992) Regional variations in formation water chemistry—major elements, Frio Formation fluids, Texas. Am Assoc Petrol Geol Bull 76(5):740–757

Madonia P, Liotta M (2010) Chemical composition of precipitation at Mt. Vesuvius and Vulcano Island, Italy: volcanological and environmental implications. Environ Earth Sci 61(1):159–171. https://doi.org/10.1007/s12665-009-0333-9

Magenheim AJ, Spivack AJ, Michael PJ, Gieskes JM (1995) Chlorine isotope composition of the ocean crust—implications for Earths distribution of chlorine. Earth Planet Sci Lett 131(3–4):427–432. https://doi.org/10.1016/0012-821x(95)00017-7

Mahara Y, Ohta T, Tokunaga T, Matsuzaki H, Nagao K, Nakata E, Miyamoto Y, Kubota T (2013) Pore-water mobility: distribution of delta Cl-37, Cl-36/Cl, I-129/I-127 and dissolved He-4 concentration in the core drilled in the Mobara gas field, Japan. Nucl Instrum Methods Phys Res. Sect B 294:597–601. https://doi.org/10.1016/j.nimb.2012.05.042

Martin JB (1999) Nonconservative behavior of Br-/Cl- ratios during alteration of volcaniclastic sediments. Geochim Cosmochim Acta 63(3–4):383–391. https://doi.org/10.1016/s0016-7037(99)00036-8

Martin JB, Gieskes JM, Torres M, Kastner M (1993) Bromine and iodine in Peru Margin sediments and pore fluids—implications for fluid origins. Geochim Cosmochim Acta 57 (18):4377–4389. https://doi.org/10.1016/0016-7037(93)90489-j

Matray JM, Lambert M, Fontes JC (1994) Stable isotope conservation and origin of saline waters from the Middle Jurassic aquifer of the Paris Basin. Appl Geochem 9(3):297–309. https://doi.org/10.1016/0883-2927(94)90040-x

Matthies D, Troll G (1990) Distribution of fluorine in recent marine-sediments related to petrographic composition—Bransfield Strait and Northwestern Weddell Sea, Antarctica. Mar Geol 91(4):313–324. https://doi.org/10.1016/0025-3227(90)90052-l

Matveev V, Peleg M, Rosen D, Tov-Alper DS, Hebestreit K, Stutz J, Platt U, Blake D, Luria M (2001) Bromine oxide—ozone interaction over the Dead Sea. J Geophys Res [Atmos] 106 (D10):10375–10387. https://doi.org/10.1029/2000jd900611

McCaffrey MA, Lazar B, Holland HD (1987) The evaporation path of seawater and the co-precipitation of Br^- and K^+ with halite. J Sediment Petrol 57(5):928–937

McDonough WF, Sun SS (1995) The composition of the Earth. Chem Geol 120(3–4):223–253. https://doi.org/10.1016/0009-2541(94)00140-4

Millot R, Guerrot C, Innocent C, Negrel P, Sanjuan B (2011) Chemical, multi-isotopic (Li-B-Sr-U-H-O) and thermal characterization of Triassic formation waters from the Paris Basin. Chem Geol 283(3–4):226–241. https://doi.org/10.1016/j.chemgeo.2011.01.020

Moghaddam AA, Fijani E (2008) Distribution of fluoride in groundwater of Maku area, northwest of Iran. Environ Geol 56(2):281–287. https://doi.org/10.1007/s00254-007-1163-2

Mohamed EA, Worden RH (2006) Groundwater compartmentalisation: a water table height and geochemical analysis of the structural controls on the subdivision of a major aquifer, the Sherwood Sandstone, Merseyside, UK. Hydrol Earth Syst Sci 10(1):49–64

Moldovanyi EP, Walter LM (1992) Regional trends in water chemistry, Smackover Formation, Southwest Arkansas—geochemical and physical controls. Am Assoc Petrol Geol Bull 76 (6):864–894

Morad S, Ismail HNB, Deros LF, Alaasm IS, Serrhini NE (1994) Diagenesis and formation water geochemistry of Triassic sandstones from Southern Tunisia. Sedimentology 41(6):1253–1272

Moran JE (1996) Origin of iodine in the Anadarko Basin, Oklahoma: an I-129 study. Am Assoc Petrol Geol Bull 80(5):685–694

Muramatsu Y, Wedepohl KH (1998) The distribution of iodine in the earth's crust. Chem Geol 147(3–4):201–216. https://doi.org/10.1016/s0009-2541(98)00013-8

Neal C, Smith CJ, Walls J, Billingham P, Hill S, Neal M (1990) Comments on the hydrochemical regulation of the halogen elements in rainfall, stemflow, throughflow and stream waters at an acidic forested area in mid-Wales. Sci Total Environ 91:1–11. https://doi.org/10.1016/0048-9697(90)90284-2

Neal C, Neal M, Davies H, Smith J (2003) Fluoride in UK rivers. Sci Total Environ 314:209–231. https://doi.org/10.1016/s0048-9697(03)00104-9

Neal C, Neal M, Hughes S, Wickham H, Hill L, Harman S (2007a) Bromine and bromide in rainfall, cloud, stream and groundwater in the Plynlimon area of mid-Wales. Hydrol Earth Syst Sci 11(1):301–312

Neal C, Neal M, Wickham H, Hill L, Harman S (2007b) Dissolved iodine in rainfall, cloud, stream and groundwater in the Plynhmon area of mid-Wales. Hydrol Earth Syst Sci 11(1):283–293

Neal M, Neal C, Wickham H, Harman S (2007c) Determination of bromide, chloride, fluoride, nitrate and sulphate by ion chromatography: comparisons of methodologies for rainfall, cloud water and river waters at the Plynlimon catchments of mid-Wales. Hydrol Earth Syst Sci 11 (1):294–300

Neilson JE, Oxtoby NH (2008) The relationship between petroleum, exotic cements and reservoir quality in carbonates—A review. Mar Petrol Geol 25(8):778–790. https://doi.org/10.1016/j.marpetgeo.2008.02.004

Nelson KH, Thompson TG (1954) Deposition of salts from sea water by frigid concentration. J Mar Res 13:166–182

Newell AJ (2006) Calcrete as a source of heterogeneity in Triassic fluvial sandstone aquifers (Otter Sandstone Formation, SW England). In: Barker RD, Tellam JH (eds) Fluid flow and solute movement in sandstones: the onshore UK Permo-Triassic red bed sequence. Geological Society Special Publication, vol 263. Geological Society, London, pp 119–127

O'Connor S, Swarbrick R, Lahann R (2011) Geologically-driven pore fluid pressure models and their implications for petroleum exploration. Introduction to thematic set. Geofluids 11(4):343–348. https://doi.org/10.1111/j.1468-8123.2011.00354.x

Osborn SG, McIntosh JC, Hanor JS, Biddulph D (2012) Iodine-129, Sr^{87}/Sr^{86}, and trace elemental geochemistry of Northern Appalachian Basin brine: evidience for basinal-scale migration and clay mineral diagenesis. Am J Sci 312(3):263–287. https://doi.org/10.2475/03.2012.01

Perez-Fodich A, Reich M, Alvarez F, Snyder GT, Schoenberg R, Vargas G, Muramatsu Y, Fehn U (2014) Climate change and tectonic uplift triggered the formation of the Atacama Desert's giant nitrate deposits. Geology 42(3):251–254. https://doi.org/10.1130/g34969.1

Peryt TM, Tomassi-Morawiec H, Czapowski G, Hryniv SP, Pueyo JJ, Eastoe CJ, Vovnyuk S (2005) Polyhalite occurrence in the Werra (Zechstein, Upper Permian) Peribaltic Basin of Poland and Russia: evaporite facies constraints. Carbonates Evaporites 20(2):182–194

Pierre C, Fritz B (1984) Early polyhalite replacement after gypsum—an example of a supratidal evaporite flat at the southeastern edge of the Ojo de Liebre Lagoon (Baja California, Mexico). Rev Geol Dynam Geog Phys 25(3):157–166

Pinti DL (2005) The origin and evolution of the oceans. In: Gargaud M, Martin H, Reisse J (eds) Lectures in astrobiology, vol 1. Advances in astrobiology and biogeophysics. Springer, Berlin, pp 83–112

Platt U, Honninger G (2003) The role of halogen species in the troposphere. Chemosphere 52:325–338

Price M (1996) Introducing groundwater, 2nd edn. Chapman and Hall, London

Price NB, Calvert SE (1977) The contrasting geochemical behaviours of iodine and bromine in recent sediments from the Namibian shelf. Geochim Cosmochim Acta 41(12):1769–1775. https://doi.org/10.1016/0016-7037(77)90209-5

Rao NS, Devadas DJ (2003) Fluoride incidence in groundwater in an area of Peninsular India. Environ Geol 45(2):243–251. https://doi.org/10.1007/s00254-003-0873-3

Rebeix R, La Salle CL, Jean-Baptiste P, Lavastre V, Fourre E, Bensenouci F, Matray JM, Landrein P, Shouakar-Stash O, Frape SK, Michelot JL, Lancelot J (2014) Chlorine transport processes through a 2000 m aquifer/aquitard system. Mar Petrol Geol 53:102–116. https://doi.org/10.1016/j.marpetgeo.2013.12.013

Reich M, Palacios C, Alvear M, Cameron EM, Leybourne MI, Deditius A (2009) Iodine-rich waters involved in supergene enrichment of the Mantos de la Luna argentiferous copper deposit, Atacama Desert, Chile. Mineral Deposita 44(6):719–722. https://doi.org/10.1007/s00126-009-0235-5

Risacher F, Fritz B, Alonso H (2006) Non-conservative behavior of bromide in surface waters and brines of Central Andes: a release into the atmosphere? Geochim Cosmochim Acta 70 (9):2143–2152. https://doi.org/10.1016/j.gca.2006.01.019

Rittenhouse G (1967) Bromine in oil-field waters and its use in determining possibilities of origin of these waters. Am Assoc Petrol Geol Bull 51(12):2430–2440

Rude PD, Aller RC (1994) Fluorine uptake by Amazon continental shelf sediment and its impact on the global fluroine cycle. Cont Shelf Res 14(7–8):883–907. https://doi.org/10.1016/0278-4343(94)90078-7

Sanders LL (1991) Geochemistry of formation waters from the Lower Silurian Clinton Formation (Albion Sandstone), eastern Ohio. Am Assoc Petrol Geol Bull 75(10):1593–1608

Schauble EA, Rossman GR, Taylor HP (2003) Theoretical estimates of equilibrium chlorine-isotope fractionations. Geochim Cosmochim Acta 67(17):3267–3281. https://doi.org/10.1016/s0016-7037(00)01375-3

Schmid S, Worden RH, Fisher QJ (2003) The origin and regional distribution of dolomite cement in sandstones from a Triassic dry river system, Corrib Field, offshore west of Ireland. J Geochem Explor 78–9:475–479. https://doi.org/10.1016/s0375-6742(03)00118-3

Schmid S, Worden RH, Fisher QJ (2004) Diagenesis and reservoir quality of the Sherwood Sandstone (Triassic), Corrib Field, Slyne Basin, west of Ireland. Mar Petrol Geol 21(3):299–315. https://doi.org/10.1016/j.marpetgeo.2003.11.015

Schmid S, Worden RH, Fisher QJ (2006) Carbon isotope stratigraphy using carbonate cements in the Triassic Sherwood Sandstone Group: Corrib Field, west of Ireland. Chem Geol 225(1–2):137–155. https://doi.org/10.1016/j.chemgeo.2005.09.006

Seda M, Svehla J, Travnicek J, Kroupova V, Konecny R, Fiala K, Svozilova M, Krhovjakova J (2012) The effect of volcanic activity of the Eyjafjallajokul volcano on iodine concentration in precipitation in the Czech Republic. Chem Erde 72(3):279–281. https://doi.org/10.1016/j.chemer.2012.04.004

Seedhouse JK, Racey A (1997) Sealing capacity of the Mercia Mudstone Group in the East Irish Sea Basin: implications for petroleum exploration. J Pet Geol 20(3):261–286. https://doi.org/10.1111/j.1747-5457.1997.tb00636.x

Selverstone J, Sharp ZD (2015) Chlorine isotope behavior during prograde metamorphism of sedimentary rocks. Earth Planet Sci Lett 417:120–131. https://doi.org/10.1016/j.epsl.2015.02.030

Shouakar-Stash O, Alexeev SV, Frape SK, Alexeeva LP, Drimmie RJ (2007) Geochemistry and stable isotopic signatures, including chlorine and bromine isotopes, of the deep groundwaters of the Siberian Platform, Russia. Appl Geochem 22(3):589–605. https://doi.org/10.1016/j.apgeochem.2006.12.005

Siemann MG (2003) Extensive and rapid changes in seawater chemistry during the Phanerozoic: evidence from Br contents in basal halite. Terra Nova 15(4):243–248. https://doi.org/10.1046/j.1365-3121.2003.00490.x

Smith MP, Yardley BWD (1999) Fluid evolution during metamorphism of the Otago Schist, New Zealand: (II) Influence of detrital apatite on fluid salinity. J Metamorph Geol 17(2):187–193

Snyder GT, Riese WC, Franks S, Fehn U, Pelzmann WL, Gorody AW, Moran JE (2003) Origin and history of waters associated with coalbed methane: I-129, Cl-36, and stable isotope results from the Fruitland Formation, CO and NM. Geochim Cosmochim Acta 67(23):4529–4544. https://doi.org/10.1016/s0016-7037(03)00380-6

Spears DA (2005) A review of chlorine and bromine in some United Kingdom coals. Int J Coal Geol 64(3–4):257–265. https://doi.org/10.1016/j.coal.2005.04.002

Starinsky A, Katz A (2003) The formation of natural cryogenic brines. Geochim Cosmochim Acta 67(8):1475–1484. https://doi.org/10.1016/s0016-7037(02)01295-4

Stewart MA, Spivack AJ (2004) The stable-chlorine isotope compositions of natural and anthropogenic materials. In: Johnson CM, Beard BL, Albarede F (eds) Geochemistry of non-traditional stable isotopes, vol 55. Reviews in mineralogy & geochemistry. Mineralogical Society of America, Washington, DC, pp 231–254. https://doi.org/10.2138/gsrmg.55.1.231

Stoessell RK, Carpenter AB (1986) Stoichiometry saturation tests of $NaCl_{1-X}Br_x$ and $KCl_{1-X}Br_X$. Geochim Cosmochim Acta 50(7):1465–1474. https://doi.org/10.1016/0016-7037(86)90320-0

Stotler RL, Frape SK, Shouakar-Stash O (2010) An isotopic survey of delta Br-81 and delta Cl-37 of dissolved halides in the Canadian and Fennoscandian Shields. Chem Geol 274(1–2):38–55. https://doi.org/10.1016/j.chemgeo.2010.03.014

Stueber AM, Walter LM (1991) Origin and chemical evolution of formation waters from Silurian-Devonian strata in the Illinois Basin, USA. Geochim Cosmochim Acta 55(1):309–325. https://doi.org/10.1016/0016-7037(91)90420-a

Sugiura T (1968) Bromine to chlorine ratios in igneous rocks. Bull Chem Soc Jpn 41(5):1133–1139. https://doi.org/10.1246/bcsj.41.1133

Svensen H, Jamtveit B, Yardley B, Engvik AK, Austrheim H, Broman C (1999) Lead and bromine enrichment in eclogite-facies fluids: extreme fractionation during lower-crustal hydration. Geology 27(5):467–470. https://doi.org/10.1130/0091-7613(1999)027<0467:labeie>2.3.co;2

Sverdrup HU, Johnson CC, Fleming RH (1942) Chapter VI: Chemistry of seawater. The oceans, their physics, chemistry and general biology. Prentice Hall, New York, pp 165–227

Symonds RB, Rose WI, Reed MH (1988) Contribution of Cl- and F-bearing gases to the atmosphere by volcanoes. Nature 334(6181):415–418. https://doi.org/10.1038/334415a0

Takamatsu N, Kato N, Matsumoto GI, Torii T (1998) The origin of salts in water bodies of the McMurdo Dry Valleys. Antarct Sci 10(4):439–448

Tellam JH (1995) Hydrochemistry of the saline groundwaters of the Lower Merseyside Basin Permo-Triassic sandstone aquifer, UK. J Hydrol 165(1–4):45–84. https://doi.org/10.1016/0022-1694(94)02583-w

Tellam JH (1996) Interpreting the borehole water chemistry of the Permo-Triassic sandstone aquifer of the Liverpool area, UK. Geol J 31(1):61–87. https://doi.org/10.1002/(sici)1099-1034(199603)31:1<61:aid-gj692>3.0.co;2-4

Tian Y, Yu CQ, Luo KL, Zha XJ, Wu JS, Zhang XZ, Ni RX (2015) Hydrochemical characteristics and element contents of natural waters in Tibet, China. J Geogr Sci 25(6):669–686. https://doi.org/10.1007/s11442-015-1195-6

Timofeeff MN, Lowenstein TK, Brennan ST, Demicco RV, Zimmermann H, Horita J, von Borstel LE (2001) Evaluating seawater chemistry from fluid inclusions in halite: examples from modern marine and nonmarine environments. Geochim Cosmochim Acta 65(14):2293–2300. https://doi.org/10.1016/s0016-7037(01)00591-9

Timofeeff MN, Lowenstein TK, da Silva MA, Harris NB (2006) Secular variation in the major-ion chemistry of seawater: evidence from fluid inclusions in Cretaceous halites. Geochim Cosmochim Acta 70(8):1977–1994. https://doi.org/10.1016/j.gca.2006.01.020

Truesdale VW, Jones SD (1996) The variation of iodate and total iodine in some UK rainwaters during 1980–1981. J Hydrol 179(1–4):67–86. https://doi.org/10.1016/0022-1694(95)02873-0

Tucker ME (1991) Sequence stratigraphy of carbonate evaporite basins—models and application to the Upper Permian (Zechstein) of North East England and adjoining North Sea. J Geol Soc 148:1019–1036. https://doi.org/10.1144/gsjgs.148.6.1019

Tweed S, Leblanc M, Cartwright I, Favreau G, Leduc C (2011) Arid zone groundwater recharge and salinisation processes; an example from the Lake Eyre Basin, Australia. J Hydrol 408(3–4):257–275. https://doi.org/10.1016/j.jhydrol.2011.08.008

Ullman WJ (1995) The fate and accumulation of bromide during playa salt deposition—an example from Lake Frome, South Australia. Geochim Cosmochim Acta 59(11):2175–2186. https://doi.org/10.1016/0016-7037(95)00099-l

Vainikka P, Hupa M (2012) Review on bromine in solid fuels. Part 1: natural occurrence. Fuel 95(1):1–14. https://doi.org/10.1016/j.fuel.2011.11.068

Vassilev SV, Eskenazy GM, Vassileva CG (2000) Contents, modes of occurrence and origin of chlorine and bromine in coal. Fuel 79(8):903–921. https://doi.org/10.1016/s0016-2361(99)00236-7

Videtich PE (1994) Dolomitization and H_2S generation in the Permian Khuff Formation, offshore Dubai, UAE. Carbonates Evaporites 9(1):42–57

Visser D, Nijland TG, Lieftink DJ, Maijer C (1999) The occurrence of preiswerkite in a tourmaline-biotite-scapolite rock from Blengsvatn, Norway. Am Mineral 84(5–6):977–982

Walna B, Kurzyca I, Bednorz E, Kolendowicz L (2013) Fluoride pollution of atmospheric precipitation and its relationship with air circulation and weather patterns (Wielkopolski National Park, Poland). Environ Monit Assess 185(7):5497–5514. https://doi.org/10.1007/s10661-012-2962-9

Walter LM, Stueber AM, Huston TJ (1990) Br-Cl-Na systematics in Illinois Basin fluids—constraints on fluid origin and evolution. Geology 18(4):315–318. https://doi.org/10.1130/0091-7613(1990)018<0315:bcnsii>2.3.co;2

Warren EA, Smalley PC (1994) North Sea formation water atlas. Geol Soc London Mem 15:208

Warren JK (1999) Evaporites: their evolution and economics. Blackwell Science, Oxford

Warren JK (2010) Evaporites through time: tectonic, climatic and eustatic controls in marine and nonmarine deposits. Earth Sci Rev 98(3–4):217–268. https://doi.org/10.1016/j.earscirev.2009.11.004

Wei XY, Wang XH, Zong ZM, Ni ZH, Zhang LF, Ji YF, Xie KC, Lee CW, Liu ZX, Chu NB, Cui JY (2004) Identification of organochlorines and organobromines in coals. Fuel 83(17–18):2435–2438. https://doi.org/10.1016/j.fuel.2004.06.018

Wen DG, Zhang FC, Zhang EY, Wang C, Han SB, Zheng Y (2013) Arsenic, fluoride and iodine in groundwater of China. J Geochem Explor 135:1–21. https://doi.org/10.1016/j.gexplo.2013.10.012

Wilson TP, Long DT (1993a) Geochemistry and isotope chemistry of Ca-Na-Cl brines in Silurian strata, Michegan Basin, USA. Appl Geochem 8(5):507–524. https://doi.org/10.1016/0883-2927(93)90079-v

Wilson TP, Long DT (1993b) Geochemistry and isotope chemistry of Michegan Basin brines—Devonian formations. Appl Geochem 8(1):81–100. https://doi.org/10.1016/0883-2927(93)90058-o

Winchester JW, Duce RA (1967) The global distribution of iodine, bromine, and chlorine in marine aerosols. Naturwissenschaften 54(5):110–113. https://doi.org/10.1007/bf00640572

Wittrup MB, Kyser TK (1990) The petrogenesis of brines in Devonian potash deposits of western Canada. Chem Geol 82:103–128. https://doi.org/10.1016/0009-2541(90)90077-K

Worden RH (1996) Controls on halogen concentrations in sedimentary formation waters. Mineral Mag 60(399):259–274. https://doi.org/10.1180/minmag.1996.060.399.02

Worden RH, Burley SD (2003) Sandstone diagenesis: the evolution from sand to stone. In: Burley SD, Worden RH (eds) Sandstone diagenesis, recent and ancient. International Association of Sedimentologists Reprint Series, vol 4. Blackwell, New York, pp 3–44

Worden RH, Brach M, Coleman ML (1994) Geochemical studies of rocks and fluids to give predictive modelling of permeability distribution in a sedimentary basin. Final Report of EC Contract JOUF-0016C

Worden RH, Smalley PC, Oxtoby NH (1996) The effects of thermochemical sulfate reduction upon formation water salinity and oxygen isotopes in carbonate gas reservoirs. Geochim Cosmochim Acta 60(20):3925–3931

Worden RH, Manning DAC, Bottrell SH (2006) Multiple generations of high salinity formation water in the Triassic Sherwood Sandstone: Wytch Farm oilfield, onshore UK. Appl Geochem 21(3):455–475. https://doi.org/10.1016/j.apgeochem.2005.12.007

Wu DS, Deng HW, Zheng BS, Wang WY, Tang XY, Xiao HY (2008) Iodine in Chinese coals and its geochemistry during coalification. Appl Geochem 23(8):2082–2090. https://doi.org/10.1016/j.apgeochem.2008.04.022

Yardley B, Gleeson S, Bruce S, Banks D (2000) Origin of retrograde fluids in metamorphic rocks. J Geochem Explor 69:281–285. https://doi.org/10.1016/s0375-6742(00)00132-1

Yechieli Y (2000) Fresh-saline ground water interface in the western Dead Sea area. Ground Water 38(4):615–623. https://doi.org/10.1111/j.1745-6584.2000.tb00253.x

Yechieli Y, Ronen D, Kaufman A (1996) The source and age of groundwater brines in the Dead Sea area, as deduced from 36Cl and 14C. Geochim Cosmochim Acta 60(11):1909–1916. https://doi.org/10.1016/0016-7037(96)00065-8

Yoshida M, Takahash K, Ozawa T, Iwasaki I (1971) Fluorine, chlorine, bromine and iodine contents of volcanic rocks in Japan. Bull Chem Soc Jpn 44(7):1844–1850. https://doi.org/10.1246/bcsj.44.1844

Yudovich YE, Ketris MP (2006) Chlorine in coal: A review. Int J Coal Geol 67(1–2):127–144. https://doi.org/10.1016/j.coal.2005.09.004

Zhang M, Frape SK, Love AJ, Herczeg AL, Lehmann BE, Beyerle U, Purtschert R (2007) Chlorine stable isotope studies of old groundwater, southwestern Great Artesian Basin. Appl Geochem 22(3):557–574. https://doi.org/10.1016/j.apgeochem.2006.12.004

Zherebtsova IK, Volkova NN (1966) Experimental study of behaviour of trace elements in the process of natural solar evaporation of Black Sea water and Sasyk-Sivash brine. Geochem Int USSR 3(4):656–670

Ziegler K, Coleman ML, Howarth RJ (2001) Palaeohydrodynamics of fluids in the Brent Group (Oseberg Field, Norwegian North Sea) from chemical and isotopic compositions of formation waters. Appl Geochem 16(6):609–632. https://doi.org/10.1016/s0883-2927(00)00057-3

Chapter 5
Halogen Geochemistry of Ore Deposits: Contributions Towards Understanding Sources and Processes

Pilar Lecumberri-Sanchez and Robert J. Bodnar

Abstract Most hydrothermal ore-forming fluids are dominantly aqueous chloride solutions. Due to the incompatible nature of halogens in most mineral phases, geofluid reservoirs commonly have distinct halogen geochemistry signatures. Comparison of the halogen geochemistry of ore-related fluids with that of geofluid reservoirs provides insights into sources of halogens and, by extension, of the fluids associated with ore formation. The halogen content of fluids has also direct effects in transport and deposition of metals. Addition of halide salts to H_2O modifies the Pressure-Volume-Temperature-Composition (PVTX) properties of hydrothermal fluids and controls the region of the Earth's crust in which metal partitioning and depositional mechanisms such as fluid immiscibility (boiling) may occur. Furthermore, addition of chloride salts to H_2O provides negatively-charged ligands that form complexes with the positively-charged metal ions, significantly increasing metal solubilities compared to solubilities in pure H_2O and enhancing the metal carrying capability of ore forming fluids. Halogens also influence the partitioning behavior of metals between different fluid phases, including liquid, vapor and melt phases and therefore determine the spatial distribution of metals in different ore deposit types and the metallogenic potential of the different fluid phases. Due to the close relationship between halogen geochemistry and the physical and chemical properties of fluids (aqueous and silicate), halogens play a significant role in ore deposit formation. As a result, some types of ore deposits show a systematic variation in time and space of halogen abundances and geochemistry, which may be used in exploration for these deposits.

P. Lecumberri-Sanchez (✉)
Inst. for Geochemistry and Petrology, ETH Zürich, 8092 Zurich, Switzerland
e-mail: lecumber@ualberta.ca

P. Lecumberri-Sanchez
Department of Geosciences, University of Arizona, 85721 Tucson, AZ, USA

R.J. Bodnar
Dept. of Geosciences, Virginia Tech, 24061 Blacksburg, VA, USA
e-mail: rjb@vt.edu

Present Address:
P. Lecumberri-Sanchez
Department of Earth and Atmospheric Sciences, University of Alberta, Alberta, Canada

D.E. Harlov and L. Aranovich (eds.), *The Role of Halogens in Terrestrial and Extraterrestrial Geochemical Processes*, Springer Geochemistry,
https://doi.org/10.1007/978-3-319-61667-4_5

5.1 Introduction

Ore deposits represent accumulations of metals or other elements of interest at concentrations that are significantly elevated relative to normal crustal abundances. The formation of economic metal deposits thus requires metal enrichment to values above crustal abundances. This usually occurs as a result of scavenging of metals from a relatively large volume of rock (or melt), transport of metals by fluids, and finally, deposition of the metals in a relatively small volume of rock to produce a high metal/rock ratio, i.e., high ore grade. A critical component in the formation of hydrothermal ore deposits is therefore the availability of a fluid with physical and chemical properties that enhance its ability to dissolve, transport, and precipitate the metals to form economic deposits. In most magmatic-hydrothermal ore deposits, the ore-forming fluid is an aqueous solution containing various amounts of highly reactive halogens that are essential for ore formation. Metals are commonly transported as metal chloride complexes in aqueous fluids (Seward et al. 2014), and therefore the behavior of halogens controls, to a large extent, the behavior of metals in the system. As such, understanding the abundance, distribution, and role of halogens in ore-forming systems has been the focus of many ore deposit-related studies. Chlorine is the most abundant halogen in most ore fluids, with F, Br and I occurring as trace components that are rarely reported (or analyzed for). Here, we discuss various aspects of ore deposits in which the halogen content of the fluid is relevant, including:

- Source of salinity and fluids in ore deposits: Some fluid reservoirs that are related to ore formation have distinct halogen signatures. These halogen signatures can, in some cases, be used to interpret the sources of ore-forming fluids as well as the physical and chemical processes associated with ore-formation. For example, Cl/Br ratios have been used extensively to infer seawater as the ultimate source of ore fluids in some deposit types (Kendrick and Burnard 2013). These same ratios can be used to infer modifications that seawater has undergone as a result of processes such as evaporation or precipitation of halite (cf., Worden 2018).
- PVTX properties of ore-forming fluids: Addition of halide salts to H_2O modifies the physical and chemical properties of the ore-forming fluid, which, in turn, affects mineralizing processes. Most natural hydrothermal fluids contain significant concentrations of salts such as NaCl, KCl, $CaCl_2$, $MgCl_2$, $FeCl_2$, and others. The amount and composition of the salts dissolved in the fluid controls the Pressure-Volume-Temperature-Composition (PVTX) properties of hydrothermal fluids and influences the PT conditions at which mineralization takes place.
- Metal transport: The solubility of metal-bearing phases increases significantly, often by several orders of magnitude, in the presence of a negatively-charged ligand that forms complexes with the positively-charged metal ions. Halogens (particularly chloride), as the most abundant anions in many geofluids, represent perhaps the most important group of ligands. The types, amounts, and

geochemical behavior of halogens in ore fluids directly control the extent of the metal enrichment and other geochemical processes related to ore deposit formation.

- The role of halogens in the genesis of specific ore deposits: Halogens play a particularly important role in some deposits in which the partitioning behavior of metals between different fluid phases, including melts, is directly controlled by the partitioning behavior of halogens; or in which the halogen content of the fluids modifies fluid phase behavior and directly controls how the system evolves. The role of halogens in some of these deposit types is discussed in detail.
- Exploration for ore deposits: In some types of ore deposits halogen abundances show a systematic variation in time and space. As such, halogen geochemistry can be an effective tool in mineral exploration.

5.2 Halogen Distribution in Ore-Forming Environments

Halogens are incompatible with most common minerals (Kendrick and Burnard 2013; Yardley and Bodnar 2014) and as a result, the halogen ratios and isotopic compositions that fluids acquire at the source are commonly preserved through most ore-forming processes. The various halogen reservoirs within the Earth show characteristic halogen concentrations, ratios and isotopic compositions (Fig. 5.1; see also Harlov and Aranovich (2018), and Hanley and Koga (2018)). Therefore, the halogen geochemistry can be used to trace the origin of the halogens and, by extension, may provide information concerning the origin of the fluids. In particular, halogens are indicators of the source of salinity in the fluid, whereas noble gases indicate the source of the solvent (water). We refer readers to the excellent paper by Kendrick and Burnard (2013) that describes in detail the application of halogen and noble gas geochemistry to constrain the sources of halogens and fluids in a wide range of ore deposit types.

A number of geochemical techniques and approaches have been used to determine the halogen geochemistry of ore deposits. The halogen contents of minerals are often obtained through electron microprobe analyses (EMPA), and are used as proxies for the halogen content of melts (e.g., F and Cl in apatite (Piccoli and Candela 1994; Mathez and Webster 2005; Webster et al. 2009)) and of hydrothermal fluids (e.g., Cl in biotite (Lentz 1994; Siahcheshm et al. 2012)). Changes in the halogen content of the fluid, the temperature, or the fluid/rock ratio can be further characterized through the study of halogen zonation in mineral replacement textures (Kusebauch et al. 2015a, b). Halogen contents in melts can be measured directly in melt inclusions by EMPA and SIMS (Ihinger et al. 1994; Hauri 2002). Halogen contents and the halogen isotopic composition of ore related fluids are commonly characterized through bulk analyses of fluid inclusions liberated by step heating or crush leach (Banks et al. 2000; Kendrick et al. 2001).

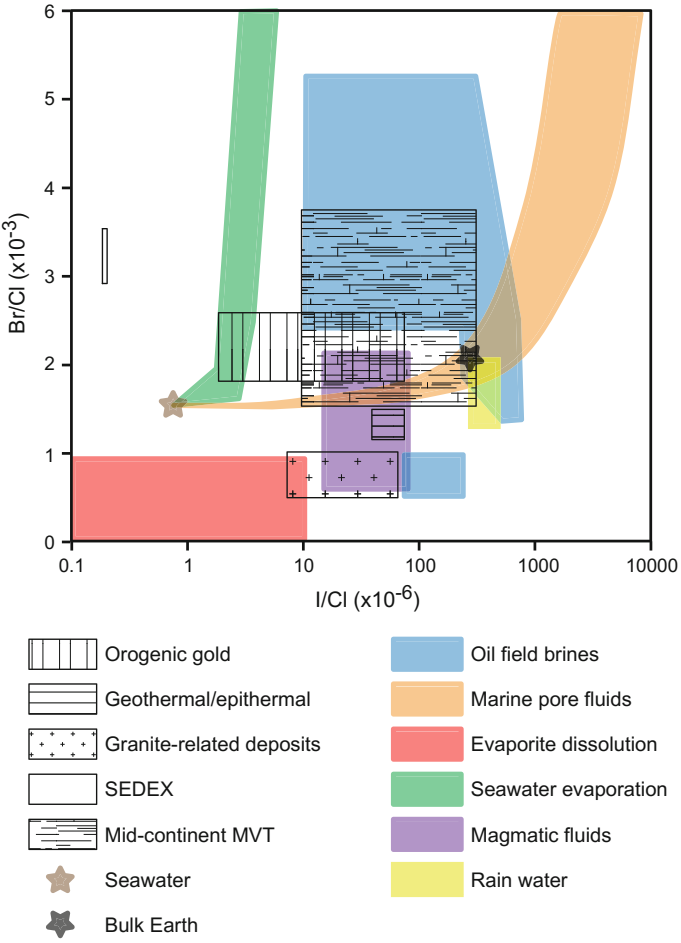

Fig. 5.1 Characteristic Br/Cl and I/Cl ratios of the different halogen reservoirs on the Earth compared to the Br/Cl and I/Cl ratios of fluids in different ore deposit types. The *green-colored band* that originates at seawater and extends to higher Br/Cl ratios represents the trend followed by seawater as a result of evaporation. The tan-colored band that extends from seawater to initially higher I/Cl ratios, and then higher Br/Cl ratios, represents the evolution in seawater halogen chemistry upon trapping as pore fluids and interaction with marine sediments (characterized by addition of organic Br and I). Modified from Yardley et al. (1992), Wilkinson (2001), Richard et al. (2014), and Kendrick and Burnard (2013)

Recent developments in laser ablation inductively coupled plasma mass spectrometry (LA-ICPMS) analyses have opened the possibility of in situ analyses of halogens in individual fluid inclusions (Seo et al. 2011; Hammerli et al. 2013), allowing for characterization of different genetic stages within a single crystal. However, quantification of F contents of fluids through LA-ICPMS analysis is not achievable due to the high ionization potential of F.

Yardley and Bodnar (2014) tabulated halogen and metal abundances in fluids from different ore forming environments. In almost every case, chloride is the most abundant halogen, usually exceeding all others by 1–3 orders of magnitude. Seawater, which represents the starting fluid composition for many types of ore systems, including the Mississippi Valley-Type (MVT) deposits and Volcanogenic Massive Sulfide deposits (VMS), contains 19,350 ppm Cl, 67.3 ppm Br, 1.3 ppm F, and 600 ppb I. Black smoker fluids in submarine hydrothermal systems have Cl contents that range from that of seawater (or slightly less) to significantly higher concentrations owing to phase separation and mixing in the sub-seafloor. Basinal brines (sometimes referred to as oilfield brines or formation waters) have chloride concentrations that range up to ~250,000 ppm, with Br ranging from several tens to a few thousand ppm (see also Worden 2018). Metamorphic fluids, including those associated with orogenic Au deposits, have Cl concentrations ranging from tens of thousands to ~200,000 ppm and Br typically from ~100 to a few thousand ppm. Magmatic fluids show a wide range in Cl contents, from a few tens of thousands to >400,000 ppm, reflecting both variations in the compositions of the exsolved magmatic fluid and the effects of fluid immiscibility and/or mixing, as discussed in more detail below. Fluids in continental geothermal systems often contain low concentrations of Cl (few thousand ppm), Br (few tens of ppm), and F (few ppm) reflecting the fact that the geothermal fluids represent meteoric water that has infiltrated the subsurface and has been heated by magmatic activity (White et al. 1984; Birkle et al. 2010). In contrast, in mid-ocean ridge environments the geothermal fluid is commonly seawater-derived, e.g., Reykjanes, Iceland (Marks et al. 2010).

The different halogen concentrations and ratios of fluids are a consequence of the original signature of the fluid and/or halogen source, sometimes modified by later processes. For example, seawater evaporation leads to partitioning of I and Br into the fluid upon salt precipitation because these elements are not incorporated into the halite structure. Therefore, bittern brines, seawater, and halogen-bearing minerals derived from seawater form a trend in Br/Cl versus I/Cl space (Fig. 5.1), whereby salts are relatively depleted in I and Br with respect to seawater, and bittern brines are relatively enriched (see also Worden 2018). The characteristic Br/Cl and I/Cl signatures of halogen reservoirs (initially compiled by Böhlke and Irwin (1992), and updated by Kendrick and Burnard (2013) and Pyle and Mather (2009)) can be compared with halogen signatures in ore deposits to determine the source of the halogens (Fig. 5.1). In addition, organic-rich sedimentary rocks constitute the main source of I and a significant source of Br such that fluid interaction with organic matter leads to relatively elevated I/Cl and Br/Cl ratios (Kendrick et al. 2011). The combination of I, Cl, and Br can be used to determine if Br has been added to the system from interaction of the fluid with organic matter (Kendrick and Burnard 2013).

In contrast with halogen elemental ratios, $\delta^{37}Cl$ is not significantly modified by fluid-only related processes (Bonifacie et al. 2005), but it can be modified by magmatic processes or by addition or removal of halogens from different sources (e.g., fluid mixing, evaporite dissolution, or precipitation) . Note that, in some cases, variation in $\delta^{37}Cl$ has been reported when boiling leads to halite precipitation

(Lüders et al. 2002; Germann et al. 2003). In this particular case, Bonifacie et al. (2005) suggest that the variation in the Cl isotopic composition is not due to boiling but to the removal of halogens associated with halite precipitation. Therefore, the Cl isotopic composition provides information on the original Cl source (and some information on later processes). Seawater-derived halogens have δ^{37}Cl isotopic compositions of around 0‰, and about 90% of Phanerozoic evaporites have δ^{37}Cl values between −0.5‰ and 0.5‰ (Eggenkamp 2014). The limited δ^{37}Cl database for continental magmatic rocks suggests that these rocks have a heterogeneous signature with δ^{37}Cl values ranging between −1‰ and +1‰ (Eggenkamp 2014). Note that the mantle δ^{37}Cl signature is still debated and MORB glasses range from −4‰ (Bonifacie et al. 2008a, b; Layne et al. 2009) to +6‰ (Magenheim et al. 1995), with a relatively good correlation between chlorinity and δ^{37}Cl (Eggenkamp 2014). Therefore, early interpretations that concluded a mantle source for Cl-bearing fluids based on the data from Magenheim et al. (1995) may need to be revisited. The Cl isotopic composition of oceanic serpentinites depends on the nature of the serpentinizing fluid. Seawater produces serpentinites with δ^{37}Cl between 0.2‰ and 0.5‰, while serpentinites derived from interaction with sedimentary pore fluids have a δ^{37}Cl between −2‰ and −0.5‰ (Barnes and Sharp 2006). Iodine isotopic compositions have been used recently as well to define the source of I in fluids associated with supergene blankets in porphyry Cu deposits (Reich et al. 2013).

The use of halogen systematics to determine fluid provenance was first applied to sedimentary environments (see Worden 2018). As a result, extensive datasets of halogen ratios and isotopic compositions are available for sediment-hosted Pb-Zn deposits, especially the MVT deposits. The halogen signature of ore fluids from the Tynagh and Silvermines Pb-Zn deposits, Ireland, is interpreted to reflect variable degrees of dilution of an original evaporative brine (Banks et al. 2000). In particular, Br/Cl ratios, higher than seawater in post-ore dolomitizing fluids at Tynagh, as well as in MVT districts in the United States midcontinent (Kendrick et al. 2002), indicate that the salinity was acquired by evaporation of seawater beyond halite saturation. The I/Cl ratios of the fluids in the United States midcontinent MVT deposits are typical of oilfield brines and are higher than can be achieved by evaporation of seawater alone, suggesting as well variable degrees of contribution of organically-sourced halogens (Kendrick et al. 2002). Interaction of fluids with organic matter is further supported by the oxygen and hydrogen isotopic compositions of water in fluid inclusions in the southern Appalachians (Kesler et al. 1997). The contribution of Br to the fluid from organic matter increases the Br/Cl ratio in a manner similar to the increase associated with the evaporation of seawater. Therefore, organic halogen input must be considered when estimating the extent of seawater evaporation or evaporite dissolution (Kendrick and Burnard 2013). Note that in localities where basinal brines and hydrothermal fluids occur synchronously the halogen signature of the fluids commonly lies in a mixing line between several endmembers (Bons et al. 2014; Fusswinkel et al. 2013, 2014; Walter et al. 2016), and that basinal brines have a high metal-carrying capability that allows leaching of metals from basement rocks in unconformity related-deposit (Essarraj et al. 2016; Pascal et al. 2016; Richard et al. 2016).

Several studies have used halogen systematics to determine the source of salinity and to identify fluid reservoirs in magmatic-hydrothermal systems. Halogen ratios and isotopic compositions in granite- and porphyry-related systems are consistent with a magmatic source for the halogens. The SW England batholith at St. Austell shows Br/Cl and I/Cl ratios of 0.85×10^{-3} and 81×10^{-6} respectively, values which are equivalent to those of modern volcanic gases (Böhlke and Irwin 1992). The range of Br/Cl ratios in the Butte, Montana, porphyry Cu deposit (Nahnybida et al. 2009) and the F/Cl ratios of biotite in the Miduk porphyry Cu deposit, Iran (Boomeri et al. 2009) are consistent with a magmatic-hydrothermal source for the halogens. In porphyry systems (in particular Bingham Canyon, Utah and Butte, Montana) the systematically negative $\delta^{37}Cl$ in all stages of mineralization is thought to have been inherited from low temperature melting of the subducting slab (Nahnybida et al. 2009). However, not all magmatic-hydrothermal systems show a purely magmatic halogen signature. At Bingham, the wide range of Br/Cl ratios suggests an additional source of halogens (Boomeri et al. 2009; Nahnybida et al. 2009), and the low Br/Cl ratios of fluid inclusions from the Capitan pluton, New Mexico, were likely the result of contributions from local Permian evaporites as a result of halite dissolution (Banks et al. 2000).

The halogen ratios and isotopic signatures in volcanogenic massive sulfide deposits indicate that most halogens in these systems are seawater-derived, and exclude any significant magmatic contribution to the halogen budget of the ore-forming fluids. The Cl and Br contents, and the $\delta^{37}Cl$ compositions of the fluid inclusions in sphalerite from the actively-forming massive sulfide mineralization in the JADE field from the Central Okinawa Trough, Japan, indicate that phase separation in the sub-seafloor resulted in the fractionation of Cl and Br into the liquid, and that the $\delta^{37}Cl$ values correlate with the extent of Cl and Br fractionation (Lüders et al. 2001). Strongly overprinted and/or metamorphosed volcanogenic massive sulfide deposits, such as Mt. Isa, Australia, have halogen signatures that indicate other (non-seawater) halogen sources. Halogen (Br/Cl and I/Cl) ratios from fluid inclusions in quartz and dolomite veins within the breccia-hosted Cu orebodies at Mt. Isa are compatible with sedimentary formation waters that originated by sub-aerial evaporation past halite saturation, and with metamorphic dehydration fluids. In combination with the Ar isotopic compositions, the halogen signature suggests that both a deeply derived metamorphic fluid produced by dehydration reactions, and a surface-derived bittern brine were present at some stage within the deposit.

Fluids from Fe-oxide-Cu-Au (IOCG) and related ore deposits worldwide have Cl/Br and $\delta^{37}Cl$ values consistent with a diversity of halogen sources including magmas, halite dissolution, and surface fluid input, which suggests that fluid mixing and/or fluid-rock interaction are significant processes in these systems (Chiaradia et al. 2006; Kendrick et al. 2007, 2008; Gleeson and Smith 2009; Smith et al. 2013; Hofstra et al. 2016; Bernal et al. 2017).

Magmatic sulfide deposits are characterized by sulfide melt/silicate melt immiscibility with halogens partitioning preferentially into the silicate melt. In these deposits, halide melts and brines can exsolve either from the sulfide melt

(Hanley et al. 2008) or the silicate melt (Gál et al. 2013). The sulfide melt/silicate melt partition coefficient of Cl is higher than those of F and Br. Therefore, fluids or halide melts that exsolved from a sulfide melt have Cl/F and Cl/Br ratios that are much higher than those of fluids that exsolved from silicate melts (Mungall and Brenan 2003). Because very high Cl/Br ratios are indicative of a sulfide melt generated as a result of sulfide/silicate melt immiscibility, the occurrence of high Cl/Br ratios has been proposed as an exploration tool for magmatic sulfide deposits (Mungall and Brenan 2003).

Few data are available for halogen concentrations (other than Cl) for epithermal ore deposits. This lack of data likely reflects the typically small size of fluid inclusions (compared to those in porphyry and MVT deposits) as well as the low salinity of the fluids, especially in the Au-rich epithermal deposits. Data for modern analogs of epithermal deposits (i.e., continental geothermal systems hosted in volcanic rocks) suggest a magmatic source for the halogens in these systems. Halogen contents in hot-spring fluids from various locations in the Central Oregon Cascade Range have Br/Cl ratios less than seawater and I/Cl ratios greater than seawater, suggesting a magmatic source for the halogens in the hot springs (Hurwitz et al. 2005). In the Taupo geothermal system, New Zealand, the geothermal fluids are dominantly heated meteoric waters, but the Cl/Br molar ratio of fluids from geothermal wells (Cl/Br from 858 to 1611) and hot springs (Cl/Br from 659 to 1664) suggests that the halogens were originally derived from a basaltic magma (Bernal et al. 2014). However, different stages of magma differentiation show slightly different halogen signatures such that rhyolite-related fluids have positive $\delta^{37}Cl$ and high Cl/Br, whereas andesite related fluids have a negative $\delta^{37}Cl$ and lower Cl/Br. Therefore, halogen systematics may potentially be useful for identifying the different magmatic sources of halogens (Bernal et al. 2014).

5.3 Effect of Halogens on Phase Equilibrium and PVTX Properties of Fluids

The circulation of hydrothermal fluids in the Earth's crust provides the most efficient means to scavenge and transport mass and energy and is therefore a key driver of ore-deposit formation and element cycling in the Earth. The dominant fluids associated with ore formation are aqueous fluids, as well as silicate and sulfide melts. Webster et al. (2018) and Dolejs and Zajacz (2018) discuss in detail the behavior of halogens in melts. In this chapter we focus on the effect of halogens (salinity) on the phase equilibria and the PVTX properties of aqueous fluids.

The single-component H_2O system is characterized by a triple point at 0.01 °C and 0.0006 MPa and a critical point at 373.95 °C and 22.064 MPa (Wagner and Pruss 1995). The liquid-vapor coexistence line extends from the triple point to the critical point, and liquid and vapor may only coexist in equilibrium within the very limited region defined by this line in PT space (Fig. 5.2). According to the Gibb's phase rule, the addition of a second component to the system H_2O increases the

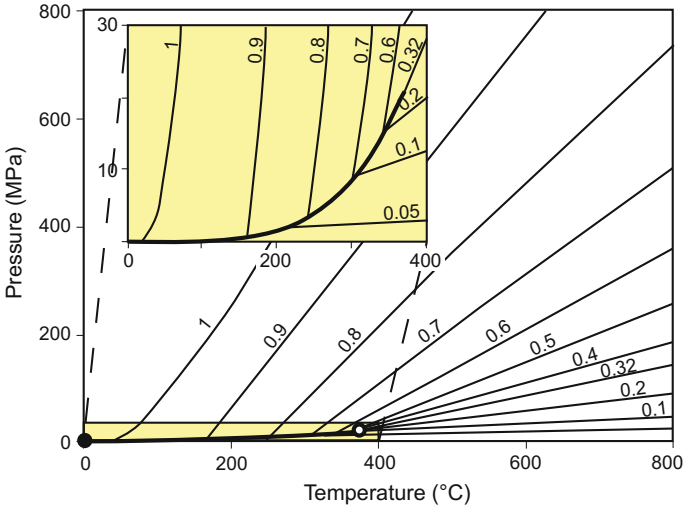

Fig. 5.2 Pressure-temperature phase diagram of H_2O. The *open circle* is the critical point of pure H_2O at 373.95 °C and 22.064 MPa (Wagner and Pruss 1995). The *filled circle* is the triple point of pure H_2O at 0.01 °C and 0.0006 MPa. The *thick line* joining the critical point and triple point is the liquid-vapor coexistence curve. Each of the *thinner lines* represents a line of constant density or isochore ($g \cdot cm^{-3}$). The *yellow-shaded* inset is an enlargement of the low temperature, low pressure portion of the diagram showing the liquid-vapor coexistence curve. From Yardley and Bodnar (2014)

number of degrees of freedom by one. Among other modifications, addition of a second component allows liquid + vapor to coexist within an area in PT space rather than being constrained to lie along a line. Stated differently, the range of temperature and pressure (depth) conditions in the Earth's crust and upper mantle where liquid + vapor immiscibility may occur is expanded greatly upon addition of salts to H_2O. This, in turn, has important implications for ore genesis because phase separation (immiscibility) is a common and important process associated with formation of ore deposits at shallow to intermediate depths in the crust, and addition of salt to water expands the region of the crust where immiscibility is possible. Phase separation generates two (or more) fluids of very different composition and density and thus modifies fluid flow behavior within the system and may also consume or produce heat. Of particular importance for ore formation is the observation that phase separation can lead to the generation of fluids that are enriched in certain metals and could potentially lead to ore precipitation (as further discussed in Sect. 5.5).

In the past several decades, a large number of experimental (Sourirajan and Kennedy 1962; Khaibullin and Borisov 1966; Hilbert 1979; Bodnar et al. 1985) and theoretical (Anderko and Pitzer 1993) studies have led to a reasonably good understanding of the effect of salt on the PVTX properties of aqueous fluids. Chloride is the major anion in most crustal and magmatic aqueous fluids. Therefore,

most studies of fluid properties have involved chloride-bearing fluids, and the systems H_2O-NaCl and H_2O-NaCl-CO_2 are now used almost universally to approximate the behavior of fluids in ore deposits.

5.3.1 The System H_2O-NaCl

The system H_2O-NaCl is the best-characterized binary aqueous fluid system, with data available from surface PT conditions up to magmatic-hydrothermal conditions. Driesner (2007) and Driesner and Heinrich (2007) compiled data on the PVTX properties of fluids in this system, and later studies have contributed new experimental data (e.g., Becker et al. 2008; Steele-MacInnis and Bodnar 2013). The system H_2O-NaCl is characterized by a continuous critical curve that extends from the critical point of H_2O to the critical point of NaCl (predicted to occur at 3568 °C and 18.2 MPa (Anderko and Pitzer 1993)). The locus of PT points for critical points of intermediate compositions between those two end members constitutes the critical curve or locus of critical points (see critical curve in Fig. 5.3) in the H_2O-NaCl system. The locus of critical points defines the maximum pressure at which liquid-vapor immiscibility might occur for a given temperature.

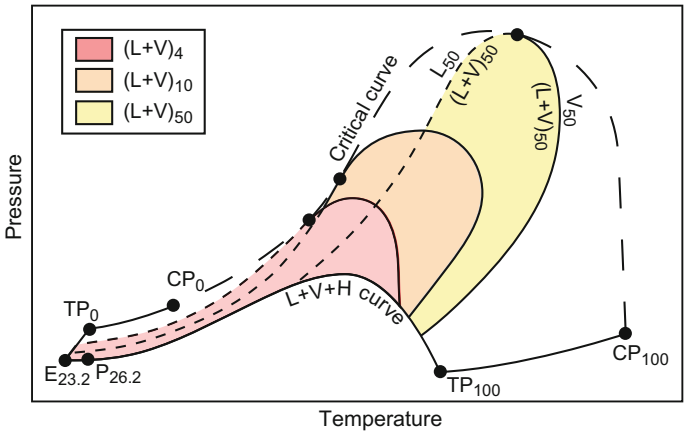

Fig. 5.3 Schematic representation of the pressure-temperature phase diagram for the system H_2O-NaCl. TP_{100} and TP_0 represent the triple point of pure NaCl and pure H_2O, respectively. CP_{100} and CP_0 represent the critical point of pure NaCl and pure H_2O, respectively. The critical curve in the H_2O-NaCl system is continuous and extends from the critical point of H_2O to the critical point of NaCl. L + V + H represents the liquid-vapor-halite coexistence curve. The *dashed lines* represent the liquid limb of the isopleths for compositions of 4, 10, and 50 wt% NaCl that separates the one-phase field (higher pressures above the dashed lines) from the two-phase (liquid-vapor) fields at pressures below the pressure represented by the dashed lines. Modified from Bodnar et al. (1985)

The three-phase curve, along which a solid (or two solids, at the eutectic and peritectic points) is in equilibrium with liquid and vapor, extends from the triple point of H_2O (0.01 °C and 0.0006 MPa; TP_0 in Fig. 5.3) to the triple point of pure NaCl (at 800.7 °C and 0.00005 MPa; TP_{100} in Fig. 5.3; Driesner and Heinrich (2007)). From the H_2O triple point to the eutectic point at −21.2 °C and ~0.0001 MPa ($E_{23.2}$ in Fig. 5.3; corresponding to a salinity of 23.2 wt% NaCl) (Bodnar et al. 1985), the solid in equilibrium with liquid and vapor is H_2O ice. From the eutectic to the peritectic at 0.1 °C ($P_{26.2}$ in Fig. 5.3), the solid in equilibrium with liquid and vapor is hydrohalite ($NaCl{\cdot}2H_2O$). From the peritectic to the triple point of NaCl (801 °C; TP_{100} in Fig. 5.3), the solid in equilibrium with liquid and vapor is halite. At the eutectic point, liquid and vapor are in equilibrium with both H_2O ice and hydrohalite, and at the peritectic point liquid and vapor are in equilibrium with both hydrohalite and halite. At temperatures >0.1 °C, the liquid + vapor + halite (L + V + H; Fig. 5.3) curve effectively defines the lowest pressure conditions at which liquid-vapor immiscibility might occur for a given temperature.

If NaCl is added to H_2O, the PT region in which liquid and vapor may coexist expands. From pure H_2O to moderate salinities of a few tens of weight percent NaCl, the PT area over which immiscibility occurs increases as salinity increases. At very high salinity (>70–80 wt% NaCl), the PT range of immiscibility decreases as the two-phase region approaches the pure NaCl liquid + vapor curve (line connecting the triple point of NaCl, TP_{100}, with the critical point of NaCl, CP_{100}, in Fig. 5.3). An important implication associated with the presence of chloride salts in hydrothermal fluids is that ore-forming processes, such as boiling, can occur at deeper levels of the crust (higher pressures and temperatures) than would be possible for pure H_2O fluids, which expands the portion of the crust in which boiling or phase separation is potentially an important ore-forming process.

5.3.2 The System H_2O-NaCl-$X^{+N}Cl_n$

Although the system H_2O-NaCl provides a reasonable approximation of the PVTX properties of many hydrothermal fluids, most natural hydrothermal fluids also contain significant concentrations of other cations, especially K, Ca, Fe and, to a lesser extent, Mg. The effect of these other chloride salts on the phase behavior of aqueous fluids has been studied to variable extents, mostly for the ternary systems H_2O-NaCl-$X^{+n}Cl_n$, where X corresponds to one of the major cations present and the subscript n represents the number of chloride ions in the formula and corresponds to the charge ($+n$) on the cation. The second-most abundant cations in most geologic fluids are K (Hall et al. 1988; Chou et al. 1992; Zezin et al. 2014a) and Ca (Oakes et al. 1990, 1995; Steele-MacInnis et al. 2011; Zezin et al. 2014b), followed by Fe (Lecumberri-Sanchez et al. 2015a; Steele-MacInnis et al. 2015) and, much less often, Mg (Dubois and Marignac 1997; Zezin et al. 2014b). The addition of other cations to the system H_2O-NaCl (i.e. H_2O-NaCl-$X^{+n}Cl_n$ systems) results in a

decrease in the solubility of halite at equivalent PT conditions as a result of the common ion effect (Steele-MacInnis et al. 2016). However, the most significant modification of phase behavior produced by the addition of other chlorides is modification of the range of PT conditions in which fluid immiscibility might occur. Whereas the PT trend of the locus of critical points is similar for most H_2O-XCl_n systems, their PT slopes vary (Liebscher 2007). For example, the critical curve for H_2O-$CaCl_2$ fluids extends to >800 bars at 500 °C, whereas the critical pressure for H_2O-$FeCl_2$ at the same temperature is ≈500 bars (Fig. 5.4). Therefore, phase separation or immiscibility in calcium chloride-dominated fluids can occur at relatively higher pressures (greater depths) compared to Fe chloride-dominated fluids of comparable salinity. At the present time, details concerning the effects of different cations on the PT limits of immiscibility and the compositions of coexisting phases in the system H_2O-NaCl-KCl-$CaCl_2$-$FeCl_2$ are poorly constrained, limiting our ability to rigorously constrain PT conditions for natural, multi-component aqueous fluids trapped in the two-phase field.

In addition to modifying the phase behavior of hydrothermal fluids, addition of cations other than Na also affects the slopes of isochores in the one-phase field. Zhang and Frantz (1987) determined the PT positions of isochores for aqueous solutions in the H_2O-$CaCl_2$, H_2O-KCl, and H_2O-NaCl systems for various salinities, and developed a model to predict the slopes of isochores for fluids containing all three salts. As an example of the effect of the cation on the slopes of the isochores, Zhang and Frantz (1987) found that H_2O-KCl fluid inclusions containing 2 molal solutions and trapped at 704 °C and 3000 bars homogenized at 370 °C, whereas H_2O-$CaCl_2$ inclusions of the same salinity homogenized at 392 °C. For comparison, H_2O-NaCl inclusions with a salinity of 2 molal (10.47 wt% NaCl) and trapped at these same PT conditions would homogenize at 356 °C according to

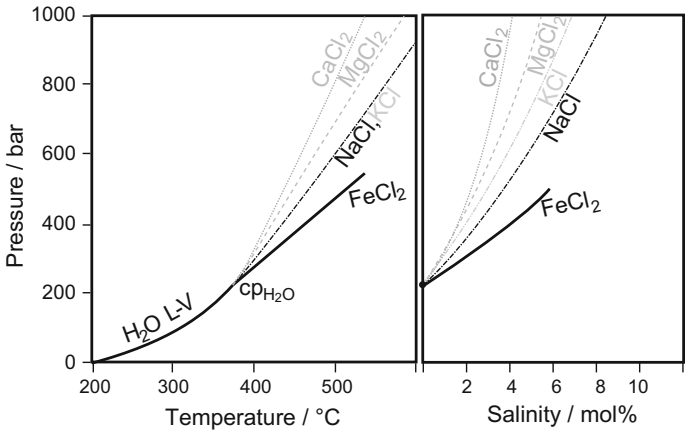

Fig. 5.4 Critical curve for the systems H_2O, H_2O-NaCl, H_2O-KCl, H_2O-$MgCl_2$, H_2O-$CaCl_2$, and H_2O-$FeCl_2$. Note that the general topology of the critical curve for all of these aqueous chloride systems is similar but their slopes vary. From Liebscher (2007) and Steele-MacInnis et al. (2015)

Bodnar and Vityk (1994). If all of these fluids had the same isochore slopes, they would show the same homogenization temperatures, ignoring the effect of small differences in pressure on the liquid-vapor curves for the three different compositions.

5.3.3 The System H_2O-NaCl-CO_2

In addition to the non-volatile solutes (defined as solutes with triple point temperatures higher than that of H_2O; Diamond (2003)), as described above, many hydrothermal fluids contain low to moderate concentrations of volatile components (defined as solutes with triple point temperatures lower than that of H_2O; Diamond (2003)). Carbon dioxide (CO_2) is the most commonly observed volatile in crustal fluids and can be abundant in some ore deposit environments (e.g., orogenic Au deposits; Bodnar et al. (2014)). Volatile solutes typically exsolve as gases upon saturation to produce a higher density phase (usually H_2O-rich) and a lower density phase (usually CO_2-rich). If chlorides are dissolved in solution, the number of H_2O molecules available to dissolve CO_2 decreases due to the clustering of water molecules around the chloride ions, and therefore the solubility of CO_2 decreases (Diamond 2003). As a consequence, the decrease in CO_2 solubility results in expansion of the PT region of fluid immiscibility (as compared to a chloride-free fluid with the same H_2O-CO_2 ratio), and increases the depth at which phase separation can occur in the crust as shown in Fig. 5.5. The dashed line labeled H_2O-CO_2 on the left side of Fig. 5.5 represents the maximum PT limits at which phase separation can occur in the salt-free H_2O-CO_2 system. As shown, the maximum temperature of immiscibility is ~374 °C at low pressure, and moves to slightly lower temperatures at higher pressures limiting the region of the crust where immiscibility can occur to relatively low temperature, lower to medium grade metamorphic environments. Also shown in Fig. 5.5 are several PTX diagrams in the ternary system H_2O-NaCl-CO_2. Each diagram shows the phase equilibria at a temperature and pressure corresponding to the region of the PT diagram where the ternary is plotted. Of importance to this discussion is the field shown in yellow and labeled "L + V". This field represents the range in compositions at which a single-phase fluid is unstable in the H_2O-NaCl-CO_2 system at that temperature and pressure, and the fluid would undergo phase separation. Note that addition of NaCl to the system H_2O-CO_2 increases the temperature at which immiscibility is possible from <375 °C to >900 °C, and also permits immiscibility at pressures up to at least 1000 MPa. As such, H_2O-CO_2 fluids containing salts can undergo immiscibility over essentially the entire range of lower-to-upper crustal PT conditions (Bodnar and Costain 1991; Schmidt and Bodnar 2000; Heinrich 2007a).

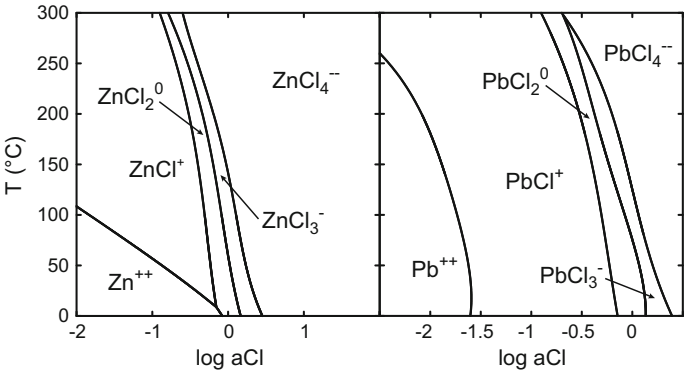

Fig. 5.5 Phase equilibria in the ternary system H_2O-CO_2-NaCl at various PT conditions representative of shallow to moderate crustal depths. The location of each ternary diagram corresponds approximately to the temperature and pressure conditions shown on the axes. The blue-shaded region corresponds to the single-phase (liquid or vapor) field. L + V corresponds to the region in which liquid and vapor would coexist. L + H corresponds to the region in which liquid and halite would coexist. V + H corresponds to the region in which vapor and halite would coexist. L + V + H corresponds to the region in which liquid, vapor, and halite would coexist. From Heinrich (2007b)

5.3.4 Effect of Other Halogens on Fluid Phase Equilibria

Halogens other than chloride rarely occur in sufficiently high concentrations to significantly modify the phase behavior of aqueous fluids. In any case, most chlorides, iodides and bromides are type 1 salts (i.e., salts with a continuous critical curve, similar to NaCl (Valyashko 2004)), and therefore the topology of the phase diagrams for aqueous solutions of most halogen salts is similar to that of the H_2O-NaCl system. Thus, most halogen salts enlarge the PT field of fluid immiscibility to variable extents, relative to pure water. There are some exceptions to this behavior, the most notable being fluoride solutions. Fluorine is the most abundant halogen in crustal rocks (Turekian and Wedepohl 1961). However, F concentrations in geologic fluids are typically orders of magnitude lower than that of Cl. This contrast in concentration between the Cl/F ratios of the crust and concentrations in geologic fluids is due to the relatively low solubility of common fluoride minerals, such as fluorite (CaF_2), and the relatively high solubility of chlorides such as halite (NaCl) and sylvite (KCl) in aqueous fluids. It is worth noting that most fluoride minerals are type 2 salts (i.e., have a discontinuous critical curve and the three phase curve intercepting the two critical curve segments (Valyashko 2004)). Therefore, H_2O-XF_n phase relations show a discontinuous critical curve that is intersected by the solidus of the XF_n salt, which results in a PT field of fluid immiscibility that is significantly smaller than that for other halide (non-fluoride) salts.

5.4 The Role of Halogens in Metal Transport and Deposition

In most ore-forming environments metal scavenging, transport, and deposition are mediated by fluids (Heinrich and Candela 2014), and halogens exert a strong influence on the ability of the fluid to transport metals. Seward and Barnes (1997), Migdisov and Williams-Jones (2014) and Seward et al. (2014) provide a thorough discussion of metal-complexation in aqueous solution. Dolejs and Zajacz (2018) and Webster et al. (2018) discuss transport of metals by silicate melts.

The type of metal complex formed in hydrothermal solutions depends on the nature of the metal and the availability of ligands. Pearson (1963) developed a conceptual model in which metals that are highly electropositive (positive charge and high charge to radius ratio) preferably associate with ligands that are highly electronegative (negative charge and high charge to radius ratio). Conversely, metals with lower charge to radius ratios tend to form complexes with ligands with lower charge to radius ratios. Although this conceptual model works best at low temperatures (<100 °C) (Seward et al. 2014), it provides a method to predict the types of metal complexes expected to form in various types of solutions. Metal-ligand association is dependent as well on the ligand availability. The complexing ligands that are most common in ore fluids are Cl^-, HS^-, and OH^- (Seward et al. 2014). Other species, such as CO_3^{2-} or SO_4^{2-}, can be as abundant as the more common ligands in some geologic fluids (Walter et al. 2017), although in many cases their potential as ligands has not been studied experimentally. In particular, concentrations of certain metals, such as Pb, Zn, Fe, and Mn, show a strong correlation with Cl concentration in geologic fluids. This correlation indicates that, for these particular elements, chloride plays a major role in their transport in geologic systems (Yardley 2005). Thus, Cl is a critical element for the transport of metals in ore fluids and directly affects ore forming processes.

5.4.1 Metal-Halogen Complexes in Hydrothermal Fluids

Metal-halogen complexes in solution are typically identified through spectrometric techniques. To study these processes at magmatic-hydrothermal conditions a combination of experimental methods, such as the hydrothermal diamond anvil cell and spectrometric techniques, are required. Recent studies have also applied ab initio modeling to predict formation of metal-halide complexes (Zajacz et al. 2011; Mei et al. 2013; Tian et al. 2014b). The results from these studies confirm that the specific complexes present in solution depend on the pressure, temperature, and composition of the fluid.

For metals that form chloride complexes, the chloride concentration of the fluid determines the extent to which chloride complexes form and the degree of chlorination of the metal (Xiao et al. 1998; Migdisov et al. 2011a). In general terms,

fluids with higher chloride concentration carry metals as higher chlorination complexes (Fig. 5.6). For example, at 300 °C Sn is transported in solution as Sn^{++} at chloride activities of 0.01 ($\log a_{Cl} = -2$), but at chloride activities of 1 ($\log a_{Cl} = 0$) Sn is transported dominantly as $SnCl_3-$ (Fig. 5.6).

The effect of temperature and pressure on the degree of chlorination of metals is related to the change in the dielectric constant of water with changing temperature and pressure. In general terms, as temperature increases, the dielectric constant of water decreases, resulting in a stronger attraction between ions (Wood and Samson 2000). In contrast, as pressure increases, the dielectric constant of water slightly increases and the attraction between ions becomes relatively weaker. Consequently, metals tend to form neutral or low-charged complexes at high temperatures. Crerar et al. (1985) suggested that the trend towards formation of neutral chloride complexes as temperature increases might be due not only to a decrease in the dielectric constant, but also to the transition from octahedral coordinated complexes to tetahedral dominated complexes, and to the reduction in the activity coefficient of anionic species.

Experimental and ab initio studies of transition metal chloride complexes (Heinrich and Seward 1990; Liu et al. 2011; Bazarkina et al. 2010; Tian et al. 2012, 2014a) corroborate the increase in the proportion of neutral or low-charged metal-chloride complexes with increasing temperature and the increase in the proportion of high chlorination complexes with increasing chloride concentration in the fluid (Fig. 5.6). Metal complexation at near-critical conditions is still not very well resolved, but recent thermodynamic modeling, X-ray absorption near edge structure (XANES), and X-ray absorption fine structure (XAFS) studies (Liu et al. 2007; Testemale et al. 2009; Hurtig and Williams-Jones 2014a) suggest that the behavior of chloride complexes in the vicinity of the critical point might differ from these general trends, likely due to the large temperature and pressure effect on the

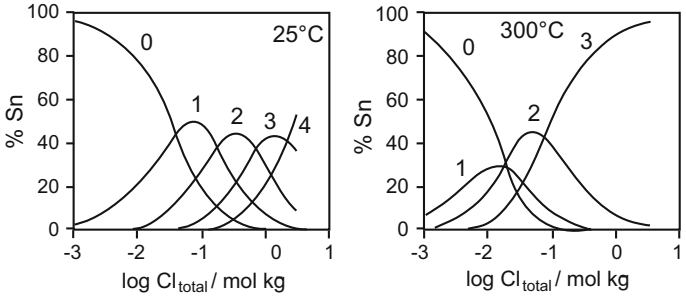

Fig. 5.6 Chloride complexation of Sn at 25 and 300 °C as a function of chloride content of the fluid. The y-axis is the percentage of the metal occurring as a given complex and the x-axis is the chloride concentration. Each of the curves represents the abundance of a *n*-chlorinated species, with *n* being the number of chloride anions per atom of metal in the complex. Thus, "0" corresponds to Sn^{++}, "1" corresponds to $SnCl^+$, etc. Note that higher chlorination species occur at higher chloride concentrations and that lower charge species occur at higher temperatures for the same chloride concentrations. From Müller and Seward (2001), Seward et al. (2014)

thermodynamic properties of fluids within this region (Johnson and Norton 1991; Klyukin et al. 2016). Copper, Ag, and Au complexing with Cl in low-density (vapor) HCl-dominated fluids is, in general, comparable to complexing in high-density liquids. The degree of chlorination increases with increasing f_{HCl} and pressure. For example, AgCl occurs as AgCl at low f_{HCl} and pressure, as AgCl(HCl) at high f_{HCl} and low pressure, and as $AgCl(HCl)_2$ at high f_{HCl} and pressure (Migdisov and Williams-Jones 2013). In a similar manner, the degree of chlorination increases with increasing temperature such that monochloride (CuCl) species are dominant at low temperatures and higher order chloride species (CuCl·HCl or $CuCl_2$) occur at high temperatures (Migdisov et al. 2014). In contrast with this behavior, at low temperature Au forms higher order chloride complexes (Au_2Cl_6) and lower order complexes at high temperature Au_2Cl_2 (Hurtig and Williams-Jones 2014b). Especially at low fluid density, increasing pressure results in higher hydration of the chloride-metal complexes and higher carrying capacity for the metal.

Recent studies suggest that multi-cation, multi-ligand complexes form in multi-component solutions (similar to ore-forming fluids) and can significantly modify the solubility of metal-bearing phases, compared to solubilities in more simple systems. For example, Zajacz et al. (2011) proposed that Cu forms Na(/K) $CuCl_2$, Na(/K)$Cu(HS)_2$, H_2SCuHS, and Na(/K)ClCuHS complexes and that their relative proportions are a function of the ratio of H_2S to chloride and of HCl to alkali chlorides in solution. Therefore, metal transport in natural hydrothermal solutions is likely to be much more complicated than is suggested by experimental and theoretical studies of simple, single-cation, single-ligand systems, and further study of metal complexation in multi-component systems is likely to significantly advance our understanding of metal transport in hydrothermal solutions.

Due to the common association of F-bearing minerals with anomalous accumulations of nominally immobile elements such as rare earth elements (REE), it was originally thought that F might be important for REE transport in solution (Salvi and Williams-Jones 1990; Wood 1990a, b). REE do form F complexes in solution. However, at hydrothermal conditions (temperature and pH), HF is strongly associated and little fluoride (F^-) is available in solution to carry REE. Therefore, most REE in hydrothermal systems are likely carried as chloride complexes (Williams-Jones et al. 2012). Fluorine is therefore more likely to act as a precipitation agent rather than as a transporting agent, due to the low solubility of REE-fluoride phases at high pH (Williams-Jones et al. 2012; Migdisov and Williams-Jones 2014). In contrast, F seems to play a significant role in mobility of elements such as Al, Zr, and Nb. The concentration of Al in solution can increase 100 times with the addition of F due to the formation of Na–Al-hydroxyfluoro complexes (Tagirov et al. 2002). In F-bearing systems, Zr and Nb are transported in solution as hydroxyl fluoride species such that the solubilities of both Zr and Nb are strongly dependent on the F content of the fluid, pH, and temperature (Migdisov et al. 2011b; Timofeev et al. 2015).

5.4.2 *Effect of Halogens on the Solubility of Metal-Bearing Phases and Precipitation Mechanisms*

The concentration of chloride-complexing metals in solution in equilibrium with their metal-bearing phases (i.e., the solubility) depends on a number of factors. For the purpose of this discussion we will focus on the solubility of sphalerite (Akinfiev and Tagirov 2014), but this discussion is generally applicable to other chloride-complexing metals.

Assuming that the dominant S species in solution is HS^-, sphalerite solubility is governed by the reaction:

$$ZnS + H^+ = Zn^{2+} + HS^- \quad K_1 = \left[a\left(Zn^{2+}\right)a(HS^-)\right]/a(H^+) \tag{5.1}$$

Some relevant Zn-chloride complexation reactions are:

$$Zn^{2+} + Cl^- = ZnCl^+ \quad K_2 = a(ZnCl^+)/\left[\left(a\left(Zn^{2+}\right)a(Cl^-)\right]\right. \tag{5.2}$$

and

$$Zn^{2+} + 2Cl^- = ZnCl_2^0 \quad K_3 = a\left(ZnCl_2^0\right)/\left(a\left(Zn^{2+}\right)a(Cl^-)^2\right) \tag{5.3}$$

If the dominant Zn-chloride complex is $ZnCl^+$, the dissolution reaction is obtained by summing reactions (5.1) and (5.2):

$$\begin{gathered} ZnS \;+ H^+ + Cl^- = \; ZnCl^+ + HS^- \\ K_4 = [a(ZnCl^+)a(HS^-)]/[(a(H^+)a(Cl^-)] \end{gathered} \tag{5.4}$$

According to LeChatelier's principle, an increase in chloride concentration displaces reaction (5.4) to the right, leading to sphalerite dissolution and increasing the Zn content of the fluid (Fig. 5.7). However, as previously discussed, the stoichiometry of metal-chloride complexes in solution depends on the chloride concentration of the fluid. Therefore, if the increase in chlorinity leads to a change in chloride-metal speciation, such that the dominant species becomes $ZnCl_2^0$, the change in Zn concentration in the fluid will be due as well to the change in the solubility constant and in the reaction coefficients. In this case the dissolution-precipitation reaction would be:

$$\begin{gathered} ZnS + H^+ + 2Cl^- = ZnCl_2^0 + HS^- \\ K_4 = a\left(ZnCl_2^0\right)a(HS^-)/\left(a(H^+)a(Cl^-)^2\right) \end{gathered} \tag{5.5}$$

where the concentration of Zn in solution is roughly proportional to the square of the chloride activity and is described by K_5 instead of K_4 (Fig. 5.7).

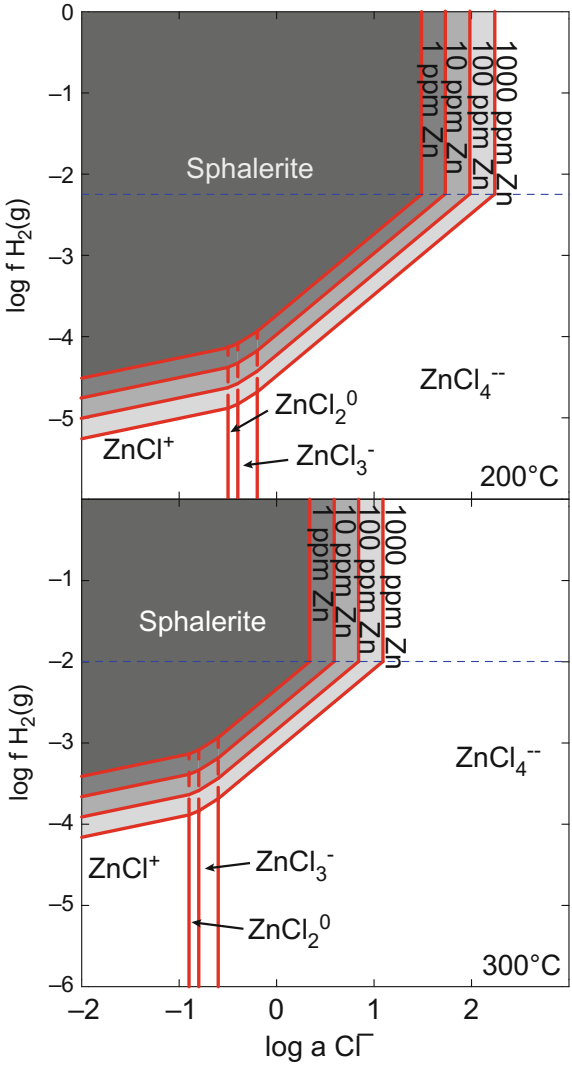

Fig. 5.7 Sphalerite solubility under quartz-K-feldspar-muscovite buffered conditions as a function of redox (f_{H2}), chloride activity (a_{Cl^-}), Zn concentration (isopleths in ppm Zn in solution), and temperature. The *unshaded areas* define the fields where various Zn chloride species are dominant under sphalerite-undersaturated conditions. The *shaded fields* define the sphalerite saturation fields for various Zn concentrations. The *horizontal dashed line* divides the field in which the dominant S species is SO_4^{2-} (above) from the field in which the dominant S species is S^{2-} (below). Note that sphalerite solubility (1) increases with increasing chloride activity for a given temperature and redox state; (2) increases with increasing temperature for a given chloride activity; and (3) varies depending on which Zn chloride species is dominant, due to the effect of chloride activity on the solubility constant (see text). Calculated with the Geochemist's Workbench (Bethke 1996) using the data compiled by Lawrence Livermore National Laboratories (1978). Recommended key values for thermodynamic calculations are taken from Baes and Mesmer (1976); Helgeson (1969); Helgeson et al. (1978, 1981), Helgeson and Kirkham (1974a, b, 1976); Tobie et al. (1978). Note that there is not unanimous agreement in the literation in chloride solutions

The solubility of metal-bearing phases varies with temperature owing to the temperature dependence of the solubility constant for the dissolution-precipitation reaction. This is because the pH and f_{H2} of fluids under rock buffered conditions vary as a function of temperature, and because metal-chloride complexation is temperature-dependent. As previously discussed, the dominant dissolution-precipitation reaction varies with metal-chloride complexation and, therefore, a different solubility constant governs the reaction. As the governing solubility constant varies, the relationship between metal and chloride concentration in solution varies. This is reflected by a change in the slope of the solubility isopleths in Fig. 5.7.

Owing to the dependence of metal solubility on, among other factors, the chlorinity, pH, f_{O2}, f_{S2}, temperature and pressure, processes that lead to variations in any of these parameters may affect the ability of the fluid to transport metals. A number of geological processes may lead to sudden changes in the chlorinity, pH, f_{O2}, f_{S2}, temperature and pressure of metal-bearing fluids, including fluid immiscibility (as further discussed in Sect. 5.1), fluid mixing, or fluid-rock interaction. These ore forming processes may cause localized changes in the solubility of metal-bearing phases and lead to metal precipitation.

5.5 Role of Halogens in Ore-Forming Systems

5.5.1 Role of Halogens in Magmatic Sulfide Deposits

Magmatic sulfide deposits are characterized by the occurrence of silicate-sulfide melt immiscibility that leads to the concentration (and potential later remobilization) of chalcophile elements. Mungall and Brenan (2003) show that upon silicate-sulfide melt immiscibility, Cl, F, Br, and I partition preferentially into the silicate melt; that the sulfide melt can accommodate up to 2000 ppm of halogens; and that saline magmatic fluids or halide melts can form by exsolution from either silicate melts or from sulfide melts.

Mungall and Brenan (2003) also report that crystallization of monosulfide solid-solutions (mss) from a mafic melt leads to progressive enrichment of Cl in the residual silicate melt. Moreover, the presence of Cl lowers the melting point of the mss, and Cl dissolves in the sulfide melt that is produced. At lower temperature, halides that exsolve from the melt can mix with externally-derived aqueous fluids to produce fluids with high Cl/F and Cl/Br ratios.

Barnes et al. (2009) attributed vesicular ore textures in the Black Swan disseminated nickel deposit, Australia, to the degassing of a sulfide melt, which produced an SO_2 and halogen-rich vapor. Upon sulfide crystallization most halogens are exsolved from the sulfide melt and generate high salinity brines or halide melts. Thus, Hanley et al. (2008) reported fluid inclusions ranging from NaCl-dominated halide melts to more complex Na-Ca-K-Fe-Mn-Ba-Si-Al-Cl brines in

the platinum group element (PGE)-rich J-M Reef in the Stillwater Complex, Montana. Brines can alternatively be derived from a silicate melt (Gál et al. 2013), though the salinity of fluids exsolved from silicate melts depends on the water/carbon dioxide ratio of the exsolved fluid. Molnár et al. (2001) reported silicate-melt derived Na-Ca-Fe-Mn-K brines at Sudbury with a later fluid stage that is more CO_2-rich and that has systematically lower and highly variable salinity. Gál et al. (2013) reported that halogens partition into the fluid, rather than the melt, when the fluid is H_2O-rich and that halogens remain in the silicate melt when the fluid is CO_2-rich. These observations are in good agreement with experimental results, which show that in the presence of a CO_2-rich fluid, the aqueous fluid/silicate melt partitioning of halogens decreases significantly (Webster et al. 2007). Finally, in some magmatic sulfide deposits there is evidence of late-stage ore fluids derived from the local groundwater.

The halogen content of aqueous fluids in magmatic sulfide deposits can be highly variable according to the fluid inclusion data (15 to 80 equivalent weight% NaCl (Hanley et al. 2008)), and based on the halogen content of minerals such as biotite, amphibole, and apatite in these deposits (Boudreau et al. 1986; Boudreau and Hoatson 2004; Hanley and Mungall 2003).

The partitioning of PGE's between silicate melt and aqueous fluid depends on the chloride content of the fluid and on the composition of the melt (Hanley et al. 2005b; Simon and Pettke 2009; Blaine et al. 2011), and the ability of the fluid to transport PGE's depends on the chloride content of the fluid. Semi-quantitative studies suggest that Pt concentrations >100 ppm can occur in chloride-bearing fluids at moderate oxygen fugacity and high temperature (Hanley et al. 2005c). Therefore, high salinity fluids may play a significant role in remobilization of PGE's, and on the final distribution of the ore minerals (Hanley et al. 2008). The correlation between ore grades and hydrothermal alteration (Hanley et al. 2008), and experimental data (Hanley et al. 2005a, b), indicate that high salinity fluids can and do remobilize PGE's in magmatic sulfide deposits.

5.5.2 *Role of Halogens in Porphyry- and Granite-Related Ore Deposits*

Among the best-studied ore deposit types in terms of halogen geochemistry are magmatic-hydrothermal deposits related to intermediate to silicic epizonal plutons, such as the porphyry-type and granite-related deposits. In such systems, pressure and melt composition (including halogen content) determine the melt/melt and fluid/melt partitioning behavior of the halogens (Cline and Bodnar 1991; Audétat et al. 2008). In magmatic-hydrothermal systems, increasing the Cl content of the melt increases the pressure at which volatile exsolution occurs (Webster 1997a) and chlorine partitioning between aqueous fluids and silicate melt determines the behavior of chloride-complexing metals (Candela and Holland 1986). In addition,

the presence of F in the melt lowers the liquidus and solidus temperatures (Manning 1981), decreases the viscosity, and increases the rate of diffusion of cations and volatiles in the melt (Hannah and Stein 1990; Webster and Holloway 1990). Furthermore, fluoride-silicate melt immiscibility reported in peralkaline granites (Vasyukova and Williams-Jones 2014, 2016) results in enrichment of REE by about two orders of magnitude (Veksler et al. 2012).

5.5.2.1 Magmatic Cl and Its Role in Melt/Fluid Metal Partitioning

The Cl content of silicate melts associated with haplogranites is commonly assumed to be around 0.2 wt% (Webster 1997b), which is in good agreement with the 0.1 to 0.6 weight percent range reported in silicate melt inclusions in porphyry- and granite-related deposits (Student and Bodnar 2004; Zajacz et al. 2008; Aiuppa et al. 2009). Note, however, that data on the Cl content of magmas associated with porphyry- and granitic-related ore deposits are scarce.

Aqueous fluids may exsolve from intermediate composition magmas either as one-phase or as two-phase (liquid + vapor) fluids, depending on the depth (pressure) of emplacement and composition of the melt. Magmatic fluids exsolved as a single phase from the silicate melt commonly have salinities of 2 to 13 wt% equivalent NaCl (Audétat et al. 2008; Zajacz et al. 2008). In porphyries where two aqueous phases exsolve from a silicate melt, the Cl content of the vapor and liquid, and the vapor/liquid mass ratios are fixed by the pressure and temperature at which exsolution occurs (Shinohara 1994; Webster and Mandeville 2007). However, several studies report brine inclusions of variable salinity coexisting with silicate melt inclusions in porphyry systems (Table 5.1) (Roedder 1992), suggesting either heterogeneous entrapment of a fluid that exsolved at PT conditions within the

Table 5.1 Salinities reported for fluid inclusions coexisting with melt inclusions and plotted on Fig. 5.8

	System	Phases present	Salinity (1)	Salinity (2)	Source
1	Mt. Malosa	M + L + V	7–13	32–35	1
2	Santa Rita	M + L + V	20	33	2
3	Cuasso al Monte	M + L + V		53–69	1
4	Capitan Mt.	M + L + V	2.2	63	2
5	Rito del medio	M + L/V	4.5–7.5	–	3
6	Ehrenfriedersdorf	M + L/V	7–8.5	–	1
7	Mole Granite	M + L/V	3.1–8	–	2
8	Canada Pinabete	M + L/V	2.6–4.8	–	3

The column labeled salinity (1) represents either the salinity of the single-phase fluid for systems in which a single aqueous phase coexists with the silicate melt, or the vapor salinity for systems in which two aqueous phases coexist with the silicate melt. Salinity (2) corresponds to the salinity of the brine in systems where two aqueous fluid phases coexist with the silicate melt. From Audétat et al. (2008). Sources of original data are: 1: Zajacz et al. (2008); 2: Audétat et al. (2008); and 3: Audétat and Pettke (2003)

two-phase field or exsolution of a single-phase, high salinity magmatic brine. Some workers (Cline and Bodnar 1994; Luo et al. 2014) have reported high-salinity (>30 wt% NaCl equivalent) brines that were interpreted to have exsolved directly from silicate melts in porphyry deposits, but there is some debate over their origin (Klemm et al. 2008). According to experimental data, exsolution of high salinity fluids from a silicate melt at the depths typical for emplacement of porphyry systems would require Cl contents of 2 wt% in the silicate melt (Webster 1997b). Therefore, questions remain regarding whether ore-related melts with sufficient Cl concentration to exsolve single phase brines exist, as well as the source of salinity variation in the brine of two-phase fluids exsolved from melts. The halogen content of the melt could potentially be sufficiently elevated to exsolve brines directly if evaporite sequences are assimilated into the magma previous to fluid exsolution (Campbell et al. 1995). Note that for most deposits in which liquid-rich, vapor-rich, and silicate melt inclusions coexist the salinities of the coexisting aqueous fluids are consistent with salinities expected at the reported PT trapping conditions where two aqueous fluid phases and melt would coexist (Fig. 5.8). For deposits where the salinity of the vapor is not reported, the vapor salinity can be estimated from PTX data for the system H_2O-NaCl. For example, in Cuasso al Monte (point 3 in Fig. 5.8), the salinity of the vapor that would coexist with the reported brines, having a salinity of ~50–60 wt% (Audétat et al. 2008), would be between 1 and 2 wt% NaCl. In the Mt. Malosa system (point 4 in Fig. 5.8), the fluid salinities reported should not be in equilibrium with a melt. If these fluids were directly exsolved from a melt, the PT conditions of trapping would be about 900 bars and 800 °C. In most deposits in which a single-phase fluid was reported to coexist with a melt the PT range reported, as expected, is systematically above the liquid-vapor curve for that salinity, i.e., in the single-phase fluid field. Some of the lower salinities reported (e.g., the Mole granite—point 7 in Fig. 5.8) would be within the two phase field, indicating that fluid immiscibility might have occurred or that the fluid composition is not properly approximated by the system H_2O-NaCl, as suggested by Steele-MacInnis et al. (2015).

The chloride content of magmatic aqueous fluids, to a large extent, controls melt-fluid partitioning of chloride-complexing metals and influences fluid flow in the system by affecting fluid density and, therefore, fluid buoyancy. At pressures below ~1.3 kbar, the salinity of a single-phase fluid exsolved from an intermediate-composition magma increases as magma crystallization proceeds, whereas at pressures above ~1.3 kbar the salinity of the single-phase fluid exsolved decreases during continued magma crystallization (Cline and Bodnar 1991; Audétat et al. 2008). Therefore, in systems emplaced at pressures lower than 1.3 kbar, the concentration of chloride-complexing metals in a single-phase fluid increases during crystallization (as the chloride content increases) and reaches its maximum at ≈80% melt crystallization. For systems emplaced at pressures higher than 1.3 kbar, the chloride content of a single-phase magmatic fluid gradually decreases as melt crystallizes (Cline and Bodnar 1991; Audétat et al. 2008). In this case, the chloride content of the magmatic fluid (and therefore the behavior of chloride-complexing metals) depends on the ratio of the initial concentration of

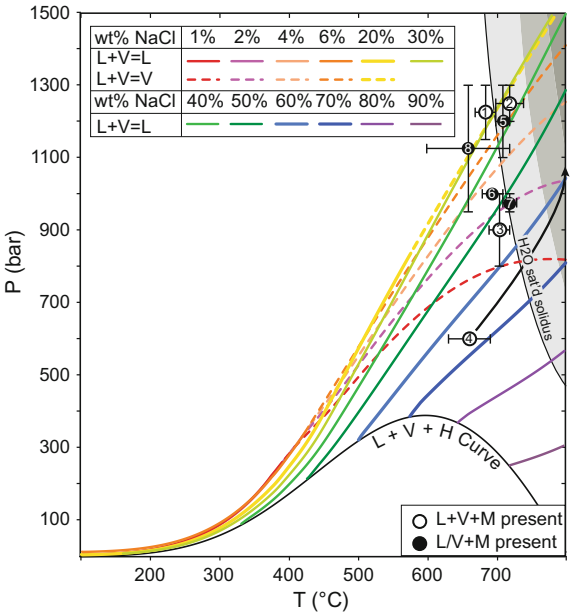

Fig. 5.8 Phase diagram of the system H_2O-NaCl showing the liquid-vapor-halite three-phase curve (L + V + H; black) and the liquid-vapor isopleths for various salinities calculated from Driesner and Heinrich (2007). For each isopleth, at PT conditions above and to the left (lower temperature or higher pressure) of the line within the PT range represented, a fluid of that composition is in the one-phase fluid field, whereas at PT conditions below and to the right (higher temperatures or lower pressures) a fluid of that composition is in the two-fluid-phase field. The *solid line* labeled "H_2O-sat'd solidus" represents the water-saturated minimum melting curve for a grantitic melt. The numbered data points represent the pressure-temperature conditions of trapping of a melt coexisting with one phase aqueous fluid *(open circles)* or with two-phase aqueous fluids *(filled circles)* for barren and mineralized porphyry systems (Audétat et al. 2008). Locations corresponding to the numbered points are *1* Mt. Malosa; *2* Santa Rita; *3* Cuasso al Monte; *4* Capitan Mt; *5* Rito del Medio; *6* Ehrenfriedersdorf; *7* Mole Granite; *8* Canada Pinabete. The salinities reported for these fluids as well as the source of the data are listed in Table 5.1

water in the melt to the water concentration at saturation. If the melt has a low initial water content, a large portion of the melt must crystallize before water saturation is achieved. Assuming that chloride remains in the melt and is not removed by crystallizing phases, the chloride concentration of the melt will increase as crystallization proceeds. Thus, water-depleted magmas will exsolve fluids later in the crystallization process and the salinity of the fluids will be relatively high, whereas water-enriched magmas will exsolve fluids earlier in the crystallization process and the salinity of the fluids will be relatively low (Cline and Bodnar 1991). In porphyries in which two-phase fluid exsolution occurs (e.g., Santa Rita, Reynolds and Beane 1985), the chloride content of the magmatic brine and vapor exsolved from a silicate melt remains constant as magma crystallization evolves (Shinohara 1994). Audétat et al. (2008) estimated the bulk metal content of two-phase fluids exsolved

from a silicate magma in the Santa Rita, New Mexico porphyry Cu deposit, and reported that the Pb concentration of the bulk fluid exsolved from the silicate melt remained roughly constant over time while the concentration of Cu decreased.

The partitioning of chloride-complexing metals between fluid and melt also depends on the composition of the silicate melt. Most notably, Sn partitioning depends on the HCl content of the fluid in equilibrium with the melt (Duc-Tin et al. 2007). The proportion of Cl exsolved as HCl (versus alkali chlorides) depends on the alumina saturation index of the melt (Urabe 1985; Frank et al. 2003). For example, up to 40% of the Cl in fluids in equilibrium with peraluminous melts at 700 °C occurs as HCl while on the order of 5–10% of the Cl in fluids in equilibrium with metaluminous melts is present as HCl. As a result, fluids exsolved from peraluminous melts at 700 °C contain up to 0.4 m HCl and up to 6000 ppm Sn (Duc-Tin et al. 2007) compared to 0.1 m HCl and $\leq$700 ppm Sn in fluids associated with metaluminous melts.

5.5.3 *Evolution of Cl in Porphyry- and Granite-Related Magmatic Fluids: Implications for Ore Transport and Deposition*

The magmatic fluid exsolved from a silicate melt constrains the initial metal signature of the different deposit types (Audétat et al. 2008). However later processes, such as fluid evolution, control the concentration of metals in specific locations and determine whether porphyry- and granite-related systems develop economic metal grades.

As previously discussed in Sect. 5.3, chloride is one of the major anions in geologic fluids and the system H_2O-NaCl is commonly used to approximate the PVTX properties of geologic fluids. A direct consequence of the range in salinities (2 to 80 wt%) and phase equilibrium behavior (one- or two-phase fluids) of hydrothermal fluids in porphyry-type deposits is that fluid density varies widely (from $\sim$0.2 to 1.1 g/cm^{-3} (Driesner 2007)) both spatially and temporally in the magmatic-hydrothermal system. This contrast in density affects fluid buoyancy and salinity evolution at the ore-deposit scale (Fournier 1987). Vapor-like and low-salinity fluids ascend whereas brines remain stationary or sink to greater depths (Henley and McNabb 1978). Recent modeling of magmatic-hydrothermal systems that implement dynamic permeability variations confirms that at lithostatic conditions brines do not ascend and that, as the permeability increases, brines tend to sink within the system (Weis et al. 2012, 2014a, b; Scott et al. 2017). In addition, halite precipitation at low pressures and high temperatures (upon entering the vapor plus halite field; Fournier 1987) is likely a common feature in porphyry-type systems and decreases the permeability (Weis 2014b; Gruen et al. 2014). Therefore, the chloride content (salinity) of the fluid controls the phase behavior and transport properties of the fluid, as well as the hydrology of the system.

Phase separation (immiscibility) of aqueous fluids is a widely reported phenomenon in greisen and porphyry deposits (Roedder 1984) and leads to the occurrence of a chloride-enriched (brine) and a chloride-depleted (vapor) phase. As previously discussed, phase separation can occur at PT conditions where the two fluid phases are in equilibrium with the silicate melt from which the fluid exsolved. Alternatively, a low-salinity single-phase fluid exsolved from a melt at depth may intercept the liquid-vapor field upon ascent (cooling and decompression) (Fig. 5.9). The specific depth at which fluid immiscibility occurs depends on the salinity of the fluid, and on the geothermal gradient in the vicinity of the cooling pluton, which in turn depends on the depth of emplacement of the pluton and the range of PT conditions at which the brittle-ductile transition occurs (Weis et al. 2012; Weis 2014a). In this sense, in deeper magmatic systems (e.g., 6 km), a single-phase fluid occurs over a relatively wide range of rock volume and time, whereas aqueous fluid immiscibility is more likely to occur over broader time and space intervals in hydrothermal systems associated with shallower plutons.

The partitioning behavior of elements between two coexisting immiscible fluids often results in efficient re-distribution of the elements, with some elements being enriched in one phase and others enriched in the other phase. As a result, the mineralizing potential of one of the resulting phases may be enhanced for some elements that are partitioned into that phase, whereas the mineralizing potential of the other fluid phase may be enhanced for other elements. Chloride-complexing

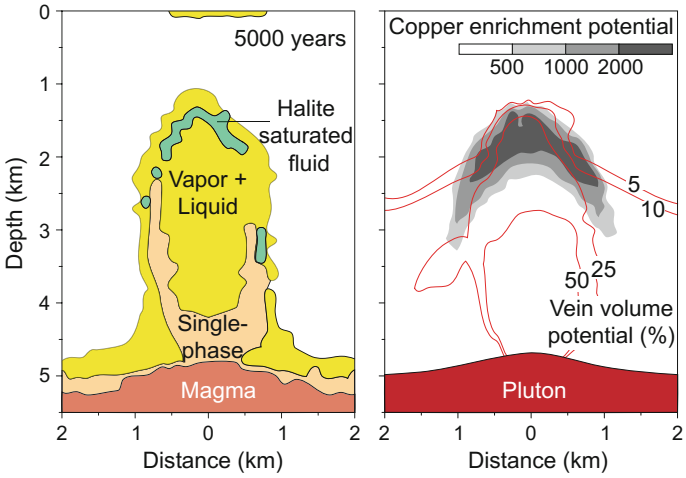

Fig. 5.9 Distribution of fluid phases above a magma body associated with the formation of a porphyry Cu deposit. The diagram on the left shows the regions where the different fluid phase assemblages are present within the magmatic-hydrothermal system 5000 years after pluton emplacement. The diagram on the right shows the areas of likely chalcopyrite precipitation (contoured in shades of *gray*) and the vein volume potential *(red contours)*. Note the coincidence of the field of halite-saturated fluid *(left)* and region of highest Cu enrichment potential *(right)*. From Weis et al. (2012)

metals (such as Fe, Pb, Zn, or Ag) partition preferentially into the brine, while elements that dominantly form hydroxyl- or sulfide-complexes (such as As or Au) partition preferentially into the vapor (Heinrich et al. 1999). Owing to the preferential partitioning of chloride into the brine, the brine has a greater mineralizing potential for chloride-complexing metals in systems where fluid immiscibility occurs.

Several mechanisms contribute to the precipitation of chloride-complexing metals in granite- and porphyry-ore deposits. Copper mineralization in porphyry deposits may be related to a steep decrease in chalcopyrite solubility during cooling at temperatures of ≈350–450 °C (Landtwing et al. 2005; Bodnar et al. 2014). This temperature range coincides as well with the brittle-ductile transition in porphyry systems (Hayba and Ingebritsen 1997). Modeling (Becker 2007; Weis et al. 2012; Weis 2014a) and phase equilibrium data suggest that, as a consequence of the steep PT gradient at the brittle-ductile transition, halite saturation commonly occurs over this same temperature range (e.g., Rottier et al. 2016). Simultaneous halite and vapor saturation, along the liquid-vapor-halite curve (L + V + H; Figs. 5.3 and 5.9), further decreases the amount of water and chloride available to transport Cu in the liquid phase and, therefore, promotes the precipitation of chalcopyrite in this temperature range (Lecumberri-Sanchez et al. 2015b), as shown by comparing the field of halite-saturated fluid (left) and region of highest Cu enrichment potential (right) on Fig. 5.9.

Other metals whose solubility is related to the chloride content of the fluid include Pb and Zn. The chloride content of the fluid constrains the pH (Yardley 2005), and the solubility of base metal sulfides (such as galena or sphalerite) is highly sensitive to the chloride content of the fluid and to pH changes. For example, low pH (acidic) fluids can carry orders of magnitude more Pb and Zn than their higher pH counterparts. Therefore, in some ore-forming systems (e.g., skarns) the neutralization of pH through fluid-rock interaction leads to base-metal precipitation (Williams-Jones et al. 2010). The change in fluid chemistry and metal-carrying capacity, which reflects the chemical interaction between fluid and rock, is directly responsible for the distribution of the alteration mineralogy observed in porphyry- and granite-related systems (Meyer and Hemley 1967; Beane and Titley 1981).

Epithermal Au-Ag-base metal deposits are generally associated with low-salinity fluids and boiling is an effective depositional process (Bodnar et al. 2014). Upon boiling, Au can be transported as a bisulfide complex in the vapor if S is present in the system. In this case, Au precipitation is coupled with sulfide precipitation and is interpreted to be the result of a decrease in the S available to form Au-S complexes when sulfides precipitate (Heinrich et al. 2004). Recent studies have shown that, in S poor systems where fluid immiscibility takes place at relatively high pressures, Au partitioning between liquid and vapor can lead to Au enrichment in the vapor and can explain Au transport and deposition by a low-density fluid (Hurtig and Williams-Jones 2014b). Despite the relatively low concentrations of Cl in epithermal systems, Ag and base metals are usually interpreted to be transported as chloride complexes and deposited as result of fluid mixing, temperature decrease,

boiling, or combinations thereof (Stefánsson and Seward 2003; Catchpole et al. 2011; Bozkaya and Banks 2015).

5.5.3.1 Effect of Halogens on Fluid-Rock Interaction

The development of alteration mineralogy in magmatic-hydrothermal systems depends on the degree of disequilibrium between the fluid and the rock and on the fluid-rock ratio. The pH of a fluid is a major control on the alteration mineralogy (Meyer and Hemley 1967), and the pH of fluids in mineral-buffered geologic systems is in turn a function of the chloride content of the fluid (Fig. 5.10) (Yardley 2005). For felsic to intermediate composition igneous rocks typical of porphyry- and greisen-type deposits, the alteration assemblage is controlled by the temperature, K activity, SiO_2 activity, and hydrogen ion activity (pH) in the fluid. The pH in turn is related to the dissociation of acids, (including HCl and, to a minor extent, HF), upon cooling of magmatic-hydrothermal fluids (Meyer and Hemley 1967; Beane and Titley 1981). High F concentrations in the fluid result in modification of the alteration mineralogy typical of porphyry- and granite-related ore deposits, prompting the growth of topaz instead of, or with, K-feldspar, muscovite, pyrophyllite, and kaolinite (Seedorff et al. 2005).

At most geological conditions some elements are commonly considered nominally immobile (e.g., Al, Zr, Nb, or REE). However, the occurrence of Al-bearing phases, such as hydrothermal garnet in skarns, suggests that under some

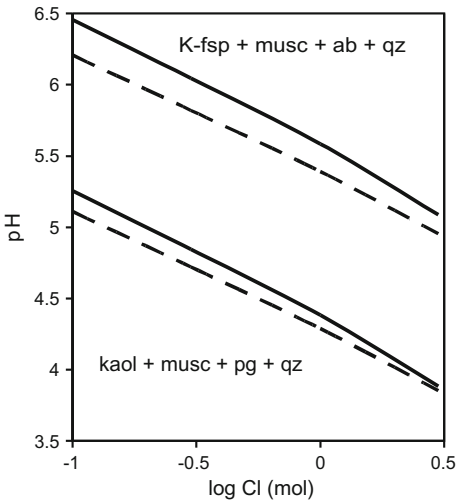

Fig. 5.10 pH versus log Cl molality of fluids in equilibrium with K-feldspar + muscovite + albite + quartz (upper curves), and with kaolinite + muscovite + paragonite + quartz (lower curves) at 275 °C *(solid lines)* and 225 °C *(dashed lines)*, at pressures on the liquid-vapor curve for H_2O. From Yardley (2005)

circumstances these elements are mobile. Mobilization of these classically immobile elements is frequently interpreted to be associated with high salinity fluids and extreme pH conditions, which are indirectly controlled by the fluid salinity, and high F contents (Gleason et al. 2000; Migdisov and Williams-Jones 2014). Therefore, the ability of a fluid to dissolve and transport nominally immobile elements is directly related to the Cl and F contents of the fluid.

Skarn deposits are examples of pH-controlled genetic processes, reflecting the interaction of a low pH fluid with a carbonate rock, resulting in carbonate dissolution and calcsilicate mineral precipitation. The low pH of the fluid is mostly a result of the S and Cl content of the fluid. Precipitation of chloride-complexing metals occurs when a low pH fluid interacts with the carbonate rock, resulting in an increase in pH, replacement of metal-Cl_n complexes in the fluid with $CaCl_2$ complexes, and incorporation of metals into the rock.

5.5.4 *Role of Halogens in Volcanogenic Massive Sulfide Deposits*

Volcanogenic massive sulfide (VMS) deposits are the fossil analogues of modern mid-ocean ridge (MOR) hydrothermal systems (Franklin et al. 2005). Kendrick (2015) discusses in detail the role that halogens play in hydrothermal processes associated with MOR systems. Therefore, in this section we limit our discussion to the effect of halogens on fluid phase behavior and mineralizing processes in VMS-type deposits. The host rock for VMS deposits is mainly basalt and the dominant source of fluid (and halogens) is seawater. The fluid salinity recorded in VMS deposits varies between about 2 and 6 wt%, although salinities up to 30 wt% have been reported in active seafloor vents (Damm et al. 1997; Bodnar et al. 2014). This salinity range is the result of phase separation (boiling) of seawater due to the high temperature and shallow depth (low pressure) occurrence of some MOR hydrothermal systems. The halogen isotopic signature of VMS fluids is roughly preserved through boiling and fluid-rock interaction processes in some cases (Bonifacie et al. 2005). Therefore, $\delta^{37}Cl$ is only slightly depleted with respect to seawater values, while in other cases there are significant changes in $\delta^{37}Cl$ associated with boiling processes.

The dominant ore metals in VMS deposits are Cu, Pb, and Zn. As discussed in Sect. 5.4, Pb and Zn are transported as chloride complexes, whereas Cu forms chloride or sulfide complexes, depending on the PTX properties of the fluids (Migdisov et al. 2014). The solubility of sphalerite (Fig. 5.7) and galena both decrease with decreasing fluid chlorinity, increasing f_{S2}, increasing pH, decreasing temperature, and decreasing f_{O2}. The dominant factors contributing to metal deposition in VMS deposits are cooling and pH increase upon mixing of hydrothermal fluids with cold seawater (Hannington 2014).

The distribution of mineralization in VMS deposits is also related to the salinity of the vent fluid, as this, in turn, affects the fluid density and buoyancy (Hannington 2014). Thus, the mixing of 350 °C hydrothermal fluids having salinities >10 wt% NaCl with cold seawater results in mixed fluids that are more dense than surrounding seawater and these fluids will descend and accumulate in brine pools to produce a laterally extensive sulfide blanket. Fluids of this same temperature but with salinities <10 wt% NaCl produce mixed fluids that are less dense than the surrounding seawater. Such fluids are buoyant and rise upwards and away from the vent region, allowing sulfide minerals to be dispersed over a wide area by near-bottom and mid-depth currents (Hannington 2014). Temporal variations in fluid density can also lead to the banding that is observed in VMS Cu-Zn ores.

Recent studies have also shown that salinity plays a major role in silica transport in the sub-seafloor feeder zones for VMS mineralization. Quartz exhibits retrograde solubility in pure H_2O at PT conditions in the vicinity of the critical point. As NaCl is added to H_2O, the region in which quartz shows retrograde solubility migrates to higher temperatures and pressures (Steele-MacInnis et al. 2012a). Additionally, at some sub-seafloor PT conditions, the H_2O-NaCl fluid undergoes phase separation, or boiling (Fig. 5.11). Fluid immiscibility leads to massive quartz precipitation, as the bulk solubility of quartz in the combined liquid + vapor phases is much lower than the solubility of quartz in the one-phase fluid before phase separation (Steele-MacInnis et al. 2012b). This region of massive quartz precipitation corresponds to the highly silicified zones found beneath VMS deposits.

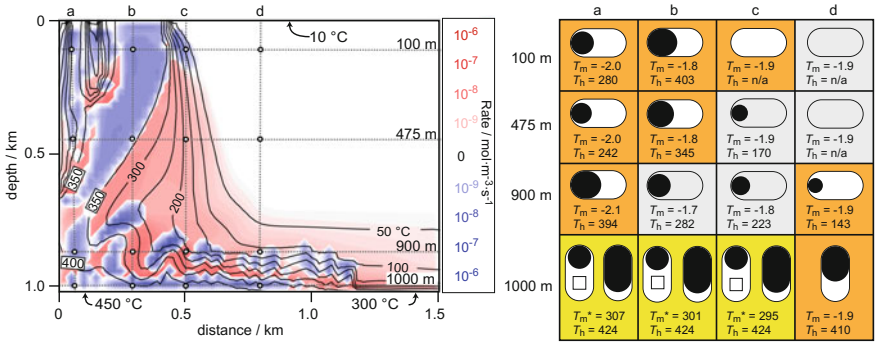

Fig. 5.11 Distribution of regions of quartz dissolution and precipitation *(left)* and fluid inclusions that would be trapped *(right)* at various locations in the sub-seafloor beneath hydrothermal vents associated with the formation of VMS deposits. Regions of quartz precipitation are shown in blue and regions of quartz dissolution are shown in *red*. The diagram on the right shows the room temperature phase relations and microthermometric properties of fluid inclusions trapped at locations shown on the left figure. T_m (°C) represents the predicted ice melting temperature. T_m* (°C) represents the predicted halite melting temperature. T_h (°C) is the liquid-vapor, homogenization temperature. Note that, in the right diagram, fluid inclusions shown with *gray* backgrounds represent locations in the sub-seafloor where quartz dissolution is occurring and therefore it is unlikely that inclusions would be trapped and/or preserved. *Orange-highlighted squares* indicate fluid inclusions trapped in the single phase field. *Yellow-highlighted squares* indicate fluid inclusions trapped in the two phase field. From Steele-MacInnis et al. (2012b)

5.5.5 Role of Halogens in Sediment-Hosted Pb-Zn Deposits

Sediment hosted Pb-Zn deposits, i.e., MVT and similar deposits, are characterized by saline ore-forming fluids typically derived from variable degrees of seawater evaporation (Kendrick and Burnard 2013; Wilkinson 2014). As a result of the high chloride content (salinity) of the fluids, significant concentrations of Pb and Zn can be carried in solution. Some fluid inclusions in these systems contain up to several hundred ppm of both Pb and Zn (Appold and Wenz 2011; Bodnar et al. 2014; Wilkinson 2010). Typically, the ore-bearing fluids are saline, low pH, high f_{O2}, low f_{S2} fluids, or combinations thereof. All of these factors contribute to the high metal-carrying capability of the fluid.

When high-salinity, metal-rich fluids interact with the carbonate host rock, the pH of the fluid increases and metals are deposited as Ca released from the carbonate host rocks replaces metals in solution to form $CaCl_2$ aqueous complexes. Interaction of metal-transporting fluids with reducing agents (such as organic matter) causes a decrease in f_{O2}, which decreases galena and sphalerite solubility. In cases where the reduced S content of the fluid is low, interaction with a reduced S source may lead to metal precipitation. The source of reduced S has proven to be, in some cases, bacterially produced sulfides from seawater sulfate reduction (Fallick et al. 2001; Wilkinson and Eyre 2005). Although some variations in the pH, $f_{O2,}$ and f_{S2} of the fluid are reported, high salinity seems to be a pre-requisite for generating a Pb- and Zn-rich fluid capable of producing sediment-hosted Pb-Zn deposits.

Basuki and Spooner (2002) compared temperatures and salinities of MVT fluid inclusions with ore grades and tonnages in the associated deposits. These researchers found that the temperature (~75 °C) and salinity (~16 wt% $CaCl_2$ equivalent) thresholds for MVT ore fluids reported by Hanor (1996) to generate metal-rich brines were applicable to MVT systems. Moreover, Basuki and Spooner (2002) reported that large tonnage districts/deposits tend to be associated with mean fluid salinities that are at the lower end (~16 to 21 wt% $CaCl_2$ equivalent) of the overall range of salinity (~16 to 26 wt% $CaCl_2$ equivalent) observed in MVT deposits (e.g., Tri-State district Stoffell et al. 2008). These workers also reported a correlation between higher ore grades and higher salinities.

5.5.6 Halogens in REE Deposits

REE deposits are commonly associated with carbonatites and peralkaline rocks (Verplanck et al. 2010). These rocks are derived from magmas formed by partial melting of metasomatized mantle originally enriched in REE, HFSEs, and halogens, and further enriched during emplacement into the crust (Verplanck et al. 2010). REE enrichment in these deposits is commonly associated with magmatic processes. However, recent studies suggest that melt-melt immiscibility can lead to significant additional enrichment of REE in one of the immiscible melt phases.

In particular, silicate-fluoride, silicate-chloride, silicate-phosphate, and silicate-sulfate melt immiscibility causes systematic depletion of REE in the silicate melt and enrichment in the coexisting non-silicate melt phase (Veksler et al. 2012). Silicate-fluoride melt immiscibility in some REE deposits results in the formation of REE-rich fluoride melts (Vasyukova and Williams-Jones 2014, 2016), and can be a critical step towards the formation of economic REE deposits.

The common association of REE deposits with abundant fluorite in hydrothermal systems suggested that F complexation in aqueous solution might be significant in the formation of these deposit types (Salvi and Williams-Jones 1990). However, the strong HF association at hydrothermal conditions implies that little F^- is available to act as a complexing agent and therefore most REE in these systems are likely transported as chloride-, carbonate-, or sulfate-complexes (Williams-Jones et al. 2012). In contrast, low pH HCl-HF bearing fluids associated with peralkaline intrusives have the capability to mobilize REE. Interaction of the low pH fluid with the rock can lead to mobilization of REE. Later interaction of that fluid with the rock (high fluid/rock ratios) can lead to deposition of REE upon pH buffering (Gysi and Williams-Jones 2013). The strong partitioning of REE into fluorite, upon precipitation from an aqueous fluid (Hinsberg 2015), implies that fluorite precipitation is an effective mechanism to concentrate REE in these deposit types.

5.6 Halogens as Exploration Tools

As a result of the critical role that halogens play in the transport and deposition of metals in ore-forming systems, halogen anomalies have been proposed as potential exploration tools. Nash (1976) suggested that the occurrence of halite-bearing fluid inclusions (high-salinity fluids) could be used as a guide to mineralization in porphyry Cu deposits. For example, in the Bingham Canyon porphyry Cu deposit, Moore and Nash (1974) reported that the zone in which halite-bearing fluid inclusions are found overlaps almost perfectly with the Cu ore zone. Similarly, Theodore and Nash (1973) found that the area in which surface outcrops contain halite-bearing fluid inclusions includes the areas representing the surface projections of the East and West orebodies in the Copper Canyon deposit, Utah.

Fuge and Andrews (1986) (and references therein) identified halogen anomalies in soil and rock as an exploration tool for porphyry Cu, MVT, and polymetallic veins based on the correlation of those anomalies with ore deposit occurrences. Böhlke and Irwin (1992) noted that, because different metals are transported as different chloride-complexes, the ratios of different halogens might be indicative of different deposit (metal) types. These descriptive observations have evolved over time as a tool to determine the source and behavior of halogens in several ore deposit types.

Specific ore deposit types have common genetic characteristics including a general range of pressure and temperature of formation and comparable fluid compositions. Therefore, the fluid phase behavior is systematically distributed in time and space

within different ore deposit types resulting in a relatively systematic distribution of fluid inclusion types. Steele-MacInnis et al. (2012b) modeled the distribution of fluid inclusion types, homogenization temperatures, and salinities in submarine hydrothermal systems using the available PVTX data for the system H_2O-NaCl (Fig. 5.11). The spatial distribution of fluid inclusions and the predicted microthermometric behavior agree with observations from VMS deposits. In the same manner, Weis et al. (2012) and Becker (2007) modeled the fluid phase behavior in porphyry Cu systems and the expected spatial distribution of fluid inclusion assemblages in these deposits (Fig. 5.9). The modeled behavior of the fluids matches the observed distribution of fluid inclusion types in porphyry Cu deposits (Rusk et al. 2008; Lecumberri-Sanchez et al. 2013). Early on, Roedder and Bodnar (1997) described a quantitative porphyry Cu-targeting index that is based partly on the presence of halite-bearing fluid inclusions and evidence of fluid immiscibility.

Fluid-phase behavior has direct implications on the dissolution-precipitation of some ore and gangue minerals (Moncada et al. 2012; Steele-MacInnis et al. 2012b). The PT range at which fluid immiscibility can occur, in particular, depends on the halogen content of the fluid. Fluid immiscibility generates characteristic mineral textures some of which can be identified in hand sample and/or under the microscope (Fig. 5.12). The various textures show close spatial and temporal associations with mineralization. As such, these systematically distributed features of ore

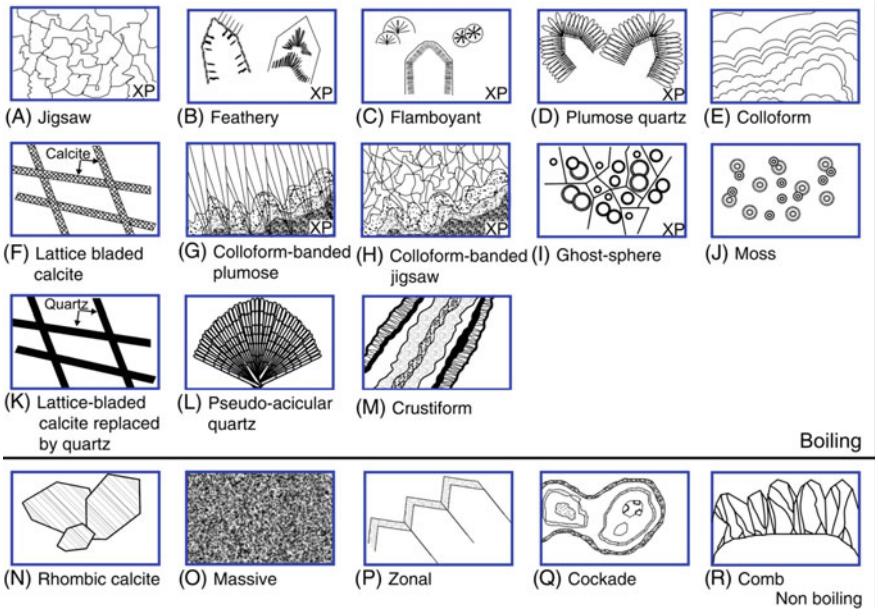

Fig. 5.12 Examples of various textures that can be used to distinguish between boiling and non-boiling fluids in the epithermal environment. All textures shown correspond to silica textures unless otherwise specified in the panels. *XP* indicates textures observed under crossed-polars. From Moncada et al. (2012)

deposits can be used as vectors towards the portion of a magmatic-hydrothermal system that is most likely to host ore. A good example of this application is textural evidence of fluid immiscibility that serves as a vector towards mineralization in low to intermediate sulfidation epithermal deposits (Moncada et al. 2012).

Acknowledgements We would like to thank Matthew Steele-MacInnis, Chris Heinrich, Philipp Weis, Thomas Driesner and the fluids group at ETH for helpful discussions on the role of halogens in ore deposits. Reviews of an earlier version of this manuscript by Anthony Williams-Jones, Terry Seward and David Banks are much appreciated and have led to a much improved manuscript. Dan Harlov and Leonid Aranovich are gratefully acknowledged for their support and patience in the editorial process. PLS was funded under the Marie Curie Intra European Fellowship 624767, and partial support for RJB during the preparation of this manuscript was provided by the U. S. National Science Foundation under grant no. EAR-1624589.

References

Aiuppa A, Baker DR, Webster JD (2009) Halogens in volcanic systems. Chem Geol 263:1–18

Akinfiev N, Tagirov B (2014) Zn in hydrothermal systems: thermodynamic description of hydroxide, chloride, and hydrosulfide complexes. Geochem Int 52(3):197–214

Anderko A, Pitzer KS (1993) Equation-of-state representation of phase equilibria and volumetric properties of the system NaCl-H_2O above 573 K. Geochim Cosmochim Acta 57:1657–1680

Appold MS, Wenz ZJ (2011) Composition of Ore Fluid Inclusions from the Viburnum Trend, Southeast Missouri District, United States: Implications for Transport and Precipitation Mechanisms. Econ Geol 106(1):55–78. https://doi.org/10.2113/econgeo.106.1.55

Audétat A, Pettke T (2003) The magmatic-hydrothermal evolution of two barren granites: a melt and fluid inclusion study of the Rito del Medio and Cañada Pinabete plutons in northern New Mexico (USA). Geochim Cosmochim Acta 67:97–121

Audétat A, Pettke T, Heinrich CA, Bodnar RJ (2008) The composition of magmatic-hydrothermal fluids in barren and mineralized intrusions. Econ Geol 103(5):877–908. https://doi.org/10.2113/gsecongeo.103.5.877

Baes CF, Mesmer RE (1976) The hydrolisis of cationes. Wiley, New York

Banks DA, Green R, Cliff RA, Yardley BWE (2000) Chlorine isotopes in fluid inclusions: determination of the origins of salinity in magmatic fluids. Geochim Cosmochim Acta 64 (10):1785–1789

Barnes J, Sharp Z (2006) A chlorine isotope study of DSDP/ODP serpentinized ultramafic rocks: insights into the serpentinization process. Chem Geol 228:246–265

Barnes SJ, Wells MA, Verrall MR (2009) Effects of magmatic processes, serpentinization, and talc-carbonate alteration on sulfide mineralogy and ore textures in the Black Swan disseminated nickel sulfide deposit, Yilgarn craton. Econ Geol 104:539–562

Basuki NI, Spooner ETC (2002) A review of fluid inclusion temperatures and salinities in mississippi valley-type Zn-Pb deposits: identifying thresholds for metal transport. Explor Min Geol 11(1–4):1–17. https://doi.org/10.2113/11.1-4.1

Bazarkina EF, Pokrovski GS, Zotov AV, Hazemann JL (2010) Structure and stability of cadmium chloride complexes in hydrothermal fluids. Chem Geol 276(1–2):1–17. https://doi.org/10.1016/j.chemgeo.2010.03.006

Beane RE, Titley SR (1981) Porphyry copper deposits Part II. Hydrothermal alteration and mineralization. In: Skinner BJ (ed) Economic geology 75th anniversary volume. The Economic Geology Publishing Company, Lancaster, PA, pp 235–269

Becker SP (2007) Fluid inclusion characteristics in magmatic-hydrothermal ore deposits. Virginia Polytechnic Institute and State University

Becker SP, Fall A, Bodnar RJ (2008) Synthetic fluid inclusions. XVII. PVTX properties of high salinith H_2O-NaCl solutions (> 30 wt% NaCl): Application to fluid inclusions that homogenize by halite disappearance from porphyry copper and other hydrothermal ore deposits. Econ Geol 103:539–554

Bernal NF, Gleeson SA, Dean AS, Liu X-M, Hoskin P (2014) The source of halogens in geothermal fluids from the Taupo Volcanic Zone, North Island, New Zealand. Geochim Cosmochim Acta 126:265–283

Bernal NF, Gleeson SA, Smith MP, Barnes JD, Pan Y (2017) Evidence of multiple halogen sources in scapolites from iron oxide-copper-gold (IOCG) deposits and regional NaCl metasomatic alteration, Norrbotten County, Sweden. Chem Geol 451:90–103

Bethke C (1996) Geochemical reaction modeling. Oxford University Press, New York

Birkle P, Marín E, Reyes R Chemical-isotopic evidences for the origin and evolution of geothermal fluids at the Tres Vírgenes geothermal field, B.C., NW-Mexico. In: World geothermal congress 2010, Bali, Indonesia, 2010. pp 1–10

Blaine FA, Linnen RL, Holtz F, Bruegmann GE (2011) The effect of Cl on Pt solubility in haplobasaltic melt: implications for micronugget formation and evidence for fluid transport of PGEs. Geochim Cosmochim Acta 75:7792–7805

Bodnar RJ, Costain JK (1991) Effect of fluid composition on mass and energy transport in the earth's crust. Geophys Res Lett 18:983–986

Bodnar RJ, Vityk MO (1994) Interpretation of microthermometric data for H_2O-NaCl fluid inclusions. In: De Vivo B, Frezzotti ML (eds) Fluid inclusions in minerals: methods and applications. Pontignano, Sienna, pp. 117–130

Bodnar RJ, Burnham CW, Sterner SM (1985) Synthetic fluid inclusions in natural quartz. III. Determination of phase equilibrium properties in the system H_2O-NaCl to 1000 °C and 1500 bars. Geochim Cosmochim Acta 49:1861–1873

Bodnar RJ, Lecumberri-Sanchez P, Moncada D, Steele-MacInnis M (2014) Fluid inclusions in hydrothermal ore deposits. In: Holland HD, Turekian KK (eds) Treatise on geochemistry, vol 13, 2nd edn. Elsevier, Oxford, pp 119–142

Böhlke JK, Irwin JJ (1992) Laser microprobe analyses of Cl, Br, I and K in fluid inclusions. Implications for sources of salinity in some ancient hydrothermal fluids. Geochim Cosmochim Acta 56:203–225

Bonifacie M, Charlou J, Jendrzejewski N, Agrinier P, Donval J (2005) Chlorine isotopic compositions of high temperature hydrothermal vent fluids over ridge axes. Chem Geol 221:279–288

Bonifacie M, Busigny V, Mével C, Philippot P, Agrinier P, Jendrzejewski N, Scambelluri M, Javoy M (2008a) Chlorine isotopic composition in seafloor serpentinites and high-pressure metaperidotites. Insights into oceanic serpentinization and subduction processes. Geochim Cosmochim Acta 72:126–139

Bonifacie M, Jendrzejewski N, Agrinier P, Humler E, Coleman M, Javoy M (2008b) The chlorine isotope composition of earth's mantle. Science 319:1518–1520

Bons PD, Fusswinkel T, Gomez-Rivas E, Markl G, Wagner T, Walter B (2014) Fluid mixing from below in unconformity-related hydrothermal ore deposits. Geology 42(12):1035–1038

Boomeri M, Nakashima K, Lentz DR (2009) The Miduk porphyry Cu deposit, Kerman, Iran: a geochemical analysis of the potassic zone including halogen element systematics related to Cu mineralization processes. J Geochem Explor 103:17–29

Boudreau AE, Hoatson DM (2004) Halogen variations in the Paleoproterozoic layered mafic-ultramafic intrusions of East Kimberley, Western Australia: implications for platinum group element mineralization. Econ Geol 99:1015–1026

Boudreau AE, Mathez EA, McCallum IS (1986) Halogen geochemistry of the Stillwater and Bushveld complexes: evidence for transport of the platinum-group elements by Cl-rich fluids. J Petrol 27(4):967–986

Bozkaya G, Banks DA (2015) Physico-chemical controls on ore deposition in the Arapucandere Pb-Zn-Cu-precious metal deposit, Biga Peninsula, NW Turkey. Ore Geol Rev 66:65–81

Campbell AR, Banks DA, Phillips RS, Yardley BWD (1995) Geochemistry of Th-U-REE mineralizing magmatic fluids, Captain Mountains, New Mexico. Econ Geol 90:1271–1287

Candela PA, Holland HD (1986) A mass transfer model for copper and molybdenum in magmatic-hydrothermal systems: the origin of porphyry-type ore deposits. Econ Geol 81:1–19

Catchpole H, Kouzmanov K, Fontboté L, Guillong M, Heinrich CA (2011) Fluid evolution in zoned Cordilleran polymetallic veins – insights from microthermometry and LA-ICP-MS of fluid inclusions. Chem Geol 281(3–4):293–304

Chiaradia M, Banks D, Cliff R, Marschik R, deHaller A (2006) Origin of fluids in South American iron oxide-copper-gold deposits: indications from delta 37Cl, 87Sr/86Sr initial and Cl/Br. Mineral Deposita 41:565–573

Chou I-M, Sterner SM, Pitzer KS (1992) Phase relations in the system NaCl-KCl-H_2O: IV. Differential thermal analysis of the sylvite liquidus in the KCl-H_2O binary, the liquidus in the NaCl-KCl-H_2O ternary, and the solidus in the NaCl-KCl binary to 2 kb pressure, and a summary of experimental data for thermodynamic-*PTX* analysis of solid-liquid equilibria at elevated *P-T* conditions. Geochim Cosmochim Acta 56:2281–2293

Cline JS, Bodnar RJ (1991) Can economic porphyry copper mineralization be generated by a typical calc-alkaline melt? J Geophys Res 96:8113–8126

Cline JS, Bodnar RJ (1994) Direct evolution of a brine from crystallizing silicic metl at the Questa, New Mexico, molybdenum deposit. Econ Geol 89:1780–1802

Crerar D, Wood S, Brantley S (1985) Chemical controls on solubility of ore-forming minerals in hydrothermal solutions. Can Mineral 23:333–352

Damm KLV, Buttermore LG, Oosting SE, Bray AM, Fornari DJ, Lilley MD, Shanks WC (1997) Direct observation of the evolution of a seafloor "black smoker" from vapor to brine. Earth and Planet Sci Lett 149:101–111

Diamond LW (2003) Introduction to gas-bearing, aqueous fluid inclusions. In: Samson I, Anderson A, Marshall D (eds) Fluid inclusions: analysis and interpretation, vol 32. Mineralogical Association of Canada Short Course Series Volume, pp 101–158

Dolejs D, Zajacz Z (2018) Halogens in silicic magmas and their hydrothermal systems. In: Harlov DE, Aranovich L (eds) The role of halogens in terrestrial and extraterrestrial geochemical processes: surface, crust and mantle. Springer, Berlin, pp 431–543

Driesner T (2007) The system H_2O-NaCl. Part II: Correlations for molar volume, enthalpy, and isobaric heat capacity from 0 to 1000 °C, 1 to 5000 bar and 0 to 1 XNaCl. Geochim Cosmochim Acta 71:4902–4919

Driesner T, Heinrich CA (2007) The system H_2O-NaCl. Part I: Correlation formulae for phase relations in temperature-pressure-composition space from 0 to 100 °C, 0 to 5000 bar, and 0 to 1 XNaC. Geochim Cosmochim Acta 71:4880–4901

Dubois M, Marignac C (1997) The H_2O-NaCl-$MgCl_2$ Ternary Phase Diagram with Special Application to Fluid Inclusion Studies. Econ Geol 92:114–119

Duc-Tin Q, Audétat A, Keppler H (2007) Solubility of tin in (Cl, F)-bearing aqueous fluids at 700 °C, 140 MPa: A LA-ICP-MS study on synthetic fluid inclusions. Geochim Cosmochim Acta 71:3323–3335

Eggenkamp H (2014) The geochemistry of stable chlorine and bromine isotopes (advances in isotope geochemistry). Springer, Berlin

Essarraj S, Boiron MC, Cathelineau M, Tarantola A, Leisen M, Boulvais P, Maacha L (2016) Basinal brines at the origin of the imiter Ag-Hg deposit (Anti-Atlas, Morocco): evidence from LA-ICP-MS data on fluid inclusions, halogen signatures, and stable isotopes (H, C, O). Econ Geol 111(7):1753–1781

Fallick AE, Ashton JH, Boyce AJ, Ellam RM, Russell MJ (2001) Bacteria were responsible for the magnitude of the world-class hydrothermal base metal sulfide orebody at Navan, Ireland. Econ Geol 96(4):885–890

Fournier RO (1987) Conceptual models of brine evolution in magmatic-hydrothermal systems. USGS Prof Pap 1350:1487–1506

Frank MR, Candela PA, Piccoli PM (2003) Alkali exchange equilibria between a silicate melt and coexisting magmatic volatile phase: an experimental study at 800 °C and 100 MPa. Geochim Cosmochim Acta 67(7):1415–1427

Franklin J, Gibson H, Jonasson I, Galley A (2005) Volcanogenic massive sulfide deposits. In: Hedenquist J, Thompson J, Goldfarb R, Richards J (eds) Economic geology: one hundredth anniversary volume 1905–2005. Society of Economic Geologists, Littleton, pp 523–560

Fuge R, Andrews MJ (1986) Chlorine and iodine, potential pathfinder elements in exploration geochemistry. Appl Geochem 1:111–116

Fusswinkel T, Wagner T, Walle M, Wenzel T, Heinrich CA, Markl G (2013) Fluid mixing forms basement-hosted Pb-Zn deposits: insight from metal and halogen geochemistry of individual fluid inclusions. Geology 41(6):679–682

Fusswinkel T, Wagner T, Wenzel T, Wälle M, Lorenz J (2014) Red bed and basement sourced fluids recorded in hydrothermal Mn-Fe-As veins, Sailauf (Germany): A LA-ICPMS fluid inclusion study. Chem Geol 363:22–39

Gál B, Molnár F, Guzmics T, Mogessie A, Szabó C, Peterson DM (2013) Segregation of magmatic fluids and their potential in the mobilization of platinum-group elements in the South Kawishiwi intrusion, Duluth complex, Minnesota – evidence from petrography, apatite geochemistry and coexisting fluid and melt inclusions. Ore Geol Rev 54:59–80

Germann K, Lüders V, Banks DA, Simon K, Hoefs J (2003) Late hercynian polymetallic vein-type base-metal mineralization in the Iberian Pyrite Belt: fluid-inclusion and stable-isotope geochemistry (S-O-H-Cl). Mineral Deposita 38:953–967

Gleason JD, Marikos MA, Barton MD, Johnson DA (2000) Neodymium isotopic study of rare earth element sources and mobility in hydrothermal Fe oxide (Fe-P-REE) systems. Geochim Cosmochim Acta 64(6):1059–1068

Gleeson SA, Smith MP (2009) The sources and evolution of mineralising fluids in iron-oxide-copper-gold systems, Norrbotten, Sweden: constrains from Br/Cl ratios and stable Cl isotopes of fluid inclusion leachates. Geochim Cosmochim Acta 73:5658–5672

Gruen G, Weis P, Driesner T, Heinrich CA, de Ronde, C. E. (2014) Hydrodynamic modeling of magmatic-hydrothermal activity at submarine arc volcanoes, with implications for ore formation. Earth Planet Sci Lett 404:307–318

Gysi AP, Williams-Jones AE (2013) Hydrothermal mobilization of pegmatite-hosted REE and Zr at Strange Lake, Canada: a reaction path model. Geochim Cosmochim Acta 122:324–352

Hall DL, Sterner SM, Bodnar RJ (1988) Freezing point depression of NaCl-KCl-H_2O solutions. Econ Geol 83:197–202

Hammerli J, Rusk B, Spandler C, Emsbo P, Oliver NHS (2013) In situ quantification of Br and Cl in minerals and fluid inclusions by LA-ICPMS: a powerful tool to identify fluid sources. Chem Geol 337–338:75–87

Hanley JJ, Koga K (2018) Halogens in terrestrial and cosmic geochemical systems: abundances, geochemical behaviours, and analytical methods. In: Harlov DE, Aranovich L (eds) The role of halogens in terrestrial and extraterrestrial geochemical processes: surface, crust and mantle. Springer, Berlin, pp 21–121

Hanley JJ, Mungall JE (2003) Chlorine enrichment and hydrous alteration of the Sudbury breccia hosting footwall Cu-Ni-PGE mineralization at the Fraser mine, Sudbury, Ontario, Canada. Can Mineral 41:857–881

Hanley JJ, Mungall JE, Pettke T, Spooner ETC, Bray CJ (2005a) Ore metal redistribution by hydrocarbon-brine and hydrocarbon-halide melt phases, North Range footwall of the Sudbury Igneous Complex, Ontario, Canada. Mineral Deposita 40:237–256

Hanley JJ, Pettke T, Mungall JE, Spooner ETC (2005b) Investigations of the behavior and distribution of platinum and gold in silicate melt-brine mixtures at 1.5 kbar, 600 to 800 °C using synthetic fluid inclusions method: a laser ablation ICPMS pilot study. Geochim Cosmochim Acta 69:2593–2611

Hanley JJ, Pettke T, Mungall JE, Spooner ETC (2005c) The solubility of platinum and gold in NaCl brines at 1.5 kbar, 600 to 800 °C: a laser ablation ICP-MS study of synthetic fluid inclusions. Geochim Cosmochim Acta 69(10):2593–2611

Hanley JJ, Mungall JE, Pettke T, Spooner ETC, Bray CJ (2008) Fluid and halide melt inclusions of magmatic origin in the ultramafic and lower banded series, Stillwater complex, Montana, USA. J Petrol 49(6):1133–1160

Hannah JL, Stein HJ (1990) Magmatic and hydrothermal processes in ore bearing systems. Geol Soc Am Spec Pap 246:1–10

Hannington M (2014) Volcanogenic massive sulfide deposits. In: Holland H, Turekian K (eds) Treatise on geochemistry, vol 13, 2nd edn. Elsevier, Oxford, pp 119–142

Harlov DE, Aranovich L (2018) The role of halogens in terrestrial and extraterrestrial geochemical processes: surface, crust, and mantle. In: Harlov DE, Aranovich L (eds) The role of halogens in terrestrial and extraterrestrial geochemical processes: surface, crust, and mantle. Springer, Berlin, pp 1–19

Hauri E (2002) SIMS analysis of volatiles in volcanic glasses: 2. Isotopes and abundances in Hawaiian melt inclusions. Chem Geol 183:117–143

Hayba DO, Ingebritsen SE (1997) Multiphase groundwater flow near cooling plutons. J Geophys Res 102(B6):12235–12252

Heinrich C, Candela P (2014) Fluids and ore formation in the Earth's crust. In: Holland H, Turekian K (eds) Treatise on geochemistry, vol 13. Elsevier, Oxford, pp 1–28

Heinrich C, Günther D, Audétat A, Ulrich T, Frischknecht R (1999) Metal fractionation between magmatic brine and vapor determined by microanalysis of fluid inclusions. Geology 27 (8):755–758

Heinrich CA (2007a) Fluid-fluid interactions in magmatic-hydrothermal ore formation. Rev Mineral Geochem 65:363–387. https://doi.org/10.2138/rmg.2007.65.11

Heinrich CA, Seward TM (1990) A spetrophotometric study of aqueous iron (II) chloride complexing from 25 °C to 200 °C. Geochim Cosmochim Acta 54:2207–2221

Heinrich CA, Driesner T, Stefansson A, Seward TM (2004) Magmatic vapor contraction and the transport of gold from the porphyry environment to epithermal. Geology 32(9):761–764

Heinrich W (2007b) Fluid immiscibility in metamorphic rocks. Rev Mineral 65:389–430

Helgeson HC (1969) Thermodynamics of hydrothermal systems at elevated temperatures and pressures. Am J Sci 267:729–804

Helgeson HC, Kirkham DH (1974a) Theoretical prediction of the thermodynamic behavior of aqueous electrolytes at high pressures and temperatures. I. Summary of the thermodynamic/ electrostatic properties of the solvent. Am J Sci 274:1089–1198

Helgeson HC, Kirkham DH (1974b) Theoretical prediction of the thermodynamic behavior of aqueous electrolytes at high pressures and temperatures. II. Debye -huckel parameters for activity coefficients and partial molal properties. Am J Sci 274:1199–1261

Helgeson HC, Kirkham DH (1976) Theoretical prediction of the thermodynamic behavior of aqueous electrolytes at high pressures and temperatures. III. Equation of state for aqueous species at infinite dilution. Am J Sci 276:97–240

Helgeson HC, Delaney JM, Nesbitt HW, Bird DK (1978) Summary and critique of the thermodynamic properties of rock-forming minerals. Am J Sci 278-A:1–229

Helgeson HC, Kirkham DH, Flowers GC (1981) Theoretical prediction of the thermodynamic behavior of aqueous electrolytes at high pressures and temperatures. IV. Calculation of activity coefficients, osmotic coefficients, and apparent molal and standard and relative partial molal properties to 600 C and 5 kb. Am J Sci 281:1249–1516

Henley RW, McNabb A (1978) Magmatic vapor plumes and ground water interaction in porphyry copper emplacement. Econ Geol 73(1):1–20

Hilbert R (1979) PVT-Daten von Easser und von Wässrigen Natriumchlorid-Lösungen bis 873 K, 4000 bar und 25 gew.-% NaCl. Thesis, 212 pp (in German)

Hinsberg VJv (2015) Reading the mineral record of fluid composition from element partitioning. Geology 38(9):847–850

Hofstra AH, Meighan CJ, Song X, Samson I, Marsh EE, Lowers HA, Emsbo P, Hunt AG (2016) Mineral thermometry and fluid inclusion studies of the pea ridge iron oxide-apatite–rare earth element deposit, Mesoproterozoic St. Francois Mountains Terrane, Southeast Missouri, USA. Econ Geol 111(8):1985–2016

Hurtig NC, Williams-Jones AE (2014a) An experimental study of the solubility of MoO3 in aqueous vapour and low to intermediate density supercritical fluids. Geochim Cosmochim Acta 136:169–193

Hurtig NC, Williams-Jones AE (2014b) An experimental study of the transport of gold through hydration of AuCl in aqueous vapour and vapour-like fluids. Geochim Cosmochim Acta 127:305–325

Hurwitz S, Mariner RH, Fehn U, Snyder GT (2005) Systematics of halogen elements and their radioisotopes in thermal springs of the Cascade Range, Central Oregon, Western USA. Earth Planet Sci Lett 235:700–714

Ihinger PD, Hervig RL, McMillan PF (1994) Analytical methods for volatiles in glasses. Rev Mineral 30:67–121

Johnson JW, Norton D (1991) Critical Phenomena in Hydrothermal Systems: State, Thermodynamic, Electrostatic, and Transport Properties of H_2O in the Critical Region. Am J Sci 291:541–648

Kendrick M (2018) Halogens in seawater, marine sediments and the altered oceanic lithosphere. In Harlov DE, Aranovich L (eds) The role of halogens in terrestrial and extraterrestrial geochemical processes: surface, crust, and mantle. Springer, Berlin, pp 591–648

Kendrick M, Burgess R, Leach D, Pattrick R (2002) Hydrothermal fluid origins in Mississippi valley-type ore districts: combined noble gas (He, Ar, Kr) and halogen (Cl, Br, I) analysis of fluid inclusions from the Illinois-Kentucky fluorspar district, Viburnum Trend, and Tri-State districts, midcontinent United States. Econ Geol 97(3):453–469

Kendrick M, Mark G, Philips D (2007) Mid-crustal fluid mixing in a Proterozoic Fe oxide-Cu-Au deposit, Ernest Henry, Austrealia: evidence from Ar, Kr, Xe, Cl, Br and I. Earth Planet Sci Lett 256:328–343

Kendrick M, Honda M, Gillen D, Baker T, Philips D (2008) New constraints on regional brecciation in the Wernecke Mountains, Canada from He, Ne, Ar, Kr, Xe, Cl, Br and I in fluid inclusions. Chem Geol 255:33–36

Kendrick M, Phillips D, Wallace M, Miller J (2011) Halogens and noble gases in sedimentary formation waters and Zn-Pb deposits: a case study from the Lennard Shelf, Australia. Appl Geochem 26:2089–2100

Kendrick MA, Burnard P (2013) Noble gases and halogens in fluid inclusions: a journey through the Earth's crust. In: Burnard P (ed) The noble gases as geochemical tracers. Advances in isotope geochemistry. Springer, Berlin, pp 319–369

Kendrick MA, Burgess R, Pattrick RAD, Turner G (2001) Fluid inclusion noble gas and halogen evidence on the origin of Cu-porphyry mineralising fluids. Geochim Cosmochim Acta 65 (16):2651–2668

Kesler SE, Vennemann TW, Frederickson C, Breithaupt A, Vazquez R, Furman F (1997) Hydrogen and oxygen isotope evidence for origin of MVT-forming brines, southern Appalachians. Geochim Cosmochim Acta 6:1513–1523

Khaibullin IK, Borisov NM (1966) Experimental investigation of the thermal properties of aqueous and vapor solutions of sodium and potassium chlorides at phase equilibrium. High Temp 4(4):489–494

Klemm LM, Pettke T, Heinrich CA (2008) Fluid and source magma evolution of the Questa porphyry Mo deposit, New Mexico, USA. Mineral Deposita 43:533–552

Klyukin YI, Driesner T, Steele-MacInnis M, Bodnar RJ (2016) Effect of salinity on mass and energy transport by hydrothermal fluids in the critical region based on the physical and thermodynamic properties of H_2O-NaCl. Geofluids (in press)

Kusebauch C, John T, Barnes JD, Klügel A, Austrheim HO (2015a) Halogen element and stable chlorine isotope fractionation caused by fluid-rock interaction (Bamble Sector, SE Norway). J Petrol 56(2):299–324

Kusebauch C, John T, Whitehouse MJ, Klemme S, Putnis A (2015b) Distribution of halogens between fluid and apatite during fluid-mediated replacement processes. Geochim Cosmochim Acta 170:225–246

Landtwing MR, Pettke T, Halter WE, Heinrich CA, Redmond PB, Einaudi MT, Kunze K (2005) Copper deposition during quartz dissolution by cooling magmatic-hydrothermal fluids; the Bingham porphyry. Earth Planet Sci Lett 235:1–2. https://doi.org/10.1016/j.epsl.2005.02.046

Layne G, Kent A, Bach W (2009) δ^{37}Cl systematics of a backarc spreading system: the Lau Basin. Geology 37:427–430

Lecumberri-Sanchez P, III MCN, Westman EC, Kamilli RJ, Canby VM, Bodnar RJ (2013) Temporal and spatial distribution of alteration, mineralization and fluid inclusions in the transitional high-sulfidation epithermal-porphyry copper system at Red Mountain, Arizona. J Geochem Explor 125: pp 80–93

Lecumberri-Sanchez P, Steele-MacInnis M, Bodnar RJ (2015a) Synthetic fluid inclusions XIX. Experimental determination of the vapor-saturated liquidus of the system H_2O-NaCl-$FeCl_2$. Geochim Cosmochim Acta 148:34–49

Lecumberri-Sanchez P, Steele-MacInnis M, Weis P, Driesner T, Bodnar RJ (2015b) Salt precipitation in magmatic-hydrothermal systems associated with upper crustal plutons. Geology 43(12):1063–1066

Lentz D (1994) Exchange interactions in hydrothermally altered rocks: examples from biotite-bearing assemblages. In: Alteration and alteration processes associated with ore forming systems, vol 11. Geological Association of Canada Short Course Notes, pp 69–99

Liebscher A (2007) Experimental studies in model fluid systems. Rev Mineral Geochem 65:15–48

Liu W, Etschmann B, Foran G, Shelley M, Brugger J (2007) Deriving formation constants for aqueous metal complexes from XANES spectra: Zn^{2+} and Fe^{2+} chloride complexes in hypersaline solutions. Am Mineral 92:761–770

Liu WH, Borg SJ, Testemale D, Etschmann B, Hazemann JL, Brugger J (2011) Speciation and thermodynamic properties for cobalt chloride complexes in hydrothermal fluids at 35-440 degrees C and 600 bar: An in-situ XAS study. Geochim Cosmochim Acta 75(5):1227–1248. https://doi.org/10.1016/j.gca.2010.12.002

Lüders V, Pracejus B, Halbach P (2001) Fluid inclusion and sulfur isotope studies in probable modern analogue Kuroko-type ores from the JADE hydrothermal field (central Okinawa Trough, Japan). Chem Geol 173(1–3):45–58

Lüders V, Banks D, Hallbach P (2002) Extreme Cl/Br and δ^{37}Cl isotope fractionation in fluids of modern submarine hydrothermal systems. Mineral Deposita 37:765–771

Luo M, Tang J, Mao J, Wang L, Chen W, Leng Q (2014) Immiscibility of magmatic fluids and their relation to Mo and Cu mineralization at the Bangpu porphyry deposit, Tibet, China. J Asian Earth Sci 7(1):13819

Magenheim A, Spivack A, Michael P, Gieskes J (1995) Chlorine stable isotope composition of the oceanic crust: implications for Earth's distribution of chlorine. Earth Planet Sci Lett 131:427–432

Manning DAC (1981) The effect of fluorine on liquidus phase relationships in the system Qz-Ab-Or with excess water at 1 Kb. Contrib Mineral Petrol 76:206–215

Marks N, Schiffman P, Zierenberg R, Elders WA, Fridleifsson GO (2010) Franzson H Isotopic evidence of hydrothermal exchange and seawater ingress from alteration minerals in the Reykjanes geothermal system: results from the IDDP. World geothermal congress, Bali, Indonesia, p 4

Mathez EA, Webster JD (2005) Partitioning behavior of chlorine and fluorine in the system apatite-silicate melt-fluid. Geochim Cosmochim Acta 69(5):1275–1286

Mei Y, Sherman DM, Liu W, Brugger J (2013) Ab initio molecular dynamics simulation and free energy exploration of copper (I) complexation by chloride and bisulfide in hydrothermal fluids. Geochim Cosmochim Acta 102:45–64

Meyer C, Hemley JJ (1967) Wall rock alteration. In: Barnes HL (ed) Geochemistry of hydrothermal ore deposits. Rinehart & Winston, Holt, pp 166–235

Migdisov A, Zezin D, Williams-Jones AE (2011a) An experimental study of Cobalt (II) complexation in Cl- and H2S-bearing hydrothermal solutions. Geochim Cosmochim Acta 75(14):4065–4079

Migdisov AA, Williams-Jones AE (2013) A predictive model for metal transport of silver chloride by aqueous vapor in ore-forming magmatic-hydrothermal systems. Geochim Cosmochim Acta 104:123–135

Migdisov AA, Williams-Jones AE (2014) Hydrothermal transport and deposition of the rare earth elements by fluorine-bearing aqueous liquids. Mineral Deposita 49:987–997

Migdisov AA, Williams-Jones AE, Hinsberg VV, Salvi S (2011b) An experimental study of the solubility of baddeleyite (ZrO_2) in fluoride-bearing solutions at elevated temperature. Geochim Cosmochim Acta 75:7426–7434

Migdisov AA, Bychkov AY, Williams-Jones AE, Hinsberg VJv (2014) A predictive model for the transport of copper by HCl-bearing water vapour in ore-forming magmatic-hydrothermal systems: implications for copper porphyry ore formation. Geochim Cosmochim Acta 129:33–53

Molnár F, Watkinson DH, Jones PC (2001) Multiple hydrothermal processes in footwall units of the north range, Sudbury igneous complex, Canada, and implications for the genesis of vein-type Cu-Ni-PGE deposits. Econ Geol 96:1645–1670

Moncada D, Mutchler S, Nieto A, Reynolds TJ, Rimstidt JD, Bodnar RJ (2012) Mineral textures and fluid inclusion petrography of the epithermal Ag-Au deposits at Guanajuato, Mexico: application to exploration. J Geochem Explor 114:20–35

Moore WJ, Nash TJ (1974) Alteration and fluid inclusion studies of the porphyry copper orebody at Bingham, Utah. Econ Geol 69:631–645

Müller B, Seward T (2001) Spectrophotometric determination of the stability of tin (II) chloride complexes in aqueous solution up to 300 °C. Geochim Cosmochim Acta 65:4187–4199

Mungall JE, Brenan JM (2003) Experimental evidence for the chalcophile behavior of the halogens. Can Mineral 41:207–220

Nahnybida T, Gleeson SA, Rusk BG, Wassenaar LI (2009) Cl/Br ratios and stable chlorine isotope analysis of magmatic-hydrothermal fluid inclusions from Butte, Montana and Bingham Canyon, Utah. Mineral Deposita 44:837–848

Nash TJ (1976) Fluid-inclusion petrology - Data from porphyry copper deposits and applications to exploration. US Geological Survey Professional Paper 907-D, pp 1–16

Oakes CS, Bodnar RJ, Simonson JM (1990) The system NaCl-$CaCl_2$-H_2O. I. The vapor-saturated ice liquidus. Geochim Cosmochim Acta 54:603–610

Oakes CS, Bodnar RJ, Simonson JM, Pitzer KS (1995) $CaCl_2$-H_2O in the supercritical and two-phase ranges. Int J Thermophys 16:483–492

Pearson RG (1963) Hard and soft acids and bases. J Am Chem Soc 85:3533–3539

Pascal M, Boiron MC, Ansdell K, Annesley IR, Kotzer T, Jiricka D, Cuney M (2016) Fluids preserved in variably altered graphitic pelitic schists in the Dufferin Lake Zone, South-central Athabasca Basin, Canada: implications for graphite loss and uranium deposition. Mineral Deposita 51(5):619–636

Piccoli P, Candela P (1994) Apatite in felsic rocks: a model for the estimation of initial halogen concentration in the Bishop tuff (Long Valley) and Tuolumne intrusive suite (Sierra Nevada batholith) magmas. Am J Sci 294:92–135

Pyle D, Mather T (2009) Halogens in igneous processes and their fluxes to the atmosphere and oceans from volcanic activity: a review. Chem Geol 263:110–121

Reich M, Snyder GT, Alvarez F, Perez A, Palacios C, Vargas G, Cameron EM, Muramatsu Y, Fehn U (2013) Using iodine isotopes to constrain supergene fluid sources in arid regions: insights from the Chuquicamata oxide blanket. Econ Geol 108:163–171

Reynolds TJ, Beane RE (1985) Evolution of hydrothermal fluid characteristics at the Santa Rita, New Mexico, porphyry copper deposit. Econ Geol 80:1328–1347

Richard A, Kendrick MA, Cathelineau M (2014) Noble gases (Ar, Kr, Xe) and halogens (Cl, Br, I) in fluid inclusions from the Athabasca Basin (Canada): Implications for unconformity-related U deposits. Precambr Res 247:110–125

Richard A, Cathelineau M, Boiron MC, Mercadier J, Banks DA, Cuney M (2016) Metal-rich fluid inclusions provide new insights into unconformity-related U deposits (Athabasca Basin and Basement, Canada). Mineral Deposita 51(2):249–270

Roedder E (1984) Fluid inclusions. Rev Mineral 12:644
Roedder E (1992) Fluid inclusion evidence for immiscibility in magmatic differentiation. Geochim Cosmochim Acta 56:5–20
Roedder E, Bodnar RJ (1997) Fluid inclusion studies of hydrothermal ore deposits. In: Barnes HL (ed) Geochemistry of hydrothermal ore deposits, 3rd edn. Wiley, New York, pp 657–698
Rottier B, Kouzmanov K, Bouvier AS, Baumgartner LP, Wälle M, Rezeau H, Bendezú R, Fontboté L (2016) Heterogeneous melt and hypersaline liquid inclusions in shallow porphyry type mineralization as markers of the magmatic-hydrothermal transition (Cerro de Pasco district, Peru). Chem Geol 447:93–116
Rusk B, Reed MH, Dilles JH (2008) Fluid inclusion evidence for magmatic-hydrothermal fluid evolution in the porphyry copper-molybdenum deposit, Butte, Montana. Econ Geol 103:307–334
Salvi S, Williams-Jones AE (1990) The role of hydrothermal processes in the granite-hosted Zr, Y, REE deposit at Strange Lake, Quebec/Labrador: evidence from fluid inclusions. Geochim Cosmochim Acta 54:2403–2418
Schmidt C, Bodnar RJ (2000) Synthetic fluid inclusions: XVI. PVTX properties in the system H_2O-NCl-CO_2 at elevated temperatures, pressures, and salinities. Geochim Cosmochim Acta 64(22):3853–3869
Scott S, Driesner T, Weis P (2017) Boiling and condensation of saline geothermal fluids above magmatic intrusion. Geophys Res Lett 44(4):1696-1706
Seedorff E, Dilles JH, Proffett JM, Einaudi MT, Zurcher L, Stavast WJA, Johnson DA, Barton MD (2005) Porphyry deposits: characteristics and origin of hypogene features. Econ Geol 100th Ann Vol: 251–298
Seo JH, Guillong M, Aerts M, Zajacz Z, Heinrich CA (2011) Microanalysis of S, Cl, and Br in fluid inclusions by LA-ICP-MS. Chem Geol 284:35–44
Seward T, Williams-Jones A, Migdisov A (2014) The chemistry of metal transport and deposition by ore-forming hydrothermal fluids. In: Holland HD, Turekian KK (eds) Treatise on geochemistry, vol 13. Elsevier, Oxford, pp 29–57
Seward TM, Barnes HL (1997) Metal transport by hydrothermal ore fludis. In: Barnes HL (ed) Geochemistry of hydrothermal ore deposits, 3rd edn. Wiley, pp 435–486
Shinohara H (1994) Exsolution of immiscible vapor and liquid phases from a crystallizing silicate melt: implications for chlorine and metal transport. Geochim Cosmochim Acta 58 (23):5215–5221
Siahcheshm K, Calagari A, Abedini A, Lentz D (2012) Halogen signatures of biotites from the Maher-Abad porphyry copper deposit, Iran: characterization of volatiles in syn- to post-magmatic hydrothermal fluids. Int Geol Rev 54(12):1353–1368
Simon AC, Pettke T (2009) Platinum solubility and partitioning in a felsic melt-vapor-brine assemblage. Geochim Cosmochim Acta 73:438–454
Smith M, Gleeson S, Yardley B (2013) Hydrothermal fluid evolution and metal transport in the Kiruna District, Sweden: contrasting metal behaviour in aqueous and aqueous-carbonic brines. Geochim Cosmochim Acta 102:89–112
Sourirajan S, Kennedy G (1962) The system H_2O-NaCl at elevated temperatures and pressures. Am J Sci 260:115–141
Steele-MacInnis M, Bodnar RJ (2013) Effect of the vapor phase on the salinity of halite-bearing aqueous fluid inclusions estimated from the halite dissolution temperature. Geochim Cosmochim Acta 115:205–216
Steele-MacInnis M, Bodnar RJ, Naden J (2011) Numerical model to determine the composition of H_2O-NaCl-$CaCl_2$ fluid inclusions based on microthermometric and microanalytical data. Geochim Cosmochim Acta 75(1):21–40
Steele-MacInnis M, Han L, Lowell RP, Rimstidt JD, Bodnar RJ (2012a) The role of fluid phase immiscibility in quartz dissolution and precipitation in sub-seafloor hydrothermal systems. Earth Planet Sci Lett 321–322:139–151. https://doi.org/10.1016/j.epsl.2011.12.037

Steele-MacInnis M, Han L, Lower RP, Rimstidt DJ, Bodnar RJ (2012b) Quartz precipitation and fluid inclusion characteristics in sub-seafloor hydrothermal systems associated with volcanogenic massive sulfide deposits. Central Eur J Geosci 4:275–286

Steele-MacInnis M, Lecumberri-Sanchez P, Bodnar RJ (2015) Synthetic fluid inclusions XX. Critical PTx properties of H_2O-$FeCl_2$ fluids. Geochim Cosmochim Acta 148:50–61

Steele-MacInnis M, Ridley J, Lecumberri-Sanchez P, Schlegel TU, Heinrich CA (2016) Application of low-temperature microthermometric data for interpreting multicomponent fluid inclusion compositions. Earth Sci Rev 159:14–35

Stefánsson A, Seward TM (2003) Stability of chloridogold(I) complexes in aqueous solutions from 300 to 600 °C and from 500 to 1800 bar. Geochim Cosmochim Acta 67(23):4559–4576

Stoffell B, Appold MS, Wilkinson JJ, McClean NA, Jeffries TE (2008) Geochemistry and evolution of mississippi valley-type mineralizing brines from the Tri-State and Northern Arkansas Districts determined by LA-ICP-MS microanalysis of fluid inclusions. Econ Geol Bull Soc Econ Geol 103(7):1411–1435. https://doi.org/10.2113/gsecongeo.103.7.1411

Student JJ, Bodnar RJ (2004) Silicate melt inclusions in porphyry copper deposits: Identification and homogenization behavior. Can Mineral 42:1563–1600

Tagirov B, Schott J, Harrichourry J-C, Salvi S (2002) Experimental study of aluminum speciation in fluoride-rich supercritical fluids. Geochim Cosmochim Acta 66(11):2013–2024

Testemale D, Brugger J, Liu WH, Etschmann B, Hazemann JL (2009) In-situ X-ray absorption study of Iron(II) speciation in brines up to supercritical conditions. Chem Geol 264(1–4):295–310. https://doi.org/10.1016/j.chemgeo.2009.03.014

Theodore TG, Nash JT (1973) Geochemical and fluid zonation at Copper Canyon, Lander County, Nevada. Econ Geol 68:565–570

Tian Y, Etschmann B, Liu WH, Borg S, Mei Y, Testemale D, O'Neill B, Rae N, Sherman DM, Ngothai Y, Johannessen B, Glover C, Brugger J (2012) Speciation of nickel (II) chloride complexes in hydrothermal fluids: In situ XAS study. Chem Geol 334:345–363. https://doi.org/10.1016/j.chemgeo.2012.10.010

Tian Y, Etschmann B, Mei Y, Grundler P, Testemale D, Hazemann J, Elliot P, Ngothai Y, Brugger J (2014a) Speciation and thermodynamic properties of manganese (II) chloride complexes in hydrothermal fluids: In situ XAS study. Geochim Cosmochim Acta 129:77–95

Tian Y, Liu W, Sherman DM, Brugger J (2014b) Metal complexation and ion hydration in low density hydrothermal fluids: ab initio molecular dynamics simulation of Cu)I) and Au(I) in chloride solutions (25–1000 °C, 1–5000 bar). Geochim Cosmochim Acta 131:196–212

Timofeev A, Migdisov AA, Williams-Jones AE (2015) An experimental study of the solubility and speciation of niobium in fluoride-bearing aqueous solutions at elevated temperature. Geochim Cosmochim Acta 158:103–111

Tobie RA, Hemingway BS, Fisher JR (1978) Thermodynamic properties of minerals and related substances at 298.15 K and 1 bar pressure and at higher temperatures. Geol Surv Bull 1452

Turekian KK, Wedepohl KH (1961) Distribution of the elements in some major units of the Earth's crust. Geol Soc Am Bull 72:175–192

Urabe T (1985) Aluminous granite as a source magma of hydrothermal ore deposits: an experimental study. Econ Geol 80:148–157

Valyashko VM (2004) Phase equilibria of water-salt systems at high temperature and pressures. In: Palmer DA, Fernandez-Prini R, Harvey AH (eds) Aqueous systems at elevated temperatures and pressures. Elsevier, Amsterdam, pp 597–641

Vasyukova O, Williams-Jones AE (2014) Fluoride-silicate melt immiscibility and its role in REE ore formation: evidence from the Strange Lake rare metal deposit, Québec-Labrador, Canada. Geochim Cosmochim Acta 139:110–130

Vasyukova O, Williams-Jones AE (2016) The evolution of immiscible silicate and fluoride melts: implications for REE ore-genesis. Geochim Cosmochim Acta 172:205–224

Veksler IV, Dorfman AM, Dulski P, Kamenetsky VS, Danyushevsky LV, Jeffries T, Dingwell DB (2012) Partitioning of elements between silicate melt and immiscible fluoride, chloride, carbonate, phosphate and sulfate melts, with implications to the origin of natrocarbonatite. Geochim Cosmochim Acta 79:20–40

Verplanck PL, Gosen BSV, Seal RR, McCafferty AE (2010) A deposit model for carbonatite and peralkaline intrusion-related rare earth element deposits. US Geological Survey Scientific Investigations Report 2010-5070-J:58

Wagner W, Pruss A (1995) The IAPWS formulation 1995 for the thermodynamic properties of ordinary water substance for general and scientific use. J Phys Chem Ref Data 31:387–535

Walter BF, Burisch M, Markl G (2016) Long-term chemical evolution and modification of continental basement brines—a field study from the Schwarzwald, SW Germany. Geofluids 16 (3):604–623

Walter BF, Steele-MacInnis M, Markl G (2017) Sulfate brines in fluid inclusions of hydrothermal veins: compositional determinations in the system H_2O-Na-Ca-Cl-SO_4. Geochim Cosmochim Ac 209:184–203

Webster JD (1997a) Chloride solubility in felsic melts and the role of chloride in magmatic degassing. J Petrol 38(12):1793–1807

Webster JD (1997b) Exsolution of magmatic volatile phases from Cl-enriched mineralizing granitic magmas and implications for ore metal transport. Geochim Cosmochim Acta 61 (5):1017–1029

Webster JD, Holloway JR (1990) Partitioning of F and Cl between magmatic hydrothermal fluids and highly evolved granitic magmas. Geol Soc Am Spec Pap 246:21–34

Webster JD, Mandeville CW (2007) Fluid immiscibility in volcanic environments. Rev Mineral Geochem 65:313–362

Webster JD, Sintoni MF, Vivo BD (2007) The dramatic effects of C-S-O-H-Cl on the melt-fluid partitioning of Cl and the challenge of accurately modeling Cl concentrations of evolving magmatic fluids. In: AGU, San Francisco,

Webster JD, Tappen CM, Mandeville CW (2009) Partitioning behavior of chlorine and fluorine in the system apatite-melt-fluid. II: Felsic silicate systems at 200 MPa. Geochim Cosmochim Acta 73(3):559–581

Webster J, Baker DR, Aiuppa A (2018) Halogens in mafic and intermediate-silica content magmas. In: Harlov DE, Aranovich L (eds) The role of halogens in terrestrial and extraterrestrial geochemical processes: surface, crust and mantle. Springer, Berlin, pp 307–430

Weis P (2014a) The dynamic interplay between saline fluid flow and rock permeability in magmatic-hydrothermal systems. Geofluids 15:350–371. https://doi.org/10.1111/gfl.12100

Weis P (2014b) The physical hydrology of ore-forming magmatic-hydrothermal systems. Soc Eco Geol Spec Publ 10(18):59–75

Weis P, Driesner T, Heinrich CA (2012) Porphyry-copper ore shells form at stable pressure-temperature fronts within dynamic fluid plumes. Science 338:1613–1616

White AF, Delany JM, Truesdell A, Janik K, Goff F, Crecraft H (1984) Fluid chemistry of the Baca geothermal field, Valles caldera, New Mexico. In: Baldridge WS, Dickerson PW, Riecker RE, Zidek J (eds) New Mexico Geological Society 35th annual fall field conference guidebook. pp 257–263

Wilkinson J (2010) A review of fluid inclusion constraints on mineralization in the irish ore field and implications for the genesis of sediment-hosted Zn-Pb deposits. Econ Geol 105:417–442

Wilkinson JJ (2001) Fluid inclusions in hydrothermal ore deposits. Lithos 55(1–4):229–272

Wilkinson JJ (2014) Sediment-hosted zinc-lead mineralization: processes and perspectives. In: Holland HD, Turekian KK (eds) Treatise on geochemistry, vol 13. Elsevier, Oxford, pp 219–249

Wilkinson JJ, Eyre SL (2005) Ore-forming processes in Irish-type carbonate-hosted Zn-Pb deposits: evidence from mineralogy, chemistry, and isotopic composition of sulfides at the Lisheen mine. Econ Geol 100(1):63–68

Williams-Jones AE, Samson IM, Ault KM, Gagnon JE, Fryer BJ (2010) The genesis of distal zinc skarns: evidence from the Mochito deposit. Honduras. Econ Geol 105(8):1411–1440

Williams-Jones AE, Migdisov AA, Samson IM (2012) Hydrothermal mobilisation of the rare elements – a tale of "Ceris" and "Yttria". Elements 8:355–360

Wood SA (1990a) The aqueous geochemistry of the rare earth elements and yttrium,2. Theoretical prediction of speciation in hydrothermal solutions to 350 °C at saturated water pressure. Chem Geol 88(1–2):99–125

Wood SA (1990b) The aqueous geochemistry of the rare-earth elements and yttrium, I. Review of available low-temperature data for inorganic complexes and the inorganic REE speciation of natural waters. Chem Geol 82:159–186

Wood SA, Samson IM (2000) The hydrothermal geochemistry of tungsten in granitoid environments: I. Relative solubilities of ferberite and scheelite as a function of T, P, pH and m(NaCl). Econ Geol 95(1):143–182

Worden RH (2018) Halogen elements in sedimentary systems and their evolution during diagenesis. In Harlov DE, Aranovich L (eds) The role of halogens in terrestrial and extraterrestrial geochemical processes: surface, crust, and mantle. Springer, Berlin, pp 185–260

Xiao Z, Gammons CH, Williams-Jones AE (1998) Experimental study of copper(I) chloride complexing in hydrothermal solutions at 40 to 300 °C and saturated water vapor pressure. Geochim Cosmochim Acta 62(17):2949–2964

Yardley BWD (2005) Metal concentrations in crustal fluids and their relationship to ore formation. Econ Geol Bull Soc Econ Geol 100(4):613–632. https://doi.org/10.2113/100.4.613

Yardley BWD, Banks DA, (1992) Munz IA Halogen compostion of fluid inclusions as tracers of crustal fluid behaviour. In: Kharaka YK, Maest AS (eds) 7th International symposium on water-rock interaction. Moderate and high temperature environments. Balkema, Rotterdam, pp 1137–1140

Yardley BWD, Bodnar RJ (2014) Fluids in the continental crust. Geochem Perspect 3(1):127

Zajacz Z, Halter WE, Pettke T, Guillong M (2008) Determination of fluid/melt partition coefficients by LA-ICPMS analysis of co-existing fluid and silicate melt inclusions: controls on element partitioning. Geochim Cosmochim Acta 72:2169–2197

Zajacz Z, Seo JH, Candela PA, Piccoli PM, Tossell JA (2011) The solubility of copper in high-temperature magmatic vapors: a quest for the significance of various chloride and sulfide complexes. Geochim Cosmochim Acta 75:2811–2827

Zezin D, Driesner T, Sanchez-Valle C (2014a) Volumetric properties of mixed electrolyte aqueous solutions at elevated temperatures and pressures. The system KCl-NaCl-H_2O to 523.15 K, 40 MPa, and ionic strength from (0.1 to 5.8) mol.kg-1. J Chem Eng Data 59(3):736–749

Zezin D, Driesner T, Scott S, Sanchez-Valle C, Wagner T (2014b) Volumetric properties of mixed electrolyte aqueous solutions at elevated temperatures and pressures. The systems $CaCl_2$-NaCl-H_2O and $MgCl_2$-NaCl-H_2O to 523.15 K, 70 MPa, and ionic strength from (0.1 to 18) mol.Kg-1. J Chem Eng Data 59(8):2570–2588

Zhang Y-G, Frantz JD (1987) Determination of the Homogenization Temperatures and Densities of Supercritical Fluids in the System KCl-$CaCl_2$-H_2O Using Synthetic Fluid Inclusions. Chem Geol 64:335–350

Chapter 6
Halogens in Mafic and Intermediate-Silica Content Magmas

James D. Webster, Don R. Baker and Alessandro Aiuppa

Abstract As volatile and variably mobile components, halogens play key roles in magmatic, metasomatic, mineralizing, and volcanic processes by influencing the physical and chemical properties of melts, fluids, and minerals. Volcanic emission of halogens to the atmosphere leads to long- and short-term impacts on atmospheric chemistry that range from global perturbation of the stratospheric O_3 budget to more localized life-threatening contamination of soils and fresh water. The concentrations of F, Cl, Br, and I in melts, fluids, and minerals provide crucial geochemical information and insights into magmatic processes ranging from partial melting to volcanic eruptions. Halogen research is useful for evaluating global-scale recycling processes involving the atmosphere, hydrosphere, lithosphere, and mantle. This study reviews halogens in basaltic to andesitic magmas and in their alkaline equivalents (basanites to phonolites). We examine and apply the results of hydrothermal experiments and thermodynamic modeling to the impacts of halogens on melting and crystallization behavior, exsolution of vapor and/or hydrosaline liquids, thermal stability of hydrous minerals, viscosity and diffusion in melts, and on melt-fluid(s) partitioning as they bear on volcanic degassing and the generation of halogen-bearing mineralizing fluids. A recurrent observation is that data for F and Cl in many of these magmas are available, but Br and I data are insufficient and much needed. It is also apparent that additional experiments on halogen-bearing

J.D. Webster (✉)
Department of Earth and Planetary Sciences, American Museum of Natural History, Central Park West at 79th St., NewYork, NY 10024-5192, USA
e-mail: jdw@amnh.org

D.R. Baker
Earth and Planetary Sciences, GEOTOP-UQAM-McGill, McGill University, H3A 2A7 Montreal, QC, Canada
e-mail: don.baker@mcgill.ca

A.Aiuppa
Dipartimento DiSTeM, Università Di Palermo, Via Archirafi 36, 90123 Palermo, Italy
e-mail: alessandro.aiuppa@unipa.it

A.Aiuppa
Istituto Nazionale di Geofisica e Vulcanologia, Via La Malfa 153, 90146 Palermo, Italy

D.E. Harlov and L. Aranovich (eds.), *The Role of Halogens in Terrestrial and Extraterrestrial Geochemical Processes*, Springer Geochemistry,
https://doi.org/10.1007/978-3-319-61667-4_6

mafic to intermediate-silica content melts and fluids are required and that thermodynamic models of magmatic and hydrothermal processes should include the role of Cl in melt-vapor-hydrosaline equilibria. We apply data on halogen behavior in magmatic systems to processes of assimilation and partial melting in magmatic seafloor environments to interpret observed glass compositions, and to processes involving halogens erupted via volcanic plumes to the atmosphere.

6.1 Introduction

Halogens in igneous systems exert controls on magmatic, magmatic-hydrothermal, metasomatic, and volcanic phenomena that are disproportionate to their terrestrial abundances (Patiño Douce et al. 2011). Fluorine and Cl alter the thermal stabilities and phase equilibria of melts, minerals, and coexisting fluids as well as the viscosities of silicate melts. They augment the concentrations of major, minor, and trace elements, including metals of potential economic interest, in aqueous and aqueous-carbonic magmatic fluids and in saline liquids, and control component transport in volcanic gases. Although the magmatic geochemistry of Br and I has received far less scrutiny, F, Cl, Br, and I have all proven to be useful as geochemical tracers of magmatic, eruptive, metasomatic, and mineralizing processes. Research involving the halogens, for example, has provided critical geochemical constraints on the cycling of volatile components between Earth's atmospheric, surface, crustal, and mantle reservoirs. Regarding the latter reservoirs, particular attention has been focused on the behavior of fluid-mobile halogens and other constituents soluble in hydrothermal fluids during subduction, mantle metasomatism, and melting, and during the ascent and evolution of magmas from deeply sourced basalts to shallowly emplaced granites.

This chapter provides a comprehensive review of the halogen concentrations of volcanic gases, fluid inclusions, silicate melt inclusions, silicate glasses, whole rocks, and halogen-enriched and volatile-poor minerals for magmatic systems with mafic compositions to those with intermediate-silica contents, including alkaline varieties. We address the solubility relationships and partitioning behavior of F, Cl, Br, and I between melts, fluids, and minerals in basaltic- to andesitic-composition magmas, as well as in their alkaline counterparts (e.g., basanites to phonolites and their plutonic equivalents, nepheline syenites). Experimental and thermodynamic approaches used to unravel magmatic halogen behavior are reviewed and applied to processes of magma differentiation, volcanic eruption, and mineralization.

6.1.1 Nomenclature

Before addressing the role of halogens in magmatic phase equilibria, their solubilities in mafic to intermediate silica-content melts, their influence on melt

viscosity and diffusion, and on the partitioning of halogens between melts, minerals, and fluids, it is useful to explain relevant terminology. Herein we abbreviate basaltic, andesitic, and equivalent alkaline melts as BAA melts. We define fluids as non-crystalline, volatile-bearing, multicomponent phases. Vapor and gas refer to the relatively low-density ($\rho < 1$) fluid phase that is largely aqueous or aqueous-carbonic in composition. Higher-density fluid phases include silicate melt and liquids such as hydrosaline or carbonate liquids. Melt refers to the highest-viscosity, aluminosilicate-dominated fluids addressed herein. We use hydrosaline liquid (also referred to as brine) to represent electrolyte-enriched aqueous or aqueous-carbonic fluids. Fluid unmixing or phase separation can occur as either the condensation of droplets of a hydrosaline liquid from vapor or immiscible separation of vapor bubbles from a hydrosaline liquid through boiling.

Solubility is used to quantify the concentration of a substance (solute) that dissolves into a solvent. This definition requires the presence of two or more distinct phases (e.g., aluminosilicate melt coexisting with vapor, or hydrosaline liquid, or vapor plus hydrosaline liquid or, perhaps, a halogen-rich mineral such as fluorite). To describe halogen solubilities in aluminosilicate melts, it is required that the melt is saturated and in thermodynamic equilibrium with at least one conjugate halogen-bearing phase (fluid, hydrosaline liquid, or crystal). The solubilities of the heavier halogens, Br and I, have not yet been determined for geologically relevant melts, but saturation values have been measured for F and Cl and in this review they derive from analyses of aluminosilicate glasses representing quenched melts that were saturated in fluoride- or chloride-salt liquids at experimental run conditions. In the case of melts coexisting with saline liquids enriched in $H_2O \pm CO_2 \pm SO_2 \pm H_2S$, the term partitioning is used to describe the concentration of a halide in fluid(s) versus that in the coexisting silicate melt or between minerals and melt or between minerals and fluid(s). Partitioning is commonly expressed as the Henrian or Nernstian partition (or distribution) coefficient, $D_i^{fluid/melt}$, which is the concentration of a species, *i*, in one phase divided by its concentration in an accompanying phase at equilibrium. The distribution of each component between a fluid and silicate melt is driven by the thermodynamic requirement that the chemical potential of component *i*, μ_i, in a system at equilibrium must be equivalent in all phases within that system. This requirement controls the solubilities of all volatiles in silicate melts and their partitioning between the fluid and melt. As noted, the maximum concentrations of Br and I reported for the various aluminosilicate melts addressed below do not involve melts saturated in molten bromide or iodide salts and the reported Br and I concentrations are not true solubilities. Rather, these maxima involve halide partitioning between fluid(s) and melt. For experiments involving silicate melt, vapor, and a hydrosaline liquid, the reported partition coefficients express the halogen concentrations in the bulk integrated vapor plus saline liquid relative to that in the melt.

Within this contribution we review the diffusivities of halogens in basaltic to andesitic melts. Confusion can arise because the abbreviation used for the diffusivity of an element is the same as that used for the partition coefficient, D. To

eliminate, or at least mitigate, this confusion values of D_i (where *i* is abbreviated as F, Cl, Br, or I) apply to partition coefficients; whereas, D_i (where *i* is spelled out as fluorine, chlorine, bromine, or iodine) refers to diffusion coefficients.

6.2 Halogens in Whole Rocks, Glasses, Melt Inclusions, Fluid Inclusions, and Minerals

Much is known about the natural abundances and geochemical behavior of F and Cl in magmatic systems, but less so for Br and I. Current understanding is based largely on analyses of matrix glasses, silicate melt inclusions (MI), fluid inclusions (FI), whole-rock samples, hydrous and halogen-bearing minerals, nominally anhydrous and halogen-poor minerals, and volcanic gases (Oppenheimer 2011; Fischer and Chiodini 2015). Application of halogen analyses from these geological materials requires examination for the potential effects of metasomatism, magmatic degassing, phenocryst fractionation, disequilibrium, and weathering. Silicate melt inclusion data must also be filtered for the effects of syn- and post-entrapment modifications, such as diffusive fractionation, host phase crystallization, leakage along cracks in the host, potential post-entrapment diffusional loss of volatiles, and other potential problems (Audetat and Lowenstern 2013). Effective constraints on halogen dissolution in melts also derive from experimental volatile solubility and phase equilibrium studies as well as empirical- and thermodynamic-based modeling.

The chemical and physical properties of F, Cl, Br, and I and their varied concentrations in the bulk silicate Earth ultimately control their behavior in natural aluminosilicate melts. The pyrolitic silicate Earth composition estimated by McDonough and Sun (1995), for example, indicates: 25, 17, 0.05, and 0.01 ppm of F, Cl, Br, and I, respectively. Halogen concentration ranges in melts are a function of the competing influences of partial melting and their concentrations at the source of melting, fractional crystallization, contamination and assimilation, magma mixing and mingling, and degassing. These processes influence the halogen contents in melts differently because of differing anion sizes and electronegativities. The Pauling electronegativities of F, Cl, Br, and I vary: 3.98, 3.16, 2.96, and 2.66, respectively. Their anionic radii vary: 133, 181, 196, and 220 pm, respectively, and hence their ability to attract electrons normalized to their ionic radii vary as well: 0.029, 0.017, 0.015, and 0.012 (1/picometer), respectively. These basic chemical properties influence the reactivity of the halogens with other ions and also their contrasting solubilities in melts and fluids, as well as their differing capacities to substitute in minerals (Dolejs and Zajacz 2018). Analogous to the ionic field strength, the comparatively larger (electronegativity/radius) ratio of F, for instance, causes it to be more reactive with cations in silicate melts, enhances its solubility in melts, and supports its fractionation from the other halogens during degassing. Moreover, the relatively larger radii of Cl and Br and their smaller (electronegativity/radius) ratios increase their fractionation from fluid-saturated melt during magmatic degassing because of their higher solubilities in aqueous fluids (Teiber et al. 2014).

6.2.1 Halogen Concentrations of Glasses and Melt Inclusions (MI)

Analyses of natural aluminosilicate glasses (i.e., matrix glass and quenched exteriors of pillow basalts) and melt inclusions (MI) report concentrations of F and Cl in silicate melts varying from sub- and low-parts per million (ppm) to weight percent (wt%) values. Concentrations of the rare and heavier halogens I and Br, on the other hand, are typically much lower and range from tens of parts per billion (ppb) to tens of ppm, respectively (Fig. 6.1). In the following discussion, we consider scrutinized and filtered glass compositions to represent those of the corresponding melts and magmatic systems. Figure 6.1 shows how the natural abundances of F, Cl, Br, and I vary with bulk silica content of glasses reported on an anhydrous basis. This figure, and several following figures, are based on a data set comprising >5600 MI and individual glass analyses; most of the data were derived from the GEOROC database (http://georoc.mpch-mainz.gwdg.de/georoc/ accessed 1 May 2014). The vast majority of glasses reported here represent magma erupted subaqueously, and they should still contain magmatic volatile contents. Before discussing the data it should be noted, however, that this dataset includes sampling biases based on the research objectives of the more than 100 separate investigations and the data should only be used to interpret halogen ranges in magmas and not the relative significance of differing magma types. For instance, this set of data includes nearly as many glass analyses from alkaline, basanitic-phonolitic volcanic systems as it does from mid ocean ridge (MOR) basalt glasses, but the former are less common on Earth. The latter, in fact, represent the most voluminous form of terrestrial magmatism. Approximately 24 km^3 of magma passes through the Earth's crust annually (Sigurdsson 2000), and approximately 75% of this volume is emplaced and/or erupts at spreading centers and hot spots so the majority of this magma is basaltic. Moreover, most of these magmas are not alkaline in composition. In addition, many of the studies of MI representing MOR, hot spot, and ocean island basalts (OIB) do not include data for F, and, as detailed below, few of the studies involved have analyzed Br or I. Finally, most but not all of the low-SiO_2 MI hosted in ferromagnesian minerals have been corrected for post-entrapment crystallization or chemical exchanges between MI and host mineral, but the influences of these corrections on halogen contents should be negligible.

For undegassed silicate melts, those that are silica poor (Fig. 6.1) generally contain the lowest magmatic halogen concentrations (Métrich and Wallace 2008). As explained below, halogen sequestration by fluids can significantly reduce their concentrations in melts. Chlorine and F contents as low as 1 to 8 ppm, for example, have been measured (Fig. 6.2) in basaltic MI and glasses (containing 48 to 50 wt% SiO_2) from mid-ocean ridges, large igneous flood basalt provinces (LIPs), and oceanic hot spots (Saal et al. 2002; Koleszar et al. 2009; Kendrick et al. 2012a, b; 2014a, b). The most F- and Cl-deficient basaltic magmas erupt at the MOR (Jambon et al. 1995; Michael and Cornell 1998) and at plume-related hot spots such as the Hawaiian islands (Hauri 2002; Coombs et al. 2004), Galapagos islands (Koleszar

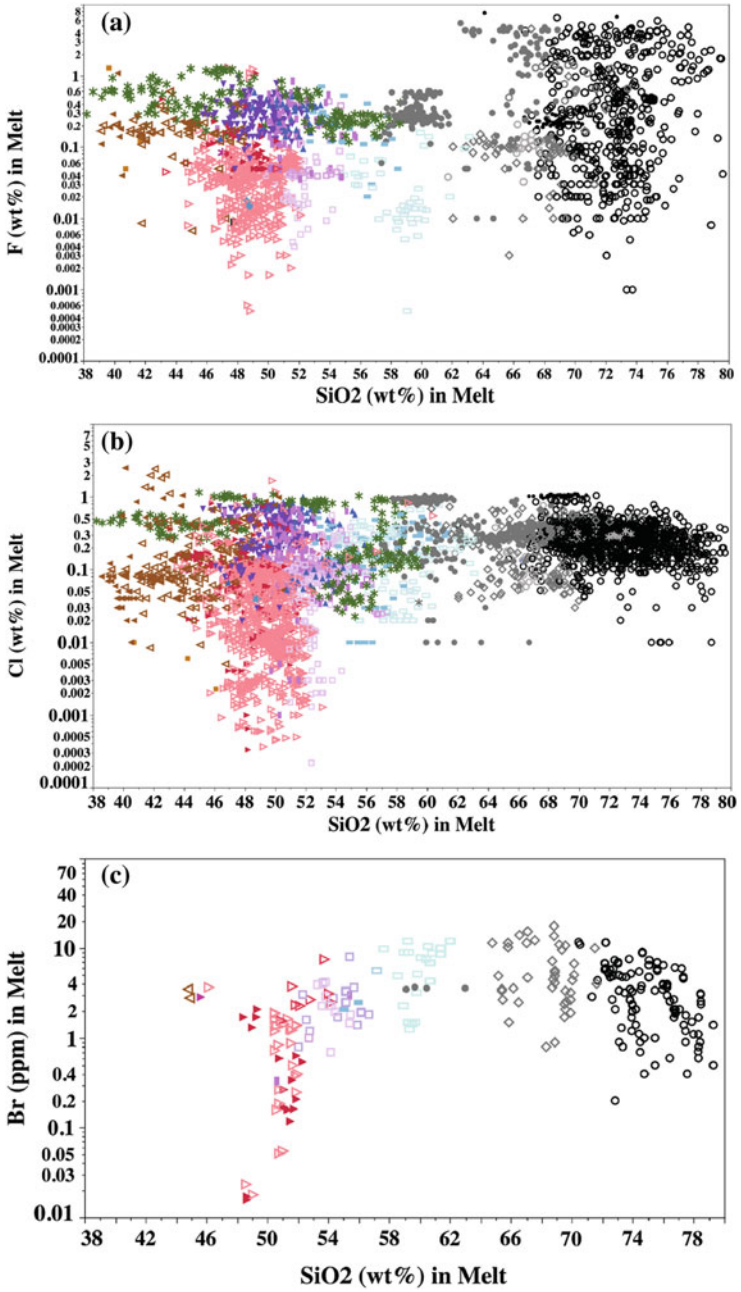

Fig. 6.1 Concentration plots of **a** wt% F (2275 data), **b** wt% Cl (4710), **c** ppm Br (175 data), and **d** ppb I (92 data) versus SiO_2 (wt%) in seafloor and matrix glasses and silicate melt inclusions (MI) representative of ultramafic-kimberlitic to high-silica magmas. **e** Samples differentiated chemically (by their symbols) as a function of ($Na_2O + K_2O$) versus SiO_2 on an anhydrous basis: *1* foidite, *2* picrobasalt, *3* basalt, *4* basaltic andesite, *5* andesite, *6* dacite, *7* rhyolite, *8* trachyte, *9* trachyandesite, *10* basaltic trachyandesite, *11* trachybasalt, *12* tephrite (basanite), *13* phonotephrite, *14* tephriphonolite, and *15* phonolite. Data sources cited in the Appendix

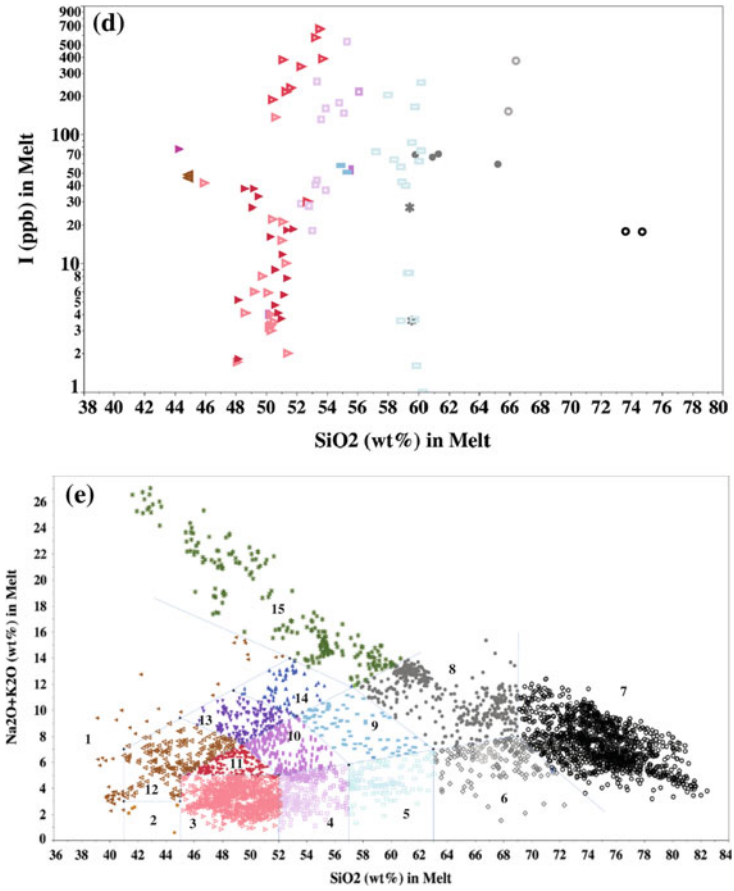

Fig. 6.1 (continued)

et al. 2009), and Iceland (Moune et al. 2007). Low-halogen basaltic volcanism on continents, some of which may involve mantle-sourced plume activity, occurs in systems such as the Parana-Etendeka large igneous province, Namibia (Marks et al. 2014), and the Rio Grande rift, New Mexico (Rowe and Lassiter 2009; Rowe et al. 2011). Minimum Cl, Br, and I concentrations increase with increasing SiO_2 in melt (Fig. 6.1); whereas, the minimum F concentrations of melts ranging from 40 to 80 wt% SiO_2 remain relatively constant at tens to hundreds of ppm.

Magmatic halogen concentrations vary with other compositional parameters such as melt alkalinity (i.e., the molar ratio of [Na+K+Ca]/Al). Fluorine contents of non-alkaline melts having basaltic- to intermediate-SiO_2 contents are generally <0.2 wt%, but melts from other BAA environments may contain more than 0.5 wt% F (Fig. 6.2, Table 6.1). These magmatic systems include ocean islands, subduction zones, flood basalts, LIPs, contaminated and/or chemically evolved

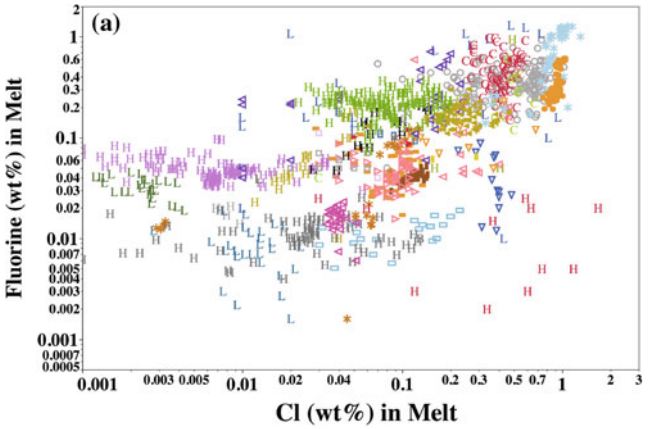
(a)
Fluorine (wt%) in Melt
Cl (wt%) in Melt

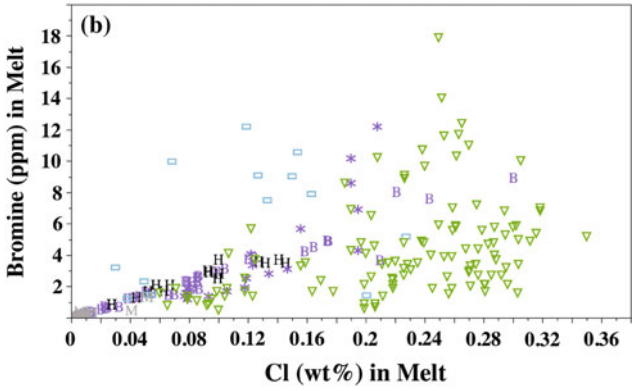
(b)
Bromine (ppm) in Melt
Cl (wt%) in Melt

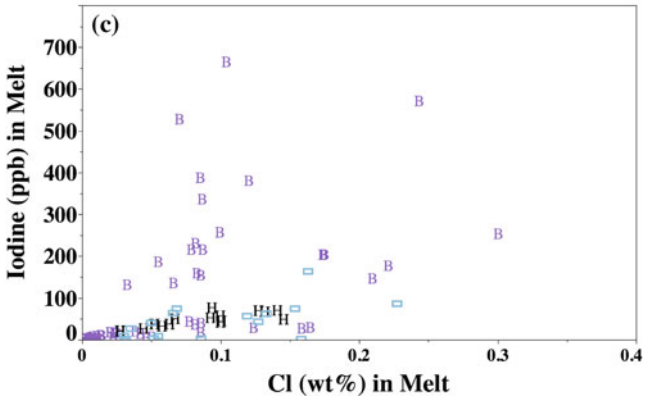
(c)
Iodine (ppb) in Melt
Cl (wt%) in Melt

◂**Fig. 6.2** Concentration plots of Cl (wt%) versus: **a** F (wt%), **b** Br (ppm), and **c** I (ppb) in natural glasses and MI from ultramafic to intermediate-silica (≤ 63 wt% SiO_2) magmas and their alkaline equivalents. The glass data are differentiated as a function of magmatic-tectonic context. In **a**, this log-log plot involving 4375 data points shows that most F-enriched magmas also contain high Cl. In **b**, most of the 118 data points show a positive correlation between Cl and Br. Some data for degassed andesite from Monserrat (*blue boxes*; Villemant et al. 2008), and the 1835 eruption of andesite from Cosiqüina volcano, Nicaragua (*violet asterisks*; Kutterolf et al. 2013) are not consistent with this trend. In **c**, most of the 86 data points for Cl correlate with I. Magmas represented include: non-alphabetic symbols = subduction environments, *H* hot spots, *L* large igneous provinces, *B* back arc basins, and *C* continental basaltic volcanoes not clearly influenced by subduction processes. Additional data sources cited in the Appendix. *Grey open circles* Mt. Vesuvius; *Blue, downward-pointing open triangles* Augustine volcano; *Yellow filled rectangles* Arenal volcano; *Orange filled rectangles* and *pink open triangles* volcanoes of Kamchatka; *Brown filled rectangles* Fuego volcano; *Brown asterisks* Mt. Shasta; *Orange filled circles* Vulcano volcano; *Pink open triangles* volcanoes of the Aeolian islands; *Orange, downward-pointing open triangles* West Sulawesi volcanic province; *Violet, left-pointing open triangles* Ponza Island; *Blue asterisks* Mt. Vesuvius; *Gray open squares* Southern Baikal volcanoes; *Orange filled circles* Phlegraean fields volcanoes; *Violet open trianges* Mt. Iwati; *Green, downward-pointing open triangles* Nicaraguan volcanoes

andesites and dacites related to MOR, and related alkaline BAA melts (e.g., those with basanitic to phonolitic compositions). Silicate melts associated with carbonatites may also contain high F contents (Sharygin et al. 2012; Mangler et al. 2014). The Cl and F concentrations of matrix glasses in Oldoinyo Lengai natrocarbonatite are 0.49 and 0.59 wt%, respectively, and similar to those reported in the MI from the same volcano (de Moor et al. 2013). The concentration ranges for F, Cl, Br, and I in *non-alkaline magmas* expand with increasing SiO_2. Other, rare felsic systems contain MI representing highly evolved felsic melts with as much as 7 wt% F. Halogens in felsic magmas are addressed by Dolejs and Zajacz (2018). Chlorine concentrations in non-alkaline basaltic to high-SiO_2 melts exhibit similar relationships. They approach and exceed 0.7 wt% in some alkaline basanites and in SiO_2-poor magmas of hot spot, LIP, subduction-zone, and chemically evolved or seawater- and/or ocean crust-contaminated dacites related to MOR (Michael and Schilling 1989) environments (Table 6.1; Fig. 6.2).

Although available data are limited, magmatic Br concentrations are commonly at ppm levels and Br maxima are typically <10 ppm for basaltic and <18 ppm for andesitic and more felsic melts. Concentrations of Br correlate positively with Cl for basaltic and basaltic-andesite melts (Fig. 6.2), but the relationship is less clear for andesitic melts. Concentrations of I in mafic melts are several orders of magnitude lower; most are <300 ppb, but some matrix glasses from andesitic back-arc basins contain >600 ppb and and others as low as 2 ppb of I (Déruelle et al. 1992). Iodine concentrations increase with increasing Cl, with <0.06 wt% Cl in melt, but the relationship shows significant dispersion with higher Cl and I concentrations in melts.

The paucity of analytical data for Br and I reflects the analytical difficulties associated with the detection of low concentrations in natural samples. In comparison, both F and Cl in glass and melt inclusions are readily determined with electron probe microanalysis (EPMA) and secondary ion mass spectrometry (SIMS) at their typical concentration levels, and new advances show promising

Table 6.1 Halogens in melt inclusions, matrix glass, glassy rims on pillow basalt, and pumiceous groundmass

Halogen concentrations	Mid-Ocean Ridge (MOR) basalt	MOR-related basaltic-andesite & andesite	Back-arc basin basalt	Back-arc basin basaltic-andesite & andesite	Hot spot basalt	Ocean island basalt	Subduction zone basalt	Subduction zone basaltic-andesite & andesite[†]	Flood and rift-related basalts	Alkaline basalts	Phonolites, Trachytes, Pantellerites
Fluorine (wt%)	0.005–0.07	0.01–0.16	0.007–0.1	0.008–0.1	0.009–0.2	0.004–0.22	0.01–0.24	0.005–0.09	0.0005–1.95	0.1–0.49	0.1–1.2
Chlorine (wt%)	0.0001–0.14	0.05–0.52	0.0003–0.23	0.05–0.84	0.0004–0.06	0.009–2.5	0.01–0.6	0.01–0.85	0.0002–0.94	0.005–0.59	0.02–1.1
Bromine (ppm)	0.06–4.5	ndl	0.018–4.9	0.7–15	0.025–4.7	0.01–4.6	0.4–2	1–300[a]	ndl	ndl	1–28
Iodine (ppb)	2–400	ndl	2–380	1–665	0.4–55	10–100	ndl	0.6[a]–11000	ndl	ndl	ndl

[a]Variably degassed glasses

ndl = no data located

References: Sobolev (1996), Aiuppa et al. (2009) and references cited therein, Déruelle et al. (1992), Sobolev et al. (2009), Rowe et al. (2011), Weston (2012), Wanless et al. (2011), Villemant et al. (pumice clasts only 2008), Rose-Koga et al. (2012), Kendrick et al. (2012a, b, 2014a, b) and references therein, Koleszar et al. (2009), Black et al. (2012), Marianelli et al. (1999), Thordarson and Self (1996), Kovalenko et al. (2006)

[†]Some data from Monserrat include partially degassed andesite glasses

results for Cl analysis via laser ablation inductively coupled mass spectrometry (LA-ICP-MS) (Seo et al. 2011). Bromine and I detection, however, require more challenging analytical methods. For example, neutron-activation analyses for Br in whole-rock samples of the Ilímaussaq intrusion of Greenland have been conducted by Krumrei et al. (2007). Bureau et al. (2000) determined Br and I concentrations of their albitic run-product glasses with PIXE. Bromine was measured in individual grains of sodalite and scapolite-group minerals by XRF microprobe by Pan and Dong (2003). In another approach, neutron-induced reactions involving Br, I, and Cl are generated, and analyses of noble gas proxy isotopes conducted in a noble gas spectrometer with the ^{40}Ar-^{39}Ar methodology (Kendrick 2012; Weston 2012; Kendrick et al. 2012b). Recently, Kutterolf et al. (2015) applied SR (synchrotron radiation) micro-XRF to measure Br in matrix and MI glasses.

6.2.2 Halogen Abundances of Whole-Rock Samples

Although they may reflect the variable influences of degassing, weathering, and phenocryst fractionation, rock samples also provide important constraints on magmatic halogen behavior. Pyle and Mather (2009) summarized halogen concentrations in whole-rock samples to characterize their behavior in terrestrial mantle and crustal reservoirs. The concentrations of F, Cl, Br, and I (in ppm) in the primitive mantle range from 18 to 25, 1.4 to 30, 0.0036 to 0.075, and 0.001 to 0.007; in the depleted mantle: 11–65, 0.5–7, and 0.02 (with no data reported for I); in the bulk continental crust: 553, 224, 0.9, and 0.7; and 557, 370, 1.6, and 1.5 for the upper continental crust, respectively. These values reflect higher halogen concentrations in increasingly felsic (and evolved) crustal materials and are qualitatively consistent with observations described previously for natural glasses and MI. Additional details on halogens in mantle rocks are available in Frezzotti and Ferrando (2018) and Klemme and Stalder (2018).

In a recent study of eruptive alkaline rocks of the Rhein Graben, Germany, Wang et al. (2014) determined F, Cl, and Br data for primitive olivine melilitites and nephelinites and their evolved products (i.e., tephrites and phonolites). They applied their data to interpret magmatic processes. The Br contents range from <0.3 ppm in the most-primitive rocks to 34 ppm for the more-evolved tephritic and phonolitic associated rocks. They also observed relatively uniform Cl/Br ratios (of 371 ± 120) that they interpreted to reflect negligible influences of partial melting, fractional crystallization, and/or degassing on the behavior of Cl and Br in the evolving alkaline melts.

Rocks containing strongly elevated F and Cl concentrations typically include halogen-enriched hydrous micas, amphiboles, and apatite, but other less common and more compositionally remarkable minerals, with halogens as essential major constituents, also occur (Fig. 6.3). These rocks are evidence of processes affecting F- and/or Cl-enriched source magmas and hydrothermal fluids. Some alkaline rocks, such as the nepheline syenites of Ilímaussaq, Greenland, contain Cl-enriched

Fig. 6.3 Photograph of common to rare halogen-enriched minerals that occur with some alkaline plutonic rocks. Minerals include from *left to right*: *top row* violet scapolite crystals in *yellow-white matrix* (AMNH 112297), *blue halite crystal* (AMNH 20238), and *yellow-white cryolite crystal* (AMNH 27675); *second row* amber fluorite crystal (AMNH 91067), *yellow sylvite crystal* (AMNH 2574), and *blue-green fluorite crystal* (AMNH 107633); *bottom* 3 cut *pink* specimens of fluorite (AMNH 1122-38,-03,-37), *dark red-brown villiaumite crystal* (AMNH 112728), and cut *deep-red* villiaumite specimen (AMNH 109320). Sample image courtesy of the Mineral and Gems collections of the American Museum of Natural History; photo credit, Beth Goldoff

magmatic sodalite ($Na_8Al_6Si_6O_{24}Cl_2$) (Krumrei et al. 2007), and other nearby alkaline intrusions contain primary magmatic as well as secondary, magmatic-hydrothermal villiaumite (NaF) and fluorite (Markl et al. 2001; Schönenberger et al. 2008). Similarly alkaline rocks containing higher SiO_2 contents, such as those at Ivigtut, Greenland, indicate a magmatic-hydrothermal genesis for cryolite (Na_3AlF_6) as well as for fluorite (Köhler et al. 2008). The latter study determined that metasomatism by F-rich, post-magmatic fluids in an A-type granitoid at Ivigtut involved a hydrous aluminofluoride liquid from which cryolite and fluorite precipitated. Alkaline natrocarbonatites also include fluorite and other more-rare halogen-enriched minerals such as sylvite (KCl), sellaite (MgF_2), neighborite ($NaMgF_3$), and others (Mangler et al. 2014). The presence of fluorite, cryolite, villiaumite, sellaite, neighborite, sylvite, and scapolite imparts elevated F and/or Cl concentrations in their host rocks (Sorensen 1974; Shchekina et al. 2013). Some of these locales represent economically viable sources for the exploitation of F;

Mangler et al. (2014), for example, report up to 9.2 wt% F, 5.9 wt% Cl, and 100 ppm Br for carbonatitic rocks of Oldoinyo Lengai, Tanzania. Details on halogens in carbonatites are given by Pirajno (2018).

Fluorine-enriched magmas, and their fluids, may also crystallize topaz ($Al_2SiO_4(OH,F)_2$) as well as fluorite (Bailey 1977). Topaz-bearing rocks may occur in late-stage greisenized granitic hypabyssal stocks, roof zones, and margins, and auto-metasomatized granites and some Li-F granites (Webster et al. 2004) and ongonite dykes (Kovalenko and Kovalenko 1976). Fluorite-enriched aluminous ongonites of the Ary-Bulak intrusion contain up to 15.5 wt% F (Peretyazhko et al. 2007). Dolejs and Zajacz (2018) address the behavior of halogens in such systems.

6.2.3 *Halogen Abundances in Fluid Inclusions*

Phenocrysts in some BAA rocks, both volcanic samples and associated mafic-ultramafic xenoliths, contain inclusions dominated by compound phase assemblages. Aqueous vapor and liquid or aqueous-carbonic vapor and liquid may coexist with melts having complex compositions, and if of primary origin, these various FI represent either supra-solidus magmatic fluids or magmatic-hydrothermal fluids that were stable at subsolidus conditions (Roedder 1984). Many of these are alkaline in composition and some are mantle sourced. For example, inclusions of halide- ± carbonate- ± sulfate- ± sulfide-melts coexisting with vapor and liquid, with or without MI, have been observed in alkali syenite, mafic, and ultramafic cumulate xenoliths from Ventotene Island, Italy (De Vivo et al. 1995); the Tubaf Seamount, Papua New Guinea (Renno et al. 2004); syenitic and associated endoskarn xenoliths representing the crystallized residue of the AD 79 eruption of Mt. Somma-Vesuvius (Fulignati et al. 2001, 2013); skarn-hosted inclusions (Fig. 6.4) of Mt. Somma-Vesuvius (Kamenetsky and Kamenetsky 2010); a spinel lherzolite xenolith suite associated with Ethiopian continental flood basalts (Frezzotti et al. 2010); and eruptive rocks of Tenerife of the Canary Islands hot spot (Frezzotti et al. 2002). Analyses of the quenched silicate glass in such inclusions constrain volatile solubilities in aluminosilicate melts and phase behavior and melting temperatures during rehomogenization (Kamenetsky and Kamenetsky 2010). Integration of this information with compositions of coexisting FI provides constraints on volatile, ore-metal, and trace-element partitioning between silicate melts, hydrosaline liquids, vapors, and sulfate liquids, with or without carbonate liquids (Audetat and Lowenstern 2013). Fluid inclusion studies have also addressed the fractionation of Br from Cl during seawater alteration of BAA volcanic host rocks (Gutzmer et al. 2003). Lastly, hydrous minerals (Kamineni 1987), brines, and associated saline groundwaters (Gascoyne et al.

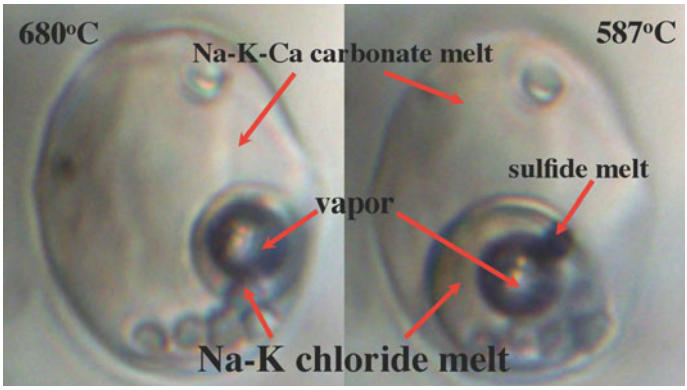

Fig. 6.4 Images of a reheated (at 587 and 680 °C) fluid inclusion with unidentified crystals, vapor bubble, globule of molten Na-K chloride phase representing a hydrosaline liquid, a small dark globule of sulfide liquid, and predominant Na-K-Ca carbonate liquid in potassium feldspar from an endoskarn xenolith from Mt. Somma-Vesuvius, Italy (Kamenetsky and Kamenetsky 2010). Images provided by V. Kamenetsky. The melt inclusion is approximately 25 microns in diameter

1987) in gabbroic plutons have been analyzed for F, Cl, and Br. The compositions of these minerals and fluids reflect anion exchanges between the plutonic rocks and pore fluids and the influence of igneous rocks on the geochemical behavior of halogens in groundwater.

The complexity of halogen-bearing FI in mafic to ultramafic and syenitic plutons also occurs in other compositional realms. Some, for example, indicate a significant role for mixed halogens and hydrocarbons in magmatic fluids such as those of the Gardar province in southern Greenland. Specifically, studies show that aqueous saline and CO_2-CH_4- and CO_2-CH_4-H_2O-bearing FI from Gardar rocks reflect highly varying oxygen fugacities in the alkaline Gardar melts (Konnerup-Madsen et al. 1982; Marks et al. 2004). Methane-bearing FI and high-salinity aqueous FI in sodalites from sodalite-bearing nepheline syenites (naujaite) from other localities at Ilimaussaq were interpreted by Krumrei et al. (2007) to represent equilibrium between CH_4-dominated vapor and a reduced, halogen-rich magma. The FI were trapped at pressures of 400–100 MPa and magmatic temperatures. Interestingly, the naujaites contain the highest gas contents of all studied Ilimaussaq rocks. Moreover, the differing behaviors of F versus those of Cl and Br in the whole-rock samples appear to result from sodalite crystallization which scavenged significant Cl and Br, but not F, from the melt (Krumrei et al. 2007).

Some halogen-bearing fluids in BAA magmas have economic significance for rare metals as well as for F. Highly saline FI in hydrothermal cryolite, quartz, siderite, and fluorite from alkaline igneous rocks of Ivigtut (Köhler et al. 2008) and chkalovite ($Na_2BeSi_2O_6$) from Ilimaussaq (Sobolev et al. 1970), for example, were

analyzed to investigate the origin of mineralizing fluids enriched in rare metals including Be, U, and REEs. Some Ivigtut FI are extremely enriched in Br and contain ca. 425–1900 ppm. Interpretation of the (Li/Br) and (Li/Cl) ratios of these FI indicates a non-marine source for the Li, Cl, and Br (Köhler et al. 2008). Most of the Ivigtut (Li/Br) ratios range from 0.3–38 and most (Li/Cl) range from 0.003–0.03, whereas these ratios in seawater are orders of magnitude lower (e.g., ca. 0.0023 and 8.8×10^{-6}, respectively). With regard to layered igneous intrusions, primary and/or secondary saline-aqueous FI (with or without CO_2 or CH_4) have been observed in quartz and other minerals at the Stillwater (Hanley et al. 2008), Bushveld (Schiffries 1990), Skaergaard (Larsen et al. 1992), Duluth (Ripley 2005), and Laramie (Frost and Touret 1989) mafic-ultramafic complexes. However, a key issue bearing on these occurrences is knowledge of the stage or stages of magma evolution coincident with saline fluid exsolution. Analysis of primary FI comprised of carbonic vapor and hydrosaline brine from the Stillwater complex, for example, returns trapping temperatures exceeding 700 °C and pressures of 430 to 560 MPa (Hanley et al. 2008). These FI were trapped in the albite-quartz core of a late-stage chemically evolved pegmatite within a gabbronorite unit. Some of the primary magmatic hydrosaline liquids were enriched in Ca, K, Fe, Mn, Ba, Si, and Al as well as Na. Certain host phenocrysts also contain highly saline, secondary FI trapped at lower temperatures of 660–800 °C (Hanley et al. 2008) indicating the Cl-rich fluids were present during much of the late-stage differentiation of the basaltic source magmas.

Inclusions of primary alkaline carbonatitic melts hosted in melilite, monticellite, olivine, and clinopyroxene from rocks of the Krestovskii intrusive massif, Siberia, contain up to 31 wt% Cl. Carbonatitic inclusions in fluorites from the Mushagai Khudak igneous complex, Mongolia, contain 5.5 wt% F (Panina and Motorina 2008). These values are consistent with the presence of F- and/or Cl-enriched minerals in some carbonatitic systems (Panina and Motorina 2008). Pirajno (2018) provides details on halogens in carbonatites and related rocks.

Lastly, particularly H_2O-enriched, aluminosilicate-poor FI have been observed to occur with F- and aluminosilicate-enriched MI, containing relatively less H_2O, in phenocrysts from some granitoids. These coexisting inclusions have been interpreted to reflect melt-liquid immiscibility in highly evolved magmas (Thomas et al. 2009). Concentrations of F approaching 6 wt%, for instance, have been measured in Li- and F-enriched MI from the Orlovka Massif, Russia (Thomas et al. 2009).

6.2.4 Halogen Abundances in Minerals

Halogen concentrations in primary, magmatic, amphiboles and biotite found in basic-to-intermediate rocks. In almost all cases, primary magmatic hydrous minerals, amphiboles, and micas are uncommon in basic rocks in comparison to other ferromagnesian phases, but become more common in intermediate rock compositions (Wones and Gilbert 1982; Speer 1984). The most common magmatic amphibole in basic-to-intermediate rocks is hornblende, however some intermediate

rock compositions contain rare cummingtonite. Alkalic rocks may contain alkali amphiboles such as riebeckite-arfedsonite solid solutions (Wones and Gilbert 1982). When micas are found in basic rocks they are commonly phlogopitic in composition and, with increasing silica concentration of the rock, become richer in the annite end-member. Muscovite is found only in more silicic rocks than considered in this review (Speer 1984).

The halogen concentrations in magmatic amphiboles and biotite are controlled by many factors (Mi and Pan 2018). Obviously the concentrations of halogens in the entire magmatic system affect the concentrations in the minerals, but so does the presence, or absence, of other halogen-bearing phases such as melt, fluid(s), apatite, and other hydrous minerals. This is because thermodynamics requires that at equilibrium the halogens must be partitioned between the phases. However, such partitioning is affected by the composition of the hydrous phases. For example, it has long been observed that Mg-Cl and Fe-F avoidance leads to higher Cl concentrations in Mg-poor hydrous phases and higher F concentrations in Fe-poor phases (see discussion in Zhu and Sverjensky 1991, 1992).

A review of the literature reveals that there are thousands of analyses of amphiboles and micas in BAA rock types, but many of these hydrous minerals are secondary and were formed, or were altered, at sub-solidus conditions. Furthermore, the vast majority of the analyses do not contain information on the halogen concentrations in these minerals. The published analyses of halogens in primary hydrous minerals in basic-to-intermediate rocks are limited to F and Cl; we remain ignorant of the other halogens' concentrations in these minerals in BAA rocks. As Giesting and Filiberto (2014) stress, such incomplete analyses make it difficult, if not impossible, to correctly assign elements to the specific crystallographic sites in the minerals and result in a loss of potential information that these minerals can provide concerning their crystallization and magmatic environment.

Selected examples of F and Cl in magmatic amphiboles. The concentrations of F and Cl in amphibole have been determined in BAA rocks varying from layered igneous intrusions through continental arcs to peralkaline and ultra-potassic compositions. Amphiboles in intrusive rocks with common BAA compositions contain halogen concentrations from below the detection limit ($\sim$100 ppm) of EPMA to concentrations approaching 1 wt%. Boudreau et al. (1986) studied late-magmatic amphiboles in the Stillwater and Bushveld layered igneous intrusions and found that whereas F varied from 0.12 to 0.76 wt%, Cl remained relatively constant at 0.12–0.27 wt%. Einali et al. (2014) study of fresh amphiboles in a diorite dike from the Chahfiruzeh porphyry of southern Iran also found a wide variation in F compared to Cl, but in this example F varied from below detection to 0.233 wt% and Cl from 0.011 to 0.020 wt%.

At least one study demonstrates that amphiboles in extrusive BAA rocks tend to display significantly higher F/Cl ratios than seen in intrusive rocks. Amphiboles in Andean basaltic-andesite rocks from the Yanacocha volcanics of Peru appear to have formed near the liquidus of the magmas, and representative compositions (determined by EPMA) from different units contain between 1.27 and 2.80 wt% F and between 0.02 and 0.11 wt% Cl (Chambefort et al. 2013). Ion probe (SIMS)

analysis of amphiboles from the same rock suite provides compositional ranges of 0.2–0.77 and 0.15–0.24 wt% F and Cl, respectively (Chambefort et al. 2013).

A number of studies report F concentrations in alkaline and ultrapotassic rocks, but unfortunately no data on Cl concentrations are reported. Amphiboles from the syenite rim of the Emerald Lake zoned pluton, Yukon Territory, Canada (Coulson et al. 2001) contain sub-equal concentrations of F and Cl. In this case, the F concentrations vary from 0.66 to 1.61 and the Cl from 0.63 to 1.05 wt%. These sub-equal concentrations of F and Cl have not been observed in the more common BAA intrusives discussed above. Shaw and Eyzaguirre (2000) analyzed amphibole megacrysts from the West Eifel volcanic field, Germany, in leucititic and nephelinitic rocks. They found F concentrations similar to those described above for amphiboles in more common rocks, 0.0–0.25 wt% F. On the other hand, Edgar et al. (1994) observed that F concentrations in amphiboles from ultra-potassic rocks average 1.98 wt% F in lamproites and 2.4 wt% F in kamafugites, although the spread in F concentrations was great in each case. These are the highest concentrations of F found for such amphiboles.

Selected examples of F and Cl in magmatic biotites. Biotites from common BAA rocks have F and Cl concentrations similar to those of amphiboles. Boudreau et al.'s (1986) investigation of halogens in the Stillwater and Bushveld complexes studied magmatic biotites in addition to the amphiboles discussed above. These authors found variations in F from 0.02 to 0.93 wt% and in Cl from 0.03 to 0.61 wt%. The Cl concentrations in these biotites were shown to have a weak, positive correlation with the Fe/(Fe + Mg + Ti) ratio as expected from F-Fe and Cl-Mg avoidance (Boudreau et al. 1986). Importantly, these biotites were found to be significantly enriched in Cl, but not F, compared to biotites in the Skaergaard and Kiglapait intrusions that were not enriched in Cl. Boudreau et al. (1986) related this remarkable enrichment in Cl to the Pt ore-forming processes in the Stillwater and Bushveld. Willmore et al. (2000) followed up on Boudreau et al. (1986) and found similar ranges in F and Cl in the Bushveld complex. Einali et al. (2014) were also able to measure halogens in biotites from the same diorite dike in which they found amphiboles (discussed above). In comparison to the amphiboles, these biotites contained significantly higher concentrations of halogens, between 0.046 to 1.49 wt % F and 0.04 to 0.05 wt% Cl. These higher concentrations might possibly be explained by late crystallization of biotite from a halogen-enriched melt that had seen little to no degassing. Braga et al. (2006) report the halogen concentrations in a single biotite megacryst found in a remarkable ultrabasic dike of the Veneto volcanic province, Italy (35.5 wt% SiO_2, 5.95 wt% FeO, 14.0 wt% MgO, 1.01 wt% Na_2O, 0.82 wt% K_2O). This single megacryst contained 0.27 wt% F and 0.01 wt% Cl. However, surrounding the megacryst were flakes of mica forming a reaction corona. These flakes contained 1.08 wt% F and 0.01 wt% Cl; the source of the enhanced F in the mica flakes was presumably the magma.

Measurements of halogen concentrations in magmatic biotites in extrusive BAA rocks from normal island arc settings were not found during the preparation of this review. However, Müller et al. (2001) measured halogens in magmatic phlogopites and biotites in alkaline rocks from Lihir Island, Papua New Guinea. They found that

phlogopites from monzodioritic to trachybasaltic rocks contained 4.7–5.22 wt% F and 0.05–0.06 wt% Cl, whereas biotites from a trachyandesitic rock had no detectable F and 0.12 wt% Cl. Biotites in the syenite rim of the Emerald Lake pluton, studied by Coulson et al. (2001), contained sub-equal concentrations of F and Cl, from 0.86 to 1.65 wt% F and from 0.64 to 1.34 wt% Cl. These halogen concentrations in biotite are not that dissimilar from those Coulsen et al. (2001) measured in coexisting amphiboles (discussed above). In comparison, biotites found in syenites from Maud Dronning Land, Antarctica, contained a larger range of F, from 0.36 to 3.30 wt%, than those of Emerald Lake, but lower concentrations and a smaller range of Cl, from 0.01 to 0.56 wt% (Markl and Piazolo 1998).

The concentrations of halogens in biotites from extremely alkaline rocks vary widely. Shaw and Eyzaguirre's (2000) study of megacrysts in the West Eifel volcanic rocks, discussed above, includes F analyses of phlogopites and biotites. The F concentrations in these minerals vary from 0.12 to 0.35 wt%, similar to the concentrations of F in the coexisting amphibole megacrysts. Edgar et al. (1994) defined average F concentrations in phlogopites from ultra-potassic rocks. These concentrations varied from 1.79 wt% F in lamprophyres through 2.18 wt% in lamproites to 3.18 wt% in kamafugites. However, Edgar et al. (1994) found a wide range in the F concentrations in biotites from each rock type. Even higher F concentrations (3.61–4.77 wt%) were found in micas from the Katwe-Kikorongo volcanic field of nephelinites and leucitites in southwest Uganda (Lloyd et al. 2002).

These few examples of halogen concentrations in amphiboles and biotites in BAA composition rocks provide an overview of the range of concentrations in the different rock types, but do not explain the mechanisms responsible for that range. These mechanisms no doubt include the composition of the source rock, the degree of partial melting that formed the primary magma, crystal fractionation, the Mg/Fe ratio of the mineral, volatile exsolution, and in some cases country rock assimilation. Although the distributions of F and Cl in magmatic amphiboles and biotites are complex, there is a general trend of increasing halogens with increasing alkalies in the host rock. This is particularly clear for F and K as stressed by Edgar et al. (1994). It is almost certainly impossible to create a general model to explain the halogen variations in hydrous minerals applicable to all BAA rocks, but as shown below, specific examples can be understood with our current level of knowledge.

Apatite. The halogen-bearing accessory phosphate mineral apatite is rare in ultramafic rocks (Mitsis and Economou-Eliopoulos 2001), present in some basaltic rocks (Watson 1979), and ubiquitous in more evolved igneous systems (Watson 1980; Piccoli and Candela 2002; Hughes 2015). With regard to the stage(s) of apatite crystallization during magma differentiation, it has been posited that most apatite crystallizes early and through a small interval of crystallization temperature as magmas cool, crystallize, and evolve (Piccoli and Candela 1994; Peng et al. 1997). The issue of the timing of apatite crystallization is crucial, because the composition of apatite that has equilibrated with melt and/or fluid(s) is invaluable for estimating concentrations and thermodynamically useful fugacities and activities of F, Cl, and Br (and other volatiles H_2O, CO_2, and SO_2) in magmatic systems (Piccoli and Candela 1994; Patiño Douce and Roden 2006; Boyce et al. 2010;

Marks et al. 2012; Teiber et al. 2014; McCubbin et al. 2011, 2015; Webster and Piccoli 2015; Stock et al. 2016). The use of apatite as a geochemical tool is supported by experiments showing that halogens and hydroxyl do not diffuse particularly quickly through apatite (Brenan 1994). As a result, apatite in rapidly cooled volcanic rocks preserves essential information on magmatic volatile geochemistry.

Most apatites in BAA rocks are F enriched, but some show wide ranges in the Cl, F, and OH contents of the mineral's halogen-hydroxyl site (Fig. 6.5). Apatites with more than 80 mol% hydroxyl or chloride component are extremely rare (Piccoli and Candela 2002). These low-F apatites contain equal to sub-equal Cl and OH, but nearly pure chloroapatites crystallize from some BAA melts (Boudreau et al. 1986; Boudreau 1995; Piccoli and Candela 2002).

Apatite compositions have been determined by bulk analysis as well as a variety of in situ analytical techniques including EPMA, SIMS, and LA-ICP-MS. Apatites are typically analyzed by EPMA as this method can determine directly the major and minor cations as well as the volatile components F and Cl. Hydroxyl contents are computed from EPMA data by assuming that the anion fractions of F, Cl, and OH in the apatite hydroxyl site sum to unity (Piccoli and Candela 2002). Analyses

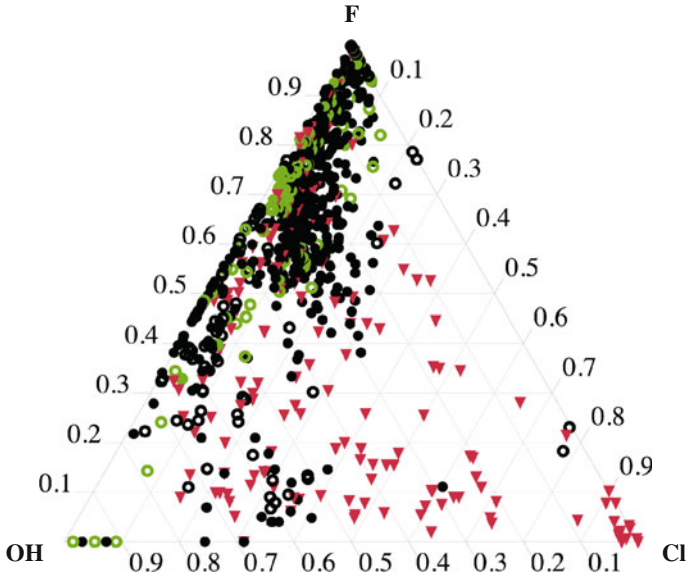

Fig. 6.5 Plot showing anion fractions of OH, F, and Cl (per formula unit) in analyses of ca. 950 apatites from >130 investigations of plutonic (*closed symbols*) and volcanic (*closed symbols*) rocks. Most apatites from plutonic non-alkaline (*black symbols*) basaltic magmas, and alkaline (*green symbols*) tephritic to phonolitic magmas, have fluorapatite compositions. Conversely, some non-alkaline volcanic basalt magmas crystallize low-Cl apatites enriched in hydroxyl. Chlorine-enriched apatites with variable (F/OH) occur in layered intrusions (*red symbols*). Data sources are listed in the Appendix

of F, Cl, Ca, and P in apatite by EPMA can be problematic, however, depending on apatite grain size, crystallographic orientation, and the analytical operating conditions (Stormer et al. 1993; Goldoff et al. 2012; Stock et al. 2015). One potential consequence of analyzing comparatively small apatite grains parallel to their c-axes with relatively high electron beam accelerating potentials and currents (i.e., far from optimal analytical conditions) is that the apparent F concentrations returned may be far too high. For example, more than 140 of the 1400 analyses of apatite summarized in the Geochemistry of Rocks of the Oceans and Continents (GEOROC4) database indicate F concentrations that exceed the maximum possible F contents (i.e., 3.76 wt%) of the hydroxyl site in apatite (Webster and Piccoli 2015).

The compositions of apatites in mafic and intermediate-SiO_2 rocks have been determined to investigate the activities of magmatic volatiles in numerous volcanic and plutonic systems. For example, F and Cl in apatites from 20 mafic to felsic volcanic systems were addressed systematically by Peng et al. (1997), and the results applied to degassing processes. Other examples include apatite-based studies of the Irazu volcano (Boyce and Hervig 2009); tephra of the Izu Bonin volcanic arc (Straub 2008); East Pacific Rise cumulates (Meurer and Natland 2001); low-SiO_2 and FeO-rich igneous rocks (e.g., nelsonites) (Piccoli and Candela 2002); intermediate- to high-SiO_2 plutons in China (Zhang et al. 2012); and mafic intrusions (Boudreau 1995), including the Munni Munni (Boudreau et al. 1993), Stillwater (Meurer and Meurer 2006), Dufek (Drinkwater et al. 1990), Sudbury (Warner et al. 1998), Duluth (Gál et al. 2013), and Kläppsjö mafic (Meurer et al. 2004) intrusive complexes and the basement sill of the Ferrar large igneous province, Antarctica (Boudreau and Simon 2007). Some apatites in layered intrusions may be particularly Cl enriched (Boudreau et al. 1986; Boudreau 1995; Meurer and Meurer 2006; Gál et al. 2013) and, therefore, consistent with the presence of highly saline FI (Mathez and Webster 2005; Hanley et al. 2008) and Cl-enriched micas and amphiboles (Boudreau et al. 1986; Willmore et al. 2000) in these systems. A related issue is determining the stages of magma evolution during which the apatite crystallizes and what magmatic conditions the apatites actually represent since differentiated granophyric rocks are also present in these systems.

Data on Br in apatite are limited. Recent analytical investigations determined ca. 6 ppm Br in apatites of Ødegården, Norway; ca. 1.5 ppm Br in the Ilimaussaq apatites; and 0.04–7.8 ppm Br in apatites from the Mt. Saint Hilaire complex, Canada (Marks et al. 2012; Teiber et al. 2015). The latter apatites also showed decreasing Cl with Br in gabbros and diorites from the complex.

Apatites in extra-terrestrial basaltic rocks have come under recent and extensive scrutiny as a geochemical tool useful for investigating halogens and other volatiles in lunar and Martian basaltic magmas (Filiberto and Treiman 2009b; Boyce et al. 2010; McCubbin et al. 2011; Ustinisik et al. 2011, 2015; Howarth et al. 2015; Tartese et al. 2013). This application is addressed for Martian rocks by Rampe et al. (2017).

A related issue is the relative ease of halogen redistribution from magmatic apatites via exchange with late-stage hydrothermal fluids. A recent study of F and Cl in coexisting magmatic apatite, biotite, and amphibole concluded that F is not as strongly influenced as Cl if hydrothermal overprinting occurs and that the larger Cl

anion appears to be more readily mobilized and re-distributed than F during some hydrothermal processes, particularly in exchanges involving biotite and amphibole (Teiber et al. 2015).

6.2.5 Halogen Abundances in Volcanic Gases

Volatiles released by degassing of mafic magmas are enriched in halogens to a variable extent. Chlorine and F have recurrently been measured in directly sampled volcanic gas condensates (Symonds et al. 1994; Gerlach 2004; Fischer 2008; Fischer and Chiodini 2015) or by remote sensing (Francis et al. 1998) or in situ (Aiuppa 2009) techniques applied to atmospheric volcanic gas plumes. In high-temperature (T > 500 °C) magmatic gases, Cl is generally fourth in order of abundance after H_2O, CO_2, and S, and typically exhibits concentrations in the 0.1–1 mol% range (Table 6.2). Thermodynamic equilibrium speciation calculations (Gerlach 2004; Martin et al. 2006) suggest that Cl is transported in such fluids essentially in the form of $HCl_{(g)}$. Metal chlorides are also present in high-temperature volcanic gases, but in comparatively far lower amounts (Symonds et al. 1987). Measurable amounts of molecular Cl ($Cl_{2(g)}$) have also recently been detected in volcanic fumaroles (Zelenski and Taran 2012), and are interpreted as the product of the catalytic oxidation of $HCl_{(g)}$ by atmospheric oxygen. Upon atmospheric release and transport, volcanic gases are dispersed within (and diluted by) ambient air, so that $HCl_{(g)}$ mixing ratios typically drop to ppmv levels in near-vent volcanic gas plumes. However, correction for background-air dilution generally returns concentrations in source magmatic gases consistent with direct sampling results (Table 6.2). Observations via spectroscopic (by Fourier Transform Infra Red spectroscopy; Francis et al. 1998) and wet-chemical (Filter packs; Aiuppa et al. 2002) techniques, and modelling (Martin et al. 2006), concur that $HCl_{(g)}$ prevails also in atmospheric gas plumes. Volcanic aerosols (Mather et al. 2003) may transport minor amounts of Cl in plumes as metal halides. Recent Differential Optical Absorption Spectroscopy (DOAS) observations indicate detectable amounts of $ClO_{(g)}$ and $OClO_{(g)}$ in near-crater volcanic plumes (Lee et al. 2005). In the plume of Etna, for instance, these Cl radicals have been measured at levels (slant-column densities) of $\sim 10^{17}$ and 10^{14} molecules/cm^2, respectively (Bobrowski et al. 2007). The presence of such large reactive Cl quantities are, however, not accounted for by current numerical models simulating halogen chemistry in volcanic plumes (von Glasow 2010), and have been questioned in light of results of more recent remote sensing DOAS observations (Kern et al. 2009). Overall, the available information suggests limited chemical processing of volcanic $HCl_{(g)}$ upon atmospheric transport of quiescent (non-eruptive) plumes (von Glasow 2010; Martin et al. 2012). In eruptive plumes, Cl can become rapidly processed by heterogeneous reactions at the volcanic ash-gas interface (Delmelle et al. 2007). These reactions lead to the fast Cl depositions seen in, for instance, some Icelandic eruptions (e.g., Bagnato et al. 2013).

Table 6.2 Selected analyses (mole fractions) of high-temperature volcanic gas samples (compiled from Gerlach 2004 and Symonds et al. 1994)

Volcanic gases[a]					
	H_2O	CO_2	SO_2	HCl	HF
Augustine (AUG)	0.96	0.0014	0.0025	0.005	0.0003
Merapi (ME)	0.883	0.0703	0.0114	0.0059	0.0004
Momotombo (MO)	0.918	0.0456	0.0095	0.0068	0.0002
Poas (PO)	0.953	0.0096	0.02	0.0104	0.0012
Kudryavy (KUD)	0.937	0.0238	0.0154	0.0074	0.00084
Tokachi (TOK)	0.93	0.0115	0.0326	0.0028	0.00035
Erta Ale (EA)	0.75	0.131	0.0784	0.0042	0.0042[b]
Kilauea Pu'O (KPO)	0.76	0.0326	0.194	0.0017	0.0018
Kilauea Summit (KS)	0.37	0.489	0.1184	0.0008	0.0008[b]
Volcanic gas plumes[c]					
	H_2O	CO_2	SO_2	HCl	HF
Etna (ET)[d]	0.78	0.087	0.026	0.013	0.00433
Stromboli (STR)[e]	0.829	0.136	0.017	0.017	
Villarica (VI)[f]	0.95	0.02	0.021	0.0063	0.0023
Masaya (MA)[f]	0.942	0.037	0.0137	0.0087	0.0019
Miyake-jima (MIY)[f]	0.949	0.02	0.027	0.0024	
Nyiragongo (NYR)[g]	0.705	0.237	0.045	0.0026	0.0011
Erebus (ER)[h]	0.579	0.364	0.014	0.0069	0.0127
Yasur (YA)[i]	0.97	0.018	0.011	0.0038	0.0014
Asama (AS)[j]	0.937	0.025	0.031	0.006	
Ambrym (AM)[k]	0.954	0.027	0.013	0.003	0.0012

Compositions of volcanic gas plumes from some selected open-conduit basaltic volcanoes are also reported
[a]From compilations of Gerlach (2004); Symonds et al. (1994) assuming a Cl/F molar ratio of 2; [b]Assuming a Cl/F molar ratio of 1; [c]Recalculated compositions on air-free basis; [d]Aiuppa et al. pers. data; [e]Burton et al. (2007); [f]Shinohara and Witter (2005); [g]Sawyer et al. (2008a); [h]Oppenheimer and Kyle (2008); [i]Métrich et al. (2011); [j]Shinohara (2013); and [k]Allard et al. (2009)
Identifying volcano abbreviations are provided in parentheses

Research has long established (Symonds et al. 1994) that H_2O-rich volcanic arc gases are typically enriched in Cl relative to the CO_2-rich gases released in a within-plate or continental rift context (Fig. 6.6). The Cl-poor composition of Erebus gas (Oppenheimer and Kyle 2008; see Fig. 6.6) suggests that this relation is probably not limited to basaltic systems, but rather extendable to more alkali-rich (phonolitic) magmas. Volcanic gas S/Cl ratios exhibit a large spread (Fig. 6.7a; Table 6.3), but still point to detectable differences between arc gases (mean S/Cl ratio of 1.7) and volcanic gases from other tectonic/geodynamic environments (mean S/Cl ratio of 3.5) (see Table 6.3). These distinct compositional signatures match those seen in corresponding magmatic glasses (cfr. 6.2.1), and demonstrate a primary control of mantle-inherited parental melt compositions on volcanic gas Cl abundances (Wallace 2005). For instance, volcanic gas Cl contents are particularly

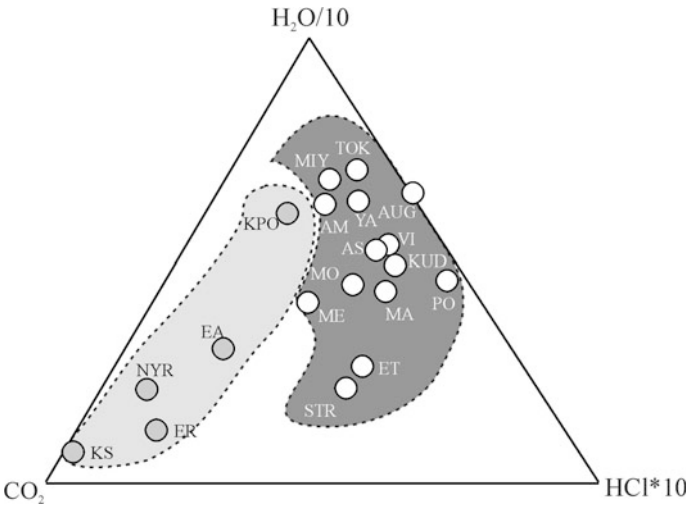

Fig. 6.6 Triangular plot illustrating the H_2O-CO_2-HCl compositions of volcanic gases and plumes from mafic volcanoes (drawn from data in Table 6.2; see Table 6.2 for abbreviations of volcano names and data provenance). *Open circles* arc volcanoes. *Grey circles* non-arc volcanoes

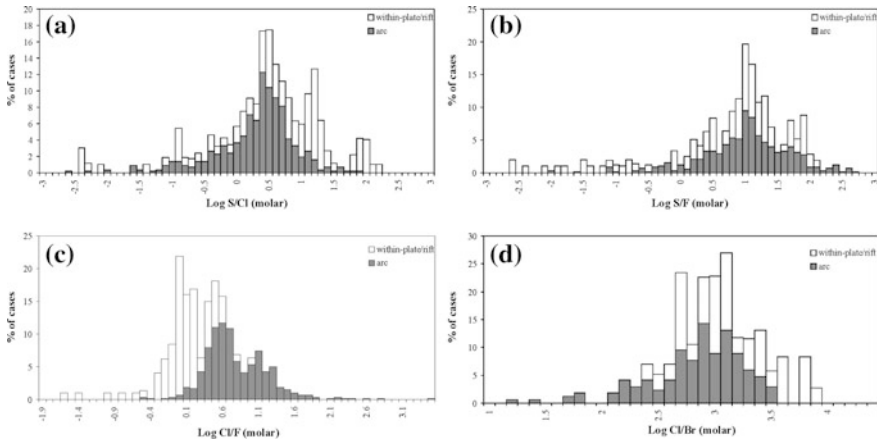

Fig. 6.7 Histograms of the logarithmic distributions of **a** S/Cl, **b** S/F, **c** Cl/F, and **d** Cl/Br (molar) ratios in gases and plumes released by within-plate (rift) and arc mafic volcanoes (dataset from Table 6.3; see Table 6.2 caption for data sources)

high at volcanoes erupting alkali Cl-rich mafic magmas with a slab-fluid signature (e.g., Etna, Stromboli), while low levels (<0.2 mol%) have been measured at hot-spot volcanoes (e.g., Kilauea) (see Fig. 6.6). These gas data are consistent with melt compositions addressed previously (Sect. 6.2.1).

Table 6.3 Statistical parameters of some relevant molar gas ratios in volcanic gas samples from mafic volcanoes

Arc Volcanoes						Non Arc Volcanoes					Global (Arc + Non arc)				
Ratio	Valid N	Mean	Median	Minimum	Maximum	Valid N	Mean	Median	Minimum	Maximum	Valid N	Mean	Median	Minimum	Maximum
S/Cl	569	1.7	2.2	0.002	66	98	3.5	5.4	0.0036	149	667	1.9	2.4	0.0024	149.0
Cl/F	527	5.5	4.3	0.289	2903	96	1.0	1.0	0.0204	8.4	623	4.2	3.9	0.0204	2902
S/F	524	9.0	9.5	0.008	1026	96	3.6	8.1	0.0024	114.2	620	7.8	9.3	0.0024	1025
Cl/Br	168	624	733	15.4	2792.9245	36	1190	1048	225	6733	204	699.9	782	15.4	6733
S/Br	152	1287	1388	25.3	18846	34	23908	20588	2458	221569	186	2195	2175	25.3	221569
S/I	78	20120	16931	992	192592	21	75128	80124	5962	614671	99	26607	28023	992.8	614671
		Flux (Tg/yr)					**Flux (Tg/yr)**					**Flux (Tg/yr)**			
SO_2		16.8[a]					1.7[a]					18.5[a]			
HCl		5.5					0.3					5.5			
HF		0.58					0.15					0.7			
HBr		0.016					0.0001					0.0105			
HI		0.0017					0.00004					0.0014			

The dataset is based on measurements of more than 600 individual gas samples, and is compiled from Gerlach (2004), Aiuppa (2009) and Aiuppa et al. (pers. data from UniPa-INGV unpublished dataset). The available number of samples in each category is indicated in the column "Valid N". The fluxes of halogens quoted in the table are calculated from the mean (S/halogen) ratios (column "Mean") and the SO_2 flux data of Shinohara (2013)

[a]From Shinohara (2013)

Fluorine is the second halogen in order of abundance in volcanic gases, and is mainly transported/emitted as $HF_{(g)}$. In the (selected) list of volcanic gas samples of Table 6.2, F concentrations range from 0.02 to 1.27 mol% (mean, 0.21 mol%). Within-plate and continental-rift volcanoes have F contents (Table 6.2) and S/F ratios (Fig. 6.7b and Table 6.3) overlapping the volcanic arc gas range. Molar ratios of Cl/F in volcanic gases show, instead, dissimilar distributions for within-plate and continental-rift volcanoes (Cl/F of ~1) and arc volcanoes (Cl/F of ~5.5) (Fig. 6.7c and Table 6.3). This once more points to a recycled (slab-derived) Cl component in arc magmas, overprinting the Cl/F MORB signature of ~1 (Pyle and Mather 2009). Fluorine enrichment (relative to Cl) is possibly highest in within-plate contexts. Fluorine is, for instance, twice as abundant as Cl in Erebus gas (Oppenheimer and Kyle 2008; Oppenheimer et al. 2009). Apart from original concentrations in parental melts, the contrasting solubilities/vapour-melt partitioning (cf., 6.3) exert an additional control on their relative Cl and F abundances in volcanic gases as described below (Aiuppa 2009).

Measurements of Br and I in volcanic gases and condensates are relatively few in number (Sugiura et al. 1963; Honda et al. 1966; Honda 1970; Snyder et al. 2002; Snyder and Fehn 2002). Existing measurements typically indicate concentrations at ppm (Br) to ppb (I) levels. $HBr_{(g)}$ is thought to dominate Br speciation in both high-temperature volcanic gases (Gerlach 2004) and near-vent volcanic plumes (Aiuppa et al. 2005; Martin et al. 2006; Oppenheimer et al. 2006a). Rapid Br atmospheric processing in atmospheric plumes (cf., 6.4.3) leads, however, to rapid formation of reactive oxidized Br ($BrO_{(g)}$), which dominates the Br budget in aged (e.g., several minutes-old) plumes (Oppenheimer et al. 2006a; Bobrowski et al. 2007; Boichu et al. 2011). Iodine speciation in gases and plumes is currently only poorly understood (Aiuppa et al. 2005).

Table 6.3 lists the statistical parameters of the trace halogen ratios in gases emitted by a selection of mafic volcanoes. These results are far less robust than those obtained for Cl and F due to the limited dataset available. There is also a disproportion between arc and non-arc volcanism in the dataset, with the former being far better represented (80% of the ≈200 individual Br volcanic gas analyses are from arc volcanoes). This suggests that at least part of the systematic trends in Figs. 6.7d and 6.8 may merely reflect an incompleteness in the database. Cl/Br ratios in volcanic gas condensates and plumes (range, 15–6700; Table 6.3) exhibit a close-to-log normal distribution (Fig. 6.7d), with arithmetic mean (700) and median (788) values that are slightly higher than the characteristic seawater (Cl/Br = 650) ratio. Based on available information, arc and non-arc volcanic gases do exhibit a factor of ≈2 Cl/Br ratio difference (means of respectively 624 and 1191; Table 6.3). The Br-poor signature of within-plate/rift volcanism (relative to volcanic arcs) is also supported by available S/Br gas information: S/Br ratios in non-arc gases plot at the upper end of the volcanic arc range and beyond (Fig. 6.8a), with typical ratios of respectively ≈1,300 and ≈23,000 (Table 6.3). Iodine systematics in volcanic gases are still very incomplete (Fig. 6.8b) (Pyle and Mather 2009; Mather et al. 2012). Available data indicate, however, a mean volcanic gas S/I ratio somewhere around 26,000–28,000 (Table 6.3). I/Cl ratios in

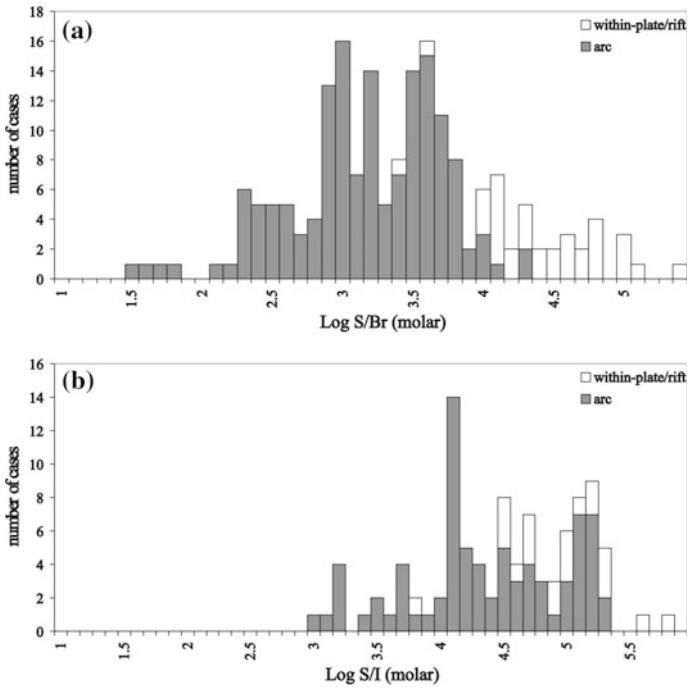

Fig. 6.8 Histograms of the logarithmic distributions of **a** S/Br and **b** S/I (molar) ratios in gases and plumes released by within-plate (rift) and arc mafic volcanoes (dataset from Table 6.3; see Table 6.3 caption for data sources)

volcanic gases are typically at $\approx 10^{-4}$ level (Snyder et al. 2002), and are therefore two orders of magnitude higher than in seawater (I/Cl $\sim 10^{-6}$). In Fig. 6.9, the Cl-Br-I compositional range of volcanic gases is put in the context of available information for a variety of geological materials related to halogen recycling at subduction zones (Kendrick et al. 2012a). These include the MORB-mantle (Kendrick et al. 2012a, b); antigorite-bearing serpentinites and their breakdown fluids (Kendrick et al. 2011); and sedimentary marine pore fluids (e.g., Muramatsu et al. 2007). Volcanic gases are distinctively more depleted in I and Br (relative to Cl) than marine pore fluids and hydrated serpentinites, which have evolved their halogen-rich signature upon alteration on the ocean floor (Kendrick et al. 2011). The majority of volcanic gas compositions cluster in a relatively narrow area between seawater and the representative MORB-mantle compositional field of Kendrick et al. (2012b). A number of volcanic gas samples diverge towards Br-poor (and I-rich) compositions that encompass the compositional field of fluids formed during late-stage breakdown of (olivine-enriched) serpentinites (Kendrick et al. 2012a). Overall, Fig. 6.9 reflects the possible heterogeneity of halogen sources in

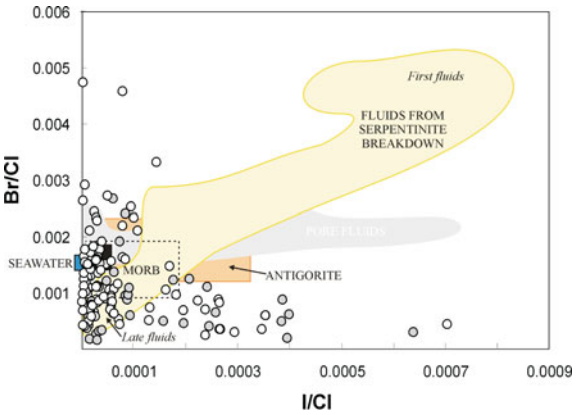

Fig. 6.9 Scatter diagram of Cl/I versus Br/Cl ratios in volcanic gases and plumes (UniPa-INGV unpublished dataset): *open circles* arc volcanoes; *grey circles* non-arc volcanoes. The compositional fields of the MORB-mantle (Kendrick et al. 2012a, b), antigorite-bearing serpentinites and their breakdown fluids (Kendrick et al. 2011), and sedimentary marine pore fluids (Muramatsu et al. 2007) are shown for comparison

volcanic gas emissions. Precise interpretation of trends in volcanic gas origins remains precluded until inter-halogen fractionations during degassing of mafic magmas become more adequately quantified (Bureau et al. 2000).

6.2.6 *Stable Isotopes of Cl, Br, and I*

The stable isotopes of Cl, Br, and I have been investigated and applied to interpretations of magmatic and hydrothermal processes in volcanic gases and BAA magmas and in their associated thermal springs (Cullen et al. 2015). The sole stable isotope for F is ^{19}F and, hence, stable isotope ratios cannot be determined for the lightest halogen. Details on isotopic fractionation and characteristics for I are available in Snyder and Fehn (2002) and Hurwitz et al. (2005) and for Br in Eggenkamp (2014). Chlorine isotopic behavior has received the most attention, and we briefly review some of this work here.

The application of $\delta^{37}Cl$ systematics to magmatic systems is supported by indications that ^{37}Cl and ^{35}Cl do not fractionate strongly from one another during high-temperature hydrothermal and magmatic processes (Liebscher et al. 2006). Thus, this geochemical tool is useful for constraining $\delta^{37}Cl$ values of and Cl isotopic fractionation during volatile transfer between the Earth's halogen-bearing reservoirs. The $\delta^{37}Cl$ composition of the depleted mantle has long remained a

matter of debate (Sharp et al. 2007; Bonifacie et al. 2008). Recent work shows that values of $\delta^{37}Cl$ apparently exhibit little variation in MORB glasses of ca. −3.0 to 0.0‰ (John et al. 2010; Eggenkamp 2014), and $\delta^{37}Cl$ ranges from −1.6 to +1.1‰ for high-$^{238}U/^{204}Pb$ OIBs and from −0.4 to +2.9‰ for enriched-mantle OIBs (John et al. 2010). Relative to this $\delta^{37}Cl$ mantle composition, recent $^{37}Cl/^{35}Cl$ measurements in arc volcanic gases (e.g., Rizzo et al. 2013) have identified the presence of an isotopically heavier Cl component, corroborating a slab-derived recycled Cl contribution to the mantle during subduction. Slab-derived Cl contributions do vary substantially along some arc segments, however. Barnes et al. (2008) determined $\delta^{37}Cl$ for volcanic gas, geothermal fluid, ash, and lava samples of the Izu Bonin-Mariana arc and observed distinct variations across the arc indicating variations in fluid sources at varying depths of the subduction zone. Barnes et al. (2009) studied the $\delta^{37}Cl$ compositions of volcanic outputs (ash, tephra, and lava samples) of 23 volcanic centers from the Central American volcanic front. They identified sizeable, systematic variations in $\delta^{37}Cl$ values (range, −2.6 to +3.0‰), along the length of the front, from mantle-like signatures at the northernmost (Guatemala and El Salvador) and southernmost (Costa Rica) ends of the front, to sediment and/or serpentinite-derived components in Nicaragua. Conversely, changes in $\delta^{37}Cl$ values in 38 thermal springs along and across the Cascades range show little variation (e.g., 0.2–1.9‰ (Cullen et al. 2015)). Moreover, Barnes and Straub (2010) applied Cl stable isotopes to constrain the relative contribution of ocean floor serpentinites to the flux of Cl passing through subduction zones for the Izu Bonin arc magmatic system.

Although Cl isotopes are important for tracing the sources of volatiles in subduction environments, care must be paid to filter out the effects of low-temperature fractionation. Sharp et al. (2010) showed that ^{37}Cl values can vary dramatically in low-temperature fumarole gases, due to fractionation in near-surface evaporation and condensation processes. Other processes involving isotopic fractionation do occur in BAA-relevant systems at lower-temperature conditions. Chlorine stable isotopes fractionate when Cl is sequestered by amphiboles during metasomatism of seafloor basalts by seawater-derived hydrothermal fluids. Altered basalts exhibit higher $\delta^{37}Cl$ relative to seawater values (Magenheim et al. 1995), and porewaters sampled at subduction zones show $\delta^{37}Cl$ as low as −8‰ (Ransom et al. 1995).

Chlorine isotopes have also been applied to mineralized magmatic systems. They have, for example, been used to determine the halogen sources in Cl-enriched layered intrusions and the fluxes involved in Cl transfer between melt, minerals, and fluids at the Stillwater complex, Montana (Boudreau et al. 1997). The behavior of these isotopes has also been investigated in FI from mineralized felsic magmas (Eastoe and Guilbert 1992). This approach shows promise for hydrothermal fluids involved with hydrothermally altered and mineralized BAA magmas. Additional details on the isotopic behavior of Cl are available in Stewart and Spivack (2004) and Eggenkamp (2014).

6.3 Experimental Observations & Theoretical Constraints

6.3.1 Fluid Exsolution in Halogen-Bearing Magmas

For halogen-bearing magmas at most mantle and mid- to deep-crustal pressures, the typical state of fluid saturation involves a single fluid phase whose density varies with pressure and whose composition is dominated, on a molar basis, by H_2O and CO_2. Such fluids also contain lesser S and halide species (Holloway 1987). However, at more shallow-crustal pressures, magmatic temperatures, and in the presence of sufficient Cl, a silicate melt may coexist with a hydrosaline liquid phase and an aqueous or aqueous-carbonic vapor (Driesner and Heinrich 2007). The presence of carbon dioxide is important in this regard. Small quantities of CO_2 expand the stability field for aqueous-carbonic vapors and hydrosaline liquids (Holloway 1973; Bowers and Helgeson 1983; Joyce and Holloway 1993; Duan et al. 1995; Shmulovich and Graham 2004; Aranovich et al. 2010).

The dissolution of volatile components in melts is controlled by the phase equilibria of the bulk system. Therefore, it is essential to review the phase equilibria of halogen-bearing BAA melts and coexisting fluids before applying the results of hydrothermal experiments on volatile solubilities, diffusion, and partitioning behaviors to natural systems. Saturation of a silicate melt in one or more fluid phases (i.e., the process of fluid exsolution) occurs when the summed partial pressures of all volatile components in the melt exceed the confining pressure on the system. Since H_2O is the dominant volatile in natural aluminosilicate melts, most coexisting magmatic fluids are, at least, partially aqueous in composition. However, as has been observed in hydrothermal experiments with CO_2 at shallow-crustal pressures (Stolper and Holloway 1998), the addition of small to moderate quantities of Cl to hydrous felsic (Webster 1992a, b), rhyodacitic (Botcharnikov et al. 2004), phonolitic (Webster et al. 2009a), and andesitic (Botcharnikov et al. 2007) systems can significantly reduce the H_2O solubility of the coexisting melts (Fig. 6.10) and, hence, increase the drive towards fluid exsolution. Although they are typically less abundant than H_2O, both Cl and CO_2 may control melt-fluid phase equilibria at specific stages of magma evolution. However, as demonstrated below, non-alkaline basaltic to andesitic melts dissolve far more Cl (wt% levels when saturated in a hydrosaline liquid) than typically occurs in most such magmas. Thus, the likelihood of Cl reducing the H_2O solubility in melt and supporting fluid exsolution in the vast majority of basaltic to andesitic magmas is low (Webster et al. 1999, 2003, 2015; Botcharnikov et al. 2007; Stelling et al. 2008; Fiege et al. 2014). Fluid-melt phase relations for chemically complex fluids have also been studied experimentally at upper-mantle pressures (Safonov et al. 2009). Coexisting diopside-composition silicate melts ± chloride liquid ± carbonate liquid were stabilized at 5 GPa and 1400–1600 °C (Safonov et al. 2007). Partially molten peridotite was observed with and without chloride and carbonate liquids at 16.5 GPa and 1200–1800 °C (Litasov and Ohtani 2009). Chlorine addition not only affects the dissolution behavior of H_2O (Beermann et al. 2015); it has also been observed that increasing Cl in basaltic

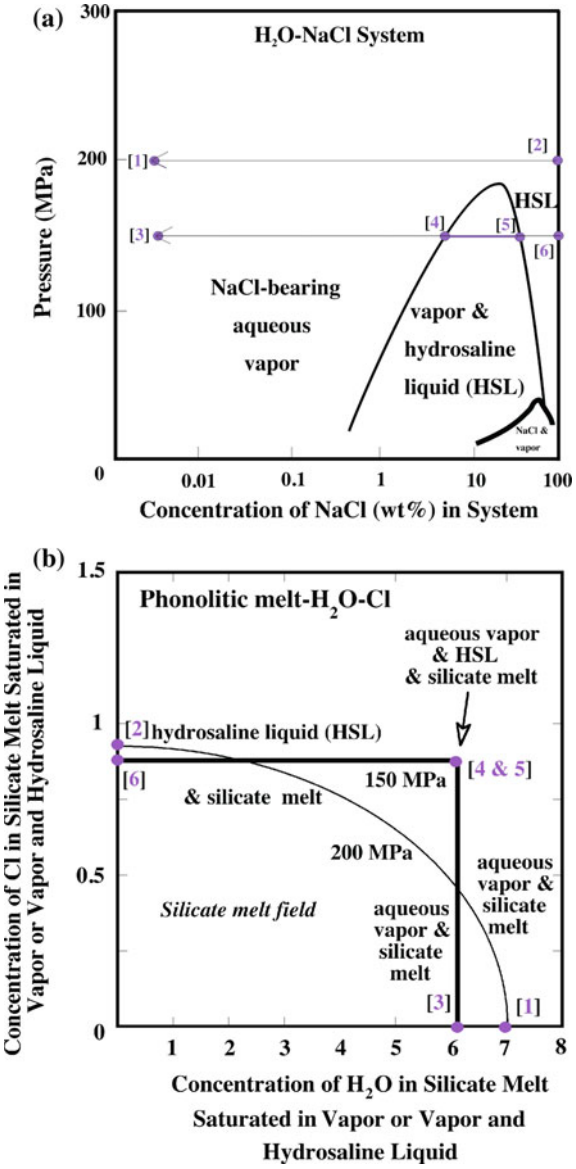
(a)
H2O-NaCl System
Pressure (MPa)
300
200
100
0
[1]
[2]
[3]
[4]
[5]
[6]
HSL
NaCl-bearing
aqueous
vapor
vapor &
hydrosaline
liquid (HSL)
NaCl &
vapor
0.01
0.1
1
10
100
Concentration of NaCl (wt%) in System
(b)
Phonolitic melt-H2O-Cl
Concentration of Cl in Silicate Melt Saturated in Vapor or Vapor and Hydrosaline Liquid
1.5
1
0.5
0
aqueous vapor
& HSL
& silicate melt
[2]hydrosaline liquid (HSL)
[6]
& silicate melt
150 MPa
[4 & 5]
200 MPa
Silicate melt field
aqueous
vapor &
silicate
melt
aqueous
vapor &
silicate
melt
[3]
[1]
1
2
3
4
5
6
7
8
Concentration of H2O in Silicate Melt
Saturated in Vapor or Vapor and
Hydrosaline Liquid

◂**Fig. 6.10** Sketches detailing: **a** phase equilibria in the system NaCl-H_2O at shallow-crustal pressures and an unconstrained magmatic temperature, and **b** dissolution behavior of Cl and H_2O in a phonolitic melt at same conditions as in (**a**) after Webster et al. (2015). The phase fields for vapor and hydrosaline liquid (HSL) are shown. *Lines* [*1*] to [*2*] and [*3*] to [*6*] express fluid phase equilibria as a function of NaCl content for the system at two pressure conditions. With increasing NaCl in the system from [*4*] to [*5*], Cl concentrations in the vapor and HSL are fixed, and the relative quantities of vapor and HSL vary. Plot **b** shows dissolution behavior of Cl and H_2O in the phonolitic melt at the same conditions as in (**a**). *Curves* [*1*] to [*2*] in (**b**) correspond to conditions of *line* [*1*] to [*2*] in (**a**). It expresses the change in Cl and H_2O dissolution in the silicate melt as the NaCl concentration of the coexisting vapor composition increases. Specifically, the addition of Cl reduces the solubility of H_2O in the melt. *Lines* [*3*] to [*4*, *5*] and [*4*, *5*] to [*6*] in (**b**) correspond to *line* [*3*] to [*6*] in (**a**). *Line* [*3*] to [*4*, *5*] shows how H_2O concentration in the melt is fixed with increasing Cl in the coexisting vapor. *Line* [*4*, *5*] to [*6*] shows how the Cl concentration in the melt is fixed with increasing Cl in the coexisting HSL. At *point* [*4*, *5*], melt coexists with conjugate vapor and HSL. These phase relations are applicable to fluid phase relations in phonolitic-trachytic magmas, but may be less relevant to fluids in basaltic and andesitic magmas

melts reduces the corresponding S contents of the melt and increases its concentrations in coexisting fluids. This relationship is enhanced as oxygen fugacity (f_{O2}) increases to $\geq$NNO+3 (Beermann 2010).

The mechanics of fluid mixing versus unmixing, as a function of chlorinity at the ionic- and molecular-species level, are influenced by a variety of forces and by the size and charge characteristics of the fluid species (Holloway 1987). As a result, the mixing processes are complicated. However, to a first-order level, the mechanics of fluid mixing can be understood as follows. For H_2O- and CO_2-dominated systems containing trace chloride ion, chemical interactions between like molecules (e.g., H_2O-H_2O, CO_2-CO_2, and Cl^{-1}-Cl^{-1}) are minor, and the predominant interactions involve H_2O molecules with CO_2 molecules, H_2O molecules with Cl^{-1} ions, and CO_2 molecules with Cl^{-1} ions. The activities (a_i) of the dominant volatile components are modestly greater than the respective mole fractions (e.g., $a_{H2O} > X_{H2O}$ and $a_{CO2} > X_{CO2}$, e.g., Aranovich and Newton 1999); the chemical drive toward volatile mixing is strong, and a single fluid is stable in this situation. The addition of Cl to the system, however, increases the proportion of interactions between similar molecules or ions (e.g., Cl^{-1}-Cl^{-1}, H_2O-H_2O, and CO_2-CO_2). Chlorine-bearing aqueous and aqueous-carbonic fluids will unmix at shallow-crustal pressures and magmatic temperatures when the $a_{Cl} \gg X_{Cl}$, $a_{H2O} \gg X_{H2O}$, and $a_{CO2} \gg X_{CO2}$ and, hence, when the activity coefficients (a_i) for these volatile components significantly exceed unity (Botcharnikov et al. 2007; Anovitz et al. 2004; Webster et al. 2015). Increasing interactions between similar molecules or ions sustain non-ideal volatile solubility in the fluid. Ultimately, i.e., with sufficient Cl in the system, strongly non-ideal conditions occur and they result in unmixing of the fluid in which a hydrosaline liquid condenses from vapor (Bodnar et al. 1985; Malinin et al. 1989; Shinohara et al. 1989; Lowenstern 1994; Webster et al. 1999; Signorelli and Carroll 2000; Botcharnikov et al. 2004; Shmulovich and Graham 2004; Mathez and Webster 2005; Webster and Mandeville 2007; Shinohara 2009). An associated consequence of non-ideal and non-Henrian activity-composition relations for these volatile components is that this situation causes elevated and sometimes fixed a_{H2O}

and a_{Cl} in coexisting melts (Botcharnikov et al. 2004, 2015; Webster and Mandeville 2007; Beermann 2010; Webster et al. 2015), as well as in fluids, even with the addition of significant Cl, and with or without CO_2 (Fig. 6.10). Moreover, for equilibria involving silicate melt and two coexisting fluids, simple changes in the H_2O and Cl contents of the system do not cause changes in the H_2O and Cl concentrations in the melt, vapor, or liquid as long as the system is maintained at a fixed pressure and temperature. Rather, it is the quantities of vapor and hydrosaline liquid that change (Fig. 6.10).

Most non-alkaline basaltic and andesitic magmas contain insufficient Cl (recall Fig. 6.1) to stabilize two fluids until they ascend to very low pressures at very shallow-crustal depths. This behavior is based on the location of the low-Cl leg of the NaCl-H_2O solvus curve (Fig. 6.10a), which shifts to lower Cl concentrations with decreasing pressure. As an example of this, Taran et al. (1995) interpreted the difference in Cl contents of comparatively dense magmatic fluids at depth versus those of the lower-density and high-temperature fumarolic gases to indicate the formation of small quantities of hydrosaline liquid in the basaltic-andesite magmas of Kudryavy volcano of the Kurile Islands. They further argued that the low-density vapor, containing less Cl than the hydrosaline liquid, separates and leaves the hydrosaline liquid behind due to the stark differences in the phase density. Associated modeling of melt-vapor-molten salt equilibria by Shmulovich and Churakov (1998) suggests that as much as 3×10^6 m^3 of anhydrous hypersaline liquid may have formed in the upper 200 m of the conduits feeding the Kudryavy volcano during magmatic crystallization and degassing over a period of 114 years.

Many alkaline tephritic, trachytic, and phonolitic magmas contain levels of Cl that influence fluid-phase equilibria during magma ascent through the crust. Hydrothermal brine (i.e., a dehydrated hydrosaline liquid), for example, was observed flowing from fissures in the phonotephritic to phonolitic rocks of the Mt. Vesuvius crater in the first decade following the 1944 eruption (Chiodini et al. 2001). The emission of molten salt was interpreted to result from the boiling and escape of aqueous-carbonic vapor from magmatic fluid, leaving behind a more-dense saline liquid that eventually ascended and breached the crater walls.

In summary, the solubility of Cl in hydrosaline liquid-saturated silicate melts, as described in Sect. 6.3.2, varies significantly with composition. Basaltic liquids can dissolve wt% levels of Cl, but such solubilities, however, far exceed the actual concentrations measured in most basaltic melts. These relationships contrast with those involving felsic magmas for which the solubility of Cl in the melt can be as low as a few thousand ppm. Natural felsic melts in such magmas do contain sufficient Cl leading to the exsolution of brine with or without a vapor phase during magma evolution and ascent towards the surface. Moreover, as demonstrated below in Sect. 6.3.3, Cl partitions subequally between basaltic melts and aqueous or aqueous-carbonic fluids, so magmatic fluids in basaltic systems are unlikely to contain sufficient Cl to support strong interactions between similar molecules and ions. It follows that the condensation of hydrosaline liquid from vapor is similarly unlikely because mafic melts dissolve and sequester most of the magmatically sourced Cl in fluid-saturated basaltic systems. Magmas, however, can derive

additional Cl by direct assimilation of seawater-derived brines. And, as discussed in Sect. 6.4.1, when seawater is heated by hot crystalline basaltic crust on the seafloor, the pressure-temperature conditions support fluid-fluid immiscibility during which seawater boils off a vapor phase and stabilizes the brine (Bischoff and Rosenbauer 1984; Fournier 1987; Foustoukos and Seyfried 2007a).

The influence of F on H_2O solubility in aqueous-fluid saturated BAA melts is poorly determined because most experimental work with F has focused on felsic melts (see Dolejs and Zajacz 2018). The investigation of volatile dissolution in molten Etna basalt shows no change in dissolved H_2O contents of the melt when the F concentration is varied from 0.1 to 1 wt% at 200 MPa (Alletti 2007). In another study, increasing F in a phonolitic melt at 200 MPa from 0.1 to 1.3 wt% has no detectable effect on the H_2O concentration dissolved in the melt (Chevychelov et al. 2008a). Thus, it appears that the addition of F does not have a significant influence on the exsolution of an aqueous fluid from hydrous, F-bearing melts.

Additional research is warranted, however, because other experiments on F-enriched systems have shown evidence of silicate melt and F-rich liquid immiscibility (Kotlova 1960; see Dolejs and Zajacz 2018), so excess F can lead to the exsolution of a F-rich fluid. Some early research has documented large fields of Si-rich melt coexisting with a F-rich liquid in anhydrous systems whose synthetic silicate melts have little relevance to magmatic systems. For example, Ershova and Olshanskii (1957) observed both an immiscible Si-rich melt and a F-rich liquid in their experimental run products in the Al-free system: MeF_2-MeO-SiO_2 (*Me* refers to Ca, Mg, Ba, and Sr) and Ershova (1957) observed the same for the system MeF_2-Al_2O_3-SiO_2. Subsequent research involving immiscible fluids has determined the melting relations and partitioning behavior of trace elements and volatile components between silicate melts and fluoride liquids (Veksler et al. 2005, 2012), silicate melts and chloride liquids (Veksler et al. 2012), two halogen-bearing silicate melts (Lester et al. 2013), and between silicate melts-carbonatitic liquids (Veksler 2004), some of which document immiscible melt and liquid at higher pressure (e.g., 5 GPa; Safonov et al. 2007). A common observation from these studies is that F apparently associates chemically with alkaline earth elements in the silicate melts and fluoride-rich liquids.

The separation of immiscible F-enriched liquids from natural, hydrous F-bearing aluminosilicate melts in mafic systems has been addressed in the geological literature (Kamenetsky and Kamenetsky 2010). For example, Klemme (2004, 2005) observed aluminosilicate blebs with 41 wt% SiO_2 and up to 12 wt% F in metasomatized mantle xenoliths. He controversially interpreted the blebs to represent quenched silicate melt that had coexisted with a conjugate fluoride liquid. Klemme (2004, 2005) concluded an origin for both F-bearing fluids involving melt-liquid immiscibility, but Dolejs (2005) and Brey et al. (2009) argued against the likelihood or stability of coexisting fluids at mantle pressures given the compositions involved. Brey et al. (2009) also noted that natural enrichments of mafic, SiO_2-poor melts in F during differentiation would be limited by saturation in the F-enriched minerals clinohumite and/or fluorphlogopite. Likewise for evolving felsic aluminosilicate

melts, the extent of F enrichment in the melt resulting from fractional crystallization would be limited by the crystallization of fluorite or topaz; these relationships are addressed by Dolejs and Baker (2004, 2006).

The influences of Br and I on fluid phase separation are not well determined for magmatic conditions. Vapor-brine experiments at 388–550 °C and 25–35 MPa show that Br partititions in favor of low-salinity vapor relative to hydrosaline liquid (Foustoukos and Seyfried 2007b).

6.3.2 *Halogen Solubility and Dissolution in Mafic and Related Melts*

Knowledge of halogen dissolution in, and exsolution from, silicate melts derives largely from experimental research and empirical as well as thermodynamic modeling (Persikov et al. 1990). Most such studies have been published in the geological literature, but results of investigations on halogen dissolution in melts have also appeared in glass technology (Köpsel 2001; Siwadamrongpong et al. 2004), ceramics (Markis et al. 1981), and archeological journals (Tanimoto and Rehren 2008).

Halogen dissolution in melts varies with pressure, temperature, melt, and fluid composition. Maximum recorded concentrations of halogens in experimentally prepared aluminosilicate melts, saturated in molten salt(s), are 16.9 wt% F in a Ca- and Mg-enriched melt containing 35.4 wt% SiO_2 and 2.4 wt% Al_2O_3 at one atm (Veksler et al. 1998), and 9 wt% Cl has been measured in Fe- and Ca-enriched basaltic melts at 2 GPa (Malinin et al. 1989). The solubilities of Br and I are not determined for BAA melts. Concentrations of Br exceed 1.1 wt% in fluid-saturated pantelleritic melt at 100–200 MPa (Bureau and Métrich 2003), and as much as 0.021 wt% I was observed to dissolve in fluid-saturated albitic melt at 200 MPa (Bureau et al. 2000).

Chlorine. The concentrations of magmatic Cl in BAA melts are typically lower than those of the primary volatile components H_2O, CO_2, and SO_2/H_2S in magmas. Nevertheless, Cl and its solubility in hydrosaline-saturated liquids and partitioning between aluminosilicate melts and fluid(s) have been investigated more so than magmatic F, Br, or I. This attention on Cl is a result of its influence on ore metal and trace-element dissolution in magmatic-hydrothermal fluids and in high-temperature volcanic gases, its control of fluid phase relations at magmatic conditions, and because of its utility as a geochemical indicator of magmatic processes.

Basaltic melts may dissolve Cl at the several wt% level. The dissolution of Cl in silicate melts varies strongly with the concentrations of network-modifying cations including the alkaline earth elements and Fe, and less so with those of the alkalis and other constituents. Chlorine dissolution increases with decreasing

concentrations of network-forming Si, decreasing concentrations of P (also as network-former) and Ti, and increasing concentrations of network-modifying cations (Iwasaki and Katsura 1967; Malinin et al. 1989; Kravchuk and Keppler 1994; Chevychelov 1999; Webster and De Vivo 2002; Chevychelov et al. 2003; Chevychelov and Suk 2003; Siwadamrongpong et al. 2004; Webster et al. 2015). Moreover, the dissolution of Cl in melts increases with increasing F contents (Webster and Holloway 1988; Webster and De Vivo 2002; Chevychelov et al. 2008a; Webster et al. 2015). For geologically relevant BAA melts, Cl dissolution in melt increases with the molar (Al + Na + Ca + Mg/Si) ratio (Fig. 6.11) (Webster et al. 1999). For example, the 200-MPa solubilities of Cl in brine- ± vapor-saturated melts increase from 0.14 wt% in the system K_2O-Al_2O_3-SiO_2-H_2O-Cl, to 0.26 wt% in the subaluminous haplogranitic system Na_2O-K_2O-Al_2O_3-SiO_2-H_2O-Cl, to 5.9 wt% for a highly alkaline basalt (Webster et al. 2015). Chlorine solubilities also increase as the melts become more alkaline (i.e., with increasing concentrations of network-modifying Na, K, and Ca relative to Al) (Koster van Groos and Wyllie 1969; Malinin et al. 1989; Metrich and Rutherford 1992; Webster 1992b; Signorelli and Carroll 2002) and as they become more aluminous (i.e., with increasing network-modifying Al contents) (Webster 1992b; Signorelli and Carroll 2000). Thus, reflecting the influences of melt aluminosity and alkalinity, the minimum Cl concentrations occur in metaluminous melts containing equivalent moles of Al and accompanying charge-balancing Na, K, and Ca (Metrich and Rutherford 1992; Carroll 2005).

Spectroscopic analyses provide direct information on the mechanisms incorporating Cl in anhydrous melts, and experimentally determined solubility relations provide indirect constraints on the speciation of Cl in hydrous to anhydrous melts. Interactions of Cl with network-modifying Ca, Mg, Fe, and alkali ions are dominant. Solid state Magic Angle Spinning (MAS) Nuclear Magnetic Resonance (NMR) spectra of felsic Cl-bearing silicate and aluminosilicate glasses, for instance, indicate that most Cl-coordination environments involve network-modifying Na, Ba, and Ca cations and that there is no clear contribution of network-forming Al and/or Si in those chloride-in-glass spectra that have been investigated (Stebbins and Du 2002; Sandland et al. 2004). A recent study of both peralkaline and peraluminous Na_2O-CaO-Al_2O_3-SiO_2 glasses by MAS-NMR spectroscopy determined that Cl exists in relatively symmetric environments dominated by Na and Ca (Baasner et al. 2014). In another study, X-ray absorption near-edge structure (XANES) analysis was applied to 25 Cl-bearing glasses, all containing ≤ 57 wt% SiO_2. The chloride ion was interpreted to form Ca-Cl, Mg-Cl, or possibly mixed Ca-Mg-Cl species of undetermined stoichiometries (Evans et al. 2008). The short-range structure that was observed is similar to that of crystalline $CaCl_2$ and $MgCl_2$ (Evans et al. 2008). Interpretations of the influence of Cl on aluminosilicate melt viscosities are also consistent with chloride ions bonding with charge-balancing Fe^{2+} (Zimova and Webb 2006). Likewise, changes in the (Fe^{3+}/Fe^{2+}+Fe^{3+}) ratio of silicate melts with addition of Cl indicates strong chemical interactions between Cl and Fe (Webb et al.

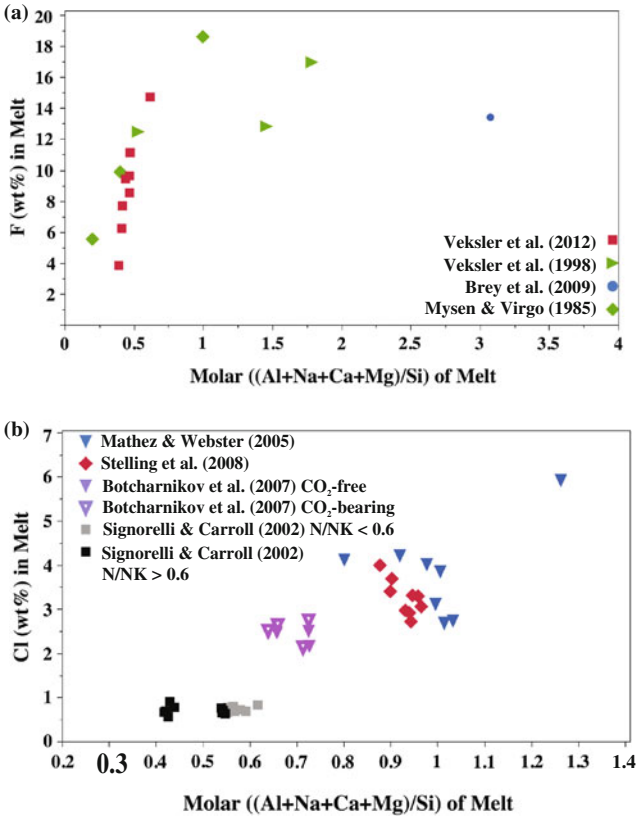

Fig. 6.11 Plots expressing experimentally determined maximum concentrations of **a** F and **b** Cl in mafic to felsic aluminosilicate melts versus the molar ((Al + Na + Ca + Mg)/(Si)) of the melt for a variety of experimental conditions. The dissolution of F and Cl is influenced strongly by the concentrations of Al, Na, Ca, and Mg in melt. In **a**, the *red squares* represent melts (with ca. 54–68 wt% SiO_2) saturated in a fluoride liquid phase at 100 MPa and 700–1050 °C (Veksler et al. 2012). These F concentrations represent saturation values. None of the other data represent silicate melts saturated in a fluoride liquid. The *green symbols* designate 1-atmosphere experiments. The *diamonds* represent melts prepared at 1550 °C (Mysen and Virgo 1985). The *triangles* are 950–1050 °C melts (Veksler et al. 1998). The *single blue circle* represents the melt of a 6-GPa and 1500 °C experiment (Brey et al. 2009). In **b**, most melts were saturated in a hydrosaline chloride-enriched liquid, with or without aqueous or aqueous-carbonic vapor. *Squares* are phonolitic melts. *Black symbols* have molar [Na/Na+K] $\leq$ 0.6. *Gray symbols* have higher [Na/Na+K]) at 25–150 MPa and 880–930 °C (Signorelli and Carroll 2002). *Triangles* (open (CO_2 + H_2O) and filled (no CO_2)) represent andesitic melts at 1200 °C and 200 MPa (Botcharnikov et al. 2007). *Diamonds* show basaltic melts at 200 MPa and 1150–1200 °C (Stelling et al. 2008). *Triangles* represent apatite-saturated basaltic melts at 200 MPa and 1075–1110 °C (Mathez and Webster 2005)

2014; Bell and Webster 2015). These spectroscopy-based constraints are consistent with experimental observations that the dominant interactions involve Cl with network-modifying alkalis, alkaline earth metals, and Fe in aluminosilicate melts, with little to no evidence of Cl forming species with silica or network-forming, 4-fold coordinated Al.

The influences of temperature, pressure, and fluid composition on Cl dissolution in melts are also well examined. The Cl concentrations in melts containing intermediate- to high-SiO_2 concentrations and those melts saturated in hydrosaline liquids or Cl-bearing aqueous fluids, increase with temperature (Webster 1992a; Webster et al. 2015). The Cl-dissolution relations involving pressure, however, are complex, and they vary with the fluid phase assemblage and f_{O2}. Some investigations have determined that the concentration of Cl in melts, apparently saturated in vapor or vapor plus hydrosaline liquid, increases with decreasing pressure (Shinohara et al. 1989; Métrich and Rutherford 1992; Chevychelov and Chevychelova 1997; Signorelli and Carroll 2000). Whereas, others have observed that the maximum Cl concentration in hydrosaline liquid- ± vapor-saturated melts increases with pressure (Webster 1992a, b, 2004; Webster and Rebbert 1998; Webster et al. 1999, 2003). This discrepancy is yet to be resolved, but strictly speaking Cl solubility in hydrosaline-liquid saturated silicate melts (with or without a coexisting vapor) definitively increases with pressure (Webster et al. 2015), whereas Cl partitioning between melt and fluid(s) responds variably to changes in pressure. However, at present, the phase relations of hydrosaline liquid versus vapor plus hydrosaline liquids, that contain cations in addition to Na and K, are poorly understood. The dissolution of Cl in melts varies with the activity of Cl in the system. The Cl activity also varies strongly with changing phase relations with vapor, hydrosaline liquid, and silicate melt ± Cl-rich minerals. Limited experimental data on fluid phase relations are available for the system H_2O-$CaCl_2$±NaCl-CO_2 (Oakes et al. 1994; Jiang and Pitzer 1996; Shmulovich and Graham 2004) and lesser data for H_2O-$MgCl_2$ (Shmulovich et al. 1995) and H_2O-$FeCl_2$±NaCl (Lecumberri-Sanchez et al. 2015; Steele-MacInnis et al. 2015), but the phase relations of geologically relevant and geochemically complex fluids: H_2O-NaCl-KCl-$FeCl_2$-$FeCl_3$-$MgCl_2$-$CaCl_2$±CO_2±F±S species are unknown. We suggest that these discrepancies in the behavior of Cl dissolution in melts as a function of pressure are largely influenced by the unknown fluid phase relations and thermodynamic activities of Cl in natural and geochemically complex fluids, and that they require systematic investigation. These relationships relating Cl solubility with pressure have a fundamental bearing on volcanic degassing and eruptive processes. Balcone-Boissard et al. (2016), for example, recently published a method for defining the storage conditions of Cl-enriched magmas based on Cl solubilities in melts as a function of pressure.

Using molten basalt from Mt. Etna, Alletti et al. (2009) determined that there was no change in the Cl contents of fluid-saturated melt with pressure for log f_{O2} of

NNO+2; whereas, the Cl concentrations of Cl-enriched melt decreased somewhat with a reduction in pressure at NNO. It is clearly established that the solubility of Cl in melts, saturated in hydrosaline liquid and lacking a coexisting aqueous vapor phase, increases with pressure (Malinin et al. 1989; Webster et al. 1999, 2015; Botcharnikov et al. 2015). The Cl concentrations of fluid-saturated, BAA melts increase, also, with increasing Cl (Webster et al. 2009a; Zajacz et al. 2012) and with decreasing S in coexisting fluids (Botcharnikov et al. 2004; Webster et al. 2006; Beermann 2010; Lesne et al. 2011). The addition of CO_2 to Cl-bearing aqueous fluids has differing effects on the measured Cl concentration of coexisting melts. With up to 35 mol% CO_2 in dominantly aqueous fluids at 200 MPa, the Cl content of conjugate phonolitic-trachytic melts is equivalent to those of CO_2-free phonolitic-trachytic melts (Webster et al. 2014). Conversely, with up to 39 mol% CO_2 in dominantly aqueous fluids at 0.001–200 MPa, the Cl content of coexisting molten Mt. Etna basalt is as much as at least 30 rel.% greater than those of CO_2-free trachybasaltic melts (Alletti et al. 2009). Similarly, Botcharnikov et al. (2007) observed progressively increasing dissolution of Cl in andesitic melt at 200 MPa with increasing CO_2 in C-O-H-Cl fluids. For example, with 24 mol% CO_2 in the fluid the increase in the Cl content of the melt is ca. 15 rel.% compared with CO_2-free fluids.

Fluorine. The influence of F on the physical properties of silicate melts and magmatic phase equilibria has led to numerous investigations of its solubility and dissolution mechanisms in aluminosilicate melts (Fig. 6.11). Fluorine is highly soluble in silicate melts. Fluorine is much more soluble than H_2O at shallow crustal pressures. The pressure dependence of F dissolution in melts is much smaller than that determined for H_2O in melts. In addition to the 16.9 wt% F that dissolved in the low-SiO_2 and Ca- and Mg-enriched melt described previously (Veksler et al. 1998), experiments involving less geologically relevant and more unusual melt compositions have determined 18.6 wt% F in Al-free melts of the system NaF-SiO_2 generated at 1 atm (Mysen and Virgo 1985), 14.7 wt% F for a melt with ca. 59 wt% SiO_2 at 100 MPa (Veksler et al. 2012), and 13.4 wt% F in a Ca- and Mg-dominated melt containing 20.7 wt% SiO_2 and <1 wt% Al_2O_3 at 6 GPa (Brey et al. 2009). Figure 6.11b shows how the maximum determined F concentration in melts increase with the molar (Al+Na+Ca+Mg/Si) of the melt. Comparison of these maxima with the F concentrations of mafic to intermediate magmas (Fig. 6.1) shows that the former far exceeds the F contents of most natural BAA glasses.

Similar to Cl, the extent to which F dissolves in silicate melts varies strongly with the concentrations of network-modifying cations. This relationship has been demonstrated for Ca and Mg in experiments conducted over the past 50 plus years (Ershova 1957; Ershova and Olshanskii 1957; Foley et al. 1986a, b; Veksler et al. 1998; Brey et al. 2009), and it covers a wide range in pressure (e.g., 1 atm to 2.8 GPa). Network-modifying Na and K in melts also correlate positively with F dissolution

(Koster van Groos and Wyllie 1968; Kogarko and Krigman 1970; Mysen and Virgo 1985; Dingwell 1985; Foley et al. 1986b), so F solubility in silicate melts saturated in a fluoride-rich liquid increases with increasing melt peralkalinity (i.e., moles [Na+K+Ca]/[Al] > 1). Likewise for peraluminous melts (i.e., moles [Na+K+Ca]/[Al] < 1), F dissolution in melt increases with increasing excess network-modifying Al in 4-fold coordination (Mysen and Virgo 1985; Dingwell 1985).

Possible speciation mechanisms for F in silicate and aluminosilicate melts have been investigated through various spectroscopic techniques primarily involving quenched glasses, but some in situ work involving melts at temperature has also provided insights on F in melts. Mysen and Virgo (1985) employed Raman spectroscopy to identify F-bearing silicate complexes in SiO_2-NaF and SiO_2-AlF_3 glasses. They determined that fluoride replaces some oxide (e.g., $2F^-$ for O^{2-}) and that Si-F bonds form in melt. They further hypothesized that Na-F complexes are more stable than Al-F complexes. Additional details on the replacement of bridging oxygens by fluoride ion pairs in some melts are described by Dolejs and Zajacz (2018). These observations are consistent with ab initio calculations that were applied to the system Na_2O-Al_2O_3-SiO_2-NaF. The results imply that F occurs in tetrahedral Si-F and $NaSiF_6$-like species in glasses (Liu and Nekvasil 2002). Application of a variety of spectroscopic methods, including high-power ^{19}F-decoupled ^{27}Al, ^{29}Si, and ^{23}Na MAS NMR spectroscopy, shows that F coordinates preferentially with Al to form octahedral AlF_6^{3-} complexes in nepheline, jadeite, and albite glasses (Schaller et al. 1992). Mysen et al. (2004) applied ^{19}F and ^{29}Si, MAS NMR spectroscopy to silica-enriched peralkaline and metaluminous glasses and melts (1400 °C) in the system Na_2O-Al_2O_3-SiO_2-NaF and found evidence of Na-F complexes; Na-Al-F complexes with Al in 4-fold coordination with F; Na-Al-F complexes with Al in 6-fold coordination with F; and Al-F complexes with Al in 6- and possibly 4-fold coordination. In a similar study that involved addition of K_2O, ^{27}Al, ^{19}F, ^{29}Si, and ^{23}Na, MAS NMR spectroscopy of SiO_2-enriched Na_2O-K_2O-Al_2O_3-SiO_2-NaF-KF glasses determined the conversion of 4-fold coordinated Al to 5- and 6-fold, network-modifying Al with concomitant formation of Al-F bonds (Karpukhina et al. 2007). With the addition of CaO to the molten Na_2O-Al_2O_3-SiO_2-NaF-AlF_3, ^{19}F NMR spectra of the quenched glasses indicate that F forms complexes with one Al and several Ca or Na neighbors (Zeng and Stebbins 2000). Reactions involving F and Ca are consistent with a Raman spectroscopy study of CaO-CaF_2-SiO_2 glasses (Luth 1988). As discussed below, many of these reactions result in weakening of the melt structure (Zeng and Stebbins 2000) and viscosity reduction.

Experimental relationships indicating high solubilities of F in alkali- and alkaline earth-enriched melts are largely congruent with these spectroscopic data. Namely, the extremely high F concentrations in the Ca- and Mg-enriched but Al- and Si-deficient melts at 1 atm (Veksler et al. 1998), and those of Brey et al. (2009) at 6 GPa support chemical interactions involving F with Ca and Mg in silicate melts over a wide range in pressure. Moreover, species involving F with 4-fold Al in melts are minor to non-detectable. This behavior is similar to that described previously for the larger halogen Cl, which exhibits minimal to no detectable chemical interactions with network-forming Al (Stebbins and Du 2002; Sandland et al.

2004). However, we note that F reacts with 4-fold Al to generate 5- and 6-fold Al-bearing species for some melt compositions.

The effects of temperature and pressure on F dissolution in BAA melts are less well understood relative to their influences on felsic melts (see Dolejs and Zajacz 2018). Although experiments on F behavior in melts have been conducted for a wide range in pressure, these studies are not sufficiently similar to one another to permit extraction of relationships between pressure and F dissolution. With regard to the influence of temperature, Chevychelov et al. (2008a) observed significantly higher concentrations of F in phonolitic melt at 1000 °C compared to those in melt at 845–865 °C with equivalent F contents in the coexisting fluids at 200 MPa. Fluorine dissolution, as a function of varying fluid composition in non-felsic melts, is also poorly constrained. The addition of CO_2 to a F-bearing, trachybasaltic melt by Alletti (2007) showed increasing F in the melt for equivalent F concentrations (on a wt% basis) in the conjugate fluid at constant pressure and temperature. The results of prior work with granitic melts provide potentially relevant constraints. Research on F-enriched, fluid-saturated topaz rhyolitic and haplogranitic melts at 200 MPa (Webster 1990; Webster and Holloway 1990) shows that the dissolution of F in melt increases with increasing F contents in coexisting fluids, with increasing temperature (i.e., similar to the results described for phonolitic melt previously), and with increasing mol% CO_2 in the fluid (i.e., similar to the results described for the basaltic melt previously). The influence of oxidized and reduced S species in aqueous fluids on F dissolution in coexisting melts is undetermined. Whereas, F in aluminosilicate melts enhances Cl dissolution levels, there is no detectable influence of Cl on F dissolution in melts.

Bromine and Iodine: True saturation values for Br and I have not been determined experimentally for aluminosilicate melts saturated in molten bromide or iodide salts. Musselwhite and Drake (2000) reacted synthetic andesitic melts with I and determined 0.1–0.62 wt% I in the run-product glasses. Cochain et al. (2015) used felsic glasses with 2.2 wt% Br in their experimental study of Br speciation in silicate melts. Otherwise, the maximum concentrations of Br and I in felsic to intermediate-SiO_2 aluminosilicate melts coexisting with halogen-bearing aqueous fluids have been measured and are addressed in Sect. 6.3.3.

6.3.3 Halogen Partitioning: Melts and Fluids

Halogen concentrations of fluids in evolving, mineralizing, and/or eruptive magmas at shallow-crustal depths are controlled primarily by their partitioning between fluids and aluminosilicate melts, but partitioning processes that involve minerals also play a role. How F, Cl, Br, and I are distributed between fluids, melts, and minerals has been determined experimentally, and partitioning models based on the experiments have been developed. This research shows that halogen partitioning behavior is complex as it varies with pressure, temperature, melt composition, and fluid composition.

Chlorine. Experiments show that Cl is highly soluble in aqueous and aqueous-carbonic fluids, and hence, it partitions in favor of fluids relative to melts (i.e., the Nernstian $D_{Cl}^{fluid/melt} > 1$) for the vast majority of terrestrial magmas at shallow-crustal pressure and temperature conditions. It is noteworthy that Cl can be measured directly in experimental run-product fluids and also computed using mass-balance modeling.

Most wt%-based experimental values of $D_{Cl}^{fluid/melt}$ for basaltic systems (Fig. 6.12a) are <10 because of the strong influence of melt composition and the extent of melt polymerization on Cl dissolution in melts (Stelling et al. 2008; Alletti et al. 2009; Beermann 2010; Baker and Alletti 2012). Several experiments on basaltic melts at 200 MPa have even returned $D_{Cl}^{fluid/melt}$ values <1 (Webster et al. 1999; Mathez and Webster 2005; Stelling et al. 2008). The experiments of Alletti et al. (2009) with trachybasaltic melt and aqueous fluids observed $D_{Cl}^{fluid/melt}$ of 8–34 at f_{O2} near NNO and $D_{Cl}^{fluid/melt}$ of 10–15 at NNO+2 log units and higher f_{O2}. At 200 MPa, these partition coefficients (Webster et al. 1999; Stelling et al. 2008; Chevychelov et al. 2008b; Alletti et al. 2009; Beermann 2010; Beermann et al. 2015) are more than 1 order-of-magnitude lower than those involving felsic melts and aqueous fluids. For example, with haplogranitic melts at this pressure, values of $D_{Cl}^{fluid/melt}$ exceeding 160 have been determined (Webster 1992a). The reaction of aqueous fluids and intermediate-SiO_2 content andesitic and phonolitic melts entails $D_{Cl}^{fluid/melt}$ >1 for most experiments (Webster et al. 1999; Botcharnikov et al. 2007, 2015). Values of $D_{Cl}^{fluid/melt}$ for the latter melts exceed those involving basaltic melts (Baker and Alletti 2012) with similar Cl concentrations in the vapor, with or without a hydrosaline liquid. These differences in $D_{Cl}^{fluid/melt}$ are consistent with the lower Cl solubilities determined for hydrosaline liquid-saturated andesitic relative to basaltic melts.

Chlorine partitioning varies strongly with the Cl concentration of the system in experiments on basaltic, andesitic, phonolitic, and felsic melts (Webster 1992a, b; Webster et al. 1999; Stelling et al. 2008), but the partitioning behavior is complex. For relatively low Cl concentrations in the system, Cl partitioning shows Henrian behavior as the increase in the Cl content of the melt varies linearly with increasing Cl in the coexisting fluid. However, the Cl concentration of the melt increases in a non-linear fashion with increasing Cl in the fluid and the system as the Cl content of the melt approaches that of its maximum Cl solubility (i.e. equivalent to that of melt saturated in hydrosaline liquid). This non-Henrian, non-ideal volatile mixing behavior also means that values of $D_{Cl}^{fluid/melt}$ increase non-linearly with the maximum Cl concentrations in the system. A result of this relationship is that at any set of fixed pressure, temperature, and bulk-melt composition conditions, (e.g., for a pluton placed in the crust), the highest concentration of Cl in a given magmatic fluid will typically be when the fluid first exsolves because the Cl content is at its maximum just prior to fluid formation and because the largest value of $D_{Cl}^{fluid/melt}$ occurs when the fluid first exsolves.

The effect of fluid composition on Cl partitioning in chemically complex C-O-H-S-Cl fluids has been studied but requires further investigation. Experiments on phonolitic, basaltic, and rhyodacitic melts and aqueous fluids (Botcharnikov

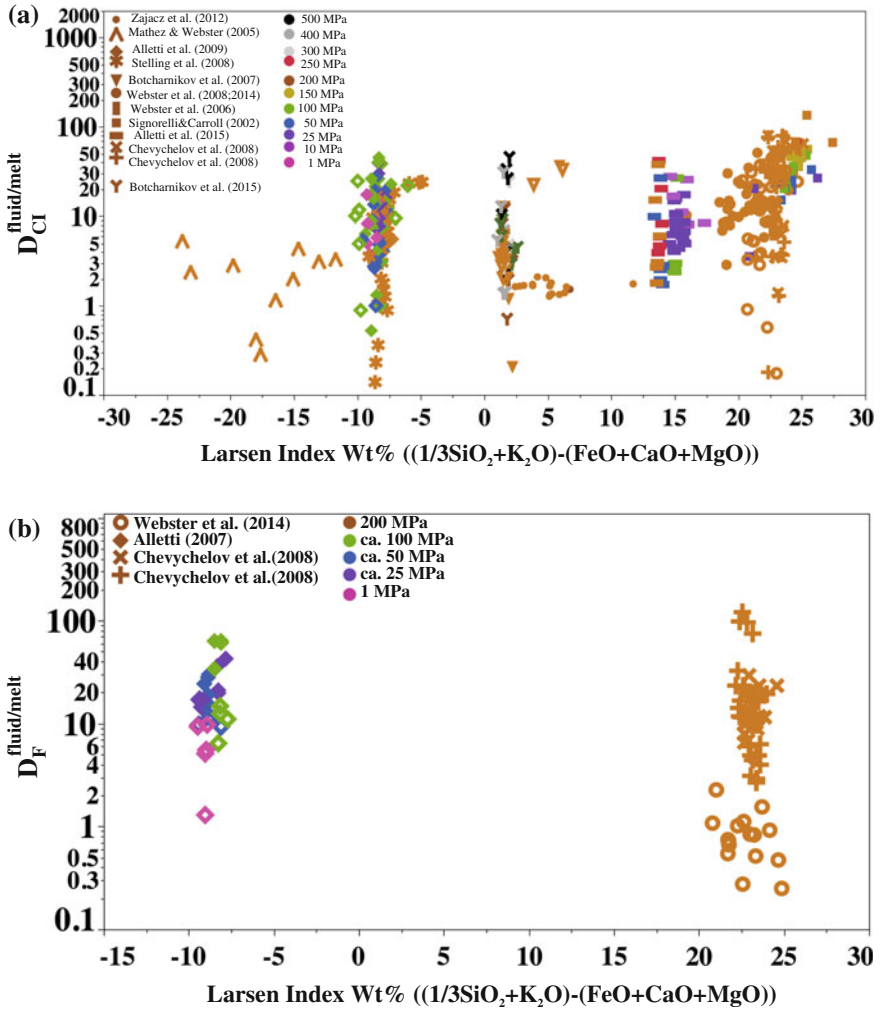

Fig. 6.12 Plots showing the fluid/melt partition coefficients (wt%-based) for (**a**) $D_{Cl}^{fluid/melt}$ and (**b**) $D_F^{fluid/melt}$ versus the Larsen Index of melt differentiation (e.g., [wt%($(K_2O + (SiO_2/3))$-(CaO + MgO + FeO)]. In **a**, the data are distinguished as a function of pressure, H_2O and CO_2 contents, and oxygen fugacity for basaltic, andesitic, and phonolitic melts. *Open symbols* are CO_2-bearing and *closed symbols* are CO_2-free. Chlorine partitioning varies strongly with the Cl content of the system. The Cl concentrations of these various experiments vary significantly, so this influence affects these values of D_{Cl}. In **b**, the data are distinguished as a function of pressure, H_2O and CO_2 contents, and oxygen fugacity for basaltic and phonolitic melts. **Open symbols** are CO_2-bearing and **closed symbols** are CO_2-free. The phonolitic data of Chevychelov et al. (2008b) show differing partitioning behavior with Pt versus Au tubing. If converted to mole fraction-based partition coefficients, the Webster et al. (2014) values of D_F are less than 1. Experimental partitioning data for Br and I with basaltic, andesitic, and tephritic-phonolitic melts are unavailable

et al. 2004; Webster et al. 2003; Beermann 2010) show values of $D_{Cl}^{fluid/melt}$ increasing with the addition of oxidized S to melts and fluids at log $f_{O2} \geq$ NNO (i.e., with $X_{SO4}^{2-} >> X_{S}^{2-}$ in melts). Research at lower f_{O2} (e.g., log f_{O2} of $\leq$NNO-0.5) shows no detectable influence of S on $D_{Cl}^{fluid/melt}$ (Zajacz et al. 2012). Interestingly, the influence of CO_2 (which dissolves largely in fluid relative to silicate melts) on $D_{Cl}^{fluid/melt}$ is variable. Botcharnikov et al. (2007) determined that CO_2 in the fluid had little influence on $D_{Cl}^{fluid/melt}$ with an andesitic melt at 200 MPa; whereas, Alletti et al. (2009) observed decreasing values of $D_{Cl}^{fluid/melt}$ with increasing CO_2 in fluids coexisting with trachybasaltic melt at 25–100 MPa. Recent experimental work on phonolitic and trachytic melts shows no clear effect of adding up to 28 mol% CO_2 in the fluids on molar values of $D_{Cl}^{fluid/melt}$ (Webster et al. 2014).

Thermodynamic models that address Cl partitioning in mixed C-O-H-S-Cl fluids and basaltic melts are currently limited. Witham et al. (2012) describe their thermodynamically based model, SolEx, which applies to amphibole-free basaltic melts containing <53 wt% SiO_2. The model can be used to predict volatile degassing at pressures of 0.5–400 MPa and is based on the assumption that Cl dissolution in basaltic melts involves ideal mixing behavior. This assumption is valid for many basaltic magmas because the Cl concentrations of most basaltic melts are $\leq$5% of their maximum solubilities at shallow-crustal pressures.

The influences of pressure and temperature on Cl partitioning between aqueous fluids and BAA melts have not been studied sufficiently in order to interpret degassing processes of ascending and cooling magmas comprehensively. Alletti et al. (2009) detected a subtle decrease in $D_{Cl}^{fluid/melt}$ with increasing pressure and quantified this relationship for trachybasaltic melts and aqueous fluids at 1200 °C and f_{O2} of NNO as:

$$D_{Cl}^{fluid/melt} = (12.73)P^{-0.0853} \tag{6.1}$$

where pressure (P) is in MPa. However, this study also determined that a negative pressure dependence is not observed with addition of CO_2 to the system. Stelling et al. (2008) investigated the influence of varying temperature (1050–1250 °C) on $D_{Cl}^{fluid/melt}$ for a trachybasaltic melt and aqueous fluids, but could not resolve a distinct relationship. Additional experimental data are available for phonolitic melts. With decreasing pressure, Cl partitions increasingly in favor of phonolitic melts relative to aqueous fluids (Signorelli and Carroll 2000), but interestingly, recent work of Alletti et al. (2014) involving Erebus volcano phonolitic compositions shows similar behavior above 50 MPa and opposite behavior at lower pressures. At and below 50 MPa, $D_{Cl}^{fluid/melt}$ decreases with decreasing pressure for the Erebus phonolitic melts (Alletti et al. 2014). Chevychelov et al. (2008a) observed no influence of temperature varying between 850 to 1000 °C on $D_{Cl}^{fluid/melt}$ for phonolitic melts. This is consistent with the observations of Stelling et al. (2008) on trachybasaltic melt.

The partitioning of Cl between fluids and BAA melts affects the solubilities of ions that associate with the chloride ion in fluids. At magmatic temperatures and shallow-crustal pressures, most components dissolved in aqueous fluids are associated chemically with one another due to the strong influence of temperature on the dielectric constant of H_2O (Pitzer 1983). Most of the dissolved chloride ion, for example, occurs in ion pairs with H^+ and other cations. For chloride-bearing fluids in equilibrium with andesitic melt, the dominant cations contributing to charge balance with Cl^- are Na^+, $Fe^{++/+++}$, K^+, as well as H^+ (Zajacz et al. 2012). Such fluid-melt reactions have been expressed as simple acid-base equilibria (Holland 1972; Ryabchikov and Hamilton 1971; Aranovich 2013; Manning and Aranovich 2014):

$$\begin{aligned} NaCl^{melt} + H_2O^{fluid} &= NaOH^{melt} + HCl^{fluid} \\ KCl^{melt} + H_2O^{fluid} &= KOH^{melt} + HCl^{fluid}, \end{aligned} \tag{6.2}$$

and also (Frank et al. 2003) as:

$$NaCl^{fluid} + HAlO_2^{melt} = NaAlO_2 + HCl^{fluid}. \tag{6.3}$$

Experiments with phonolite melt suggest the chloride ion associates primarily with Na^+, K^+, Ca^{++}, and H^+ in fluids (Webster et al. 2009a). With oxidized S present, the relevant equilibria may include:

$$2CaSO_4 + NaCl + KCl(+H_2O) = 2CaCl^+_{aq} + NaSO^-_{4aq} + KSO^-_{4aq}(+H_2O). \tag{6.4}$$

The major chloride species in aqueous (aq) fluids in equilibrium with basaltic melts are not as well constrained, but experiments involving S-bearing saline fluids involve enhanced concentrations of Na, K, and Ca in such fluids (Beermann 2010).

Fluorine. The distribution of F between BAA melts and fluids is not nearly as well established as that for Cl, but it has been determined that F concentrations in aqueous and aqueous-carbonic fluids at magmatic conditions are generally much lower than those of the other halogens. It should be noted that most experimental studies on F partitioning estimate the F contents of the fluids by mass balance. The F concentrations of the run fluids are not measured directly. In addition, the major fluoride species in melt-saturated aqueous fluids are not well constrained.

For trachybasaltic melts coexisting with aqueous fluids (Fig. 6.12b), values of $D_F^{fluid/melt}$ range from ca. 3 to 38 (Alletti 2007). The data suggest that $D_F^{fluid/melt}$ increases in favor of fluid with increasing pressure, and they show significant reductions in $D_F^{fluid/melt}$ with the addition of CO_2 to the system. Given that the solubilities of F in mafic-composition aluminosilicate melts, which are saturated in a fluoride-dominated liquid, range from ca. 15–21 wt%, as described previously, this strong tendency for F to partition in favor of an aqueous fluid phase is interesting. Furthermore, such elevated F contents of fluids coexisting with basaltic melts appear

surprising when it is considered that $D_F^{fluid/melt}$ with more-polymerized felsic melts are typically well below unity (Webster and Holloway 1990; Dolejs and Baker 2007a, b). As described previously, SiO_2-enriched melts dissolve less F than SiO_2-poor melts do. Fluorine partitioning between fluids and andesitic melts is undetermined.

Experiments on F partitioning with phonolitic systems show inconsistencies. All such experiments have been conducted at 200 MPa. One study with phonolitic melts and F- and Cl-bearing aqueous fluids returns values of $D_F^{fluid/melt}$ that exceed unity at temperatures of 1000 °C and 845–865 °C (Chevychelov et al. 2008a). This study also determined $D_F^{fluid/melt}$ values >100, but the study also noted problematic experimental issues involving the types of precious metal tubing that were used. In contrast, in another study with phonolitic-trachytic melts, values of less than unity were determined for $D_F^{fluid/melt}$ (Webster et al. 2014). The cause for the discrepancy between these two studies is unknown. The composition of the starting glass in the latter study is quite similar to that used by Chevychelov et al. (2008a) except that the glass of Webster et al. (2014) was modestly more enriched in (Na/Na+K) relative to that of Chevychelov et al. (2008a). In addition, the run durations of both studies were similar. Interestingly, however, is the observation that the runs of Chevychelov et al. (2008a), with high $D_F^{fluid/melt}$, began with all of the F added to the fluids of the starting charges; whereas, the experiments of Webster et al. (2014) showing low $D_F^{fluid/melt}$ began with all of the F in the starting melt.

Additional experimentation is clearly required because the absence or presence of elevated F in BAA magmas bears on the longevity of magmatic processes in F-enriched shallow-crustal magmas that have degassed most of their H_2O. Fluorine-rich melts that retain some F, after melt—fluid(s) interaction, may maintain an extensive crystallization interval by remaining stable to low temperatures (Koster van Groos and Wyllie 1968). This is a consequence of the fluxing influence of F on silicate melts (Sect. 6.3.4). Moreover, because F is typically the last volatile element to undergo strong degassing from most melts and because F concentrations in high-temperature volcanic gases are at least an order of magnitude less than those of Cl and other volatiles (Fischer and Chiodini 2015), magmatic F may provide important information on magma genesis for partially degassed systems (Wu and Koga 2013).

Bromine and I. Published fluid-melt partitioning data for Br and I are largely limited to felsic melts, and both halogens partition strongly in favor of the aqueous fluid. Experiments with Br have involved fluid-saturated albitic melts at 200 MPa (Bureau et al. 2000), synthetic Fe-free melts at 100–200 MPa (Bureau and Métrich 2003), and haplogranitic melts at 650–1700 MPa (Bureau et al. 2010). Although these compositions are not representative of low- to intermediate-SiO_2 content melts, the scarcity of experimental results for these halogens warrants a brief review of the relevant data as their partitioning relations may provide insights for BAA magmas. The presence of 2800–3900, 4300–5900, 9700–11300, and 5400–7900 ppm Br in the haplogranitic, rhyolitic, pantelleritic, and albitic melts of Bureau and Métrich (2003), respectively, shows Br dissolution in melts increasing, generally with decreasing SiO_2 but the variations in pressure, temperature, (Na/Na+K) in melt, and melt alkalinity of these experiments complicate interpretation of

the data. The relationship between melt composition and Br partitioning is consistent with observed effects of melt composition (i.e., SiO_2) on Cl dissolution in aluminosilicate melts generally. In this regard, Cochain et al. (2015) applied X-ray absorption spectroscopy to experimental glasses fused at 2.1–7.6 GPa to determine that Br forms NaBr complexes in hydrous felsic melts at high pressure. Equivalent data for I are restricted to aqueous fluid and albitic melt. Interestingly, a comparison of Nernst-style partition coefficients determined by Bureau et al. (2000) shows D_{Cl}, D_{Br}, and D_I increasing from 8 to 18 to 104 at 200 MPa and 900 °C, respectively. Thus, the distribution of Cl, Br, and I between fluids and molten albite increasingly favors the fluid as the ionic radii increase while their dissolution in melt relative to fluid decreases as their ionic radii increase. The experimentally determined partitioning behaviors of Br and I are consistent with the observation that maximum Br and I concentrations of these glasses and melt inclusions level off and eventually decrease (Fig. 6.2c) with increasing silica contents of the melts. This may reflect sequestration of Br and I by magmatic fluids during progressive melt evolution.

6.3.4 *Halogens and Melt-Mineral-Fluid Phase Equilibria in Basaltic, Andesitic and Equivalent Alkaline Melts*

The phase equilibria of halogen-bearing silicate melt, aqueous and aqueous-carbonic vapor, and hydrosaline liquid were reviewed in Sect. 6.3.1. Fluorine and Cl also exert strong controls on experimental mineral-melt and mineral-fluid equilibria, but the concentration ranges of F and Cl involved in some experimental investigations (i.e., up to wt% levels) exceed those of typical non-alkaline basaltic and andesitic magmas and this issue bears on the geologic relevance of some experimental work. Most F concentrations vary between 5 to 600 ppm, in OIBs and MORBs, and 100 to 5000 ppm in arc basalts. Chlorine concentrations in OIBs and MORBs generally vary from 5 to 1000 ppm, and from to 1000–5000 ppm with arc basalts (Fig. 6.2). For comparison, recall from Sect. 6.2.2 that the F and Cl concentrations in the upper mantle vary from 18 to 25, and 0.5 to 7 ppm, respectively (Pyle and Mather 2009). At their highest concentrations, F and Cl might be expected to affect the phase equilibria of mafic rocks, however in comparison to the multitude of studies investigating the effects of CO_2 and H_2O on the phase relations and partial melt compositions of mafic rocks, only a few studies have investigated this influence of F or Cl.

Studies on the effect of halogens on the melting and crystallization of mafic rocks at crustal pressures are rare even though the effects of F on the phase equilibria and partial melt compositions of ultrapotassic igneous compositions at mantle pressures (1 GPa and above—see Frezzotti and Ferrando (2018) and Klemme and Stalder (2018)) were actively pursued by A. Edgar and colleagues (e.g., Edgar et al. 1994, 1996) and by S. Foley and collaborators (e.g., Foley et al. 1986a, b) in the 1980s and 1990s. Fluorine can reach approximately 1 wt% in mafic ultrapotassic

rocks (Foley et al. 1986b; Edgar et al. 1996), and F concentrations often positively correlate with K_2O, which reflects processes of magma evolution (Aoki et al. 1981). Bromine and I concentrations in mafic rocks are much less, at the ppm level or even lower, in basic rocks (Aiuppa et al. 2009) and, hence, are not expected to affect the formation and crystallization of mafic magmas. This does not preclude, however, that Br dissolved in saline aqueous fluids from felsic magmas may conceivably contribute to unmixing of Cl-bearing vapor and hydrosaline liquid.

The effect of F on phase relationships. Early experimental work by Koster van Groos and Wyllie (1968), Anfiligov et al. (1973), and Manning (1981) showed reduced solidus and/or liquidus temperatures with the addition of F to felsic melts. The results are summarized by Dolejs and Zajacz (2018). In subsequent research involving basaltic melts, increasing F was demonstrated to reduce olivine stability relative to that of pyroxene (Foley et al. 1986b; Filiberto and Treiman 2009a). Filiberto et al. (2012) investigated the phase relations and partial melts of a mafic composition representative of Martian basaltic magma. Filiberto et al. (2012) demonstrated that addition of ~2 wt% F depresses the olivine-pigeonite saturated liquidus by 95 °C and 200 MPa (from 1375 °C, 1.2 GPa, to 1280 °C, 1.0 GPa) as can be seen in Fig. 6.13. They further demonstrated that the addition of F to the system significantly increases the pigeonite/liquid and olivine/liquid Fe-Mg partition coefficient ($K_D^{Fe/Mg}$) and attributed this difference to F-Mg complexing in the melt, consistent with previous NMR studies. This supposition is consistent with observations of Veksler et al. (1998) and Brey et al. (2009) on F behavior in alkaline earth element-bearing melts discussed previously. Regarding the latter study, supplementing the F contents of experiments on molten carbonate-bearing garnet-wehrlite with up to 16 wt% F in the melt, depresses the solidus temperature by 300 °C at 10 GPa and 150 °C at 6 GPa and supports crystallization of F-clinohumite at solidus temperatures.

Related research on hydroxyl-bearing and other minerals has shown increased thermal stability with increasing F in amphibole (Johnson and Fegley 2003). Augmenting the kalsilite-forsterite-quartz system with up to 4 wt% F, stabilizes

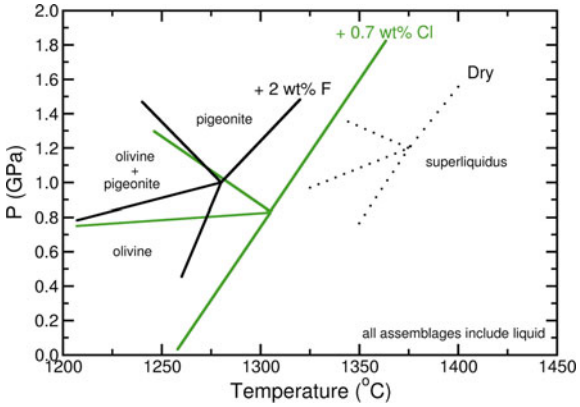

Fig. 6.13 Phase equilibrium diagram showing the effects of adding F or Cl to basaltic melts of Filiberto and Treiman (2009b), Filiberto et al. (2012, 2014). Phase relations for halogen-free equivalent melts also shown for comparison

phlogopite in equilibrium with the melts at 2.8 GPa (Foley et al. 1986b). Experiments with phonolitic melt at 100 MPa show that increasing F (up to 2.7 wt %) stabilizes fluorite and the rare Zr-silicate mineral hiortdahlite ($(Ca,Na)_{13}Zr_3Si_9(O,OH,F)_{33}$) at the expense of the Ca content of the melt and clinopyroxene, and also modifies the liquid line of descent of evolving phonolitic magmas (Giehl et al. 2014).

The effect of F on the depression of liquidus surfaces in simplified carbonatitic compositions at crustal pressures was first discovered by Kuellner et al. (1966), but it was Jago and Gittins (1991) who conclusively demonstrated the importance of this effect and its potential role in the evolution of carbonatites. Jago and Gittins (1991) found that the addition of F to the system Na_2CO_3-K_2CO_3-$CaCO_3$ allows low-alkali, Ca-rich carbonatitic magmas (similar to those found in most intrusive carbonatite complexes) to evolve to alkali-rich, Ca-poor carbonatitic magmas similar to those found at the Oldoinyo Lengai volcano, Tanzania. Chapter 12 of this volume provides more details on the role of halogens in the formation of carbonatitic magmas.

Because of the ability of F to easily substitute for OH in hydrous minerals, a number of studies have investigated the impact of this replacement on the stability of amphibole. Bowen and Schairer (1935) were apparently the first to report the synthesis of fluor-amphibole at 1 atm pressure. Comeforo and Kohn (1954) published results on the synthesis of large fluor-tremolite crystals (5 mm in length) at one atmosphere and final experimental temperatures near 1100 °C using crucibles containing up to 9 kg of starting materials. These authors also report research by van Valkenburg and Pike (1952) that found the upper stability limit of fluor-tremolite to be near 1145 °C at 1 atm (Comeforo and Kohn 1954). A similar temperature limit for fluor-tremolite at one atmosphere was found by Troll and Gilbert (1974), who also predicted a maximum temperature stability for this mineral of 1175 °C at 175 MPa. Holloway and Ford (1975) investigated the effect of partially replacing OH with F in pargasite on the melting of this mineral. They found that under fluid-absent conditions, a fluorhydroxyl pargasite with 43 mol% F and 57 mol% OH was stable in the mantle to above 3.0 GPa, or 1–1.5 GPa above the stability of the end-member hydrous pargasite. The thermal stability of this fluorhydroxyl paragasite is 1060 °C at 500 MPa and increases to a maximum of 1290 °C at 3 GPa before falling to 1285 °C at 3.5 GPa. The maximum thermal stability of fluorhydroxyl pargasite at 500 MPa is enhanced significantly, 30 °C or more, compared to the stability of a hydroxy pargasite at low water activity (Holloway and Ford 1975).

Mahood and Baker (1986) tentatively identified kaersutite in experiments performed at 1026 °C, 1 atmosphere, to study the crystallization of an alkali-olivine basalt and suggested that it was a fluor-amphibole (or an oxy-amphibole). This phase crystallizes at near-solidus conditions, was found in trace abundances, and did not play a significant role in affecting the compositions of residual melts. However, Mahood and Baker's (1986) results suggest the possibility that high-F basic magmas could crystallize a F-rich amphibole below the minimum pressures generally understood to limit amphibole stability. The crystallization of significant

quantities of such a F-rich amphibole would be expected to have a profound effect on the liquid line of descent of F-bearing magmas that have solidi below approximately 1050 °C.

The effect of Cl on phase relationships. Filiberto and Treiman (2009a, b) and Filiberto et al. (2014) have been pioneers in the investigation of the effects of Cl on the phase equilibria of mafic melts at crustal and shallow mantle pressures. These studies concentrated on studying the same Fe-Mg-rich analogue Martian basalt as Filiberto et al. (2012) except with the addition of Cl rather than F. Filiberto and Treiman (2009a, b) demonstrated that the addition of 0.7 wt% Cl shifts the olivine + pigeonite multiply saturated liquidus point from 1375 °C and 1.2 GPa to 1305 °C and 0.85 GPa (Fig. 6.13). They also found that the addition of Cl to the system reduces the olivine/liquid and pigeonite/liquid exchange $K_D^{Fe/Mg}$, in contrast to what is observed in F-bearing systems (Filiberto et al. 2012). This effect was attributed to Cl-Fe complexation in the melt.

Filiberto et al. (2014) demonstrated that the effect of Cl on the liquidus depression of a basaltic melt was significantly affected by bulk composition. Whereas Filiberto and Treiman (2009a, b) demonstrated that Cl and H_2O had similar effects on the reduction of the liquidus temperature of the composition they used, Filiberto et al. (2014) study of a composition richer in MgO and SiO_2, but poorer in Al_2O_3 and FeO, found that the effect of Cl on liquidus reduction was measurably less than that of H_2O. These authors also demonstrated that the olivine + orthopyroxene multiple-saturation point on the liquidus shifted from 1.4 GPa, 1450 °C for the Cl-free system to 0.7 GPa, 1350 °C with 1.63 wt% Cl.

Although studies on the role of halogens in the evolution of mafic magmas are rare, Filiberto and colleagues have demonstrated that F and Cl may have significant effects on the temperatures of crystallization, the points of multiple saturation of liquidi, and the partitioning of Fe and Mg between melts and crystals. Such effects on Earth are most likely to occur in island arc magmas, where the concentrations of F and Cl are typically the highest and on Mars, where Cl concentrations in magmas are expected to be significantly higher than on Earth (Filiberto and Treiman 2009a, b, Filiberto et al. 2014; Howarth et al. 2015).

Investigations of alkaline systems also show strong influences of Cl on phase relations. Giehl et al. (2014) experiments show that addition of up to 0.5 wt% Cl to phonolitic melt enhances the stability of sodalite, hiortdahlite, and the rare Zr-silicate mineral eudialyte ($Na_4(Ca, Ce, Fe, Mn)_2ZrSi_6O_{17}(OH, Cl)_2$). It follows that Cl addition also modifies the liquid line of descent of related magmas.

6.3.5 Halogen Partitioning: Melts and Minerals

Because the hydroxl anion in hydrous minerals (e.g., amphiboles, apatite, and micas) has a similar size and charge to F^-, and a similar charge to Cl^-, significant substitution of these halogens for hydroxls in hydrous minerals has been observed. And, despite the rarity of hydrous minerals in basic-to-intermediate magmatic

systems, they can occasionally be present and constitute significant repositories of halogens in these magmas and rocks.

The partitioning of halogens between crystals that incorporate large amounts of halogens in their hydroxyl sites, such as apatite, biotite and muscovite micas, and amphiboles has been studied for many decades (e.g., Munoz and Ludington 1974, 1977; Munoz 1984, 1992; Zhu and Sverjensky 1991, 1992). These studies demonstrated the ability to use the concentrations of halogens and water in the crystals to constrain the relative activities of HCl and HF in the system through thermodynamic calibrations of reactions such as:

$$\underset{}{2HCl} + \underset{\text{phlogopite}}{KMg_3AlSi_2O_{10}(OH)_2} = \underset{\text{chlor-phlogopite}}{KMg_3AlSi_2O_{10}(Cl)_2} + \underset{}{2H_2O} \tag{6.5}$$

and

$$\underset{\text{chlor-phlogopite}}{KMg_3AlSi_3O_{10}(Cl)_2} + \underset{\text{fluor-annite}}{KFe_3AlSi_3O_{10}(F)_2} = \underset{\text{fluor-phlogopite}}{KMg_3AlSi_3O_{10}(F)_2} + \underset{\text{chlor-annite}}{KFe_3AlSi_3O_{10}(Cl)_2} \tag{6.6}$$

Hydroxyl ions, Cl^-, and F^- in the hydroxyl site and Mg-Fe-Al in the mica octahedral site were considered to mix ideally by Munoz (1984) and Zhu and Sverjensky (1991, 1992). These same studies also demonstrated the need to use reciprocal site mixing energetics (Wood and Nicholls 1978) in the activity-composition calculations of the micas due to Mg-Cl and Fe-F avoidance. These reciprocal site mixing energies, $\sim$18–42 kJ mol^{-1} (Zhu and Sverjensky 1992), have significant effects on the calculated partitioning of halogens between micas and fluids and cannot be ignored.

Icenhower and London (1997) illustrated the effect of Mg-Cl and Fe-F avoidance in their study on halogen (F, Cl) partitioning between biotite and silicic melts. They demonstrated that with increasing Mg/Fe in the mica, the partition coefficient of F increases and that of Cl decreases, consistent with the thermodynamic treatment of Munoz (1984, 1992) and Zhu and Sverjensky (1991, 1992). Sato et al. (2005) investigated Cl/OH partitioning between a dacitic melt and amphibole at 185–300 MPa, and 800 and 850 °C, which also demonstrated a dependence of the partitioning upon the Mg concentration of the amphibole. Although neither of these studies investigated BAA systems, they demonstrate that the non-ideal mixing of Mg-Cl-Fe-F, seen in the early low-temperature studies, exists up to magmatic temperatures and indicates that the complexity of the interactions between halogens, silicate melts, and aqueous fluids needs to be quantified. As shown below, we are well on the way to such quantification, but much more work needs to be done.

Experiments on the partitioning of F between fluid and mica coexisting with a phonolite melt at 200 MPa and 845–865 °C produce a global average of $D_F^{fluid/mica} = 11.3 \pm 6.6$ (Chevychelov et al. 2008c). The range of Mg and Fe concentrations in these experiments was not great enough to discern an effect of these

elements on the partitioning. The measurements clearly show a positive dependence of the partition coefficient on the F concentration of the fluid such that $D_F^{fluid/mica}$ is between 5 and 7 when the concentration of F in the fluid is 2 to 3 wt%, but increases to 29 when the fluid contains 18 wt% F (Fig. 6.14). Clearly, the partitioning is non-Henrian. Chevychelov et al.'s (2008c) measurements of Cl partitioning between fluid and mica from the same experiments demonstrate a linear relationship between the partition coefficient and Cl concentration in the fluid:

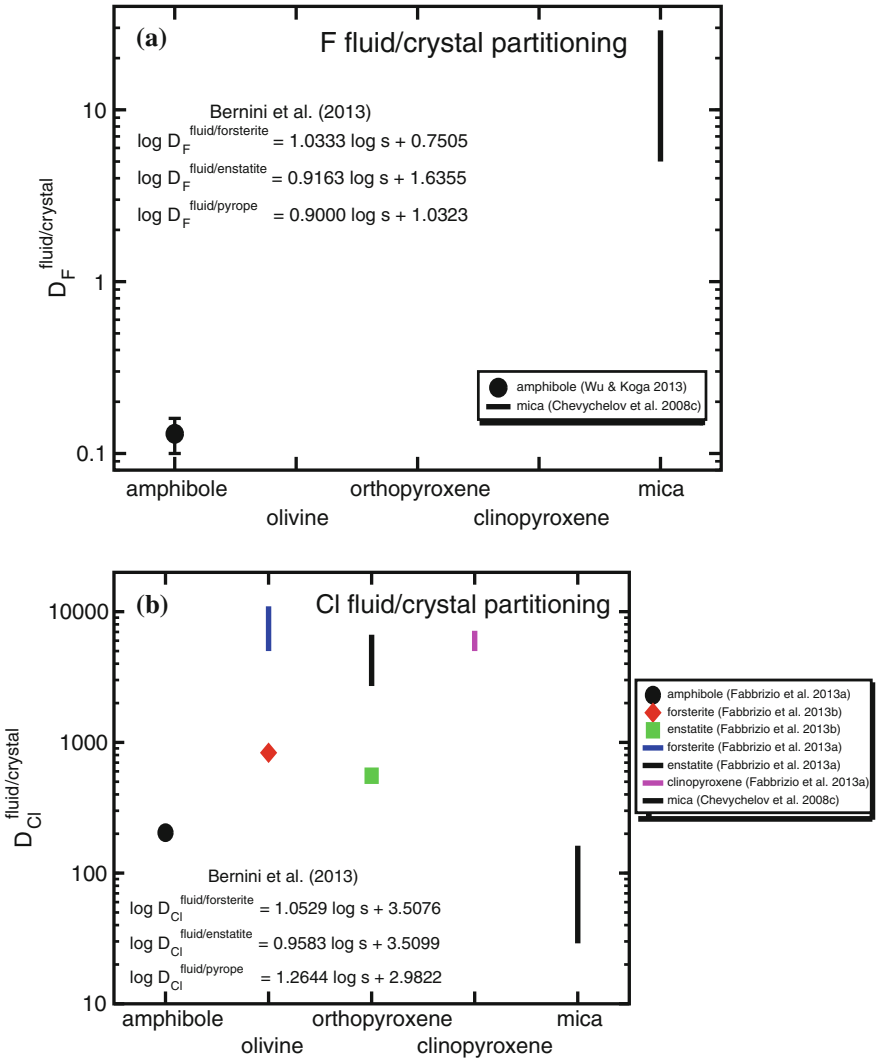

Fig. 6.14 Plots of partition coefficients, $D^{fluid/crystal,}$ between aqueous fluids and silicate minerals. **a** Fluorine partition coefficients. **b** Chlorine partition coefficients. The *vertical bars* in both figures show the range of partition coefficients found in the cited study, and the equations describing the partitioning mentioned by Bernini et al. (2013) are also shown. See the text for further discussion

$$D_{Cl}^{\frac{fluid}{mica}} = 7.11(wt\%Cl^{fluid}). \quad (6.7)$$

This linear relationship has a correlation coefficient of 0.908 and appears valid for Cl concentrations in the fluid up to ~20 wt%. At higher Cl concentrations, i.e. 39 wt% Cl in the fluid, the fluid/mica partition coefficient for Cl was 162.

Recently, Wu and Koga (2013) measured the partitioning of F between hydrous fluids and hornblende and humite group minerals at 1 GPa, 770–947 °C. They found $D_F^{fluid/amphibole}$ equal to 0.13 ± 0.03 (Fig. 6.14a). Fabbrizio et al. (2013a) measured $D_{Cl}^{fluid/amphibole}$ at 2.0 GPa, 900 °C to be 204, but neither of these studies investigated the effect of amphibole composition on the partition coefficient (Fig. 6.14b).

Unfortunately, only three partitioning studies of halogens between basaltic melts and hydrous minerals have been made (see Fig. 6.15). Hauri et al. (2006) report F and Cl partitioning between basaltic melts and amphibole and mica in 2 experiments. At 1.5 GPa and 1050 °C, Hauri et al. (2006) found the $D_F^{amphibole/melt}$ = 0.85 and $D_{Cl}^{amphibole/melt}$ = 0.046, whereas $D_F^{mica/melt}$ = 1.64 and $D_{Cl}^{mica/melt}$ = 0.056. At 0.5 GPa, 1000 °C, the partition coefficients were similar: $D_F^{amphibole/melt}$ = 1.19, $D_{Cl}^{amphibole/melt}$ = 0.038, $D_F^{mica/melt}$ = 2.54, and $D_{Cl}^{mica/melt}$ = 0.054.

Chevychelov et al. (2008c) also measured the partitioning of F and Cl between mica and a fluid-saturated phonolitic melt at 200 MPa and 845–865 °C. Although there is some evidence of a small effect of the F concentration on the partitioning of F between mica and melt, the average of their measurements yields $D_F^{mica/melt}$ = 1.6 ± 0.6, in agreement with the two measurements of Hauri et al. (2006), as shown in Fig. 6.15a. $D_{Cl}^{mica/melt}$ varies from 0.17 to 0.35. Although there is evidence for a correlation between the Cl concentration in the fluid and the partition coefficient (Chevychelov et al. 2008c), the average of their experiments produces $D_{Cl}^{mica/melt}$ = 0.25 ± 0.07 (Fig. 6.15b). These values are about four times those of Hauri et al. (2006), and are attributed to differences in the compositions of the melts and micas and the experimental conditions.

Dalou et al. (2014) measured F and Cl partitioning between amphibole and melt at 1.2 GPa, 1180 and 1200 °C. At 1180 °C, Dalou et al. (2014) found $D_F^{amphibole/melt}$ = 0.360 and $D_{Cl}^{amphibole/melt}$ = 0.119; at 1200 °C $D_F^{amphibole/melt}$ = 0.635 and $D_{Cl}^{amphibole/melt}$ = 0.378. The origin of differences in the partition coefficients measured in Hauri et al. (2006) and Dalou et al. (2014) remain unknown, but may be due to different experimental conditions. Nevertheless, these partition coefficients all indicate that amphibole and mica may significantly fractionate F from Cl during magmatic processes.

An example application of the use of halogen concentrations in hydrous minerals to constrain the activities of magmatic halogens is the study of Coulson et al. (2001) who applied the thermodynamic treatment of Zhu and Sverjensky (1991, 1992) to investigate the evolution of halogens in the Emerald Lake pluton (Yukon, Canada) through the study of biotite and apatite. This pluton is concentrically zoned from an augite syenite at its margins to a core of biotite granite and contains late-stage

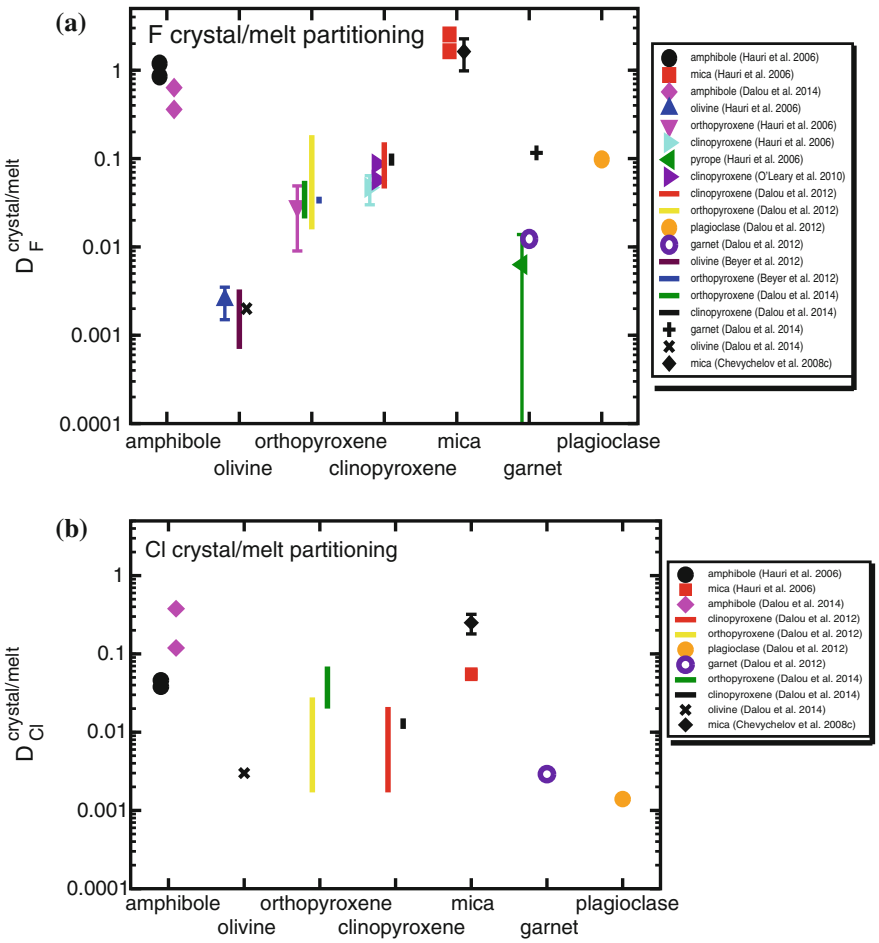

Fig. 6.15 Plots of partition coefficients, $D^{mineral/melt,}$ between minerals and silicate melts. **a** Fluorine partition coefficients. **b** Chlorine partition coefficients. The *vertical bars* in both figures show the range of partition coefficients found in the cited study. The observed variations have been linked by several authors to changes in the composition of the mineral or the silicate melt. See the text for further discussion

pegmatitic segregations. After carefully selecting non-altered crystals, Coulson et al. (2001) found only a decrease in the log (a_{HCl}/a_F) ratio of the fluid through the zoned pluton from ~ 0.6 to -0.1. Coulson et al. (2001) interpreted these results to indicate that the fluid was magmatic and relatively homogeneous throughout the pluton during crystallization. Coulson et al. (2001) also investigated the halogens in amphiboles and found that they displayed patterns similar to those seen in the other minerals.

Zhang et al. (2012) combined studies of crystal-fluid partitioning of halogens (e.g., Munoz 1984, 1992; Zhu and Sverjensky 1991, 1992) with crystal-melt

partitioning of halogens to estimate the halogen concentrations in the melt during the crystallization of the Liujiawa pluton, China. The studied rocks from this pluton varied from a gabbronorite, through a two-pyroxene diorite to a clinopyroxene diorite and hornblende gabbro. These authors found that the Cl and F concentrations in the melt remained relatively constant until near the solidus where the Cl concentration decreased strongly. The decrease in Cl, while the F remained constant, was interpreted to reflect fluid exsolution from the melt and preferential sequestration of Cl by the fluid.

Recently Giesting and Filiberto (2014) outlined a model for the determination of Cl/OH partitioning between amphibole and melt. These authors repeatedly warn the reader of the potential pitfalls in using amphiboles to determine the concentrations of volatiles in the melt because of the combination of amphibole's "flexible" composition and because most analyses of amphibole do not include all of the possible components, e.g., ferric versus ferrous Fe or the oxy-amphibole component. Despite these challenges, the authors present a framework for the construction of future models that provide the promise of using amphiboles to determine the precise concentrations of halogens in their magmatic melts. However, the work of Giesting and Filiberto (2014) makes it clear that one key to using any hydrous mineral to investigate the composition of the coexisting melt or fluid is the accurate analysis of all of the components comprising the mineral.

Halogens in apatite. Experimental studies have been conducted to investigate how volatile components are exchanged between apatite and basaltic melts with or without fluids (Konzett and Frost 2009), but many aspects of halogen exchange are not yet sufficiently well understood. These experiments have determined the distribution of: (1) F and Cl between apatite, basaltic melts, and vapor with or without hydrosaline liquid at 200 MPa (Mathez and Webster 2005); (2) F and OH between apatite and haplobasaltic-andesite melt at 1 GPa (Huh 2013); (3) F, Cl, and OH between apatite and a synthetic shergottite melt at 1 GPa (Vander Kaaden et al. 2012); (4) F, Cl, and OH between apatite and basaltic melts at 1 GPa (McCubbin et al. 2014); (5) F, Cl, and OH between apatite and Fe-enriched basaltic melt at 1.5 GPa (McCubbin et al. 2014); and (6) F, Cl, and OH between apatite and Fe-enriched basaltic melt at 1.0–1.2 GPa (McCubbin et al. 2015). Related experimental research on apatite not involving BAA melts has explored how: (1) F and Cl partition between apatite, rhyolitic melts, and vapor with or without hydrosaline liquid at 200 MPa (Webster et al. 2009b) and 50 MPa (Doherty et al. 2014; Webster et al. 2017); (2) F, Cl, and OH partition between apatite and saline aqueous fluids at 20 and 100 MPa (Latil and Maury 1977); (3) F, Cl, and OH partition between apatite and saline aqueous and aqueous-carbonic fluids at 1 and 2 GPa (Brenan 1993); (4) F and OH partition between apatite, phlogopite, and fluid at 2 GPa (Vukadinovic and Edgar 1993); and (5) Cl and OH partition between apatite, amphibole, and phlogopite coexisting with sub-solidus basalt at 3–15 GPa (Konzett et al. 2012). Another experimental study explored the partitioning of Br, Cl, F, and OH between apatite and anhydrous mixtures of CaF_2-, $CaCl_2$-, and NaBr-bearing salt melts at 1 bar (Dong 2005). Some of these studies have also addressed the

distribution of CO_2 and/or S between magmatic apatite and coexisting volatile-bearing phases. Partitioning data for I were not located.

The partitioning of F and Cl between melt and apatite ± fluids varies with the Cl concentration of the system, melt composition, pressure, and temperature. The partitioning of Cl between fluid and melt varies from Henrian to non-Henrian behavior in high-Cl magmatic systems (Beermann et al. 2015), and similarly the distribution of Cl between apatite and melt transitions from Henrian to non-Henrian behavior (Fig. 6.16) as the Cl content of the system increases relative to the solubility of Cl in melt (Mathez and Webster 2005). This is consistent with the observation that the solubilities of halogens in melts influence mineral/melt partitioning of the halogens (Dalou and Mysen 2015). The partitioning of F between Cl-bearing to Cl-enriched basaltic melts and apatite shows Henrian behavior in most of the 200 MPa experiments of Mathez and Webster (2005), but Huh (2013) observe non-linear, non-Henrian behavior of F partitioning in Cl-free experiments at 1 GPa (Fig. 6.17). In addition to Cl, there are other differences in apatite composition between these two studies. Apatites that precipitated in the experiments of Mathez and Webster (2005) involved apparent (calculated) mole fractions of OH ranging from 0.03–0.39 whereas those of Huh (2013) range from 0.41–1.0. Although not determined, we suggest that the differing mixing behavior for F in apatite, shown in both studies, reflects the different Cl and OH contents of the apatites, the different pressures involved, and differences in fluid phase relations at the differing pressures.

Given the strong influence of melt composition on F and Cl dissolution in melts and on the partitioning of these halogens between fluid and melt, it is not surprising that the distribution of F and Cl between apatite and melt also varies with melt composition (Figs. 6.16 and 6.17). The influence of pressure on the uptake of halogens by apatite is poorly determined. Brenan's (1993) work shows strong changes in the exchange of F, Cl, and OH between apatite and NaCl-bearing and HCl-bearing aqueous fluids as pressure varies between 1 and 2 GPa, but these experiments did not include silicate melt. Subsequent research demonstrated that Cl partitions increasingly in favor of apatite relative to felsic melts as pressure decreases from 200 to 28 MPa with fixed Cl contents of coexisting vapor or vapor plus brine (Webster and Piccoli 2015), but this relationship has not been explored for BAA melts. Fluorine partitioning between apatite and felsic melts shows no clear dependence on pressure (Doherty et al. 2014), but this is unconstrained for BAA melts. The influence of temperature on halogen partitioning has not been investigated systematically, but it is known that the lattice of apatite expands with increasing temperature, which indirectly influences the incorporation of F versus Cl versus OH within the mineral structure (Tacker and Stormer 1989). It is likely, therefore, that changes in temperature will affect halogen exchange and partitioning behaviors.

Previous studies have established Nernstian partition coefficients for F and Cl between apatite and melt. Fewer data are available for F partitioning between fluids and apatite because of the difficulties in measuring F in fluids at experimental conditions and also in computing the F contents of apatite-saturated fluids via mass

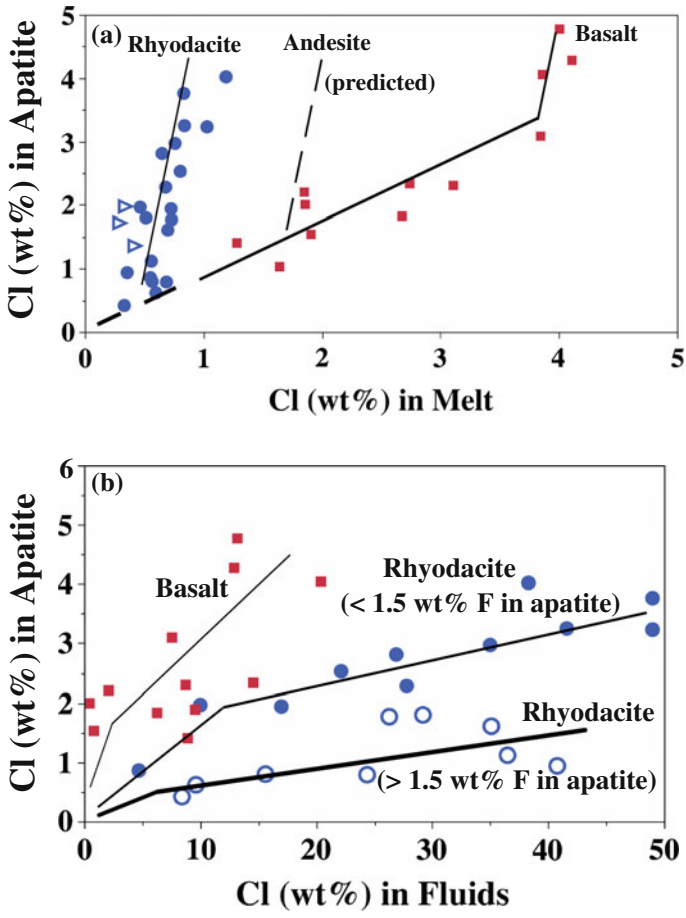

Fig. 6.16 Plots of experimentally determined 200-MPa partitioning data for Cl between apatite and melt (**a**) and apatite and fluids (**b**). In **a**, *red squares*, fit with *bold lines* represent partitioning with fluid-saturated basaltic melts at 1060–1150 °C (Mathez and Webster 2005). *Blue circles* represent fluid-saturated rhyodacitic melts and *blue triangles* are fluid-absent runs with rhyodacitic melts at ca. 900–924 °C (Webster et al. 2009b). *Dashed curve* is predicted Cl partitioning behavior between apatite and a fluid-saturated, calc-alkaline andesitic melt with 60 wt% SiO_2 and 3 wt% total alkalies at 200 MPa, based on computed Cl solubility for a hydrosaline, liquid-saturated melt of this composition (Webster et al. 2015). In **b**, Cl partitioning varies with F contents of apatites. *Faint lines* and *red symbols* for basaltic melts (*square* = 1–2.5 wt% F in apatite, *horizontal box* = apatite with 2.7 wt% F, and *vertical box* = apatite with <1 wt% F). *Blue symbols* are for rhyodacitic melts. The *filled circles*, fit with a medium line, represent runs with apatites containing <1.5 wt% F. The *open circles*, fit with bold lines, represent runs with apatites containing >1.5 wt% F

balance. When F-bearing minerals (i.e., apatite) are present in experiments, accurate mass-balance computations require precise knowledge of the volumetric abundances of apatite in each run product (as well as accurate F contents in the apatite),

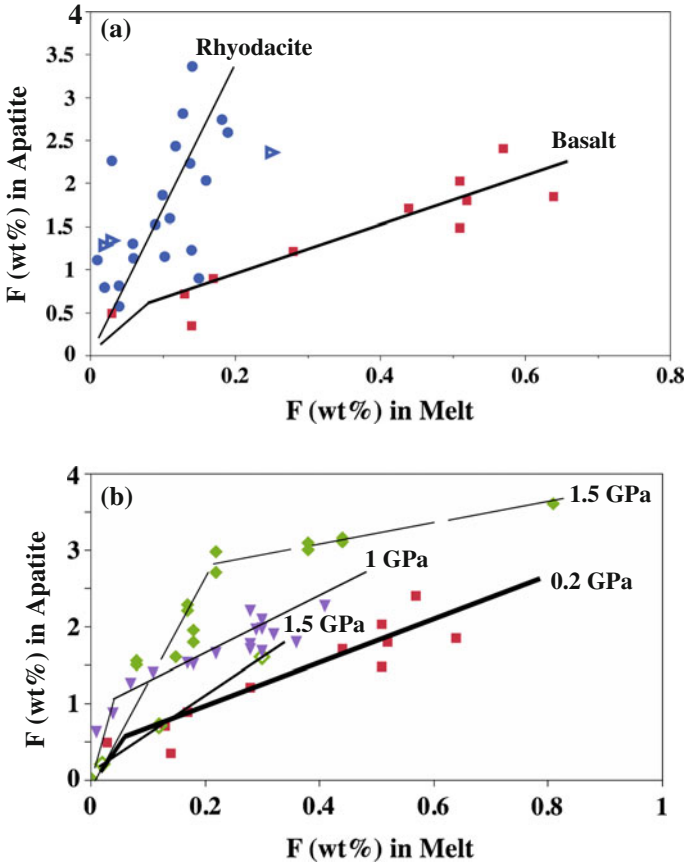

Fig. 6.17 Plots of experimentally determined partitioning data for F between apatite and melt as a function of melt composition at 200 MPa (**a**) and pressure with basaltic melts at 0.2–1.5 GPa (**b**). Fluorine generally partitions more strongly in favor of apatite than melt. In **a**, F partitions more strongly into the basaltic melt than the rhyodacitic melt for equivalent F in coexisting apatites. In **b**, basaltic melt compositions vary between experiments. *Green symbols* fit with faint lines represent the 1.5-GPa data of McCubbin et al. (2014, 2015). *Open diamonds* represent runs in Mo capsules with log f_{O2} near that of the Fe-wüstite buffer, and *closed diamonds* represent runs in graphite capsules with log f_{O2} ca. 2 log units greater than that of the Fe-wüstite buffer. The *purple symbols*, fit with medium-density lines, are 1 GPa partitioning data (Huh 2013). The *red symbols*, fit with bold lines, are 200 MPa data from Mathez and Webster (2005) for runs with ≤ 14 wt% CaO in the melt

otherwise the errors become excessive. Experimental partition coefficients have been used to interpret compositions of natural igneous apatites that preserve and record the halogen concentrations of melts and fluids of apatite-bearing magmas. For example, one can apply simple Nernst-style partition coefficients as long as the experimental pressures and temperatures, and the general ranges in F, Cl, and OH for experimentally generated apatites, are sufficiently consistent with those of the

natural system of interest. Alternatively, however, it is well established that the incorporation of F versus Cl versus OH in apatite is controlled by crystal chemical constraints (Tacker and Stormer 1989) and that these relationships lead to non-Henrian solution behavior for F, Cl, and OH in apatite because these components are typically not present at the trace-element level typically expected for Henrian behavior. Moreover, given that 3 components are involved in the anion exchanges between apatite and other phases, Boyce et al. (2010) conclude that use of equilibrium constants, K, (e.g., $K^{F-H} = (F_{melt}/F_{apatite})/(H_{melt}/H_{apatite})$) for exchange reactions involving F and hydrogen), such as:

$$F_{melt} + H_{apatite} = F_{apatite} + H_{melt}, \tag{6.8}$$

is a more thermodynamically valid method for quantifying F, Cl, and OH partitioning.

An equally rigorous approach for the application of halogen partitioning data to natural systems entails determination of the fugacities of halogens in fluid or melt in equilibrium with apatite (Piccoli and Candela 1994; Webster and Piccoli 2015). Such thermodynamic interpretations and modeling of apatite support the application of apatite compositional data to studies resolving magma geochemistry and magmatic, volcanic, and mineralizing processes. Much of this research is based on thermodynamic interpretation of the mixing behavior of F, Cl, and OH in apatite. Korzhinskiy (1981), for example, used the atomic fractions of F and Cl of hydrothermal apatites to compute relative fugacity ratios of HCl and HF (e.g., f_{HCl}/f_{HF}) in the associated hydrothermal fluids for reactions such as:

$$\begin{aligned} &Ca_5(PO_4)_3F_{fluorapatite} + H_2O = Ca_5(PO_4)_3OH_{hydroxylapatite} + HF, \\ &Ca_5(PO_4)_3Cl_{chlorapatite} + H_2O = Ca_5(PO_4)_3OH_{hydroxylapatite} + HCl, \text{ and} \\ &Ca_5(PO_4)_3F_{fluorapatite} + HCl = Ca_5(PO_4)_3Cl_{chlorapatite} + HF. \end{aligned} \tag{6.9}$$

Tacker and Stormer (1989) applied regular solution modeling of OH and Cl in apatite and determined their mixing behavior to be ideal above 500 °C. Furthermore, the extent of anionic interactions between OH and F that they determined allowed them to interpret the OH-F mixing behavior as ideal, and they applied their model to the exchange of hydroxyl and halogens in apatites and fluids at hydrothermal conditions. Following on the work of Candela (1986), Piccoli and Candela (1994) developed a thermodynamic model for volatiles in apatites, silicic melts, and fluids. They used the halogen concentrations of rhyolitic and granitic apatites to track changes in the fugacity ratios (f_{HF}/f_{OH}), (f_{HCl}/f_{OH}), and f_{HCl}/f_{HF}) in magmas of the extrusive Bishop Tuff and the intrusions of the Tuolomne Intrusive Suite. Their model also supports determination of the temperatures and crystallization behavior of apatite in felsic magmas as well as computation of the F and Cl concentrations of the coexisting melts and aqueous fluids. The apatite-constrained halogen contents of the Bishop Tuff melts agree well with the halogen concentrations determined through analysis of the Bishop Tuff melt

inclusions. Future thermodynamically based models for apatite, however, must account for recent observations on mixing properties in apatite. Acalorimetric study of mixing between the F and Cl end members shows asymmetric mixing and non-ideal behavior for these components (Hovis and Harlov 2010), and some non-ideal mixing has been shown for F-OH (Hovis et al. 2014). Calorimetric-based data for Cl-OH and F-Cl-OH mixing do not yet exist, however.

6.3.6 *Fluid-Crystal Partitioning for Nominally Halogen-Free Minerals*

In recent years, interest has turned towards the partitioning of halogens between fluids, silicate melts, and nominally anhydrous and nominally halogen-free minerals (NAMs) that contain halogens as trace elements (e.g., olivine, pyroxene, plagioclase). These studies have become possible because of the ability of analytical instruments, primarily ion microprobes, to analyze halogens at concentration levels near 1 ppm (e.g., Dalou et al. 2012; Le Voyer et al. 2014b). These studies demonstrate that although the concentrations of halogens in NAMs may be low, the abundance of these crystals may be high enough for them to form the major halogen reservoir (Roberge et al. 2015) in basic rocks and mantle peridotites.

Three studies on the partitioning of halogens between hydrous fluids and nominally halogen-free crystals were published in 2013 (Fig. 6.14). Bernini et al. (2013) performed experiments at 2.6 GPa, 1100 °C, in the system forsterite-enstatite-pyrope-H_2O with either $MgCl_2$ or MgF_2. The Cl concentrations in the experimentally produced crystals vary from only 2.1–11.4 ppm and do not depend upon the salinity of the fluid, which varies from 0.3 to 30 wt% Cl. The F concentrations in enstatite vary from 170 to 3336 ppm and 510 to 1110 ppm in pyrope, and do not depend upon the F concentration of the fluid. However, olivine dissolves 1750 to 1900 ppm F in equilibrium with fluids with up to 1.6 wt% F, but at higher F concentrations the forsterite is replaced by humite group minerals. These results yield fluid/crystal partition coefficients of F from 1 to 100 and for Cl from 1000 to 10^5 that can be expressed by:

$$\begin{aligned}
\log D_{Cl}^{\frac{fluid}{forsterite}} &= 1.0529 \log s + 3.5076,\\
\log D_{Cl}^{\frac{fluid}{enstatite}} &= 0.9583 \log s + 3.5099,\\
\log D_{Cl}^{\frac{fluid}{pyrope}} &= 1.2644 \log s + 2.9822,\\
\log D_{F}^{\frac{fluid}{forsterite}} &= 1.0333 \log s + 0.7505,\\
\log D_{F}^{\frac{fluid}{enstatite}} &= 0.9163 \log s + 1.6355,\\
\log D_{F}^{\frac{fluid}{pyrope}} &= 0.9 \log s + 1.0323,
\end{aligned} \tag{6.10}$$

where *s* is the salinity of Cl or F in wt%. Bernini et al. (2013) then applied these partition coefficients to investigate the composition of mantle brines and their role in island arc volcanism. Note that the dependence of the partition coefficient upon the salinity of the fluid indicates non-Henrian behavior of the two halogens, even though their concentrations in the crystals are less than 2000 ppm. Furthermore, no Fe was present in the experiments so the importance of Mg-Cl and Fe-F avoidance in the partitioning is unknown but likely important.

Fabbrizio et al. (2013b) measured Cl partitioning between forsterite and enstatite and an aqueous fluid in the system $MgO\text{-}SiO_2\text{-}H_2O\text{-}NaCl\text{-}BaO\text{-}C \pm CaCl_2 \pm TiO_2 \pm Al_2O_3 \pm F$ at 2 GPa and 900–1300 °C. They were able to measure Cl in the crystals by EPMA and found a mean value of $D_{Cl}^{fluid/forsterite} = 841$ (±609, 1–σ uncertainty about the mean) and mean value of $D_{Cl}^{fluid/enstatite} = 644$ (±544, 1–σ uncertainty about the mean) for fluids with less than 5 wt% Cl. No effects of temperature were found. Fabbrizio et al. (2013b) found that the addition of Al, Ca, or F increases the amount of Cl dissolved in the olivine by approximately a factor of 4. They also found that the fluid/forsterite partition coefficient is a strong function of the Cl content of the fluid at 1200 °C. At Cl concentrations in the fluid of less than 5 wt%, $D_{Cl}^{fluid/forsterite}$ is ∼1000, whereas at high salinities $D_{Cl}^{fluid/forsterite}$ increases to 10,000. They also discovered that addition of Al, Ca, or F decreases the partition coefficient to ∼1000. They interpreted the changes at greater than 5 wt% Cl in the fluid as evidence of the system being outside the range where Henry's law can be applied and only calculated partition coefficients for salinities less than 5 wt%. Fabbrizio et al. (2013a) expanded their studies of Cl partitioning by performing additional experiments to determine fluid/crystal partitioning for clinopyroxene and amphibole by investigating the partitioning using a natural composition doped with TiO_2 and NaCl or NaF_2. They found that $D_{Cl}^{fluid/forsterite}$ varies from 5000 to 11000, $D_{Cl}^{fluid/enstatite}$ from 2700 to 6666, and $D_{Cl}^{fluid/clinopyroxene}$ from 5000 to 7142.

These studies of halogen fluid/crystal partitioning all demonstrate that although halogens are strongly partitioned into fluids, their concentrations in nominally halogen-free minerals are sufficiently large to make these minerals significant repositories of halogens in the mantle and possibly in crustal intrusions. However, the application of the measured partition coefficients to natural systems must be performed with caution because of the non-Henrian behavior observed and the lack of quantification of the effects of varying Fe/Mg ratios on the partition coefficients.

6.3.7 *Crystal-Melt Partitioning for Nominally Halogen-Free Crystals*

Measurements of halogen partitioning between silicate melts and NAMs are less advanced than between fluids and NAMs. Up to the writing of this chapter, only six published studies investigating the partitioning of halogens between NAMs and silicate melts have been found in the literature (Fig. 6.15).

Hauri et al. (2006) measured partition coefficients for F between water-undersaturated, hydrous (4–9 wt% H_2O) melts and olivine, orthopyroxene and clinopyroxene at 1–4 GPa and 1000–1380 °C. Their results yield no obvious correlations with either temperature or pressure and the results suggest Henrian behavior for the halogens. Hauri et al.'s (2006) 7 measurements of F distribution between olivine and melt yield $D_F^{olivine/melt} = 0.0025 \pm 0.0010$. Their 11 experiments with orthopyroxenes produce an order of magnitude higher partition coefficient, $D_F^{opx/melt} = 0.029 \pm 0.010$, as do their 8 experiments with clinopyroxene, $D_F^{cpx/melt} = 0.047 \pm 0.017$. However, for garnet their 4 experiments yield a $D_F^{garnet/melt}$ with a large scatter, 0.0063 ± 0.0075. These results demonstrate that $D_F^{cpx/melt} > D_f^{opx/melt} > D_F^{garnet/melt} > D_F^{olivine/melt}$, although the scatter in the data for garnet is great and may possibly reflect non-Henrian behavior.

O'Leary et al. (2010) produced halogen partition coefficients as a by-product of their study of H_2O partitioning between hydrous melts and clinopyroxene. They performed one set of experiments using a high-alumina basalt, with H_2O concentrations from 0.2 to 4.9 wt%, to crystallize clinopyroxenes at 1.5 GPa and 1275 °C. In these experiments, $D_F^{cpx/melt}$ varies from 0.0507 ± 0.0014 to 0.087 ± 0.004. Although they show a positive correlation with the $^{IV}Al^{3+}$ in the clinopyroxene, there is no evidence that the partition coefficients are affected by the melt's H_2O concentration. O'Leary et al. (2010) also performed experiments on an alumina-free basaltic composition and demonstrated that $D_F^{cpx/melt}$ is significantly lower than in high-alumina basalt. Interestingly, they also demonstrated that $D_F^{olivine/melt}$ in this Al-free composition is 0.00024 and 0.00054, significantly below values measured by Hauri et al. (2006) or in more recent, Al-bearing experiments.

Dalou et al. (2012) measured the partitioning of F and Cl (as well as a suite of other trace elements) between a basaltic melt and olivine, orthopyroxene, clinopyroxene, plagioclase, and garnet from 0.8 to 2.5 GPa and 1265 to 1430 °C. They found that $D_F^{crystal/melt}$ is universally greater than $D_{Cl}^{crystal/melt}$ and that clinopyroxene has the highest partition coefficients and plagioclase the lowest. In no instance could Dalou et al. (2012) find evidence of a systematic pressure or temperature effect upon their measured partition coefficients. The $D_F^{cpx/melt}$ in 5 experiments vary from 0.0428 to 0.153 and in the same experiments the $D_{Cl}^{cpx/melt}$ varies from 0.0017 to 0.021. The values of $D_F^{opx/melt}$ in 11 experiments vary from 0.0158 to 0.1841 and the $D_{Cl}^{opx/melt}$ of 14 experiments varies from 0.0017 to 0.0278. Olivine, plagioclase, and garnet were each found in only one experiment. The partition coefficient of F between olivine and melt is 0.1164 and for Cl it is 0.0012. For plagioclase, the same two partition coefficients are 0.0980 and 0.0014 and for garnet are 0.0123 and 0.0029, respectively. The lower values of $D_F^{cpx/melt}$, $D_F^{opx/melt}$, and $D_F^{garnet/melt}$ found by Dalou et al. (2012) are similar to those of Hauri et al. (2006), but Dalou et al.'s (2012) value of $D_F^{olivine/melt}$ is almost 2 orders of magnitude greater than that of Hauri et al. (2006) and was later "dismissed" by Dalou et al. (2014).

Beyer et al. (2012) investigated F partitioning in the Fe-free, synthetic systems CaO-MgO-Al_2O_3-SiO_2-F and Na_2O-CaO-MgO-Al_2O_3-SiO_2-F, as well as in a natural, Fe-bearing ankaramitic bulk composition, at pressures up to 2.5 GPa and temperatures between 1285 and 1445 °C. These authors found that F is

significantly more compatible in orthopyroxene ($D_F^{opx/melt}$ between 0.031 and 0.037) than in olivine ($D_F^{ol/melt}$ between 7×10^{-4} and 3.3×10^{-3}). Beyer et al. (2012) determined no effect of bulk composition, temperature, or pressure on their 8 measured partition coefficients and found that their values for $D_F^{opx/melt}$ and $D_F^{ol/melt}$ are similar to those determined by Hauri et al. (2006), and that only their $D_F^{opx/melt}$ is similar to that of Dalou et al. (2012). Beyer et al. (2012) found a correlation between the concentration of Al_2O_3 and F in orthopyroxenes, similar to Dalou et al.'s (2012) finding for clinopyroxenes, and pointed out that their lowest $D_F^{ol/melt}$ is similar to $D_H^{ol/melt}$, i.e. 6×10^{-4}. Using their measured partition coefficients, Beyer et al. (2012) calculated similar F concentrations in the sources of MORBs and in sub-continental spinel lherzolites (6–15 ppm), but found that the sources of ocean-island basalts may be enriched in F with up to 31 ppm.

Dalou et al. (2014) performed 5 experiments to measure the partitioning of F and Cl between hydrous basaltic melt and olivine, orthopyroxene, clinopyroxene, garnet, and amphibole at pressures from 1.2 to 2.5 GPa and temperatures between 1180 and 1430 °C. Comparing results from experiments at 1.2 GPa with temperatures from 1180 to 1240 °C, Dalou et al. (2014) demonstrated that with increasing H_2O concentration from 2.6 to 5.9 wt% in the melt, the $D_F^{opx/melt}$ decreases from 0.056 to 0.021 and the $D_F^{cpx/melt}$ decreases from 0.114 to 0.083. On the other hand, in the same experiments $D_{Cl}^{opx/melt}$ increases from 0.020 to 0.069 and $D_{Cl}^{cpx/melt}$ slightly increases from 0.011 to 0.015. Dalou et al. (2014) suggest that these changes may be due to differing H_2O concentrations in the melts, differing temperatures between the experiments, or different melt compositions in the experiments. At 2.5 GPa and 1340 °C, Dalou et al. (2014) found a surprisingly high $D_F^{garnet/melt}$ of 0.116 compared to Hauri et al.'s (2006) value of 0.0063 ± 0.0075. Dalou et al. (2014) also measured $D_F^{ol/melt}$ of 0.002 ± 0.1 and $D_{Cl}^{ol/melt}$ of 0.003 ± 0.004 in an experiment at 1.2 GPa and 1240 °C that contained 2.9 wt% H_2O in the melt. Dalou et al. argue for a correlation between the number of non-bridging oxygens per tetrahedral cation (NBO/T) in the melt with the partition coefficients such that with increasing NBO/T, $D_F^{mineral/melt}$ decreases and $D_{Cl}^{mineral/melt}$ increases. Furthermore, they argue that the main effect on NBO/T is due to H_2O dissolution in the melt. Dalou et al. (2014) used their data to model the melting of hydrous lherzolite and compared their models to the F and Cl concentrations in melt inclusions from arc rocks.

Joachim et al. (2015) measured the partitioning of F and Cl between melt and both olivine and orthopyroxene at temperatures between 1350 and 1600 °C at pressures between 1.0 and 2.3 GPa. They found a significant positive correlation between the temperature and the partition coefficient of each halogen studied. At 1350 °C the partition coefficients of F and Cl between olivine and melt were both 0.005 and at 1600 °C the partition coefficient of F increases to 0.31 and that of Cl to 0.17. Over the temperature range of 1450–1600 °C the partition coefficients of F and Cl between orthopyroxene and melt increase from 0.06 to 0.2 and from 0.015 to 0.16, respectively.

Although the number of experimental studies on the partitioning of halogens between nominally halogen-free crystals and melts are few, all agree that the partitioning of F into the crystals is significantly greater than Cl and that clinopyroxene/

melt partition coefficients ($D_F^{cpx/melt} \sim 0.05$, $D_{Cl}^{cpx/melt} \sim 0.015$) are the highest, followed in decreasing order by the orthopyroxene/melt ($D_F^{opx/melt} \sim 0.035$, $D_{Cl}^{opx/melt} \sim 0.02$), and olivine/melt ($D_F^{ol/melt} \sim 0.003$, $D_{Cl}^{ol/melt} \sim 0.003$). The large differences described for the partitioning results from Hauri et al. (2006) and Dalou et al. (2014) for garnet, require further investigation to determine halogen partitioning for this mineral. However, these studies also make clear the importance of the mineral, and probably the melt composition, on the partition coefficients. Thus, even though halogens appear to display Henrian (or at least near-Henrian) behavior in crystal/melt partitioning, application of the experimental results to petrogenetic modeling still must be done with caution.

6.3.8 Solubility Mechanisms of Halogens in Nominally Halogen-Free Crystals

The general consensus is that the dissolution mechanism for halogens in the crystal structure of halogen-free minerals is some form of coupled replacement. Many authors (see below) suggest the replacement of oxygen by halogens, although Bernini et al. (2013) and Joachim et al. (2015) also suggest the possibility of the replacement of one SiO_4^{4-} group, by four halogens, as previously observed in low pressure garnets. Halogens can also be found in halogen-free minerals as "chain length defects", such as the amphibole lamellae detected by Mosenfelder and Rossman (2013a) in natural F-bearing orthopyroxenes. Additionally, many authors have suggested the incorporation of halogens into mafic NAMs occurs as clinohumite-like defects and have searched for them.

Beyer et al. (2012) failed to find evidence of F-clinohumite in olivine and suggested that F replaces oxygen in the olivine structure. Mosenfelder and Rossman (2013b) found no evidence of amphibole lamellae in the clinopyroxenes they studied (unlike orthopyroxene), but they found a clear correlation between the F concentration and the sum of (Na+K+$^{IV}Al^{3+}$) per formula unit in clinopyroxene that they interpreted as suggesting two mechanisms for F substitution:

$$^{IV}Al^{3+} + F^{-} \leftrightarrow {}^{IV}Si^{4+} + O^{2-} \tag{6.11}$$

and

$$^{M2}Na^{+} + F^{-} \leftrightarrow {}^{M2}Ca^{2+} + O^{2-}. \tag{6.12}$$

Crépisson et al. (2014) investigated natural and experimentally produced forsterites enriched in OH (up to 2000 ppm H_2O) and F (up to 1700 ppm) by a variety of techniques and concluded that F is incorporated in their olivines as clumped OH/F defects.

Dalou et al. (2012) found systematic correlations between the jadeitic component of their orthopyroxene and the Ca-tschermak component of the clinopyroxene

with the Cl partition coefficient. They interpreted this behavior as a coupled substitution in which Cl^{-} and Al^{3+} substitute for Si^{4+} and O^{2-}. Based upon their modeling of the partition coefficients and Raman spectroscopy, Dalou et al. (2012) proposed that Cl substitutes into O3 sites that are more closely associated with the M2 sites in orthopyroxene. Fluorine is in the O1 site and associated with the M1 site. In clinopyroxene, they suggest that F is in the O3 site and Cl is in the O1 or O2 sites. Fabbrizio et al. (2013b) found evidence that Cl is incorporated into synthetic forsterite through the stabilization of point defects similar to Ti-clinohumite, but could find no such evidence for this substitution mechanism in natural olivines (Fabbrizio et al. 2013a) or in synthetic orthopyroxene (Fabbrizio et al. 2013b).

6.3.9 *Effect of Halogens on Viscosity of Mafic Melts*

Melt viscosity plays an important role in controlling the transport rate of silicate melts, including their extraction from partially molten source regions; their transport in dikes and sills through the upper mantle and crust; their eruption at the surface of the Earth; and their possible thermal and mechanical convection in magma chambers. Materials scientists studying the effects of halogens on the viscosity of industrial melts in the mid 20th century demonstrated that addition of F decreases melt viscosity (see summary by Dingwell et al. 1985), in some cases substantially, but Cl addition may enhance melt viscosity (Hirayama and Camp 1969). Because of the importance of halogens in magmatic systems, the study of their effect on melt viscosities became an active research topic of the late 20th century and continues to this day. However, only the effects of F and Cl have been studied.

Fluorine's effect on melt viscosity. The effect of F on the viscosity of basic-to-intermediate magmatic melts has been studied for 20 years, primarily by D. Dingwell and colleagues. Although most viscosity studies concentrated on silicic melts because of their potential to possess high halogen concentrations (Aiuppa et al. 2009), some of these investigations still provide insight into the effects of halogens in more mafic melts.

In their pioneering work, Dingwell et al. (1985) investigated the viscosities of albitic, jadeiitic, and nephelinitic melts, with approximately 5 wt% added F, at 1 atm. and 1000–1600 °C. Their results clearly demonstrated that addition of F to these melts reduces melt viscosity by between 0.16 log units (nepheline melt) to 0.26 log units (albite melt) for each weight percent of F added to the melt. Dingwell et al. (1985) also found that the addition of F reduces the activation energies for viscous transport in these melts and that the viscosity reducing effects of H_2O and F addition are similar. Dingwell (1987) followed up with a study on the combined effects of F and H_2O on the viscosity of albite melt and found that not only are the combined effects additive, but that the viscosity reduction of melts, containing both H_2O and F, are up to 0.5 log units greater than expected from the effects of F or H_2O alone. Dingwell and Hess (1998) measured the viscosities of melts in the

system Na_2O-Fe_2O_3-SiO_2-F with up to 4 wt% F and established that even in alumina-free systems the addition of F results in strong viscosity reductions.

Giordano et al.'s (2004) extensive study of the effects of F and H_2O on the viscosity of albite melt demonstrated that at 1200 K addition of 3–4 wt% F decreases the viscosity of the melt, but that F is less effective at reducing viscosity than H_2O at equivalent molar concentrations in the melt. They also found that the influence of added F (>7 wt%) on the viscosity is minor, unlike H_2O addition that continues to significantly lower melt viscosity up to the highest concentrations studied, i.e., approximately 20 mol%. These authors found that the viscosities of F + H_2O-bearing melts are very similar to melts only containing H_2O. Giordano et al. (2008) combined their earlier results with data in the literature to create an empirical model to calculate the viscosity of multicomponent magmatic melts that contain both H_2O and F. This model is now often used for the calculation of H_2O- and F -bearing silicate melt viscosities.

Zimova and Webb (2007) measured the viscosity of fluorinated melts in the system Na_2O-Fe_2O_3-Al_2O_3-SiO_2 containing 1100–9000 ppm F and 54–57 wt% SiO_2. They demonstrated that F-addition decreases the viscosity of these mafic melts, but the effects of F on melt viscosity are smaller than seen by Giordano et al. (2004) in the Fe-free, more silicic, albite melts.

Baasner et al. (2013a, b) measured the viscosities of mafic to silicic F-bearing melts in the system Na_2O-CaO-Al_2O_3-SiO_2. Baasner et al. (2013a) found that 1 mol % F decreases the viscosity of a peraluminous melt by 0.31 log units and a peralkaline melt by 0.57 log units. Baasner et al. (2013b) found that the viscosity-reducing effect of F is much greater in peraluminous than in peralkaline melts. In the latter melts, the first few percent of F addition leads to a significant decrease in viscosity but higher F concentrations have minimal effects. Whereas, in peraluminous melts F continues to reduce viscosity to the highest concentrations studied (18 mol%). These authors also found the combined effects of H_2O and F on the viscosity of the peraluminous melts are not independent of each other.

The effects of Cl and Cl + F on melt viscosity. In contrast to F, little is known about the effects of Cl on the viscosity of silicate melts. However, the interactions between Cl and silicate melts are complex and less understood than F. For some compositions the addition of Cl results in a viscosity increase and for other compositions a decrease in viscosity. Early work in materials science by Hirayama and Camp (1969) found that addition of Cl increases the viscosity of a K_2O-BaO-silicate melt. Baker and Vaillancourt (1995) demonstrated that the addition of Cl to an albitic melt increases viscosity from 1060 Pa s for the Cl-free melt to 1523 Pa s for a melt with ~5000 ppm Cl at 1400 °C, 1.5 GPa. Further studies by Dingwell and Hess (1998) on alumina-free melts in the system Na_2O-Fe_2O_3-SiO_2-F-Cl demonstrated that addition of Cl up to 3.2 wt% increases the viscosity at high temperatures, but decreases it at low temperatures. They also found that in comparison to equivalent F additions, the viscosity decreasing effect of Cl at low temperatures is much less.

More recently, S. Webb and colleagues investigated the effects of Cl on melt viscosity in simple but geologically relevant systems at one atmosphere and

temperatures between ~600 and 800 °C. Zimova and Webb (2006) demonstrated that Cl addition to Na_2O-Fe_2O_3-Al_2O_3-SiO_2 melts could either increase, or decrease, the melt viscosity depending upon the composition. Their study investigated melts with Cl concentrations reaching 5700 ppm. In general, the viscosities of peralkaline melts increase with Cl addition and those of peraluminous melts decrease, however there were exceptions for both types of melt compositions. Notably, the effects of Cl addition are minor, i.e. the changes in viscosity (either positive or negative) are no more that 0.3 log units. Zimova and Webb (2007) investigated the combined effects of F and Cl on the viscosities of aluminosilicate melts in the Na_2O-Fe_2O_3-Al_2O_3-SiO_2 system. They found that addition of up to ~1 wt% F always results in a decrease in viscosity, but the addition of Cl + F (2850 ppm Cl and 3660 ppm F) results in an increase in the viscosity of peraluminous melts and a decrease in the viscosity of peralkaline melts, the opposite of the effects seen for Cl by Zimova and Webb (2006). Nevertheless, for the range of the halogen concentrations studied by Zimova and Webb (2007), the effects of the added halogens on the viscosity are 1 log unit or less.

Baasner et al. (2013a) demonstrated that Cl addition in haplo-phonolitic melts in the Na_2O-CaO-Al_2O_3-SiO_2 system results in viscosity increases for peralkaline melts (Fig. 6.18) and decreases for peraluminous melts. However, Cl has no effect on the viscosity of an alumina-free Na_2O-CaO-SiO_2 melt. These authors also found that the effects of F and Cl are additive when both halogens are dissolved in the peraluminous melt and that the viscosity increases caused by Cl addition could be negated by adding equal moles of F. Baasner et al. (2013b) found that the addition of Cl to hydrated and fluorinated peralkaline, haplo-phonolitic melts in the

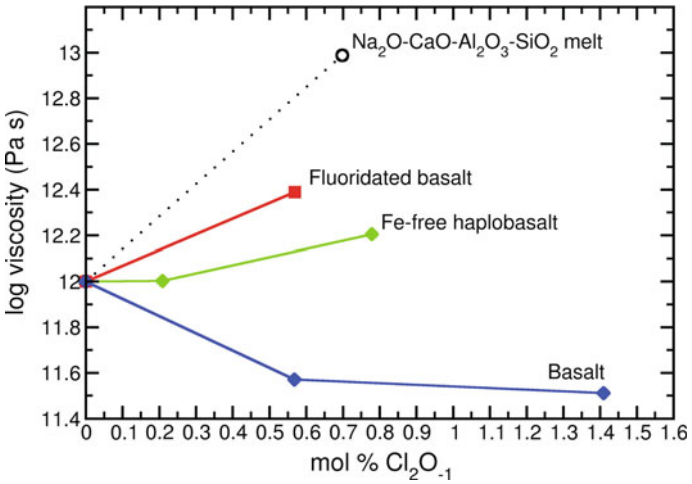

Fig. 6.18 The effect of Cl addition on the viscosity of basaltic melts at low temperatures (drawn after Webb et al. 2014). Chlorine addition by itself is interpreted to increase the viscosity of melts, but the decrease of viscosity in the basaltic melt is attributed the reduction of Fe^{3+} to Fe^{2+} by Cl addition resulting in an increase of network-modifying ions (Webb et al. 2014)

Na_2O-CaO-Al_2O_3-SiO_2 system increases melt viscosity and has no influence on the viscosity reduction effect of added H_2O. Furthermore, the effects of Cl and H_2O are additive such that the viscosity increases caused by Cl addition could be compensated for by the viscosity decreases due to H_2O addition. Addition of Cl to F- and H_2O-bearing peraluminous melts does not have a significant effect on the measured melt viscosities.

Webb et al. (2014) studied the effect of Cl on the viscosity of a basaltic melt and a similar, Fe-free, haplo-basaltic melt (Fig. 6.18). They found that in the Fe-free system the addition of Cl results in a viscosity increase, but in the Fe-bearing melt Cl addition decreases the viscosity. However, addition of Cl to a fluoridated basaltic melt results in a viscosity increase. They concluded that addition of Cl reacts with the melt structure to enhance viscosity, but they also found that Cl addition resulted in the conversion of Fe^{3+} to Fe^{2+}, thus increasing the network-modifying cations in the melt and producing an overall reduction in the viscosity of the melt studied.

The effects of Cl on viscosity and its interactions with silicate melt structure remain an active topic of investigation, particularly at magmatic temperatures for basic melts where almost nothing is known. Unlike F, where the viscosity measurements span the concentration range of this element in natural melts (Figs. 6.1 and 6.2) and we have a robust model for the calculation of its viscosity effects in magmatic melt (Giordano et al. 2008), there are no models that can be used to estimate the viscosity of Cl- or Cl + F-bearing melts. Nor will any models be forthcoming until more measurements of the effects of Cl on silicate melt viscosity are performed. Nevertheless, because of its low concentrations in magmatic melts (Figs. 6.1 and 6.2) and its modest effects on melt viscosity, the Cl concentration can probably be safely ignored in the calculations of BAA melt viscosities in most cases.

6.3.10 *Halogen Diffusion and Halogens's Effects upon Diffusion of Other Elements*

Diffusion in silicate melts often controls rates of growth and dissolution of new phases (e.g., crystals or bubbles of a fluid or gas phase). Diffusion also controls the homogenization rate of two magmas in the absence of strong physical mixing and/or at small length scales, as in the case of the contact between basaltic enclaves and granitic magmas. The diffusion of halogens may control the rates of halide or fluoride mineral growth and dissolution in magmas. Alletti et al. (2007) proposed the possibility of diffusive fractionation of halogens during rapid bubble growth due to differing diffusion coefficients between H_2O, F, and Cl.

Fluorine diffusion in basic-to-intermediate melt compositions. Dingwell and Scarfe (1985) measured the diffusion of F in a fluoridated melt of jadeitic composition at 1 atm in air, but at conditions resulting in the loss of F and Si from the melt (Fig. 6.19, Table 6.4). They also measured F diffusion at 1.0–1.5 GPa by

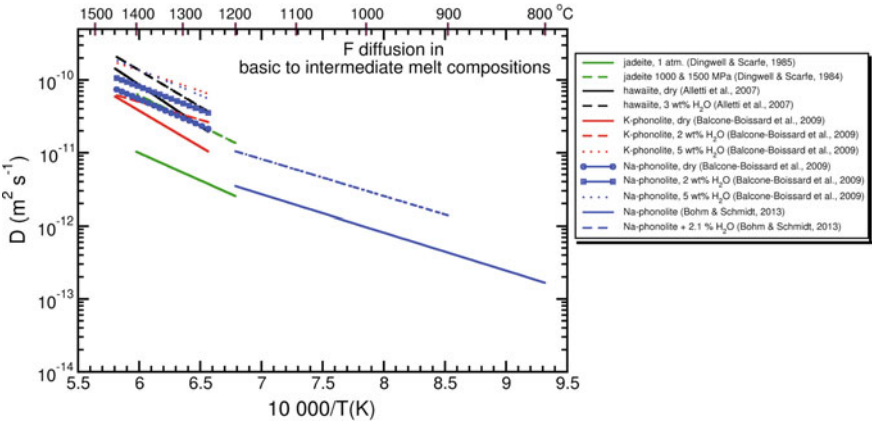

Fig. 6.19 Fluorine diffusion in basic-to-intermediate melt compositions at crustal to upper-mantle pressures

juxtaposing the F-bearing jadeitic melt with a normal, F-free melt (Dingwell and Scarfe 1984). Although Dingwell and Scarfe (1984) found no evidence of a pressure effect between 1.0 and 1.5 GPa, the small difference in the Arrhenius equations for F diffusion at 1 atm and at 1.0–1.5 GPa (Fig. 6.19) results in an order of magnitude difference in $D_{fluorine}$ at 1300 °C. This difference may be attributable to changes in the F diffusion mechanism between the two types of experiments, to a small pressure effect between 1 atm and 1.0 GPa, to differences in the experimental techniques (i.e., loss of F at 1 atm as SiF_4), or to a small amount of H_2O in the high-pressure melts.

Alletti et al. (2007) measured F diffusion in a hawaiitic basaltic melt from Mt. Etna at 0.5 and 1.0 GPa under anhydrous conditions and with 3 wt% H_2O in the melts at temperatures of 1250–1450 °C (Fig. 6.19). No effect of pressure on F diffusion was found, but the addition of H_2O results in a $D_{fluorine}$ approximately twice that found in the anhydrous experiments. They investigated the diffusion of F, Cl, and Br individually and also when combined in the melt, and found that addition of other diffusing halogens (Cl and Br) does not significantly affect the diffusion of F, for example.

Balcone-Boissard et al. (2009) studied F diffusion in Na-rich and K-rich phonolite melts containing 0, 2, and 5 wt% H_2O at 0.5 and 1 GPa (Fig. 6.19). Fluorine was found to have a higher activation energy for diffusion in the K-phonolite than in the Na-phonolite melt under anhydrous conditions, but $D_{fluorine}$ is slightly lower in the K-phonolite. The E_a determined for F diffusion in the Na-phonolitic melt (133 kJ/mol) is similar to that for other sodic compositions, e.g., 120 kJ/mol in albite (Dingwell and Scarfe 1985) and 144 or 159 kJ/mol in jadeite (Dingwell and Scarfe 1984, 1985). The effect of pressure on F diffusion was not measurable. The addition of H_2O enhanced F diffusion, but only by a relatively small amount compared to the effect of H_2O on major- and trace-element cation

Table 6.4 Diffusion coefficients for F and Cl in basaltic, jadeitic, phonolitic, and other mafic melts and for Br in basaltic melt

			$D = D_o \exp(E_a/RT)$			
	T (°C)	P (MPa)	H_2O (wt%)	D_o (m^2 s^{-1})	E_a (kJ mol^{-1})	Reference
Fluorine diffusion in melts of						
Jadeite	1200–1400	0.001	0	3.2×10^{-7}	143.9 ± 14.2	Dingwell and Scarfe (1985)
Jadeite	1200–1400	1000–1500	0	5.9×10^{-6}	159.0 ± 11.2	Dingwell and Scarfe (1984)
Hawaiitic basalt	1250–1450	500–1000	0	5.9×10^{-4}	218.2 ± 33.5	Alletti et al. (2007)
Hawaiitic basalt	1250–1450	500–1000	3	1.4×10^{-4}	191.9 ± 30.7	Alletti et al. (2007)
K-phonolite	1250–1450	500–1000	0	3.4×10^{-5}	215.0 ± 29.5	Balcone-Boissard et al. (2009)
K-phonolite	1250–1450	500–1000	2	4.5×10^{-8}	94.3 ± 32.1	Balcone-Boissard et al. (2009)
K-phonolite	1250–1450	500–1000	5	3.5×10^{-7}	108.9 ± 36.6	Balcone-Boissard et al. (2009)
Na-phonolite	1250–1450	500–1000	0	1.2×10^{-6}	133.2 ± 14.8	Balcone-Boissard et al. (2009)
Na-phonolite	1250–1450	500–1000	2	5.5×10^{-7}	122.3 ± 42.7	Balcone-Boissard et al. (2009)
Na-phonolite	1250–1450	500–1000	5	2.2×10^{-6}	134.1 ± 45.3	Balcone-Boissard et al. (2009)
Na-phonolite	800–1200	100	0	1.2×10^{-8}	99.8 ± 7.4	Böhm and Schmidt (2013)
Na-phonolite	900–1200	100	2.1	2.9×10^{-8}	97.1 ± 4.7	Böhm and Schmidt (2013)
Chlorine diffusion in melts of						
Hawaiitic basalt	1250–1450	500–1000	0	3.3×10^{-2}	277.2 ± 8.1	Alletti et al. (2007)
Hawaiitic basalt	1250–1450	500–1000	3	2.3×10^{-2}	259.4 ± 8.6	Alletti et al. (2007)
K-phonolite	1250–1450	500–1000	0	2.2×10^{-6}	164.0 ± 33.1	Balcone-Boissard et al. (2009)
K-phonolite	1250–1450	500–1000	2	6.7×10^{-1}	330.3 ± 111.2	Balcone-Boissard et al. (2009)
K-phonolite	1250–1450	500–1000	5	5.8×10^{-1}	306.7 ± 103	Balcone-Boissard et al. (2009)
Na-phonolite	1250–1450	500–1000	0	4.7×10^{-5}	215.7 ± 54.4	Balcone-Boissard et al. (2009)
Na-phonolite	1250–1450	500–1000	2	1.3×10^{-6}	148.4 ± 53.8	Balcone-Boissard et al. (2009)
Na-phonolite	1250–1450	500–1000	5	2.3×10^{-5}	178.3 ± 63.3	Balcone-Boissard et al. (2009)

(continued)

Table 6.4 (continued)

Chlorine diffusion in melts of						
Na-phonolite	900–1200	100	0	1.4×10^{-7}	153.1 ± 7.2	Böhm and Schmidt (2013)
Na-phonolite	900–1200	100	2.4	1.1×10^{-6}	154.4 ± 14.0	Böhm and Schmidt (2013)
Na–Ca-Al–Si-O	1100–1300	600–1800	0	3.4×10^{-4}	207	Watson and Bender (1980)
Bromine diffusion in melts of						
Hawaiitic basalt	1250–1450	500–1000	0	7.5×10^{-5}	191.1 ± 33.3	Alletti et al. (2007)

diffusion in other compositions. For example, the addition of 5 wt% H_2O to the Na-phonolitic melt only increases F diffusion at 1250 °C from 2.7×10^{-11} to 5.3×10^{-11} m^2 s^{-1}, instead of the orders of magnitude increase seen for elements such as Zr and P (Watson 1994). The enhancement of $D_{fluorine}$ with H_2O addition is quantitatively similar to the measurements of Alletti et al. (2007) in basaltic melt. Interestingly, when H_2O is added, the $D_{fluorine}$ values and Arrhenius equations are similar in both melt compositions (Table 6.4).

Böhm and Schmidt (2013) measured F diffusion in a Na-phonolite melt at lower temperatures than Balcone-Boissard et al. (2009). The activation energies for F diffusion at anhydrous conditions and with 2 wt% H_2O were similar to those Balcone-Boissard et al. (2009) found for their Na-phonolitic melt (Table 6.4, Fig. 6.19). Furthermore, both studies are consistent in the finding that the addition of H_2O has little-to-no effect on the activation energy for diffusion. However, the pre-exponential factors found by Böhm and Schmidt (2013) are one to two orders of magnitude less than those of Balcone-Boissard et al. (2009), resulting in similarly lower values of $D_{fluorine}$ at equivalent temperatures. The differences may be due to the lower pressure used by Böhm and Schmidt (2013), 100 MPa as compared to 500 and 1000 MPa used by Balcone-Boissard et al. (2009), and/or due to compositional differences between the different phonolitic melts used in the studies.

Chlorine diffusion in basic-to-intermediate melts. Watson and Bender (1980) measured Cl tracer diffusion in an anhydrous, geologically relevant but simple melt (Fig. 6.20), with a Na-Ca-Al-Si-O composition containing 56 wt% silica at 1100–1300 °C and 0.6–1.8 GPa. There was no measurable pressure dependence on Cl diffusion over this pressure range.

Alletti et al. (2007) measured Cl diffusion in the same basaltic melt from Etna and at the same conditions used for their measurements of F diffusion (Figs. 6.19 and 6.20). $D_{chlorine}$ is a little lower than $D_{fluorine}$ in most cases at temperatures below 1400 °C, but because of its higher activation energy (Table 6.4) $D_{chlorine}$ is approximately equal to $D_{fluorine}$ at high temperatures. The addition of 3 wt% H_2O increases $D_{chlorine}$ by a factor of two, but has a small effect on the Arrhenius parameters (Table 6.4).

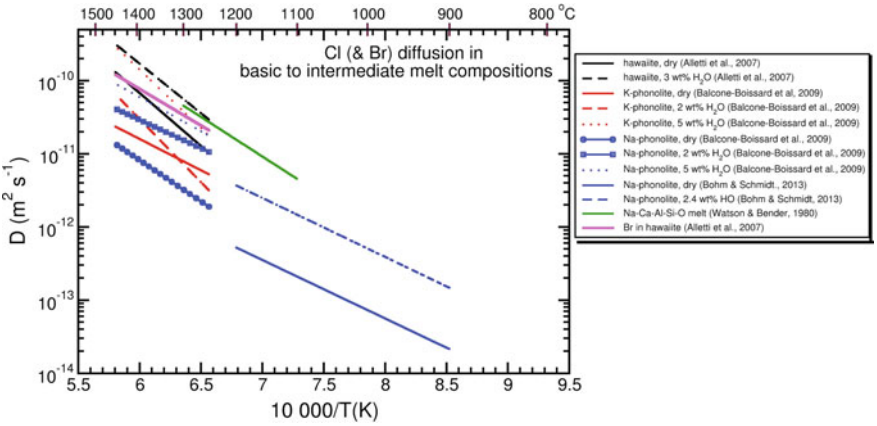

Fig. 6.20 Chlorine and Br diffusion in basic-to-intermediate melt compositions at crustal to upper-mantle pressures. All data apply to diffusion of Cl, except for the single study on Br by Alletti et al. (2007)

Balcone-Boissard et al.'s (2009) study of Cl diffusion in Na- and K-rich phonolite melts demonstrated that $D_{chlorine}$ is similar in both compositions (Fig. 6.20). Water addition increases $D_{fluorine}$ and $D_{chlorine}$ in both compositions, but the influence of H_2O on Cl diffusion is much greater than its effect on F diffusivity. Balcone-Boissard et al. (2009) demonstrated that the effect of H_2O on $D_{chlorine}$ is greater in phonolitic melts than in the basaltic melt studied by Alletti et al. (2007), as expected considering the more silica-rich compositions of the phonolitic melts. Perhaps importantly, the addition of H_2O increases the activation energy for Cl diffusion in the K-phonolites. Chlorine diffusion in these melts displays a greater enhancement between 2 and 5 wt% H_2O than between 0 and 2 wt%. This is unlike observations for most elements in silicate melts, where the diffusivity increases the most when small amounts of H_2O are added (Watson 1994).

Böhm and Schmidt (2013) also measured Cl diffusion in the same Na-phonolite melt used for their measurements of F diffusion (Fig. 6.20). Their results for Cl diffusion, both the pre-exponential factor and activation energy for diffusion (Table 6.4), are more similar to those of Balcone-Boissard et al. (2009) than their Arrhenius parameters for F diffusion. The activation energy for Cl diffusion was also found to be little (if at all) affected by the addition of H_2O to the melt, but the pre-exponential factor increases by an order of magnitude (Table 6.4).

Diffusion of other halogens. The diffusion of the other naturally occurring halogens, Br and I, is poorly known. No measurements of I diffusion in basic to intermediate melts appear to have been made, and only one study of Br diffusion in a basic melt has been published. Alletti et al. (2007) measured Br diffusion under anhydrous conditions in the same basaltic melt as used for the measurement of F and Cl diffusion. This study found that $D_{bromine}$ is slightly less than $D_{chlorine}$, but that its activation energy for diffusion is similar to that of F (Table 6.4, Fig. 6.19).

Comparison of halogen diffusivities in melt. The diffusivities of Cl are typically lower than those of F at magmatic temperatures and Br appears similar to Cl (Figs. 6.19 and 6.20). The effect of size on halogen diffusion appears to become more significant with increasing SiO_2 in the melt. This trend is attributed to the structural roles (or "sites" or coordinating ions) of F and Cl (and Br) in silicate melts (Balcone-Boissard et al. 2009). Balcone-Boissard et al. (2009) hypothesized that the differences between the behaviour of F and Cl are due to their roles in the melt structure. Here, F replaces coordinating oxygen and Cl associates with alkalies, alkali-earths, and H_2O (Schaller et al. 1992; Zeng and Stebbins 2000; Liu and Nekvasil 2002; Mysen et al. 2004; Sandland et al. 2004; Kiczenski and Stebbins 2006). Chlorine possibly forms an alkali-H_2O complex outside of the melt structure, perhaps as some form of nano-emulsion. Importantly, however, there is no visible evidence of an immiscible chloride phase present.

Halogens and the diffusion of other elements in silicate melts. Although no studies have expressly determined the effect of halogen addition on the diffusion of major elements in mafic to intermediate melts, the results of Baker (1993) for silicic melts provide some clues as to what might be expected. Baker (1993) found that the addition of 1.3 wt% F to melts, containing 61–73 wt% SiO_2, increases the Si-Al effective binary diffusion coefficient by less than an order of magnitude and only slightly reduces the activation energy for diffusion. On the other hand, Cl appears to increase the activation energy for diffusion in the silicic melts investigated (Baker 1993). Such effects on diffusion are consistent with the effects of F and Cl on melt viscosity (discussed above) and the connection between melt viscosity and Si-Al interdiffusion in melts by the Eyring equation (see Baker 1992):

$$D = \frac{kT}{\eta\lambda}, \tag{6.13}$$

where k is Boltzmann's constant; T is the temperature (in K); η is the melt viscosity (in Pa second); and λ is the diffusive jump distance, taken to be 100 pm (Baker 1992). The effects of F and Cl addition on the Si-Al effective binary diffusion coefficient are expected to be similar in other BAA melt compositions, although no experimental data currently exist. Nevertheless, the effect of F addition on the Si-Al effective binary diffusion coefficient of fluoridated and hydrous fluoridated BAA melts can be at least semi-quantitatively calculated from the Eyring equation and the viscosity model of Giordano et al. (2008) and used for petrological calculations of non-alkali diffusivities in basic-to-intermediate melt compositions.

6.4 Applications & Case Studies

6.4.1 Halogen Behavior in Layered Mafic Intrusions

Over the length of Earth's history, rare but immense volumes of mafic- to ultramafic-composition magmas have intruded into the crust. These magmas cool and form mineralogically and chemically layered mafic intrusions, some of which are mineralized with, and exploited for valuable Pt group elements (PGE), V, Cr, Ti, Fe, and Sn (Kanitpanyacharoen and Boudreau 2013). A variety of petrologic and geochemical evidence indicates that these magmatic rocks were partially recrystallized and chemically altered by Cl-bearing volatile phases (Boudreau et al. 1986; Hanley et al. 2008).

Two classic examples of layered intrusions are the Bushveld igneous complex of South Africa and the Stillwater complex of Montana, USA, but more than a dozen others have been recognized. Rock samples from select horizons within these intrusions are variably enriched in S and Cl ± C (Mathez et al. 1989). However, determining the volatile contents of any given stage of magma evolution associated with ore formation, represented by these rocks, is challenging because of the scarcity of fluid inclusions and volatile-bearing MI in these plutonic rocks. With careful sample selection and inspection, Hanley et al. (2008) were able to locate and describe fluid inclusions indicating a continuum of magmatic-hydrothermal processes evolving from magmatic temperatures to sub-solidus metasomatic conditions. In the Stillwater, magma-sourced fluids ranged from NaCl-dominated hydrosaline liquids to geochemically complex, mixed Na-Ca-K-Fe-Mn-Ba-Al-Si saline liquids with or without significant CO_2 and CH_4. This transition in fluid composition occurred during differentiation of the initially basaltic melt to more-evolved, residual, granophyric compositions.

Research on the Bushveld, and other smaller intrusions, has identified associations of Cl-enriched phlogopites, amphiboles, and apatites with PGE sulfide-mineralized horizons. Experiments (Blaine et al. 2011) and some volcanic gas and mineral compositions (MacKenzie and Canil 2011; Mazziotti et al. 2012) imply chemical associations of Cl with Pt, Re, and other metals at elevated temperatures, so knowledge of the abundances and behavior of these volatiles is important for understanding processes of magma evolution, fluid(s) exsolution, and ore formation in such plutons. Hydrous apatites ± amphiboles have been studied extensively from some of these systems. They provide records of volatile behavior during magma evolution and processes leading to mineralization. Interestingly, some apatites from the Bushveld complex are among the most Cl-enriched igneous apatites known (Boudreau 1995; Piccoli and Candela 2002). Others show up to 50% of the OH component in the anion site. Hydroxyl-poor apatites range from nearly pure fluoro- to chloroapatite end-member compositions. This broad range in apatite compositions is unique to magmatic systems. The compositions of apatites also vary systematically with stratigraphic height within the intrusions. Chemical zoning within apatite is unreported, however, for these slowly cooled magmatic

systems, but different grains of apatite located within individual thin sections (of the same rock sample) may show significant compositional variations (Boudreau 1995). Through the 9-km thick Bushveld complex, for example, the mole fraction of Cl (X_{Cl}^{apat}) varies but remains generally >0.5 from the base to the PGE-mineralized Merensky Reef located ca. 3.2 km above the base. Conversely, X_{Cl}^{apat} decreases immediately above the PGE-mineralization, varies less with increasing stratigraphic distance from the base, and remains generally <0.4 to the top where X_{Cl}^{apat} is nearly null. Also for the Bushveld, and for layered intrusions in general, the apatites show decreasing (Cl/F) in the more evolved cumulate rocks. The larger, cross-system chemical variations are still undergoing interpretation, but it has been suggested that exsolution of Cl-rich fluid(s) helped to fractionate Cl from F in the melt (Boudreau 1995). It has also been argued that these Cl-bearing fluids ascended and reacted with increasingly evolved melt, forcing changes in the chemistry and textures of the rocks.

Boudreau and co-workers have used the F and Cl concentrations in apatite to model the evolution of magmatic halogen behavior in a number of these layered igneous intrusions (e.g., Boudreau et al. 1986, 1993; Boudreau and Simon 2007) through application of the exchange reaction:

$$Fluorapatite^{crystal} + HCl^{aqueous\ fluid} \leftrightarrow Chlorapatite^{crystal} + HF^{aqueous\ fluid}. \quad (6.14)$$

By estimating the equilibrium constant for this reaction, $K_{exchange}$, and approximating the activity coefficients of halogens in apatites as unity above 500 °C, the activities of the halogens in the coexisting fluid can be calculated:

$$\frac{a_{HF}^{aqueous\ fluid}}{a_{HCl}^{aqueous\ fluid}} = K_{exchange}\left(\frac{X_F^{fluorapatite}}{X_{Cl}^{chlorapatite}}\right). \quad (6.15)$$

Similar reactions and equations for the exchange of OH and F between apatite and fluid can also be written. Recent research, however, has observed evidence of non-ideal thermodynamic mixing of F and OH in hydroxyl-enriched apatite (Hovis et al. 2014), and results of another study suggest that non-ideal mixing of F and Cl may occur in OH-free apatite (Hovis and Harlov 2010). The results of the latter study require confirmation, but both investigations suggest that the activity coefficients of halogens in some magmatic apatites may indeed vary from unity. Although the thermodynamic relations between halogens in the melts are even less well constrained, Boudreau and Simon (2007) hypothesized that that changes in ($a_{HF}^{aqueous\ fluid}/a_{HCl}^{aqueous\ fluid}$) and ($a_{HF}^{aqueous\ fluid}/a_{OH}^{aqueous\ fluid}$) should reflect similar changes in the melt.

Boudreau and Simon (2007) analyzed apatites from Antarctic sills and demonstrated that the observed variations in HF/HCl and HF/OH fugacity ratios in the apatites could be explained either by changes in the fugacities of H_2O, F, and Cl in these magmatic complexes (i.e., by an order of magnitude) or by changing the apatite crystallization temperature by 500 °C. The latter interpretation, however, is

inconsistent with the prior arguments of Boudreau et al. (1993) suggesting that temperature changes of 500 °C during apatite crystallization in a layered intrusion were unlikely to be the cause of the observed variations in $X_F^{apatite}/X_{Cl}^{apatite}$ and $X_F^{apatite}/X_{OH}^{apatite}$. This is because apatite crystallization is controlled by P concentrations in the melt and those are a strong function of the degree of crystallization of the magma (Piccoli and Candela 2002). Thus, most apatite should crystallize at similar temperatures throughout most of a magmatic intrusion, but not necessarily at the same time because the walls of intrusions cool faster than the center. Combining the apatite compositions with a model of the evolution of the major elements, a C-O-H-S fluid, and halogens during crystallization, Boudreau and Simon (2007) demonstrated that increases in the Cl/F and OH/F ratios seen in apatites near the center of the sill could be due to the upward migration of a Cl-rich fluid from the base of the sill. The rapidly cooling base, near the cold country rocks, should crystallize sooner than the center and also become saturated in fluid earlier. This Cl-enriched aqueous fluid would subsequently ascend towards the center of the sill where fluid-undersaturated melt would resorb the fluid, leading to a melt enriched in Cl and OH relative to the initial bulk melt composition of the sill. Apatites that crystallize from such volatile-enriched melt would be similarly enriched in Cl and OH compared to those at the base.

6.4.2 *Halogen Enrichment in Basaltic Magmas of Seafloor Environments*

Determining the compositions of mantle source reservoirs and processes involved in decompression-driven partial melting at oceanic and crustal spreading centers, and during volatile-fluxed partial melting in subduction zone environments, is of significant research interest. This information is needed to understand how much of the subducted ocean crust is retained in the mantle and how much is incorporated into, and recycled by, partial melts as they ascend through the crust. Also important is the role of volatile components in magma generation and evolution at spreading centers and oceanic islands.

Retention of chemically altered oceanic crust in the mantle during subduction and partial melting (Wysoczanski et al. 2006) influences heterogeneity in depleted versus enriched mantle reservoirs. This impacts the compositions of basaltic magmas (e.g., normal MORB versus enriched MORB) that are generated at spreading centers (Koleszar et al. 2009). These reservoirs and melting processes have been investigated geochemically with trace elements (Kent et al. 2002), isotopes (Eggenkamp 2014), and volatile components (Rose-Koga et al. 2012; Le Voyer et al. 2014a). Although the basaltic melts generated at oceanic spreading centers typically do not contain high volatile contents, some magmas contain highly variable enrichments in halogens, and Cl in particular (Michael and Schilling 1989). Chlorine over-enrichments have also been observed in a number of intraplate ocean

island basalts (OIBs), including hot spot related systems, their more evolved eruptive products (Kent et al. 1999; Lassiter et al. 2002; Saal et al. 2007), and, interestingly, in some rare flood basalts of rift-related continental environments (Black et al. 2012). The processes of magma contamination by seawater and seawater-altered crustal components have also been considered. Variable Cl enrichment related to seawater contamination also occurs in subduction-related basaltic magmas and back-arc basins involving components from subduction processes (Peate et al. 2001; Kent et al. 2002; Hahm et al. 2012; Kendrick et al. 2013b, 2014b).

Rocks in the source regions of mantle melting contain low halogen contents, which influence the halogen concentrations of mantle-sourced basaltic magmas as well as the larger issue of halogen recycling between the mantle, crust, hydrosphere, and atmosphere (Saal et al. 2002; Kovalenko et al. 2006). Joachim et al. (2014) recently calculated that mantle sources for spreading center magmas contain ca. 3–15 ppm F and 0.5–14 ppm Cl and those supporting OIB magma generation contain ca. 35–65 ppm F and 21–55 ppm Cl. These ranges are consistent with other estimates (see chapters by Frezzotti and Ferrando (2018) and Klemme and Stalder (2018)). Concentrations of Br and I are less well constrained, but mantle MORB sources beneath Iceland, for example, contain as little as ca. 60 ppb Br and <10 ppb I (Weston 2012). The primitive mantle is heterogeneous, however Hoffman (1977) and Nielsen et al. (2000) measured Cl concentrations and select incompatible trace elements in Galapagos platform basalts, that are ultradepleted in these components, in order to investigate heterogeneities bearing on the origin of normal-MORB magmas.

The halogen contents of most seafloor and ocean island basaltic rocks, MI, and glasses, however, rarely reflect their lower concentrations in the mantle because of the effects of variable partial melting, fractional crystallization, assimilation and/or contamination, magma mixing, and degassing (Saal et al. 2002; Le Voyer et al. 2014a, b). This is particularly true for Cl (Michael and Cornell 1998). These processes influence magmatic Cl concentrations strongly, with lesser impacts on F, Br, and I. Quantitatively determining the relation of these processes on Cl in seafloor and ocean island basalts has been the object of intense scrutiny, and we attempt to summarize some of the relevant observations and relationships here. Figure 6.21a, b addresses Cl in basaltic to dacitic glasses and MI from seafloor environments and in submarine-Kilauea basalts. Figure 6.21 c, d addresses those in OIBs and two Cl-enriched continental rift-related basalts. These figures compare the (Cl/K_2O) with the measured Cl concentrations normalized to their computed maximum Cl solubilities. The latter parameter was computed for each glass and MI composition at fixed, shallow-crustal pressure of 50 MPa and temperature of 1150 °C using the Cl solubility model of Webster et al. (2015). It represents the maximum Cl concentration of a silicate melt in equilibrium with a Cl-dominated hydrosaline liquid. When the (measured Cl concentration)/(modeled Cl solubility) ratio is unity, the silicate melt is saturated in hydrosaline liquid (as expressed by dashed lines in [a] and [c]). It is important to note that the Cl-enriched to over-enriched magmas addressed here are volumetrically less than that of most Cl-poor basaltic magmas erupted on seafloors and in continental land masses.

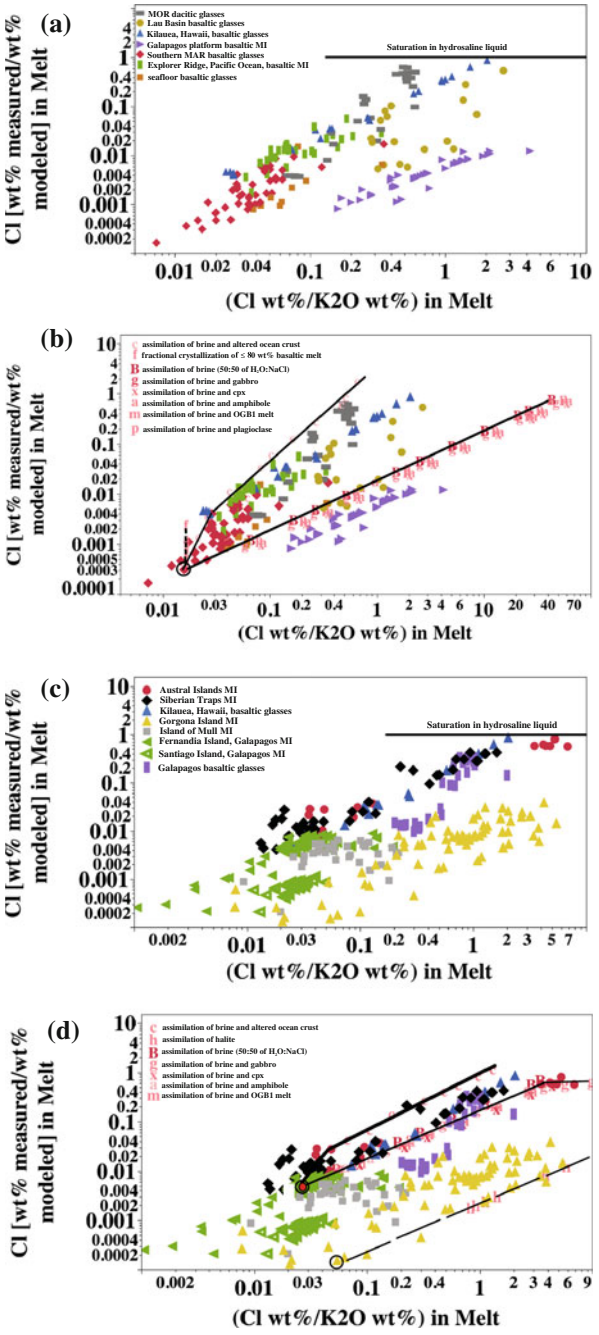
(a)
MOR dacitic glasses
Lau Basin basaltic glasses
Kilauea, Hawaii, basaltic glasses
Galapagos platform basaltic MI
Southern MAR basaltic glasses
Explorer Ridge, Pacific Ocean, basaltic MI
seafloor basaltic glasses
Saturation in hydrosaline liquid
Cl [wt% measured/wt% modeled] in Melt
(Cl wt%/K2O wt%) in Melt
(b)
assimilation of brine and altered ocean crust
fractional crystallization of ≤ 80 wt% basaltic melt
assimilation of brine (50:50 of H2O:NaCl)
assimilation of brine and gabbro
assimilation of brine and cpx
assimilation of brine and amphibole
assimilation of brine and OGB1 melt
assimilation of brine and plagioclase
Cl [wt% measured/wt% modeled] in Melt
(Cl wt%/K2O wt%) in Melt
(c)
Austral Islands MI
Siberian Traps MI
Kilauea, Hawaii, basaltic glasses
Gorgona Island MI
Island of Mull MI
Fernandia Island, Galapagos MI
Santiago Island, Galapagos MI
Galapagos basaltic glasses
Saturation in hydrosaline liquid
Cl [wt% measured/wt% modeled] in Melt
(Cl wt%/K2O wt%) in Melt
(d)
assimilation of brine and altered ocean crust
assimilation of halite
assimilation of brine (50:50 of H2O:NaCl)
assimilation of brine and gabbro
assimilation of brine and cpx
assimilation of brine and amphibole
assimilation of brine and OGB1 melt
Cl [wt% measured/wt% modeled] in Melt
(Cl wt%/K2O wt%) in Melt

◄ **Fig. 6.21** Log-log plots of measured wt% Cl in melt/modeled, maximum Cl solubility in hydrosaline ± vapor-saturated melt at 50 MPa versus (wt% Cl)/(wt% K_2O in melt) based on glasses and silicate melt inclusions from a variety of seafloor (**a**, **b**) and oceanic island, hot spot, and continental crustal (**c**, **d**) systems. Most data are basaltic but several glasses are andesitic to dacitic. Most data show positive correlations between these variables, but the associated dispersion varies. Plot (**a**) applies to glasses from submarine seafloor systems. The *line* represents the (measured concentration of Cl)/(modeled Cl solubility in the melt) where melts are saturated in a hydrosaline liquid. Several seafloor Lau Basin dacitic glasses and one submarine Kilauea basaltic glass contain >60% and >85%, respectively, of the Cl content required for equilibration with hydrosaline liquids. Plot (**b**) includes results of modeling of a Cl-poor MOR basaltic melt composition (circled datum) as this melt assimilates brine only (*bold solid line*) or brine plus altered ocean crust (*fine solid curve*). Other potential contaminants for assimilation are also shown. Consequences of fractional crystallization are shown as a *short dashed line*. Plot (**c**) applies to oceanic islands and submarine Kilauea glasses and melt inclusions. The *line* represents melts saturated in a hydrosaline liquid. Several Austral Island melt inclusions contain >60% of the Cl content required for equilibration with hydrosaline liquid. Plot (**d**) displays results of modeling an Austral Island basaltic melt composition (circle 1) as it assimilates brine plus altered ocean crust (*fine solid curve*) and brine plus clinopyroxene- and anorthite-dominated gabbro (*bold curve*). Austral melt inclusion data are consistent with contamination by variable partial melting of brine-bearing gabbro (as concluded by Lassiter et al. 2002). Circle 2 shows the effects of Gorgona Island basaltic melt as it assimilates NaCl (*dashed line*). Symbols used include fractional crystallization of basaltic melt or basaltic melt composition assimilating brine and altered ocean floor crust (**c**); brine only (**b**); brine and plagioclase-clinopyroxene gabbro (**g**); brine and clinopyroxene (cpx) only (x); brine and altered, Cl-enriched amphibole (**a**); brine and gabbroic partial melt glass composition OGB1 of (Kvassnes and Grove 2008); and brine plus plagioclase (*p*). Additional data sources are provided in the Appendix

The effects of crystallization-driven differentiation on the halogen contents of evolving, seafloor and OIB magmas—dominated by olivine, pyroxene, plagioclase, and Fe oxide precipitation—has been quantified through plots involving F and Cl versus MgO and TiO_2 in basaltic glasses and MI (Michael and Schilling 1989). More recent studies have determined and applied trace-element ratios such as (Cl/Nb) and (F/Zr) to resolve this issue (le Roux et al. 2006). It was observed for many seafloor basalt and OIB samples, particularly those from slow-spreading ridges, that the rate of Cl increase correlates with the extent of crystallization of the above mineral assemblage. Hence, fractional crystallization is the dominant process of magma evolution (and the primary process increasing Cl in the residual melt) involved for most of these magmas. However, the Cl concentrations increase more sharply with decreasing MgO for some oceanic MORB glasses associated with ridges involving relatively fast spreading rates (Michael and Schilling 1989). Fractional crystallization-based modeling of Cl behavior in the latter system. which treats Cl as a perfectly incompatible trace element, predicts modest increases in the Cl contents of residual aliquots of melt that are far less than the observed over-enrichments that are present in the associated glasses (Michael and Schilling 1989). Moreover, Michael and Cornell (1998) predicted that (Cl/K_2O) ratios should remain constant in primitive, fluid-undersaturated, basaltic magmas as they evolve via fractional crystallization. This is because Cl and K behave as incompatible trace elements in this Cl- and K-deficient mineral assemblage. Figure 6.21b includes the

results from petrological modeling of fractional crystallization operating alone on a basaltic melt. The observed effect is to increase the Cl concentration of the evolving melt while decreasing the Cl solubility in the residual fractions of melt (as explained in Sect. 6.3.2) that become increasingly evolved. The (Cl/K_2O) does indeed remain constant with changing melt composition, and the overall effect of fractional crystallization on the Cl content and Cl dissolution in the melt is to force the evolving melt composition (and resultant glass and MI data) along a vertical vector.

Some oceanic MORB glasses associated with ridges involving fast-spreading rates and a relatively high magma flux exhibit widely varying (Cl/K_2O) ratios (Michael and Cornell 1998; Nielsen et al. 2000). Similar observations bear on a number of OIBs and hot spot magmatic systems (Kent et al. 1999; Coombs et al. 2004). These observations have been interpreted to indicate that fractional crystallization is not the sole process involved in generating variable Cl contents in basaltic magmas in these environments (Michael and Schilling 1989; Wanless et al. 2010).

Pre-eruptive contamination of seafloor and ocean island basaltic magmas by seawater-derived brines (i.e., hydrosaline liquids) also enhances Cl contents of such magmas and reduces their K concentrations by dilution. This process may occur by direct magmatic assimilation of a K-poor hydrosaline liquid, assimilation of hydrothermally altered, hydrosaline, liquid-bearing, low-K basaltic rocks, or by partial melting of an altered, hydrosaline, liquid-bearing, low-K basalt. As noted previously, immiscibility involving vapor plus hydrosaline liquid occurs when seawater is heated by hot crystalline basaltic crust and it boils (Bischoff and Rosenbauer 1984; Fournier 1987; Foustoukos and Seyfried 2007a). After boiling, the buoyant separation of vapor leaves behind a more-dense hydrosaline liquid in the hydrothermal systems that develop within the hot basaltic crust (Fontaine and Wilcock 2006). Mechanistically, interfacial tensions involving the fluid and mineral phases of altered basaltic and gabbroic seafloor crust develop and may favor preferential segregation of vapor into primary fractures and of brine into smaller fissures forming brine layers (Fontaine and Wilcock 2006). These processes are consistent with the presence of hydrosaline FI in hydrothermally altered gabbroic rocks from the seafloor (Kelly and Delaney 1987).

The presence of elevated Cl levels, i.e., more than 1000 ppm Cl in the matrix glasses and MI sampled at the Loihi seamount of Hawaii (Kent et al. 1999) and up to 1.68 wt% Cl in glasses collected from the submarine flank of Kilauea volcano, Hawaii (Coombs et al. 2004), has been interpreted to reflect the direct assimilation of hydrosaline liquids dominated by H_2O, Na, and Cl. The former study also determined that higher H_2O and B contents accompanied Cl. The latter study determined that K, Ca, Ba, Rb, Sr, and Pb, in addition to Na as the dominant cation, were also dissolved in the hydrothermal fluids at Loihi and Kilauea. The Hawaiian glass compositions reported by Coombs et al. (2004) are compared with the modeled results of brine assimilation in Fig. 6.21b, d, using the circled southern mid-Atlantic ridge glass with a Cl/K_2O ratio of 0.016 as a representative, Cl-poor starting basaltic melt composition prior to melt-brine interaction. The modeled results show an increase in the Cl content with assimilation of up to 1 wt% of a hydrosaline liquid containing 50 wt% NaCl and 50 wt% H_2O. Direct brine assimilation produces a

linear increase in the (measured Cl concentration)/(modeled Cl solubility) ratio with increasing Cl/K_2O. Assimilation of 1 wt% of brine, for example, increases the Cl/K_2O ratio by a factor of 315 and generates a melt with a Cl/K_2O ratio of 5.1. It is noteworthy that the extent of Cl enrichment is limited, however. The modeled and brine-contaminated melt composition with the highest Cl content dissolved only 9% of its Cl saturation value, indicating that the melt did not achieve equilibrium with the hydrosaline liquid. Additional modeling, not included in the figure, shows that saturation of this melt composition in hydrosaline liquid requires the assimilation of 11 wt% of a 50:50 NaCl- and H_2O-bearing brine and that a melt of this composition would dissolve ca. 3 wt% Cl at brine saturation. This value is nearly twice that of the maximum recorded Cl concentration from the Kilauea glasses, so although the basaltic melts involved appear to have interacted with hydrosaline liquids, the melts did not actually equilibrate with such liquids. The predicted brine-assimilation trend is consistent with that shown by the Kilauea glass data, and this supports the interpretation of Coombs et al. (2004) for direct assimilation of the hydrosaline liquid. In addition, the Kilauea glass data show little dispersion along the trend that is consistent with that of the modeled trend. This uniformity involving low dispersion implies that other processes did not play a significant role in magma differentiation as brine assimilation occurred. These observations contrast with the other data sets in Fig. 6.21. They show positive correlations between the (measured Cl concentration)/(modeled Cl solubility in melt) ratio versus Cl/K_2O. The trends include much greater dispersion implying processes in addition to, or other than, assimilation of brine. In passing, we also note that the work of Kendrick et al. (2012a, b) shows that K/Cl, Br/Cl, and I/Cl ratios of some basaltic glasses are largely unmodified by partial melting and crystallization of basalt melt even though Le Voyer et al. (2014a, b) correlated the degree of partial melting with variable Cl/Nb in some equatorial, mid-Atlantic MORB samples. Kendrick et al. (2012a, b) further suggest that the application of all 3 of these halogens may prove to be better for assessing the role of seawater assimilation.

More broadly, glass-based investigations of basaltic melt-brine interactions have determined that the assimilation process involves hydrosaline liquids with 40–70 wt% salts that are generated in convecting hydrothermal systems on and below the seafloor at ca. 50–60 MPa and 500–700 °C (Le Roux et al. 2006; Wanless et al. 2011; Kendrick et al. 2013a). At locations proximal to ocean-ridge systems, these interactions likely occur at crustal levels and pressures close to those of the axial magma chamber and in the diabase dikes of the sub-seafloor layer 2B (Le Roux et al. 2006). Regarding the former, Coogan et al. (2003) consider such assimilation at the roof of the axial magma chambers to be a common process. These interactions may also occur during distal off-axis eruptions that take place through altered basaltic, diabasic, and gabbroic crust, which contains hydrosaline liquid and salt crystals in fluid inclusions and cracks and other pore space in the rocks (Le Roux et al. 2006). Other evidence of brine incorporation comes from the analysis of Cl-rich apatites (0.66–3.05 wt% Cl) in cumulates from the East Pacific Rise, from the mid-Atlantic ridge near the Kane transform (0.05–1.22 wt% Cl), and from the southwest Indian ridge (Meurer and Natland 2001) (0.16–1.46 wt% Cl).

These Cl-enriched apatites may also have reacted with seafloor hydrosaline liquids (Meurer and Natland 2001).

Some magma-brine interactions also involve partial incorporation of hydrothermally altered rocks that contain hydrosaline liquid trapped along grain boundaries (Kent et al. 1999), in pockets in the rock, and in FI in the minerals (Le Roux et al. 2006). These interactions lead to chemical contamination of the magma by altered seafloor crust and/or altered amphiboles as well as brine. The results from geochemical modeling of a basaltic melt are included in Fig. 6.21. The melts are characterized by a low (Cl/K_2O), assimilating brine with 0.01–1 wt% of a 50:50 H_2O-NaCl liquid along with a fixed quantity of 25 wt% hydrothermally altered amphiboles and/or the assimilation of a similar brine plus 25 wt% of hydrothermally altered crust. Magma interaction with brine and altered amphiboles involves two sources of added Cl. Whole-mineral Cl concentrations of amphibolite-grade hornblendes in altered ocean crust range from 0.1 to 0.6 wt%. Chlorine in some internal sectors of rare hastingsite crystals in actinolite-bearing metasomatized ocean floor rocks from the Mathematician Ridge, East Pacific Ocean, exceed 3 wt% (Vanko 1986). This Cl enrichment in amphibole is attributed to interaction with seafloor hydrosaline liquids. Chemical interaction of these components generates positive correlations between the (measured concentration)/(modeled Cl solubility in the melt) ratio versus (Cl/K_2O) that exhibit minimal dispersion about the trend. Conversely, assimilation of altered, brine-laden basaltic crust at the roof, and along the walls of axial magma chambers, generates melt compositions that are less mafic than that of the starting basalt. This bulk compositional change decreases the Cl solubility in the melt and increases the (measured concentration)/(modeled Cl solubility in melt) ratio. The interaction with brine increases the Cl content of the contaminated melt. The combined effects shift the resultant melt compositions such that the increase in the ordinate with increasing Cl/K_2O exceeds that observed for brine assimilation alone. The overall effect is to increase the dispersion of the data supporting the positive correlation. These processes, working in concert, have been considered to have been operative within many ocean-floor ridges and particularly within those characterized by fast to intermediate spreading rates (Michael and Schilling 1989; Michael and Cornell 1998). These processes may also have affected magmas supporting the growth of hot spot-related, volcanic ocean islands including the Galapagos (Koleszar et al. 2009), Loihi (Kent et al. 1999), and Gorgona islands (Shimizu et al. 2009), given the similarities in modeled trends and in glass and MI data (Fig. 6.21). Should this assimilation occur concurrently with fractional crystallization, the resulting magmas evolve via AFC processes (coupled assimilation and fractional crystallization). Clearly, fractional crystallization working in concert with these other processes will broaden the dispersion of the correlation to higher (measured concentration)/(modeled Cl solubility) ratios with increasing Cl/K_2O ratios in the ensuing fractions of melt. For example, the significant spread in the positively correlated data for the Galapagos Islands (Fig. 6.21c, d) may reflect AFC processes involving assimilation of altered ocean crust and brine.

Alternatively, the interaction of magma with hydrothermally altered, brine-bearing basaltic to gabbroic rocks encompassing the axial magma chambers may lead to

low-degree partial melting of the host rocks and subsequent assimilation and mixing of the Cl-enriched partial melt into the magma chamber (Coogan et al. 2003; Wanless et al. 2010, 2011; Lassiter et al. 2002). Partial melting of altered Cl-bearing host rocks is supported energetically by the latent heat released during crystallization of the basaltic magmas and by the fluxing effects of H_2O dissolved in the brine (Wanless et al. 2010, 2011; Lassiter et al. 2002). To represent this process, we have modeled a low-Cl/K_2O basaltic melt assimilating brine plus plagioclase only, clinopyroxene only, a gabbro-like mixture of anorthite and clinopyroxene, and a basaltic partial melt (Fig. 6.21). The latter composition (partial melt OGB1) was determined experimentally by Kvassnes and Grove (2008); it represents a melt of the phase assemblage plagioclase, augite, and olivine that is dominated by plagioclase and augite. Our modeling involves variable quantities (e.g., 0.01–1 wt%) of a 50:50 H_2O-NaCl brine and fixed quantities (e.g., 20 wt%) of assimilated silicate materials for the plagioclase-only, clinopyroxene-only, and the OGB1 melt calculations. The modeled results show positive, linear correlations mimicking those of the oceanic island and seafloor glass data, but the former involve minimal dispersion, which contrasts with the data for oceanic island and seafloor basalts showing significant dispersion about their positive correlations. This variability must reflect the coupled influences of fractional crystallization; brine assimilation; and contamination by altered amphiboles, altered seafloor crust, and/or basaltic partial melts. Furthermore, some MOR glasses from the East Pacific Rise, Juan de Fuca Ridge, and the Galapagos spreading center involve compositions ranging from basalt to dacite. These have been postulated to form via AFC-related partial melting at the tops of the axial magma chambers (Wanless et al. 2010). The spread in the silica content from these MOR glasses is derived from fractional crystallization. Moreover, the glasses show significant dispersion (Fig. 6.21) because the reduction in the Cl dissolution in the evolving melts induces strong increases in the (measured concentration)/(modeled Cl solubility in melt) ratio as the mixed melts become increasingly felsic and their Cl solubility drops.

The MI from the Austral Islands (Lassiter et al. 2002) display a minor dispersion about their positive correlation between the (measured concentration)/(modeled Cl solubility in melt) ratio versus Cl/K_2O. Interestingly, the most Cl-enriched MI show a distinct break-in-slope with Cl/K_2O ratios that exceed 2 (Fig. 6.21). This pattern is consistent with that of the positive correlation shown by the modeled relation for partial melting of the gabbro-like, plagioclase-clinopyroxene mixture, which also shows a break-in-slope. The modeled slope change occurs when the (measured concentration)/(modeled Cl solubility in melt) ratio exceeds 0.5, i.e., when the molten mixture of the primary basaltic melt, the brine, and the partial melt of plagioclase plus clinopyroxene achieves half of its maximum Cl solubility. The modeling for this partial melting process contrasts with all the others in that it involves variable quantities (e.g., 0.01–1 wt%) of a 50:50 H_2O-NaCl brine that increase proportionally with the quantities (e.g., 20–35 wt%) of plagioclase plus clinopyroxene. Given the change in the relationship between Cl/K_2O versus the (measured concentration)/(modeled Cl solubility in melt) ratio as the brine/(plagioclase + pyroxene) ratio varies, we suggest that the presence of tens of wt% Cl in the brine phase enhances the extent of partial melting of crustal rocks. Moreover, the potential

actions of Cl as a flux during partial melting is consistent with the observed influence of Cl on basaltic liquidus phase relations (Filiberto and Treiman 2009a) and with the apparent chemical interaction of Cl with Mg, Ca, and Fe in silicate melts (Webster et al. 2015). This mechanism is also consistent with the interpretations of Lassiter et al. (2002) for their variably Cl-enriched Austral Island samples.

We also include data for continental flood basalts, which include the large igneous provinces of the Permian Siberian traps, Russia and the Paleogene flood basalts, Mull, Scotland (Fig. 6.21). Both systems are far removed from potential seawater sources of Cl. MI from the former show strong enrichments in F as well as Cl. These have been interpreted using trace-element and isotopic data to indicate widespread assimilation of crustal rocks containing evaporates and carbonates by the basaltic magmas (Black et al. 2012). Volcanic degassing of the trap-forming magmas is estimated to have released thousands of gigatons of Cl and F to the atmosphere, potentially contributing to the degradation of global environmental conditions (Black et al. 2012). In this case the solubilities of Cl and F in fluids versus melts are of particular importance. The MI show a wide range in Cl/K_2O and a linear correlation with the measured/modeled Cl ratio. They are also characterized by wide variations in their Larsen index values (e.g., wt% $[K_2O + 1/3/SiO_2]$-[CaO + MgO + FeO]) with some values <−30. Those Siberian trap MI with the lowest Larsen indices involve melts with extreme enrichments in Mg and correspondingly high Cl solubilities (e.g., Cl concentrations exceeding 4.8 wt%). As a result, these data also show the largest range in the (measured concentration)/(modeled Cl solubility in melt) ratio. In contrast, the MI compositions for Mull are clustered and show little evidence of a positive correlation between Cl/K_2O and the (measured concentration)/(modeled Cl solubility in melt) ratio (Peate et al. 2012). The modest changes in Cl/K_2O, are accompanied by minor changes in the measured/modeled Cl ratio, which are consistent with the lack of seawater input during AFC processes at Mull as discussed by Peate et al. (2012).

Although most of the predicted trends in Fig. 6.21 show similar correlations and slopes with the MI and glass data, a selection of the most relevant type of assimilation and or partial melting processes involved, accompanied by fractional crystallization with or without degassing, also requires comparison of the bulk compositions (i.e., MgO, CaO, SiO_2, FeO, and other major components) of the final contaminated mixes of the initial 'starting' basalt melt, brine, and assimilated silicate components with those of the MI and basaltic glasses. We do not address this issue herein, but these additional considerations have been explored in detail by Le Roux et al. (2006), Koepke et al. (2007), Wanless et al. (2010), and others.

6.4.3 *Volcanic Processes/Halogen Degassing*

Processes controlling halogens in volcanic gases. Studying halogens in volcanic gases can contribute to deciphering the mechanisms of volatile exsolution, as well as the ascent and release of magmatic volatiles, and therefore can help to interpret the

dynamics of magma storage, ascent, and eruption. While the volcano-to-volcano variability in the halogen gas compositions mainly reflects diversity in gas origin and abundance in parental magmas (cf., 6.2.4), the temporal variations in gas chemistry, seen at each given volcano, are controlled by processes inside the volcano, and respond to variations in the state of volcano activity (Giggenbach 1996). The idea that halogens in volcanic gases can contribute to eruption forecasting was presented quite some time ago (Menyailov 1975). However, our limited understanding of halogen solubility/dissolution in BAA melts and vapour/melt partitioning (see above), and the multiplicity of processes (degassing, hydrothermal-magmatic gas interactions, scrubbing, mixing of distinct fluids) that together control gas chemistry (Giggenbach 1996; Oppenheimer et al. 2014; Fischer and Chiodini 2015), have prevented us from achieving rigorous quantitative models of halogen behaviour in volcanic gases, and from using them as reliable precursors of eruptions.

A substantial impetus for improved models of volcanic halogen degassing has been the recent progress in halogen measurements in both magmatic gases (e.g., Burton et al. 2007; cfr 2.4), and MI (Métrich and Wallace 2008; cfr 6.2.1). The emerging new models (e.g., Spilliaert et al. 2006a; Edmonds et al. 2009) are particularly useful for the interpretation of magmatic gas chemistry at mafic volcanoes where, compared to silicic volcanoes, the perturbing action of hydrothermal reactions (and consequent halogen scrubbing) is commonly less intense (Symonds et al. 2001).

Spilliaert et al. (2006b) used the volatile composition of a suite of MI from Mount Etna to derive a model of the pressure-related degassing behaviour of halogens during ascent, differentiation, and extrusion of H_2O-CO_2-rich alkali basalts. The pressure-dependent model of magmatic S-Cl-F gas evolution was constructed by applying (i) a H_2O-CO_2 saturation model (Newman and Lowenstern 2002) to dissolved concentrations of CO_2 and H_2O, and (ii) a step-by-step best-fitting procedure to S, Cl, and F contents in MI where K_2O was used to account for crystallization. Results indicated that halogens begin to exsolve at shallower pressures (100 MPa for Cl and $\leq$ 10 MPa for F) than S (140 MPa) during ascent of H_2O-rich basalts (see also Aiuppa et al. 2004a, b). An important consequence of this observation is that, although the evolutionary path of the magmatic gas phase actually depends on the dynamics (e.g., closed vs. open) of ascent, differentiation, and degassing of the magma, the magmatic gas S/Cl and S/F ratios invariably correlate with pressure, being high at high pressure (S/Cl > 30) and low at 0.1 MPa (S/Cl = 0.2–9; depending on conditions of magma ascent). These model results, corroborated by similar findings obtained at other arc volcanoes such as Stromboli (Métrich et al. 2001, 2010; Burton et al. 2007) and Yasur (Métrich et al. 2011), offer a reference framework for interpreting variations in S, Cl, and F in gas emissions from basaltic volcanoes; and, in particular, help explain the high S/halogen and CO_2/halogen ratios of magmatic gases seen during Hawaiian-style (Etna: Allard et al. 2005; Piton de la Fournaise: Allard et al. 2013), Strombolian-style (Yasur: Oppenheimer et al. 2006b; Stromboli: Burton et al. 2007), and Vulcanian-style (Eyjafjallajökull: Allard et al. 2010) explosive mafic eruptions. In all such instances, comparison between observations and models strongly suggests a deep derivation of gases erupted during basaltic explosive eruptions. On Stromboli

volcano, for example, the measured gas compositions suggest confining pressures of ~70–80 MPa (most energetic explosions) to ~20 MPa (smallest explosions) for the "syn-explosive gas source region", which correspond to depths between ~2.7 and 0.8 km below the vents (Burton et al. 2007). Similarly on Etna, quantitative modeling of the S/Cl ratio of the magmatic gas phase supports the idea that lava fountaining episodes are triggered by gas accumulation at about 1.5 km depth below the vent (Allard et al. 2005). The fact that explosions are driven by deeply originating gas implies a transition from closed- to open-system degassing and differential gas bubble transfer from depth (Burton et al. 2007). In contrast, the far-lower S/halogens ratios (S/Cl ~2; S/F ~4–9; see Table 6.3), seen in the majority of the quiescent, open-vent emissions of mafic volcanos, are suggestive of a shallower derivation for the emitted gases, consistent with near-surface, gas-melt separation during continuous shallow magma convective circulation (Shinohara 2008, 2013). Halogens only prevail over S (e.g., S/Cl and S/F gas ratios of <1) in the late stages of (residual) degassing, such as at lateral (secondary) vents and in the final phases of effusive eruptions (Aiuppa et al. 2002; Aiuppa 2009; Oppenheimer et al. 2011a; Mather et al. 2012).

Edmonds et al. (2009) extended the models of halogen degassing to H_2O-poor (Kilauea-like) basalts. These authors (and Edmonds and Gerlach 2007) characterised the halogen compositions of gases released at the Pu u Ō ō vent on Kilauea volcano with FTIR that they found to cover a range between S-rich, F-poor compositions and S-poor, F-rich compositions. Starting from compositions of silicate glasses (both MI and glass matrixes, as did Spilliaert et al. 2006b), they constructed a degassing model for halogens for closed- and open-system conditions, which demonstrated that the onset of halogen degassing in H_2O-poor basaltic magmas only occurs at shallow levels in the conduit (from pressures <1 MPa, or around 35 m depth below the magma-air interface). This behavior reflects low vapour/melt partition coefficients (≈1.5) for both Cl and F. Based on these model results, Edmonds et al. (2009) suggested that the range and trends in gas compositions merely reflect variable depths of the last gas-melt equilibration in the conduit during open-system degassing (see also Edmonds and Gerlach 2007), with more halogen-rich compositions prevailing during effusive phases (low-pressure, gas-melt separation at ≈0.1 MPa) and more S-rich, halogen-poor compositions prevailing during lava spattering (higher-pressure, gas-melt separation at ≈0.3 MPa). The authors also concluded that the differing diffusivities of S and halogens play little role in controlling the gas phase composition.

The results of Edmonds et al. (2009) are in qualitative agreement with those of Spilliaert et al. (2006a, b) for more hydrous basalts. This agreement indicates that some consensus has been reached for volcanic gases being poor in halogens and with high SO_2/HCl and SO_2/HF ratios at places where volatile-rich magmas supply deeply sourced gas bubbles, such as during (or shortly before; Aiuppa and Federico 2004) basaltic paroxysmal events (Allard 2010). Pulsatory supply of deeply-derived, halogen-poor magma/gas to the Erebus phonolitic lava lake possibly also controls the periodic fluctuations in gas compositions seen at this persistently degassing open-vent volcano (Oppenheimer et al. 2009, 2011b). Chlorine-

and F-rich gases are characteristic of late, shallow volcanic degassing, as in the concluding stages of basaltic eruptions, or during periods of reduced magma supply at persistently degassing volcanoes (see Aiuppa 2009).

The extent to which similar arguments apply to trace halogens (Br, I) is unfortunately unknown. Recent research at Etna volcano (Bobrowski and Giuffrida 2012), however, first reported the existence of cyclic changes in plume BrO/SO_2 ratios that possibly correlate with changes in volcanic activity style. Lübcke et al. (2014) also demonstrated a sizeable BrO/SO_2 ratio decrease in the weeks prior to major eruptive activity at Nevado del Ruiz volcano in Colombia. These observations are intriguing, because volcanic BrO can routinely be monitored from remote (i.e., safe) locations via conventional scanning-DOAS instruments. However, BrO is likely to make up only a fraction of the total, emitted volcanic Br in plumes (see 5.2c below). Additional research is needed to confirm the value of BrO/SO_2 observations for volcano monitoring.

Fluxes of volcanic halogens to the atmosphere. In contrast to S and CO_2, whose global budgets are dominated by anthropogenic emissions, halogens have their global geochemical cycles controlled (F, Br)—or at least substantially contributed (Cl, I)—by volcanism (Pyle and Mather 2009). Characterizing halogen emissions from volcanoes contributes, therefore, to our understanding of the mechanisms and rates of volatile transport from the mantle to the crust and atmosphere (see Frezzotti and Ferrando 2018), and brings profound insights into the extent of halogen recycling at convergent margins (see Barnes et al. 2018). The magnitude of halogen emissions also controls the environmental impacts of volcanic degassing and is key to understanding volcanic behaviour.

Volcanic halogen fluxes to the atmosphere can be estimated using two alternative and complementary methods. The petrological method (first established by Devine et al. 1984) determines volcanic halogen fluxes by combining knowledge of pre- (from MI) and post-eruptive (from matrix glasses) halogen contents in magmas (cfr 6.2.1) with estimates of eruption magnitude. With this technique, halogens fluxes from a given eruption can be established, or even time-averaged magma eruption rates for either a given volcano or a volcanic segment. Uncertainties in the technique include, among others: (i) the representativeness of MI, in which a variety of pre- and post-entrapment processes may render the volatile contents unrepresentative of the original magmatic volatile contents in the primitive magmas (Métrich and Wallace 2008); (ii) the difficulty in quantifying the contribution of non-erupted (intruded) magma to the volatile budget; and (iii) the lack of constraints on possible contributions from a separate magmatic vapour phase. Despite these uncertainties, the petrological method is unique in that it allows for estimation of the halogen yield of past eruptions (e.g., Kutterolf et al. 2013), and paves the way to obtaining time-averaged halogen fluxes integrated over long-term (*geological*) timescales. Wallace (2005), for example, has presented the currently most widely accepted "petrological" estimate of the Cl arc output that he assessed at 4–7 Tg/yr.

The alternative approach is to estimate *present-day* volcanic halogen emissions from the measurement of gas compositions (SO_2/halogen ratios) and spectroscopically derived SO_2 fluxes at actively degassing volcanoes (see Oppenheimer et al.

2014 for a review). Attempts to quantify volcanic halogen fluxes using volcanic gas compositions started in the 1970s (Cadle 1975), but have been complicated by uncertainties in volcanic SO_2 flux inventories (Oppenheimer et al. 2014) and large heterogeneities in SO_2/halogens ratios in volcanic gases (Figs. 6.8–6.9). The ranges in published global volcanic halogen inventories span two orders of magnitude for Cl and F, and up to four orders of magnitude for trace halogens (Br and I) (Fig. 6.22). Symonds et al. (1988) used an annual volcanic flux of 18.7 Tg of SO_2 and SO_2/halogens ratios in the 1–100 range to evaluate annual volcanic HCl and HF emissions at 0.4–11 and 0.06–6 Tg, respectively. Similarly uncertain fluxes of 0.7–8.6 Tg/yr for HF and 1.2–170 for HCl Tg/yr were more recently obtained by Halmer et al. (2002) using similar magmatic gas SO_2/halogen proxies. Results from these earlier studies demonstrated the urgent need to better constrain the characteristic (mean) SO_2/halogen signature of volcanic gas emissions. This task was undertaken by Pyle and Mather (2009), who critically reviewed the current volcanic gas dataset, and discussed the limiting factors for better constraining global volcanic fluxes. The authors identified two main issues. The first is that the available gas dataset is sparse and incomplete, and somewhat biased toward individual fumarole compositions. Since fumaroles at any given volcano are often diverse in composition, and potentially influenced by secondary processes (e.g., reactions with external fluids/wall-rocks and scrubbing of reactive components; Symonds et al. 2001), it remains uncertain to what extent their SO_2/halogen ratios are representative of the volcanic system as a whole. The second issue is that volcanic gas halogen compositions show not only large spatial diversity (within each volcano and from one volcano to another), but are also highly variable in time. Large changes in halogen gas compositions, from rapid (Allard et al. 2005; Burton et al. 2007; Oppenheimer and Kyle 2008; Oppenheimer et al. 2009) to more sluggish (Aiuppa et al. 2002, 2005), are observed at volcanoes that are routinely monitored for gas. Ultimately, Pyle and Mather (2009) calculated both geometric and flux-weighted means of SO_2/halogen ratios from their revised dataset to determine (using a global SO_2 output of 15 Tg/yr) the halogen output from arc volcanoes at 4.3 ± 1.0 Tg/yr for HCl and 0.5 ± 0.2 Tg/yr for HF (Fig. 6.22). The authors did not provide numbers for the Cl-F contribution from non-arc (within plate and/or rift-related) volcanoes, whose contribution to the total Cl budget was, however, considered to be modest (Sawyer et al. 2008a, b; Mather et al. 2012; Zelenski et al. 2013). The volcanic arc fluxes of Pyle and Mather (2009) are in reasonable agreement with those quoted by Fischer (2008) (5.6 and 0.24 Tg/yr for HCl and HF, respectively), and with the petrologically estimated Cl arc output of Wallace (2005) (4–7 Tg/yr) (Fig. 6.22). More recently, Shinohara (2013) inferred a globally averaged S_t/HCl (molar) ratio for arc volcanism of ~ 2, which combined with an updated SO_2 global emission inventory (total arc output, 16.8 Tg/yr) yields a global HCl output from persistently degassing arc volcanoes of 4.1 Tg/yr that is very close to the Pyle and Mather (2009) value.

We compiled a dataset of volcanic gas SO_2/halogens ratios from mafic volcanoes, based on measurements from more than 600 individual gas samples (Table 6.3). Data are compiled from Gerlach (2004), Aiuppa (2009), and Aiuppa

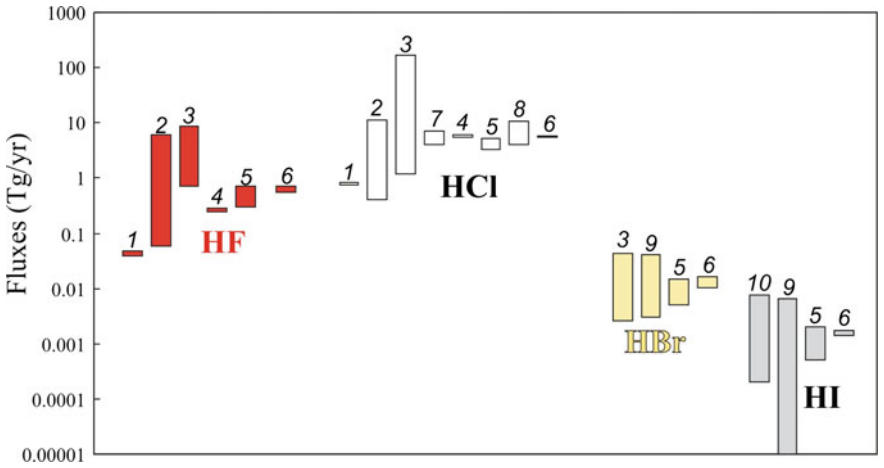

Fig. 6.22 A comparison of published and new (this study) inventories of global volcanic halogen fluxes (in Tg/yr). Data sources: (1) Cadle (1975); (2) Symonds et al. (1988); (3) Halmer et al. (2002); (4) Fischer (2008); (5) Pyle and Mather (2009); (6) this study (data from Table 6.2); (7) Wallace (2005); (8) Shinohara (2013); (9) Aiuppa et al. (2005); and (10) Snyder and Fehn (2002)

et al. (personal data from a UniPa-INGV unpublished dataset). This dataset is larger than that of Pyle and Mather (2009), suggesting that the quoted statistical parameters (mean, median, minimum, maximum; see Table 6.3), that we calculated for each SO_2/halogen ratio, are potentially more robust. The inferred mean S_t/HCl (molar) ratio for arc volcanism in our compilation is 1.7 (Table 6.3) or slightly lower than that quoted by Shinohara (2013) ($\sim$2). This leads to a global arc HCl output of 5.5 Tg/yr (Table 6.3 and Fig. 6.9). We also infer from data in Table 6.3 a global arc HF output of 0.58 Tg/yr, with an additional contribution of 0.15 Tg/yr from rift/within-plate volcanism (total output: 0.7 Tg/yr). Non-arc volcanism appears to contribute a trivial fraction of the total volcanic Cl output (Table 6.3).

One implication of the above studies is that, if a consensus can be reached on a global arc HCl output of 4.1–5.5 Tg/yr, then the efficiency of Cl recycling at subduction zones can be evaluated from comparison with input fluxes at the slab. Jarrard (2003) presented new measurements and mass-balance calculations to constrain the global-scale flux of Cl entering the slab (bound to sediments and crust materials) at $\sim$25 Tg/yr. Although uncertainties in both input and output fluxes remain large, these results appear to unambiguously suggest that only a fraction ($\sim$20%) of subducted Cl is re-emitted at volcanic arcs. The remaining fraction is transported back into the mantle (Kendrick et al. 2012a, b, 2013a, b; Barnes et al. 2018).

One new aspect that the studies of Shinohara (2013) and Taran (2009) revealed is that, in addition to persistent degassing, transport via hot and cold volcanic groundwater needs also to be considered to fully constrain the total volcanic Cl emission budget. Shinohara (2013) calculated that the annual amount of volcanic Cl, transported in the hydrological cycle, can be on the order of $\sim$6.1 Tg, raising

the total global volcanic Cl flux to ~10.6 Tg/yr. This total output also accounts for the (modest) Cl output contribution from explosive volcanism of 0.44 Tg/yr, of which 0.16 Tg/yr is from mafic explosive volcanism. These new results demonstrate that regional studies of Cl transport via cold and hot springs and groundwater should be prioritized in future years (Taran 2009). Note that the fraction of Cl recycled by arc volcanoes increases to ~50% if the total output (persistent degassing + hot/cold groundwater transport + explosive degassing) of Shinohara (2013) is used in the calculations.

The Br and I volcanic budgets have been less studied, and uncertainties associated with estimates will remain large until a more-comprehensive volcanic gas compositional dataset becomes available. Pyle and Mather (2009), for example, evaluated the global arc fluxes of HBr and HI at 0.005–0.0150 Tg/yr and 0.005–0.002 Tg/yr, respectively, based on gas plume compositions measured at only two actively degassing volcanoes in Nicaragua (Witt et al. 2008). Iodine isotope studies (Snyder and Fehn 2002) suggest, however, that gas emissions in Central American may not represent global arc mean emissions, given the I-rich nature of the subducted sediment component to this arc (Pyle and Mather 2009). We use a more complete trace halogen dataset, illustrated in Table 6.3 and Fig. 6.8, to attempt our own quantification of global trace halogen volcanic fluxes. We calculate ~0.0105 Tg/yr for HBr and ~0.0014 Tg/yr for HI. Most values are right in the middle of Pyle and Mather's (2009) range (Fig. 6.22). Our results suggest a dominant contribution from arc volcanism to trace halogen volcanic budgets (Table 6.3). We admit, however, that our volcanic gas dataset is unacceptably incomplete for non-arc volcanism; implying that the numbers may need extensive revision as new data become available.

Impacts. The emission and subsequent deposition of volcanogenic halogens result in a variety of environmental impacts, from the local and regional (Delmelle 2003; von Glasow 2010) to the global scale (Oppenheimer et al. 2014). One commonly evoked large-scale effect of explosive silicic eruptions is alteration of the stratospheric halogen cycle (Coffey 1996). The formation of volcanic aerosols, plus, eventually, the injection of sizeable quantities of volcanogenic halogens into the lower stratosphere (Solomon et al. 1993; Theys et al. 2009, 2014), is thought to lead to the "activation" of stratospheric halogens into reactive forms that in turn trigger large ozone depletion events, as seen in the case of Pinatubo from 1991 to 1993 (McCormick et al. 1995). Given the focus of this chapter on mafic volcanism, we refer to the above references and Robock (2000) for discussion of these Pinatubo-type impacts, and we concentrate instead on the effects of effusive/explosive basaltic volcanism. Although mafic plinian eruptions are relatively uncommon in nature, the "hot" convective plumes (Kaminski et al. 2011), formed during far more common lava fountaining episodes and/or large lava flow eruptions, still make basaltic eruptions prone to produce global-scale impacts. Long-range tropospheric dispersion of volcanic halogens in eruptive clouds is still debated (Tabazadeh and Turco 1993; Textor et al. 2003a; Prata et al. 2007), because it is unclear to what extent these water-soluble species can survive the scavenging action by hydrometeors. Modelling results (Textor et al. 2003b) indicate that

eruptions occurring in a relatively dry troposphere, such as near the poles, where the tropopause is also at a lower altitude, can meet the circumstances favourable for large scale-halogen dispersion. Icelandic eruptions are obviously good candidates. Significant stratospheric injection of volcanogenic halogens has, for example, been detected during the February 26th eruption of Hekla in 2000, which resulted in enhanced formation of active halogens (ClO_x and BrO_x) and strong stratospheric ozone loss (Rose et al. 2006). The strong ozone depletion detected in the tropospheric volcanic plume from Eyjafjallajökull in 2010 has also been attributed to catalytic heterogeneous reactions initiated by volcanic halogens (Vance et al. 2010). Icelandic eruptions are also known to have produced large-scale impacts that go beyond ozone depletion. The long-lived effusive eruption of Laki in 1783–1784 is famous for having injected 122 Tg of SO_2, 7 Tg of HCl and 15 Tg of HF in the upper troposphere-lower stratosphere (Thordarson et al. 1996). These massive volcanic emissions resulted in severe pollution in northern Europe that caused extreme weather and agricultural damage (Thordarson and Self 2003), which in turn eventually increased human mortality (Grattan et al. 2003; Witham and Oppenheimer 2005) and was a possible contributing factor to the French Revolution. While SO_2 was the likely trigger for the volcanic fog ("vog") events registered during such volcanic eruptions (Baxter 2000), HF probably played a central role in the poisoning of livestock (Thorarinsson 1979). HF is readily adsorbed onto volcanic ash particles (Óskarsson 1980; Delmelle et al. 2007), and is therefore scavenged as tephra settles out from eruptive plumes. Ingestion of bioavailable F (CaF_2) by grazing animals, and bioaccumulation in bone tissues, can eventually lead to deformity, lesions, and eventually death (Cronin et al. 2003). This happened during the 1970 eruption of Hekla (Óskarsson 1980), but fortunately was not repeated in 2010 during the Eyjafjallajökull eruption, possibly because hydromagmatic interactions during the vulcanian phase of the eruption prevented massive F release into the atmosphere (Gislason et al. 2011; Bagnato et al. 2013). Impacts from the recent (2014–2015) effusive Holuhraun eruption, the largest in Iceland for more than 200 years with 1.5 km^3 of lava erupted, were also minimised by the lower HF and HCl emissions (relative to the more evolved Laki magma), very minor explosivity (no ash production), and by the location and timing of the eruption, which occurred far away from the inhabited parts of the island, just north of the Vatnajökull glacier (Gislason et al. 2015; Pfeffer et al. 2015). This notwithstanding, the Bárðarbunga eruption in 2014–2015, which is thought to have released $\sim$11 Tg of SO_2 and $\leq$1 Tg of HCl, resulted in environmental pressure on the surface waters, soils, and vegetation of Iceland. This led to acidic precipitation (the lowest pH of precipitation, 105 km away from the source, was 3.2) and elevated dissolved H_2SO_4, HCl, HF, and metal concentrations in snow and precipitation (Gislason et al. 2015).

The large impacts produced by some Icelandic eruptions raise the question of what the environmental consequence could have been from the far more massive continental flood basalt eruptions. Extensive research on LIPs, such as the Deccan volcanic province (Self et al. 2008) and the Siberian Traps (Black et al. 2012), has indicated a huge release of halogens (e.g., $\sim$1 Tg of HCl per km^3 of erupted lava).

The environmental effects from such LIPs eruptions are hardly predictable, however, because they would have primarily depended upon the rate of gas emission (e.g., on gas fluxes), and ultimately on the poorly constrained, temporal distribution (e.g., total duration) and continuity (e.g., frequency of eruptions) of eruptive activity. Still, given the large lava productivity of LIPs (e.g., 800,000 km^3 for the Deccan Traps; Self et al. 2006), conservative calculations predict annual Cl emissions of $\sim$5 Mt/year that should have certainly resulted in measurable impacts, and that may have possibly initiated global environmental change (Font et al. 2011, 2014). The recent discovery of Cl-rich Fe hydroxides (akaganeite: ß-$Fe_2[OH]_3Cl$) in Cretaceous-Paleogene boundary sections in Europe (Font et al. 2011, 2014) has, for instance, been related to long-large transport, and severe climate-effects (i.e., acid rains), of magmatic Cl release from Deccan traps volcanism.

Passive (quiescent) degassing is a less spectacular, but certainly more continuous, mode of volcanic halogen release, and may eventually result in considerable, although more localized, effects. Halogens are deposited on the ground from tropospheric volcanic plumes via both dry and wet processes (Delmelle 2003). In a set of key papers, Delmelle et al. (2001, 2002, 2003) reported on the unusually high rate of acidic halogen deposition downwind from Masaya volcano, Nicaragua. Effects included visible damage to cultivation and acidification of soils. At Mount Etna, it was demonstrated that recurrent plume fumigation of the upper volcano flanks leads to 0.6–17 tons of HCl and 0.02–0.6 tons of HF being dry deposited daily. This corresponds to 0.1–10% of the daily halogen release from the summit craters (Aiuppa et al. 2004b). Since halogen acids are extremely water soluble, wet deposition is an additional major pathway for atmospheric deposition. The manifestly acidic nature of volcanic rainwaters (Harding and Miller 1982; Johnson and Parnell 1986; Kawaratani and Fujita 1990; Aiuppa et al. 2006; Calabrese et al. 2011) is typically a by-product of high HCl and HF depositions. Wet deposition of volcanogenic HF has been associated (Allibone et al. 2012) with anomalous occurrences of dental fluorosis in communities living downwind from the massive volcanic plumes emissions of Ambrym volcano in Vanuatu (Allard et al. 2015). Upon their deposition, halogens are partially trapped by volcanic soils. HF, in particular, shows a strong affinity for Al and Fe oxyhydroxides and allophanes present in andosols (Delmelle et al. 2003; D'Alessandro et al. 2012). This process may eventually protect volcanic groundwaters from acidification (Bellomo et al. 2007). Halogen sorption from such acidified soils, however, eventually combined with direct respiration of acid gases by stomata from foliage, can enrich vegetation in halogens living in the areas surrounding the volcanoes. There have been reports of high volcanic halogen contents in a variety of biological media, including lichens (Garrec et al. 1984; Notcutt and Davies 1989; Varrica et al. 2000), chestnut leaves, and pine needles (Bellomo et al. 2007). The effects (harmful or beneficial) of these unusually high F contents in plants are yet to be fully understood, as are the potential impacts on humans (D'Alessandro 2006).

One additional effect that has only recently been brought to light is that volcanic halogens do not only destroy ozone in the stratosphere during large-scale explosive eruptions (see above), but also in quiescent tropospheric plumes (Mather 2008; von

Glasow et al. 2009; Oppenheimer et al. 2010; Vance et al. 2010; von Glasow 2010; von Glasow and Crutzen 2014). This impact was originally evoked by Bobrowski et al. (2003) after their first discovery of reactive Br (BrO) in a volcanic plume. This initial detection was supported later by ground-based (Oppenheimer et al. 2006a; Bobrowski et al. 2007; Bobrowski and Platt 2007; Bani et al. 2009; Boichu et al. 2011; Kelly et al. 2013; General et al. 2014) and satellite (Hörmann et al. 2013) observations that demonstrated the regular presence of BrO in aged (minutes to hours old), tropospheric, volcanic plumes, along with other reactive halogen species such as ClO (Lee et al. 2005; Bobrowski et al. 2007) and OClO (Bobrowski et al. 2007). Measurements have failed to detect BrO at "hot" actively degassing vents (Oppenheimer et al. 2006a), suggesting that this species is not directly emitted by volcanoes, but rather produced by in-plume reactions between volcanic and atmospheric gases/aerosols. The role played by atmospheric reactions in forming BrO is, in fact, consistent with observations showing that plumes' BrO/SO_2 ratios (that typically fall in the 10^{-5} to 10^{-3} range) increase with increasing transport distances from volcanic craters (Bobrowski et al. 2007). There have been considerable efforts in modelling in an attempt to establish paths, mechanisms, and rates of reactions leading to BrO formation in plumes (Gerlach 2004; Oppenheimer et al. 2006a; Martin et al. 2006; Bobrowski et al. 2007; Roberts et al. 2009; Glasow 2010). Consensus has been reached that an essential step in BrO formation takes place at the magma-air interface in the so-called "effective source region" (von Glasow 2010), where a high-temperature volcanic gas-air mixture is formed at nearly thermodynamic equilibrium conditions, and sizeable amounts of Br radicals can initially develop (Gerlach 2004; Martin et al. 2006, 2009). In this source region, and in the later ambient-temperature downwind regime, the process is additionally initiated by reaction of volcanic HBr_g either in the gas (by reaction with OH radicals) or in acidic volcanic aerosols (Roberts et al. 2009; von Glasow 2010). These reactions form the radicals (Br_2, Br, HOBr, and $BrNO_2$; the latter after reaction with NO_x) that then fuel an autocatalytic cycle of BrO generation ("BrO explosion") and ozone depletion via reaction of Br with O_3 (Bobrowski et al. 2003, 2007, 2015). These models predict BrO/SO_2 ratios that match well the magnitude and rate of increase of BrO/SO_2 ratios measured in volcanic plumes (Roberts et al. 2009; von Glasow 2010). Simulations also foresee levels of O_3 depletion that are in agreement with those measured in tropospheric volcanic plumes (Oppenheimer et al. 2010; Vance et al. 2010; Kelly et al. 2013).

6.5 Concluding Remarks

Although most basaltic and andesitic magmas contain minor to trace-element levels of F and Cl and far lower Br and I contents, it is well demonstrated that F and Cl exert fundamental controls on magmatic, metasomatic, mineralizing, and volcanic processes; on melt properties including viscosity and diffusion; and on melt-mineral-vapor-hydrosaline liquid phase relations in mafic to intermediate magmatic systems.

Fluorine and Cl may also affect the dissolution of other components (including elements of economic significance) in hydrothermal fluids and eruptive vapors. The halogen contents of alkaline equivalents of these magmas (i.e., basanites to phonolites) are also variable, but they tend to contain higher concentrations than non-alkaline basaltic magmas. The concentration ranges of F and Cl in basaltic and andesitic magmas vary by as much as 4 orders-of-magnitude and those of Br and I by 3 orders-of-magnitude. Halogen contents in these magmas vary with, and hence serve as, geochemical indicators of partial melting, fractional crystallization, magma mixing, magmatic contamination, fluid exsolution, and weathering processes.

We have made great strides in understanding the partitioning of halogens between minerals, silicate melts, and fluids. In many cases we have enough partitioning data to understand the distribution of F and Cl between these phases. However, as yet, there is no general model for the prediction of F and Cl partitioning applicable to the common compositions of melts, crystals, and fluids at crustal P-T conditions. Our knowledge of the partitioning of the heavier halogens Br and I is even less. The effects of F on viscosity are well understood and incorporated into a current model for the calculation of magmatic melt viscosity. The effects of Cl appear much more complicated then those of F, but minor in magnitude, and, in most cases, any effect of Cl on melt viscosity can be ignored. The effects of Br and I on melt viscosity are unknown but, presuming they behave similarly to Cl, are expected to be minor. Fluorine and Cl affect the phase equilibria of BAA melts by complexing with alkaline earths and Fe. Although their effects on phase equilibria do not appear as great as those of H_2O and CO_2, they are significant and may explain the petrogenesis of halogen-rich (and often alkali-rich) magmas on terrestrial planets.

The diffusion of F and Cl in BAA magmas is known for a few melt compositions, but significant gaps in our knowledge exist for andesitic bulk compositions. Furthermore, the effects of F and Cl on the diffusion of major elements in BAA magmas are still relatively unknown.

Experimental contraints on the partitioning of F and Cl between BAA melts and fluids are reasonably well established, but equivalent data for F and Cl between melts-fluids-amphiboles-micas-apatites are quite limited and insufficient to fully investigate geochemical and petrologic interpretations of magmatic, metasomatic, mineralizing, and volcanic processes. Likewise, such data for Br and I are virtually non-existent for mafic to intermediate-silica melts, whether alkaline or not.

Improved experimental constraints, and associated thermodynamic and empirical modeling of halogen partitioning between silicate melts and the various relevant fluids are much needed to better understand volcanic degassing. Within igneous systems, halogen abundances also vary as a function of their concentrations in mantle source regions and the tectonic environment involved, which reflects the process of partial melting. With regard to eruptive systems, the global-scale variations of halogen abundances in volcanic gases are reasonably well known for Cl and F, but far less so for Br and I. Consequently, the relative contributions of mantle, crust, and recycled subducted materials (sediments/oceanic crust/serpentinites) to Br and I in volcanic gases remain poorly constrained, as are the global volcanic Br and I fluxes.

There have been major improvements in our ability to predict Cl and F abundances in volcanic gases using quantitative empirical models of halogen behaviour during decompression-driven degassing of mafic melts. Consensus has been reached for a relatively shallow release of halogens from ascending basaltic melts. However, a general thermodynamic model is still missing that can quantitatively link the evolution of halogens in melts with that in the coexisting magmatic gas phase.

The emission of volcanic halogens into the atmosphere produces a variety of long- to short-range impacts, both during eruptions and quiescence. The paths and consequences of this volcanic contribution to the air, water, and soil have been intensively studied in the past decades, but will require additional efforts before they become accurately understood.

Acknowledgements We acknowledge thoughtful reviews by Alan Boudreau, Michael Carroll, Tobias Fischer, Daniel Harlov, and Leonid Aranovich. We appreciate assistance in accessing and organizing data sets provided by Beth Goldoff. The following individuals kindly provided access to their data for publications in review and in press: Francis McCubbin, Roman Botcharnikov, Celia Dalou, and Marina Alletti. Phil Piccoli shared his apatites database, and Vladim Kamenetsky shared images of fluid inclusions. AA acknowledges the European Research Council for funding (ERC grant agreement No. 305377), JDW acknowledges support from NSF award EAR-1219484, and DRB thanks NSERC for their continued research support. Rock and mineral sample images courtesy of the Mineral and Gems collections of the American Museum of Natural History and provided by Jamie Newman and Beth Goldoff. AA dedicates this chapter to the memory of Roland Von Glasow, halogen-lover, generous man, and excellent scientist.

Appendix

References providing data for select figures.

Figure 6.1: Métrich et al. (1999, 2010, 2011), Wallace and Anderson (1999, 2010, 2011)), Fedele (2002), Horn and Schmincke (2000), Del Carlo and Pompilio (2004), Suh et al. (2008), Signorelli et al. (1999), Fulignati and Marianelli (2007), Fulignati et al. (2004, 1991), Frezzotti et al. (2004, 1991), Spilliaert et al. (2006a, b), Chazot et al. (1996), Marianelli et al. (1995), Elburg et al. (2006), Solovova et al. (2005), Salvioli-Mariani et al. (2002), Vaggelli et al. (1993), Cioni et al. (1998), Schiano et al. (2004), Churikova et al. (2007), Self and King (1996), Tolstykh et al. (2001, 2003), Vigouroux et al. (2009), Collins et al. (2009), Saito et al. (2010), Johnson et al. (2009), Naumov et al. (2003, 2008), Fourmentraux et al. (2012), Neave et al. (2012), Panina et al. (2011), Andreeva and Kovalenko (2011), Perfit et al. (1999), Michael et al. (1989, 1994), Yang and Scott (2005), Wade et al. (2006), Eschenbacher (1998), Webster et al. (1997, 2003, 2004, 2010), Webster and Duffield (1994), Cervantes and Wallace (2003), Humphreys et al. (2008, 2009), Blundy and Cashman (2001, 2005), Blundy et al. (2008), Straub and Layne (2003), Michael and Cornell (1998), Tappen et al. (2009), Webster and Rebbert (1998), Black et al. (2012), Bouvier et al. (2010), Coombs et al. (2004), Déruelle et al. (1992), Hansteen and Gurenko (1998), Hauri (2002), Jambon et al. (1995), Kendrick et al. (2012a, b, 2013a, b, 2014a, b), Kent et al. (1999, 2002), Kilgour

et al. (2013), Koleszar et al. (2009), Kovalenko et al. (2006), Lassiter et al. (2002), Lloyd et al. (2013), Lowenstern (1994), Mandeville et al. (2009), Mangler et al. (2014), Marks et al. (2014), Métrich and Wallace (2008), Michael and Schiling (1989), De Moor et al. (2013), Moune et al. (2007), Nadeau et al. (2013), Nielsen et al. (2000), Oppenheimer et al. (2011b), Peate et al. (2012), Portnyagin et al. (2012), Raffone et al. (2008), Renno et al. (2004), Rose-Koga et al. (2014), Le Roux et al. (2006), Rowe et al. (2011), Rowe and Lassiter (2009), Ruscitto et al. (2011), Saal et al. (2002), Sharygin et al. (2012), Shimizu et al. (2009), Sobolev et al. (2009), Straub (2008), Sugiura et al. (1963), Thomas et al. (2009), Thordarson and Self (1996), Thordarson et al. (1996), Villemant et al. (2008), Le Voyer et al. (2010), Wang et al. (2014), Wanless et al. (2010, 2011), Weston (2012), Kutterolf et al. (2015).

Figure 6.2: Kutterolf et al. (2013, 2015), Métrich et al. (1999, 2010), Fedele (2002), Horn and Schmincke (2000), Del Carlo and Pompilio (2004), Suh et al. (2008), Signorelli et al. (1999), Fulignati and Marianelli (2007), Fulignati et al. (2004), Frezzotti et al. (1991, 2004), Spilliaert et al. (2006a, b), Chazot et al. (1996), Marianelli et al. (1995), Cervantes and Wallace (2003), Elburg et al. (2006), Solovova et al. (2005), Salvili-Mariani et al. (2002), Vaggelli et al. (1993), Cioni et al. (1998), Schiano et al. (2004), Churikova et al. (2007), Self and King (1996), Tolstykh et al. (2001, 2003), Vigouroux et al. (2009), Collins et al. (2009), Saito et al. (2010), Johnson et al. (2009), Naumov et al. (2003), Fourmentraux et al. (2012), Neave et al. (2012), Panina et al. (2011), Andreeva and Kovalenko (2011), Perfit et al. (1999), Michael et al. (1989, 1994), Yang and Scott (2005), Wade et al. (2006), Eschenbacher (1998), Michael and Cornell (1998), Humphreys et al. (2009), Straub and Layne (2003), Webster et al. (2003), Black et al. (2012), Bouvier et al. (2010), Coombs et al. (2004), Déruelle et al. (1992), Hansteen and Gurenko (1998), Hauri (2002), Humphreys et al. (2008), Jambon et al. (1995), Kendrick et al. (2012a, b, 2013a, b, 2014a, b), Kent et al. (1999, 2002), Kilgour et al. (2013), Koleszar et al. (2009), Kovalenko et al. (2006), Lassiter et al. (2002), Lloyd et al. (2013), Lowenstern (1994), Mangler et al. (2014), Marks et al. (2014), Métrich and Wallace (2008), Michael and Schiling (1989), De Moor et al. (2013), Moune et al. (2007), Nadeau et al. (2013), Naumov et al. (2008), Neave et al. (2012), Nielsen et al. (2000), Spilliaert et al. (2006a, b), Oppenheimer et al. (2011b), Peate et al. (2012), Portnyagin et al. (2012), Raffone et al. (2008), Renno et al. (2004), Rose-Koga et al. (2014), Le Roux et al. (2006), Rowe et al. (2011), Rowe and Lassiter (2009), Ruscitto et al. (2011), Saal et al. (2002), Salvioli-Mariani et al. (2002), Sharygin et al. (2012), Shimizu et al. (2009), Sobolev et al. (2009), Straub (2008), Sugiura et al. (1963), Suh et al. (2008), Thordarson and Self (1996), Thordarson et al. (1996), Villemant et al. (2008), Le Voyer et al. (2010), Wade et al. (2006), Wang et al. (2014), Wanless et al. (2010, 2011), Weston (2012), Yang and Scott (2005), Kutterolf et al. (2015).

Figure 6.5: Most data sourced in Piccoli and Candela (2002) with additional analyses of Parat et al. (2011), Tang et al. (2012), Panina et al. (2011), Sheth et al. (2011), Boyce and Hervig (2009), Bryan (2006), Timina et al. (2006), Solovova et al. (2009), Patino Douce et al. (2011), Larrea et al. (2013), Orejana et al. (2008),

Arzamastesev et al. (2009), Rosatelli et al. (2007), Boudreau and Simon (2007), Delpech et al. (2004), Meurer et al. (2004), Heaman et al. (2006), Prelević et al. (2005).

Figure 6.21: Lassiter et al. (2002), Coombs et al. (2004), Jambon et al. (1995), Kent et al. (2002), Michael et al. (1989, 1994), Michael and Cornell (1998), Perfit et al. (1999), Wanless et al. (2010), Black et al. (2012), Koleszar et al. (2009), Peate et al. (2012), Shimizu et al. (2009).

References

Aiuppa A (2009) Degassing of halogens from basaltic volcanism: insights from volcanic gas observations. Chem Geol 263:99–109. https://doi.org/10.1016/j.chemgeo.2008.08.022

Aiuppa A, Federico C (2004) Anomalous magmatic degassing prior to the 5th April 2003 paroxysm on Stromboli. Geophys Res Lett 31:L14607. https://doi.org/10.1029/2004GL020458

Aiuppa A, Federico C, Paonita A, Pecoraino G, Valenza M (2002) S, Cl and F degassing as an indicator of volcanic dynamics: the 2001 eruption of Mount Etna. Geophys Res Lett 29(11): 1559. https://doi.org/10.1029/2002GL015032

Aiuppa A, Federico C, Giudice G, Gurrieri S, Paonita A, Valenza M (2004a) Plume chemistry provides insights into the mechanisms of sulfur and halogen degassing at basaltic volcanoes. Earth Planet Sci Lett 222:469–483

Aiuppa A, Bellomo S, D'Alessandro W, Federico C, Ferm M, Valenza M (2004b) Volcanic plume monitoring at Mount Etna by passive air sampling. J Geophys Res 109(D21):D21308

Aiuppa A, Federico C, Franco A, Giudice G, Gurrieri S, Inguaggiato S, Liuzzo M, McGonigle AJS, Valenza M (2005) Emission of bromine and iodine from Mount Etna volcano. Geochem Geophys Geosyst 6:Q08008. https://doi.org/10.1029/2005GC000965

Aiuppa A, Bellomo S, Brusca L, D'Alessandro W, Di Paola R, Longo M (2006) Major-ion bulk deposition around an active volcano (Mt. Etna, Italy). Bull Volcanol 68:255–265. https://doi.org/10.1007/s00445-005-0005-x

Aiuppa A, Baker DR, Webster JD (2009) Halogens in volcanic systems. Chem Geol 263:1–18

Allard P (2010) A CO_2-rich gas trigger of explosive paroxysms at Stromboli volcano, Italy. J Volcanol Geotherm Res 189:363–374

Allard P, Burton M, Muré F (2005) Spectroscopic evidence for a lava fountain driven by previously accumulated magmatic gas. Nature 433:407–410. https://doi.org/10.1038/nature03246

Allard P, Aiuppa A, Bani P, Métrich N, Bertagnini A, Gauthier PG, Parello F, Sawyer GM, Shinohara H, Bagnato R, Mariet C, Garaebiti E, Pelletier B (2009) Ambrym basaltic volcano (Vanuatu Arc): Volatile fluxes, magma degassing rate and chamber depth. AGU abs. V24C-04

Allard P, Burton MR, Oskarsson N, Michel A, Polacci M (2010) Chemistry and fluxes of magmatic gases powering the explosive trachyandesitic phase of Eyjafjallajökull 2010 eruption: constraints on degassing magma volumes and processes. In: Proceed AGU Fall Mtg, December, 2010

Allard P, La Spina A, Tamburello G, Aiuppa A, Di Muro A, Coppola D, Battaglia J, Burton M, Brenguier F, Staudacher T (2013) First measurement of magma degassing processes and co-varying seismic tremor during an eruption of Piton de la Fournaise hot spot basaltic volcano, Reunion island. In: Proceed IAVCEI 2013 Sci Assem, July 20–24, Kagoshima, Japan, Abs. 3A1_2G-O6

Allard P, Aiuppa A, Bani P, Métrich N, Bertagnini A, Gauthier P-J, Shinohara H, Sawyer G, Parello F, Bagnato E, Pelletier B, Garaebiti E (2015) Prodigious emission rates and magma

degassing budget of major, trace and radioactive volatile species from Ambrym basaltic volcano, Vanuatu island Arc. J Volcanol Geotherm Res 304:378–402
Alletti M (2007) Experimental investigation of halogen diffusivity and solubility in Etnean basaltic melts. PhD diss., University of Palermo, Italy, p 92
Alletti M, Baker DR, Freda C (2007) Halogen diffusion in a basaltic melt. Geochim Cosmochim Acta 71:3570–358
Alletti M, Baker DR, Scaillet B, Aiuppa A, Moretti R, Ottolini L (2009) Chlorine partitioning between a basaltic melt and H_2O-CO_2 fluids at Mount Etna. Chem Geol 263:37–50
Alletti M, Burgisser A, Scaillet B, Oppenheimer C (2014) Chloride partitioning and solubility in hydrous phonolites from Erebus volcano: a contribution towards a multi-component degassing model. Geo Res J 3–4:27–45
Allibone R, Cronin SJ, Charley DT, Neall VE, Stewart RB, and Oppenheimer C (2012) Dental fluorosis linked to degassing of Ambrym volcano, Vanuatu: a novel exposure pathway. Environ Geochem Health 34(2):155–170. https://doi.org/10.1007/s10653-010-9338-2
Andreeva IA, Kovalenko VI (2011) Evolution of the trachydacite and pantellerite magmas of the bimodal volcanic association of Dzarta-Khuduk, Central Mongolia: investigation of inclusions in minerals. Petrololgy 19:348–369
Anfiligov VN, Glyuk DS, Trufanova LG (1973) Phase relations in the interaction between granite and sodium fluoride at water vapor pressure of 1000 mg/cm^2. Geokhym 1:44–48
Anovitz LM, Labotka TC, Blencoe JG, Horita J (2004) Experimental determination of the activity-composition relations and phase equilibria of H_2O-CO_2-NaCl fluids at 500 °C, 500 bars. Geochim Cosmochim Acta 68:3557–3567
Aoki K, Ishiwaka K, Kanisawa S (1981) Fluorine geochemistry of basaltic rocks from continental and oceanic regions and petrogenetic application. Contrib Mineral Petrol 76:53–59
Aranovich LY (2013) Fluid–mineral equilibria and thermodynamic mixing properties of fluid systems. Petrol 21:539–549
Aranovich LY, Newton RC (1999) Experimental determination of CO_2–H_2O activity–composition relations at 600–1000 °C and 6–14 kbar by reversed decarbonation and dehydration reactions. Am Mineral 84:1319–1332
Aranovich LY, Zakirov IV, Sretenskaya NG. Gerya TV (2010) Ternary system H_2O-CO_2-NaCl at high T-P parameters: an empirical mixing model. Geochem Int 48:446–455
Aranovich LY, Newton RC, Manning CE (2013) Brine-assisted anatexis: experimental melting in the system haplogranite–H_2O–NaCl–KCl at deep-crustal conditions. Earth Planet Sci Lett 374:111–120
Arzamastsev AA, Arzamastseva LV, Bea F, Montero P (2009) Trace elements in minerals as indicators of the evolution of alkaline ultrabasic dike series: LA-ICP-MS data for the magmatic provinces of Northeastern Fennoscandia and Germany. Petrol 17(1):46–72
Audétat A, Lowenstern JB (2014) Melt Inclusions. In: Holland HD, Turekian KK (eds) Treatise on geochemistry, 2nd edn, vol 13, pp 143–173
Baasner A, Schmidt BC, Webb SL (2013a) Compositional dependence of the rheology of halogen (F, Cl) bearing-aluminosilicate melts. Chem Geology 346(C):172–183
Baasner A, Schmidt BC, Webb SL (2013b) The effect of chlorine, fluorine and water on the viscosity of aluminosilicate melts. Chem Geology 357:134–149
Baasner J, Hung I, Kemp TF, Dupree R, Schmidt BC, Webb SL (2014) Contraints on the incorporation mechanism of chlorine in peralkaline and peraluminous Na_2O-CaO-Al_2O_3-SiO_2 glasses. Am Mineral 99:1713–1723
Bagnato E, Aiuppa A, Bertagnini A, Bonadonna C, Cioni R, Pistolesi M, Pedone M, Hoskuldsson A (2013) Scavenging of sulphur, halogens and trace metals by volcanic ash: the 2010 Eyjafjallajökull eruption. Geochim Cosmochim Acta 103:138–160
Bailey JC (1977) Fluorine in granitic rocks and melts: a review. Chem Geol 19(1–4):1–42
Baker DR (1992) Estimation of diffusion coefficients during interdiffusion of geologic melts: calculations using transition state theory. Chem Geol 98:11–21
Baker DR (1993) The effect of F and Cl on the interdiffusion of peralkaline intermediate and silicic melts. Am Mineral 78:316–324

Baker DR, Alletti M (2012) Fluid saturation and volatile partitioning between melts and hydrous fluids in crustal magmatic systems: the contribution of experimental measurements and solubility models. Earth Sci Rev 114:298–324

Baker DR, Vaillancourt J (1995) Cl in albite melt: a volatile which increases melt viscosity. EOS 76:F-646 (abstract)

Balcone-Boissard H, Baker DR, Villemant B, Boudon G (2009) F and Cl diffusion in phonolitic melts: influence of the Na/K ratio. Chem Geol 263:89–98

Balcone-Boissard H, Boudon G, Cioni R, Webster JD, Zdanowicz G, Orsi G, Civetti L (2016) Chlorine as a geobarometer for alkaline magmas: evidence from a systematic study of the eruptions of Mount Somma-Vesuvius. Sci Rep 6:21726. https://doi.org/10.1038/srep21726

Bani P, Oppenheimer C, Tsanev V, Carn S, Cronin S, Crimp R, Calkins J, Charley D, Lardy M, Roberts T (2009) Surge in sulphur and halogen degassing from Ambrym volcano, Vanuatu. Bull Volcanol 71:1159–1168

Barnes JD, Straub SM (2010) Chlorine stable isotope variations in Izu Bonin tephra: implications for serpentinite subduction. Chem Geol 272:62–74

Barnes JD, Sharp ZD, Fischer TP (2008) Chlorine isotope variations across the Izu-Bonin-Mariana arc. Geol 36(11):883–886

Barnes JD, Sharp ZD, Fischer TP, Hilton DR, Carr MJ (2009) Chlorine isotope variations along the Central American volcanic front and back arc. Geochem Geophys Geosyst 10:Q11S17. https://doi.org/10.1029/2009GC002587

Barnes JD, Manning C, Scambelluri M, Selverstone J (2018) The behavior of halogens during subduction-zone processes. In: Harlov DE, Aranovich L (eds) The role of halogens in terrestrial and extraterrestrial geochemical processes: surface, crust, and mantle. Springer, Berlin, pp 545–590

Baxter PJ (2000) Impacts of eruptions on human health. In: Sigurdsson H, Houghton BF, McNutt SR, Rymer H, Stix J (eds) Encyclopedia of volcanoes. Academic Press, San Diego, pp 1035–1043

Beermann O (2010) The solubility of sulfur and chlorine in H_2O-bearing dacites of Krakatau and basalts of Mt. Etna. PhD diss., Leibniz Universität Hannover, Germany, p 107

Beermann O, Botcharnikov RE, Nowak M (2015) Partitioning of sulfur and chlorine between aqueous fluid and basaltic melt at 1050 °C, 100 and 200 MPa. Chem Geol 418:132–157

Bell AS, Webster JD (2015) Dissolved Cl, oxygen fugacity, and their effects on Fe behavior in a hydrous rhyodacite. Am Mineral 100:1595–1599

Bellomo S, Aiuppa A, D'Alessandro W, Parello F (2007) Environmental impact of magmatic fluorine emission in the Mt. Etna area. J Volcanol Geotherm Res 165:87–101

Bernini D, Wiedenbeck M, Dolejs D, Keppler H (2013) Partitioning of halogens between mantle minerals and aqueous fluids: implications for the fluid flow regime in subduction zones. Contrib Mineral Petrol 165:117–128

Beyer C, Klemme S, Wiedenbeck M, Stracke A, Vollmer C (2012) Fluorine in nominally fluorine-free mantle minerals: Experimental partitioning of F between olivine, orthopyroxene and silicate melts with implications for magmatic processes. Earth Planet Sci Lett 337–338:1–9

Bischoff JL, Rosenbauer RJ (1984) The critical point and two-phase boundary of seawater, 200 °C–500 °C. Earth Planet Sci Lett 68:172–180

Black BA, Elkins-Tanton LT, Rowe MC, Ukstins Peate I (2012) Magnitude and consequences of volatile release from the Siberian Traps. Earth Planet Sci Lett 317–318:363–373

Blaine FA, Rl L, Holtz F, Bruegmann GE (2011) The effect of Cl on Pt solubility in haplobaslatic melt: implications for micronugget formation and evidence for fluid transport of the PGEs. Geochim Cosmochim Acta 75:7792–7805

Blundy JD, Cashman KV (2001) Magma ascent and crystallization at Mount St. Helens, 1980–1986. Contrib Mineral Petrol 140:631–650

Blundy JD, Cashman KV (2005) Rapid decompression-driven crystallization recorded by melt inclusions from Mount St. Helens volcano. Geology 33:793–796

Blundy JD, Cashman KV, Berlo K (2008) Evolving magma storage conditions beneath Mount St. Helens inferred from chemical variations in melt inclusions from the 1980–1986 and current (2004–2006) eruptions. USGS Prof Pap 1750:755–790

Bobrowski N, Giuffrida G (2012) Bromine monoxide/sulphur dioxide ratios in relation to volcanological observations at Mt. Etna 2006–2009. Solid Earth 3:433–445

Bobrowski N, Platt U (2007) SO_2/BrO ratios studied in five volcanic plumes. J Volcanol Geotherm Res 166(3–4):147–160

Bobrowski N, Hönninger G, Galle B, Platt U (2003) Detection of bromine monoxide in a volcanic plume. Nature 423:273–276

Bobrowski N, von Glasow R, Aiuppa A et al (2007) Reactive halogen chemistry in volcanic plumes. J Geophys Res 112:D06311

Bobrowski N, von Glasow R, Giuffrida GB, Tedesco D, Aiuppa A, Yalire M, Arellano S, Johansson M, Galle B (2015) Gas emission strength and evolution of the molar ratio of BrO/SO_2 in the plume of Nyiragongo in comparison to Etna. J Geophys Res D: Atmos 120(1): 277–291

Bodnar RJ, Burnham CW, Sterner SM (1985) Synthetic fluid inclusions in natural quartz. III. Determination of phase equilibrium properties in the system H_2O-NaCl to 1000 °C and 1500 bars. Geochim Cosmochim Acta 49:1861–1873

Böhm A, Schmidt BC (2013) Fluorine and chlorine diffusion in phonolitic melt. Chem Geol 346:162–171

Boichu M, Oppenheimer C, Roberts TJ, Tsanev V, Kyle PR (2011) On bromine, nitrogen oxides and ozone depletion in the tropospheric plume of Erebus volcano (Antarctica). Atmos Environ 45(23):3856–3866

Bonifacie M, Endrzejewski N, Agrinier P, Humler E, Coleman M, Javoy M (2008) The chlorine isotopic composition of Earth's mantle. Science 319:1518–1520

Botcharnikov RE, Behrens H, Holtz F, Koepke J, Sato H (2004) Sulfur and chlorine solubility in Mt. Unzen rhyodacitic melt at 850 °C and 200 MPa. Chem Geol 213:207–225

Botcharnikov RE, Holtz F, Behrens H (2007) The effect of CO_2 on the solubility of H_2O-Cl fluids in andesitic melt. Eur J Mineral 19:671–680

Botcharnikov RE, Holtz F, Behrens H (2015) Solubility and fluid-melt partitioning of H_2O and Cl in andesitic magmas as a function of pressure between 50 and 500 MPa. Chem Geol 388:112–129. https://doi.org/10.1016/j.chemgeo.2015.07.019

Boudreau AE (1995) Fluid evolution in layered intrusions: evidence from the chemistry of the halogen-bearing minerals. In: Thompson JFH (ed) Magmas, fluids and ore deposits, Geol Soc Can Short Course Series, vol 23. pp 25–46

Boudreau A, Simon A (2007) Crystallization and degassing in the Basement Sill, McMurdo Dry Valleys. Antarctica. J Petrol 48(7):1369–1386

Boudreau AE, Mathez EA, McCallum IS (1986) Halogen geochemistry of the Stillwater and Bushveld complexes: evidence for transport of the platinum-group elements by Cl-rich fluids. J Petrol 27:967–986

Boudreau AE, Love C, Hoatson DM (1993) Variation in the composition of apatite in the Munni Munni Complex and associated intrusions of the West Pilbara Block, Western Australia. Geochim Cosmochim Acta 57:4467–4477

Boudreau AE, Stewart MA, Spivack AJ (1997) Stable Cl isotopes and origin of high-Cl magmas of the stillwater complex. Montana Geol 25(9):791–794

Bouvier A-S, Métrich N, Deloule E (2010) Light elements, volatiles, and stable isotopes in basaltic melt inclusions from Grenada, Lesser Antilles: inferences for magma genesis. Geochem Geophys Geosys 11(9):Q09004

Bowen NL, Schairer JF (1935) Grünerite from Rockport, Massachusetts, and a series of synthetic fluor-amphiboles. Am Mineral 20:543–551

Bowers TS, Helgeson HC (1983) Calculation of the thermodynamic and geochemical consequences of nonideal mixing in the system H_2O-CO_2-NaCl on phase relations in geologic systems: metamorphic equilibria at high pressures and temperatures. Am Mineral 68:1059–1075

Boyce JW, Hervig RL (2009) Apatite as a monitor of late-stage magmatic processes at Volcán Irazú, Costa Rica. Contrib Mineral Petrol 157:135–145
Boyce JW, Liu Y, Rossman GR, Guan Y, Eiler JM, Stolper EM, Taylor LA (2010) Lunar apatite with terrestrial volatile abundances. Nature 466(7305):466–469
Braga R, Morten L, Zanetti A (2006) Origin of a mica megacryst in an alkaline dyke from the Veneto volcanic province, Italy. Eur J Mineral 18:223–231
Brenan J (1994) Kinetics of fluorine, chlorine and hydroxyl exchange in fluorapatite. Chem Geol 110:195–210
Brenan JM (1993) Partitioning of fluorine and chlorine between apatite and aqueous fluids at high pressure and temperature: implications for the F and Cl content of high P-T fluids. Earth Planet Sci Lett 117:251–263
Brey GP, Bulatov VK, Girnis AV (2009) Influence of water and fluorine on melting of carbonated peridotite at 6 and 10 GPa. Lithos 112S:249–259
Bryan SE (2006) Petrology and geochemistry of the Quaternary caldera-forming, phonolitic Granadilla eruption, Tenerife (Canary Islands). J Petrol 47(8):1557–1589
Bureau H, Métrich N (2003) An experimental study of bromine behavior in water-saturated silicic melts. Geochem Cosmochim Acta 67(9):1689–1697
Bureau H, Keppler H, Métrich N (2000) Volcanic degassing of bromine and iodine: experimental fluid/melt partitioning data and applications to stratospheric chemistry. Earth Planet Sci Lett 183:51–60
Bureau H, Foy E, Raepsaet C, Somogyi A, Munsch P, Simon G, Kubsky (2010) Bromine cycle in subduction zones through in situ Br monitoring in diamond anvil cells. Geochem Cosmochim Acta 74:3839–3850
Burton M, Allard P, Muré F, La Spina A (2007) Magmatic gas composition reveals the source depth of slug-driven Strombolian explosive activity. Science 317:227–230
Cadle RD (1975) Volcanic emissions of halides and sulfur compounds to the troposphere and stratosphere. J Geophys Res 80:1650–1652
Calabrese S, Aiuppa A, Allard P, Bagnato E, Bellomo S, Brusca L, D'Alessandro W, Parello F (2011) Atmospheric sources and sinks of volcanogenic elements in a basaltic volcano (Etna, Italy). Geochim Cosmochim Acta 75(23):7401–7425
Candela PA (1986) Towards a thermodynamic model for the halogens in magmatic systems: an application to melt-vapor-apatite equilibria. Chem Geol 57:289–301
Carroll MR (2005) Chlorine solubility in evolved alkaline magmas. Ann Geophys 48(4/5): 619–631
Cervantes P, Wallace PJ (2003) Role of H_2O in subduction-zone magmatism: new insights from melt inclusions in high-Mg basalts from central Mexico. Geol 31(3):235–238
Chambefort I, Dilles JH, Longo AA (2013) Amphibole geochemistry of the Yanacocha Volcanics, Peru: evidence for diverse sources of magmatic volatiles related to gold ores. J Petrol 54:1017–1046. https://doi.org/10.1093/petrology/egt004
Chazot G, Menzies MA, Harte B (1996) Silicate glasses in spinel lherzolites from Yemen: origin and chemical composition. Chem Geol 134:159–179
Chevychelov VY (1999) Calcium effect on chlorine solubility in fluid-saturated granitic magmas. Geokhim 5:522–535
Chevychelov VY, Chevychelova TK (1997) Partitioning of Pb, Zn, W, Mo, Cl, and major elements between aqueous fluid and melt in the systems granodiorite (granite, leucogranite)-H_2O-NaCl-HCl. Neues Jahrb Mineral Abhand 172:101–115
Chevychelov VY, Suk NI (2003) Influence of the composition of magmatic melt on the solubility of metal chlorides at pressures of 0.1–3.0 kbar. Petrology 11:62–74
Chevychelov VY, Simakin AG, Bondarenko GV (2003) Mechanism of chlorine dissolution in water-saturated model granodiorite melt: applications of IR spectroscopic methods. Geochim Int 41(4):395–409
Chevychelov VY, Botcharnikov RE, Holtz F (2008a) Partitioning of Cl and F between fluid and hydrous phonolitic melt of Mt. Vesuvius at 850–1000 °C and 200 MPa. Chem Geol 256:172–184

Chevychelov VY, Botcharnikov RE, Holtz R (2008b) Experimental study of fluorine and chlorine partitioning between fluid and subalkaline basaltic melt. Dok Earth Sci 422(7):1089–1092
Chevychelov VY, Botcharnikov RE, Holtz R (2008c) Experimental study of fluorine and chlorine contents in mica (biotite) and their partitioning between mica, phonolite melt, and fluid. Geochem Int 46(11):1081–1089
Chiodini G, Marini L, Russo M (2001) Geochemical evidences of high-temperature hydrothermal brines at Vesuvio Volcano (Italy). Geochim Cosmochim Acta 65:2129–2147
Churikova TG, Woerner G, Mironov NL, Kronz A (2007) Volatile (S, Cl and F) and fluid mobile trace element compositions in melt inclusions: implications for variable fluid sources across the Kamchatka arc. Contrib Mineral Petrol 154:217–239
Cioni R, Marianelli P, Santacroce R (1998) Thermal and compositional evolution of the shallow magma chambers of vesuvius: evidence from pyroxene phenocrysts and melt inclusions. J Geophys Res B103:18277–18294
Cochain B, Sanloup C, de Grouchy C, Crépisson C, Bureau H, Leroy C, Kantor I, Irifune T (2015) Bromine speciation in hydrous silicate melts at high pressure. Chem Geol 404:18–26
Coffey MT (1996) Observations of the impact of volcanic activity on stratospheric chemistry. J Geophys Res 101:6767–6780
Collins SJ, Pyle DM, Maclennan J (2009) Melt inclusions track pre-eruption storage and dehydration of magmas at Etna. Geology 37:571–574
Comeforo JE, Kohn JA (1954) Synthetic asbestos investigations, I: study of synthetic fluor-tremolite. Am Mineral 39:537–548
Coogan LA, Mitchell NC, O'Hara MJ (2003) Roof assimilation at fast spreading ridges: an investigation combining geophysical, geochemical, and field evidence. J Geophys Res 108. https://doi.org/10.1029/2001JB001171
Coombs ML, Sisson TW, Kimura J-I (2004) Ultra-high chlorine in submarine Kilauea glasses: evidence for direct assimilation of brine by magma. Earth Planet Sci Lett 217:297–313
Coulson IM, Dipple GM, Raudsepp M (2001) Evolution of HF and HCl activity in magmatic volatiles of the gold-mineralized Emerald Lake pluton, Yukon Territory, Canada. Mineral Deposita 36:594–606
Crépisson C, Blanchard M, Bureau H, Sanloup C, Withers AC, Khodja H, Surblé S, Raepsaet C, Béneut K, Leroy C, Giur P, Balan E (2014) Clumped fluoride-hydroxl defects in forsterite: implications for the upper-mantle. Earth Planet Sci Lett 390:287–295
Cronin SJ, Neall VE, Lecointre JA, Hedley MJ, Loganathan P (2003) Environmental hazards of fluoride in volcanic ash: a case study from Ruapehu volcano, New Zealand. J Volcanol Geotherm Res 121:271–291
Cullen JT, Barnes JD, Hurwitz S, Leeman WP (2015) Tracing chlorine sources of thermal and mineral sprins along and across the Cascade Range using halogen concentrations and chlorine isotope compositions. Earth Planet Sci Lett 426:225–234
D'Alessandro W (2006) Human fluorosis related to volcanic activity: a review. In: Kungolos AG, Brebbia CA, Samaras CP, Popov V (eds), Environmental toxicology. WIT Press, Southampton, UK, pp 21–30. http://www.earthprints.org/handle/2122/2590
D'Alessandro W, Bellomo S, Parello F (2012) Fluorine adsorption by volcanic soils at Mt. Etna, Italy. Appl Geochem 27:1179–1188
Dalou C, Mysen BO (2015) The effect of H_2O on F and Cl solubility and solution mechanisms of in aluminosilicate melts at high pressure and high temperature. Am Mineral 100:633–643
Dalou C, Koga KT, Shimizu N, Boulon J, Devidal J-L (2012) Experimental determination of F and Cl partitioning between lherzolite and basaltic melt. Contrib Mineral Petrol 163:591–609
Dalou C, Koga KT, Le Voyer M, Shimizu N (2014) Contrasting partition behavior of F and Cl during hydrous mantle melting: implications for Cl/F in arc magmas. Prog Earth Planet Sci 1(1):26. https://doi.org/10.1186/s40645-014-0026-1
De Vivo B, Torok K, Ayuso RA, Lima A, Lirer L (1995) Fluid inclusion evidence for magmatic silicate/saline/CO_2 immiscibility and geochemistry of alkaline xenoliths from Ventotene Island, Italy. Geochim Cosmochim Acta 59(14):2941–2953

Del Carlo P, Pompilio M (2004) The relationship between volatile content and the eruptive style of basaltic magma: the Etna Case. Ann Geophys 47:1423–1432

Delmelle P (2003) Environmental impacts of tropospheric volcanic gas plumes. In: Oppenheimer C, Pyle DM, and Barclay J (eds) Volcanic degassing, vol 213. Geol Soc Spec Publ, pp 381–399

Delmelle P, Stix J, Bourque CPA, Baxter PJ, Garcia Alvarez J, Barquero J (2001) Loading in the vicinity of Masaya Volcano, a major sulfur and chlorine source in Nicaragua. Environ Sci Technol 35:1289–1293

Delmelle P, Stix J, Baxter PJ, Garcia-Alvarez J, Barquero J (2002) Atmospheric dispersion, environmental effects and potential health hazard associated with the low-altitude gas plume of Masaya volcano, Nicaragua. Bull Volcanol 64:423–434

Delmelle P, Delfosse T, Delvaux B (2003) Sulfate, chloride and fluoride retention in andosols exposed to volcanic acid emissions. Environ Pollut 126:445–457

Delmelle P, Lambert M, Dufrene Y, Gerind P, Oskarsson N (2007) Gas/aerosol–ash interaction in volcanic plumes: new insights from surface analyses of fine ash particles. Earth Planet Sci Lett 259:159–170

Delpech G, Grégoire M, O'Reilly SY, Cottin JY, Moine B, Michon G, Giret A (2004) Feldspar from carbonate-rich silicate metasomatism in the shallow oceanic mantle under Kerguelen Islands (South Indian Ocean). Lithos 75(1–2):209–237

Déruelle B, Dreibus G, Jambon A (1992) Iodine abundances in oceanic basalts: implications for Earth dynamics. Earth Planet Sci Lett 108(4):217–227

Devine JD, Sigurdsson H, Davis AN (1984) Estimate of sulphur and chlorine yield to the atmosphere from volcanic eruptions and potential climatic effects. J Geophys Res 89:6309–6325

Dingwell D (1987) Melt viscosities in the system $NaAlSi_3O_8$–H_2O–F_2O_{-1}. In: Mysen BO (ed) Magmatic processes; physicochemical principles. Geochemical Society, University Park, pp 423–431

Dingwell DB (1985) The structures and properties of fluorine-rich magmas: a review of experimental studies. In: Taylor RP, Strong DF (eds) Recent advances in the geology of granite-related mineral deposits, vol 39. Can Inst Mineral Metal, pp 1–12

Dingwell DB, Hess K-U (1998) Melt viscosities in the system Na-Fe-Si-O-F-Cl: Contrasting effects of F and Cl in alkaline melts. Am Mineral 83:1016–1021

Dingwell DB, Scarfe CM (1984) Chemical diffusion of fluorine in jadeite melt at high pressure. Geochim Cosmochim Acta 48:2517–2525

Dingwell DB, Scarfe CM (1985) Chemical diffusion of fluorine in melts in the system Na_2O-Al_2O_3-SiO_2. Earth Planet Sci Lett 73:377–384

Dingwell DB, Scarfe CM, Cronin DJ (1985) The effect of fluorine on viscosities in the system Na_2O-Al_2O_3-SiO_2: implications for phonolites, trachytes and rhyolites. Am Mineral 70:80–87

Doherty AL, Webster JD, Goldoff BA, Piccoli PM (2014) Partitioning behavior of chlorine and fluorine in felsic melt-fluid(s)-apatite systems at 50 MPa and 850–950 °C. Chem Geol. https://doi.org/10.1016/j.chemgeo.2014.06.023

Dolejs D (2005) Evidence for fluoride melts in Earth's mantle formed by liquid immiscibility: comment and reply. Geology 33:e76–e77. https://doi.org/10.1130/0091-7613-33.1e76

Dolejs D, Baker DR (2004) Thermodynamic analysis of the system Na_2O-K_2O-CaO-Al_2O_3-SiO_2-H_2O-F_2O_{-1}: stability of fluorine-bearing minerals in felsic igneous suites. Contrib Mineral Petrol 146:762–778

Dolejs D, Baker DR (2006) Fluorite solubility in hydrous haplogranitic melts at 100 MPa. Chem Geol 225:40–60

Dolejs D, Baker DR (2007a) Liquidus equilibria in the system K_2O-Na_2O-Al_2O_3-SiO_2-F_2O_{-1}-H_2O to 100 MPa: I. Silicate-fluoride liquid immiscibility in anhydrous systems. J Petrol 48(4): 785–806

Dolejs D, Baker DR (2007b) Liquidus equilibria in the system K_2O-Na_2O-Al_2O_3-SiO_2-F_2O_{-1}-H_2O to 100 MPa: II. Differentiation paths of fluorosilicic magmas in hydrous systems. J Petrol 48(4):807–828

Dolejs D, Zajacz Z (2018) Halogens in silicic magmas and their hydrothermal systems. In: Harlov DE, Aranovich L (eds) The role of halogens in terrestrial and extraterrestrial geochemical processes: surface, crust, and mantle. Springer, Berlin, pp 431–543

Dong P (2005) Halogen-element behaviour in apatites, scapolite, and sodalite: an experimental investigation with field applications. Unpub PhD diss., Univ. Saskatchewan, p 222

Driesner T, Heinrich CA (2007) The system H_2O-NaCl. Part. I: correlation formulae for phase relations in temperature-pressure-composition space from 0 to 1000 °C, 0 to 5000 bar, and 0 to 1 X_{NaCl}. Geochim Cosmochim Acta 71:4880–4901

Drinkwater JL, Czamanski GK, Ford AB (1990) Apatite of the Dufek intrusion: Distribution, parageneis, and chemistry. Can Mineral 28:835–855

Duan Z, Moller N, Weare JH (1995) Equation of state for the NaCl-H2O-CO_2 system: prediction of phase equilibria and volumetric properties. Geochim Cosmochim Acta 59:2869–2882

Eastoe CJ, Guilbert JM (1992) Stable chlorine isotopes in hydrothermal processes. Geochim Cosmochim Acta 56(12):4247–4255

Edgar AD, Lloyd FE, Vukadinovic D (1994) The role of fluorine in the evolution of ultrapotassic magmas. Mineral Petrol 51:173–193

Edgar AD, Pizzolato LA, Sheen J (1996) Fluorine in igneous rocks and minerals with emphasis on ultrapotassic mafic and ultramafic magmas and their mantle source regions. Mineral Mag 60:243–257

Edmonds M, Gerlach TM (2007) Vapor segregation and loss in basaltic melts. Geo 35:751–754

Edmonds M, Gerlach TM, Herd RA (2009) Halogen degassing during ascent and eruption of water-poor basaltic magma. Chem Geol 263:122–130

Eggenkamp H (2014) The geochemistry of stable chlorine and bromine isotopes. In: Advances in isotope geochemistry. Springer, Berlin, p 142

Einali M, Alirezaei S. Zaccarini F (2014) Chemistry of magmatic and alteration minerals in the Chahfiruzeh porphyry copper deposit, south Iran: implications for the evolution of the magmas and physicochemical conditions of the ore fluids. Turkish J Earth Sci 23:147–165. https://doi.org/10.3906/yer-1301-1

Elburg MA, Kamenetsky VS, Nikogosian IK, Foden JD, Sobolev AV (2006) Coexisting high- and low-calcium melts identified by mineral and melt inclusion studies of a subduction-influenced syncollisional magma from South Sulawesi, Indonesia. J Petrol 47:2433–2462

Ershova ZP (1957) Equilibrium of immiscible liquids in the systems of the MeF_2-Al_2O_3-SiO_2 type. Geochemistry 4:350–358

Ershova ZP, Olshanskii YI (1957) Equilibrium of immiscible liquids in the systems of the MeF_2-MeO-SiO_2 type. Geochemistry 3:257–266

Eschenbacher, A (1998) Open-system degassing of a fractionating, alkaline magma, Mount Erebus, Ross Island, Antarctica. Unpublished Master's Thesis, New Mexico Institute of Mining and Technology, Socorro

Evans KA, Mavrogenes JA, O'Neill HS, Keller NS, Jang L-Y (2008) A preliminary investigation of chlorine XANES in silicate glasses. Geochem Geophys Geosys 9(10). https://doi.org/10.1029/2008GC002157

Fabbrizio A, Stalder R, Hametner K, Günther D, Marquardt K (2013a) Experimental partitioning of halogens and other trace elements between olivine, pyroxenes, amphibole and qaqueous fluid at 2 GPa and 900–1300°C. Contrib Mineral Petrol 166:639–653

Fabbrizio A, Stalder R, Hametner K, Günther D (2013b) Experimental chlorine partitioning between forsterite, enstatite and aqueous fluid at upper mantle conditions. Geochim Cosmochim Acta 121:684–700

Fedele L (2002) Studies of magmatic systems. PhD Diss., Virginia Polytechnic Institute, State University, Blacksburg, VA, pp 1–69

Fiege A, Behrens H, Holtz F, Adams F (2014) Kinetic vs. thermodynamic control of degassing of H_2O-S ± Cl-bearing andesitic melts. Geochim Cosmochim Acta 125:241–264

Filiberto J, Treiman AH (2009a) The effect of chlorine on the liquidus of basalt: first results and implications for basalt genesis on Mars and Earth. Chem Geol 263(1–4):60–68

Filiberto J, Treiman AH (2009b) Martian magmas contained abundant chlorine, but little water. Geology 37(12):1087–1090

Filiberto J, Wood J, Dasgupta R, Shimizu N, Le L, Treiman AH (2012) Effect of fluorine on near-liquidus phase equilibria of a Fe-Mg rich basalt. Chem Geol 312–313:118–126

Filiberto J, Dasgupta R, Gross J, Treiman AH (2014) Effect of chlorine on near-liquidus phase equilibria of an Fe-Mg-rich tholeiitic basalt. Contrib Mineral Petrol 168:1027

Fischer TP (2008) Fluxes of volatiles (H_2O, CO_2, N_2, Cl, F) from arc volcanoes. Geochem Int 42:21–38

Fischer TP, Chiodini G (2015) Volcanic, magmatic and hydrothermal gases. In: The encyclopedia of volcanoes, 2nd edn, Elsevier, pp. 779–796. https://doi.org/10.1016/B978-0-12-385938-9.00045-6

Foley SF, Taylor WR, Green DH (1986a) The role of fluorine and oxygen fugacity in the genesis of the ultrapotassic rocks. Contrib Mineral Petrol 94:183–192

Foley SF, Taylor WR, Green DH (1986b) The effect of fluorine on phase relationships in the system $KAlSiO_4$-Mg_2SiO_4-SiO_2 at 28 kbar and the solution mechanism of fluorine in silicate melts. Contrib Mineral Petrol 93:46–55

Font E, Nédélec A, Ellwood BB, Mirao J, Silva PF (2011) A new sedimentary benchmark for the Deccan Traps volcanism? Geophys Res Lett 38:L24309. https://doi.org/10.1029/2011GL049824

Font E, Fabre S, Nédélec A, Adatte T, Keller G, Veiga-Pires C, Ponte J, Mirao J, Khozyem H, Spangenberg JE (2014) Atmospheric halogen and acid rains during the main phase of Deccan eruptions: Magnetic and mineral evidence. Geol Soc Am Spec Pap 505. https://doi.org/10.1130/2014.2505(18)

Fontaine FJ, Wilcock WSD (2006) Dynamics and storage of brine in mid-ocean ridge hydrothermal systems. J Geophys Res 111:B06102. https://doi.org/10.1029/2005JB003866

Fourmentraux C, Metrich N, Bertagnini A, Rosi M (2012) Crystal fractionation, magma step ascent, and syn-eruptive mingling: the Averno 2 eruption (Phlegraean Fields, Italy). Contrib Mineral Petrol 163:1121–1137

Fournier RO (1987) Conceptual models of brine evolution ion magmatic-hydrothermal systems. US Geol Surv Prof Paper 1350:1487–1506

Foustoukos DI, Seyfried WE Jr (2007a) Fluid phase separation processes in submarine hydrothermal systems. Rev Mineral Geochem 65:213–239

Foustoukos DI, Seyfried WE Jr (2007b) Trace element partitioning between vapor, brine and halite under extreme phase separation conditions. Geochim Cosmochim Acta 71:2056–2071

Francis P, Burton MR, Oppenheimer C (1998) Remote measurements of volcanic gas compositions by solar occultation spectroscopy. Nature 396:567–570

Frank MR, Candela PA, Piccoli PM (2003) Alkali exchange equilibria between a silicate melt and coexisting magmatic volatile phase: An experimental study at 800 °C and 100 MPa. Geochim Cosmochim Acta 67(7):1415–1427

Frezzotti ML, Ferrando S (2018) The role of halogens in the lithospheric mantle. In: Harlov DE, Aranovich L (eds) The role of halogens in terrestrial and extraterrestrial geochemical processes: surface, crust, and mantle. Springer, Berlin, pp 805–845

Frezzotti ML, De Vivo B, Clocchiatti R (1991) Melt-mineral-fluid interactions in ultramafic nodules from alkaline lavas of Mount Etna (Sicily, Italy): melt and fluid inclusion evidence. J Volcanol Geotherm Res 47:209–219

Frezzotti ML, Andersen T, Neumann ER, Simonsen SL (2002) Carbonatite melt-CO_2 fluid inclusions in mantle xenoliths from Tenerife, Canary Islands: a story of trapping, immiscibility and fluid-rock interaction in the upper mantle. Lithos 64:77–96

Frezzotti M-L, Peccerillo A, Zanon V, Nikogosian IK (2004) Silica-rich melts in quartz xenoliths from Vulcano island and their bearing on processes of crustal anatexis and crust-magma interaction beneath the Aeolian Arc, Southern Italy. J Petrol 45:3–26

Frezzotti ML, Ferrando S, Peccerillo A, Petrelli M, Tecce F, Perucchi A (2010) Chlorine-rich metasomatic H_2O-CO_2 fluids in amphibole-bearing peridotites from Inhjibara (Lake Tana region, Ethiopian plateau): nature and evolution of volatiles in the mantle of a region of continental flood basalts. Geochim Cosmochim Acta 74:3023–3039

Frost BR, Touret JLR (1989) Magmatic CO_2 and saline melts from the Sybille monzosyenite, Laramie anorthosite complex, Wyoming. Contrib Mineral Petrol 103:178–186

Fulignati P, Marianelli P (2007) Tracing volatile exsolution within the 472 AD 'Pollena' magma chamber of Vesuvius (Italy) from melt inclusion investigation. J Volcanol Geotherm Res 161:289–302

Fulignati P, Kamenetsky VS, Marianelli P, Sbrana A, Mernagh TP (2001) Melt inclusion record of immiscibility between silicate, hydrosaline, and carbonate melts: applications to skarn genesis at Mount Vesuvius. Geology 29:1043–1046

Fulignati P, Marianelli P, Santacroce R, Sbrana A (2004) Probing the Vesuvius magma chamber-host rock interface through xenoliths. Geol Mag 141:417–428

Fulignati P, Kamenetsky VS, Marianelli P, Sbrana A (2013) PIXE mapping on multiphase fluid inclusions in endoskarn xenoliths of AD 472 eruption of Vesuvius (Italy). Period Mineral 82(2):291–297

Gál B, Molnár F, Guzmics T, Mogessie A, Scabó C, Peterson DM (2013) Segregation of magmatic fluids and their potential in the mobilization of platinum-group elements in the South Kawishiwi Intrusion, Duluth Complex, Minnesota—Evidence from petrography, apatite geochemistry and coexisting fluid and melt inclusions. Ore Geol Rev 54:59–80

Garrec JP, Plebin R, Faivre-Pierret RX (1984) Impact of volcanic fluoride and SO_2 emissions from moderate activity volcanoes on surrounding vegetation. Bull Volcanol 47:491–496

Gascoyne M, Davison CC, Ross JD, Pearson R (1987) Saline groundwaters and brines in plutons in the Canadian Shield. In: Fritz P, Frape SK (eds) Saline water and gases in crystalline rocks, vol 33. Geol Assoc Canada Spec Pap, pp 53-68

General S, Bobrowski N, Pöhler D, Weber K, Fischer C, Platt U (2014) Airborne I-DOAS measurements at Mt. BrO and OClO evolution in the plume, J Volcanol Geotherm Res. https://doi.org/10.1016/j.jvolgeores.2014.05.012

Gerlach TM (2004) Volcanic sources of tropospheric ozone-depleting trace gases. Geochem Geophys Geosyst 5:Q09007. https://doi.org/10.1029/2004GC000747

Giehl C, Marks MAW, Nowak M (2014) An experimental study on the influence of fluorine and chlorine on phase relations in peralkaline phonolitic melts. Contrib Mineral Petrol 167:977

Giesting PA, Filiberto J (2014) Quantitative models linking igneous amphibole composition with magma Cl and OH content. Am Mineral 99:852–865

Giggenbach WF (1996) Chemical composition of volcanic gases. In: Scarpa R, Tilling RI (eds) Monitoring and mitigation of volcanic hazards. Springer, Berlin

Giordano D, Romano C, Dingwell DB, Poe B, Behrens H (2004) The combined effects of water and fluorine on the viscosity of silicic magmas. Geochim Cosmochim Acta 68:5159–5168

Giordano D, Russell JK, Dingwell DB (2008) Viscosity of magmatic liquids: a model. Earth Planet Sci Lett 271:123–134

Gíslason SR, Hassenkam T, Nedel S, Bovet N, Eiriksdottir ES, Alfredsson HA, Hem CP, Balogh ZI, Dideriksen K, Oskarsson N, Sigfusson B, Larsen G, Stipp LS (2011) Characteriztion of Eyjafiallajokull volcanic ash particles and a protocol for rapid risk assessment. Proc Natl Acad Sci 3:7307–7312. https://doi.org/10.1073/pnas.1015053108

Gíslason SR, Stefánsdóttir G, Pfeffer MA, Barsotti S, Jóhannsson T, Galeczka I, Bali E, Sigmarsson O, Stefánsson A, Keller NS, Sigurdsson A, Bergsson B, Galle B, Jacobo VC, Arellano S, Aiuppa A, Jónasdóttir EB, Eiríksdóttir ES, Jakobsson S, Guofinnsson GH, Halldórsson SA, Gunnarsson H, Haddadi B, Jónsdóttir I, Thordarson T, Riishuus M, Högnadóttir T, Dürig T, Pedersen GBM, Höskuldsson A, Gudmundsson MT (2015) Environmental pressure from the 2014–2015 eruption of Bároarbunga volcano, Iceland. Geochem Perspect Lett 1:84–93

Goldoff B, Webster JD, Harlov DE (2012) Characterization of fluor-chlorapatites by electron probe microanalysis with a focus on time-dependent intensity variation of halogens. Am Mineral 97:1103–1115

Grattan JP, Durand M, Taylor S (2003) Illness and elevated human mortality coincident with volcanic eruptions. In: Oppenheimer C, Pyle DM, Barclay J (eds) Volcanic Degassing, vol 213. Geol Soc Lond Spec Publ, pp 401–414

Gutzmer J, Banks DA, Lüders V, Hoefs J, Beukes NJ, von Bezing KL (2003) Ancient sub-seafloor alteration of basaltic andesites of the Ongeluk Formation, South Africa: implications for the chemistry of Paleoproterozoic seawater. Chem Geol 201:37–53

Hahm D, Hilton DR, Castillo PR, Hawkins JW, Hanan BB, Hauri EH (2012) An overview of the volatile systematics of the Lau Basin—resolving the effects of source variation, magmatic degassing and crustal contamination. Geochim Cosmochim Acta 85:88–113

Halmer MM, Schmincke HU, Graf HF (2002) The annual volcanic gas input into the atmosphere, in particular into the stratosphere: a global dataset for the past 100 years. J Volcanol Geotherm Res 115:511–528

Hanley JJ, Mungall JE, Pettke T, Spooner ETC, Bray CJ (2008) Fluid and halide melt inclusions of magmatic origin in the ultramafic and Lower Banded Series, Stillwater Complex, Montana, USA. J Petrol 49(6):1133–1160

Hansteen TH, Gurenko AA (1998) Sulfur, chlorine, fluorine in glass inclusions in olivine and clinopyroxene from basaltic hyaloclastites representing the Gran Canaria shield stage at sites 953 and 956. In: Weaver PPE, Schmincke H-U, Firth JV, Duffield W (eds) Proceedings of the ocean drilling program, scientific results, vol 157. Ocean Drilling Program, College Station, pp 403–410

Harding D, Miller JM (1982) The influence on rain chemistry of the Hawaiian volcano Kilauea. J Geophys Res 87(C2):1225–1230

Hauri EH (2002) SIMS analysis of volatiles in silicate glasses, 2: isotopes and abundances in Hawaiian melt inclusions. Chem Geol 183:115–141

Hauri EH, Gaetani GA, Green TH (2006) Partitioning of water during melting of the Earth's upper mantle at H_2O-undersaturated conditions. Earth Planet Sci Lett 248:715–734

Heaman LM, Creaser RA, Cookenboo HO, Chacko T (2006) Multi-stage modification of the Northern Slave mantle lithosphere: evidence from zircon- and diamond-bearing eclogite xenoliths entrained in Jericho kimberlite. Can J Pet 47:821–858

Hirayama C, Camp FE (1969) Effect of fluorine and chlorine on viscosity and fining of soda-lime and potassium-barium silicate glass. Glass Technol 10:123–127

Hoffman AW (1977) Mantle geochemistry; the message from oceanic volcanism. Nature 385(6613):219–229

Holland HD (1972) Granites, solutions, and base metal deposits. Econ Geol 67:281–301

Holloway JR (1973) The system pargasite-H_2O-CO_2: a model for melting of a hydrous mineral with a mixed-volatile fluid-I. Experimental results to 8 kbar. Geochim Cosmochim Acta 37:651–666

Holloway JR (1987) Igneous fluids. In: Carmichael ISE, Eugster HP (eds) Thermodynamic modeling of geological materials: minerals, fluids and melts. Rev Mineral, vol 17, pp 211–233

Holloway JR, Ford CE (1975) Fluid-absent melting of the fluoro-hydroxy amphibole pargasite to 35 kilobars. Earth Planet Sci Lett 25:44–48

Honda F (1970) Geochemical study of iodine in volcanic gases. II. Behaviour of iodine in volcanic gases. Geochem J 3:201–211

Honda F, Mizutani Y, Sugiura T, Oana S (1966) A geochemical study of iodine in volcanic gases. Bull Chem Soc Japan 39:2690–2695

Hörmann C, Sihler H, Bobrowski N, Beirle S, Penning de Vries M, Platt U, Wagner T (2013) Systematic investigation of bromine monoxide in volcanic plumes from space by using the GOME-2 instrument. Atmos Chem Phys 13:4749–4781

Horn S, Schmincke H-U (2000) Volatile emission during the eruption of Baitoushan Volcano (China/North Korea) ca. 969 AD. Bull Volcanol 61:537–555

Hovis GL, Harlov DE (2010) Solution calorimetric investigation of fluor-chlorapatite crystalline solutions. Am Mineral 95:946–952
Hovis GL, McCubbin FM, Nekvasil H, Ustunisik G, Woerner WR, Lindsley DH (2014) A novel technique for fluorapatite synthesis and the thermodynamic mixing behavior of F-OH apatite crystalline solutions. Am Mineral 99:890–897
Howarth GH, Pernet-Fisher JF, Bodnar RJ, Taylor LA (2015) Evidence for the exsolution of Cl-rich fluids in martian magmas: apatite petrogenesis in the enriched lherzolite shergottite Northwest Africa 7755. Geochim Cosmochim Acta 166:234–248
Hughes JM (2015) The many facets of apatite. Am Mineral 100:1033–1039
Huh MC (2013) Experimental determination of fluorine and hydrogen partitioning between apatite and basaltic melt. PhD diss., UCLA, p 56
Humphreys MCS, Blundy JD, Sparks RSJ (2008) Shallow-level decompression crystallization and deep magma supply at Shiveluch Volcano. Contrib Mineral Petrol 155:45–61
Humphreys MCS, Edmonds M, Christopher T, Hards V (2009) Chlorine variations in the magma of Soufrière Hills Volcano, Montserrat: insights from Cl in hornblende and melt inclusions. Geochim Cosmochim Acta 73:5693–5708. https://doi.org/10.1016/j.gca.2009.06.014
Hurwitz S, Mariner RH, Fehn U, Snyder GT (2005) Systematics of halogen elements and their radioisotopes in thermal springs of the Cascade Range, Central Oregon, Western USA. Earth Planet Sci Lett 235:700–714
Icenhower JP, London D (1997) Partitioning of fluorine and chlorine between biotite and granitic melt: experimental calibration at 200 MPa H_2O. Contrib Mineral Petrol 127:17–29
Iwasaki B, Katsura T (1967) The solubility of hydrogen chloride in volcanic rock melts at a total pressure of one atmosphere and at temperatures of 1200 °C and 1290 °C under anhydrous conditions. Bull Chem Soc Japan 40:554–561
Jago BC, Gittins J (1991) The role of fluorine in carbonatite magma evolution. Nature 349:56–58
Jambon A, Déruelle B, Dreibus G, Pineau F (1995) Chlorine and bromine abundance in MORB: the contrasting behaviour of the Mid-Atlantic Ridge and East Pacific Rise and implications for chlorine geodynamic cycle. Chem Geol 126:101–117
Jarrard RD (2003) Subduction fluxes of water, carbon dioxide, chlorine, and potassium. Geochem Geophys Geosyst 4(50):8905. https://doi.org/10.1029/2002GC000392
Jiang S, Pitzer KS (1996) Phase equilibria and volumetric properties of aqueous $CaCl_2$ by an equation of state. AI Ch E J 42:585–594
Joachim B, Pawley A, Lyon I, Henkel T, Clay PL, Ruzié L, Burgess R, Ballentine CJ (2014) Partial separation of halogens during the subduction of oceanic crust (abs.) EGU Gen Assemb, Vienna, Austria id. 7371
Joachim B, Pawley A, Lyon IC, Marquardt (nee Nartmann) K, Henkel T, Clay PL, Ruzié L, Burgess R, Ballentine CJ (2015) Experimental partitioning of F and Cl between olivine, orthopyroxene and silicate melt at Earth's mantle conditions. Chem Geol 416:65–78
John T, Layne GD, Haase KM, Barnes JD (2010) Chlorine isotope evidence for crustal recycling into the Earth's mantle. Earth Planet Sci Lett 298(1–2):175–182
Johnson N, Parnell RA (1986) Composition, distribution and neutralization of "acid rain" derived from Masaya volcano, Nicaragua. Tellus 38B:106–117
Johnson NM, Fegley B Jr (2003) Longevity of fluorine-bearing tremolite on Venus. Icarus 165(2):340–348
Johnson ER, Wallace PJ, Delgado-Granados H, Manea VC, Kent AJR, Bindeman IN, Donegan CS (2009) Subduction-related volatile recycling and magma generation beneath central Mexico: insights from melt inclusions, oxygen isotopes and geodynamic models. J Petrol 50:1729–1764
Joyce DR, Holloway JR (1993) An experimental determination of the thermodynamic properties of H_2O-CO_2-NaCl fluids at high pressures and temperatures. Geochim Cosmochim Acta 57:733–746
Kamenetsky VS, Kamenetsky MB (2010) Magmatic fluids immiscible with silicate melts: examples from inclusions in phenocrysts and glasses, and implications for magma evolution and metal transport. Geofluids 10:293–311

Kamineni DC (1987) Halogen-bearing minerals in plutonic rocks: a possible source of chlorine in saline groundwater in the Canadian Shield. In: Fritz P, Frape SK (eds) Saline water and gases in crystalline rocks, vol 33. Geol Assoc Can Spec Pap, pp 69–79

Kaminski E, Chenet AL, Jaupart C, Courtillot V (2011) Rise of volcanic plumes to the stratosphere aided by penetrative convection above large lava flows. Earth Planet Sci Lett 301(1):171–178

Kanitpanyacharoen W, Boudreau AE (2013) Sulfide-associated mineral assemblages in the Bushveld Complex, South Africa: platinum-group element enrichment by vapor refining by chloride-carbonate fluids. Mineral Deposita 48:193–210

Karpukhina NG, Werner-Zwanziger U, Zwanziger JW, Kiprianov AA (2007) Preferential binding of fluorine to aluminum in high peralkaline aluminosilicate glasses. J Phys Chem B 111(35):10413–10420

Kawaratani RK, Fujita S (1990) Wet deposition of volcanic gases and ash in the vicinity of Mount Sakurajima. Atmos Environ 24A:1487–1492

Kelley DS, Delaney JR (1987) Two-phase separation and fracturing in mid-ocean ridge gabbros at temperatures greater than 700 °C. Earth Planet Sci Lett 83(1–4):53–66

Kelly PJ, Kern C, Roberts TJ, Lopez T, Werner C, Aiuppa A (2013) Rapid chemical evolution of tropospheric volcanic emissions from Redoubt Volcano, Alaska, based on observations of ozone and halogen-containing gases. J Volcanol Geotherm Res 259:317–333

Kendrick MA (2012) High precision Cl, Br and I determinations of mineral standards using the noble gas method. Chem Geol 292–293:116–126

Kendrick MA, Scambelluri M, Honda M, Phillips D (2011) High abundances of noble gas and chlorine delivered to the mantle by serpentinite subduction. Nat Geosci 4:807–812

Kendrick MA, Woodhead JD, Kamenetsky VS (2012a) Tracking halogens through the subduction cycle. Geology 40(12):1075–1078

Kendrick MA, Kamenetsky VS, Phillips D, Honda M (2012b) Halogen systematics (Cl, Br, I) in Mid-Ocean Ridge Basalts: a Macquarie Island case study. Geochim Cosmochim Acta 81:82–93

Kendrick MA, Arculus RJ, Burnard P, Honda M (2013a) Quantifying brine assimilation by submarine magmas: examples from the Galápagos Spreading Centre and Lau Basin. Geochim Cosmochim Acta 123:150–165

Kendrick MA, Honda M, Pettke T, Scambelluri M, Phillips D, Giuliani A (2013b) Subduction zone fluxes of halogens and noble gases in seafloor and forearc serpentinites. Earth Planet Sci Lett 365:86–96

Kendrick MA, Jackson MG, Kent AJR, Hauri EH, Wallace PJ, Woodhead J (2014a) Contrasting behaviours of CO_2, S, H_2O and halogens (F, Cl, Br, and I) in enriched-mantle melts from Pitcairn and Society seamounts. Chem Geol 370:69–81

Kendrick MA, Arculus RJ, Danyushevsky LV, Kamenetsky VS, Woodhead JD, Honda M (2014b) Subduction-related halogens (Cl, Br and I) and H_2O in magmatic glasses from Southwest Pacific Backarc Basins. Earth Planet Sci Lett 400:165–176

Kent AJR, Norman MD, Hutcheon ID, Stolper EM (1999) Assimilation of seawater-derived components in an oceanic volcano: evidence from matrix glasses and glass inclusions from Loihi seamount. Hawaii Chem Geol 156:299–319

Kent AJR, Peate DW, Newman S, Stolper EM, Pearce JA (2002) Chorine in submarine glasses from the Lau Basin: seawater contamination and constraints on the composition of slab-derived fluids. Earth Planet Sci Lett 202:361–377

Kern C, Sihler H, Vogel L, Rivera C, Herrera M, Platt U (2009) Halogen oxide measurements at Masaya volcano, Nicaragua using active long path differential optical absorption spectroscopy. Bull Volcanol 71:659–670. https://doi.org/10.1007/s00445-008-0252-8

Kiczenski TJ, Stebbins JF (2006) The effect of fictive temperature on the structural environment of fluorine in silicate and aluminosilicate glasses. J Am Ceramic Soc 89:57–64

Kilgour G, Blundy J, Cashman K, Mader HM (2013) Small volume andesite magmas and melt-mush interactions at Ruapehu, New Zealand: evidence from melt inclusions. Contrib Mineral Petrol 166:371–392

Klemme S (2004) Evidence for fluoride melts in Earth's mantle formed by liquid immiscibility. Geology 32(5):441–444
Klemme S (2005) Evidence for fluoride melts in Earth's mantle formed by liquid immiscibility: comment and reply. Geology. https://doi.org/10.1130/0091-7613-33.1e76
Klemme S, Stalder R (2018) Halogens in the Earth's mantle: what we know and what we don't. In: Harlov DE, Aranovich L (eds) The role of halogens in terrestrial and extraterrestrial geochemical processes: surface, crust, and mantle. Springer, Berlin, pp 847–869
Koepke J, Berndt J, Feig ST, Holtz F (2007) The formation of SiO_2-rich melts within the deep oceanic crust by hydrous partial melting of gabbros. Contrib Mineral Petrol 153:67–84
Kogarko LN, Krigman LD (1970) Phase equilibria in the system nepheline-NaF. Geochem Int 7:103–107
Köhler J, Konnerup-Madsen J, Markl G (2008) Fluid geochemistry in the Ivigtut cryolite deposit, South Greenland. Lithos 103:369–392
Koleszar AM, Saal AE, Hauri EH, Nagle AN, Lliang Y, Kurz MD (2009) The volatile contents of the Galapagos plume: evidence for H_2O and F open system behavior in melt inclusions. Earth Planet Si Lett 287:442–452
Konnerup-Madsen J, Rose-Hansen J (1982) Volatiles associated with alkaline igneous rift activity: fluid inclusions in the Ilimaussaq intrusion and the Gardar granitic complexes (south Greenland). Chem Geol 37:79–93
Konzett J, Frost DJ (2009) The high P-T stability of hydroxyl-apatite in natural and simplified MORB—an experimental study to 15 GPA with implications for transport and storage of phosphorus and halogens in subduction zones. J Petrol 50(11):2043–2062
Konzett J, Rhede D, Frost DJ (2012) The high PT stability of apatite and Cl partitioning between apatite and hydrous potassic phases in peridotite: an experimental study to 19 GPa with implications for the transport of P, Cl and K in the upper mantle. Contrib Mineral Petrol 163:277–296
Köpsel D (2001) Solubility and vaporization of halides. Proc Int Cong Glass, Edinburgh, Scotland, p 330
Korzhinskiy MA (1981) Apatite solid solution as indicators of the fugacity of HCl° and HF° in hydrothermal fluids. Geochem Int 18:44–60
Koster van Groos AF, Wyllie PJ (1968) Melting relationships in the system $NaAlSi_3O_8$-NaF-H_2O to four kilobars pressure. J Geol 76(1):50–70
Koster van Groos AF, Wyllie PJ (1969) Melting relationships in the system $NaAlSi_3O_8$-NaCl-H_2O at one kilobar pressure with petrological applications. J Geol 77(5):581–605
Kotlova AG (1960) Ol'Shanskii YI, Tsvetkov AI. Some trends in immiscibility effects in binary silicate and borate systems. Mineral Geokhim Tr Inst Geol Rudn Mest An SSSR 42:3–9
Kovalenko VI, Kovalenko NI (1976) Ongonites. Nauka, Moscow
Kovalenko VI, Naumov VB, Girnis AV, Dorofeeva VA, Yarmolyuk VV (2006) Estimation of the average contents of H_2O, Cl, F, and S in the depleted mantle on the basis of the compositions of melt inclusions and quenched glasses of Mid-Ocean Ridge Basalts. Geochem Int 44(3): 209–231
Kravchuk IF, Keppler H (1994) Distribution of chloride between aqueous fluids and felsic melts at 2 kbar and 800 °C. Eur J Mineral 6(6):913–924
Krumrei TV, Pernicka E, Kaliwoda M, Markl G (2007) Volatiles in a peralkaline system: Abiogenic hydrocarbons and F-Cl-Br systematics in the naujite of the Ilímaussaq intrusion, South Greenland. Lithos 95:298–314
Kuellner FJ, Vispcky AP, Tuttle OF (1966) Preliminary survey of the system barite-calcite-fluorite at 500 bars. In: Tuttle OF, Gittins J (eds) Carbonatites. Interscience, New York, pp 353–364
Kutterolf S, Hansteen TH, Appel K, Freundt A, Krüger K, Pérez W, Wehrmann H (2013) Combined bromine and chlorine release from large explosive volcanic eruptions: a threat to stratospheric ozone? Geology 41(6):707–710
Kutterolf S, Hansteen TH, Freundt A, Wehrmann H, Appel K, Krüger K, Pérez W (2015) Bromine and chlorine emissions from plinian eruptions along the Central American volcanic arc: from source to atmosphere. Earth Planet Sci Lett 429:234–246

Kvassnes AJS, Grove TL (2008) How partial melts of mafic lower crust affect ascending magmas at oceanic ridges. Contrib Mineral Petrol 156:49–71

Larrea P, Widom E, Galé C, Ubide T, Lago M, Franca Z (2013) New Sr-Nd-Pb isotopic data on Graciosa island lavas (Azores). Mineral Mag 77(5):1547–1563

Larsen RB, Brooks CK, Bird DK (1992) Methane-bearing, aqueous, saline solutions in the Skaergaard intrusion, east Greenland. Contrib Mineral Petrol 112:428–437

Lassiter JC, Hauri EH, Nikogosian IK, Barsczus HG (2002) Chlorine-potassium variations in melt inclusions from Raivavae and Rapa, Austral Islands: constraints on chlorine recycling in the mantle and evidence for brine-induced melting of oceanic crust. Earth Planet Sci Lett 202:525–540

Latil C, Maury R (1977) Contribution a l'étude des échanges d'ions OH-, Cl-, et F- et de leur fixation dans les apatites hydrothermales. Bull Soc Fran Minéral Cristall 100:246–250 (in French)

Lecumberri-Sanchez P, Steel-MacInnis M, Bodnar RJ (2015) Synthetic fluid inclusions XIX. Experimental determination of the vapor-saturated liquidus of the system H_2O-NaCl-$FeCl_2$. Geochim Cosmochim Acta 148:34–49

Le Roux PJ, Shirey SB, Hauri EH, Perfit MR, Bender JF (2006) The effects of variable sources, processes and contaminants on the composition of northern EPR MORB (8-10°N and 12-14 N): Evidence from volatiles (H_2O, CO_2, S) and halogens (F, Cl). Earth Planet Sci Lett 251:209–231

Lee C, Kim YJ, Tanimoto H, Bobrowski N, Platt U, Mori T, Yamamoto K, Hong CS (2005) High ClO and ozone depletion observed in the plume of Sakurajima volcano, Japan. Geophys Res Lett 32:21809. https://doi.org/10.1029/2005GL023785

Le Voyer M, Rose-Koga EF, Shimizu N, Grove TL, Schiano P (2010) Two contrasting H_2O-rich components in primary melt inclusions from Mount Shasta. J Petrol 51(7):1571–1595

Le Voyer M, Cottrell E, Kelley KA, Brounce M, Hauri EH (2014a) The effect of primary versus secondary processes on the volatile content of MORB glasses: an example from the equatorial Mid-Atlantic Ridge (5°N-3°S). J Geophys Res Solid Earth 120. https://doi.org/10.1002/2014JB011160

Le Voyer M, Asimow PD, Mosenfelder JL, Guan Y, Wallace PJ, Schiano P, Stolper E, Eiler JM (2014b) Zonation of H_2O and F concentrations around melt inclusions in olivine. J Petrol 55(4):685–707

Lesne P, Kohn SC, Blundy J, Witham F, Botcharnikov RE, Behrens H (2011) Experimental simulation of closed-system degassing in the system Basalt-H_2O-CO_2-S-Cl. J Petrol 52(9):1737–1762

Lester GW, Kyser TK, Clark AH, Layton-Matthews D (2013) Trace element partitioning between immiscible silicate melts with H_2O, P, S, F, and Cl. Chem Geol 357:178–185

Liebscher A, Barnes JD, Sharp ZD (2006) Chlorine isotope vapor-liquid fractionation during experimental fluid-phase separation at 400 °C/23 MPa to 450 °C/42 MPa. Chem Geol 234:340–345

Litasov KD, Ohtani E (2009) Phase relations in the peridotite-carbonate-chloride system at 7–16.5 GPa and the role of chlorides in the origin of kimberlite and diamond. Chem Geol 262:29–41

Liu Y, Nekvasil H (2002) Si-F bonding in aluminosilicate glasses: inferences from ab initio NMR calculations. Am Mineral 87:339–346

Lloyd FE, Woolley AR, Stoppa F, Eby GN (2002) Phlogopite-biotite parageneses from the K-mafic-carbonatite effusive magmatic association of Katwe-Kikorongo, SW Uganda. Mineral Petrol 74:299–322

Lloyd AS, Plank T, Ruprecht P, Hauri EH, Rose W (2013) Volatile loss from melt inclusions in pyroclasts of differing sizes. Contrib Mineral Petrol 165:129–153

Lowenstern JB (1994) Chlorine, fluid immiscibility, and degassing in peralkaline magmas from Pantelleria, Italy. Am Mineral 79:353–369

Lübcke P, Bobrowski N, Arellano S, Galle B, Garzón G, Vogel L, Platt U (2014) BrO/SO_2 molar ratios from scanning DOAS measurements in the NOVAC network. Solid Earth 5:409–424

Luth RW (1988) Raman spectroscopic study of the solubility mechanisms of F in glasses in the system CaO-CaF_2-SiO_2. Am Mineral 73:297–305
MacKenzie JM, Canil D (2011) Fluid/melt partitioning of Re, Mo, W, Tl and Pb in the system haplobasalt-H_2O-Cl and the volcanic degassing of trace metals. J Volcanol Geotherm Res 204:57–65
Magenheim AJ, Spivack AJ, Michael PJ, Gieskes JM (1995) Chlorine stable isotope composition of the oceanic crust: implications for Earth's distribution of chlorine. Earth Planet Sci Lett 131 (3–4):427–432
Mahood GA, Baker DR (1986) Experimental constraints on depths of fractionation of mildly alkalic basalts and associated felsic rocks: Pantelleria, Strait of Sicily. Contrib Mineral Petrol 83:251–264
Malinin SD, Kravchuk IF, Delbove F (1989) Chloride distribution between phases in hydrated and dry chloride-aluminosilicate melt systems as a function of phase composition. Geochem Int 26:32–38
Mandeville CW, Webster JD, Tappen C, Taylor BE, Timbal A, Sasaki A, Hauri E, Bacon CR (2009) Stable isotopic and petrologic evidence for open-system degassing during the climactic and pre-climactic eruptions of Mt Mazama Crater Lake Oregon. Geochim Cosmochim Acta 73:2978–3012
Mangler MF, Marks MAW, Zaitzev AN, Eby GN, Markl G (2014) Halogens (F, Cl and Br) at Oldoinyo Lengai volcano (Tanzania): Effects of magmatic differentiation, silicate-natrocarbonatite melt separation and surface alteration of natrocarbonatite. Chem Geol 365:43–53
Manning DAC (1981) The effect of fluorine on liquidus phase relationships in the system Qz-Ab-Or with excess water at 1 kb. Contrib Mineral Petrol 76:257–262
Manning CE, Aranovich LY (2014) Brines at high pressure and temperature: Thermodynamic, petrologic and geochemical effects. Precambr Res 253:6–16
Marianelli P, Metrich N, Santacroce R, Sbrana A (1995) Mafic magma batches at Vesuvius: a glass inclusion approach to the modalities of feeding stratovolcanoes. Contrib Mineral Petrol 120:159–169
Marianelli P, Métrich N, Sbrana A (1999) Shallow and deep reservoirs involved in magma supply of the 1944 eruption of Vesuvius. Bull Volcanol 61:48–63
Markis JH, Clemens K, Tomozawa M (1981) Effect of fluorine on the phase separation of Na_2O-SiO_2 glasses. J Am Ceram Soc 64(1):C-20
Markl G, Piazolo S (1998) Halogen-bearing minerals in syenites and high-grade marbles of Dronning Maud Land, Antarctica: monitors of fluid compositional changes during late-magmatic fluid-rock interaction processes. Contrib Mineral Petrol 132:246–268
Markl G, Marks M, Schwinn G, Sommer H (2001) Phase equilibrium constraints on intensive crystallization parameters of the Ilímaussaq Complex, South Greenland. J Petrol 42:2231–2258
Marks M, Halama R, Wenzel T, Markl G (2004) Nd-, O-, and H-isotopic evidence for complex, closed-system fluid evolution of the peralkaline Ilimaussaq Intrusion, South Greenland. Geochim Cosmochim Acta 68:3379–3395
Marks MAW, Wenzel T, Whitehouse MJ, Loose M, Zack T, Barth M, Worgard L, Krasz V, Eby GN, Stosnach H, Markl G (2012) The volatile inventory (F, Cl, Br, S, C) of magmatic apatite: an integrated analytical approach. Chem Geol 291:241–255
Marks L, Keiding J, Wenzel T, Trumbull RB, Veksler I, Weidenbeck M, Markl G (2014) F, Cl, and S concentrations in olivine-hosted melt inclusions from mafic dikes in NW Namibia and implications for the environmental impact of the Paraná-Etendeka Large Igneous Province. Earth Planet Sci Lett 392:39–49
Martin RS, Mather TA, Pyle DM (2006) Modeling the chemistry of high temperature mixtures of magmatic and atmospheric gases. Geochem Geophys Geosyst 7:Q04006. https://doi.org/10.1029/2005GC001186
Martin RS, Roberts TJ, Mather TA, Pyle DM (2009) The implications of H_2S and H_2 stability in high-T mixtures of magmatic and atmospheric gases for the production of oxidized trace species (e.g., BrO and NO_x). Chem Geol 263:143–150

Martin RS, Wheeler JC, Ilyinskaya E, Braban CF, Oppenheimer C (2012) The uptake of halogen (HF, HCl, HBr and HI) and nitric (HNO_3) acids into acidic sulphate particles in quiescent volcanic plumes. Chem Geol 296–297:19–25

Mather TA (2008) Volcanoes and the atmosphere: the potential role of the atmosphere in unlocking the reactivity of volcanic emissions. Philos Trans R Soc A 366:4581–4595

Mather TA, Pyle DM, Oppenheimer C (2003) Tropospheric volcanic aerosol. In: Robock A, Oppenheimer C (eds) Volcanism and the Earth's atmosphere. Geophysical Monograph, vol 139. American Geophysical Union, Washington, DC, pp 189–212

Mather TA, Witt MLI, Pyle DM, Quayle BM, Aiuppa A, Bagnato E, Martin RS, Sims KWW, Edmonds M, Sutton AJ, Ilyinskaya E (2012) Halogens and trace metal emissions from the ongoing 2008 summit eruption of Kīlauea volcano, Hawaii. Geochim Cosmochim Acta 83:292–323

Mathez EA, Webster JD (2005) Partitioning behavior of chlorine and fluorine in the system apatite-silicate melt-fluid. Geochim Cosmochim Acta 69(5):1275–1286

Mathez EA, Dietrich VJ, Holloway JR, Boudreau AE (1989) Carbon distribution in the stillwater complex and evolution of vapor during crystallization of stillwater and bushveld magmas. J Petrol 30:153–173

Mazziotti Tagliani S, Nicotra E, Viccaro M, Gianfagna A (2012) Halogen-dominant mineralization at Mt. Calvario dome (Mt. Etna) as a response of volatile flushing into the magma plumbing system. Mineral Petrol 106:89–105

McCormick MP, Thomason LW, Trepte CR (1995) Atmospheric effects of the Mt. Pinatubo eruption Nature 373:399–404

McCubbin FM, Jolliff BJ, Nekvasil H, Carpenter PK, Zeigler RA, Steele A, Elardo SM, Lindsley DH (2011) Fluorine and chlorine abundances in lunar apatite: implications for heterogeneous distributions of magmatic volatiles in the lunar interior. Geochim Cosmochim Acta 75:5073–5093

McCubbin FM, Vander Kaaden KE, Tartése R, Whitson ES, Anand M, Franchi IA, Mikhail S, Ustunisik G, Hauri EH, Want J, Boyce JW (2014) Apatite-melt partitioning in basaltic magmas: The importance of exchange equilibria and the incompatibility of the OH component in halogen-rich apatite. 45th Lunar Planet Sci Conf #2741

McCubbin FM, Vander Kaaden KE, Tartése R, Boyce JW, Mikhail S, Whitson ES, Bell AS, Anand M, Franchi IA, Wang J, Hauri EH (2015) Experimental investigation of F, Cl, an OH partitioning between apatite and Fe-rich basaltic melt at 1.0–1.2 GPa and 950–1000 °C. Am Mineral 100:1790–1802

McDonough WF, Sun S-S (1995) The composition of the Earth. Chem Geol 120:223–253

Menyailov IA (1975) Prediction of eruptions using changes in composition of volcanic gases. Bull Volcanol 39(1):112–125

Métrich N, Rutherford MJ (1992) Experimental study of chlorine behavior in hydrous silicic melts. Geochim Cosmochim Acta 56:606–607

Métrich N, Wallace P (2008) Volatile abundances in basaltic magmas and their degassing paths tracked by melt inclusions. In: Putirka K, Tepley F (eds) Minerals, inclusions and volcanic processes. Mineralogical Society of America, vol 69. Reviews in Mineralogy and Geochemistry, pp 363–402

Métrich N, Schiano P, Clocchiatti R, Maury RC (1999) Transfer of sulfur in subduction settings: an example from Batan Island (Luzon Volcanic Arc, Philippines). Earth Planet Sci Lett 167:1–14

Métrich N, Bertagnini A, Landi P, Rosi M (2001) Crystallisation driven by decompression and water loss at Stromboli volcano (Aeolian Islands). J Petrol 42:1471–1490

Métrich N, Bertagnini A, Di Muro A (2010) Conditions of magma storage, degassing and ascent at Stromboli: new insights into the volcano plumbing system with inferences on the eruptive dynamics. J Petrol 51:603–626. https://doi.org/10.1093/petrology-egp083

Métrich N, Allard P, Aiuppa A, Bani P, Bertagnini A, Shinohara H, Parello F, Di Muro A, Garaebiti E, Belhadj O, Massare D (2011) Magma and volatile supply to post-collapse

volcanism and block resurgence in Siwi caldera (Tanna Island, Vanuatu arc). J Petrol 52(6):1077-1105
Meurer WP, Meurer MES (2006) Using apatite to dispel the "trapped liquid" concept and to understand the loss of interstitial liquid by compaction in mafic cumulates: an example from the Stillwater Complex, Montana. Contrib Mineral Petrol 151:187–201
Meurer WP, Natland JH (2001) Apatite compositions from oceanic cumulates with implications for the evolution of mid-ocean ridge magmatic systems. J Volcanol Geotherm Res 110:281–298
Meurer WP, Hellström FA, Claeson DT (2004) The relationship between chloroapatite and PGE-rich cumulats in layered intrusions: the Kläppsjö gabbro, North-Central Sweden, as a case study. Can Mineral 42:279–289
Mi J-X, Pan Y (2018) Halogen-rich minerals: crystal chemistry and geological significances. In: Harlov DE, Aranovich L (eds) The role of halogens in terrestrial and extraterrestrial geochemical processes: surface, crust, and mantle. Springer, Berlin, pp 123–184
Michael PJ, Cornell WC (1998) Influence of spreading rate and magma supply on crystallization and assimilation beneath mid-ocean ridges: evidence from chlorine and major element chemistry of mid-ocean ridge basalts. J Geophys Res 103(B8):18325–18356
Michael PJ, Schilling J-G (1989) Chlorine in mid-ocean ridge magmas: evidence for assmilation of seawater-influenced components. Geochim Cosmochim Acta 53(12):3131–3143
Michael PJ, Chase RL, Allan JF (1989) Petrologic and geologic variations along the Southern Explorer Ridge, northeast Pacific Ocean. J Geophys Res 94:13895–13918
Michael PJ, Forsyth DW, Blackman DK, Fox PJ, Hanan BB, Harding AJ, Macdonald KC, Neumann GF, Orcutt JA, Tolstoy M, Weiland CM (1994) Mantle control of a dynamically evolving spreading center: Mid-Atlantic Ridge 31–34°S. Earth Planet Sci Lett 121:451–468
Mitsis I, Economou-Eliopoulos M (2001) Occurrence of apatite associated with magnetite in an ophiolite complex (Othrys), Greece. Am Mineral 86:1143–1150
de Moor JM, Fisher TP, King PL, Botcharnikov RE, Hervig RL, Hilton DR, Barry PH, Mangasini F, Ramirez C (2013) Volatile-rich silicate melts from Oldoinyo Lengai volcano (Tanzania): implications for carbonatite genesis and eruptive behavior. Earth Planet Sci Lett 361:379–390
Mosenfelder JL, Rossman GR (2013a) Analysis of hydrogen and fluorine in pyroxenes: I. Orthopyroxene. Am Mineral 98:1026–1041
Mosenfelder JL, Rossman GR (2013b) Analysis of hydrogen and fluorine in pyroxenes: II. Clinopyroxene. Am Mineral 98:1042–1054
Moune S, Sigmarsson O, Thordarson T, Gauthier P-J (2007) Recent volatile evolution in the magmatic system of Hekla volcano, Iceland. Earth Planet Sci Lett 255:373–389
Müller D, Leander F, Herzig PM, Hunt S (2001) Potassic igneous rocks from the vicinity of epithermal gold mineralization, Lihir Island, Papua New Guinea. Lithos 57:163–186
Munoz JL (1984) F-OH and Cl-OH exchange in micas with applications to hydrothermal ore deposits. In: Bailey SW (ed) Micas. Rev Mineral, vol 13, pp 469–493
Munoz JL (1992) Calculation of HF and HCl fugacities from biotite compositions: revised equations. Geological Society of America, Abstracts with programs 26:A221
Munoz JL, Luddington SD (1974) Fluorine-hydroxyl exchange in biotite. Am J Sci 274:396–413
Munoz JL, Luddington SD (1977) Fluorine-hydroxyl exchange in synthetic muscovite and its application to muscovite-biotite assemblages. Am Mineral 62:304–308
Muramatsu Y, Doi T, Tomaru H, Fehn U, Takeuchi R, Matsumoto R (2007) Halogen concentrations in porewaters and sediments of the Nankai Trough, Japan: implications for the origin of gas hydrates. Appl Geochem 22:534–556
Musselwhite DS, Drake MJ (2000) Early outgassing of Mars: implications from experimentally determined solubility of iodine in silicate magmas. Icarus 148:160–175
Mysen BO, Virgo D (1985) Interaction between fluorine and silica in quenched melts on the joins SiO_2-AlF_3 and SiO_2-NaF determioned by Raman spectroscopy. Phys Chem Mineral 12:77–85

Mysen BO, Cody GD, Smith A (2004) Solubility mechanisms of fluorine in peralkaline and meta-aluminous silicate glasses and in melts to magmatic temperatures. Geochim Cosmochim Acta 68(12):2745–2769

Nadeau O, Williams-Jones AE, Stix J (2013) Magmatic-hydrothermal evolution and devolatilization beneath Merapi volcano, Indonesia. J Volcanol Geotherm Res 261:50–68

Naumov VB, Portnyagin MV, Tolstykh ML, Yarmolyuk VV (2003) Composition of magmatic melts from the southern Baikal volcanic region: a study of inclusions in olivine from trachybasalts. Geochem Int 41:213–223

Naumov VB, Tolstykh ML, Grib EN, Leonov VL, Kononkova NN (2008) Chemical composition, volatile components, and trace elements in melts of the Karymskii Volcanic Center, Kamchatka, and Golovnina Volcano, Kunashir Island: Evidence from Inclusions in Minerals. Petrology 16(1):1–18

Neave DA, Fabbro G, Herd RA, Petrone CM, Edmonds M (2012) Melting, differentiation and degassing at the Pantelleria Volcano, Italy. J Petrol 53:637–663

Newman S, Lowenstern JB (2002) Volatilecalc: a silicate melt–H_2O–CO_2 solution model written in VISUAL BASIC Excel. Comput Geosci 28(5):597–604

Nielsen RL, Sours-Page RE, Harpp KS (2000) Role of a Cl-bearing flux in the origin of depleted ocean floor magmas. Geochem Geophys Geosys 3(11):1–9. https://doi.org/10.1029/1999GC00001

Notcutt G, Davies F (1989) Accumulation of volcanogenic fluoride by vegetation—Mt Etna, Sicily. J Volcanol Geotherm Res 39(4):329–333

Oakes CS, Bodnar RJ, Simonson JM, Pitzer KS (1994) Critical and supercritical properties for 0.3-3.0 mol kg^{-1} $CaCl_{2(aq)}$. Geochim Cosmochim Acta 75:2421–2431

O'Leary JA, Gaetani GA, Hauri EH (2010) The effect of tetrahedral Al^{3+} on the partitioning of water between clinopyroxene and silicate melt. Earth Planet Sci Lett 297:111–120

Oppenheimer C (2011) Volcanic degassing. In: Holland JD, Turekian KK (eds.) Geochemistry of earth systems. Academic Press, pp 1–44

Oppenheimer C, Kyle PR (2008) Probing the magma plumbing of Erebus volcano, Antarctica, by open-path FTIR spectroscopy of gas emissions. J Volcanol Geotherm Res 177:743–754

Oppenheimer C, Tsanev VI, Braban CF, Cox RA, Adams JW, Aiuppa A, Bobrowski N, Delmelle P, Barclay J, McGonigle AJS (2006a) BrO formation in volcanic plumes. Geochim Cosmochim Acta 70:2935–2941

Oppenheimer C, Bani P, Calkins JA, Burton MR, Sawyer GM (2006b) Rapid FTIR sensing of volcanic gases released by Strombolian explosions at Yasur volcano, Vanuatu. Appl Phys B Lasers Opt 85:453–460. https://doi.org/10.1007/s00340-006-2353-4

Oppenheimer C, Lomakina A, Kyle PR, Kingsbury NG, Boichu M (2009) Pulsatory magma supply to a phonolite lava lake. Earth Planet Sci Lett 284:392–398

Oppenheimer C, Kyle P, Eisele F, Crawford J, Huey G, Tanner D, Kim S, Mauldin L, Blake D, Beyersdorf A, Buhr M, Davis D (2010) Atmospheric chemistry of an Antarctic volcanic plume. J Geophys Res 115:D04303. https://doi.org/10.1029/2009JD011910

Oppenheimer C, Scaillet B, Martin RS (2011a) Sulfur degassing from volcanoes: source conditions, surveillance, plume chemistry and impacts. Rev Mineral Geochem 73:363–421

Oppenheimer C, Moretti R, Kyle PR, Eschenbacher A, Lowenstern JB, Hervig RL, Dunbar NW (2011b) Mantle to surface degassing of alkalic magmas at Erebus volcano, Antarctica. Earth Planet Sci Lett 306:261–271

Oppenheimer C, TP Fischer, B Scaillet (2014) Volcanic degassing: process and impact. In: Treatise on geochemistry, 2nd edn. https://doi.org/10.1016/B978-0-08-095975-7.00304-1

Orejana D, Villaseca C, Billström K, Paterson BA (2008) Petrogenesis of Permian alkaline lamprophyres and diabases from the Spanish Central System and their geodynamic context within western Europe. Contrib Mineral Petrol 156(4):477–500

Oskarsson N (1980) The interaction between volcanic gases and tephra: fluorine adhering to tephra of the 1970 Hekla eruption. J Volcanol Geotherm Res 8:251–266

Pan Y, Dong P (2003) Bromine in scapolite-group minerals and sodalite: XRF microprobe analysis, exchange experiments, and application to skarn deposits. Can Mineral 41:529–540

Panina LI, Motorina IV (2008) Liquid immiscibility in deep-seated magmas and the generation of carbonatitic melts. Geochem Int 46(5):448–464

Panina LI, Nikolaeva AT, Rokosova EY (2011) Crystallization conditions of the alkaline-basic dike from the Yllymakh Massif, central Aldan: evidence from melt inclusion data in minerals. Geochem Int 49:120–138

Parat F, Holtz F, Klügel A (2011) S-rich apatite-hosted glass inclusions in xenoliths from La Palma: contraints on the volatile partitioning in evolved alkaline magmas. Contrib Mineral Petrol. https://doi.org/10.1007/s00410-011-0606-7

Patiño Douce AE, Roden MF (2006) Apatite as a probe of halogen and water fugacities in the terrestrial planets. Geochim Cosmochim Acta 70:3173–3196

Patiño Douce AE, Roden MF, Chaumba J, Fleisher C, Yogodzinski G (2011) Compositional variability of terrestrial mantle apatites, thermodynamic modeling of apatite volatile contents, and the halogen and water budgets of planetary mantles. Chem Geol 288:14–31

Peate DW, Kokfelt TF, Hawkesworth CJ, van Calsteren PW, Hergt JM, Pearce JA (2001) U-series isotope data on Lau Basin glases: the role of subduction-related fluids during melt generation in back-arc basins. J Petrol 42(8):1449–1470

Peate DW, Ukstins Peate I, Rowe MC, Thompson JM, Kerr AC (2012) Petrogenesis of high-MgO lavas of the Lower Mull Plateau Group, Scotland: Insights from melt inclusions. J Petrol 53 (9):1867–1886

Peng G, Luhr JF, McGee JJ (1997) Factors controlling sulfur concentrations in volcanic apatite. Am Mineral 82:1210–1224

Peretyazhko IS, Zagorsky VY, Tsareva EA, Sapozhnikov AN (2007) Immiscibility of calcium fluoride and aluminosilicate melts in ongonite from the Ary-Bulak intrusion, eastern Transbaikal region. Dok Earth Sci 413(2):315–320

Perfit MR, Ridley WI, Jonasson IR (1999) Geologic, petrologic and geochemical relationships between magmatism and massive sulfide mineralization along the eastern Galapagos Spreading Center Rev. Econ Geol 8:75–99

Persikov ES, Zharikov VA, Bukhtiyarov PG, Pol'skoy SF (1990) The effect of volatiles on the properties of magmatic melts. Eur J Mineral 2:621–642

Pfeffer MA et al. (2015) Ground-based measurements of the emission rate and composition of gases from the Holuhraun eruption, Geophysical Research Abstracts. 17, EGU2015-7373, Abstract presented at the EGU General Assembly 2015

Piccoli PM, Candela PA (1994) Apatite in felsic rocks: a model for the estimation of initial halogen concentrations in the Bishop Tuff (Long Valley) and Tuolomne Intrusive Suite (Sierra Nevada Batholith) magmas. Am J Sci 294:92–135

Piccoli PM, Candela PA (2002) Apatite in igneous systems. In: Kohn MJ, Rakovan J, Hughes JM (eds) Phosphates: geochemical, geobiological, and materials importance. Mineralogical Society of America, pp 255–292

Pirajno F (2018) Halogens in hydrothermal fluids and their role in the formation and evolution of hydrothermal mineral systems. In: Harlov DE, Aranovich L (eds) The role of halogens in terrestrial and extraterrestrial geochemical processes: surface, crust, and mantle. Springer, Berlin, pp 959–995

Pitzer KS (1983) Dielectric constant of water at very high temperature and pressure. Proc Natl Acad Sci USA 80:4575–4576

Portnyagin M, Hoernle K, Storm S, Mironom N, van den Bogaard C, Botcharnikov R (2012) H_2O-rich melt inclusions in fayalitic olivine from Hekla volcano: implications for phase relationships in silicic systems and driving forces for explosive volcanism on Iceland. Earth Planet Sci Lett 357–358:337–346

Prata AJ, Carn SA, Stohl A, Kerkmann J (2007) Long range transport and fate of a stratospheric volcanic cloud from Soufrière Hills volcano, Montserrat. Atmos Chem Phys 7:5093–5103. https://doi.org/10.5194/acp-7-5093-2007

Prelević D, Foley SF, Romer RL, Cvetković V, Downes H (2005) A Tertiary ultrapotassic province in Serbia: constraints on the scale and character of the sources. J Petrol 46:1443–1487

Pyle DM, Mather TA (2009) Halogens in igneous processes and their fluxes to the atmosphere and oceans from volcanic activity: a review. Chem Geol 263:110–121. https://doi.org/10.1016/j.chemgeo.2008.11.013

Raffone N, Ottolini L, Tonarini S, Gianelli G, Fridleifsson GO (2008) A SIMS study of lithium, boron and chlorine in basalts from Reykjanes (southwestern Iceland). Microchim Acta 161:307–312

Rampe EB, Ming DW, Blake DF et al (2017) Mineralogy of an ancient lacustrine mudstone succession from the Murray formation, Gale crater, Mars. Earth Planet Sci Lett 171:172–185. https://doi.org/10.1016/j.epsl.2017.04.021

Ransom B, Spivack AJ, Kastner M (1995) Stable Cl isotopes in subduction-zone porewaters: implications for fluid rock interactions and the cycling of chlorine. Geology 23:715–718

Renno AD, Franz L, Witzke T, Herzig PM (2004) The coexistence of melts of hydrous copper chloride, sulfide and silicate compositions in a magnesiohastingsite cumulate, Tubaf Seamount, Papua New Guinea. Can Mineral 42:1–16

Ripley EM (2005) Re/Os isotopic and fluid inclusion studies of fluid-rock interaction in the contact aureole of the Duluth Complex, Minnesota. Geochim Cosmochim Acta 69(10):332

Rizzo AL, Caracausi A, Liotta M, Paonita A, Barnes JD, Corsaro RA, Martelli M (2013) Chlorine isotope composition of volcanic gases and rocks at Mount Etna (Italy) and inferences on the local mantle source. Earth Planet Sci Lett 371–372:134–142

Roberge M, Bureau H, Bolfan-Casanova N, Frost DJ, Raepsaet C, Surble S, Khodja H, Auzende A-L, Fiquet G (2015) Is the transition zone a deep reservoir for fluorine? Earth Planet Sci Lett 429:25–32

Roberts T, Braban C, Martin R, Oppenheimer C, Adams J, Cox R, Jones R, Griffiths P (2009) Modelling reactive halogen formation and ozone depletion in volcanic plumes. Chem Geol 263:151–163

Robock A (2000) Volcanic eruptions and climate. Rev Geophys 38:191–219

Roedder E (1984) Fluid inclusions. Rev Mineral 12:644

Rosatelli G, Wall F, Stoppa F (2007) Calcio-carbonatite melts and metasomatism in the mantle beneath Mt. Vulture (Southern Italy). Lithos 99:229–248

Rose WI, Millard GA, Mather TA, Hunton DE, Anderson B, Oppenheimer C, Thornton BF, Gerlach TM, Viggiano AA, Kondo Y, Miller TM, Ballenthin JO (2006) The atmospheric chemistry of a 33–34 hour old volcanic cloud from Hekla Volcano (Iceland): insights from direct sampling and the application of chemical box modeling. J Geophys Res Atm 111(20): D20206. https://doi.org/10.1029/2005JD006872

Rose-Koga, EF, Koga KT, Schiano P, Le Voyer M, Shimizu N, Whitehouse MJ, Clocchiatti R (2012) Mantle source heterogeneity for South Tyrrhenian magmas revealed by Pb isotopes and halogen contents of olivine-hosted melt inclusions. Chem Geol 334:266–279

Rose-Koga EF, Koga KT, Schiano P, Hamada M, Hélouis T, Whitehouse MJ, Shimizu N (2014) Volatile (F and Cl) concentrations in Iwate olivine-hosted melt inclusions indicating low-temperature subduction. Earth Planets Space 66:81

Rowe MC, Lassiter JC (2009) Chlorine enrichment in central Rio Grande Rift basaltic melt inclusions: Evidence for subduction modification of the lithospheric mantle. Geology 37 (5):439–442

Rowe MC, Peate DW, Newbrough A (2011) Compositional and thermal evolution of olivine-hosted melt inclusions in small-volume basaltic eruption: a “simple” example from Dotsero Volcano, NW Colorado. Contrib Mineral Petrol 161:197–211

Ruscitto DM, Wallace PJ, Kent AJR (2011) Revisiting the compositions and volatile contents of olivine-hosted melt inclusions from the Mount Shasta region: implications for the formation of high-Mg andesites. Contrib Mineral Petrol 162:109–132

Ryabchikov ID, Hamilton DL (1971) Possibility of concentrated chloride solutions in course of acid magma crystallization. Dokl Akad Nauk SSSR 197:933–937

Saal AE, Hauri EH, Langmuir CH, Perfit MR (2002) Vapour undersaturation in primitive mid-ocean ridge basalt and the volatile content of Earth’s upper mantle. Nature 419:451–455

Saal AE, Kurz MD, Hart SR, Blusztaijn JS, Blichert-Toft J, Liang Y, Geist DJ (2007) The role of lithospheric gabbros on the composition of Galapagos lavas. Earth Planet Sci Lett 257 (304):391–406

Safonov OG, Perchuk LL, Litvin YA (2007) Melting relations in the chloride-carbonate silicate systems at high-pressure and the model for formation of alkali diamond-forming liquids in the upper mantle. Earth Planet Sci Lett 253:112–128

Safonov OG, Chertkova NV, Perchuk LL, Litvin YA (2009) Experimental model for alkalic chloride-rich liquids in the upper mantle. Lithos 112S:260–273

Saito G, Morishita Y, Shinohara H (2010) Magma plumbing system of the 2000 eruption of Miyakejima Volcano, Japan, deduced from volatile and major component contents of olivine-hosted melt inclusions. J Geophys Res B115. https://doi.org/10.1029/2010JB007433

Salvioli-Mariani E, Mattioli M, Renzulli A, Serri G (2002) Silicate melt inclusions in the cumulate minerals of gabbroic nodules from Stromboli Volcano (Aeolian Islands, Italy): main components of the fluid phase and crystallization temperatures. Mineral Mag 66:969–984

Sandland TO, Du DL, Stebbins JF, Webster JD (2004) Structure of Cl-containing silicate and aluminosilicate glasses: A 35Cl MAS-NMR study. Geochim Cosmochim Acta 68:5059–5069

Sato H, Holtz F, Behrens H, Botcharnikov R, Nakada S (2005) Experimental petrology of the 1991-1995 Unzen dacite, Japan. Part II: Cl/OH partitioning between hornblende and melt and its implications for the origin of oscillatory zoing of hornblende phenocrystas. J Petrol 46:339–354

Sawyer GM, Carn SA, Tsanev VI, Oppenheimer C, Burto M (2008a) Investigation into magma degassing at Nyiragongo volcano, Democratic Republic of the Congo. Geochem Geophys Geosys 9:Q02017. https://doi.org/10.1029/2007GC001829

Sawyer GM, Oppenheimer C, Tsanev VI, Yirgu G (2008b) Magmatic degassing at Erta 'Ale volcano, Ethiopia. J Volcanol Geotherm Res 178:837–846

Schaller T, Dingwell DB, Keppler H, Knöller W, Merwin L, Sebald A (1992) Fluorine in silicate glasses: A multinuclear nuclear magnetic resonance study. Geochim Cosmochim Acta 56:701–707

Schiano P, Clocchiatti R, Ottolini L, Sbrana A (2004) The relationship between potassic, calc-alkaline and na-alkaline magmatism in south Italy volcanoes: a melt inclusion approach. Earth Planet Sci Lett 220:121–137

Schiffries CM (1990) Liquid-absent aqueous fluid inclusions and phase equilibria in the system $CaCl_2$-NaCl-H_2O. Geochim Cosmochim Acta 54:611–619

Schönenberger J, Köhler J, Markl G (2008) REE systematics of fluorides, calcite and siderite in peralkaline plutonic rocks from the Gardar Province, South Greenland. Chem Geol 247:16–35

Self S, King AJ (1996) Petrology and sulfur and chlorine emissions of the 1963 eruption of Gunung Agung, Bali, Indonesia. Bull Volcanol 58:263–285

Self S, Widdowson M, Thordarson T, Jay AE (2006) Volatile fluxes during flood basalt eruptions and potential effects on the global environment: a Deccan perspective. Earth Planet Sci Lett 248(1–2):518–532

Self S, Blake S, Sharma K, Widdowson M, Sephton S (2008) Sulfur and chlorine in late Cretaceous Deccan magmas and eruptive gas release. Science 319:1654–1657

Seo JH, Guillong M, Aerts M, Zajacz Z, Heinrich CA (2011) Microanalysis of S, Cl, and Br in fluid inclusions by LA-ICP-MS. Chem Geol 284:35–44

Sharp ZD, Barnes JD, Brearley AJ, Chaussidon M, Fischer TP, Kamenetsky VS (2007) Chlorine isotope homogeneity of the mantle, crust and carbonaceous chondrites. Nature 446:1062–1065. https://doi.org/10.1038/nature05748

Sharp ZD, Barnes JD, Fischer TP, Halick M (2010) An experimental determination of chlorine isotope fractionation in acid systems and applications to volcanic fumaroles. Geochim Cosmochim Acta 74:264–273

Sharygin VV, Kamenetsky VS, Zaitsev AN, Kamenetsky MB (2012) Silicate-natrocarbonatite liquid immiscibility in 1917 eruption combeite-wollastonite nephelinite, Oldoinyo Lengai volcano, Tanzania: melt inclusion study. Lithos 152:23–39

Shaw CSJ, Eyzaguirre J (2000) Origin of megacrysts in the mafic alkaline lavas of the West Eifel volcanic field, Germany. Lithos 50:75–95

Shchekina TI, Gramenitskiy EN, Alferyeva YO (2013) Leucocratic magmatic melts with the maximum fluorine concentrations: experiment and relations in nature. Petrol 21(5):454–470

Sheth HC, Choudhary AK, Bhattacharyya S, Cucciniello C, Laishram R, Gurav T (2011) The Chogat-Chamardi subvolcanic complex, Saurashtra, northwestern Deccan Traps: geology, petrochemistry, and petrogenetic evolution. J Asian Earth Sci 41:307–324

Shimizu K, Shimizu N, Komiya T, Suzuki K, Murayama S, Tatsumi Y (2009) CO_2-rich komatiitic melt inclusions in Cr-spinels within beach sand from Gorgona Island, Colombia. Earth Planet Sci Lett 288:33–43

Shinohara H (2008) Excess degassing from volcanoes and its role on eruptive and intrusive activity. Rev Geophys 46:RG4005. https://doi.org/101029/2007RG000244

Shinohara H (2009) A missing link between volcanic degassing and experimental studies on chloride partitioning. Chem Geol 263:51–59

Shinohara H (2013) Volatile flux from subduction zone volcanoes: Insights from a detailed evaluation of the fluxes from volcanoes in Japan. J Volcanol Geotherm Res 268:46–63

Shinohara H, Witter JB (2005) Volcanic gases emitted during mild Strombolian activity of Villarrica volcano, Chile. Geophys Res Lett 32:L20308. https://doi.org/10.1029/2005GL024131

Shinohara H, Ilyama JT, Matsuo S (1989) Partition of chlorine compounds between silicate melt and hydrothermal solutions: partition of NaCl-KCl. Geochim Cosmochim Acta 53:2617–2630

Shmulovich KI, Churakov SV (1998) Natural fluid phases at high temperatures and low pressures. J Geochem Explor 62:183–191

Shmulovich KI, Graham CM (2004) An experimental study of phase equilibria in the systems H_2O-CO_2-$CaCl_2$ and H_2O-CO_2-NaCl at high temperatures and pressures (500–800 °C, 0.5–0.9 GPa) geological and geophysical applications. Contrib Mineral Petrol 146:450–462

Shmulovich KI, Tkachenko SI, Plyasunova NV (1995) Phase equilibria in fl uid systems at high pressures and temperatures. In: Shmulovich KI, Yardley BWD, Gonchar GG (eds) Fluids in the crust. Chapman and Hall, New York, pp 193–214

Signorelli S, Carroll MR (2000) Solubility and fluid-melt partitioning of Cl in hydrous phonolitic melts. Geochim Cosmochim Acta 64(16):2851–2862

Signorelli S, Carroll MR (2002) Experimental study of Cl solubility in hydrous alkaline melts: constrains on the theoretical maximum amount of Cl in trachytic and phonolitic melts. Contrib Mineral Petrol 143:209–218

Signorelli S, Vaggelli G, Francalanci L, Rosi M (1999) Origin of magmas feeding the plinian phase of the Campanian Ignimbrite eruption, Phlegrean Fields (Italy): constraints based on matrix-glass and glass-inclusion compositions. J Volcanol Geotherm Res 91:199–220

Sigurdsson H (2000) Volcanic episodes and rates of volcanism. In: Sigurdsson H, Houghton BF, McNutt SR, Rymer H, Stix J (eds) Encyclopedia of volcanoes. Academic Press, San Diego, pp 271–279

Siwadamrongpong S, Koide M, Matusita K (2004) Prediction of chloride solubility in CaO-Al_2O_3-SiO_2 glass systems. J Non-Cryst Solids 347:114–120

Snyder GT, Fehn U (2002) Origin of iodine in volcanic fluids: ^{129}I results from the Central American Volcanic arc. Geochim Cosmochim Acta 21:3827–3838

Snyder GT, Fehn U, Goff F (2002) Iodine isotope ratios and halide concentrations in fluids of the Satsuma-Iwojima volcano, Japan. Earth Planets Space 54:265–273

Sobolev AV (1996) Melt inclusions in minerals as a source of principle petrological information. Petrology 4(3):209–222

Sobolev VS, Bazarova TY, Shugurova NA, Bazarov LS, Dolgov YA, Sorensen H (1970) A preliminary examination of fluid inclusions in nepheline, sorensenite, tugtukpite and chkalovite from the Ilímaussaq alkaline intrusion, South Greenland. Medd Grøn 181(11):32p

Sobolev AV, Krivolutskaya NA, Kuzmin DV (2009) Petrology of the parental melts and mantle sources of Siberian Trap magmatism. Petrology 17:253–286

Solomon S, Sanders RW, Garcia RR, Keys JG (1993) Increased chlorine dioxide over Antarctica caused by volcanic aerosols from Mount Pinatubo. Nature 363:245–248
Solovova IP, Girnis AV, Kogarko LN, Kononkova NN, Stoppa F, Rosatelli G (2005) Compositions of magmas and carbonate-silicate liquid immiscibility in the Vulture Alkaline Igneous Complex, Italy. Lithos 85:113–128
Solovova IP, Girnis AV, Ryabchikov ID, Kononkova NN (2009) Mechanisms of formation of barium-rich phlogopite and strontium-rich apatite during the final stages of alkaline magma evolution. Geochem Int 47(6):578–591
Sorensen H (1974) The alkaline rocks. Wiley, New York, p 622
Speer JA (1984) Micas in igneous rocks. In: Bailey SW (ed) Rev Mineral, vol 13, pp 299–356
Spilliaert N, Metrich N, Allard P (2006a) S-Cl-F degassing pattern of water rich alkali basalt: modelling and relationship with eruption styles of Mount Etna volcano. Earth Planet Sci Lett 248:772–786
Spilliaert N, Allard P, Metrich N, Sobolev A V (2006b) Melt inclusion record of the conditions of ascent, degassing, and extrusion of volatile-rich alkali basalt during the powerful 2002 flank eruption of Mount Etna (Italy). J Geophys Res B111. https://doi.org/10.1029/2005JB003934
Stebbins JF, Du L-S (2002) Choride ion sites in silicate and aluminosilicate glasses: a preliminary study by ^{35}Cl solid-state NMR. Am Mineral 87:359–363
Steel-MacInnis M, Lecumberri-Sanchez P, Bodnar RJ (2015) Synthetic fluid inclusions XX. Critical PT*x* properties of H_2O-$FeCl_2$ fluids. Geochim Cosmochim Acta 148:50–61
Stelling J, Botcharnikov RE, Beermann O, Nowak M (2008) Solubility of H_2O- and chlorine-bearing fluids in basaltic melt of Mount Etna at T = 1050–1205 °C and P = 200 MPa. Chem Geol 256:102–110
Stewart MA, Spivack AJ (2004) The stable-chlorine isotope compositions of natural and anthropogenic materials. Rev Mineral Geochem 55:231–254
Stock MJ, Humphreys MCS, Smith VC, Johnson RD, Pyle DM, EIMF (2015) New constraints on electron-beam induced halogen migration in apatite. Am Mineral 100:281–293
Stock MJ, Humphreys MCS, Smith VC, Isaia R, Pyle DM (2016) Late-stage volatile saturation as a potential trigger for explosive volcanic eruptions. Nat Geosci. https://doi.org/10.1038/NGEO2639
Stolper E, Holloway JR (1988) Experimental determination of the solubility of carbon dioxide in molten basalt at low pressure. Earth Planet Sci Lett 87(4):397–408
Stormer JC, Pierson ML, Tacker RC (1993) Variation of F-X-rays and Cl-X-ray intensity due to anisotropic diffusion in apatite furing electron microprobe analysis. Am Mineral 78:641–648
Straub SM (2008) Uniform processes of melt differentiation in the central Izu Bonin volcanic arc (NW Pacific). In: Annen C, Zellmer GF (eds) Dynamics of crustal magma transfer, storage and differentiation, vol 304. Geol Soc Lond Spec Publ, pp 261–283
Straub SM, Layne GD (2003) The systematics of chlorine, fluorine and water in Izu arc front volcanic rocks. Geochim Cosmochim Acta 67:4179–4204
Sugiura T, Mizutani Y, Oana S (1963) Fluorine, chlorine, bromine and iodine in volcanic gases. J Earth Sci Nagoya Univ 11:272
Suh CE, Luhr JF, Njome MS (2008) Olivine-hosted glass inclusions from scoriae erupted in 1954-2000 at Mount Cameroon Volcano, West Africa. J Volcanol Geotherm Res 169:1–33
Symonds RB, Rose WI, Reed MH, Lichte F, Finnegan DL (1987) Volatilization, transport and sublimation ofmetallic and non-metallic elements in high temperature gases at Merapi Volcano, Indonesia. Geochim Cosmochim Acta 51:2083–2101. https://doi.org/10.1016/0016-7037(87)90258-4
Symonds R, Rose WI, Reed MH (1988) Contribution of Cl- and F-bearing gases to the atmosphere by volcanoes. Nature 334:415–418
Symonds RB, Rose WI, Bluth GJS, Gerlach TM (1994) Volcanic-gas studies: methods, results and applications. In: Carroll MR, Holloway JR (eds) Volatiles in magmas. Rev Mineral, vol 30, pp 1–66
Symonds RB, Gerlach TM, Reed MH (2001) Magmatic gas scrubbing: implications for volcano monitoring. J Volcanol Geotherm Res 108:303–341

Tabazadeh A, Turco RP (1993) Stratospheric chlorine injection by volcanic emissions: HCl scavenging and implications for ozone. Nature 260:1082–1086
Tacker RC, Stormer JC (1989) A thermodynamic model for apatite solid-solutions, applicable to high-temperature geologic problems. Am Mineral 74:877–888
Tang M, Wang X-L, Xu X-S, Zhu C, Cheng T, Yu Y (2012) Neoproterozoic subducted materials in the generation of Mesozoic Luzong volcanic rocks: evidence from apatite geochemistry and Hf-Nd isotopic decoupling. Gondwana Res 21:266–280
Tanimoto S, Rehren T (2008) Interactions between silicate and salt melts in LBA glassmaking. J Archeol Sci 35:2566–2573
Tappen C, Webster JD, Roderick D, Mandeville CW (2009) Petrology and geochemistry of ca 2100–1000 aBP magmas of Augustine volcano Alaska. J Volcanol Geotherm Res 183:42–62
Taran YA (2009) Geochemistry of volcanic and hydrothermal fluids and volatile budget of the Kamchatka-Kuril subduction zone. Geochim Cosmochim Acta 73:1067–1094
Taran YA, Hedenquist JW, Korzhinsky MA, Tkachenko SI, Shmulovich KI (1995) Geochemistry of magmatic gases from Kudryavy volcano, Iturup, Kuril Islands. Geochim Cosmochim Acta 59(9):1749–1761
Tartese R, Anand M, Barnes JJ, Starkey NA, Franchi IA, Sano Y (2013) The abundance, distribution, and isotopic composition of hydrogen in the Moon as revealed by basaltic lunar samples: implications for the volatile inventory of the Moon. Geochim Cosmochim Acta 122:58–74
Teiber H, Marks MAW, Wenzel T, Siebel W, Altherr R, Markl G (2014) The distribution of halogens (F, Cl, Br) in granitoid rocks. Chem Geol 374–375:92–109
Teiber H, Scharrer M, Marks MAW, Arzamastsev AA, Wenzel T, Markl G (2015) Equilibrium partitioning and subsequent re-distribution of halogens among apatite-biotite-amphibole assemblages from mantle-derived plutonic rocks: complexities revealed. Lithos 220–223: 221–237
Textor C, Graf HF, Herzog M (2003a) Injection of gases into the stratosphere by explosive volcanic eruptions. J Geophys Res 108:D19. https://doi.org/10.1029/2002JD002987
Textor C, Sachs PM, Graf H-F, Hansteen TH (2003b) The 12900 years BP Laacher See eruption: estimation of volatile yields and simulation of their fate in the plume. In: Oppenheimer C, Pyle DM, Barclay J (eds) Volcanic degassing, vol 213. Geol Soc Lond Spec Publ, pp 307–328
Theys N, Van Roozendael M, Dils B, Hendrick F, Hao N, De Maziére M (2009) First satellite detection of volcanic bromine monoxide emission after the Kasatochi eruption. Geophys Res Lett 36(3):L03809
Theys N, De Smedt I et al (2014) First satellite detection of volcanic OClO after the eruption of Puyehue-Cordõn Caulle. Geophys Res Lett 41(2):667–672
Thomas R, Davidson P, Badanina E (2009) A melt and fluid inclusion assemblage in beryl from pegmatite in the Orlovka amazonite granite, East Transbaikalia, Russia: Implications for pegmatite-forming melt systems. Mineral Petrol 96:129–140
Thorarinsson S (1979) On the damage caused by volcanic eruptions with special reference to tephra and gases. In: Sheets PD, Grayson DK (eds) Volcanic activity and human ecology. Academic Press, New York, pp 125–159
Thordarson T, Self S (1996) Sulfur, chlorine and fluorine degassing and atmospheric loading by the Roza eruption, Columbia River Basalt Group, Washington, USA. J Volcanol Geotherm Res 784(1.2):49–73
Thordarson T, Self S (2003) Atmospheric and environmental effects of the 1783–1784 Laki eruption: a review and reassessment. J Geophys Res 108(D1):4011
Thordarson T, Self S, Oskarsson N, Hulsebosch T (1996) Sulfur, chlorine and fluorine degassing and atmospheric loading by the 1783–1784 Ad Laki (Skaft´ar Fires) eruption. Bull Volcanol 55:233–263
Timina TY, Sharygin VV, Golovin AV (2006) Melt evolution during the crystallization of basanites of the Tergesh Pipe, Northern Minusinsk Depression. Geochem Int 44(8):752–770

Tolstykh ML, Naumov VB, Yu Ozerov A, Kononkova NN (2001) Composition of magmas of the 1996 eruption at the Karymskii volcanic center, Kamchatka: evidence from melt inclusions. Geochem Int 39:447–458

Tolstykh ML, Naumov VB, Babanskii AD, Bogoyavlenskaya GE, Khubunaya SA (2003) Chemical composition, volatile components, and trace elements in andesitic magmas of the Kurile-Kamchatka Region. Petrology 11:407–425

Troll G, Gilbert MC (1974) Stability of fluorine Tremolite. EOS Trans Am Geophys Union 55:481 (abstract)

Ustinisik G, Nekvasil H, Lindsley DH (2011) Differential degassing of H_2O, Cl, F, and S: potential effects on lunar apatite. Am Mineral 96:1650–1653

Ustinisik G, Nekvasil H, Lindsley DH, McCubbin FM (2015) Degassing pathways of Cl-, F-, H-, and S-bearing magmas near the lunar surface: Implications for the composition and Cl isotopic values of lunar apatite. Am Mineral 100:1717–1727

Vaggelli G, De Vivo B, Trigila R (1993) Silicate-melt inclusions in recent Vesuvius lavas (1631–1944): II analytical chemistry. J Volcanol Geotherm Res 58(1):367–376

Van Valkenburg A, Pike RG (1952) Synthesis of mica. J Res Nat Bur Stan 48:360–369

Vance A, McGonigle AJS, Aiuppa A, Stith JL, Turnbull K, Von Glasow R (2010) Ozone depletion in tropospheric volcanic plumes. Geophys Res Lett 37(22):L22802

Vander Kaaden KE, McCubbin FM, Whitson ES, Hauri EH, Wang J (2012) Partitioning of F, Cl, and H_2O between apatite and a synthetic Shergottite liquid (QUE 94201) at 1.0 Gpa and 990–1000 °C. 43rd Lunar Planet Sci Conf, abs 1247

Vanko DA (1986) High-chlorine amphiboles from oceanic rocks: product of highly saline hydrothermal fluids? Am Mineral 71:51–59

Varrica D, Aiuppa A, Dongarrà G (2000) Volcanic and anthropogenic contribution to heavy metal content in lichens from Mt. Etna and Vulcano island (Sicily). Environ Pollut 108:153–162

Veksler IV (2004) Liquid immiscibility and its role at the magmatic-hydrothermal transition: a summary of experimental studies. Chem Geol 210:7–31

Veksler IV, Fedorchuk YM, Nielsen TFD (1998) Phase equilibria in the silica-undersaturated part of the $KAlSiO_4$-Mg_2SiO_4-Ca_2SiO_4-SiO_2-F system at 1 atm and the larnite-normative trend of melt evolution. Contrib Mineral Petrol 131:347–363

Veksler IV, Dorfman AM, Kamenetsky M, Dulski P, Dingwell DB (2005) Partitioning of lanthanides and Y between immiscible silicate and fluoride melts, fluorite and cryolite and the origin of the lanthanide tetrad effect in igneous rocks. Geochim Cosmochim Acta 69(11): 2847–2860

Veksler IV, Dorfman AM, Dulski P, Kamenetsky VS, Danyushevsky LV, Jeffries T, Dingwell DB (2012) Partitioning of elements between silicate melt and immiscible fluoride, chloride, carbonate, phosphate and sulfate melts, with implications to the origin of natrocarbonatite. Geochim Cosmochim Acta 79:20–40

Vigouroux N, Williams-Jones AE, Wallace PJ, Staudacher T (2009) The November 2002 eruption of Piton De La Fournaise, Reunion: tracking the pre-eruptive thermal evolution of magma using melt inclusions. Bull Volcanol 71:1077–1089

Villemant B, Mouatt J, Michel A (2008) Andesitic magma degassing investigated through H_2O vapour-melt partitioning of halogens at Soufriére Hills Volcano, Montserrat (Lesser Antilles). Earth Planet Sci Lett 269:212–229

von Glasow R (2010) Atmospheric chemistry in volcanic plumes. PNAS 107(15):6594–6599

von Glasow R, Crutzen PJ (2014) Tropospheric halogen chemistry. Treatise on geochemistry, 2nd edn. https://doi.org/10.1016/B978-0-08-095975-7.00402-2

von Glasow R, Bobrowski N, Kern C (2009) The effects of volcanic eruptions on atmospheric chemistry. Chem Geol 263(1–4):131–142

Vukadinovic D, Edgar AD (1993) Phase relations in the phlogopite-apatite system at 20 kbar: implications for the role of fluorine in mantle melting. Contrib Mineral Petrol 114:247–254

Wade JA, Plank T, Melson WG, Soto GJ, Hauri EH (2006) The volatile content of magmas from Arenal volcano, Costa Rica. J Volcanol Geotherm Res 157:94–120

Wallace PJ (2005) Volatiles in subduction zone magmas: concentrations and fluxes based on melt inclusion and volcanic gas data. J Volcanol Geotherm Res 140:217–240
Wallace PJ, Anderson AT (1999) Gradients in H_2O, CO_2, and exsolved gas in a large-volume silicic magma system: interpreting the record preserved in melt inclusions from the Bishop Tuff. J Geophys Res 104(B):20097–20122
Wang L-X, Marks MAW, Keller J, Markl G (2014) Halogen variations in alkaline rocks from the Upper Rhine Graben (SW Germany): insights into F, Cl and Br behavior during magmatic processes. Chem Geol 380:133–144
Wanless VD, Perfit MR, Ridley WI, Klein E (2010) Dacite petrogenesis on mid-ocean ridges: evidence for oceanic crustal melting and assimilation. J Petrol 51(12):2377–2410
Wanless VD, Perfit MR, Ridley WI, Wallace PJ, Grimes CB, Klein EM (2011) Volatile abundances and oxygen isotopes in basaltic to dacitic lavas on mid-ocean ridges: the role of assimilation at spreading centers. Chem Geol 287:54–65
Warner S, Martin RF, Abdel-Rahman A-FM, Doig R (1998) Apatite as a monitor of fractionation, degassing, and metamorphism in the Sudbury igneous complex, Ontario. Can Mineral 36:981–999
Watson EB (1979) Apatite saturation in basic to intermediate magmas. Geophys Res Lett 6:937–940
Watson EB (1980) Apatite and phosphorus in mantle source regions: An experimental study of apatite/melt equilibria at pressures to 25 kbar. Earth Planet Sci Lett 51:322–335
Watson EB (1994) Diffusion in volatile-bearing magmas, In: Carroll MR, Holloway JR (eds) Volatiles in magmas. Rev Mineral, vol 30, pp 371–411
Watson EB, Bender JF (1980) Diffusion of cesium, samarium, strontium, and chlorine in molten silicate at high temperatures and pressures, Geological Society of America, Abstracts with programs 12, 545
Webb SL, Murton BJ, Wheeler AJ (2014) Rheology and the Fe^{3+}-chlorine reaction in basaltic melts. Chem Geol 366:24–31
Webster JD (1990) Partitioning of F between H_2O and CO_2 fluids and topaz rhyolite melt. Contrib Mineral Petrol 104:424–438
Webster JD (1992a) Fluid-melt interactions involving Cl-rich granites: Experimental study from 2 to 8 kbar. Geochim Cosmochim Acta 56:659–678
Webster JD (1992b) Water solubility and chlorine partitioning in Cl-rich granitic systems: effects of melt composition at 2 kbar and 800 °C. Geochim Cosmochim Acta 56:679–687
Webster JD (2004) The exsolution of magmatic hydrosaline melts. Chem Geol 210:33–48
Webster JD, De Vivo B (2002) Experimental and modeled solubilities of chlorine in aluminosilicate melts, consequences of magma evolution, and implications for exsolution of hydrous chloride melt at Mt. Somma-Vesuvius. Am Mineral 87:1046–1061
Webster JD, Duffield WA (1994) Extreme halogen abundances in tin-rich magma of the Taylor Creek rhyolite New Mexico. Econ Geol 89:840–850
Webster JD, Holloway JR (1988) Experimental constraints on the partitioning of Cl between topaz rhyolite melt and H_2O and H_2O + CO_2 fluids: new implications for granitic differentiation and ore deposition. Geochim Cosmochim Acta 52:2091–2105
Webster JD, Holloway JR (1990) Partitioning of F and Cl between magmatic hydrothermal fluids and highly evolved granitic magmas. Geol Soc Am Spec Pap 246:21–34
Webster JD, Mandeville CW (2007) Fluid immiscibility in volcanic systems. In: Leibscher A, Heinrich C (eds) Fluid-fluid equilibria in the crust. Rev Mineral Geochem, vol 65, pp 313–362
Webster JD, Piccoli PM (2015) Magmatic apatite: a powerful, yet deceptive, mineral. Elements 11:185–190
Webster JD, Thomas R, Rhede D, Foerster H-J, Seltmann R (1997) Melt inclusions in quartz from an evolved peraluminous pegmatite: geochemical evidence for strong tin enrichment in fluorine-rich and phosphorus-rich residual liquids. Geochim Cosmochim Acta 61:2589–2604
Webster JD, Rebbert CR (1998) Experimental investigation of H_2O and Cl solubilities in F-enriched silicate liquids: implications for volatile saturation of topaz rhyolite magmas. Contrib Mineral Petrol 132:198–207

Webster JD, Kinzler RJ, Mathez EA (1999) Chloride and water solubility in basalt and andesite liquids and implications for magmatic degassing. Geochim Cosmochim Acta 63:729–738
Webster JD, De Vivo B, Tappen C (2003) Volatiles, magmatic degassing and eruptions of Mt. Somma-Vesuvius: constraints from silicate melt inclusions, solubility experiments and modeling. In: De Vivo B, Bodnar RJ (eds) Melt inclusions in volcanic systems: methods, applications and problems, vol 5. Elsevier, Amsterdam, pp 207–226
Webster JD, Thomas R, Förster H-J, Seltmann R, Tappen C (2004) Geochemical evolution of halogen-enriched granite magmas and mineralizing fluids of the Zinnwald tin-tungsten mining district, Erzgebirge, Germany. Mineral Deposita 39:452–472
Webster JD, Sintoni MF, De Vivo B (2006) The role of sulfur in promoting magmatic degassing and volcanic eruption at Mt. Somma-Vesuvius. In: De Vivo B (ed) Volcanism in the Campania Plain: Vesuvius, Campi Flegrei and ignimbrites. Elsevier, Amsterdam, pp 219–233
Webster JD, Sintoni MF, De Vivo B (2009a) The partitioning behavior of Cl and S in aqueous fluid- and saline-liquid saturated phonolitic and trachytic melts at 200 MPa. Chem Geol 263:19–36
Webster JD, Tappen C, Mandeville CW (2009b) Partitioning behavior of chlorine and fluorine in the system apatite-melt-fluid: II. Felsic silicate systems at 200 MPa. Geochim Cosmochim Acta 73:559–581
Webster JD, Mandeville CW, Goldoff B, Coombs ML, Tappen C (2010) Augustine volcano Alaska: the influence of volatile components in magmas erupted AD 2006 to 2100 years before present In: J Power ML Coombs J Freymueller (eds) The 2006 Eruption of Augustine Volcano. US Geol Surv Prof Pap 1769:383–423
Webster JD, Goldoff B, Sintoni MF, Shimizu N, De Vivo B (2014) C-O-H-Cl-S-F volatile solubilities, partitioning, and mixing in phonolitic-trachytic melts and aqueous-carbonic vapor ± saline liquid at 200 MPa. J Petrol 55(11):2217–2248
Webster JD, Vetere F, Botcharnikov RE, Goldoff B, McBirney A, Doherty AL (2015) Experimental and modeled chlorine solubilities in aluminosilicate melts at 1 to 7000 bars and 700 to 1250 °C: Applications to magmas of Augustine Volcano, Alaska. Am Mineral 100:522–535
Webster JD, Goldoff BA, Flesch RN, Nadeau PA, Silbert ZW (2017) Hydroxyl, Cl, and F partitioning between highsilica rhyolitic melts-apatite-fluid(s) at 50–200 MPa and 700–1000 ° C. Am Mineral 102:61–74
Weston BM (2012) Noble gases and halogens in Icelandic basalts. PhD Dissertation, University of Manchester, p 225
Willmore CC, Boudreau AE, Kruger FJ (2000) The halogen geochemistry of the Bushveld complex, Republic of South Africa: Implications for the chalcophile element distribution in the lower and critical zones. J Petrol 41:1517–1539
Witham CS, Oppenheimer C (2005) Mortality in England during the 1783–4 Laki Craters eruption. Bull Volcanol 67:15–26
Witham F, Blundy J, Kohn SC, Lesne P, Dixon J, Churakov SV, Botcharnikov R (2012) SolEx: a model for mixed COHSCl-volatile solubilities and exsolved gas compositions in basalt. Comp Geosci 45:87–97
Witt MLI, Mather TA, Pyle DM, Aiuppa A, Bagnato E Tsanev VI (2008) Mercury and halogen emissions from Masaya and Telica volcanoes, Nicaragua. J Geophys Res 113:B06203
Wones DR, Gilbert MC (1982) Amphiboles in the igneous environment. In: Veblen DR, Ribbe PH (eds) Rev Mineral 9B:355–390
Wood BJ, Nicholls J (1978) The thermodynamic properties of reciprocal solid solutions. Contrib Mineral Petrol 66(4):389–400
Wu J, Koga KT (2013) Fluorine partitioning between hydrous minerals and aqueous fluid at 1 GPa and 770–947 ºC: a new constraint on slab flux. Geochim Cosmochim Acta 119:77–92
Wysocznski RJ, Wright IC, Gamble JA, Hauri EH, Luhr JF, Eggins SM, Handler MR (2006) Volatile contents of Kermadec Arc-Havre Trough pillow glasses: fingerprinting slab-derived

aqueous fluids in the mantle sources of arc and back-arc lavas. J Volcanol Geotherm Res 152:51–73

Yang K, Scott SD (2005) Vigorous exsolution of volatiles in the magma chamber beneath a hydrothermal system on the modern sea floor of the eastern Manus back-arc basin, Western Pacific: evidence from melt inclusions. Econ Geol 100:1085–1096

Zajacz Z, Candela PA, Piccoli PM, Sanchez-Valle C (2012) The partitioning of sulfur and chlorine between andesite melts and magmatic volatiles and the exchange coefficients of major cations. Geochim Cosmochim Acta 89:81–101

Zelenski M, Taran Y (2012) Volcanic emissions of molecular chlorine. Geochim Cosmochim Acta 87:210–226. https://doi.org/10.1016/j.gca.2012.03.034

Zelenski M, Fischer TP. de Moor JM, Marty B, Zimmermann L, Ayalew D, Nekrasov AN, Karandashev VK (2013) Trace elements in gas emissions from the Erta ale volcano, Afar, Ethiopia. Chem Geol 357:95–116

Zeng Q, Stebbins JF (2000) Fluoride sites in aluminosilicate glasses: High-resolution ^{19}F NMR results. Am Mineral 85:863–867

Zhang C, Holtz F, Ma C, Wolff PE, Li X (2012) Tracing the evolution and distribution of F and Cl in plutonic systems from volatile-bearing minerals: a case study from the Liujiawa pluton (Dabie orogeny, China). Contrib Mineral Petrol 164:859–879

Zhu C, Sverjensky DA (1991) Partitioning of F-Cl-OH between minerals and hydrothermal fluids. Geochim Cosmochim Acta 55:1837–1858

Zhu C, Sverjensky DA (1992) F-Cl-OH partitioning between biotite and apatite. Geochim Cosmochim Acta 56:3435–3467

Zimova M, Webb S (2006) The effect of chlorine on the viscosity of Na_2O-Fe_2O_3-Al_2O_3-SiO_2 melts. Am Mineral 91:344–352

Zimova M, Webb S (2007) The combined effects of chlorine and fluorine on the viscosity of aluminosilicate melts. Geochim Cosmochim Acta 71:1553–1562

Chapter 7
Halogens in Silicic Magmas and Their Hydrothermal Systems

David Dolejš and Zoltán Zajacz

Abstract Halogens, mainly F and Cl, play key roles in the evolution and rheology of silicic magmas, magmatic-hydrothermal transition, partitioning of metals into aqueous fluids, and formation of ore deposits. Similarity of ionic radii of O, hydroxyl, and F, and a much greater size of Cl are responsible for (i) higher solubility, hence compatibility of F in silicate melts, (ii) greater lattice energies of fluorides, therefore their more refractory character and lower solubilities in fluids, and (iii) higher hardness of F as ligand for complexing, leading to a distinct spectrum of metal-fluoride versus metal-chloride complexes. In the F-rich systems, the interaction of F with rock-forming aluminosilicates corresponds to progressive fluorination by the thermodynamic component F_2O_{-1}. Formation of F-bearing minerals first occurs in peralkaline and silica-undersaturated systems that buffer F concentrations at very low levels (villiaumite, fluorite). The highest concentrations of F are reached in peraluminous silica-saturated systems, where fluorite or topaz are stable. Coordination differences and short-range order effects between [NaAl]–F, Na–F versus Si–O lead to the fluoride-silicate liquid immiscibility, which extends from the silica–cryolite binary to the peralkaline albite–silica–cryolite ternary and to peraluminous topaz-bearing systems, where it may propagate to solidus temperatures in the presence of other components such as Li. Differentiation paths of silicic magmas diverge, depending on the Ca-F proportions. In the Ca-rich systems, the F enrichment is severely limited by fluorite crystallization, whereas the Ca-poor magmas evolve to the high F concentrations and saturate with topaz, cryolite, or immiscible multicomponent fluoride melts (brines). These liquids preferentially partition and decouple high-field strength elements and rare-earth

D. Dolejš (✉)
Institute of Earth and Environmental Sciences, University of Freiburg, 79104 Freiburg i.Br., Germany
e-mail: david.dolejs@minpet.uni-freiburg.de

Z. Zajacz
Department of Earth Sciences, University of Toronto, ON M5S 3B1 Toronto, Canada
e-mail: zajacz@es.utoronto.ca

D.E. Harlov and L. Aranovich (eds.), *The Role of Halogens in Terrestrial and Extraterrestrial Geochemical Processes*, Springer Geochemistry,
https://doi.org/10.1007/978-3-319-61667-4_7

elements (REE), and are responsible for the appearance of non-chondritic element ratios and/or lanthanide tetrad effects. Continuous transition from volatile-rich silicate melts to hydrothermal fluids is unlikely, although two fluids—hydrous halide melts and solute-poor aqueous fluids—may often exsolve simultaneously. The fluoride ligand is responsible for the effective sequestration of hard cations, mainly REE, Th, U, and Zr, into the hydrothermal fluids. In the Cl-dominated systems, the maximum concentrations in silicate melts are significantly lower than those of F due to the absence of bonding between Cl and network-forming cations in the melt structure. The typical Cl-rich phase in felsic magmas is an aqueous ± carbonic fluid phase; the saturation of which limits the attainable concentration of Cl in the silicate melt. The more depolymerized the structure of the silicate melt is, the more easily metal-chloride species are accommodated. Therefore, metaluminous rhyolites are characterized by the highest fluid/melt partition coefficients for Cl as well as the lowest maximum dissolved Cl concentration. Chlorine is dominantly present as NaCl, KCl, $CaCl_2$, $FeCl_2$, and HCl species in aqueous magmatic fluids; their relative proportions are strongly influenced by silicate melt composition, pressure and total dissolved chloride concentration. The activity coefficients of metal-chloride species in the aqueous fluid are strongly dependent on pressure and total chloride concentration, and so is the volatile/melt partition coefficient of Cl. The increase of pressure strongly promotes Cl partitioning into the fluid phase, whereas increased chloride concentrations in the fluid work against it, especially if vapor-brine immiscibility occurs anchoring the activity of major chloride species in the system. Chloride ions are dominant, or at least take the form of significant complex forming ligands for a broad range of economically important elements found in magmatic-hydrothermal ore deposits such as Cu, Au, Mo, Pb, Zn, Sn, and W. Therefore, Cl has significant effect on the volatile/melt and vapor/brine partition coefficients of these elements, and at least partially controls the likelihood of the formation of economic ore mineralization.

7.1 Introduction

Highly differentiated silicic igneous rocks represent the genetic link between magmatic and hydrothermal processes. Granitic rocks of A- or S-type affinity commonly exhibit enrichment in a combination of volatile components (F, B), rare alkalies (Li, Rb, Cs), and high-field strength elements (Zr, Nb, Ta, U, Th) as a consequence of the overall incompatibility of these constituents in rock-forming minerals or an aqueous fluid phase, and protracted differentiation in these magmatic systems (e.g., Linnen and Cuney 2005; Linnen et al. 2012). The abundance of incompatible volatile constituents including halogens may reach levels that significantly affect both the chemical and physical properties of evolving granite or pegmatite systems. In addition to F, silicate magmas contain minor quantities of other halogens with greater ionic radii (Cl, Br, I), which strongly partition into hydrothermal fluid phase upon volatile saturation (Bureau and Keppler 1999).

Despite the same valence state, strong differences in ionic radii and polarizability of halide ions underlie the different roles these elements play during magmatic-hydrothermal transition. The similarity of ionic radius of F and that of O is universally responsible for its greater solubility in silicate melts (e.g., Bureau and Keppler 1999). This fact, therefore, implies the generally more compatible behavior of F during fluid saturation and consequent effects for the structure and rheology of residual melts. In addition, the smaller ionic radius of F, when compared to other halogens, leads to larger lattice energies for the fluorides as opposed to the chlorides. This phenomenon determines the more refractory (high-temperature) nature of F compounds relative to chlorides, and it dictates the generally larger solubility of chlorides in aqueous fluids. As a consequence, the small solubility of Cl in silicate melts and its greater solubility in aqueous fluids lead to dramatically different partitioning behavior during magmatic-hydrothermal transitions. These fundamental chemical properties underlie the profound differences in the behavior of F and Cl as the two most abundant halogens in the Earth's magmatic and hydrothermal systems (Wenk and Bulakh 2004).

In this chapter we examine the chemical characteristics of halogens and their impact on solubility in silicate magmas, stability of halogen-bearing minerals, and/or immiscible halide melts, as well as mechanisms of magmatic-hydrothermal transition and element partitioning. We first present thermodynamic analysis of F-bearing silicate systems and predict the stabilities of diverse fluoride minerals in natural igneous rocks. Experimental phase equilibria are used to constrain the differentiation paths of fluorosilicate magmas and the conditions favourable for fluoride–silicate liquid–liquid immiscibility. Chemographic and thermodynamic analysis of the silicate–halide–H_2O systems is then used to predict the nature of the magmatic-hydrothermal transition, that is, exsolution of halide liquids, brines, and dilute aqueous fluids. We subsequently discuss how various physical-chemical variables affect the element partitioning between silicate melts and aqueous magmatic fluids, with the main attention being paid to the speciation of Cl in magmatic fluids, which controls the exchange of major cations and hydrogen between the melt and the fluid phase. We also provide an overview of the effect of Cl on the sequestration of the most important magmatic-hydrothermal ore forming metals from felsic melts and the partitioning of these metals between the vapor and brine phases in subcritical salt–H_2O fluids.

7.2 Behavior and Distribution of Halogens in Silicate Magmas

7.2.1 Chemical Characteristics of Halogens

Halogens belong to the volatile constituents in silicate melts, which also comprise H_2O, CO_2, B, and to a lesser extent S (Carroll and Holloway 1994). Individual concentrations of volatile constituents may exceed 5 wt% (e.g., F or H_2O; Webster

et al. 1997; Dolejš and Baker 2004; Thomas et al. 2005), but some remain less than 1 wt% (e.g., Cl or CO_2, S; Carroll and Webster 1994; Holzheid and Grove 2002; O'Neill and Mavrogenes 2002). These differences impart variable effects on the physical properties and equilibria of silicate magmas, and may be rationalized by two general observations:

(i) The solubilities of halogens and other volatiles increase with increasing melt depolymerization. This trend is related to an increasing number of available sites which are either electrostatically terminated and/or host network formers (Pelton et al. 1993; Pelton and Wu 1999). In turn, such sites act as source of low-valence cations for the formation of halide, carbonate, or hydroxide complexes, thus promoting the volatile solubilities (Brooker et al. 2001; Webster et al. 2015).

(ii) The solubility of halogens and chalcogens decreases with a progressive mismatch between the ionic radius of the substituent and that of O as part of the aluminosilicate network (cf., Bureau et al. 2000). These differences in solubilities become much more significant when considered on a molar basis. Consider 5 wt% F dissolved in an albitic melt, which corresponds to 42 mol% F when using F and $NaAlSi_3O_8$ as components. That is, the melt contains nearly one fluoride per four aluminosilicate tetrahedra or one tetrahedral quadruplet. This example underlies the substantial effect of light volatiles on the properties of silicate melts, in particular, phase equilibria, element partitioning, melt density, and viscosity (Korzhinskiy 1959, 1960; Kushiro 1975; Dingwell et al. 1996; Giordano et al. 2004).

Fluorine, Cl, Br, and I exhibit variable concentrations in the silicate melt, which generally decrease with increasing ionic radius (Bureau et al. 2000). Radii of halide anions decrease from 2.20 (I^-) to 1.33 Å (F^-), the latter being very close to O and hydroxyl radii (1.40 and 1.37 Å, respectively; Shannon 1976; Fig. 7.1a). Subject to steric requirements and short-range order, F can readily substitute for O on the vertices of aluminate or silicate tetrahedra, which promotes its solubility in the melt (Webster 1990; Dolejš and Baker 2007a) whereas incorporation of I or S (1.84 Å) is restricted to interstitial or network-modifier sites, and this limits their solubility in the melt. This effect, when combined with differences in halide solubilities in aqueous fluids, leads to a linear relationship between the the fluid/melt partitioning coefficients of halogens and their ionic radius (Bureau et al. 2000; Fig. 7.1b; for symbol explanation see Table 7.1).

7.2.2 *Structure and Short-Range Ordering in Halogen-Bearing Melts*

Silicate melts contain cations and anions with a wide range of electronic polarizabilities that affect the chemical compatibility of species and short-range order. The transfer of electrons from the shell of a cation to the bonding sphere of

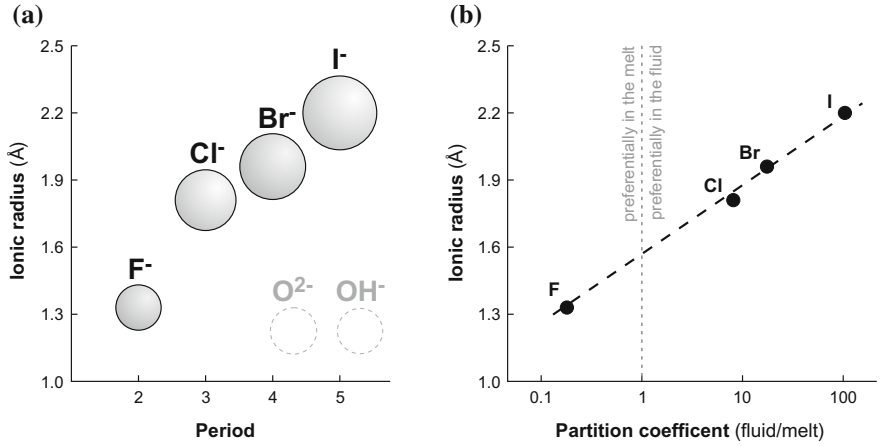

Fig. 7.1 Ionic radii of halogens. **a** Comparison with those of O and hydroxyl (Shannon 1976). **b** Illustration of halogen incompatibility in silicate melts and their preferential partitioning into aqueous fluid as the ionic radius increases (Bureau et al. 2000)

Table 7.1 Notation

Symbol	Definition
a_i^j	Activity of component *i* in phase *j*
ASI	Alumina saturation index, molar Al/(Na + K + 2Ca)
b	Brine
C_i^j	Concentration of solute *i* in phase *j*
$D_i^{j/k}$	Mass fraction-based partition coefficient of element *i* between phases *j* and *k*
e	Eutectic
f	Fluid, generally refers to aqueous fluid phase
fl	Fluoride melt or component
G	Molar Gibbs energy
K	Equilibrium constant
m	Melt
m_i^j	Molality of solute *i* in phase *j*
s	Solid
sil	Silicate melt or component
v	Vapor
V	Molar volume
X_i^j	Mole fraction of constituent *i* in phase *j*
γ_i^j	Activity coefficient of constituent *i* in phase *j*

an anion results in greater thermodynamic stability of ionic compounds (e.g., Navrotsky 1994) and can be regarded as an acid-base reaction by the Lewis definition (Lewis 1938; Flood and Förland 1947).

The Lewis acidity or basicity is quantitatively defined by two alternative scales: (i) cation and anion bonding strength for crystalline solids (Brown 1981; Hawthorne 1985, 1992), or (ii) optical basicity for oxide glasses and melts (Duffy and Ingram 1971; Duffy 1993, 1996). In the former, the bonding strength of the cation is a measure of its ability to donate electrons (Lewis definition of an acid; Lewis 1923), hence cation bond strengths positively correlate with electronegativity (Zhang 1982; Brown 1988; Brown and Skowron 1990).

For practical applications, the values of bond valences around a specific cation are calculated as the cation valence divided by its coordination number (e.g., Brown 1981, 2000). As an example, consider P^{5+}, which is exclusively found in the tetrahedral coordination, whose bond valence is 5/4 = 1.25 valence units. In a wide range of crystal structures, cation valences vary by ~20% from the mean value only, which provides a basis for the assessment of the compatibilities of individual cations with specific anionic groups. To illustrate, Na^+ has a bonding strength of 0.16 valence units, which fits very well with that of Cl^- = 0.14 indicating that NaCl forms a stable periodic structure (Brown 2000). This matching principle is applied to various combinations of cations with anionic groups (Fig. 7.2). It also allows for the qualitative estimate of the compound or species stability (e.g., forsterite, apatite vs. K_3PO_4). Comparison of the Lewis acid-base properties greatly simplifies considerations about compound stability, appropriate species in aqueous fluids or choice of thermodynamic components (Brown 1992, 2000).

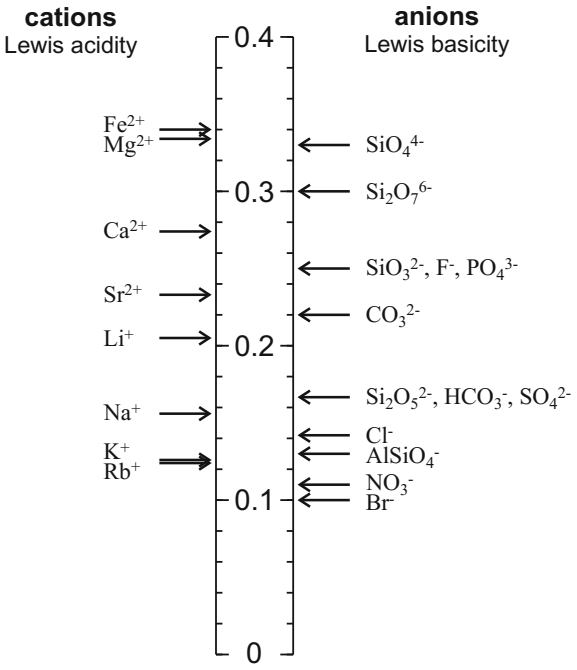

Fig. 7.2 Illustration of the bond valence matching principle between cations (Lewis acids) and anions (Lewis bases). Note, for instance, the compatibility of Na–$AlSiO_4$, K–$AlSiO_4$, Mg–SiO_4, Ca–PO_4 etc. (Brown 2000)

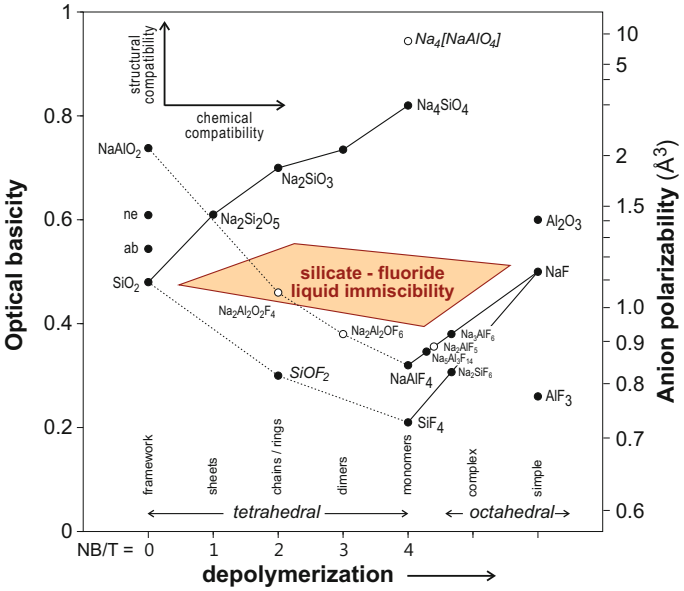

Fig. 7.3 Optical basicity versus structural variation for compounds in the system Na_2O–$NaAlO_2$–SiO_2–F_2O_{-1} (Dolejš and Baker 2005). Optical basicities of individual species were calculated according to Duffy (1989, 1993) and the anion polarizability scale is based on data of Duffy (1989). Symbols: *solid circles*—solid phases and species, *open circles*—melt species (Sterten 1980; Zhang et al. 2002). Equilibria proceed in order to minimize differences in optical basicity, i.e., chemically compatible compounds plot at the same vertical level. The large central field, represented by the chemical and structural gap, corresponds to the liquid–liquid immiscibility in the SiO_2–NaF system (Anfilogov et al. 1979)

For compounds and complex species, optical basicity (Duffy 1993, 1996; Fig. 7.3) provides a quantitative scale for the Lewis acid-base properties, whereby chemical equilibria proceed towards products with minimal differences in optical basicity. This approach replaced previous attempts to predict compatibility and speciation in fluorosilicate melts using the thermodynamic data of solids and gases in hypothetical reaction equilibria (Kogarko et al. 1968; Snow and Welch 1972; Bragina and Anfilogov 1980; Rutlin and Grande 1997, 1998; Siljan et al. 2001). The use of the optical basicity scale is particularly suitable for liquids because of its derivation from spectroscopic measurements of glasses (rather than crystalline phases). It is independent of the availability or accuracy of thermodynamic data and is linear with composition.

Various applications of the optical-basicity concept to phase equilibria are discussed by Duffy (1993, 1996) and we illustrate this approach by several examples. In the silicate systems with F, the equilibrium between free fluoride ions (F^-) and

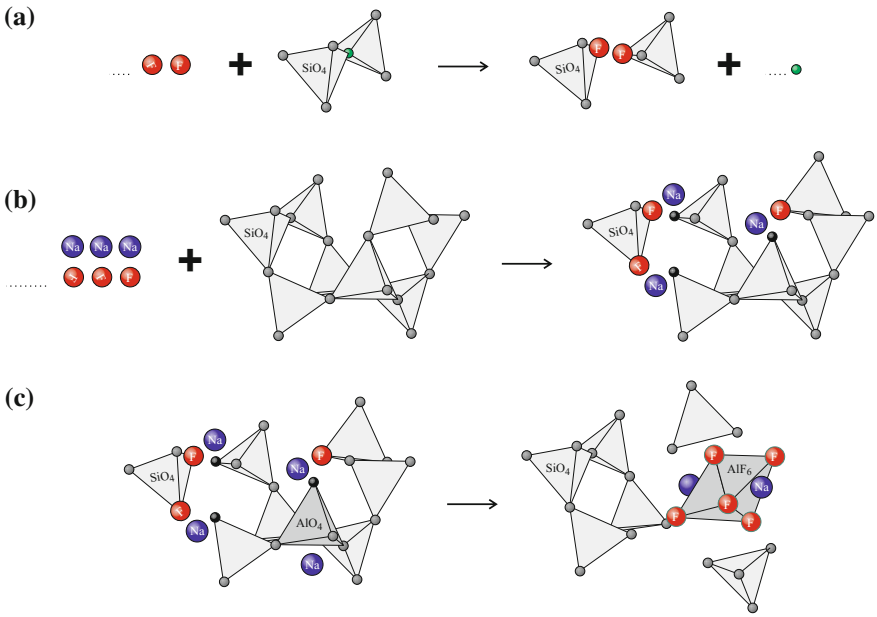

Fig. 7.4 Schematic representation of F interaction with silicate framework. **a** Depolymerization of the network of silicate tetrahedra by replacement of the bridging O atom by a pair of terminal F atoms. **b** Addition of alkali fluoride leading to network depolymerization by converting the bridging O atom into a non-bridging one, charge-balanced by Na, and a terminal F atom (Eq. 7.1). c Short-range ordering between Na cations and AlF_6 octahedra, as a pre-requisite of separation between aluminofluoride and silicate melt

anions of silicate tetrahedra—bridging O (O^0), non-bridging O (O^-), and terminal F atoms (F^0) can be represented as follows (Fig. 7.4):

$$F^- \,(\text{free}) + O^0 \,(\text{bridging}) = O^- \,(\text{non-bridging}) + F^0 \,(\text{terminal}). \tag{7.1}$$

In the molecular-species notation, this homogeneous equilibrium corresponds, for instance, to:

$$\text{NaF}(0.50) + 1/2\,\text{SiO}_2(0.48) = 1/4\,\text{Na}_4\text{SiO}_4(0.82) + 1/4\,\text{SiF}_4(0.21) \tag{7.2}$$

where numbers in parentheses indicate non-dimensional values of optical basicity (Duffy 1989, 1996). The reactions proceed in order to minimize differences in basicity, thus, Na–F and Si–O^0 bonds are compatible (difference in basicities is 0.02) and Si–O^- and Si–F^0 bonds are relatively unstable (difference in basicities is 0.61; Fig. 7.3). This trend is characteristic for all alkali fluoride-alkali silicate systems and indicates that the extent of formation of Si-F bonds is small. This prediction is in agreement with spectroscopic measurements in F-bearing aluminosilicate systems (Mysen and Virgo 1985a, b; Schaller et al. 1992; Mysen et al. 2004).

In the Al_2O_3-bearing systems, short-range order between tetrahedron centers (Si and [NaAl]) and terminations (O^0 and F^0) is described by:

$$[\mathrm{NaAl}]-\mathrm{F}^0\big|\mathrm{F}^0-[\mathrm{NaAl}]+\mathrm{Si}-\mathrm{O}^0-\mathrm{Si}=[\mathrm{NaAl}]-\mathrm{O}^0-[\mathrm{NaAl}]+\mathrm{Si}-\mathrm{F}^0\big|\mathrm{F}^0-\mathrm{Si}. \tag{7.3}$$

Note that one O bridge, –O°–, must be replaced by a pair of F terminations, –F° |F°–, in order to maintain the charge balance. In the species notation, this equilibrium (Eq. 7.3) has the following form:

$$1/2\,\mathrm{NaAlF_4}\,(0.32)+1/2\,\mathrm{SiO_2}\,(0.48)=1/2\,\mathrm{NaAlO_2}\,(0.74)+1/2\,\mathrm{SiF_4}\,(0.21) \tag{7.4}$$

where the numbers in parentheses indicate values of optical basicity (Duffy 1989, 1996). The differences in optical basicity for original and resulting configurations are 0.16 and 0.53, respectively, and predict the shift in equilibrium to the left, i.e., resulting in ordering of F terminal atoms to aluminate tetrahedra and Si–F avoidance. This prediction is supported by results of spectroscopic studies (Mysen and Virgo 1985a, b; Schaller et al. 1992; Stebbins and Zeng 2000; Mysen et al. 2004).

7.2.3 Halogen Complexing in Aqueous Fluids

Chemical elements, and in particular, economic metals in magmatic fluids are commonly associated with various ligands, most notably Cl^-, F^-, HCl^o, OH^-, HS^-, H_2S^o, and potentially SO_4^{2-} (e.g., Candela and Piccoli 1995; Barnes 1997; Williams-Jones and Heinrich 2005). Therefore, the concentration of these ligands in magmatic fluids significantly impacts their fluid/melt partition coefficients. The affinities of various metal cations to associate with various ligands are highly variable. A simple way to predict relative stabilities of aqueous complexes is the application of the hard-soft acid-base (HSAB) theory (Pearson 1968a, b). The HSAB theory distinguishes Lewis acids (electron acceptors, usually metal cations) and Lewis bases (electron donors, or ligands). Hard acids and bases have high electronegativity, low polarizability and generally high valence state, whereas soft acids and soft bases have low electronegativity, high polarizability and low valence state. Therefore, cations with small ionic radii and high positive charge behave as hard acids, whereas cations with large ionic radii and low positive charge are typically soft acids. Similar statements can be made for bases except their valence state is negative. Hard acids tend to form stable complexes with hard bases through ionic bonds whereas soft acids make stable covalently bonded complexes with soft bases. When considering aqueous geologic fluids, the most significant examples for hard acids are the following: H^+, Na^+, K^+, Si^{4+}, Al^{3+}, Fe^{2+}, Ca^{2+}, Mg^{2+}, Sr^{2+}, Mo^{6+}, Sn^{4+}, U^{6+}, ions of rare earth elements (REE) and other cations

with high field strength. Geologically important soft acids are Au^{+}, Cu^{+}, Ag^{+}, Pt^{2+}, Pd^{2+}, Hg^{2+}, and Cd^{2+} (Pearson 1968a, b; Parr and Pearson 1983). Halogens become softer bases with increasing ionic radius as their electronegativity decreases. The fluoride ion is one of the hardest bases, whereas the iodide ion is a soft base. The chloride and bromide ions show borderline properties between hard and soft bases. Consider the complexing between halogens and Au as an example. Gold is a soft acid in its monovalent state, and the stability constants of Au(I) halogenide complexes increase as the participating halogens become softer. At ambient conditions, the stability constants of Au halogenide complexes are as follows: $\log K_{AuCl_2^-} = 9.6$, $\log K_{AuBr_2^-} = 12.4$, $\log K_{AuI_2^-} = 19$ (Seward 1989; Akinfiev and Zotov 2010). Though, as the above example shows, Br and I are expected to form stronger complexes with soft acids such as Au^{+}, their significance in the transport of such metals in magmatic and hydrothermal systems will likely be severely limited by their much lower abundance relative to Cl and F in geological systems.

A representative example to demonstrate the borderline base properties of chloride ions is the stability of REE chloride complexes in hydrothermal fluids. The REE(III) ions are in general hard acids but they become smaller and harder from La to Lu. Migdisov et al. (2009) showed that the formation constants of $REECl^{2+}$ aqueous complexes gradually increase from Lu to La, i.e., from a harder hard acid to a softer hard acid. Increasing stability of REE-chloride complexes with increasing REE cation radius were also observed in high-density aqueous fluids in the P-T regime of slab dehydration by Tsay et al. (2014). Another example for such borderline behavior of Cl^{-} can be demonstrated using the solubility and partitioning behavior of Cu. Though Cu is classified as a soft acid, it has been shown that in most high temperature geologic fluids, chloride ions form strong complexes with Cu and therefore primarily control the fluid/melt partition coefficients of Cu (Candela and Holland 1984; Williams et al. 1995; Zajacz et al. 2011, 2012b; Lerchbaumer and Audétat 2012). On the other hand, many hard acids, such as alkali and alkali-earth cations, Fe^{2+}, U^{6+}, and Mo^{6+}, can also form strong chloride complexes in high-temperature fluids as discussed in detail below (e.g., Candela and Piccoli 1995; Zajacz et al. 2008; Bali et al. 2011, 2012).

7.2.4 Concentrations of Halogens in Silicic Magmas

Fluorine and Cl are generally present as minor elements in felsic magmas. Figures 7.5, 7.6, 7.7, 7.8 and 7.9 are a compilation of a substantial amount of data on F and Cl concentrations in geologic silicate melts, which are mainly based on the analysis of silicate melt inclusions (SMI) with some additional data on matrix glass compositions. The behavior of F and Cl during the late stages of magmatic evolution in highly fractionated systems is remarkably different (Fig. 7.5). While the Cl concentrations generally cease to increase in the silicate melt at some instant along the liquid line of descent, F is progressively accumulated and can reach extremely

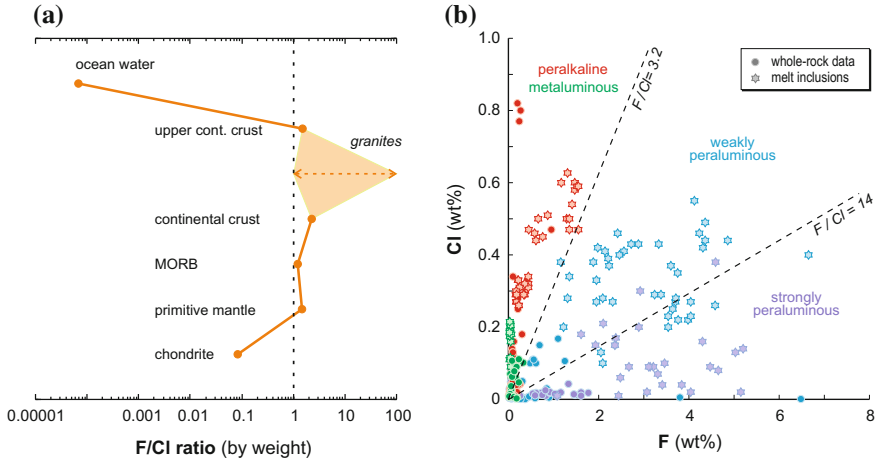

Fig. 7.5 Fluorine versus Cl concentrations in **a** global geochemical reservoirs, and **b** silicic igneous rocks and melt inclusions. Data sources are listed in Dolejš and Baker (2004)

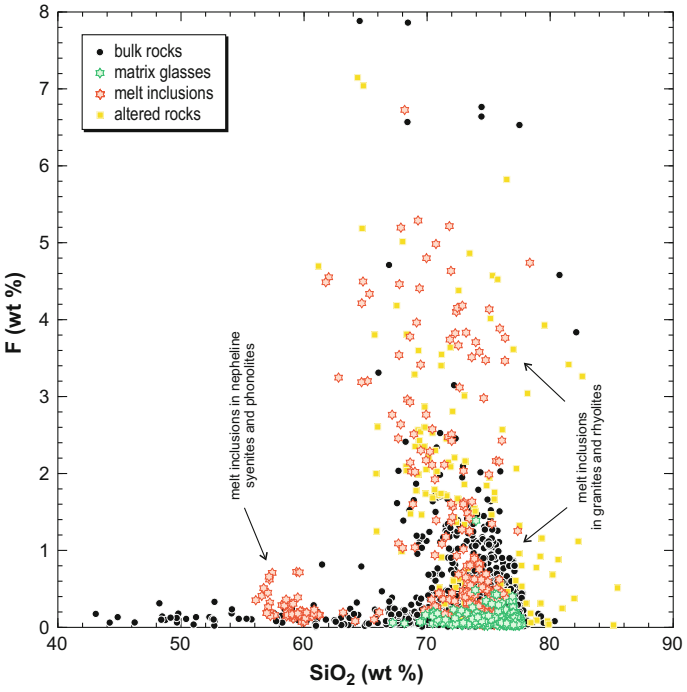

Fig. 7.6 Abundances of F in igneous rocks, melt inclusions, matrix glasses, and hydrothermally altered rocks. Data sources are listed in Dolejš and Baker (2004)

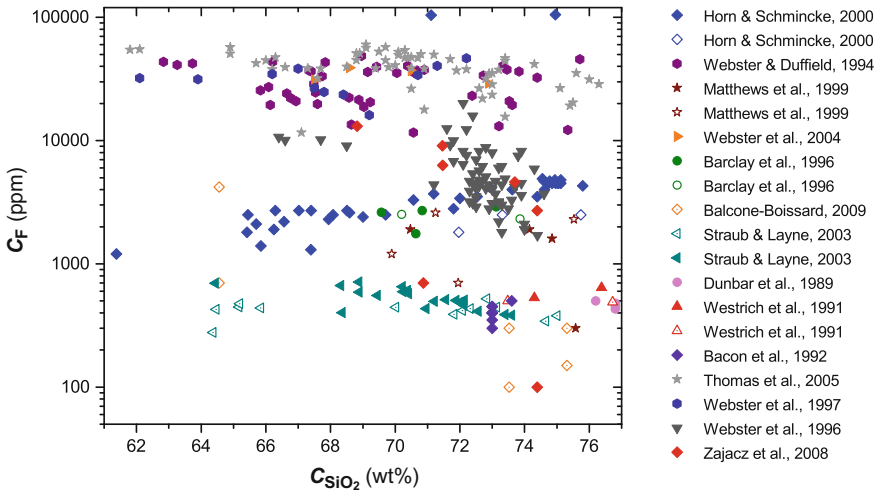

Fig. 7.7 The concentration of F in silicate melt inclusions (*filled symbols*) and matrix glasses (*open symbols*) from natural samples. Fluorine can be present in much higher concentrations in highly fractionated melts than Cl. Note that wt%-level F concentrations would noticeable reduce C_{Sio_2} in the melt

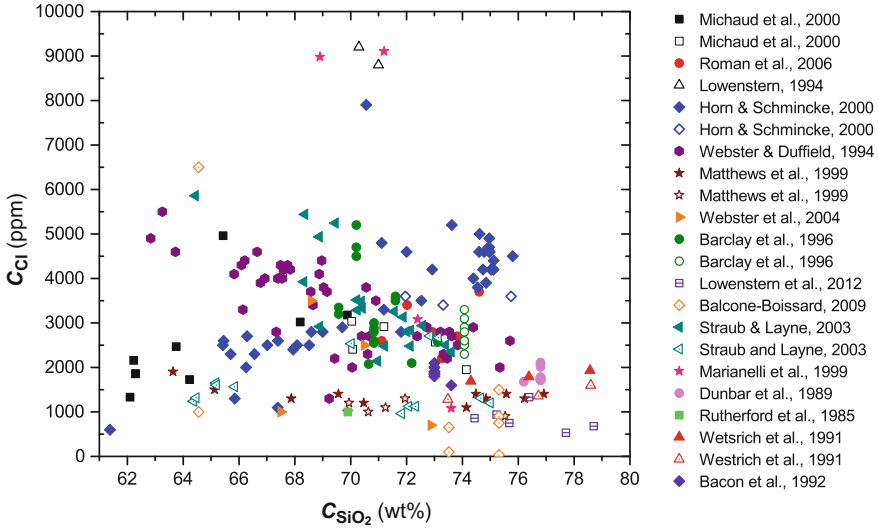

Fig. 7.8 The concentration of Cl in natural silicate melts based on data from silicate melt inclusions in minerals (*filled symbols*) and from groundmass glasses in volcanic rocks (*open symbols*). No systematic correlation is apparent between the SiO_2 and Cl concentrations in felsic magmas. In addition, the concentration of Cl in the groundmass glasses is generally not much lower than in the silicate melt inclusions from the same localities, indicating inefficient syn-eruptive Cl degassing

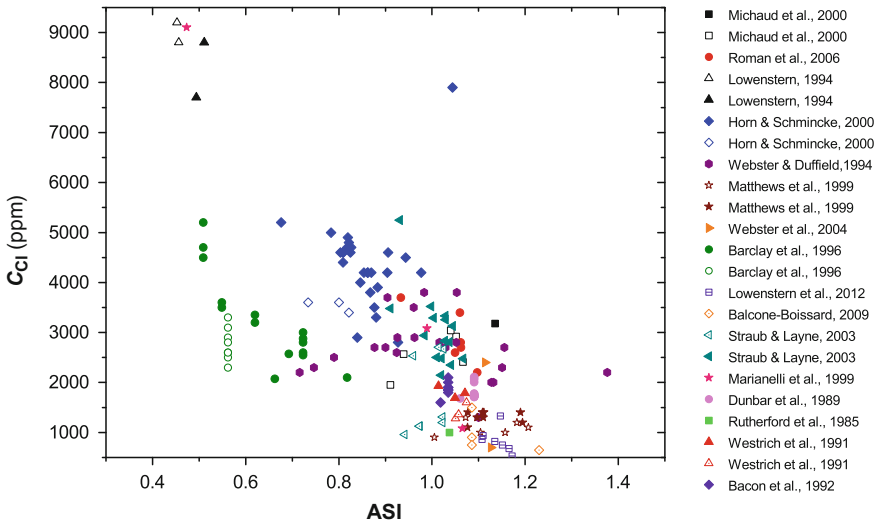

Fig. 7.9 The variation of Cl concentrations in natural silicate melts as a function of alumina saturation index [ASI = Al/(Na + K + 2Ca) in molar units]. The data is from the same sources as those in Fig. 7.8, except only glass compositions with $C_{Sio_2} > 69$ wt% are plotted as ASI is generally only used for granitic melts. The reasons for this are that the Ca/(Na + K) ratios increase rather significantly towards more mafic compositions, as well as the concentration of other network modifier cations

high concentrations (several wt%) in highly fractionated melts (e.g., Webster and Duffield 1994; Webster et al. 1996; Thomas and Webster 2000; Thomas et al. 2005; Zajacz et al. 2008; Agangi et al. 2012) (Figs. 7.6 and 7.7). This contrasting behavior between F and Cl relates to the melt-fluid equilibrium, and will be discussed in detail in the following sections.

Chlorine concentrations can vary broadly between 500 and 9000 ppm, based on the SMI data, without overall correlation with the SiO_2 concentration in the silicate melt, at least within the felsic compositional regime (Fig. 7.8). This variation in the Cl concentration is likely controlled by its abundance in the source region of the magmas as well as the partitioning of Cl between the melt, mineral, and fluid phases during magma evolution. Both F and Cl behave as incompatible elements with respect to most major rock-forming silicate and oxide minerals, except for biotite, amphibole, and apatite, and therefore, their concentrations are expected to rise during magma evolution (Icenhower and London 1997; Piccoli and Candela 2002; Chevychelov et al. 2008; Webster et al. 2009; Zhang et al. 2012a). This is well represented by the elevated abundances of these elements in felsic rather than in mafic melts in arc settings, as deducted from silicate melt inclusion data (Wallace 2005).

Remarkably, however, Cl concentrations in the silicate melt inclusions correlate with the alumina saturation index [ASI = Al/(Na + K + 2Ca)] of the silicate melt (Fig. 7.9). While the Cl concentrations in metaluminous and peraluminous granitic melts rarely rise above 3000 ppm, Cl-rich melt inclusions, with up to 9000 ppm Cl,

were found in peralkaline systems. In addition, F-rich melts may also be characterized by higher Cl concentrations even in peraluminous systems. This is well demonstrated by the data of Webster and Duffield (1994) where the Cl concentrations can be as high as 3800 ppm even in highly evolved metaluminous melt inclusions.

There is much less available data on the concentrations of Br and I in magmas due to the analytical challenges posed by their low concentration levels. In addition, much of the available data is not derived from silicate melt inclusions, but matrix glasses in volcanic rocks. Therefore the reported Br and I concentrations may be affected by syn-eruptive degassing. Villemant and Boudon (1999) and Balcone-Boissard et al. (2010) have reported so far the most comprehensive datasets on Br and I concentrations from matrix glasses in felsic volcanics. The Br and I concentrations reported by Villemant and Boudon (1999), from the matrix glass in volcanic clasts from Mt. Pelée, range from 1 to 12 ppm and 27–164 ppb, respectively. A characteristic Cl/Br ratio of 177 ± 64 and a Cl/I ratio of $16{,}700 \pm 8200$ can be defined based on their dataset. Similar concentration ranges were reported by Balcone-Boissard et al. (2010) from Vesuvius, Fogo, and Mt. Pelée and even lower concentrations were found for Santa Maria-Santiaguito. Within this latter dataset, it is apparent that Br and I are present at relatively elevated concentrations, along with Cl, in the more alkaline Plinian clasts from Vesuvius and Fogo relative to the other locations. The range of concentrations and the Cl/Br and Cl/I ratios in all these felsic volcanics overlap with those reported from quenched sea floor back arc basalt glasses (Kendrick et al. 2014).

7.3 Differentiation and Crystallization of F-Bearing Magmas

7.3.1 Geological Setting and Sources of F-Bearing Magmas

Fluorine-bearing granites and rhyolites are typical of continental collisional or intra-plate settings and are frequently associated with Li, Sn–W and Ta–Nb ore deposits (Clarke 1992; Borodin 2004). The characteristic enrichment in volatile constituents (F, $H_2O \pm B$, Cl), incompatible (Rb, Cs, Li) and rare metal (Sn, W, Nb, Ta, U) elements results from their strong incompatibility and protracted magmatic fractionation. The F-bearing silicic suites are subdivided into the following categories:

1. Strongly peraluminous high-Li granites (S-type), derived from metasedimentary sources, displaying a fractionation sequence of biotite monzogranites through two-mica and Li–mica–topaz varieties towards topaz–albite–lepidolite granites with Sn–W greisen-style mineralization (e.g., Manning and Hill 1990; Štemprok and Seltmann 1994; Förster et al. 1999; Breiter et al. 1999);

2. Weakly peraluminous and metaluminous low-Li-P silicic rocks (I/S-type, aluminous A-type), derived from quartzofeldspathic precursors, which evolve from biotite granodiorites, biotite granites, and two-mica granites (rhyolites) towards topaz rhyolites, ongonites, and quartz topazites with Ta, Nb, and U disseminated mineralization. The quartz topazites represent the highest enrichments in F produced by magmatic processes (Kortemeier and Burt 1988; Antipin et al. 1999; Liu et al. 1999; Gioncada et al. 2014);
3. Peralkaline low-Ca granites (alkaline A-type) characterized by biotite-fayalite, aegirine-arfvedsonite, or aegirine-riebeckite varieties evolving to fluorite- or cryolite-bearing granites (Horbe et al. 1991; Kovalenko et al. 1995). Subsequent alkali-carbonic metasomatism may lead to decomposition of rock-forming silicates into additional fluorides and carbonates (chiolite, siderite; Bailey 1980; Charoy and Raimbault 1994; Pauly and Bailey 1999; Goodenough et al. 2000);
4. Metaluminous, high-Ca (calc-alkaline, I-type) suites, which include amphibole-biotite tonalites, granodiorites, and biotite granites with titanite, magnetite, and accessory fluorite, which buffers melt concentrations of F at low levels (Hogan and Gilbert 1995; Price et al. 1999).

The extreme geochemical specialization of F-rich granites is a consequence of the crystal fractionation of rock-forming silicates (Kostitsyn 2000). The concentrations of the most incompatible elements, Ta, Cs, and Rb (Pollard et al. 1995; Antipin et al. 1999), provide a minimum estimate of the degree of crystal fractionation. For example, typical concentrations of Ta vary from 0.3 to 9 ppm (granites) through 37–43 ppm (ongonites) to 77–179 ppm (quartz topazites), and imply that ongonites represent <10% of the residual liquids from F-bearing granites. Quartz topazites in the Tonto basin, Arizona (Kortemeir and Burt 1988) represent $\sim$1% residual liquids from parental ongonites. Similarly, the colinear increase in Ta and Sn concentrations over three orders of magnitude in the Phuket (Thailand) fractionated I-type granites indicates more than 99% fractionation (Pollard et al. 1995).

The progressive increase in F concentrations provides a comparable estimate of the degree of magmatic differentiation. Fluorine abundances increase from biotite granites (0.11 $\pm$ 0.07 wt% F) to topaz granites with ongonites (1.09 $\pm$ 0.69 and 0.89 $\pm$ 0.57 wt% F, respectively) and quartz topazites (3.85 $\pm$ 2.12 wt% F; Dolejš and Baker 2004). The increase from $\sim$0.1 (parental granites) to $\sim$1.90 wt% F (aphyric ongonites; Kovalenko and Kovalenko 1976; Štemprok 1991) provides the following estimates of Rayleigh fractionation: 5.3% ($D_F^{s/m} = 0$) and 1.5% residual melt ($D_F^{s/m} = 0.3$, London 1997). Furthermore, F concentrations in melt inclusions (3.10 $\pm$ 1.12 wt% F; Webster and Duffield 1994; Webster et al. 1997; Thomas et al. 2000) are about three times higher than those of their host rocks (0.99 $\pm$ 0.89 wt% F), which attests to significant partitioning of F into hydrothermal fluids and its incorporation in greisens (2.58 $\pm$ 1.79 wt% F).

These levels of magmatic differentiation provide challenging questions about the nature of the fractionation process: (i) are parental low-F granites cumulates, strongly depleted in incompatible and volatile elements? (ii) Are the most-evolved alkali-free quartz topazites representative of liquid compositions? (iii) Can the enrichment in F,

large-ion lithophile and high-field strength elements be produced by silicate-fluoride liquid-liquid immiscibility? Since the nature of the differentiation process is directly related to the interactions between F and the aluminosilicate melt via melt-solid-fluid equilibria, we present major-element compositional trends in the granite, topaz-granite, ongonite (including xianghualingite, kalgutite, selengite) and quartz-topazite sequences (Figs. 7.10, 7.11 and 7.12). The compiled geochemical data are presented in cation units of major elements and simultaneously recalculated into normative minerals in F-bearing rocks (Dolejš and Štemprok 2001).

The magmatic and hydrothermal evolution of F-bearing magmas and rocks can be summarized as follows:

1. The F concentrations increase with increasing peraluminosity in melt inclusions, glasses, and whole rocks (Fig. 7.10). This trend is interpreted as a consequence of two factors—melt derivation from different sources and a progressive decrease in CaO concentration. With increasing peraluminosity, the increasing contribution from metasedimentary crustal protoliths provides F by the dehydration breakdown of micas (Peterson et al. 1991; Skjerlie and Johnston 1992). The CaO concentrations vary inversely with the melt peraluminosity and decrease from I- and A-type granites and rhyolites towards S-types;
2. Intrusive rocks are more peraluminous than melt inclusions and glasses (Fig. 7.11). This phenomenon is typical of peraluminous granitic rocks in general (Castro et al. 1999). The solubility of excess alumina in granitic melts is fairly low (Puziewicz and Johannes 1988; Holtz et al. 1992; Joyce and Voigt 1994). The aluminosilicate minerals (micas, topaz) represent restites or products of preceding crystal fractionation which fail to separate and remain in the magma suspension. It is noteworthy that, with the exception of the Macusani and Spor Mountain occurrences (Pichavant et al. 1987, 1988a, b; Christiansen et al. 1984; Webster et al. 1987), peraluminous obsidians are virtually unknown (Macdonald et al. 1992);
3. Melt inclusions, glasses, and whole rocks are enriched in alkalies and Al (alkali feldspar) compared to the hydrous haplogranite minimum at 100 MPa (Tuttle and Bowen 1958; Fig. 7.12). This shift reflects increasing volatile abundances (H_2O, F) in the melt, which displace the haplogranitic minimum towards the albite composition and increase the stability of quartz (Manning et al. 1980; Manning 1981; Johannes and Holtz 1996). As a consequence, the whole-rock SiO_2 concentrations decrease with increasing F contents (Fig. 7.6);
4. Topaz granites, topaz rhyolites, and ongonites (Štemprok 1991; Dergachev 1992) evolve by fractionation of quartz and K-feldspar towards enrichment in albite and topaz. Total alkali concentrations remain approximately constant whereas alumina contents slightly increase (Fig. 7.11b);
5. High-F rocks (quartz topazites, silexites, xianghualingites, and elvans) are very rare, compared to ongonites. They form two distinct differentiation trends. Xianghualinigites, elvans, kalgutites, and selengites (Stone 1968; Hall 1970; Henley 1974; Du and Huang 1985; Vladimirov et al. 1991; Dergachev 1990, 1992; Zhu et al. 1993) evolve by fractionation of plagioclase towards

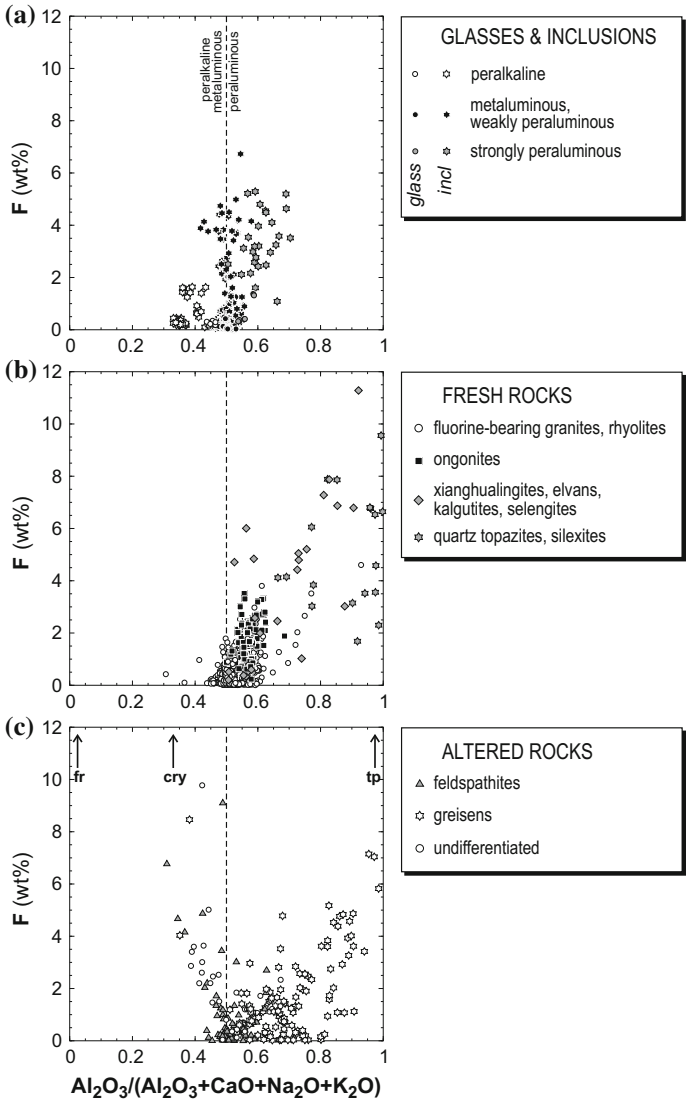

Fig. 7.10 Variations in the F concentration as a function of aluminosity in **a** matrix glasses (obsidians) and melt inclusions, **b** fresh igneous rocks, and **c** hydrothermally altered rocks. The molar ratio $Al_2O_3/(Al_2O_3 + CaO + Na_2O + K_2O)$ replaces the alumina saturation index (Shand 1927), which attains very high or infinite values for strongly peraluminous compositions. Note the differences in inidividual F abundances as well as the systematic shift to more peraluminous compositions from melts towards altered rocks. Mineral abbreviations: *fr* fluorite, *cry* cryolite, *tp* topaz. Data sources are listed in Dolejš and Baker (2004)

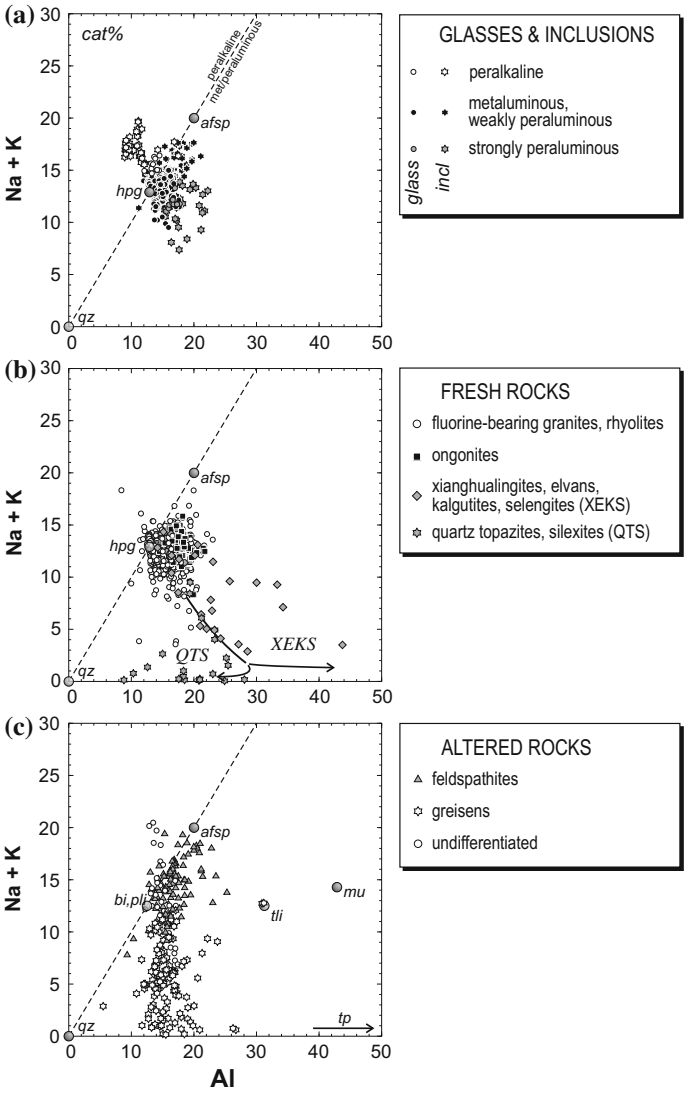

Fig. 7.11 Na + K versus Al variation diagrams (cation %) with distribution of **a** glasses and melt inclusions, **b** fresh igneous rocks, and **c** hydrothermally altered rocks. Note (i) the systematic enrichment in feldspar in all the graphs, with respect to the haplogranite composition, (ii) displacement of ongonites towards higher alumina concentrations at constant alkali contents (topaz and feldspar enrichment), (iii) divergence of alkali-depleted differentiation trends of quartz topazites (quartz enrichment) and xianghualingites, elvans, kalgutites, and selengites (muscovite and Li–mica enrichment), and (iv) the Al-conservative nature of the hydrothermal-alteration trends. Abbreviations: *hpg* haplogranite (hydrous minimum at 100 MPa; Tuttle and Bowen 1958), *afsp* alkali felspar, *qz* quartz, *bi* annite-phlogopite, *mu* muscovite, *pli* polylithionite, *tri* trilithionite. Data sources are listed in Dolejš and Baker (2004)

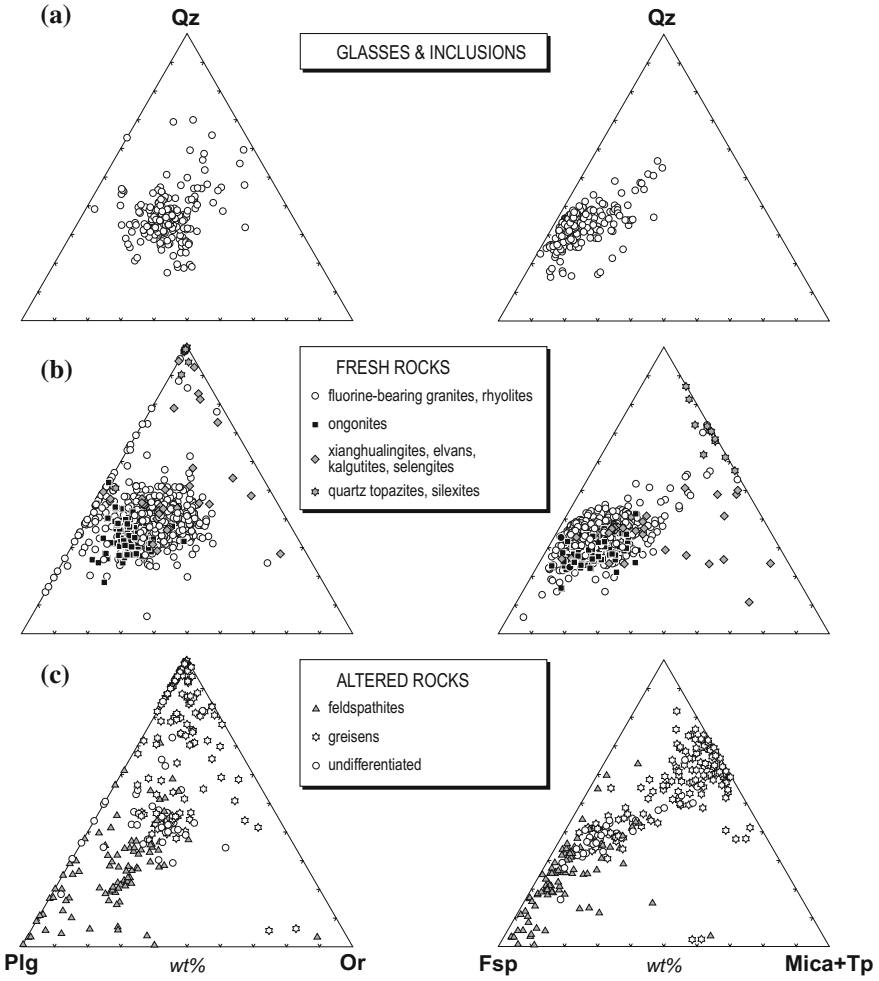

Fig. 7.12 Normative composition of **a** glasses and melt inclusions, **b** fresh igneous rocks, and (c) hydrothermally altered rocks. Mineral abbreviations: *Fsp* feldspar, *Mica* biotite + muscovite + lepidolite, *Or* K-feldspar, *Plg* plagioclase, *Qz* quartz, *Tp* topaz. Normative proportions were recalculated from the major-element whole-rock data using the procedure by Dolejš and Štemprok (2001). Note (i) the large scatter of whole-rock data when compared to the glasses and melt inclusions as well as departures of fresh rocks towards the quartz-plagioclase assemblage, and (ii) the enrichment in the feldspar (plagioclase) component in ongonites versus feldspar depletion in quartz topazites, silexites, xianghualingites, and related rock types. Data sources are listed in Dolejš and Baker (2004)

quartz-muscovite/Li-mica enrichment. Quartz topazites and silexites form by feldspar removal. Complete alkali loss leads to a quartz-topaz bimineralic assemblage (Eadington and Nashar 1978; Birch 1984; Kortemeier and Burt 1988; Johnston and Chappell 1992);

6. Subsolidus alteration by hydrothermal fluids is Al-conservative. Changes in the alumina saturation index (Shand 1927) depend on the removal or addition of alkalies (Fig. 7.11c).

Magmatic differentiation of subaluminous topaz rhyolites and ongonites culminates with the formation of alkali-free quartz topazites ($\sim$30% topaz and 70% quartz). These occur as fine-grained dyke rocks with chilled margins, magmatic flow banding, and without significant alteration aureoles (Eadington and Nashar 1978; Kortemeier and Burt 1988; Liu et al. 1999; Antipin et al. 1999). Compositionally, the quartz topazites represent a F analogue of lepidolite-quartz pegmatites (Černý 1991, 1992) or quartz tourmalinites (London and Manning 1995). The formation of quartz topazites requires either the crystallization of the peraluminous assemblage from a residual alkali-rich liquid (not preserved) or the unmixing into an alkali-poor, peraluminous silicate melt and a conjugate alkali-rich liquid or fluid (cf., Glyuk and Shinakin 1986; Wang et al. 1997, 2000). In both cases, the alkali association requires the presence of a weakly polarizing anionic ligand (strong Lewis acid). The *relatively* high polarizability of F (Duffy 1989) leads to a significant [NaAl]–F association (cf., Kohn et al. 1991; Schaller et al. 1992; Stebbins and Zeng 2000), which does not promote aluminosilicate saturation. It appears necessary that a stronger Lewis acid or oxyanions not coordinating with Al such as Cl_2O_{-1}, B_2O_3, and CO_2, are responsible for alkali complexing and their removal into residual or exsolving liquids or fluids. This is in agreement with the preservation of alkali-carbonate fluids in granite-pegmatite systems (Anderson et al. 2001; Sirbescu and Nabelek 2003a, b). This reversal of *early* alkali (feldspathic) enrichment in F-, B-, or P-bearing systems (Manning 1981; Pichavant et al. 1987; London et al. 1993; Johannes and Holtz 1996) to subsequent alkali loss and peraluminous crystallization represents a long-standing problem of the late-magmatic crystallization of volatile-rich granitic systems.

In contrast to igneous centers in continental or anorogenic settings, the Ca-bearing intermediate and silicic suites in island or continental arcs often lack any F enrichment (Barton 1996). In the I-type granodiorites and granites, the F concentrations do not exceed $\sim$0.2 wt% F (e.g., Norman et al. 1992), because F is hosted by amphibole, biotite, and/or accessory fluorite (CaF_2). Since fluorite is the most common fluoride mineral in silicic magmatic rocks and their metamorphic and metasomatic successors (Burt 1972; Bohlen and Essene 1978; Hogan and Gilbert 1995; Haapala 1997; Marshall et al. 1998; Sallet et al. 2000), the observed variability in F contents may be related to several factors. These include (i) magmatic crystallization of fluorite and its F-buffering effect; (ii) formation of fluorite during subsolidus cooling via closed-system equilibria between Ca-bearing silicates and OH–F silicates; and (iii) precipitation or removal of fluorite during open-system hydrothermal alteration.

The fluorite abundance varies from accessory amounts in metaluminous granitic rocks and high-grade metamorphic rocks (Buddington and Leonard 1962; Bohlen and Essene 1978; Hogan and Gilbert 1995), to volume-percent proportions in peralkaline granites and rhyolites (Marshall et al. 1998; Sallet et al. 2000; Abdel-Rahman et al. 2001) and becomes irregularly distributed in topaz granites and rhyolites, pegmatites, and greisens (Simmons and Heinrich 1975; Webster et al. 1987; Haapala 1997). In peralkaline systems, fluorite occurs as phenocrysts in rhyolites, microlites in melt inclusions, and solid inclusions in phenocrysts in granites (e.g., Marshall et al. 1998; Webster and Rebbert 2001). Additionally, fluorite is common in peralkaline A-type granites (Sallet et al. 2000). These natural observations and experimental results by Scaillet and Macdonald (2001, 2004) confirm that fluorite forms as an *early* magmatic phase in peralkaline silicic melts.

7.3.2 Mineral Stabilities in F-Bearing Magmas

Formation of the individual F-bearing minerals in silicate magmas and rocks is dictated by the occurrence and relative order of fluorination reactions. For example:

$$Al_2SiO_5\,(\text{andalusite}) + F_2 = Al_2SiO_4F_2\,(\text{topaz}) + 1/2\,O_2, \tag{7.5}$$

or

$$CaSiO_3\,(\text{wollastonite}) + F_2 = CaF_2\,(\text{fluorite}) + SiO_2\,(\text{quartz}) + 1/2\,O_2. \tag{7.6}$$

As written, these equilibria indicate that the formation of F-bearing minerals depends on the redox state of the system, and is preferred by more reducing conditions. However, none of the major elements (cations) changes its valence state. In addition, the fact that F is the most electronegative compared to all other elements ensures that F will always be present in the negative one valence state, even if redox state(s) of any other element(s) may vary. The above equilibria simply represent an anion exchange—replacement of one or more O atoms by F, with the ratio of stoichiometric coefficients between F and O dictated by their charge ratio, i.e., 2:1. It is advantageous to condense these two elements into a single entity as an exchange operator (cf., Burt 1972, 1974). Equations (7.10) and (7.11) can now be written as:

$$Al_2SiO_5\,(\text{andalusite}) + F_2O_{-1} = Al_2SiO_4F_2\,(\text{topaz}), \tag{7.7}$$

or

$$CaSiO_3\,(\text{wollastonite}) + F_2O_{-1} = CaF_2\,(\text{fluorite}) + SiO_2\,(\text{quartz}). \tag{7.8}$$

This notation provides a unique parameter for the fluorination state, F_2O_{-1}, and it eliminates the dependence of equilibria on the O fugacity because no element effectively changes its valence. For true redox reactions, for instance,

$$\begin{aligned} &6\,CaFeSi_2O_6\,(\text{hedenbergite}) + 6\,F_2O_{-1} + 3\,O_2 = \\ &6\,CaF_2\,(\text{fluorite}) + 2\,Fe_3O_4\,(\text{magnetite}) + 12\,SiO_2\,(\text{quartz}). \end{aligned} \tag{7.9}$$

The balancing O species is effectively related to Fe oxidation between hedenbergite and magnetite, and it does not interfere with the formation of fluorite.

In natural systems, the principle of compound-basicity and bond-valence equalization dictates that common aluminosilicate melts and mineral assemblages are chemically compatible and in equilibrium with alkali or alkali-earth fluorides ± aluminofluorides (Fig. 7.3). In silicates, F is only incorporated as a substituent and in minor quantities, mainly for the hydroxyl group. Mutual stabilities and sequence of formation of F-bearing minerals, predominantly fluorite, villiaumite, cryolite, topaz etc., thus require the most basic components such as Na_2O and CaO to represent the principal variables. We will show below how the chemical potentials (activities) of these components are linked to feldspar equilibria. The stabilities of F-bearing minerals in common mineral assemblages will be linked in the system Na_2O–CaO–Al_2O_3–SiO_2 (+H_2O). As discussed by Anovitz et al. (1987) and Dolejš and Baker (2004), all fluorination equilibria have an approximately similar temperature dependence. Hence the relative order of fluorination reactions is independent of temperature. The following discussion is applicable to a temperature range of 400–800 °C and a pressure of 100 MPa.

The chemical compatibility principles between aluminosilicate and fluorides also dictate that the fluoride minerals are first formed in the most basic bulk composition, i.e., peralkaline silica-undersaturated systems, by the general reaction:

$$Na_2O + F_2O_{-1} = 2\,NaF\,(\text{villiaumite}), \tag{7.10}$$

which indicates consumption of the most basic component. In the presence of common rock-forming silicates, the formation of villiaumite will occur, for instance, by the following reaction:

$$\begin{aligned} &2\,NaAlSiO_4\,(\text{nepheline}) + 2\,Na_2Si_2O_5 + 2\,F_2O_{-1} = \\ &4\,NaF\,(\text{villiaumite}) + 2\,NaAlSi_3O_8\,(\text{albite}). \end{aligned} \tag{7.11}$$

The sodium-disilicate component formally represents excess alkalies in a peralkaline melt or in the mineral assemblage (presence of sodic amphibole and/or clinopyroxene). When the F concentration in the system is allowed to further increase due to the lack of buffering effects during crystallization, villiaumite will be replaced by a less basic fluoride phase–cryolite, as follows:

$$4\,\mathrm{NaF}\,(\text{villiaumite}) + 3\,\mathrm{NaAlSiO_4}\,(\text{nepheline}) + 4\,\mathrm{F_2O_{-1}} = 2\,\mathrm{Na_3AlF_6}\,(\text{cryolite}) + 1\,\mathrm{NaAlSi_3O_8}\,(\text{albite}), \quad (7.12)$$

and analogously for the silica-saturated systems:

$$2\,\mathrm{NaF}\,(\text{villiaumite}) + 1\,\mathrm{NaAlSi_3O_8}\,(\text{albite}) + 2\,\mathrm{F_2O_{-1}} = 1\,\mathrm{Na_3AlF_6}\,(\text{cryolite}) + 3\,\mathrm{SiO_2}\,(\text{quartz}). \quad (7.13)$$

When the chemical potential of F_2O_{-1} continues to increase, F will be incorporated into the aluminosilicates:

$$1\,\mathrm{Al_2SiO_5}\,(\text{andalusite}) + 1\,\mathrm{F_2O_{-1}} = 1\,\mathrm{Al_2SiO_4F_2}\,(\text{topaz}), \quad (7.14)$$

as observed in F-bearing peraluminous granites or rhyolites. The order of formation with decreasing basicity, from alkali fluorides through aluminofluorides to fluoroaluminosilicates also implies that F concentrations in the system will systematically vary. They will remain very low during villiaumite crystallization, but reach their maxima during the formation of topaz.

7.3.2.1 System Na_2O–Al_2O_3–SiO_2–F_2O_{-1}

The quaternary system Na_2O–Al_2O_3–SiO_2–F_2O_{-1} provides a first approximation for F-bearing felsic magmatic systems for several reasons (Dolejš and Baker 2004), i.e.: (i) It contains important rock-forming minerals such as quartz, albite and nepheline, and it covers a wide range of silica activities, $a(SiO_2)$; (ii) It continuously covers peralkaline to peraluminous compositions; (iii) It includes the major fluoride phases found in nature: topaz, cryolite, chiolite, villiaumite, and malladrite. Because the stabilities of F-bearing minerals are directly related to the peralkalinity or peraluminosity of the system, we portray the fluorination of quartzofeldspathic assemblages as a function of the chemical potential of Na_2O (Fig. 7.13a). Its lower limit is constrained by the breakdown of albite to andalusite:

$$\mathrm{Na_2O} + \mathrm{Al_2SiO_5}\,(\text{andalusite}) + 5\,\mathrm{SiO_2}\,(\text{quartz}) = 2\,\mathrm{NaAlSi_3O_8}\,(\text{albite}), \quad (7.15)$$

and the upper limit is defined by the transformation of quartz to sodium disilicate:

$$\mathrm{Na_2O} + 2\,\mathrm{SiO_2}\,(\text{quartz}) = \mathrm{Na_2Si_2O_5}. \quad (7.16)$$

The chemical-potential space of Na_2O and F_2O_{-1} is limited by the saturation boundary of villiaumite (Eq. 7.15), which is, however, only reached under

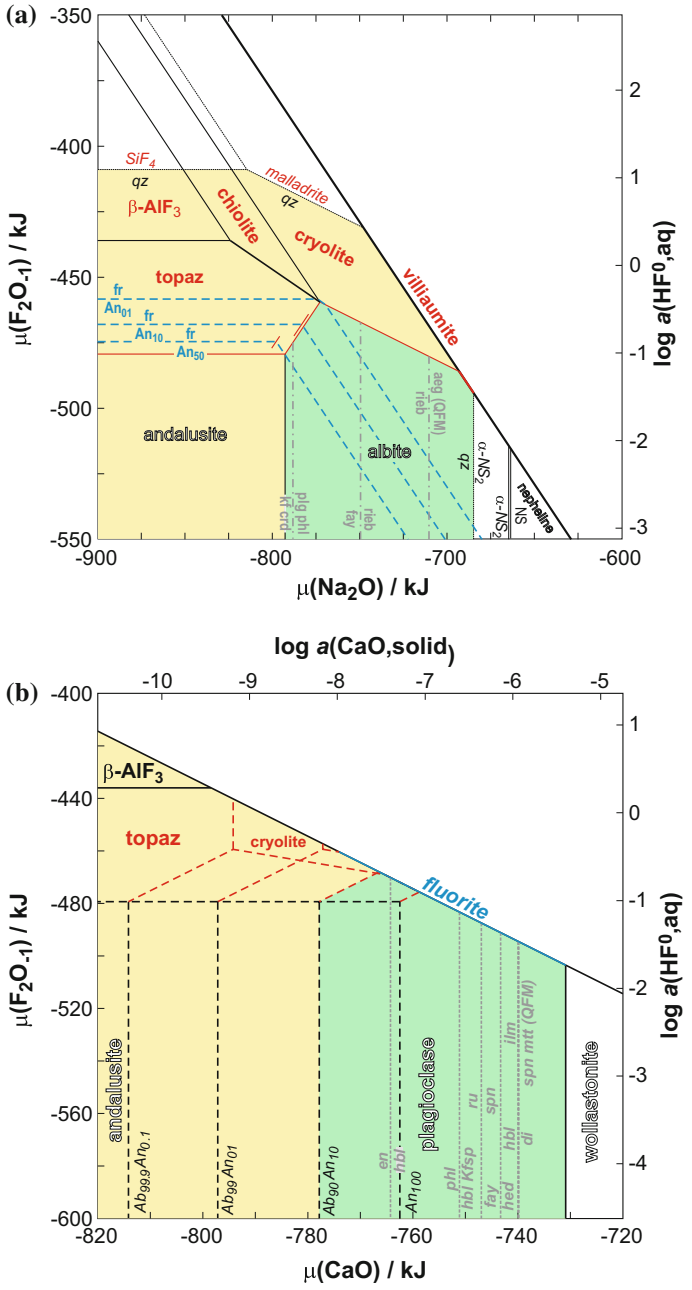
(a)
SiF4
qz
β-AlF3
chiolite
malladrite
qz
cryolite
villaumite
topaz
fr
An01
fr
An10
fr
An50
andalusite
albite
aeg (QFM)
rieb
zb
α-NS2
NS
α-NS
nepheline
plg phl
Kf crd
fay
rieb
μ(F2O-1) / kJ
μ(Na2O) / kJ
log a(HF0,aq)
(b)
log a(CaO,solid)
β-AlF3
topaz
cryolite
fluorite
andalusite
Ab99An0.1
Ab99An01
Ab90An10
en
hbl
An100
plagioclase
phl
hbl Kfsp
ru
fay
spn
hed
hbl
ilm
di
spn mtt (QFM)
wollastonite
μ(F2O-1) / kJ
μ(CaO) / kJ
log a(HF0,aq)

◂**Fig. 7.13** Chemical-potential diagrams illustrating the stability of principal Na- and Ca-bearing minerals and topaz at 600 °C and 100 MPa (Dolejš and Baker 2004). **a** $\mu(Na_2O)$ versus $\mu(F_2O_{-1})$ diagram for the system Na_2O–Al_2O_3–SiO_2–F_2O_{-1}. The *yellow* field indicates the presence of quartz. The *green* field corresponds to quartz + albite assemblage. The *blue dashed lines* represent the contours of fluorite saturation in the Ca-bearing system as function of plagioclase composition. Bulk composition: SiO_2:Al_2O_3 = 10:1 molar. Mobile components: Na_2O, F_2O_{-1}. **b** $\mu(CaO)$ *versus* $\mu(F_2O_{-1})$ projection of the system Na_2O–CaO–Al_2O_3–SiO_2–F_2O_{-1} at quartz saturation. The *yellow* field indicates the presence of the assemblage albite + quartz. The *green* field corresponds to the plagioclase (An_{10}) + quartz assemblage. Note the shrinking of the andalusite and topaz stability fields with the decreasing plagioclase An-content and the closing of the cryolite stability field at $An_{>3}$. Mineral abbreviations: *aeg* aegirine, *crd* cordierite, *di* diopside, *en* enstatite, *fay* fayalite, *hbl* hornblende, *ilm* ilmenite, *kf* K-feldspar, *mtt* magnetite, *phl* phlogopite, *plg* plagioclase, *rieb* riebeckite, *ru* rutile, *spn* titanite, and *QFM* quartz–fayalite–magnetite buffer

extremely peralkaline conditions (Fig. 7.13a). In peralkaline systems, the formation of villiaumite is preceded at a lower F_2O_{-1} chemical potential by the formation of cryolite due to the fluorination of plagioclase:

$$\begin{aligned} &NaAlSi_3O_8\,(\text{plagioclase}) + Na_2O + 3\,F_2O_{-1} \\ &\quad = Na_3AlF_6\,(\text{cryolite}) + 3\,SiO_2\,(\text{quartz}). \end{aligned} \tag{7.17}$$

In peraluminous silicic systems, topaz becomes the first stable F-bearing phase,

$$2\,NaAlSi_3O_8\,(\text{plagioclase}) + F_2O_{-1} = Al_2SiO_4F_2\,(\text{topaz}) + 5\,SiO_2\,(\text{quartz}) + Na_2O. \tag{7.18}$$

The formation of chiolite or β-AlF_3 requires a high chemical potential for F_2O_{-1}, beyond the stability of plagioclase. These transformations can occur in systems where the F behavior is unbuffered and/or it can be considered a perfectly mobile component.

7.3.2.2 System CaO–Na_2O–Al_2O_3–SiO_2–F_2O_{-1}

Addition of CaO to the system Na_2O–Al_2O_3–SiO_2–F_2O_{-1} introduces fluorite to the system and permits consideration of plagioclase control on equilibria among F-bearing minerals. The fluorite occurrence is universally controled by the equilibrium (Fig. 7.13b):

$$CaO + F_2O_{-1} = CaF_2\,(\text{fluorite}). \tag{7.19}$$

Here the variation in the range of the CaO chemical potential in natural magmas and rocks is limited by the saturation of andalusite (in the presence of plagioclase) at the lower limit:

$$\mathrm{CaO} + \mathrm{Al_2SiO_5\ (andalusite)} + \mathrm{SiO_2} = \mathrm{CaAl_2Si_2O_8\ (plagioclase)}, \tag{7.20}$$

and by the formation of wollastonite at the upper limit:

$$\mathrm{CaO} + \mathrm{SiO_2} = \mathrm{CaSiO_3\ (wollastonite)}. \tag{7.21}$$

In Fig. 7.13, these equilibria are indicated for a complete range of plagioclase composition (0.1–100 mol% An) and the chemical potential space is conveniently subdivided by additional buffers of CaO activity, such as enstatite-hornblende, phlogopite-hornblende-K-feldspar, rutile-titanite, fayalite-hedenbergite, blende-diopside, and ilmenite-magnetite-titanite, which allow application to a horn-wide variety of igneous systems.

The chemical-potential spaces illustrated in Fig. 7.13 represent two limiting cases with respect to the plagioclase composition. As albite–anorthite proportions vary in nature, the equilibria and saturation limits of F-bearing minerals will continuously change. Increasing the anorthite content of plagioclase in peralkaline and metaluminous environments will promote the preferential saturation with fluorite (as opposed to villiaumite or cryolite) due to the equilibrium:

$$\begin{aligned}\mathrm{CaAl_2Si_2O_8\ (plagioclase)} + 4\,\mathrm{SiO_2} + \mathrm{Na_2O} + \mathrm{F_2O_{-1}} \\ = \mathrm{CaF_2\ (fluorite)} + 2\,\mathrm{NaAlSi_3O_8\ (plagioclase)}.\end{aligned} \tag{7.22}$$

In peraluminous compositions, the plagioclase composition controls the crystallization of fluorite versus topaz by the following invariant equilibrium:

$$\mathrm{CaAl_2Si_2O_8\ (plagioclase)} + 2\,\mathrm{F_2O_{-1}} = \mathrm{CaF_2\ (fluorite)} + \mathrm{Al_2SiO_4F_2\ (topaz)} + \mathrm{SiO_2}. \tag{7.23}$$

These effects are illustrated by dashed phase boundaries in Fig. 7.13a, b, which in a complementary manner show that fluorite is a ubiquitous saturation phase in Ca-bearing systems, whereas the crystallization of topaz, cryolite, and villiaumite (in the order of decreasing peraluminosity) requires very Ca-poor conditions, consistent with the extremely evolved nature of highly differentiated granites or nepheline and sodalite syenites. These predictions are consistently summarized in Fig. 7.14. The chemical-potential space of $\mathrm{Na_2O}$ and CaO covers the full variability of plagioclase-bearing igneous rocks, from peralkaline to peraluminous varieties, because the activity of alumina is self-consistently buffered by

$$\mathrm{Na_2O} + \mathrm{Al_2O_3} + 6\,\mathrm{SiO_2} = 2\,\mathrm{NaAlSi_3O_8\ (plagioclase)}, \tag{7.24}$$

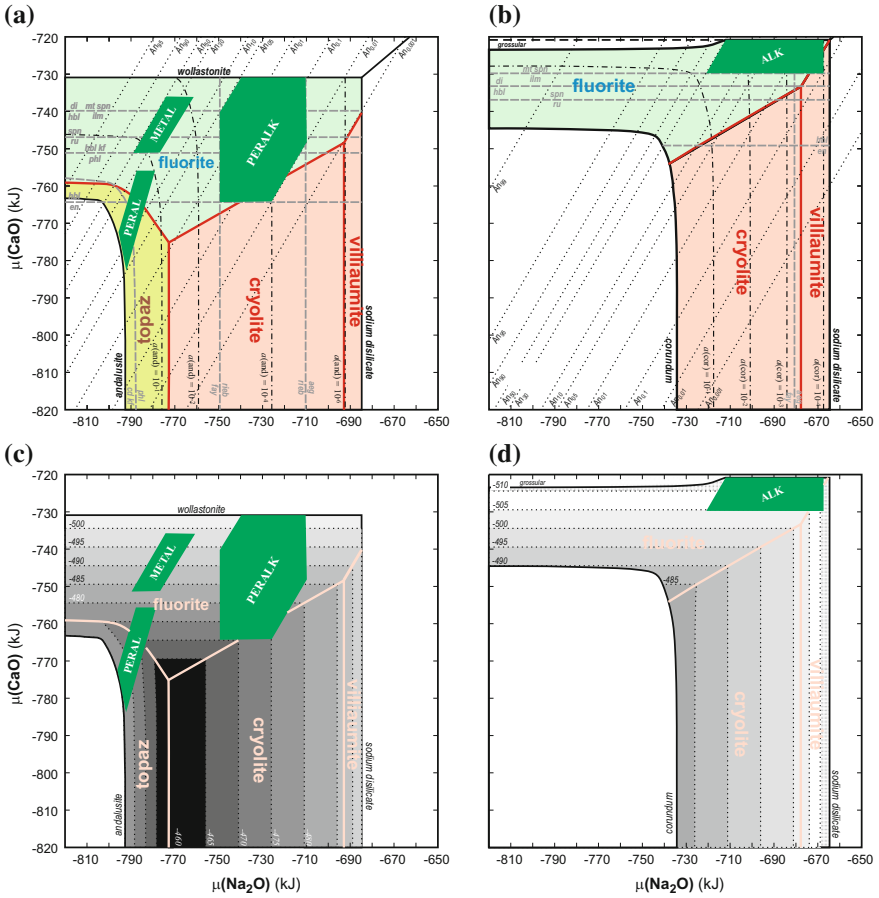

Fig. 7.14 The chemical-potential $\mu(Na_2O)$ *versus* $\mu(CaO)$ projection of the system Na_2O–CaO–Al_2O_3–SiO_2–F_2O_{-1} at 600 °C and 100 MPa illustrating the compatibilities between the granitic or nepheline-syenitic rock types and F-bearing minerals (Dolejš and Baker 2004): **a** $a(SiO_2) = 1$, i.e. at quartz saturation. Chemical potentials of Na_2O and CaO are related through plagioclase equilibrium (*dotted lines*): $[CaO] + 2\ NaAlSi_3O_8(ss) = [Na_2O] + CaAl_2Si_2O_8(ss) + 4\ SiO_2(s)$, and that of F_2O_{-1} by the coexistence of quartz, plagioclase, and the fluoride phase. Abbreviations for rock groups: *ALK* alkaline nepheline syenites, *PERAL* peraluminous granites, *METAL* metaluminous granodiorites to tonalities, and *PERALK* peralkaline granites. **b** $a(SiO_2) = 1$. Isopleths of $\mu(F_2O_{-1})$ in kJ at quartz, plagioclase, and F-bearing phase equilibrium. **c** $a(SiO_2) = 0.25$, i.e. at nepheline-albite equilibrium. **d** $a(SiO_2) = 0.25$. Isopleths of $\mu(F_2O_{-1})$ in kJ for nepheline, plagioclase, and fluoride phase equilibria

and

$$\mathrm{CaO} + \mathrm{Al_2O_3} + 2\,\mathrm{SiO_2} = \mathrm{CaAl_2Si_2O_8}\ (\text{plagioclase}). \tag{7.25}$$

The plagioclase composition, together with additional rock-forming mineral buffers, permits delineation of the stability fields of common peraluminous, metaluminous, and peralkaline silica-saturated and -undersaturated rocks. On this framework, the stability fields of the *first stable* F-bearing mineral are imposed, together with the isopleths of chemical potential of F_2O_{-1} that scale with the F concentration in the system (Fig. 7.14).

In granitic and rhyolitic rocks with the silica activity near unity, crystallization of topaz, fluorite, cryolite, or villiaumite is controlled by alkalinity and Ca abundance in the system. Villiaumite is stable under extremely peralkaline conditions, coexisting with pure albite ($An_{<0.001}$) at 600 °C and 1 kbar. Similarly, cryolite stability requires coexistence with nearly pure albite ($An_{<02}$). Cryolite is predicted to occur in aegirine-, riebeckite-, and/or fayalite-bearing granites (Fig. 7.14a). Silicic rocks with Ca-bearing plagioclase ($An_{>05}$) saturate with topaz and fluorite. The stability of topaz is restricted to peraluminous conditions, with the andalusite activity greater than 0.1, which is consistent with the presence of Li-micas or anhydrous aluminosilicates such as cordierite or garnet. Crystallization of fluorite requires high Ca/Na environments and this mineral becomes stable in peraluminous biotite granites, amphibole-, clinopyroxene-, or titanite-bearing calc-alkaline rocks as well as in peralkaline granites and rhyolites (Dolejš and Baker 2004; Fig. 7.14a). In silica-undersaturated rocks, buffered by the albite–nepheline equilibrium at $a(SiO_2) = 0.25$, the stability field of corundum eliminates the occurrence of topaz in nepheline and sodalite syenites and phonolites (Fig. 7.14b). The cryolite stability field slightly expands with the decreasing activity of silica at the expense of villiaumite and fluorite due to the equilibria:

$$\begin{aligned} &6\,\mathrm{NaF}\ (\text{villiaumite}) + \mathrm{NaAlSi_3O_8}\ (\text{plagioclase}) \\ &\quad = \mathrm{Na_3AlF_6}\ (\text{cryolite}) + 2\,\mathrm{Na_2O} + 3\,\mathrm{SiO_2}, \end{aligned} \tag{7.26}$$

and

$$\begin{aligned} &3\,\mathrm{CaF_2}\ (\text{fluorite}) + 7\,\mathrm{NaAlSi_3O_8}\ (\text{plagioclase}) \\ &= \mathrm{Na_3AlF_6}\ (\text{cryolite}) + 3\,\mathrm{CaAl_2Si_2O_8}\ (\text{plagioclase}) + 2\,\mathrm{Na_2O} + 15\,\mathrm{SiO_2}. \end{aligned} \tag{7.27}$$

The levels of the F_2O_{-1} chemical potential at the feldspar–F-bearing mineral boundary, used as a proxy for the F concentration in the system (Fig. 7.14c, d), provide an explanation for the highly variable F enrichment observed in natural magmas (e.g., Dolejš and Baker 2004; Fig. 7.6). The lowest levels of F concentration are predicted in Ca-rich or strongly peralkaline environments. The chemical potential of F_2O_{-1} increases towards low-Ca and peraluminous conditions and reaches its maximum at the cryolite-topaz-fluorite invariant point in silicic rocks. Consequently, villiaumite-saturated magmas will strongly inhibit F enrichment,

whereas low-Ca topaz- or cryolite-bearing magmas will evolve towards the highest F concentrations. Similarly, the maximum F solubility increases from peralkaline through metaluminous to peraluminous conditions. These results are consistent with F melt concentrations increasing from 1.5 to 3.5 wt% F, observed in natural peralkaline rhyolites (Webster and Rebbert 2001) versus topaz-bearing rhyolites and ongonites, respectively (Kovalenko and Kovalenko 1984; Štemprok 1991). In the silica-undersaturated systems, corundum-bearing nepheline syenites reach the highest F concentrations before they crystallize cryolite (Fig. 7.14d). By contrast, titanite-bearing nepheline-syenite magmas may achieve very low F concentrations, buffered by fluorite. Overall, the chemical potential of F_2O_{-1} is buffered at 10–50 kJ · mol^{-1} less than in silica-saturated rocks (Fig. 7.14c, d), which explains the substantially lower F concentrations in melt inclusions from evolved nepheline syenites and phonolites than those found in granites and rhyolites (e.g., Harms and Schmincke 2000; Fig. 7.6).

7.3.3 Silicate-Fluoride Liquid Immiscibility

The strong, short range order resulting in the formation of alkali- and alkali-aluminofluoride versus silicate species (Eqs. 7.2 and 7.4) creates a structural incompatibility due to the distinct coordination of the alkali cation and Si. In the alkali fluoride end-member, the alkali cation is in an octahedral coordination (Strunz and Nickel 2001) and all alkali-F bonds have the electrostatic bond valence = 1/6. In the SiO_2 end-member, Si has a tetrahedral coordination at low pressures (e.g., Hemley et al. 1994) and the Si-O bonds possess an electrostatic bond valence = 1. This difference precludes the occurrence of fluoride polyhedra and silicate tetrahedra as neighbours and leads to alkali-fluoride and silicate clustering producing liquid-liquid immiscibility (Kogarko and Krigman 1975; Anfilogov et al. 1979; Gramenitskiy and Shchekina 2001; Veksler 2004; Dolejš and Baker 2007a; Lester et al. 2013; Shchekina et al. 2013; Figs. 7.3 and 7.15).

The silicate-fluoride liquid-liquid immiscibility has been advocated as the principal petrogenetic mechanism to explain:

1. The strongly variable F concentrations in natural silicic rocks and melt inclusions, in particular topaz granites, rhyolites, ongonites, and quartz topazites, which span nearly two orders of magnitude (Kovalenko and Kovalenko 1976; Eadington and Nashar 1978; Kortemeier and Burt 1988; Štemprok 1991; Johnston and Chappell 1992; Dergachev 1992; Antipin et al. 1999; Thomas et al. 2005; Peretyazhko et al. 2007). This would otherwise require extreme levels of crystal fractionation and abundant complementary, more primitive cumulates.
2. The unconventional trace-element patterns, including tetrad effects in the REE distribution and/or strong enrichment and decoupling of high field strength elements (Gramenitskiy and Shchekina 2001; Peretyazhko and Savina 2010).

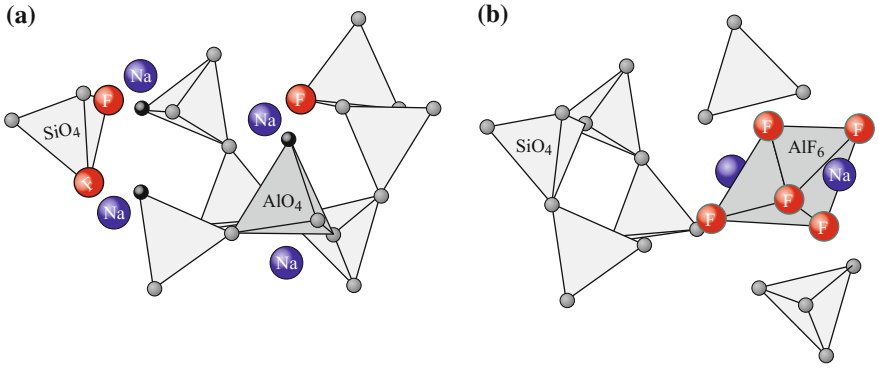

Fig. 7.15 Schematic illustration of **a** Na–F disorder in the aluminosilicate network versus **b** Na–F ordering toward the aluminate species producing cryolite-like octahedral structures, which become immiscible within a polymerizing silicate framework

Previous experimental attempts to locate the silicate-fluoride liquid immiscibility in a number of HF-, LiF-, KF-, NaF-, Na_3AlF_6-, and AlF_3-bearing silicate systems yielded contradictory results, as discussed by Dolejš and Baker (2007a). These disagreements persist from simple binaries, such as albite–NaF (e.g., Koster van Groos and Wyllie 1968; Rutlin 1998), to multicomponent composition (e.g., Kovalenko et al. 1975; Danckwerth 1981; Gramenitskiy and Shchekina 1994; Xiong et al. 2002). Some of the controversies may have resulted from the misinterpretation of round fluoride crystals as immiscible liquid globules, or the assignment of solute-rich stable or quench fluids to immiscible fluoride liquids (e.g., microliquation; Anfilogov et al. 1973; Glyuk and Anfilogov 1973a, b). In order to be petrogenetically significant, the postulated liquid-liquid miscibility gaps must be intersected by relevant liquid lines of descent. That is, they are located on an appropriate liquidus surface (or volume), which occur under realistic temperatures. Numerous experimental studies, which report the occurrence of silicate and fluoride immiscible melts, were hindered by inappropriate choices of fluoride additives, and these compositions substantially depart from the liquid lines of descent or intersect the Alkemade compatibilities, that is, penetrate potential thermal barriers (Dolejš and Baker 2007a).

We discuss the topological features of the silicate-fluoride liquid-liquid immiscibility by tracing its extension from the silica–cryolite binary systém into the cryolite- and topaz-bearing quaternary and fluorohaplogranitic quinary systems (Dolejš and Baker 2007a, b). This approach provides constraints on the differentiation paths of the fluid-undersaturated F-bearing granitic and rhyolitic magmas. Mechanisms of exsolution of hydrohalide liquids during fluid saturation will be discussed in Sect. 7.4.

The existence of a liquid-liquid immiscibility in the SiO_2–Na_3AlF_6 system has remained inconclusive (Weill and Fyfe 1964; Grjotheim et al. 1971; Kogarko and Krigman 1975, 1981). However, carefully reversed experiments by Dolejš and Baker (2007a) demonstrated a large stability field for silica polymorphs (quartz,

tridymite) and the strongly asymmetric location of the binary eutectic at ~95 wt% cryolite (Fig. 7.16). The fluoride-silicate miscibility gap has not been detected below 1100 °C, but the liquid-liquid immiscibility in the SiO_2–Na_3AlF_6 binary has been documented at 1200 °C at 1 atm and 6 kbar (Kogarko and Krigman 1975; Robert and Dolejš, unpublished experimental results). These observations imply that a high-temperature, two-liquid miscibility gap exists on the tridymite liquidus surface, and its extension and/or closure into the albite- and topaz-bearing systems is of fundamental significance for the differentiation of peralkaline cryolite- and peraluminous topaz-bearing granites and rhyolites.

The liquidus relations in the SiO_2–$NaAlSi_3O_8$–Na_3AlF_6 ternary system are shown in Fig. 7.16a. The silicate-fluoride miscibility gap extends over the entire ternary space, but in the $NaAlSi_3O_8$–Na_3AlF_6 binary subsystem, it is located on the cryolite liquidus. As a consequence, the silica–cryolite cotectic represents a thermal minimum for the miscibility gap, which is located at ~970 °C. The ternary quartz–albite–cryolite eutectic occurs at ~5 wt% F and ~770 °C at 1 kbar in an H_2O-absent system (Fig. 7.16a). Peralkaline F-bearing silicic magmas are expected to fractionate along the quartz–albite cotectic while progressively increasing the F content in the melt until they reach cryolite saturation at the quartz–albite–cryolite eutectic point and completely crystallize. The silicate-fluoride liquid miscibility gap

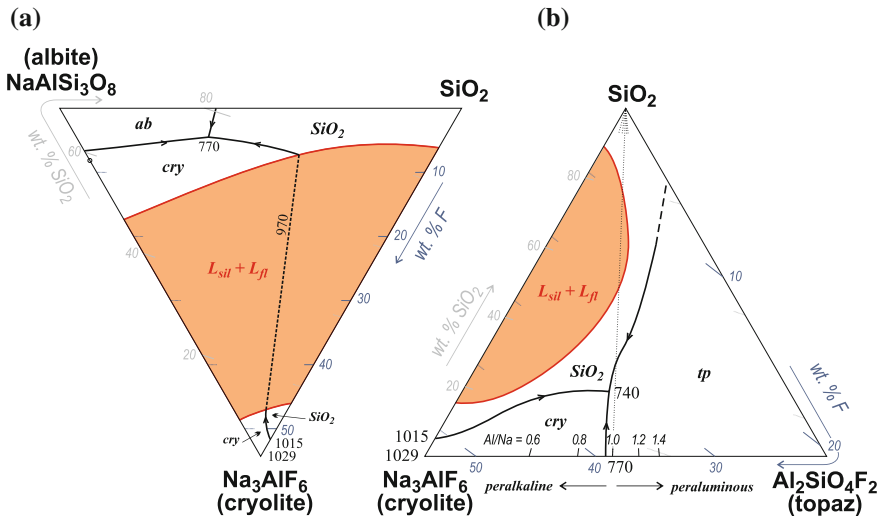

Fig. 7.16 Liquidus projections of the **a** silica–albite–cryolite and **b** silica–topaz–cryolite ternary systems in weight per cent at 100 MPa (Dolejš and Baker 2007a). The fluoride-silicate miscibility gap extends from the silica liquidus in the silica–cryolite binary to the cryolite liquidus (in the albite-rich portion of the diagram). The albite–quartz cotectic leads to the ternary eutectic at 770 °C and does not reach the liquid miscibility gap. Similarly, the fluoride-liquid immiscibility extends from the silica–cryolite binary to the topaz-bearing ternary and closes at 960 °C on the quartz liquidus surface. The ternary quartz–cryolite–topaz eutectic is located at 740 °C (30.6 wt% SiO_2, 31.8 wt% F, Al/Na = 0.96). SiO_2 concentrations of F and variations in the alumina saturation index (Al/Na ratio) are shown on the sides

is located at very high temperatures and on the cryolite liquidus surface. It is, thus, inaccessible to peralkaline quartz-and feldspar-crystallizing magmas.

In contrast, the SiO_2–$Al_2SiO_4F_2$–Na_3AlF_6 ternary system covers a wide range of peralkaline to peraluminous compositions, and it serves as transition to the multicomponent fluorohaplogranitic system. Topaz and cryolite represent products of the first fluorination step of albitic feldspar. Hence, they are potential F buffers during crystallization of silicate magmas. In addition, the SiO_2–$Al_2SiO_4F_2$–Na_3AlF_6 space is pierced by the albite–F_2O_{-1} and nepheline–F_2O_{-1} joins. The existence of albite or nepheline pseudoternary fields would indicate the occurrence of a peritectic transition, which would allow for very high F enrichment in the residual melts and the formation of feldspar-free products, e.g., quartz topazites.

The topaz–cryolite assemblage forms a simple binary eutectic with 39.2 wt% F at nearly subaluminous composition (molar Al/Na $\sim$0.95), 770 °C, and 1 kbar, indicating closure of the SiO_2–Na_3AlF_6 miscibility gap as it extends into the topaz-bearing composition space (Fig. 7.16b). The SiO_2–Na_3AlF_6 two-liquid field, as it propagates into a more aluminous ternary system, is underlain by the ternary assemblage of tridymite/quartz + silicate liquid + fluoride liquid, but remains exclusively located on the silica polymorph liquidus surface. The miscibility gap closes at 960 °C and it is not intersected by the silica–cryolite or silica–topaz cotectic curves. These two cotectic curves converge to the ternary eutectic composition with 31.9 wt% F and molar Al/Na $\sim$0.95, located at 740 °C and 1 kbar in anhydrous system (Fig. 7.16b). Increasing the aluminosity of the system thus restricts and closes the silicate-fluoride miscibility gap at high temperatures and on the silica liquidus, while allowing quartz-saturated fractionation paths to reach extremely high concentrations of F in the residual melts of nearly subaluminous composition. The SiO_2–$Al_2SiO_4F_2$–Na_3AlF_6 ternary system does not contain any additional, pseudoternary phases, such as albite or nepheline. Thus it represents a thermal barrier in the Na_2O–Al_2O_3–SiO_2–F_2O_{-1} quaternary system, and the stability fields of the "high-fluorination" phases (e.g., chiolite, maladrite) are not accessible by magmatic crystal fractionation (Dolejš and Baker 2007a).

The liquidus equilibria of quartz, albite, topaz, and cryolite are schematically summarized in Fig. 7.17 as a model for differentiation paths of peralkaline to peraluminous F-bearing haplogranitic and haplorhyolitic magmas. This anhydrous quaternary system consists of four liquidus volumes (of the above mineral phases) and one liquid miscibility gap that continuously extends from the quartz to the cryolite field. Natural silicic magmas, with initially low concentrations of F, are situated close to the albite–quartz binary eutectic (E_{AQ}; Fig. 7.17). Magmatic fractionation of quartz and feldspar will, depending on the initial alkali/Al ratio, promote the peralkaline or peraluminous nature of the evolving melts. Peralkaline melts will be first saturated with cryolite, whereas their peraluminous counterparts will crystalize topaz. Both the cryolite- or topaz-bearing ternary eutectics (E_{AQC}, E_{AQT}; Fig. 7.17) are located at low F contents (<5 wt% F). By contrast, the quaternary eutectic (E_{AQTC}) is displaced to much higher F levels. Therefore, the evolving melts, upon reaching cryolite or topaz saturation, will continue to fractionate to high levels of F enrichment and their alkali/Al ratios will converge. In the

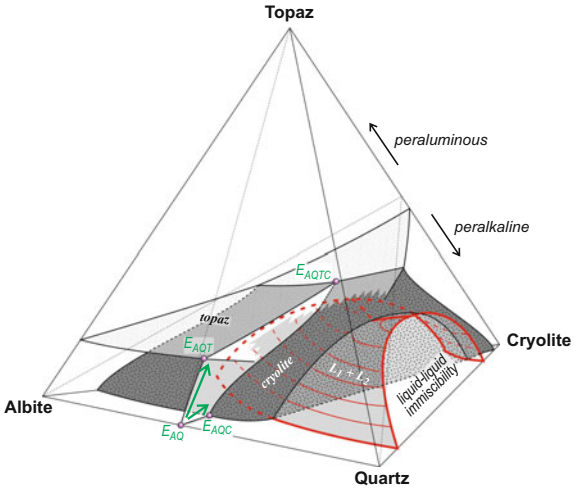

Fig. 7.17 Schematic liquidus projection of the quaternary quartz–albite–cryolite–topaz system in weight per cent at 100 MPa (Dolejš and Baker 2007a). The fluoride-silicate liquid miscibility gap is located within the cryolite and quartz volumes. Symbols: E_{AQ} binary albite–quartz eutectic, E_{AQC} ternary albite–quartz–cryolite eutectic, E_{AQT} ternary albite–quartz–topaz eutectic, E_{AQTC} quaternary albite–quartz–topaz–cryolite eutectic. *Arrows* indicate the fractionation paths for the peraluminous and peralkaline quartz–albite-precipitating melts, respectively. Note that the quartz–albite cotectic surface does not reach the liquid miscibility gap

absence of aluminosilicate mineral buffers, the initial peralkaline or peraluminous divergence will subsequently be reversed, and all the residual melts will reach a very weakly peralkaline composition. The fluoride-silicate liquid miscibility gap remains inaccessible to any feldspar-precipitating liquid line of descent in this anhydrous model system (Dolejš and Baker 2007a; Fig. 7.17).

The behavior of alkalis and the partitioning of halogens in natural highly evolved F-bearing magmatic rocks remain unconstrained by the above phase equilibrium studies. The rock sequence granite/rhyolite–topaz granite/ongonite–quartz topazite is characterized by alkali depletion and Na–K decoupling. Topaz rhyolites and ongonites become K-poor (<3.5 wt% K_2O), transitional topaz tronhjemites are implicitly sodic and K-depleted ($\sim$0.4 wt% K_2O; Kortemeier and Burt 1988), and quartz topazites are effectively alkali-free (0.1–0.5 wt% $K_2O + Na_2O$; Zhu and Liu 1990; Johnston and Chappell 1992). The alkali loss was attributed to the separation of an immiscible alkali-fluoride melt or alkali-halide fluid (Kortemeir and Burt 1988), which was facilitated by a peritectic transition albite + melt = quartz + topaz + cryolite or chiolite (Kovalenko and Kovalenko 1976; Kogarko and Krigman 1981). In order to address these issues, the quaternary system $Na_2O–Al_2O_3–SiO_2–F_2O_{-1}$ has been extended by the addition of K_2O and H_2O into a six-component F-bearing haplogranitic system (Dolejš and Baker 2007b).

The limiting binary systems haplogranite ($Qz_{38}Ab_{33}Or_{29}$ by weight)-topaz and haplogranite-cryolite at fluid saturation demonstrate that the maximum F

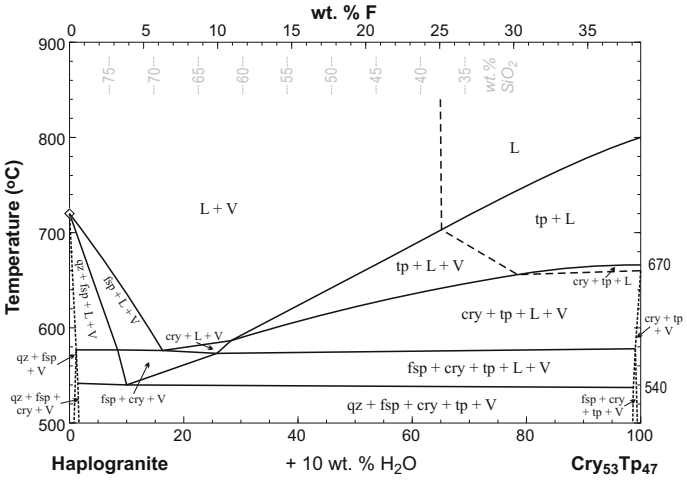

Fig. 7.18 Phase-diagram section extending from the haplogranite minimum composition ($Qz_{38}Or_{29}Ab_{33}$ by weight; Tuttle and Bowen 1958) with 10 wt% H_2O at 100 MPa (Dolejš and Baker 2007b). The binary section connects the silicate system with the subaluminous (molar Al/Na = 1) cryolite–topaz mixture. The haplogranite–H_2O eutectic temperature at 720 °C (Tuttle and Bowen 1958) is lowered to the quartz–albite–K-feldspar–cryolite–topaz–H_2O eutectic at 540 °C (weakly peraluminous)

solubilities remain low and temperature-dependent (Dolejš and Baker 2007b). Topaz saturation occurs at ~1.7 wt% F at 690 °C, whereas cryolite saturates at ~3.9 wt% F at 670 °C and 100 MPa. In addition, Clarke et al. (2009) experimentally demonstrated that the crystallization of andalusite is succeded by topaz at 1 wt% F in the melt. Strong liquidus depression in the hydrous cryolite–topaz binary, in the absence of quartz and feldspar to 660 °C at 100 MPa, suggests additional liquidus depression from the simple haplogranite-topaz and haplogranite–cryolite binaries as well as high F solubility in cotectic, cryolite-, and topaz-saturated melts. The differentiation paths of residual fluorogranitic melts terminate at a pseudoternary, haplogranite–topaz–cryolite eutectic at 540 °C and 100 MPa, with ~4.5 wt% F and ASI ~1.12 (Dolejš and Baker 2007b; Figs. 7.18 and 7.19a). Progressive release of aqueous fluids near the solidus is expected to slightly decrease the SiO_2 content of the melt and increase its peraluminosity due to incongruent partitioning of major components to the fluid phase.

In natural multicomponent systems, the differentiation of F-bearing granitic and rhyolitic magmas may differ due to alumina buffering imposed by coprecipitation of aluminosilicate minerals. Crystallization of andalusite (or sillimanite) in the presence of quartz buffers the activity of alumina via the following equilibrium:

$$Al_2SiO_5\,(\text{andalusite, sillimanite}) = SiO_2\,(\text{quartz}) + Al_2O_3\,(\text{melt}), \qquad (7.28)$$

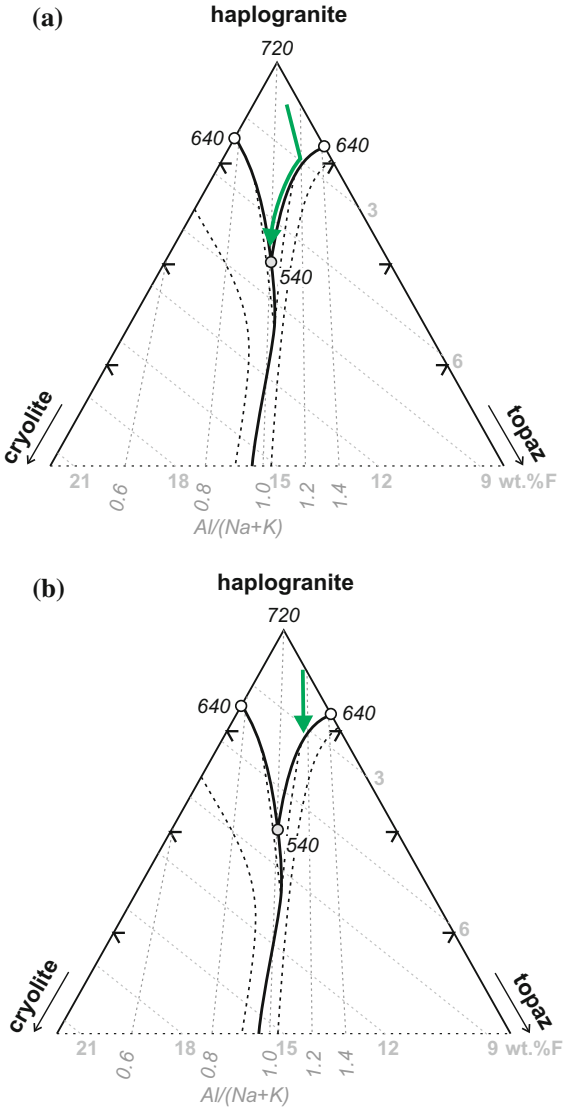

Fig. 7.19 Schematic liquidus projection and evolutionary paths of F-bearing residual melts **a** in the absence of alumina buffering, applicable to leucogranites and rhyolites, and **b** in the presence of additional mineral phases such as micas, cordierite, or garnet, which buffer the activity of alumina

and, analogously, for white mica and K-feldspar:

$$KAl_2AlSi_3O_{10}(OH)_2\,(\text{muscovite}) = KAlSi_3O_8\,(\text{K-feldspar}) + H_2O + Al_2O_3\,(\text{melt}). \tag{7.29}$$

Numerous additional equilibria involving cordierite, garnet, and other common rock-forming minerals are listed by Barton et al. (1991) and Barton (1996). When the alumina activity is buffered by simultaneous stability of other aluminosilicates,

the liquid line of descent in the pseudoternary system haplogranite–topaz–cryolite will follow an ASI isopleth, reach the topaz saturation surface, and invariantly terminate (Fig. 7.19b). In this scenario, the evolving melts will not experience residual enrichment in F and will precipitate topaz at the solidus.

Silicate-fluoride liquid-liquid immiscibility (Kogarko and Krigman 1981; Veksler et al. 2005, 2012; Dolejš and Baker 2007a) does not propagate to the low-temperature haplogranitic systems, which are poor in additional components including Li. The above equilibria thus define the differentiation paths of Li-, Ca-, and Fe-poor F-bearing leucogranites, rhyolites, ongonites, and their differentiates (quartz topazites, xianghualingites, elvans) (Fig. 7.20). Fluorine-bearing natural rocks are moderately to strongly peraluminous, whereas peralkaline varieties are nearly absent. Fluorine-bearing granites and ongonites follow the feldspar-aluminosilicate (andalusite–topaz) [+quartz] cotectic curves and represent magmatic liquids. On the other hand, the compositions of the quartz topazites and xianghualingites overlap with the quartz–topaz boundary. This is consistent with their bimineralic nature and representative of crystalizing assemblages, which are products of disequilibrium or zonal crystallization in pegmatite-forming melts or were affected by hydrothermal alteration, mainly alkali loss (cf., Birch 1984; Kleeman 1985; Hervig et al. 1987; Kortemeier and Burt 1988; Johnston and Chappell 1992; Dolejš and Baker 2007b; Fig. 7.20).

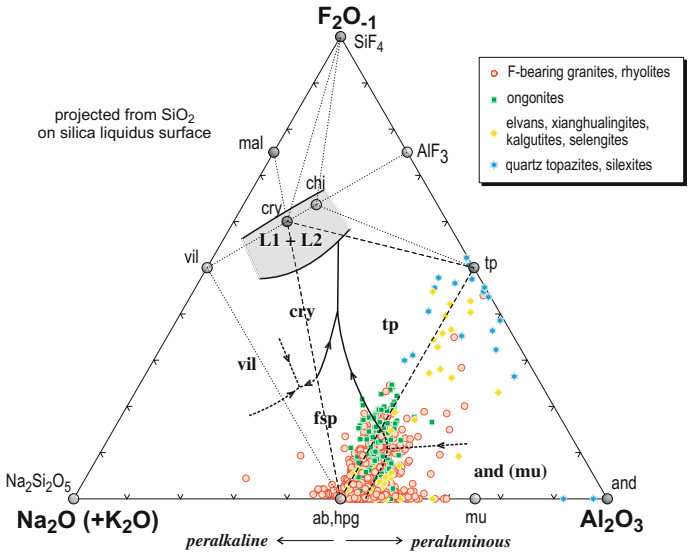

Fig. 7.20 Liquidus projection of the $Na_2O + K_2O–Al_2O_3–SiO_2–F_2O_{-1}$ system from the SiO_2 apex onto the silica saturation surface (Dolejš and Baker 2007b). The position of the haplogranite-aluminosilicate eutectic is based on Joyce and Voigt (1994). Sources for the whole-rock data are listed in the electronic appendix of Dolejš and Baker (2004)

Additional rock-forming constituents (Ca, Mg, Fe or Li) are expected to affect the model of fluorohaplogranitic differentiation by saturation in new F-bearing phases (e.g., fluorite or Li-fluoromicas), which may limit the F enrichment and promote its partitioning to other phases. Highly evolved Li- and B-rich granitic and pegmatitic melts are Ca-poor (Černý 1998; Stilling 1998), hence fluorite crystallization is restricted to near-solidus conditions (Webster et al. 1987; Weidner and Martin 1987; Lukkari and Holtz 2007). Lithium micas and amblygonite-montebrasite solid solutions may act as sinks for F during magmatic fractionation (Icenhower and London 1995; London 1997; London et al. 2001), but the amount of precipitating solid phases is likely to be very limited by the Li or P available in the melt. On the other hand, Li significantly depresses the crystallization temperatures, by 100–240 °C at 1 kbar under hydrous conditions (Muñoz 1971; Stewart 1978; London 1986), and it increases the extent and the low-temperature limit of the fluoride-silicate, liquid-liquid immiscibility. The fluoride-silicate liquid immiscibility occurs at less than 4 wt% F in the melt, and it is located on the quartz liquidus through a divariant two-liquid + quartz field (Gramenitskiy and Shchekina 1994; Gramenitskiy et al. 2005; Veksler et al. 2012).

In contrast to simple systems, which saturate with one fluoride mineral and no immiscible fluoride melt, natural multicomponent magmas may, in the presence of other, mainly alkali cations and/or chlorides, produce immiscible salt melts (or brines) due to the strong solidus depression in multicomponent fluoride-chloride systems (Dolejš and Baker 2006a). Villiaumite is compatible with halite (eutectic temperature, T_e = 678–680 °C at 1 atm), with halite and cryolite (T_e = 674 °C), or halite and sylvite (T_e = 590–606 °C) (Sauerwald and Dombois 1954; Phillips et al. 1955; Kuvakin and Kusakin 1959; Bukhalova and Mal'tsev 1965). In the presence of H_2O, these halide melts will have a limited fraction of dissolved H_2O due to very high vapor pressure, and will plaussibly evolve to aqueous fluids by boiling (Urusova and Ravich 1966; Kotelnikova and Kotelnikov 2002). This mechanism is consistent with the formation and preservation of fluoride hydrosaline liquids, enriched in Ca and/or REE fluorides, in nature (Klemme 2004; Badanina et al. 2004, 2006; Peretyazhko et al. 2007; Peretyazhko and Savina 2010; Vasyukova and Williams-Jones 2014; cf., Veksler and Thomas 2002).

7.3.4 *Inhibition of F Enrichment by Fluorite Saturation*

Simple fluoride minerals, such as villiaumite (NaF) or fluorite (CaF_2) are potential buffers or moderators of F enrichment during magma differentiation due to the universal availability of Na_2O and CaO in natural magmas. The refractory nature of fluorite, with its high melting temperature of 1372 °C at 1 atm and low enthalpy of melting, is responsible for its low solubility in silicate melts at magmatic temperatures (Kojima et al. 1968; Dolejš and Baker 2006b), and make it an important candidate for buffering the range of F concentrations. Fluorite is a very common mineral in silicic magmatic rocks and their metamorphic and metasomatic

successors (e.g., Bohlen and Essene 1978; Hogan and Gilbert 1995; Haapala 1997). Its amount varies from accessory to percent amounts in granites and rhyolites (e.g., Marshall et al. 1998; Sallet et al. 2000; Abdel-Rahman and El-Kibbi 2001), but it is rather irregularly distributed in pegmatites or greisens (Lentz and Gregoire 1995; Sakoma et al. 2000; Frindt and Poutainen 2002). There is no obvious textural relationship between fluorite and bulk-rock Ca or F contents, but the formation of fluorite appears to be linked to the magma aluminosity (Gabitov et al. 2005; Dolejš and Baker 2006b). In peralkaline systems, fluorite forms solid inclusions in magmatic phenocrysts, microlites in melt inclusions, or phenocrysts in volcanic rocks (e.g., Marshall et al. 1998; Webster and Rebbert 2001). In metaluminous granites, and their metamorphic equivalents, it occurs as a rare accessory phase (Buddington and Leonard 1962; Bohlen and Essene 1978; Hogan and Gilbert 1995; Price et al. 1999). In peraluminous topaz-bearing granites and rhyolites, fluorite is frequently an abundant, but secondary phase produced during hydrothermal alteration (Taylor et al. 1984; Lentz and Gregoire 1995; Sakoma et al. 2000; Frindt and Poutainen 2000; cf., Barton 1982; Ryabchikov et al. 1996; Dolejš and Baker 2004). Similar relationships between the fluorite stability and the melt aluminosity have been documented in experimental studies. Fluorite is an early liquidus phase in peralkaline rhyolites (Scaillet and Macdonald 2001, 2004). In metaluminous systems, fluorite is a rare interstitial accessory phase in granites and their metamorphic equivalents (Buddington and Leonard 1962; Bohlen and Essene 1978; Hogan and Gilbert 1995). An observed incompatibility between titanite, clinopyroxene and fluorite can be explained by the following equilibrium:

$$\mathrm{CaTiSiO_5 + F_2O_{-1} = TiO_2 + CaF_2 + SiO_2}, \tag{7.30}$$

which occurs at 1.0 wt% F (in the melt) at 850 °C and 200 MPa buffered to NNO oxygen fugacity (Price et al. 1999). An experimental study of the Spor Mountain vitrophyre (Webster et al. 1987) located the fluorite liquidus about 150–200 °C above the solidus at 50–200 MPa, indicating its late magmatic origin. In peraluminous systems, represented by topaz-bearing granites, rhyolites, and ongonites, fluorite is commonly a secondary phase formed during subsolidus alteration. Two mechanisms lead to the formation of subsolidus fluorite (Dolejš and Baker 2004)—open-system fluorination (Haapala 1997):

$$\mathrm{CaAl_2Si_2O_8\,(ss) + 4\,HF\,(aq) = CaF_2(s) + Al_2SiO_4F_2(ss) + SiO_2(s) + 2\,H_2O\,(aq)}, \tag{7.31}$$

and hydration during cooling (Barton 1982; Ryabchikov et al. 1996):

$$\begin{aligned}\mathrm{CaAl_2Si_2O_8(ss) + 2\,KAlSi_3O_8(ss) + Al_2SiO_4F_2(ss) + 2\,H_2O}\\ \mathrm{= 2\,KAl_3Si_3O_{10}(OH)_2(s) + CaF_2(s) + 3\,SiO_2(s)}.\end{aligned} \tag{7.32}$$

This suggestion is corroborated by results from experimental studies on topaz granites. Here, fluorite is identified as a near-solidus phase, which melts completely

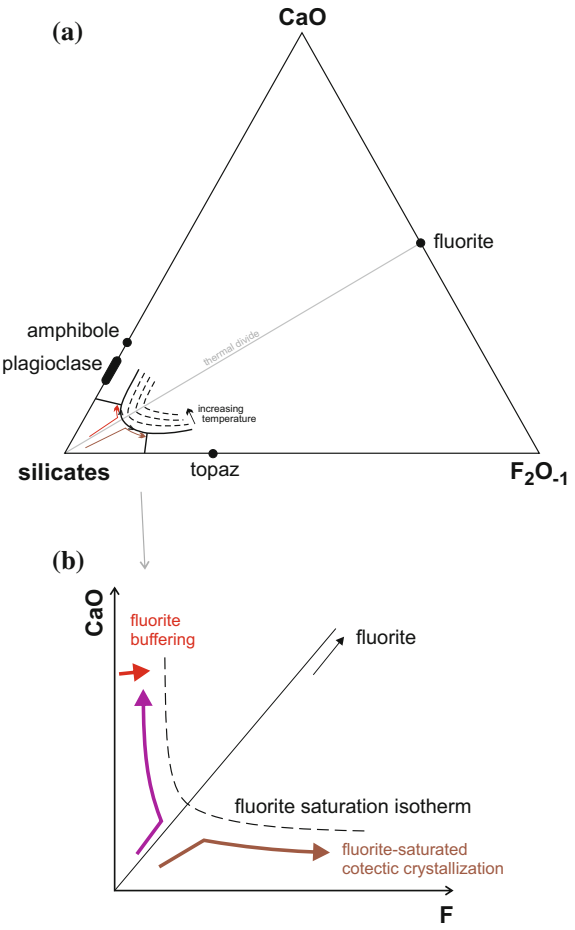

Fig. 7.21 Schematic illustration of **a** the liquidus equilibrium in the system silicate–CaO–F_2O_{-1}, and **b** its transformation into the CaO versus F bivariate space with fluorite saturation isotherms. The silicate-fluorite join represents a stable mineral assemblage, hence the thermal barrier, which divides the fluorite cotectic boundary into two diverging segments. Colored trends indicate magma differentiation paths with variable CaO and F contents

within 25 and 40 °C above the solidus temperature (Weidner and Martin 1987; Xiong et al. 2002; Lukkari and Holtz 2007). In the latter study, the fluorite stability field rapidly expands to a high temperature with addition of F to the system, thus confirming that Ca and F behave as independent components controlling the saturation (Eq. 7.24).

If fluorite moderates the evolution and F concentrations of residual granitic and rhyolitic magmas, the nature and location of cotectic curves, where fluorite is stable, must be found experimentally. Owing to the refractory nature of fluorite, its solubility in silicate melts under magmatic conditions is expected to be low, as illustrated in Fig. 7.21a. Subsequently, the fluorite saturation isotherms will acquire a hyperbolic form in the orthogonal composition space CaO versus F, in accordance with the solubility product of Eq. (7.24).

At 800 °C and 100 MPa, the fluorite solubilities on the fluid-saturated, haplogranite-fluorite join are low: 1.05 (peralkaline), 0.82 (subaluminous), and

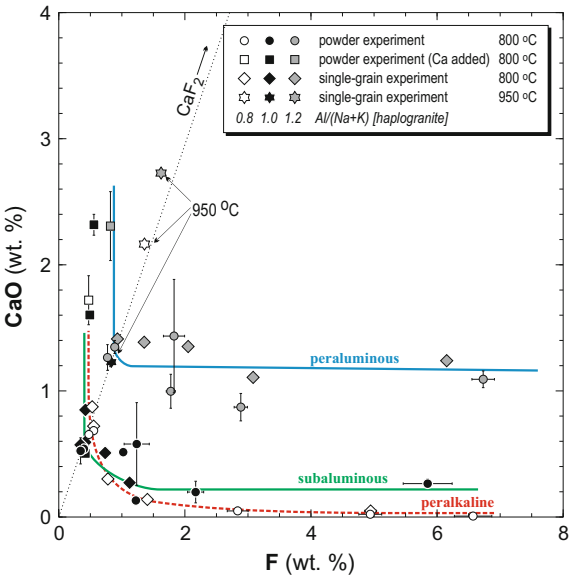

Fig. 7.22 Fluorite solubility isotherms (in weight per cent on an anhydrous basis) at 800–950 °C, 100 MPa, and 10 wt% H_2O in the peraluminous, subaluminous, and peralkaline systems (Dolejš and Baker 2006b)

1.92 wt% CaF_2 (peraluminous). Whereas, at 950 °C and 100 MPa, the solubilities increase to 2.90 (peralkaline), 1.71 (subaluminous), and 3.57 wt% CaF_2 (peraluminous) (Dolejš and Baker 2006b; Fig. 7.22). In addition, these values indicate a solubility minimum near the subaluminous composition and more than a twofold increase in the fluorite solubility in the peraluminous melts (ASI $\sim$1.2). The experimentally determined hyperbolic shape of the saturation isotherms confirms partial or complete decoupling of CaO and F_2O_{-1} in the silicate melt structure.

The concentrations of CaO and F in natural volcanic glasses and melt inclusions show a similar hyperbolic trend (Fig. 7.23). Importantly, peralkaline and metaluminous melts are characterized by elevated Ca contents (up to 3.6 wt% CaO), but very low F concentrations (<0.2 wt% F). By contrast, peraluminous systems are Ca-poor, with a negative correlation to peraluminosity, but produce F-rich residual melts (up to 5 wt%) (Fig. 7.23). These features are in excellent agreement with experimental saturation isotherms, and confirm that a number of natural silicic magmas become saturated in fluorite during progressive crystallization. An asymptotic approach of the solubility isotherm to the diagram axes in Fig. 7.22 implies that when one component is substantially more abundant than the other (F $\gg$ 2 Ca or 2 Ca $\gg$ F in molar quantities), fluorite crystallization is controlled by the less-abundant component and it is essentially independent of the more-abundant component. Cotectic fractionation of fluorite with rock-forming silicates will buffer the concentration of the less-abundant component, whereas the contents of the other one will continue to rise. In peraluminous granites, which are also frequently Ca-poor, the fluorite saturation is dictated by the CaO concentration and will generally appear very late at low temperatures. In calc-alkaline and Ca-rich peralkaline magmas, fluorite crystallization buffers the F concentration in the melt at

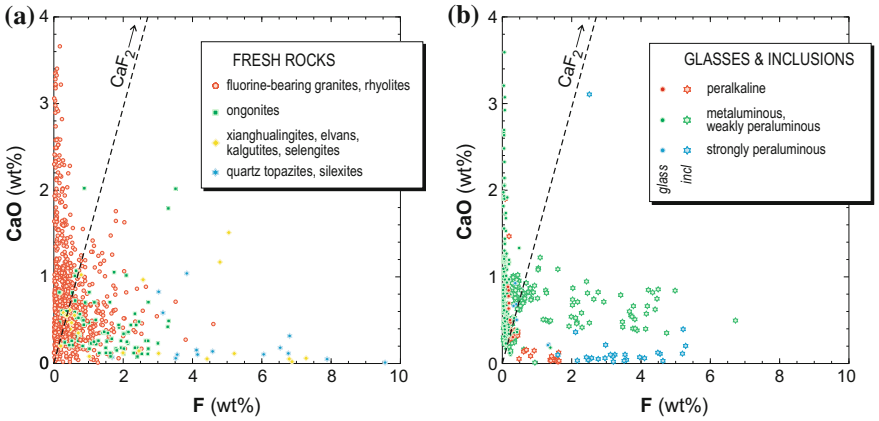

Fig. 7.23 CaO versus F concentrations in **a** granitic and rhyolitic rocks and **b** in matrix glasses and melt inclusions. Note (i) the dichotomy between the CaO-rich F-poor granites and F-rich CaO-poor suites, and (ii) increasing melt peraluminosity with increasing F content. Data sources are given in Dolejš and Baker (2004, 2006b)

very low levels inihibiting the formation of F-rich residual melts. The silicate-fluorite immiscibility has not been encountered in peralkaline through peraluminous compositions (ASI = 0.8–1.2) up to at least 950 °C at 100 MPa and aqueous fluid saturation, but it is predicted to occur above 1230–1300 °C (Dolejš and Baker 2006b; cf., Webster et al. 1998; Ueda and Maeda 1999). The occurrence of silicate-fluoride liquid-liquid immiscibility at common magmatic temperatures requires the presence of other fluoride (or chloride) components, which will lower the melting temperature of the fluoride assemblage and produce fluoride (or hydrous fluoride) liquid as discussed in the preceding section.

7.4 Magmatic-Hydrothermal Evolution of Halogen-Bearing Systems

The nature of late-stage evolution of magmatic systems and the formation of aqueous or halide fluids is fundamental to interpreting the magma crystallization temperatures, the timing of fluid saturation and mass-transfer, and the ore-forming potential of the media that are involved. For instance, an increase in H_2O solubility extends magma fractionation, delays saturation with aqueous fluid phase, and restricts the dispersal of economically important constituents. As a consequence, fluid-mobile elements and ligands continue to be enriched in residual melt until fluid saturation is reached. The efficiency of element partitioning to the fluid phase will be a function of the halide/H_2O ratio in the residual melt as it dictates the concentration of complexing ligands (e.g., Audétat et al. 2008; Heinrich and

Candela 2014). The course of the magmatic to hydrothermal evolution is a complex interplay between: (i) halogen-H_2O interaction in the silicate melt structure; (ii) phase equilibria in the halide-H_2O system; and (iii) halogen-silicate interaction in the silicate melt.

In the following discussion we use the terms liquid, melt, brine, fluid, and vapor in general accordance with Stalder et al. (2000), Wyllie and Ryabchikov (2000), and Dolejš and Baker (2007b). Namely, a liquid has a general meaning and sensu stricto it refers to media where H_2O is not the predominant component such as in melts and brines. Melt represents a silicate, halosilicate, or halide medium with a definite amount of dissolved H_2O. Brine is a hydrous halide liquid. Vapor is an aqueous phase with a low solute content, generally of low density. This terminology is primarily based on chemical composition of the medium rather than emphasizing its physical properties such as density.

7.4.1 *Silicate-Halide-H_2O System as Model for Devolatilization*

The evolution of halogen-bearing, hydrous silicate melts, with decreasing temperature and/or pressure, is primarily dictated by phase equilibria of all three components—silicate, halide, and H_2O, which are usually portrayed in the form of a pseudoternary system (Koster van Groos and Wyllie 1968, 1969; Webster 1997a, 2004; Fig. 7.23). This model system allows us to predict changes in halogen and H_2O solubility and to evaluate the evolutionary paths of individual media (liquids and aqueous fluids). It also allows us to inspect the potential for and mechanisms of continuous or discrete transition between hydrous silicate melts, halide brines, and solute-bearing vapors.

The general topology of the silicate–halide–H_2O ternary system is, to a large extent, defined by equilibria in the two binary systems silicate-halide and halide-H_2O. It is affected by the refractory versus volatile behavior of halides and the halide-silicate liquid immiscibility (Fig. 7.24). For halides with high melting temperature and low solubility in aqueous fluids, e.g., NaF, Na_3AlF_6, and CaF_2, the silicate-halide binary system is characterized by low halogen solubility at saturation by halide mineral. The halide liquidus surface may be overlain by a silicate-halide liquid miscibility gap (Koster van Groos and Wyllie 1968; Rutlin 1998; Dolejš and Baker 2006b). Qualitative topology of the ternary system corresponds to the albite–NaF–H_2O system (Koster van Groos and Wyllie 1968; Kotelnikova and Kotelnikov 2002; Fig. 7.24a). During fractionation of silicate minerals, magmas with a high halogen/H_2O ratio reach the silicate-fluoride cotectic, i.e., precipitate a solid halide phase (e.g., fluorite, cryolite). With continuing cotectic crystallization, the halogen concentration in the melt remains buffered, but the H_2O content in the melt increases. Magmatic evolution is terminated at the ternary silicate + halide + melt + fluid eutectic, with exsolution of a solute-poor, aqueous vapor. By contrast, magmas with a low halogen/H_2O ratio, undergoing silicate fractionation, reach the melt-vapor

miscibility gap, and steadily exsolve aqueous vapor while the halogen content in the melt continues to rise. In this latter case, magmatic fractionation is terminated at the ternary eutectic by saturation with the solid halide phase (Fig. 7.24a). The location of the halide-silicate two-liquid miscibility gap on the fluoride liquidus makes it inaccessible, i.e., irrelevant to any differentiation paths for natural magmas. Halide liquids or brines cannot form because the silicate-halide monotectic and the hydrous halide solidus are located above common magmatic temperatures (above 850 °C).

Halides with a moderate melting temperature and high solubility in aqueous fluids include NaCl. The silicate–NaCl binary system saturates with an NaCl liquid or brine. The general topology of this ternary system is approximated by the albite–NaCl–H_2O system (Koster van Groos and Wyllie 1969). It can be further applied to highly soluble chloride, fluoride, and carbonate salts, which are separated from the silicate melt by a liquid–liquid miscibility gap with the eutectic close to the salt end member (Fig. 7.24b). The evolutionary sequence of magmas with low halogen/H_2O ratios remains the same as described in the previous discussion. However, note that the solute content in the aqueous fluid *increases* with decreasing temperature. Magmas with high halogen/H_2O ratios reach, by fractionation of silicate minerals, the salt-silicate miscibility gap and start to exsolve a hydrosaline liquid (brine). The monotectic unmixing buffers the halogen concentration in the melt, but the H_2O concentration in both the silicate melt and the halide liquid continue to rise. When relevant, subcritical phenomena in the salt–H_2O binary will lead to a discontinuous decrease in the fluid salinity by boiling (Sourirajan and Kennedy 1962; Koster van Groos and Wyllie 1968, 1969; Bodnar et al. 1985; Koster van Groos 1991). This scenario is particularly relevant for multicomponent F- and Cl-bearing systems, where fluoride and chloride salts may form mixtures with low melting temperatures (cf., Chartrand and Pelton 2001; Heyrman and Chartrand 2007; Renaud et al. 2009, 2011). In this case, the existence of a halide "liquid immiscibility" is controlled by a multiphase salt liquidus depression as discussed by Dolejš and Baker (2006a).

Halide salts or other volatile substances with moderate to very low melting temperatures are completely miscible with H_2O, e.g., KF or HF. The silicate-halide binary system is characterized by a high halogen solubility due to a simple eutectic behavior. The topology of the ternary system depends on the interaction between the halide and silicate liquid components: (i) when the halide component does not significantly affect the H_2O solubility in the melt, the magmas with high halogen/H_2O ratios will reach saturation by a hydrosaline liquid, which subsequently moderates the halogen abundance in the melt, and crystallization leading to the discrete exsolution of a solute-poor vapor; and (ii) when the halide component substantially increases the H_2O solubility in the melt, i.e., leads to the formation of a hydrohalosilicate liquid, protracted magmatic-hydrothermal transition will occur. The qualitative topology of such a ternary system is based on the albite–$Na_2Si_2O_5$–H_2O system (Mustart 1972; Fig. 7.24c). It is applicable when the upper critical end point on the binary or ternary solidus curve occurs at very low pressures or the critical curve is continuous (Morey and Chen 1956; Urusova and Ravich 1966). Magmas with high halogen/H_2O ratios will saturate with a hydrosaline liquid (brine). With decreasing temperature, this cotectic assemblage will evolve toward a

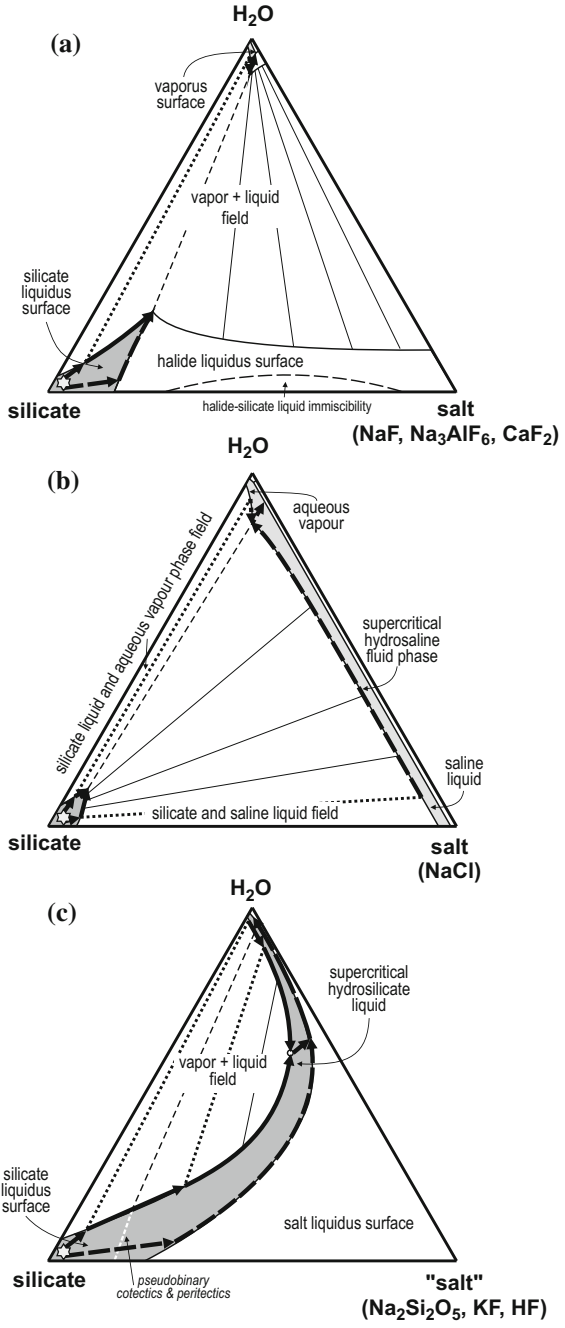

Fig. 7.24 Isobaric liquidus projections with general topologies of the ternary silicate–salt–H_2O systems. **a** System, which contains an ionic salt with a high melting point and subcritical behavior along the salt–H_2O join. This system illustrates buffering of F concentrations in the melt by crystallization of the solid fluoride phase. **b** System, which contains an ionic salt with a low melting point and silicate-salt liquid-liquid immiscibility. This system buffers halide concentrations in the melt by exsolving a (hydro)saline immiscible liquid. **c** Systems, which contain either salt or a volatile substance with the upper critical end point at very low pressures. In this scenario, the liquid-vapor miscibility gap closes and gives rise to the continuous supercritical transition from the hydrous melt to the solute-rich fluid phase

hydrohalosilicate residual melt and a halide fluid with progressively decreasing salinity. By contrast, magmas with the low halogen/H_2O ratios will reach the melt-vapor miscibility gap and start exsolving a solute-poor aqueous vapor by the time minerals start to fractionate out. Upon cooling, the residual melt and aqueous vapor approach each other compositionally until they coincide in the critical gap closure as a hydrohalosilicate liquid. This liquid will continue to fractionate silicates and evolve towards a low-temperature aqueous fluid with a low solute content. This ternary topology is significant for the continuous protracted evolution of a hydrous silicate melt towards a hydrohalosilicate liquid as well as for the formation of these media from an initially aqueous vapor. The other scenarios above do not produce halosilicate liquid media. Existence of such halosilicate mixtures has not been demonstrated under natural conditions yet, as it possibly requires strong mixing or association interaction between the two components.

The formation of pseudobinary solid phases along the silicate-halide binary (e.g., topaz, scapolite, sodalite) leads to the occurrence of cotectic (thermal barriers) or peritectic transitions, which moderate halogen concentrations and potentially prevent the accessibility of the critical closure of the melt-fluid miscibility gap. The albite–HF and granite–HF binaries contain pseudobinary liquidus fields of quartz or topaz (Wyllie and Tuttle 1961; Wyllie 1979; Danckwerth 1981) which either limit the maximum F concentration by cotectic feldspar–quartz–topaz buffering and prevent attainment of the ternary critical point (Kovalenko and Kovalenko 1976), or leave the F concentrations unbuffered by passing through the feldspar and quartz fields by peritectic transitions (Kogarko and Krigman 1981).

7.4.2 Magmatic-Hydrothermal Evolution of F-Bearing Systems

7.4.2.1 Experimental Constraints

The nature of magmatic-hydrothermal transition in F-bearing systems depends on the relationship between H_2O solubility and F enrichment in residual melts, and on the solubility of aluminosilicates in F-bearing fluids at near-solidus temperatures. The experimental results of Dingwell (1985) and Webster (1990) indicated a decrease or a negligible change in the H_2O solubility for up to 8 wt% F in granitic melt, but numerous other studies have documented a positive correlation between H_2O and F concentrations in the melt. Holtz et al. (1993) and Webster and Rebbert (1998) determined experimentally an increase of 0.5–0.8 wt% H_2O for each wt% F at 200 MPa, for F concentrations less than 5 wt% in the melt. At higher F contents, the gradient of increasing solubility slightly declines to to 0.3 wt% H_2O per each wt% F at 100 MPa, leading to a solubility of 12.5 wt% H_2O at 29.5 wt% F in the melt (Dolejš and Baker 2007b). These results do not support the continuous transition from volatile-rich melts to solute-rich, hydrofluorosilicate fluids in subaluminous systems.

The solubility of aluminosilicates in F-bearing fluids is strongly dependent on the bulk composition and speciation of the system of interest. In granitic melts and magmas, the coexisting aqueous fluid is enriched in dissolved aluminosilicates (Dingwell 1985; Webster 1990). The presence of SiO_2-rich melt or gel inclusions in quartz topazites and greisens (Eadington and Nashar 1978; Williamson et al. 1997, 2002) is independently supported by increasing solubilities of quartz, andalusite, and topaz in high-temperature aqueous fluids (Haselton et al. 1988; Aksyuk and Zhukovskaya 1998; Dolejš 2006, 2014). In the multicomponent systems, the solute concentration and composition are expected to be complex, and likely to change from peralkaline to peraluminous or acidic conditions. These principal variables, other relevant species, and solid phases are illustrated in Fig. 7.25.

In alkali-poor, strongly peraluminous systems, the solubility of aluminosilicates in an aqueous fluid increases as a result of the formation of aluminofluoride and silicofluoride complexes (Haselton et al. 1988; Aksyuk and Zhukovskaya 1998; Tagirov et al. 2002; Dolejš 2006, 2014). At very high F concentrations, HF and SiF_4 are expected to be the dominant solutes because they are volatile, low-density constituents forming supercritical mixtures with H_2O (Franck and Spalthoff 1957; Devyatykh et al. 1999). Such residual media would also form by extensive crystallization of silicates at the solidus.

In strongly peralkaline systems, the melt-fluid equilibria are mainly dictated by interaction between H_2O and alkali silicates. The solubility of H_2O in peralkaline granitic melts rapidly increases (Dingwell et al. 1997). Alkali silicates are extensively soluble in the aqueous fluids (Luth and Tuttle 1969) and have very low melting temperatures under hydrous conditions (Tuttle and Bowen 1958; Rowe et al. 1967). This leads to a complete miscibility between peralkaline silicate melts and aqueous fluids at low pressures (Mustart 1972), and the consequent transition from the hydrous melts to alkali silicate-rich fluids by protracted and continuous crystallization.

In broadly subaluminous and weakly peralkaline systems, aqueous speciation is dominated by HF, NaF, and KF. The HF–H_2O system is supercritical (Mootz et al. 1981). The KF–H_2O binary exhibits a continuous transition from hydrous molten salt (brine) to aqueous vapor, with a maximum vapor pressure of 190 MPa (Urusova and Ravich 1966). These experimental data imply that a supercritical, continuous transition from hydrous fluorosilicate melts through alkali-silicofluoride brine to low-temperature solute-bearing aqueous fluid is expectable in K-dominated systems. By contrast, the NaF–H_2O system is subcritical at pressures below 400 MPa (Ravich and Valyashko 1965; Koster van Groos and Wyllie 1968; Kotelnikova and Kotelnikov 2002). Thus in Na-dominated systems, residual hydrous fluorosilicate melts are likely to encounter progressive crystallization of fluoride minerals (e.g., chiolite, cryolite, or villiaumite) near the solidus and discontinuously release F-poor and other solute-poor aqueous fluid (Fig. 7.25). This remarkably contrasting behavior of KF-bearing versus NaF-bearing systems indicates a complexity, which will also arise in Cl-bearing systems. Here, the interaction between Cl in the fluid phase and

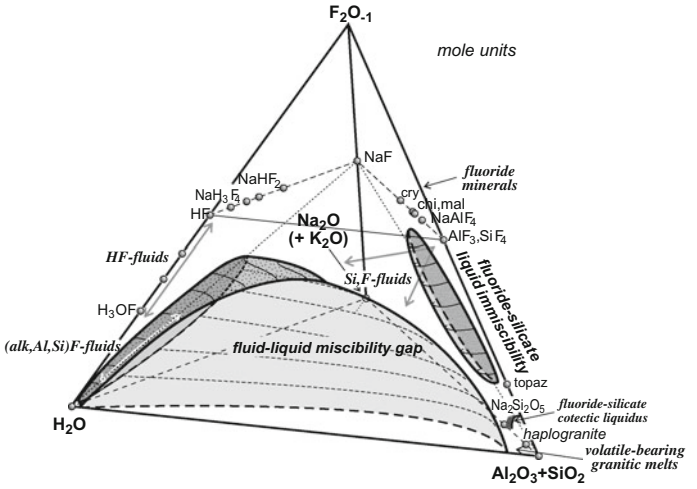

Fig. 7.25 Topology of the liquid–fluid and the fluoride–silicate liquid–liquid miscibility gaps in the system (Na_2O + K_2O)–(Al_2O_3 + SiO_2)–H_2O–F_2O_{-1} (mole units) (Dolejš and Baker 2007b). The liquid–fluid miscibility gap originates at the haplogranite–H_2O join (front edge) and closes by the critical curve, which connects hydrous fluoride liquids (left face) and HF–SiF_4 vapors (front face). The silicate-fluoride cotectic surfaces schematically illustrate buffering effects on the F concentrations in the melt and the composition of the coexisting fluid phase (see text for detailed discussion). *Arrows* indicate the compositions of the various types of fluids. Additional sources of experimental data include haplogranite–H_2O: Luth and Tuttle (1969); albite–$Na_2Si_2O_5$–H_2O: Mustart (1972); NaF–H_2O: Ravich and Valyashko (1965); KF–H_2O: Urusova and Ravich (1966); HF–H_2O: Mootz et al. (1981); NaF–HF: Adamczak et al. (1959); KF–HF: Cady (1934); and fluoride–silicate liquid–liquid immiscibility: Rutlin (1998)

aluminosilicates is negligible. The super- versus subcritical equilibria and saturation limits of chloride brines will become the driving force of magmatic-hydrothermal evolution.

7.4.2.2 Hydrothermal Alteration Styles Associated with F-Rich Granitic Systems

Fluorine-bearing granite plutons commonly develop extensive alteration and/or mineralization aureoles where hydrothermal crystallization of topaz, fluorite, F-rich micas, or cryolite in F-poor country rocks gives a clear record of the transfer of F by hydrothermal fluids. These alteration aureoles include vein and stockwork swarms and massive greisen, albite apogranite (Pollard et al. 1987), or alkali amphibole-cryolite systems (Horbe et al. 1991).

Extensive alkali metasomatism (cryolitization) is restricted to peralkaline F-bearing granitic aureoles (Horbe et al. 1991; Kovalenko et al. 1995; Goodenough et al. 2000). In terms of a_{Na^+}/a_{H^+}, the formation of cryolite overlaps with the stability of alkali amphiboles and pyroxenes (Dolejš and Baker 2004) and requires

small aqueous concentrations of F due to the low solubilities of aluminofluorides (Bailey 1980). At the world's F-richest system (Ivigtut, Greenland), alkali metasomatism proceeded from albitization to cryolitization with precipitation of siderite and base-metal sulfides (Pauly 1960, 1974; Bailey 1980; Pauly and Bailey 1999). This complex suite records a concomitant fluorination and carbonation of its silicate precursors as a consequence of changing oxygen fugacity (Stormer and Carmichael 1970).

In peraluminous suites, the origin of alkali feldspathites (albitization) has been explained as: (i) alteration by saline aqueous solutions due to H_2O–CO_2 unmixing (Schwartz and Surjono 1990); (ii) magmatic-feldspar replacement due to pressure decrease (Witt 1988); (iii) low-temperature Na metasomatism associated with quartz leaching (Cathelineau 1986) in a F-rich environment (Charoy and Pollard 1989); (iv) alteration due to dilution or mixing of fluoride- and chloride-bearing fluids (Pollard et al. 1987); and (v) interaction with NaF-bearing fluids (Kotov et al. 1981). The formation of nearly monomineralic albitites and alkali feldspathites must be accompanied by a strong decrease in the activity of silica in the hydrothermal fluid, related to the destabilizing effect of F (Charoy and Pollard 1989) due to the formation of soluble $Si(OH,F)_4$ complexes (Aksyuk and Zhukovskaya 1998) or thermal reversals in quartz solubility (Walther and Helgeson 1977; Fournier and Potter 1982; Fournier 1985; Nichols and Wiebe 1998; Dolejš and Manning 2010).

Hydrolytic alteration (greisenization) develops as a pervasive endogranitic replacement as well as overlying stockwork systems. It is characterized by a progressive increase in hydrogen activity leading to the destabilization of feldspars (mica-quartz greisens), subsequent destruction of micas (topaz–quartz greisens), and the formation of monomineralic quartz greisens (Štemprok 1987). This sequence of sericitic through advanced argillitic alteration stages represents a common down-temperature hydrolytic, chloride-dominated alteration style with very low concentrations of F ($\sim$2 wt% NaF equiv. in the fluid; Klemm 1994). The appearance of F-bearing phases (Li micas, topaz, fluorite) is related to their low solubility products and precipitation at low fluid F/Cl ratios (e.g., Richardson and Holland 1979; Malinin and Kurovskaya 1996).

The alteration zones in the apical parts of the granitic plutons are commonly found as an upward sequence of microclinization, albitization, and greisenization (Pollard 1983, 1989). The temperature dependence of Na–K fluid-feldspar equilibria (Lagache and Weisbrod 1977) is augmented by the increase of the Na/K aqueous ratios buffered by subsolvus feldspars in the presence of F (Barton and Frantz 1983). That is, preferential removal of fluoride ligands during precipitation of fluorite and/or topaz produces albitization. On the other hand, rare late-stage feldspathization (Beus and Zalashkova 1964) is probably related to the boiling of aqueous or aqueous-carbonic fluids (cf., Dilles and Einaudi 1992).

The overall albitization-greisenization trend is interpreted as due to the influx of meteoric waters into the interior of the pluton (Dolejš and Štemprok 2001) in the upward temperature gradient followed by cooling outflow. The convection model with temperature-pressure gradients has been favoured over the isothermal-isobaric titration models of greisenization and Sn precipitation (Heinrich 1990, 1995; Halter

et al. 1998), which do not reproduce the initial Na depletion characteristic of greisens (Hall 1971; Štemprok 1987; Wasternack et al. 1995).

7.4.3 Exsolution of Cl-Bearing Aqueous Fluids

Limited solubility of Cl in silicate melts (Koster van Gross and Wyllie 1969; Webster and De Vivo 2002; Webster 2004; Aranovich et al. 2013; Webster et al. 2015) and relatively low melting temperatures of alkali chlorides augmented by depression in the liquidus due to H_2O (Bodnar et al. 1985; Chou 1987; Chou et al. 1992; Sterner et al. 1992; Aranovich and Newton 1997) imply strong partitioning of Cl from silicate melts to aqueous fluids and diverse solid-brine-vapor equilibria. The saline aqueous fluids range from concentrated brines to dilute vapors and dictate metal complexing, ore deposition, and various alteration styles *en route*. From intrusive towards shallow epithermal settings, the salinity and composition of hydrothermal fluids is expected to change dramatically, and this is partly due to subcritical phase separation in the H_2O–NaCl system (Bodnar et al. 1985; Heinrich 2005; Driesner and Heinrich 2007). Despite these advances it is still unclear (i) how the salinity of exsolving magmatic fluids is linked to the volatile contents, e.g., Cl/H_2O ratio, of the parental melt, (ii) whether one or two fluid phases can simultaneously separate from magmas, and (iii) how their proportions, salinities and alkali ratio change during progressive devolatilization.

This task relates to a quantitative understanding of the multicomponent granite–halide–H_2O system, which has so far only been interpreted graphically (e.g., Koster van Groos and Wyllie 1968; Webster 2004). This obscures relationships between polymineralic (multivariant) crystallization and exsolution, tie lines between the Cl and H_2O concentrations in the melt, and the fluid salinity (Fig. 7.26). Quantitative modeling of magmatic devolatilization has been hindered by a lack of a thermodynamic model for halogens in silicate melts. Both the conventional Margules-type formalism or the Pelton-Reddy-Blander model for chloride capacities have disadvantages when applied to very small chloride solubilities in strongly polymerized melts (Reddy and Blander 1987; Pelton et al. 1993; Pelton 1999). We therefore explore a recent solution model for Cl in silica-rich melts (Dolejš 2007) that is based on Darken's quadratic formalism for a solute in a multicomponent solvent, extended from the hydrous haplogranitic melt model of Holland and Powell (2001). In the linearly independent set of end-member melt species, Cl is represented by NaCl. For application in the quinary system Qz-Or-Ab-H_2O–Cl_2O_{-1}, definition of the configurational properties of the Cl-bearing haplogranitic melt must allow for the substitution of Na and K on silicate and halide sites (Fig. 7.27). Activity coefficients for all melt end-members were obtained by differentiation of the excess

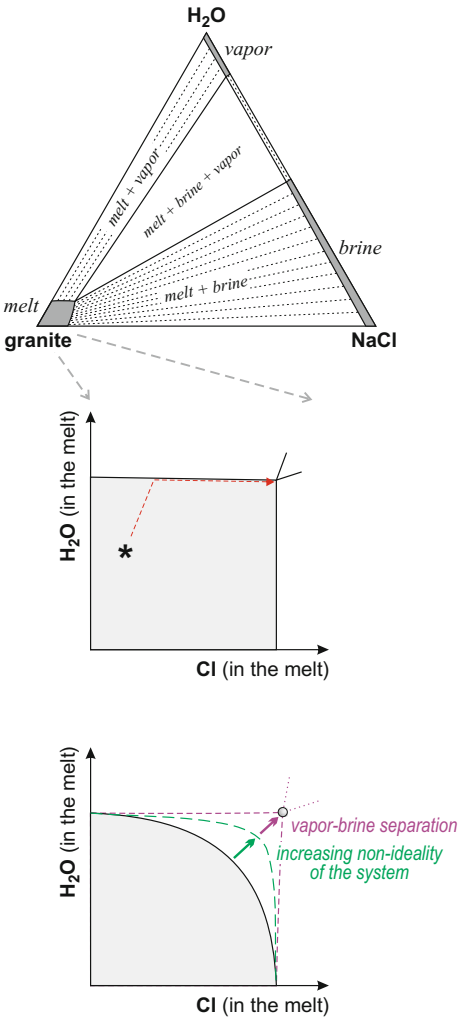

Fig. 7.26 Illustration of Cl and H_2O solubilities in silicate melts as part of the silicate–salt–H_2O ternary system

Gibbs energy. The thermodynamic properties of NaCl in the aluminosilicate framework were related to the molten-salt standard state via Darken's energetic increment:

$$\begin{aligned} I_{\mathrm{NaCl}}(\mathrm{J}) &= \Delta_{\mathrm{f}} G_{\mathrm{NaCl,silicate\,melt}} - \Delta_{\mathrm{f}} G_{\mathrm{NaCl,molten\,salt}} \\ &= 10850 + 31.126\,\mathrm{T\,(K)} - 1.333\,\mathrm{P(bar)}, \end{aligned} \tag{7.33}$$

which was calibrated by experimental data on Cl solubility in granitic melts at 800–1060 °C and 0.5–2 kbar (Webster 1992, 1997a; Fig. 7.28a). Interaction between

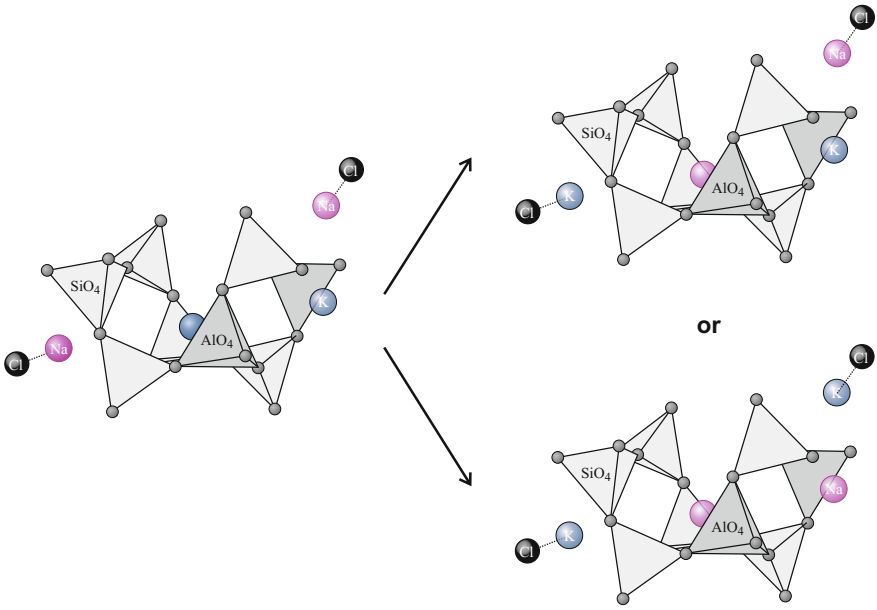

Fig. 7.27 Schematic illustration of Na and K exchange in the aluminosilicate melt structure. The two different configurations lead to additional configurational entropy contributions

NaCl and H_2O in the melt structure is described by the regular solution parameter as follows:

$$W_{\mathrm{NaCl-H2O}}(\mathrm{J}) = -53385 + 42.507\,T\,(\mathrm{K}) + 2.667P\,(\mathrm{bar}). \tag{7.34}$$

Properties of H_2O–NaCl–KCl fluids, including vapor-brine separation and Na–K partitioning, were described by the Kosinski–Anderko–Pitzer equation of state (Anderko and Pitzer 1993a, b; Kosinski and Anderko 2001). Phase equilibria in the SiO_2–Al_2O_3–Na_2O–K_2O–H_2O–Cl_2O_{-1} system were computed by Gibbs free energy minimization using linear simplex switching, followed by second-order, steepest descent refinement (De Capitani and Brown 1987; Powell et al. 1998). The computational results include the proportions and composition of all the phases in equilibrium. As a practical illustration, supraliquidus equilibria between a fluid-saturated granitic melt and saline fluid (or fluids) are illustrated in Fig. 7.28b. This projection allows for the rapid graphical estimation of the fluid salinity as a function of the H_2O and Cl concentrations of the parental magma.

The phase equilibrium computations further enable incremental calculation of proportions and compositions of coexisting solid, melt, and fluid phases and predict fluid saturation during equilibrium or fractional crystallization or decompression. Figure 7.29 illustrates phase equilibria for the haplogranite–H_2O–NaCl system at 800 °C. At 200 MPa, fluid forms a single supercritical phase ranging from 0 to 80 wt% NaCl + KCl (Fig. 7.29a). H_2O solubility in the melt decreases from 5.5 to

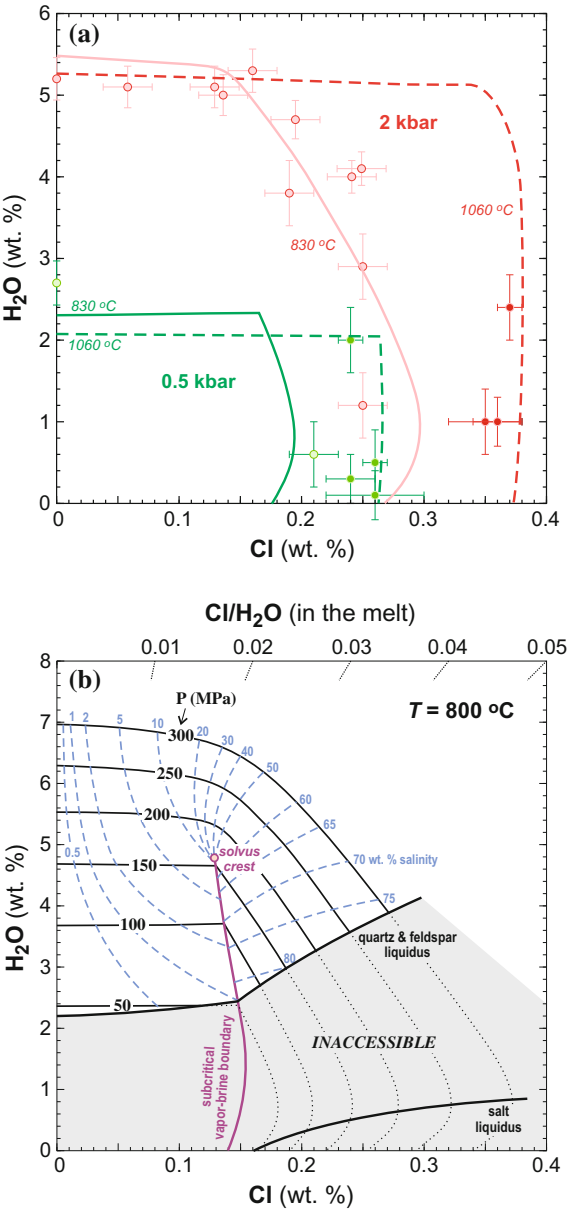

Fig. 7.28 **a** The solubilities of Cl and H_2O in granitic and rhyolitic melts at 830–1060 °C and 0.5–2.0 kbar. *Point symbols* indicate experimental data from Webster (1992, 1997a), whereas *solid* and *dashed curves* are calculated with the thermodynamic model. **b** Fluid saturation curves for haplogranitic melts at T = 800 °C and P = 50–300 MPa as a function of the H_2O and Cl concentration in the melt. *Blue dashed curves* indicate salinity of the exsolving fluid phase. In the gray region, the melt is unstable at 800 °C and would partially crystallize due to the low H_2O activity

3.2 wt% as the Cl concentration increases. Alkemade triangles imply existence of a temperature minimum where the tie-lines of the melt-fluid and melt-crystal assemblages become colinear (5.4 wt% H_2O and 0.13 wt% Cl in the melt). In the vicinity of the minimum, the tie-lines between coexisting melt and fluid show a strong curvature, which implies that very small changes in the melt Cl/H_2O ratio

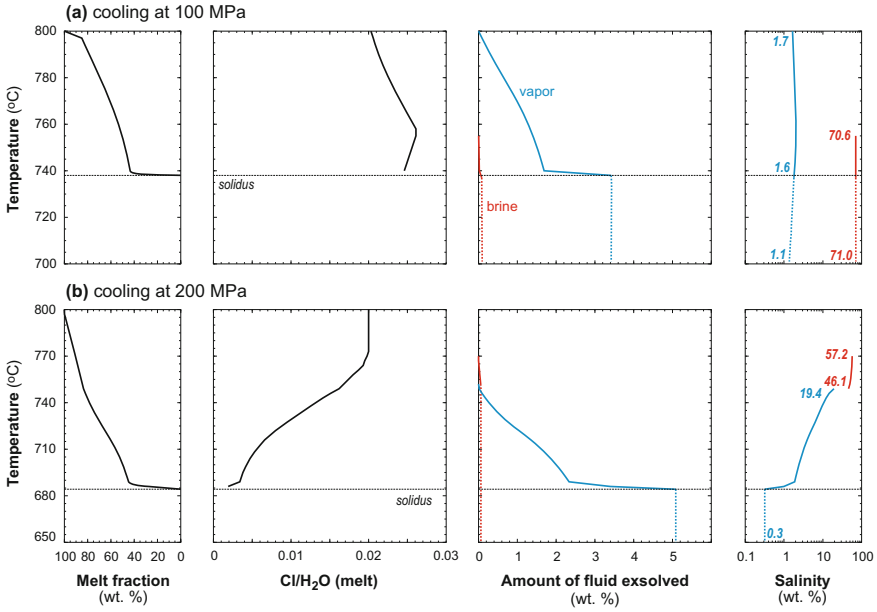

Fig. 7.29 Evolution of an alkali feldspar-saturated haplogranitic melt and its magmatic fluid phase(s) from 800 °C and **a** 100 MPa and **b** 200 MPa during isobar cooling. The initial melt composition is Cl/H_2O = 0.02 (by weight)

produce large variations in the fluid salinity. The partitioning coefficient for Cl is not a constant but decreases by two orders of magnitude as the melt Cl/H_2O ratio decreases. This is a consequence of the non-Henrian behavior of Cl (major constituent in the fluid phase). At 800 °C and 100 MPa, the H_2O–NaCl system is subcritical and consists of an aqueous vapor and a saline brine with salinities of 0–2 and 72–82 wt% NaCl + KCl, respectively (Fig. 7.29b). As a result, the thermal minimum becomes an invariant point where all the differentiation paths for Cl-bearing granitic melts terminate (Cl/H_2O = 0.037). As natural silicic melts display Cl/H_2O = 0.01–0.08 by mass, these magmas will saturate with two fluids consecutively. At the invariant point, the Cl and H_2O concentrations in the melt remain constant despite that the system continues to exsolve two fluid phases simultaneously. At this stage, composition of natural melt inclusions cannot provide information on the devolatilization progress and amounts of released fluids.

Fractional devolatilization during isothermal decompression and isobaric crystallization is illustrated using a haplogranitic minimum melt with 3 wt% H_2O and 300 ppm Cl (Fig. 7.30a). At 75 MPa (~3 km), saturation with low-salinity vapor occurs and the amount of vapor increases with magma crystalinity. At 47 MPa, the residual melt solidifies by the reaction: melt = crystals + brine. This scenario is applicable to the segregation of near-eutectic melts in highly evolved plutons. The saturation with brine at the solidus only allows for the incompatible enrichment of

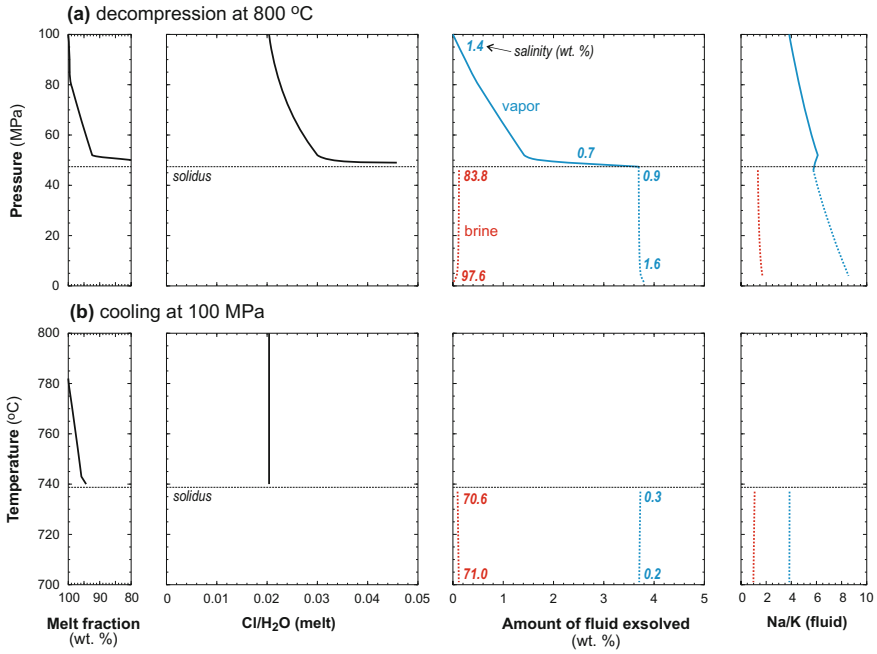

Fig. 7.30 Evolution of an minimum haplogranitic melt $Qz_{38}Ab_{33}Or_{29}$ (by weight) and its magmatic fluid phase(s) from 800 °C and 100 MPa at fluid saturation during **a** isothermal fractional decompression, and **b** isobaric cooling. The initial melt composition is $Cl/H_2O = 0.02$ (by weight)

the ore and minor elements in the residual melt. These elements are efficiently sequestered by the high-salinity brine upon solidification. In Fig. 7.30b, a feldspar-saturated melt with $Cl/H_2O = 0.04$ crystallizes isobarically at 100 MPa. Over a temperature interval of 65 °C, the magma simultaneously exsolves an aqueous vapor and a saline brine. The fluid compositions are dictated by the H_2O–NaCl + KCl solvus. At the solidus, the amounts of exsolved fluids proportionally increase but their salinities do not change. This case is applicable to crystallizing plutons after final emplacement. Early saturation with brine may sequester metals and trace elements before their enrichment in the residual melt. Such geological settings are likely to remain poorly mineralized or barren.

The thermodynamic model for Cl-bearing hydrous haplogranitic systems demonstrates that (i) experimental data require only minor deviations from mixing of halide and aqueous components in the melt, i.e., the trends of Cl and H_2O solubilities can be explained by non-ideal activity-composition relationships in the aqueous fluid; (ii) natural silicic magmas with $Cl/H_2O < 0.04$ first saturate with dilute aqueous vapor and subsequently exsolve concentrated brines at the solidus; (iii) the "vapor-then-brine" mechanism of exsolution promotes enrichment of incompatible and ore elements in the residual melts and their efficient removal by

late-stage brines; this is an important prerequisite for the formation of economic mineralization; and (iv) simultaneous exsolution of two fluids invariantly buffers the melt composition. Therefore, at this stage, the composition of melt inclusions becomes invariant despite the progressive release of fluids.

7.5 Speciation, Solubility and Partitioning of Elements Between Halogen-Bearing Melts and Fluids

7.5.1 Fluorine-Bearing Systems

7.5.1.1 Speciation and Solubility of Trace Elements in F-Bearing Silicate Melts

Fluorine-rich rocks are frequently highly evolved and enriched in incompatible constituents including large-ion lithophile, high-field strength and rare-earth elements (e.g., Linnen and Cuney 2005; Linnen et al. 2012). In addition, some element pairs, such as Nb–Ta, Zr–Hf, or the lanthanides, show departures from universal, chondritic ratios (e.g., Veksler et al. 2012). These departures are controlled by the competing effects of F on speciation of trace elements in the melt structure, and the saturation limits of accessory minerals (e.g., zircon, hafnon, columbite, and tantalite) or Fe and Ti oxides (e.g., magnetite, ilmenite, rutile), which selectively partition the high-field strength elements.

Halogens play a significant role in the speciation and transport of metal cations (Keppler and Wyllie 1991; Linnen 1998; Linnen and Cuney 2005). Their behavior and mobility, during late-magmatic hydrothermal processes, depends on the local chemical environment. In peralkaline systems, the high-field strength elements are highly soluble, which promotes their late crystallization at low temperatures (e.g., Linnen and Keppler 1997) as well as their transport in alkaline fluids, e.g., fenitizing aqueous fluids. By contrast, in peraluminous and silica-saturated systems, the behavior of high-field strength elements is moderated by crystallization of Ti-bearing minerals or may reach saturation in columbite or tantalite during late pegmatitic evolution. As the associated hydrothermal systems are more acidic, the high-field strength elements remain useful, immobile, geochemical tracers except in the case of very F-rich environments.

Incorporation mechanisms in silicate melts and glasses. Zirconium in silicate glasses is present in the form of tetravalent $Zr^{4+}O_6$, $Zr^{4+}O_7$ and $Zr^{4+}O_8$ moieties. There is no clear evidence for Zr–F or Zr–Cl complexing in alkali silicate and aluminosilicate glasses (Farges et al. 1991). The local Zr environment is more affected by bonding requirements than by the network topology. In F-bearing albitic melts, the number of O ligands around Zr decreases, from ZrO_8 to ZrO_6 while promoting saturation with zircon (Farges and Calas 1991). In addition, the halogens have an indirect, opposite depolymerizing effect and tend to stabilize the $Zr^{4+}O_6$

moieties in the melt, resulting in an increase in the compatibility of Zr in the melt (Farges et al. 1991).

Niobium is present in hydrous, F-bearing glasses as $Nb^{5+}O_6$ moieties, which are corner-shared by aluminosilicate tetrahedra through a non-bridging O apex (Piilonen et al. 2005, 2006). In peraluminous granitic glasses, the presence of F leads to a more distorted environment around the Nb atom, consistent with an increase in the non-bridging O atoms due to depolymerization of the melt structure by F (Piilonen et al. 2006). In peralkaline granitic glasses, the halogen effect is reversed and the NbO_6 environment becomes more ordered, which may be related to the charge-balancing role of excess alkalies for Nb^{5+}.

Molybdenum occurs in anhydrous silicate glasses of variable composition as molybdate $Mo^{6+}O_4$ moieties (Farges et al. 2006a). Under reducing conditions (approximately one log unit below the Fe-wustite buffer), its valence decreases to the 5+ and 4+ state. Therefore, Mo^{6+} is the dominant valence state in magmatic environments. Fluorine and Cl have no detectable effect on the valence state of Mo in the silicate glass, no preferential ordering between Mo and halogens, but impart a distinct radially distorted coordination environment documented by EXAFS spectroscopy (Farges et al. 2006b).

No evidence for direct complexation of Zr, Th, Sn, U, Nb, and Mo by F has been documented by spectroscopic methods (Farges et al. 1991, 1992; Farges and Rossano 2000; Piilonen et al. 2005, 2006; Farges et al. 2006a, b, c). However, structural depolymerization, induced by the presence of halogens and an increase in the number of non-bridging O atoms, probably plays a key role in stabilizing the high-field strength elements in the melt structure.

Solubility of accessory minerals in F-bearing melts. Despite the stoichiometric simplicity of many accessory minerals (e.g., $ZrSiO_4$, $MnNb_2O_6$), their cations frequently occur in distinct coordination environments in silicate melts. As a consequence, solubility and saturation of these minerals is controlled by activities of two or more chemical components independently, for instance:

$$ZrSiO_4\,(\text{zircon}) = ZrO_2\,(\text{melt}) + SiO_2\,(\text{melt}) \tag{7.35}$$

or

$$MnNb_2O_6\,(\text{columbite}) = MnO\,(\text{melt}) + Nb_2O_5\,(\text{melt}), \tag{7.36}$$

where the equilibrium constant corresponding to Eq. (7.41) will have the following form:

$$K = \frac{a^{melt}_{MnO} \cdot a^{melt}_{Nb_2O_5}}{a^{columbite}_{MnNb_2O_6}} = \frac{X^{melt}_{MnO} \cdot \gamma^{melt}_{MnO} \cdot X^{textmelt}_{Nb_2O_5} \cdot \gamma^{melt}_{Nb_2O_5}}{a^{columbite}_{MnNb_2O_6}}. \tag{7.37}$$

The activity coefficients of the melt components, γ, become a function of the melt composition (e.g., alumina saturation index) or the concentration of volatiles including halogens.

Solubilities of various accessory or economic minerals have been experimentally investigated in anhydrous and hydrous silicate melts with variable amounts of F (e.g., Keppler 1993; Linnen 1998; Maar et al. 1998; Bhalla et al. 2005; Bartels et al. 2010; Van Lichtervelde et al. 2010; Fiege et al. 2011; Dong Che et al. 2013), and these results were summarized by Linnen et al. (2014) and Aseri et al. (2015). In general, melt alkalinity or aluminosity, temperature, and oxygen fugacity, where appropriate, are the principal factors governing the solubility of high-field strength-bearing minerals. The effects of F's presence in the melt were found to be subordinate (e.g., Aseri et al. 2015).

The solubilities of zircon and hafnon [(Zr,Hf)SiO_4] in volatile-bearing silicic melts remain unclear. Keppler (1993) determined increasing solubility of zircon with the increasing F abundances, whereas Baker et al. (2002) and Van Lichtervelde et al. (2010) did not detect any substantial effects. Recent experimental results by Aseri et al. (2015) demonstrate increasing solubilities of zircon and hafnon up to 8 wt% F in a fluid-saturated subaluminous granitic melt. This trend may be explained by Zr–F complexing in the melt structure (cf., Farges et al. 1991; Farges 1996), or by F-induced depolymerization and availability of non-bridging O atoms for the formation of ZrO_x and HfO_y moieties. In an experimental study with peralkaline silica-undersaturated melts, Marr et al. (1998) documented experimentally that the presence of F in the melt decreases the solubility of zircon and promotes the crystallization of baddeleyite over wadeite [$K_2CaZr(SiO_3)_4$].

Fluorine has a negligible effect on the solubility of the wolframite end-members, ferberite [$FeWO_4$] and hubnerite [$MnWO_4$], in evolved granitic melts at 800 °C and 200 MPa (Dong Che et al. 2013), and no conclusive effect on the solubility of cassiterite in granitic melts, although under highly oxidizing conditions a positive correlation may be expected (Bhalla et al. 2005).

Relative solubilities of columbite and tantalite strongly depend on melt composition (Linnen and Keppler 1997). Keppler (1993) reported increasing columbite and tantalite solubilities with increasing F contents in the melt in contrast to Fiege et al. (2011) and Aseri et al. (2015) who observed no halogen effect. These more recent observations are consistent with the presence of F-free tantaloaluminosilicate moieties in the melt structure as proposed by Van Lichtervelde et al. (2010) and Mayanovic et al. (2013). In addition, Nb and Ta are highly compatible in Li fluoromicas as opposed to a Li–F-rich rhyolite melt, with $D_{Nb}^{mica/melt} = 2.7-5.8$ and $D_{Ta}^{mica/melt} = 0.4-2.9$ (Kovalenko et al. 1977; Raimbault and Burnol 1998). Both elements, however, remain largely incompatible (D $\sim$ 0.02–0.09) during crystal fractionation owing to a very small fraction of mica in the crystallizing assemblage. Protracted fractionation of a mica-bearing assemblage may be responsible for the decrease of Nb/Ta ratios found in evolved peraluminous granites (Raimbault and Burnol 1998).

The absence of spectroscopic evidence and experimental observations on mineral solubilities indicate that no significant complexing between F and high-field strength elements occurs in aluminosilicate melts under magmatic conditions. Zircon and hafnon, the only silicates in the preceding discussion, show a positive

correlation between solubility and increasing F contents in the melt (Aseri et al. 2015). Fluorine tends to increase the activity of silica through preferential ordering of alkalies and Al in the melt structure (Schaller et al. 1992; Zeng and Stebbins 2000; Mysen et al. 2004). Hence increasing F concentrations are expected to indirectly promote zircon saturation and decrease its solubility. The predicted increase in the silica activity is, however, an indirect consequence of increasing the activity of bridging O atoms. In zircon and hafnon, all O atoms are non-bridging, which explains the opposite effect of F on their solubility in F-bearing melts. This consideration also explains why non-silicate melts, bonded by "free" O atoms, remain relatively insensitive to structural effects in the melt induced by the addition of F.

7.5.1.2 Element Partitioning Between Silicate and Fluoride Melts

Highly evolved granitic rocks are frequently characterized by: (i) extreme enrichment of some trace elements, including high-field strength and/or REE; (ii) variable proportions of light versus heavy REE and the presence of the tetrad distribution pattern; and (iii) decoupling of geochemically similar elements such as Y–Ho, Zr–Hf, or Nb–Ta (Peretyazhko and Savina 2010; Veksler et al. 2012; Vasyukova and Williams-Jones 2014). The formation of the tetrad effect has been attributed to partitioning between the silicate melt and an aqueous fluid (Irber 1999; Monecke et al. 2002), the stability of fluoride complexes in aqueous fluids (Bau 1996), or the partitioning between immiscible silicate and fluoride melts (Veksler et al. 2005, 2012). These irregularities cannot be consistently explained by extended fractionation of rock-forming minerals, but may have resulted from the following processes: (i) fractionation of exotic solid phases (e.g., fluoride minerals); (ii) partitioning from the silicate melt to aqueous fluid; (iii) percolation of aqueous fluids; (iv) partitioning between silicate and fluoride melts; and (v) subsolidus hydrothermal alteration (Peretyazhko and Savina 2010; Veksler et al. 2012).

Partitioning of trace elements between silicate and fluoride melts was experimentally investigated in anhydrous and hydrous F-bearing systems by Gramenitskiy and Shekina (2002) and Veksler et al. (2005, 2012) (Fig. 7.31). At T = 700–950 °C and P < 100 MPa, the partition coefficients for elements between fluoride and silicate melts range from 0.009 to 500 (Gramenitskiy et al. 2005; Veksler et al. 2012). Partitioning of alkalies to a fluoride melt sharply increases with decreasing ionic radius from $D_{\mathrm{Cs}}^{\mathrm{fl/sil}} = 0.04{-}0.07$ to $D_{\mathrm{Li}}^{\mathrm{fl/sil}} = 10{-}24$. Alkali earths are compatible in the fluoride melt, with $D^{\mathrm{fl/sil}} > 18$, reaching a maximum at $D_{\mathrm{Ca,Mg}}^{\mathrm{fl/sil}} = 69{-}94$. Despite the refractory nature of fluorite, this indicates that Ca and Mg are preferentially sequestered from the silicate melt to form a Ca- and Mg-rich fluoride melt. The partition coefficients of tetravalent, high-field strength elements sharply decrease with decreasing ionic radius, from $D_{\mathrm{Th}}^{\mathrm{fl/sil}} = 49$ to $D_{\mathrm{Sn}}^{\mathrm{fl/sil}} = 0.07$. The same quantitative trend is observed for Nb and Ta, with $D_{\mathrm{Nb}}^{\mathrm{fl/sil}} = 3.7 - 0.08$

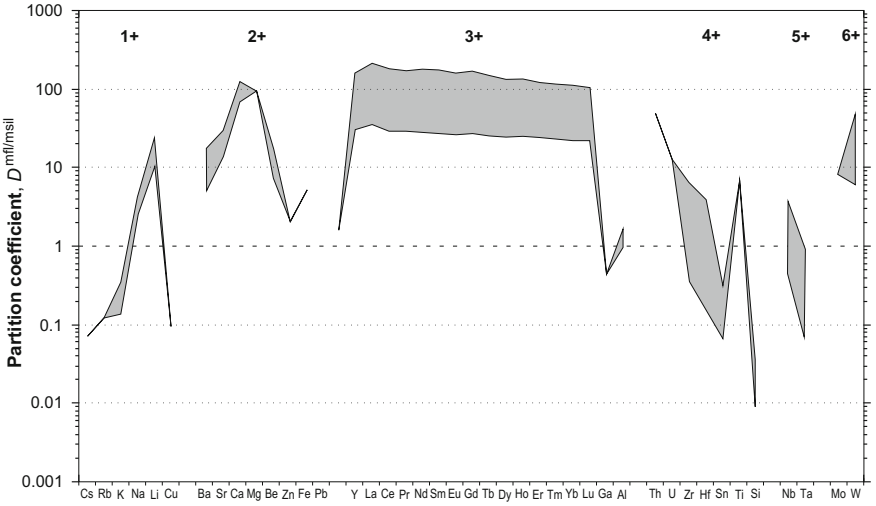

Fig. 7.31 Element partition coefficients between immiscible fluoride and silicate melts (Veksler et al. 2012)

and $D_{Ta}^{fl/sil} = 0.9 - 0.02$, whereas Mo and W are compatible in the fluoride melt ($D_{Mo,W}^{fl/sil} = 8.4 - 48$). It is noteworthy that the partition coefficients of conventional chemical pairs, i.e., ions with identical charge and a very similar radius (Th–U, Zr–Hf, Nb–Ta, Mo–W) are remarkably different. As a consequence, the fluoride-silicate liquid immiscibility is expected to decouple these pairs and produce significant departures from chondritic ratios (Veskler et al. 2012).

The partition coefficients of the REE are very high, $D_{REE}^{fl/sil} = 85 - 500$, though generally 100–200 (Fig. 7.31). Individual D_{REE} decrease with decreasing ionic radius, that is, light rare earths (LREE) are prefentially partitioned to the fluoride melt, whereas the silicate melt is enriched in heavy rare earths (HREE) (Veksler et al. 2012). The partial reduction of Eu^{3+} to Eu^{2+} appears to be responsible for a weak negative Eu anomaly observed in fluoride melts. Subtle periodic differences in partition coefficients for individual REE lead to the formation of the tetrad effect (cf., Bau 1996; Irber 1999; Monecke et al. 2002; Veksler et al. 2005, 2012; Badanina et al. 2006). The tetrad effect in the REE distribution is due to variations in the configuration of the 4f electron shell (Fidelis and Siekierski 1966; Peppard et al. 1969). As a result, the sequence of REE is subdivided into four tetrads: La–Nd, Pm–Gd, Gd–Ho and Er–Lu. However, the second tetrad is obscured by the absence of a stable Pm nuclide and by the distinct geochemical behavior of Eu^{2+}. The anomalous behavior of Ce^{4+} under highly oxidizing conditions may affect the pattern and limit the interpretation of the first tetrad as well. The most characteristic examples of the REE tetrad patterns are documented from highly evolved Li- and F-rich granites, rhyolites, and associated greisens (Bau 1996; Irber 1999; Monecke et al. 2002; Peretyazhko and Savina 2010).

7.5.1.3 Element Partitioning Between Silicate Melts and Aqueous Fluids

Phase equilibrium studies in the fluoride-H_2O binary systems indicate that NaF, Na_3AlF_6, and CaF_2, excluding KF, are characterized by a discontinuous vapor-pressure curve at low pressures and exhibit a discrete solidus of hydrous fluoride melt and a stable coexistence of the latter with dilute F-bearing aqueous fluid (Koster van Groos and Wyllie 1968; Valyashko and Urusova 2003; Dolejš and Baker 2007b). This effect may be further promoted by isobaric retrograde solubility of ionic salts, which decreases fluoride solubility in aqueous fluid with increasing temperature as documented for the systems NaF–H_2O and CaF_2–H_2O (Dolejš and Manning 2010). As a consequence, fluoride–H_2O systems are not characterized by a continuous transition from hydrous fluoride melts to dilute aqueous fluids, since these two are immiscible and the former crystallize at a fluid-saturated solidus. In the following text we concentrate on element partitioning between F-bearing silicate melts and aqueous fluids, pertaining to systems where the F abundance in the melt is insufficient to reach saturation in a hydrous fluoride melt or such a melt is no longer stable at the temperature of interest.

Fluorine. Experimental studies of element partitioning between F-bearing melts and aqueous fluids have concentrated on F behavior in peraluminous to peralkaline granitic or rhyolitic systems at T = 650–1000 °C and P = 1–4 kbar (Webster 1990; Webster and Holloway 1990; Kravchuk and Slutskii 2001; Kravchuk et al. 2004; Borodulin et al. 2009) and have been summarized by Carroll and Webster (1994) and Baker and Alletti (2012). The partition coefficient for F between hydrous silicic melt and aqueous fluid is largely independent of temperature and pressure, but varies as a function of the alumina saturation index and F concentration in the melt (e.g., Webster 1990; Borodulin et al. 2009; Fig. 7.32). In weakly peraluminous systems, it broadly follows Henry's law up to 4.5 wt% F in the melt, with $D_F^{fl/m} = 0.3-0.7$. Above 4.5 wt% F in the melt, the partition coefficient rises sharply and exceeds unity at ~6.5 wt% F in the melt (Fig. 7.32).

Major elements. In the absence of experimental data on major- or trace-element partitioning into F-bearing aqueous fluids, the speciation of F in hydrothermal solutions remains largely controversial (e.g., Icenhower and London 1997). Initial studies of mineral stabilities using various F buffers, OH–F fluid-mineral partitioning, and thermodynamic calculations identified HF^0 as the predominant fluoride species (Muñoz and Ludington 1974; Jackson and Helgeson 1985; Zhu and Sverjensky 1991, 1992; Halter et al. 1998). On the other hand, mineral solubility measurements have revealed the presence of silicohydroxyfluoride and aluminosilicofluoride complexes (Haselton et al. 1988; Aksyuk and Zhukovskaya 1998; Dolejš 2006; cf., Webster 1990). In addition, partitioning experiments in the system albite–F_2O_{-1}–H_2O have produced SiO_2-rich and F-poor fluids (10.0 wt% SiO_2, 2.8 wt% Al_2O_3, 2.1 wt% Na_2O, 1.8 wt% F), coexisting with a hydrous albitic melt with 4 wt% F at 800 °C and 100 MPa (Dolejš 2004), which do not cause alkali-alumina decoupling or F depletion in the melt ($D_F^{fl/melt} = 0.43$). Findings

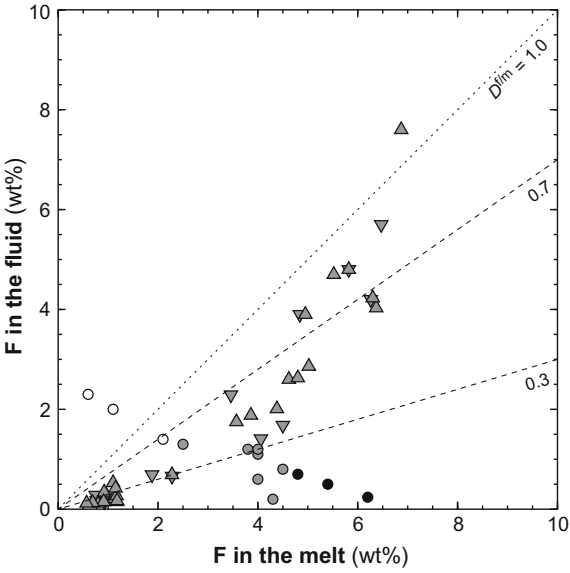

Fig. 7.32 Experimental concentrations of F in coexisting silicate melts and aqueous fluids. Symbols: *gray upright triangles*—800–1000 °C, 200–500 MPa; Webster (1990); *gray inverted triangles*—800 °C, 200 MPa, Webster and Holloway (1990); *open circles*—peralkaline granites, 650–850 °C, 100 MPa, Borodulin et al. (2009); *gray circles*—weakly peraluminous granites, 650–850 °C, 100 MPa, Borodulin et al. (2009); *closed circles*—strongly peraluminous granites, 650–850 °C, 100 MPa, Borodulin et al. (2009)

from SiO_2-rich fluid inclusions in greisens (Williamson et al. 1997) and quartz topazites (Eadington and Nashar 1978) also suggest the presence of Si ± F-rich solutes or silicothermal gels (Wilkinson et al. 1996, Williamson et al. 2002; Thomas and Davidson 2012).

The solubility of aluminosilicates in high-temperature aqueous fluids is very low at crustal pressures (Luth and Tuttle 1969; Frantz et al. 1981; Walther 1986; Woodland and Walther 1987; Eugster and Baumgartner 1987; Paillat et al. 1992; Manning 1994), but it rapidly increases with increasing F contents (Webster 1990) due to the formation of aqueous fluoride complexes. The fluid-melt partitioning here has two petrogenetic implications:

1. Selective loss of elements during aqueous devolatilization. This relates to the role of alkali loss in the formation of quartz topazites or the formation of solute-rich fluid inclusions (silicothermal gels) observed in greisens (Williamson et al. 1997, 2002).
2. Progressive closure, with increasing F contents, of the melt-fluid miscibility gap, potentially leading to the supercritical transition from hydrous silicate melts to fluorosilicate aqueous fluids.

Owing to the increasing knowledge of fluid-melt partitioning in F-bearing aluminosilicate systems (Dingwell 1985; Haselton et al. 1988; Webster 1990), and the stability of aluminofluoride and silicofluoride aqueous species (Aksyuk and Zhukovskaya 1998; Tagirov and Schott 2001; Tagirov et al. 2002), we can use thermodynamic modeling to calculate solute contents and speciation in aqueous fluids buffered by the cotectic assemblage quartz, albite, K-feldspar, and topaz. These calculations are in good agreement with the total solute contents

experimentally determined by Webster (1990) and provide important constraints on the compositional changes of fluid-saturated residual melts.

The six-component system K_2O–Na_2O–Al_2O_3–SiO_2–F_2O_{-1}–H_2O contains five model phases: quartz, albite (solid solution), K-feldspar (solid solution), topaz, and aqueous fluid. Alkali feldspars are considered to be non-ideal solid solutions (Fuhrman and Lindsley 1988; Wen and Nekvasil 1994). At the pressure and temperature of interest, the remaining degree of freedom is the chemical potential of F_2O_{-1}. Its range is, however, bracketed by the occurrence of another silicate phase (lower limit) or a second fluoride phase (upper limit). For the F-bearing haplogranite system at 600 °C and 100 MPa, these additional limiting phases are sodium disilicate and cryolite, respectively (Dolejš and Baker 2004). In the presence of six phases, the chemical potentials of the six components are determined and charge-balance constraints define $\mu(H^+)$. The chemical potentials, and hence the activities and molalities of any aqueous species, are calculated as follows, for instance:

$$SiO_2 + 2\,H_2O = Si(OH)_4^0, \tag{7.38}$$

$$Na_2O + Al_2O_3 + 4\,H_2O = 2\,NaAl(OH)_4^0, \tag{7.39}$$

$$Al_2O_3 + H_2O + 2\,F_2O_{-1} = 2\,AlOHF_2^0, \tag{7.40}$$

$$Al_2O_3 + 2\,H_2O + 2\,F_2O_{-1} = 2\,Al(OH)_2F_2^- + 2\,H^+. \tag{7.41}$$

Thermodynamic data for aqueous species were retrieved from Ryzhenko et al. (1985), Shock and Helgeson (1988), Shock et al. (1989), Johnson et al. (1992), and Tagirov and Schott (2001). They are based on the Helgeson–Kirkham–Flowers model for aqueous electrolytes at high temperatures and pressures (Helgeson et al. 1981; Tanger and Helgeson 1988; Shock et al. 1992). Activity coefficients for ionic and neutral species were calculated using the extended Debye-Hückel equation, with a temperature-independent extended term of 0.03 (Walther 2001). The H_2O activity was corrected for the solute content and osmotic coefficient (Helgeson et al. 1981; Tanger and Helgeson 1988). The speciation calculation was iteratively repeated to simultaneously satisfy chemical-potential and charge-balance constraints. The results are presented in Fig. 7.33.

Neutral complexes $Si(OH)_2F_2^0$ and HF^0 are the dominant aqueous species. As $\mu(F_2O_{-1})$ decreases, their concentrations decrease and become comparable to that of aqueous silica for SiO_2 at ~0.3 wt% F (Fig. 7.33a). Alkalis and Al are transported as fluoride and hydroxyfluorides complexes (cf., Tagirov and Schott 2001; Tagirov et al. 2002), but the concentrations of alkali aluminate species are very low (10^{-5}–10^{-3} molal). The concentrations of K-bearing species are one to two orders of magnitude lower than those of Na-bearing species. This incongruent partitioning and the high Na/K ratio in the aqueous fluid (~13–17) are characteristic of halide and carbonate aqueous systems (e.g., Webster and Holloway 1988; Shinohara 1994;

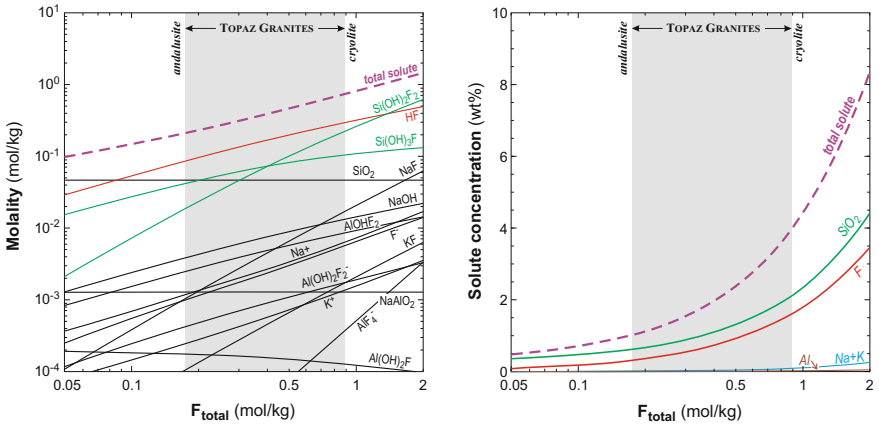

Fig. 7.33 Calculated compositions of aqueous fluids coexisting with a quartz–K-feldspar–albite–topaz assemblage at 600 °C and 100 MPa. The range of F concentrations is bracketed by the lowest and the highest value of $\mu(F_2O_{-1})$ at the andalusite and the cryolite buffer, respectively. **a** Molal concentrations of individual species. **b** Total concentrations of individual elements. Concentrations of Al_2O_3 are smaller than those of $(Na,K)_2O$

Student and Bodnar 1999; Frank et al. 2003). The total [Na + K]/Al ratio is close to unity at very low F concentrations but increases to ~3 in the F-rich fluids.

The total element concentrations in wt% are recalculated in Fig. 7.33b. The total solute content varies from 2 wt% at the quartz–alkali feldspar–topaz–andalusite buffer to 20 wt% at the quartz–alkali feldspar–topaz–cryolite buffer and the total dissolved F concentration increases from 0.7 to 7 wt%. These results and element proportions are in good agreement with experimental determinations by Dingwell (1985) and Webster (1990). Since the total alkali and Al budgets transported by the fluid are very small (Fig. 7.33b), the variations in the [Na + K]/Al ratio are unimportant and the F-rich fluids are unlikely to affect the melt alumina saturation index. The pH is independent of the F concentration, and its value (7.0–7.1) is approximately half an order of magnitude above neutral conditions at 600 °C and 100 MPa (Marshall and Franck 1981). Due to significant SiO_2 and F enrichment in the fluid phase, the aqueous devolatilization of highly evolved granitic and rhyolitic melts may lead to their SiO_2- and F-depletion at very high F contents. This trend is suggested by the increasing value of the partition coefficient, $D_F^{f/m}$, as the F content in the system increases (Webster 1990; Webster and Holloway 1990; Fig. 7.32). Consequently, late-stage fluids may sequester a significant portion of the F from the residual melts, which becomes recorded as solute-rich inclusions (e.g., silicothermal gels; Williamson et al. 1997, 2002; Thomas and Davidson 2012). In view of these observations, HF^o appears to represent a subordinate species in both aqueous and hydrous silicate-melt systems (Kohn et al. 1991; Schaller et al. 1992; Dolejš 2006, 2014). Therefore, applications of OH–F partitioning between biotite or apatite, silicate melt, and/or aqueous fluid may underestimate the total F concentrations by

several orders of magnitude (Förster and Tischendorf 1989; Sallet 2000; cf., Icenhower and London 1997; London 1997).

Trace elements. Partitioning of trace elements between hydrous silicate melt and F-bearing aqueous fluid was evaluated in several experimental studies up to 800 °C and 4 kbar (Keppler and Wyllie 1991; Bai and Koster van Gross 1999). Copper shows no preferential partitioning between hydrous granitic melts and F-bearing aqueous fluid, $D_{Cu}^{f/m} = 1.0-5.4$, unlike in Cl-bearing systems (Candela and Holland 1984; Keppler and Wyllie 1991; Bai and Koster van Groos 1999). The effect of F on the Sn partitioning to the fluid phase has remained inconclusive (Keppler and Wyllie 1991), although the experimental data on cassiterite solubility suggested a positive correlation with the HF concentration (Eugster 1986; Barsukov et al. 1987). Over a wide range of the HF concentrations, Sn remains strongly melt-compatible, with $D_{Sn}^{f/m} = 0.004-0.020$ (Keppler and Wyllie 1991). Tungsten partitions preferentially to the aqueous fluid in the absence of halide ligands, $D_{W}^{f/m} = 2.8-4.1$, but becomes less soluble in the fluid with increasing HF or NaF concentrations, with $D_{W}^{f/m} = 0.4-1.0$ (Keppler and Wyllie 1991; Bai and Koster van Groos 1999). This is probably due to the destabilization of the neutral aqueous tungstate complex (H_2WO_4) as the pH of the fluid changes with the rising HF concentration. The behavior of Mo is very similar to that of W, with its strongest compatibility in a halogen-free fluid, $D_{Mo}^{f/m} = 3.9-7.2$, but it decreases and remains constant at 1–2 molal fluoride concentration, $D_{Mo}^{f/m} = 0.3-2.4$ (Keppler and Wyllie 1991; Bai and Koster van Groos 1999). Uranium is very insoluble in a halogen-free aqueous fluid, $D_{U}^{f/m} < 0.002$, but the partition coefficient rises with the square root of the HF concentration in the fluid ($D_{U}^{f/m} = 0.45$ at 4 molal hydrogen fluoride), consistent with the presence of neutral aqueous UO_2F_2. The partitioning of Th is quantitatively similar to that of U, with $D_{U}^{f/m} = 0.003$ in the halogen-free fluid and $D_{U}^{f/m} \leq 0.39$ at elevated contents of hydrogen fluoride (Keppler and Wyllie 1991). The partitioning behavior of Zr remains unconstrained, but recent experimental data on the solubility of baddeleyite in F-bearing aqueous fluids support the existence of zirconohydroxyfluoride complexes $ZrF(OH)_3$ and $ZrF_2(OH)_2$ up to 400 °C and 700 bar (Migdisov et al. 2011). Complexing between Nb or Ta and F was demonstrated, using Ta(V) oxide and columbite solubilities, in F-bearing fluids at 300–550 °C by Zaraisky et al. (2010). At magmatic conditions, and in F-bearing granitic systems, $D_{Nb}^{f/m} < 0.1$ and $D_{Ta}^{f/m} < 0.08$ (London et al. 1988; Chevychelov et al. 2005). In an initial study, Bai and Koster van Groos (1999) did not observe any effect of F on the partitioning of La and Ce between a silicate melt and an aqueous fluid, $D_{La,Ce}^{f/m} = 0.01-0.03$.

These results are in general agreement with qualitative prediction by the Pearson's acid-base theory (Wood and Samson 1998). Fluorine represents a very hard ligand, which is preferentially bonded to comparably hard cations such as

Th, U, and REE (Wood and Samson 1998; Migdisov et al. 2009, 2011; Linnen et al. 2014; Tsay et al. 2014). The efficiency of the F ligand in hydrothermal sequestration and transport, however, still remains incompletely unconstrained. This is due to the fact that (i) very few direct and reliable experimental data exist on speciation and complex stability in aqueous fluids (e.g., Migdisov et al. 2009, 2011), and (ii) that the stability of fluoride complexes is clearly a function of F speciation in the fluid. Some of the differences encountered in previous studies are due to the use of different fluoride additives, HF versus NaF, and the ensuing compositional shifts including peralkaline versus peraluminous melt compositions (cf., Keppler and Wyllie 1991; Bai and Koster van Groos 1999). Furthermore, the presence of F strongly increases the amount of aluminosilicate solutes, which may provide sites for incorporation and substantially increase the solubility of high-field strength elements (e.g., Antignano and Manning 2008; Hayden and Manning 2011).

7.5.2 Partitioning and Speciation in Chloride-Bearing Systems

As Cl is one of the most important constituents of magmatic and hydrothermal fluids for metal complexation, we first consider the physical-chemical controls on the fluid/melt partition coefficient of Cl, its speciation in magmatic fluids, and the effect it exerts on ore metal extraction from magmas.

7.5.2.1 Partitioning of Cl Between Silicate Melts and Magmatic Fluids

Starting from the pioneering studies of Holland (1972) and Kilinc and Burnham (1972), many researchers have investigated the partitioning of Cl between silicate melts and exsolving aqueous magmatic fluids, mainly due to the significance of Cl in the extraction of ore metals from magmas. Despite abundant experimental work defining the effect of various physical-chemical parameters on $D_{\mathrm{Cl}}^{\mathrm{f/m}}$, no forward thermodynamic model has yet been constructed that is capable of predicting $D_{\mathrm{Cl}}^{\mathrm{f/m}}$ in pressure–temperature–composition (*P*–*T*–*X*) space.

The following basic mass action expression describing the partitioning of Cl between silicate melts and aqueous fluids can be envisaged as:

$$\mathrm{MCl}_x(\mathrm{m}) = \mathrm{MCl}_x(\mathrm{f}), \tag{7.42}$$

where M stands for metal or hydrogen with a valence state of x. Basically, Cl is present as either HCl or a metal-chloride species in both the silicate melt and the aqueous fluid phase. The proportion of various chloride species dissolved in the

melt and the fluid is likely not identical, and it is dominantly controlled by the following type of exchange reactions:

$$\mathrm{M(I)O_{x/2}\,(m) + x/yM(II)Cl_y\,(f) = M(I)Cl_x(f) + x/yM(II)O_{y/2}(m).} \qquad (7.43)$$

There is a large amount of experimental data to constrain the equilibrium constants for Eq. (7.48) for various M(I)–M(II) pairs. These will be discussed in details in Sect. 7.5.2.2.

Thermodynamic modeling of the aqueous fluid/silicate melt partitioning of Cl is rather challenging for the following reasons: (i) Cl may be present in the form of various metal chloride and HCl species in the magmatic volatile phase (MVP; Gammon et al. 1969; Holland 1972; Williams et al. 1997; Shinohara 2009) and likely in the silicate melt as well (Sandland et al. 2004); (ii) metal-chlorides in particular display non-ideal behavior in aqueous fluids with complex activity-composition relationships (Anderko and Pitzer 1993a, b; Shinohara 1994; Driesner 2007; Driesner and Heinrich 2007; Aranovich and Newton 1996, 1997); (iii) metal chloride–H_2O systems exhibit liquid (brine)-vapor immiscibility in a large fraction of the typical *P–T–X* regime of upper crustal magma reservoirs (Bodnar et al. 1985; Driesner and Heinrich 2007; Liebscher and Heinrich 2007); (iv) the presence of molecular gas species with low dipole moments increases the activity coefficients of dissolved metal chloride species, and therefore affects $D_{Cl}^{f/m}$ as well as the miscibility gap between liquid and vapor (e.g., Frantz et al. 1992; Joyce and Holloway 1993; Gibert et al. 1998a; Schmidt and Bodnar 2000; Shmulovich and Graham 2004; Liebscher and Heinrich 2007); (v) metal chlorides in aqueous fluids have negative partial molar volumes, which may depend on the fluid density and composition, therefore the prediction of volume change associated with Cl transfer from the silicate melt to the fluid phase is challenging, yet necessary to model the rather pronounced pressure dependence of $D_{Cl}^{f/m}$ (Shinohara et al. 1989; Anderko and Pitzer 1993a; Driesner 2007); and (vi) it is unclear if metal chloride species, dissolved in silicate melts, obey Henry's law as the strong variation in activity coefficients for metal chloride species in the MVP may mask smaller variations in the silicate melt.

Fortunately, abundant experimental data have been collected on $D_{Cl}^{f/m}$ in the past several decades allowing for a fairly quantitative understanding of the effect of P-T and melt composition on this variable. In the following sections we discuss the available data on felsic systems and assess the effect of the most important physical-chemical variables on $D_{Cl}^{f/m}$.

Effect of Cl concentration. For the sake of simplicity, we first investigate the effect of dissolved chloride concentrations on $D_{Cl}^{f/m}$ in supercritical fluids. A large number of experiments have been conducted above the solvus in the salt–H_2O system. As $D_{Cl}^{f/m}$ is pressure dependent, we compiled data obtained at nearly constant pressure of 200–220 MPa for comparison (Fig. 7.34). This pressure is well

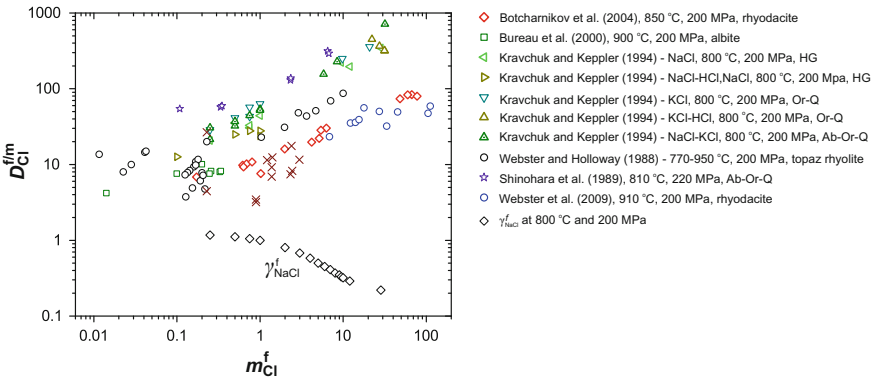

Fig. 7.34 The variation of $D_{Cl}^{f/m}$ in felsic systems as a function of the total Cl concentration in the aqueous fluid phase. It is apparent that above an m_{Cl}^{f} of about 0.5, the value of $D_{Cl}^{f/m}$ increases with m_{Cl}^{f}. For comparison, the variation of the activity coefficients of dissolved NaCl (γ_{NaCl}^{f}) in the aqueous fluid is shown, as computed by Kravchuk and Keppler (1994) using the equation of state of Anderko and Pitzer (1993a). It is apparent that the trend seen in γ_{NaCl}^{f} is the inverse of that shown by $D_{Cl}^{f/m}$. The concentration of Cl had to be recalculated to molality units in several studies, which required an estimation of the speciation of Cl in the fluid phase. For this we used the reported silicate melt compositions and assumed a $K_{K,Na}^{f/m} = 0.6$, and $K_{H,Na}^{v/m}$ from Williams et al. (1997) to predict HCl/NaCl ratios. The potential presence of $FeCl_2$ and other minor chloride species was ignored. We only compare experiments, which were conducted at 200 or 220 MPa in order to eliminate the effect of pressure from this comparison

above the critical curve in the NaCl–H_2O system for all experimental temperatures. Therefore, it is likely that all experiments in the comparison contained supercritical fluids. The most complete datasets were available for haplogranite, F-bearing rhyolite (topaz rhyolite), and rhyodacite melt compositions (Webster and Holloway 1988; Shinohara et al. 1989; Kravchuk and Keppler 1994; Bureau et al. 2000; Botcharnikov et al. 2004; Webster et al. 2009). Figure 7.34 clearly shows that $D_{Cl}^{f/m}$ rapidly increases with the concentration of Cl in the fluid phase. The trends are shifted relative to each other, however, the slope of the fits appear nearly identical for various melt compositions. One must note that for identical Cl concentrations in the fluid phase, the Cl concentration in the silicate melt is about an order of magnitude higher in the rhyodacite melts than in the haplogranitic ones. The observation that the slope of the m_{Cl}^{f} versus $D_{Cl}^{f/m}$ fit is nearly identical for different melt compositions, despite the large difference in C_{Cl}^{m}, indicates that the primary factor causing the variation of $D_{Cl}^{f/m}$ as a function of Cl concentration, may be the variation in the activity coefficients of major chloride species in the fluid phase. This has been most clearly suggested by Kravchuk and Keppler (1994) who assumed that Cl obeyed Henry's law in the silicate melt and used the experimen-

tally determined $D_{Cl}^{f/m}$ values to derive variations in the activity coefficients of NaCl in the fluid phase. Kravchuk and Keppler (1994) has also calculated the activity coefficients of $NaCl^{o}$ species in the NaCl–H_2O system at $T = 800$ °C and $P = 200$ MPa using the equation of state of Anderko and Pitzer (1993a) to support their hypothesis. We plotted their data in Fig. 7.34. The slope of the variation in γ_{NaCL}^{f}, as a function of m_{Cl}^{f}, nearly resembles the inverse of the trends shown by $D_{Cl}^{f/m}$ at $m_{Cl}^{f} \geq 1$. Therefore, it is likely that the variation of $D_{Cl}^{f/m}$, as a function of the total Cl concentration of the system, can be well described with an activity model for dissolved chloride species in the fluid phase. It appears that the equation of state of Anderko and Pitzer (1993a) for the NaCl–H_2O system may successfully be used as a first approximation despite the more complex chloride speciation in aqueous fluids co-existing with geologic silicate melts.

Many upper crustal magma reservoirs are characterized by *P-T* conditions where immiscibility between low-density, salt-poor vapor and high-density, salt-rich liquid (brine) phases in the salt–H_2O system is likely. Upon the entry of a new phase, the number of the degrees of freedom in the system decreases, and the primary response to the addition of metal-chlorides to the bulk aqueous fluid will be an increase in the brine/vapor mass ratio (Shinohara et al. 1989; Shinohara 1994; Webster 2004). At the same time, the activity of metal-chlorides, and therefore the salt concentrations in the vapor, brine, and silicate melt phases remain fixed as long as *P* and *T* and the chemical potential of the other components of the system remain constant.

In addition, one may consider the possibility of a shallow magmatic reservoir or volcanic conduit falling in a *P-T* regime, which allows for salt-vapor coexistence. This would require *T* below the liquidus of the salt mixture co-existing with the silicate melt, whereas *P* would need to be below about 300 bars based on the phase diagram of the NaCl–H_2O binary (Bodnar et al. 1985; Driesner and Heinrich 2007). The melting point of NaCl at these relatively low *P* is at 801–810 °C, which would still allow many felsic magmas to fall in the salt-vapor coexistence field. However, as discussed in detail below, most magmatic fluids contain major KCl and $FeCl_2$ components, which will affect the salt liquidus. Indeed, the NaCl–KCl system has an eutectic point at ~660 °C and $X_{NaCl} = 0.45$, whereas the liquidus temperature is near 700 °C and $X_{NaCl} = 0.7$, which is typical of magmatic fluids at ambient pressure (Chou et al. 1992; Aranovich and Newton 1997). These fall well below the eruption temperature of most magmas and the H_2O saturated haplogranite solidus at the relevant pressures (Johannes and Holtz 1996). Therefore, it is likely that saturation of solid salts will only rarely occur during magma evolution.

Effects of pressure and temperature. Many previous studies on $D_{Cl}^{f/m}$ in felsic systems were conducted at constant pressure. A few studies used variable pressure, but unfortunately temperature and silicate melt composition varied significantly as well among the experiments. Therefore, much of the existing experimental data cannot be directly applied to constrain the pressure dependence of $D_{Cl}^{f/m}$ due to the lack of a model that at least accounts for the effect of melt composition. To

systematically investigated the effect of P on $D_{Cl}^{f/m}$, Shinohara et al. (1989) studied the partitioning of Cl between haplogranite melts and aqueous chloride-bearing fluids in the pressure range 60–600 MPa and found a strong positive correlation between $D_{Cl}^{f/m}$ and pressure. The values of $D_{Cl}^{f/m}$ varied from as low as ~3 at P = 60 MPa up to ~500 at 600 MPa. Similarly, Signorelli and Carroll (2000, 2002) studied the pressure dependence of Cl partitioning between phonolitic and trachytic melts and aqueous fluids between 50 and 250 MPa, and have also observed the positive effect of pressure on $D_{Cl}^{f/m}$. For example, when considering dilute supercritical fluids equilibrated with Vesuvius phonolite melts, $D_{Cl}^{f/m}$ increased from about 0.6 at P = 50 MPa to about 20 at P = 250 MPa. The experiments of Webster and Holloway (1988), using rhyolitic melts, also encompassed a wide pressure range from 50 to 500 MPa, but experimental run temperatures and the ASI of the run product glasses varied significantly. Nevertheless, when considering only experiments with dilute supercritical fluids, $D_{Cl}^{f/m}$ increased from about 4 at P = 100 MPa to about 23 at P = 500 MPa.

In Fig. 7.35, we plotted $D_{Cl}^{f/m}$ as a function of pressure only from experiments where the aqueous phase was a vapor or a relatively dilute supercritical fluid. Complete datasets, with internally consistent melt composition and temperature, were only available in two studies (Shinohara et al. 1989; Signorelli and Carroll 2000). We found that when these data are plotted in logarithmic space, a simple

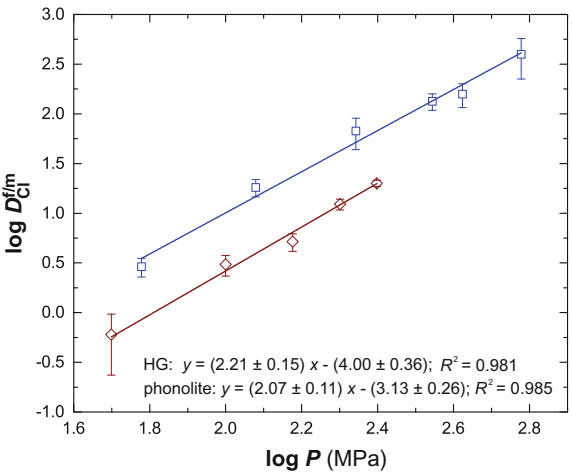

Fig. 7.35 The pressure dependence of $D_{Cl}^{f/m}$ with respect to low-salinity aqueous fluids. The *blue symbols* represent haplogranite melt compositions from Shinohara et al. (1989), whereas the *red symbols* are the phonolite melt compositions from Signorelli and Carroll (2000). The plotted data represent only dilute fluids with the following criteria for the estimated fluid composition at run conditions: for P $\leq$ 120 MPa—the fluid is single phase vapor; for 120 MPa $\leq$ P $\leq$ 220 MPa —m_{Cl} > 1.36; and for P > 220 MPa—m_{Cl}^{f}< 2.5

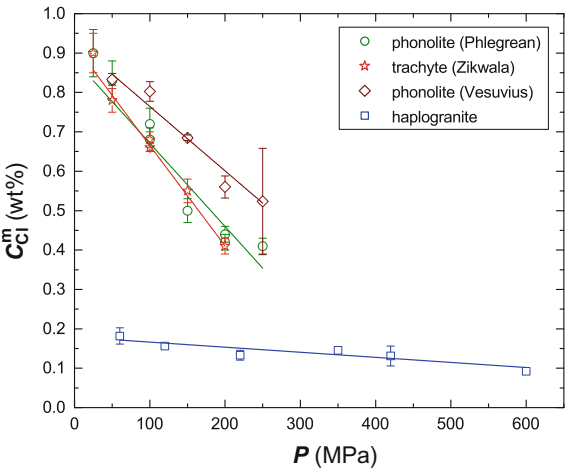

Fig. 7.36 The pressure dependence of the Cl concentration in silicate melts at saturation with high salinity aqueous fluids $m_{Cl} > 6$. Data sources are the following: Vesuvius phonolite—Signorelli and Carroll (2000); Phlegrean Phonolite and Zikwala trachyte—Signorelli and Carroll (2002); and haplogranite—Shinohara et al. (1989)

linear correlation exists between log P and $D^{f/m}_{Cl}$. The slope of the fitted lines is nearly identical for the two different melt compositions (haplogranite and phonolite) suggesting that the thermodynamic properties of the aqueous fluid phase are exerting the primary control on the pressure dependence of $D^{f/m}_{Cl}$. The linear correlation in logarithmic space is purely empirical. However, it may provide practical means to simple parameterization of the effect of pressure on $D^{f/m}_{Cl}$ at low salt concentrations in the aqueous fluid phase.

To investigate the effect of pressure on $D^{f/m}_{Cl}$ at high fluid salinities, we used the data of Shinohara et al. (1989), and Signorelli and Carroll (2000, 2002). As the aqueous fluids were in the vapor/hydrosaline liquid immiscibility field in many of the experiments, $D^{f/m}_{Cl}$ could not be directly derived by mass balance. However, following the practice of Signorelli and Carroll (2002), the concentration of Cl in silicate melts coexisting with two-phase aqueous fluids can be compared. In addition, we included experiments at relatively high pressures that contained supercritical fluids with >6 m Cl. As the C^f_{Cl} versus C^m_{Cl} slope is rather flat at high chloride activities (Shinohara et al. 1989; Webster 2004), the C^m_{Cl} values can be used as a proxy to understand the effect of pressure on $D^{f/m}_{Cl}$ in systems with high-salinity aqueous fluids (Signorelli and Carroll 2002). It is apparent in Fig. 7.36, that the concentration of Cl in silicate melts in equilibrium with high-salinity fluids drops moderately with increasing pressure indicating a slight increase in $D^{f/m}_{Cl}$. The relative effect seems slightly more pronounced for experiments with phonolitic and trachytic melts than for those with rhyolites. However in both cases, it is much more modest than that observed in the case of low-salinity fluids.

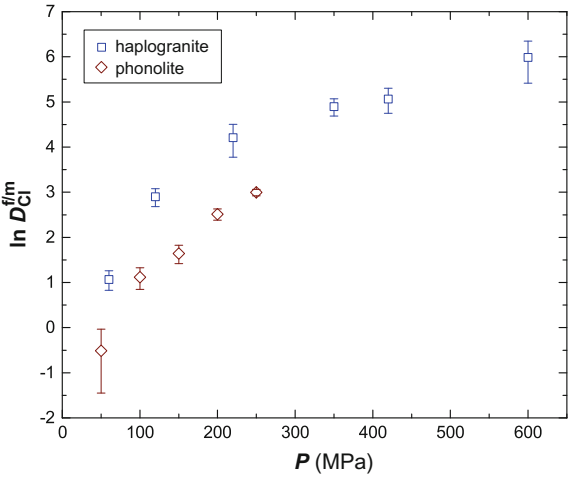

Fig. 7.37 The variation in $D_{Cl}^{f/m}$ as a function of pressure for haplogranite (Shinohara et al. 1989) and phonolite melts (Signorelli and Carroll 2000). The slope of the curve connecting the points should be proportional to the molar volume change for the NaCl (m) = NaCl (f) reaction, as shown in Fig. 7.38

In order to interpret the pressure dependence of $D_{Cl}^{f/m}$, we consider the pressure dependence of the equilibrium constant of the mass-action law describing the transfer of Cl from the silicate melt to the fluid phase, as follows:

$$\left(\frac{\partial \ln K}{\partial P}\right)_T = -\frac{1}{RT}\left(\frac{\partial \Delta_r G^o}{\partial P}\right)_T = -\frac{\Delta_r V^o}{RT}. \tag{7.44}$$

As there is a positive correlation between the equilibrium constant K and $D_{Cl}^{f/m}$, the observation that $D_{Cl}^{f/m}$ increases with pressure requires that the standard molar volume change during the mass transfer reaction is negative. The observation that the $\partial \ln D_{Cl}^{f/m}/\partial P$ slope decreases with increasing P suggests that the value of $\Delta_r V^o$ becomes less negative with increasing P (Fig. 7.37). The negative $\Delta_r V^o$ is a consequence of the hydration of strong dipole metal chloride ion pairs (i.e., NaCl, KCl, $FeCl_2$) in the aqueous fluid as the H_2O molecules in the hydration shell are more densely packed than in pure H_2O. We used the correlation formulae of Driesner (2007) and Driesner and Heinrich (2007) to predict the partial molar volume of NaCl in aqueous fluids at 800 °C in the pressure range of 50 to 500 MPa at low (0.2–1 wt%) and high (60–85 wt%) NaCl concentrations in the fluid. These data were combined with an assumed partial molar volume of 25 $cm^3\ mol^{-1}$ for NaCl (m) species to estimate $\Delta_r V^o$ (Fig. 7.38). This latter value was based on the estimate of Shinohara et al. (1989). Two key observations can be made from Fig. 7.38: (i) the variaton of $\Delta_r V^o$ as a function of P, corresponds well to the observed

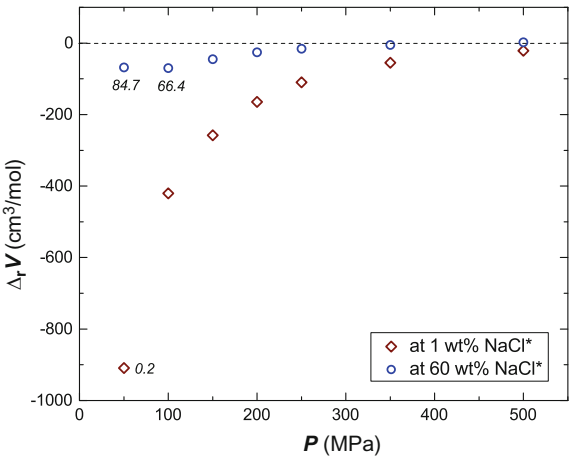

Fig. 7.38 The molar volume change for the reaction NaCl (m) = NaCl (f) at 800 °C as estimated by the calibration of Driesner (2007) and Driesner and Heinrich (2007). The values were calculated for low salinity (1 wt% NaCl) and high-salinity (60 wt% NaCl) aqueous fluids. Exceptions are the values with a salinity label, where slightly different salt concentrations had to be used in order to remain in the single phase field

$\partial \ln D_{Cl}^{f/m}/\partial P$ slope in Fig. 7.37, and (ii) $\Delta_r V^o$ becomes less negative with increasing salt concentration in the aqueous fluid phase, which is consistent with the observation that the effect of pressure on $D_{Cl}^{f/m}$ is much more moderate in systems with high-salinity than in systems with low-salinity fluids.

Effect of silicate melt composition. Figure 7.34 shows that the trends describing $D_{Cl}^{f/m}$ as a function of m_{Cl}^{f} are shifted relative to each other. The values of $D_{Cl}^{f/m}$ are the highest in the haplogranite systems of Shinohara et al. (1989) and Kravchuk and Keppler (1994). At the same time, $D_{Cl}^{f/m}$ is about an order of magnitude lower for rhyodacite melts. The large drop in $D_{Cl}^{f/m}$, in response to a relatively small change in silicate melt composition, indicates that the activity coefficients of the dissolved chloride species in the silicate melt are rather sensitive to the composition and/or structure of the silicate melt in the felsic compositional regime. As expected, this corresponds well to the trend observed in the maximum dissolved chloride concentrations in silicate melts. For example, the most chloride-rich fluids of Botcharnikov et al. (2004) ($m_{Cl}^{f} \approx 70$), coexist with a silicate melt containing about 0.8 wt% Cl, whereas the same value for the slightly peralkaline to slightly peraluminous haplogranite melts of Kravchuk and Keppler (1994) is in the range of 0.15–0.30 wt%. The $D_{Cl}^{f/m}$ values are correspondingly higher in the study of Kravchuk and Keppler (1994) by about a factor of 4 to 5 at identical Cl concentrations in the fluid phase. Taking advantage of this relationship, we will use the concentration of Cl in the silicate melt, in equilibrium with high-salinity fluids, as a proxy for $D_{Cl}^{f/m}$. This way, a much larger number of data points can be compared because at least the effect of Cl concentration in the fluid phase is eliminated from the set of variables affecting $D_{Cl}^{f/m}$. Several studies have been conducted with this approach using a wide variety of melt compositions (Metrich and Rutherford 1992;

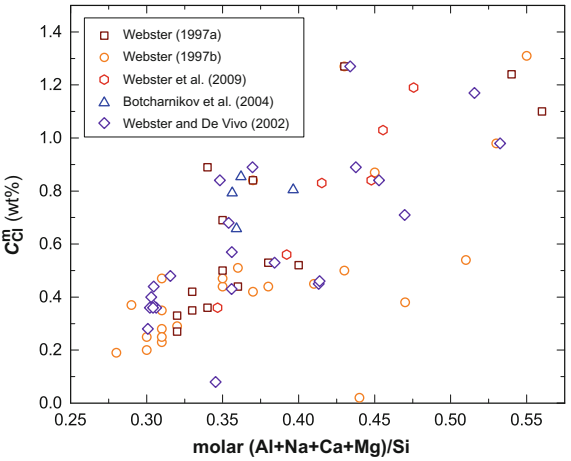

Fig. 7.39 The effect of silicate melt composition on chloride solubilities in silicate melts. Only data obtained at $P = 200 \pm 10$ MPa were plotted. The experiments of Webster et al. (1997a, b) and Webster and De Vivo (2002) were saturated in hydrous chloride melts, though the exact composition of these were not reported. From the study of Botcharnikov et al. (2004) and Webster et al. (2009), we plotted only experiments, which contained a volatile phase with chloride concentration over 30 molal

Webster 1997b; Webster and De Vivo 2002; Bureau and Metrich 2003). Webster and De Vivo (2002) and Metrich and Rutherford (1992) pointed out the effect of the alumina saturation index (ASI) on $D_{Cl}^{f/m}$ in granitic systems. They showed that $D_{Cl}^{f/m}$ is the highest at ASI = 1, and decreases towards both more peralkaline and more peraluminous melt compositions. Webster (1997a, b) proposed the molar (Al + Na + Ca + Mg)/Si ratio to be a suitable proxy for compositional effects on chloride solubility in multicomponent silicate melts. Webster and De Vivo (2002) further developed this model using a wide variety of synthetic melt compositions. They concluded that silicate melt constituents affect chloride solubility in the following order of importance: Mg $\sim$ Ca > Fe > Na > K > network-forming Al. The proposed model for chloride solubility in silicate melts reproduced their experimental dataset with typically less than 10% relative differences between the predicted and measured values. As the model is rather convolute with distinct formulations for different melt compositional intervals, the reader is referred to the article for further details. Here, we just show near chloride-saturation Cl concentrations at $P = 200$ MPa compiled from a number of experimental studies as a function of the (Al + Na + Ca + Mg)/Si ratio. This parameter was chosen because some of the experimental studies did not report the run product glass compositions in full, only the (Al + Na + Ca + Mg)/Si ratios. Figure 7.39 documents a fairly good positive correlation between the (Al + Na + Ca + Mg)/Si ratio and the chloride solubility values with the exception of a few outliers. Melt compositions at the lower end of the trend are rhyolites, whereas the highest plotted Cl concentrations are from latite melt compositions. More mafic compositions are discussed in the article on mafic and intermediate systems by Webster et al. (2015) and in a companion chapter.

Effects of other volatile constituents. Carbon dioxide is known to increase the activity coefficient of NaCl species in aqueous fluids, which is, for example,

manifested by the expansion of the solvus in the NaCl–H_2O system in response to the addition of CO_2 (Frantz et al. 1992; Shmulovich and Graham 1999, 2004; Schmidt and Bodnar 2000; Aranovich et al. 2010). One may expect, therefore, that CO_2 addition to aqueous metal chloride-bearing fluids will have a negative effect on $D_{Cl}^{f/m}$. However, only a few studies have addressed the effect of CO_2 on Cl partitioning with somewhat contradictory results. Botcharnikov et al. (2007) and Alletti et al. (2009) have shown that $D_{Cl}^{f/m}$ decreases by about a factor of 2 in response to the addition of about 20 mol% CO_2 to the fluid phase in equilibrium with andesitic and basaltic melts, respectively. At the same time, Webster (1997a) reported that the addition of CO_2 to salt-rich fluids at 200 MPa did not have a noticeable effect on $D_{Cl}^{f/m}$. This apparent contradiction may be assigned to the likely different relative effect of CO_2 on the activity coefficients of metal chloride species in dilute and concentrated solutions, as most of the data of Botcharnikov et al. (2007) and Alletti et al. (2009) were obtained at significantly lower fluid salinities than those of Webster (1997a). For example, CO_2 is known to have a much larger relative effect on the NaCl concentration in the vapor than in the brine phase at *P-T* conditions below the critical curve in the NaCl–H_2O–CO_2 system (Schmidt and Bodnar 2000; Frank et al. 2003; Liebscher and Heinrich 2007).

Only a few studies have investigated the effect of F on $D_{Cl}^{f/m}$ (Webster 1997a, b; Webster and Rebbert 1998). Webster (1997a) concluded that F had little effect on chloride solubilities in silicate melts at F concentrations below 1.2 wt%, but a rather significant one at higher F concentrations. For example, about 1.5 to 3 times higher chloride solubilities were determined in silicate melts with dissolved F concentrations of 5.1–7.8 wt% compared to F-free silicate melts of otherwise similar composition (Webster 1997a, b). The concentration of F in the silicate melt also appears as a positive term in the formula of Webster and De Vivo (2002) to predict chloride solubilities in silicate melts. The positive effect of F on chloride solubilities was attributed to Al-F complexing in the melt structure and the related release of network modifier cations from the charge balancing role for the Al^{3+}–Si^{4+} substitution (Webster 1997a, b). Due to the increased chloride solubilities in the silicate melt, it is expected the F addition reduces $D_{Cl}^{f/m}$. This may be seen in Fig. 7.34, wherein the topaz–rhyolite samples of Webster and Holloway (1988) display significantly lower $D_{Cl}^{f/m}$ than the haplogranitic compositions. These melts contained about 1–1.2 wt% F, but also some CaO (0.4 wt%) and FeO ($\sim$1wt%), which may also affect $D_{Cl}^{f/m}$. Nevertheless, Webster and Holloway (1988) also conducted some F-free experiments with otherwise identical melt compositions, and pointed out that $D_{Cl}^{f/m}$ decreases the most in response to F addition at low chloride activities.

7.5.2.2 Speciation of Cl in Magmatic Fluids

Thermodynamic formulation. Chlorine may be present in the form of various chemical species in magmatic fluids and the relative proportion of these species may affect the fluid/melt partitioning of ore metals, as well as sub-solidus fluid/rock interaction in the associated hydrothermal systems. Therefore, it is essential to understand what the main chloride species in magmatic fluids are and how their proportions relate to the composition of the silicate melt, temperature, and pressure.

The pioneering studies of Gammon et al. (1969) and Holland (1972) established a basic framework for understanding Cl speciation in high-pressure magmatic fluids. Here we follow the formulation of Holland (1972), further developed by Candela (1990), to describe the partitioning of chloride-complexed metals between silicate melts and magmatic fluids. The partitioning of the major elements in particular are best expressed in the form of exchange coefficients between the melt and the fluid phase since they compete for the available total Cl budget in the fluid phase. One may consider the following exchange reaction between melt and fluid:

$$KO_{0.5}\,(\mathrm{m}) + NaCl\,(\mathrm{f}) = KCl\,(\mathrm{f}) + NaO_{0.5}\,(\mathrm{m}). \tag{7.45}$$

Reaction (7.50) has the following equilibrium constant:

$$K_{7.50} = \frac{a^{f}_{KCl} \cdot a^{m}_{NaO0.5}}{a^{m}_{KO0.5} \cdot a^{f}_{Nacl}}, \tag{7.46}$$

which can be expanded as

$$K_{7.50} = \frac{\gamma^{f}_{KCl} \cdot X^{f}_{KCl} \cdot \gamma^{m}_{NaO0.5} \cdot X^{m}_{NaO0.5}}{\gamma^{m}_{KO0.5} \cdot X^{m}_{KO0.5} \cdot \gamma^{f}_{NaCl} \cdot X^{f}_{NaCl}}, \tag{7.47}$$

and rearranged as follows

$$K_{7.50} = \frac{X^{m}_{NaO0.5}}{X^{f}_{NaCl}} \cdot \frac{X^{f}_{KCl}}{X^{m}_{KO0.5}} \cdot \frac{\gamma^{f}_{KCl}}{\gamma^{f}_{KO0.5}} \cdot \frac{\gamma^{m}_{NaO0.5}}{\gamma^{f}_{NaCl}}. \tag{7.48}$$

Assuming that the product of the activity coefficients is constant, Eq. (7.53) can be rewritten as

$$K_{7.50} = \frac{D^{f/m}_{K}}{D^{f/m}_{Na}} \cdot G \cdot Z, \tag{7.49}$$

where G is the product of the activity coefficients in Eq. (7.53), and Z is a constant relating to the conversion of molar based concentration units to mass based

concentration units. One may eliminate the constants from the equation and call the $K_{7.50}/(G\cdots Z)$ quantity $K^{\mathrm{f/m}}_{\mathrm{K,Na}}$, i.e., the fluid/melt exchange coefficient of K and Na.

Similar exchange reactions can be written for any elements that are dominantly present as chloride species in the fluid and as oxide species in the silicate melt. If the valence state of element i is n, the same derivation as above leads to the following general formula:

$$K^{f/m}_{i,Na} = \frac{D^{f/m}_{i}}{\left(D^{f/m}_{Na}\right)^{n}}. \tag{7.50}$$

These fluid/melt *exchange* coefficients are much more stable quantities than the Nernst-type *partition* coefficients as much of the dependence on total chloride concentration, and, to some extent, on pressure, temperature, and melt composition, are eliminated. Note that Eq. (7.55) suggests that elements with valence states higher than one will partition with exponential dependence into chloride-rich fluids with increasing $D^{\mathrm{f/m}}_{\mathrm{Na}}$.

It is more challenging to address the HCl/total metal chloride ratio in magmatic fluids. Candela (1990) proposed a comprehensive thermodynamic formulation to describe hydrogen/metal exchange equilibria between fluids and peraluminous haplogranitic melts. This formulation is based on the following exchange reaction:

$$\mathrm{NaCl\,(f) + 0.5\,H_2O\,(m) + 0.5\,Al_2O_3(m) + 3\,SiO_2(m) = HCl\,(f) + NaAlSi_3O_8(m).} \tag{7.51}$$

The same reaction could be written with any other feldspar component in the melt. The Al_2O_3 (m) component in this exchange reaction represents the Al in the silicate melt that is present in excess of what can be incorporated into the feldspar components. So, basically this is Al^{3+} replacing Si^{4+} in the silicate melt structure for which the substitution reaction cannot be compensated by charge balancing by Na, K, or Ca. The formulation of Candela (1990) assumes that H^+ plays the charge balancing role of Na^+, K^+, and Ca^{2+} for this excess Al_2O_3 component in peraluminous melts, and calls this a "fictive hydrous aluminosilicate [H(fasc)]" component. The concentration of the H(fasc) component can easily be calculated using stoichiometric constraints as follows:

$$X^{\mathrm{m}}_{\mathrm{H(fasc)}} = X^{\mathrm{m}}_{\mathrm{Al}} - \left(X^{\mathrm{m}}_{\mathrm{Na}} + X^{\mathrm{m}}_{\mathrm{K}} + 2X^{\mathrm{m}}_{\mathrm{Ca}}\right). \tag{7.52}$$

Replacing Al_2O_3 by H(fasc) in Eq. (7.56), and assuming unit activities of H_2O and SiO_2 and a constant product for the activity coefficients of all the other components, yields the following expression:

$$K_{\mathrm{H,Na}}^{\mathrm{f/m}} = \frac{X_{\mathrm{Hcl}}^{\mathrm{f}} \cdot X_{\mathrm{Na}}^{\mathrm{melt}}}{X_{\mathrm{H(fasc)}}^{\mathrm{melt}} \cdot X_{\mathrm{Nacl}}^{\mathrm{f}}} \cdot Z * \mathrm{P} \tag{7.53}$$

where G is the product of the activity coefficients and Z is a constant relating to the conversion of concentration units. For practical use, these constants are eliminated from the equation. One must note that the H(fasc) quantity directly relates to the ASI of the melt in the following manner:

$$ASI = C_{\mathrm{H(fasc)}}^{\mathrm{m}} / \left(C_{\mathrm{Na}}^{\mathrm{m}} + C_{\mathrm{K}}^{\mathrm{m}} + 2C_{\mathrm{Ca}}^{\mathrm{m}}\right) + 1. \tag{7.54}$$

Therefore, the HCl/metal chloride ratios are expected to positively correlate with ASI.

K/Na exchange. Holland (1972) has produced the most comprehensive experimental dataset of cation exchange coefficients between silicate melts and chloride-bearing aqueous fluids to date. He determined $K_{\mathrm{K,Na}}^{\mathrm{f/m}} = 0.74 \pm 0.06$ at T = 810–855 °C and P = 180–230 MPa in equilibrium with granitic melts. Similar values have been determined for $K_{\mathrm{K,Na}}^{\mathrm{f/m}}$ by a number of other studies in granitic systems in the P-T range of upper crustal magmas reservoirs (Gammon et al. 1969; Shinohara et al. 1989; Bai and Koster van Groos 1999; Schafer et al. 1999; Student and Bodnar 1999). The reported $K_{\mathrm{K,Na}}^{\mathrm{f/m}}$ values for granitic melts span the range of 0.4–0.75 without systematic dependence on chloride concentrations in the fluid phase or the ASI of the melt. However, the only study that systematically investigated the effect of the HCl concentration on $K_{\mathrm{K,Na}}^{\mathrm{f/m}}$ for melt-brine equilibrium reported that, in the presence of more than 1 wt% HCl in the brine phase, the value of $K_{\mathrm{K,Na}}^{\mathrm{f/m}}$ decreases to 0.4 ± 0.03 from the approximate 0.6 observed at HCl concentrations of 0–0.5 wt% (Frank et al. 2003). These authors suggested that this observation is due to the preferential formation of NaOH species over KOH species in the structure of hydrous silicate melts, and therefore preferential Na transfer to the brine phase by the following reaction:

$$\mathrm{NaOH\,(m) + HCl\,(b) = NaCl\,(b) + H_2O\,(system)}. \tag{7.55}$$

They proposed the following formula to describe the effect of HCl in the brine, $K_{\mathrm{K,Na}}^{\mathrm{f/m}} = 0.4(\pm 0.03) + 0.03/C_{\mathrm{HCl}}^{\mathrm{brine}}$, where $C_{\mathrm{HCl}}^{\mathrm{brine}}$ is expressed in wt%. The ASI of the run product glasses of Frank et al. (2003) falls between 0.91 and 1.09, and this should positively correlate with $C_{\mathrm{HCl}}^{\mathrm{f}}$ according to Williams et al. (1997). Therefore, ASI is a practical parameter to assess if the proposition of Frank et al. (2003) is consistent with other experimental studies. Student and Bodnar (1999) and Schafer et al. (1999) determined that $K_{\mathrm{K,Na}}^{\mathrm{f/m}} = 0.4 \pm 0.06$ and 0.48 ± 0.13, respectively, for haplogranitic melts at an ASI of 0.94–0.95, which is broadly consistent with the

data of Frank et al. (2003). Interestingly, no clear correlation can be identified between the ASI of the run product glass and $K^{f/m}_{K,Na}$ in the data reported by Bai and Koster van Groos (1999), even though this study covered an extremely wide range in ASI from 0.53 to 50. Unfortunately Gammon (1969), Holland (1972), and Shinohara et al. (1989) did not fully report their run product glass compositions. Therefore, the value of ASI in these studies, which reported the highest $K^{f/m}_{K,Na}$ values of about 0.75, cannot be calculated. To our knowledge, no $K^{f/m}_{K,Na}$ have been reported for felsic melts other than granitic in composition. However, Zajacz et al. (2012a) determined an $K^{f/m}_{K,Na}$ of 1.23 ± 0.10 for andesite melts, indicating that $K^{f/m}_{K,Na}$ increases towards more mafic, more depolymerized melt compositions.

Fe/Na exchange. Iron is the third most abundant metallic element described from high temperature magmatic fluids as sampled by fluid inclusions (Ulrich et al. 1999; Audétat and Pettke 2003; Kamenetsky et al. 2004; Yardley 2005; Klemm et al. 2007; Zajacz et al. 2008; Seo et al. 2009; Yardley and Bodnar 2014). Despite this observation, very few data exist on Fe partitioning between chloride-bearing fluids and silicate melts. Simon et al. (2004) studied the solubility of magnetite in rhyolitic melts and co-existing chloride-bearing aqueous vapors and brines. The salinities of the vapor and brine phases were varied along a pressure vector from 100 to 145 MPa at 800 °C. We used their data to derive partition coefficients for Fe. Interestingly, the Fe/Na ratios in the fluid phase are only slightly dependent on the total chloride concentration, which is inconsistent with Eq. (7.55). Therefore, it is impractical to calculate $K^{f/m}_{Fe,Na}$ according to Eq. (7.55) as the resulting value is strongly dependent on the total chloride concentration. Instead, the quantity $K^{f/m}_{Fe(II),Na'} = \frac{D^{f/m}_{Fe}}{D^{f/m}_{Na}}$ can be used. Note that the denominator is $D^{f/m}_{Na}$ instead of $\left(D^{f/m}_{Na}\right)^2$. Also, as Fe is expected to be dominantly present in ferrous form in the fluid phase, it is logical to use Fe(II) concentrations from the silicate melt as well. An Fe^{2+}/Fe^{total} ratio of 0.8 was calculated for a system buffered to a NNO oxygen fugacity in the study of Simon et al. (2004) using the equation of Kress and Carmichael (1991). The calculated $K^{f/m}_{Fe(II),Na'}$ values based on Simon et al. (2004) are shown in Fig. 7.40 as a function of the total chloride molality in the fluid phase. It is apparent that the Fe/Na ratios, and therefore, $K^{f/m}_{Fe(II),Na'}$, is slightly lower for brines in coexisting vapor/brine pairs. Also, for unknown reason, the 110 MPa experiment shows significantly lower $K^{f/m}_{Fe(II),Na'}$ than those at higher pressures. Similar data can also be derived from the composition of co-existing silicate melt and fluid inclusions trapped in quartz crystals in miarolitic cavities. Using the data of Zajacz et al. (2008), an average $K^{f/m}_{Fe(II),Na'}$ value of 3.2 can be derived from such samples. This should be considered as a minimum estimate of $K^{f/m}_{Fe(II),Na'}$, because the total Fe concentration was used for the silicate melt instead of only Fe(II) due to the lack of good constraints on fO_2 for the natural samples. It is apparent in

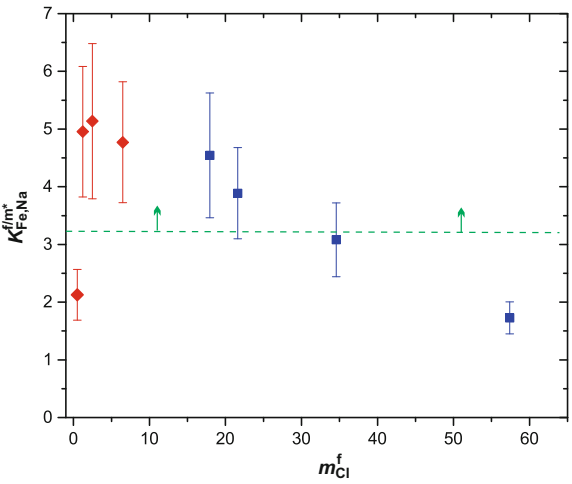

Fig. 7.40 The exchange coefficient of Fe and Na between granitic silicate melts and aqueous fluids. The symbols represent data from the experiments of Simon et al. (2004). *Red diamonds* stand for vapor phase fluids, whereas *blue squares* represent brines. The *green line* represents the minimum value derived based on co-existing fluid and melt inclusions by using the data of Zajacz et al. (2008). It is a minimum estimate because all Fe in the silicate melt was assumed to be present as Fe^{2+} for the calculation due to the lack of precise constraints on fO_2

Fig. 7.40, that $K^{f/m}_{Fe(II),Na'}$ most likely falls between 3 and 5 for rhyolitic melts. Zajacz et al. (2012) determined $K^{f/m}_{Fe(II),Na'}$ for andesitic melts and also found a chloride concentration independent value for this quantity. The determined $K^{f/m}_{Fe(II),Na'} = 1.08 \pm 0.16\,(1\sigma)$ is much smaller than those for the rhyolite melts indicating that $K^{f/m}_{Fe(II),Na'}$ decreases towards more mafic melt compositions.

Ca,Mg/Na exchange. To our knowledge, only Holland (1972) determined exchange coefficients between Ca, Mg, and Na. He observed a parabolic correlation between the total chloride concentration in the fluid and the fluid/melt partition coefficients of Ca and Mg as expected based on Eq. (7.55). This is required by Eq. (7.55) because $D^{f/m}_{Na}$ is linearly proportional to the total chloride concentration in the fluid phase. This can be considered as a confirmation of the assumption that the product of the activity coefficients in Eq. (7.53) is constant and that Ca and Mg are present as $CaCl_2$ and $MgCl_2$ species in the fluid, respectively. The following exchange coefficients were determined: $K^{f/m}_{Ca,Na} = 0.38 \pm 0.09$ and $K^{f/m}_{Mg,Na} = 0.16 \pm 0.04\,(1\sigma)$. The fluid/melt partition coefficients for Ca and Mg reached values as high as 3 and 1.2 for a total chloride concentration of 6 mol/kg of solution.

Hydrogen chloride/metal chloride ratios. Williams et al. (1997) used the thermodynamic framework established by Candela (1990) and determined

$K^{f/m}_{H,Na}$ for haplogranitic melts with ASI in the range of 1.02–1.25 at T = 800 °C and P = 100 MPa and T = 850 °C and P = 50 MPa. At these conditions, the fluid phase was in the brine–vapor stability field, and therefore, $K^{f/m}_{H,Na}$ values, in reference to both the vapor ($K^{v/m}_{H,Na}$) and brine phase ($K^{b/m}_{H,Na}$), were defined. The following values were reported at 850 °C and 50 MPa—$K^{v/m}_{H,Na}$= 19 ± 7 and $K^{b/m}_{H,Na}$= 3.9 ± 2.3, whereas at 800 °C and 100 MPa—$K^{v/m}_{H,Na}$= 26 ± 1.3 and $K^{b/m}_{H,Na}$= 1.6 ± 0.7. Williams et al. (1997) argued that the value of $K^{v/m}_{H,Na}$ is only slightly affected by pressure, contradicting Shinohara (1987), who observed a significant pressure effect on the HCl/alkali metal chloride ratios coexisting with identical haplogranitic melts. One could explain such pressure effects by the higher dipole moment of the alkali chloride ion pairs relative to HCl leading to the formation of stronger hydration shells around the ion pairs and a larger associated drop in free energy. A consequence of this would be that the increasing density of the aqueous fluid phase with increasing pressure would preferentially stabilize hydrated metal chloride ion pairs relative to HCl in the fluid phase. Indeed, this is consistent with the observation of Williams et al. (1997) that $K^{f/m}_{H,Na}$ is much larger with respect to vapors than it is for brines. To our knowledge, no experimental data exists to constrain the HCl/metal chloride ratio for melt compositions other than haplogranite in the felsic compositional regime. In the case of andesitic melts, Zajacz et al. (2012a) found a positive correlation between the molar (Al + Fe(III))/(Na + K) ratio of the melt and the HCl/metal chloride ratios in the coexisting aqueous fluids. This is identical to that observed for haplogranite melts. However, much more experimental data are needed to allow for the construction of a thermodynamic model that can accurately predict $K^{f/m}_{H,Na}$ as a function of melt composition.

Chloride speciation in fluids exsolving from evolved granitic melts. As the understanding of the practical implications inherent in the above exchange coefficients is not completely intuitive, we conducted some model calculations to show the expected speciation of Cl in equilibrium with granitic melts as a function of ASI. We used a granite melt with ASI = 1.00 and C_{CaO} = 0.25 wt% and $C_{Fe(II)O}$ = 0.5 wt%. The FeO and CaO concentrations were based on typical silicate melt inclusion compositions described from fluid-saturated granites (Zajacz et al. 2008). As the $K^{f/m}_{H,Na}$ values of Williams et al. (1997) are only applicable to melts with an ASI > 1, we modeled a series of fluid compositions coexisting with melts with the ASI ranging from 1.00 to 1.25. The variation in ASI was induced by symmetric stepwise variation of the Al_2O_3, Na_2O, and K_2O concentrations around their concentration in the starting granite composition. Chloride speciation was calculated for both vapor and brine phases at T = 800 °C and P = 100 MPa and the results are shown in Fig. 7.41. It is apparent that in the vapor NaCl > KCl ~ $FeCl_2$ are the major metal chloride species, but with increasing ASI, HCl rapidly takes the

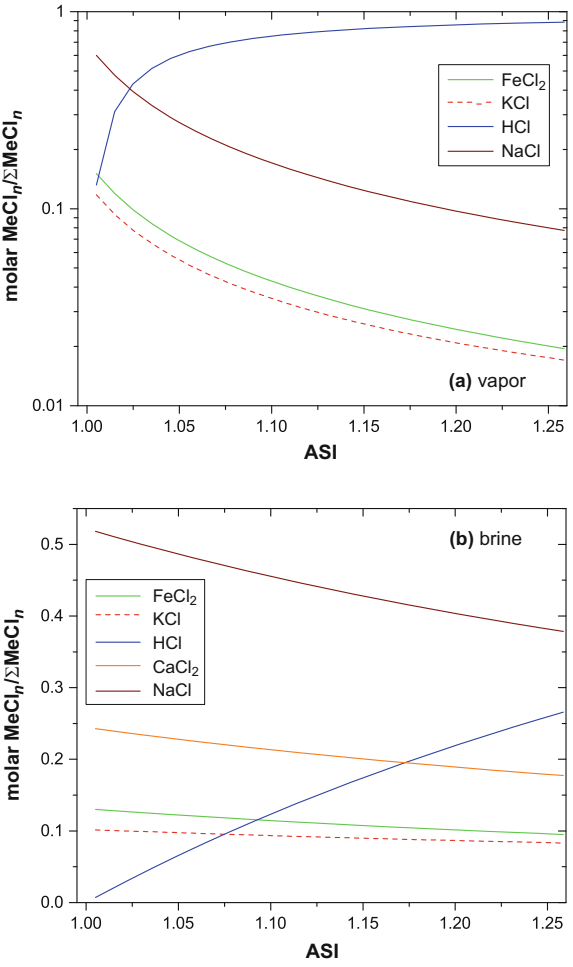

Fig. 7.41 The predicted relative abundance of major chloride species in aqueous vapor and brine exsolving from a typical granitic melt at 800 °C and 100 MPa as a function of the alumina saturation index of the melt (*ASI*). The assumed granite melt composition at *ASI* = 1 was the following: SiO_2 = 78.35 wt%, Al_2O_3 = 12.4 wt%, Na_2O = 4.4 wt%, K_2O = 4.2 wt%, FeO = 0.5 wt%, and CaO = 0.3 wt%. To yield *ASI* > 1, the molar proportion of Al and Na, and K and Ca was varied symmetrically around the initial composition. The cation exchange coefficients used for the calculation are the following: $K^{f/m}_{K,Na} = 0.4$, $K^{f/m}_{Fe,Na^*} = 4.0$, $K^{f/m}_{Ca,Na} = 0.38$, $K^{v/m}_{H,Na} = 26$, and $K^{b/m}_{H,Na} = 1.6$

place of metal chlorides over, such that vapors in equilibrium with melts with ASI > 1.03 are predicted to be HCl-dominated. Two remarkable differences can be observed in brines relative to vapors: (i) a much smaller fraction of Cl is present in the form of HCl; and (ii) $CaCl_2$ becomes an important chloride species in the fluid. Observation no. 2 is due to the $D^{f/m}_{Na}{}^{n}$ term in the denominator of Eq. (7.55) as $n = 2$ for Ca. Interestingly, the composition of brine inclusions in quartz trapped in the same assemblages with silicate melt inclusions from multiple locations contain much smaller concentrations of Ca than the predicted values (Audétat and Pettke 2003; Zajacz et al. 2008).

It is important to note that the concentrations of Mn, Zn, and Pb can also reach wt% levels in magmatic brines as determined by LA–ICP–MS analysis of natural fluid inclusions (e.g., Audétat et al. 1998; Ulrich et al. 1999; Audétat and Pettke 2003; Klemm et al. 2007; Zajacz et al. 2008; Seo et al. 2009). The experiments of Holland (1972) yielded $K^{f/m}_{Mn,Na} = 6.5 \pm 1.6\,(1\sigma)$, whereas Zajacz et al. (2008) determined $K^{f/m}_{Mn,Na} = 2.9 \pm 0.2\,(1\sigma)$ based on the composition of coexisting silicate melt and fluid inclusions. The partitioning of Zn and Pb will be discussed in the following section.

7.5.2.3 The Role of Cl in the Partitioning of Ore Metals Between Silicate Melt and Aqueous Fluid Phases

Lead and Zinc. Lead and Zn commonly occur in relatively high concentrations (up to about 1 wt%) in magmatic-hydrothermal fluids though they tend to precipitate only at lower epithermal temperatures (Ulrich et al. 1999; Audétat and Pettke 2003; Klemm et al. 2007; Zajacz et al. 2008; Yardley and Bodnar 2014). Relatively few experimental data exist on the fluid/melt partitioning of these elements (Holland 1972; Urabe 1985, 1987). All these studies found a strong positive correlation between C^{fluid}_{Cl} and $D^{f/m}_{Zn}$ and/or $D^{f/m}_{Pb}$. Holland (1972; 810–855 °C, 180–230 MPa, haplogranite) found that $D^{f/m}_{Zn}$ was a parabolic function of C^{fluid}_{Cl} [mol/kg of solution] and calculated a $K^{f/m}_{Zn,Na}$ value of 9.5 ± 2.4. Urabe (1985; 800 °C, 350 MPa) proposed that the ASI of the silicate melt greatly affects $D^{f/m}_{Zn}$ and $D^{f/m}_{Pb}$ in systems with chloride-bearing fluids. We recalculated the results of Urabe (1985) to exchange coefficients with Na. The resulting values for peraluminous melts are $K^{f/m}_{Zn,Na} = 43$ and $K^{f/m}_{Pb,Na} = 10$, whereas for peralkaline melts $K^{f/m}_{Zn,Na} = 0.38$ and $K^{f/m}_{Pb,Na} = 0.22$. These values suggest that Zn and Pb can only be effectively extracted from peraluminous melts by chloride-bearing fluids. In addition, Urabe (1987; 800 °C, 160–500 MPa) found that $D^{f/m}_{Zn}$ and $D^{f/m}_{Pb}$ decreases by about an order of magnitude as pressure increases from 160 to 500 MPa. Zajacz et al. (2008) used coexisting fluid and melt inclusions in quartz from natural samples to obtain fluid/melt partition coefficients for Zn and Pb amongst other elements. As opposed to experimental studies, they found a linear correlation between $D^{f/m}_{Zn}$ and $D^{f/m}_{Pb}$ and $C^{f/m}_{Cl}$ [mol/kg of solution], which were described by using the following equations: $D^{f/m}_{Zn} = 8.2 + 8.25\,C^{fluid}_{Cl}$; $D^{f/m}_{Pb} = 6.2 C^{fluid}_{Cl}$. The linear relationship between $D^{f/m}_{Zn}$ and $D^{f/m}_{Pb}$ may be explained by either a metal/Cl ratio of 1 in the stable complexes (e.g., mixed hydroxide–chloride complexes), or potentially with increasing activity coefficients of $ZnCl_2$ and $PbCl_2$ complexes with increasing fluid salinity. The empirical fits of Zajacz et al. (2008) are broadly consistent with the $D^{f/m}_{Zn}$ and $D^{f/m}_{Pb}$ values determined by others using coexisting

fluid and melt inclusions in quartz and topaz (Audétat et al. 2000; Audétat and Pettke 2003; Audétat 2010).

Copper. All experimental studies identified a positive linear correlation between C_{Cl}^{fluid} and $D_{Cu}^{f/m}$. However, the slope of the fitted line varies significantly between the previous studies. For example, Candela and Holland (1984; 750 °C, 140 MPa, NNO) found $D_{Cu}^{f/m}$ around 40 at $C_{Cl}^{fluid} = 4$ mol/kg of dissolved chloride concentration solution, while Keppler and Wyllie (1991; 750 °C, 200 MPa, NNO) found similarly high $D_{Cu}^{f/m}$ at as low as 0.48–0.96 mol/kg of solution dissolved chloride concentration. Candela and Holland (1984) added Cl to the starting solution in the form of NaCl and KCl, whereas Keppler and Wyllie (1991) used HCl instead. Therefore, considering the high fluid/melt mass ratios in both studies, it is likely that the run fluids of Keppler and Wyllie (1991) had high HCl/metal chloride ratios at run conditions even after alkali metal–hydrogen exchange between fluid and melt. This is supported by the peraluminous composition of the run product glasses of Keppler and Wyllie (1991). Therefore, the higher $D_{Cu}^{f/m}$ in this study is likely a consequence of the higher HCl/metal chloride ratios in the aqueous fluid phase. Bai and Koster van Groos (1999; 750–800 °C, 100–400 MPa) also used HCl in the starting fluid and found $D_{Cu}^{f/m}$ on the same order of magnitude as Keppler and Wyllie (1991) had, though with a significantly larger scatter. Zajacz et al. (2011; 1000 °C, 150 MPa, NNO-0.4) studied the solubility of Cu in magmatic vapors and found that it was highest in mixed NaCl–HCl fluids, and proposed the stability of Cu-chloride species associated with alkali metal or hydrogen ions (i.e. $NaCuCl_2$, $HCuCl_2$). The formation of such complexes is consistent with static ab initio quantum chemistry calculations as well as ab initio molecular dynamics simulations (Zajacz et al. 2011; Mei et al. 2014).

In addition to the effect of fluid chemistry, Williams et al. (1995; 800 °C, 50–100 MPa, HG) identified an approximately 20 fold increase in $D_{Cu}^{f/m}$ in a system with two-phase chloride-bearing fluids as pressure increased from 50 MPa to 100 MPa. The effect of pressure, however, does not seem entirely systematic when the data of Williams et al. (1995) is compared to that of Candela and Holland (1984). Both datasets were recast by the authors into exchange coefficients and compared: $K_{Cu,Na}^{f/m}$ is 11 ± 6 at 850 °C and 50 MPa and 215 ± 73 at 800 °C and 100 MPa (Williams et al. 1995), and $K_{Cu,Na}^{f/m} = 20 \pm 6$ at 750 °C and 140 MPa (Candela and Holland 1984). The reason for this apparent contradiction is unclear. The fact that vapor and brine coexist in the experiments of Williams et al. (1995) should not significantly affect the determined $K_{Cu,Na}^{f/m}$ values as $K_{Cu,Na}^{v/b}$ is close to 1. Simon et al. (2006) determined $K_{Cu,Na}^{f/m} = 33 \pm 21$ for Cl-bearing, S-free vapor phase fluids at 800 °C and 140 MPa, which is consistent, within error, with the data of Candela and Holland (1984).

The vapor/brine partitioning behavior of Cu and the effect of S on Cu partitioning and solubilities have been a focus of attention over the past two decades. Data obtained on co-existing vapor and brine inclusions from natural high-temperature fluid inclusion assemblages indicated that Cu preferentially partitions into the vapor phase. This observation was attributed to the presumed positive effect of S on Cu solubilities in aqueous fluids (Heinrich et al. 1999; Williams-Jones and Heinrich 2005; Seo et al. 2009). Nevertheless, high P-T experiments systematically showed preferential Cu partitioning into the brine phase even in S-bearing systems (Pokrovski et al. 2005, 2008; Simon et al. 2006; Frank et al. 2011), with the exception of the study of Nagaseki and Hayashi (2008), which was later shown to be erroneous by Lerchbaumer and Audétat (2012). Zajacz et al. (2009) have shown that cations with a valance state of 1+ and a radius smaller or equal to that of Na^+ and Ag^+ can rapidly diffuse through the structure of quartz and therefore the ratio of such elements (including Cu/Na and Cu/H) can be readily modified in fluid and melt inclusions after entrapment. Li et al. (2009) specifically demonstrated post entrapment modification of Cu/Na ratios in synthetic fluid inclusions, whereas Lerchbaumer and Audétat (2012) experimentally reproduced post entrapment Cu enrichment of S-bearing vapor inclusions, which lead to the empirical observation of artificially elevated apparent vapor/brine partition coefficients for Cu when analyzing co-existing vapor and brine inclusions. Seo and Heinrich (2013) revisited the question of Cu partitioning between vapor and brine by analyzing co-existing natural vapor and brine inclusions in topaz and confirmed that Cu preferentially partitions into the brine.

Experimental data on $D_{Cu}^{v/b}$ shows that Cu and Na partitions into the brine approximately to the same extent, i.e. $K_{Cu,Na}^{v/b}$ is close to 1 (Williams et al. 1995; Simon et al. 2006; Frank et al. 2011; Lerchbaumer and Audétat 2012). In addition, Tattich et al. (2015) have shown that this statement remains valid even when significant amounts of CO_2 X_{co_2}(X_{CO2} = 0.4) is added to the fluid and therefore the solvus in the salt–H_2O system significantly expands.

Gold. Though Au forms the most stable complexes with reduced S species in high-temperature aqueous fluids (e.g., Benning and Seward 1996; Gibert et al. 1998b; Simon et al. 2007; Zezin et al. 2007; Pokrovski et al. 2009b; Williams-Jones et al. 2009; Zajacz et al. 2010), most previous experimental fluid/melt partitioning studies using chloride-bearing fluids identified a clear positive correlation between C_{Cl}^{fluid} and $D_{Au}^{f/m}$ (e.g., Henley 1973; Frank et al. 2002; Simon et al. 2005, 2007; Pokrovski et al. 2009a; Zajacz et al. 2010). It is practical to first look at the effect of Cl on Au concentrations in the magmatic fluids, because the $D_{Au}^{f/m}$ values reported in many previous studies may be affected by uncertainties on the concentration of Au in the silicate melt due to the presence of Au nuggets in the run product glasses. The Au concentrations in the fluids are directly comparable as most experiments were conducted in Au capsules and therefore determined Au solubilities in both the

silicate melt and the aqueous fluid phase. Frank et al. (2002; 800 °C, 100 MPa, NNO) equilibrated granitic melts with brines ($C_{Cl}^{fluid} \approx 44$ molal) with HCl/total chloride ratios between 0.0007 and 0.09. They found that the solubility of Au in the fluid phase showed little variability within the range of 25–80 ppm at $m_{HCl}^{fluid} < 1.5$ but increased parabolically to about 2000 ppm with increasing C_{HCl}^{fluid} at higher HCl concentrations. Frank et al. (2002) attributed this trend to the presence of an $HAuCl_2$ complex in HCl-rich fluids. Simon et al. (2007; 800 °C, 120 MPa, NNO) investigated a system with vapor phase fluids with $m_{Cl}^{fluid} \approx 0.3$. They determined Au solubilities in the range of 23–39 ppm, nearly identical to those in the low-HCl brines of Frank et al. (2002). The ASI of the melt in the experiments of Simon et al. (2007) was in the range of 1.07–1.13. Therefore, the vapors were likely HCl-rich (Fig. 5.8), which may explain the relatively high Au solubilities. Zajacz et al. (2010, 1000 °C, 150 MPa, NNO-0.6) studied the solubility of Au in magmatic vapors. They identified a positive linear correlation between the solubility of Au and C_{HCl}^{fluid} and attributed this to Au dissolution as a neutral AuCl complex. More interestingly, they found an Au solubility maximum at intermediate NaCl/(NaCl + HCl) ratios in the fluid and inferred that the dominant Au species is $NaAuCl_2$ in vapors containing both NaCl and HCl in significant concentrations. The range of determined Au solubilities, normalized to fO_2 = NNO, was 3–31 ppm (assuming a monovalent state for Au), which is broadly consistent with the results of Simon et al. (2007) at lower T. Interestingly, Hanley et al. (2005; 600–800 °C, 150 MPa, NNO) found a negative correlation between the solubility of Au and total dissolved chloride concentration in supercritical aqueous fluids. They attributed this to the salting-out effect, wherein stronger dipole NaCl ion pairs successfully compete against weaker-dipole Au chloride complexes for H_2O molecules to form hydration shells around them. The range of Au solubilities determined by Hanley et al. (2005) is consistent with that of Frank et al. (2002), despite the fact that Hanley inferred much lower HCl concentrations in their experiments. However, these authors used very different methodologies to estimate C_{HCl}^{fluid} in their experiments and the one experiment of Hanley et al. (2005) that contained a silicate melt phase would suggest much more HCl-rich fluids if the method of Williams et al. (1997) was used to estimate C_{HCl}^{fluid} based on the ASI of the melt.

Existing data on $D_{Au}^{f/m}$ for S-free systems indicates that the lowest values are expected in more mafic melt compositions where the concentration of Cl in the equilibrium fluids is relatively low, with $D_{Au}^{f/m} \approx 20$ (Zajacz et al. 2012b). Whereas the highest $D_{Au}^{f/m}$, on the order of a few thousands, were found in granitic systems with HCl-rich aqueous fluids (Frank et al. 2002; Hanley et al. 2005). However, the presence of reduced S species may enhance these values significantly (Zajacz et al. 2010).

Relatively few data exist on the vapor/brine partitioning of Au at magmatic temperatures. Simon et al. (2005; 800 °C, 110–145 MPa, NNO) investigated Au

partitioning between NaCl–KCl–$FeCl_2$-bearing vapors and brines and determined $K^{b/v}_{Au,Na}$ in the range of 0.22–0.75, meaning that Au was preferentially partitioned into the brine, but to a smaller extent than Na. Frank et al. (2011; 800 °C, 100 MPa, NNO) found a similar $K^{b/v}_{Au,Na}$ in the range of 0.12–1.65 in a S-bearing system. At sub-magmatic temperatures, the density model of Pokrovski et al. (2005) predicts the preferential partitioning of Au into the brine phase, but to a relatively smaller extent compared to that of Na, which is consistent with the above experiments at magmatic temperatures. However, Pokrovski et al. (2008; 450 °C, 39–41 MPa) noted that Au partitioning greatly increases towards the vapor phase in the presence of reduced S-species in acidic systems. This is consistent with the preferential partitioning of Au into the vapor phase as determined by LA–ICPMS analysis of co-existing brine and vapor inclusions in natural samples from porphyry-type ore deposits (Heinrich et al. 1999; Ulrich et al. 1999).

Molybdenum. Existing data on the effect of Cl on $D^{f/m}_{Mo}$ and on Mo solubilities in hydrothermal fluids is somewhat controversial. Experimental studies directly investigating the fluid/melt partitioning of Mo have concluded that the concentration of Cl in the fluid either does not affect or even reduces $D^{f/m}_{Mo}$ (Candela and Holland 1984; Keppler and Wyllie 1991). A similar observation was made by Zajacz et al. (2008) by analyzing coexisting fluid and melt inclusions in miarolitic quartz. Candela and Holland (1984) defined $D^{f/m}_{Mo} = 2.5 \pm 1.6$ independent of C^{fluid}_{Cl}, whereas the HCl-bearing experiments of Keppler and Wyllie (1991) yielded $D^{f/m}_{Mo} = 1.8 \pm 0.8$ as opposed to $D^{f/m}_{Mo}$ = 5.5 in the chloride-free experiment. The data derived from natural samples by Zajacz et al. (2008, $D^{f/m}_{Mo} = 2-24$) and by Audétat (2010, $D^{f/m}_{Mo} = 17-20$) are in general somewhat higher but broadly consistent with the experimental values. On the other hand, experimental studies on the solubility of MoO_2 and MoS_2 in high-T hydrothermal fluids observed increasing dissolved Mo with increasing C^{fluid}_{NaCl} and C^{fluid}_{HCl}. In the case of S-free systems, the positive effect of chloride concentrations were either explained by the effect of Na (present as NaCl) leading to the formation of Na_2MoO_4 or $NaHMoO_4$ complexes (Cao 1989; Ulrich and Mavrogenes 2008), or by the direct effect of Cl leading to the formation of Mo oxo-chloride complexes of the form MoO_2Cl_2 or $MoO_2(OH)Cl$ (Rempel et al. 2008; Ulrich and Mavrogenes 2008). A positive effect of C^{fluid}_{NaCl} on $D^{f/m}_{Mo}$ was also identified in S-bearing systems, and was attributed to the formation of a Na-bearing thiomolybdate complex of the form $NaHMoO_2S_2$ (Zhang et al. 2012b).

In systems with two-phase aqueous fluids, Mo always strongly partitions into the brine phase to a similar or greater extent than Na does (Heinrich et al. 1999; Ulrich et al. 1999; Audétat and Pettke 2003; Audétat 2010). This is consistent with the formation of Na molybdate or Mo-oxo-chloride type complexes in the brine.

Tungsten and Sn. Experimental studies on the effect of fluid chlorinity on $D^{f/m}_{W}$ yielded controversial results. Manning and Henderson (1984) investigated the partitioning of W between haplogranitic melts and various aqueous fluids at

800 °C and 100 MPa. They identified a strong positive correlation between $D_W^{f/m}$ and m_{Cl}^{f} with $D_W^{f/m}$ increasing from 1.5 to 6.7 as m_{Cl}^{f} changed from 0.5 to 3.4. Unfortunately, all the Cl concentration series experiments fell into the two phase field in the salt–H_2O system. Therefore, the quench fluid compositions represent the average composition of vapor and brine, and the observed increasing $D_W^{f/m}$ only reflect the preferential partitioning of W into the brine phase relative to the vapor. Keppler and Wyllie (1991) observed the opposing effect of fluid chlorinity on $D_W^{f/m}$ at 750 °C and 200 MPa. Here $D_W^{f/m}$ dropped rapidly with increasing HCl from 3.5 ± 0.9 at m_{Cl}^{f} = 0 to 0.81 at m_{Cl}^{f} = 2 in equilibrium with haplogranitic melts. The apparent contradiction between the above two studies could possibly be resolved by the fact that Keppler and Wyllie (1991) loaded Cl in the form of HCl into the capsule, whereas Manning and Henderson (1984) used NaCl. Bai and Koster van Groos (1999) used both NaCl and HCl-bearing starting solutions at 750 °C and 200 MPa. Including data at m_{HCl}^{f}= 0, $D_W^{f/m}$ showed no correlation with m_{Cl}^{f} when an HCl solution was loaded into the capsule. Furthermore, it showed a negative correlation with m_{Cl}^{f} when NaCl solution was loaded into the capsules as opposed to that seen by Manning and Henderson (1984). Overall, the above experimental data can be considered inconclusive regarding the effect of dissolved chlorides on $D_W^{f/m}$. However, Zajacz et al. (2008) identified a general positive correlation between $D_W^{f/m}$ and the concentration of Cl in the fluid phase by analysis of the composition of co-existing granitic melt and aqueous fluid inclusions. They defined the following relationship: $D_W^{f/m} = -4.9 + 5.4\ {}^{*}m_{Cl}^{*fluid}$ for ${}^{*}m_{Cl}^{*fluid} < 3$ Tungsten shows a preferential partitioning into the brine phase relative to the vapor to the same extent as Na at near magmatic temperatures (Audétat et al. 1998; Heinrich et al. 1999; Zajacz et al. 2008), which is also consistent with chloride complexation of W. All in all, it seems likely that fluid chlorinity has a significant positive impact on W extraction from magmas. However, the details of the interaction between W and chloride ligands and the identity of the dominant complexes are yet to be determined.

The experimental study of Sn partitioning has been hampered by rapid alloying between Sn and most noble metals commonly used as capsule material for hydrothermal experiments. Nevertheless, most fluid/melt partitioning studies found a positive correlation between fluid chlorinity and $D_{Sn}^{f/m}$ (Nekrasov et al. 1980; Keppler and Wyllie 1991; Hu et al. 2008). Nekrasov et al. (1980, 850 °C and 100 MPa) found that fO_2 very significantly affects $D_{Sn}^{f/m}$, including systems with chloride bearing fluids. Candela and Piccoli (1995) recast the results of Keppler and Wyllie (1991) and Nekrasov et al. (1980) into $K_{Sn,Na}^{f/m}$ assuming that Sn dissolved in

the aqueous fluid as an $SnCl_2$ complex. At fO_2 = NNO, the experiments of Keppler and Wyllie (1991) and Nekrasov et al. (1980) yield $K^{f/m}_{Sn,Na}$= 0.3 and 0.7, respectively indicating that Sn only moderately partitions into the fluid phase. However, at the more reducing W-WO_2 buffer, Nekrasov et al. (1980) determined $K^{f/m}_{Sn,Na}\approx 8$. This difference could be attributed to the effect of fO_2, which induced a change in the oxidation state of Sn in the silicate melt and potentially in the fluid phase as well (Linnen et al. 1995; Bhalla et al. 2005; Farges et al. 2006c). Hu et al. (2008, 800 °C, 100 MPa), however, found that at relatively high fO_2 (NNO) that $D^{f/m}_{Sn}$ increased from $7.4 \pm 0.9{\cdot}10^{-4}$ to as high as 50 ± 6 while M_{HCl} in the starting solution of their experiments were raised from 0.01 to 4. Though the reported data does not allow for the estimation of NaCl/HCl ratios in the fluid phase during the experiment, a minimum range of 6–50 can be derived for $K^{f/m}_{Sn,Na}$ from this set of experiments assuming that all HCl is converted to NaCl in the fluid by H–Na exchange between the melt and fluid. These values are much higher than those determined by Keppler and Wyllie (1991) and Nekrasov et al. (1980) at similar P and T and melt compositions. Tin is more soluable in silicate melts in 2+ than in 4 + oxidation state (Linnen 1995, 1996), but one would expect Sn^{2+} form stronger chloride complexes relative to Sn^{4+} based on the similar electronic structure of Sn^{2+} and Pb^{2+}. Therefore, the net effect of fO_2 on $D^{f/m}_{Sn}$ is hard to predict, and the inconsistency between the above studies is challenging to interpret as a function of fO_2. Duc-Tin et al. (2007) studied the solubility of cassiterite in aqueous NaCl- and HCl-bearing fluids with a technique that eliminated complications caused by diffusive loss of Sn to the noble metal capsule. They found that NaCl, and in particular HCl, had a strong positive effect on the solubility of cassiterite in aqueous fluids. These solubility data were combined with previous data on cassiterite solubilities in granitic melts. Model $D^{f/m}_{Sn}$ values in the range 0.1–4.0 were proposed for natural systems with moderately saline fluids. These values are higher than those of Keppler and Wyllie (1991) and Nekrasov et al. (1980) at fO_2 = NNO, but compare well with those determined by the analysis of co-existing fluid and melt inclusions in quartz (Audétat and Pettke 2003; Zajacz et al. 2008). In systems with two phase fluids at magmatic or near magmatic temperatures, Sn always preferentially partitions into the brine phase over the vapor phase to the approximated same extent as Na (Audétat et al. 1998; Heinrich et al. 1999; Audétat and Pettke 2003). The evidence seems conclusive that Cl plays an important role in the extraction of Sn into aqueous magmatic fluids. However, $D^{f/m}_{Sn}$ is low enough for most geologically relevant conditions to allow for the enrichment of Sn in highly fractionated felsic melts as evidenced by the composition of silicate melt inclusions in quartz from plutonic settings (Thomas and Webster 2000; Audétat and Pettke 2003; Rickers et al. 2006; Zajacz et al. 2008).

7.5.3 The Partitioning of Br and I

To our knowledge, only the study of Bureau et al. (2000) has addressed directly the partitioning of Br and I between silicate melts and magmatic fluids. This study used an albite melt composition and dilute fluids ($m_{Cl} < 0.2$) at $T = 900$ °C and $P = 200$ MPa. They determined the following fluid/melt partition coefficients: $D_{Cl}^{f/m} = 8.1 \pm 0.2$; $D_{Br}^{f/m} = 17.5 \pm 0.6$; and $D_{I}^{f/m} = 104 \pm 7$. The natural logarithm of the fluid/melt partition coefficients for these elements were shown to have an excellent positive linear correlation with the ionic radii of the respective anions. In addition, Bureau and Metrich (2003) investigated the "bromide solubility" in silicate melts as a function of melt composition and pressure. They found that Br shows similar systematics to Cl, including the solubility minimum at metaluminous compositions relative to peraluminous and peralkaline melts, as well as a negative pressure dependence.

7.6 Implications for Future Research

The behavior of halogens in silicic magmas, and their hydrothermal systems, has been supported by tremendous amount of experimental work including phase equilibria and element partitioning and has been connected with significant advances in analytical and modeling methodology. These studies have substantially improved our understanding of the solubility and partitioning behavior of halogens during magma evolution, their effect on the structure and physical properties of silicate melts, late-magmatic phase equilibria, and the mobility of ore forming elements in the magmatic-hydrothermal environment. This emerging knowledge has direct implications for the development of genetic ore deposit models, which aid exploration for mineral resources, mechanisms of global element cycling, or impact assessment of magmatic events.

Halogens, mainly F and Cl due to their larger global abundances, play substantially different roles in magmatic and hydrothermal processes, which simply reflect variations in their ionic radius and a concomitant effect on their hardness. Fluorine is highly soluble in silicate melts, which allows for strong control on melt rheology and transport properties, protracted magmatic differentiation due to the presence of additional major component, and liquidus depression. The small ionic radius of F is responsible for large lattice energies, hence greater stabilities of fluoride minerals (in contrast to other halides), which are as a result more refractory and less soluble in aqueous fluids. The fluoride–H_2O systems thus more frequently exhibit large miscibility gaps, where F-poor aqueous fluids and molten fluorides separate. The existence and occurrence of immiscible fluoride melts may represent an intervening step during magmatic-hydrothermal evolution of F-bearing magmas, and it poses a considerable interpretation challenge. Experimental data suggest a

rather complex extent of the liquid–liquid immiscibility from simple high-temperature systems to multicomponent, often Li-bearing compositions, at temperatures relevant to the final stages of magma evolution. Studies of phase equilibria are prone to metastabilities related to crystal nucleation and sluggish kinetics in peraluminous systems that rapidly change in alkali- and volatile-rich systems obscured by quench and preservation difficulties. Although no coherent view of the fluoride-silicate liquid–liquid immiscibility exists yet, recent advances in quasichemical modeling of multicomponent molten silicate-halide systems, and applications of solution thermodynamics to molten salt–H_2O mixtures at elevated temperatures, may provide important, self-consistent constraints in the future (Wang et al. 2010, 2013; Lambotte and Chartrand 2013a, b; Chartrand et al. 2014).

Partitioning of major, minor and trace elements between silicate melts and halogen-bearing liquids (melts and aqueous fluids) is critical for understanding the roles these media play in element transport and decoupling during silicate melt-molten salt (brine) or silicate melt-aqueous fluid fractionation. Element partitioning in F-bearing systems is very little known (Gramenitskiy et al. 2005; Veksler et al. 2012), although a number of peculiar geochemical enrichment or decoupling patterns, including the lanthanide tetrad effect, were observed in natural magmatic suites (Peretyazhko et al. 2007; Peretyazhko and Savina 2010; Vasyukova and Williams-Jones 2014). These natural observations have provided impetus for the development of new experimental, frequently in situ techniques or atomistic simulations, which address phase equilibria, structure-property relations, and chemical speciation in halogen-bearing fluids (e.g., Wilke et al. 2013; Louvel et al. 2014; Migdisov and Williams-Jones 2014; Jahn et al. 2015; Timofeev et al. 2015), and start to define new constraints on the solubility and speciation of high-field strength and REE as important petrogenetic tracers in natural systems.

Transport of numerous ore-forming elements from magmas into exsolving aqueous fluids, which are in turn major contributors to the metal budget of magmatic-hydrothermal systems, is fundamentally controlled by Cl. The partitioning and deposition are facilitated by metal-chloride complexing, but also by indirect effects where chloride species constrain hydrothermal alteration styles and reactions or, as a co-solvent, control the hydrodynamics of fluid flow. In the future, additional studies will be required to better link the effects of silicate melt composition, pressure, and temperature on Cl partitioning between the melts and aqueous fluids, possibly in the form of a comprehensive thermodynamic model. Furthermore, our understanding of the Cl speciation in magmatic fluids needs to be extended along additional compositional vectors, as most of our knowledge is now limited to haplogranitic melts, predominantly of metaluminous or peraluminous composition. A particularly important variable to constrain is the HCl/total chloride ratio, which is expected to have the greatest impact on economic metal solubilities and hydrothermal alteration styles. Previous experimental data on this critical variable is rather limited in pressure-temperature-composition space, as is the partitioning of other major elements, such as Fe and Ca, despite their significant concentrations in magmatic fluid inclusions. In addition, these elements may limit transfer of S to lower-temperature hydrothermal environments due to Fe sulfide and

anhydrite precipitation, or may significantly modify the nature of the brine-vapor solvus in the multicomponent chloride–H_2O system (Zhang and Frantz 1989; Shmulovich and Graham 2004; Lecumberri-Sanchez et al. 2015; Steele-MacInnis et al. 2015). Additional complexities arise from the presence of dissolved volatile species with low dipole moments, such as CO_2 and probably H_2S, the effect of which on vapor-brine immiscibility and Cl partitioning is even less constrained. Emerging research opportunities are expected to provide new avenues towards the relative stabilities of chloride and various sulfur-bearing, hydroxide, and/or alkali metal-bearing oxycomplexes of numerous relevant elements (e.g., Cu, Au, Mo, Sn) in pressure-temperature-composition space.

Acknowledgements Preparation of this contribution was financially supported by the Czech Science Foundation Project Nr. P210/12/0986 (to D.D.) and by a Discovery Grant from the Natural Sciences and Engineering Research Council of Canada (to Z.Z.). Reviews by Hans Keppler, David London, and Jake Lowerstern, coupled with editoral work by Daniel Harlov and Leonid Aranovich, helped to improve the manuscript over all.

References

Abdel-Rahman AFM, El-Kibbi MM (2001) Anorogenic magmatism: chemical evolution of the Mount El-Sibai A-type complex (Egypt), and implications for the origin of within-plate felsic magmas. Geol Mag 138:67–85

Adamczak RL, Mattern JA, Tieckelmann H (1959) A partial phase study of the system NaF–HF. J Phys Chem 63:2063–2065

Agangi A, Kamenetsky VS, McPhie J (2012) Evolution and emplacement of high fluorine rhyolites in the Mesoproterozoic Gawler silicic large igneous province, South Australia. Precambr Res 208:124–144

Akinfiev NN, Zotov AV (2010) Thermodynamic description of aqueous species in the system Cu–Ag–Au–S–O–H at temperatures of 0–600 °C and pressures of 1–3000 bar. Geochem Int 48:714–720

Aksyuk AM, Zhukovskaya TN (1998) The solubility of quartz in aqueous solutions of hydrofluoric acid at temperatures 500–1,000 °C and pressures 100–500 MPa. Dokl Earth Sci 361:745–748

Alletti M, Baker DR, Scaillet B, Aiuppa A, Moretti R, Ottolini L (2009) Chlorine partitioning between a basaltic melt and H_2O–CO_2 fluids at Mount Etna. Chem Geol 263:37–50

Anderko A, Pitzer KS (1993a) Equation of state representation of phase equilibria and volumetric properties of the system NaCl–H_2O above 573 K. Geochim Cosmochim Acta 57:1657–1680

Anderko A, Pitzer KS (1993b) Phase-equilibria and volumetric properties of the systems KCl–H_2O and NaCl–KCl–H_2O above 573 K—Equation of State representation. Geochim Cosmochim Acta 57:4885–4897

Anderson AJ, Clark AH, Gray S (2001) The occurrence and origin of zabuyelite (Li_2CO_3) in spodumene-hosted fluid inclusions: implications for the internal evolution of rare-element granitic pegmatites. Can Mineral 39:1513–1527

Anfilogov VN, Glyuk DS, Trufanova LG (1973) Phase relations in interaction between granite and sodium fluoride at water vapor pressure of 1000 kg/cm^2. Geochem Int 10(1):30–33

Anfilogov VN, Bragina GI, Bobylev IB, Zyuzeva NA (1979) Structural position of fluorine and chlorine in a silicate melt. Geochem Int 16:17–22

Anovitz LM, Hemmingway BS, Westrum EF Jr, Metz GW, Essene EJ (1987) Heat capacity measurements for cryolite (Na_3AlF_6) and reactions in the system Na–Fe–Al–Si–O–F. Geochim Cosmochim Acta 51:3087–3103

Antignano A, Manning CE (2008) Rutile solubility in H_2O, H_2O–SiO_2, and H_2O–$NaAlSi_3O_8$ fluids at 0.7–2.0 GPa and 700–1000 °C: implications for mobility of nominally insoluble elements. Chem Geol 255:283–293

Antipin VS, Savina EA, Mitichkin MA, Perelyaev VI (1999) Rare-metal lithium-fluorine granites, ongonites and topazites of the Southern Baikal region. Petrology 7:147–159

Aranovich LY, Newton RC (1996) H_2O activity in concentrated NaCl solutions at high pressures and temperatures measured by the brucite–periclase equilibrium. Contrib Mineral Petrol 125:200–212

Aranovich LY, Newton RC (1997) H_2O activity in concentrated KCl and KCl–NaCl solutions at high temperatures and pressures measured by the brucite–periclase equilibrium. Contrib Mineral Petrol 127:261–271

Aranovich LY, Zakirov IV, Sretenskaya NG, Gerya TV (2010) Ternary system H_2O–CO_2–NaCl at high T-P parameters: an empirical mixing model. Geochem Int 48:446–455

Aranovich LY, Newton RC, Manning CE (2013) Brine-assisted anatexis: experimental melting in the system haplogranite–H_2O–NaCl–KCl at deep-crustal conditions. Earth Planet Sci Lett 374:111–120

Aseri AA, Linnen RL, Dong Che X, Thibault Y, Holtz F (2015) Effects of fluorine on the solubilities of Nb, Ta, Zr and Hf minerals in highly fluxed water-saturated haplogranitic melts. Ore Geol Rev 64:736–746

Audétat A (2010) Source and evolution of molybdenum in the porphyry Mo(-Nb) deposit at Cave Peak, Texas. J Petrol 51:1739–1760

Audétat A, Pettke T (2003) The magmatic-hydrothermal evolution of two barren granites: a melt and fluid inclusion study of the Rito del Medio and Canada Pinabete plutons in northern New Mexico (USA). Geochim Cosmochim Acta 67:97–121

Audétat A, Gunther D, Heinrich CA (1998) Formation of a magmatic-hydrothermal ore deposit: insights with LA-ICP-MS analysis of fluid inclusions. Science 279:2091–2094

Audétat A, Gunther D, Heinrich CA (2000) Magmatic-hydrothermal evolution in a fractionating granite: a microchemical study of the Sn-W-F-mineralized Mole Granite (Australia). Geochim Cosmochim Acta 64:3373–3393

Audétat A, Pettke T, Heinrich CA, Bodnar RJ (2008) The composition of magmatic-hydrothermal fluids in barren and mineralized intrusions. Econ Geol 103:877–908

Bacon CR, Newman S, Stolper E (1992) H_2O, CO_2, Cl, and F in melt inclusions in phenocrysts from 3 holocene explosive eruptions, Crater Lake, Oregon. Am Mineral 77:1021–1030

Badanina EV, Veksler IV, Thomas R, Syritso LF, Trumbull RB (2004) Magmatic evolution of Li-F, rare-metal granites: a case study of melt inclusions in the Khangilay complex, Eastern Transbaikalia (Russia). Chem Geol 210:113–133

Badanina EV, Trumbull RB, Dulski P, Wiedenbeck M, Veksler IV, Syritso LF (2006) The behavior of rare-earth and lithophile trace elements in rare-metal granites: a study of fluorite, melt inclusions, and host rocks from the Khangilay complex, Transbaikalia, Russia. Can Mineral 44:667–692

Bai TB, Koster van Groos AF (1999) The distribution of Na, K, Rb, Sr, Al, Ge, Cu, W, Mo, La, and Ce between granitic melts and coexisting aqueous fluids. Geochim Cosmochim Acta 63:1117–1131

Bailey JC (1980) Formation of cryolite and other aluminofluorides: a petrological review. Bull Geol Soc Denmark 29:1–45

Baker DR, Alletti M (2012) Fluid saturation and volatile partitioning between melts and hydrous fluids in crustal magmatic systems: the contribution of experimental measurements and solubility models. Earth-Sci Rev 114:298–324

Baker DR, Conte AM, Freda C, Ottolini L (2002) The effect of halogens on Zr diffusion and zircon dissolution in hydrous metaluminous granitic melts. Contrib Mineral Petrol 142:666–678

Balcone-Boissard H, Villemant B, Boudon G, Michel A (2008) Non-volatile vs. volatile behaviours of halogens during the AD 79 Plinian eurption of Mt. Vesuvius, Italy. Earth Planet Sci Lett 269:66–79

Balcone-Boissard H, Villemant B, Boudon G (2010) Behavior of halogens during the degassing of felsic magmas. Geochem Geophys Geosyst 11:Q00905

Bali E, Audétat A, Keppler H (2011) The mobility of U and Th in subduction zone fluids: an indicator of oxygen fugacity and fluid salinity. Contrib Mineral Petrol 161:597–613

Bali E, Keppler H, Audétat A (2012) The mobility of W and Mo in subduction zone fluids and the Mo–W–Th–U systematics of island arc magmas. Earth Planet Sci Lett 351:195–207

Barclay J, Carroll MR, Houghton BF, Wilson CJN (1996) Pre-eruptive volatile content and degassing history of an evolving peralkaline volcano. J Volcan Geotherm Res 74:75–87

Barnes HL (ed) (1997) Geochemistry of hydrothermal ore deposits, 3rd edn. Wiley, New York, p 992

Barsukov VL, Durasova NA, Kovalenko NI, Ryabchikov ID, Ryzhenko BN (1987) Oxygen fugacity and tin behavior in metals and fluids. Geol Zb 38:723–733

Bartels A, Holtz F, Linnen RL (2010) Solubility of manganotantalite and manganocolumbite in pegmatitic melts. Am Mineral 95:537–544

Barton MD (1982) The thermodynamic properties of topaz solid solutions and some petrologic applications. Am Mineral 67:956–974

Barton MD (1996) Granitic magmatism and metallogeny of southwestern North America. Geol Soc Am Spec Pap 315:261–280

Barton MD, Frantz JD (1983) Exchange equilibria of alkali feldspars with fluoride-bearing fluids. Carnegie Inst Wash Yearb 82:377–381

Barton MD, Iichik RP, Marikos MA (1991) Metasomatism. Rev Mineral 26:321–349

Bau M (1996) Controls on the fractionation of isovalent trace elements in magmatic and aqueous systems: evidence from Y/Ho, Zr/Hf and lanthanide tetrad effect. Contrib Mineral Petrol 123:323–333

Benning LG, Seward TM (1996) Hydrosulphide complexing of Au(I) in hydrothermal solutions from 150–400 °C and 500–1500 bar. Geochim Cosmochim Acta 60:1849–1871

Beus AA, Zalashkova NY (1964) Post-magmatic high temperature metasomatic processes in granitic rocks. Int Geol Rev 6:668–681

Bhalla P, Holtz F, Linnen RL, Behrens H (2005) Solubility of cassiterite in evolved granitic melts: effect of T, fO_2, and additional volatiles. Lithos 80:387–400

Birch WD (1984) Quartz-topaz-loellingite rocks near Eldorado, Victoria. Aust J Earth Sci 31:269–278

Bodnar RJ, Burnham CW, Sterner SM (1985) Synthetic fluid inclusions in natural quartz. III. Determination of phase equilibrium properties in the system H_2O–NaCl to 1000 °C and 1500 bars. Geochim Cosmochim Acta 49:1861–1873

Bohlen SR, Essene EJ (1978) The significance of metamorphic fluorite in the Adirondacks. Geochim Cosmochim Acta 42:1669–1678

Borodin LS (2004) Model system of petrochemical and metallogenic trends of granitoids as a basis for the prognosis of Sn, Li, Ta, Nb, W, Mo, and Cu deposits. Geol Ore Depos 46:3–26

Borodulin GP, Chevychelov VY, Zaraisky GP (2009) Experimental study of partitioning of Ta, Nb, Mn, and F between aqueous fluoride fluid and granitic and alkaline melts. Dokl Earth Sci 427:868–873

Botcharnikov RE, Behrens H, Holtz F, Koepke J, Sato H (2004) Sulfur and chlorine solubility in Mt. Unzen rhyodacitic melt at 850 °C and 200 MPa. Chem Geol 213:207–225

Botcharnikov RE, Holtz F, Behrens H (2007) The effect of CO_2 on the solubility of H_2O–Cl fluids in andesitic melt. Eur J Mineral 19:671–680

Bragina GI, Anfilogov VN (1980) Phase relations and unmixing in the Na_2O–Al_2O_3–SiO_2–NaF system. Geochem Int 17:71–75

Breiter K, Förster HJ, Seltmann R (1999) Variscan silicic magmatism and related tin–tungsten mineralization in the Erzgebirge-Slavkovský les metallogenic province. Mineral Depos 34:505–521

Brooker RA, Kohn SC, Holloway JR, McMillan PF (2001) Structural controls on the solubility of CO_2 in silicate melts. Part II: IR characteristics of carbonate groups in silicate glasses. Chem Geol 174:241–254

Brown ID (1981) The bond-valence method: an empirical approach to chemical structure and bonding. In: O'Keefe M, Navrotsky A (eds) Structure and bonding in crystals, vol II. Acad Press, New York, pp 1–30

Brown ID (1988) What factors determine cation coordination numbers? Acta Crystall B44:545–553

Brown ID (1992) Chemical and steric constraints in inorganic solids. Acta Crystall B48:553–572

Brown ID (2000) The bond valence model as a tool for teaching inorganic chemistry: the ionic model revisited. J Chem Educ 77:1070–1075

Brown ID, Skowron A (1990) Electronegativity and Lewis acid strength. J Am Chem Soc 112:3401–3403

Buddington AF, Leonard BF (1962) Regional geology of the St. Lawrence County magnetite district, Northwest Adirondacks, New York. US Geol Surv Prof Pap 376:1–145

Bukhalova GA, Mal'tsev VT (1965) The K, Na || AlF_6. Russ J Inorg Chem 10:100–102

Bureau H, Keppler H (1999) Complete miscibility between silicate melts and hydrous fluids in the upper mantle: experimental evidence and geochemical implications. Earth Planet Sci Lett 165:187–196

Bureau H, Metrich N (2003) An experimental study of bromine behaviour in water-saturated silicic melts. Geochim Cosmochim Acta 67:1689–1697

Bureau H, Keppler H, Metrich N (2000) Volcanic degassing of bromine and iodine: experimental fluid/melt partitioning data and applications to stratospheric chemistry. Earth Planet Sci Lett 183:51–60

Burt DM (1972) The influence of fluorine on the facies of Ca–Fe–Si skarns. Carnegie Inst Wash Yearb 71:443–449

Burt DM (1974) Concepts of acidity and basicity in petrology—the exchange operator approach. Geol Soc Am Abstr Progr 6:674–676

Cady GH (1934) Freezing points and vapor pressures of the system potassium fluoride-hydrogen fluoride. J Am Chem Soc 56:1431–1434

Candela PA (1990) Theoretical constraints on the chemistry of the magmatic aqueous phase. In: Stein HJ, Hannah JL (eds) Ore-bearing granite systems; petrogenesis and mineralizing processes. Geol Soc Am Spec Pap 246:11–19

Candela PA, Holland HD (1984) The partitioning of copper and molybdenum between silicate melts and aqueous fluids. Geochim Cosmochim Acta 48:373–380

Candela PA, Piccoli PM (1995) Model ore-metal partitioning from melts into vapor and vapor/brine mixtures. In: Thompson JFH (ed) Model ore-metal partitioning from melts into vapor and vapor/brine mixtures in magmas, fluids and ore deposits. Min Assoc Can Short Course 23:101–127

Cao X (1989) Solubility of molybdenite and the transport of molybdenum in hydrothermal solutions. Doctoral dissertation, Iowa State University, p 103

Carroll M, Holloway JR (eds) (1994) Volatiles in magmas. Rev Mineral 30:517

Carroll M, Webster JD (1994) Solubilities of sulfur, noble gases, nitrogen, chlorine, and fluorine in magmas. Rev Mineral 30:231–279

Castro A, Patiño-Douce AE, Corretgé LG, de la Rosa JD, El-Biad M, El-Hmidi H (1999) Origin of peraluminous granites and granodiorites, Iberian massif, Spain: an experimental test of granite petrogenesis. Contrib Mineral Petrol 135:255–276

Cathelineau M (1986) The hydrothermal alkali metasomatism effects on granitic rocks: quartz dissolution and related subsolidus changes. J Petrol 27:945–965

Černý P (1991) Rare-element pegmatites: I. Anatomy and internal evolution of pegmatite deposits. Geosci Can 18:49–67

Černý P (1992) Geochemical and petrogenetic features of mineralization in rare element granitic pegmatites in the light of current research. Appl Geochem 7:393–416

Černý P (1998) Magmatic vs. metamorphic derivation of rare-element granitic pegmatites. Krystalinikum 24:7–36

Charoy B, Pollard PJ (1989) Albite-rich, silica-depleted metasomatic rocks at Emuford, northeast Queensland: mineralogical, geochemical, and fluid inclusion contraints on hydrothermal evolution and tin mineralization. Econ Geol 84:1850–1874

Charoy B, Raimbault L (1994) Zr-, Th-, and REE-rich biotite differentiates in the A-type granite pluton of Suzhou (eastern China): the key role of fluorine. J Petrol 35:919–962

Chartrand P, Pelton AD (2001) Thermodynamic evaluation and optimization of the Li, Na, K, Mg, Ca//F, Cl reciprocal system using the modified quasi-chemical model. Met Mater Trans 32A:1417–1430

Chartrand P, Gemme F, Robelin C (2014) A thermodynamic model for the NH_4^+, $K^+//H_2PO_4^-$, $H_2P_2O_7^-$, NO_3^-, Cl^-–H_2O system. Proc Eng 83C:250–258

Che XD, Linnen RL, Wang RC, Aseri A, Thibault Y (2013) Tungsten solubility in evolved granitic melts: an evaluation of magmatic wolframite. Geochim Cosmochim Acta 106:84–98

Chevychelov VY, Zaraiskii GP, Borisovskii SE, Borkov DA (2005) Effect of melt composition and temperature on the partitioning of Ta, Nb, Mn, and F between a granitic (alkaline) melt and fluorine-bearing aqueous fluid: fractionation of Ta and Nb and conditions of ore formation in rare-metal granites. Petrologiya 13:339–357

Chevychelov VY, Botcharnikov RE, Holtz F (2008) Experimental study of fluorine and chlorine contents in mica (biotite) and their partitioning between mica, phonolite melt, and fluid. Geochem Int 46:1081–1089

Chou IM (1987) Phase relation in the system NaCl–KCl–H_2O. III. Solubilities of halite in vapor-saturated liquids above 445 °C and redetermination of phase equilibrium properties in the system NaCl–H_2O to 1000 °C and 1500 bars. Geochim Cosmochim Acta 51:1965–1975

Chou IM, Sterner SM, Pitzer KS (1992) Phase relations in the system NaCl–KCl–H_2O IV. Differential thermal analysis of the sylvite liquidus in the KCl–H_2O binary, the liquidus in the NaCl–KCl–H_2O ternary, and the solidus in the NaCl–KCl binary to 2 kb pressure, and a summary of experimental data for thermodynamic PTX analysis of solid-liquid equilibria at elevated P-T conditions. Geochim Cosmochim Acta 56:2281–2293

Christiansen EH, Bikun JV, Sheridan MF, Burt DM (1984) Geochemical evolution of topaz rhyolites from the Thomas Range and Spor Mountain, Utah. Am Mineral 69:223–236

Clarke DB (1992) Granitoid rocks. Chapman & Hall, London, p 283

Clarke DB, Wunder B, Förster HJ, Rhede D, Hahn A (2009) Experimental investigation of near-liquidus andalusite-topaz relations in synthetic peraluminous haplogranites at 200 MPa. Mineral Mag 73:997–1007

Danckwerth PA (1981) Phase relations in the system Na_2O–Al_2O_3–SiO_2–H_2O–HF at 15 kbar. Carnegie Inst Wash Yearb 80:350–352

De Capitani C, Brown TH (1987) The computation of chemical equilibrium in complex systems containing non-ideal solutions. Geochim Cosmochim Acta 51:2639–2652

Dergachev VB (1990) Rare-metal ongonites and elvanites and their possible analogues in southwestern England. Russ Geol Geophys 31:69–73

Dergachev VB (1992) Classification of rare-metal rocks of the ongonite group. Russ Geol Geophys 33:89–96

Devyatykh GG, Pryakhin DA, Bulanov AB, Balabanov VV (1999) Phase diagram of silicon tetrafluoride. Dokl Chem 364:4–5

Dilles JH, Einaudi MT (1992) Wall-rock alteration and hydrothermal flow paths about the Ann-Mason porphyry copper deposit, Nevada. A 6-km vertical reconstruction. Econ Geol 87:1963–2001

Dingwell DB (1985) The structure and properties of fluorine-rich silicate melts: implications for granite petrogenesis. In: Taylor RP, Strong DF (eds) Granite-related mineral deposits: geology, petrogenesis and tectonic setting. Canadian Institute of Mining, Metallurgy and Petroleum, Halifax, pp 72–81

Dingwell DB, Hess KU, Knoche R (1996) Granite and granitic pegmatite melts: volumes and viscosities. Trans R Soc Edinb Earth Sci 87:65–72

Dingwell DB, Holtz F, Behrens H (1997) The solubility of H_2O in peralkaline and peraluminous granitic melts. Am Mineral 82:434–437

Dolejš D (2004) Thermodynamics and phase equilibria of the silicate-fluoride-H_2O systems: implications for fluorine-bearing granites. Ph.D. dissertation, McGill University, Montreal, p 358

Dolejš D (2006) Quartz solubility in fluorine-bearing aqueous fluids. Bay Geoinst Ann Rep 2005:84–86

Dolejš D (2007) Thermodynamic model of chlorine in silicic melts: a quantitative approach to magmatic devolatilization. Bay Geoinst Ann Rep 2006:112–116

Dolejš D (2014) Si-F complexing in aqueous fluids: experimental study and implications for transport of immobile elements. Geophys Res Abstr 16:EGU2014-7221

Dolejš D, Baker DR (2004) Thermodynamic analysis of the system Na_2O–K_2O–CaO–Al_2O_3–SiO_2–H_2O–F_2O_{-1}: stability of fluorine-bearing minerals in felsic igneous suites. Contrib Mineral Petrol 146:762–778

Dolejš D, Baker DR (2005) Thermodynamic modeling of melts in the system Na_2O–$NaAlO_2$–SiO_2–F_2O_{-1}. Geochim Cosmochim Acta 69:5537–5556

Dolejš D, Baker DR (2006a) Phase transitions and volumetric properties of cryolite, Na_3AlF_6: differential thermal analysis to 100 MPa. Am Mineral 91:97–103

Dolejš D, Baker DR (2006b) Fluorite solubility in hydrous haplogranitic melts at 100 MPa. Chem Geol 225:40–60

Dolejš D, Baker DR (2007a) Liquidus equilibria in the system K_2O–Na_2O–Al_2O_3–SiO_2–F_2O_{-1}–H_2O to 100 MPa: I. Silicate-fluoride liquid immiscibility in anhydrous systems. J Petrol 48:785–806

Dolejš D, Baker DR (2007b) Liquidus equilibria in the system K_2O–Na_2O–Al_2O_3–SiO_2–F_2O_{-1}–H_2O to 100 MPa: II. Differentiation paths of fluorosilicic magmas in hydrous systems. J Petrol 48:807–828

Dolejš D, Manning CE (2010) Thermodynamic model for mineral solubility in aqueous fluids: theory, calibration and application to model fluid-flow systems. Geofluids 10:20–40

Dolejš D, Štemprok M (2001) Magmatic and hydrothermal evolution of Li-F granites: Cínovec and Krásno intrusions, Krušné hory batholith, Czech Republic. Bull Czech Geol Surv 76:77–99

Driesner T (2007) The system H_2O-NaCl. Part II: correlations for molar volume, enthalpy, and isobaric heat capacity from 0 to 1000 °C, 1 to 5000 bar, and 0 to 1 X-NaCl. Geochim Cosmochim Acta 71:4902–4919

Driesner T, Heinrich CA (2007) The system H_2O-NaCl. Part I: correlation formulae for phase relations in temperature-pressure-composition space from 0 to 1000 °C, 0 to 5000 bar, and 0 to 1 X-NaCl. Geochim Cosmochim Acta 71:4880–4901

Du S, Huang Y (1985) Hisanghuagite—a new type of magmatic rocks. Scient Sin B 28:537–546

Duc-Tin Q, Audétat A, Keppler H (2007) Solubility of tin in (Cl, F)-bearing aqueous fluids at 700 °C, 140 MPa: a LA-ICP-MS study on synthetic fluid inclusions. Geochim Cosmochim Acta 71:3323–3335

Duffy JA (1989) A common optical basicity scale for oxide and fluoride glasses. J Non-Crystal Sol 109:35–39

Duffy JA (1993) A review of optical basicity and its applications to oxidic systems. Geochim Cosmochim Acta 57:3961–3970

Duffy JA (1996) Optical basicity: a practical acid-base theory for oxides and oxyanions. J Chem Educ 73:1138–1142

Duffy JA, Ingram MD (1971) Establishment of an optical scale for Lewis basicity in inorganic oxyacids, molten salts, and glasses. J Am Chem Soc 93:6448–6454

Dunbar NW, Hervig RL, Kyle PR (1989) Determination of pre-eruptive H_2O, F and Cl contents of silicic magmas using melt inclusions—examples from Taupo Volcanic Center, New Zealand. Bull Volcanol 51:177–184

Eadington PJ, Nashar B (1978) Evidence for the magmatic origin of quartz-topaz rocks from the New England batholith, Australia. Contrib Mineral Petrol 67:433–438

Eugster HP (1986) Minerals in hot water. Am Mineral 71:655–673
Eugster HP, Baumgartner L (1987) Mineral solubilities and speciation in supercritical metamorphic fluids. Rev Mineral 17:367–404
Farges F (1996) Does Zr–F "complexation" occur in magmas? Chem Geol 127:253–268
Farges F, Calas G (1991) Structural analysis of radiation damage in zircon and thorite: an X-ray absorption spectroscopic study. Am Mineral 76:60–73
Farges F, Rossano S (2000) Water in Zr-bearing synthetic and natural glasses. Eur J Mineral 12:1093–1107
Farges F, Ponader CW, Brown GE Jr (1991) Structural environments of incompatible elements in silicate glass/melt systems: I. Zirconium at trace levels. Geochim Cosmochim Acta 55:1563–1574
Farges F, Ponader CW, Calas G, Brown GE Jr (1992) Local environment around incompatible elements in silicate glass/melt systems. II. U(VI), U(V) and U(IV). Geochim Cosmochim Acta 56:4205–4220
Farges F, Siewert R, Brown GE Jr, Guesdon A, Morin G (2006a) Structural environments around molybdenum in silicate glasses and melts. I. Influence of composition and oxygen fugacity on the local structure of molybdenum. Can Mineral 44:731–753
Farges F, Siewert R, Ponader CW, Brown GE Jr, Pichavant M, Behrens H (2006b) Structural environments around molybdenum in silicate glasses and melts. II. Effect of temperature, pressure, H_2O, halogens and sulfur. Can Mineral 44:755–773
Farges F, Linnen RL, Gordon EB Jr (2006c) Redox and speciation of tin in hydrous silicate glasses: a comparison with Nb, Ta, Mo and W. Can Mineral 44:795–810
Fidelis I, Siekierski S (1966) The regularities in stability constants of some rare earth complexes. J Inorg Nucl Chem 28:185–188
Fiege A, Kirchner C, Holtz F, Linnen RL, Dizony W (2011) Influence of fluorine on the solubility of manganotantalite ($MnTa_2O_6$) and manganocolumbite ($MnNb_2O_6$) in granitic melts—an experimental study. Lithos 122:165–174
Flood H, Förland T (1947) The acidic and basic properties of oxides. Acta Chem Scand 1:592–604
Förster HJ, Tischendorf G (1989) Reconstruction of the volatile characteristics of granitoidic magmas and hydrothermal solutions on the basis of dark micas: the Hercynian postkinematic granites and associated high-temperature mineralizations of the Erzgebirge (G.D.R.). 1. Communication: calculation procedure and results. Chemie Erde 49:7–20
Förster HJ, Tischendorf G, Trumbull RB, Gottesmann B (1999) Late-collisional granites in the Variscan Erzgebirge, Germany. J Petrol 40:1613–1645
Fournier RO (1985) Silica minerals as indicators of conditions during gold deposition. US Geol Surv Bull 1649:15–26
Fournier RO, Potter RW (1982) An equation correlating the solubility of quartz in water from 25° to 900°C at pressures up to 10,000 bars. Geochim Cosmochim Acta 46:1969–1973
Franck EU, Spalthoff W (1957) Hydrogen fluoride. I. Specific heat, vapor pressure, and density up to 300° and 300 atmospheres. Zeitschr Elektrochem 61:348–357
Frank MR, Candela PA, Piccoli PM, Glascock MD (2002) Gold solubility, speciation, and partitioning as a function of HCl in the brine-silicate melt-metallic gold system at 800 °C and 100 MPa. Geochim Cosmochim Acta 66:3719–3732
Frank MR, Candela PA, Piccoli PM (2003) Alkali exchange equilibria between a silicate melt and coexisting magmatic volatile phase: an experimental study at 800 °C and 100 MPa. Geochim Cosmochim Acta 67:1415–1427
Frank MR, Simon AC, Pettke T, Candela PA, Piccoli PM (2011) Gold and copper partitioning in magmatic-hydrothermal systems at 800 °C and 100 MPa. Geochim Cosmochim Acta 75:2470–2482
Frantz JD, Popp RK, Boctor NZ (1981) Mineral-solution equilibria—V. Solubilities of rock-forming minerals in supercritical fluids. Geochim Cosmochim Acta 45:69–77
Frantz JD, Popp RK, Hoering TC (1992) The compositional limits of fluid immiscibility in the system H_2O–NaCl–CO_2 as determined with the use if synthetic fluid inclusions in conjunction with mass spectrometry. Chem Geol 98:237–255

Frindt S, Poutiainen M (2002) P-T path fluid evolution in the Gross Spitzkoppe granite stock, Namibia. Bull Geol Soc Finland 74:103–114

Fuhrman ML, Lindsley DH (1988) Ternary-feldspar modeling and thermometry. Am Mineral 73:201–215

Gabitov R, Price JD, Watson EB (2005) Solubility of fluorite in haplogranitic melt of variable alkalis and alumina content at 800–1000 °C and 100 MPa. Geochem Geophys Geosys 6: Q03007

Gammon JB, Borcsik M, Holland HD (1969) Potassium-sodium ratios in aqueous solutions and coexisting silicate melts. Science 163:179–181

Gibert F, Guillaume D, Laporte D (1998a) Importance of fluid immiscibility in the H_2O–NaCl–CO_2 system and selective CO_2 entrapment in granulites: experimental phase diagram at 5–7 kbar, 900 °C and wetting textures. Eur J Mineral 10:1109–1123

Gibert F, Pascal ML, Pichavant M (1998b) Gold solubility and speciation in hydrothermal solutions: experimental study of the stability of hydrosulphide complex of gold (AuHSo) at 350 to 450 °C and 500 bars. Geochim Cosmochim Acta 62:2931–2947

Gioncada A, Orlandi P, Vezzoli L, Omarini RH, Mazzuoli R, Lopez-Azarevich V, Sureda R, Azarevich M, Acocella V, Ruch J (2014) Topaz magmatic crystallization in rhyolites of the Central Andes (Chivinar volcanic complex, NW Argentina): constraints from texture, mineralogy and rock chemistry. Lithos 184–187:62–73

Giordano D, Romano C, Dingwell DB, Poe B, Behrens H (2004) The combined effects of water and fluorine on the viscosity of silicic magmas. Geochim Cosmochim Acta 68:5159–5168

Glyuk DS, Anfilogov VN (1973a) Phase equilibria in the system granite–H_2O–HF at a pressure of 1000 kg/cm^2. Geochem Int 10:321–325

Glyuk DS, Anfilogov VN (1973b) Phase equilibria in the granite–H_2O–KF system at a steam pressure of 1000 kg/cm^2. Geochem Int 10:1169–1170

Glyuk DS, Shinakin BM (1986) The role of liquid-immiscibility differentiation in the pegmatite process. Geochem Int 23:38–49

Goodenough KM, Upton BGJ, Ellam RM (2000) Geochemical evolution of the Ivigtut granite, South Greenland: a fluorine-rich "A-type" intrusion. Lithos 51:205–221

Gramenitskiy YN, Shchekina TI (1994) Phase relationships in the liquidus part of a granitic system containing fluorine. Geochem Int 31:52–70

Gramenitskiy EN, Shchekina TI (2001) Geochemistry of tantalum, niobium, zirconium, and hafnium in fluorine-enriched granites and alkaline rocks according to experimental data. Geokhim 2001:621–635 (in Russian)

Gramenitskiy EN, Shekina TI (2002) Experimental data on geochemistry of REE and Y in the fluorine-bearing granite and nepheline syenite magmas. 9th Int Symp Exper Mineral Petrol Geochem, p 40

Gramenitskiy EN, Shchekina TI, Devyatova VN (2005) Phase relations in the fluorine-bearing granite and nepheline syenite systems and the element distribution between phases (experimental research). GEOS, Moscow, p 186 (in Russian)

Grjotheim K, Matiašovský K, Fellner P, Silný A (1971) Electrolytic deposition of silicon and of silicon alloys. Part I: physicochemical principles of the Na_3AlF_6–Al_2O_3–SiO_2 mixtures. Can Metall Q 10:79–82

Haapala I (1997) Magmatic and postmagmatic processes in tin-mineralized granites: topaz-bearing leucogranite in the Eurajoki rapakivi stock, Finland. J Petrol 38:1645–1659

Hall A (1970) The composition of Cornish quartz-porphyry ("elvan") dykes. Proc Ussher Soc 2 (3):205–208

Hall A (1971) Greisenisation in the granite of Cligga Head Cornwall. Proc Geol Assoc 82:209–230

Halter WE, Williams-Jones AE, Kontak DJ (1998) Modeling fluid-rock interaction during greisenization at the East Kemptville tin deposit: implications for mineralization. Chem Geol 150:1–17

Hanley JJ, Pettke T, Mungall JE, Spooner ETC (2005) The solubility of platinum and gold in NaCl brines at 1.5 kbar, 600 to 800 °C: a laser ablation ICP-MS pilot study of synthetic fluid inclusions. Geochim Cosmochim Acta 69:2593–2611

Harms E, Schmincke HU (2000) Volatile composition of the phonolitic Laacher See magma (12,900 yr BP): implications for syn-eruptive degassing of S, F, Cl and H_2O. Contrib Mineral Petrol 138:84–98

Haselton HT Jr, Cygan GL, D'Angelo WM (1988) Chemistry of aqueous solutions coexisting with fluoride buffers in the system K_2O–Al_2O_3–SiO_2–H_2O–F_2O_{-1} (1 kbar, 400°–700°C). Econ Geol 83:163–173

Hawthorne FC (1985) Towards a structural classification of minerals: the $^{VI}M^{IV}T_2\Phi_n$ minerals. Am Mineral 70:455–473

Hawthorne FC (1992) The role of OH and H_2O in oxide and oxysalt minerals. Z Kristall 201:183–206

Hayden LA, Manning CE (2011) Rutile solubility in supercritical $NaAlSi_3O_8$–H_2O fluids. Chem Geol 284:74–81

Heinrich CA (1990) The chemistry of tin (-tungsten) ore deposition. Econ Geol 85:529–550

Heinrich CA (1995) Geochemical evolution and hydrothermal mineral deposition in (Sn-W-base metal) and other granite-related ore systems: some conclusions from Australian examples. In Thompson JFH (ed) Magmas, fluids, and ore deposits. Mineral Assoc Canada Short Course 23:203–219

Heinrich CA (2005) The physical and chemical evolution of low-salinity magmatic fluids at the porphyry to epithermal transition: a thermodynamic study. Miner Depos 39:864–889

Heinrich CA, Candela PA (2014) Fluids and ore formation in the Earth's crust. In Scott SD (ed) Treatise on geochemistry. Geochemistry of mineral deposits, vol 13, 2nd edn. Elsevier, Amsterdam, p 1–28

Heinrich CA, Gunther D, Audétat A, Ulrich T, Frischknecht R (1999) Metal fractionation between magmatic brine and vapor, determined by microanalysis of fluid inclusions. Geology 27:755–758

Helgeson HC, Kirkham DH, Flowers GC (1981) Theoretical prediction of the thermodynamic behavior of aqueous electrolytes at high pressures and temperatures: IV. Calculation of activity coefficients, osmotic coefficients, and apparent molal and standard and relative partial molal properties to 600 °C and 5 kb. Am J Sci 281:1249–1516

Hemley RJ, Prewitt CT, Kingma KJ (1994) High-pressure behavior of silica. Rev Mineral 29:41–81

Henley RW (1973) Solubility of gold in hydrothermal chloride solutions. Chem Geol 11:73–87

Henley S (1974) Geochemistry and petrogenesis of elvan dykes in the Perranporth area, Cornwall. Proc Ussher Soc 3:136–145

Hervig RL, Kortemeier WT, Burt DM (1987) Ion-microprobe analyses of Li and B in topaz from different environments. Am Mineral 72:392–396

Heyrman M, Chartrand P (2007) A thermodynamic model for the NaF–KF–AlF_3–NaCl–KCl–$AlCl_3$ system. TMS Light Metals 2007:519–524

Hogan JP, Gilbert MC (1995) The A-type Mount Scott granite sheet: importance of crustal magma traps. J Geophys Res 100:15779–15792

Holland HD (1972) Granites, solutions, and base metal deposits. Econ Geol 67:281–301

Holland T, Powell R (2001) Calculation of phase relations involving haplogranitic melts using an internally consistent thermodynamic dataset. J Petrol 42:673–683

Holtz F, Johannes W, Pichavant M (1992) Effect of excess aluminium on phase relations in the system Qz–Ab–Or: experimental investigation at 2 kbar and reduced H_2O-activity. Eur J Mineral 4:137–152

Holtz F, Dingwell DB, Behrens H (1993) Effects of F, B_2O_3 and P_2O_5 on the solubility of water in haplogranite melts compared to natural silicate melts. Contrib Mineral Petrol 113:492–501

Holzheid A, Grove TL (2002) Sulfide saturation limits in silicate melts and their implications to core formation scenarios for terrestrial planets. Am Mineral 87:227–237

Horbe MA, Horbe AC, Costi HT, Teixeira JT (1991) Geochemical characteristics of cryolite-tin-bearing granites from the Pitinga Mine, northwestern Brazil—a review. J Geochem Explor 40:227–249

Horn S, Schmincke HU (2000) Volatile emission during the eruption of Baitoushan Volcano (China/North Korea) ca. 969 AD. Bull Volcanol 61:537–555

Hu X, Bi X, Hu R, Shang L, Fan W (2008) Experimental study on tin partition between granitic silicate melt and coexisting aqueous fluid. Geochem J 42:141–150

Icenhower J, London D (1995) An experimental study of element partitioning among biotite, muscovie, and coexisting peraluminous silicic melt at 200 MPa H_2O. Am Mineral 80:1229–1251

Icenhower JP, London D (1997) Partitioning of fluorine and chlorine between biotite and granitic melt: experimental calibration at 200 MPa H_2O. Contrib Mineral Petrol 127:17–29

Irber W (1999) The lanthanide tetrad effect and its correlation with K/Rb, Eu/Eu*, Sr/Eu, Y/Ho, and Zr/Hf of evolving peraluminous granite suites. Geochim Cosmochim Acta 63:489–508

Jackson KJ, Helgeson HC (1985) Chemical and thermodynamic constraints on the hydrothermal transport and deposition of tin: II. Interpretation of phase relations in the Southeast Asian tin belt. Econ Geol 80:1365–1378

Jahn S, Dubrail J, Wilke M (2015) Complexation of Zr and Hf monomers in supercritical aqueous solutions: insights from ab initio molecular dynamics simulations. Chem Geol 418:30–39

Johannes W, Holtz F (1996) Petrogenesis and experimental petrology of granitic rocks. Springer, Berlin, p 335

Johnson JW, Oelkers EH, Helgeson HC (1992) SUPCRT92: a software package for calculating the standard molal thermodynamic properties of minerals, gases, aqueous species, and reactions from 1 to 5000 bar and 0 to 1000°C. Comp Geosci 18:899–947

Johnston C, Chappell BW (1992) Topaz-bearing rocks from Mount Gibson, North Queensland, Australia. Am Mineral 77:303–313

Joyce DB, Holloway JR (1993) An experimental determination of the thermodynamic properties of H_2O–CO_2–NaCl fluids at high pressures and temperatures. Geochim Cosmochim Acta 57:733–746

Joyce DB, Voigt DE (1994) A phase equilibrium study in the system $KAlSi_3O_8$–$NaAlSi_3O_8$–SiO_2–Al_2SiO_5–H_2O and petrogenetic implications. Am Mineral 79:504–512

Kamenetsky VS, Naumov VB, Davidson P, van Achterbergh E, Ryan CG (2004) Immiscibility between silicate magmas and aqueous fluids: a melt inclusion pursuit into the magmatic-hydrothermal transition in the Omsukchan Granite (NE Russia). Chem Geol 210:73–90

Kendrick MA, Arculus RJ, Danyushevsky LV, Kamenetsky VS, Woodhead JD, Honda M (2014) Subduction-related halogens (Cl, Br and I) and H_2O in magmatic glasses from Southwest Pacific Backarc Basins. Earth Planet Sci Lett 400:165–176

Keppler H (1993) Influence of fluorine on the enrichment of high field strength trace elements in granitic rocks. Contrib Mineral Petrol 114:479–488

Keppler H, Wyllie PJ (1991) Partitioning of Cu, Sn, Mo, W, U, and Th between melt and aqueous fluid in the systems haplogranite–H_2O–HCl and haplogranite–H_2O–HF. Contrib Mineral Petrol 109:139–150

Kilinc IA, Burnham CW (1972) Partitioning of chloride between a silicate melt and a coexisting aqueous phase from 2 to 8 kilobars. Econ Geol 67:231–235

Kleeman JD (1985) Origin of disseminated woltramite-bearing quartz-topaz rock at Torrington, New South Wales, Australia. High-heat production (HHP) granites, hydrothermal circulation and ore genesis. Institute of Mining and Metallurgy, London, pp 197–201

Klemm W (1994) Chemical evolution of hydrothermal solutions during Variscan and post-Variscan mineralization in the Erzgebirge, Germany. In: Seltmann R, Kämpf H, Möller P (eds) Metallogeny of collisional orogens. Czech Geological Survey, Prague, pp 150–158

Klemm LM, Pettke T, Heinrich CA, Campos E (2007) Hydrothermal evolution of the El Teniente deposit, Chile: Porphyry Cu–Mo ore deposition from low-salinity magmatic fluids. Econ Geol 102:1021–1045

Klemme S (2004) Evidence for fluoride melts in Earth's mantle formed by liquid immiscibility. Geology 32:441–444
Kogarko LN, Krigman LD (1975) Immiscibility in fluorosilicate systems. Phys Chem Glasses 1:61–65
Kogarko LN, Krigman LD (1981) Fluorine in silicate melts and magmas. Nauka, Moscow, p 126 (in Russian)
Kogarko LN, Krigman LD, Sharudilo NS (1968) Experimental investigations of the effect of alkalinity of silicate melts on the separation of fluorine into the gas phase. Geochem Int 5:782–790
Kohn SC, Dupree R, Mortuza MG, Henderson CMB (1991) NMR evidence for five- and six-coordinated aluminum fluoride complexes in F-bearing aluminosilicate glasses. Am Mineral 76:309–312
Kojima H, Whiteway SG, Masson CR (1968) Melting points of inorganic fluorides. Can J Chem 46:2968–2971
Kortemeier WT, Burt DM (1988) Ongonite and topazite dikes in the Flying W ranch area, Tonto basin, Arizona. Am Mineral 73:507–523
Korzhinskiy DS (1959) Acid-base interaction of the components in silicate melts and the direction of cotectic lines. Dokl Akad Nauk SSSR, Earth Sci Sect 128:821–823
Korzhinskiy DS (1960) Acidity-alkalinity in magmatic processes. 21st international geological congress, Report of the 21st session, Copenhagen, pp 160–170
Kosinski JJ, Anderko A (2001) Equation of state for high-temperature aqueous electrolyte and noneletrolyte systems. Fluid Phase Equilib 183–184:75–86
Koster van Groos AF (1991) Differential thermal analysis of the liquidus relations in the system NaCl–H_2O to 6 kbar. Geochim Cosmochim Acta 55:2811–2817
Koster van Groos AF, Wyllie PJ (1968) Melting relationships in the system $NaAlSi_3O_8$–NaF–H_2O to 4 kilobars pressure. J Geol 76:50–70
Koster van Groos AF, Wyllie PJ (1969) Melting relationships in the system $NaAlSi_3O_8$–NaCl–H_2O at 1 kilobar pressure, with petrological applications. J Geol 77:581–605
Kostitsyn YuA (2000) Sources of rare metals in peraluminous granites: a review of geochemical and isotopic data. Geochem Int 39:S43–S59
Kotelnikova ZA, Kotelnikov AR (2002) Synthetic NaF-bearing fluid inclusions. Geochem Int 40:594–600
Kotov NV, Domnina MI, Vorob'yev PV, Kovnurko GM, Galibin VA (1981) Experimental determination of the composition of the albitizing solution during hydrothermal transformation of granite in the presence of NaF. Geochem Int 18:47–54
Kovalenko VI, Kovalenko NI (1976) Ongonites: subvolcanic analogues of rare-metal Li–F granites. Nauka, Moscow, p 127 (in Russian)
Kovalenko VI, Kovalenko NI (1984) Problems of the origin, ore-bearing and evolution of rare-metal granitoids. Phys Earth Planet Inter 35:51–62
Kovalenko NI, Kovalenko VI, Belykh LA (1975) Experimental study of the fusion and crystallization of topaz-bearing quartz keratophyre (ongonite) in the presence of water and hydrofluoric acid. Dokl Akad Nauk SSSR 215:129–132
Kovalenko VI, Antipin VS, Konusova VV, Smirnova YV, Petrov LL, Vladykin NV, Kunzetsova AI, Kostyukova YS, Pisarskaya VA (1977) Partition coefficients of fluorine, niobium, tantalum, lanthanum, ytterbium, yttrium, tin and tungsten in ongonite. Dokl Akad Nauk SSSR 233:203–205
Kovalenko VI, Tsaryeva GM, Goreglyad AV, Yarmolyuk VV, Troitsky VA, Hervig RL, Farmer GL (1995) The peralkaline granite-related Khaldzan-Buregtey rare metal (Zr, Nb, REE) deposit, western Mongolia. Econ Geol 90:530–547
Kravchuk IF, Keppler H (1994) Distribution of chloride between aqueous fluids and felsic melts at 2 kbar and 800 °C. Eur J Mineral 6:913–923
Kravchuk IF, Slutskii AB (2001) Fluorine behavior in fluid-magmatic systems. Geochem Int 39:609–614

Kravchuk IF, Kotelnikov AR, Senin VG (2004) Partitioning of volatile (Cl, F, and S) and rare alkali (Rb and Cs) elements in the system aluminosilicate melt-fluid. Geokhimiya 2004:1213–1219

Kress VC, Carmichael ISE (1991) The compressibility of silicate liquids containing Fe_2O_3 and the effect of composition, temperature, oxygen fugacity and pressure on their redox states. Contrib Mineral Petrol 108:82–92

Kushiro I (1975) On the nature of silicate melt and its significance in magma genesis: regularities in the shift of the liquidus boundaries involving olivine, pyroxene and silica minerals. Am J Sci 275:411–431

Kuvakin MA, Kusakin PS (1959) The sodium-fluoride-aluminum fluoride-sodium chloride system. Russ J Inorg Chem 4:1188–1190

Lagache M, Weisbrod A (1977) The system two alkali feldspars–KCl–NaCl–H_2O at moderate to high temperatures and low pressures. Contrib Mineral Petrol 62:77–101

Lambotte G, Chartrand P (2013a) Thermodynamic modeling of the (Al_2O_3 + Na_2O), (Al_2O_3 + Na_2O + SiO_2), and (Al_2O_3 + Na_2O + AlF_3 + NaF) systems. J Chem Thermodyn 57:306–334

Lambotte G, Chartrand P (2013b) A thermodynamic approach to the corrosion of the cathode refractory lining in aluminium electrolysis cells: modelling of the Al_2O_3–Na_2O–SiO_2–AlF_3–NaF–SiF_4 system. TMS Light Met 2013:911–916

Lecumberri-Sanchez P, Steele-MacInnis M, Bodnar RJ (2015) Synthetic fluid inclusions XIX. Experimental determination of the vapor-saturated liquidus of the system H_2O–NaCl–$FeCl_2$. Geochim Cosmochim Acta 148:34–49

Lentz DR, Gregoire C (1995) Petrology and mass-balance constraints on major-, trace-, and rare-earth-element mobility in porphyry-greisen alteration associated with the epizonal True Hill granite, southwestern New Brunswick, Canada. J Geochem Expl 52:303–331

Lerchbaumer L, Audétat A (2012) High Cu concentrations in vapor-type fluid inclusions: an artifact? Geochim Cosmochim Acta 88:255–274

Lester GW, Clark AH, Kyser TK, Naslund HR (2013) Experiments on liquid immiscibility in silicate melts with H_2O, P, S, F and Cl: implications for natural magmas. Contrib Mineral Petrol 166:329–349

Lewis GN (1923) Valence and the structure of atoms and molecules. Chem Catal Comp, New York, p 172

Lewis GN (1938) Acids and bases. J Franklin Inst 226:293–313

Li Y, Audétat A, Lerchbaumer L, Xiong XL (2009) Rapid Na, Cu exchange between synthetic fluid inclusions and external aqueous solutions: evidence from LA-ICP-MS analysis. Geofluids 9:321–329

Liebscher A, Heinrich CA (2007) Fluid-fluid interactions in the Earth's lithosphere. Rev Mineral Geochem 65:1–13

Linnen RL (1998) The solubility of Nb–Ta–Zr–Hf–W in granitic melts with Li and Li + F: constraints for mineralization in rare metal granites and pegmatites. Econ Geol 93:1013–1025

Linnen RL, Cuney M (2005) Granite-related rare-element deposits and experimental constraints on Ta–Nb–W–Sn–Zr–Hf mineralization. Geol Assoc Can Short Course Notes 17:45–68

Linnen RL, Keppler H (1997) Columbite solubility in granitic melts: consequences for the enrichment and fractionation of Nb and Ta in the Earth's crust. Contrib Mineral Petrol 128:213–227

Linnen RL, Pichavant M, Holtz F, Burgess S (1995) The effect of fO_2 on the solubility, diffusion, and speciation of tin in haplogranitic melt at 850 °C and 2 kbar. Geochim Cosmochim Acta 59:1579–1588

Linnen RL, Van Lichtervelde M, Černý P (2012) Granitic pegmatites as sources of strategic metals. Elements 8:275–280

Linnen RL, Samson IM, Williams-Jones AE, Chakhmouradian AR (2014) Geochemistry of the rare-earth element, Nb, Ta, Hf, and Zr deposits. In Scott SD (ed) Treatise on geochemistry. Geochemistry of mineral deposits, vol 13, 2nd edn. Elsevier, Amsterdam, pp 543–568

Liu CS, Ling HF, Xiong XL, Shen WZ, Wang DZ, Huang XL, Wang RC (1999) An F-rich, Sn-bearing volcanic-intrusive complex in Yanbei, South China. Econ Geol 94:325–342
London D (1986) Magmatic-hydrothermal transition in the Tanco rare-element pegmatite: evidence from fluid inclusions and phase-equilibrium experiments. Am Mineral 71:376–395
London D (1997) Estimating abundances of volatile and other mobile components on evolved silicic melts through mineral-melt equilibria. J Petrol 38:1691–1706
London D, Manning DAC (1995) Chemical variation and significance of tourmaline from southwest England. Econ Geol 90:495–519
London D, Hervig RL, Morgan VIGB (1988) Melt-vapor solubilities and elemental partitioning in peraluminous granite-pegmatite systems: experimental results with Macusani glass at 200 MPa. Contrib Mineral Petrol 99:360–373
London D, Morgan GBVI, Babb HA, Loomis JL (1993) Behavior and effects of phosphorus in the system Na_2O–K_2O–Al_2O_3–SiO_2–P_2O_5–H_2O at 200 MPa (H_2O). Contrib Mineral Petrol 113:450–465
London D, Morgan GBVI, Wolf MB (2001) Amblygonite-montebrasite solid solutions as monitors of fluorine in evolved granitic and pegmatitic melts. Am Mineral 86:225–233
Louvel M, Sanchez-Valle C, Malfait W, Cardon H, Testemale D, Hazemann JL (2014) Constraints on the mobilization of Zr in magmatic-hydrothermal processes in subduction zones from in site fluid-melt partitioning experiments. Am Mineral 99:1616–1625
Lowenstern JB (1994) Chlorine, fluid immiscibility, and degassing in peralkaline magmas from Pantelleria, Italy. Am Mineral 79:353–369
Lowenstern JB, Bleick H, Vazquez JA, Castro JM, Larson PB (2012) Degassing of Cl, F, Li, and Be during extrusion and crystallization of the rhyolite dome at Volcan Chaiten, Chile during 2008 and 2009. Bull Volcanol 74:2303–2319
Lukkari S, Holtz F (2007) Phase relations of a F-enriched peraluminous granite: an experimental study of the Kymi topaz granite stock, southern Finland. Contrib Mineral Petrol 153:273–288
Luth WC, Tuttle OF (1969) The hydrous vapor phase in equilibrium with granite and granite magmas. Geol Soc Am Memoir 115:513–548
Maar RA, Baker DR, Williams-Jones AE (1998) Chemical controls on the solubility of Zr-bearing phases in simplified peralkaline melts and application to the Strange Lake intrusion, Quebec–Labrador. Can Mineral 36:1001–1008
Macdonald R, Smith RL, Thomas JE (1992) Chemistry of the subalkalic silicic obsidians. US Geol Surv Prof Paper 1523, p 224
Malinin SD, Kurovskaya NA (1996) The effect of pressure on mineral solubility in aqueous chloride solutions under supercritical conditions. Geokhimiya 1:51–58 (in Russian)
Manning DAC (1981) The effect of fluorine on liquidus phase relationships in the system Qz-Ab-Or with excess water at 1 kb. Contrib Mineral Petrol 76:206–215
Manning CE (1994) The solubility of quartz in H_2O in the lower crust and upper mantle. Geochim Cosmochim Acta 58:4831–4839
Manning DAC, Henderson P (1984) The behavior of tungsten in granitic melt-vapor systems. Contrib Mineral Petrol 86:286–293
Manning DAC, Hill PI (1990) The petrogenesis and metallogenetic significance of topaz granite from the southwest England ore field. Geol Soc Am Spec Paper 246:51–69
Manning DAC, Hamilton DL, Henderson CMB, Dempsey MJ (1980) The probable occurrence of interstitial Al in hydrous, F-bearing and F-free aluminosilicate melts. Contrib Mineral Petrol 75:257–262
Marianelli P, Metrich N, Sbrana A (1999) Shallow and deep reservoirs involved in magma supply of the 1944 eruption of Vesuvius. Bull Volcanol 61:48–63
Marshall WL, Franck EU (1981) Ion product of water substance, 0–1000°C, 1–10,000 bars, new international formulation and its background. J Phys Chem Ref Data 10:295–304
Marshall AS, Hinton RW, Macdonald R (1998) Phenocrystic fluorite in peralkaline rhyolites, Olkaria, Kenya Rift Valley. Mineral Mag 62:477–486

Matthews SJ, Sparks RSJ, Gardeweg MC (1999) The Piedras Grandes-Soncor eruptions, Lascar Volcano, Chile; Evolution of zoned magma chamber in the central Andean upper crust. J Petrol 40:1891–1919

Mayanovic RA, Yan H, Anderson AJ, Solferino G (2013) Investigation of the structural environment of Ta in a silicate glass and water system under high P-T conditions. J Non-Cryst Solids 368:71–78

Mei Y, Liu W, Sherman DM, Brugger J (2014) Metal complexation and ion hydration in low density hydrothermal fluids: Ab initio molecular dynamics simulation of Cu(I) and Au(I) in chloride solutions (25–1000 °C, 1–5000 bar). Geochim Cosmochim Acta 131:196–212

Metrich N, Rutherford MJ (1992) Experimental study of chlorine behavior in hydrous silicic melts. Geochim Cosmochim Acta 56:607–616

Michaud V, Clocchiatti R, Sbrana S (2000) The Minoan and post-Minoan eruptions, Santorini (Greece), in the light of melt inclusions: chlorine and sulphur behaviour. J Volcanol Geotherm Res 99:195–214

Migdisov AA, Williams-Jones AE (2014) Hydrothermal transport and deposition of the rare earth elements by fluorine-bearing aqueous liquids. Mineral Deposita 49:987–997

Migdisov AA, Williams-Jones AE, Wagner T (2009) An experimental study of the solubility and speciation of the rare earth elements (III) in fluoride- and chloride-bearing aqueous solutions at temperatures up to 300 °C. Geochim Cosmochim Acta 73:7087–7109

Migdisov AA, Williams-Jones AE, van Hinsberg V, Salvi S (2011) An experimental study of the solubility of baddeleyite (ZrO_2) in fluoride-bearing solutions at elevated temperature. Geochim Cosmochim Acta 75:7426–7434

Monecke T, Kempe U, Monecke J, Sala M, Wolf D (2002) Tetrad effect in rare earth element distribution patterns: a method of quantification with application to rock and mineral samples from granite-related rare metal deposits. Geochim Cosmochim Acta 66:1185–1196

Mootz D, Ohms U, Poll W (1981) Schmelzdiagramm H_2O–HF und Strukturen der 1:1- und einer 1:2-Phase. Z Anorg Allg Chem 479:75–83

Morey GW, Chen WT (1956) Pressure-temperature curves in systems containing water and a salt. J Am Chem Soc 78:4249–4252

Muñoz JL (1971) Hydrothermal stability relations of synthetic lepidolite. Am Mineral 56:2069–2078

Muñoz JL, Ludington DS (1974) Fluorine-hydroxyl exchange in biotite. Am J Sci 274:396–413

Mustart DA (1972) Phase relations in the peralkaline portion of the system Na_2O–Al_2O_3–SiO_2–H_2O. Ph.D. dissertation, Stanford University, p 202

Mysen BO, Virgo D (1985a) Interaction between fluorine and silica in quenched melts on the joins SiO_2–AlF_3 and SiO_2–NaF determined by Raman spectroscopy. Phys Chem Mineral 12:77–85

Mysen BO, Virgo D (1985b) Structure and properties of fluorine-bearing aluminosilicate melts: the system Na_2O–Al_2O_3–SiO_2–F at 1 atm. Contrib Mineral Petrol 91:205–220

Mysen BO, Cody GD, Smith A (2004) Solubility mechanisms of fluorine in peralkaline and meta-aluminous silicate glasses and in melts to magmatic temperatures. Geochim Cosmochim Acta 68:2745–2769

Nagaseki H, Hayashi KI (2008) Experimental study of the behavior of copper and zinc in a boiling hydrothermal system. Geology 36:27–30

Navrotsky A (1994) Physics and chemistry of earth materials. Cambridge University Press, Cambridge, p 417

Nekrasov IY, Epel'baum MB, Sobolev VP (1980) Partition of tin between melt and chloride fluid in the granite–SnO–SnO_2–fluid system. Dokl Earth Sci Sect 252:165–168

Nichols GT, Wiebe R (1998) Desilication veins in the Cadillac Mountain granite (Maine, USA): a record of reversals in the SiO_2 solubility of H_2O-rich vapour released during subsolidus cooling. J Metamorph Geol 16:795–808

Norman MD, Leeman WP, Mertzman SA (1992) Granites and rhyolites from the northwestern USA: temporal variation in magmatic processes and relations to tectonic setting. Trans R Soc Edin Earth Sci 83:71–81

O'Neill HSC, Mavrogenes JA (2002) The sulfide capacity and the sulfur content at sulfide saturation of silicate melts at 1400°C and 1 bar. J Petrol 43:1049–1087

Paillat O, Elphick SC, Brown WL (1992) The solubility of water in $NaAlSi_3O_8$ melts: a re-examination of Ab-H_2O phase relationships and critical behavior at high pressures. Contrib Mineral Petrol 112:490–500

Parr RG, Pearson RG (1983) Absolute hardness: companion parameter to absolute electronegativity. J Am Chem Soc 105:7512–7516

Pauly H (1960) Paragenetic relations in the main cryolite ore of Ivigtut, South Greenland. Neu Jahrb Mineral Abh 94:121–139

Pauly H (1974) Ivigtut cryolite deposit, SW-Greenland. In Štemprok M (ed) Metallization associated with acid magmatism, vol 1. Czech Geological Survey, Prague, pp 393–399

Pauly H, Bailey JC (1999) Genesis and evolution of the Ivigtut cryolite deposit, SW Greenland. Meddelelser om Grønland, Geosci 37:60

Pearson RG (1968a) Hard and soft acids and bases. HSAB, Part I. Fundamental principles. J Chem Educ 45:581–587

Pearson RG (1968b) Hard and soft acids and bases. HSAB, Part II. Underlying theories. J Chem Educ 45:643–648

Pelton AD (1999) Thermodynamic calculations of chemical solubilities of gases in oxide melts and glasses. Glass Sci Tech 72:214–226

Pelton AD, Wu P (1999) Thermodynamic modeling in glass-forming melts. J Non-Crystal Solids 253:178–191

Pelton AD, Eriksson G, Romero-Serrano A (1993) Calculation of sulfide capacities in multicomponent slags. Metall Trans 24B:817–825

Peppard DF, Mason GW, Lewey S (1969) A tetrad effect in liquid-liquid extraction ordering of lanthanides(III). J Inorg Nucl Chem 31:2271–2272

Peretyazhko IS, Savina EA (2010) Tetrad effects in the rare earth element patterns of granitoid rocks as an indicator of fluoride-silicate liquid immiscibility in magmatic systems. Petrology 18:514–543

Peretyazhko IS, Vye Zagorsky, Tsareva EA, Sapozhnikov AN (2007) Immiscibility of calcium fluoride and aluminosilicate melts in ongonite from the Ary-Bulak Intrusion, Eastern Transbaikal Region. Dokl Earth Sci 413:315–320

Peterson JW, Chako T, Kuehner SM (1991) The effects of fluorine on the vapor-absent melting of phlogopite + quartz: implications for deep-crustal processes. Am Mineral 76:470–476

Phillips NWF, Singleton RH, Hollingshead EA (1955) Liquidus curves for aluminum cell electrolyte. II. Ternary systems of cryolite-alumina with sodium fluoride, sodium chloride, and aluminum fluoride. J Electrochem Soc 102:688–690

Piccoli PM, Candela PA (2002) Apatite in igneous systems. Rev Mineral 48:255–292

Pichavant M, Valencia Herrera J, Boulmier S, Briqueu L, Joron JL, Juteau M, Marin L, Michard A, Sheppard SMF, Treuil M, Vernet M (1987) The Macusani glasses, SE Peru: evidence of chemical fractionation in peraluminous magmas. In Mysen BO (ed) Magmatic processes: physicochemical principles. Geochem Soc Spec Publ 1:359–373

Pichavant M, Kontak DJ, Valencia Herrera J, Clark AH (1988a) The Miocene-Pliocene Macusani volcanics, SE Peru. I. Mineralogy and magmatic evolution of a two-mica aluminosilicate-bearing ignimbrite suite. Contrib Mineral Petrol 100:300–324

Pichavant M, Kontak DJ, Briqueu L, Valencia Herrera J, Clark AH (1988b) The Miocene-Pliocene Macusani volcanics, SE Peru. II. Geochemistry and origin a felsic peraluminous magma. Contrib Mineral Petrol 100:325–338

Piilonen PC, Farges F, Linnen RL, Brown GE Jr (2005) Tin and niobium in dry and fluid-rich (H_2O, F) silicate glasses. Phys Scr T115:405–407

Piilonen PC, Farges F, Linnen RL, Brown GE Jr, Pawlak M, Pratt A (2006) Structural environment of Nb^{5+} in dry and fluid-rich (H_2O,F) silicate glasses: a combined XANES and EXAFS study. Can Mineral 44:775–794

Pokrovski GS, Roux J, Hazemann JL, Testemale D (2005) An X-ray absorption spectroscopy study of argutite solubility and aqueous Ge(IV) speciation in hydrothennal fluids to 500 °C and 400 bar. Chem Geol 217:127–145

Pokrovski GS, Borisova AY, Harrichoury J-C (2008) The effect of sulfur on vapor-liquid fractionation of metals in hydrothermal systems. Earth Planet Sci Lett 266:345–362

Pokrovski GS, Tagirov BR, Schott J, Bazarkina EF, Hazermann JL, Proux O (2009a) An in situ X-ray absorption spectroscopy study of gold-chloride complexing in hydrothermal fluids. Chem Geol 259:17–29

Pokrovski GS, Tagirov BR, Schott J, Hazemann JL, Proux O (2009b) A new view on gold speciation in sulfur-bearing hydrothermal fluids from in situ X-ray absorption spectroscopy and quantum-chemical modeling. Geochim Cosmochim Acta 73:5406–5427

Pollard PJ (1983) Magmatic and postmagmatic processes in the formation of rocks associated with rare-element deposits. Trans Inst Min Metall B Appl Earth Sci 92:B1–B9

Pollard PJ (1989) Geologic characteristics and genetic problems associated with the development of granite-hosted deposits of tantalum and niobium. In: Möller P, Černý P, Saupé F (eds) Lanthanides, tantalum and niobium. Mineralogy, geochemistry, characteristics of primary ore deposits, prospecting, processing and applications. Springer, Berlin, pp 240–256

Pollard PJ, Pichavant M, Charoy B (1987) Contrasting evolution of fluorine- and boron-rich tin systems. Mineral Depos 22:315–321

Pollard PJ, Nakapadungrat S, Taylor RG (1995) The Phuket supersuite, southwest Thailand: fractionated I-type granites associated with tin-tantalum mineralization. Econ Geol 90:586–602

Powell R, Holland T, Worley B (1998) Calculating phase diagrams involving solid solutions via non-linear equations, with examples using THERMOCALC. J Metamorph Geol 16:577–588

Price JD, Hogan JP, Gilbert MC, London D, Morgan GBVI (1999) Experimental study of titanite-fluorite equilibria in the A-type Mount Scott granite: implications for assessing F contents of felsic magma. Geology 27:951–954

Puziewicz J, Johannes W (1988) Phase equilibria and compositions of Fe–Mg–Al minerals and melts in water-saturated peraluminous granitic systems. Contrib Mineral Petrol 100:156–168

Raimbault L, Burnol L (1998) The Richemont rhyolite dike, Massif Central, France: a subvolcanic equivalent of rare-metal granites. Can Mineral 36:265–282

Ravich MI, Valyashko VM (1965) Solubility of sodium fluoride at elevated temperatures. Russ J Inorg Chem 10:107–109

Reddy RG, Blander M (1987) Modeling of sulfide capacities of silicate melts. Metal Trans 18B:591–596

Rempel KU, Williams-Jones AE, Migdisov AA (2008) The solubility of molybdenum dioxide and trioxide in HCl-bearing water vapour at 350 °C and pressures up to 160 bars. Geochim Cosmochim Acta 72:3074–3083

Renaud E, Robelin C, Heyrman M, Chartrand P (2009) Thermodynamic evaluation and optimization of the ($LiF + NaF + KF + MgF_2 + CaF_2 + SrF_2$) system. J Chem Thermodyn 41:666–682

Renaud E, Robelin C, Gheribi AE, Chartrand P (2011) Thermodynamic evaluation and optimization of the Li, Na, K, Mg, Ca, Sr//F, Cl reciprocal system. J Chem Thermodyn 43:1286–1298

Richardson CK, Holland HD (1979) The solubility of fluorite in hydrothermal solutions, an experimental study. Geochim Cosmochim Acta 43:1313–1325

Rickers K, Thomas R, Heinrich W (2006) The behavior of trace elements during the chemical evolution of the H_2O-, B-, and F-rich granite-pegmatite-hydrothermal system at Ehrenfriedersdorf, Germany: a SXRF study of melt and fluid inclusions. Mineral Deposita 41:229–245

Roman DC, Cashman KV, Gardner CA, Wallace PJ, Donovan JJ (2006) Storage and interaction of compositionally heterogeneous magmas from the 1986 eruption of Augustine Volcano, Alaska. Bull Volcanol 68:240–254

Rowe JJ, Fournier RO, Morey GW (1967) The system water-sodium oxide-silicon dioxide at 200, 250, and 300°. Inorg Chem 6:1183–1188

Rutherford MJ, Sigurdsson H, Carey S, Davis A (1985) The May 18, 1980 eruption of Mount St. Helens 1. Melt composition and experimental phase equilibria. J Geophys Res 90:2929–2947

Rutlin JL (1998) Chemical reactions and mineral formation during sodium aluminium fluoride attack on aluminosilicate and anorthite based refractories. Dr-Ing. Thesis, Norwegian University of Science and Technology, Trondheim, p 167

Rutlin J, Grande T (1997) Fluoride attack on alumino-silicate refractories in aluminium electrolysis cells. Light Metals 1997:295–301

Rutlin J, Grande T (1998) Molten fluoride attack on anorthite based powder barrier materials in aluminum electrolysis cells. Light Metals 1998:589–595

Ryabchikov ID, Solovova IP, Babanskii AD, Fauzi K (1996) Fluorine mobilization and bonding at magmatic and postmagmatic stages in rare-metal granites: evidence from the Homrat Akarem deposit (Egypt). Geochem Int 34:347–350

Ryzhenko BN, Bryzgalin OV, Artamkina IY , Spasennykh MY, Shapkin AI (1985) An electrostatic model for the electrolytic dissociation of inorganic substances dissolved in water. Geochem Int 22:138–144

Sakoma EM, Martin RF, Williams-Jones AE (2000) The late stages of evolution of the Kwandonkaya A-type granite complex, Nigeria, as deduced from mafic minerals. J Afr Earth Sci 30:329–350

Sallet R (2000) Fluorine as a tool in the petrogenesis of quartz-bearing magmatic associations: applications of an improved F–OH biotite-apatite thermometer grid. Lithos 50:241–253

Sallet R, Moritz R, Fontignie D (2000) Fluorite $^{87}Sr/^{86}Sr$ and REE constraints on fluid-melt relations, crystallization time span and bulk D_{Sr} of evolved high-silica rhyolites, Tabuleiro granites, Santa Catarina, Brazil. Chem Geol 164:81–92

Sandland TO, Du LS, Stebbins F, Webster JD (2004) Structure of Cl-containing silicate and aluminosilicate glasses: a Cl-35 MAS–NMR study. Geochim Cosmochim Acta 68:5059–5069

Sauerwald F, Dombois HE (1954) Über die allgemeinen Formen der Dreistoff-Diagramme mit zwei eutektischen binären Systemen und einem binären Mischkristallsystem mit Mischungslücke und kritischem Punkt, sowie das System KCl–NaCl–NaF. Z Anorg Allg Chem 277:60–72

Scaillet B, Macdonald R (2001) Phase relations of peralkaline silicic magmas and petrogenetic implications. J Petrol 42:825–845

Scaillet B, Macdonald R (2004) Fluorite stability in silicic magmas. Contrib Mineral Petrol 147:319–329

Schafer B, Frischknecht R, Gunther D, Dingwell DB (1999) Determination of trace-element partitioning between fluid and melt using LA-ICP-MS analysis of synthetic fluid inclusions in glass. Eur J Mineral 11:415–426

Schaller T, Dingwell DB, Keppler H, Knoeller W, Merwin L, Sebald A (1992) Fluorine in silicate glasses: a multinuclear nuclear magnetic resonance study. Geochim Cosmochim Acta 56:701–707

Schmidt C, Bodnar RJ (2000) Synthetic fluid inclusions: XVI. PVTX properties in the system H_2O–NaCl–CO_2 at elevated temperatures, pressures, and salinities. Geochim Cosmochim Acta 64:3853–3869

Schwartz MO, Surjono (1990) Greisenization and albitization at the Tikus tin-tungsten deposit, Belitung, Indonesia. Econ Geol 85:691–713

Seo JH, Heinrich CA (2013) Selective copper diffusion into quartz-hosted vapor inclusions: evidence from other host minerals, driving forces, and consequences for Cu–Au ore formation. Geochim Cosmochim Acta 113:60–69

Seo JH, Guillong M, Heinrich CA (2009) The role of sulfur in the formation of magmatic-hydrothermal copper-gold deposits. Earth Planet Sci Lett 282:323–328

Seward TM (1989) The hydrothermal chemistry of gold and its implications for ore formation: boiling and conductive cooling as examples. Econ Geol Monogr 6:398–404

Shand SJ (1927) Eruptive rocks: their genesis, composition, and classification with a chapter on meteorites. Wiley, New York, p 360

Shannon RD (1976) Revised effective ionic radii and systematic studies of interatomic distances in halides and chalcogenides. Acta Crystallogr A32:751–767

Shchekina TI, Gramenitskiy EN, Alferyeva Y (2013) Leucocratic magmatic melts with the maximum fluorine concentrations: experiment and relations in nature. Petrology 21:454–470

Shinohara H (1987) Partition of chlorine compounds in the system silicate melt and hydrothermal solutions. Doctoral dissertation, Tokyo Institute of Technology, p 192

Shinohara H (1994) Exsolution of immiscible vapor and liquid phases from a crystallizing silicate melt—implications for chlorine and metal transport. Geochim Cosmochim Acta 58:5215–5221

Shinohara H (2009) A missing link between volcanic degassing and experimental studies on chloride partitioning. Chem Geol 263:51–59

Shinohara H, Iiyama JT, Matsuo S (1989) Partition of chlorine compounds between silicate melt and hydrothermal solutions 1. Partition of NaCl–KCl. Geochim Cosmochim Acta 53:2617–2630

Shmulovich KI, Graham CM (1999) An experimental study of phase equilibria in the system H_2O–CO_2–NaCl at 800 °C and 9 kbar. Contrib Mineral Petrol 136:247–257

Shmulovich KI, Graham CM (2004) An experimental study of phase equilibria in the systems H_2O–CO_2–$CaCl_2$ and H_2O–CO_2–NaCl at high pressures and temperatures (500–800 °C, 0.5-0.9 GPa): geological and geophysical applications. Contrib Mineral Petrol 146:450–462

Shock EL, Helgeson HC (1988) Calculation of the thermodynamic and transport properties of aqueous species at high pressures and temperatures: correlation algorithms for ionic species and equation of state predictions to 5 kb and 1000°C. Geochim Cosmochim Acta 52:2009–2036

Shock EL, Helgeson HC, Sverjensky DA (1989) Calculation of the thermodynamic properties of aqueous species at high pressures and temperatures: standard partial molal properties of inorganic neutral species. Geochim Cosmochim Acta 53:2157–2183

Shock EL, Oelkers EH, Johnson JW, Sverjensky DA, Helgeson HC (1992) Calculation of the thermodynamic properties of aqueous species at high pressures and temperatures. Effective electrostatic radii, dissociation constants and standard partial molal properties to 1000°C and 5 kbar. J Chem Soc Faraday Trans 88:803–826

Signorelli S, Carroll MR (2000) Solubility and fluid-melt partitioning of Cl in hydrous phonolitic melts. Geochim Cosmochim Acta 64:2851–2862

Signorelli S, Carroll MR (2002) Experimental study of Cl solubility in hydrous alkaline melts: constraints on the theoretical maximum amount of Cl in trachytic and phonolitic melts. Contrib Mineral Petrol 143:209–218

Siljan OJ, Grande T, Schøning C (2001) Refractories for aluminium electrolysis cells. Part I: deterioration mechanisms based on phase equilibria. Aluminium 77:294–300

Simmons WB Jr, Heinrich EW (1975) A summary of the petrogenesis of the granite-pegmatite system in the northern end of the Pikes Peak batholith. Forschr Mineral 52:251–264

Simon AC, Pettke T, Candela PA, Piccoli PM, Heinrich CA (2004) Magnetite solubility and iron transport in magmatic-hydrothermal environments. Geochim Cosmochim Acta 68:4905–4914

Simon AC, Frank MR, Pettke T, Candela PA, Piccoli PM, Heinrich CA (2005) Gold partitioning in melt-vapor-brine systems. Geochim Cosmochim Acta 69:3321–3335

Simon AC, Pettke T, Candela PA, Piccoli PM, Heinrich CA (2006) Copper partitioning in a melt-vapor-brine-magnetite-pyrrhotite assemblage. Geochim Cosmochim Acta 70:5583–5600

Simon AC, Pettke T, Candela PA, Piccoli PM, Heinrich CA (2007) The partitioning behavior of As and Au in S-free and S-bearing magmatic assemblages. Geochim Cosmochim Acta 71:1764–1782

Sirbescu MLC, Nabelek PI (2003a) Dawsonite: an inclusion mineral in quartz from the Tin Mountain pegmatite, Black Hills, South Dakota. Am Mineral 88:1055–1059

Sirbescu MLC, Nabelek PI (2003b) Crustal melts below 400 °C. Geology 31:685–688

Skjerlie KP, Johnston AD (1992) Vapor-absent melting at 10 kbar of a biotite- and amphibole-bearing tonalitic gneiss: implications for the generation of A-type granites. Geology 20:263–266

Snow RJ, Welch BJ (1972) Reactions in the cryolite-silica system. Proc Australas Inst Min Metall 241:81–86

Sourirajan S, Kennedy GC (1962) The system H_2O–NaCl at elevated temperatures and pressures. Am J Sci 260:115–141

Stalder R, Ulmer P, Thompson AB, Günter D (2000) Experimental approach to constrain second critical end-points in fluid silicate systems: near-solidus fluids and melts in the system albite-H_2O. Am Mineral 85:68–77

Stebbins JF, Zeng Q (2000) Cation ordering at fluoride sites in silicate glasses: a high-resolution ^{19}F NMR study. J Non-Crystal Solids 262:1–5

Steele-MacInnis M, Lecumberri-Sanchez P, Bodnar RJ (2015) Synthetic fluid inclusions XX. Critical PTx properties of H_2O–$FeCl_2$ fluids. Geochim Cosmochim Acta 148:50–61

Štemprok M (1987) Greisenization (a review). Geol Rundsch 76:169–175

Štemprok M (1991) Ongonite from Ongon Khairkhan, Mongolia. Mineral Petrol 43:255–273

Štemprok M, Seltmann R (1994) The metallogeny of the Erzgebirge (Krušné hory). In: Seltmann R, Kämpf H, Möller P (eds) Metallogeny of collisional orogens. Czech Geological Survey, Prague, pp 61–69

Sterner SM, Chou IM, Downs RT, Pitzer KS (1992) Phase relations in the system NaCl–KCl–H_2O: V. Thermodynamic-PTX analysis of solid-liquid equilibria at high temperatures and pressures. Geochim Cosmochim Acta 56:2295–2309

Sterten Å (1980) Structural entities in NaF–AlF_3 melts containing alumina. Electrochim Acta 25:1673–1677

Stewart DB (1978) Petrogenesis of lithium-rich pegmatites. Am Mineral 63:970–980

Stilling AB (1998) Bulk composition of the Tanco pegmatite at Bernic Lake, Manitoba, Canada. M.Sc. thesis, University of Manitoba, Winnipeg, p 76

Stone M (1968) A study of the Praa Sands elvan and its bearing on the origin of elvans. Proc Ussher Soc 2:37–42

Stormer JC Jr, Carmichael ISE (1970) Villiaumite and the occurrence of fluoride minerals in igneous rocks. Am Mineral 55:126–134

Straub SM, Layne GD (2003) The systematics of chlorine, fluorine, and water in Izu arc front volcanic rocks: implications for volatile recycling in subduction zones. Geochim Cosmochim Acta 67:4179–4203

Strunz H, Nickel EH (2001) Strunz mineralogical tables. Chemical-structural classification system, 9th edn. Schweizerbart, Stuttgart, p 870

Student JJ, Bodnar RJ (1999) Synthetic fluid inclusions XIV: coexisting silicate melt and aqueous fluid inclusions in the haplogranite–H_2O–NaCl–KCl system. J Petrol 40:1509–1525

Tagirov B, Schott J (2001) Aluminum speciation in crustal fluids revisited. Geochim Cosmochim Acta 65:3965–3992

Tagirov B, Schott J, Harrichoury JC, Salvi S (2002) Experimental study of aluminum speciation in fluoride-rich supercritical fluids. Geochim Cosmochim Acta 66:2013–2024

Tanger JC IV, Helgeson HC (1988) Calculation of the thermodynamic and transport properties of aqueous species at high pressures and temperatures: revised equations of state for the standard partial molal properties of ions and electrolytes. Am J Sci 288:19–88

Tattich BC, Candela PA, Piccoli PM, Bodnar RJ (2015) Copper partitioning between felsic melt and H_2O–CO_2 bearing saline fluids. Geochim Cosmochim Acta 148:81–89

Taylor M, Smith RW, Ahler BA (1984) Gorceixite in topaz greisen assemblages, Silvermine area, Missouri. Am Mineral 69:984–986

Thomas R, Davidson P (2012) Evidence of a water-rich silica gel state during the formation of a simple pegmatite. Mineral Mag 76:2785–2801

Thomas R, Webster JD (2000) Strong tin enrichment in a pegmatite-forming melt. Mineral Deposita 35:570–582

Thomas R, Webster JD, Heinrich W (2000) Melt inclusions in pegmatite quartz: complete miscibility between silicate melts and hydrous fluids at low pressure. Contrib Mineral Petrol 139:394–401

Thomas R, Förster HJ, Rückers K, Webster JD (2005) Formation of extremely F-rich hydrous melt fractions and hydrothermal fluids during differentiation of highly evolved tin-granite magmas: a melt/fluid-inclusion study. Contrib Mineral Petrol 148:582–601

Timofeev A, Migdisov AA, Williams-Jones AE (2015) An experimental study of the solubility and speciation of niobium in fluoride-bearing aqueous solutions at elevated temperature. Geochim Cosmochim Acta 158:103–111

Tsay A, Zajacz Z, Sanchez-Valle C (2014) Efficient mobilization and fractionation of rare-earth elements by aqueous fluids upon slab dehydration. Earth Planet Sci Lett 398:101–112

Tuttle OF, Bowen NL (1958) Origin of granite in the light of experimental studies in the system $NaAlSi_3O_8$–$KAlSi_3O_8$–SiO_2–H_2O. Geol Soc Am Mem 74:153

Ueda S, Maeda M (1999) Phase-diagram study for the Al_2O_3–CaF_2–SiO_2 system. Metall Mater Trans 30B:921–925

Ulrich T, Mavrogenes J (2008) An experimental study of the solubility of molybdenum in H_2O and KCl–H_2O solutions from 500 °C to 800 °C, and 150 to 300 MPa. Geochim Cosmochim Acta 72:2316–2330

Ulrich T, Gunther D, Heinrich CA (1999) Gold concentrations of magmatic brines and the metal budget of porphyry copper deposits. Nature 399:676–679

Urabe T (1985) Aluminous granite as a source magma of hydrothermal ore deposits—an experimental study. Econ Geol 80:148–157

Urabe T (1987) The effect of pressure on the partitioning ratios of lead and zinc between vapor and rhyolite melts. Econ Geol 82:1049–1052

Urusova MA, Ravich MI (1966) Phase equilibria in the potassium fluoride-water system at elevated temperatures. Russ J Inorg Chem 11:353–357

Valyashko V, Urusova M (2003) Solubility behavior in ternary water-salt systems under sub- and supercritical conditions. Monatsh Chem 134:679–692

Van Lichtervelde M, Holtz F, Hanchar JM (2010) Solubility of manganotantalite, zircon and hafnon in highly fluxed peralkaline to peraluminous pegmatitic melts. Contrib Mineral Petrol 160:17–32

Vasyukova O, Williams-Jones AE (2014) Fluoride-silicate melt immisciblity and its role in REE ore formation: evidence from the Strange Lake rare metal deposit, Québec-Labrador, Canada. Geochim Cosmochim Acta 139:110–130

Veksler IV (2004) Liquid immiscibility and its role at the magmatic-hydrothermal transition: a summary of experimental studies. Chem Geol 210:7–31

Veksler IV, Thomas R (2002) An experimental study of B-, P- and F-rich synthetic granite pegmatite at 0.1 and 0.2 GPa. Contrib Mineral Petrol 143:673–683

Veksler IV, Dorfman AM, Kamenetsky M, Dulski P, Dingwell DB (2005) Partitioning of lanthanides and Y between immiscible silicate and fluorite melts, fluorite and cryolite and the origin of the lanthanide tetrad effect in igneous rocks. Geochim Cosmochim Acta 69:2847–2860

Veksler IV, Dorfman AM, Dulski P, Kamenetsky VS, Danyushevsky LV, Jeffries T, Dingwell DB (2012) Partitioning of elements between silicate melt and immiscible fluorie, chloride, carbonate, phosphate and sulfate melts, with implications to the origin of natrocarbonatite. Geochim Cosmochim Acta 79:20–40

Villemant B, Boudon G (1999) H_2O and halogen (F, Cl, Br) behaviour during shallow magma degassing processes. Earth Planet Sci Lett 168:271–286

Vladimirov AG, Kruk NN, Chupin VP, Turkina ON, Rudnev SM, Vladimirov VG, Titov AV (1991) Topaz-protolithionite granites and ongonites of the Bazardara ore formation (south-eastern Pamir). Soviet Geol Geophys 32:34–41

Wallace PJ (2005) Volatiles in subduction zone magmas: concentrations and fluxes based on melt inclusion and volcanic gas data. J Volcanol Geotherm Res 140:217–240

Walther JV (1986) Mineral solubilities in supercritical H_2O solutions. Pure Applied Chem 58:1585–1598

Walther JV (2001) Experimental determination and analysis of the solubility of corundum in 0.1 and 0.5 m NaCl solutions between 400 and 600 °C from 0.5 to 2.0 kbar. Geochim Cosmochim Acta 65:2843–2851

Walther JV, Helgeson HC (1977) Calculation of the thermodynamic properties of aqueous silica and the solubility of quartz and its polymorphs at high pressures and temperatures. Am J Sci 277:1315–1351

Wang L, Wang H, Huang Z (1997) Discovery of three-end member components in Li-F granites and the origin of their liquid segregation. Geol Explor 33:11–20 (in Chinese)

Wang L, Wang H, Huang Z (2000) REE geochemical indicatrices of Li–F granite liquid segregation. Chinese J Geochem 19:203–216

Wang P, Anderko A, Springer RD, Kosinski JJ, Lencka MM (2010) Modeling chemical and phase equilibria in geochemical systems using a speciation-based model. J Geochem Expl 106:219–225

Wang P, Kosinski JJ, Lencka MM, Anderko A, Springer RD (2013) Thermodynamic modeling of boric acid and selected metal borate systems. Pure Appl Chem 85:2117–2144

Wasternack J, Martens S, Gottesmann B (1995) Field and petrographic study of brecciation and greisenization phenomena in the Gottesberg tin deposit (Saxony, Germany). Z Geol Wiss 23:619–642

Webster JD (1990) Partitioning of F between H_2O and CO_2 fluids and topaz rhyolite melt. Implications for mineralizing magmatic-hydrothermal fluids in F-rich granitic systems. Contrib Mineral Petrol 104:424–438

Webster JD (1992) Fluid-melt interactions involving Cl-rich granites: experimental study from 2 to 8 kbar. Geochim Cosmochim Acta 56:659–678

Webster JD (1997a) Chloride solubility in felsic melts and the role of chloride in magmatic degassing. J Petrol 38:1793–1807

Webster JD (1997b) Exsolution of magmatic volatile phases from Cl-enriched mineralizing granitic magmas and implications for ore metal transport. Geochim Cosmochim Acta 61:1017–1029

Webster JD (2004) The exsolution of magmatic hydrosaline chloride liquids. Chem Geol 210:33–48

Webster JD, De Vivo B (2002) Experimental and modeled solubilities of chlorine in aluminosilicate melts, consequences of magma evolution, and implications for exsolution of hydrous chloride melt at Mt. Somma-Vesuvius. Am Mineral 87:1046–1061

Webster JD, Duffield WA (1994) Extreme halogen abundances in tin-rich magma of the Taylor Creek Rhyolite, New Mexico. Econ Geol 89:840–850

Webster JD, Holloway JR (1988) Experimental constraints on the partitioning of Cl between topaz rhyolite melt and H_2O and H_2O + CO_2 fluids: new implications for granitic differentiation and ore deposition. Geochim Cosmochim Acta 52:2091–2105

Webster JD, Holloway JR (1990) Partitioning of F and Cl between magmatic hydrothermal fluids and highly evolved granitic magmas. Geol Soc Am Spec Pap 246:21–34

Webster JD, Rebbert CR (1998) Experimental investigation of H_2O and Cl- solubilities in F-enriched silicate liquids; implications for volatile saturation of topaz rhyolite magmas. Contrib Mineral Petrol 132:198–207

Webster JD, Rebbert CR (2001) The geochemical signature of fluid-saturated magma determined from silicate melt inclusions in Asension Island granite xenoliths. Geochim Cosmochim Acta 65:123–136

Webster JD, Holloway JR, Hervig RL (1987) Phase equilibria of a Be, U and F-enriched vitrophyre from Spor Mountain, Utah. Geochim Cosmochim Acta 51:389–402

Webster JD, Burt DM, Aguillon RA (1996) Volatile and lithophile trace-element geochemistry of Mexican tin rhyolite magmas deduced from melt inclusions. Geochim Cosmochim Acta 60:3267–3283

Webster JD, Thomas R, Rhede D, Forster HJ, Seltmann R (1997) Melt inclusions in quartz from an evolved peraluminous pegmatite: geochemical evidence for strong tin enrichment in fluorine-rich and phosphorus-rich residual liquids. Geochim Cosmochim Acta 61:2589–2604

Webster JD, Thomas R, Veksler I, Rhede D, Seltmann R, Förster HJ (1998) Late-stage processes in P- and F-rich granitic magmas. Acta Univ Carol Geol 42:181–188

Webster J, Thomas R, Förster HJ, Seltmann R, Tappen C (2004) Geochemical evolution of halogen-enriched granite magmas and mineralizing fluids of the Zinnwald tin-tungsten mining district, Erzgebirge, Germany. Mineral Deposita 39:452–472

Webster JD, Tappen CM, Mandeville CW (2009) Partitioning behavior of Cl and F in the system apatite-melt-fluid. II: felsic silicate systems at 200 MPa. Geochim Cosmochim Acta 73:559–581

Webster JD, Vetere F, Botcharnikov RE, Goldoff B, McBirney A, Doherty AL (2015) Experimental and modeled chlorine solubilities in aluminosilicate melts at 1 to 7000 bars and 700 to 1250 °C: applications to magmas of Augustine Volcano, Alaska. Am Mineral 100:522–535

Weidner JR, Martin RF (1987) Phase equilibria of a fluorine-rich leucogranite from the St. Austell pluton. Cornwall. Geochim Cosmochim Acta 51:1591–1597

Weill DF, Fyfe WS (1964) The 1010° and 800° isothermal sections in the system Na_3AlF_6–Al_2O_3–SiO_2. J Electrochem Soc 111:582–585

Wen S, Nekvasil H (1994) SOLVCALC: an interactive graphics program package for calculating the ternary feldspar solvus and for two-feldspar geothermometry. Comp Geosci 20:1025–1040

Wenk HR, Bulakh A (2004) Minerals. Their constitution and origin. Cambridge Univ Press, Cambridge, p 666

Westrich HR, Eichelberger JC, Hervig RL (1991) Degassing of the 1912 Katami magmas. Geophys Res Lett 18:1561–1564

Wilke M, Jahn S, Schmidt C, Dubrail J, Appel K, Borchert M, Kvashnina K, Pascarelli S, Manning CE (2013) Insights from X-ray absorption-fluorescence spectroscopy and ab-initio molecular dynamics on concentration and complexation of Zr and Hf in aqueous fluids at high pressure and temperature. J Phys Conf Ser 430:012122

Wilkinson JJ, Nolan J, Rankin AH (1996) Silicothermal fluid: a novel medium for mass transport in the lithosphere. Geology 24:1059–1062

Williams TJ, Candela PA, Piccoli PM (1995) The partitioning of copper between silicate melts and two-phase aqueous fluids: an experimental investigation at 1 kbar, 800 °C and 0.5 kbar, 850 °C. Contrib Mineral Petrol 121:388–399

Williams TJ, Candela PA, Piccoli PM (1997) Hydrogen-alkali exchange between silicate melts and two-phase aqueous mixtures: an experimental investigation. Contrib Mineral Petrol 128:114–126

Williams-Jones AE, Bowell RJ, Migdisov AA (2009) Gold in solution. Elements 5:281–287

Williams-Jones AE, Heinrich CA (2005) Vapor transport of metals and the formation of magmatic-hydrothermal ore deposits. Econ Geol 100:1287–1312

Williamson BJ, Stanley CJ, Wilkinson JJ (1997) Implications from inclusions in topaz for greisenisation and mineralisation in the Hensbarrow topaz granite, Cornwall, England. Contrib Mineral Petrol 127:119–128

Williamson BJ, Wilkinson JJ, Luckham PF, Stanley CJ (2002) Formation of coagulated colloidal silica in high-temperature mineralizing fluids. Mineral Mag 64:547–553

Witt WK (1988) Evolution of high-temperature hydrothermal fluids associated with greisenization and feldspathic alteration of a tin-mineralized granite, northeast Queensland. Econ Geol 83:310–334

Wood SA, Samson IM (1998) Solubility of ore minerals and complexation of ore metals in hydrothermal solutions. Rev Econ Geol 10:33–80

Woodland AB, Walther JV (1987) Experimental determination of the solubility of the assemblage paragonite, albite, and quartz in supercritical H_2O. Geochim Cosmochim Acta 51:365–372

Wyllie PJ (1979) Magmas and volatile components. Am Mineral 64:469–500

Wyllie PJ, Ryabchikov ID (2000) Volatile components, magmas, and critical fluids in the upwelling mantle. J Petrol 41:1195–1206

Wyllie PJ, Tuttle OF (1961) Experimental investigation of silicate systems containing two volatile components. Part II. The effects of NH_3 and HF, in addition to H_2O, on the melting temperatures of albite and granite. Am J Sci 259:128–143

Xiong XL, Rao B, Chen FR, Zhu JC, Zhao ZH (2002) Crystallization and melting experiments of a fluorine-rich leucogranite from the Xianghualing Pluton, South China, at 150 MPa and H_2O-saturated conditions. J Asian Earth Sci 21:175–188

Yardley BWD (2005) Metal concentrations in crustal fluids and their relationship to ore formation. Econ Geol 100:613–632

Yardley BWD, Bodnar RJ (2014) Fluids in the continental crust. Geochem Perspect 3:1–123

Zajacz Z, Halter WE, Pettke T, Guillong M (2008) Determination of fluid/melt partition coefficients by LA-ICP MS analysis of co-existing fluid and silicate melt inclusions: controls on element partitioning. Geochim Cosmochim Acta 72:2169–2197

Zajacz Z, Hanley JJ, Heinrich CA, Halter WE, Guillong M (2009) Diffusive reequilibration of quartz-hosted silicate melt and fluid inclusions: are all metal concentrations unmodified? Geochim Cosmochim Acta 73:3013–3027

Zajacz Z, Seo JH, Candela PA, Piccoli PM, Heinrich CA, Guillong M (2010) Alkali metals control the release of gold from volatile-rich magmas. Earth Planet Sci Lett 297:50–56

Zajacz Z, Seo JH, Candela PA, Piccoli PM, Tossell JA (2011) The solubility of copper in high-temperature magmatic vapors: a quest for the significance of various chloride and sulfide complexes. Geochim Cosmochim Acta 75:2811–2827

Zajacz Z, Candela PA, Piccoli PM, Sanchez-Valle C (2012a) The partitioning of sulfur and chlorine between andesite melts and magmatic volatiles and the exchange coefficients of major cations. Geochim Cosmochim Acta 89:81–101

Zajacz Z, Candela PA, Piccoli PM, Sanchez-Valle C, Wälle M (2012b) Gold and copper in volatile saturated mafic to intermediate magmas: solubilities, partitioning and implications for ore deposit formation. Geochim Cosmochim Acta 91:140–159

Zaraisky GP, Korzhinskaya V, Kotova N (2010) Experimental studie of Ta_2O_5 and columbite-tantalite solubility in fluoride solutions from 300 to 550°C and 50 to 100 MPa. Mineral Petrol 99:287–300

Zeng Q, Stebbins JF (2000) Fluoride sites in aluminosilicate glasses: high-resolution ^{19}F NMR results. Am Mineral 85:863–867

Zezin DY, Migdisov AA, Williams-Jones AE (2007) The solubility of gold in hydrogen sulfide gas: an experimental study. Geochim Cosmochim Acta 71:3070–3081

Zhang Y (1982) Electronegativities of elements in valence states and their applications. 2. A scale for strength of Lewis acids. Inorg Chem 21:3889–3893

Zhang Y, Frantz JD (1989) Experimental determination of the compositional limits of immiscibility in the system $CaCl_2$–H_2O–CO_2 at high temperatures and pressures using synthetic fluid inclusions. Chem Geol 74:289–308

Zhang Y, Gupta S, Sahai Y, Rapp RA (2002) Modeling of the solubility of alumina in the NaF–AlF_3 system at 1300 K. Metall Mater Trans 33B:315–319

Zhang C, Holtz F, Ma C, Wolff PE, Li X (2012a) Tracing the evolution and distribution of F and Cl in plutonic systems from volatile-bearing minerals: a case study from the Liujiawa pluton (Dabie orogen, China). Contrib Mineral Petrol 164:859–879

Zhang L, Audétat A, Dolejš D (2012b) Solubility of molybdenite (MoS_2) in aqueous fluids at 600–800 °C, 200 MPa: a synthetic fluid inclusion study. Geochim Cosmochim Acta 77:175–185

Zhu JC, Liu W (1990) Topazite-ongonite relationships and its bearing on vertical zonatio in rare-metal granites: evidence from Xianghualing district, Hunan Province, China. In: Proceedings of the 8th quadrennial IAGOD symposium. Schweizerbart, Stuttgart, pp 303–313

Zhu C, Sverjensky DA (1991) Partitioning of F–Cl–OH between minerals and hydrothermal fluids. Geochim Cosmochim Acta 55:1837–1858

Zhu C, Sverjensky DA (1992) F–Cl–OH partitioning between biotite and apatite. Geochim Cosmochim Acta 56:3435–3467

Zhu J, Liu W, Zhou F (1993) Ongonite and topazite in dike no. 431 of Xianghualing district and their spatial zonation and genetic relationship. Acta Petrol Sin 9:158–166 (in Chinese)

Chapter 8
The Behavior of Halogens During Subduction-Zone Processes

Jaime D. Barnes, Craig E. Manning, Marco Scambelluri and Jane Selverstone

Abstract Halogens (Cl, F, I, Br) are enriched in surface reservoirs compared to the mantle. The subduction of these reservoirs in the form of sedimentary pore fluids, sediments, altered oceanic crust, and serpentinized mantle lithosphere returns halogens to the mantle and to regions of arc magma genesis. Pore fluids are particularly enriched in I, yet shallow pore fluid loss in subduction zones due to compaction, as indicated by $^{129}I/I$ ratios, makes pore fluids a negligible halogen source at depths $> \sim 5$ km. Sediments can host large quantities of halogens, particularly I. However, serpentinites $\pm$ altered oceanic crust subduct the largest amount of halogens to depths of magma genesis. Due to their hydrophilic nature, halogens are lost to aqueous slab-derived fluids during prograde metamorphic reactions. The addition of halogens, particularly Cl, increases the ability of subduction-zone fluids to transport metals and trace elements. The amount of Cl in solution is a function of the P-T conditions of the subduction zone, such that higher temperatures at a given depth and lower pressures at a given temperature favor ion pair formation ($NaCl_{aq}$, KCl_{aq}). Therefore, ion pairing will be more important in subduction zones with warmer geotherms, such as Cascadia, compared to those with cooler geotherms, such as Alaska. High halogen concentrations in melt inclusions and volcanic gas emissions from the arc front support the efficiency of fluid loss and transport from the slab to the region of magma genesis. Despite this high efficiency, mass balance calculations and halogen concentrations in back-arc

J.D. Barnes (✉)
Department of Geological Sciences, University of Texas, Austin, TX 78712, USA
e-mail: jdbarnes@jsg.utexas.edu

C.E. Manning
Department of Earth, Planetary and Space Sciences, University of California, Los Angeles, CA 90095-1567, USA

M. Scambelluri
Dipartimento di Scienze Della Terra, Ambiente e Vita DISTAV- Universita di Genova, Corso Europa 26, 16132 Genoa, Italy

J. Selverstone
Department of Earth and Planetary Sciences, University of New Mexico, Albuquerque, NM 87131-0001, USA

D.E. Harlov and L. Aranovich (eds.), *The Role of Halogens in Terrestrial and Extraterrestrial Geochemical Processes*, Springer Geochemistry,
https://doi.org/10.1007/978-3-319-61667-4_8

basalts and ocean island basalts show that more halogens are subducted than returned to the Earth's surface through volcanic arc fronts, implying transport of halogens into the upper mantle. Chlorine is the halogen most efficiently recycled to the surface, and F the least. Shallow loss of I and Br, through fore-arc fluids that are not accounted for in the mass balance calculation, likely explain the imbalance in these cycles.

8.1 Introduction

Halogens (F, Cl, Br, and I) are highly mobile in fluids, making them effective tracers of fluid sources within subduction zones. Despite their incompatibility, the relatively small ionic radii of Cl and F permit them to be incorporated into hydrous minerals (e.g., apatite, amphibole, serpentine, micas) in moderate amounts, primarily by exchange for OH^-. In contrast, the large ionic radii of Br and I make them highly incompatible. Serpentine is the notable exception among hydrous minerals because of its ability to incorporate up to 45 μg/g I in its structure (Kendrick et al. 2013). The breakdown of different halogen hosts (e.g., amphibole in altered oceanic crust or serpentine in hydrated mantle peridotite) along a subduction zone P-T gradient can be used to trace fluid sources based on diagnostic halogen ratios (F/Cl, I/Cl, Br/Cl) (Fig. 8.1), stable Cl isotope compositions, and $^{36}Cl/Cl$ and $^{129}I/I$ ratios of various reservoirs.[1]

The transport of halogens from the subducting slab to the overlying mantle wedge likely occurs primarily via dissolution in an H_2O-rich fluid produced from the dehydrating slab (e.g., Manning 2004). The addition of halogens, particularly Cl, to subduction-zone fluids changes the physical properties and solute structure compared to pure H_2O (Mantegazzi et al. 2013; Sakuma and Ichiki 2015). For example, saline solutions will suppress the onset of slab melting and cause dehydration reactions to proceed at shallower depths compared to pure H_2O or H_2O-CO_2 fluids (e.g., Aranovich et al. 2013). Additionally, Cl and F complex with metals, suggesting that halogen-rich subduction fluids may be critical in the transport of metals within subduction zones (Keppler 1996, 2017).

The enrichment of halogens in arc magmas has long been cited as evidence for subduction of surface reservoirs. For example, melt inclusions from basaltic arc

[1]Halogens can also be transported via melt and "slab diapirs" (Behn et al. 2011; Gerya et al. 2003). For example, F may be more mobilized in melt compared to fluid (Straub and Layne 2003). However, in general, halogens will strongly partition into a fluid phase compared to a melt (Bureau et al. 2000). Therefore, in this review, the focus is on halogen transport via fluids from the dehydrating slab. In addition, the use of halogen ratios and halogen isotopes to trace slab-derived fluid sources has traditionally assumed transport through the mantle wedge in a near vertical manner and therefore outputs across the arc represent depth to the subducting slab. This assumption ignores potential complications due to non-vertical transport along the slab-mantle interface and within the mantle wedge (Hoernle et al. 2008; Marschall and Schumacher 2012).

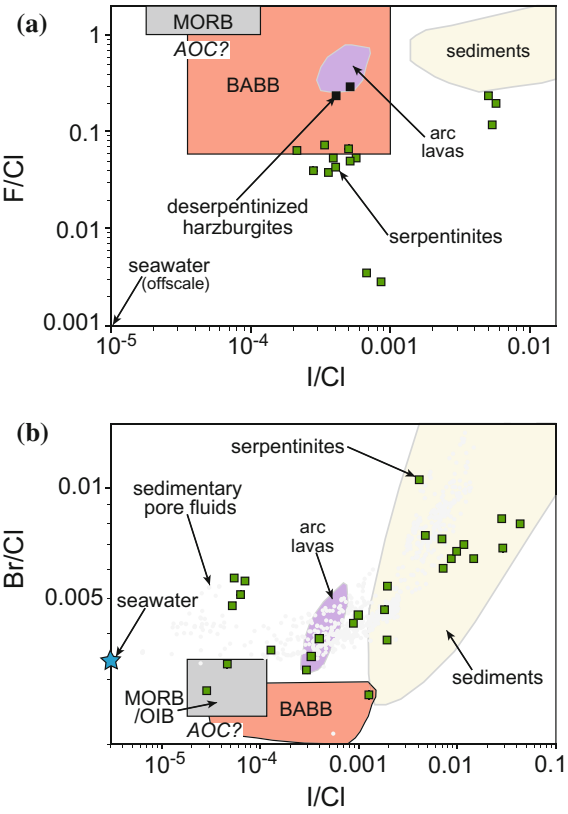

Fig. 8.1 **a** F/Cl versus I/Cl and **b** Br/Cl versus I/Cl of various subduction-zone reservoirs (modified from John et al. 2011; Kendrick et al. 2014a). Arc lava and subducting sediment data from John et al. (2011). F/Cl back arc basalt (BABB) glass data from Bézos et al. (2009); Br/Cl and I/Cl BABB data from Kendrick et al. (2014a). Serpentinite data in a from John et al. (2011) and in **b** from Kendrick et al. (2013). The I concentration in altered oceanic crust (AOC) is unknown. Here we assume it to be lower than that of MORB (Kendrick et al. 2014a). Halogen ratios of sedimentary pore fluids from Fehn et al. (2006, 2007), Muramatsu et al. (2001) and references therein

volcanoes have Cl concentrations up to ~5800 μg/g (St. Augustine, Aleutians; Zimmer et al. 2010) and F concentrations up to ~2500 μg/g (Irazú, Central America; Benjamin et al. 2007). Although halogens are extremely hydrophilic, there is increasing evidence that they may survive within the slab past the arc volcanic front despite extensive slab dehydration (~65% global average of water loss by subarc depths; Hacker 2008). Recent work has also shown halogen enrichment in back-arc basalts and ocean-island basalts compared to MORB (e.g., Kendrick et al. 2012b, 2014a, b; Kent et al. 2002; Sun et al. 2007).

Here we review halogen reservoirs, movement, and geochemistry in subduction systems. We begin by providing an overview of the concentrations of halogens in inputs (pore fluids, sediments, altered oceanic crust, and serpentinites) into the subduction system and how these halogens are lost during subduction zone metamorphism. Halogen concentrations in outputs (volcanic gas and melt inclusions) are summarized, allowing for calculations to be made of halogen flux through the volcanic front and evidence of halogen transport into the upper mantle. We also discuss the role halogens have on subduction-zone fluid chemistry and the transport of metals and trace elements. Finally, we discuss the use of halogen isotopes as tracers of volatile sources in subduction zones.

8.2 Halogen Sources into the Subduction Zone

8.2.1 Pore Fluids

It is estimated that pore fluid in subducted sediments and altered oceanic crust (AOC) accounts for ~60% of the total water entering subduction zones (Jarrard 2003). Pore fluids are enriched in halogens, especially I (Kastner et al. 1991; Martin et al. 1993; Muramatsu et al. 2007). This I enrichment is due to the breakdown of organic sediments during diagenesis with some samples having I concentrations >100 μg/g (Fehn et al. 2007; Martin et al. 1993; Muramatsu et al. 2001; Snyder et al. 2005; Tomaru et al. 2007). These high concentrations are well above the seawater concentration of 55 ng/g (Geochemical Reference Model, earthref.org/GERM). In general, the Br concentration in pore fluids ranges from near that of seawater to twice the concentration of seawater (Fehn et al. 2007; Martin et al. 1993; Muramatsu et al. 2007). Chlorine concentrations are also high, ranging from near seawater concentration (≈19,500 μg/g) to about 50% of seawater concentration (Kastner et al. 1991; Mottl et al. 2004). Sedimentary pore fluids have Br/Cl ratios of 0.0035−0.009 and I/Cl ratios of 0.000003−0.01 (both ratios are characteristically higher than that of seawater) (Kendrick et al. 2014b) (Fig. 8.1). To our knowledge, little work has been done to determine F concentrations in pore fluids.

It is commonly assumed that pore fluids are expelled at shallow levels in subduction zones (by ~5 km depth) due to porosity collapse and compaction (e.g., Jarrard 2003; Kastner et al. 1991; van Keken et al. 2011). Pore fluids are thus typically ignored in elemental budgets of subduction zone cycling. Some work suggests that pore fluids may survive to ~100 km depth in subduction zones, based on noble gas and high I/Cl and Br/Cl ratios in fluid inclusions in a mantle wedge peridotite (Sumino et al. 2010). However, recent studies have shown that serpentinites are a large, hitherto unknown sink of I and that high I/Cl and Br/Cl ratios in fore-arc serpentinites can explain these halogen trends in fluid inclusions (Kendrick et al. 2011, 2013). There are two different interpretations regarding pore fluid interaction with serpentinites: (1) pore fluids serpentinize peridotite under low-T as a result of fluid infiltration in a bending fault in outer rise settings (John et al. 2011; Kendrick et al. 2011), or (2) pore fluids are squeezed from the compacting sediment and infiltrate the peridotite above the subduction channel, driving low-T serpentinization (Kendrick et al. 2011; Scambelluri and Tonarini 2012). These elements are then recycled in high-pressure fluids without the need to subduct pore fluids to 100 km (Kendrick et al. 2011, 2013).

8.2.2 Sediments

Estimates of Cl and F concentration in marine sediments vary widely. Measured Cl concentrations in marine sediments (e.g., hemipelagic mud, marls, pelagic clay)

from various DSDP/ODP/IODP drill sites range from ~40 to ~2000 μg/g (Barnes et al. 2008, 2009b; John et al. 2011) and F concentrations range from ~400 to ~1250 μg/g (John et al. 2011). Ito et al. (1983) used a Cl concentration of 1200 μg/g in clays and carbonates to calculate that 3.2×10^{12} g of Cl are subducted globally each year in marine sediments. Subsequent flux estimates of Cl and F derived from subducting sediments, are based on their average concentration in the upper continental crust (Cl = 640 μg/g and F = 611 μg/g; Gao et al. 1998; Wedepohl 1995), resulting in the estimate that 1.6×10^{12} g of Cl and 1.5×10^{12} g of F are globally subducted in sediments each year (John et al. 2011; Straub and Layne 2003).

70% of the Earth's I is hosted in marine sediments due to the accumulation of I in organic material (Muramatsu and Wedepohl 1998). Estimated and measured I concentrations in marine sediments range from <1 to 28 μg/g (John et al. 2010; Li and Schoomaker 2003; Muramatsu et al. 2007; Muramatsu and Wedepohl 1998). Muramatsu and Wedepohl (1998) estimate 30 ppm I in marine carbonates. Because I concentrations in marine sediments are directly linked to the presence of organic material and because most subducting sediments were deposited under deep sea conditions, sediments entering the subduction system are likely to have I concentrations near the lower end of this range (Fehn 2012). If one uses 5 μg/g I in subducting marine sediments, then an estimated 1.2×10^{10} g of I in marine sediments is subducted annually.[2]

Bromine concentrations in marine sediments are poorly known. Li (1982) estimates concentrations of 70 μg/g in marine pelagic clays. Analyses of marine sediments indicate that values range from 0.3 to 70 μg/g Br (John et al. 2011; Muramatsu et al. 2007). Using 20 μg/g Br (average of values reported in John et al. (2011) and Muramatsu et al. (2007)), an estimated 4.9×10^{10} g of Br is subducted annually in marine sediments.

With the exception of I, little work has been done on halogen loss from sediments during subduction. Data from metasedimentary gneisses, mica schists, and granulites show that sediments likely lose 75 to 95% of their I by about 400 °C (Muramatsu and Wedepohl 1998). Iodine enrichment in fore-arc waters and gases is largely due to the loss of I from marine sediments during the early stages of subduction (e.g., Muramatsu et al. 2001; Tomaru et al. 2007). Despite the ability of sediments to host large amounts of halogens, sediments constitute a relatively small percentage of the subducted material and, in the case of I, halogens may be lost from sediments early in the subduction process.

[2]For consistency and ease of comparing input fluxes, all calculated fluxes in this contribution use the parameters outlined in Straub and Layne (2003) and John et al. (2011): convergence rate of 5 cm/yr, bulk crust density of 2.8 g/cm^3, 44,000 km of trench length, 400 m thickness of sediment, 6 km thickness of AOC, and 5% serpentinization of the upper 6 km of lithospheric mantle (or 100% serpentinization of 300 m) to 15% serpentinization of the upper 3 km of lithospheric mantle (or 100% serpentinization of 450 m).

8.2.3 Altered Oceanic Crust (AOC)

Most work on halogen concentrations in AOC has focused on Cl and to a lesser extent F. However, Cl and F concentrations in AOC remain poorly constrained due to limited accessibility of the deeper crust; scarcity of Cl and F abundance data of bulk rock and secondary minerals in the literature; and the chemical heterogeneity of the crust (Straub and Layne 2003). Metasomatism of oceanic crust results in the formation of secondary hydrous minerals (e.g., clays, chlorite, amphiboles, talc, epidote), which can incorporate Cl and F into their mineral structure (e.g., Ito et al. 1983; Philippot et al. 1998; Vanko 1986). Amphibole is commonly assumed to be the major sink for Cl and F in AOC. Chlorine concentrations of amphibole range from below electron microprobe detection limits (typically ~0.01 wt%) to as high as 4 wt% (Gillis 1996; Gillis and Meyer 2001; Ishizuka 1989; Laverne et al. 1995; Pertsev et al. 2015; Vanko 1986; Vanko and Stakes 1991); whereas F concentrations range from below electron microprobe detection limits (typically ~0.2 wt%) to as high as 0.54 wt% (Gillis 1996; Gillis and Meyer 2001; Vanko 1986). Estimates of the Cl concentration in AOC, based on assumed Cl concentrations and modal abundances of secondary minerals, range from 50 to 78 μg/g Cl (Ito et al. 1983; Straub and Layne 2003). These values yield an estimated 2.5 to 2.9 $\times$ 10^{12} g of Cl in AOC subducted globally each year (Ito et al. 1983; Jarrard 2003). Analyses of bulk Cl concentrations in AOC are limited to three studies (Barnes and Cisneros 2012; Bonifacie et al. 2007a; Sano et al. 2008). Barnes and Cisneros (2012) propose 207 μg/g Cl in AOC based on a weighted average of bulk Cl concentrations in extrusive lavas, sheeted dikes, and gabbros from seven DSDP/ODP/IODP drill sites for a subducted Cl budget of 8.1 $\times$ 10^{12} g/yr from AOC. Bulk-rock Cl contents in eclogite-facies AOC rocks range from 10 to 95 μg/g (Marschall et al. 2009; Selverstone and Sharp 2013); bulk Cl concentrations determined from Cl concentrations in eclogite-facies minerals yield similar estimates (71–79 μg/g; Debret et al. 2016). Most of the Cl is hosted in amphiboles, with smaller amounts contained in chlorite, talc, chloritoid, garnet, and omphacite (Debret et al. 2016; Selverstone and Sharp 2013). Calculated F concentration for AOC, based on F concentrations in minerals, is 216 μg/g with an estimated 8.0 $\times$ 10^{12} g of F in AOC globally subducted each year (John et al. 2011; Straub and Layne 2003). Bulk F concentrations in eclogite-facies AOC, also based on F concentrations in minerals, ranges from 10 to 16 μg/g, suggesting loss of F to the fore-arc from amphibole breakdown (Debret et al. 2016).

The Br and I content of AOC is virtually unknown. Muramatsu and Wedepohl (1998) estimate that AOC hosts about 9 ng/g I (nearly identical to the I concentration in MORB, see Sect. 8.5.1) based on analyses of bulk mafic rock. This suggests that a calculated 3.3 $\times$ 10^{8} g of I in AOC are globally subducted each year. Kendrick et al. (2014a) hypothesized that AOC has lower Br/Cl and I/Cl ratios than MORB due to hydrothermal alteration, which increases the Cl concentration in AOC. They suggest a Br/Cl of <0.0025, but do not speculate on the I/Cl ratio

(Kendrick et al. 2014a) (Fig. 8.1). For our flux calculations (Table 8.1), we use a Br concentration of 150 ng/g. This value is based on Br concentrations in MORB (see Sect. 8.5.1) and is consistent with the Br/Cl ratio used by Kendrick et al. (2014a).

Fluids released by amphibole breakdown were long thought to be the primary fluid source for arc magmatism and the control on the location of the volcanic front (Davies and Stevenson 1992; Tatsumi 1986; Tatsumi and Eggins 1995). Additionally, amphibole breakdown may produce the Cl-rich fluids found in eclogites (Philippot and Selverstone 1991). However, experimental constraints indicate that equilibrium amphibole breakdown occurs at shallower depths than most arc volcano fronts, so amphibole-derived, Cl-rich fluids likely primarily affect the forearc mantle (Schmidt and Poli 1998). Therefore, a slab-derived saline fluid source which is stable to greater depths in a subduction zone is needed to account for the transport of Cl to sub-arc depths (e.g., Scambelluri and Philippot 2001).

8.2.4 Serpentinites

In the last 20 years, it has become clear that serpentinites play a key role in the transport of water, carbon, fluid-mobile elements (FME; e.g., B, As, Sb, Li, Pb), and halogens into subduction zones. Serpentinites form via the hydration of mantle rocks in different geodynamic environments (Fig. 8.2a) and host up to 13 wt% water. Historically, serpentinite formation was attributed to seawater-driven alteration of mid-ocean ridge mantle. Such abyssal serpentinites are more widespread in modern slow- and ultraslow-spreading oceans, where they can cover 25% of the seafloor (Cannat et al. 1995). Past Alpine subduction largely involved this type of oceanic lithosphere (Lagabrielle and Cannat 1990). In fast spreading oceans, like the present-day Pacific, a thick crustal layer prevents seawater interaction with deep-seated mantle peridotite, unless transform faults and bend faults at outer rises (Fig. 8.2a) enable deep seawater infiltration and mantle serpentinization (Kerrick 2002; Ranero et al. 2003). The extent of mantle serpentinization within bend faults has yet to be properly quantified. At convergent plate margins, rising slab fluids form kilometer-thick serpentinite layers in the supra-subduction forearc mantle (Bostock et al. 2002; Hyndman and Peacock 2003; Rüpke et al. 2004; Savov et al. 2005; Tatsumi 1989).

Serpentine (antigorite) stability over a large pressure range provides a means to transport water and FME to depths of 150–200 km (Fig. 8.2b) (Ulmer and Trommsdorff 1995; Wunder and Schreyer 1997), thus affecting global geochemical cycles (e.g., Barnes and Straub 2010; Cannaò et al. 2015; Deschamps et al. 2013; Luth 2014; Ryan and Chauvel 2014; Scambelluri et al. 1997, 2004; Scambelluri and Tonarini 2012; Schmidt and Poli 1998; Straub and Layne 2003). In addition, the trace element and rare earth element (REE) compositions of serpentinites can be used to fingerprint the tectonic setting of formation and the fluid-rock interactions occurring during subduction (Fig. 8.2a) (Deschamps et al. 2013; Kodolányi et al. 2012). Compared to abyssal serpentinites from mid-ocean ridges, the geochemistry

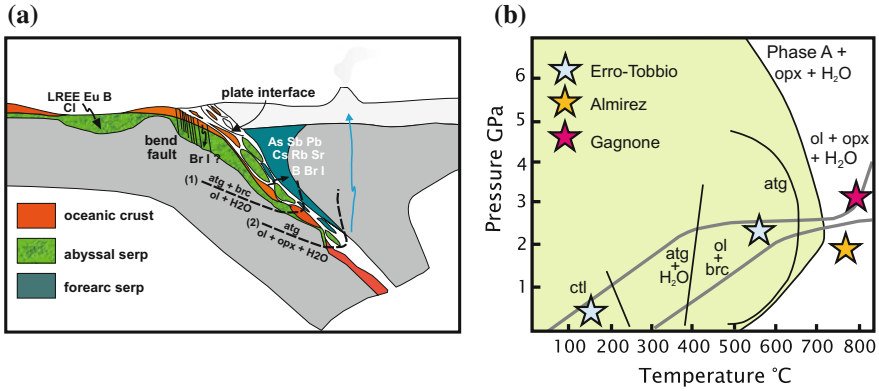

Fig. 8.2 **a** Schematic sketch (not to scale) showing serpentinite from various environments: (1) abyssal serpentinite, (2) bend-fault serpentinite, and (3) forearc mantle serpentinite. Also shown are subducting serpentinites and the plate interface subduction channel and the possible fluxes of elements in abyssal and forearc serpentinites (after Deschamps et al. 2013). Still unknown is the effective elemental influx related to bend faults. The hypothesized flux shown here in bend faults is after John et al. (2011) and Kendrick et al. (2011). Serpentinite in the subduction plate interface becomes enriched in a comparable set of elements as the forearc serpentinite (Cannaò et al. 2015; Deschamps et al. 2013; Scambelluri et al. 2014). **b** P-T diagram showing the stability field of chrysotile, antigorite + brucite, antigorite, and olivine + orthopyroxene assemblages. The stability of antigorite is influenced by the Al content that shifts antigorite stability to higher T (Ulmer and Trommsdorff 1995). Model subduction-zone gradients at the top of the slab from Syracuse et al. (2010) are represented by the *dark grey curves*. The subduction zone gradients reported here correspond to the ones shown in Fig. 8.10. The *stars* indicate the P-T crystallization conditions of Erro-Tobbio (shallow serpentinization overprinted by high-pressure recrystallization) (Scambelluri et al. 2004), Almirez (Trommsdorff et al. 1998) and Gagnone (Scambelluri et al. 2014). Abbreviations: *atg* antigorite, *brc* brucite, *ol* olivine, *opx* orthopyroxene

of serpentinites from convergent margins suggests significant involvement of sedimentary material, either present on top of the bending faults or in the subduction channel, located at the interface between the subducting and the overriding plates (Fig. 8.2a) (Deschamps et al. 2013; John et al. 2011; Kendrick et al. 2011; Lafay et al. 2013; Scambelluri et al. 2014).

The uptake of water, C, FME, and halogens into serpentinites and the cycling of these elements during subduction can be determined using coupled field and geochemical studies of serpentinites recording P-T conditions from shallow to deep levels within subduction zones. Low-P and low-T ($T < 300$ °C; Fig. 8.2b) serpentinization generally produces lizardite and/or chrysotile pseudomorphs (with variable amounts of chlorite, magnetite $\pm$ talc, actinolite) after the primary mantle minerals (Fig. 8.3a). During subduction, fluids and elements are lost from serpentinite during the chrysotile-antigorite transition (Kodolányi and Pettke 2011) and via the following prograde dehydration reactions:

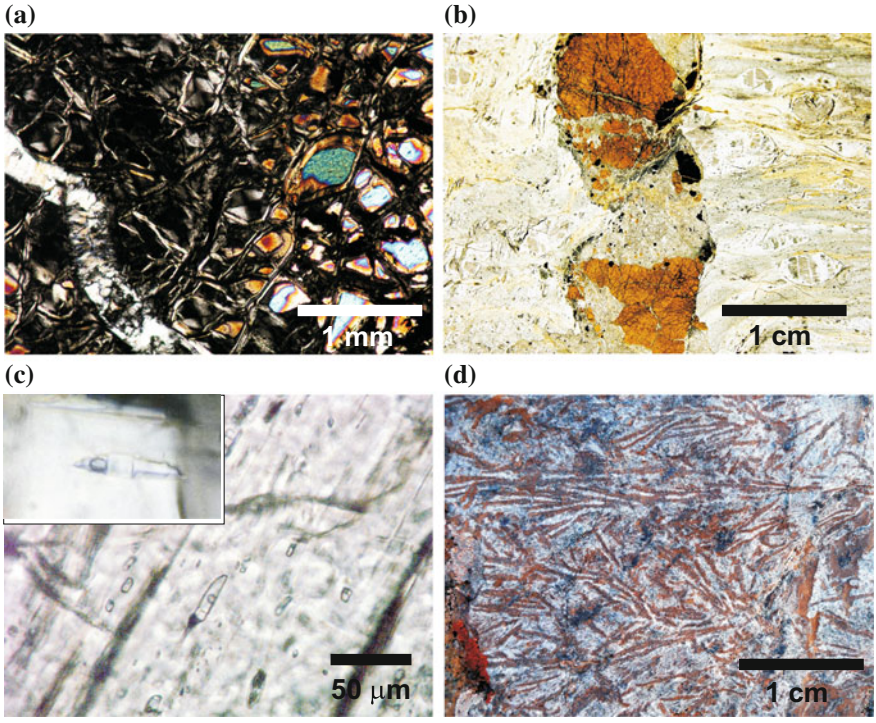

Fig. 8.3 **a** Shallow Erro-Tobbio serpentinite showing serpentine after mantle olivine (present as relict grains in a mesh serpentine texture). Chrysotile is cut by an antigorite vein (left corner of the picture). Crossed nicols. **b** Ti-clinohumite (*red*), olivine (*white*), minor diopside, and magnetite vein in a foliated Erro-Tobbio antigorite serpentinite with clasts of relict mantle clinopyroxene. The vein is a dehydration fluid conduit. **c** Fluid inclusions in diopside from an Erro-Tobbio vein. The inclusions contain H_2O liquid, a vapour bubble and salt (NaCl and MgCl) daughter crystals (visible in the inset). **d** Olivine (*brown elongate crystals*) and orthopyroxene + chlorite (*grey areas* in between olivine) from an Almirez spinifex chlorite harzburgite, which derived from antigorite breakdown. The recrystallization conditions of the rocks reported here are shown by the *yellow* and *red stars* in Fig. 8.2b (i.e., the peak P-T conditions of Gagnone and Almirez chlorite harzburgites)

$$\text{antigorite} + \text{brucite} = \text{olivine} + \text{fluid} \tag{8.1}$$

and

$$\text{antigorite} = \text{olivine} + \text{orthopyroxene} + \text{fluid} \tag{8.2}$$

Reaction (8.1) involves dehydration of antigorite and brucite and leads to consumption of the less abundant reactant (brucite) to produce metamorphic olivine and fluid (Fig. 8.2b). It is recorded by most eclogite-facies Alpine serpentinites (e.g., Erro-Tobbio and Lanzo peridotite, Western Alps), showing rock- and vein-forming antigorite + olivine-bearing parageneses overgrowing early generations of low-T

chrysotile serpentine (Fig. 8.3b) (Debret et al. 2013; Scambelluri et al. 1995, 1997). Pressure-temperature estimates of the Alpine eclogites coexisting with olivine-bearing high-pressure serpentinite yield estimates in the range of 2–2.5 GPa, indicating that reaction (8.1) occurs at approximately 80 km depths (Angiboust et al. 2009, 2012; Bucher et al. 2005; Hermann et al. 2000; Li et al. 2004; Pelletier and Müntener 2006; Rebay et al. 2012). The fluid produced at this stage is preserved as salty aqueous inclusions in veins (Fig. 8.3c) (Scambelluri et al. 1997). Although the high salinity of this fluid may be caused by fluid/rock interaction before and/or during inclusion entrapment, this evidence demonstrates recycling of Cl and associated halogens in subduction fluids (Scambelluri et al. 2004). A larger amount of fluid is released by reaction (8.2), experimentally reproduced at pressure-temperature conditions which may range, depending on subduction gradients, from subarc (110 km) to 200 km depths (Ulmer and Trommsdorff 1995; Wunder and Schreyer 1997). Reaction (8.2) is recorded in two localities: Cerro del Almirez (SE Spain) and Cima di Gagnone (Swiss Central Alps) (Evans and Trommsdorff 1978; Scambelluri et al. 2014; Trommsdorff et al. 1998). These rocks display olivine, orthopyroxene and chlorite in spinifex-like or in a granular equilibrium texture (Fig. 8.3d) (Padròn-Navarta et al. 2010; Scambelluri et al. 2014). These dehydrated serpentinites also preserve relics of the fluid phase released during antigorite breakdown in the form of solid polyphase inclusions hosting an aqueous liquid phase (Scambelluri et al. 2001).

Serpentinites are major hosts of Cl and I (Fig. 8.2a) (Barnes and Sharp 2006; Debret et al. 2014; John et al. 2011; Kendrick et al. 2011, 2013; Scambelluri et al. 1997, 2004; Sharp and Barnes 2004). Abyssal serpentinites have average Cl concentrations of ~2000 μg/g structurally bound in serpentine (Anselmi et al. 2000; Barnes and Sharp 2006; Kendrick et al. 2013; Kodolányi and Pettke 2011; Sharp and Barnes 2004). Fluorine concentrations in serpentinites are rarely reported, but average around 204 μg/g (Mével 2003; Stueber et al. 1968). Only recently have Br and I concentrations been measured in serpentinites (Kendrick et al. 2011, 2013), with Br and I concentrations in seafloor and forearc serpentinites of 1.3–24 μg/g (average = 6.4 μg/g) and 0.02–45 μg/g (average = 7.6 μg/g), respectively. Figure 8.4a shows the Br/Cl versus I/Cl ratios of serpentinites from modern mid-ocean ridges, passive and convergent plate margins, along with ophiolitic peridotites serpentinized in shallow settings (Internal and External Liguride Ophiolites, Apennine, and part of Erro-Tobbio, Alps; data after Kendrick et al. 2013; John et al. 2011). I/Cl and Br/Cl ratios in serpentinites are similar to ratios of sedimentary marine pore fluids (Figs. 8.1b and 8.4a), implying a contribution of pore fluids to the serpentinizing fluid. The Br and I contents of these rocks increase relative to Cl from abyssal to forearc serpentinites. This is likely a result of the involvement of a (meta)sedimentary component in the serpentinization fluids due to the loss of fluids from sediments at shallow depths within the subduction zone hydrating the forearc mantle wedge. Interestingly, the Northern Apennine ophiolitic serpentinites that escaped subduction show significantly higher Br and I than modern abyssal serpentinites. High Br and I concentrations are also recorded in early chrysotile relics preserved in the subducted Erro-Tobbio unit.

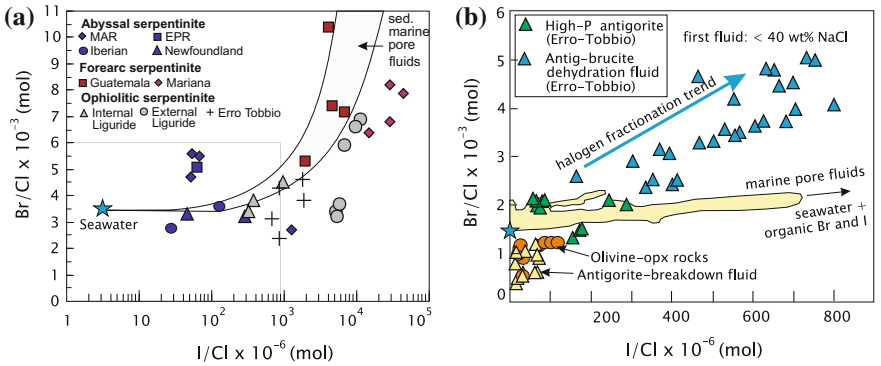

Fig. 8.4 **a** Br/Cl versus I/Cl element plots showing chrysotile–lizardite serpentinites from abyssal (Mid Atlantic Ridge, MAR; East Pacific Rise, EPR; Iberian and Newfoundland), forearc (Guatemala and Mariana), and ophiolitic settings (Internal and External Liguride, Northern Apennine; Erro-Tobbio, Alps). Reference fields include the compositional range of sedimentary marine pore fluids and of seawater (modified from Kendrick et al. 2013; data from Kendrick et al. 2013; John et al. 2011). **b** inset of Fig. 8.4a (*light grey line*) showing the compositions of high-pressure antigorite and saline fluid inclusions from Erro-Tobbio (released from reaction 8.1 in Fig. 8.2b; see for instance Fig. 8.3d) together with the compositions of the Almirez harzburgites and associated fluid inclusions (released from reaction 8.2 in Fig. 8.2b). The field of sedimentary pore fluids is also reported (after Kendrick et al. 2011)

This geochemical feature indicates the involvement of sedimentary marine pore fluids during shallow serpentinization of these mantle rocks (Kendrick et al. 2013). These data lead to the conclusion that shallow serpentinization took place in outer rises, accretionary complexes, or in the mantle wedge (i.e., settings quite distant from mid ocean ridges) (Kendrick et al. 2011, 2013; John et al. 2011; Scambelluri and Tonarini 2012). A contribution of pore fluids to the serpentinizing fluid is also supported by noble gas data (Kendrick et al. 2011) and Cl isotope data (Barnes et al. 2006; Barnes and Sharp 2006).

Halogens can be lost (up to 90% of Cl) during the chrysotile-to-antigorite transition during the early stages of subduction (<30 km) (Kodolányi and Pettke 2011). However, work on exhumed high-pressure serpentinites shows that despite progressive dehydration and halogen loss during the early stages of subduction, high-pressure serpentinites retain significant concentrations of halogens (Bonifacie et al. 2008a; John et al. 2011; Scambelluri et al. 2004; Selverstone and Sharp 2013). The extent of Cl recycling during serpentinite subduction is illustrated in Fig. 8.5, which shows the concentrations measured in minerals crystallized at increasing pressure-temperature conditions. Here the Erro-Tobbio and Almirez subducted units record dehydration reactions (8.1) and (8.2), respectively (see Fig. 8.2b for P-T equilibration conditions; Scambelluri et al. 2004). Subduction results in a decrease in Cl and B concentrations in minerals due to the progressive release of such elements into the fluids. The estimated bulk-rock Cl budgets are shown in Fig. 8.5b. Overall, Fig. 8.5 shows that, despite Cl and B loss to subduction fluids,

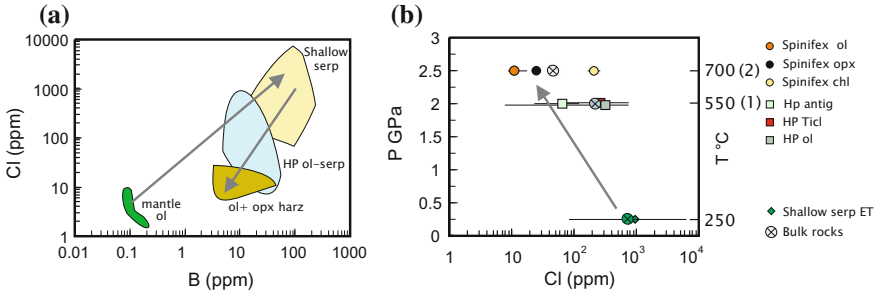

Fig. 8.5 **a** Boron versus Cl composition of mantle olivine, early shallow chrysotile, and high-pressure minerals in olivine-serpentinite formed after reaction (8.1), and in deserpentinized olivine + orthopyroxene + chlorite harzburgite formed after reaction (8.2). Data are from the Erro-Tobbio high-pressure serpentinite and in the Almirez chlorite harzburgite (Scambelluri et al. 2004). **b** Mineral and bulk-rock Cl variability in the above samples as a function of the estimated metamorphic pressures and temperatures and the reference reactions (8.1) and (8.2)

the most dehydrated rocks still retain appreciable amounts of such elements. Detailed variations in the halogen compositions from subduction-zone serpentinite and fluids from Erro-Tobbio and Almirez are shown in Fig. 8.4b. In general, the residual high-pressure serpentinites show decreasing concentrations of Cl, Br, and I with increasing dehydration (John et al. 2011; Kendrick et al. 2011). In samples from Almirez, the above scenario is complicated by the recently documented exchange of radiogenic Sr and ^{11}B between ultramafic rocks and the surrounding metasediments during subduction (Harvey et al. 2014). This suggests caution when reconstructing element loss from these rocks compared with other units evolved at different pressure-temperature conditions. However, the constant halogen loss between Erro-Tobbio and Almirez (Fig. 8.5) and the halogen variations shown in Fig. 8.4b encourage the use of these rocks to assess halogen behavior during serpentinite subduction.

Halogen loss from subducting serpentinite is counterbalanced by increased halogen concentrations in veins and in fluid inclusions, suggesting that halogens are preferentially released to the fluid during dehydration. The variation between rock residues and fluids is shown by the halogen fractionation trend in Fig. 8.4b (John et al. 2011; Kendrick et al. 2011), with Br and I progressively depleted relative to Cl (Kendrick et al. 2011). Interestingly, the halogen signature of the Erro-Tobbio high-pressure antigorite serpentinite, formed after shallow-level chrysotile serpentinite (see Fig. 8.4a), can be tracked back to the original marine pore fluid signature (Fig. 8.4b). With increasing grade, F/Cl ratios increase in the residual rock (John et al. 2011). This increase in F may be due to the formation of Ti-clinohumite (John et al. 2011), which is able to host large concentrations of F with increasing metamorphic grade (Evans and Trommsdorff 1983; Lopez Sánchez-Vizcaíno et al. 2005), as evidenced by correlations between F and Ti concentrations.

Overall, Fig. 8.5 shows that, despite Cl and B loss to subduction fluids, the most dehydrated rocks still retain appreciable amounts of such elements.

The rock forming olivine, orthopyroxene and chlorite from the Almirez chlorite harzburgite contain 10 μg/g Cl on average, which corresponds to an average bulk estimate of 40 μg/g Cl (Fig. 8.5b; Scambelluri et al. 2004). Bulk analyses of such rocks show that they can contain up to ~250 μg/g Cl, ~40–50 μg/g F, 0.2 μg/g Br, and ~700 ng/g I (John et al. 2011; Kendrick et al. 2011), thus introducing detectable halogen anomalies into the upper mantle.

8.3 Halogen Outputs from the Subduction Zone

Halogens are recycled to the Earth's surface through the forearc, volcanic front, and the backarc. Fluxes through the fore-arc are very poorly constrained, in part due to limited accessibility of venting fore-arc gases and fluids, and therefore are ignored in all published volatile cycling budgets (e.g., Ito et al. 1983; Jarrard 2003; John et al. 2011; Straub and Layne 2003; Wallace 2005). In this section, we focus on the better constrained halogen fluxes through the volcanic arc from measurable halogen concentrations in volcanic gases and melt inclusions.

8.3.1 Volcanic Gas Data

Halogen concentrations in gas plumes are determined using halogen to SO_2 ratios and SO_2 flux measurements. SO_2 is the most commonly measured gas because of its high abundances in volcanic plumes, low atmospheric background and strong absorption in UV (e.g., Fischer 2008; Wallace 2005). Improvements in SO_2 flux measurements will therefore result in better quantification of other gas fluxes. SO_2 flux measurements have traditionally been made using the ground-based UV correlation spectrometer (COSPEC). More recently, rapid advances have been made in SO_2 flux measurements using UV spectrometry by application of differential optical absorption spectrometry (Shinohara 2008) and satellite remote sensing techniques (Pieri 2015).

Halogens are commonly degassed as hydrogen halides (HCl, HF, HBr, HI) (Aiuppa et al. 2005; Symonds et al. 1988), although other trace halogen compounds are possible (e.g., BrO, ClO) (Bobrowski et al. 2003; Platt and Bobrowski 2015). Measurements of Cl and F concentrations in volcanic gases are not common and those of Br and I are rare (Aiuppa et al. 2005, 2009; Fischer 2008; Snyder and Fehn 2002). Despite the limited concentration data in the literature, several studies have attempted to estimate the halogen flux from arc volcanoes based on volcanic gas data (Table 8.1). Errors associated with these estimates reflect possible modification of halogen concentrations during transport from the magma to the surface, limited data from some arcs, and how to "scale up" to an estimation of total arc volcanic output starting with variable halogen concentrations among fumaroles at an individual volcano (Fischer 2008; Pyle and Mather 2009). In addition, with the

Table 8.1 Calculated input and output budgets for various reservoirs

Calculations from this contribution[a]									
	Thickness (m)	Cl (ppm)	F (ppm)	I (ppb)	Br (ppm)	Subduction influx (g Cl/yr)	Subduction influx (g F/yr)	Subduction influx (g I/yr)	Subduction influx (g Br/yr)
Sediments	400	640	611	5000	20	1.6×10^{12}	1.5×10^{12}	1.2×10^{10}	4.9×10^{10}
Altered oceanic crust	6000	207	216	9	0.15	7.7×10^{12}	8.0×10^{12}	3.3×10^{8}	5.5×10^{9}
Serpentinites	300–450	2000	204	7600	6.4	$3.7–5.5 \times 10^{12}$	$3.8–5.7 \times 10^{11}$	$1.4–2.1 \times 10^{10}$	$1.2–1.8 \times 10^{10}$
Total						**$13–15 \times 10^{12}$**	**$9.9–10 \times 10^{12}$**	**$2.6–3.3 \times 10^{10}$**	**$6.7–7.3 \times 10^{10}$**
Prior work[b]									
						Subduction influx (g Cl/yr)	Subduction influx (g F/yr)	Subduction influx (g I/yr)	Subduction influx (g Br/yr)
Straub and Layne (2003)						3.7×10^{12}	7.9×10^{12}		
Ito et al. (1983)						$3.6–8.6 \times 10^{12}$			
Jarrard (2003)						4.5×10^{12}			
Snyder and Fehn (2002)								2.0×10^{10}	
						Arc outflux (g Cl/yr)	Arc outflux (g F/yr)	Arc outflux (g I/yr)	Arc outflux (g Br/yr)
Jarrard (2003)						$7–22 \times 10^{12}$			
Straub and Layne (2003)						$2.9–3.8 \times 10^{12}$	$0.3–0.4 \times 10^{12}$		
Ito et al. (1983)						$4.3–9.5 \times 10^{12}$			
Wallace (2005)						$4–7 \times 10^{12}$			
Ruscitto et al. (2012)						5.6×10^{12}			

(continued)

Table 8.1 (continued)

Calculations from this contribution[a]									
	Thickness (m)	Cl (ppm)	F (ppm)	I (ppb)	Br (ppm)	Subduction influx (g Cl/yr)	Subduction influx (g F/yr)	Subduction influx (g I/yr)	Subduction influx (g Br/yr)
Pyle and Mather (2009)						4.2×10^{12}	0.5×10^{12}	$0.5–2 \times 10^{9}$	$4.9–14.8 \times 10^{9}$
Fischer (2008)						5.5×10^{12}	0.2×10^{12}		
Shinohara (2013)						1.1×10^{13}			

[a]Details for calculations and references for values used are summarized in the text in Sect. 8.2

[b]None of the prior influx calculations for any halogen includes contributions from serpentinites or pore fluids. Arc outflux estimates are based on gas data with the exception of Straub and Layne (2003) and Ruscitto et al. (2012), which are based on volatile contents in magma (melt inclusion data) and magma production rates. Shinohara (2013) is the only estimate to include volatile data from thermal spring discharge

exception of Shinohara (2013), none of these estimates include halogen fluxes through thermal springs, which may be significant (e.g., Taran 2009). Instead, they focus solely on high temperature fumarole fluxes (Fischer 2008; Pyle and Mather 2009). Despite these possible errors, the estimated outputs are remarkably consistent, especially given that some of the estimates are based on volcanic gas data (e.g., Fischer 2008; Pyle and Mather 2009) and others on melt inclusion data (Ruscitto et al. 2012; Straub and Layne 2003).

8.3.2 Melt Inclusions

The last ~15 years have seen a rapidly growing database of halogen contents in melt inclusions[3] (e.g., Wallace 2005), including those from arc volcanoes (e.g., Cervantes and Wallace 2003; Esposito et al. 2014; Johnson et al. 2009; Portnyagin et al. 2007; Ruscitto et al. 2010; Sadofsky et al. 2008; Shaw et al. 2008). Halogen contents are enriched in arc lavas compared to MORB (Fig. 8.6) and this enrichment is commonly cited as strong evidence for the contribution of slab-derived fluids to arc volcanism (e.g., Wallace 2005). The highest Cl concentrations reported in olivine-hosted melt inclusions from arc basalts are ~5800 μg/g from Augustine in the Aleutian arc (Fig. 8.6a) (Zimmer et al. 2010). Published F data are sparse, but include concentrations up to ~2500 μg/g from Irazú (Fig. 8.6b) (Benjamin et al. 2007). Due to the high solubility of Cl and F in mafic (basaltic) melts (e.g., Webster et al. 1999) and no diffusive re-equilibration of Cl and F through host olivine (Bucholz et al. 2013), these values are believed to reflect initial melt compositions (e.g., Benjamin et al. 2007; Wade et al. 2006). Reported Br concentrations in melt inclusions is limited to Central America with concentrations up to 13 μg/g (Kutterolf et al. 2013). To our knowledge, there are no published data on I concentrations in melt inclusions.

Chlorine contents in many arc basalts have been explained by mixing between a mantle source and slab-derived fluid with a Cl/H_2O ratio similar to that of seawater (Johnson et al. 2009; Ruscitto et al. 2010; Wallace 2005). Many melt inclusions from arc samples have Cl/H_2O ratios consistent with the salinity of a fluid derived from serpentinites (4–8 wt% NaCl) (Scambelluri et al. 2004) or altered oceanic crust (~4 wt% NaCl for the upper crust and ~35 wt% for the lower crust) (Nehlig 1993; Philippot et al. 1998) (cf., Johnson et al. 2009). Volcanic magmas with

[3]For purposes of comparison, only olivine melt inclusion data from arc basalts are presented and discussed; however, melt inclusions from other mineral phases (e.g., plagioclase) and volcanic glass shards also provide viable and valuable data. For example, Balcone-Boissard et al. (2010) show that Cl/Br/I ratios are constant in pumice from felsic explosive eruptions, suggesting that these halogens are not fractionated from each other during rapid magma decompression and can be used to trace mantle source compositions.

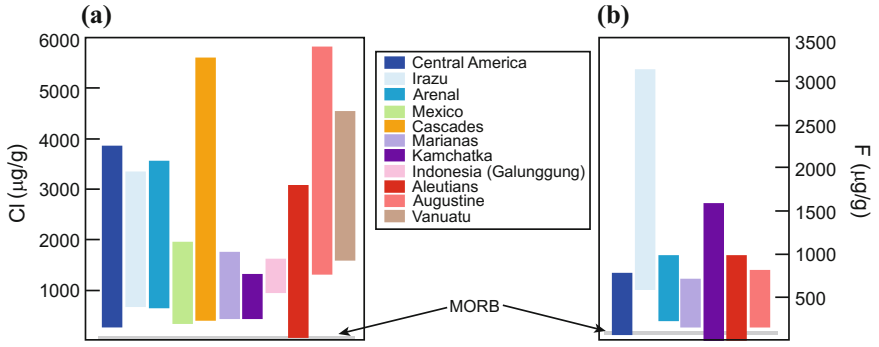

Fig. 8.6 **a** Cl and **b** F concentrations in olivine-hosted melt inclusions from arc basalts. Fields enclose data from Central America (Benjamin et al. 2007; Kutterolf et al. 2013; Roggensack et al. 1997; Sadofsky et al. 2008; Wade et al. 2006), Mexico (Cervantes and Wallace 2003; Johnson et al. 2009), Cascades (Ruscitto et al. 2010), Marianas (Shaw et al. 2008), Kamchatka (Auer et al. 2009; Portnyagin et al. 2007), Indonesia (Sisson and Bronto 1998), Aleutians (Zimmer et al. 2010) and Vanuatu (Métrich and Deloule 2014). Halogen concentrations in MORB are given for comparison

unusually high Cl/H_2O ratios, such as those from Irazú (up to 0.48) (Benjamin et al. 2007) and Galunggung, western Java, Indonesia (0.25–0.53) (Sisson and Bronto 1998), are explained as having contribution from a highly saline fluid or melt. However, recent work has shown that water can be lost or gained in olivine-hosted melt inclusions via proton diffusion through the host crystal (e.g., Bucholz et al. 2013; Gaetani et al. 2012; Portnyagin et al. 2008). Halogen/H_2O ratios determined from melt inclusions are valid *only* if water content is unmodified, thus correlations between water and halogen species should be treated with extreme caution (Bucholz et al. 2013). In addition to water loss via proton diffusion, the initial halogen/H_2O ratios of melt inclusions may be complicated due to halogen fractionation from H_2O during devolatilization of the subducting slab or during transport of slab-derived fluids through the mantle wedge (Wallace 2005) or late-stage magma interaction with brine (Métrich and Deloule 2014).

8.4 Consequences for Evolution of the Mantle—Evidence of a Subducted Component

Because of their high fluid affinity, halogens strongly partition into subduction-zone fluids. As a result, halogens are generally predicted to be removed from the slab by devolatilization reactions prior to reaching subarc depths. However, increasing evidence shows that halogens can survive past the volcanic arc front.

8.4.1 Halogen Concentrations in the Depleted Upper Mantle (DMM) and Mid-Ocean Ridge Basalts (MORB)

The concentration of Cl in the upper mantle (depleted MORB mantle, DMM) is estimated to range between 3 and 10 μg/g (Burgess et al. 2002; Jambon et al. 1995; Lassiter et al. 2002; Schilling et al. 1980). However, others suggest Cl concentrations in the DMM as low at 0.4–1 μg/g (Saal et al. 2002; Salters and Stracke 2004; Workman and Hart 2005; Frezzotti and Ferrando 2018; Klemme and Stalder 2018). Most MORB glasses contain ~20–50 μg/g Cl (Jambon et al. 1995; Michael and Schilling 1989; Schilling et al. 1980). Estimates of F concentrations in the DMM and MORB range from 11 to 65 μg/g (Salters and Stracke 2004; Schilling et al. 1980) and from 16 to 109 μg/g (Saal et al. 2002; Schilling et al. 1980), respectively. Bromine concentrations in the DMM range from 8 to 20 ng/g (Burgess et al. 2002; Jambon et al. 1995; Schilling et al. 1980) and 100 to 200 ng/g for MORB (Jambon et al. 1995; Schilling et al. 1980). Iodine concentrations in the DMM are estimated between 0.4 to 0.8 ng/g (Burgess et al. 2002; Deruelle et al. 1992). MORB glasses average 8 ng/g I (Deruelle et al. 1992). MORB F/Cl, Br/Cl and I/Cl ratios are ~1–10, 2.2–3.4 × 10^{-3}, and 3–9 × 10^{-5}, respectively (Kendrick et al. 2012a, 2014b) (Fig. 8.1).

8.4.2 Halogens in Back-Arc Basin Basalts (BABB)

BABB are enriched in halogens compared to MORB (Fig. 8.7). Manus Basin (Papua New Guinea) and Valu Fa Ridge (Lau Basin, Tonga Arc) basalt glasses have particularly high Cl concentrations (Kendrick et al. 2012b, 2014a; Kent et al. 2002; Sun et al. 2007). Sun et al. (2007) estimate that ~80% of the Cl in Manus glasses are derived from slab fluids. However, the Cl enrichment is too great to be explained by Cl released from amphibole, phlogopite, or apatite (Kent et al. 2002). High I/Cl ratios (10 times the MORB value) in BABB glasses from the Manus Basin and the Valu Fa Ridge imply halogen contribution from serpentinite-derived fluids. MORB-like I/Cl and Br/Cl ratios in other BABB glasses (Woodlark Basin, North Fiji Basin, Fonualei Spreading Center (Lau Basin)) suggest a halogen contribution from the AOC (Kendrick et al. 2014a) (Fig. 8.1).

8.4.3 Halogens in Ocean Island Basalts (OIB)

One way Cl recycling into the deeper mantle has been assessed is on the basis of Cl/K ratios in OIB. Chlorine has a similar compatibility to K during magmatic processes (Michael and Cornell 1998). Therefore, Cl/K ratios of uncontaminated basalts reflect assimilation of crustal material in the mantle source (e.g., Stroncik

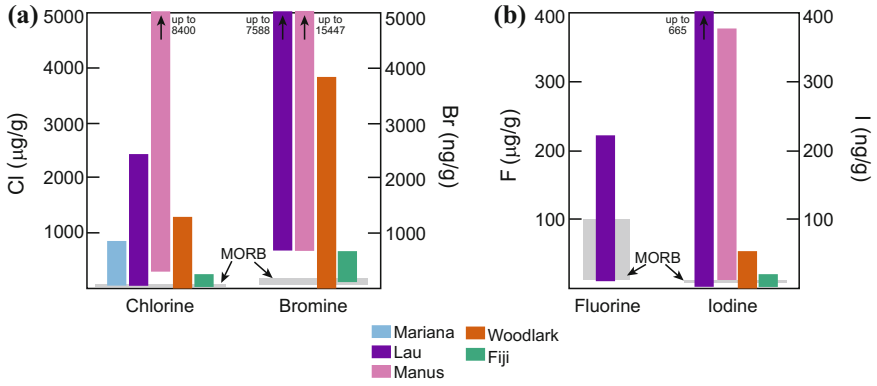

Fig. 8.7 **a** Chlorine and Br concentrations and **b** F and I concentrations in back-arc basalt glasses from various back-arc basins. Halogen concentrations in MORB are given for comparison. Data from Bézos et al. (2009), Kendrick et al. (2014a), Kent et al. (2002), Stolper and Newman (1994) and Sun et al. (2007)

and Haase 2004). Normal MORB has Cl/K ratios as low as 0.01, whereas enriched MORB has Cl/K ratios of 0.05–0.08. Cl/K ratios >0.08 are due to either seawater alteration or assimilation of hydrothermally altered crustal material (Michael and Cornell 1998). Correlations between Cl/K ratios and radiogenic isotope ratios ($^{87}Sr/^{86}Sr$ and $^{206}Pb/^{204}Pb$) in OIB glasses and EM-type lavas are interpreted to reflect recycling of crustal material into OIB sources (Stroncik and Haase 2004; Workman et al. 2006) (Fig. 8.8b). The Cl isotope composition of OIB glasses also show trends with Cl/K ratios. For example, HIMU samples have a positive correlation between $\delta^{37}Cl$ values and Cl/K, whereas enriched MORB samples have high $\delta^{37}Cl$ values and low Cl/K ratios. This provides additional evidence for the survival of Cl into the upper mantle (John et al. 2010) (Fig. 8.8c). However, HIMU-type lavas from the Austral Islands have a relatively low Cl/K ratio of $\sim$0.04, which is interpreted to reflect the effective removal of Cl during subduction and minimal recycling of Cl into the mantle via crustal residues (Lassiter et al. 2002). Discrepancies in the interpretation of Cl/K ratios in OIB basalts are partially due to uncertainty in the accepted value for the mantle K concentration (J. C. Lassiter, pers. comm.). Instead, Cl/Nb ratios may be a more effective tracer of Cl mobility (Sun et al. 2007).

As with BABB glasses, recent studies have used F, Cl, Br, and I concentrations in OIB glasses to assess halogen cycling into the deeper mantle (Kendrick et al. 2012b, 2014b). Cl/K, Br/K, and I/K in OIB glasses are all low and show correlations with $^{87}Sr/^{86}Sr$ suggesting the presence of a subducted component. Interestingly, F/Nd does not correlate with $^{87}Sr/^{86}Sr$ (this is also noted in basalt glasses from Samoa (Workman et al. 2006)), suggesting preferential subduction of F compared to the other halogens (Kendrick et al. 2014b).

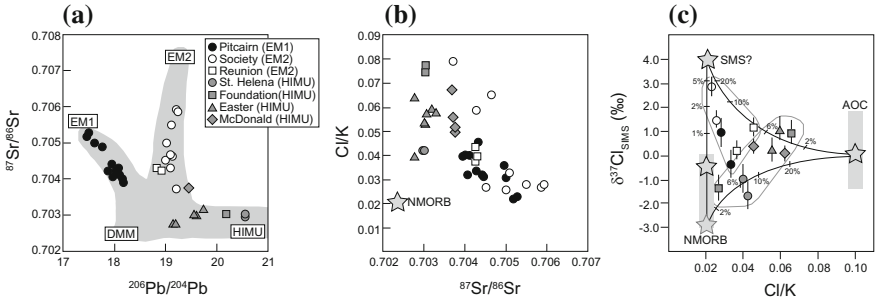

Fig. 8.8 **a** $^{206}Pb/^{204}Pb$ and $^{87}Sr/^{86}Sr$ source characteristics of OIB glasses used in the halogen studies of John et al. (2010), Kendrick et al. (2014b) and Stroncik and Hasse (2004). *Light gray* area highlights mantle end members (Hofmann 2003). **b** Strong correlation between Cl/K ratios and Sr isotope ratios supports recycling of crustal material in OIB sources. Br/K and I/K ratios (not shown) show nearly identical trends with $^{87}Sr/^{86}Sr$ as Cl/K. F/Nd shows no correlation with $^{87}Sr/^{86}Sr$ (not shown). Data from Stroncik and Hasse (2004) and Kendrick et al. (2014b). **c** $\delta^{37}Cl$ values (determined by SIMS) versus Cl/K ratios of OIB glasses (modified from John et al. 2010). EM1 and EM2 samples tend to have low Cl/K ratios and high $\delta^{37}Cl$ values, whereas, HIMU samples have higher Cl/K ratios and lower $\delta^{37}Cl$ values. AOC has a range of $\delta^{37}Cl$ values from −1.4 to +1.8‰ (averaging ~0‰), overlapping well with the range observed in HIMU glasses (Barnes and Cisneros 2012). The $\delta^{37}Cl$ value of the upper mantle has not been agreed upon and ranges from −0.2 to −3‰ (Bonifacie et al. 2008b; Layne et al. 2009; Sharp et al. 2007, 2013). We prefer the value of −0.2‰ (Sharp et al. 2007, 2013), but note that modelling presented in this figure (John et al. 2010) uses the extreme end member of −3‰ (Layne et al. 2009). SMS is the hypothetical end member of deeply subducted sediments proposed by John et al. (2010), but not documented in other studies (e.g., Selverstone and Sharp 2013, 2015). (More details on Cl stable isotopes are presented in Sect. 8.7.1.)

8.5 Mass Budget Calculations

A summary of halogen inputs and outputs is presented in Figs. 8.9 and 8.10. The halogen budget of the global subduction system remains highly uncertain, chiefly because the only output at convergent margins that currently is reasonably well characterized is that from arc volcanoes. However, as with H_2O, CO_2 and other volatiles (e.g., Kelemen and Manning 2015), additional output pathways are likely but are extremely difficult to quantify. For example, contributions from the fore-arc, including geothermal systems, may be substantial, yet are poorly known. Magma ponding beneath or within the crust will lead to the generation and migration of a halogen-bearing fluid phase. While the fate of these halogens remains largely unknown, the participation of halogen-rich, magma-derived fluids in metamorphism and ore generation attests to the importance of this process. In addition, the contribution of crustal material eroded from the upper plate via mechanical coupling (e.g., Clift and Vannucchi 2004; Scholl and von Huene 2007) is not included in the halogen input estimates. Future work is necessary to achieve a robust halogen mass balance in convergent margins. Nevertheless, it is possible to evaluate preliminary constraints from the sources and sinks that can currently be estimated.

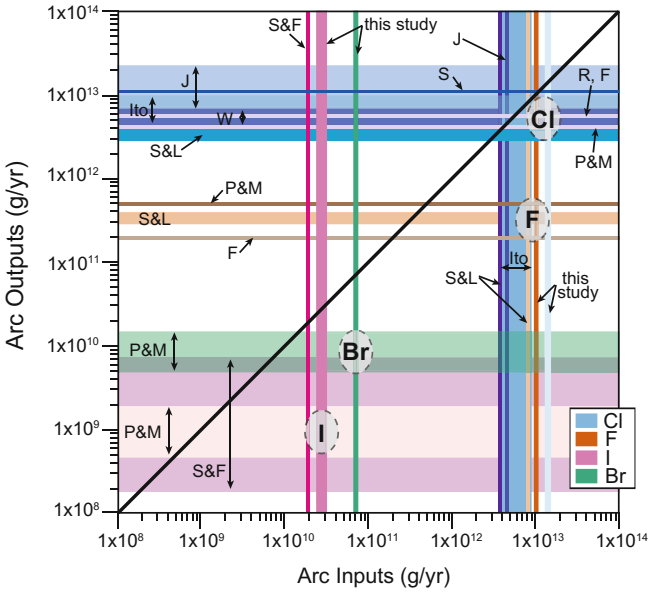

Fig. 8.9 Halogen mass balance through the volcanic arc front. Chlorine fluxes are shown in shades of *blue*, F in shades of *orange-brown*, I in shades of *pink*, and Br in shades of *green*. *Gray ovals* enclose areas of input and output overlap with selected inputs from estimates that include halogen concentrations in serpentinites. Chlorine is the only halogen that is nearly in balance through the arc front, with some Cl likely returned to the mantle and some unaccounted for fraction lost beneath the fore-arc. Fluorine is returned to the mantle in greater proportion than Cl. Bromine and I have significant losses before the arc front that are unaccounted for in these calculations. *S&L* (Straub and Layne 2003), *J* (Jarrard 2003), *Ito* (Ito et al. 1983), *W* (Wallace 2005), *F* (Fischer 2008), *R* (Ruscitto et al. 2012), *P&M* (Pyle and Mather 2009), *S&F* (Snyder and Fehn 2002), *S* (Shinohara 2013)

8.5.1 *Chlorine Flux Through Subduction Zones*

Early mass balance calculations implied that the global Cl budget is nearly balanced, with Cl almost entirely returned to the Earth's surface (Ito et al. 1983; Jarrard 2003; Ruscitto et al. 2012; Straub and Layne 2003). However, these studies did not include serpentinites in the calculations. Serpentinites are now known to be a major Cl host (e.g., Barnes and Sharp 2006; Kendrick et al. 2011; Scambelluri et al. 2004) and stable to great depths (up to 200 km) in subduction zones (Ulmer and Trommsdorff 1995; see Sect. 8.2.4). More recent calculations that include serpentinites suggest that Cl inputs may exceed outputs at subduction zones, thus allowing Cl to be recycled back into the mantle (Barnes and Straub 2010; John et al. 2011). Updated calculations (this contribution) also support the survival of Cl past the arc front (Table 8.1; Fig. 8.9). This conclusion is consistent with observations of saline fluid inclusions found in eclogitic terranes in the Alps (Philippot et al. 1998; Philippot and Selverstone 1991; Scambelluri et al. 1997; Selverstone et al. 1992);

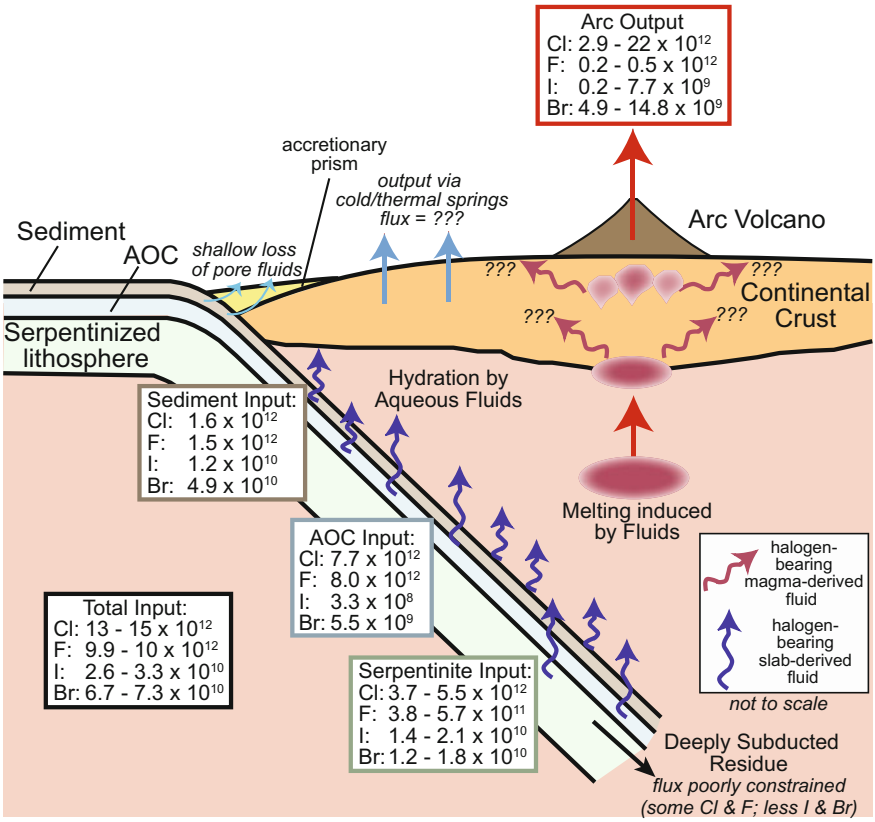

Fig. 8.10 Schematic diagram illustrating halogen fluxes through the subduction zone. Arc output flux values are from references given in Table 8.1. Influx calculations are from this contribution. Pore fluids are assumed to be lost at very shallow depths (by ~5 km) and are therefore ignored in the calculations. The unknown extent of serpentinization of the subducting oceanic lithosphere leads to uncertainties in the serpentinite halogen input. Halogen loss via progressive metamorphic dehydration reactions of sediments, altered oceanic crust, and serpentinites is poorly constrained leading to uncertainties in the halogen content in the residual slab. Despite these uncertainties, there is clear evidence for the return of halogen from surficial reservoirs into the upper mantle

high Cl concentrations retained in high-pressure dehydrated residues of serpentinites (John et al. 2011; Kendrick et al. 2011; Scambelluri et al. 2004); and high concentrations of Cl in back-arc glasses (Bézos et al. 2009; Kendrick et al. 2014a; Kent et al. 2002; Stolper and Newman 1994; Sun et al. 2007). There is also evidence for deep Cl recycling into the upper mantle by Cl/K, Br/Cl, and I/Cl ratios and δ^{37}Cl values measured in plume-related basalts (John et al. 2010; Kendrick et al. 2014b; Stroncik and Haase 2004; Workman et al. 2006). Based on halogen concentrations in OIB, BABB, and MORB glasses, up to 10% of the total subducted Cl may survive into the upper mantle (Kendrick et al. 2014b).

8.5.2 Fluorine Flux Through Subduction Zones

Mass balance calculations overwhelmingly suggest that F is efficiently returned to the mantle (Table 8.1; Fig. 8.9). These calculations are supported by F concentrations in BABB and OIB glasses and arc front melt inclusions, which suggest that F is decoupled from Cl during the subduction process and preferentially returned to the mantle (Kendrick et al. 2014b; Straub and Layne 2003). Kendrick et al. (2014b) speculate that the preferential subduction of F versus Cl may be due to the higher solubility of F in nominally anhydrous minerals produced during subduction-driven dehydration (Bernini et al. 2013; Beyer et al. 2012; Dalou et al. 2012; Fabbrizio et al. 2013) and the higher compatibility of F in micas and amphiboles relative to Cl (e.g., Morrison 1991; Munoz 1984; Volfinger et al. 1985). Preferential retention of F in subducted lithologies may also be due to the sequestration of F in Ti-clinohumite (cf., Evans and Trommsdorff 1983; John et al. 2011). Future studies addressing F behavior in subduction zones should help address the decoupling of Cl and F.

8.5.3 Iodine and Br Fluxes Through Subduction Zones

Mass balance calculations show a greater input of Br and I into the subduction system than is returned to the surface via arc volcanism (Table 8.1; Fig. 8.9). Calculations by Snyder and Fehn (2002) estimate that up to 38% of the total subducted I may reach the volcanic arc front. I/Cl and Br/Cl ratios of OIB glasses suggest that <4–10% of the total subducted I and Br reaches the upper mantle (Kendrick et al. 2014b). Work on halogen concentrations in serpentinites demonstrates that I and Br are lost from serpentinites at shallower depths than either Cl or F (John et al. 2011; Kendrick et al. 2011, 2013). Loss of Br and I at depths shallower than the arc front is the likely explanation for the imbalance. Little work has been done on Br loss during subduction, but I shows dramatic losses at shallow depths. Marine sediments, the major iodine reservoir, lose 75–95% of their I by ~400 °C (Muramatsu and Wedepohl 1998). This estimate is supported by cosmogenic ^{129}I data of fore-arc fluids which imply mobilization of I from subducting sediments (Muramatsu et al. 2001; Tomaru et al. 2007) (see Sect. 8.7.2).

8.6 Halogens and Fluid Chemistry

High concentrations of halogens in subduction-zone fluids (estimated chlorine concentrations >1 wt% (Kent et al. 2002; Portnyagin et al. 2007; Stolper and Newman 1994; Straub and Layne 2003) and F concentrations up to ~1 wt% (Portnyagin et al. 2007)) have important consequences for the transport of metals and trace elements (Keppler 1996, 2017; Manning 2004; Webster 2004).

8.6.1 Physical Properties and Solute Structure

The addition of salts, such as NaCl and KCl, to H_2O changes fluid physical properties and the solute structure relative to pure H_2O. Recent experimental and theoretical studies at subduction-zone conditions (Mantegazzi et al. 2013; Sakuma and Ichiki 2015) show that at a given P and T, increasing salinity in NaCl-H_2O solutions causes the sound speed in the fluid to decrease. This translates to increases in the fluid density at all subduction-zone pressures and temperatures. For example, at 800 °C and 3 GPa, the density of pure H_2O is 1160 kg/m^2. NaCl concentrations of 1 and 3 molal yield solution densities of 1250 and 1350 kg/m^2, respectively, or 7 and 16% higher (Mantegazzi et al. 2013). As discussed below, salt solutions are strongly ionized at all subduction conditions. The increases in density with rising salt concentration arise from the volume reduction associated with ion solvation by H_2O (Sakuma and Ichiki 2015). Mantegazzi et al. (2013) derived thermodynamic and transport properties from an equation of state based on their sound speed determinations. Results indicate that, as NaCl concentration rises from 0 to 3 molal at 800 °C and 3 GPa, thermal expansivity and isothermal compressibility decrease, whereas adiabatic compressibility increases. It is important to note that the inferred isobaric heat capacity does not change systematically with salinity and is highly discrepant with pure H_2O at high pressure (Wagner and Pruß 2002).

8.6.2 Effects on Phase Equilibria

The addition of salts to metamorphic H_2O has a very different effect on phase equilibria than addition of CO_2 and other non-polar gases (Manning and Aranovich 2014). This is because in mixtures of NaCl and H_2O, the H_2O activity displays negative departures from ideality at high pressure and temperature (e.g., Aranovich and Newton 1996, 1997; Mantegazzi et al. 2013; Shmulovich and Graham 1996; Tropper and Manning 2004), whereas CO_2-H_2O mixtures show comparatively larger, and positive, departures from ideality (Aranovich and Newton 1999; Halbach and Chatterjee 1982; Holloway 1977; Kerrick and Jacobs 1981; Saxena and Fei 1987). Although studies of mixing properties of metamorphic fluids typically focus on pressures lower than those attained during subduction, limited investigations at high pressure (e.g., Mantegazzi et al. 2013; Tropper and Manning 2004) confirm the conclusions above.

The contrasting properties of mixing H_2O with salts (e.g., NaCl, KCl) versus CO_2 and other non-polar gases have several important petrologic consequences (Manning and Aranovich 2014; Mantegazzi et al. 2013). The first is that, at a given pressure and concentration of salt or CO_2, the melting temperature of the coexisting mineral assemblage will be higher in the presence of the salt solution. Aranovich et al. (2013) showed that at 1 GPa and in the presence of a (Na,K)Cl solution with an H_2O mole fraction of 0.7, the haplogranite melting temperature is 100 °C higher

than when coexisting with an H_2O-CO_2 fluid of the same H_2O mole fraction. Their experimental results suggest that the disparity should increase at higher pressures. Thus, high-salinity aqueous solutions can be expected to suppress the onset of slab melting relative to pure H_2O or H_2O-CO_2. Second, dehydration reactions involving key hydrous minerals will proceed at lower temperatures (i.e., generally shallower depths) than would be the case in the presence of pure H_2O or H_2O-CO_2 mixtures. Finally, the different mixing properties lead to the persistence of a large miscibility gap at high concentrations of salt and CO_2 in the bulk fluid (e.g., Aranovich et al. 2010; Heinrich 2007; Liebscher 2010; Manning et al. 2013). At sufficiently high concentrations of CO_2 and salt, this can lead to the creation of two fluid phases, one of which is a brine with a high carrying capacity for metals derived from the slab.

8.6.3 Aqueous Geochemistry of Halogens

8.6.3.1 Alkali-Chloride Solutions

The main rock-forming alkali metals are Na and K. The most abundant halogen is Cl. These elements will play major roles in governing the effects of halogens on fluid-mediated processes in subduction zones. Here we evaluate the effects of subduction-zone pressures and temperatures on these dissolved solutes. At any pressure and temperature, NaCl or KCl ion pairs in an aqueous solution ($NaCl_{aq}$, KCl_{aq}) will partly dissociate to their constituent ions

$$NaCl_{aq} = Na^+ + Cl^- \tag{8.1}$$

$$KCl_{aq} = K^+ + Cl^- \tag{8.2}$$

Polynuclear clusters (e.g., $NaCl_2^-$, K_2Cl^+, $NaKCl_2$) may be present at elevated salinity at low pressure and high temperature (Oelkers and Helgeson 1993); however, their concentrations are likely negligible at high-pressure subduction conditions (Sakuma and Ichiki 2015).

The extent of dissociation in Eq. 8.1 governs the availability of Cl^- to interact with other metals in solution and is influenced by homogeneous equilibria among dissolved solutes. In an aqueous NaCl solution, these are

$$NaOH_{aq} = Na^+ + OH^- \tag{8.3}$$

$$HCl_{aq} = H^+ + Cl^- \tag{8.4}$$

$$H_2O = H^+ + OH^- \tag{8.5}$$

The distribution of species, pH and extent of dissociation can be determined for a given NaCl concentration by combining equilibrium constants for Eqs. 8.1–8.5, solute activity models, and the charge balance constraint. Taking the standard state of aqueous species to be the unit activity of the hypothetical 1 molal solution referenced to infinite dilution, species concentrations and activity coefficients were calculated using the Güntelberg equation for ion activities and assuming unit activity coefficients of neutral species (Manning 2013). Pressures and temperatures were taken from the thermal models of Syracuse et al. (2010) for Alaska and Cascadia slab-top sediments (D80 models, Fig. 8.11), corresponding respectively to relatively cool and warm subduction geotherms. The Deep Earth Water Model (v 11.0.1) of Sverjensky et al. (2014) was used to calculate equilibrium constants, as well as the density and dielectric constant of H_2O for calculation of the solvent A parameter.

Figure 8.12 a shows the distribution of species in a 1 molal NaCl solution at the temperature of the Alaska sediment top. Note that pressure increases with temperature as well (Fig. 8.11). It can be seen that Na^+ and Cl^- are the predominant species everywhere along this subduction geotherm. The concentrations of HCl_{aq} and $NaOH_{aq}$ ion pairs increase with temperature and pressure but are always lower in abundance than Na^+ and Cl^-. The rise in OH^- concentration with temperature and pressure signals an increasingly alkaline pH (see below).

KCl has a greater tendency to form ion pairs than does NaCl. Comparison of Fig. 8.12a, b shows that, along the Alaskan sediment geotherm, KCl_{aq}

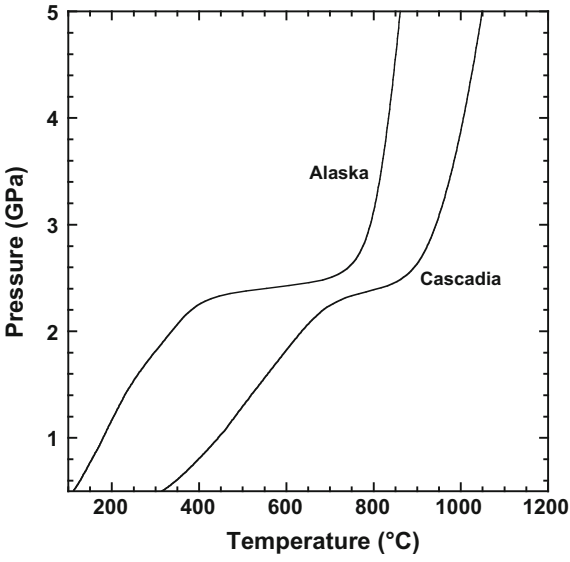

Fig. 8.11 Model subduction-zone geothermal gradients from Syracuse et al. (2010). P-T conditions correspond to the sediments at the slab top, using the D80 set of models in which thermomechanical coupling between the slab and mantle wedge begins at 80 km depth

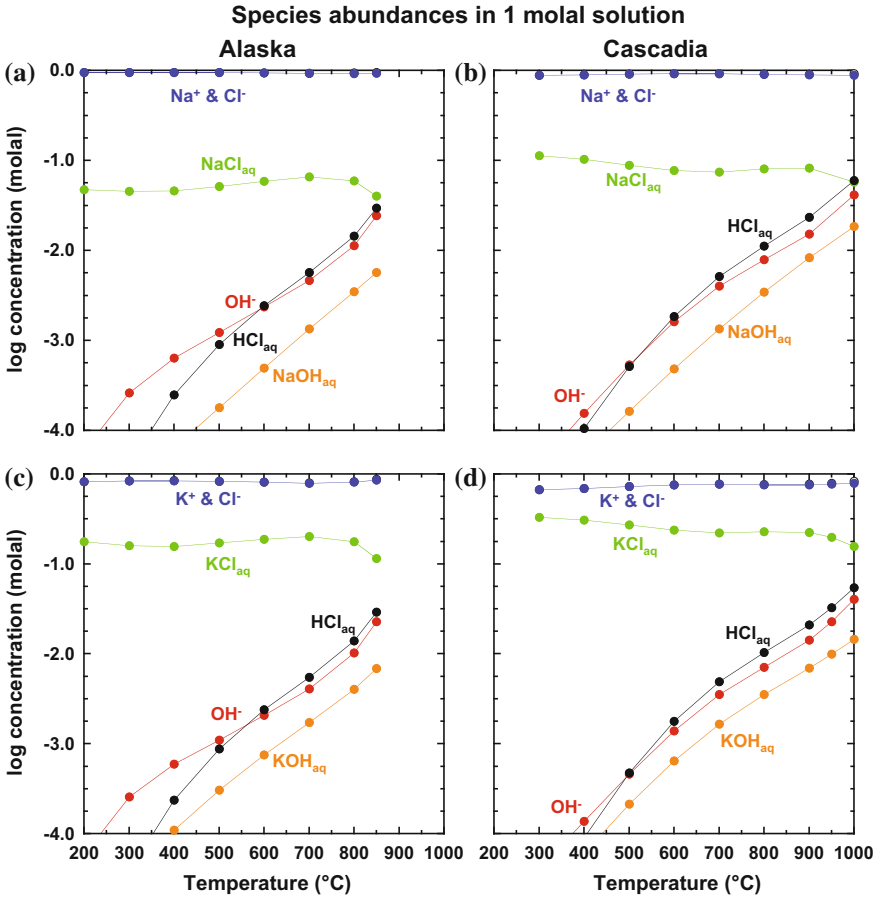

Fig. 8.12 Results of thermodynamic modeling of 1 molal NaCl and KCl solutions. Conditions correspond to model slab-top geotherms from Fig. 8.11, i.e., pressure and temperature co-vary. *Filled circles* represent conditions at which modeling was conducted. Equilibrium constants and solvent parameter A were calculated from the DEW model 11.0.1 (Sverjensky et al. 2014), to a maximum pressure of 6 GPa. Ion activities were computed using the Güntelberg equation. Neutral species were assumed to have a unit activity (Manning 2013). Activity coefficients and species concentrations were calculated using a modified version of the program EQBRM (Anderson and Crear 1993). For many lithologies, parts of both thermal models are likely metastable with respect to H_2O-saturated melting

concentration is everywhere greater than that of $NaCl_{aq}$. Concentrations of K^+ and Cl^- are correspondingly slightly lower.

In general, the thermodynamic data indicate that higher temperatures, at a given depth, and lower pressures, at a given temperature, favor ion pair formation. The implication for subduction geotherms is that NaCl and KCl will be more associated along hotter subduction geotherms, such as that of the sediment top in the Cascadia

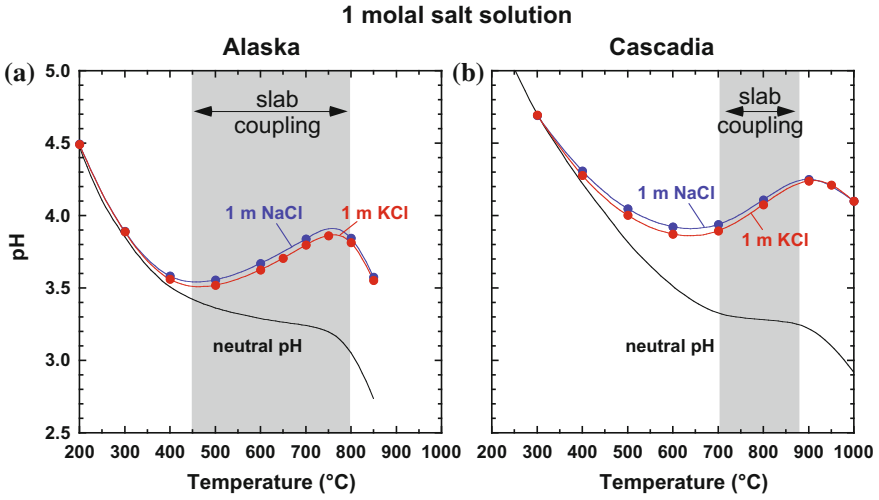

Fig. 8.13 pH of fluids in thermodynamic models shown in Fig. 8.12. Neutral pH at high P and T is much lower than 7 due to a greater extent of dissociation of H_2O (e.g., Manning 2013). The pH of 1 molal NaCl and KCl solutions is always more alkaline than acid-base neutrality, and becomes increasingly so with depth in both subduction zones. This is due to the increasing stability of HCl_{aq} (see text). The temperature range of thermomechanical slab coupling is shown in the *shaded regions* (Syracuse et al. 2010)

subduction zone (Fig. 8.12c, d). It can be seen in Fig. 8.12 that the relative abundance of $NaCl_{aq}$ and KCl_{aq} in 1 molal salt solutions is greater on the Cascadia path relative to the Alaska path, due to the lower pressure at each temperature in the former system (Fig. 8.11).

The pH of 1 molal salt solutions varies with temperature and depth along slab geotherms (Fig. 8.13). Neutral pH, as determined by the equilibrium constant for Eq. 8.5, decreases from 7 at ambient conditions to less than 4 at moderate temperature and high pressure of the sediment top along the Alaskan and Cascadian geotherms. This indicates that, at subduction zone conditions, H_2O exhibits a much stronger propensity to ionize relative to shallow crustal conditions. The concentration of HCl_{aq} is always greater than that of $NaOH_{aq}$ (Fig. 8.12). Therefore, the pH of 1 molal NaCl or KCl solution is everywhere alkaline due to the greater concentration of Na^+ or K^+ than Cl^-. The two salts exhibit similar pH changes along slab geotherms, though it can be seen that KCl yields slightly less alkaline conditions than does NaCl due to the greater association of the former salt (Fig. 8.12). All else being equal, the more dissociated the salt, the more alkaline the solution.

At low temperatures where HCl_{aq} concentration is very low, the pH differs negligibly from neutrality. However, as temperature increases with depth along subduction paths, the growing concentration of HCl_{aq} ion pairs drives the solution to progressively more alkaline pH. Notably, where the slab and overriding mantle

begin to couple mechanically, the resultant nearly isobaric temperature increase leads to greater HCl_{aq} formation relative to $NaOH_{aq}$ or KOH_{aq}, resulting in a significant increase in alkalinity in this region of the subduction zone. Maximum departure from neutral pH is predicted at the deepest, highest temperature conditions. At these conditions, a 1 molal salt solution would have pH $\sim$0.8 and $\sim$1.2 units greater than the acid-base neutrality at the most extreme Alaskan and Cascade sediment top conditions calculated.

The relationships portrayed in Figs. 8.12 and 8.13 depend on salt concentration. This is illustrated in Fig. 8.14, which shows the variation in calculated species abundance as a function of total NaCl concentration at 700 °C and 2.5 GPa, along the Alaskan sediment top. The solution is always dominated by ionic species. However, the relative abundance of the ion pairs controls the pH, regardless of concentration. As the HCl_{aq} concentration rises, the pH is forced to increase as H^+ is consumed relative to OH^-.

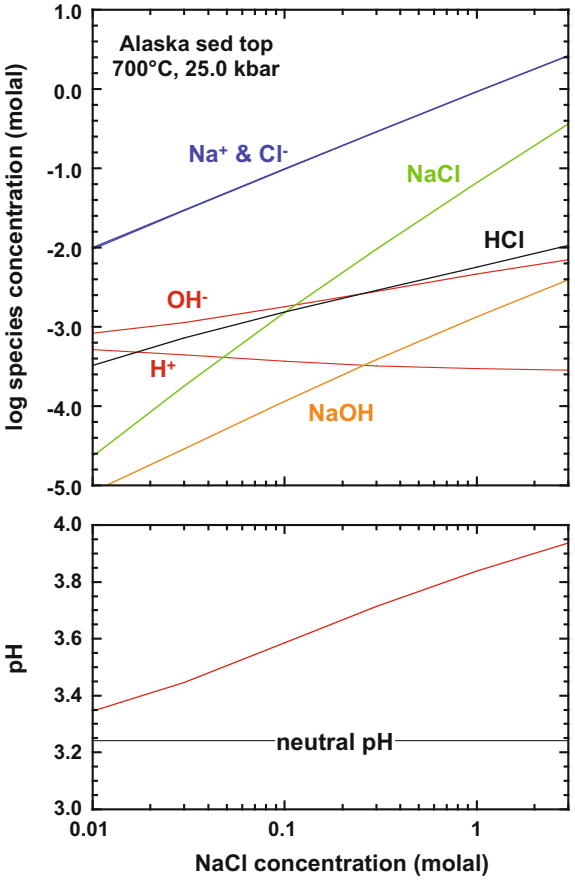

Fig. 8.14 Variation in species abundance with NaCl concentration at Alaskan slab-top conditions of 700 °C, 2.5 GPa. Variations in equilibrium constants with P and T lead to small differences between Na^+ and Cl^- concentration that are unresolvable at the scale of plotting. Compensating variations in OH^- and H^+ yield charge balance and changing pH with NaCl. All model parameters as in Fig. 8.12

8.6.3.2 Role of Saline Fluids in Metal Transport

It is well known that halogen-rich fluids are responsible for significant metal transport and deposition in shallow crustal environments, such as hydrothermal ore deposits. In general, metal-Cl^- and F^- complex stability are not strongly pressure dependent. Halogen complexing can therefore be expected to play an important role in metal mobility in subduction-zone environments.

Keppler (1996) showed that trace-element partitioning between clinopyroxene and a 5 m (NaK)Cl solution indicate higher solubility of Rb, Ba, U, K, Pb, and Sr relative to pure H_2O, and that fluid-clinopyroxene partition coefficients yield trace-element patterns (relative to NMORB) that are similar to subduction-zone volcanics. He concluded that Cl^- fluids could be responsible for trace element transport in subduction zones.

The thermodynamic basis for this behavior is the relative stability of metal-halogen complexes in the aqueous phase. For example, divalent metal M^{+2} and Cl^- will form Cl^- complexes via the stepwise association reactions

$$M^{+2} + Cl^- = MCl^+ \tag{8.6}$$

$$MCl^+ + Cl^- = MCl_{2aq} \tag{8.7}$$

A generic hydrolysis reaction for the oxide of metal M can be written as

$$MO + 2H^+ = M^{+2} + H_2O \tag{8.8}$$

It is evident that formation of MCl^+ and MCl_{2aq} complexes requires forward progress of reaction Eq. (8.7). Thus, more positive equilibrium constants for reactions Eqs. (8.6) and (8.8) indicate an increase in the transport susceptibility of a particular metal by Cl^- complexes.

Figure 8.15 compares equilibrium constants for the first association reaction (8.5) for a range of divalent metals along the Alaskan and Cascadian slab-top P-T paths (Fig. 8.11). Equilibrium constants for reactions involving alkaline earth and transition metals increase with temperature (and depth) along both paths. The equilibrium constants are broadly similar regardless of the path, indicating relatively little dependence on pressure. Of the alkaline earths, values of logK for Mg, Sr, and Ba Cl^- complex formation are very similar, but values for Ca are higher. Regardless of the temperature of the path, Ca will be more strongly mobilized and redistributed by Cl^--bearing fluids. Of the transition metals for which data are available, Zn, Mn, and Pb display a stronger tendency to form Cl^- complexes than do the alkaline earth metals. It can be expected that these elements are strongly mobilized by Cl^- solutions in subduction-zone settings. This simple analysis shows that, with the recent publication of robust thermodynamic models for high pressure fluids (Sverjensky et al. 2014), it will soon be possible to attempt more quantitative analyses of the role of alkali halides on metal cycling in subduction zones.

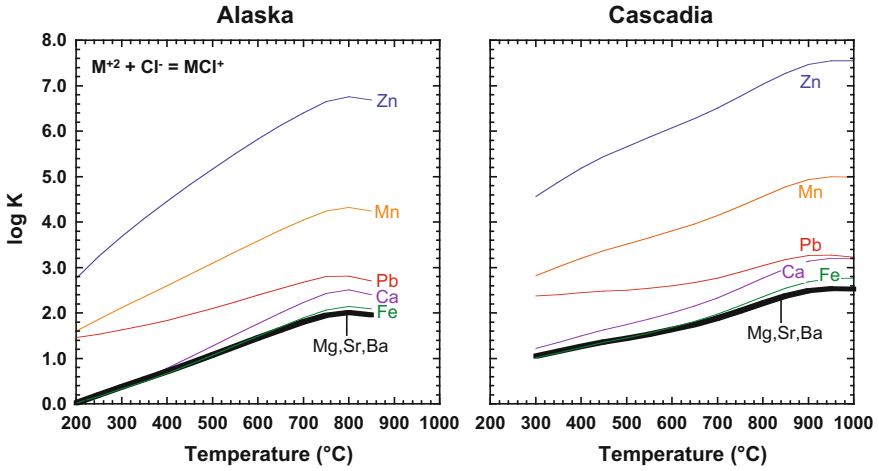

Fig. 8.15 Logarithms of equilibrium constants for the first association reaction involving divalent metal (M) chlorides. Data from the DEW model 11.0.1 (Sverjensky et al. 2014)

8.7 Halogen Isotopes

In the last ~15 years, stable Cl isotopes (^{35}Cl and ^{37}Cl) and cosmogenic halogen isotopes (^{36}Cl and ^{129}I) have been used to trace volatile sources through subduction zones. Studies employing Br stable isotopes (^{79}Br and ^{81}Br; Aston 1920) are limited and to date no published work has used Br isotopes as tracers in subduction zones.

8.7.1 Stable Cl Isotopes (^{35}Cl and ^{37}Cl)

Chlorine has two stable isotopes, ^{35}Cl and ^{37}Cl, with relative abundances of 75.77% and 24.23%, respectively. Chlorine isotope ratios are reported in standard per mil notation (δ^{37}Cl) relative to Standard Mean Ocean Chloride (SMOC), which is defined to be 0‰ (Kaufmann et al. 1984). In the last 20 years, much work has focused on defining the Cl isotope composition of various Cl reservoirs (Fig. 8.16).

The Cl isotope composition of the upper mantle has been a subject of debate in recent years. Sharp et al. (2007) proposed a relatively homogeneous MORB mantle δ^{37}Cl value of -0.2 ± 0.5‰. Bonifacie et al. (2008b) argued that the mantle has a value of ≤ -1.6‰, based on the observation of lower δ^{37}Cl values in samples with lower Cl concentration. However, these low δ^{37}Cl values may not reflect uncontaminated samples, but rather analytical error associated with the analysis of small samples (Sharp et al. 2013). Layne et al. (2009) proposed a δ^{37}Cl value of −3.0‰ based on SIMS measurements of two MORB samples. Recently, using new analyses of mantle and chondritic material, Sharp et al. (2013) convincingly argued

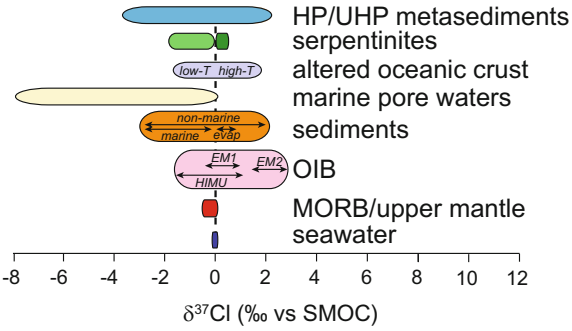

Fig. 8.16 δ^{37}Cl values of various crustal and mantle reservoirs. δ^{37}Cl values from Arcuri and Brimhall (2003), Barnes and Cisneros (2012), Barnes et al. (2006, 2008, 2009a, b), Barnes and Sharp (2006), Bonifacie et al. (2007b), Boschi et al. (2013), Godon et al. (2004), John et al. (2010), Ransom et al. (1995), Selverstone and Sharp (2013, 2015), Sharp et al. (2007, 2013) and Spivack et al. (2002)

for a mantle value of -0.2 ± 0.3‰, analytically indistinguishable from a chondrite value of -0.3 ± 0.3‰. However, the mantle likely preserves some heterogeneities due to the subduction of crustal material (John et al. 2010; Sharp et al. 2007).

Seawater, brines, and evaporites have average δ^{37}Cl values of 0.0 ± 0.5‰ with minimal change through geologic time (e.g., Eastoe et al. 1999, 2007; Eastoe and Peryt 1999; Eggenkamp et al. 1995; Kaufmann et al. 1984). Marine sedimentary pore fluids are negative, down to −7.8‰ (Bonifacie et al. 2007b; Godon et al. 2004; Ransom et al. 1995; Spivack et al. 2002). Marine and non-marine sedimentary material has δ^{37}Cl values ranging from −3.0‰ to +2.0‰ (n = 82) with most non-evaporite marine samples having values between ∼−2‰ and 0‰ (Arcuri and Brimhall 2003; Barnes et al. 2008, 2009b; Selverstone and Sharp 2015). AOC has δ^{37}Cl values ranging from −1.6 to +1.8‰ (Barnes and Cisneros 2012; Bonifacie et al. 2007a). Negative values are dominantly from low-temperature altered, clay-bearing AOC. High-temperature altered, amphibole-bearing AOC is isotopically positive (Barnes and Cisneros 2012). Most seafloor serpentinization results from interaction with seawater producing serpentinites with δ^{37}Cl values between ∼0.0 and +0.5‰ (Barnes et al. 2009a; Barnes and Sharp 2006; Boschi et al. 2013). However, serpentinites can interact with isotopically negative pore fluids, producing rare isotopically negative serpentinites (Barnes et al. 2006; Barnes and Sharp 2006).

The role of subduction metamorphism on the modification of the Cl isotope composition of high-pressure, subducted material is an area of current research. Theoretical calculations predict that little to no Cl isotope fractionation should occur at elevated temperatures (Schauble et al. 2003) and δ^{37}Cl values are thus expected to remain unaltered during metamorphic devolatilization and Cl loss. Work on high-pressure serpentinites and deserpentinized peridotites from the Alps confirm that no significant Cl isotope fractionation occurs during dehydration of the serpentinites (John et al. 2011; Selverstone and Sharp 2013). However, Selverstone

and Sharp (2013) showed that the $\delta^{37}Cl$ values of serpentinites can be modified at lower pressures during exhumation following subduction. High-pressure and ultra high-pressure sedimentary rocks have $\delta^{37}Cl$ values ranging from −3.7 to +2.2‰ (n = 33) (John et al. 2010; Selverstone and Sharp 2013), in good agreement with data from unmetamorphosed sedimentary rocks ($\delta^{37}Cl = -3.0$ to +1.7‰) (Selverstone and Sharp 2015). John et al. (2010) hypothesize that deeply subducted sediments may be characterized by high $\delta^{37}Cl$ values, possibly up to +4‰, but other studies have yet to document such elevated values.

A study of metasomatized, suprasubduction-zone mantle preserved in the Finero complex in the Alps documented two distinct fluid infiltration events characterized by two different $\delta^{37}Cl$ values (Selverstone and Sharp 2011). One fluid endmember had $\delta^{37}Cl \leq -2$‰, was associated with low δD, had high O-fugacity, and had elevated Si, Al, and Ca contents. This fluid produced amphibole-rich segregations in the peridotites. The other fluid had $\delta^{37}Cl$ values $\geq +2$‰; high δD and $\delta^{18}O$ values; and high alkali, HFSE, LILE, Cr, and Cl contents. This latter fluid resulted in pervasive growth of phlogopite in the peridotites.

Previous work employing Cl stable isotopes as a tracer of source in subduction zones has been limited to the Izu-Bonin-Mariana (IBM), and the Central and South America systems (Barnes et al. 2008, 2009b; Barnes and Straub 2010; Chiaradia et al. 2014). $\delta^{37}Cl$ values of outputs from across the IBM system (fore-arc serpentinites, volcanic front ash, back-arc lavas) vary and were interpreted to imply fluid sources at different depths within the subduction zone (Barnes et al. 2008).[4] Volcanic front ash data show little variation in $\delta^{37}Cl$ values along the length of the arc and indicate a fluid contribution from sediments and altered oceanic crust. $\delta^{37}Cl$ values of outputs from both forearc seamounts and reararc cross-chains (chain of seamounts at high angles to the arc front) suggest a serpentinite-derived fluid source. Fluids released at shallow depths, due to the transition from chrysotile/lizardite to antigorite in subducting lithospheric serpentinite, contribute to forearc seamounts. In contrast, fluids released at ∼200 km depth from the breakdown of antigorite contribute to rear arc cross-chains (Barnes et al. 2008). Subsequent work focusing solely on 0–44 Ma tephras from the Izu-Bonin arc show no correlation between $\delta^{37}Cl$ values and either ^{207}Pb or Sr isotopes, which are controlled by fluids from subducting sediment and igneous crust, respectively. This lack of correlation was used as an argument for a serpentinite Cl reservoir (Barnes and Straub 2010).

In contrast to the IBM arc, ashes from the Central America volcanic front record large Cl isotope variations along the length of the arc (–2.6 to +3.0‰), consistent with different Cl sources (Barnes et al. 2009b). Nicaraguan ashes record interaction

[4]The Cl isotope composition of volcanic outputs has focused on lavas, tephras, and glasses. Volcanic gases can have unusually high $\delta^{37}Cl$ values (up to +12‰). Volcanoes with these high values are distinguished by high-T fumaroles (>100 ºC) and large volcanic lakes and/or hydrothermal systems. These high values are explained by kinetic fractionation in which ^{35}Cl-enriched HCl preferentially dissolves in the aqueous condensate along the flow path producing a ^{37}Cl-enriched HCl vapor (Sharp et al. 2010). As a consequence, volcanic gas samples, particularly those from high-T systems, are avoided for use as a tracer of source.

with sediment and/or serpentinite-derived fluids, whereas samples from the northern and southern ends of the arc reflect a more mantle-like signature, consistent with conclusions from other geochemical tracers, such as $\delta^{15}N$, $\delta^{18}O$, and Ba/La (e.g., Patino et al. 2000; Fischer et al. 2002; Eiler et al. 2005).

Recent work on across arc Cl isotope variations in Ecuadorian lavas show that changes in $\delta^{37}Cl$ values across the arc correlate well with slab fluid indices (e.g., Ba/La, Pb/Ce). The overall decrease in $\delta^{37}Cl$ values away from the trench can be interpreted in the frame of previous petrogenetic models of Ecuadorian volcanoes. Here magmas are formed by a steadily decreasing melt fraction of the mantle induced by a steadily decreasing amount of fluids released by the subducted slab away from the trench (Chiaradia et al. 2014).

8.7.2 Cosmogenic Halogen Isotopes (^{36}Cl and ^{129}I)

Iodine has one stable isotope (^{127}I) and one long-lived isotope (^{129}I). ^{129}I is a cosmogenic nuclide with a half-life of 15.7 Myr, allowing for age determinations up to 80 Ma. ^{129}I forms either from interaction with cosmic rays with Xe isotopes in the atmosphere or by the spontaneous fission of ^{238}U in the crust (Fabryka-Martin et al. 1985). Anthropogenic ^{129}I is also produced as a byproduct of nuclear weapons testing and nuclear fuel reprocessing (e.g., Muramatsu and Ohmomo 1986). Due to the high concentration of I in marine sediments and pore fluids, most studies use ^{129}I as a tracer of sediment and/or sedimentary pore fluid recycling through the fore-arc (e.g., Fehn and Snyder 2003; Fehn et al. 2007; Muramatsu et al. 2001; Tomaru et al. 2007). Previous work on I cycling through the oceans has pointed out a large I imbalance in the marine cycle. There is a large flux of iodine from marine organic material into sediments. In addition, the oceans lose I to the atmosphere in the form of iodinated hydrocarbons. Flux of I from river input into the ocean cannot balance ocean I loss (Muramatsu et al. 2001; Muramatsu and Wedepohl 1998). However, the release of I from subducting sediments into fore-arc fluids and ultimately back into the oceans may address this imbalance (Muramatsu et al. 2001). Many I-enriched brines and fluids are documented within the forearc of Japan and New Zealand (e.g., Fehn and Snyder 2003; Fehn et al. 2007; Muramatsu et al. 2001; Tomaru et al. 2007), as well as in the continental slope of Peru (Martin et al. 1993). In New Zealand, $^{129}I/I$ ratios suggest an old I source to the fore-arc fluids, possibly sourced from the accretionary wedge and not derived from actively subducting sediments (Fehn and Snyder 2003; Fehn et al. 2007). However, in several localities in Japan, ^{129}I data support I sourced from subducting marine sediments and not by derivation from accretionary host rock (Muramatsu et al. 2001; Tomaru et al. 2007). Their similar geochemistry with respect to other fore-arc brines has led others to suggest that these Japanese fore-arc fluids may in fact be derived from the upper plate (Fehn 2012).

A few studies have used ^{129}I to address sediment recycling at or near the arc volcanic front (e.g., Fehn et al. 2002; Snyder and Fehn 2002). $^{129}I/I$ ratios in fluids

from hydrothermal springs, crater lakes, and fumaroles from the Central American arc front suggest I is predominantly sourced from subducting sediments and diluted by groundwater or modified by older crustal I (Snyder and Fehn 2002). ^{129}I/I ratios from crater lakes from White Island, New Zealand and Copahue, Argentina also support the derivation of I from subducted sediments (Fehn et al. 2002). Although data is limited, ^{129}I indicates a subducted marine sedimentary source for all arc volcanic fluids studied (Fehn 2012).

In addition to the two Cl stable isotopes discussed in Sect. 8.7.1, Cl has one long-lived isotope (^{36}Cl) with a half-life of 0.301 Myr. ^{36}Cl is produced by the interaction of cosmic rays with Ar isotopes in the atmosphere and by cosmic ray interaction with stable Cl, Ca, and K in the crust. Like ^{129}I, ^{36}Cl is also produced anthropogenically as a waste product of nuclear reactors and nuclear explosions (Bentley et al. 1986; Phillips 2000). The use of ^{36}Cl as a tracer of source in subduction zones is surprisingly limited. A ^{36}Cl/Cl and ^{129}I/I study of volcanic arc thermal springs and a non-thermal mineral spring in the fore-arc of the Cascade Range show that halogens discharged through these springs are primarily derived from magmatic sources, rather than underlying sedimentary units (Hurwitz et al. 2005). Br/Cl and I/Cl ratios and ^{36}Cl and ^{129}I data are consistent with halogens fluxed from the subducting slab (Hurwitz et al. 2005).

8.8 Summary

Our knowledge of the behavior of halogens in subduction zones has greatly increased in the last couple of decades. Chlorine stable isotopes and cosmogenic halogen isotopes (^{36}Cl and ^{129}I) have been employed to successfully trace fluid sources from subduction inputs to arc outputs. Serpentinites have been identified as major halogen sources, particularly for Cl ($\sim$2000 μg/g) and I (up to 45 μg/g), to sub-arc depths in subduction zones. High halogen concentrations in melt inclusions are strong evidence for the subduction of surficial reservoirs. Recent work on halogen concentrations in BABB and OIB also supports the survival of halogens into the upper mantle.

Despite these advances, halogen loss through the fore-arc and through hydrothermal systems is poorly constrained, leading to potentially large uncertainties in mass balance calculations. Our knowledge of the Cl cycle is the best understood, likely followed by F. Bromine and I arc outputs are poorly constrained with a few measurements from volcanic gas emissions and limited published data from melt inclusions. The extent to which these elements are lost to subduction-zone fluids and melts, and how they are fractionated from one another during subduction are areas of active research. The addition of halogens to aqueous slab fluids and the resultant effects on phase equilibria, as a function of the subduction geothermal gradient, may have profound implications for elemental transport within subduction zones.

Acknowledgements The authors thank M. Kendrick for discussions and providing a draft of Fig. 8.1, and R. Esposito for discussions on melt inclusions. The authors gratefully acknowledge thorough and helpful reviews by S. Straub, N. Metrich, and H. Marschall. We also thank D.E. Harlov and L. Aranovich for editorial handling, comments, and patience. This work was supported by the Deep Carbon Observatory and U.S. National Science Foundation grant EAR-1347987 to CEM.

References

Aiuppa A, Federico C, Franco A, Giudice G, Gurrieri S, Inguaggiato S, Liuzzo M, McGonigle AJS, Valenza M (2005) Emission of bromine and iodine from Mount Etna volcano. Geochem Geophys Geosyst 6:Q08008. https://doi.org/08010.01029/02005GC000965

Aiuppa A, Baker DR, Webster JD (2009) Halogens in volcanic systems. Chem Geol 263:1–18

Anderson G, Crear D (1993) Thermodynamics in geochemistry. Oxford University Press, New York, p 588

Angiboust S, Agard P, Jolivet L, Beyssac O (2009) The Zermatt-Saas ophiolite: the largest (60-km wide) and deepest (c. 70–80 km) continuous slice of oceanic lithosphere detached from a subduction zone? Terra Nova 21:171–180

Angiboust S, Langdon R, Agard P, Waters D, Chopin C (2012) Eclogitization of the Monviso ophiolite (W. Alps) and implications on subduction dynamics. J Metamorph Geol 30:37–61

Anselmi B, Mellini M, Viti C (2000) Chlorine in the Elba, Monti Livornesi and Murlo serpentines: evidence for sea-water interaction. Eur J Mineral 12(1):137–146

Aranovich LY, Newton RC (1996) H_2O activity in concentrated solutions at high pressures and temperatures measured by the brucite-periclase equilibrium. Contrib Mineral Petrol 125:200–212

Aranovich LY, Newton RC (1997) H_2O activity in concentrated KCl and solutions at high temperatures and pressures measured by the brucite-periclase equilibrium. Contrib Mineral Petrol 127:261–271

Aranovich LY, Newton RC (1999) Experimental determination of CO_2-H_2O activity-composition relations at 600–1000 C and 6–14 kbar by reversed decarbonation and dehydration reactions. Am Mineral 84(9):1319–1332

Aranovich LY, Zakirov IV, Sretenskaya NG, Gerya TV (2010) Ternary system H_2O-CO_2-NaCl at high T-P parameters: an empirical mixing model. Geochem Int 48:446–455

Aranovich LY, Newton RC, Manning CE (2013) Brine-assisted anatexis: experimental melting in the system haplogranite-H_2O-NaCl-KCl at deep-crustal conditions. Earth Planet Sci Lett 374:111–120

Arcuri T, Brimhall G (2003) The chloride source for atacamite mineralization at the Radomiro Tomic porphyry copper deposit, northern Chile. Econ Geol 98:1667–1681

Aston FW (1920) The mass-spectra of chemical elements Part 2. Philos Mag 40:628–634

Auer S, Bindeman I, Wallace P, Ponomareva V, Portnyagin M (2009) The origin of hydrous, high-$\delta^{18}O$ voluminous volcanism: diverse oxygen isotope values and high magmatic water contents within the volcanic record of Klyuchevskoy volcano, Kamchatka, Russia. Contrib Mineral Petrol 157:209–230

Balcone-Boissard H, Villemant B, Boudon G (2010) Behavior of halogens during the degassing of felsic magmas. Geochem Geophys Geosyst 11:9

Barnes JD, Cisneros M (2012) Mineralogical control on the chlorine isotope composition of altered oceanic crust. Chem Geol 326–327:51–60

Barnes JD, Sharp ZD (2006) A chlorine isotope study of DSDP/ODP serpentinized ultramafic rocks: insights into the serpentinization process. Chem Geol 228:246–265

Barnes JD, Straub SM (2010) Chlorine stable isotope variations in Izu Bonin tephra: implications for serpentinite subduction. Chem Geol 272:62–74

Barnes JD, Selverstone J, Sharp ZD (2006) Chlorine chemistry of serpentinites from Elba, Italy, as an indicator of fluid source and subsequent tectonic history. Geochem Geophys Geosyst 7: Q08015. https://doi.org/08010.01029/02006GC001296

Barnes JD, Sharp ZD, Fischer TP (2008) Chlorine isotope variations across the Izu-Bonin-Mariana arc. Geology 36:883–886

Barnes JD, Paulick H, Sharp ZD, Bach W, Beaudoin G (2009a) Stable isotope (^{18}O, D, ^{37}Cl) evidence for multiple fluid histories in mid-Atlantic abyssal peridotites (ODP Leg 209). Lithos 110:83–94

Barnes JD, Sharp ZD, Fischer TP, Hilton DR, Carr MJ (2009b) Chlorine isotope variations along the Central American volcanic front and back arc. Geochem Geophys Geosyst 10:Q11S17. https://doi.org/10.1029/2009GC002587

Behn MD, Kelemen PB, Hirth G, Hacker BR, Massonne HJ (2011) Diapirs as the source of the sediment signature in arc lavas. Nat Geosci 4:641–646

Benjamin ER, Plank T, Wade JA, Kelley KA, Hauri EH, Alvarado GE (2007) High water contents in basaltic magmas from Irazu Volcano, Costa Rica. J Volcanol Geotherm Res 168:68–92

Bentley HW, Phillips FM, Davis SN (1986) ^{36}Cl in the terrestrial environment. In: Fritz P, Fontes J-C (eds) Handbook of environmental geochemistry, vol 2b. Elsevier Science, New York, pp 422–475

Bernini D, Wiedenbeck M, Dolejš D, Keppler H (2013) Partitioning of halogens between mantle minerals and aqueous fluids: implications for the fluid flow regime in subduction zones. Contrib Miner Petrol 165:117–128

Beyer C, Klemme S, Wiedenbeck M, Stracke A, Vollmer C (2012) Fluorine in nominally fluorine-free mantle minerals: experimental partitioning of F between olivine, orthopyroxene and silicate melts with implications for magmatic processes. Earth Planet Sci Lett 337:1–9

Bézos A, Escrig S, Langmuir CH, Michael PJ, Asimow PD (2009) Origins of chemical diversity of back-arc basin basalts: a segment-scale study of the Eastern Lau Spreading Center. J Geophys Res 114:B06212. https://doi.org/06210.01029/02008JB005924

Bobrowski N, Hönninger G, Galle B, Platt U (2003) Detection of bromine monoxide in a volcanic plume. Nature 423:273–276

Bonifacie M, Jendrzejewski N, Agrinier P, Coleman M, Pineau F, Javoy M (2007a) Pyrohydrolysis-IRMS determination of silicate chlorine stable isotope compositions. Application to oceanic crust and meteorite samples. Chem Geol 242:187–201

Bonifacie M, Monnin C, Jendrzejewski N, Agrinier P, Javoy M (2007b) Chlorine stable isotopic composition of basement fluids of the eastern flank of the Juan de Fuca Ridge (ODP Leg 168). Earth Planet Sci Lett 260:10–22

Bonifacie M, Busigny V, Mével C, Philippot P, Agrinier P, Jendrzejewski N, Scambelluri M, Javoy M (2008a) Chlorine isotopic composition in seafloor serpentinites and high-pressure metaperidotites. Insights into oceanic serpentinization and subduction processes. Geochim Cosmochim Acta 72:126–139

Bonifacie M, Jendrzejewski N, Agrinier P, Humler E, Coleman M, Javoy M (2008b) The chlorine isotope composition of the Earth's mantle. Science 319:1518–1520

Boschi C, Bonatti E, Ligi M, Brunelli D, Dallai L, D'Orazio M, Früh-Green G, Tonarini S, Barnes JD, Bedini R (2013) A 10 Ma year old window into deep hydrothermal circulation at the Vema Fracture Zone (11ºN, MAR). Lithos 178:3–23

Bostock MG, Hyndman RD, Rondenay S, Peacock SM (2002) An inverted continental Moho and serpentinization of the forearc mantle. Nature 417:536–538

Bucher K, Fazis Y, Capitani CD, Grapes R (2005) Blueschists, eclogites, and decompression assemblages of the Zermatt-Saas ophiolite: high-pressure metamorphism of subducted Tethys lithosphere. Am Mineral 90:821–835

Bucholz CE, Gaetani GA, Behn MD, Shimizu N (2013) Post-entrapment modification of volatiles and oxygen fugacity in olivine-hosted melt inclusions. Earth Planet Sci Lett 374:145–155

Bureau H, Keppler H, Métrich N (2000) Volcanic degassing of bromine and iodine: experimental fluid/melt partitioning data and applications to stratospheric chemistry. Earth Planet Sci Lett 183:51–60

Burgess R, Layzelle E, Turner G, Harris JW (2002) Constraints on the age and halogen composition of mantle fluids in Siberian coated diamonds. Earth Planet Sci Lett 197:193–203
Cannaò E, Agostini S, Scambelluri M, Tonarini S, Godard M (2015) B, Sr and Pb isotope geochemistry of high-pressure Alpine metaperidotites monitors fluid-mediated element recycling during serpentinite dehydration in subduction mélange (Cima di Gagnone, Swiss Central Alps). Geochim Cosmochim Acta 163:80–100
Cannat M, Karson JA, Miller DJ, et al (1995) Proc. ODP, Init. Repts. In, vol 153. Ocean Drilling Program, College Station, TX, p 798
Cervantes P, Wallace PJ (2003) Role of H_2O in subduction-zone magmatism: new insights from melt inclusions in high-Mg basalts from central Mexico. Geology 31:235–238
Chiaradia M, Barnes JD, Cadet-Voisin S (2014) Chlorine isotope variations across the Quaternary volcanic arc of Ecuador. Earth Planet Sci Lett 396:22–33
Clift P, Vannucchi P (2004) Controls on tectonic accretion versus erosion in subduction zones: implications for the origin and recycling of the continental crust. Rev Geophys 42:1
Dalou C, Koga KT, Shimizu N, Boulon J, Devidal JL (2012) Experimental determination of F and Cl partitioning between lherzolite and basaltic melt. Contrib Mineral Petrol 163:591–609
Davies JH, Stevenson DJ (1992) Physical model for the source region of subduction zone volatiles. J Geophys Res 97:2037–2070
Debret B, Nicollet C, Andreani M, Schwartz S, Godard M (2013) Three steps of serpentinisation in an eclogitized oceanic serpentinization front (Lanzo Massif—Western Alps). J Metamorph Geol 31:165–186
Debret B, Koga KT, Nicollet C, Andreani M, Schwartz S (2014) F, Cl and S input via serpentinite in subduction zones: implications for the nature of the fluid released at depth. Terra Nova 26:96–101
Debret B, Koga KT, Cattani F, Nicollet C, Van den Bleeken G, Schwartz S (2016) Volatile (Li, B, F and Cl) mobility during amphibole breakdown in subduction zones. Lithos 244:165–181
Deruelle B, Dreibus G, Jambon A (1992) Iodine abundances in oceanic basalts: implications for Earth dynamics. Earth Planet Sci Lett 108:217–227
Deschamps F, Godard M, Guillot S, Hattori K (2013) Geochemistry of subduction zone serpentinites: a review. Lithos 178:96–127
Eastoe CJ, Peryt T (1999) Stable chlorine isotope evidence for non-marine chloride in Badenian evaporites, Carpathian mountain region. Terra Nova 11(2/3):118–123
Eastoe CJ, Long A, Knauth LP (1999) Stable chlorine isotopes in the Palo Duro Basin, Texas: evidence for preservation of Permian evaporite brines. Geochim Cosmochim Acta 63(9): 1375–1382
Eastoe CJ, Peryt TM, Petrychenko OY, Geisler-Cussey D (2007) Stable chlorine isotopes of Phanerozoic evaporites. Appl Geochem 22:575–588
Eggenkamp HGM, Kreulen R, Koster van Groos AF (1995) Chloride stable isotope fractionation in evaporites. Geochim Cosmochim Acta 59(24):5169–5175
Eiler JM, Carr MJ, Reagan M, Stolper E (2005) Oxygen isotope constraints on the sources of Central American arc lavas. Geochem Geophys Geosyst 6:Q07007. https://doi.org/10.1029/2004GC000804
Esposito R, Hunter J, Schiffbauer JD, Shimizu N, Bodnar RJ (2014) An assessment of the reliability of melt inclusions as recorders of the pre-eruptive volatile content of magmas. Am Mineral 99:976–998
Evans BW, Trommsdorff V (1978) Petrogenesis of garnet lherzolite, Cima di Gagnone, Lepontine Alps. Earth Planet Sci Lett 40:333–348
Evans BW, Trommsdorff V (1983) Fluorine hydroxyl titanian clinohumite in Alpine recrystallized garnet peridotite: compositional controls and petrologic significance. Am J Sci 283:355–369
Fabbrizio A, Stalder R, Hametner K, Günther D, Marquardt K (2013) Experimental partitioning of halogens and other trace elements between olivine, pyroxenes, amphibole and aqueous fluid at 2 GPa and 900–1,300 °C. Contrib Mineral Petrol 166:639–653
Fabryka-Martin J, Bentley H, Elmore D, Airey PL (1985) Natural iodine-129 as an environmental tracer. Geochim Cosmochim Acta 49:337–347

Fehn U (2012) Tracing crustal fluids: applications of natural ^{129}I and ^{36}Cl. Ann Rev Earth Planet Sci 40:45–67

Fehn U, Snyder GT (2003) Origin of iodine and ^{129}I in volcanic and geothermal fluids from the North Island of New Zealand: implications for Subduction Zone Processes. Spec Publ Soc Econ Geol 10:159–170

Fehn U, Snyder GT, Varekamp JC (2002) Detection of recycled marine sediment components in crater lake fluids using ^{129}I. J Volcanol Geotherm Res 115:451–460

Fehn U, Lu Z, Tomaru H (2006) 129I/I ratios and halogen concentrations in pore water of Hydrate Ridge and their relevance for the origin of gas hydrates: a progress report. In: Trehu AM, Bohrmann G, Torres ME, Colwell FS (eds) Proceedings of the ocean drilling program, Scientific results, vol 204, pp 1–25

Fehn U, Snyder GT, Muramatsu Y (2007) Iodine as a tracer of organic material: ^{129}I results from gas hydrate systems and fore arc fluids. J Geochem Explor 95:66–80

Fischer TP (2008) Fluxes of volatiles (H2O, CO_2, N_2, Cl, F) from arc volcanoes. Geochem J 42:21–38

Fischer TP, Hilton DR, Zimmer MM, Shaw AM, Sharp ZD, Walker JA (2002) Subduction and recycling of nitrogen along the Central American margin. Science 297:1154–1157

Gaetani GA, O'Leary JA, Shimizu N, Bucholz CE, Newville M (2012) Rapid reequilibration of H_2O and oxygen fugacity in olivine-hosted melt inclusions. Geology 40:915–918

Gao S, Luo TC, Zhang BR, Zhang HF, Han YW, Zhao ZD, Hu YK (1998) Chemical composition of the continental crust as revealed by studies in East China. Geochim Cosmochim Acta 62:1959–1975

Gerya TV, Yuen DA (2003) Rayleigh-Taylor instabilities from hydration and melting propel 'cold plumes' at subduction zones. Earth Planet Sci Lett 212:47–62

Gillis KM (1996) Rare element constraints on the origin of amphibole in gabbroic rocks from Site 894, Hess Deep. In: Mevel C, Gillis KM, Allan JF, Meyer PS (eds) Proceedings of the ocean drilling program, Scientific results, vol 147. Ocean Drilling Program, pp 59–75

Gillis KM, Meyer PS (2001) Metasomatism of oceanic gabbros by late stage melts and hydrothermal fluids: evidence from rare earth element composition of amphiboles. Geochem Geophys Geosyst 2:2000GC000087

Godon A, Jendrzejewski N, Castrec-Rouelle M, Dia A, Pineau F, Boulègue J, Javoy M (2004) Origin and evolution of fluids from mud volcanoes in the Barbados accretionary complex. Geochim Cosmochim Acta 68(9):2153–2165

Hacker BR (2008) H_2O subduction beyond arcs. Geochem Geophys Geosyst 9:Q03001. https://doi.org/03010.01029/02007GC001707

Halbach H, Chatterjee ND (1982) An empirical Redlich-Kwong-type equation of state for water to 1000 °C and 200 kbar. Contrib Mineral Petrol 79:337–345

Harvey J, Garrido CJ, Savov I, Agostini S, Padrón-Navarta JA, Marchesi C, Sánchez-Vizcaíno VL, Gómez-Pugnaire MT (2014) ^{11}B-rich fluids in subduction zones: the role of antigorite dehydration in subducting slabs and boron isotope heterogeneity in the mantle. Chem Geol 376:20–30

Heinrich W (2007) Fluid immiscibility in metamorphic rocks. Rev Mineral Geochem 65:389–430

Hermann J, Müntener O, Scambelluri M (2000) The importance of serpentinite mylonites for subduction and exhumation of oceanic crust. Tectonophysics 327:225–238

Hoernle K, Abt DL, Fischer KM, Nichols H, Hauff F, Abers GA, van den Bogaard P, Heydolph K, Alvarado G, Protti M, Strauch W (2008) Arc-parallel flow in the mantle wedge beneath Costa Rica and Nicaragua. Nature 451:1094–1097

Hofmann AW (2003) Sampling mantle heterogeneity through oceanic basalts: isotopes and trace elements. In: Carlson RL (ed) The core and mantle: treatise on geochemistry, vol 2. Elsevier Ltd., Oxford, pp 61–101

Holloway JR (1977) Fugacity and activity of molecular species in supercritical fluids, vol 10. Springer, New York

Hurwitz S, Mariner RH, Fehn U, Snyder GT (2005) Systematics of halogen elements and their radioisotopes in thermal springs of the Cascade Range, Central Oregon, Western USA. Earth Planet Sci Lett 235:700–714

Hyndman RD, Peacock SM (2003) Serpentinization of the forearc mantle. Earth Planet Sci Lett 212:417–432

Ishizuka H (1989) Mineral paragenesis of altered basalts from Hole 504B, ODP Leg 111. In: Becker K, Sakai H, et al (eds) Proceedings of the ocean drilling program, Scientific results, vol. Ocean Drilling Program, pp 61–76

Ito E, Harris DM, Anderson AT Jr (1983) Alteration of oceanic crust and geologic recycling of chlorine and water. Geochim Cosmochim Acta 47:1613–1624

Jambon A, Déruelle B, Dreibus G, Pineau F (1995) Chlorine and bromine abundance in MORB: the contrasting behaviour of the Mid-Atlantic Ridge and East Pacific Rise and implications for chlorine geodynamic cycle. Chem Geol 126:101–117

Jarrard RD (2003) Subduction fluxes of water, carbon dioxide, chlorine, and potassium. Geochem Geophys Geosyst 4(5):8905. https://doi.org/8910.1029/2002GC000392

John T, Layne GD, Haase KM, Barnes JD (2010) Chlorine isotope evidence for crustal recycling into the Earth's mantle. Earth Planet Sci Lett 298:175–182

John T, Scambelluri M, Frische M, Barnes JD, Bach W (2011) Dehydration of subducting serpentinite: implications for halogen mobility in subduction zones and the deep halogen cycle. Earth Planet Sci Lett 308(1):65–76. https://doi.org/10.1016/j.epsl.2011.1005.1038

Johnson ER, Wallace PJ, Granados HD, Manea VC, Kent AJ, Bindeman IN, Donegan CS (2009) Subduction-related volatile recycling and magma generation beneath Central Mexico: insights from melt inclusions, oxygen isotopes and geodynamic models. J Petrol 50:1729–1764

Kastner M, Elderfield H, Martin JB (1991) Fluids in convergent margins: what do we know about their composition, origin, role in diagenesis and importance for oceanic chemical fluxes? Philos Trans R Soc Lond 335:243–259

Kaufmann R, Long A, Bentley H, Davis S (1984) Natural chlorine isotope variations. Nature 309:338–340

van Keken PE, Hacker BR, Syracuse EM, Abers GA (2011) Subduction factory: 4. Depth-dependent flux of H2O from subducting slabs worldwide. J Geophys Res 116: B01401. https://doi.org/01410.01029/02010JB007922

Kelemen PB, Manning CE (2015) Reevaluating carbon fluxes in subduction zones, what goes down, mostly comes up. Proc Natl Acad Sci. https://doi.org/10.1073/pnas.1507889112

Kendrick MA, Scambelluri M, Honda M, Phillips D (2011) High abundances of noble gas and chlorine delivered to the mantle by serpentinite subduction. Nat Geosci 4(11):807–812

Kendrick MA, Kamenetsky VS, Phillips D, Honda M (2012a) Halogen systematics (Cl, Br, I) in mid-ocean ridge basalts: a Macquarie Island case study. Geochim Cosmochim Acta 81:82–93

Kendrick MA, Woodhead JD, Kamenetsky VS (2012b) Tracking halogens through the subduction cycle. Geology 40:1075–1078

Kendrick MA, Honda M, Pettke T, Scambelluri M, Phillips D, Giuliani A (2013) Subduction zone fluxes of halogens and noble gases in seafloor and forearc serpentinites. Earth Planet Sci Lett 365:86–96

Kendrick MA, Arculus RJ, Danyushevsky LV, Kamenetsky VS, Woodhead JD, Honda M (2014a) Subduction-related halogens (Cl, Br and I) and H_2O in magmatic glasses from Southwest Pacific Backarc Basins. Earth Planet Sci Lett 400:165–176

Kendrick MA, Jackson MG, Kent AJ, Hauri EH, Wallace PJ, Woodhead J (2014b) Contrasting behaviours of CO_2, S, H_2O and halogens (F, Cl, Br, and I) in enriched-mantle melts from Pitcairn and Society seamounts. Chem Geol 370:69–81

Kent AJR, Peate DW, Newman S, Stolper EM, Pearce JA (2002) Chlorine in submarine glasses from the Lau Basin: seawater contamination and constraints on the composition of slab-derived fluids. Earth Planet Sci Lett 202:361–377

Keppler H (1996) Constraints from partitioning experiments on the composition of subduction-zone fluids. Nature 380:237–240

Keppler H (2017) Fluids and trace element transport in subduction zones. Am Mineral 102:5–20

Kerrick D, Jacobs G (1981) A modified Redlich-Kwong equation for H_2O, CO_2, and H_2O-CO_2 mixtures at elevated pressures and temperatures. Am J Sci 281(6):735–767

Kerrick DM (2002) Serpentinite seduction. Science 298:1344–1345

Klemme S, Stalder R (2018) Halogens in the Earth's mantle: what we know and what we don't. In: Harlov DE, Aranovich L (eds) The role of halogens in terrestrial and extraterrestrial geochemical processes: surface, crust, and mantle. Springer, Berlin, pp 847–869

Kodolányi J, Pettke T (2011) Loss of trace elements from serpentinites during fluid-assisted transformation of chrysotile to antigorite—an example from Guatemala. Chem Geol 284:351–362

Kodolányi J, Pettke T, Spandler C, Kamber BS, Gméling K (2012) Geochemistry of ocean floor and fore-arc serpentinites: constraints on the ultramafic input to subduction zones. J Petrol 53:235–270

Kutterolf S, Hansteen TH, Appel K, Freundt A, Krüger K, Perez W, Wehrmann H (2013) Combined bromine and chlorine release from large explosive volcanic eruptions: a threat to stratospheric ozone? Geology 41:707–710

Lafay R, Deschamps F, Schwartz S, Guillot S, Godard M, Debret B, Nicollet C (2013) High-pressure serpentinites, a trap-and-release system controlled by metamorphic conditions: example from the Piedmont zone of the western Alps. Chem Geol 343:38–54

Lagabrielle Y, Cannat M (1990) Alpine Jurassic ophiolites resemble the modern central Atlantic basement. Geology 18(4):319–322

Lassiter JC, Hauri EH, Nikogosian IK, Barsczus HG (2002) Chlorine-potassium variations in melt inclusions from Raivavae and Rapa, Austral Islands: constraints on chlorine recycling in the mantle and evidence for brine-induced melting of oceanic crust. Earth Planet Sci Lett 202:525–540

Laverne C, Vanko DA, Tartarotti P, Alt JC (1995) Chemistry and geothermometry of secondary minerals from the deep sheeted dike complex, Hole 504B. In: Erzinger J, Becker K, Dick HJB, Stokking LB (eds) Proceedings of the ocean drilling program, Scientific results, vol 137/140. Ocean Drilling Program, pp 167–189

Layne GD, Kent AJR, Bach W (2009) δ^{37}Cl systematics of a backarc spreading system: the Lau Basin. Geology 37:427–430

Li XP, Rahn M, Bucher K (2004) Serpentinites of the Zermatt-Saas ophiolite complex and their texture evolution. J Metamorph Geol 22:159–177

Li Y-H (1982) A brief discussion on the mean oceanic residence time of elements. Geochim Cosmochim Acta 46:2671–2675

Li Y-H, Schoomaker JE (2003) Chemical composition and mineralogy of marine. Treatise Geochem 7:1–35

Liebscher A (2010) Aqueous fluids at elevated pressure and temperature. Geofluids 10:3–19

Lopez Sánchez-Vizcaíno VL, Trommsdorff V, Gómez-Pugnaire MT, Garrido CJ, Müntener O, Connolly JAD (2005) Petrology of titanian clinohumite and olivine at the high-pressure breakdown of antigorite serpentinite to chlorite harzburgite (Almirez Massif, S. Spain). Contrib Mineral Petrol 149:627–646

Luth R (2014) Volatiles in Earth's Mantle. In: Holland HD, Turekian KK (eds) Treatise on Geochemistry, vol 3, 2nd edn. Elsevier, Oxford, pp 355–379

Manning CE (2004) The chemistry of subduction-zone fluids. Earth Planet Sci Lett 223:1–16

Manning CE (2013) Thermodynamic modeling of fluid-rock interaction at conditions of the earth's middle crust to upper mantle. Rev Mineral Geochem 76:135–164

Manning CE, Aranovich LY (2014) Brines at high pressure and temperature: thermodynamic, petrologic and geochemical effects. Precambr Res 253:6–16

Manning CE, Shock EL, Sverjensky DA (2013) The chemistry of carbon in aqueous fluids at crustal and upper-mantle conditions: experimental and theoretical constraints. Rev Mineral Geochem 75:109–148

Mantegazzi D, Sanchez-Valle C, Driesner T (2013) Thermodynamic properties of aqueous solutions to 1073 K and 4.5 GPa, and implications for dehydration reactions in subducting slabs. Geochim Cosmochim Acta 121:263–290

Marschall HR, Schumacher JC (2012) Arc magmas sourced from mélange diapirs in subduction zones. Nat Geosci 5:862–867

Marschall HR, Altherr R, Gméling K, Kasztovszky ZS (2009) Lithium, boron and chlorine as tracers for metasomatism in high-pressure metamorphic rocks: a case study from Syros (Greece). Mineral Petrol 95:291–302

Martin JB, Gieskes JM, Torres M, Kastner M (1993) Bromine and iodine in Peru margin sediments and: implications for fluid origins. Geochim Cosmochim Acta 57:4377–4389

Métrich N, Deloule E (2014) Water content, δD and $\delta^{11}B$ tracking in the Vanuatu arc magmas (Aoba Island): insights from olivine-hosted melt inclusions. Lithos 206:400–408

Mével C (2003) Serpentinization of abyssal peridotites at mid-ocean ridges. C R Geosci 335:825–852

Michael PJ, Cornell WC (1998) Influence of spreading rate and magma supply on crystallization and assimilation beneath mid-ocean ridges: evidence from chlorine and major element chemistry of mid-ocean ridge basalts. J Geophys Res 103(B8):18325–18356

Michael PJ, Schilling J-G (1989) Chlorine in mid-ocean ridge magmas: evidence for assimilation of seawater-influenced components. Geochim Cosmochim Acta 53:3131–3143

Morrison J (1991) Compositional contraints on the incorporation of Cl into amphiboles. Am Mineral 76:1920–1930

Mottl MJ, Wheat CG, Fryer P, Gharib J, Martin JB (2004) Chemistry of springs across the Mariana forearc shows progressive devolatilization of the subducting plate. Geochim Cosmochim Acta 68:4915–4933

Munoz JL (1984) F-OH and Cl-OH exchange in micas with applications to hydrothermal ore deposits. In: Bailey SW (ed) Reviews in mineralogy: micas, vol 13. Mineralogical Society of America, Washington, D.C., p 584

Muramatsu Y, Ohmomo Y (1986) Iodine-129 and iodine-127 in environmental samples collected from Tokaimura/Ibaraki, Japan. Sci Total Environ 48:33–43

Muramatsu Y, Wedepohl KH (1998) The distribution of iodine in the earth's crust. Chem Geol 147:201–216

Muramatsu Y, Fehn U, Yoshida S (2001) Recycling of iodine in fore-arc areas: evidence from the iodine brines in Chiba, Japan. Earth Planet Sci Lett 192:583–593

Muramatsu Y, Doi T, Tomaru H, Fehn U, Takeuchi R, Matsumoto R (2007) Halogen concentrations in pore waters and sediments of the Nankai Trough, Japan: implications for the origin of gas hydrates. Appl Geochem 22:534–556

Nehlig P (1993) Interactions between magma chambers and hydrothermal systems: oceanic and ophiolitic constraints. J Geophys Res Solid Earth 98(B11):19621–19633

Oelkers EH, Helgeson HC (1993) Multiple ion association in supercritical aqueous solutions of single electrolytes. Science 261:888–891

Padròn-Navarta JA, Tommasi A, Garrido CJ, Lopez Sanchez-Vizcaìno V, Gòmez-Pugnaire MT, Jabaloy A, Vauchez A (2010) Fluid transfer into the wedge controlled by high-pressure hydrofracturing in the cold top-slab mantle. Earth Planet Sci Lett 297:271–286

Patino LC, Carr MJ, Feigenson MD (2000) Local and regional variations in Central American arc lavas controlled by variations in subducted sediment input. Contrib Mineral Petrol 138:265–283

Pelletier L, Müntener O (2006) High-pressure metamorphism of the Lanzo peridotite and its oceanic cover, and some consequences for the Sesia-Lanzo zone (northwestern Italian Alps). Lithos 90:111–130

Pertsev AN, Aranovich LY, Prokofiev VY, Bortnikov NS, Cipriani A, Simakin SS, Borisovskiy SE (2015) Signatures of residual melts, magmatic and seawater-derived fluids in oceanic lower-crust gabbro from the vema lithospheric section, central Atlantic. J Petrol 56:1069–1088

Philippot P, Selverstone J (1991) Trace-element-rich brines in eclogitic veins: implications for fluid composition and transport during subduction. Contrib Mineral Petrol 106:417–430

Philippot P, Agrinier P, Scambelluri M (1998) Chlorine cycling during subduction of altered oceanic crust. Earth Planet Sci Lett 161(1–4):33–44

Phillips FM (2000) Chlorine-36. In: Cook PG, Herczeg AL (eds) Environmental tracers in subsurface hydrology. Kluwer Academic Publishing, Boston, pp 299–348

Pieri D (2015) Satellite and aircraft-based techniques to measure volcanic emissions and hazards. In: Schmidt A, Fristad K, Elkins-Tanton L (eds) Volcanism and global environmental change. Cambridge University Press, Cambridge, pp 133–146

Platt U, Bobrowski N (2015) Quantification of volcanic reactive halogen emissions. In: Schmidt A, Fristad K, Elkins-Tanton L (eds) Volcanism and global environmental change. Cambridge University Press, Cambridge, pp 111–132

Portnyagin M, Hoernle K, Plechov P, Mironov N, Khubunaya S (2007) Constraints on mantle melting and composition and nature of slab components in volcanic arcs from volatiles (H_2O, S, Cl, F) and trace elements in melt inclusions from the Kamchatka Arc. Earth Planet Sci Lett 255:53–69

Portnyagin M, Almeev R, Matveev S, Holtz F (2008) Experimental evidence for rapid water exchange between melt inclusions in olivine and host magma. Earth Planet Sci Lett 272:541–552

Pyle DM, Mather TA (2009) Halogens in igneous processes and their fluxes to the atmosphere and oceans from volcanic activity: a review. Chem Geol 263:110–121

Ranero CR, Morgan JP, McIntosh K, Reichert C (2003) Bending-related faulting and mantle serpentinization at the Middle America trench. Nature 425:367–373

Ransom B, Spivack AJ, Kastner M (1995) Stable Cl isotopes in subduction-zone pore waters: implications for fluid-rock reactions and the cycling of chlorine. Geology 23(8):715–718

Rebay G, Spalla MI, Zanoni D (2012) Interaction of deformation and metamorphism during subduction and exhumation of hydrated oceanic mantle: insights from the Western Alps. J Metamorph Geol 30:687–702

Roggensack K, Hervig RL, McKnight SB, Williams SN (1997) Explosive basaltic volcanism from Cerro Negro volcano: influence of volatiles on eruptive style. Science 277:1639–1642

Rüpke LH, Morgan JP, Hort M, Connolly JAD (2004) Serpentine and the subduction zone water cycle. Earth Planet Sci Lett 223:17–24

Ruscitto DM, Wallace PJ, Johnson ER, Kent AJR, Bindeman IN (2010) Volatile contents of mafic magmas from cinder cones in the Central Oregon High Cascades: implications for magma formation and mantle conditions in a hot arc. Earth Planet Sci Lett 298:153–161

Ruscitto DM, Wallace PJ, Cooper LB, Plank T (2012) Global variations in H_2O/Ce: 2. Relationships to arc magma geochemistry and volatile fluxes. Geochem Geophys Geosyst 13: Q03025

Ryan JG, Chauvel C (2014) The subduction-zone filter and the impact of recycled materials on the evolution of the mantle. In: Holland HD, Turekian KK (eds) The mantle and core. Treatise on geochemistry, vol 3. Elsevier, Oxford, pp 479–508

Saal AE, Hauri EH, Langmuir CH, Perfit MR (2002) Vapour undersaturation in primitive mid-ocean-ridge basalt and the volatile content of the Earth's upper mantle. Nature 419:451–455

Sadofsky SJ, Portnyagin M, Hoernle K, van den Bogaard P (2008) Subduction cycling of volatiles and trace elements through the Central American volcanic arc: evidence from melt inclusions. Contrib Mineral Petrol 155:433–456

Sakuma H, Ichiki M (2015) Density and isothermal compressibility of supercritical H_2O-NaCl fluid: molecular dynamics study from 673 to 2000 K, 0.2 to 2 GPa, and 0 to 22 wt% NaCl concentrations. Geofluids 16(2016):89–102

Salters VJM, Stracke A (2004) Composition of the depleted mantle. Geochem Geophys Geosyst 5: Q05B07. https://doi.org/10.1029/2003GC000597

Sano T, Miyoshi M, Ingle S, Banerjee NR, Ishimoto M, Fukuoka T (2008) Boron and chlorine contents of upper oceanic crust: basement samples from IODP Hole 1256D. Geochem Geophys Geosyst 9:Q12O15. https://doi.org/10.1029/2008GC002182

Savov IP, Ryan JG, D'Antonio M, Kelley K, Mattie P (2005) Geochemistry of serpentinized peridotites from the Mariana forearc Conical seamounts, ODP Leg 125: implications for the elemental recyclng at subduction zones. Geochem Geophys Geosyst 6:4

Saxena SK, Fei Y (1987) High pressure and high temperature fluid fugacities. Geochim Cosmochim Acta 51:783–791

Scambelluri M, Philippot P (2001) Deep fluids in subduction zones. Lithos 55:213–227
Scambelluri M, Tonarini S (2012) Boron isotope evidence for shallow fluid transfer across subduction zones by serpentinized mantle. Geology 40:907–910
Scambelluri M, Muntener O, Hermann J, Piccardo GB, Trommsdorff V (1995) Subduction of water into the mantle: history of an alpine peridotite. Geology 23(5):459–462
Scambelluri M, Piccardo GB, Philippot P, Robbiano A, Negretti L (1997) High salinity fluid inclusions formed from recycled seawater in deeply subducted alpine serpentinite. Earth Planet Sci Lett 148(3–4):485–499
Scambelluri M, Bottazzi P, Trommsdorff V, Vannucci R, Hermann J, Gomez-Pugnaire MT, Vizcaino VLS (2001) Incompatible element-rich fluids released by antigorite breakdown in deeply subducted mantle. Earth Planet Sci Lett 192(3):457–470
Scambelluri M, Müntener O, Ottolini L, Pettke TT, Vannucci R (2004) The fate of B, Cl and Li in the subducted oceanic mantle and in the antigorite breakdown fluids. Earth Planet Sci Lett 222:217–234
Scambelluri M, Pettke T, Rampone E, Godard M, Reusser E (2014) Petrology and trace element budgets of high-pressure peridotites indicate subduction dehydration of serpentinized mantle (Cima di Gagnone, Central Alps, Switzerland). J Petrol 55:459–498
Schauble EA, Rossman GR, Taylor HPJ (2003) Theoretical estimates of equilibrium chlorine-isotope fractionations. Geochim Cosmochim Acta 67(17):3267–3281
Schilling J-G, Bergeron MB, Evans R (1980) Halogens in the mantle beneath the North Atlantic. Phil Trans R Soc Lond A297:147–178
Schmidt MW, Poli S (1998) Experimentally based water budgets for dehydrating slabs and consequences for arc magma generation. Earth Planet Sci Lett 163:361–379
Scholl DW, von Huene R (2007) Crustal recycling at modern subduction zones applied to the past—issues of growth and preservation of continental basement crust, mantle geochemistry, and supercontinent reconstruction. Geol Soc Am Mem 200:9–32
Selverstone J, Sharp ZD (2011) Chlorine isotope evidence for multicomponent mantle metasomatism in the Ivrea Zone. Earth Planet Sci Lett 310:429–440
Selverstone J, Sharp ZD (2013) Chlorine isotope constraints on fluid-rock interactions during subduction and exhumation of the Zermatt-Saas ophiolite. Geochem Geophys Geosyst 14: 4370–4391. https://doi.org/10.1002/ggge.20269
Selverstone J, Sharp ZD (2015) Chlorine isotope behavior during prograde metamorphism of sedimentary rocks. Earth Planet Sci Lett 417:120–131
Selverstone J, Franz G, Thomas S, Getty S (1992) Fluid variability in 2 GPa eclogites as an indicator of fluid behavior during subduction. Contrib Mineral Petrol 112:341–357
Sharp ZD, Barnes JD (2004) Water soluble chlorides in massive seafloor serpentinites: a source of chloride in subduction zones. Earth Planet Sci Lett 226:243–254
Sharp ZD, Barnes JD, Brearley AJ, Chaussidon M, Fischer TP, Kamenetsky VS (2007) Chlorine isotope homogeneity of the mantle, crust and carbonaceous chondrites. Nature 446:1062–1065
Sharp ZD, Barnes JD, Fischer TP, Halick M (2010) A laboratory determination of chlorine isotope fractionation in acid systems and applications to volcanic fumaroles. Geochim Cosmochim Acta 74:264–273
Sharp ZD, Mercer JA, Jones RH, Brearley AJ, Selverstone J, Bekker A, Stachel T (2013) The chlorine isotope composition of chondrites and earth. Geochim Cosmochim Acta 107:189–204
Shaw AM, Hauri EH, Fischer TP, Hilton DR, Kelley KA (2008) Hydrogen isotopes in Mariana arc melt inclusions: implications for subduction dehydration and the deep-Earth water cycle. Earth Planet Sci Lett 275:138–145
Shinohara H (2008) Excess degassing from volcanoes and its role on eruptive and intrusive activity. Rev Geophys 46:1–31
Shinohara H (2013) Volatile flux from subduction zone volcanoes: insights from a detailed evaluation of the fluxes from volcanoes in Japan. J Volcanol Geotherm Res 268:46–63
Shmulovich KI, Graham CM (1996) Melting of albite and dehydration of brucite in H2O-NaCl fluids to 9 kbars and 700–900 °C: implications for partial melting and water activities during high pressure metamorphism. Contrib Mineral Petrol 124(3–4):370–382

Sisson TW, Bronto S (1998) Evidence for pressure-release melting beneath magmatic arcs from basalt at Galunggung, Indonesia. Nature 391:883–886

Snyder GT, Fehn U (2002) Origin of iodine in volcanic fluids: ^{129}I results from the Central American Volcanic Arc. Geochim Cosmochim Acta 66:3827–3838

Snyder GT, Savov IP, Muramatsu Y (2005) Iodine and boron in Mariana serpentinite mud volcanoes (ODP Legs 125 and 195): Implications for forearc processes and subduction recycling. Proceedings of the ocean drilling program, Scientific results 195

Spivack AJ, Kastner M, Ransom B (2002) Elemental and isotopic chloride geochemistry and fluid flow in the Nankai Trough. Geophys Res Lett 29(14):6-1–6-4

Stolper EM, Newman S (1994) The role of water in the petrogenesis of Mariana trough magmas. Earth Planet Sci Lett 121:293–325

Straub SM, Layne GD (2003) The systematics of chlorine, fluorine, and water in Izu arc front volcanic rocks: implications for volatile recycling in subduction zones. Geochim Cosmochim Acta 67(21):4179–4203

Stroncik NA, Haase KM (2004) Chlorine in oceanic intraplate basalts: constraints on mantle sources and recycling processes. Geology 32:945–948

Stueber AM, Huang WH, Johns WD (1968) Chlorine and fluorine abundances in ultramafic rocks. Geochim Cosmochim Acta 32:353–358

Sumino H, Burgess R, Mizukami T, Wallis SR, Holland G, Ballentine CJ (2010) Seawater-derived noble gases and halogens preserved in exhumed mantle wedge peridotite. Earth Planet Sci Lett 294:163–172

Sun WD, Binns RA, Fan AC, Kamenetsky VS, Wysoczanski R, Wei GJ, Hu YH, Arculus RJ (2007) Chlorine in submarine volcanic glasses from the eastern Manus basin. Geochim Cosmochim Acta 71:1542–1552

Sverjensky DA, Harrison B, Azzolini D (2014) Water in the deep Earth: the dielectric constant and the solubilities of quartz and corundum to 60 kb and 1200 °C. Geochim Cosmochim Acta 129:125–145

Symonds RB, Rose WI, Reed MH (1988) Contribution of Cl- and F-bearing gases to the atmosphere by volcanoes. Nature 334:415–418

Syracuse EM, van Keken PE, Abers GA (2010) The global range of subduction zone thermal models. Phys Earth Planet Inter 183(1–2):73–90

Taran YA (2009) Geochemistry of volcanic and hydrothermal fluids and volatile budget of the Kamchatka-Kuril subduction zone. Geochim Cosmochim Acta 73:1067–1094

Tatsumi Y (1986) Formation of the volcanic front in subduction zones. Geophys Res Lett 17:717–720

Tatsumi Y (1989) Migration of fluid phases and genesis of basalt magmas in subduction zones. J Geophys Res 94:4697–4707

Tatsumi Y, Eggins S (1995) Subduction zone magmatism. Blackwell Science, Boston

Tomaru H, Ohsawa S, Amita K, Lu Z, Fehn U (2007) Influence of subduction zone settings on the origin of forearc fluids: Halogen concentrations and ^{129}I/I ratios in waters from Kyushu, Japan. Appl Geochem 22:676–691

Trommsdorff V, Lòpez Sànchez-Vizcaìno V, Gomez-Pugnaire MT, Muntener O (1998) High pressure breakdown of antigorite to spinifex-textured olivine and orthopyroxene, SE Spain. Contrib Mineral Petrol 132:139–148

Tropper P, Manning C (2004) Paragonite stability at 700 °C in the presence of H2O–NaCl fluids: constraints on H2O activity and implications for high pressure metamorphism. Contrib Mineral Petrol 147(6):740–749

Ulmer P, Trommsdorff V (1995) Serpentine stability to mantle depths and subduction-related magmatism. Science 268:858–861

Vanko DA (1986) High-chlorine amphiboles from oceanic rocks: product of highly-saline hydrothermal fluids? Am Mineral 71:51–59

Vanko DA, Stakes DS (1991) Fluids in oceanic layer 3: evidence from veined rocks, Hole 735B, Southwest Indian Rdige. In: Von Herzen RP, Robinson PT, et al (eds) Proceedings of the ocean

drilling program, Scientific results, vol 118. Ocean Drilling Program, College Station, TX, pp 181–215
Volfinger M, Robert J-L, Vielzeuf D, Neiva AMR (1985) Structural control of the chlorine content of OH-bearing silicates (micas and amphiboles). Geochim Cosmochim Acta 49:37–48
Wade JA, Plank T, Melson MG, Soto GJ, Hauri EH (2006) The volatile content of magmas from Arenal volcano, Costa Rica. J Volcanol Geotherm Res 157:94–120
Wagner W, Pruß A (2002) The IAPWS formulation 1995 for the thermodynamic properties of ordinary water substance for gen- eral and scientific use. J Phys Chem Ref Data 31:387–535
Wallace PJ (2005) Volatiles in subduction zone magmas: concentrations and fluxes based on melt inclusion and volcanic gas data. J Volcanol Geotherm Res 140:217–240
Webster JD (2004) The exsolution of magmatic hydrosaline chloride liquids. Chem Geol 210:33–48
Webster JD, Kinzler RJ, Mathez EA (1999) Chloride and water solubilitiy in basalt and andesite melts and implications for magma degassing. Geochim Cosmochim Acta 63:729–738
Wedepohl KH (1995) The composition of the continental crust. Geochim Cosmochim Acta 59:1217–1232
Workman RK, Hart SR (2005) Major and trace element composition of the depleted MORB mantle (DMM). Earth Planet Sci Lett 231:53–72
Workman RK, Hauri E, Hart SR, Wang J, Blusztajn J (2006) Volatile and trace elements in basaltic glasses from Samoa: implications for water distribution in the mantle. Earth Planet Sci Lett 241:932–951
Wunder B, Schreyer W (1997) Antigorite: high-pressure stability in the system MgO-SiO_2-H_2O (MSH). Lithos 41:213–227
Zimmer MM, Plank T, Hauri EH, Yogodzinski GM, Stelling P, Larsen J, Singer B, Jicha B, Mandeville C, Nye CJ (2010) The role of water in generating the calc-alkaline trend: new volatile data for Aleutian magmas and a new tholeiitic index. J Petrol 51:2411–2444

Chapter 9
Halogens in Seawater, Marine Sediments and the Altered Oceanic Lithosphere

Mark A. Kendrick

Abstract This chapter aims to provide a framework for understanding the distribution of halogens in the oceanic lithosphere. It reviews the concentrations of F, Cl, Br and I in seawater, marine sediment pore waters, hydrothermal vent fluids, fluid inclusions from deeper in the crust, and the complementary solid-phase reservoirs of organic matter and minerals present in sediments and crustal/mantle rocks from varying depths. Seawater (3.4–3.5 wt% salt) is depleted in F, weakly enriched in I and strongly enriched in Cl and Br compared to the primitive mantle. Sequestration of I and Br by phytoplankton lead to the storage of these elements in marine sediments, which are the Earths dominant I reservoir. Regeneration of organic matter during diagenesis releases I^- and Br^- to marine sediment pore waters, which acquire Br/Cl and I/Cl ratios of higher than seawater and can be advected into the underlying crust and lithosphere. In contrast, Cl is usually assumed to behave conservatively in pore waters and F is precipitated in authigenic sedimentary minerals meaning it is not significantly advected into the underlying basement. Vent fluids have salinities of 0.1–6 wt% salts, which provide evidence for phase separation and segregation of vapours and brines in hydrothermal systems. The majority of vent fluids have Br/Cl ratios within 10% of the seawater value. However, elevated Br/Cl and I/Cl ratios indicate that some vent fluids interact with organic-rich sediments, and low Br/Cl ratios suggest some vent fluids leach Cl from glassy volcanic rocks or halite. Vent fluids have F/Cl ratios scattered around the seawater value which reflects the generally low mobility of F during diagenesis and hydrothermal alteration. In comparison to vent fluids, fluid inclusions also provide evidence for phase separation but preserve a much greater range of salinity including brines with salinities as high as $\sim$50 wt% salt. The altered ocean crust has a F concentration of close to its initial value. In contrast, Cl is mobilised within layer 2 pillows and dykes and strongly enriched in layer 3 gabbros subjected to high temperature alteration. Amphibole is the dominant Cl host in the oceanic crust, with Cl concentrations of <500 ppm under greenschist conditions and up to wt% levels under amphibolite conditions. The increasing Cl

M.A. Kendrick (✉)
Research School of Earth Sciences, The Australian National University, Canberra 2601, ACT, Australia
e-mail: mark.kendrick@anu.edu.au

D.E. Harlov and L. Aranovich (eds.), *The Role of Halogens in Terrestrial and Extraterrestrial Geochemical Processes*, Springer Geochemistry,
https://doi.org/10.1007/978-3-319-61667-4_9

content of amphibole as a function of metamorphic grade most likely reflects a decreasing water/rock ratio and a general increase in fluid salinity as a function of depth in the crust. Amphibole preferentially incorporates Cl relative to Br and I; however, I is enriched in absolute terms, and relative to Cl, in clay-rich alteration and biogenic alteration of glassy rocks in the upper crust. Serpentinites formed in the oceanic lithosphere can contain thousands of ppm Cl and some serpentinites preserve Br/Cl and I/Cl signatures very similar to sedimentary pore waters, indicating that all halogens have high compatibilities in serpentine. Fluorine is slightly enriched in some serpentinites compared to peridotites, which may indicate minor mobilisation of F from igneous lithologies in the overlying crust. The altered oceanic crust and mantle lithosphere reaching subduction zones have poorly defined halogen concentrations. However, the average Cl concentration could be as high as $\sim$400 ppm. And it may have a F/Cl ratios as low as $\sim$0.25 compared to $\sim$2 in pristine crust. It is estimated that approximately 90% of the Cl present in altered oceanic lithosphere is introduced during seawater alteration.

9.1 Introduction

As a chemical group, the halogens (F, Cl, Br, I) are united by the ability to form negatively charged anions; however, Cl is uniquely important within this group because it is the dominant ligand that enables metal transport in the majority of hydrothermal solutions (Bischoff and Dickson 1975; Seyfried and Bischoff 1981; Yardley 2005). Fluid salinity is consequently of profound importance to the mass transfer processes operating during hydrothermal alteration of the oceanic lithosphere. There is wide interest in the scale of seafloor alteration processes and metasomatism because alteration of the oceanic lithosphere moderates the composition of seawater (Bischoff and Dickson 1975; Edmond et al. 1979) and determines the chemical composition of the slab that is subducted into the mantle at convergent plate margins. Seafloor alteration is therefore critical to the geological cycles of all elements (Bischoff and Dickson 1975; Edmond et al. 1979; Spandler and Pirard 2013).

In comparison to Cl, the other halogens exhibit systematically different behaviours in the oceanic lithosphere that are related to their ionic sizes or elemental abundances. Fluorine and Cl are similarly abundant on Earth with primitive mantle concentrations on the order of $\sim$15–30 ppm (Table 9.1; Kendrick et al. 2017; Pyle and Mather 2009). However, the F^- anion is significantly smaller than the heavier halogens and F is strongly electronegative, being the only element in the periodic table that is more electronegative than oxygen. These properties result in F having a much higher compatibility than Cl in many hydrous and nominally anhydrous minerals (Bernini et al. 2013; Carpenter 1969; Dalou et al. 2012; Frohlich et al. 1983; Ichikuni 1979; Seyfried and Ding 1995). Consequently, F is distinguished from the heavier halogens by a low solubility in aqueous fluids (Seyfried and Ding 1995).

Bromine and I have even higher solubilities in aqueous fluids than Cl, but they are trace constituents on Earth with primitive mantle concentrations of $\sim$76 ppb for

Table 9.1 Halogens in seawater and the primitive mantle

	F ppm	Cl ppm	Br ppb	I ppb
Primitive mantle	17 ± 6	26 ± 8	76 ± 25	7 ± 4
Seawater	1.3	19,350	67,300	58
Seawater/PM	~0.08	~740	~890	~8

References: Drever (1997); Elderfield and Truesdale (1980); Huang et al. (2005); primitive mantle concentrations of Kendrick et al. (2017), see also McDonough and Sun (1995), Kamenetsky and Eggins (2012) and Pyle and Mather (2009)

Br and ~7 ppb for I (Table 9.1). Iodine is a weakly electronegative redox sensitive element that is important in a number of biochemical pathways, which together with its low abundance mean it is regarded as an essential element for life (Elderfield and Truesdale 1980; Fuge and Johnson 1986; Leblanc et al. 2006).

The contrasting solubilities of F, Cl, Br and I in aqueous fluids mean that their relative abundances, or the F/Cl, Br/Cl and I/Cl, ratios of a fluid, can provide useful information about a number of hydrogeochemical processes relevant to alteration of the oceanic lithosphere. These include the roles of phase separation, crustal-hydration, dissolution of evaporites, or precipitation of hydrothermal-halite in controlling vent fluid salinity (Campbell and Edmond 1989; Oosting and Von Damm 1996; Seyfried et al. 2003; You et al. 1994). In addition, the presence of organic matter can be inferred from high I abundances (Campbell and Edmond 1989; Gieskes et al. 2002; Kawagucci et al. 2011). This information is of considerable importance to investigating the role of fluids in alteration of the oceanic lithosphere and the depth of the biosphere (Campbell and Edmond 1989; Mottl et al. 2011; Oosting and Von Damm 1996; Reeves et al. 2011; Wu et al. 2012; You et al. 1994).

The current chapter aims to show how the different geochemical behaviours of the halogens control their abundances in both hydrothermal fluids and the complementary reservoirs of the oceanic lithosphere and how salts, and acids generated by hydrolysis of salts, facilitate transport of metals in solution (Seyfried and Bischoff 1981). The majority of data for both altered oceanic rocks and fluids are for Cl, with more limited data available for F and Br, and very limited data for I. Therefore while the aim is to provide a framework for understanding the distribution of halogens in the oceanic lithosphere, an important role of this chapter is also to identify current gaps in our knowledge. Improving constraints on the absolute and relative abundances of F, Cl, Br, and I in different lithospheric reservoirs (e.g., sediments, altered basalt, serpentinites) is critical for optimal use of halogen abundance ratios in tracking halogens through the subduction cycle (Kendrick et al. 2012b, 2017; Straub and Layne 2003) and will further contribute to our understanding of marine halogen cycling (Frohlich et al. 1983; Leblanc et al. 2006; Seyfried et al. 1986; Seyfried and Ding 1995).

9.2 Halogen Chemistry in Seawater and Marine Sediments

The halogen composition of seawater and the more evolved fluids that have interacted with sediments and could be advected into the mafic portions of the oceanic lithosphere is controlled by the unique chemical properties of each halogen and their abundances on Earth.

The concentrations of F, Cl and Br in seawater, present as the fluoride (F^-), chloride (Cl^-), and bromide (Br^-) anions, is fairly constant over thousand-year timescales with minor variations related to salinity which fluctuates around ~3.4–3.5 wt% salts (Drever 1997; Pinet 1992). In contrast, I is unique among the halogens because its predominant species in seawater is iodate (IO_3^-) and iodide (I^-) is only important in surface waters and small anoxic basins (Elderfield and Truesdale 1980; Huang et al. 2005; Wong and Brewer 1977). The concentration of iodate, which is taken up by a number of marine organisms, is correlated with other nutrients such as nitrate and phosphate and varies as a function of water depth and latitude (Elderfield and Truesdale 1980; Huang et al. 2005). In addition to iodate and iodide, dissolved organic I is significant at shallow and intermediate depths accounting for up to ~5 ppb of the total I at depths of 400 m in the north Pacific (Huang et al. 2005). The total I concentration of seawater varies from about 44 ppb up to 76 ppb with a mean of ~58 ppb (Elderfield and Truesdale 1980; Huang et al. 2005; Nakayama et al. 1989; Zheng et al. 2012).

The average abundances of halogens in seawater (Drever 1997; Elderfield and Truesdale 1980; Huang et al. 2005) and estimated abundances of halogens in the primitive mantle (Kendrick et al. 2017; McDonough and Sun 1995; Palme and O'Neill 2003; Sharp and Draper 2013) are given in Table 9.1. These data illustrate that F is unique among the halogens because it is depleted in seawater relative to the primitive mantle (Table 9.1). In comparison, I exhibits a modest enrichment in seawater and Cl and Br are both enriched by hundreds of times in seawater compared to the primitive mantle (Table 9.1).

9.2.1 Fluorine's Low Solubility

The low solubility of F in aqueous fluids means that in contrast to the heavy halogens (Cl, Br and I), F is inefficiently transported by rivers, and is removed from solution once in the ocean (Carpenter 1969). Important F sinks in the oceanic environment include marine carbonates, phosphates, and alumina-silicates (clay minerals) (cf., Carpenter 1969; Frohlich et al. 1983; Matthies and Troll 1990; Rude and Aller 1994). Calcite can contain hundreds of ppm of F and magnesium-calcite and aragonite have maximum F concentrations in excess of 1000 ppm that represent a 1000-fold enrichment over seawater and demonstrate the high compatibility of F in carbonate (Fig. 9.1; Ohde and Kitano 1980;

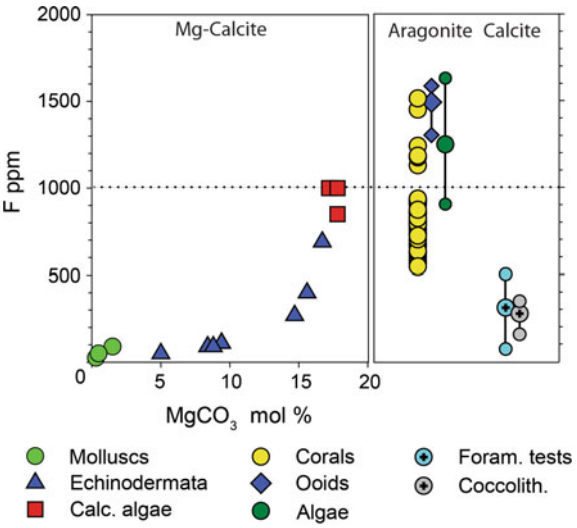

Fig. 9.1 The F content (ppm) of different types of carbonate. Mg carbonates and aragonite have higher F contents than calcite (Carpenter 1969; Ohde and Kitano 1980; Ramos et al. 2005; Rude and Aller 1991; Tanaka et al. 2013)

Okumura et al. 1983; Opdyke et al. 1993; Rude and Aller 1991; Tanaka et al. 2013). An exchange reaction has been proposed in which two F^- anions substitute for CO_3^{2-} (Ichikuni 1979):

$$CaCO_3 + 2F^- = CaF_2 + CO_3^{2-} \tag{9.1}$$

Given the conservative nature of F^- in seawater, this reaction indicates that the F content of aragonite can be used to monitor the CO_2 content of seawater, which exhibits significant spatial and temporal variation (e.g., Ichikuni 1979; Ramos et al. 2005; Tanaka et al. 2013).

Carbonate fluorapatite (CFA) in marine phosphates with concentrations of 1–3 wt% F contains an order of magnitude more F than carbonate (Li and Schoonmaker 2003; Rude and Aller 1991). However, because phosphorite deposits are restricted to zones of nutrient rich water upwelling they are estimated to account for only ~20% of F uptake from the ocean (Frohlich et al. 1983). Fluorine also substitutes for the hydroxyl group in alumina-silicates (clay minerals); however, the relative importance of this sink is disputed (cf., Carpenter 1969; Matthies and Troll 1990; Rude and Aller 1994).

Fluorine is mobilised during diagenesis of marine carbonates but it is fixed into newly formed carbonates, apatite, or clay minerals, meaning the fluids occupying sediment pore spaces have low ppm levels of F and F/Cl ratios similar to seawater (Frohlich et al. 1983; Mahn and Gieskes 2001; Rude and Aller 1994).

Fluorine is further distinguished from the heavier halogens by its relative compatibility in the mantle. Fluorine has a compatibility comparable to moderately incompatible elements like Nd or Pr (Kendrick et al. 2017; Workman et al. 2006), whereas the heavy halogens (Cl, Br and I) have incompatibilities comparable to more strongly incompatible elements such as K, La or Nb (Kendrick et al. 2012a, 2017;

le Roux et al. 2006; Schilling et al. 1980). This difference cannot explain the F depletion of seawater but it explains why the surface reservoirs of seawater and sediments are less enriched in F than the heavy halogens (cf., Table 9.1; Kendrick et al. 2017).

9.2.2 Chlorine in Halite

In contrast to F, Cl is usually regarded as a conservative element in sedimentary marine pore waters, meaning that its concentration is not easily altered. Chlorine and Br have very low compatibilities in marine carbonate (Kitano et al. 1975; Okumura et al. 1986) and low concentrations in other sedimentary minerals such as carbonate fluorapatite. As a result, evaporites formed by evaporation of seawater beyond the point of halite saturation (30–35 wt% salt; McCaffrey et al. 1987; Zherebtsova and Volkova 1966), commonly represent the only significant mineral reservoir of Cl in sedimentary settings (Hanor 1994; Worden 1996). Evaporite deposits are important sedimentary units in some ocean basins and dissolution of evaporites is indicated as an important source of salinity for hydrothermal fluids in Red Sea brine pools (e.g., Pierret et al. 2001; Shanks and Bischoff 1977; Zierenberg and Shanks III 1986). In addition, halite could be important in some hydrothermal settings where precipitation of hydrothermal halite is possible (Butterfield et al. 1997; Foustoukos and Seyfried 2007).

Evaporitic salt deposits are characterised by very low Br/Cl and I/Cl ratios (Bein et al. 1991; Fontes and Matray 1993; McCaffrey et al. 1987). Halite has relative partition coefficients ($D = [X/Cl]_{salt}/[X/Cl]_{fluid}$) of ~ 0.03 for Br/Cl and <0.003 for I/Cl, whereas Br can be accommodated more easily in sylvite ($D \sim 0.2$), carnalite, and other potash salts (Fontes and Matray 1993; Hermann 1980; Holser 1979; Siemann and Schramm 2000). As a result, the actual concentrations of Br and I in evaporite deposits vary depending on the salts present; the presence of organic material and fluid inclusions, which contain significant Br and I; and on the diagenetic history of the deposit (Bein et al. 1991; Fontes and Matray 1993). Experimental studies suggest that Br is excluded from the halite lattice under hydrothermal conditions (Berndt and Seyfried 1997; Foustoukos and Seyfried 2007). This means that fluid interaction with either sedimentary or hydrothermal halite has the potential to strongly alter Cl concentrations and fluid Br/Cl and I/Cl ratios.

9.2.3 Iodine and Bromine in Organic Matter

The marine I cycle is dominated by accumulation of I in algae: Kelp (a type of seaweed, which is multicellular macroalgae) is the main I accumulator in coastal environments, whereas phytoplankton is the main I accumulator at sea (Iwamoto and Shiraiwa 2012; Leblanc et al. 2006).

Iodine is seasonally variable and heterogeneously distributed in Kelp (Gall et al. 2004). Maximum concentrations of ~ 6 wt% I have been reported in parts of a Kelp

plant (Laminaria Digitalis; Kuepper et al. 2013), but an average I content of 1 wt% has been suggested (Gall et al. 2004). Other seaweeds contain ~1–500 ppm I (Muramatsu and Wedepohl 1998; Yang et al. 2014). Several species of coral have skeletons in which organic components can have very high halogen concentrations of 5–6 wt% I, 1–2 wt% Br, and <1000 ppm Cl (Collins 1969; Goldberg et al. 1994). The Br/I weight ratios of seaweeds and corals range from ~0.1 to 2.5 (Collins 1969; Kuepper et al. 2013). In comparison, plankton has variable halogen contents ranging from sub-ppm to typical values of ~200–300 ppm I and 1000–4000 ppm Br. Plankton have Br/I weight ratios of 3–24 and $I/C_{organic}$ of 0.0002–0.002 (Bobrov et al. 2005; Iwamoto and Shiraiwa 2012; Martin et al. 1993; Price and Calvert 1977).

Iodine accumulated by algae is either emitted to the atmosphere as I_2 gas (or volatile iodocarbon compounds) or buried in marine sediment, which has previously been estimated to contain ~70% of the I present in the crust and seawater (Leblanc et al. 2006; Muramatsu and Wedepohl 1998). Regeneration of organic matter releases iodide (I^-), bromide (Br^-), and CH_4 into sedimentary pore waters in the subsurface (Kennedy and Elderfield 1987a, b; Muramatsu et al. 2007; Price and Calvert 1973, 1977). Studies of cosmosgenic ^{129}I indicate pore waters can migrate laterally over many km (e.g., Fehn et al. 2006; Muramatsu et al. 2001, 2007). However, pore waters also seep gradually upwards toward the seafloor (Wong and Brewer 1977). In typical oxic basins, iodide in escaping pore waters is oxidised and, together with seawater iodate, is then adsorbed back onto organic detritus close to the sediment surface (Fig. 9.2; Price and Calvert 1973, 1977). If present, additional adsorption may also occur on Fe-hydroxides (Ullman and Aller 1985) and clay minerals (Montavon et al. 2014). As a result sediment profiles in oxic basins can have very high I concentrations of 100–2000 ppm close to the surface (Fig. 9.2a; Price and Calvert 1977), along with elevated $I/C_{organic}$ and I/Br ratios, but at depths of more than a metre below the surface, sediments have more typical concentrations of ~5–50 ppm I, along with $I/C_{organic}$ and I/Br ratios similar to plankton (Kennedy and Elderfield 1987a, b; Price and Calvert 1973, 1977; Upstillgoddard and Elderfield 1988).

Halogen regeneration processes result in pore water Br and I concentrations tending to increase with depth and solid phase Br and I concentrations tending to decrease with depth and sediment maturity (Fig. 9.2). Pelagic sediments have typical I concentrations of ~5–50 ppm I in the solid phase (Kennedy and Elderfield 1987b; Muramatsu et al. 2007). However, Murumatsu et al. (2007) reported that sediments from the Nankai Trough contain 3–4 times more Br and I in pore waters than in the solid phase. In contrast to unconsolidated sediment, lithified marine sediments have much lower halogen concentrations. For example, the median I concentration of twenty limestones and shales analysed by Muramatsu and Wedepohl (1998) is 2^{+2}_{-1} ppm. The Callovian-Oxfordian clay of France contains 1–7 ppm I and 0.4–1.2 wt% organic C (Claret et al. 2010). The organic rich Kimmeridge clay of England contains 6–34 ppm I and 16–55 wt% organic C (Cosgrove 1970). Taken together, these data give a combined average of 4 ± 3 ppm I in lithified marine sediments (Table 9.2) and suggest that variable depletion of I occurs relative to C in lithified sediments, compared with organic I/C ratios.

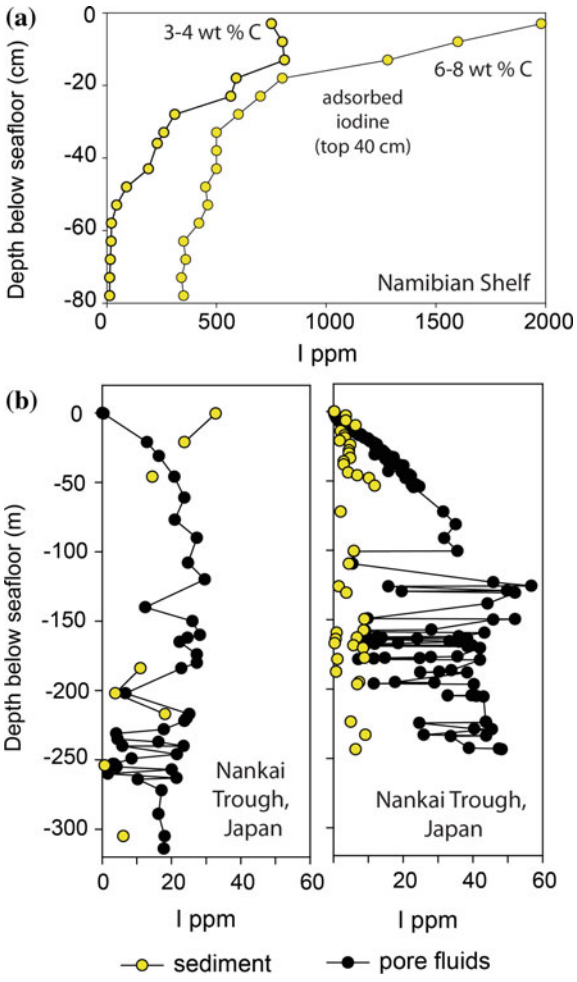

Fig. 9.2 Iodine in dry sediments (solid phase) and sedimentary pore waters as a function of depth. **a** The top 80 cm of sediments on the Namibian Shelf that contain 2–8 wt% organic carbon are exceptionally enriched in I (Price and Calvert 1977), but show a typical surface enrichment of I resulting from iodate adsorption (Kennedy and Elderfield 1987a, b; Price and Calvert 1977). **b** Complex deep sediment profiles on the Nankai Trough show that deeper pore fluids have generally higher I concentrations than shallower pore fluids; this trend is seen most clearly in the top 100 m of the second profile (Muramatsu et al. 2007)

A large database is now available for Cl, Br and I in sedimentary marine pore waters (Fig. 9.3; Fehn et al. 2000, 2003, 2006, 2007a, b; Gieskes and Mahn 2007; Mahn and Gieskes 2001; Martin et al. 1993; Muramatsu et al. 2001, 2007; Tomaru et al. 2007a, b, c, 2009). These studies have shown that sedimentary pore waters have a relatively narrow range in salinity (~1–5 wt% salt), which reflects the modification of seawater salinity (3.5 wt% salts) by formation and destruction of gas hydrate (Fig. 9.3b). Plotting pore water Cl, Br, and I data as ratios in a three element plot, which removes the effects of salinity variation, enables the sediment-derived halogen component to be fully resolved from seawater (Fig. 9.3a). The slopes in Fig. 9.3a indicate that the sediment-derived halogen component has a fairly constant seawater-corrected Br/I weight ratio of ~0.3–1.6 (Fig. 9.3a; Kendrick et al. 2011a). Presumably the low seawater-corrected Br/I ratio of sedimentary pore waters

Table 9.2 Representative concentrations of halogens in marine reservoirs

	H_2O wt%	Cl wt%	F ppm	Br ppm	I ppm
Fluids and sediments					
Seawater	96.5	1.93	1.3	67	0.06
Pore fluids	>95	0.17–2.3	0.5–7	2–260	0.1–220
Unlithified pelagic sediments (*including pore fluids)	30*	1*	1000 ± 300	60 ± 60	30 ± 25
Lithified marine sediments		700 ± 500	1000 ± 300	12 ± 10	4 ± 3
Mineral and organic components					
Seaweed				<200 ppm	1–500
Seaweed (Kelp)				1000–2000	10,000
Plankton			1000 ± 500	1000–4000	200–300
Calcite			300 ± 200		<2 ppm
Aragonite			1000 ± 500		
Mg-carbonate			800 ± 500		
Fluorapatite			0.6–2.6		
Clay minerals	5–15	<100 ppm	1000 ± 300		(I adsorbed?)
Mn-crusts/nodules		0.6–1.1	390	28–140	100–900

References: Baturin (1988); Carpenter (1969); Fehn et al. (2000, 2003, 2006); Gieskes and Mahn (2007); Glasby (1973); Glasby et al. (1978); Hein and Koschinsky (2014); John et al. (2011); Kennedy and Elderfield (1987a, b); Lu et al. (2008); Mahn and Gieskes (2001); Muinos et al. (2013); Muramatsu et al. (2001, 2007); Muramatsu and Wedepohl (1998); Ohde and Kitano (1980); Pyle and Mather (2009); Rude and Aller (1991); Tanaka et al. (2013); Tomaru et al. (2007a, b, c, 2009)

(0.3–1.6), compared to plankton (3–24; Bobrov et al. 2005; Collins 1969; Martin et al. 1993), reflects the surface-adsorbed I component acquired on the seafloor under oxic conditions (Francois 1987; Martin et al. 1993; Upstillgoddard and Elderfield 1988). In comparison, the solid sedimentary phases preserve higher Br/I ratios, which overlap planktonic values (Fig. 9.3; Muramatsu et al. 2007).

9.2.4 *Iodine Adsorption and Substitution in Carbonate*

In addition to I sorption onto organic detritus at the sediment-seawater interface (Price and Calvert 1973, 1977), I is significantly adsorbed onto the surfaces of a number of reactive minerals (Ullman and Aller 1985). Available data indicate that hydrogenetic Fe–Mn crusts formed on igneous substrates, and nodules formed in sedimentary environments, contain up to 390 ppm F, 1.1 wt% Cl, 200 ppm Br and 900 ppm I which represent a factor of ~2 depletion of Cl, a factor of ~3

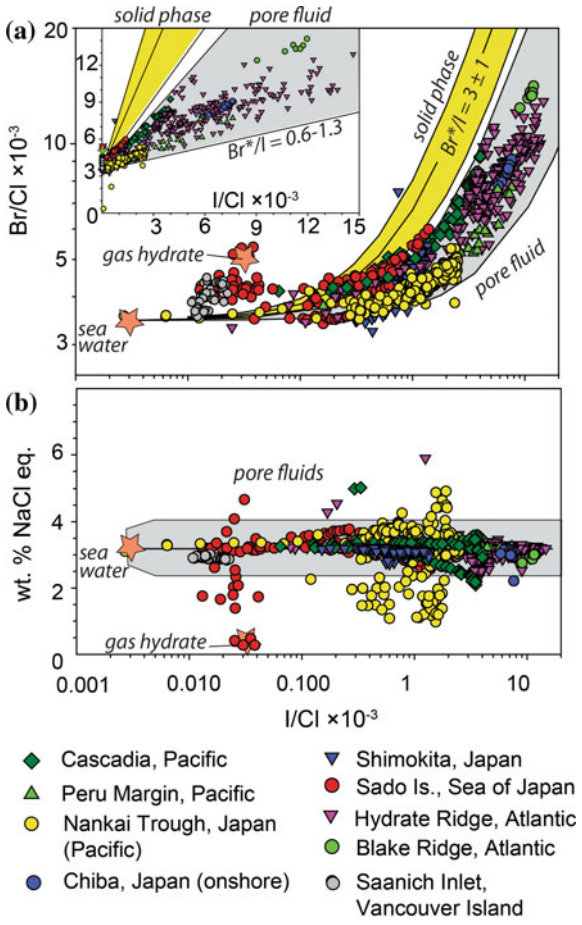

Fig. 9.3 Chlorine, Br and I in sediments and sedimentary pore waters. **a** Pore water Br/Cl versus I/Cl on a log-log scale (with linear scale inset). Pore waters define an envelope (*shaded grey*) extending from seawater (*star*) and bounded by Br*/I slopes of 0.6 and 1.3 [Br* denotes seawater-corrected Br where $Br^* = Br_{total} - Br_{seawater}$; $Br_{seawater} = 0.0035 \times Cl$ (Kendrick et al. 2011a)]. In contrast to pore waters, the solid phase in Nankai Trough sediments has a higher Br*/I of 3 ± 1 shown by the *yellow envelope*. **b** I/Cl versus salinity expressed as wt% NaCl equivalent. Pore fluid chlorinity is close to seawater in most cases, but is significantly altered by the formation and destruction of gas hydrate in some locations. Note that the pore waters have been sampled from IODP drill holes on both passive and convergent continental margins (see Fehn et al. 2000, 2003, 2006; Lu et al. 2008; Mahn and Gieskes 2001; Muramatsu et al. 2001, 2007; Tomaru et al. 2007b, c, 2009)

enrichment of Br, a factor of ~300 enrichment of F and a factor of ~2000 enrichment of I compared to seawater (Table 9.2; Glasby 1973; Glasby et al. 1978; Hein and Koschinsky 2014; Rude and Aller 1991). Hydrogenetic Fe–Mn crusts and nodules include detrital minerals such as fluorapatite and a mixture of MnO_2 and FeOOH precipitated from cold seawater (with a varying hydrothermal component in some cases; Baturin and Dubinchuk 2011; Hein and Koschinsky 2014). The crusts have slow growth rates, very high porosities, and large reactive surface areas that enable efficient scavenging of reactive trace elements from seawater (Hein and Koschinsky 2014). The experiments of Ullman and Aller (1985) confirm iodate, but not iodide, is strongly adsorbed onto Fe-oxyhydroxides and the same may be true for Mn oxide crusts.

Clay minerals such as montmorillonite $[(Na,Ca)_{0.33}(Al,Mg)_2(Si_4O_{10})(OH)_2.nH_2O]$ have reactive surfaces that adsorb variable quantities of water (e.g., nH_2O) and other substances. Due to the environmental significance of radioactive iodide, which is one of the most mobile radioisotopes present in nuclear waste, a number of investigations have been conducted to evaluate the sorption of iodine to clay. Experimental results showing significant iodine sorption have been controversial because of uncertainties regarding the speciation of iodine in the experiments (Glaus et al. 2008), and the potential of iodine to be irreversibly bound in carbonate formed during the experiment (Claret et al. 2010). However, a recent study that controlled for these factors reported reversible sorption of iodide onto clay minerals under controlled PCO_2 (Montavon et al. 2014).

Claret et al. (2010) suggested carbonate within Callovian-Oxfordian clay rock (France) contains ~2 ppm I. Recent experimental data suggest that IO_3^- but not I^- can substitute for CO_3^{2-} in calcite (Lu et al. 2010) and the iodate mineral lautarite $[Ca(IO_3)_2]$ is known from I-rich nitrate deposits (Jackson and Ericksen 1997). In contrast, $2F^-$ can readily substitute for CO_3^{2-}, but Br^- and Cl^- (like I^-) have low compatibilities in carbonate (Kitano et al. 1975; Okumura et al. 1986). It should however, be noted that while the maximum I concentration of 2 ppm reported for carbonate represents a considerable enrichment over seawater I concentration of ~58 ppb, it is 100 times less than the maximum I concentration of ~220 ppm in sedimentary pore waters (Table 9.2). Further work is clearly required to understand the interactions of I species, clay minerals and carbonates.

9.2.5 Summary

Two distinct fluids that could be advected into the mafic portions of the oceanic crust have been identified and are relatively well defined: (i) seawater and (ii) sedimentary marine pore water. Sedimentary marine pore waters comprise seawater modified by the addition of organic components and adsorbed I present in marine sediments. The majority of pore waters preserve salinities close to seawater, but salinities of 1–5 wt% salts can be explained by fluid interaction with gas hydrate (Fig. 9.3). Fluorine has a low solubility in aqueous fluids and is retained by or

incorporated into several marine minerals during diagenesis. In contrast, diagenesis releases considerable Br and I from the solid phase in organic-rich sediments to the fluid phase. It is usually assumed that Cl has a negligible concentration in the solid phase of marine sediment (Martin et al. 1993; Muramatsu et al. 2007; Gieskes and Mahn 2007). However, the few data available for Cl in lithified sedimentary rock indicate surprisingly high Cl concentrations ranging up to ~1000's of ppm, which might be partly explained by the variable presence of salt derived from seawater or sedimentary pore waters (Table 9.2; John et al. 2011; Turekian and Wedepohl 1961). Further data are therefore required to evaluate the significance of water soluble halogens in marine sediment and to improve the constraint on the Cl content of the solid phase. Water soluble halogens might be included in estimates of bulk silicate Earth concentrations, but removal of pore waters during sediment compaction suggests that sedimentary pore waters (and therefore salt in dry sediments) are not relevant for estimation of deep subduction budgets (Peacock 1990).

9.3 The Oceanic Crust-Lithosphere and the Scale of Fluid Infiltration

As a first step toward evaluating the behaviour of halogens during alteration and metasomatism of the oceanic crust, it is desirable to review current knowledge concerning the structure of the oceanic crust and the scale of fluid infiltration.

It is now recognised that the character of the oceanic crust generated along the Earth's 67,000 km long system of oceanic spreading centres varies as a function of spreading rate (Bird 2003; Dick et al. 2006; Snow and Edmonds 2007). The classic 'Penrose' style of oceanic crust, as defined by the participants of the 1972 Penrose conference (Conference Participants 1972), which has a homogenous layered structure where sediments are underlain by pillow basalts, sheeted dykes, and layered intrusives, is only generated at fast spreading centres (>60 mm/yr; Dick et al. 2006). In these cases, the rate of magma supply exceeds the rate of plate divergence and the seismic Moho at depths of 6–7 km represents a petrological transition from layered gabbro to peridotite (Fig. 9.4; Dick et al. 2006).

In contrast, extremely heterogenous crust is generated at ultra-slow spreading centres, which have rates of divergence of <20 mm/yr, and account for more than 20,000 km of the global ridge system (Bird 2003; Dick et al. 2003). In some cases, ultra-slow spreading centres are completely amagmatic and characterised by tectonic extension with hydrated ultramafic rocks (serpentinites) exposed on the seafloor (Dick et al. 2006; Snow and Edmonds 2007). In other cases, a thin and/or patchy carapace of volcanic rock lies directly on top of layered intrusives or mantle peridotites (Fig. 9.4; Dick et al. 2006) and the seismic Moho at depths of only 1–4 km could represent a hydration front between serpentine and mantle peridotite, as originally suggested by Hess (1962).

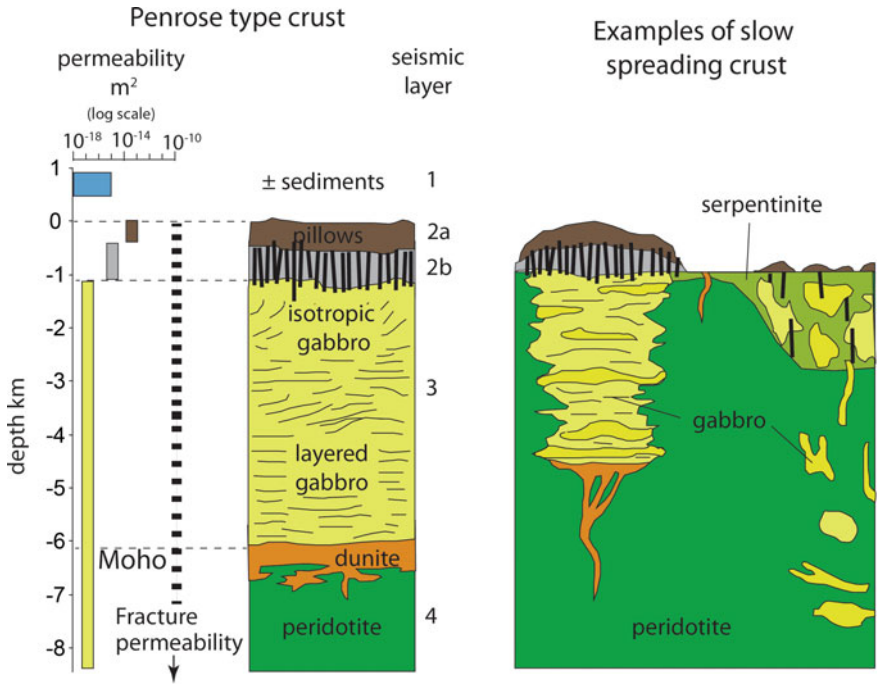

Fig. 9.4 Schematic diagram showing two end-member styles of oceanic crust. Penrose style homogenous oceanic crust with a well defined layered seismic structure is generated at fast spreading centres (Conference Participants 1972; Dick et al. 2006). Crustal styles vary at slow spreading centres and may include poorly developed gabbros and dykes or a missing volcanic carapace; peridotites exposed on the seafloor are hydrated to serpentinites and the seismic Moho could represent the hydration front. The diagrams are modified after Dick et al. (2006) with permeability data from Anderson et al. (1985, 2012), Fisher (1998), and Fisher and Becker (2000). Note that fracture permeability continues to variable and poorly defined depths (see text)

Finally, slow spreading ridges, such as the Mid-Atlantic Ridge, with rates of divergence of between 20 mm/yr and 60 mm/yr, are characterised by alternating segments of the two crustal styles implying the Penrose model is inadequate for a large portion of the oceanic crust (Dick et al. 2006; Larsen et al. 2009; Snow and Edmonds 2007).

9.3.1 Crustal Permeability

Pillow lavas and hyaloclastite breccias in seismic layer 2a of the oceanic crust have relatively high permeability ($\sim 10^{-13}$ m^2), meaning that the upper 500 m of the crustal basement enjoys good connectivity with cold seawater and is subject to low-temperature 'brownstone' facies weathering at very high water/rock ratios (e.g., w/r > 100; Anderson et al. 1985; Fisher 1998). In situ borehole permeability

measurements indicate permeability decreases to 10^{-18}–10^{-15} m^2 at greater depths, but numerical heat flow models imply that localised fracture generated permeabilities of up to 10^{-9} m^2 control the effective permeability in the deeper crust (Fig. 9.4; Anderson et al. 2012; Fisher 1998; Fisher and Becker 2000; Nehlig 1994). Unlithified sediments represent a low permeability barrier to vertical fluid flow (Fig. 9.4) and hydrothermal systems on the ridge flanks are therefore connected to seawater, and each other, through fractures exposed on basement outcrops (Anderson et al. 2012; Hutnak et al. 2008).

9.3.2 High Temperature Hydrothermal Vent Systems

High temperature (350–400 °C) black smoker vent systems, where precipitation of Fe, Cu, and Zn sulphides generate vent chimneys and sulphide mounds, are found along mid-ocean ridges, back arc basin spreading centres and at intra-plate submarine volcanoes (Baker and German 2004; Edmond et al. 1979; Hannington et al. 2011; Staudigel et al. 2004; Von Damm et al. 1985). The majority of high temperature hydrothermal fields at spreading centres occur on the ridge axes, but off-axis systems linked to crustal fractures are known at distances of up to several km from the axis (Melchert et al. 2008; Rona et al. 1990; Zierenberg et al. 1995). The circulation of hydrothermal fluids is responsible for up to 80% of the geothermal heat lost in these settings, meaning it is the major mechanism by which the oceanic crust cools (e.g., Williams et al. 1974).

Heat flow calculations and the distribution of hydrothermal plumes in the water column indicate that independent vent fields and associated ore deposits (e.g., hydrothermal outflow zones) occur at intervals of as little as 25 km along fast spreading centre ridge axes and as far apart as 200 km on slow spreading centre ridge axes (Baker 2007; Hannington et al. 2011). Seawater is drawn into the oceanic crust to feed these systems through fractures, gaps between pillow lavas or dykes, and breccia zones over wide but poorly defined areas between the vent fields and on the ridge flanks (Anderson et al. 2012; Hutnak et al. 2008).

Seismic evidence for brittle deformation suggests that hydrothermal fluids penetrate to maximum depths of $\sim$10 km on parts of the Mid-Atlantic Ridge (Glasby 1998). The TAG hydrothermal field at 26° N on the Mid-Atlantic Ridge is situated above a 15 km long detachment fault that penetrates >7 km into the crust to near Moho depths (de Martin et al. 2007). Periodic reactivation of the fault has supplied heat to the overlying hydrothermal system and enabled sporadic hydrothermal activity over tens to hundreds of thousands of years in this area (Humphris and Cann 2000; Kleinrock and Humphris 1996; Tivey et al. 2003).

In comparison, seismic evidence suggests that hydrothermal fluids penetrate only $\sim$3 km into the fast spreading East Pacific Rise (Glasby 1998). Melt lenses at depths of 1–3 km on the East Pacific Rise supply heat to the overlying hydrothermal system but represent a barrier to deeper fluid flow. The duration of hydrothermal activity is difficult to constrain but is commonly related to magmatism

on fast spreading ridges, and individual vent fields are probably sustained over periods of only ten's to hundred's of years (Stakes and Moore 1991).

9.3.3 *Serpentinite Hosted Systems*

The Lost City Hydrothermal Field on the Atlantis Facture Zone occurs 15 km from the Mid-Atlantic ridge axis at 30° N (Kelley et al. 2001). This system is hosted by ultramafic rocks and is characterised by carbonate vent chimneys and low temperature (40–90 °C) alkaline fluids (pH 9–10) (Kelley et al. 2001, 2007). The alkalinity of the fluids and the presence of hydrogen, methane and abiogenic hydrocarbons are characteristics of fluids produced by serpentinisation of ultramafic lithologies (Kelley et al. 2007; Proskurowski et al. 2008). The discovery of this system was significant because it is driven by heat generated by exothermic serpentinisation reactions, rather than magmatism, and similar reactions could potentially drive numerous hydrothermal systems distal to ridge axes, implying a much higher level of seafloor hydrothermal activity than previously recognised (Kelley et al. 2001). Serpentinites are commonly exposed along transform faults and low angle detachments related to oceanic core complexes, providing evidence for widespread fluid activity at varying distance from oceanic spreading axes (Fryer 2002).

The slab bend formed immediately before subduction is now recognised as an additional site of important hydrothermal alteration (Fig. 9.5). Seismic evidence suggests faults cut at least 20 km below the seafloor in this location, with the

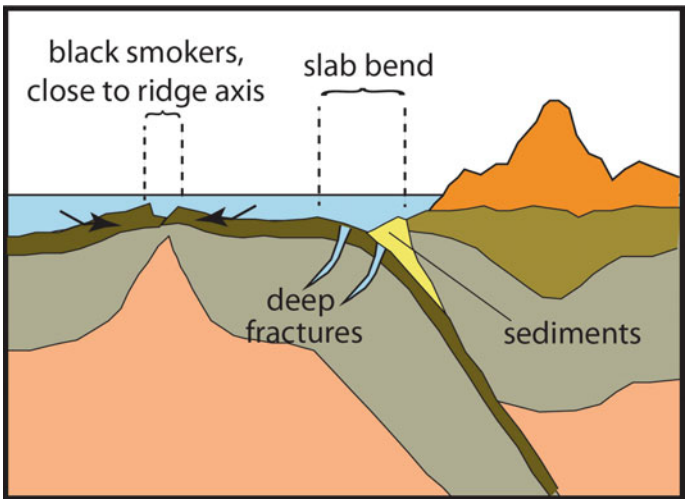

Fig. 9.5 Schematic diagram highlighting the slab bend as an important site for deep (>20 km) fractures and hydrothermal alteration of the lithospheric mantle (see text). Note that fractures at the slab bend provide a possible pathway for sedimentary pore waters to infiltrate the lithosphere

potential for large scale serpentinisation of the lithospheric mantle (Fig. 9.5; Ranero et al. 2003). Heat flow measurements off shore Nicaragua and Central Chile indicate these areas are characterised by unexpectedly low heat flow consistent with heat loss by hydrothermal activity (Grevemeyer et al. 2005).

9.4 Black Smoker Vent Fluid Chemistry and Halogens

In comparison to seawater, high temperature black smoker vent fluids contain negligible Mg or SO_4^{2-} (dissolved sulphur is S^{2-}), and are often depleted in U, P and F (Fig. 9.6). In contrast, they are enriched in trace elements, dissolved SiO_2 and contain 5–10 times more K and Ca relative to Na, than seawater (Fig. 9.7). Typical vent fluids have pH of 3–4, maximum temperatures of close to 400 °C and salinities that range from 0.1 to 6 wt% salts (Fig. 9.8).

The composition of hydrothermal vent fluids results from chemical reaction of seawater with the oceanic crust and the mobilisation of trace elements and silica made possible by the high temperature of the fluid, acidity, and presence of the chloride ligand (Bischoff and Dickson 1975; Humphris and Thompson 1978; Seyfried and Bischoff 1981). The take up of Mg into Mg-rich hydrous-silicate minerals, including smectite, chlorite, amphibole, and talc, is important because Mg-metasomatism is the primary source of vent fluid acidity and leads to extensive hydration of the crust (reaction 9.2; Bischoff and Dickson 1975; Seyfried and Mottl 1982).

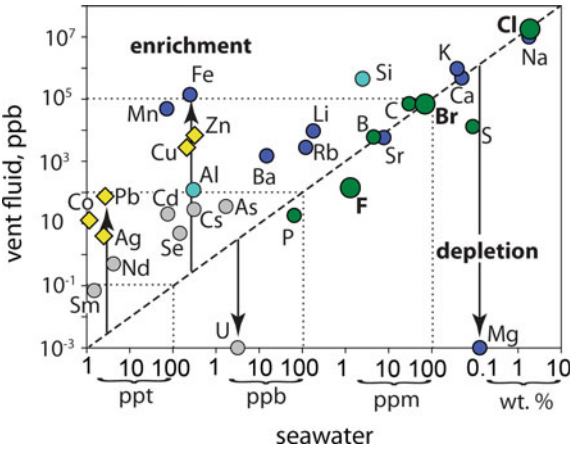

Fig. 9.6 Comparison of selected elements in seawater and Hanging Garden vent fluids from 21° N on the East Pacific Rise (Von Damm et al. 1985; Li and Schoonmaker 2003). The diagram shows that relative to the 1:1 line (*dashed*), most trace elements are strongly enriched in the vent fluids, but that S, F, and P are slightly depleted and Mg is quantitatively removed from the vent fluids. Note that the Hanging Garden Vent fluids have near seawater salinity and that this diagram uses a log scale meaning that small variations in concentration (e.g., a factor of 2) cannot be easily evaluated (see Fig. 9.7)

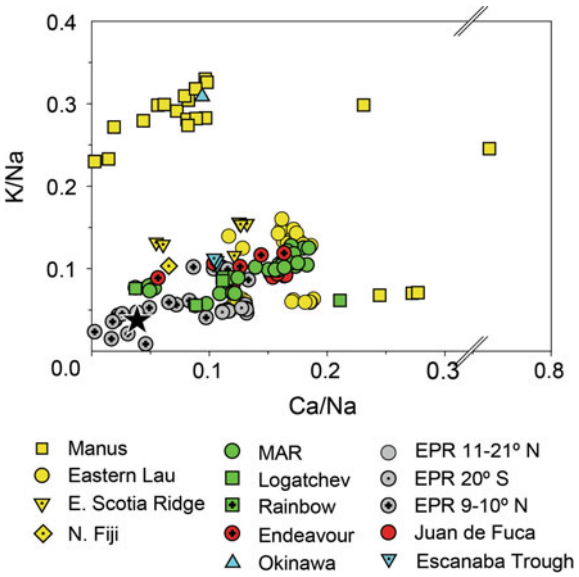

Fig. 9.7 Ca/Na versus K/Na weight ratios of vent fluids for which Cl and Br data are available (below). Vent fluids are variably enriched in K and Ca, relative to Na in seawater; the seawater ratios are shown by the *star* (Butterfield et al. 1990; Ishibashi et al. 1994; James et al. 1995, 2014; Mottl et al. 2011; Pester et al. 2012; Reeves et al. 2011; Seyfried et al. 2003; Von Damm 1997, 1998, 2000, 2003)

$$3MgCl_{2(aq)} + 4SiO_{2(aq)} + 4H_2O_{(l)} = Mg_3Si_4O_{10}(OH)_{2(s)} + 6HCl_{(aq)} \quad (9.2)$$

SO_4^{2-} is removed from solution by reduction to sulphide and precipitation with Ca as anhydrite; Ca is released to the fluid by albitisation of plagioclase and the Ca/Na ratio of the fluid is subsequently controlled by plagioclase and epidote solid solution (Berndt et al. 1989). Potassium is incorporated into K-minerals at low temperature but it is released to the fluid at temperatures of >150 °C, which means most high temperature vent fluids have K/Cl ratios higher than seawater. The K/Cl ratio of the vent fluid is usually limited by the low K content of the basaltic crust, but relatively high K/Cl ratios of ~0.3 occur in the Manus basin vent fluids where more evolved K-rich rocks are present on the seafloor (Fig. 9.7; Reeves et al. 2011).

The growth of Mg-rich hydrous minerals causes a finite increase in the salinity of hydrothermal fluids; however, this is only detectable at low water-rock ratios of <1 (e.g., Kelley and Robinson 1990; Seyfried et al. 1986; Seyfried and Mottl 1982). Therefore, the occurrence of vent fluids with salinities of less than seawater, and in some cases the dominance of vent fluids with lower than seawater salinity over many years of observation (Campbell et al. 1988), has been interpreted as strong evidence for phase separation and segregation of brines and vapours in submarine hydrothermal systems (Bischoff and Rosenbauer 1989; Butterfield et al. 1997; Seyfried et al. 2003; Von Damm et al. 1997) (Table 9.3).

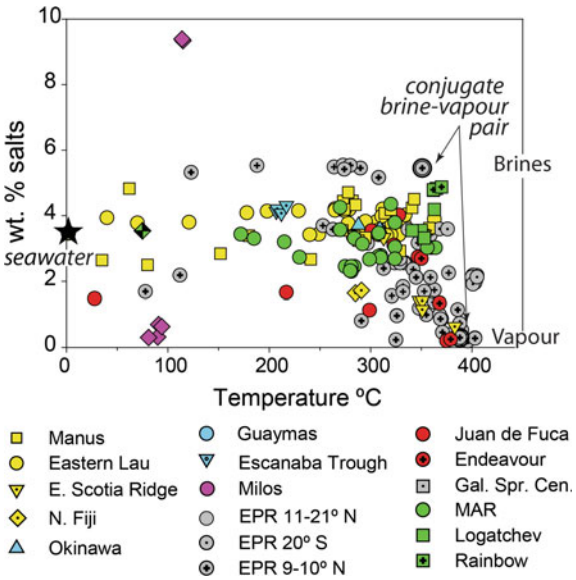

Fig. 9.8 Temperature and salinity data for selected vent fluids. Note that the data show maximum vent temperature and that most of the salinities are for end-member hydrothermal fluids with zero Mg (e.g., uncontaminated by seawater). A conjugate brine and vapour pair emitted from vent F at 9° N on the East Pacific Rise is indicated (below; Von Damm et al. 1997 the other data are from Butterfield et al. 1990; Edmond et al. 1979; Ishibashi et al. 1994; James et al. 1995, 2014; Kawagucci et al. 2011; Mottl et al. 2011; Pester et al. 2012; Reeves et al. 2011; Seyfried et al. 2003, 2011; Von Damm et al. 1997, 1998, 2000, 2003, 2005; Wu et al. 2012)

Table 9.3 Halogen signatures of fluids in the oceanic lithosphere

	Salinity	F/Cl	Br/Cl	I/Cl
Seawater	3.5	0.00007	0.0035	0.000003
Sedimentary pore fluids	1–5	0.00005–0.0002	SW^a–0.014	SW^a–0.04
Vent fluids	0.1–7	0.000006–0.0005	0.001–0.005	SW^a–0.001
Crustal brines (fluid inclusions)	10–60	<0.0001	SW^a–0.005	SW^a–0.00012

SW^a = seawater
References are given in Table 9.1 and Figs. 9.3, 9.11 and 9.15

9.4.1 *Phase Relations in the H_2O-NaCl System*

The phase relations of sub-marine hydrothermal systems are strongly controlled by the presence of salts. Pure water exists as a homogenous supercritical fluid above its critical point (374 °C; 220 bars). In contrast, a critical curve extends beyond the critical point of pure H_2O in any binary H_2O-salt system, and the two-phase region is vastly expanded (Fig. 9.9; e.g., Bischoff and Pitzer 1989; Driesner and Heinrich 2007). The critical point of seawater (407 °C; 220 bars) lies on the critical curve of

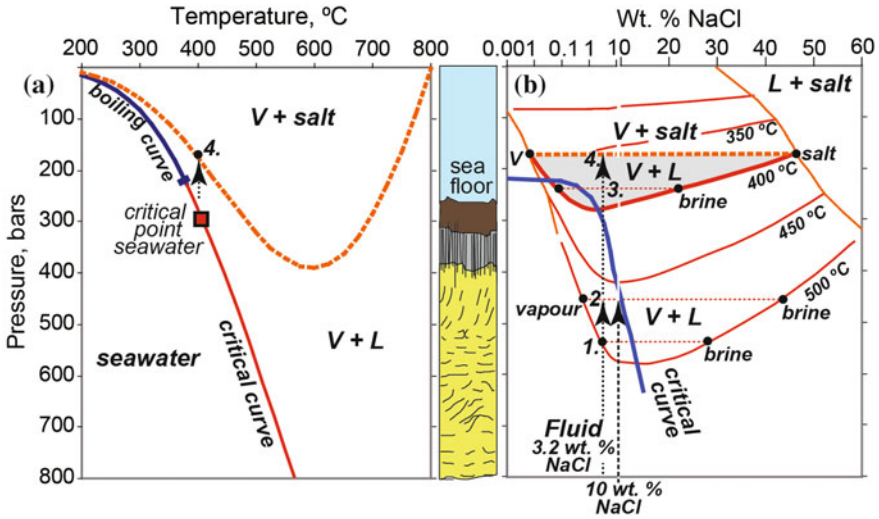

Fig. 9.9 Phase diagrams for the binary H_2O-NaCl system. **a** Pressure versus temperature and **b** pressure versus wt% NaCl. Note that the approximate depth of different crustal units under hydrostatic pressure is shown and that the wt% NaCl scale switches from log to linear at 10 wt%. Part a shows the critical curve, with the critical point of seawater estimated from 3.2 wt% NaCl solution, and the L-V-S boundary that separates the vapour-salt and vapour-liquid fields. Part **b** shows the critical curve, liquid-salt field, and isotherms that define the two phase field at selected temperatures. The effects of depressurisation are shown for 4 different pressure-temperature regimes (see text). Data and equations used to construct the figures are from Bischoff and Pitzer (1989) and Driesner and Heinrich (2007)

the H_2O-NaCl system and joins the boiling curve to the condensation curve in Fig. 9.9a (e.g., Bischoff and Pitzer 1989; Bischoff and Rosenbauer 1984; Driesner and Heinrich 2007). Sub-critical phase separation occurring below the critical point of seawater produces a small quantity of vapour, whereas super-critical phase separation occurring above the critical point of seawater produces a small quantity of brine (Fig. 9.9).

The slope of the critical curve implies that phase separation will produce progressively more saline brines at higher pressures and temperatures deeper within the oceanic crust (Fig. 9.9). The salinity of brines also increases as the L-V isotherms are overstepped, such that at 500 °C and 540 bars the first brine exsolved has a salinity of 28 wt%, but further decompression to 450 bars would yield a brine of 44 wt% NaCl (points 1 and 2; Fig. 9.9b). It is important to note that the salinities of the vapours and brines produced at different temperature and pressure conditions are controlled exclusively by the shape of the liquid-vapour envelope. For example at 500 °C and 450 bars, parental fluids with salinities of either 3.2 wt% NaCl (seawater) or 10 wt% NaCl, would both exsolve into conjugate fluids with identical

salinities, but at different proportions that can be estimated using the lever rule (point 2; Fig. 9.9b).

In addition to the well documented phenomena of liquid-vapour immiscibility, precipitation of hydrothermal-halite is possible under some circumstances (e.g., point 4; Fig. 9.9). This is possible for seawater, which is approximated by the H_2O-NaCl system (Fig. 9.9), because hydrostatic pressures above spreading centres at typical water depths of 2000–2500 m are only ~200–250 bars and seawater heated above ~400 °C would separate into steam and halite (Fig. 9.9). Butterfield et al. (1997) presented photomicrographic evidence for halite coating glass surfaces and intergrown with TiO_2, AlO(OH), and sphalerite, that was interpreted as evidence for precipitation of hydrothermal halite during high temperature interaction of seawater with seafloor lavas. The precipitation of hydrothermal halite has also been suggested as a possible cause of Br and Cl fractionation in some hydrothermal vent fluids (Berndt and Seyfried 1997; Foustoukos and Seyfried 2007). However, it should be noted that the vapour-salt field is probably restricted to much shallower depths in the multi-component salt systems that are relevant for hydrothermal fluids than in the H_2O-NaCl system that is relevant for seawater (below).

9.4.2 *Complex Salt Systems and Hydrolysis*

Hydrothermal vent fluids are better modelled in the ternary H_2O-NaCl-$CaCl_2$ system than in the NaCl-H_2O system (Vanko et al. 1988) because they have Ca/Na and K/Na ratios elevated by 5–10 times compared to seawater (Fig. 9.7). The two phase field is even larger in these complex salt systems than in the H_2O-NaCl system. The critical curve for H_2O-K/Cl is similar to that of H_2O-NaCl, but the critical curve for H_2O-$CaCl_2$ moves to significantly higher pressure at any given temperature than in the H_2O-NaCl system (Fig. 9.10; Bischoff et al. 1996; Driesner and Heinrich 2007; Hovey et al. 1990). In addition, at temperatures of 400–450 °C, the vapour-salt field shrinks back from pressures of 180–250 bars in the H_2O-NaCl system (that overlap the seafloor; Fig. 9.10), to 130–170 bars in the H_2O-KCl system and to as little as ~40–65 bars in the H_2O-$CaCl_2$ system (Fig. 9.10; Driesner and Heinrich 2007; Hovey et al. 1990; Keevil 1942; Ketsko et al. 1984).

In addition to the role of Cl as an important ligand for metal transport in hydrothermal solutions (e.g., Yardley 2005), hydrolysis reactions in H_2O-salt systems can have a significant influence on the pH of hydrothermal fluids (e.g., reaction 9.3; Bischoff et al. 1996; Seyfried et al. 1988; Seyfried and Bischoff 1981). Hydrolysis reactions in binary salt systems have the general form:

$$xH_2O + M^{x+}Cl_x^- = xHCl + M^{x+}(OH)_x^- \tag{9.3}$$

The equilibrium lies to the left under Earth's surface conditions, meaning salt solutions have a neutral pH, but the equilibrium can be significantly shifted to the right under some crustal conditions. Bischoff et al. (1996) demonstrated that at

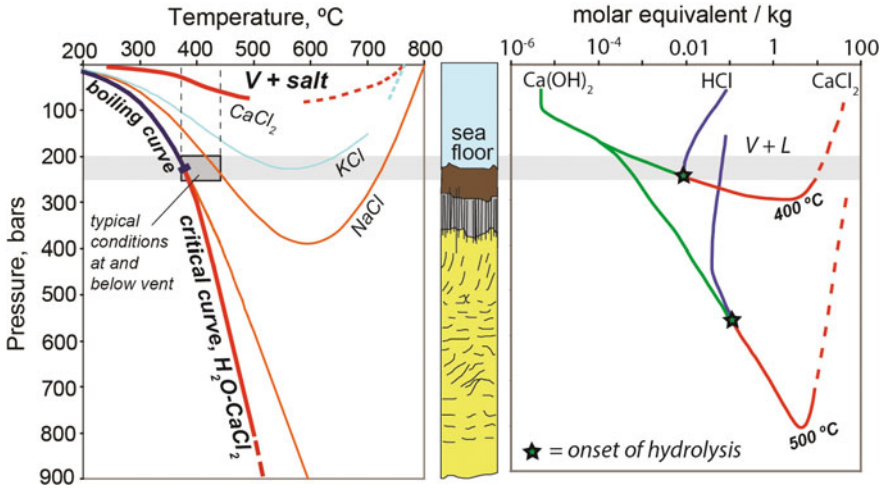

Fig. 9.10 Phase diagrams for various binary salt systems. **a** Pressure versus temperature plot showing the critical curves for H_2O-NaCl and H_2O-$CaCl_2$, and the L-V-S curves for the H_2O-NaCl, K/Cl, and $CaCl_2$ systems. Note that the vapour-salt field shrinks back from a maximum size in the H_2O-NaCl system to a minimum size in the H_2O-$CaCl_2$ system. **b** Pressure versus molar equivalent $CaCl_2$, HCl, and $Ca(OH)_2$. The binary H_2O-$CaCl_2$ system differs to the H_2O-NaCl system in that hydrolysis occurs under high temperature—low pressure conditions (see text). Data and equations used to construct the figures are from Bischoff and Pitzer (1989), Bischoff et al. (1996), Driesner and Heinrich (2007), Hovey et al. (1990) and Ketsko et al. (1984)

temperatures of 350–500 °C hydrolysis is significantly more important in the $CaCl_2$-H_2O system than in the binary NaCl-H_2O system. Fournier and Thompson (1993) reported that hydrolysis does not occur in the liquid-vapour region of the H_2O-NaCl-KCl system, but that HCl is a significant component of the steam in equilibrium with halite in the vapour-salt region of the H_2O-NaCl and H_2O-NaCl-KCl systems. The varying degrees of hydrolysis in the different salt systems are related to the relative solubilities of the metal hydroxide produced by hydrolysis: $Ca(OH)_2$ has a low solubility meaning it is removed from solution more efficiently than NaOH and as a result reaction 9.3 is pushed further to the right (Bischoff et al. 1996).

In nature, the hydroxide component produced by hydrolysis reacts with silicates to form hydrous silicate minerals in the oceanic crust. For example, hydrolysis of $MgCl_2$ leads to Mg being fixed in hydrous silicate minerals under prograde conditions as seawater is drawn into hydrothermal systems (reaction 9.2; Seyfried et al. 1988). The reactivity of Mg in the oceanic crust means that it is quickly removed from solution and Mg is not present in the hydrothermal fluids that reach the high temperature reaction zone above the magma chamber. In the absence of $MgCl_2$, hydrolysis of $CaCl_2$ becomes the main acid generating reaction and is important in the hydrothermal upflow zones; hydrolysis of NaCl can be locally important in zones of Na metasomatism (Seyfried et al. 1988). The generation of acidity by hydrolysis reactions is important because it enables mobilisation of heavy metals

from seafloor lithologies (Seyfried and Bischoff 1981). Furthermore, HCl partitions into the vapour produced by phase separation (Fig. 9.10; Bischoff et al. 1996), meaning segregation of vapours and brines enables discrete zones of alkali or acid metasomatism to develop in different parts of the oceanic crust, or waves of acid metasomatism to pass through a hydrothermal system (Kigai and Tagirov 2010).

9.4.3 Halogen Abundance Ratios in Vent Fluids

There has been considerable interest in the relative abundances of halogens in hydrothermal vent fluids. The existing data show vent fluids have F concentrations ranging from ~0.1 to 7 ppm, compared to the seawater value of 1.3 ppm F, and that F varies independently of Cl with vent fluid F/Cl ratios varying by almost two orders of magnitude around the seawater value (Fig. 9.11a; Edmond et al. 1979;

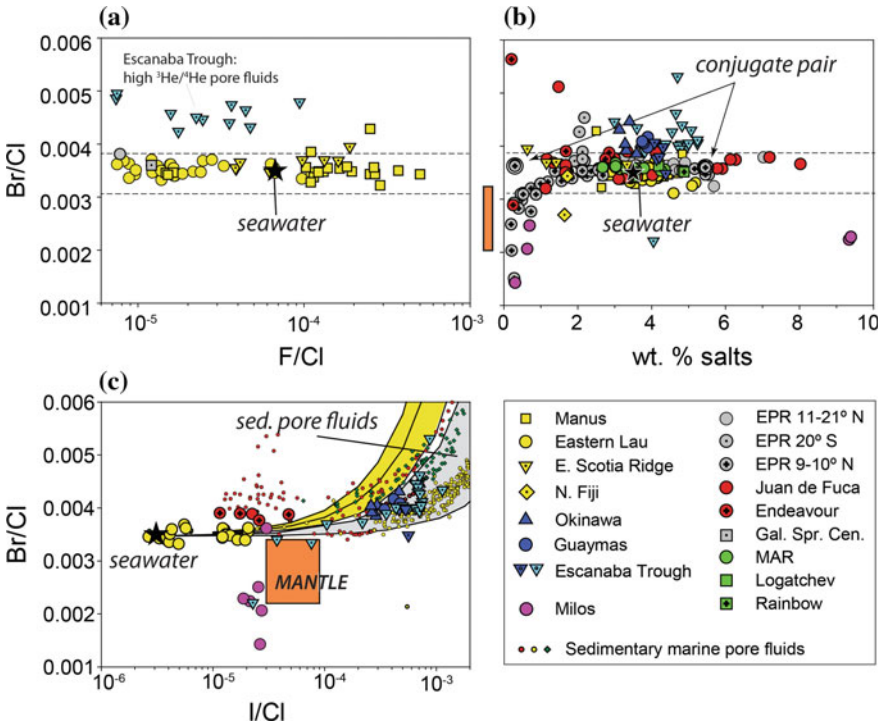

Fig. 9.11 The halogen systematics of hydrothermal vent fluids: **a** F/Cl versus Br/Cl; **b** Br/Cl versus salinity; and **c** I/Cl versus Br/Cl (Butterfield et al. 1990; Campbell and Edmond 1989; Campbell et al. 1994; Edmond et al. 1979; Gieskes et al. 2000; 2002; Ishibashi et al. 2002; James et al. 1999, 2014; Kawagucci et al. 2011; Mottl et al. 2011; Oosting and Von Damm 1996; Reeves et al. 2011; Seyfried et al. 2003; Von Damm et al. 1985, 1997, 1998, 2000, 2003, 2005; Wu et al. 2012; You et al. 1994)

Gieskes et al. 2000, 2002; James et al. 2014; Mottl et al. 2011; Reeves et al. 2011; Von Damm et al. 1985). The reported variation in F fits well with experimental studies that demonstrate F is removed from solution as seawater interacts with basalt and is heated from 150 to 250 °C, but re-enters solution with further heating to 300 °C (Seyfried and Ding 1995). Fluorine is incorporated into Mg-carbonate (cf., Fig. 9.1) and hydrous minerals at low temperature but the direction of hydroxyl-fluoride and carbonate-fluoride exchange reactions reverses at high temperature when the speciation of dissolved F changes from $F^-_{(aq)}$ to $HF_{(aq)}$, which reduces the chemical activity of the F^- anion (Seyfried and Ding 1995). Consequently the experimental studies imply that while magmatic F might be mobilised in deeper parts of the crust as $HF_{(aq)}$, it is likely that seawater $F^-_{(aq)}$ is removed from solution during heating and is not advected deeply into the crust (Seyfried and Ding 1995). The co-depletion of some hydrothermal fluids in P as well as F suggests that precipitation of fluorapatite is also important (Fig. 9.6; Gieskes et al. 2002).

A number of studies have investigated Br in hydrothermal fluids and demonstrated that the Br/Cl ratio of the vent fluids is usually within 10% of the seawater value and that it does not vary systematically as a function of salinity (Fig. 9.11b). Furthermore, conjugate vapours and brines from vent F at 9°16' N on the East Pacific Rise (Von Damm et al. 1997) and Milos Island in the Hellenic Arc (Wu et al. 2012) have similar Br/Cl ratios (Fig. 9.11b). Taken together these data strongly suggest that the Br/Cl ratio is not strongly or systematically altered by liquid-vapour phase separation in the majority of hydrothermal systems investigated (Fig. 9.11b). This conclusion is consistent with experiments on NaCl solutions that show no systematic fractionation of Br and Cl during sub-critical phase separation (Berndt and Seyfried 1997). Experiments under other conditions have shown fractionation of Br relative to Cl into either vapours or brines during phase separation (see Berndt and Seyfried 1990; Foustoukos and Seyfried 2007; Liebscher et al. 2006). However, the results from the different laboratories are not in agreement and the available Br/Cl data summarised for vent fluids in Fig. 9.11 are more easily explained by the conservation of Br/Cl during phase separation with unusual Br/Cl ratios of fluids in specific settings being explained by fluid-rock reactions (below).

The unusually high Br/Cl ratios in fluids from a small number of vents (Fig. 9.11b) can be explained by fluid interaction with sedimentary material, because where Br/Cl and I/Cl data are both available these ratios co-vary in a manner comparable to that observed for sedimentary pore waters (Fig. 9.11c; Campbell and Edmond 1989; Campbell et al. 1994; Gieskes et al. 2002; Kawagucci et al. 2011; Mottl et al. 2011; You et al. 1994). Furthermore, I concentrations are correlated with NH_4 and other sediment-derived components in these fluids (Campbell et al. 1994; You et al. 1994). Note that limited data are available for I or F in vent fluids and halogen data for sedimentary pore fluids with mantle-like $^3He/^4He$ signatures, which are believed to represent hydrothermal fluids from beneath the Escanaba Trough hydrothermal system (Hole 1038B-H; Ishibashi et al. 2002; James et al. 1999), are included in Fig. 9.11 as light blue symbols (Gieskes

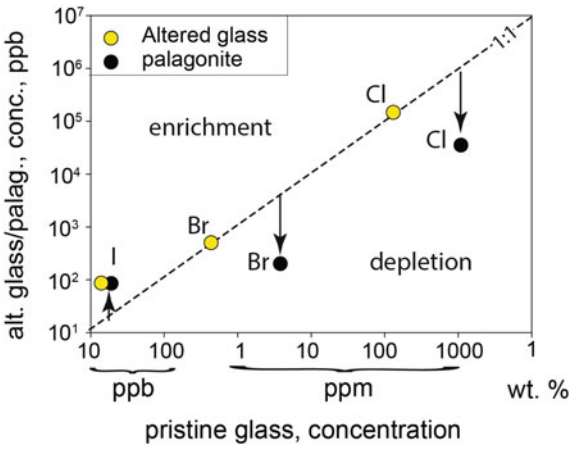

Fig. 9.12 Halogens in pristine glasses and their weakly altered or palagonitised counterparts from Macquarie Island and Samoa (Kendrick et al. 2012a, 2015a)

et al. 2000, 2002). These 'hydrothermal pore fluids' have Br/Cl and I/Cl values overlapping the range reported for Escanaba Trough vent fluids (Fig. 9.11c; Campbell and Edmond 1989; Campbell et al. 1994; You et al. 1994).

Unusually low Br/Cl ratios are restricted to a few locations between 9° and 10° N on the East Pacific Rise (Oosting and Von Damm 1996) and Milos Island in the Hellenic Arc (Fig. 9.11b; Wu et al. 2012). It is possible that vent fluids acquired low Br/Cl ratios in these settings by fluid interaction with sedimentary halite or by leaching glassy magmatic rocks that are typically characterised by Br/Cl of less than seawater (see mantle field in Fig. 9.11c; Jambon et al. 1995; Kendrick et al. 2013a, 2017; Schilling et al. 1980). Similarly low Br/Cl ratios have been reported for unusual sediment pore waters that have interacted with glassy volcaniclastic rocks in the Aoba Basin of the New Hebrides convergent margin (Martin 1999). Strongly altered, palagonitised glasses can also be depleted in Cl and Br relative to pristine glasses (Fig. 9.12; Kendrick et al. 2015a) confirming that these elements are mobilised during low temperature alteration of glass.

Finally, the fact that most vent fluids have Br/Cl ratios within 10% of seawater (Fig. 9.11) implies that in most cases, fluid-rock ratios are sufficiently high that Br and Cl behave conservatively in hydrothermal vent fluids and are not significantly altered by phase separation or reaction with mafic lithologies (Br concentrations are more readily altered by interaction with sediments; Fig. 9.3; Muramatsu et al. 2007; Price and Calvert 1977). However, leaching of Cl > Br from glassy rocks is possible and has the potential to lower the Br/Cl ratio of a fluid. Furthermore, at low water-rock ratios, precipitation of OH > Cl > Br in Fe/Mg-hydroxy chlorides, or amphibole, has the potential of increasing a fluid's salinity and Br/Cl ratio (Kendrick et al. 2015b; Seyfried et al. 1986; Svensen et al. 1999, 2001; Vanko 1986). Therefore, it should not be assumed that Br and Cl behave conservatively under all hydrothermal conditions.

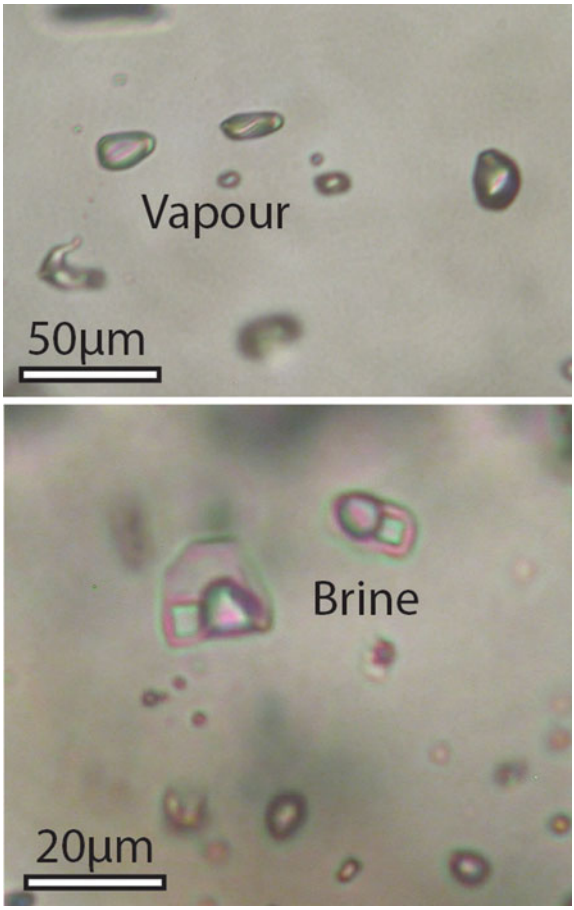

Fig. 9.13 Photomicrographs of vapour and brine fluid inclusions in a quartz vein hosted by amphibolite metagabbro from layer 3 of the crust. This sample (7–45), dredged from the Mathematician Ridge of the Pacific Ocean, has been described in detail by Vanko (1988) and Kendrick et al. (2015b). The vapour bubbles have a high degree of fill in the vapour inclusions. In contrast, brine inclusions have much smaller vapour bubbles and visible halite daughter minerals which have a *bright green hue* and *cubic form*

9.5 Fluids in the Deeper Crust

Evidence for the nature of fluids in deeper parts of the oceanic crust comes from mineral alteration (Gillis and Meyer 2001; Vanko 1986), fluid inclusions (Fig. 9.13; Kelley et al. 1992, 1993; Kendrick et al. 2015b; Nehlig 1991; Vanko 1988; Vanko et al. 1992), and studies of magmatic glass that contain assimilated halogens (below; Kendrick et al. 2013a, 2015a, 2017). Fluid inclusions have been investigated in minerals such as quartz, anhydrite, sphalerite, epidote, amphibole, and chlorite from a number of dredges and ophiolites. These include samples from within and just below the vent chimney all the way down to upper amphibolite facies metagabbros from layer 3 of the oceanic crust (Castelain et al. 2014; Juteau et al. 2000; Kelley and Delaney 1987; Kelley and Robinson 1990; Kelley et al. 1992, 1993; Lécuyer et al. 1999; Nehlig 1991; Nehlig and Juteau 1988; Vanko 1986, 1988, 1992, 2004).

Collectively these studies demonstrate the predominance of low salinity Na-Ca-Cl fluids throughout the oceanic crust that are broadly similar to vent fluids. For example, Nehlig (1991) reported that more than 95% of the fluid inclusions examined in samples taken from crustal sections through the Semail and Trinity ophiolites of Oman and California, and in samples from the Gorringe Bank of the East Pacific Rise, had salinities within 1 wt% of seawater. However, in addition to the dominant fluid inclusions with salinities of 0.1–6 wt%, which are similar to vent fluids, fluid inclusions with extreme Ca enrichment (Ca/Na = 1), which is stronger than known from vent fluids (Fig. 9.7), have been reported (Vanko et al. 1992) and brine inclusions with salinities of up to ~50 wt% salts appear to be a common minor component at all levels of the oceanic crust (Fig. 9.13; Juteau et al. 2000; Kelley and Delaney 1987; Lécuyer et al. 1999; Vanko 1988, 2004; Aranovich et al. 2015).

Brine inclusions with salinities of ~30 wt% salts have been reported in the vent chimneys of several systems in the Lau Basin and within a few hundred metres of the seafloor beneath the Pacmanus system of the Manus Basin, demonstrating that high salinity brines are not restricted to deep parts of the oceanic crust (Lécuyer et al. 1999; Vanko et al. 2004). However, high salinity brine inclusions are most commonly reported from deeper amphibolite settings (Vanko 1988; Kendrick et al. 2015b) and above newly emplaced gabbroic intrusions (Kelley and Delaney 1987) or plagiogranites that form in the roof zones of crustal magma chambers (Kelley and Robinson 1990; Nehlig 1991; Vanko et al. 1992). In many cases the brine inclusions co-exist with more abundant low salinity vapour inclusions that provide evidence for their origin by phase separation (e.g., Juteau et al. 2000; Kelley and Delaney 1987; Vanko 1988). The dominance of vapour inclusions is the expected result of seawater undergoing phase separation (e.g., point 2 in Fig. 9.9; Bischoff and Pitzer 1989). However, the vapour inclusions can have salinities that are even greater than seawater suggesting complex multi-stage histories and/or input of a magmatic component.

In some cases, brine inclusions dominate samples recovered from layer 3 of the crust. These inclusions have been interpreted as brines that have been segregated from their conjugate vapours, but their origin by phase separation cannot be proven (Kelley and Robinson 1990; Vanko et al. 1992). The fluid inclusion evidence for possible segregation of brines in layer 3 of the oceanic crust is significant because brine segregation and double diffusive convection of fluids in the oceanic crust has previously been invoked to explain the predominance of fluids with lower than seawater salinity emitted from vents on the seafloor (Fig. 9.14; Bischoff and Rosenbauer 1989). It is suggested the brines would be segregated because of the different wetting properties and buoyancies of vapours and brines in a micro-scale fracture network. Buoyant vapours would be preferentially lost to the overlying hydrothermal system, whereas dense brines could be trapped in the lower crust. If correct, this model implies brines generated by multiple episodes of phase separation gradually accumulate in the deeper crust and they are implied to have long residence times in the crust at very low effective water-rock ratios (Fig. 9.14). The ultimate fate of brines within this model is unknown but brines might eventually be flushed out of the crust by advection of more typical low salinity fluids in the

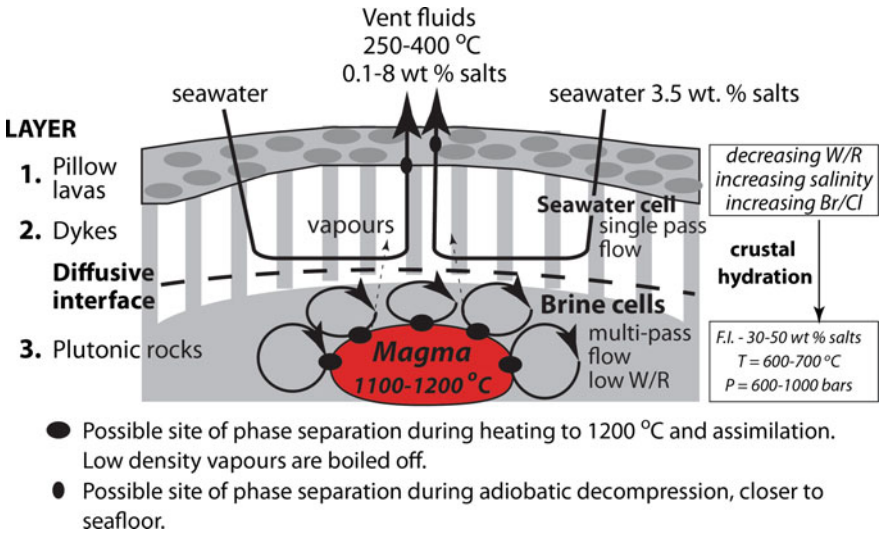

Fig. 9.14 Schematic diagram illustrating the double diffusive convection concept of Bischoff and Rosenbauer (1989). This model predicts brines are segregated from vapours and preferentially retained in deeper portions of the crust. The presence of brines may help explain some styles of alteration and Cl-rich amphiboles. The ultimate fate of the brines may be to be diluted by lower salinity fluids and flushed out of the crust, to migrate laterally and leak from ridge flanks or be assimilated by magmas (Fig. 9.16)

waning stages of hydrothermalism or they might be transported laterally and leak out of the ridge flanks away from the vents (Bischoff and Rosenbauer 1989). In addition, a portion of these brines could be assimilated by magmas driving the hydrothermal system (Kendrick et al. 2013a, 2015a, 2017) or involved in flux melting and the genesis of plagiogranites (Aranovich et al. 2010, 2015).

A major uncertainty related to the brine fluid inclusions is whether they originate purely from evolved seawater or include a component derived from late-stage magmatic fluids. Magmatic fluids exsolved from basic rocks are dominated by CO_2 with a low salinity aqueous component (Dixon et al. 1995; Webster et al. 1999). However, more saline fluids might sometimes be exsolved from evolved intrusive rocks such as plagiogranites in magma chamber roof zones (Kelley and Robinson 1990; Kelley et al. 1992). If magmatic fluids enter the two-phase field, their salinity depends on the shape of the liquid-vapour envelope in the relevant water-salt system (e.g., Fig. 9.9 and 9.10), meaning that it is not possible to infer the source of the fluid (e.g., seawater or magmatic) from the measured salinity. Vanko et al. (1992) suggested that a minor magmatic component could be present in high salinity CO_2-bearing fluid inclusion assemblages from the Oceanographer Transform, but favoured an origin entirely from evolved seawater for brines trapped without accompanying CO_2 on the Mathematician Ridge (Vanko 1988, 1992; Kendrick et al. 2015b). Reeves et al. (2011) suggested that unusually high F/Cl

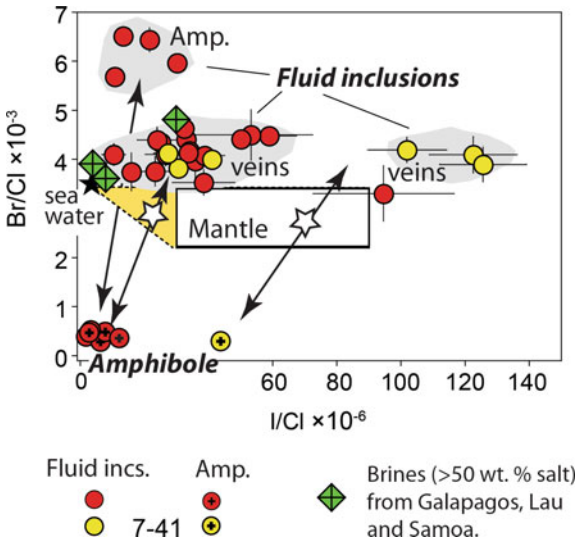

Fig. 9.15 Halogens in fluid inclusions and amphibole separated from Mathematician Ridge amphibolites and metagabbros. Fluid inclusions where analysed by crushing vein minerals (quartz and epidote) and the amphibole wall-rock in vacuum (Kendrick et al. 2015b). Note that the range of fluid inclusion compositions is very similar to the composition of brines assimilated by submarine magmas dredged from the Lau Basin, Galapagos Spreading Centre and Samoa (Fig. 9.16; Kendrick et al. 2013a, 2015a)

ratios in Manus Basin vent fluids could result from the input of magmatic volatiles (Fig. 9.11).

9.5.1 Halogens in Brines and Assimilation by Magmas

The systematics of Br/Cl, I/Cl, and F/Cl in brine inclusions can be inferred from two separate lines of inquiry. Kendrick et al. (2015b) investigated halogens and noble gases in high salinity brine and vapour fluid inclusions in six quartz/epidote veins from the Mathematician Ridge of the NE Pacific using a bulk extraction technique. The fluid inclusions in all the veins were shown to have a similar range of Br/Cl and I/Cl irrespective of the relative proportions of brine and vapour fluid inclusions (Fig. 9.15). In addition, Br/Cl was not correlated with Ar/Cl, which is strongly fractionated by phase separation (Kendrick et al. 2015b). Taken together these data suggest that Br/Cl and I/Cl were not fractionated during phase separation of Mathematician Ridge fluids, consistent with the behaviour of Br/Cl in vent fluids (Sect. 9.4.3). On average the Mathematician Ridge fluids have Br/Cl ~20% higher than seawater and I/Cl intermediate of seawater and the mantle (Fig. 9.15; Kendrick et al. 2015b). These compositions were attributed to mixing halogens introduced by seawater with halogens mobilised from the crust and preferential exclusion of Br and I relative to Cl from amphibole crystallised at low water/rock ratios (Fig. 9.15; Kendrick et al. 2015b). Proton Induced X-ray Emission (PIXE) has been used to analyse some individual brine inclusions from the Mathematician Ridge, Oceanographer Transform and Oman ophiolite (Juteau et al. 2000; Vanko et al. 2001). The majority of the fluid inclusions investigated by PIXE are indicated to

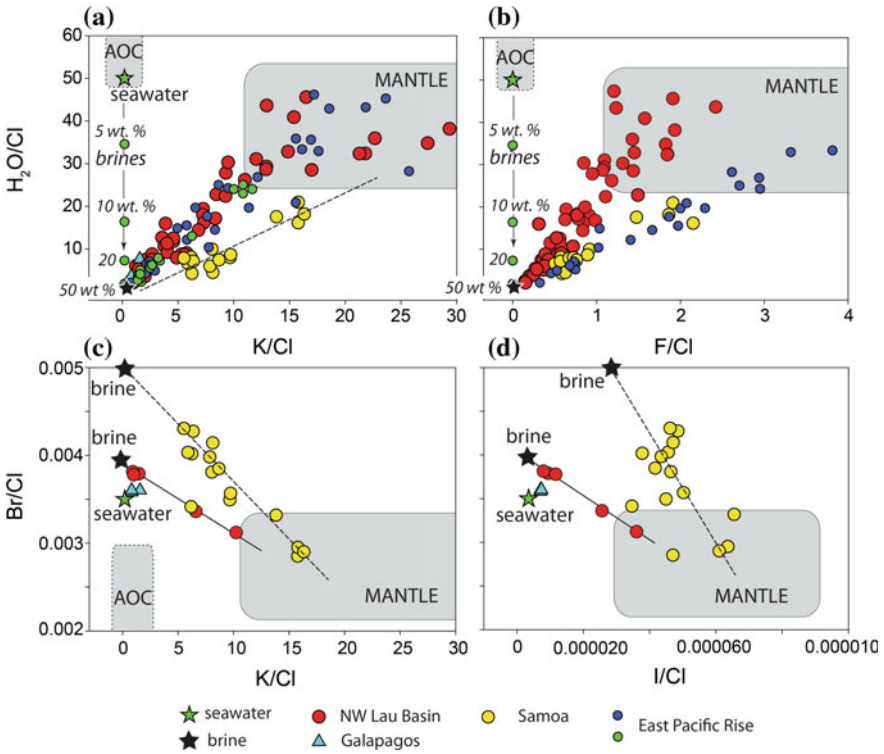

Fig. 9.16 Halogens in magmatic glasses affected by brine assimilation. **a** K/Cl versus H_2O/Cl; **b** F/Cl versus H_2O/Cl; **c** Br/Cl versus K/Cl; and **d** Br/Cl versus I/Cl (Kendrick et al. 2013a, 2015a; le Roux et al. 2006; Lytle et al. 2012). The mantle field is defined by Kendrick et al. (2013a, 2014, 2015a, 2017). Brines have K/Cl and F/Cl of <0.1 (e.g., Fig. 9.8) and H_2O/Cl that is proportional to salinity (parts **a** and **b**). The altered ocean crust (AOC) is assumed to have low K/Cl and high H_2O/Cl based on existing data and the relatively low compatibility of Cl in hydrous minerals compared to H_2O (Ito et al. 1983; Sano et al. 2008)

have Br/Cl close to or above seawater, but the precision of the analyses is low (Juteau et al. 2000; Vanko et al. 2001).

The second constraint on the halogen composition of high salinity brines in the oceanic crust comes from recent studies of volcanic glass (Kendrick et al. 2013a, 2015a, 2017). It has long been recognised that some volcanic glasses contain 'excess Cl' introduced by the assimilation of seawater-derived components (Michael and Cornell 1998; Michael and Schilling 1989). Most workers have favoured the assimilation of hydrothermally altered crust to account for excess Cl. However, plotting the H_2O/Cl and K/Cl ratios of all known glasses, identified as containing excess seawater-derived Cl (Coombs et al. 2004; Freund et al. 2013; Kent et al. 1999a, b, 2002; le Roux et al. 2006; Lytle et al. 2012; Wanless et al. 2010), shows that Cl is introduced into these melts by high salinity brines (e.g., Fig. 9.16; Kendrick et al. 2013a). This is shown by the data in Fig. 9.16 which

extend from a range of compositions representative of the mantle to converge on a single component with very low ratios of H_2O/Cl, K/Cl, and F/Cl that are characteristic of a Na-Ca-K-Cl brine with salinity of >50 wt% salts (Fig. 9.16; Kendrick et al. 2013a, 2015a, 2017). In contrast, altered crustal material would have much higher H_2O/Cl (Ito et al. 1983). The Br and I data available for glasses, affected by brine assimilation from the NW part of the Lau Basin, the Galapagos, and Samoa, define coherent mixing trends with K, Cl, and H_2O, demonstrating that the assimilated brines are characterised by Br/Cl and I/Cl ratios a few 10's of percent higher than seawater (Fig. 9.16), that are very similar to the range of compositions determined for Mathematician Ridge fluid inclusions (Fig. 9.15; Kendrick et al. 2015b).

The brine assimilation data are significant because: (i) some of the glasses affected have high concentrations of H_2O and CO_2, which demonstrate that assimilation must have occurred at depth in crustal magma chambers rather than on the seafloor (Coombs et al. 2004; Kendrick et al. 2013a; le Roux et al. 2006), and (ii) the data provide evidence that seawater-derived brines, with Br/Cl and I/Cl distinct from the mantle, not only penetrate the lower crust but come into direct contact with, and are assimilated by crustal magmas (Fig. 9.16). Mass balance calculations suggest the affected magmas from the NW part of the Lau Basin, the Galapagos, and Samoa assimilated up to 0.5% of their total mass in brine which introduced 0–70% of their total Cl and 0–30% of their total H_2O (Kendrick et al. 2013a, 2015a, b). Therefore, assimilation of brines generated in hydrothermal systems can alter the concentrations of halogens and relative abundance ratios (F/Cl, Br/Cl and I/Cl) of newly forming crust (e.g., magma), even before the new crust has been accreted. In addition, the ductile zone, surrounding the magma chambers, is not a complete barrier to assimilation of seawater-derived volatiles.

9.6 Halogens in Altered Oceanic Crust and Lithosphere

A relatively small number of studies have investigated the bulk halogen content of the altered ocean crust with the majority of studies focused on Cl (Barnes and Cisneros 2012; Bonifacie et al. 2007; Chavrit et al. 2016; Floyd and Fuge 1982; Ito and Anderson 1983; Ito et al. 1983; Kendrick et al. 2015b; Magenheim et al. 1995; Sano et al. 2008). The earliest estimates for whole rock Cl concentration were made by electron microprobe measurements of Cl in individual mineral phases, followed by estimation of the modal abundances of the minerals in the rock (Ito et al. 1983). Major problems with this approach are that intra-granular Cl and fluid inclusion hosted Cl, which can account for 100–200 ppm Cl in the bulk sample (Kendrick et al. 2015b), or Cl present in volumetrically minor phases such as Fe hydroxychlorides are not included in the analysis. In addition, although detection limits of better than 50 ppm Cl can be achieved with sufficiently long counting times (e.g., Michael and Cornell 1998) most minerals have Cl concentrations of less than the typical 100–300 ppm detection limits for Cl achieved by routine electron microprobe analysis.

Direct measurements of Cl have been achieved by various instrumental neutron activation techniques that provide modest 2σ precision of 15–20% (Sano et al. 2008) or 200 ppm Cl (Barnes and Cisneros 2012), but have the significant advantage of requiring minimal sample processing.

Direct measurements of F, Cl, and I have also been achieved by digestion of powders and spectrophotometry (Floyd and Fuge 1982) and more recently by combining pyrohydrolysis for halogen extraction from powders with ion chromatography for F and Cl analysis (Bonifacie et al. 2007; John et al. 2011; Magenheim et al. 1995; Sharp and Barnes 2004) and ICP-MS for Br and I analysis (John et al. 2011). These techniques can provide accurate results with internal precision of better than 5%. However, Bonifacie et al. (2007) demonstrated that Cl yields during pyrohydrolysis can vary between labs with yields as low as 40% in some of the early studies, implying that significant unquantified fractionation of halogens during extraction is possible.

Kendrick et al. (2011a, b, 2013a, 2015b) and Chavrit et al. (2016) employed 'the noble gas method' for analysis of Cl, Br, I, and K in rock chips and mineral separates whereby neutron irradiation is used to generate noble gas proxy isotopes for the halogens, which can be precisely measured by noble gas mass spectrometry (Böhlke and Irwin 1992; Johnson et al. 2000; Kendrick 2012). This technique combines the advantages of neutron activation analysis, by avoiding wet chemical extraction of halogens (or K), with very high internal precision of ~5% (2σ).

Finally, the external precision of all methods is currently limited by the availability of well characterised standards for Br and I (Kendrick 2012; Kendrick et al. 2013a; Marks et al. 2017). In addition, some differences between laboratories could be introduced by sample washing procedures, which might completely remove water soluble components from powdered samples. Water soluble halogens are especially important in marine sediments (Turekian and Wedepohl 1961) and serpentinites (e.g., Sharp and Barnes 2004).

9.6.1 Mineralogy and Cl Content of Oceanic Crust

The altered oceanic crust comprises relict glass and nominally anhydrous minerals typical of basalts and gabbros (e.g., plagioclase, pyroxene and olivine) and their hydrous alteration products. Parts of the crust that have interacted with cold seawater contain clay minerals (smectites including montmorillonite, and saponite), zeolites, and Fe-hydroxides. Glassy rocks present in hyaloclastites in Layer 2a of the crust can be extensively replaced by palagonite, which is defined as a heterogenous mixture of clays, zeolite, and oxides (Staudigel et al. 2008; Staudigel and Hart 1983; Stroncik and Schmincke 2002). At temperatures of 200–300 °C, prehnite, pumpellyite, and chlorite are important. Actinolite, tremolite, albite, epidote, and sphene become important at >300 °C, and hornblende and phlogopite can be important at >400 °C (Alt and Honnorez 1984; Bideau et al. 1991; Talbi et al. 1999). In addition, a number of minerals, including carbonate and quartz, form over

Table 9.4 Halogens and water in selected minerals of the altered oceanic lithosphere

Mineral	H_2O wt.%	Cl ppm	F ppm	Br ppm	I ppb
Low to intermediate temperature[a]					
Clay minerals	5–15	21–23	150–400		(adsorbed I?)
Palagonite	40–50	10's		<20	50–20,000
Zeolites	9–20				(adsorbed I?)
Fe-hydroxides	25–40	>4000–8000 (?)		$D_{Br/Cl} < 1$	
High temperature[b]					
Amphibole	2	<100–60,000	<100–70,000	<0.5–2	<5–70
Wide temperature range[c]					
Carbonate			1000 ± 300 (?)		<20,000 ?
Talc	5–9	400–900 (?)			
Serpentine	12–14	100–10,000	1–100	1–24	50–45,000
Fluorapatite	0–1	1000–2000	10,000–30,000		
Fluid inclusions—contribution to bulk Cl concentration					
1 vol.%	0.35	70–200		0.3–0.6	<1–20

References
[a]Kendrick et al. (2015a); Magenheim et al. (1995); Seyfried et al. (1986); Stroncik and Schmincke (2002)
[b]Bideau et al. (1991); Cortesogno et al.(2004); Gillis and Meyer (2001); Ito and Anderson (1983); Jacobson (1975); Nehlig and Juteau (1988); Prichard and Cann (1982); Vanko (1986); Kendrick et al. (2015b)
[c]Barnes et al. (2009); Bonifacie et al. (2008); Claret et al. (2010); Debret et al. (2014); John et al. (2011); Kendrick et al. (2013b); Sharp and Barnes (2004)

wide temperature ranges. The polymorphs of serpentine (chrysotile, lizardite, and antigorite) form in olivine-rich rocks between 100 and 500 °C (Bideau et al. 1991) and talc forms by silica metasomatism under all prograde conditions (Seyfried et al. 1988). Typical water contents and what is known about the halogen contents of some common alteration minerals are summarised in Table 9.4.

9.6.2 Low Temperature Seawater Alteration

Clay minerals contain a lot of water and significant F, but typically very little Cl (Table 9.4). For example smectites contain 5–15 wt% H_2O and the smectite veins analysed by Magenheim et al. (1995) had 150–400 ppm F but only ~20 ppm Cl. Kendrick et al. (2015a) reported that palagonite crusts on Samoan glass contain 35 ppm Cl which represented a 97% depletion compared to the pristine glass (Fig. 9.12). Although it is usually assumed that Cl is introduced into the oceanic crust during hydrothermal alteration, the very low Cl content of these clay minerals and palagonite demonstrates that parts of the oceanic crust could be depleted in Cl

during low temperature alteration. Alternatively, halogens might be remobilised on a local scale (Floyd and Fuge 1982), with for example, Cl released during clay alteration taken up by Fe-hydroxy chlorides (Table 9.4; Seyfried et al. 1986).

In comparison to Cl and F, even fewer data are available for Br or I. The palagonite investigated by Kendrick et al. (2015a) was less depleted in Br, than Cl, and it was enriched in I relative to pristine glass. Chavrit et al. (2016) also demonstrated I enrichment in some clay-bearing samples of altered basalt. Therefore parts of the crust could be enriched in I relative to unaltered crust, both relative to Cl and in absolute terms (e.g., high I and high I/Cl). Iodine could be trapped in altered ocean crust preferentially relative to Cl if it is adsorbed onto clay minerals (Claret et al. 2010; Montavon et al. 2014) or zeolites, which are micro-porous adsorbants. Alternatively, I is a biophilic element and there is growing evidence that microbes are involved in some styles of glass alteration (Alt and Mata 2000; Fisk et al. 1998; Kruber et al. 2008; Staudigel et al. 2008; Stroncik and Schmincke 2002) and alteration of some minerals (Ivarsson et al. 2008). Kruber et al. (2008) reported that palagonite formed by the bio-alteration of glass can contain up to 1 wt% organic C ($\delta^{13}C = -22‰$). If the microbes responsible for this alteration have an $I/C_{organic}$ similar to plankton (0.0002–0.002; Bobrov et al. 2005; Iwamoto and Shiraiwa 2012; Martin et al. 1993; Price and Calvert 1977) this would imply that exceptionally high I concentrations of ~2–20 ppm might be expected in biogenic palagonite.

In summary, low temperature alteration of the crust leading to hydration and formation of clays causes a finite increase in fluid salinity and some remobilisation of heavy halogens from the crust. However, because this alteration takes place at very high water-rock ratios the effects are difficult to discern in alteration fluids (Sect. 5.4). Low temperature alteration of mafic lithologies, either by biological processes or by adsorbtion of I onto reactive minerals, might be significant for the marine I cycle (cf., Leblanc et al. 2006).

9.6.3 High Temperature Hydrothermal Alteration

Amphibole and serpentine are usually the only minerals in which Cl (and more rarely F) can be detected by electron microprobe. Other hydrous minerals such as prehnite, pumpellyite, chlorite and epidote are assumed to contain <100 ppm Cl but remove water from the system implying that they cause a finite increase in the salinity of alteration fluids. In addition to mineral matrices, a number of minerals can be important hosts of fluid inclusions. Fluid inclusions are often estimated to account for up to 1 vol.% of coarse minerals with abundant inclusions. If these fluid inclusions trapped fluids with average salinities and densities similar to seawater, the fluid inclusions can be estimated to contribute up to 70 ppm Cl and 250 ppb Br but negligible F or I toward the mineral's bulk composition (Table 9.4). In comparison, Kendrick et al. (2015b) reported bulk halogen concentrations of

100–200 ppm Cl, 300–600 ppb Br and 4–20 ppb I for fluid inclusions bearing vein minerals from the Mathematician Ridge.

The concentrations of F and Cl in amphiboles within the oceanic crust are extremely variable ranging from concentrations of 10's of ppm Cl and 100's ppm F in igneous amphibole up to wt% levels of Cl in late-stage hydrothermal veins (Fig. 9.17; Cortesogno et al. 2004; Gillis and Meyer 2001; Jacobson 1975; Nehlig and Juteau 1988; Vanko 1986). Actinolite, present under greenschist facies conditions, generally contains <500 ppm Cl (Vanko 1986), which is consistent with the concentration range of 100–300 ppm expected to result from hydration by fluids with seawater salinity (Cortesogno et al. 2004; Kendrick et al. 2015b). In contrast, amphibolite grade hornblendes contain hundreds to thousands of ppm Cl (Cortesogno et al. 2004; Ito and Anderson 1983; Nehlig and Juteau 1988; Prichard and Cann 1982; Tribuzio et al. 2014; Vanko 1986; Silantyev et al. 2008). The variability of amphibole Cl concentrations under amphibolite conditions could reflect equilibration with segregated vapours and brines produced by phase separation of seawater that is heterogeneously distributed through this part of the crust (Cortesogno et al. 2004). Amphiboles with 1 to 6 wt% Cl have been reported from several locations but are always a volumetrically minor component of the rock, which is commonly associated with late-stage veins and/or mylonites (Bideau et al. 1991; Honnorez and Kirst 1975; Jacobson 1975; Vanko 1986). The effect of hydrothermal alteration is to introduce seawater Cl and redistribute igneous Cl and F between a growing number of amphiboles. As a result, amphiboles formed during progressive hydrothermal alteration are distinguished from igneous amphiboles by progressively higher Cl contents and Cl/Na ratios, and lower F/Cl ratios (Fig. 9.17; Coogan et al. 2001; Mevel 1988).

Crystal chemistry exerts an important control on amphibole halogen concentration. For example, the negative correlation between F/Cl and Cl in Fig. 9.17 results in part from F and Cl competing to occupy the same site in amphibole. It has long been assumed that the large Br^- and I^- anions would be preferentially

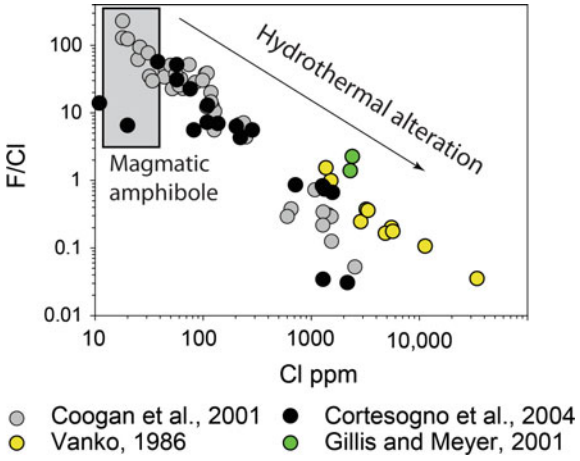

Fig. 9.17 F/Cl versus Cl concentration for amphiboles in the oceanic crust. The data of Coogan and Cullen (2009) and Cortesogno et al. (2004) were obtained by ion microprobe, whereas the data of Gillis and Meyer (2001) and Vanko (1986) are based on electron microprobe analyses

excluded from amphibole relative to Cl^- and F^- (Svensen et al. 1999, 2001), and this has recently been confirmed by the analysis of amphibole and related fluid inclusions in amphibolites and metagabbros from the Mathematician Ridge (Kendrick et al. 2015b).

In addition to crystal chemistry, it is now generally agreed that high Cl amphiboles can only form when the chemical activity of Cl is high and the chemical activity of H_2O is low, such as occurs in the presence of saline fluids (Kullerud and Erambert 1999; Markl and Bucher 1998; Vanko 1986). Therefore, Cl-rich amphiboles do not provide a mechanism for reducing fluid salinity; rather, they provide evidence for the presence of high salinity fluids in the crust.

If phase separation is the major control on fluid salinity (Kelley and Delaney 1987; Vanko 1988), the increase in amphibole Cl content from greenschist to amphibolite facies can be interpreted as evidence for efficient segregation of brines and vapours and support for the idea that brines are preferentially stored in the deeper crust (e.g., Fig. 9.14). However, while it has been recognised that crustal hydration can lead to appreciable increases in fluid salinity, the effect of 'drying up' or 'fluid desiccation' on salinity has not been evaluated within the context of the oceanic crust. For example, Kelley and Delaney (1987) suggest that formation of hydrous minerals could increase seawater salinity by a factor of two but favoured phase separation in the generation of ultra-saline brines. In contrast to this, it is well known that at water/rock ratios of less than 0.1–0.01 'drying up' leads to substantial increases in the concentration of all dissolved components (Reed 1997). Furthermore, desiccation of metamorphic fluids is implicated in the generation of Cl-rich amphiboles and metamorphic salt in granulites in northern Norway, which provides strong evidence for the generation of ultra-saline fluids (up to 100% salt) by this process in some settings (Kullerud and Erambert 1999; Markl and Bucher 1998). The high Cl content of amphibolite facies amphiboles can therefore also be interpreted as indicating fluid/rock ratios approach zero at the limit of the seafloor hydrothermal system (cf., Fig. 9.14).

The relative importance of phase separation and 'drying up' might be tested in future studies of Cl, Br, and I in fluid inclusions and minerals. As Br and I are excluded from amphibole relative to Cl (Kendrick et al. 2015b), drying up should produce fluids with very high Br/Cl and I/Cl ratios (Svensen et al. 2001). Whereas because Br/Cl does not appear to be strongly fractionated by phase separation (Fig. 9.11), phase separation might yield brines with Br/Cl and I/Cl much closer to seawater values (Kendrick et al. 2015b). This line of reasoning suggests that phase separation was the dominant process responsible for the generation of brines in the Mathematician Ridge hydrothermal system (Kendrick et al. 2015b) and brines assimilated by magmas which are all inferred to have Br/Cl ratios of only slightly higher than seawater (Fig. 9.15; Kendrick et al. 2013a, 2015a, 2017).

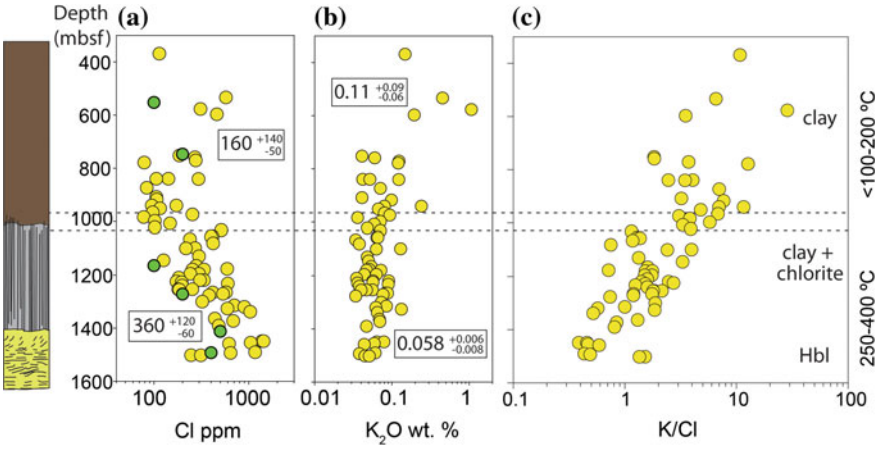

Fig. 9.18 The concentrations of **a** Cl and **b** K and **c** the K/Cl ratio of whole rock samples from IODP Hole 1256D in the East Pacific is shown as a function of depth below the seafloor. The data are from Sano et al. (2008) and Barnes and Cisneros (2012) (*green dots* in part **a**). The alteration mineralogy shown on the figure is simplified. The median Cl and K concentrations of low and high temperature alteration zones, with 2σ uncertainties, are shown for comparison

9.6.4 The Bulk Halogen Content of the Oceanic Crust

Sano et al. (2008) sampled core from Hole 1256D drilled in the Eastern Pacific at intervals of <50 m, over more than 1000 m of core, providing high density Cl concentration data that show a broad increase in Cl as a function of depth in the oceanic basement sampled by this hole (Fig. 9.18). Four additional studies have investigated Cl and Cl isotopes in seven different cores drilled in the Pacific, Atlantic, and Indian Oceans but sampling within each core is at a much lower density (Barnes and Cisneros 2012; Bonifacie et al. 2007; Chavrit et al. 2016; Magenheim et al. 1995). These studies show similar Cl concentration ranges as observed in Hole 1256D, in which low temperature alteration has a median Cl concentration of 160 ppm and high temperature alteration has a median concentration of 360 ppm Cl, but individual samples contain as little as 11 ppm or as much as 2000 ppm Cl (Fig. 9.18; Barnes and Cisneros 2012; Bonifacie et al. 2007; Chavrit et al. 2016; Magenheim et al. 1995; Sano et al. 2008). These studies indicate that the real concentration of Cl in the oceanic crust is much higher than was initially estimated (50 ± 25 ppm Cl) on the basis of electron microprobe data (Ito et al. 1983).

Unfortunately, because crustal lithologies have extremely variable Cl concentrations (e.g., 200–1200 ppm Cl at 1500 m in Hole 1256D; Fig. 9.18), the low density of data available from the majority of IODP holes means that it is difficult to assess if the broad increase in Cl observed with depth in Hole 1256D (Fig. 9.18; Sano et al. 2008) is a general feature of the oceanic crust (cf., Barnes and Cisneros 2012). However, the following observations suggest that Cl concentrations are

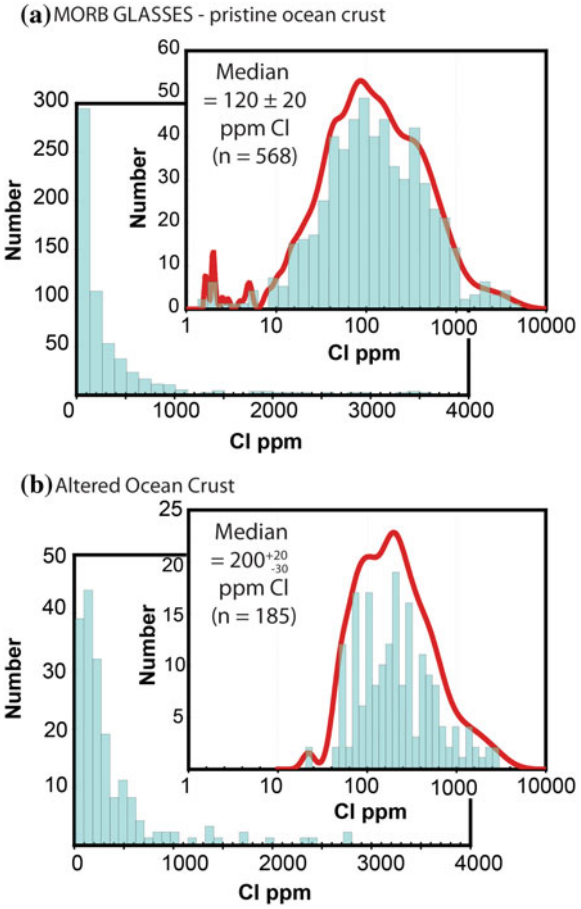

Fig. 9.19 The Cl concentrations of pristine MORB glasses and altered ocean crust. The data define log-normal distributions that are typical of trace elements. The AOC is indicated to have twice the Cl content of pristine crust on average. Glass data include N-MORB, E-MORB, and evolved glasses from the Galapagos spreading centre that have assimilated seawater Cl (Danyushevsky et al. 2000; Kamenetsky and Eggins 2012; Kendrick et al. 2012a, 2013a; le Roux et al. 2002; Michael and Cornell 1998; Saal et al. 2002; Sims et al. 2002, 2003). Altered Ocean Crust data are from Barnes and Cisneros (2012), Bonifacie et al. (2007), Floyd and Fuge (1982), Magenheim et al. (1995), and Sano et al. (2008)

likely to increase with depth: (i) Cl and Br are mobilised into the fluid during alteration of glass (Fig. 9.12; Floyd and Fuge 1982; Kendrick et al. 2015a); (ii) low temperature alteration minerals have very low Cl concentrations (Sect. 9.6.2; Table 9.4); and (iii) amphibole Cl concentrations increase from greenschist- to amphibolite-facies providing evidence for fluids becoming increasingly saline at depth in the oceanic crust (Sect. 9.6.3).

Finally, the concentration range of Cl in pristine mid-ocean ridge glasses is contrasted with the concentration range in altered oceanic rocks in Fig. 9.19. The pristine glasses include N-MORB and E-MORB and are variably evolved, with MgO mainly between 4 and 9 wt% but including some dacites from the Galapagos Spreading Centre with 1 wt% MgO. The median Cl concentration of these glasses (120 ± 20 ppm) is suggested here as a proxy for the 'initial' concentration of Cl in layer 2 (lavas and dykes) of the oceanic crust. In contrast, cumulate minerals in layer 3 gabbros will have a much lower initial concentration of Cl (and other incompatible elements) implying much lower initial Cl concentrations in deeper

portions of the crust. The suggested initial Cl concentration of layer 2 (120 ± 20 ppm Cl) is just within uncertainty of the median obtained for the upper portion of Hole 1256D (160^{+140}_{-50} ppm Cl; Figs. 9.18 and 9.19). Considering the high flux of seawater and very high water/rock ratios in this part of the crust, the lack of pronounced Cl enrichment demonstrates that the dominant effect of low temperature alteration is probably halogen remobilisation and exchange of halogens between seawater and the crust, rather than halogen enrichment. In contrast, the median concentration of Cl in the lower portion of Hole 1256D (360^{+120}_{-60} ppm Cl) is probably >3–30 times higher than the initial concentration of Cl in the gabbro cumulates (Fig. 9.18). Therefore, it appears that hydrothermal alteration may mobilise Cl in the upper crust and strongly enrich Cl in the lower crust (Figs. 9.18 and 9.19). In contrast to Cl, K exhibits the opposite behaviour, being most enriched during low temperature alteration in the upper crust. Therefore, the K/Cl ratio, which is commonly used to measure relative Cl enrichment, changes with increasing crustal depth and alteration much more sharply than the absolute abundance of either element (Fig. 9.18c).

9.6.5 *Halogens in Serpentinites*

The halogen content of seafloor serpentinites formed at varying distances from the mid-ocean ridges, including forearc settings, has been investigated in several studies (Barnes et al. 2009; Barnes and Sharp 2006; Bonifacie et al. 2008; Boschi

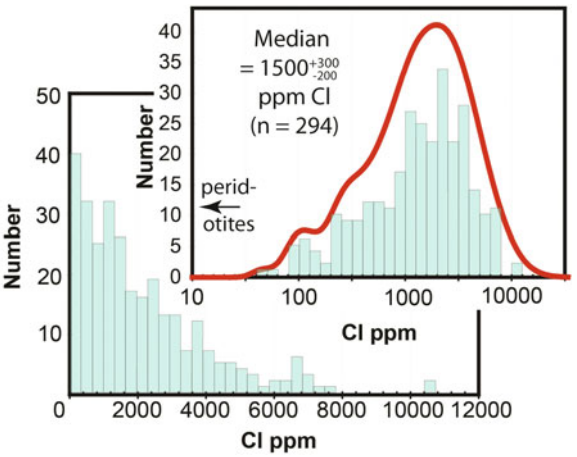

Fig. 9.20 Histogram and probability density function of serpentinite Cl concentration data. As with all trace elements, Cl tends toward a log-normal distribution, meaning the median is better defined than the mean. Data from Barnes et al. (2006, 2009), Bonifacie et al. (2008), Debret et al. (2014), John et al. (2011), Kendrick et al. (2013b), Kodolányi et al. (2012), Scambelluri et al. (2004) and Sharp and Barnes (2004)

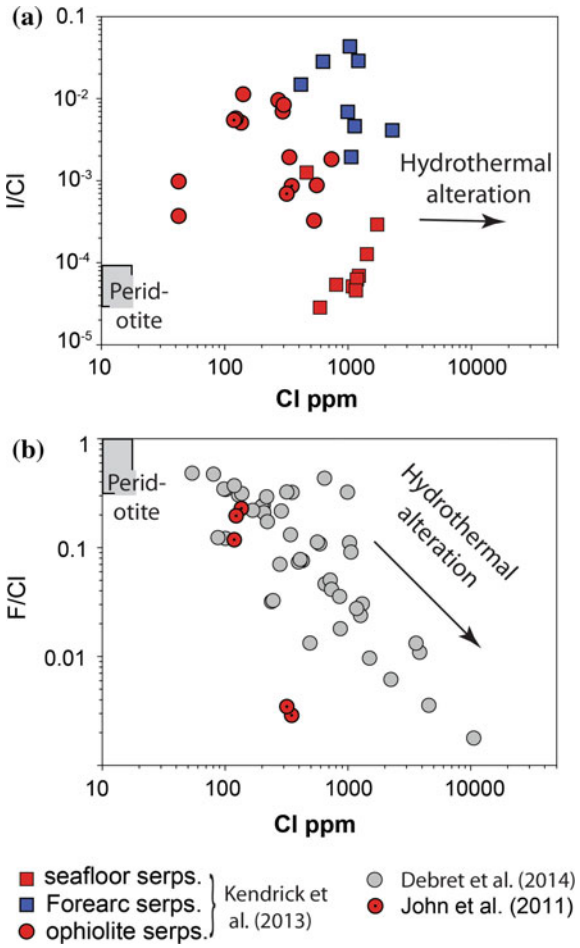

Fig. 9.21 Halogen abundance ratios as a function of Cl concentration (ppm) in lizardite and chrysotile 'pre-subduction' serpentinites. **a** I/Cl and **b** F/Cl (antigorite serpentinites are not included in these plots). The data of Kendrick et al. (2013b) are differentiated the same way as in Fig. 9.22. Additional data are from John et al. (2011) and Debret et al. (2014)

et al. 2013; Debret et al. 2014; John et al. 2011; Kendrick et al. 2013b; Kodolányi et al. 2012; Scambelluri et al. 2004; Sharp and Barnes 2004). Taken together the data show serpentinites contain from ~100 ppm to 1 wt% Cl, with a median concentration of 1500^{+300}_{-200} ppm Cl (Fig. 9.20). The maximum concentration of Cl in serpentine is somewhat less than amphibole, but serpentinite rocks, wholly dominated by serpentine, have a higher H_2O and Cl content than any other major subduction zone lithology (Scambelluri et al. 1997; Schmidt and Poli 1998).

The I/Cl ratio of serpentinites is not correlated with Cl concentration (Fig. 9.21a); however, serpentinites have combined Br/Cl and I/Cl that overlap the range of sedimentary marine pore waters and the serpentinites formed at the greatest distances from mid-ocean ridges have the highest I/Cl ratios (Fig. 9.22; Kendrick et al. 2013b). These data can be explained if sedimentary marine pore waters, as well as seawater, are involved in serpentinisation (Kendrick et al. 2011b, 2013b).

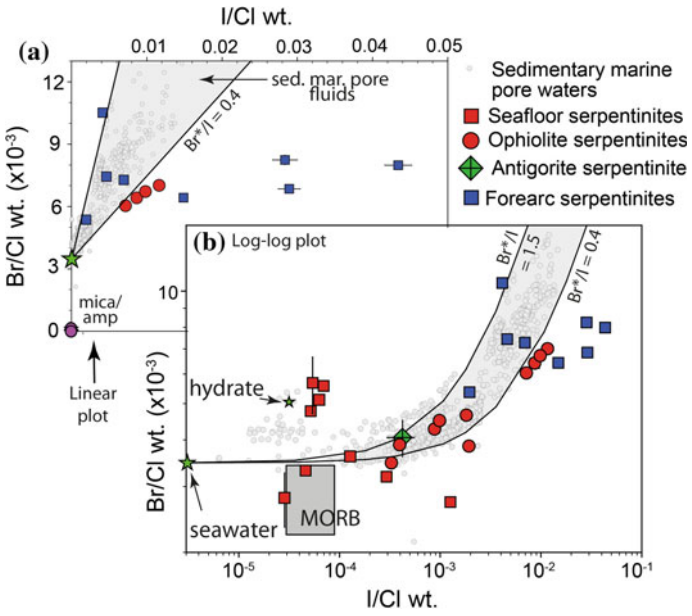

Fig. 9.22 Br/Cl versus I/Cl for serpentinites: **a** linear scale and **b** log-log scale. The trend of sedimentary marine pore waters (Fig. 9.3), gas hydrate, MORB, and the compositions on amphibole and mica are shown for reference. Serpentinite data from Kendrick et al. (2011b, 2013b); MORB field from Kendrick et al. (2013a, 2017); mica/amphibole data from Kendrick (2012) and Kendrick et al. (2015b), see Fig. 9.15

Sedimentary marine pore waters could be particularly important during serpentinisation at the slab bend and in the forearc (Fig. 9.5; Ranero et al. 2003). The small mismatch between serpentinite Br/Cl-I/Cl and sedimentary marine pore waters could be explained in several ways. The high I and Br content of the serpentinites attests to the high compatibility of all halogens in serpentine. However, it is likely that halogen abundance ratios are fractionated between serpentinites and serpentinising fluids to some degree. Alternatively, if serpentinites preserve Br/Cl and I/Cl ratios close to that of the serpentinising fluids, the data indicate that in addition to seawater and sediment-derived halogens, some serpentinites contain an additional small 'mantle' component that could be mobilised from igneous lithologies in the overlying crustal rocks (Figs. 9.22 and 9.23). Slab fluids with fractionated I/Cl are then required to explain the highest I/Cl of 0.04 in forearc serpentinites because it is greater than observed in sedimentary pore waters (Fig. 9.22a; Kendrick et al. 2013b).

In contrast to I/Cl and Br/Cl, the F/Cl ratio is negatively correlated with Cl in serpentinites (Fig. 9.21b) in a similar manner to that observed for amphibole (Fig. 9.17). It is likely that the compatibility of F is at least as high as the heavy halogens in serpentine, but the negative relationship between F/Cl and Cl can be explained if serpentinising fluids introduce variable quantities of seawater and sediment-derived Cl, Br, and I, and relatively little F (Figs. 9.22 and 9.23). There

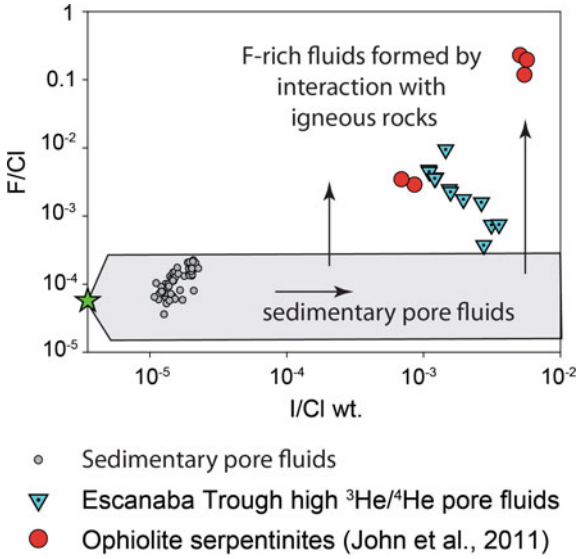

Fig. 9.23 Serpentinite F/Cl versus I/Cl data. Serpentinite data from John et al. (2011). Pore fluid data from Gieskes and Mahn (2007). Escanaba Trough high $^{3}He/^{4}He$ pore fluid data (representative of hydrothermal fluids) from Gieskes et al. (2002)

are very few combined F/Cl and I/Cl data available for sedimentary pore waters (Mahn and Gieskes 2001). However, the low solubility of F in sedimentary pore waters (Frohlich et al. 1983; Rude and Aller 1994) suggests F/Cl is likely to be maintained fairly close to the seawater value. Therefore, the higher F/Cl of serpentinites and some hydrothermal fluids, relative to seawater, probably results from mobilisation of F from igneous lithologies in the crust (Fig. 9.23).

The median Cl concentration of 1500^{+300}_{-200} ppm in serpentinites corresponds to a H_2O/Cl weight ratio of ~ 80 that is greater than the seawater H_2O/Cl value of 50. Serpentinites with much higher Cl concentrations are probably produced as the water 'drys up' and the salinity of the serpentinising fluid increases (e.g., H_2O/Cl decreases). Kendrick et al. (2011a, b, 2013b) suggested a water/rock ratio of <0.1 and that the fluid being spent during serpentinisation (e.g., dried up) might be required to explain the preservation of sediment pore water halogen signatures (Fig. 9.22) and high noble gas concentrations in serpentine. However, metamorphic salts produced by complete drying up (e.g., Markl and Bucher 1998) have not been identified in crushed serpentinites. The nature of the 'water soluble Cl component' in serpentinites is still unclear (Kodolányi et al. 2012) and experimental studies are required to determine halogen partitioning in serpentinites.

9.7 Synthesis and Future Directions

As shown above there are a relatively large number of data available for F, Cl, Br, and I in sedimentary pore waters and hydrothermal fluids, but the data base for multiple halogens in minerals within sediments and the crustal basement is much

smaller. As a result, while Cl, Br, and I are known to exhibit systematic behaviour in sedimentary pore waters and the organic phase within unconsolidated sediment (Figs. 9.2 and 9.3), the relative abundance ratios of F/Cl, Br/Cl, and I/Cl and the halogen concentrations in lithified sediments are less well known. Chlorine and F data, and limited Br and I data, are available for altered basalts and gabbros, and serpentinites. Despite the limitations imposed by data availability, some general statements about the most important lithologies and guestimates of likely concentration ranges in key crustal lithologies are possible. This is undertaken below for each of the halogens in a 'representative crustal section' entering a subduction zone. This is undertaken for the crust immediately prior to subduction, because the final state of the oceanic crust is relevant for assessing possible fluxes of halogens into the deep mantle and through magmatic arcs, which is a critical parameter given the role of halogens in complexing metals and facilitating trace element transport in slab-derived fluids (Migdisov and Williams-Jones 2014; Yardley 2005).

The representative crustal section investigated comprises 400 m of marine sediment, 1500 m of layer 2 lavas and dykes, 4500 m of layer 3 gabbros, and 500 m of serpentinites (Fig. 9.24). These thicknesses are based on average crust (Chen 1992; Snow and Edmonds 2007) and a band of serpentinite, which could represent either intense local zones of serpentinisation, or diffuse serpentinisation of

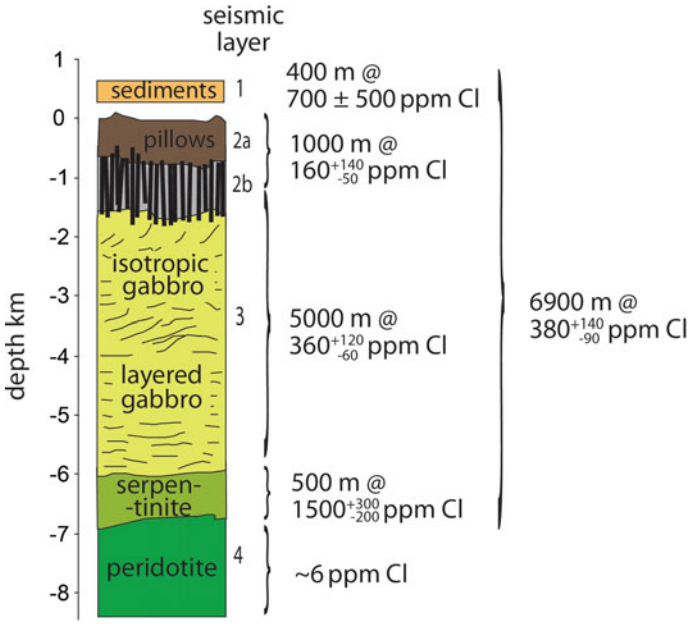

Fig. 9.24 Schematic diagram of a representative, oceanic lithospheric cross section with estimated Cl concentrations at the point of subduction. Note that the average extent of alteration in the deep crust and lithospheric mantle are poorly defined and these figures assume significant alteration at the slab bend prior to subduction (see text for discussion)

the uppermost 10 km of the lithospheric mantle formed at the slab bend (Fig. 9.5). The degree of lithospheric serpentinisation is still poorly known, and given that additional serpentinisation occurs in the forearc (Bostock et al. 2002), this figure is considered a conservative lower limit for the amount of serpentinite subducted into the mantle.

The existing data suggest that Cl concentrations increase with depth in the altered oceanic crust (Fig. 9.18). However, for simplicity we assume that the upper 1000 m of the oceanic crust, which has been subjected to relatively low temperature alteration, has a median concentration of 160^{+140}_{-50} ppm Cl, and that the lower 5000 m has a median concentration of 360^{+120}_{-60} ppm Cl (cf., Figs. 9.18 and 9.24). It is possible that away from the subduction zones a large portion of the crust, at depths of 4–6 km, could be unaltered. However, it is assumed that at the point of subduction, fluids have penetrated the entire crustal section, which is consistent with seismic evidence for serpentinisation of the mantle lithosphere at the slab bend (Fig. 9.5; Ranero et al. 2003) and heat flow measurements (Grevemeyer et al. 2005). In this scenario, it is likely that at increasing depths, zones of relatively unaltered crust are transected by increasingly Cl-rich zones of alteration, reflecting channelized fluid flow within deep fracture systems. This would lead to extremely variable concentrations of Cl in the deeper crust, similar to that observed in existing drill hole data and dredge samples; for example, Fig. 9.18 shows concentrations ranging from 200 to 1200 ppm Cl at ~1200 m in Hole 1256D (Sano et al. 2008). In comparison to the oceanic crust, sediments are assumed to have a poorly defined Cl concentration of 700 ± 500 ppm (cf., Table 9.2; Muramatsu and Wedepohl 1998) and serpentinites are assigned the median value of 1500^{+300}_{-200} ppm Cl (Figs. 9.20 and 9.24). These figures suggest that the subducting lithosphere could have a bulk Cl concentration on the order of 400 ppm (Fig. 9.24). This figure is close to the median value suggested for altered ocean crust (Fig. 9.24), and implies that due to its size, the altered ocean crust could be the largest single Cl reservoir in subducting slabs (Fig. 9.25). However, it should be stressed that there is considerable uncertainty concerning the degree of deep-crust and lithosphere alteration, and that the relative sizes of the altered ocean crust and serpentinite reservoirs in Fig. 9.24 could be substantially different.

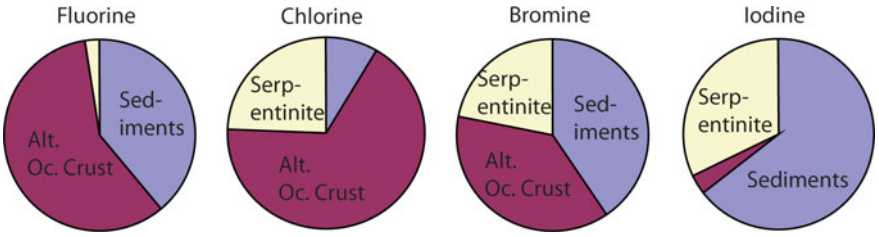

Fig. 9.25 Pie charts showing the relative importance of sediments, altered ocean crust and serpentinites as reservoirs for F, Cl, Br and I in the oceanic lithosphere, under the assumptions used to construct Fig. 9.24 (Table 9.5; Sect. 9.7)

Table 9.5 Summary of halogens in sediments, altered ocean crust, and serpentinites

	Thickness (km)	F ppm	Cl ppm	Br ppm	I ppm
Marine sediments	0.4	1000 ± 300	700 ± 500	60 ± 60	30 ± 25
Mature/lith. seds		1000 ± 300	700 ± 500	12 ± 10	4 ± 3
AOC—layer 2	1–1.5	260 ± 160	160^{+140}_{-50}	$0.3^{+0.3}_{-0.2}$	$0.02^{+0.02}_{-0.01}$
AOC—layer 3	4.5–5	50 ± 40	360^{+120}_{-60}	0.7 ± 0.4	0.01 ± 0.01
Serpentinites	0.5	50 ± 40	1500^{+300}_{-200}	5 ± 1	1.5 ± 1.5
Bulk lithosphere	6.9	100 ± 50	380^{+140}_{-90}	3 ± 2	1.6 ± 1.5

Data from Tables 9.2 and 9.4 and Figs. 9.1, 9.2, 9.3, 9.4, 9.5, 9.6, 9.7, 9.8, 9.9, 9.10, 9.11, 9.12, 9.13, 9.14, 9.15, 9.16, 9.17, 9.18, 9.19, 9.20, 9.21, 9.22 and 9.23. *AOC* Altered Ocean Crust

In contrast to Cl, there are fewer data available for F. However, because F is mobilised over relatively short distances during alteration and is not significantly introduced by seawater, we assume the F concentration in layer 2 of altered ocean crust is similar to that of MORB. The average F concentration of MORB is estimated as 260 ± 160 ppm F, based on a F/Nd = 20 ± 12 (Workman et al. 2006) and Nd of ~13 ppm, which is 10 times the primitive mantle value (Hofmann 2003). Serpentinites have typical F concentrations of 1–100 ppm (Debret et al. 2014; John et al. 2011), which overlap depleted mantle values of 11–16 ppm F (Pyle and Mather 2009). We assume that where a F enrichment is observed, the F has been mobilised from overlying lithologies in layers 2–3 of the crust (Fig. 9.23). Marine sediments are assigned a concentration of 1000 ± 300 ppm F (Fig. 9.1; Li 1991; Rude and Aller 1991). These assumptions suggest that taken as a whole the altered oceanic lithosphere contains on the order of 100 ± 50 ppm F (Table 9.5). Therefore, the altered oceanic lithosphere has a F/Cl weight ratio of ~0.25 compared to ~2 for median MORB, with the difference resulting from up to ~90% of crustal Cl being introduced by hydrothermal alteration.

The Br and I content of altered oceanic crust is poorly known. It has been suggested that low temperature clay-rich alteration could be enriched in I and have higher I/Cl than MORB, whereas high temperature amphibole alteration has Br/Cl and I/Cl of less than MORB (Sects. 9.6.2 and 9.6.3; Chavrit et al. 2016; Kendrick et al. 2015b). If the altered oceanic crust retains Br/Cl and I/Cl within a factor of 2 of MORB, we can estimate it has ppb-levels of Br and I. In contrast, sediments and serpentinites both have extremely variable Br/Cl and I/Cl ratios with ppm levels of Br and I (Tables 9.2 and 9.5). In contrast to the altered oceanic crust, serpentinites formed in the mantle lithosphere can incorporate substantial Br and I and may even preserve the Br/Cl, I/Cl, and F/Cl ratios of the serpentinising fluids (cf., Figs. 9.22 and 9.23). The small amount of data available mean that the average Br/Cl and I/Cl of the serpentinites is not known (Fig. 9.22). However, even under the conservative assumptions made above regarding the extent of lithospheric serpentinisation

(Fig. 9.24), serpentinite rocks rich in chrysotile or lizardite have the potential to be a major reservoir of Br and I (Table 9.5; Fig. 9.25). As a result, serpentinites have the potential to be an important pathway for Br and I into subduction zones, however, it has been suggested that Br and I are preferentially lost relative to Cl during high grade metamorphism and antigoritisation of serpentine meaning that Br and I are unlikely to be strongly subducted into the deep mantle (cf., Fig. 9.25; John et al. 2011; Kendrick et al. 2011b, 2013b, 2014, 2017).

Further work combining the analysis of multiple halogens in hydrothermal fluids is now desirable. In particular, analysis of I in hydrothermal fluids together with Br and Cl would help confirm if hydrothermal fluids with elevated Br/Cl ratios have interacted with sediments (cf., Fig. 9.11). In addition, it is important to improve linkages in understanding between the behaviour of halogens in hydrothermal fluids and changes in alteration mineralogy. This is required to test the range of conditions under which Br and Cl can be safely regarded as behaving conservatively. The possible importance of low temperature alteration for the marine I cycle is yet to be evaluated and further data are required for all the halogens in bulk rock samples, individual mineral phases, and fluid inclusions within the oceanic crust and lithospheric mantle. The extreme heterogeneity of alteration in the oceanic crust and lithosphere implies a high density of data is required to identify broad trends in changing halogen concentrations laterally or as a function of depth (e.g., Fig. 9.18).

Acknowledgements Mark A. Kendrick is supported by an Australian Research Council Future Fellowship (FT130100141). I am grateful to Zach Sharp and Michael Mottl for their constructive reviews of this chapter and also to several colleagues whom I have collaborated with, or discussed halogen geochemistry, over the years.

References

Alt J, Honnorez J (1984) Alteration of the upper oceanic crust, DSDP site 417: mineralogy and chemistry. Contrib Mineral Petrol 87:149–169

Alt JC, Mata P (2000) On the role of microbes in the alteration of submarine basaltic glass: a TEM study. Earth Planet Sci Lett 181:301–313

Aranovich LY, Bortnikov NS, Serebryakov NS, Sharkov EV (2010) Conditions of the formation of plagiogranite from the Markov trough, Mid-Atlantic Ridge, 5A degrees 52′-6A degrees 02′ N. Dokl Earth Sci 434(1):1257–1262

Aranovich LYa, Prokofiev VYu, Pertsev AN, Bortnikov NS, Ageeva OA, Bel'tenev VE, Borisovsky SE, Simakin SG (2015) Composition and origin of a K_2O-rich granite melt in the mid-Atlantic Ridge, 13°34′ N: evidence from the analysis of melt inclusions and minerals of the gabbro–plagiogranite association. Dokl Earth Sci 460:174–178

Anderson BW, Coogan LA, Gillis KM (2012) The role of outcrop-to-outcrop fluid flow in off-axis oceanic hydrothermal systems under abyssal sedimentation conditions. J Geophys Res Solid Earth 117(B05):103

Anderson RN, Zoback MD, Hickman SH, Newmark RL (1985) Permeability versus depth in the upper oceanic crust—in situ measurements in DSDP Hole 504B, Eastern Equatorial Pacific. Earth Planet Sci Lett 90:3659–3669

Baker ET (2007) Hydrothermal cooling of midocean ridge axes: do measured and modeled heat fluxes agree? Earth Planet Sci Lett 263:140–150

Baker ET, German CR (2004) On the global distribution of hydrothermal vent fields. In: German CR, Lin J, Parson LM (eds) Mid-ocean ridges: hydrothermal interactions between the lithosphere and oceans. American Geophysical Union, Washington, pp 245–266

Barnes JD, Cisneros M (2012) Mineralogical control on the chlorine isotope composition of altered oceanic crust. Chem Geol 326–327:51–60

Barnes JD, Sharp ZD (2006) A chlorine isotope study of DSDP/ODP serpentinized ultramafic rocks: Insights into the serpentinization process. Chem Geol 228:246–265

Barnes JD, Paulick H, Sharp ZD, Bach W, Beaudoin G (2009) Stable isotope ($\delta^{18}O$, δD, $\delta^{37}Cl$) evidence for multiple fluid histories in mid-Atlantic abyssal peridotites (ODP Leg 209). Lithos 110:83–94

Baturin GN (1988) The geochemistry of manganese and manganese nodules in the ocean. D. Reidel Publishing Company, Boston, 342 pp

Baturin GN, Dubinchuk VT (2011) Mineralogy and chemistry of ferromanganese crusts from the Atlantic Ocean. Geochem Int 49:578–593

Bein A, Hovorka SD, Fisher RS, Roedder E (1991) Fluid inclusions in bedded permian halite, Palo Duro Basin, Texas—Evidence for modification of seawater in evaporite brine-pools and subsequent early diagenesis. J Sediment Petrol 61:1–14

Berndt ME, Seyfried WE (1990) Boron, bromine and other trace-elements as clues to the fate of chlorine in midocean ridge vent fluids. Geochim Cosmochim Acta 54:2235–2245

Berndt ME, Seyfried WE (1997) Calibration of Br/Cl fractionation during subcritical phase separation of seawater: possible halite at 9 to 10° N East Pacific Rise. Geochim Cosmochim Acta 61:2849–2854

Berndt ME, Seyfried WE Jr, Janecky DR (1989) Plagioclase and epidote buffering of cation ratios in mid-ocean ridge hydrothermal fluids: experimental results in and near the supercritical region. Geochim Cosmochim Acta 53:2283–2300

Bernini D, Wiedenbeck M, Dolejs D, Keppler H (2013) Partitioning of halogens between mantle minerals and aqueous fluids: implications for the fluid flow regime in subduction zones. Contrib Mineral Petrol 165:117–128

Bideau D, Hebert R, Hekinian R, Cannat M (1991) Metamorphism of deep seated rocks from the Garrett ultrafast transform (East Pacific Rise near 13°25'S). J Geophys Res Solid Earth Planet 96:10079–10099

Bird P (2003) An updated digital model of plate boundaries. Geochem Geophys Geosyst 4:1027

Bischoff JL, Dickson FW (1975) Seawater-basalt interaction at 200 °C and 500 bars—Implications for the origin of seafloor heavy-metal deposits and regulation of seawater chemistry. Earth Planet Sci Lett 25:385–397

Bischoff JL, Pitzer KS (1989) Liquid-vapor relations for the system NaCl-H_2O; summary of the P-T-x surface from 300° to 500° C. Am J Sci 289:217–248

Bischoff JL, Rosenbauer RJ (1984) The critical point and two-phase boundary of seawater, 200–500°C. Earth Planet Sci Lett 68:172–180

Bischoff JL, Rosenbauer RJ (1989) Salinity variations in submarine hydrothermal systems by layered double diffusive convection. J Geol 97:613–623

Bischoff JL, Rosenbauer RJ, Fournier RO (1996) The generation of HCl in the system $CaCl_2$-H_2O: Vapor-liquid relations from 380-500° C. Geochim Cosmochim Acta 60:7–16

Bobrov VA, Phedorin MA, Leonova GA, Kolmogorov YP (2005) SR XRF element analysis of sea plankton. Nuclear Instruments & Methods in Physics Research Section a-Accelerators Spectrometers Detectors and Associated Equipment 543:259–265

Böhlke JK, Irwin JJ (1992) Laser microprobe analyses of noble gas isotopes and halogens in fluid inclusions: Analyses of microstandards and synthetic inclusions in quartz. Geochim Cosmochim Acta 56:187–201

Bonifacie M, Jendrzejewski N, Agrinier P, Coleman M, Pineau F, Javoy M (2007) Pyrohydrolysis-IRMS determination of silicate chlorine stable isotope compositions. Application to oceanic crust and meteorite samples. Chem Geol 242:187–201

Bonifacie M, Busigny V, Mevel C, Philippot P, Agrinier P, Jendrzejewski N, Scambelluri M, Javoy M (2008) Chlorine isotopic composition in seafloor serpentinites and high-pressure metaperidotites. Insights into oceanic serpentinization and subduction processes. Geochim Cosmochim Acta 72:126–139

Boschi C, Bonatti E, Ligi M, Brunelli D, Cipriani A, Dallai L, D'Orazio M, Früh-Green GL, Tonarini S, Barnes JD, Bedini RM (2013) Serpentinization of mantle peridotites along an uplifted lithospheric section, Mid Atlantic Ridge at 11° N. Lithos 178:3–23

Bostock MG, Hyndman RD, Rondenay S, Peacock SM (2002) An inverted continental Moho and serpentinization of the forearc mantle. Nature 417:536–538

Butterfield DA, Massoth GJ, McDuff RE, Lupton JE, Lilley MD (1990) Geochemistry of hydrothermal fluids from axial seamount hydrothermal emissions study vent field, Juan de Fuca Ridge: subseafloor boiling and subsequent fluid-rock interaction. J Geophys Res 95 (B8):12895

Butterfield DA, Jonasson IR, Massoth GJ, Feely RA, Roe KK, Embley RE, Holden JF, McDuff RE, Lilley MD, Delaney JR, Pyle D (1997) Seafloor eruptions and evolution of hydrothermal fluid chemistry [and discussion]. Philos Trans Math Phys Eng Sci 355:369–386

Campbell AC, Edmond JM (1989) Halide systematics of submarine hydrothermal vents. Nature 342:168–170

Campbell AC, Bowers TS, Measures CI, Falkner KK, Khadem M, Edmond JM (1988) A time series of vent fluid compositions from 21° N, East Pacific Rise (1979, 1981, 1985), and the Guaymas Basin, Gulf of California (1982, 1985). J Geophys Res Solid Earth Planet 93:4537–4549

Campbell AC, German C, Palmer MR, Gamo T, Edmond JM (1994) Chapter 11. Geochemistry of hydrothermal fluids from escanaba trough, gorda ridge, geological, hydrothermal and biologic studies at escanaba trough, gorda ridge, offshore Northern California. USGS Bulletin. USGS, pp 201–221

Carpenter R (1969) Factors controlling the marine geochemistry of fluorine. Geochim Cosmochim Acta 33:1153–1167

Castelain T, McCaig AM, Cliff RA (2014) Fluid evolution in an oceanic core complex: a fluid inclusion study from IODP Hole U1309 D-Atlantis Massif, 30° N, Mid-Atlantic Ridge. Geochem Geophys Geosyst 15:1193–1214

Chavrit D, Burgess R, Sumino H, Teagle DAH, Droop G, Shimizu A, Ballentine CJ (2016) The contribution of hydrothermally altered ocean crust to the mantle halogen and noble gas cycles. Geochim Cosmochim Acta 183:106–124

Chen YJ (1992) Oceanic crustal thickness versus spreading rate. Geophys Res Lett 19:753–756

Claret F, Lerouge C, Laurioux T, Bizi M, Conte T, Ghestem JP, Wille G, Sato T, Gaucher EC, Giffaut E, Tournassat C (2010) Natural iodine in a clay formation: Implications for iodine fate in geological disposals. Geochim Cosmochim Acta 74:16–29

Collins AG (1969) Chemistry of some Andarko Basin brines containing high concentrations of iodine. Chem Geol 4:169–187

Conference Participants (1972) Penrose field conference: ophiolites. Geotimes 17:24–25

Coogan LA, Wilson RN, Gillis KM, MacLeod CJ (2001) Near-solidus evolution of oceanic gabbros: insights from amphibole geochemistry. Geochim Cosmochim Acta 65:4339–4357

Coombs ML, Sisson TW, Kimura JI (2004) Ultra-high chlorine in submarine Kilauea glasses: evidence for direct assimilation of brine by magma. Earth Planet Sci Lett 217:297–313

Cortesogno L, Gaggero L, Zanetti A (2004) Rare earth and trace elements in amphiboles of oceanic gabbros (MARK area, mid-atlantic ridge) at medium to low-temperature seafloor alteration. Ofioliti 29:107–123

Cosgrove ME (1970) Iodine in bituminous kimmeridge shales of Dorset coast, England. Geochim Cosmochim Acta 34:830–836

Dalou Cl, Koga K, Shimizu N, Boulon J, Devidal JL (2012) Experimental determination of F and Cl partitioning between lherzolite and basaltic melt. Contrib Mineral Petrol 163:591–609

Danyushevsky LV, Eggins SM, Falloon TJ, Christie DM (2000) H_2O abundance in depleted to moderately enriched mid-ocean ridge magmas; Part I: incompatible behaviour, implications for mantle storage, and origin of regional variations. J Petrol 41:1329–1364

Debret B, Koga KT, Nicollet C, Andreani M, Schwartz S (2014) F, Cl and S input via serpentinite in subduction zones: implications for the nature of the fluid released at depth. Terra Nova 26:96–101

de Martin BJ, Sohn RA, Canales JP, Humphris SE (2007) Kinematics and geometry of active detachment faulting beneath the trans-atlantic geotraverse (TAG) hydrothermal field on the mid-atlantic ridge. Geology 35:711–714

Dick HJB, Lin J, Schouten H (2003) An ultraslow-spreading class of ocean ridge. Nature 426:405–412

Dick HJB, Natland JH, Ildefonse B (2006) Past and future impact of deep drilling in the oceanic crust and mantle. Oceanography 19:72–80

Dixon JE, Stolper EM, Holloway JR (1995) An experimental study of water and carbon dioxide solubilities in mid ocean ridge basaltic liquids.1. Calibration solubility models J Petrol 36:1607–1631

Drever JI (1997) The geochemistry of natural waters: surface and groundwater environments, 3rd edn. Prentice-Hall Inc., Upper Saddle River, NJ

Driesner T, Heinrich CA (2007) The system H_2O–NaCl. Part I: Correlation formulae for phase relations in temperature-pressure-composition space from 0 to 1000 °C, 0 to 5000 bar, and 0 to 1 XNaCl. Geochim Cosmochim Acta 71:4880–4901

Edmond JM, Measures C, McDuff RE, Chan LH, Collier R, Grant B, Gordon LI, Corliss JB (1979) Ridge crest hydrothermal activity and the balances of the major and minor elements in the ocean—Galapagos data. Earth Planet Sci Lett 46:1–18

Elderfield H, Truesdale VW (1980) On the biophilic nature of iodine in seawater. Earth Planet Sci Lett 50:105–114

Fehn U, Snyder G, Egeberg PK (2000) Dating of pore waters with I-129: relevance for the origin of marine gas hydrates. Science 289:2332–2335

Fehn U, Snyder GT, Matsumoto R, Muramatsu Y, Tomaru H (2003) Iodine dating of pore waters associated with gas hydrates in the Nankai area, Japan. Geology 31:521–524

Fehn U, Lu Z, Tomaru H (2006) ^{129}I/I ratios and halogen concentrations in pore water of Hydrate Ridge and their relevence for the origin of gas hydrates: a progress report. In: Trehu AM, Bohrmann G, Torres ME, Colwell FS (eds) Proceedings of the Ocean Drilling Program, Scientific Results, pp 1–25

Fehn U, Moran JE, Snyder GT, Muramatsu Y (2007a) The initial ^{129}I/I ratio and the presence of 'old' iodine in continental margins. Nucl Instrum Methods Phys Res Sect B 259:496–502

Fehn U, Snyder GT, Muramatsu Y (2007b) Iodine as a tracer of organic material: ^{129}I results from gas hydrate systems and fore arc fluids. J Geochem Explor 95:66–80

Fisher AT (1998) Permeability within basaltic oceanic crust. Rev Geophys 36:143–182

Fisher AT, Becker K (2000) Channelized fluid flow in oceanic crust reconciles heat-flow and permeability data. Nature 403:71–74

Fisk MR, Giovannoni SJ, Thorseth IH (1998) Alteration of oceanic volcanic glass: textural evidence of microbial activity. Science 281:978–980

Floyd PA, Fuge R (1982) Primary and secondary alkali and halogen element distribution in Iceland research drilling project basalts from Eastern Iceland. J Geophys Res 87:6477–6488

Fontes JC, Matray JM (1993) Geochemistry and origin of formation brines from the Paris Basin, France 1. Brines associated with triassic salts. Chem Geol 109:149–175

Fournier RO, Thompson JM (1993) Composition of steam in the system NaCl-KCl-H_2O-quartz at 600 °C. Geochim Cosmochim Acta 57:4365–4375

Foustoukos DI, Seyfried WE (2007) Trace element partitioning between vapor, brine and halite under extreme phase separation conditions. Geochim Cosmochim Acta 71:2056–2071

Francois R (1987) The influence of humic substances on the geochemistry of iodine in nearshore and hemipelagic marine-sediments. Geochim Cosmochim Acta 51:2417–2427

Freund S, Beier C, Krumm S, Haase KM (2013) Oxygen isotope evidence for the formation of andesitic–dacitic magmas from the fast-spreading Pacific-Antarctic Rise by assimilation–fractional crystallisation. Chem Geol 347:271–283

Frohlich PN, Kim KH, Jahnke R, Burnett WC, Soutar A, Deakin M (1983) Pore water fluoride in Peru continental margin sediments: uptake from seawater. Geochim Cosmochim Acta 47:1605–1612

Fryer P (2002) Recent studies of serpentinite occurrences in the oceans: Mantle-ocean interactions in the plate tectonic cycle. Chem Erde Geochem 62:257–302

Fuge R, Johnson CC (1986) The geochemistry of iodine—a review. Environ Geochem Health 8:31–54

Gall EA, Kupper FC, Kloareg B (2004) A survey of iodine content in Laminaria digitata. Bot Mar 47:30–37

Gieskes JM, Mahn C (2007) Halide systematics in interstitial waters of ocean drilling sediment cores. Appl Geochem 22:515–533

Gieskes JM, Mahn CL, Schnetzger B (2000) Data report: trace element geochemistry of I^-, Br^-, F^-, HPO_4^{2-}, Ba^{2+}, and Mn^{2+} in pore waters of Escanaba Trough, sites 1037 and 1038. In: Zierenberg RA, Fouquet Y, Miller DJ, Normark WR (eds) Proceedings of the ocean drilling program scientific results. Texas A&M University, College Station, TX, pp 1–16

Gieskes JM, Simoneit BRT, Goodfellow WD, Baker PA, Mahn C (2002) Hydrothermal geochemistry of sediments and pore waters in Escanaba Trough—ODP Leg 169. Appl Geochem 17:1435–1456

Gillis KM, Meyer PS (2001) Metasomatism of oceanic gabbros by late stage melts and hydrothermal fluids: evidence from the rare earth element composition of amphiboles. Geochem Geophys Geosyst 2:2000GC000087

Glasby GP (1973) Mechanisms of enrichment of the rarer elements in marine manganese nodules. Mar Chem 1:105–125

Glasby GP (1998) The relation between earthquakes, faulting, and submarine hydrothermal mineralization. Mar Georesour Geotechnol 16:145–175

Glasby GP, Keays RR, Rankin PC (1978) Distribution of rare earth, precious metal and other trace elements in recent and fossil deep manganese nodules. Geochem J 12:229–243

Glaus MA, Muller W, Van Loon LR (2008) Diffusion of iodide and iodate through Opalinus Clay: monitoring of the redox state using an anion chromatographic technique. Appl Geochem 23:3612–3619

Goldberg WM, Hopkins TL, Holl SM, Schaefer J, Kramer KJ, Morgan TD, Kim K (1994) Chemical-composition of the sclerotized black coral skeleton (coelenterata, Antipatharia)—A comparison of 2 species. Comp Biochem Physiol B Biochem Mol Biol 107:633–643

Grevemeyer I, Kaul N, Diaz-Naveas JL, Villinger HW, Ranero CR, Reichert C (2005) Heat flow and bending-related faulting at subduction trenches: case studies offshore of Nicaragua and Central Chile. Earth Planet Sci Lett 236:238–248

Hannington M, Jamieson J, Monecke T, Petersen S, Beaulieu S (2011) The abundance of seafloor massive sulfide deposits. Geology 39:1155–1158

Hanor JS (1994) Origin of saline fluids in sedimentary basins. In: Parnell J (ed) Geofluids: origin, migration and evolution of fluids in sedimentary basins. Geological Society Special Publication, London, pp 151–174

Hein JR, Koschinsky A (2014) 13.11—Deep-ocean ferromanganese crusts and nodules. In: Turekian HDHK (ed) Treatise on geochemistry, 2nd edn. Elsevier, Oxford, pp 273–291

Hermann AG (1980) Bromide distribution between halite and NaCl-saturated seawater. Chem Geol 28:171–177

Hess HH (1962) History of Ocean basins. In: Engel AEJ, James HL, Leonard BF (eds) Petrologic sudies: a volume to honour A.F. Buddington. Geological Society of America, pp 599–620

Hofmann AW (2003) Sampling mantle heterogeneity through oceanic basalts: isotopes and trace elements. In: Carlson RL (ed) Treatise of geochemistry, vol 2: the core and mantle. Elsevier, Amsterdam, pp 61–101

Holser WT (1979) Trace elements and isotopes in evaporites. In: Burns RG (ed) Marine minerals. Mineralogical Society of America short course notes, pp 295–346

Honnorez J, Kirst P (1975) Petrology of rodingites from equatorial mid-Atlantic fracture zones and their geotectonic significance. Contrib Mineral Petrol 49:233–257

Hovey JK, Pitzer KS, Tanger JC, Bischoff JL, Rosenbauer RJ (1990) Vapour-liquid phase equilibria of potassium chloride-water mixtures: equation-of-state representation for KCl-H_2O and NaCl-H_2O. J Phys Chem 94:1175–1179

Huang Z, Ito K, Morita I, Yokota K, Fukushi K, Timerbaev AR, Watanabe S, Hirokawa T (2005) Sensitive monitoring of iodine species in sea water using capillary electrophoresis: vertical profiles of dissolved iodine in the Pacific Ocean. J Environ Monit 7:804–808

Humphris SE, Cann JR (2000) Constraints on the energy and chemical balances of the modern TAG and ancient Cyprus seafloor sulfide deposits. J Geophys Res Solid Earth 105:28477–28488

Humphris SE, Thompson G (1978) Hydrothermal alteration of oceanic basalts by seawater. Geochim Cosmochim Acta 42:107–125

Hutnak M, Fisher AT, Harris R, Stein C, Wang K, Spinelli G, Schindler M, Villinger H, Silver E (2008) Large heat and fluid fluxes driven through mid-plate outcrops on ocean crust. Nat Geosci 1:611–614

Ichikuni M (1979) Uptake of fluoride by aragonite. Chem Geol 27:207–214

Ishibashi J, Grimaud D, Nojiri Y, Auzende JM, Urabe T (1994) Fluctuation of chemical compositions of the phase-separated hydrothermal fluid from the North Fiji Basin Ridge. Mar Geol 116(1–2):215–226

Ishibashi J-I, Sato M, Sano Y, Wakita H, Gamo T, Shanks Iii WC (2002) Helium and carbon gas geochemistry of pore fluids from the sediment-rich hydrothermal system in Escanaba trough. Appl Geochem 17:1457–1466

Ito E, Anderson AT Jr (1983) Submarine metamorphism of gabbros from the Mid-Cayman Rise: petrographic and mineralogic constraints on hydrothermal processes at slow-spreading ridges. Contrib Mineral Petrol 82:371–388

Ito E, Harris DM, Anderson AT (1983) Alteration of oceanic-crust and geologic cycling of chlorine and water. Geochim Cosmochim Acta 47:1613–1624

Ivarsson M, Lindblom S, Broman C, Holm NG (2008) Fossilized microorganisms associated with zeolite-carbonate interfaces in sub-seafloor hydrothermal environments. Geobiology 6:155–170

Iwamoto K, Shiraiwa Y (2012) Characterization of intracellular iodine accumulation by iodine-tolerant microalgae. Procedia Environ Sci 15:34–42

Jackson JC, Ericksen GE (1997) An X-ray diffraction method for semiquantitative mineralogical analysis of Chilean nitrate ore. Rev Geol Chile 24:45–53

Jacobson S (1975) Dashkesanite: high-chlorine amphibole from St. Pauls Rocks equatorial Atlantic and Transcaucasia, USSR. Smithsonian Contrib Earth Sci 14:17–22

Jambon A, Deruelle B, Dreibus G, Pineau F (1995) Chlorine and bromine abundance in MORB: the contrasting behaviour of the Mid-Atlantic Ridge and East Pacific Rise and implications for chlorine geodynamic cycle. Chem Geol 126:101–117

James RH, Elderfield H, Palmer MR (1995) The chemistry of hydrothermal fluids from the Broken Spur site, 29°N Mid-Atlantic ridge. Geochim Cosmochim Acta 59(4):651–659

James RH, Rudnicki MD, Palmer MR (1999) The alkali element and boron geochemistry of the Escanaba trough sediment-hosted hydrothermal system. Earth Planet Sci Lett 171:157–169

James RH, Green DRH, Stock MJ, Alker BJ, Banerjee NR, Cole C, German CR, Huvenne VAI, Powell AM, Connelly DP (2014) Composition of hydrothermal fluids and mineralogy of associated chimney material on the East Scotia Ridge back-arc spreading centre. Geochim Cosmochim Acta 139:47–71

John T, Scambelluri M, Frische M, Barnes JD, Bach W (2011) Dehydration of subducting serpentinite: implications for halogen mobility in subduction zones and the deep halogen cycle. Earth Planet Sci Lett 308:65–76

Johnson L, Burgess R, Turner G, Milledge JH, Harris JW (2000) Noble gas and halogen geochemistry of mantle fluids: comparison of African and Canadian diamonds. Geochim Cosmochim Acta 64:717–732

Juteau T, Manac'h G, Moreau O, Lécuyer C, Ramboz C (2000) The high temperature reaction zone of the Oman ophiolite: new field data, microthermometry of fluid inclusions, PIXE analyses and oxygen isotopic ratios. Mar Geophys Res 21(3–4):351–385

Kamenetsky VS, Eggins SM (2012) Systematics of metals, metalloids, and volatiles in MORB melts: effects of partial melting, crystal fractionation and degassing (a case study of Macquarie Island glasses). Chem Geol 302:76–86

Kawagucci S, Chiba H, Shibash J-I, Yamanaka T, Toki T, Muramatsu Y, Ueno Y, Makabe A, Inoue K, Yoshida N, Nakagawa S, Nunoura T, Takai K, Takahata N, Sano Y, Narita T, Teranishi G, Obata H, Gamo T (2011) Hydrothermal fluid geochemistry at the Iheya North field in the mid-Okinawa Trough: implication for origin of methane in subseafloor fluid circulation systems. Geochem J 45:109–124

Keevil NB (1942) Vapor pressures of aqueous solutions at high temperatures. J Am Chem Soc 64:841–850

Kelley DS, Delaney JR (1987) 2-phase separation and fracturing in mid-ocean ridge gabbros at temperatures greater than 700-degrres-C. Earth Planet Sci Lett 83:53–66

Kelley DS, Robinson PT (1990) Development of a brine dominated hydrothermal system at temperatures of 400–500° C in the upper level plutonic sequence, Troodos Ophiolite, Cyprus. Geochim Cosmochim Acta 54:653–661

Kelley DS, Robinson PT, Malpas JG (1992) Processes of brine generation and circulation in the oceanic crust—fluid inclusion evidence from the Troodos Ophiolite, Cyprus. J Geophys Res Solid Earth 97:9307–9322

Kelley DS, Gillis KM, Thompson G (1993) Fluid evolution in submarine magma-hydrothermal systems at the Mid-Atlantic Ridge. J Geophys Res-Solid Earth 98:19579–19596

Kelley DS, Karson JA, Blackman DK, Fruh-Green GL, Butterfield DA, Lilley MD, Olson EJ, Schrenk MO, Roe KK, Lebon GT, Rivizzigno P, Party ATS (2001) An off-axis hydrothermal vent field near the Mid-Atlantic Ridge at 30° N. Nature 412:145–149

Kelley DS, Fruh-Green GL, Karson JA, Ludwig KA (2007) The lost city hydrothermal field revisited. Oceanography 20:90–99

Kendrick MA (2012) High precision Cl, Br and I determination in mineral standards using the noble gas method. Chem Geol 292–293:116–126

Kendrick MA, Phillips D, Wallace M, Miller JM (2011a) Halogens and noble gases in sedimentary formation waters and Zn-Pb deposits: a case study from the Lennard Shelf, Australia. Appl Geochem 26:2089–2100

Kendrick MA, Scambelluri M, Honda M, Phillips D (2011b) High abundances of noble gas and chlorine delivered to the mantle by serpentinite subduction. Nat Geosci 4:807–812

Kendrick MA, Kamenetsky VS, Phillips D, Honda M (2012a) Halogen (Cl, Br, I) systematics of mid-ocean ridge basalts: a Macquarie Island case study. Geochim Cosmochim Acta 81:82–93

Kendrick MA, Woodhead JD, Kamenetsky VS (2012b) Tracking halogens through the subduction cycle. Geology 40:1075–1078

Kendrick MA, Arculus RJ, Burnard P, Honda M (2013a) Quantifying brine assimilation by submarine magmas: Examples from the Galápagos Spreading Centre and Lau Basin. Geochim Cosmochim Acta 123:150–165

Kendrick MA, Honda M, Pettke T, Scambelluri M, Phillips D, Giuliani A (2013b) Subduction zone fluxes of halogens and noble gases in seafloor and forearc serpentinites. Earth Planet Sci Lett 365:86–96

Kendrick MA, Arculus RJ, Danyushevsky L, Kamenetsky VS, Woodhead J, Honda M (2014) Subduction-related halogens (Cl, Br and I) and H_2O in magmatic glasses from Southwest Pacific Backarc Basins. Earth Planet Sci Lett 400:165–176

Kendrick MA, Jackson MG, Hauri E, Phillips D (2015a) The halogen (F, Cl, Br, I) and H_2O systematics of Samoan lavas: assimilated seawater, EM2 and high $^3He/^4He$ components. Earth Planet Sci Lett 410:197–209

Kendrick MA, Honda M, Vanko DA (2015b) Halogens and noble gases in Mathematician Ridge metagabbros: Implications for oceanic hydrothermal root zones and global volatile cycles. Contrib Miner Petrol 170:1–20

Kendrick MA, Hémond C, Kamenetsky VS, Danyushevsky L, Devey C, Rodemann T, Jackson MG, Perfit MR (2017) Seawater cycled throughout earth's mantle in partially serpentinized lithosphere. Nat Geosci 10:222–228

Kennedy HA, Elderfield H (1987a) Iodine diagenesis in non-pelagic deep sea sediments. Geochem Cosmochem Acta 51:2505–2514

Kennedy HA, Elderfield H (1987b) Iodine diagenesis in pelagic deep sea sediments. Geochemi Cosmochem Acta 51:2489–2504

Kent AJR, Clague DA, Honda M, Stolper EM, Hutcheon ID, Norman MD (1999a) Widespread assimilation of a seawater-derived component at Loihi Seamount, Hawaii. Geochim Cosmochim Acta 63:2749–2761

Kent AJR, Norman MD, Hutcheon ID, Stolper EM (1999b) Assimilation of seawater-derived components in an oceanic volcano: evidence from matrix glasses and glass inclusions from Loihi seamount, Hawaii. Chem Geol 156:299–319

Kent AJR, Peate DW, Newman S, Stolper EM, Pearce JA (2002) Chlorine in submarine glasses from the Lau Basin: seawater contamination and constraints on the composition of slab-derived fluids. Earth Planet Sci Lett 202:361–377

Ketsko VA, Urusova MA, Valyashko VM (1984) Solubility and vapour-pressure of solutions in the $CaCl_2$–H_2O system at 250–400 °C. Zh Neorg Khim 29:2443–2445

Kodolányi J, Pettke T, Spandler C, Kamber BS, Gméling K (2012) Geochemistry of ocean floor and fore-arc serpentinites: constraints on the ultramafic input to subduction zones. J Petrol 53 (2):235–270

Kigai IN, Tagirov BR (2010) Evolution of acidity of hydrothermal fluids related to hydrolysis of chlorides. Petrology 18:252–262

Kitano Y, Okumura M, Idogaki M (1975) Incorporation of sodium, chloride and sulfate with calcium carbonate. Geochem J 9:75–84

Kleinrock MC, Humphris SE (1996) Structural control on seafloor hydrothermal activity at the TAG active mound. Nature 382:149–153

Kruber C, Thorseth IH, Pedersen RB (2008) Seafloor alteration of basaltic glass: textures, geochemistry, and endolithic microorganisms. Geochem Geophys Geosyst 9:Q12002

Kuepper FC, Carpenter LJ, Leblanc C, Toyama C, Uchida Y, Maskrey BH, Robinson J, Verhaeghe EF, Malin G, Luther GW III, Kroneck PMH, Kloareg B, Meyer-Klaucke W, Muramatsu Y, Megson IL, Potin P, Feiters MC (2013) In vivo speciation studies and antioxidant properties of bromine in Laminaria digitata reinforce the significance of iodine accumulation for kelps. J Exp Bot 64:2653–2664

Kullerud K, Erambert M (1999) Cl-scapolite, Cl-amphibole, and plagioclase equilibria in ductile shear zones at Nusfjord, Lofoten, Norway: implications for fluid compositional evolution during fluid-mineral interaction in the deep crust. Geochim Cosmochim Acta 63:3829–3844

Larsen HC, Cannat M, Ceuleneer G, Fruh-Green GL, Kodaira S, MacLeod C, Miller JM, Seama N, Tatsumi Y, Toomey D (2009) Oceanic crustal structure and formation: IODP and ODP Achievements November 2002–December 2005. In: Szarek R (ed)

le Roux PJ, le Roex AP, Schilling JG, Shimizu N, Perkins WW, Pearce NJG (2002) Mantle heterogeneity beneath the southern Mid-Atlantic Ridge: trace element evidence for contamination of ambient asthenospheric mantle. Earth Planet Sci Lett 203:479–498

le Roux PJ, Shirey SB, Hauri EH, Perfit MR, Bender JF (2006) The effects of variable sources, processes and contaminants on the composition of northern EPR MORB (8–10° N and 12–14° N): evidence from volatiles (H_2O, CO_2, S) and halogens (F, Cl). Earth Planet Sci Lett 251:209–231

Leblanc C, Colin C, Cosse A, Delage L, La Barre S, Morin P, Fiévet B, Voiseux C, Ambroise Y, Verhaeghe E, Amouroux D, Donard O, Tessier E, Potin P (2006) Iodine transfers in the coastal marine environment: the key role of brown algae and of their vanadium-dependent haloperoxidases. Biochimie 88:1773–1785

Lécuyer C, Dubois M, Marignac C, Gruau G, Fouquet Y, Ramboz C (1999) Phase separation and fluid mixing in subseafloor back arc hydrothermal systems: a microthermometric and oxygen isotope study of fluid inclusions in the barite-sulfide chimneys of the Lau Basin. J Geophys Res Solid Earth 104:17911–17927

Li YH (1991) Distribution patterns of the elements in the ocean—a synthesis. Geochim Cosmochim Acta 55:3223–3240

Li Y-H, Schoonmaker JE (2003) Chemical composition and mineralogy of marine sediments. In: Treatise on geochemistry, pp 1–35

Liebscher A, Luders V, Heinrich W, Schettler G (2006) Br/Cl signature of hydrothermal fluids: liquid-vapour fractionation of bromine revisited. Geofluids 6:113–121

Lu ZL, Hensen C, Fehn U, Wallmann K (2008) Halogen and ^{129}I systematics in gas hydrate fields at the northern Cascadia margin (IODP Expedition 311): insights from numerical modeling. Geochem Geophys Geosyst 9(10):n/a–n/a

Lu ZL, Jenkyns HC, Rickaby REM (2010) Iodine to calcium ratios in marine carbonate as a paleo-redox proxy during oceanic anoxic events. Geology 38:1107–1110

Lytle ML, Kelley KA, Hauri EH, Gill JB, Papia D, Arculus RJ (2012) mantle sources and Samoan influence in the northwestern lau back-arc basin. Geochem Geophys Geosyst 13:2012GC004233

Magenheim AJ, Spivack AJ, Michael PJ, Gieskes JM (1995) Chlorine stable isotope composition of the oceanic crust: Implications for Earth's distribution of chlorine. Earth Planet Sci Lett 131:427–432

Mahn CL, Gieskes JM (2001) Halide systematics in comparison with nutrient distributions in sites 1033B and 1034B, Saanich Inlet: ODP Leg 169S. Mar Geol 174:323–339

Markl G, Bucher K (1998) Composition of fluids in the lower crust inferred from metamorphic salt in lower crustal rocks. Nature 391:781–783

Marks MAW, Kendrick, MA, Eby NG, Zack T, Wenzel T (2017) The F, Cl, Br and I contents of reference glasses BHVO-2G, BIR-1G, BCR-2G, GSD-1G, GSE-1G, NIST SRM 610 and NIST SRM 612. Geostand Geoanal Res 41:107–122. doi:10.1111/ggr.12128

Martin JB (1999) Nonconservative behavior of Br-/Cl- ratios during alteration of volcaniclastic sediments. Geochim Cosmochim Acta 63:383–391

Martin JB, Gieskes JM, Torres M, Kastner M (1993) Bromine and iodine in Peru margin sediments and pore fluids: implications for fluid origins. Geochim Cosmochim Acta 57:4377–4389

Matthies D, Troll G (1990) Distribution of fluorine in recent marine-sediments related to petrographic composition—bransfield strait and Northwestern Weddell Sea, Antarctica. Mar Geol 91:313–324

McCaffrey MA, Lazar B, Holland HD (1987) The evaporation path of seawater and the composition of Br^- and K^+ with halite. J Sediment Petrol 57:928–937

McDonough WF, Sun S-S (1995) The composition of the earth. Chem Geol 120:223–253

Melchert B, Devey CW, German CR, Lackschewitz KS, Seifert R, Walter M, Mertens C, Yoerger DR, Baker ET, Paulick H, Nakamura K (2008) First evidence for high-temperature off-axis venting of deep crustal/mantle heat: the Nibelungen hydrothermal field, southern Mid-Atlantic Ridge. Earth Planet Sci Lett 275:61–69

Mevel C (1988) Metamorphism in oceanic layer 3, gorringe bank, Eastern Atlantic. Contrib Mineral Petrol 100:496–509

Michael PJ, Cornell WC (1998) Influence of spreading rate and magma supply on crystallization and assimilation beneath mid-ocean ridges: Evidence from chlorine and major element chemistry of mid-ocean ridge basalts. J Geophys Res Solid Earth 103:18325–18356

Michael PJ, Schilling J-G (1989) Chlorine in mid-ocean ridge magmas: evidence for assimilation of seawater-influenced components. Geochim Cosmochim Acta 53:3131–3143

Migdisov AA, Williams-Jones AE (2014) Hydrothermal transport and deposition of the rare earth elements by fluorine-bearing aqueous liquids. Mineral Deposita 49:987–997

Montavon G, Sabatié-Gogova A, Ribet S, Bailly C, Bessaguet N, Durce D, Giffaut E, Landesman C, Grambow B (2014) Retention of iodide by the callovo-oxfordian formation: an experimental study. Appl Clay Sci 87:142–149

Mottl MJ, Seewald JS, Wheat CG, Tivey MK, Michael PJ, Proskurowski G, McCollom TM, Reeves E, Sharkey J, You CF, Chan LH, Pichler T (2011) Chemistry of hot springs along the Eastern Lau Spreading Center. Geochim Cosmochim Acta 75:1013–1038

Muramatsu Y, Wedepohl KH (1998) The distribution of iodine in the earth's crust. Chem Geol 147:201–216

Muramatsu Y, Fehn U, Yoshida S (2001) Recycling of iodine in fore-arc areas: evidence from the iodine brines in Chiba, Japan. Earth Planet Sci Lett 192:583–593

Muramatsu Y, Doi T, Tomaru H, Fehn U, Takeuchi R, Matsumoto R (2007) Halogen concentrations in pore waters and sediments of the Nankai trough, Japan: implications for the origin of gas hydrates. Appl Geochem 22:534–556

Nakayama E, Kimoto T, Isshiki K, Sohrin Y, Okazaki S (1989) Determination and distribution of iodide- and total-iodine in the North Pacific Ocean—by using a new automated electrochemical method. Mar Chem 27:105–116

Nehlig P (1991) Salinity of oceanic hydrothermal fluids: a fluid inclusion study. Earth Planet Sci Lett 102:310–325

Nehlig P (1994) Fracture and permeability analysis in magma-hydrothermal transition zones in the Samail Ophiolite (Oman). J Geophys Res Solid Earth 99:589–601

Nehlig P, Juteau T (1988) Deep crustal seawater penetration and circulation at ocean ridges—Evidence from the Oman ophiolite. Mar Geol 84:209–228

Ohde S, Kitano Y (1980) Incorporation of fluoride into Ca-Mg carbonate. Geochem J 14:321–324

Okumura M, Kitano Y, Idogaki M (1983) Incorporation of fluoride ions into calcite—effect of organic materials and magnesium ions in a parent solution. Geochem J 17:257–263

Okumura M, Kitano Y, Idogaki M (1986) Behavior of bromide ions during the formation of calcium carbonate. Mar Chem 19:109–120

Oosting SE, Von Damm KL (1996) Bromide/chloride fractionation in seafloor hydrothermal fluids from 9–10°N East Pacific Rise. Earth Planet Sci Lett 144:133–145

Opdyke BN, Walter LM, Huston TJ (1993) Fluoride content of foraminiferal calcite: relations to life habitat, oxygen isotope composition, and minor element chemistry. Geology 21:169–172

Palme H, O'Neill HSC (2003) Cosmochemical estimates of mantle composition. In: Holland H, Turekian KK (eds) Treatise on geochemistry. Elsevier, New York, pp 1–38

Peacock SM (1990) Fluid processes in subduction zones. Science 248:329–337

Pester NJ, Reeves EP, Rough ME, Ding K, Seewald JS, Seyfried WE (2012) Subseafloor phase equilibria in high-temperature hydrothermal fluids of the Lucky Strike Seamount (Mid-Atlantic Ridge, 37°17′N). Geochim Cosmochim Acta 90:303–322

Pierret MC, Clauer N, Bosch D, Blanc G, France-Lanord C (2001) Chemical and isotopic ($^{87}Sr/^{86}Sr$, $\delta^{18}O$, δD) constraints to the formation processes of Red-Sea brines. Geochim Cosmochim Acta 65:1259–1275

Pinet PR (1992) Oceanography: an introduction to the planet oceanus. West Publishing Company, New York

Price NB, Calvert SE (1973) The geochemistry of iodine in oxidised and reduced recent marine sediments. Geochim Cosmochim Acta 37:2149–2158

Price NB, Calvert SE (1977) Contrasting geochemical behaviours of iodine and bromine in recent sediments from the Namibian Shelf. Geochim Cosmochim Acta 41:1769–1775

Prichard HM, Cann JR (1982) Petrology and mineralogy of dredged gabbro from Gettysburg Bank, Eastern Atlantic. Contrib Mineral Petrol 79:46–55

Proskurowski G, Lilley MD, Seewald JS, Fruh-Green GL, Olson EJ, Lupton JE, Sylva SP, Kelley DS (2008) Abiogenic hydrocarbon production at lost city hydrothermal field. Science 319:604–607

Pyle DM, Mather TA (2009) Halogens in igneous processes and their fluxes to the atmosphere and oceans from volcanic activity: a review. Chem Geol 263:110–121

Ramos AA, Ohde S, Hossain MMM, Ozaki H, Sirirattanachai S, Apurado JL (2005) Determination of fluorine in coral skeletons by instrumental neutron activation analysis. J Radioanal Nucl Chem 266:19–29

Ranero CR, Phipps Morgan J, McIntosh K, Reichert C (2003) Bending-related faulting and mantle serpentinization at the Middle America trench. Nature 425:367–373

Reed MH (1997) Hydrothermal alteration and its relationship to ore fluid composition. In: Barnes HL (ed) Geochemistry of hydrothermal ore deposits. Wiley, New York, pp 303–366

Reeves EP, Seewald JS, Saccocia P, Bach W, Craddock PR, Shanks WC, Sylva SP, Walsh E, Pichler T, Rosner M (2011) Geochemistry of hydrothermal fluids from the PACMANUS, Northeast Pual and Vienna Woods hydrothermal fields, Manus Basin, Papua New Guinea. Geochim Cosmochim Acta 75:1088–1123

Rona PA, Denlinger RP, Fisk MR, Howard KJ, Taghon GL, Klitgord KD, McClain JS, McMurray GR, Wiltshire JC (1990) Major off-axis hydrothermal activity on the northern Gorda Ridge. Geology 18:493–496

Rude PD, Aller RC (1991) Fluorine mobility during early diagenesis of carbonate sediment: an indicator of mineral transformations. Geochim Cosmochim Acta 55:2491–2509

Rude PD, Aller RC (1994) Fluorine uptake by Amazon continental shelf sediment and its impact on the global fluorine cycle. Cont Shelf Res 14:883–907

Saal AE, Hauri EH, Langmuir CH, Perfit MR (2002) Vapour undersaturation in primitive mid-ocean-ridge basalt and the volatile content of earth's upper mantle. Nature 419:451–455

Sano T, Miyoshi M, Ingle S, Banerjee NR, Ishimoto M, Fukuoka T (2008) Boron and chlorine contents of upper oceanic crust: basement samples from IODP Hole 1256D. Geochem Geophys Geosyst 9:Q12O15

Scambelluri M, Piccardo GB, Philippot P, Robbiano A, Negretti L (1997) High salinity fluid inclusions formed from recycled seawater in deeply subducted alpine serpentinite. Earth Planet Sci Lett 148:485–499

Scambelluri M, Müntener O, Ottolini L, Pettke TT, Vannucci R (2004) The fate of B, Cl and Li in the subducted oceanic mantle and in the antigorite breakdown fluids. Earth Planet Sci Lett 222:217–234

Schilling JG, Bergeron MB, Evans R (1980) Halogens in the mantle beneath the North Atlantic. Philos Trans R Soc Lond Ser A Math Phys Eng Sci 297:147–178

Schmidt MW, Poli S (1998) Experimentally based water budgets for dehydrating slabs and consequences for arc magma generation. Earth Planet Sci Lett 163:361–379

Seyfried WE, Bischoff JL (1981) Experimental seawater-basalt interaction at 300 °C, 500 bars, chemical-exchange, secondary mineral formation and implications for the transport of heavy-metals. Geochim Cosmochim Acta 45:135–147

Seyfried WE, Ding K (1995) The hydrothermal chemistry of fluoride in seawater. Geochim Cosmochim Acta 59:1063–1071

Seyfried WE, Mottl MJ (1982) Hydrothermal alteration of basalt by seawater under seawater-dominated conditions. Geochim Cosmochim Acta 46:985–1002

Seyfried WE, Berndt ME, Janecky DR (1986) Chloride depeletions and enrichments in seafloor hydrothermal fluids—constraints from experimental basalt alteration studies. Geochim Cosmochim Acta 50:469–475

Seyfried WE, Berndt ME, Seewald JS (1988) Hydrothermal alteration processes at mid-Ocean Ridges—constraints from diabase alteration experiments, hot spring fluids and composition of the oceanic crust. Can Mineral 26:787–804

Seyfried WE Jr, Seewald JS, Berndt ME, Ding K, Foustoukos DI (2003) Chemistry of hydrothermal vent fluids from the main endeavour field, northern Juan de Fuca Ridge: geochemical controls in the aftermath of June 1999 seismic events. J Geophys Res 108:2429

Shanks WC, Bischoff JL (1977) Ore transport and deposition in Red Sea geothermal systems—geochemical model. Geochim Cosmochim Acta 41:1507–1519

Sharp ZD, Barnes JD (2004) Water-soluble chlorides in massive seafloor serpentinites: a source of chloride in subduction zones. Earth Planet Sci Lett 226:243–254

Sharp ZD, Draper DS (2013) The chlorine abundance of earth: implications for a habitable planet. Earth Planet Sc Lett 369–370:71–77

Siemann MG, Schramm M (2000) Thermodynamic modelling of the Br partition between aqueous solutions and halite. Geochim Cosmochim Acta 64:1681–1693

Silantyev SA, Kostitsyn YA, Cherkashin DV, Kononkova NN, Kornienko EM, Dick HJB, Kelemen PB (2008) Magmatic and metamorphic evolution of the oceanic crust in the western flank of the MAR crest zone at 15°44′N: investigation of cores from sites 1275B and 1275D, JOIDES resolution Leg 209. Petrology 16:353–375 "http://elibrary.ru/item.asp?id=13581157"

Sims KWW, Goldstein SJ, Blichert-toft J, Perfit MR, Kelemen P, Fornari DJ, Michael P, Murrell MT, Hart SR, DePaolo DJ, Layne G, Ball L, Jull M, Bender J (2002) Chemical and isotopic constraints on the generation and transport of magma beneath the East Pacific Rise. Geochim Cosmochim Acta 66:3481–3504

Sims KWW, Blichert-Toft J, Fornari DJ, Perfit MR, Goldstein SJ, Johnson P, DePaolo DJ, Hart SR, Murrell PJ, Michael PJ, Layne GD, Ball LA (2003) Aberrant youth: chemical and isotopic constraints on the origin of off-axis lavas from the East Pacific Rise, 9°–10° N. Geochem Geophys Geosyst 4:2002GC000443

Snow JE, Edmonds HN (2007) Ultraslow-spreading ridges rapid paradigm changes. Oceanography 20:90–101

Spandler C, Pirard C (2013) Element recycling from subducting slabs to arc crust: a review. Lithos 170:208–223

Stakes D, Moore WS (1991) Evolution of hydrothermal activity on the Juan de Fuca Ridge—Observations, mineral ages and Ra isotope ratios. J Geophys Res Solid Earth 96:21739–21752

Staudigel H, Hart SR (1983) Alteration of basaltic glass—mechanisms and significance for the oceanic-crust seawater budget. Geochim Cosmochim Acta 47:337–350

Staudigel H, Hart SR, Koppers AAP, Constable C, Workman R, Kurz M, Baker ET (2004) Hydrothermal venting at Vailulu'u seamount: the smoking end of the Samoan chain. Geochem Geophys Geosyst 5:Q02003

Staudigel H, Furnes H, McLoughlin N, Banerjee NR, Connell LB, Templeton A (2008) 3.5 billion years of glass bioalteration: volcanic rocks as a basis for microbial life? Earth Sci Rev 89:156–176

Straub SM, Layne GD (2003) The systematics of chlorine, fluorine, and water in Izu arc front volcanic rocks: implications for volatile recycling in subduction zones. Geochim Cosmochim Acta 67:4179–4203

Stroncik N, Schmincke HU (2002) Palagonite—a review. Int J Earth Sci 91:680–697

Svensen H, Jamtveit B, Yardley B, Engvik AK, Austrheim H, Broman C (1999) Lead and bromine enrichment in eclogite-facies fluids: extreme fractionation during lower-crustal hydration. Geology 27:467–470

Svensen H, Banks DA, Austreim H (2001) Halogen contents of eclogite facies fluid inclusions and minerals: Caledonides, western Norway. J Metamorph Geol 19:165–178

Talbi ELH, Honnorez J, Clauer N, Gauthier-Lafaye F, Stille P (1999) Petrology, isotope geochemistry and chemical budgets of oceanic gabbros-seawater interactions in the equatorial Atlantic. Contrib Mineral Petrol 137:246–266

Tanaka K, Ono T, Fujioka Y, Ohde S (2013) Fluoride in non-symbiotic coral associated with seawater carbonate. Mar Chem 149:45–50

Tivey MA Schouten H, Kleinrock MC (2003) A near-bottom magnetic survey of the mid-Atlantic ridge axis at 26° N: implications for the tectonic evolution of the TAG segment. J Geophys Res Solid Earth 108: B5 2277

Tomaru H, Fehn U, Lu ZL, Matsumoto R (2007a) Halogen systematics in the Mallik 5L-38 gas hydrate production research well, Northwest territories, Canada: implications for the origin of gas hydrates under terrestrial permafrost conditions. Appl Geochem 22:656–675

Tomaru H, Lu Z, Snyder GT, Fehn U, Hiruta A, Matsumoto R (2007b) Origin and age of pore waters in an actively venting gas hydrate field near Sado Island, Japan Sea: interpretation of halogen and ^{129}I distributions. Chem Geol 236:350–366

Tomaru H, Lu ZL, Fehn U, Muramatsu Y, Matsumoto R (2007c) Age variation of pore water iodine in the Eastern Nankai trough, Japan: evidence for different methane sources in a large gas hydrate field. Geology 35:1015–1018

Tomaru H, Fehn U, Lu ZL, Takeuchi R, Inagaki F, Imachi H, Kotani R, Matsumoto R, Aoike K (2009) Dating of dissolved iodine in pore waters from the gas hydrate occurrence offshore Shimokita Peninsula, Japan: 129I results from the D/V Chikyu Shakedown Cruise. Resour Geol 59:359–373

Tribuzio R, Renna MR, Dallai L, Zanetti A (2014) The magmatic–hydrothermal transition in the lower oceanic crust: clues from the Ligurian ophiolites, Italy. Geochim Cosmochim Acta 130:188–211

Turekian KK, Wedepohl KH (1961) Distribution of the elements in some major units of the earth's crust. Geol Soc Am Bull 72:175–192

Ullman WJ, Aller RC (1985) The geochemistry of iodine in near-shore carbonate sediments. Geochim Cosmochim Acta 49:967–978

Upstillgoddard RC, Elderfield H (1988) The role of diagenesis in the Estuarine budgets of iodine and bromine. Cont Shelf Res 8:405–430

Vanko DA (1986) High-chlorine amphiboles from oceanic rocks: product of highly-saline hydrothermal fluids? Am Mineral 71:51–59

Vanko DA (1988) Temperature, pressure, and composition of hydrothermal fluids, with their bearing on the magnitude of tectonic uplift at mid-ocean ridges, inferred from fluid inclusions in oceanic layer 3 rocks. J Geophys Res Solid Earth 93:4595–4611

Vanko DA, Bodnar RJ, Sterner SM (1988) Synthetic fluid inclusions: VIII. vapor-saturated halite solubility in part of the system NaCl-$CaCl_2$-H_2O, with application to fluid inclusions from oceanic hydrothermal systems. Geochim Cosmochim Acta 52:2451–2456

Vanko DA, Griffith JD, Erickson CL (1992) Calcium-rich brines and other hydrothermal fluids in fluid inclusions from plutonic rocks, Oceanographer Transform, mid-Atlantic Ridge. Geochim Cosmochim Acta 56:35–47

Vanko DA, Bonnin-Mosbah M, Philippot P, Roedder E, Sutton SR (2001) Fluid inclusions in quartz from oceanic hydrothermal specimens and the Bingham, Utah porphyry-Cu deposit: a study with PIXE and SXRF. Chem Geol 173:227–238

Vanko DA, Bach W, Roberts S, Yeats CJ, Scott SD (2004) Fluid inclusion evidence for subsurface phase separation and variable fluid mixing regimes beneath the deep-sea PACMANUS hydrothermal field, Manus Basin back arc rift, Papua New Guinea. J Geophys Res Solid Earth 109:B03201

Von Damm KL (2000) Chemistry of hydrothermal vent fluids from 9° to 10° N, East Pacific Rise: "Time zero," the immediate posteruptive period. J Geophys Res Solid Earth 105 (B5):11203–11222

Von Damm KL, Edmond JM, Grant B, Measures CI, Walden B, Weiss RF (1985) Chemistry of submarine hydrothermal solutions at 21°N, East Pacific Rise. Geochim Cosmochim Acta 49:2197–2220

Von Damm KL, Buttermore LG, Oosting SE, Bray AM, Fornari DJ, Lilley MD, Shanks Iii WC (1997) Direct observation of the evolution of a seafloor 'black smoker' from vapor to brine. Earth Planet Sci Lett 149:101–111

Von Damm KL, Bray AM, Buttermore LG, Oosting SE (1998) The geochemical controls on vent fluids from the Lucky Strike vent field, Mid-Atlantic Ridge. Earth Planet Sci Lett 160 (3–4):521–536

Von Damm KL, Lilley MD, Shanks WC, Brockington M, Bray AM, O'Grady KM, Olson E, Graham A, Proskurowski G (2003) Extraordinary phase separation and segregation in vent fluids from the southern East Pacific Rise. Earth Planet Sci Lett 206(3–4):365–378

Von Damm KL, Parker CM, Zierenberg RA, Lilley MD, Olson EJ, Clague DA, McClain JS (2005) The Escanaba Trough, Gorda Ridge hydrothermal system: temporal stability and subseafloor complexity. Geochim Cosmochim Acta 69(21):4971–4984

Wanless VD, Perfit MR, Ridley WI, Klein E (2010) Dacite petrogenesis on mid-ccean Ridges: evidence for oceanic crustal melting and assimilation. J Petrol 51:2377–2410

Webster JD, Kinzler RJ, Mathez EA (1999) Chloride and water solubility in basalt and andesite melts and implications for magmatic degassing. Geochim Cosmochim Acta 63:729–738

Williams DL, Von Herzen RP, Sclater JG, Anderson RN (1974) The galapagos spreading centre: lithospheric cooling and hydrothermal circulation. Geophys J Int 38:587–608

Wong GTF, Brewer PG (1977) Marine chemistry of iodine in anoxic basins. Geochim Cosmochim Acta 41:151–159

Worden RH (1996) Controls on halogen concentrations in sedimentary formation waters. Mineral Mag 60:259–274

Workman RK, Hauri E, Hart SR, Wang J, Blusztajn J (2006) Volatile and trace elements in basaltic glasses from Samoa: implications for water distribution in the mantle. Earth Planet Sci Lett 241:932–951

Wu S-F, You C-F, Valsami-Jones E, Baltatzis E, Shen M-L (2012) Br/Cl and I/Cl systematics in the shallow-water hydrothermal system at Milos Island, Hellenic Arc. Mar Chem 140–141: 33–43

Yang M, Her N, Ryu J, Yoon Y (2014) Determination of perchlorate and iodide concentrations in edible seaweeds. Int J Environ Sci Technol 11:565–570

Yardley BWD (2005) 100th Anniversary special paper: metal concentrations in crustal fluids and their relationship to ore formation. Econ Geol 100:613–632

You CF, Butterfield DA, Spivack AJ, Gieskes JM, Gamo T, Campbell AJ (1994) Boron and halide systematics in submarine hydrothermal systems: effects of phase separation and sedimentary contributions. Earth Planet Sci Lett 123:227–238

Zheng J, Takata H, Tagami K, Aono T, Fujita K, Uchida S (2012) Rapid determination of total iodine in Japanese coastal seawater using SF-ICP-MS. Microchem J 100:42–47

Zherebtsova IK, Volkova NN (1966) Experimental study of behaviour of trace elements in the process of natural solar evaporation of Black Sea water and Lake Sasky-Sivash brine. Geochem Int 3:656–670

Zierenberg RA, Shanks Iii WC (1986) Isotopic constraints on the origin of the Atlantis II, Suakin and Valdivia brines, Red Sea. Geochim Cosmochim Acta 50:2205–2214

Zierenberg RA, Schiffman P, Jonasson IR, Tosdal R, Pickthorn W, McClain J (1995) Alteration of basalt hyaloclastite at the off-axis sea cliff hydrothermal field, Gorda Ridge. Chem Geol 126:77–99

Chapter 10
The Role of Halogens During Regional and Contact Metamorphism

Johannes Hammerli and Mike Rubenach

Abstract Halogens are important elements for a range of geological processes during metamorphism from stabilizing mineral phases to being important ligands for mass transfer. Halogens are highly incompatible in most minerals, which makes it difficult to unravel their presence in the past. Minerals useful for understanding halogen behaviour during metamorphism include: scapolite, apatite, titanite, biotite, and amphibole. However, their ability to incorporate halogens depends on parameters such as bulk rock composition, fluid properties, and water-rock ratios. Comprehensive studies of halogens in regional metamorphic rocks and minerals, such as the Clearwater Region, Idaho, USA or the Mary Kathleen Fold Belt, Mt Isa Inlier, Australia, show that halogen contents are highly variable on a bulk rock- and rock layer-scale, reflecting protolith variations. Where low fluid-rock ratios occurred during regional metamorphism, pre-exisiting variations in halogen compositions and ratios across individual layers were not eliminated, resulting in large differences between halogen concentrations on a mineral- and rock-layer scale. Research on F and Cl in apatite in siliceous marbles from five classic aureoles highlights the use of this mineral regarding rock or fluid buffering, and in establishing fluid sources. Chlorine enrichment in biotite and amphibole, associated with regional albitization observed in Cloncurry, Australia or the Bamble Sector Norway, demonstrate advection of saline fluids during albitization and K-feldspar metasomatism that occur in association with regional mineralization. Chlorine-bearing fluids are capable of mobilizing large amounts of metals during large-scale metamorphism on a regional, whole rock, and mineral scale. Consequently, fluid flow could be an essential prerequisite to actively discharge metals from the metamorphic rocks. Recent analytical advancements allow for more routine analyses of halogen contents in minerals and fluid inclusions. For instance, in situ LA-ICP-MS analyses of Cl and

J. Hammerli (✉) · M. Rubenach
Economic Geology Research Centre (EGRU), Geoscience, College of Science and Engineering, James Cook University, Townsville, QLD 4811, Australia
e-mail: Johannes.hammerli@my.jcu.edu.au

J. Hammerli
Centre for Exploration Targeting, School of Earth Sciences, The University of Western Australia, Perth, Australia

D.E. Harlov and L. Aranovich (eds.), *The Role of Halogens in Terrestrial and Extraterrestrial Geochemical Processes*, Springer Geochemistry,
https://doi.org/10.1007/978-3-319-61667-4_10

Br allow for the reconstruction of the interaction of halogen-bearing fluids with crustal rocks in complex geological settings that have undergone multiple hydrothermal events. In such cases, scapolite can be used as an archive for fluid properties during metamorphism. For example, within the Mount Isa Inlier, it was found that the fluids, which interacted with calc-silicates in the Mary Kathleen Fold Belt, were of bittern brine derivation contrasting with the Cloncurry Region, where the fluids show evidence of dissolved halite. Magmatic fluid interaction with calc-silicate rocks was found to be localized.

10.1 Introduction

This chapter reviews studies of halogens (Cl, F, Br, I) in both regional, and thermal metamorphism. We address halogen contents in metamorphic rocks, their distribution in common metamorphic minerals, the role of fluids in halogen distribution and transport, and the role of metamorphic protolithic compositions as well as halogen sources during metamorphic processes.

Examples from regional metamorphic terranes that are considered in this chapter concentrate mainly on greenschist to amphibolite facies metamorphic conditions, with a focus on well-studied areas such as the Mount Isa Inlier in Australia and the Clearwater Region, Idaho, USA. The role of halogens in subduction related processes and high-grade metamorphism are discussed in Chaps. 8 and 11, respectively (cf., Barnes et al. 2018; Aranovich and Safonov 2018). Metasomatic rocks are also considered, with the exception of the alteration associated with mineralization and skarns, which are reviewed in Chaps. 5 and 12 (cf., Lecumberri and Bodnar 2018; Pirajno 2018).

The study of halogen concentrations in minerals and fluid inclusions can help to understand a range of first order geological processes. Chlorine, I, and Br have much higher incompatibilities than F and hence partition strongly into the fluid or melt phase, so that their concentrations and ratios can be important tracers that are useful for identifying fluid sources in the crust. The presence of halogens can also control the stability of minerals and affect solidus temperatures (e.g., Stormer and Carmichael 1971; Manning 1981). Furthermore, Cl has been widely recognized as an important ligand for metal transport in hydrothermal (crustal) fluids (e.g., Barrett and Anderson 1982; Hemley et al. 1992; Yardley 2005). However, quantitative analysis of halogens, especially I and Br, is challenging due to their low concentrations in most geological materials. In addition, electron probe microanalysis (EPMA) of F can be difficult due to F migration in the crystals during analysis, especially for apatite (cf., Goldoff et al. 2012). Non-routine methods such as instrumental neutron activation analyses (INAA) (e.g., Heinrich et al. 1993), leachate ion chromatography analyses (e.g., Bottrell et al. 1988), laser micro-probe noble gas mass spectrometry (Böhlke and Irwin 1992; Kendrick et al. 2008), proton-induced X-ray emission (PIXE) (e.g., Heinrich et al. 1992; Ryan et al. 1993), secondary ion mass spectrometry (SIMS) (e.g., Marks et al. 2012), or synchrotron X-ray

fluorescence (SXRF) (e.g., Vanko et al. 2001), have been successfully applied to determine low levels of halogen concentrations in fluid inclusions and minerals. Nevertheless, systematic studies are rare, especially in a metamorphic context. Recent analytical developments for more routine quantification of halogens by LA-ICP-MS (e.g., Seo et al. 2011; Hammerli et al. 2013, 2014) hold great promise for enabling more systematic studies on the behaviour of halogens during metamorphism, and may help to resolve halogen characteristics of different fluid inclusion assemblages and mineral zones not resolvable by bulk rock techniques.

10.2 Halogen Distribution in Metamorphic Rocks: Provenance Effects and Modifications During Metamorphism

10.2.1 Bulk Rock Content

The halogen inventory in rocks in general is poorly constrained. Our limited understanding of the halogen distribution in rocks and minerals is mainly due to low halogen concentrations, and, with the exception of Cl, the requirement for non-routine analytical procedures to obtain meaningful results. In particular, quantification of F contents in apatite and other F-rich minerals is challenging because diffusion and matrix effects during EPMA can result in inaccurate concentrations (Stormer et al. 1993; Ottolini et al. 2000). Unfortunately, much of the existing halogen data were generated prior to 1960, and more sensitive techniques show that these early analyses were often erroneous, with halogen concentrations, especially Br and I, regularly overestimated (Fuge 1988).

With rather limited data, various attempts have been made to estimate the halogen content in metamorphic rocks and the continental crust (Table 10.1). Boness et al. (1991) measured halogen concentrations in metasedimentary rocks and obtained concentrations of $\leq$3100 ppm Cl, $\leq$0.25 ppm Br, and $\leq$0.48 ppm I in metapelites and 70–120 ppm Cl, 0.25 ppm Br, and $\sim$0.17 ppm I in greywackes. Muramatsu and Wedepohl (1998) and Wedepohl (1987) reported average values of $\sim$0.024 ppm I and $\sim$300 ppm Cl for a variety of metamorphic rocks (gneisses, schists, amphibolites, and marbles) (Table 10.1). In a recent study, Selverstone and Sharp (2015) systematically quantified Cl contents in two sedimentary sequences and their metamorphic equivalents. Their results show a range of Cl bulk rock contents between a few ppm to $\sim$100 ppm. Average concentrations of 182 ppm Cl and 524 ppm F for the middle crust (equivalent to amphibolite-facies rocks) were suggested by Gao et al. (1998), which is in agreement with average F contents in mid-amphibolite facies metamorphic rocks ($\sim$560 ppm F, Hammerli et al. 2016). The concentrations of halogens in the bulk continental crust are inferred to $\sim$525 ppm F, $\sim$472 ppm Cl, $\sim$0.8 ppm I, and $\sim$1 ppm Br (Table 10.1; Wedepohl 1995).

Table 10.1 Concentration of halogens in crustal rocks and estimated bulk crust values

	Average concentr. (ppb) iodine	Average concentr. chlorine (ppm)	Average concentr. bromine (ppm)	Average concentr. fluorine (ppm)	Source
Organic-rich shales	16,700		≤200*		Fuge (2005), *Martin et al. (1993)
Carbonates	2700	320	10.2	330	Fuge (1988)
Shales	2300	160	14.8	740	Fuge (1988)
Shales	1800	1100			Muramatsu and Wedepohl (1998) *Chai and Muramatsu (2007)
Limestones	260*, 2500	720	0.07*		
Sandstones	136	1340			
Sandstones	800	200	6.7	270	Fuge (1988)
Dolomites	710		0.53		Chai and Muramatsu (2007)
Metapelites	≤480	≤3100	≤0.25	~550*	Boness et al. (1991), *Hammerli et al. (2016)
Greywackes	90–170	70–120	0.25	~550*	Boness et al. (1991), *Hammerli et al. (2016)
Gneisses	24	320			
Mica schists	25	320			Muramatsu and Wedepohl (1998)
Amphibolites	23	300			
Marbles	31	300			
Schists		~2–100			Selverstone and Sharp (2015)
Average metamorpic rock	2.4	300			Muramatsu and Wedepohl (1998)
Middle Crust		182		524	Gao et al. (1998)
Continental crust	119	448			Muramatsu and Wedepohl (1998)
Continental crust	800	472	1	525	Wedepohl (1995)

The Br value from Martin et al. (1993) represent maximum concentrations in continental margin sediments

10.2.2 Halogen Distribution and Host Minerals in Metamorphic Rocks

10.2.2.1 Iodine and Br

The most common and important halogen host minerals in metamorphic rocks are summarized in Table 10.2 where we distinguish between psammopelites, calc-silicates (including marbles), and metabasites. A full list of halogen-bearing

minerals can be found in Chap. 3. Overall, similar to the incomplete halogen dataset for rocks, Br and I are seldom measured in minerals. Halogens are likely to be incorporated only in a handful of common metamorphic minerals (e.g., Fuge 1974a, b, c) such as apatite, micas, amphiboles, and in less common minerals such as scapolite, humite-group minerals, tourmaline, and titanite in calcsilicate rocks (Tables 10.2 and 10.3). Bromine concentrations of ~0.2 ppm have been measured in feldspars (Fuge 1974b) whilst concentrations in the ppm range have been measured in amphibole, mica, apatite, and several hundreds of ppm Br has been quantified in scapolite (Kendrick 2012; Hammerli et al. 2014; Kusebauch et al. 2015a, b, c). Halite can incorporate a few hundreds of ppm Br, while sylvite and carnallite can take up to 10 times higher Br concentrations (Braitsch and Hermann 1963; Fuge 1974b and references therein). Iodine may reach concentrations of 170 ppb in biotite and up to 100 ppb in hornblende, and similar concentration levels have been measured in apatite while more than 1000 ppb has been quantified in scapolite (Kendrick 2012). Sulfide minerals, such as galena and pyrite, have been found to incorporate up to 6 ppm I, while evaporites generally contain I contents in the sub-ppm level (e.g., Fuge 1974c; Fuge and Johnson 1984).

Sparse datasets make it particularly challenging to establish the distribution of I and Br between minerals during metamorphism. Nonetheless, studies have shown a high partitioning of I and Br into organic matter (Table 10.1) so that residual organic compounds not only have the potential to control I, but also might have a significant impact on the Br (re-) distribution in (meta-) sedimentary rocks (e.g., Correns 1956; Cosgrove 1970; Boness et al. 1991; Martin et al. 1993; see also Worden 2018). Hence, the depositional environment and the presence of organic material have a direct impact on the Br and I budget during subsequent metamorphism. During metamorphism, increasing temperatures and subsequent decomposition of organic compounds leads to a liberation of Br and I into pore-water (e.g., Hurai et al. 2008; Kendrick et al. 2011). Bromine, similar to Cl or F, although to lesser degree due to its

Table 10.2 Major halogen-host minerals in psammopelitic rocks, calc-silicates/marbles, and metabasites

	Meta-psammopelites	Calc-silicates	Metabasites
F	**Biotite, apatite**	**Apatite, titanite, (fluorite), amphibole, biotite,** (humite), (cuspidine)	**Amphibole, biotite, titanite, apatite**
Cl	**Biotite, apatite**	**(Scapolite), apatite, amphibole, biotite**	**(Scapolite), amphibole, biotite, apatite**
I	**Feldspar? biotite,** apatite	**(Scapolite), feldspar? amphibole, biotite,** apatite	**(Scapolite), amphibole, biotite,** apatite
Br	**Feldspar? biotite,** apatite	**(Scapolite), feldspar? amphibole, biotite,** apatite	**(Scapolite), amphibole, biotite,** apatite

Minerals in bold are the most important halogen hosts while scapolite might be an important halogen sink if formed during saline-fluid-rock interaction

Table 10.3 EPMA of typical halogen bearing metamorphic minerals

Humite	
$(Mg,Fe)_7(SiO_4)_3(F,OH)_2$	
Piazolo & Markl (1999)	
SiO_2	37.52
TiO_2	0.00
FeO	3.05
MgO	55.08
Cl	0.00
F	5.43
Total	101.08
O=F	2.27
Total F corr.	98.81
Si	3.05
Ti	0.00
Mg	6.68
Fe^{2+}	0.21
Cl	0.00
F	1.40
Sum cations	9.95

Structural formula based on 26 cation charges

Amphibole (Hornblende)	
(formula see below)	
Oliver et al. (1992)	
SiO_2	39.65
TiO_2	0.97
Al_2O_3	12.93
Fe_2O_3	5.42
FeO	13.74
MnO	1.18
MgO	8.36
CaO	11.53
Na_2O	0.86
K_2O	2.15
Cl	1.21
Total	98.00
O=Cl	0.27
Total Cl corr.	97.73
Si	6.11
Ti	0.11
Al	2.35
Fe^{3+}	0.63
Fe^{2+}	1.77
Mn	0.15
Mg	1.92
Ca	1.90
Na	0.26
K	0.42
Cl	0.31

Structural formula based on 23 (O, OH, Cl)

$(K,Na)_{0-1}(Ca,Na,Fe,Mg)_2(Mg,Fe,Al)_5(Al,Si)_8O_{22}(OH)_2$

Scapolite	
$Na_4Al_3Si_9O_{24}Cl$*	
Satish-Kumar et al. (2006)	
SiO_2	53.80
Al_2O_3	24.32
FeO	0.03
MgO	0.00
CaO	10.07
Na_2O	6.78
K_2O	2.30
Cl	2.57
O=Cl	1.16
Total Cl corr.	98.71
Si	7.87
Al	4.19
Fe	0.00
Mg	0.00
Ca	1.58
Na	1.92
K	0.43
Cl	0.64

Structural formula based on 16 cations

**marialite (see text)*

Apatite	
$Ca_5(PO_4)_3(F,Cl,OH)$	
Satish-Kumar et al. (2006)	
SiO_2	0.00
TiO_2	0.00
Al_2O_3	0.00
Cr_2O_3	0.00
FeO	0.00
CaO	53.93
P_2O_5	42.82
F	3.00
Cl	0.81
H_2O*	0.08
Total	100.64
O=F	1.26
O=Cl	0.18
Total F, Cl corr.	99.20
Si	0.00
Ti	0.00
Al	0.00
Cr	0.00
Fe	0.00
Ca	5.06
P	3.18
F	0.83
Cl	0.12
OH*	0.05

Structural formula based on 13 O

**calculated*

Biotite	
$K(Mg,Fe^{2+})_3[AlSi_3O_{10}](OH,Cl,F)_2$	
Rubenach (2005)	
SiO_2	33.83
TiO_2	2.01
Al_2O_3	16.94
FeO	21.65
MnO	0.00
MgO	7.40
CaO	0.00
Na_2O	0.00
K_2O	9.49
Cl	1.49
Total	92.81
O=Cl	0.34
Total Cl corr.	92.47
Si	5.43
^{IV}Al	2.57
^{VI}Al	0.47
Fe	2.91
Mn	0.00
Mg	1.77
Ti	0.24
K	1.94
Cl	0.41
Total	15.90

Structural formula based on 22 O

Titanite	
$CaTiSiO_5$	
Sengupta et al. (2004)	
SiO_2	30.00
TiO_2	30.94
Al_2O_3	6.47
Cr_2O_3	0.05
Fe_2O_3	0.32
FeO	0.00
MnO	0.03
MgO	0.04
CaO	29.2
Na_2O	0.03
K_2O	0.01
F	2.24
O=F	0.94
Total F corr.	98.35
Si	0.97
Ti	0.75
Al	0.25
Fe^{3+}	0.01
Mg	0.00
Ca	1.01
F	0.23
OH	0.03

Structual formula based on 3 cations and charge balance

large ionic size, potentially replaces OH groups in crystal structures and thus might be recycled into hydrous minerals (see also Sect. 10.2.3.3). The size of the I^- ion on the other hand, is probably too large to replace OH-groups in rock-forming minerals. Boness et al. (1991) speculated that instead, I might bond to the crystal surfaces or may fill crystal lattice defects. Provided that rare data for I and Br in feldspars, hornblende, and biotite can be trusted (Fuge 1974b), and in the absence of organic material, these minerals might be the more common hosts for Br and I in higher-grade rocks. Due to its low modal abundance, apatite is likely to be only a minor host for the bulk rock Br and I content.

10.2.2.2 Fluorine and Cl

While Br and I values in common rock-forming minerals are equally sparse, more data are available for F and Cl. Chlorine can be incorporated in metamorphic apatite, amphibole, micas, and scapolite at weight percent levels (Table 10.3) (e.g., Nijland et al. 1993; Lieftink et al. 1993; Oliver et al. 1992; Hammerli et al. 2014). Fluorine concentrations can reach weight-precent levels in apatite, titanite, micas, and amphibole (Table 10.3) (Petersen et al. 1982 and references therein; Markl and Piazolo 1998, 1999; Čopjaková et al. 2009; Harlov and Förster 2002a, b; Hansen and Harlov 2007). These minerals are typically the major hosts for Cl and F in metamorphic rocks (see Fig. 10.1 and Sect. 10.2.3.1). Fluorine contents in tourmaline from most metamorphic environments are likely to be in the trace element range (e.g., Van den Bleeken et al. 2007), as F is preferably incorporated into coexisting micas and titanite (Torres-Ruiz et al. 2003). However, under certain conditions, tourmaline contains elevated F concentrations (Henry and Dutrow 2011). A case where tourmaline concentrates high amounts of F, and thus might be the major F host, is reported by Čopjaková et al. (2009) from the Bohemian Massif where F-enriched metasedimentary rocks are inferred to be the geochemical source for significant tourmaline formation. Primary talc minerals can incorporate considerable amounts of F (e.g., ~0.5 wt%, Ross et al. 1968; Petersen et al. 1982; Abercrombie et al. 1987). High F contents can also be present in humite-group minerals, although restricted to marbles, impure dolomites, and calc-silicates (Tell 1974; Piazolo and Markl 1999; Tables 10.2 and 10.3). Cuspidine, a hydroxyl-silicate, although not very common, can be a major F host. It is found in a contact metamorphic setting such as calcareous contact metamorphic rocks in the Oslo Rift where cuspidine hosts ~10.5 wt% F (Jamtveit et al. 1997). Depending on the modal abundances of fluorapatite, biotite, and muscovite, fluorite is naturally the principal F host in metamorphic rocks. In the absence of fluorite, fluorapatite is generally the major host for F in most metasedimentary rocks (see Sect. 10.2.3.1 and Fig. 10.1). Fluorite is impossible to precipitate from seawater as a primary mineral phase (Möller et al. 1980; see also Worden 2018 in this volume) and in general dolomitization and the extraction of Mg from pore-water is necessary in order to split MgF^+ complexes—presumably the most important F binding complexes in brines (see Möller et al. 1980 and references therein). The increased Ca^{2+}

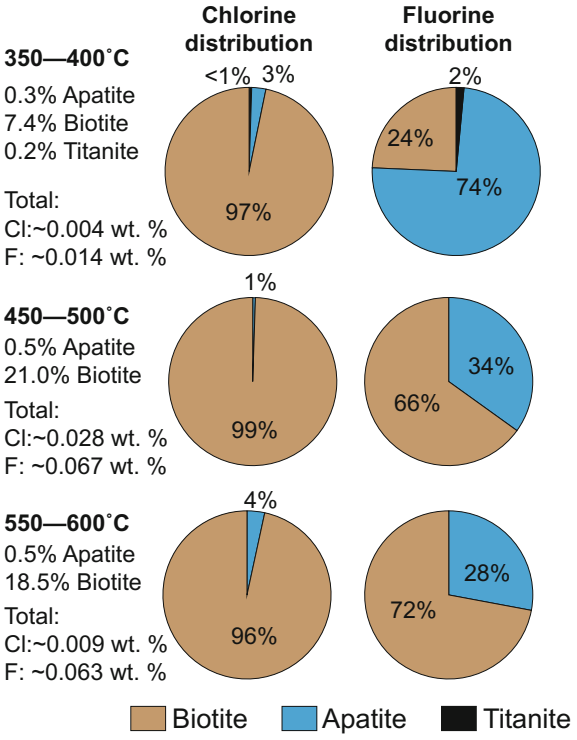

Fig. 10.1 Distribution of F and Cl in typical meta-psammopelites from the Eastern Mt. Lofty Ranges, Australia (Hammerli et al. 2016). The low-grade sample contains a modal abundance of 7.4% biotite whereas the higher-grade samples contain ~20% biotite. Apatite, biotite, and titanite are the only halogen-bearing minerals from which the bulk rock F and Cl can be estimated

concentration in the pore water due to dolomitization and the higher F^- ion content resulting from the Mg–F breakup can lead to CaF_2 supersaturation and subsequent fluorite formation, as disseminated grains, which can later be remobilised and re-precipitated in various forms (Möller et al. 1980). Due to this process, fluorite in metamorphic rocks is mostly restricted to calcareous horizons unless transported in vein and fault systems to different lithologies. Overall, metamorphic fluids require high F contents in order to form fluorite in e.g., granulite-facies rocks (e.g., Markl and Piazolo 1998; Sengupta et al. 2004). Other processes include the mixing of different fluid types with an example given by Sanchez et al. (2009) from fluorite deposits in Asturias (Spain), where F is inferred to be leached from volcanic rocks with subsequent fluorite precipitation during fluid mixing between deep brines and surfical fluids in carbonates.

Halogen bearing evaporite minerals, such as halite or carnallite, are unlikely to survive regional metamorphism as primary precipitation products due to their alteration, dissolution or recrystallization during low-grade metamorphism (e.g., Warren 1997, 1999).

10.2.3 Controlling Factors of Halogen Distribution During Metamorphism

Experiments and field studies have shown that the degree of halogen incorporation into minerals, and their distribution, is controlled by three major variables: (A) bulk rock composition, (B) pressure–temperature conditions, and (C) halogen availability/presence of fluids and their properties (e.g., pH, fluid/rock ratios). Whereas a detailed description of mineral chemistry and crystal structural changes for all the halogen-bearing phases upon variations in the above factors is beyond the scope of this chapter, we try to summarize the most important controlling factors on those minerals that are expected to control significant quantities of halogens in metamorphic rocks.

10.2.3.1 Bulk Rock Composition

The chemical composition of a rock is a crucial factor when it comes to sequestering halogens in environments with relatively low to moderate fluid-rock ratios, where fluids do not significantly change and re-equilibrate mineral assemblages (e.g., as in skarns, see Pirajno (2018)). Fluid-mineral ratios and their consequences are discussed in Sect. 10.3.1. The impact of the bulk rock chemistry on the ability of a rock and its minerals to host halogens is exemplified by marbles and orthogneisses from the amphibolite- and granulite-facies rocks of the Adirondack Mountains, New York, where the marbles contain higher Mg contents than the associated orthogneisses. This difference resulted in higher Mg/Fe ratios in biotite from the marbles compared to biotite from the orthogneisses (Valley et al. 1990). The ability of hydroxyl silicates to incorporate Cl and F is strongly dependent on the host mineral's Fe and Mg content such that F and Fe "avoid" each other and the high Mg contents lower the tolerance of Cl incorporation (Munoz and Swenson 1981; Valley et al. 1982; Volfinger et al. 1985; Hawthrone and Oberti 2007 and references therein). This leads to the situation where amphibole and biotite in marbles contain higher F contents than in the associated orthogneisses, which are relatively Cl rich (Valley et al. 1990).

Another example of the controlling factor in the bulk rock composition for halogen sequestration is given by Hammerli et al. (2016) who studied regionally metamorphosed psammopelites from the Kanmantoo Group from the Adelaide Fold Belt, Mount Lofty Ranges, Australia. This study shows that biotite and apatite control Cl and F in the host rock. While the vast majority of F is always hosted in apatite, irrespective of the metamorphic grade, the importance of apatite as a Cl sink strongly depends on the modal abundance of biotite (Fig. 10.1). Moreover, the bulk Cl and F contents of metasedimentary rocks seem to be correlated with the modal abundance of apatite and biotite and hence the rock's provenance. In other words, rocks with more pelitic protoliths are likely to contain elevated Cl contents compared to psammopelites. However, besides the chemical composition, P–T

conditions play an important role by stabilizing potential halogen hosts such as biotite (see Sect. 10.2.3.2).

The role of a rock's chemical composition in order to retain halogens becomes even more obvious by looking at marbles from the same metamorphic sequence in the Mt Lofty Ranges. Impure marbles show a much more diverse halogen-bearing mineral assemblage. Scapolite in marbles from an amphibolite-facies zone contain Cl in the weight percent-range (Kwak 1977; Hammerli et al. 2013; Hammerli unpublished data) and seems to be the most important Cl host as apatite contains low Cl concentrations (<200 ppm). Fluorine is distributed amongst minute grains of fluorite, titanite (~2.5 wt% F), and apatite (~4.5 wt% F).

Metabasites have a significantly different bulk rock composition than metamorphic rocks from the above examples. Nijland et al. (1993) investigated halogen content and distribution in metabasites from within the amphibolite- to granulite-facies transition zone in the Bamble Sector, South Norway. The authors established partitioning orders for F and Cl, where F is preferentially incorporated into apatite and is least favourably integrated into amphibole and titanite (apatite > titanite > biotite $\geq$ amphibole), whereas the order for Cl partitioning is apatite > amphibole $\geq$ biotite $\geq$ titantite.

10.2.3.2 Pressure and Temperature Conditions

Pressure and temperature effects on the halogen distribution between apatite and biotite have been studied both experimentally and by thermodynamic modelling by Korzhinskiy (1981), Zhu and Sverjensky (1991, 1992), and Sallet (2000). These results confirm observations that F is strongly partitioned into apatite over biotite. The degree of partitioning strongly depends on the Fe content of the biotite and the temperature. Higher temperatures lead to lower partitioning coefficients for F into apatite. Chlorine shows the same trend, being preferentially incorporated into apatite, although at high-temperatures it is possible that there is no particular preference for Cl incorporation between apatite and biotite (Zhu and Sverjensky 1991, 1992). The above studies further found that with increasing pressure and temperature, the hydroxyl-apatite member stability field expands and the fluorapatite and chlorapatite fields become smaller. However, chlorapatite becomes stable relative to fluorapatite at high temperatures. The partitioning of F between minerals and fluids, on the other hand, seems to be independent of pressure (Zhu and Sverjensky 1991, 1992).

Enami et al. (1993) studied the stability of titanite compositions with respect to different pressure and temperature conditions based on a comprehensive dataset of natural titanite occurrences. The data show that with increasing pressure and temperature, the F and Al concentrations in titanite increase. This increase is potentially linked with a negative volume change due to incorporation of F and Al into the titanite crystal structure where the smaller F ions replace the larger OH ions (Enami et al. 1993 and references therein). However, other studies (e.g., Markl and Piazolo 1999) have shown that other variables, such as fluid properties and bulk rock

compositions, especially low TiO_2/Al_2O_3 ratios, play a major part in F uptake. Hence, aluminous F-rich titanite might be stable over a wide pressure–temperature range. Tropper et al. (2002) perfomed experiments to investigate Al and F substitution in titanite at relatively high pressures and temperatures (900–1000 °C and 1.1–4 GPa). They confirmed earlier suggestions that the bulk rock and mineral assemblage play important roles for F subsitution into titanite. Their findings showed that the maximum subsitution of AlF^{2+} for TiO^{2+} in titanite ($CaTi[SiO_4](O,OH,F)$ is reached when titanite reacts with fluorite and anorthite or Al_2SiO_5.

The solubility of fluorite in an H_2O-fluid was found to be positively correlated with pressure and temperature (Tropper and Manning 2007, and references therein). However, fluorite solubility also increases with increasing salinity, which indicates that the salinity of the fluid is likely to be the controlling factor in many geological environments (see section below and 10.2.5).

10.2.3.3 Fluid Properties

Halogen availability plays a central role on how and in which minerals halogens are distributed. Chlorine and F behave substantially differently during geological processes that involve fluid-rock interaction. While Cl (and also I and Br) is strongly partitioned into aqueous fluids, F is preferentially incorporated into solid phases (e.g., Zhu and Sverjensky 1991). For instance, Kusebauch et al. (2015b) experimentally showed that apatite/fluid partition coefficients for F can reach 300. The larger ions Br and I, on the other hand, have partition coefficients that are up to 5 orders of magnitude smaller than F, and hence Br and I are concentrated in the fluid phase. Interestingly, Kusebauch et al.'s (2015b) study showed that OH preferably replaces Cl in apatite at high temperatures, irrespective of the fluid's NaCl concentration (see also Harlov and Förster 2003). Zhu and Sverjensky (1991) also suggested an increasing stability of OH-apatite at elevated pressures and temperatures; however, their conclusions are based on fixed HCl activities.

When hydroxyl minerals such as apatite, biotite, amphibole, or scapolite contain high levels of Cl, it is generally understood that fluids with high salinities must have interacted with that particular rock (Volfinger et al. 1985). Importantly, Munoz and Swenson (1981) and Zhu and Sverjensky (1991) pointed out that the Cl content in biotite is not only a function of NaCl in the fluid and/or the mineral composition (see Sect. 10.2.3.1), but also depends on the Cl speciation e.g., HCl in the fluid, which is sensitive to the pH of the fluid. Zhu and Sverjensky (1991) showed that decreasing the pH of a fluid favours the partitioning of Cl into annite (biotite) with respect to the fluid. In general and, with the exception of scapolite, which can be a major halogen host and only contains small amounts of OH (see Sect. 10.4.6), rock forming minerals that contain OH are the most likely hosts of the halogens, since the halogens can partially replace OH in e.g., apatite, amphibole, or biotite (see Eqs. 10.1 and 10.4):

$$\mathrm{OH}_{(\mathrm{Mineral})} + \mathrm{HCl}_{(\mathrm{aq})} = \mathrm{Cl}_{(\mathrm{Mineral})} + \mathrm{H_2O}_{(\mathrm{aq})} \tag{10.1}$$

$$K_{T,P} = \left(\frac{a\mathrm{Cl}_{(\mathrm{Mineral})}}{a(\mathrm{OH})_{(\mathrm{Mineral})}}\right) \Big/ \left(\frac{a\mathrm{HCl}_{(\mathrm{aq})}}{a\mathrm{H_2O}_{(\mathrm{aq})}}\right) \tag{10.2}$$

$$K_{T,P} = \left(\frac{X\mathrm{Cl}_{(\mathrm{Mineral})}}{X(\mathrm{OH})_{(\mathrm{Mineral})}}\right) \Big/ \left(\frac{a\mathrm{HCl}_{(\mathrm{aq})}}{a\mathrm{H_2O}_{(\mathrm{aq})}}\right) \tag{10.3}$$

$$(\mathrm{OH})_{2(\mathrm{Mineral})} + (2\mathrm{HF})^{0}_{(\mathrm{aq})} = \mathrm{F}_{2(\mathrm{Mineral})} + 2\mathrm{H_2O}_{(\mathrm{aq})} \tag{10.4}$$

$$K_{T,P} = \left(\frac{a\mathrm{F}_{2(\mathrm{Mineral})}}{a(\mathrm{OH})_{2(\mathrm{Mineral})}}\right) \Big/ \left(\frac{a\mathrm{HF}^{0}_{(\mathrm{aq})}}{a\mathrm{H_2O}_{(\mathrm{aq})}}\right)^{2} \tag{10.5}$$

$$K_{T,P} = \left(\frac{X\mathrm{F}_{2(\mathrm{Mineral})}}{X(\mathrm{OH})_{2(\mathrm{Mineral})}}\right) \Big/ \left(\frac{a\mathrm{HF}^{0}_{(\mathrm{aq})}}{a\mathrm{H_2O}_{(\mathrm{aq})}}\right)^{2} \tag{10.6}$$

Equations 10.2 and 10.5 show the equilibrium constant relationship between halogens in aqueous fluids and OH-bearing minerals for Cl and F, respectively. Under the assumption of ideal mixing of F–OH and Cl–OH in the anion site, Eqs. 10.3 and 10.6 can be justified where *X replaces the activity (a)* and stands for the molar fraction of F, Cl, or OH in the mineral (Korzhinskiy 1981; Zhu and Sverjensky 1991). A decrease in the water activity, coupled with an increase in the halogen content, in the hydrothermal fluid is one way to incorporate higher concentrations of halogens in OH-bearing minerals. For OH-bearing minerals, an increasing NaCl content in the fluid alone will not significantly increase their Cl and F content, as the fluid-mineral reactions are controlled by HF and HCl (Eqs. 10.1 and 10.4). This is consistent with observations by, e.g., Rubenach (2005) (see also Sect. "Albitization in the Mt Isa Inlier") where NaCl-rich fluids lead to albitisation but the halogen content of the biotite varies considerably across the outcrop and between the different albitization areas.

The incorporation of Cl or F into OH-bearing silicates, such as biotite or amphibole, generally extends their stability field to higher temperatures (e.g., Stormer and Charmichael 1971; Valley et al. 1982). In calc-silicate rocks, elevated F levels in talc can increase the stability of calcite and talc to sillimanite-grade conditions (Abercrombie et al. 1987), whereas the presence of NaCl can lead to scapolite formation over a wide range of pressure–temperature conditions (e.g., Shaw 1960; Ellis 1978).

10.2.3.4 Summary of Halogen Distribution in Metamorphic Rocks

As nicely exemplified by titanite, biotite, apatite, and amphibole, the presence, stability, and composition of most halogen-bearing minerals strongly depends on key parameters, such as bulk rock composition, pressure–temperature conditions, fluid

properties, and water-rock ratios, as briefly discussed in the above sections. However, once the key parameters (e.g., equilibrium constants) are thermodynamically constrained, halogen-bearing minerals, such as biotite, apatite, and scapolite, can be used to gain insights into the fluid properties, such as halogen fugacities, in coexisting hydrothermal fluids (see Sect. 10.2.6 below, as well as Ellis (1978); Munoz and Swenson (1981); Munoz (1984, 1992); Zhu and Sverjensky (1991, 1992)).

Despite the complexity of rock-water interaction and P–T dependence, simplified conclusions for the affinity of halogens in minerals during metamorphism can be drawn from natural observations and experimental results. In order to generalize halogen distribution amongst minerals, we distinguish between three bulk rock systems: (i) psammo-pelites, (ii) calc-silicate/marbles, and (iii) metabasites (Table 10.2). In psammo-pelitic rocks, F is strongly partitioned into apatite and phlogopite (e.g., Munoz and Eugster 1969) leading to the following simplified F distribution: apatite > biotite $\geq$ amphibole, while in calc-silicates and marbles, the presence of fluorite and/or humite minerals can lead to the following distribution of F (fluorite) > (humite) > apatite > titanite > amphibole $\geq$ biotite. The distribution for Cl is more variable and strongly dependent on bulk rock compositions. In calcic rocks, if present, scapolite and amphibole are likely to sequester the highest concentrations of Cl followed by apatite and biotite, whereas in psammopelitic rocks, apatite often acts as the main Cl sink closely followed by biotite. In mafic rocks (metabasites, e.g., Nijland et al. 1993), F is preferably incorporated into apatite and least favourably integrated into biotite and amphibole (apatite > titanite > biotite $\geq$ amphibole). The order for Cl partitioning is the following: apatite > amphibole $\geq$ biotite $\geq$ titanite, however, if present, scapolite is likely to be the most important Cl-host (Lieftink et al. 1993).

10.2.4 Halogen Content of Rocks During Metamorphism

The complexity of halogen uptake during metamorphism makes it difficult for a general statement to be made as to whether rocks gain or lose halogens during metamorphism. Boness et al. (1991) concluded, based on a series of metapelitic rocks ranging from the biotite-isograd zone to anatexis, that Cl, I, and Br concentrations are not correlated with metamorphic grade. Hammerli et al. (2016) made a similar observation for F where bulk rock F concentrations in metapsammopelites range between $\sim$100 and 900 ppm irrespective of metamorphic grade. Muramatsu and Wedepohl (1998) analysed regional metamorphic rocks (>450 °C; >5 kbar) and concluded that the bulk rock I content decreases by $\geq$80% during prograde metamorphism. The loss of I during relatively low-grade metamorphism can be explained by the decomposition of organic matter that liberates I into hydrothermal fluids whereas the large atomic size of I generally prohibits its incorporation into metamorphic OH-bearing minerals (e.g., Boness et al. 1991). A recent study (Selverstone and Sharp 2015) agrees with Muramatsu and Wedepohl's (1998) findings that the Cl content of metasedimentary rocks does not change systematically with metamorphic

grade. Moreover, their findings showed that the primary heterogeneities of the Cl isotope and Cl concentration in the protoliths persist throughout metamorphism. This also means that Cl is recycled into newly formed or recrystallized mineral phases rather than being released into the devolatilization fluid. Although no data are available, a similar scenario for Br as for I can be assumed as its ion size is too large to be incorporated to a great extent in metamorphic OH-bearing minerals (Correns 1956). However, it has been shown that hydrothermal alteration can impart elevated I and other halogen contents in rocks compared to fresh equivalents (Boness et al. 1991; Muramatsu and Wedepohl 1998). In some cases this may be explained by the formation of hydrothermal sulfides that can take up elevated concentrations of I (Fuge and Johnson 1984).

10.2.5 Halogen-Bearing Fluids and Mineral Solubility

Experimental data and thermodynamic modelling imply that the presence of halogens in fluids can significantly influence the solubility of major and minor mineral phases at the P–T conditions present during regional and thermal metamorphism. Evidence for mass transfer, associated with aqueous fluids during metamorphism, can be observed in the form of, for example, (syn-) metamorphic quartz (Fig. 10.2a) or calcite veins. The solubility of quartz in hydrothermal fluids has been studied extensively over a wide range of P–T conditions and fluid properties (e.g., Anderson and Burnham 1967; Rimstidt and Barnes 1980; Newton and Manning 2000; Shmulovich et al. 2001, 2006). The experiments have shown that the solubility of quartz in saline solutions strongly depends on the P–T conditions and the salt content of the fluid. In principle, two mechanisms have been observed: the so-called salting-in and salting-out effects. Salting-out behaviour leads to a situation in which the quartz solubility in the saline solution is lower than in pure water, whereas salting-in means that the quartz solubility is higher compared to a pure H_2O–quartz system. Figure 10.2 shows a compilation of experimental data for quartz solubility in H_2O–NaCl (Fig. 10.2b, c) and H_2O–$CaCl_2$ (Fig. 10.2b) systems. In H_2O–NaCl–quartz experiments at 700 °C and <4 kbar, the quartz solubility correlates positively with the NaCl content of the fluid until an *X*NaCl of 0.1 is reached in the fluid (salting-in, Fig. 10.2b, c and references therein). With increasing NaCl contents, the quartz solubility decreases and salting-out behaviour takes over. At higher pressures (>4 kbar) at 700 °C, no initial increase in the quartz solubility with increasing NaCl contents can be observed and the system shows a continuous salting-out behaviour (Fig. 10.2c). Shmulovich et al. (2006) produced an extensive data set for quartz solubility in fluids of different compositions, including H_2O–NaCl and H_2O–$CaCl_2$ solutions. Their experiments show that the solubility of quartz correlates with the properties of cations of the chloride species where larger electrostatic radii correlate with higher quartz

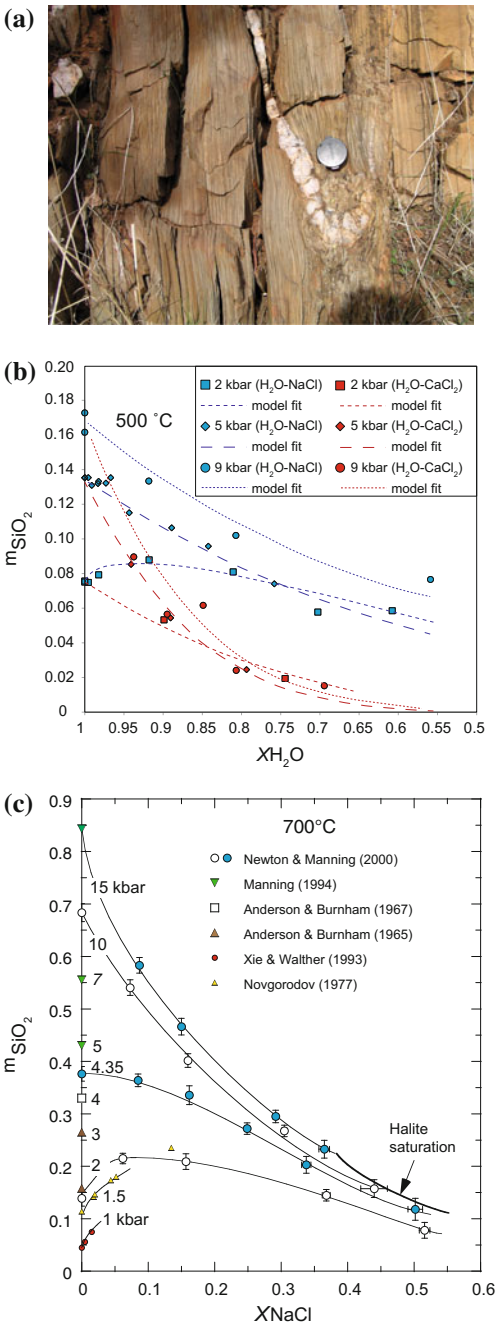

Fig. 10.2 **a** Typical folded (syn-) metamorphic quartz vein often found in metamorphic terranes. **b** Experimentally determined solubility of quartz in m SiO_2 with increasing salt content (decreasing XH_2O) at different pressures and salt compositions with monovalent and divalent cations (NaCl and $CaCl_2$), data taken from Shmulovich et al. (2006). **c** Solubility of quartz (m SiO_2) with increasing NaCl (XNaCl) at 700 °C under different pressures showing the pressure dependence of the salting-in and salting-out effect. At low pressures, quartz solubility initially increases (salting-in) with increasing XNaCl. This is not seen at pressures >4 kbar. This implies that especially at higher pressures, NaCl depresses mass transfer of quartz and plagioclase in the lower crust. (Figure modified after Newton and Manning 2000)

solubilities. Their experiments also showed that monovalent cations (e.g., NaCl) lead to higher quartz solubilities compared to divalent cation-chloride pairs (e.g., $CaCl_2$) at the same P–T conditions (Fig. 10.2b).

The experiments by Shmulovich et al. (2001) suggest that the solubility behaviour of albite in H_2O–NaCl fluid is very similar to that of quartz whereas diopside behaves differently and shows an increased solubility with increasing *X*NaCl in the fluid.

In contrast to quartz and albite, the solubility of calcite increases drastically in saline fluids. In a series of experiments, Ellis (1963) studied the solubility of calcite in aqueous fluids to temperatures of 300 °C and Fein and Walther (1989) performed calcite solubility experiments in supercritical saline fluids at 400–600 °C and 2 kbar. More recently, Newton and Manning (2002) studied calcite solubility in saline fluids at P–T conditions of the lower crust/upper mantle. All of these studies collectively demonstrated that, over this temperature range, NaCl is the driving factor for calcite dissolution. Newton and Manning (2002) further showed that increasing the pressure (6–14 kbar at 700 °C) leads to only a relatively small increase in calcite solubility (20%).

The solubility of calcite, and its precipitation, is shown impressively in large-scale areas such as the Mary Kathleen Fold Belt, Australia (Oliver 1996) or the Bamble Sector, Norway (Dahlgren et al. 1993) where vast areas have undergone carbonate metasomatism, often related to large-scale shear zones. Evidence for carbonate mobility on a smaller scale include calcite veins that can often be found in metamorphic rocks. Given the comparably very low solubility of calcite in "pure-water" (Fein and Walther 1989), it can only be speculated that saline fluids are likely involved in most metamorphic situations with significant $CaCO_3$ mass transfer. However it should also be noted that under certain circumstances, cooling and decompression of a saline-deficient fluid might still be able to precipitate significant amounts of carbonate (Caciagli and Manning 2003).

Similar to calcite, experimental studies have shown that the solubility of fluorite is positively correlated with fluid salinity where increased NaCl contents lead to the formation of NaF, CaF^+, MgF^+ and $CaCl^+$ complexes (e.g., Rimstidt 1997; Tropper and Manning 2007 and references therein).

Accessory phases, such as xenotime, monazite, and rutile, that are increasingly used as geochronometers for metamorphic events, have been investigated experimentally and on natural samples for their stability during interaction with hydrothermal/metasomatic fluids (e.g., Hetherington et al. 2010; Rapp et al. 2010; Harlov and Hetherington 2010; Budzyn et al. 2011; Harlov et al. 2011; Williams et al. 2011; Tropper et al. 2011, 2013). It has been shown that fluids rich in F or Cl can lead to partial dissolution of these accessory minerals and subsequent reprecipitation, which can at least partially and locally reset the radiogenic clock and, in the case of rutile, lead to highly elevated solubilities (e.g., Harlov et al. 2011; Williams et al. 2011).

10.2.6 The Use of Halogen-Bearing Minerals to Constrain Halogen Contents in (Metamorphic) Hydrothermal Fluids

The experimental work of Ellis (1978) on scapolite and fluid interaction in calcite-buffered systems at 750 °C and 4 kbar showed that the Cl and CO_2 contents of the scapolite (Cl/Cl + CO_3) are controlled by the fluid composition. Ellis (1978) proposed an equation to calculate the equilibrium constant for these conditions: $\ln K_D = -0.0028(X_{Al})^{-5.5580}$ where X_{Al} is the atomic ratio of Al/(Al + Si) in scapolite. The equilibrium constant can then be used in the following equation to determine the NaCl component in the fluid:

$$K_D = \frac{Xcc_{Sc} \times X\mathrm{NaCl}_{Fl}}{X\mathrm{NaCl}_{Sc}} \tag{10.7}$$

Xcc_{Sc} is the activity of $CaCO_3$ in scapolite, $X\mathrm{NaCl}_{Sc}$ is the activity of NaCl in scapolite and $X\mathrm{NaCl}_{Fl}$ is the fraction of NaCl in the fluid given as (NaCl/(NaCl + H_2O)). Ellis (1978) suggested that the activity coefficients in this system are close to 1. Therefore the activities of the individual components can be treated as mole fractions (see e.g., Oliver et al. 1992 or Hammerli et al. 2014 for examples and applications). However, due to the lack of thermodynamic data on scapolite, $X\mathrm{NaCl}_{fluid}$ approximations are limited to the experimental conditions, i.e., 750 °C and 4 kbar. Scapolite group minerals, their stability, and their occurrences are discussed in more detail later in Sect. 10.4.6.3.

Based on the partitioning coefficient for F–OH exchange between apatite and biotite, equations have been developed to calculate metamorphic and magmatic temperatures. The early geothermometer (Stormer and Carmichael 1971) has been improved throughout the years thanks to the availability of more thermodynamic data (e.g., Munoz and Ludington 1974, 1977; Ludington 1978; Zhu and Sverjensky 1991, 1992). The equation used to calculate temperatures from 300 to 1100 °C, put forward by Zhu and Sverjensky (1992), is:

$$T(^\circ\mathrm{C}) = \frac{8852 - 0.024P(\mathrm{bars}) + 5000X_{Fe}}{1.987 \ln K_{D,F}^{Ap/Bt} + 3.3666} - 273.15 \tag{10.8}$$

where X_{Fe} is the Fe fraction in biotite and $K_{D,F}^{Ap/Bt}$ is the partition coefficient for F between apatite and biotite (cf., Zhu and Sverjensky 1991, 1992). One of the main uncertainties in using this equation is the analytical error, especially if EPMA values are not drift corrected (Stormer et al. 1993). When applying the equation, it has to be kept in mind that biotite alteration can significantly influence the calculated temperatures. Additionally, Fe^{3+} seems to have an effect on the F–OH partitioning, which is not fully understood (Zhu and Sverjensky 1992).

Together with Munoz and Swenson's (1981) experiments and modelling, Zhu and Sverjensky's (1991, 1992) work allowed Munoz (1992) to reformulate his

equations from Munoz and Swenson (1981) that corrected the calculation of halogen fluid fugacities (f) in the fluid based on the biotite composition:

$$\log(fH_2O/fHF) = 1000/T * \left(2.37 + 1.1X_{Mg}\right) + 0.43 - \log(X_F/X_{OH}) \quad (10.9)$$

$$\log(fH_2O/fHCl) = 1000/T * \left(1.15 - 0.55X_{Mg}\right) + 0.68 - \log(X_{Cl}/X_{OH}) \quad (10.10)$$

$$\log(fHF/fHCl) = -1000/T * \left(1.22 + 1.65X_{Mg}\right) + 0.25 + \log(X_F/X_{Cl}) \quad (10.11)$$

where T (in Kelvin) is the estimated temperature of the halogen exchange equilibrium and X_{Mg} stands for Mg/(sum octahedral cations) in biotite. X_F, X_{Cl}, and X_{OH} are the mole fractions of F, Cl, and OH on the hydroxyl site of biotite. Examples for halogen fugacity calculations based on biotite chemistry can be found in e.g., Coulson et al. (2001), Harlov and Förster (2002a), and Hammerli et al. (2015).

10.3 Fluid or Rock Buffering and Origin of Fluids and Processes

10.3.1 Rock Versus Fluid Buffering

The overall low compatibility of Cl, Br, and I in most rock-forming minerals, and their high affinity for fluid phase, means that metamorphic fluids will contain concentrations of these elements that are relatively high compared to the minerals. During the metamorphic cycle, the fluid/rock ratio decreases during compaction and diagenesis at elevated temperatures when pore spaces are reduced and the equilibria of halogen consuming reactions are shifted towards the fluid component due to, e.g., exhaustion of the halogen supply from evaporites (halite). During diagenesis, the halogen content of the rock reflects the depositional/sedimentary environment where a general trend can be expected from dense bittern brines sinking to lower sedimentary sequences (e.g., Warren 1997; Fig. 10.14, see Sect. 10.6). During this process, fluid-rock interaction and equilibration with excess Ca and Na bearing minerals, e.g., via albitization, can control the fluid properties (e.g., Houston et al. 2011, see also Yardley and Bodnar 2014). In the case of excess NaCl due to, for example, halite dissolution reactions, the fluid composition might not change significantly despite the consumption of Ca-bearing feldspars via albitization. Such fluids/brines were termed mass-limited by Houston et al. (2011) (see also Sect. 10.4.4).

However, if considerable amounts of external fluids are pumped through the pore-space and/or fractures during metamorphism, fluid/rock ratios, and hence time-intergrated fluid flux, can increase again. Increased time integrated fluid flux or, in other words, higher fluid/rock ratios (e.g., Greenwood 1975; Ferry and Dipple 1991; Oliver et al. 1992) can be directly linked to the degree of fluid buffering (e.g., Symmes and Ferry 1991). Fluid buffering is here defined as a system in which the

fluid, rather than the primary rock composition, controls the approach to local equilibrium of the system. In some cases, the fluid can be externally derived. An example of external fluid buffering is given in the study by Hammerli et al. (2014) that describes mafic rocks which have been almost entirely replaced by scapolite during fluid-rock interaction. In mineral assemblages where scapolite is present, a direct link between fluid salinity, fluid/rock ratios, and the halogen bulk rock content might be present (see Sect. 10.2.6; Oliver et al. 1992; Hammerli et al. 2014). However, the speciation of Cl and F is crucial for halogen incorporation in OH-bearing minerals such as biotite (Rubenach 2005, see Sects. 10.2.3.3 and "Albitization in the Mt Isa Inlier"). In the case of rock buffering, the minerals in the rock regulate the metamorphic reactions and control the fluid composition, including the halogen contents. Such scenarios can also be described as systems with low fluid/rock ratios or low time integrated fluid flux. Fluid- or rock-buffered systems might commonly be restricted to individual rock layers, as indicated by the varying progress of infiltration-driven metamorphic reactions (e.g., Oliver et al. 1992; Ferry 1994; Ferry et al. 2001; Evans et al. 2013; Hammerli et al. 2014). Most regional metamorphic belts probably remain rock-buffered (low fluid/rock ratios) systems (e.g., Greenwood 1975; Rumble 1977; Mora and Valley 1989; Oliver et al. 1992; Hammerli et al. 2014), while relatively high fluid fluxes might be restricted to focussed/channelized fluid flow paths, often seen as e.g., quartz veins (e.g., Ague 1994; Ferry and Gerdes 1998; Masters and Ague 2005, Fig. 10.2a). Smith and Yardley (1999) describe a classic example of rock buffering in the low-grade metamorphic rocks of the Otago Schist, New Zealand. They suggest that equilibration of Cl-rich detrital apatite with a diluted pore-fluid during metamorphism could significantly contribute to the fluid salinity. Another example is given by metasedimentary rocks from the Mary Kathleen Fold Belt, where Oliver et al. (1992) claimed that variable Cl-concentrations, on a layer-scale, in minerals and fluids, were the result of the original heterogeneous protolithic compositions where halite would have controlled the salinity of the fluids and the Cl contents of the minerals. Another process that potentially significantly alters the salinity of pore-water under rock buffered conditions is the leakage of fluid inclusions from earlier igneous or metamorphic events (Nordstrom et al. 1989). Fluid inclusions in general can be a major halogen reservoir. Fuge and Johnson (1984) found that >30% of a "mineral's" I can be stored in fluid inclusions. In contrast to "internal" halogen reservoirs, some metamorphic belts show evidence of widespread metasomatism resulting from the advection of fluids. Examples include the Mount Isa Inlier (Rubenach 2012) and the Bamble Zone in Norway (Nijland et al. 2014 and references therein) (see Sects. 10.4.4.2 and 10.4.6.3).

10.3.2 Fluids in Metamorphic Rocks and Their Origins

During sedimentation and diagenesis, halogens, especially Cl, Br, and I, are mainly concentrated in pore-waters and/or halogen-bearing evaporites. Compaction,

resulting in decreasing pore volumes, will automatically decrease the halogen reservoir in a sedimentary pile (Yardley 2009). Dehydration reactions during subsequent prograde metamorphism are expected to lead to a dilution effect, and hence lower the salinity of the pore-fluids. This concept is supported in a recent study by Selverstone and Sharp (2015) who found that dehydration reactions do not release halogens. However, Yardley and Graham's (2002) study on metamorphic fluids showed that the degree of dilution of saline fluids by water, released during dehydration reactions, is less pronounced than expected. Moreover, their dataset shows a notable persistence in fluid salinity during metamorphism. While early dehydration of, for example, clay in relatively porous rocks allows for the recharge of saline fluids via pores, and hence limits fluid dilution, the persistance of saline fluids in rocks with low porosity is more difficult to explain. One possibility is that a so-called "dual porosity" network controls the pore water properties and the dehydration discharge. Saline fluids might occur as isolated pores while fluid released by dehydration reactions escapes via a network of microfractures (Holness and Clemens 1999; Yardley and Graham 2002). Based on a comprehensive dataset of fluid inclusions and fluids sampled from drill holes, Yardley and Graham (2002) also showed that the salinity of metamorphic fluids is strongly correlated with the geodynamic setting of sedimentation. Overall, metamorphic fluids evolved in metasedimentary rocks, which were accumulated in oceanic or accretionary settings, contain significantly lower salinities, typically <10 wt% NaCl, compared to metamorphic fluids in rocks originally deposited on continental crust. The authors conclude that this difference is derived from the presence and distribution of an evaporitic horizon and/or connate waters in continental sedimentary environments. In evaporite-present sequences, the dissolution of halite during metamorphism can lead to higher salinities in metamorphic fluids with increasing metamorphic temperatures—the opposite effect of dehydration reactions. While evaporite minerals in general are unlikely to survive regional metamorphism, due to their alteration, dissolution, or recrystallization during low-grade metamorphism (e.g., Warren 1997, 1999), it is possible that fluids with salinities close to halite saturation remain in the pore-spaces during metamorphism.

Other processes that can lead to high-salinity brines are hydration reactions or phase separation via CO_2 boiling. This has been observed in siliceous carbonate rocks from the Alps that underwent lower amphibolite-facies metamorphism. Phase separation of fluids, that originally were close to halite saturation, can lead to the precipitation of solid halite and sylvite minerals in regional and contact metamorphic rocks (Trommsdorf et al. 1985; Trommsdorf and Skippen 1986, also see Sect. 10.4.1). More recently, Ferry and Gottschalk (2009) have demonstrated that halide minerals can form during infiltration-driven decarbonation reactions under regional metamorphic conditions, provided that the decarbonation reactions take place at least partly in the unmixed fluid field and that the infiltrated fluid has a salinity similar to seawater or greater. The precipitation of halide minerals during metamorphism might be a more common scenario than generally assumed. Markl and Bücher (1998) observed NaCl–KCl solids in granulites from the lower crust. The halide minerals were interpreted to have formed during a "dewatering process"

in which amphibole formed from pyroxene and Fe–Ti oxides. During this process, amphiboles preferably incorporate H_2O and therefore enrich the fluid's Cl content until halide saturation is reached. The lack of observations of halite crystals in high-grade metamorphic rocks might be strongly related to routine thin section preparation techniques, which generally involve water, that would dissolve minute halite grains (Manning and Aranovich 2014). Nevertheless, halite crystals in ultra-high temperature granulites (Huizenga, pers. comm.) would further imply the presence of saline fluids over a large range of pressure and temperature conditions.

Unfortunately, no comparable data exist for F, I, and Br. Nevertheless, F concentrations in fluids from metamorphic environments are generally expected to be low and not correlated with the salinity of the fluid (e.g., Yardley 1996).

As mentioned in Sect. 10.3.1, throughout the metamorphic history of a rock the pore-water chemistry does not only change due to attempted equilibration with the constituent minerals, rather the infiltrating fluids can also replace and change the pore-water's geochemical properties. The infiltration of external fluids has been recognised in various regional and contact metamorphic terranes (e.g., Ferry and Dipple 1991; Ague 2003; Masters and Ague 2005; Aranovich et al. 2010; Hammerli et al. 2015). Potential external halogen-rich fluid sources include: (a) seawater, (b) saline fluids derived from halite dissolution processes, (c) residual fluids after halite extraction (bittern brine fluids), and (d) magmatic fluids.

Besides seawater and seawater-related fluids, such as residual bittern brines (see Sect. 10.3.3), magmatic fluids, and associated hydrothermal systems, have been recognized as important halogen sources in the Earth's crust (e.g., Böhlke and Irwin 1992; Irwin and Roedder 1995; Kendrick et al. 2001a, b; Hammerli et al. 2014). These fluids can be observed in currently active hydrothermal systems linked to igneous activity. Such magmatic fluids can contribute halogens to contemporaneous (thermal) metamorphic processes (Penniston-Dorland and Ferry 2005). A well-studied example of an active hydrothermal system, and related saline fluid production, is the Taupo Volcanic Zone (TVZ), North Island, New Zealand. The TVZ sits in a zone of active subduction of the Pacific plate under the Australian plate (e.g., Giggenbach 1995; Reyes and Trompetter 2012; Bernal et al. 2014 and references therein). Bernal et al. (2014) measured a range of fluid tracers including Cl and Br in hydrothermal fluids. The study showed that it might be possible to distinguish between andesitic and rhyolitic magma sources by examining hydrothermal fluids. In their study, they concluded that the hydrothermal fluids and Cl have two different sources. In the east of the TVZ, hydrothermal fluids are related to andesitic magmas, while in the west hydrothermal fluids are linked with rhyolitic magmatism. Under favourable conditions, exsolving magmatic fluids can be responsible for strong metasomatism and skarn formation, which is discussed in detail in Chap. 12 (Pirajno 2018).

Besides the introduction of halogens into metamorphic terranes from the above sources (a–d), recycling of the crust in complexly evolving tectonic regimes and the release of highly saline fluids can be significant. Glassley et al. (2010) present an example where K-rich brines were produced during the continental collision responsible for the Nagssugtoqidian Orogen in West Greenland. Hypersaline K-rich fluids, that metasomatically altered rocks via a crustal-scale shear zone (Nordre Stromfjord Shear zone), were produced when serpentinized lithospheric mantle was

trapped during continental collision. Dehydration reactions and the mobilization of trapped saline pore fluids are the likely source for the K-rich brines. The altered rocks are rich in K-feldspar, tourmaline, fluorapatite, and zircon. It was argued that the enhanced fluorapatite and zircon levels in the altered rocks could have resulted from the dissolution of these minerals in the fluid source region via interaction with hypersaline fluids and have subsequently crystallized in the altered rocks.

10.3.3 Halogen Ratios and Cl Isotopes

10.3.3.1 Halogen Ratios

In order to understand mass movement, fluid flow, and associated element mobility, that in some cases lead to mineralization events of economic significance, halogen ratios, especially Br/Cl and I/Cl, in fluid inclusions and minerals have been used to constrain and identify fluid- and halogen origins during regional and contact metamorphism. For illustrative purposes, we use molar log Br/Cl and I/Cl ratios in Fig. 10.3 (Table 10.4 shows the conversion of different halogen ratios alternatively used in other studies). When seawater evaporates (Br/Cl ~ -2.81, I/Cl ~ -6.06) to the point of halite precipitation, the residual bittern brines contain high concentrations of Br and I due to the incompatibility of Br and I in halite (e.g., Holser, 1979a; McCaffery et al. 1987; see also Worden 2018 in this volume). It follows that bittern brine fluids contain high Br/Cl ratios (>-2.81) and high I/Cl ratios ($\gg -6.06$) (Fig. 10.3). Such fluids have been recognized in several regional metamorphic terranes such as the Mt. Isa Inlier or the Adelaide Fold Belt, Australia (Heinrich et al. 1993, Kendrick et al. 2006, 2007; Hammerli et al. 2013, 2014). Fluids that contain a substantial dissolved halite component show low Br/Cl ratios ($\ll -2.81$) and low I/Cl ratios (<-6.06) (Holser 1979a; McCaffery et al. 1987; Böhlke and Irwin 1992). Examples where the dissolution of halite contributed significantly to the halogen content of the fluid during metamorphism include the Emerald fields in Colombia (Banks et al. 2000; Fig. 10.3) and the Cloncurry district in the Mt. Isa region (Kendrick et al. 2011). Typical S-type granitic fluids are inferred to have Br/Cl log ratios between ~ -3.22 and -2.85 and I/Cl log ratios of around -4 (e.g., Böhlke and Irwin 1992; Irwin and Roedder 1995), while mantle fluids/juvenile magmatic fluids are confined to Br/Cl log ratios between -3 and -2.7 and I/Cl log ratios of -5 and -4.15 (Jambon et al. 1995; Johnson et al. 2000; Kendrick et al. 2001a). However, besides fluid mixing, several processes potentially alter fluid end-members. Organic material, high in Br and I, can strongly influence the fluid's Br and I contents upon fluid interaction during metamorphism. Examples include fluids that gained some of their Br content via the decomposition of organic material at temperatures <200 °C during Alpine metamorphism (Hurai et al. 2008).

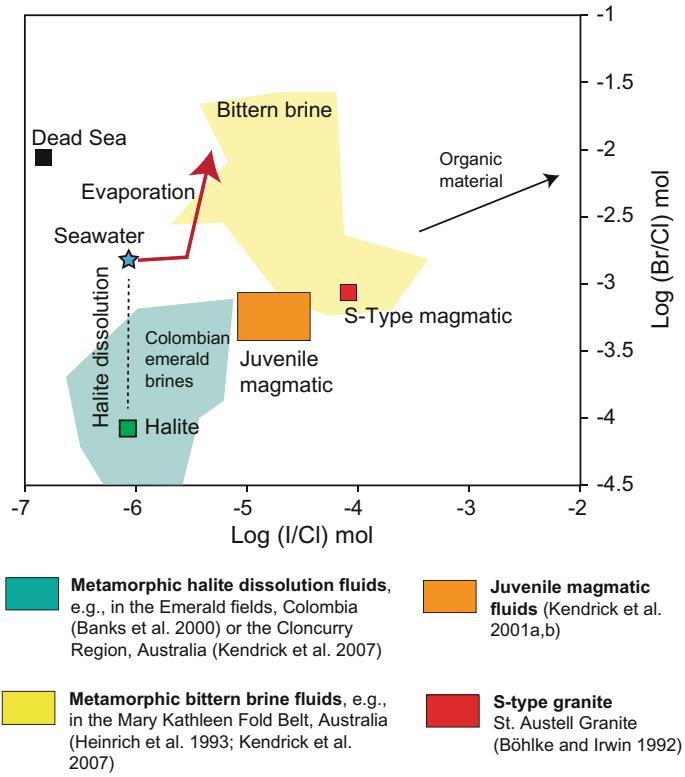

Fig. 10.3 Characteristic halogen ratios for fluids from different sources

Furthermore, Bons and Gomez-Rivas (2013) have shown that Cl and Br can potentially fractionate during gravitational infiltration into the crust as a result of the greater mass of Br compared to Cl. Br/Cl ratios can therefore be significantly increased if this process continues for several tens of million of years. Halogen fractionation during vapour-liquid phase separation has been poorly studied and the outcomes are controversial. Phase separation in the presence of CO_2 in fluids with relatively high halogen contents potentially plays a more important role than is generally assumed (e.g., Liebscher et al. 2006 and references therein). The most common problem, however, when assigning fluids to their original sources, is how halogens fractionate between minerals and between minerals and fluids. This has to be specifically considered in rock-buffered environments with low fluid fluxes and hence low fluid/rock ratios. To date, only a very small database of Cl, I, and Br contents in minerals, other than scapolite, is available, which makes it difficult to assess the degree of fractionation resulting from different distribution coefficients between fluids and minerals. The importance of future studies focusing on halogen fractionation has been shown in a pilot study by Mark et al. (2005), which indicates significant fractionation of halogens between biotite and scapolite.

Table 10.4 Reference halogen ratios of crustal fluids and their conversion to different notations commonly used in the literature

	Cl/Br	Cl/Br(m) #	Br/Cl (m)*10^{-3}	Br/Cl (log m)	I/Cl(m)*10^{6}	I/Cl*10^{6}	I/Cl(log m)	Reference
Seawater	~288	~648	1.54	~−2.81	0.87	~3.1	~−6.06	Riley and Chester (1971)
Halite	>4450	>10,000	<0.1	<−4	≪−0.87	≪3.1	≪6.06	Holser (1979a); McCaffery et al. (1987)
Halite dissolution fluid	≫288	≫647	≪1.54	≪−2.81	<0.87	<3.1	<6.06	Holser (1979a); McCaffery et al. (1987); Böhlke and Irwin (1992)
Bittem brine	<288	<648	>1.54	>−2.81	>0.87	>3.1	>−6.06	Holser (1979b); McCaffery et al. (1987)
Magmatic fluid	310 to 735	~700 to 1650	0.6 to 1.43	~−3.22 to −2.85	~100	~358	~−4	Böhlke and Irwin (1992), Irwin and Roedder (1995)
Mantle fluid	220 to 445	~500 to 1000	1 to 2	~ −3 to −2.7	~10 to 71	~37.8 to 254	~−5 to −4.15	Jambon et al. (1995); Johnson et al. 2000); (Kendrick et al. (2001a)

#(m) stands for mol

10.3.3.2 Halogen Isotopes

In addition to halogen ratios, stable Cl isotopes, and to a much lesser degree, stable Br isotopes have been used to constrain fluid sources and rock–water interaction processes (see Eggenkamp 2014 for a comprehensive review). Both elements have two stable isotopes (^{35}Cl, ^{37}Cl and ^{79}Br, ^{81}Br). Stable Cl and Br isotope ratios are usually reported as $\delta^{37}Cl$ SMOC and $\delta^{81}Br$ SMOB where SMOC and SMOB stand for standard mean ocean chloride and standard mean ocean bromide, respectively. These two values are defined as 0‰ whereas positive $\delta^{37}Cl$ and $\delta^{81}Br$ values show enrichment in the heavy isotopes relative to seawater. Eggenkamp (2014) summarized $\delta^{37}Cl$ signatures for sedimentary pore-waters. He showed that most published values are negative with the majority being around −0.2‰, while $\delta^{81}Br$ tended to be positive in pore water. Early halite is slightly enriched in ^{37}Cl ($\delta^{37}Cl > 0$) compared to the residual brine. Whereas subsequently formed evaporite minerals, have negative $\delta^{37}Cl$ values, resulting in evaporite deposits with Cl isotope signatures between −1 and 1 $\delta^{37}Cl$ (mostly between −0.5 and 0.5) (Eggenkamp et al. 1995; Eggenkamp 2014 and references therein; see also Worden 2018). Hence, by dissolving evaporite sequences, Cl isotope signatures similar to seawater can be expected. As yet, there is no general agreement on the Cl isotope signature of the mantle (see Eggenkamp 2014 for a summary on published data; Barnes and Sharp 2017; see also Chap. 14, Klemme and Stalder (2018)). The continental crust has a heterogeneous Cl isotope signature, as demonstrated by Selverstone and Sharp (2015) who measured variable isotope ratios in metamorphic rocks between −3 and 2.4‰ that seem to be unaffected by metamorphic grade.

10.4 Halogen-Rich Fluids and Related Processes

10.4.1 Fluid Immiscibility

In a binary H_2O−salt system, phase separation (boiling) is prominent at low pressures (<2 kbar) and hence restricted to contact metamorphic conditions (see Heinrich 2007 for a review). However, if non-polar phases such as CO_2 and CH_4/N_2 are added to a saline fluid, in the resulting ternary system (e.g., H_2O−CO_2−NaCl), the immiscibility field expands drastically under most conditions of regional metamorphism (e.g., Trommsdorf and Skippen 1986). In many metamorphic environments, it can be expected that the (infiltrating) fluids contain CO_2 and Cl, the latter probably prominently bound to Na but also to other salts such as $MgCl_2$, KCl, $CaCl_2$, as well as HCl. Various metal-chloride complexes might also be present (e.g., Sisson and Hollister 1990; Walther and Orville 1982; Hemley et al. 1992; Yardley 2005). The presence of NaCl in metamorphic fluids almost certainly leads to a two fluid system in the course of decarbonation reactions in carbonate-bearing rocks during prograde metamorphism (Fig. 10.4). During fluid infiltration driven decarbonation processes, the progress of decarbonation is strongly influenced by the fluid's halogen content.

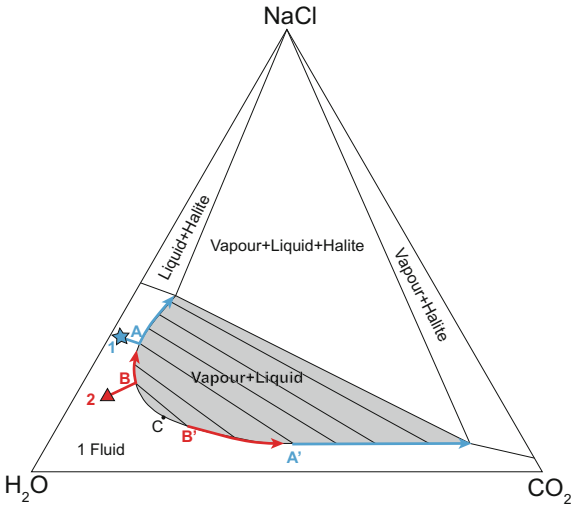

Fig. 10.4 Fluid immiscibility at amphibolite facies conditions in the system NaCl–H_2O–CO_2 modified from Bowers and Helgeson (1983), Trommsdorf and Skippen (1986), and Heinrich (2007). Fluid 1 (*star symbol*) evolves upon decarbonation (increasing CO_2) towards the two fluid slovus where fluid A coexists with Vapour A'. Further decarbonation allows the fluid to evolve along the solvus until the fields are reached where fluids (liquid and vapour phase) are saturated with vapour and lead to halite precipitation. Fluid 2 (*triangle symbol*) demonstrates the scenario for hydration reactions where H_2O is lost and hence the 1 phase fluid hits the solvus where it evolves and eventually reaches the same composition as fluid 1 upon decarbonation

Ferry and Gottschalk (2009) investigated how the infiltration of saline fluids affects the spatial progress of typical decarbonation reactions such as calcite + quartz = wollastonite + CO_2 and dolomite = periclase + calcite + CO_2 in contact metamorphic settings. Their results showed that for fluids with salinities ≥ 5 times higher than seawater, significantly higher fluid fluxes (up to ~ 8 times higher) are required to achieve the same spatial decarbonation progress as pure H_2O fluids. Fluids with lower salinities ($X_{NaCl} \leq 0.05$) require 1.1–1.5 times the fluid flux to produce the same spatial extent of decarbonation compared to pure H_2O systems. These observations are directly linked with fluid phase separations (Fig. 10.4) as the CO_2-rich fluid phase limits the progression of the above reactions to the right.

10.4.2 The Presence of NaCl and Its Consequences for Fluid Flow

The role of NaCl during metamorphic fluid flow has been investigated experimentally in detail over the past few decades. In order to understand the potential of fluid flow in (meta-) sedimentary rocks, the study of dihedral angles along grain boundaries, also called "wetting angles", is critical. These angles define whether

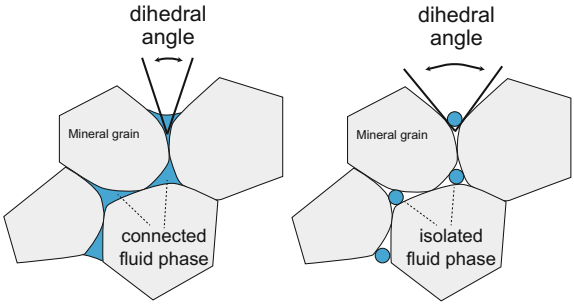

Fig. 10.5 Dihedral angles in (meta-) sedimentary rocks. Low angles lead to pore-water connectivity and hence permit pervasive fluid flow whereas high dihedral angles result in isolated pore-waters. (modified from Minarik 2003)

porewaters are connected and enhance fluid flow or whether porewater occurs as isolated droplets at grain triple junctions (Fig. 10.5). Many studies have investigated dihedral angle systematics in H_2O–CO_2–NaCl–carbonate and quartz–CO_2–H_2O–NaCl systems over a wide range of pressure–temperature conditions (Watson and Brenan 1987; Laporte and Watson 1991; Holness and Graham 1991, 1995; Holness 1992; Gibert et al. 1997; Heinrich 2007). The results show that connected fluid phases (pore-water) in marble, and hence pervasive fluid flow, is only expected if the fluid compositions are close to $X\mathrm{CO}_2 \sim 0.5$ or if the NaCl content is ≥ 30 wt%. Such high salinities might be reached during fluid immiscibility processes (Fig. 10.4). Other fluid compositions in monomineralic carbonate rocks lead to larger dihedral angles and hence pore-water will occur as isolated fluids (Fig. 10.5) so that fluid flow or fluid infiltration is more dependent on higher porosity; on fluid overpressure and subsequent hydrofracturing or tectonic (micro-) fractures (e.g., Oliver et al. 1990; Rubenach 2012); and/or reaction enhanced permeability via processes such as albitization (Hövelmann et al. 2010). In rocks where quartz is the major mineral, fluids with $\mathrm{CO}_2/(\mathrm{CO}_2 + \mathrm{H}_2\mathrm{O}) > 0.3$ tend to be restricted to isolated pores. Based on these studies, at shallow crustal levels fluid is theoretically only expected to circulate via porewater connectivity if the salinity is high. At lower crustal levels (i.e., up to <25 km), the salinity becomes less important and weaker brines and fluids with low CO_2 contents might be able to migrate via porewater connectivity. Overall it has to be kept in mind that the above studies mostly looked at synthetic, monomineralic rocks with synthetic grain boundaries and porosity. In nature, mineral assemblages are typically more complicated and hence the above findings might be only one factor, out of many, that control fluid flow. Moreover, Connelly and Podladchikov (2013) pointed out that compaction is likely a driving force for fluid flow at lower crustal depths where fluid might be accumulated on certain horizons that potentially act as large-scale lateral fluid conduits.

10.4.3 Halogen Behaviour During Thermal Metamorphism

Besides rock buffered scenarios, where halogen contents often were not significantly changed by external fluids, thermal contact aureole rocks are commonly

influenced by the infiltration of magmatic and meteoric fluids, and/or by the formation of metamorphic fluids. Fluid flow may occur away from plutons, toward plutons, or along circulatory patterns. Although our understanding of fluid-rock interaction in contact aureoles has benefited greatly from isotopic and fluid inclusion studies, systematic research on halogens in thermal metamorphic rocks has been mainly restricted to calc-silicate rocks and skarns (see Pirajno 2018).

Studies of halogens in pelitic rocks subjected to thermal metamorphism are quite limited. An exception is work on the Ponder Pluton and its aureole (British Columbia, Canada) by Sisson (1987). She documents halogens in biotite, amphibole, and apatite in both the pluton and the surrounding thermal metamorphic rocks (Fig. 10.6). The concentration of Cl in the minerals increases towards the contact with the pluton and decreases continuing on into the pluton, whereas the reverse is true for F (Fig. 10.6). Fluid inclusions in quartz veins and quartz in granite samples show high salinity values. This observation is interpreted as an influx of a Cl-rich/F-poor fluid towards and into the pluton (up-temperature fluid flow), resulting in exchange of Cl for F in granite minerals.

A different scenario is proposed by Markl and Piazzolo (1998) who studied a marble and calcsilicate bearing meta-sedimentary sequence in Central Dronning Maud Land, East Antarctica. These rocks underwent granulite facies metamorphism ($\sim$830 °C and $\sim$6.8 kbar), followed by the post-metamorphic intrusion of a syenite. The marbles and calcsilicates were interpreted to represent metamorphosed evaporite sequences that formed anhydrite, gypsum, and scapolite during metamorphism. The study proposed that aqueous fluids were liberated when the melt reached H_2O saturation at $\sim$650 °C and $\sim$4.5 kbar. The released fluid led to retrogressive mineral reactions in the surrounding meta-sedimentary rocks. However, the retrogression of scapolite was relatively limited and hence it is assumed that potential Cl-liberation upon scapolite breakdown was minor. In contrast to Sisson's (1987) study, Markl and Piazolo (1998) propose down-temperature fluid flow towards and into the surrounding country rocks. During fluid-rock interaction, F was actively removed from the fluid via the formation of fluorite and other F-bearing phases such as humite group minerals. The extraction of F from the fluid is reflected by the trend of increasing H_2O/HF fugacity ratios away from the intrusion. Chlorine on the other hand behaved differently and remained in the fluid phase. This is supported by the similar H_2O/HCl fugacity ratios obtained from biotite in the syenite and in the surrounding marbles/calcsilicates.

In a study of biotite from pelitic rocks in the Ballachulisch aureole (Scotland), Pattison (1987) found no relationship between the F content and metamorphic grade. The highest F values (>0.7 wt%, up to 1.4 wt%) occur in anomalous magnesian samples.

The most detailed study on halogens in contact-metamorphosed siliceous carbonates is that of Penniston-Dorland and Ferry (2005). They studied the F and Cl contents of apatite from the Ballachulisch and Beinn and Dubhaich aureoles, Scotland; the Monzoni and Predazzo aureoles, Italy; and the Ritter Range roof pendant, California. A correspondence was found between apatite compositions (Cl, F, OH) and the X_{CO_2} calculated from the metamorphic assemblages (Fig. 10.6). In samples with high X_{CO_2}, the apatite grains are enriched in Cl. This is a consequence

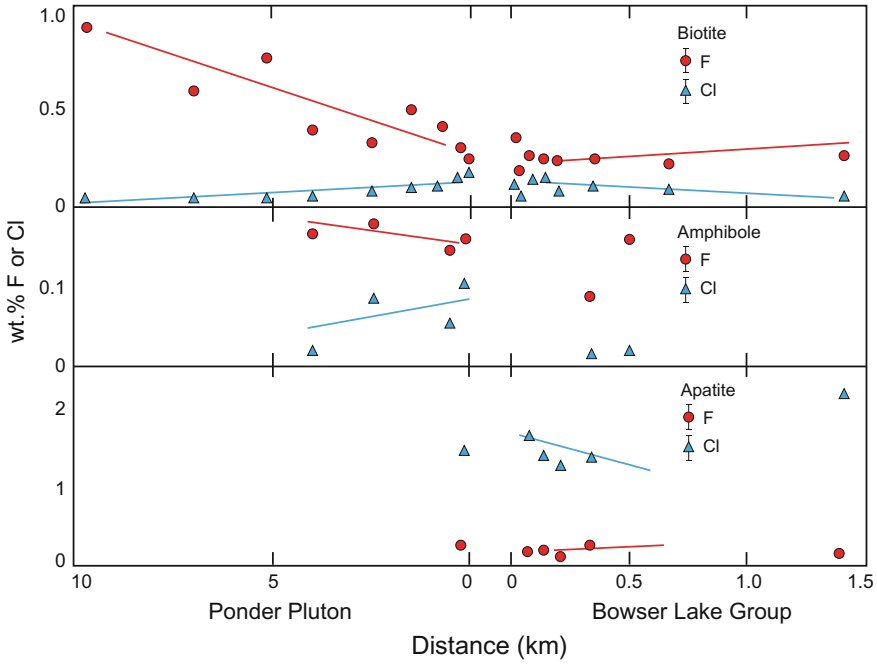

Fig. 10.6 Fluorine and Cl concentration variations in biotite, amphibole, and apatite versus distance from the contact between the Ponder Pluton and Bowser Lake Group sediments. The contact of the Ponder Pluton and the sediments is at "0" on the x-axis. (Figure modified from Sisson 1987)

of rock buffered metamorphic reactions, where the high Cl is probably the result of a low a_{H2O} and low F relative to Cl. In contrast, a second group of apatite grains is close to the F–OH mixing line, corresponding to infiltration of low XCO_2, relatively F-rich magmatic fluids (Fig. 10.6). Samples of contrasting compositions can be as little as 1 m apart, but are generally on the order of 100 m. Their study also summarizes apatite compositions from a variety of metamorphic and skarn lithologies.

The fluid buffered scenario in metamorphic rocks requires significant time integrated fluid fluxes, and hence high fluid-rock ratios. This is commonly achieved in contact metamorphic settings at the interface between the intrusion and the host lithology that frequently results in skarns. Detailed information on the role of halogens during skarn-forming processes can be found in Lecumberri-Sanchez and Bodnar (2018) and Pirajno (2018; Fig. 10.7).

10.4.4 Albitization

10.4.4.1 Mechanisms

Besides forming during fluid migration in sedimentary basins, and in some cases underlying crystalline basement, albitites may also form during regional

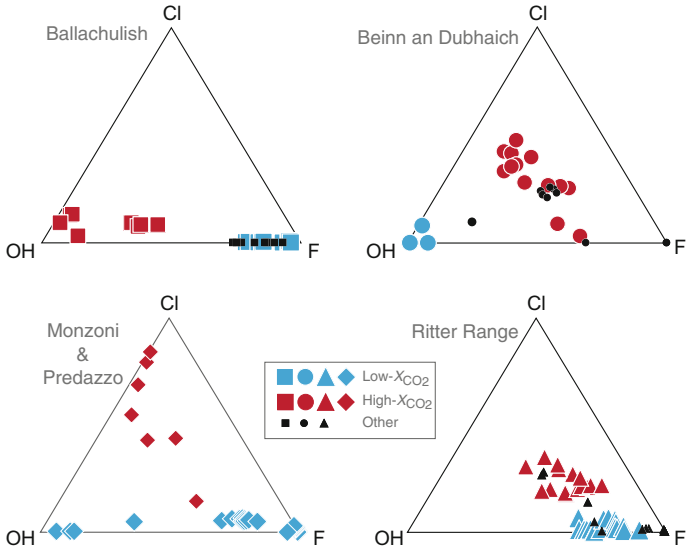

Fig. 10.7 Apatite compositions separated by location and rock type. XCO_2 refers to the rock type and fluid the minerals were in equilibrium with. All aureoles show the same trend of Cl-poor apatite in low-XCO_2 systems. Apatite from the high XCO_2-group show distinctly higher Cl contents and are Cl–F–OH solid solutions as opposed to F–OH solid solutions of apatite from the XCO_2-poor group. Apatite from rocks, without clear evidence for high or low XCO_2 fluid infiltration, is marked as "others". (Figure modified from Penniston-Dorland and Ferry 2005)

metamorphism (Engvik et al. 2011; Rubenach 2012). Albitization involves the conversion of plagioclase, K-feldspar, scapolite, or muscovite into albite. As discussed below, halogen-bearing minerals, such as biotite and amphibole, may form in association with albitites. Yet in some cases these minerals, where associated with albitization, show low Cl contents (e.g., Bamble Sector, Norway, Kusebauch et al. 2015c). In other examples, high values of Cl occur in biotite adjacent to albitites (e.g., Snake Creek Anticline, Queensland, Australia, Rubenach 2005). Experimental and observational studies have shown that the replacement of Ca-plagioclase by albite is dominated by the coupled exchange reaction $Ca^{2+} + Al^{3+} = Na^{+} + Si^{4+}$. Based on experiments, Hövelmann et al. (2010) and Engvik et al. (2008) concluded that the mechanism is best explained by pseudomorphic replacement of plagioclase and/or K-feldspar via an interface coupled dissolution-precipitation mechanism (Putnis 2002, 2009; Putnis et al. 2007; Norberg et al. 2011, 2013). Their results showed that during albitization, Al is likely to be mobilised in the form of Na–Al complexes such as $NaAl(OH)_4^0$.

Albitization of K-feldspar via the reaction $KAlSI_3O_8 + (Na^+)_{fluid} = NaAlSi_3O_8 + (K^+)_{fluid}$ is strongly dependent both on the Na^+/K^+ ratio of the fluid, and on temperature, as albitization is favoured at high temperatures (e.g., Orville 1963; Lagache and Weisbrod 1977; Norberg et al. 2011).

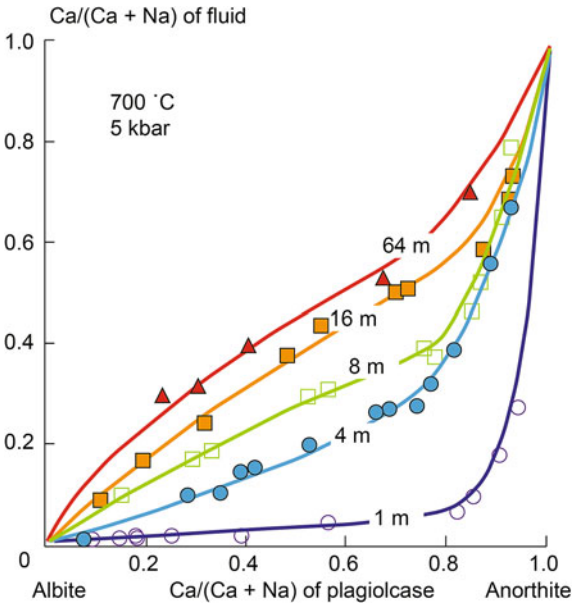

Fig. 10.8 Ca/Na ratios in the fluid versus the composition of coexisting plagioclase. The salinity of the experimental fluids ranges from 1 m to 64 m. If the concentrations of salts increase at a constant Na/Ca ratio, the equilibrium compositions shift towards albites (sodic plagioclases). (Modified from Shmulovich and Graham 2008)

Shmulovich and Graham (2008) have recently extended the classic work of Orville (1972) on Ca–Na partitioning between plagioclase and fluid to higher pressures (0.5 Gpa) and higher bulk salt concentrations in the fluid phase (1–64 m solutions). In dilute solutions, an increase in salinity results in the strong partitioning of Na into the fluid phase while the Na/Ca ratio in a fluid in equilibrium with plagioclase will always be lower than the Na/Ca ratio in the plagioclase (Fig. 10.8), resulting in a maximum albitization effect. In experiments with high salinity fluids, the Na/Ca ratio in the fluid and plagioclase approach similar values, resulting in a less pronounced compositional change in plagioclase with variable fluid salinities (Fig. 10.8).

Houston et al. (2011) observed a positive correlation between the Ca and Cl concentration in pore water, which is likely linked to fluid-mineral interaction, such as albitization. One explanation for this trend is the following relationship where increasing salinity, and therefore higher Na activity, necessitates a stronger increase in Ca in order to maintain the equilibrium: $CaAl_2Si_2O_8 + 4SiO_2 + 2Na^+ = 2NaAlSi_3O_8 + Ca^{2+}$, where the (aCa^{2+}/a^2Na^+) ratio is fixed due to buffering by both Na and Ca-bearing minerals. This correlation is also supported by the experiments of Shmulovich and Graham (2008). In situations where halite dissolution processes take place, the Ca-educt, in the form of plagioclase (for example), can become exhausted, which leads to a decrease in the Ca/Na ratio in the fluid as a result of fluid buffering. Albitization is often related with high-salinity fluids that provide the extensive amounts of Na required for widespread sodic alteration. The source of the fluid's salinity can be all of the possibilities discussed in Sect. 10.3.2. In the case of regional albitization of psammopelites, e.g., the Eastern Succession,

Mount Isa Inlier, metasomatic, Cl-rich biotite has commonly formed adjacent to albitites demonstrating that the metasomatizing fluids were saline and relatively acidic (see Sect. 10.4.4.2; Rubenach 2005). Albitization related to high-saline fluids is commonly implicated in element mobility. It is often associated with ore deposits of metals that strongly complex with Cl allowing for high solubility in saline solutions (see Sect. 10.5, e.g., Charoy and Pollard 1989; Oliver et al. 2004).

Anderson and Burnham (1983) and Hövelman et al. (2010) suggested that hot alkaline (high-pH) albitizing fluids can mobilize "immobile" elements, such as Al, Ti, and potentially REE, via OH^- and Na^+ complexes. In order to mobilize Al, for example, the fluid's salinity can be a limiting factor, as Cl competes to form Na–Cl complexes, which limits the formation of the soluble $NaAl(OH)_4^0$ complexes, hence lowering the Al mobility potential.

Other than evaporates, the source of Na can be the release of Na by mineral reactions e.g., liberation of Na during kaolinization of micas and chloritization of smectite (e.g., Morad et al. 1990). Drummond et al. (1986) suggested that metamorphic fluids gained Na from the breakdown of paragonitic muscovite in metasedimenatry rocks that had undergone amphibolite facies metamorphism. These Na-rich fluids then interacted with granites, which resulted in the exchange of Na for K in feldspar and mica leading to trondhjemitic rock compositions.

10.4.4.2 Examples of Regional Albitization

Albitization is a well-recognised phenomenon during diagenesis at temperatures <200 °C e.g., Ramseyer et al. (1992), which is commonly linked to the presence of saline fluids from which the required Na is sourced (e.g., González-Acebrón et al. 2010). In contrast, albitization at higher temperatures and pressures is generally associated with contact metamorphism. However, a few studies indicate that regional albitization can be related to large-scale hydrothermal systems that are not immediately related with an intrusion and accompanying magmatic fluids. An example of widespread regional albitization is found in the French Pyrénées where granites and metamorphic rocks are extensively albitized and talcisized (Boulvais et al. 2006; Poujol et al. 2010). Albitization and talcization took place over a time span of 20 Ma at the beginning of the Alpine orogeny ($\sim$100–50 Ma) in a transtensional tectonic regime when the Iberian plate rotated around Europe. During that time the North Pyrenean Fault was active and appears to have been related with massive talc-chlorite enrichments in the region. The saline mineralizing fluids contained up to 30 wt% NaCl at the estimated pressure–temperature conditions of 2 kbar and 250–300 °C (Boulvais et al. 2006 and references therein, Poujol et al. 2010). Based on fluid inclusions and stable isotope data, a model is proposed that suggests that seawater infiltrated into the mid crustal regions where it reacted with Triassic evaporites resulting in highly saline fluids. It is inferred that a single crustal-scale hydrothermal system subsequently developed that resulted in talc-chlorite mineralization and regional albitization (Poujol et al. 2010 and references therein).

Albitization in the Mt Isa Inlier

Albitization is widespread in the Eastern Succession, Mt Isa region, Australia, and occurred during two discrete events. An older group of albitites (e.g., the Snake Creek Anticline and the Osborne Mine) is locally quite abundant in metapsammopelitic rocks from the lower units (mainly rhythmically-bedded metaturbidites) of the Soldiers Cap Group along a belt 140 km in length (de Jong and Williams 1995; Rubenach 2012). Although initially thought to have formed during the peak metamorphic D_2 event ($\sim$1580–1590 Ma) of the Isan Orogeny, subsequent work and age determinations demonstrated that these albitites formed before or during the D_1/first metamorphic events of $\sim$1650 Ma (Rubenach et al. 2008; Rubenach 2012; Abu Sharib and Sanislav 2013). Mafic intrusions may have overlapped with this event and could have acted as heat engines that helped in the fluid circulation, but they probably did not supply the saline fluids responsible for the extensive albitization. In contrast to the albitized gabbros from the Bamble Sector in Norway (Engvik et al. 2011), the mafic rocks from the Snake Creek area, Mt. Isa region, Australia show very minor metasomatic alteration (mainly to cummingtonite-oligoclase rocks) even where they are in contact with highly albitized metasedimentary rocks. Porphyroblast assemblages in the albitites include (1) cordierite $\pm$ andalusite $\pm$ staurolite $\pm$ sillimanite, or (2) garnet + staurolite $\pm$ gedrite $\pm$ andalusite. Albite grains occur in the earliest porphyroblasts (cordierite or garnet $\pm$ staurolite), along with monazite grains dated at 1649 Ma (Abu Sharib and Sanislav 2013). The albitization was probably synchronous with porphyroblast growth or possibly preceded it (Rubenach 2012). Albitization involved removal of muscovite, and decrease in or removal of quartz, resulting in albite, accessory rutile, with or without small biotite grains. Albitites selectively formed in metasedimentary rocks adjacent to metadolerite sills or along shear zones. Where more intense, e.g., between two sills or along some shear zones, metapelitic rocks were also replaced. Extending for metres to tens of metres away from the albitized shear zones, muscovite schists were replaced by biotite-rich schists containing variable albite contents (Fig. 10.9), whereas metapsammitic beds are typically albitized for tens to hundreds of metres. The Cl content of biotite from the biotite-rich schists is mainly in the range 0.3–1.4 wt% and the Fe/(Fe + Mg) ratios range between 0.24 and 0.62 (Rubenach 2005). The higher values occur in albitized areas in the central and southern parts of the Snake Creek Anticline. By contrast, typical biotite from non-metasomatized schists in the Snake Creek Anticline generally shows low Cl contents, averaging 0.21 wt%, where above detection limits. Although there are limited data, the F content of biotite in biotite-rich rocks is generally less than 0.5 wt% with one sample showing 1.2 wt% (unpublished data).

An important observation is that, in contrast with the adjacent biotite-rich schists, the Cl contents of biotite from the albitite shear zones are commonly low, even though high saline fluids caused all the metasomatism. What is important is that partitioning of Cl into minerals depends on the HCl content of the fluids, not simply the salinity (Munoz and Swenson 1981). The reaction forming albite-bearing biotite-rich schists from muscovite-rich schists is as follows: muscovite + quartz + H_2O + K^+ + (Mg^{++}, Fe^{++}) = biotite + H^+. It is suggested

Fig. 10.9 Albitite with adjacent, biotite-rich, fold hinge schist, Snake Creek Anticline, Queensland, Australia. The biotite in this photo is enriched in Cl (up to 1.4 wt%). Fluorine is up to 1.2 wt%. *1* Albitite "shear-zone" *2* Selectively albitized metapsammite layer. *3* Biotite-rich pelite, containing cordierite pseudomorphs and andalusite. *4* Biotite-bearing metapsammite layers. Typical unmetasomatized muscovite schists (with andalusite and garnet porphyroblasts) and muscovite metapsammites occur adjacent to this outcrop to the left and bottom right

that this extra H^+ contributed locally to the infiltrating fluids so that higher amounts of Cl were partitioned into the biotite.

In the Snake Creek Anticline, many andalusite grains show clear evidence of multiple growth events. A few studied biotite grains from the biotite-rich schists show differing populations for Cl and Mg/(Mg + Fe) for the various zones and the matrix, suggesting changing rock/fluid equilibria during the various deformation/metamorphic events (Rubenach 2005).

The Corella/Doherty formations in the Selwyn (Cloncurry) Zone of the Eastern Fold Belt, Mount Isa Inlier consist dominantly of calc-silicate rocks. These have been subjected to giant-scale, hydrothermal brecciation associated with the Williams-Naraku batholiths that intruded in the period 1490–1530 Ma (de Jong and Williams 1995; Rubenach 2012). In the Snake Creek area, the breccias formed contemporaneously with the Saxby Granite at 1527 Ma (Rubenach et al. 2008). The breccias and adjacent bedded calc-silicate rocks have been subjected to Na–Ca metasomatism, with assemblages consisting dominantly of hematite-stained albite, calcite, biotite, amphiboles, and clinopyroxene. Only limited work has been done on the halogens in the amphiboles and sheet silicates. For example, in the Snake Creek area biotite contains up to 1.5 wt% F and 0.7 wt% Cl (Rubenach unpublished data). In a study of fluid inclusions in quartz, which included noble gases and

halogens (Br, Cl, I), Kendrick et al. (2008) concluded that the metasomatizing fluids were halite dissolution sedimentary formation waters with a probable magmatic component.

In the Cloncurry Region, saline fluids were involved with both albitization and scapolitization (see Sect. 10.4.6.3). However, heavily albitized zones are often scapolite-absent. The absence of scapolite in albitite schists can be explained by the low Ca-activity. However, this is not the case for calc-silicate rocks that have calcic amphibole and pyroxene. It is possible that $X\mathrm{CO_2}$ is low in all albitites from the Cloncurry Region such that the low $\mathrm{CO_2}$ does not stabilize scapolite at these temperatures.

Albitization in Southern Norway

Vast areas in southern Norway have undergone intense fluid-rock interaction resulting in widespread albitization and scapolitization. The high-grade Bamble and Kongsberg sectors (amphibolite- to granulite facies rocks), currently separated by the Permian Oslo Graben, have been studied in detail over the years for the mechanisms and origins of the metasomatizing fluids during the geodynamic history of the region (e.g., Elliott 1966; Bodart 1968; Munz et al. 1994, 1995; Engvik et al. 2011, 2014). Extensive albitization has been observed in the Bamble sector where metasedimentary and meta-igneous rocks (including metagabbros) reached peak P–T conditions of 7 kbar and 800 °C (Harlov 2000; Nijland et al. 2014) at 1150–1125 Ma (Cosca et al. 1998; Bingen et al. 2008). This high-grade metamorphism was overprinted by amphibolite-facies metamorphism at 1105−1080 Ma (Cosca et al. 1998), which is most evident in amphibolite-facies metapelitic rocks. Large-scale fluid circulation, associated with amphibolite-facies metamorphism, led to regional-scale metasomatism including extensive albitization that is spatially associated with widespread scapolitization (also see Sect. 10.4.6).

Munz et al. (1994, 1995) studied fluid rock-interaction in the Modum Complex within the Kongsberg sector where postmetamorphic quartz veins are interpreted to have formed at ∼250–300 °C and 1–2 kbar. These veins are associated with albitization in the form of extensive albite replacement in metasedimentary rocks and metagabbros. Hydrocarbon-rich fluid inclusions, together with the halogen ratios from saline aqueous fluid inclusions, led to the suggestion that unmetamorphosed sedimentary rocks acted as a fluid source for the albitizing fluid. This scenario is supported by the findings of Gleeson et al. (2003) who concluded that the quartz-vein fluids were heterogeneous sedimentary formation waters (brines). The penetration of the fluid into deeper crustal levels was hypothesized to be initiated by uplift during late Precambrian or Permian rifting of the nearby Oslo-Graben (Munz et al. 1995), which separated the Bamble Sector from the Kongsberg Sector.

10.4.5 K-Feldspathization

K-feldspathization describes the processes by which feldspars are transformed to K-feldspar via the reaction $NaAlSi_3O_8 + K^+ = KAlSi_3O_8 + Na^+$, where K can be introduced via KCl in solution. Orville (1962, 1963) experimentally investigated K and Na exchange between alkali-feldspars and alkali chloride solutions (2 M and 0.2 M) between 350 and 700 °C at 200 MPa in the system $KAlSi_3O_8$–$NaAlSi_3O_8$–NaCl–KCl–H_2O, where the ion exchange reaction can be written as $NaAlSi_3O_8 + KCl = KAlSi_3O_8 + NaCl$. Lagache and Weisbrod (1977) conducted a similar study at 20–200 MPa and 300–660 °C with chloride contents ranging from 0.05–14 M. The results show that the K/(K + Na) ratio of the fluid equilibrated with two feldspars drops with decreasing temperatures, implying that more potassic-feldspar is formed. Orville (1962, 1963) found that increasing pressure has the same effect as falling temperatures on the K/(K + Na) ratio in the fluid. Additionally, Lagache and Weisbrod (1977) showed that an isothermal pressure decrease could lead to fluid unmixing, resulting in increased potassic alteration, and, hence, lower the K/(K + Na) ratio in the fluid. Variable total concentrations of the alkali chlorides in the solution seem to have only minor implications on the composition of the feldspars.

K-feldspathization can occur over a broad temperature range. It is commonly found during diagenesis where K-rich fluids might be sourced from potash salts, volcanic sediments, or mudrocks. The latter have been considered as a potential source for feldspathization in carbonates from the northern Alps (Spötl et al. 1996). Earlier albitization can enrich the residual saline fluids significantly in K (e.g., Salton sea; Hardie 1990) leading to high (Ca + K)/(Na + Mg) ratios that might be lowered during successive potassic alteration. Furthermore, K can be released by the hydrothermal chloritization of smectite and illites from siltstones and shales. K-Feldspar from arkose has been proposed as a viable source of K^+ for potential potassic alteration upon fluid rock interaction at elevated temperatures (Mahon 1966; Hardie 1990).

Extensive K-metasomatism is commonly associated with extensional regimes where volcanoclastic sediments undergo potassic alteration at low temeratures (<150 °C) via prolonged interaction with alkali-rich saline fluids (e.g., Beratan 1999; Ennis et al. 2000). However, K-feldspathization is not only restricted to sedimentary and diagenetic environments. Helvaci and Griffin (1983) reported K-feldspathization and silicification of felsic metavolcanics and the albitization of granitoids, basic-intermediate metavolcanics, and mica-schists. The authors observed that the granitoids had intruded into the metavolcanics and they therefore concluded that feldspathization and silicification could not be diagenetic processes. The above study suggests that the metavolcanics and granitoids formed the seafloor into which seawater penetrated via fractures during low-grade Alpine metamorphism. One possible scenario for the genetically related K-feldspathization and albitization is that albitization of the lower parts of the metavolcanic rocks, together

with the albitization of the granitoids, liberated K that led to K-feldspathization in the upper parts of the metavolcanics. However, the presence of large local variations in the degree of K-feldspathization and albitization might infer variable permeabilities in the rock layers or protolithic variations.

K-metasomatism at deeper crustal levels has been recognised in several terranes such as the Nordre Strømfjord Shear Zone of West Greenland, and the Shevaroy Hills Massif, India (Harlov et al. 1998; Hansen and Harlov 2007; Glassley et al. 2010). Studies of K-rich rocks in the lower crust (e.g., Newton et al. 1998; Harlov et al. 1998; Glassley et al. 2010; see also Aranovich and Safonov 2018) have shown that a K-rich saline brine with low H_2O activity can interact with minerals via grain-boundary fluid migration or along shear-zones. This leads to the formation of K-rich feldspars, in some cases almost pure orthoclase, in the form of K-feldspar veins along quartz-plagioclase grain boundaries in the deep crust.

10.4.6 Scapolitization

10.4.6.1 Scapolite-Minerals

Besides saline fluid inclusions, Cl-bearing scapolite minerals might be the best indicator for the presence of high-salinity fluids during metamorphism. The scapolite-mineral group is best expressed via the formula $M_4(T_{12}O_{24})A$, where M represents Na, K, Ca, Sr, Ba, and Fe^{2+}, T represents Si, Al and Fe^{3+}, and A stands for Cl, CO_3, SO_4 or Br. The composition of scapolite is generally written in the literature as meionite ($Ca_4(Al_6Si_6O_{24})CO_3$) equivalent% (Me% = 100 [$\sum$(divalent cations/4)].

Minerals of the scapolite group generally fall into the simplified non-linear solid-solution between marialite $Na_4(Al_3Si_9O_{24})Cl$ and meionite $Ca_4(Al_6Si_6O_{24})CO_3$ (Sokolova and Hawthorne 2008), although there can be significant substitution of K and Sr for Na; Ba for Ca; Fe^{3+} for Al and Br; OH for Cl; and SO_4 for CO_3. Furthermore, Teertstra and Sherriff (1996, 1997) distinguished between three subseries (A, B, C, Fig. 10.10). Here the subseries joins are located at Me20–25% and Me60–67% with the apparent mizzonite endmember ($NaCa_3Al_5Si_7O_{24}CO_3$) plotting around the join between subseries B and C (Fig. 10.10). High meionite numbers, in general, correlate with elevated CO_2 and/or S contents, while low meionite numbers characteristically reflect high Cl contents (e.g., Teertstra and Sherriff 1997). The pure meionite or marialite endmembers have yet to be found in nature. Experimental work (e.g., Moecher and Essene 1990) has shown that their stability is restricted to high temperatures.

Monovalent for divalent cation substitutions mainly take place on the M site in the form of $Ca(Na + K)^{-1}$, whereas 1:1 substitutions of the trivalent for tetravalent cations occur on the T site. Scapolite chemistry on the A site (Cl, CO_3, Br, SO_4, and H_2O) is influenced by: (i) fluid compositions; (ii) site occupancy and charge balance issues arising from Ca–Na–Al coupled substitutions; and (iii) P–T conditions and

coexisting minerals (Haughton 1970; Orville 1975; Ellis 1978; Kwak 1977; Moecher and Essene 1991; Teertstra and Sherriff 1997; Sokolova and Hawthorne 2008).

Scapolite can provide information about the fluid chemistry for a given pressure, temperature, and mineral assemblage if the effects of site occupancy and solid solution can be isolated from the potential controls of the fluid chemistry such as quantitative calculations of the salt content in the coexisting fluids (Ellis 1978; Oliver et al. 1992; Satish-Kumar et al. 2006; Hammerli et al. 2014, see Sect. 10.2.6). Furthermore, experimental work (Pan and Dong 2003) has shown that scapolite probably does not fractionate Br and Cl, and this can be directly used to determine the origin of the fluid. These findings have been supported by Hammerli et al. (2014) who showed that the halogen contents in scapolite are not correlated with the major element composition of the scapolite group minerals. In situ quantification of trace elements, including Cl and Br in scapolite, is promising as mineral zoning can reveal how fluid compositions varied during metamorphism and provides a complementary tool to fluid inclusion studies (e.g., Satish-Kumar et al. 2006; Hammerli et al. 2013, 2014). Figure 10.11 shows a zoned scapolite grain from a shear zone where three fluid pulses can be distinguished (see Hammerli et al. 2014 for details).

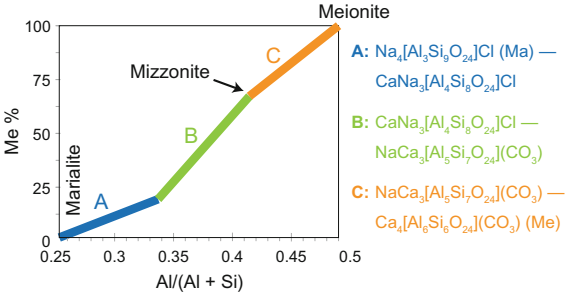

Fig. 10.10 Simplified non-linear solid-solution between marialite $Na_4(Al_3Si_9O_{24})Cl$ and meionite $Ca_4(Al_6Si_6O_{24})CO_3$ with three subseries. (Modified after Teertstra and Sherriff 1996, 1997; Sokolova and Hawthorne 2008)

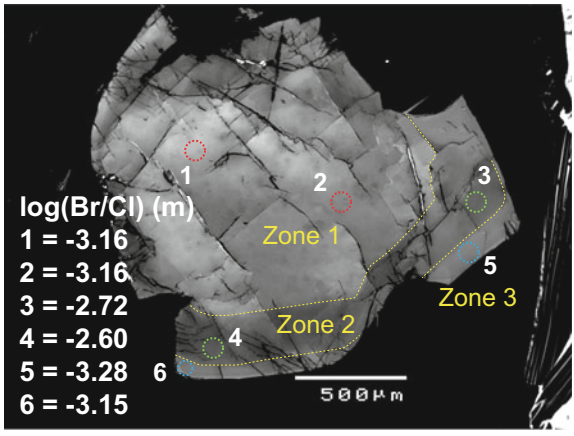

Fig. 10.11 Scapolite porphyroblast from a shear-zone shows three different zones (*1, 2,* and *3*). Changing Br/Cl ratios between the mineral zones indicate the presence of different fluids during mineral growth. (Modified from Hammerli et al. 2014)

The presence of scapolite in metamorphic rocks (largely calc-silicate rocks) is not unexpected if we consider the stability field of scapolite at regional metamorphic conditions (e.g., Orville 1975). However, experimental and thermodynamic data are very limited for scapolite group minerals and some of the thermodynamic approaches are in poor agreement (Oterdoom and Wenk 1983; Komada et al. 1996; Kuhn et al. 2005). Nevertheless, the studies by Orville (1975) and Goldsmith and Newton (1977) on scapolite-plagioclase stability relations can provide some constraints on the theoretical stability of scapolite in regional metamorphic rocks. The thermodynamic data from Orville's (1975) experiments in the system $NaAlSi_3O_8$–$CaAl_2Si_2O_8$–NaCl–$CaCO_3$ at 400 MPa and 750 °C suggest that scapolite is stable relative to calcite + NaCl + plagioclase over a relatively wide range of "bulk compositions". Orville (1975) also showed that for a given temperature and pressure condition, NaCl-deficient environments tie the scapolite to a relatively narrow mizzonitic composition and that coexisting plagioclase should be either of a sodic or calcic composition. The experimental data preclude the occurrence of a plagioclase composition between the two end points and the occurrence of scapolite if calcite is present in excess. Goldsmith and Newton (1977) showed that marialite is stable relative to albite + NaCl at pressures between 8 and 15 kbar at a minimum temperature of 800 °C. Experiments in the system $NaAlSi_3O_8$–$CaAl_2Si_2O_8$–$CaCO_3$–$CaSO_4$ showed that under these same P–T conditions, Na stabilizes scapolite to lower temperatures, whereas pure meionite is not stable at temperatures lower than 875 °C (Goldsmith and Newton 1977). Oterdoom and Wenk (1983) also showed that CO_3-rich scapolite requires high temperatures (>550 °C) in order to be stable.

10.4.6.2 Examples of Extensive Scapolitization

Widespread scapolitization has been recognized in various regional- and contact metamorphic belts and terranes. For example, scapolite group minerals have been described in impure marbles and calc-silicate rocks from regional metamorphic terranes in Antarctica (Piazolo and Markl 1999; Satish-Kumar et al. 2006), the Swiss Alps (Frank 1983), the Betic Cordilleras (Gomez-Pugnaire et al. 1994), the Adelaide Fold Belt, South Australia (Kwak 1977), the Mt. Isa Inlier, Australia (Oliver et al. 1992), and the Lufilian-Zambezi Belt, Zambia (Katongo et al. 2011), as well as in contact aureole settings such as the St. Joe-Clearwater Region, Idaho (Hietanen 1967; Mora and Valley 1989). Despite the discussed significance of scapolite in constraining fluid properties and origins during metamorphism, only a few systematic studies (Hietanen 1967; Kwak 1977; Frank 1983; Mora and Valley 1989) have focused on scapolite in rocks from low-, to high metamorphic grades, ranging from greenschist facies to (upper) amphibolite facies conditions.

Scapolite in St Joe-Clearwater Region, Idaho

Scapolitized metasedimentary rocks from the Wallace Formation in the St. Joe-Clearwater Region, Idaho, have been studied in detail by Hietanen (1967) and Mora and Valley (1989). Here, the calcareous shales, sandstones, mudstone, and quartzite underwent regional metamorphism followed by a contact metamorphic event that reached peak conditions of 5–5.5 kbar and 600 °C. Contact metamorphism is related to the Idaho batholith that led to concentric isograds around the intrusion. Most of the regional metamorphic minerals were completely recrystallised during contact metamorphism. However, some relict regional metamorphic staurolite isograds might still be present in the region (Lang and Rice 1985).

In these rocks, scapolite ranges from fine-grained xenomorphic grains on the micron scale to cm-scale porphyroblasts, is layer-based, and distributed parallel to the bedding. Heitanen (1967) noticed that the scapolite-absent layers are chemically very similar to those that have scapolite and contain the same mineral assemblage; the only difference is the lack of Cl. Variable Cl contents on a layer-scale point towards limited mass transfer between layers. Furthermore, scapolite modal abundance decreases with increasing metamorphic grade from ~40% in low grade rocks to ~10% in high-grade rocks. Based largely on optical properties, Hietanen (1967) observed that the meionite content in scapolite increases over a distance of ~60 km from 35% at an estimated temperature of ~300 °C to 65% at ~600 °C (Fig. 10.12). EPMA confirmed this general trend of an increasing meionite component (Evans et al. 1969). However, the meionite content is significantly higher in high-grade rocks (Fig. 10.12). An increase in the meionite component, as a function of higher metamorphic temperatures in the same region, was also confirmed by Mora and Valley (1989). This gain in the meionite component, as a function of increasing temperature, is not linear as a rapid increase in the meionite content can be observed close to the epidote-facies to amphibolite-facies to upper amphibolite-facies boundary (Fig. 10.12). Plagioclase is commonly present in these samples and has an anorthite content that is mostly ~20–25% lower (more sodic) than the anorthite equivalent in coexisting scapolite. Hietanen (1967) observed that the Ca content in plagioclase increases with increasing temperature, but at a different rate than in scapolite, which has been speculated to be pressure as well as temperature controlled.

Scapolite Occurrence in the Eastern Mt Lofty Ranges, South Australia

A second systematic study was carried out by Kwak (1977) on a series of scapolite-bearing metamorphic rocks from the Kanmantoo Group, eastern Mount Lofty Ranges, which belong to the Adelaide Fold Belt in South Australia. Scapolite was studied in rocks of variable compositions ranging from sulfide-rich veins to meta-dolerite to pelitic schists to impure marbles. The rocks underwent regional metamorphism with temperatures from ~350 to ~700 °C and pressures from 3 to 5 kbar. The results show a very similar trend as observed in the St Joe-Clearwater

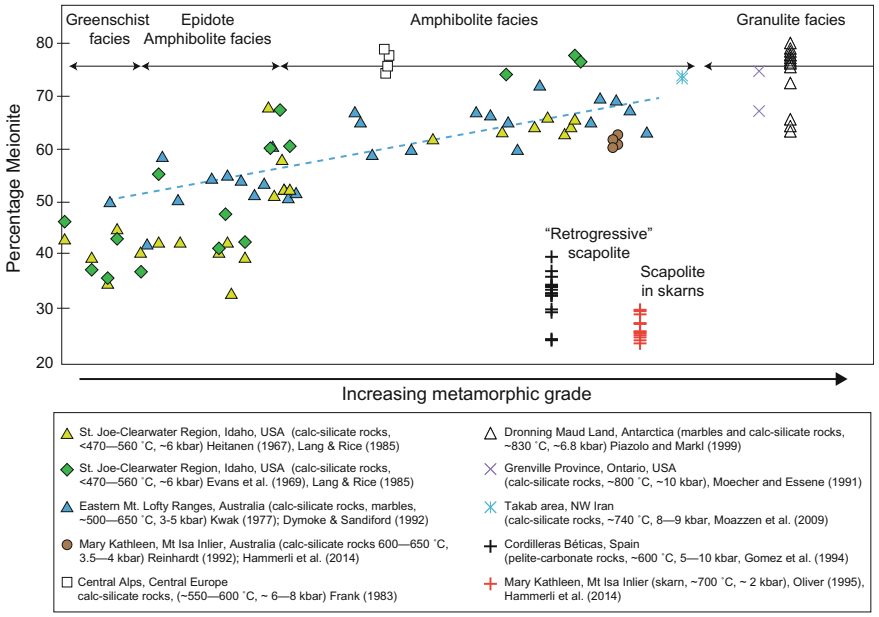

Fig. 10.12 Scapolite composition data (in percentage meionite) versus estimated metamorphic grade. The *blue dashed line* is a linear trend for the data from the Eastern Mt. Lofty Ranges (Kwak 1977)

Region with meionite values increasing during prograde metamorphism where a ~10 km stretch sees an increase in the meionite component from ~50 to 66%. Compared to Heitanen's (1967) study, this trend is almost linear (Fig. 10.12). Kwak observed an interesting fact that the scapolite composition is not correlated with the mineralogy or the bulk rock composition. For instance, no S was detected in scapolite in contact with sulfide minerals. This indicates that the SO_3 content in scapolite is strongly controlled by the P–T conditions, such that higher temperatures than in the Mt. Lofty Ranges (>650 °C) would be required to form S-rich scapolite, though redox reactions might also play a strong role regarding the formation and stability of S-rich scapolite (Lovering and Widdowson 1969). This has been also suggested by experiments (Goldsmith and Newton 1977; Kotel'nikov et al. 1987) and natural S-rich scapolite occurrences in granulite-facies rocks (von Knorring and Kennedy 1958). It should also be noted that in NaCl-deficient systems, the incorporation of minor S might be able to stabilize CO_3-rich scapolite to unusually low temperatures, as speculated by Pan et al. (1994).

It is likely that the fluid source responsible for widespread scapolitization is different in the above examples. While there is strong evidence that the Wallace Formation in Idaho contained evaporites at some point during its development, as evidenced by salt casts and skeletal halite within the formation at lower grades, the protolith of the impure marble from the Kanmantoo Group is a limestone that was

formed at the height of a marine transgression. Furthermore, the 7–8 km thick sequence of turbiditic Kanmantoo Group sediments contains no evidence of evaporitic horizons (Dyson et al. 1996; Preiss 2000; Haines et al. 2001; Jago et al. 2003). Thus, scapolite formation in the Eastern Mount Lofty Ranges is unlikely to be related to primary halite. It is more likely that saline external fluids infiltrated the sediments, which subsequently led to scapolitization during regional metamorphism. The scapolite forming fluids are inferred to be bittern brines as based on their Br/Cl ratios (Hammerli et al. 2013). In the case of the Idaho sequence, it has been suggested that the salt content required for scapolitization was directly derived from halite. However, it seems unlikely that primary halite survives low-grade metamorphism until temperatures of 300 °C are reached—the minimum temperature inferred to be required for marialitic scapolitization (e.g., Otherdoom and Wenk 1983). Moreover, in the Idaho region primary evaporitic halite would have had to survive initial regional metamorphism prior to contact metamorphism with which scapolite formation is associated. Mass balance calculations have shown that only a trace amount of halite is required to form heavily scapolitized rocks (Hietanen 1967; Mora and Valley 1989). Mora and Valley (1989) demonstrated that in a closed system a 1.5% modal abundance of halite could form a rock with 20% scapolite. In an open system, where halite is dissolved, much higher quantities of halite are necessary to maintain the required NaCl activity in the scapolitizing fluid. However, in carbonate-bearing scapolite-rich rocks, it is possible that fluid phase separation played an important role that could have led to secondary halite deposition prior to scapolite formation. Hence, it is feasible that primary halite dissolved during regional metamorphism and that upon fluid unmixing, secondary halite precipitated. It can be speculated that this secondary halite could have been the source of NaCl during scapolitization in the course of contact metamorphism. The general increase in the meionite values in both terranes (Fig. 10.12) is likely a result of carbonate–plagioclase–NaCl–scapolite stability relationships, where meionitic scapolite becomes more stable in rock-buffered environments with increasing temperatures (Goldsmith and Newton 1977).

Extensive Scapolitization in the Mt Isa Inlier

Probably the most extensively scapolitized region known is found in the Eastern succession of the Proterozoic Mt. Isa Inlier, Queensland, Australia. This Eastern part of the Mt. Isa Inlier can be subdivided into the Mary Kathleen Fold Belt and the Cloncurry district to the East. The Mary Kathleen Fold Belt consists of the calc-silicates, marbles, metasiltstones, and metaquartzites of the Corella Formation (e.g., Matheson and Searl 1956; Oliver et al. 1992, 1994). Since its deposition at $\sim$1750 Ma, these metasediments underwent at least four deformation events and were intruded by granites, dolerites, and diorites. The Corella Formation, and the emplaced igneous rocks, underwent several large-scale alteration events, with the most prominent being scapolitization and albitization. The earliest scapolitization event can be correlated with the early intrusions of granite and dolerite ($\sim$1740 Ma,

e.g., Oliver et al. 1992, 1994) shortly after the deposition of the Corella formation. Scapolite in the granitic dikes contains a very distinct magmatic fluid signature whereas scapolite that occurs as acicular needles in garnet-clinopyroxene skarns, proximal to the granitic intrusions, shows a mixed fluid signature between bittern brine fluids and exsolving magmatic fluids (Hammerli et al. 2014). Preserved contact metamorphic scapolite in skarns around the Burstall granite ($\sim$1740–1730 Ma), that formed at $\sim$700 °C and $\sim$2 kbar (Oliver 1995), shows no evidence for recrystallization during the main deformation event during regional metamorphism ($\sim$1580–1550 Ma, at 550–650°C and 3–4 kbar, Oliver et al. 1991), probably resulting from structural deformation partitioning.

The bittern brine fluid component in the skarn-scapolite demonstrates that the Corella Formation was saturated with a bittern brine fluid, at least in the Mary Kathleen Region, during the time of early granitic intrusion (Hammerli et al. 2014). Scapolite formation during regional metamorphism occurred mostly via the following reaction: plagioclase + calcite + NaCl = scapolite at temperatures of around 500 °C (Oliver et al. 1992). Metamorphic rocks from the Mary Kathleen Fold Belt contain scapolite porphyroblasts aligned within, and locally cross-cutting, the 1580 Ma regional metamorphic foliations. They are interpreted to be unrelated to pre-regional metamorphic intrusions (Oliver et al. 1992). Scapolite can also be present as fine-grained, xenomorphic grains, typically within K-feldspar and calcite-rich layers, but they are also present in the calcic amphibole-rich layers. Halogen ratios in metamorphic scapolite show no evidence for halite being an important halogen source during scapolitization (Hammerli et al. 2014), which has also been confirmed by fluid inclusion studies (Kendrick et al. 2006, 2008). This observation leads to the conclusion that the Corella Formation in the Mary Kathleen Region, at least at the current level of erosion, was halite-deficient. Highly saline fluids could have been transported laterally from evaporitic horizons or more likely vertically as suggested by Hammerli et al. (2014) (see Sect. 10.6 and Fig. 10.14).

Oliver et al. (1992) reported large compositional variations in scapolite, biotite, and amphibole on the layer-scale in metasediments that can be attributed to differences in the activities of volatiles (H_2O, CO_2, Cl, SO_4) within the rock layers in a rock-buffered environment. Oliver et al. (1992) suggested that this difference is due to variable halite contents and calculated that $2.4*10^{18}$ g NaCl is stored within the $\geq$180 km^3 of scapolitized rocks in the Mary Kathleen Belt alone. This is the equivalent of $\sim 2 \times 10^9$ m^3 of halite and implies that >15 vol.% of the Corella Formation would have been halite. In the alternative scenario that no primary halite precipitated in the Corolla Formation in the currently exposed Mary Kathleen Fold Belt, the total volume of halite had to be significantly higher in order to produce the amount of residual bittern brine necessary to form the observed volumes of scapolite. A large volume of evaporites (incl. halite) could possibly have been present in stratigraphically higher beds and transported/removed during diagenesis and deformation (Kendrick et al. 2006; Hammerli et al. 2014)

The Cloncurry district, east of the Mary Kathleen Fold Belt, contains, along with the Corella Formation, the Soldiers-cap Group that consists of metamorphosed

siliciclastic turbidites. Scapolite in the Corella/Doherty formation from the Cloncurry district has Br/Cl values (Hammerli, unpublished data) that clearly point to a halite component in the saline fluid, and this is also confirmed by fluid inclusion studies (Kendrick et al. 2008). These results point towards the presence of halite layers in the sedimentary sequence of the Corella/Doherty formation in the Cloncurry district. Maximum deposition ages, derived from detrital zircon studies, indicate that the Doherty formation formed late ($\sim$1740 Ma, Withnall and Hutton 2012) relative to the Corella Formation in the Mary Kathleen Fold Belt. It is therefore possible that the Doherty Formation was deposited after the Wonga event and intrusion by plutons at $\sim$1740 Ma (Oliver et al. 1999 and references therein). It can be speculated that halite-bearing evaporitic layers that formed after $\sim$1740 Ma were more likely to be preserved until regional metamorphism started.

Scapolitization of Mafic Rocks (Bamble Sector, Southern Norway)

Scapolite can also be prominently present in mafic rocks. It has been described in the Bamble Sector, southern Norway, which represents a region that underwent high-grade amphibolite-facies metamorphism in the Proterozoic, reaching granulite-facies metamorphic conditions in certain parts (e.g., Nijland et al. 2014 and references therein, also see Sect. 10.4.4.1). Scapolitized metagabbros and amphibolites contain marialitic scapolite (up to 3.9 wt% Cl) that occurs together with Cl-rich apatite (Lieftink et al. 1993). It has been suggested that the saline fluid that resulted in heavily scapolitized rocks (up to 85 vol.%) was derived from neighbouring metasedimentary rocks where synmetamorphic intrusions mobilized metamorphic saline fluids (Lieftink et al. 1993; Nijland et al. 1993). Cl/Br ratios from heavily scapolitized rocks (Lieftink et al. 1993 and Hammerli unpublished data) are typical for bittern brine fluids, which supports the idea that an influx of saline metamorphic fluids interacted with basic rocks.

Kusebauch et al. (2015c) sampled variably altered meta-gabbros from the Bamble Sector, that contain shear zones, in order to investigate the interplay between pervasive and localized fluid flow. Their detailed study includes the quantification of halogens on bulk rock samples and mineral separates. In addition, oxygen isotopes and Cl isotopes were measured. Based on halogen concentrations and their ratios, the study concluded that the saline fluids responsible for regional scale alteration (including scapolitization) most likely originated from marine pore fluids. Kusebauch et al. (2015c) found that local, fluid-mineral reactions, such as scapolitization, can lead to desalination effects meaning that the alteration mineral assemblage influences the halogen budget of the evolving fluid. The spatial association of albitites and scapolite in the region suggests that the albitizing and scapolitizing fluid might be genetically related over a broad range of temperatures up to 700 °C (Nijland and Touret 2001; Engvik et al. 2011). Interestingly, Austrheim et al. (2008) and Engvik et al. (2011, 2014) reported that albitization and scapolitization led to Fe mobility, which implies that the abundant Fe-ore deposits in the region might be genetically linked with Na-metasomatism and scapolitization.

However, the recent study of Kusebauch et al. (2015c) also pointed out the remaining challenges in understanding the fractionation of halogens between major mineral phases such as amphibole, biotite, and scapolite. Despite these uncertainties, in fluid dominated situations, scapolite likely provides the best proxy for deciphering the origin of the fluids (Pan and Dong 2003; Hammerli et al. 2013, 2014).

Strongly scapolitized meta-amphibolites are also present in the Mt. Isa Inlier, (Oliver et al. 1994; Hammerli et al. 2014) where the scapolite reactions start in a rock with excess clinopyroxene that drives the (unbalanced) reaction to the right, i.e. clinopyroxene + H_2O + $NaCl_{fluid}$ = calcic amphibole + scapolite. Some of these meta-amphibolites are almost fully scapolitized with more than 90% of the rock being scapolite. This high modal abundance of scapolite suggests that in some cases extensive amounts of saline fluids were available and that most or all of the pyroxene was consumed. The formation of scapolite in these rocks is similar to that from the Bamble Sector where bittern brine fluids also led to scapolitization of mafic rocks.

Scapolite in NaCl-Deficient Regional Metamorphic Terranes

In NaCl-deficient systems, scapolite forms at higher temperatures. This is due to the absence of the stabilizing effects by NaCl at lower temperatures. Frank (1983) studied metamorphic evolution of calcareous schists and silicious dolomites during Alpine metamorphism. Meionitic scapolite ~Me75 was found to replace calcite and anorthite via the following reaction: 3 anorthite + calcite = meionite at temperatures estimated to be >550 °C (Fig. 10.11).

10.4.6.3 Scapolite Formation During Retrogression

Highly scapolitized layers (up to 60 modal %), formed during the retrogressive metamorphic path followed by high-pressure metapelitic rocks from the Cordillera Béticas, Spain, have been analysed in detail by Gómez-Pugnaire et al. (1994). Scapolite in various forms, including cm-large porphyroblasts in a biotite matrix, has been described in metapelites that were inferred to contain evaporitic minerals. Interestingly, and similar to the findings of Mora and Valley (1989) in scapolite sequences in the contact aureole, St. Joe-Clearwater Region, Idaho, scapolite-rich and scapolite-deficient layers studied by Gómez-Pugnaire et al. (1994) are chemically almost indistinguishable except for the higher Cl contents in the scapolite-bearing sections.

The metapelitic rocks from the Cordillera Béticas contain variable Cl and F concentrations in biotite and apatite (up to 6.5 wt% Cl and 3.3 wt% F) implying that the fluid was not homogeneous in terms of halogen concentrations. This indicates low fluid-rock ratios or spatially variable permeabilities so that the fluid was not able to homogenise halogen concentrations between different layers. Subsequently, different fluid/rock ratios resulted in different degrees of fluid- or rock-buffering.

The initial prograde metamorphic path of the rocks from the Cordillera Béticas led to peak conditions of $\geq$18 kbar and ~650 °C resulting in a mineral assemblage consisting of plagioclase, kyanite, talc, biotite, phengite, Na–Ca amphibole, garnet, carbonate, and possibly quartz and paragonite. Subsequent retrogression/decompression is suggested to have resulted in porphyroblastic, albite-rich plagioclase as a result of early breakdown of the phengite component in the white mica that also led to the release of H_2O. Retrogressive Scapolite forms later than plagioclase, and is assumed to coincide with late chlorite and quartz. The scapolite grains are Na-rich and CO_3-poor, and range between ~#Me30 and #Me40 (Fig. 10.11). The conclusion that plagioclase was not involved in the scapolite forming reactions is supported by the low meionite numbers, compared to scapolite that typically forms via NaCl + plagioclase reactions at similar pressure–temperature conditions (Fig. 10.12), and by the presence of stable albite. It is proposed that scapolite formed via the reaction: Al-biotite + $CaCO_3$ + NaCl + SiO_2 = Al-poor biotite + scapolite + $MgCO_3$ + KCl + $MgCl_2$ + H_2O. This reaction requires high NaCl contents during decompression of the rocks.

In those same rocks, Gómez-Pugnaire et al. (1994) report the presence of minute KCl and NaCl crystals within quartz microstructures, which led to the conclusion that evaporitic halide minerals were present during scapolite formation. This means that halide minerals would have survived metamorphic conditions of $\geq$18 kbar and 600 °C. Such situations can be explained either by fluid-absent circumstances or by situations of fluid unmixing or H_2O consumption processes where subsequent halide mineral precipitation might be an alternative scenario (e.g., Trommsdorf et al. 1985; Trommsdorf and Skippen 1986; Markl and Bücher 1998). Gómez-Pugnaire et al. (1994) suggest that the release of H_2O during the white mica breakdown reactions and albite formation could have locally led to the dissolution of the evaporitic halide-rich minerals producing a dense brine fluid, close to halite saturation. The formation of scapolite might have continuously depleted the brine in NaCl until scapolite-formation stopped.

10.5 The Role of Halogens in Element Mobility During Regional and Contact Metamorphism

The presence of halogens can strongly increase the solubility of a range of elements of economic interest. Despite the fact that Br and I are more likely to build complexes with some metals (e.g., Seward and Barnes 1997), Cl is, due to its much higher concentration in most cases, a much more important ligand for base metal complexing. The correlation between Cl and increased solubilities of metals has been clearly demonstrated experimentally in the past (e.g., Barrett and Anderson 1982; McKibben and Williams 1989; Ilton and Eugster 1990; Hemley et al. 1992; see also Lecumberri-Sanchez and Bodnar 2018). Fluorine and Cl can also be crucial in the transport of elements such as Ti, Zr, REE, and HFSE that are regarded as

immobile under most conditions (Alderton et al. 1980; Michard and Albarede 1986; Giere 1990; Keppler 1993; Tropper et al. 2011, 2013).

Experiments by Rapp et al. (2010) and Tanis et al. (2015, 2016) on rutile have shown that its solubility strongly increases in saline fluids compared to pure H_2O. Rapp et al. (2010) showed that the F content is especially critical, along with temperature, in enhancing the solubility of rutile up to 100 times that in H_2O as measured by Tropper and Manning (2005). The experiments performed by Tanis et al. (2015, 2016) additionally showed that if both NaCl and NaF are present in the fluid, the rutile solubility increases more dramatically than in fluids with only NaCl or NaF. Titanite grains in hydrothermal veins are evidence for Ti mobility where extraction of Cl or F from the fluid via apatite formation (for example), could be a trigger for titanite precipitation in hydrothermal veins.

Most studies on metal element mobility focus on magmatic-hydrothermal settings, Mississippi Valley Type environments, or sedimentary exhalative Pb-Zn deposit (MVT-SEDEX) formation at relatively low P–T conditions (e.g., Holland 1972; Leach et al. 2005 and references therein; see also Lecumberri-Sanchez and Bodnar 2018 and Pirajno 2018). The transport of base metals and other trace elements, however, has also been identified in regional metamorphic settings (e.g., Haack et al. 1984; Pitcairn et al. 2006; Hammerli et al. 2015). Clear evidence for metal transport is often challenging to recognise in metamorphic terranes as protolithic variations can make comparisons between low and high-grade rocks hard to distinguish (e.g., Cardenas et al. 1996; Cullers 2002). Nevertheless, detailed studies of fluid inclusions and bulk rock- and mineral chemistry have shown that metamorphic fluids could contain significant amounts of base metal elements. Yardley (2005) reviewed the relationship between the salinity of fluids, temperature, and the concentration of the transition metals (Fe, Mn, Zn, Pb). The compiled data clearly show a positive correlation between metal solubility, the Cl content, and temperature. Accordingly, the metal content of crustal fluids is generally controlled by the host-rock during metamorphism. Hammerli et al. (2015) confirmed the conclusions of Yardley (2005) and the experimental results of workers, such as Ilton and Eugster (1990) or Hemley et al. (1992), regarding the increased metal content in saline fluids during fluid-rock interaction with increasing temperatures. Decreasing Pb and Zn contents in the bulk rock are consistent with the model of Pb and Zn extraction from the micas (Fig. 10.13). Such metal-mobilizing fluids, upon entering favourable geodynamic settings, can lead to mineralizations of economic significance. Besides base-metal mobilization, U has been identified as being mobilized during metamorphism as indicated by U deposits associated with regional metamorphic terranes (e.g., Kish and Cuney 1981; Oliver et al. 1992). A recent fluid inclusion study by Eglinger et al. (2014) has elegantly shown that highly saline fluids, with salinities close to 60 wt% $CaCl_2$ and $\sim$15 wt% NaCl, were present during amphibolite-facies metamorphism, which transported high concentrations of Cu and tens of ppm U. Evaporites within the same sedimentary sequence, where the U is concentrated, are regarded as the NaCl source during metamorphism.

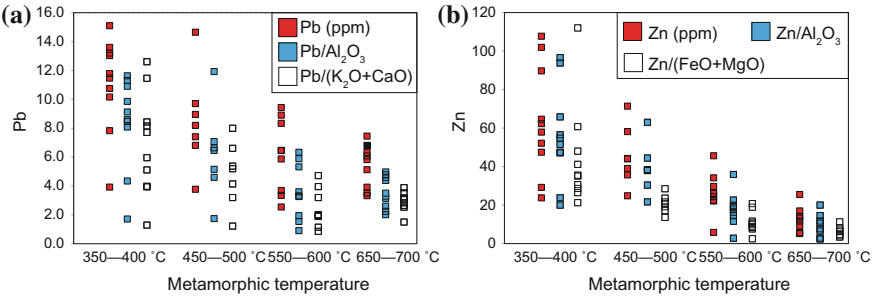

Fig. 10.13 Bulk rock Pb (A), and Zn (B) concentrations versus metamorphic temperature. Both metal concentrations (ppm) and ratios (to account for protolith variability) are shown. Metal contents decrease with increasing metamorphic temperatures in both cases. For graphical purposes, only absolute concentrations are shown. (Modified after Hammerli et al. 2015)

◂**Fig. 10.14** **a** Evaporation of an enclosed basin of (sea) water leads to the precipitation of evaporites such as gypsum and halite. Residual dense bittern brine fluids, rich in Ca, K, Mg, and Br, infiltrate deeper sediments (A-1) where fluid-rock interaction can lead to fluorite formation (A-4), albitization (A-3), and K-feldspathization. Impervious rock layers might lead to overpressure and lateral fluid flow. Buried organic-rich layers can act as major Br and I sources during diagenesis and metamorphism upon their decomposition and fluid interaction (A-2). More details on sedimentary environments and halogen distribution and behaviour can be found in Worden (2018). The presence of highly saline fluids during regional metamorphism can lead to elevated Cl-contents in apatite, amphibole, and biotite, such that scapolite might form in calc-silicate rocks and metabasites. Scapolite might be present in isolated layers, depending on the mineralogy and Cl-availability, where it occurs as small, xenomorphic grains (B-1) or porphyroblasts (B-2). Multiple metamorphic events potentially lead to a recrystallization of scapolite or distinct zonation (B-2). Shear-zones and/or faults can lead to focussed fluid flow during peak or post-peak metamophism where, under certain circumstances, K-rich saline fluids can lead to the extensive formation of biotite and porphyroblastic scapolite (B-4). Alternatively, a sodic fluid can lead to significant albitization in or around shear-zones (e.g., Rubenach 2012, Fig. 10.9, B-3). Syn- or post-metamorphic intrusions can lead to complicated fluid flow regimes where fluid mixing of metamorphic fluids and igneous fluids can take place (B-5)

10.6 Summary

Halogens play an important role during the metamorphic cycle of a rock from diagenesis throughout metamorphism and metasomatism and up to partial melting. Their presence influences the mineral compositions and stabilities and can control mass-transfer during diagenesis (see Worden 2018), regional and contact metamorphism (Fig. 10.14), and subduction-zone processes (see Barnes et al. 2018).

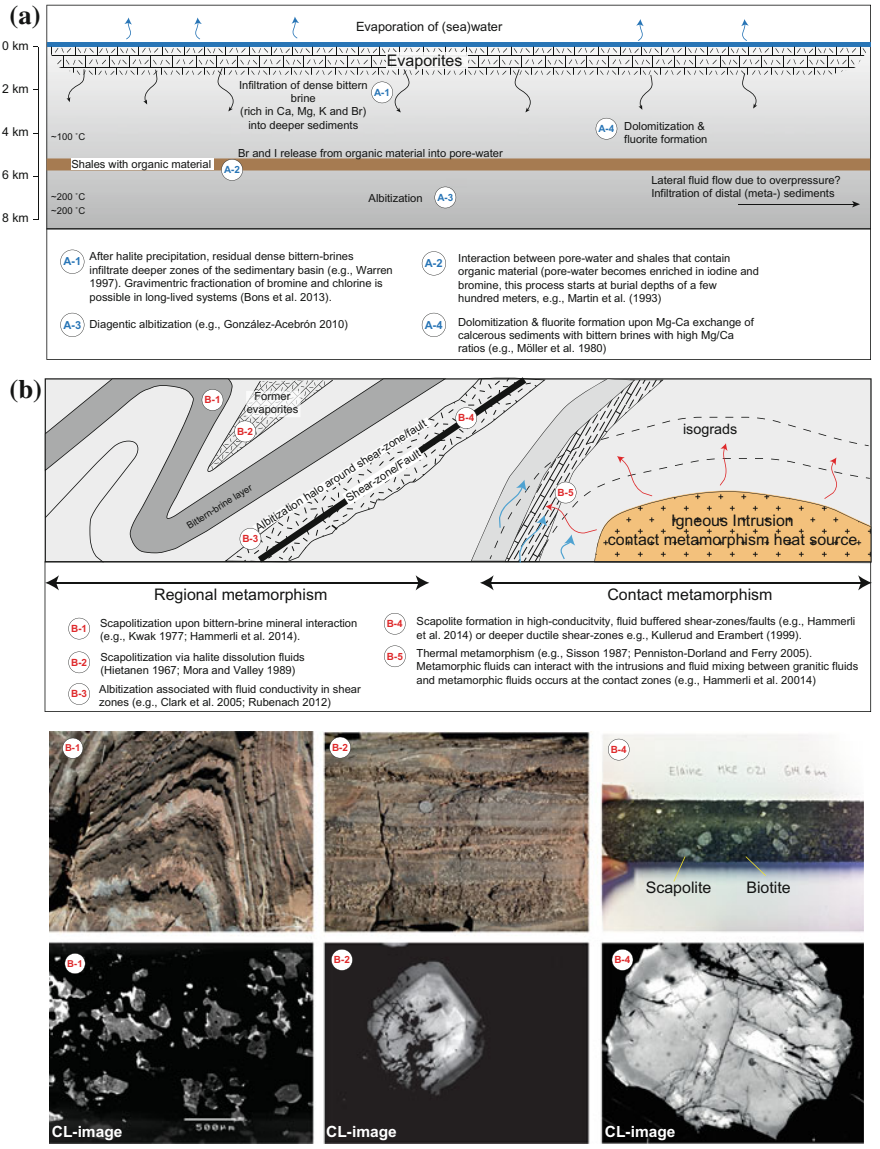

Despite the widely recognized importance of halogens in metal mobility, surprisingly little is known about their behaviour during metamorphism. Moreover, to date no study has addressd the exact behaviour of F during the evaporation of seawater.

Identifying the origin of saline fluids is particularly challenging as their sources, such as dissolved evaporitic layers, or non-exposed intrusions, are often no longer present or visible. Nevertheless, approaches that combine stable isotope signatures,

noble gases, and halogen ratios in minerals and fluids seem to be the most reliable tools to identify halogen sources and related geochemical processes (e.g., Banks et al. 2000; Böhlke and Irwin 1992; Kendrick et al. 2001a; Hammerli et al. 2014; Bernal et al. 2014; Kusebauch et al. 2015c).

The studies by Heitanen (1967), Mora and Valley (1989), Oliver et al. (1992), Gómez-Pugnaire et al. (1994), Kullerud and Erambert (1999), and Hammerli et al. (2014), all observed considerable variations in halogen contents and their hosts on a layer- and thin-section scale. These observations suggest that in rock-buffered environments, typical for regional metamorphism, local equilibrium was achieved on a relatively small scale, where fluid-rock interaction was not enough to smooth the halogen distribution out. This is also reflected by fluid compositions calculated based on halogen-bearing minerals as well as by the spread of fluid inclusion compositions. The above variations might be a result of limited fluid flow via porewater connectivity in marbles and (meta-) psammopelites. Fluid circulation and exchange via (tectonic-) hydro-fracture networks may allow for only local equilibration with minerals (e.g., Holness and Graham 1991, 1995; Holness 1992; Evans et al. 2013).

On a stratigraphic-scale, the halogen contents, and their ratios, can vary significantly between sedimentary units (Fig. 10.14a, explained in detail by Warren 1997). Residual, dense, bittern brine fluids likely gravimetrically penetrate deeper lying sedimentary layers (Warren 1997; Bons and Gomez-Rivas 2013; see also Worden 2018) where impermeable layers, such as halite, can lead to lateral fluid flow. It is possible that, although stratigraphically separated, both residual bittern brine fluids, and fluids with dissolved halite components, may coexist in (meta-) sedimentary units (Fig. 10.14). During subsequent metamorphism, these fluids can interact with their host lithologies, which, depending on their chemical composition, can lead to the formation of halogen-rich minerals (Tables 10.2 and 10.3). Such a scenario might have occurred in the Mt. Isa Inlier where in the Mary Kathleen section residual bittern brine fluids supplied halogens to the hydrothermal fluids. Fluids in the Corella/Doherty Formation in the Cloncurry district, on the other hand, contain a major halite component (Kendrick et al. 2007; Hammerli unpublished data), which might have been provided by stratigraphically higher halite-rich evaporites. During metamorphism, shear-zones or faults, and the contacts between mafic intrusions and (meta-) sedimentary rocks, can act as major fluid flow paths that can lead to associated albitization (e.g., Clark et al. 2005; Rubenach 2012; Fig. 10.14)

The recognition of saline fluids during metamorphism is critical in terms of evaluating potential mass transport and for a range of considerations regarding metamorphic reactions, mineral phase stability, and minimum melting temperatures (e.g., Aranovich et al. 2013; Manning and Aranovich 2014 and references therein). However, the lack of key halogen-bearing minerals, such as micas, amphibole, scapolite, fluorite, or apatite, or the lack of fluid inclusions, makes it difficult to recognise the presence of saline fluids. Quantitative analyses of apatite or micas might be the key to gain insights into fluid properties. More studies should include both regional and local considerations, investigating halogen distribution in relation

to varying lithologies, different layers, metamorphic grade, distance from igneous contacts, and possible structural features such as faults, shear-zones, and strain heterogeneities.

In order to understand the behaviour of halogens during metamorphism (e.g., changes with metamorphic grade, rock buffering versus fluid buffering, partitioning between minerals and fluid, sources of fluids) accurate analyses are essential. Attempts at integrating halogen studies with fluid inclusion and stable isotope work have shown great potential for elucidating metamorphic and metasomatic processes (e.g., Bernal et al. 2014; Kusebauch et al. 2015c).

Acknowledgements We would like to thank Nick Oliver for early discussions and Carl Spandler for helpful suggestions and comments as well as B. Yardley, H. Austrheim and W. Glassley for their reviews that helped to improve this chapter considerably. The editors D.E. Harlov and L. Aranovich are thanked for their help and patience.

References

Abercrombie HJ, Skippen GB, Marshall DD (1987) F-OH substitution in natural tremolite, talc, and phlogopite. Contrib Mineral Petrol 97:305–312

Abu Sharib ASAA, Sanislav IV (2013) Polymetamorphism accompanied switching in horizontal shortening during Isan Orogeny: example from the Eastern Fold Belt, Mount Isa Inlier, Australia. Tectonophysics 587:146–167

Ague JJ (1994) Mass transfer during bavorrian metamorphism of pelites, South-Central Connecticut. I: evidence for changes in composition and volume. Am J Sci 294:989–1057

Ague JJ (2003) Fluid infiltration and transport of major, minor, and trace elements during regional metamorphism of carbonate rocks, Wepawaug Schist, Connecticut, USA. Am J Sci 303:753–816

Alderton DHM, Pearce JA, Potts PJ (1980) Rare earth element mobility during granite alteration: evidence from south-west England. Earth Planet Sci Lett 49:149–165

Anderson GM, Burnham CW (1965) The solubility of quartz in supercritical water. Am J Sci 263:494–511

Anderson GM, Burnham CW (1967) Reaction of quartz and corundum with aqueous chloride and hydroxide solutions at high temperatures and pressures. Am J Sci 265:12–27

Anderson GM, Burnham CW (1983) Feldspar solubility and the transport of aluminum under metamorphic conditions. Am J Sci 238:283–297

Aranovich L, Safonov O (2018) Halogens in high-grade metamorphism. In: Harlov DE, Aranovich L (eds) The role of halogens in terrestrial and extraterrestrial geochemical processes: surface, crust, and mantle. Springer, Berlin, pp 713–757

Aranovich LY, Dubinina EO, Avdeenko AS, Lebedeva YM, Bushmin SA, Dolivo-Dobrovol'skii DD (2010) Oxygen isotopic composition of coexisting minerals of sillimanite-hypersthene rocks from the Por'ya bay area: evidence of fluid involvement in granulite-facies metamorphism. Geochem Int 48:739–751

Aranovich LY, Newton RC, Manning CE (2013) Brine-assisted anatexis: experimental melting in the system haplogranite–H_2O–NaCl–KCl at deep-crustal conditions. Earth Planet Sci Lett 374:111–120

Austrheim H, Putnis CV, Engvik AK, Putnis A (2008) Zircon coronas around Fe–Ti oxides: a physical reference frame for metamorphic and metasomatic reactions. Contrib Mineral Petrol 156:517–527

Banks DA, Giuliani G, Yardley BWD, Cheilletz A (2000) Emerald mineralisation in Colombia: fluid chemistry and the role of brine mixing. Mineral Dep 35:699–713

Barnes JD, Sharp ZD (2017) Chlorine isotope geochemistry. Rev Mineral Geochem 82 (1):345–378

Barnes J, Manning C, Scambelluri M, Selverstone J (2018) The behaviour of halogens during subduction-zone processes. In: Harlov DE, Aranovich L (eds) The role of halogens in terrestrial and extraterrestrial geochemical processes: surface, crust, and mantle. Springer, Berlin, pp 545–590

Barrett TJ, Anderson GM (1982) The solubility of sphalerite and galena in NaCl brines. Econ Geol 77:1923–1933

Beratan KK (1999) Miocene potassium metasomatism, Whipple Mountains, southeastern California: a datable tracer of extension-related fluid transport. Geology 27:259–262

Bernal NF, Glesson SA, Dean AS, Liu XM, Hoskin P (2014) The source of halogens in geothermal fluids from the Taupo Volcanic Zone, North Island, New Zealand. Geochim Cosmochim Acta 126:265–283

Bingen B, Davis WJ, Hamilton MA, Engvik AK, Stein HJ, Skar O, Nordgulen O (2008) Geochronology of high-grade metamorphism in the Sveconorwegian belt, S. Norway: U–Pb, Th–Pb and Re–Os data. Norwegian Journal of Geology 88:13–42

Bodart DE (1968) On the paragenesis of albitites. Nor Geol Tidskr 48:269–280

Böhlke JK, Irwin JJ (1992) Laser microprobe analyses of Cl, Br, I, and K in fluid inclusions: Implications for sources of salinity in some ancient hydrothermal fluids. Geochim Cosmochim Acta 56:203–225

Boness M, Heumann KG, Haack U (1991) Cl, Br and I analyses of metamorphic and sedimentary rocks by isotope dilution mass spectrometry. Contrib Mineral Petrol 107:94–99

Bons PD, Gomez-Rivas E (2013) Gravitational fractionation of isotopes and dissolved components as a first-order process in crustal fluids. Econ Geol 106:1195–1201

Bottrell SH, Yardley BWD, Buckley F (1988) A modified crush-leach method for the analysis of fluid inclusion electrolytes. Bull Minér 111:279–290

Boulvais P, de Parseval P, D'Hulst A, Paris P (2006) Carbonate alteration associated with talc-chlorite mineralization in the eastern Pyrenees, with emphasis on the St. Barthelemy Massif. Mineral Petrol 88:499–526

Bowers TS, Helgeson HC (1983) Calculation of the thermodynamic and geochemical consequences of nonideal mixing in the system H_2O-CO_2-NaCl on phase relations in geological systems: equation of state for H_2O-CO_2-NaCl fluids at high pressures and temperatures. Geochim Cosmochim Acta 47:1247–1275

Braitsch O, Herrmann AG (1963) Zur Geochemie des Broms in Salinaren Sedimenten, 1. Experimentelle Bestimmung der Br-Verteilung in verschiedenen natürlichen Salzsystemen. Geochim Cosmochim Acta 27:361–391

Budzyn B, Harlov DE, Williams ML, Jercinovic MJ (2011) Experimental determination of stability relations between monazite, fluorapatite, allanite, and REE-epidote as a function of pressure, temperature, and fluid composition. Am Mineral 96:1547–1567

Caciagli NC, Manning CE (2003) The solubility of calcite in water at 5–16 kbar and 500–800 °C. Contrib Mineral Petrol 146:275–285

Cardenas AA, Girty GH, Hanson AD, Lahren MM, Knaack C, Johnson D (1996) Assessing differences in composition between low metamorphic grade mudstones and high-grade schists using log ratio techniques. J Geol 104:279–293

Chai JY, Muramatsu Y (2007) Determination of bromine and iodine in twenty-three geochemical reference materials by ICP-MS. Geostand Geoanal Res 31:143–150

Charoy B, Pollard PJ (1989) Albite-rich, silica-depleted metasomatic rocks at Emuford, northeast Queensland: Mineralogical, geochemical, and fluid inclusion constraints on hydrothermal evolution and tin mineralization. Econ Geol 84:1850–1874

Clark C, Schmidt-Mumm A, Faure K (2005) Timing and nature of fluid flow and alteration during mesoproterozoic shear zone formation, Olary domain, South Australia. J Metamorph Geol 23:147–164

Connolly JAD, Podladchikov YY (2013) A hydromechanical model for lower crustal fluid flow. In: Harlov DE, Austrheim H (eds) Metasomatism and the chemical transformation of rock: the role of fluids in terrestrial and extraterrestrial processes. Springer, Berlin, pp 599–658

Čopjaková R, Buriánek D, Škoda R, Houzar S (2009) Tourmalinites in the metamorphic complex of the Svratka Unit (Bohemian Massif) a study of compositional growth of tourmaline and considerations related to genesis. J Geosci 54:221–243

Correns CW (1956) The geochemistry of the halogens. In: Ahrens LH, Rankama K, Runcom SK (eds) Physics and chemistry of the earth 1. Pergamon Press, London

Cosca MA, Mezger K, Essene EJ (1998) The Baltica-Laurentia connection: Sveconorwegian (Grenvillian) metamorphism, cooling, and unroofing in the Bamble Sector, Norway. J Geol 106:539–552

Cosgrove ME (1970) Iodine in the Bituminous Kimmeridge shales of the Dorset coast, England. Geochim Cosmochim Acta 34:830–836

Coulson IM, Dipple GM, Raudsepp M (2001) Evolution of HF and HCl activity in magmatic volatiles of the gold-mineralized Emerald Lake pluton, Yukon Territory, Canada. Miner Dep 36:594–606

Cullers RL (2002) Implications of elemental concentrations for provenance, redox conditions, and metamorphic studies of shales and limestones near Pueblo, CO, USA. Chem Geol 191:305–327

Dahlgren S, Bogoch R, Magaritz M, Michard A (1993) Hydrothermal dolomite marbles associated with charnockitic magmatism in the Proterozoic Bamble Shear Belt, south Norway. Contrib Mineral Petrol 113:394–408

de Jong G, Williams PJ (1995) Giant metasomatic system formed during exhumation of mid-crustal Proterozoic rocks in the vicinity of the Cloncurry Fault, northwest Queensland. Aust J Earth Sci 42:281–290

Drummond MS, Ragland PC, Wesolowski D (1986) An example of trondhjemite genesis by means of alkali metasomatism: rockford Granite, Alabama Appalachians. Contrib Mineral Petrol 93:98–113

Dyson IA, Gatehouse CG, Jago JB (1996) Sequence stratigraphy of the Talisker Calc-siltstone and lateral equivalents in the Cambrian Kanmantoo Group. Geol Surv S Aust Q Geol Notes 129:27–41

Eggenkamp H (2014) The geochemistry of stable chlorine and bromine isotopes. Springer, Heidelberg, p 172

Eggenkamp HGM, Kreulen R, Koster Van Groos AF (1995) Chlorine stable isotope fractionation in evaporites. Geochim Cosmochim Acta 59:5169–5175

Eglinger A, Ferraina C, Tarantola A, Andre-Mayer SA, Vanderhaeghe O, Boiron M-C, Dubessy J, Richard A, Brouand M (2014) Hypersaline fluids generated by high-grade metamorphism of evaporites: fluid inclusion study of uranium occurrences in the Western Copperbelt. Contrib Mineral Petrol 167:967

Elliott RB (1966) The association of amphibolite and albitite, Kragerö, south Norway. Geol Mag 103:1–7

Ellis AJ (1963) The solubility of calcite in sodium chloride solutions at high temperatures. Am J Sci 261:259–267

Ellis DE (1978) Stability and phase equilibria of chloride and carbonate bearing scapolites at 750° C and 400 bar. Geochim Cosmochim Acta 42:1271–1281

Enami M, Suzuki K, Liou JG, Bird DK (1993) Al-Fe^{3+} and F-OH substitutions in titanite and constraints on their P-T dependence. Eur J Mineral 5:219–231

Engvik AK, Putnis A, Fitz Gerald JD, Austrheim H (2008) Albitisation of granitic rocks: the mechanism of replacement of oligoclase by albite. Can Mineral 46:1401–1415

Engvik AK, Mezger K, Wortelkamp S, Bast R, Corfu F, Korneliussen A, Ihlen P, Bingen B, Austrheim H (2011) Metasomatism of gabbro—mineral replacement and element mobilization during the Sveconorwegian metamorphic event. J Metam Geol 29:399–423

Engvik AK, Ihlen PM, Austrheim H (2014) Charactersiation of Na-metasomatism in the Sveconorwegian Bamble Sector of South Norway. Geosci Front 5:659–672

Ennis DJ, Dunbar NW, Campbell AR, Chapin CE (2000) The effects of K-metasomatism on the mineralogy and geochemistry of silicic ignimbrites near Socorro, New Mexico. Chem Geol 167:285–312

Evans BW, Shaw DM, Haughton DR (1969) Scapolite stroichiometry. Contrib Mineral Petrol 24:293–305

Evans KA, Powell R, Frost BR (2013) Using equilibrium thermodynamics in the study of metasomatic alteration, illustrated by an application to serpentinites. Lithos 168–169:67–84

Fein JB, Walther JV (1989) Calcite solubility and speciation in supercritical NaCl-HCl aqueous fluids. Contrib Mineral Petrol 103:317–324

Ferry JM (1994) Overview of the petrologic record of fluid flow during regional metamorphism in northern New England. Am J Sci 294:905–988

Ferry JM, Dipple GM (1991) Fluid flow, mineral reactions and metasomatism. Geology 19:211–214

Ferry JM, Gerdes ML (1998) Chemically reactive fluid flow during metamorphism. Ann Rev Earth Planet Sci 26:255–287

Ferry JM, Gottschalk M (2009) The effect of fluid salinity on infiltration-driven contact metamorphism of carbonate rocks. Contrib Mineral Petrol 158:619–636

Ferry JM, Wing BA, Rumble D (2001) Formation of wollastonite by chemically reactive fluid flow during contact metamorphism, Mt. Morrison pendant, Sierra Nevada, California, USA. J Petrol 42:1705–1728

Frank E (1983) Alpine metamorphism of calcareous rocks along a cross-section in the Central Alps: occurence and breakdown of muscovite, margarite and paragonite. Schweiz Mineral Petrogr Mitt 63:37–93

Fuge R (1974a) Chlorine. In: Wedepohl KH (ed) Handbook of geochemistry, Chapter 17. Springer, Berlin

Fuge R (1974b) Bromine. In: Wedepohl KH (ed) Handbook of geochemistry, Chapter 35. Springer, Berlin

Fuge R (1974c) Iodine. In: Wedepohl KH (ed) Handbook of geochemistry, Chapter 53. Springer, Berlin

Fuge R (1988) Sources of halogens in the environment, influences on human and animal health. Environ Geochem Health 10:51–61

Fuge R (2005) Soils and iodine deficiency. In: Selinus O, Alloway B, Centeno JA, Finkelman RB, Fuge R, Lindh U, Smedley P (eds.) Essentials of medical geology. Elsevier, San Diego, pp 417–433

Fuge R, Johnson CC (1984) Evidence for the chalcophile nature of iodine. Chem Geol 43:347–352

Gao S, Luo T-C, Zhang B-R, Zhang H-F, Han Y-W, Hu Y-K, Zhao Z-D (1998) Chemical composition of the continental crust as revealed by studies in east China. Geochim Cosmochim Acta 62:1959–1975

Giere R (1990) Hydrothermal mobility of Ti, Zr, and REE: examples from the Bergell and Adamello contact aureoles (Italy). Terra Nova 2:60–67

Giggenbach WF (1995) Variations in the chemical and isotopic composition of fluids discharged from the Taupo Volcanic Zone, New Zealand. J Volcanol Geoth Res 68:89–116

Gilbert F, Guillaume D, Laporte D (1997) Importance of fluid immiscibility in the H_2O-CO_2-NaCl system and selective CO_2 entrapment in granulites: experimental phase diagram at 5–7 kbar, 900 °C and wetting textures. Eur J Mineral 10:1109–1123

Glassley WE, Korstgard JA, Sorensen K (2010) K-rich brine and chemical modification of the crust during continent–continent collision, Nagssugtoqidian Orogen, West Greenland. Precambr Geol 180:47–62

Gleeson SA, Yardley BWD, Munz IA, Boyce AJ (2003) Infiltration of basinal fluids into high-grade basement, south Norway: sources and behaviour of waters and brines. Geofluids 3:33–48

Goldoff B, Webster JD, Harlov DE (2012) Characterization of fluor-chlorapatites by electron probe microanalysis with a focus on time-dependent intensity variation of halogens. Am Mineral 97:1103–1115

Goldsmith JR, Newton RC (1977) Scapolite-plagioclase stability relations at high pressures and temperatures in the system $NaAlSi_3O_8$-$CaAl_2Si_2O_8$-$CaCO_3$-$CaSO_4$. Am Mineral 62:1063–1081

Gomez-Pugnaire MT, Franz G, Sanchez-Vizcaino VL (1994) Retrograde formation of NaCl-scapolite in high pressure metaevaporites from Cordilleras Beticas (Spain). Contrib Mineral Petrol 116(4):448–461

González-Acebrón L, Arribas J, Maas R (2010) The role of sandstone provenance in diagenetic albitization of feldspars. A case study in the Jurassic Tera Group sandstones (Cameros Basin, NE Spain). Sed Geol 229:53–63

Greenwood HJ (1975) Buffering of pore fluids by metamorphic reactions. Am J Sci 275:573–593

Haack U, Heinrichs H, Boness M, Schneider A (1984) Loss of metals from pelites during regional metamorphism. Contrib Mineral Petrol 85:116–132

Haines PW, Jago JB, Gum JC (2001) Turbidite deposition in the Cambrian Kanmantoo Group, South Australia. Aust J Earth Sci 48:465–478

Hammerli J, Rusk B, Spandler C, Emsbo P, Oliver NHS (2013) In situ quantification of Br and Cl in minerals and fluid inclusions by LA-ICP-MS: a powerful tool to identify fluid sources. Chem Geol 337–338:75–87

Hammerli J, Spandler C, Oliver NHS, Rusk B (2014) Cl/Br of scapolite as a fluid tracer in the earth's crust: insights into fluid sources in the Mary Kathleen Fold Belt, Mt. Isa Inlier. Australia. J Metamorph Geol 32:93–112

Hammerli J, Spandler C, Oliver NHS, Sossi P, Dipple G (2015) Zn and Pb mobility during metamorphism of sedimentary rocks and potential implications for some base metal deposits. Miner Dep 50:657–664

Hammerli J, Spandler C, Oliver NHS (2016) Element mobility and redistribution during upper crustal metamorphism: an example from the Eastern Mt Lofty Ranges, South Australia. Contrib Mineral Petrol. https://doi.org/10.1007/s00410-016-1239-7

Hansen EC, Harlov DE (2007) Whole-rock, phosphate, and silicate compositional trends across an amphibolite- to granulite-facies transition, Tamil Nadu, India. J Petrol 48:1641–1690

Hardie LA (1990) The roles of rifting and hydrothermal $CaCl_2$ brines in the origin of potash evaporites. Am J Sci 290:43–106

Harlov DE (2000) Pressure–temperature estimation in orthopyroxene–garnet bearing granulite facies rocks, Bamble Sector, Norway. Mineral Petrol 69:11–33

Harlov DE, Förster H-J (2002a) High-grade fluid metasomatism on both a local and regional scale: the Seward Peninsula, Alaska and the Val Strona di Omegna, Ivrea-Verbano Zone, Northern Italy Part I: petrography and silicate mineral chemistry. J Petrol 43:769–799

Harlov DE, Förster H-J (2002b) High-grade fluid metasomatism on both a local and regional scale: the Seward Peninsula, Alaska and the Val Strona di Omegna, Ivrea-Verbano Zone, Northern Italy Part II: phosphate mineral chemistry. J Petrol 43:801–824

Harlov DE, Förster H-J (2003) Fluid-induced nucleation of (Y + REE)-phosphate minerals within apatite: nature and experiment. part II. fluorapatite. Am Mineral 88:1209–1229

Harlov DE, Hetherington CJ (2010) Partial high-grade alteration of monazite using alkali-bearing fluids: experiment and nature. Am Miner 95:1105–1108

Harlov DE, Hansen EC, Bigler C (1998) Petrologic evidence for K-feldspar metasomatism in granulite facies rocks. Chem Geol 151:373–386

Harlov DE, Wirth R, Hetherington CJ (2011) Fluid-mediated partial alteration in monazite: the role of coupled dissolution-reprecipitation in element redistribution and mass transfer. Contrib Mineral Petrol 162:329–348

Haughton DR (1970) Plagioclase-Scapolite equilibrium. Can Mineral 10:854–870

Hawthorne FC, Oberti R (2007) Amphiboles: crystal chemistry. Rev Mineral Geochem 67:1–54

Heinrich W (2007) Fluid immiscibility in metamorphic rocks. Rev Mineral 65:389–430

Heinrich CA, Ryan CG, Mernagh TP, Eadington PJ (1992) Segregation of ore metals between magmatic brine and vapor—a fluid inclusion study using PIXE microanalysis. Econ Geol 87:1566–1583

Heinrich CA, Bain JHC, Fardy JJ, Waring CL (1993) Br/Cl geochemistry of hydrothermal brines associated with Proterozoic metasediment-hosted copper mineralization at Mount Isa, northern Australia. Geochim Cosmochim Acta 57:2991–3000

Helvaci C, Griffin WL (1983) Metamorphic feldspathization of metavolcanics and granitoids, Avnik area, Turkey. Contrib Mineral Petrol 83:309–319

Hemley JJ, Cygan GL, Fein JB, Robinson GR, D'Angelo WM (1992) Hydrothermal ore-forming processes in the light of studies in rock-buffered systems: 1 Iron-copper-zinc-lead sulfide solubility relations. Econ Geol 87:1–22

Henry DJ, Dutrow BL (2011) The incorporation of fluorine in tourmaline: internal crystallographic controls or external environmental influences? Can Mineral 49:41–56

Hetherington CJ, Harlov DE, Budzyn B (2010) Experimental metasomatism of monazite and xenotime: mineral stability, REE mobility and fluid composition. Mineral Petrol 99:165–184

Hietanen A (1967) Scapolite in the Belt Series in the St. Joe-Clearwater region, Idaho. Geol Soc Am Spec Paper 86:1–56

Holland H (1972) Granite, solutions and base metal deposits. Econ Geol 67:281–301

Holness MB (1992) Equilibrium dihedral angles in the system quartz–H_2O–CO_2–NaCl at 800°C and 1–15 kbar: the effect of pressure and fluid composition on the permeability of quartzites. Earth Planet Sci Lett 114:171–184

Holness MB, Clemens JC (1999) Partial melting of the Appin quartzite driven by fracture-controlled H_2O infiltration in the aureole of the Ballachulish igneous complex, Scottish Highlands. Contrib Mineral Petrol 136:154–168

Holness MB, Graham CM (1991) Equilibrium dihedral angles in the system H_2O–CO_2–NaCl–calcite, and implications for fluid flow during metamorphism. Contrib Mineral Petrol 108:368–383

Holness MB, Graham CM (1995) P-T-X effects on equilibrium carbonate–H_2O–CO_2–NaCl dihedral angles: constraints on carbonate permeability and the role of deformation during fluid infiltration. Contrib Mineral Petrol 119:301–313

Holser WT (1979a) Trace elements and isotopes in evaporites. Mineral Soc Amer: Rev Mineral 6:295–346

Holser WT (1979b) Mineralogy of evaporites. In: Burns RG (ed) Marine minerals: reviews in Mineralogy, vol 6. Mineralogical Society of America, Washington D.C., pp 211–294

Houston SJ, Smalley PC, Laycock A, Yardley BWD (2011) The relative importance of buffering and brine inputs in controlling the abundance of Na and Ca in sedimentary formation waters. Mar Petrol Geol 28:1242–1251

Hövelmann J, Putnis A, Geisler T, Schmidt B, Golla-Schindler U (2010) The replacement of plagioclase feldspars by albite: observations from hydrothermal experiments. Contrib Mineral Petrol 159:43–59

Hurai V, Lexa O, Schulmann K, Montigny R, Prochaska W, Frank W, Konečný P, Kráľ J, Thomas R, Chovan M (2008) Mobilization of ore fluids during Alpine metamorphism: evidence from hydrothermal veins in the Variscan basement of Western Carpathians, Slovakia. Geofluids 8:181–207

Ilton ES, Eugster HP (1990) Partitioning of base metals between silicates, oxides, and a chloride-rich hydrothcrmal fluid. I. Evaluation of data derived from experimental and natural assemblages. In: Spencer RJ, Ming Chou I (eds) Fluid-mineral interactions: a tribute to H. P. Eugster. Geochem Soc, Spec Publ 2, pp. 157–169

Irwin JJ, Roedder E (1995) Diverse origins of fluid in magmatic inclusions at Bingham (Utah, USA), Butte (Montana, USA), St. Austell (Cornwall, UK), and Ascension Island (mid-Atlantic, UK), indicated by laser microprobe analysis of Cl, K, Br, I, Ba + Te, U, Ar, Kr, and Xe. Geochim Cosmochim Acta 59:295–312

Jago JB, Gum JC, Burtt AC, Haines PW (2003) Stratigraphy of the Kanmantoo Group: a critical element of the Adelaide Fold Belt and the Palaeo-Pacific plate margin, Eastern Gondwana. Aust J Earth Sci 50:343–363

Jambon A, Deruelle B, Dreibus G, Pineau F (1995) Chlorine and bromine abundance in MORB: the contrasting behaviour of the Mid-Atlantic Ridge and East Pacific Rise and implications for chlorine geodynamic cycle. Chem Geol 126:101–107

Jamtveit B, Dahlgren S, Austrheim H (1997) High grade contact metamorphism of calcareous rocks from the Oslo Rift, Southern Norway. Am Mineral 82:1241–1254

Johnson L, Burgess R, Turner G, Milledge HJ, Harris JW (2000) Noble gas and halogen geochemistry of mantle fluids: comparison of African and Canadian diamonds. Geochim Cosmochim Acta 64:717–732

Katongo C, Koller F, Ntaflos T, Koeberl C, Tembo F (2011) Occurrence and origin of Scapolite in the Neoproterozoic Lufilian–Zambezi Belt, Zambia: evidence/role of brine-rich fluid infiltration during regional metamorphism. In: Ray J, Sen G, Gosh B (eds) Topics in igneous petrology. Springer, Dordrecht, pp 485

Kendrick MA (2012) High precision Cl, Br and I determinations in mineral standards using the noble gas method. Chem Geol 292–293:116–126

Kendrick MA, Burgess R, Pattrick RAD, Turner G (2001a) Fluid inclusion noble gas and halogen evidence on the origin of Cu-porphyry mineralizing fluids. Geochim Cosmochim Acta 65:2651–2668

Kendrick MA, Burgess R, Pattrick RAD, Turner G (2001b) Halogen and Ar-Ar age determinations of fluid inclusions in quartz veins from porphyry copper deposits using complementary noble gas extraction techniques. Chem Geol 177:351–370

Kendrick MA, Duncan RJ, Phillips D (2006) Noble gas and halogen constraints on mineralizing fluids of metamorphic versus surficial origin. Mt Isa, Australia. Chem Geol 235:325–351

Kendrick MA, Mark G, Phillips D (2007) Mid-crustal fluid mixing in a Proterozoic Fe oxide-Cu-Au deposit, Ernest Henry, Australia: evidence from Ar, Kr, Xe, Cl, Br, and I. Earth Planet Sci Lett 256:328–343

Kendrick MA, Baker T, Fu B, Philips D, Williams PJ (2008) Noble gas and halogen constraints on regionally extensive mid-crustal Na-Ca metasomatism, the Proterozoic Eastern Mount Isa Block, Australia. Precambr Res 163:131–150

Kendrick MA, Phillips D, Wallace M, Miller JMcL (2011) Halogens and noble gases in sedimentary formation waters and Zn-Pb deposits: a case study from the Lennard Shelf, Australia. Appl Geochem 26:2089–2100

Keppler H (1993) Influence of fluorine on the enrichment of high field strength trace elements in granitic rocks. Contrib Mineral Petrol 114:479–488

Kish L, Cuney M (1981) Uraninite-albite veins from the Mistamisk Valley of the Labrador Trough Quebec. Mineral Mag 44:471–483

Klemme S, Stalder R (2018) Halogens in the Earth's mantle: what we know and what we don't. In: Harlov DE, Aranovich L (eds) The role of halogens in terrestrial and extraterrestrial geochemical processes: surface, crust, and mantle. Springer, Berlin, pp 847–869

Komada N, Moecher DP, Westrum EF (1996) Thermodynamic properties of Scapolites at temperatures ranging from 10 K to 1000 K. J Chem Thermodyn 28:941–973

Korzhinskiy MA (1981) Apatite solid solution as indicators of the fugacity of HCl and HF in hydrothermal fluids. Geochem Int 3:45–60

Kotel'nikov AR (1987) Hydrothermal stability of sulfur bearing scapolite. Geochem Inter 24 (2):80–90

Kuhn BK, Reuser E, Powell R, Günther D (2005) Metamorphic evolution of calc-silicates in the Central Alps, Switzerland. Mineral Petrol Mitt 85:175–190

Kullerud K, Erambert M (1999) Cl-scapolite, Cl-amphiboles, and plagioclase equilibria in ductile shear zones at Nusfjord, Lofoten, Norway: implications for fluid compositional evolution during fluid–mineral interactions in the deep crust. Geochim Cosmochim Acta 63:3829–3844

Kusebauch C, John T, Whitehouse MJ, Engvik AK (2015a) Apatite as probe for the halogen composition of metamorphic fluids (Bamble Sector, SE Norway). Contrib Mineral Petrol 170 (4):34

Kusebauch C, John T, Whitehouse MJ, Klemme S, Putnis A (2015b) Distribution of halogens between fluid and apatite during fluid-mediated replacement processes. Geochim Cosmochim Acta 170:225–246

Kusebauch C, John T, Barnes JD, Klügel S, Austrheim HO (2015c) Halogen element and stable chlorine isotope fractionation caused by fluid-rock interaction (Bamble Sector, SE Norway). J Petrol 56(2):299–324. https://doi.org/10.1093/petrology/egv001

Kwak TAP (1977) Scapolite compositional change in a metamorphic gradient and ist bearing on the identification of meta-evaporite sequences. Geol Mag 114(5):343–354

Lagache M, Weisbrod A (1977) The system: two alkali feldspar-KCI-NaCI-H, O at moderate to high temperatures and low pressures. Contrib Mineral Petrol 62:77–101

Lang HM, Rice JM (1985) Metamorphism of pelitic rocks in the Snow Peakarea, northern Idaho: sequence of events and regional implications. Geol Soc Am Bull 96:73l–736

Laporte D, Watson EB (1991) Direct observation of near-equilibrium pore geometry in synthetic quartzites at 600–800°C and 2–10.5 kbar. J Geol 99:873–878

Leach DL, Sangster DF, Kelley KD, Large RR, Garven G. Allen CR, Gutzmer J, Walters S (2005) Sediment-hosted lead–zinc deposits: a global perspective. Econ Geol 100th Anniversary 100:561–607

Lecumberri-Sanchez P, Bodnar R (2018) Halogen geochemistry of ore deposits: contributions towards understanding sources and processes. In: Harlov DE, Aranovich L (eds) The role of halogens in terrestrial and extraterrestrial geochemical processes: surface, crust, and mantle. Springer, Berlin, pp 261–305

Liebscher A, Luders V, Heinrich W, Schettler G (2006) Br/Cl signature of hydrothermal fluids: liquid-vapour fractionation of bromine revisited. Geofluids 6:113–121

Lieftink DJ, Nijland TG, Maijer C (1993) Cl-rich scapolite from Ødegårdens Verk, Bamble, Norway. Norsk Geologisk Tidsskrift 73:55–57

Lovering JF, Widdowson JR (1969) Electron microprobe determination of sulphur coordination in minerals. Lithos 1:264–267

Ludington S (1978) The biotite-apatite geothermometer revisited. Am Mineral 63:551–553

Mahon WAJ (1966) Natural hydrothermal systems and the reaction of hot water with sedimentary rocks. New Zealand J Sci 10:206–221

Manning CE (1994) The solubility of quartz in H_2O in the lower crust and upper mantle. Geochim Cosmochim Acta 58:4831–4839

Manning DAC (1981) The effect of fluorine on liquidus phase relationships in the system Qz-Ab-Or with excess water at 1 kb. Contrib Mineral Petrol 76:206–215

Manning CE, Aranovich LY (2014) Brines at high pressure and temperature: thermodynamic, petrologic and geochemical effects. Precambr Res 253:6–16

Mark G, Williams PJ, Blake KL, Van Achterberg E, Ryan CG (2005) Br–Cl fractionation in mid-crustal fluid–rock systems. Geochim Cosmochim Acta 69S:A843

Markl G, Bücher K (1998) Composition of fluids in the lower crust inferred from metamorphic salt in lower crustal rocks. Nature 391:781–783

Markl G, Piazolo S (1998) Halogen-bearing minerals in syenites and high grade marbles of Dronning Maud Land, Antarctica: monitors of fluid compositional changes during late-magmatic fluid–rock interaction processes. Contrib Mineral Petrol 132:246–268

Markl G, Piazolo S (1999) Stability of high–Al titanite from low-pressure calc-silicates in light of fluid and host rock composition. Am Mineral 84:37–47

Marks MAW, Wenzel T, Whitehouse MJ, Loose M, Zack T, Barth M, Worgard L, Krasz V, Eby GN, Stosnach H, Markl G (2012) The volatile inventory (F, Cl, Br, S, C) of magmatic apatite: an integrated analytical approach. Chem Geol 291:241–255

Martin JB, Gieskes JM, Torres M, Kastner M (1993) Bromine and iodine in Peru margin sediments and pore fluids: implications for fluid origin. Geochim Cosmochim Acta 57:4377–4389

Masters RL, Ague JJ (2005) Regional-scale fluid flow and element mobility in Barrow's metamorphic zones, Stonehaven, Scotland. Contrib Mineral Petrol 150:1–18

Matheson RS, Searl RA (1956) Mary Kathleen Uranium Deposit, Mont Isa-Cloncurry District, Queensland, Australia. Econ Geol 51:528–540
McCaffrey MA, Lazar B, Holland HD (1987) The evaporation path of seawater and the coprecipitation of Br^- and K^+ with halite. J Sed Res 57:928–937
McKibben AE, Williams AE (1989) Metal speciation and solubility in saline hydrothermal fluids: an empirical approach based on geothermal brine data. Econ Geol 84:1996–2007
Michard A, Albarede F (1986) The REE content of some hydrothermal fluids. Chem Geol 55:51–60
Minarik B (2003) Planetary science: the core of planet formation. Nature 422(6928):126–128
Moazzen M, Oberhänsli R, Hajialioghli R, Möller A, Bousquet R, Droop GTR, Jahangiri A (2009) Peak and post-peak P-T conditions and fluid composition for scapolite clinopyroxene–garnet cac-slicate rocks from the Takab area, NW Iran. Eur J Mineral 21:149–162
Moecher PD, Essene EJ (1990) Phase equilibria for calcic scapolite, and implications of variable A1-Si disorder for P-T, T-XCO_2, and a-X relations. J Petrol 31:99–124
Moecher PD, Essene EJ (1991) Calculation of CO_2 activities using scapolite equilibria: constraints on the presence and composition of a fluid phase during high grade metamorphism. Contrib Mineral Petrol 108:219–240
Mora CI, Valley JW (1989) Halogen-rich scapolite and biotite: implications for metamorphic fluid-rock interaction. Am Mineral 74:721–737
Morad S, Morten B, Knarud R, Nystuen J (1990) Albitization of detrital plagioclase in Triassic reservoir sandstones from the Snorre Field, Norwegian North Sea. J Sed Petrol 60:411–425
Möller P, Schulz S, Jacob KH (1980) Formation of fluorite in sedimentary basins. Chem Geol 31:97–117
Munoz JL (1984) F-OH and Cl–OH exchange in micas with applications to hydrothermal ore deposits. Micas. Rev Mineral Soc Am 13:469–494
Munoz JL (1992) Calculation of HF and HCl fugacities from biotite compositions: revised equations. Geol Soc Am Abstr Progr 26:221
Munoz JL, Eugster HP (1969) Experimental control of fluorine reactions in hydrothermal systems. Am Mineral 54:943–959
Munoz JL, Ludington SD (1974) Fluoride-hydroxyl exchange in biotite. Am J Sci 274:396–413
Munoz JL, Ludington SD (1977) Fluorine-hydroxyl exchange in synthetic muscovite, with application to muscovite-biotite assemblages. Am Mineral 62:304–308
Munoz JL, Swenson A (1981) Chloride-hydroxyl exchange in biotite and estimation of relative HCl/HF activities in hydrothermal fluids. Econ Geol 76:2212–2221
Munz IA, Wayne D, Austrheim H (1994) Retrograde fluid infiltration in the high-grade Modum Complex, South Norway—evidence for age, source and REE mobility. Contrib Mineral Petrol 116:32–46
Munz IA, Yardley BWD, Banks DA, Wayne D (1995) Deep penetration of sedimentary fluids in basement rocks from southern Norway—evidence from hydrocarbon and brine inclusions in quartz veins. Geochim Cosmochim Acta 59:239–254
Muramatsu Y, Wedepohl KH (1998) The distribution of iodine in the earth's crust. Chem Geol 147:201–216
Newton RC, Manning CE (2000) Quartz solubility in H_2O-NaCl and H_2O-CO_2 solutions at deep crust-upper mantle pressures and temperature: 2–15 kbar and 500–900 °C. Geochim Cosmochim Acta 64:2993–3005
Newton RC, Manning CE (2002) Experimental determination of calcite solubility in H_2O-NaCl solutions at deep crust/upper mantle pressures and temperatures: implications for metasomatic processes in shear zones. Am Mineral 87:1401–1409
Newton RC, Aranovich LY, Hansen EC, Vandenheuvel BA (1998) Hypersaline fluids in Precambrian deep-crustal metamorphism. Precambr Res 91:41–63
Nijland TG, Touret JLR (2001) Replacement of graphic pegmatite by graphic albite–actinolite–clinopyroxene intergrowths (Mjavatn, southern Norway). Eur J Mineral 13:41–50

Nijland TG, Jansen JB, Maijer C (1993) Halogen geochemistry of fluid during amphibolite-granulite metamorphism as indicate by apatite and hydrous silicates in basic rocks from the Bamble Sector, South Norway. Lithos 30:167–189
Nijland TJ, Harlov DE, Andersen T (2014) The Bamble sector, south Norway: a review. Geosci Front 5:635–658
Norberg N, Neusser G, Wirth R, Harlov D (2011) Microstructural evolution during experimental albitization of K-rich alkali feldspar. Contrib Mineral Petrol 162:531–546
Norberg N, Harlov D, Neusser G, Wirth R, Rhede D, Morales L (2013) Experimental development of patch perthite from synthetic cryptoperthite: microstructural evolution and chemical re-equilibration. Am Mineral 98:1429–1441
Nordstrom DK, Lindblom S, Donahue RJ, Barton CC (1989) Fluid inclusions in the Stripa granite and their possible influence on the groundwater chemistry. Geochim Cosmochim Acta 53:1741–1755
Novgorodov PG (1977) On the solubility of quartz in H_2O + CO_2 and H_2O + NaCl at 700 °C and 1.5 kb pressure. Geochem Inter 14:191–193
Oliver NHS (1995) Hydrothermal history of the Mary Kathleen Fold Belt, Mt Isa Block, Queensland. Aust J Earth Sci 42:267–279
Oliver NHS (1996) Review and classification of structural controls on fluid flow during regional metamorphism. J Metam Geol 14:477–492
Oliver NHS, Valenta RK, Wall VJ (1990) The effect of heterogeneous stress and strain on metamorphic fluid flow, Mary Kathleen, Australia, and a model for large-scale fluid circulation. J Metam Geol 8:311–331
Oliver NHS, Holcombe RJ, Hill EJ, Pearson PJ (1991) Tectono-metamorphic evolution of the Mary Kathleen Fold Belt, northwest Queensland: a reflection of mantle plume processes? Aust J Earth Sci 38:425–455
Oliver NHS, Wall VJ, Cartwright I (1992) Internal control of fluid compositions in amphibolite-facies scapolitic calc-silicates, Mary Kathleen, Australia. Contrib Mineral Petrol 111:94–112
Oliver NHS, Rawling TJ, Cartwright I, Pearson P (1994) High-temperature fluid-rock interaction and scapolitization in an extension-related hydrothermal system, Mary Kathleen, Australia. J Petrol 35:1455–1491
Oliver NHS, Pearson PJ, Holcombe RJ, Ord A (1999) Mary Kathleen metamorphic–hydrothermal uranium-rare-earth deposit: ore genesis and a numerical model of coupled deformation and fluid flow. Aust J Earth Sci 46:467–484
Oliver NHS, Cleverley JS, Mark G, Pollard PJ, Fu B, Marshall LJ, Rubenach MJ, Williams PJ, Baker T (2004) Modeling the role of sodic alteration in the genesis of iron oxide–copper–gold deposits; eastern Mt. Isa Block, Australia. Econ Geol 99:1145–1176
Orville PM (1962) Alkali metasomatism and feldspars. Norsk Geol Tidsskr 42(2) Halvbind (Feldspar vol):283–316
Orville PM (1963) Alkali ion exchange between vapor and feldspar phases. Am J Sci 261:201–237
Orville PM (1972) Plagioclase cation exchange equilibria with aqueous chloride solutions: results at 700 °C and 2000 bars in the presence of quartz. Am J Sci 272:234–272
Orville PM (1975) Stability of scapolite in the system Ab-An-NaCl-$CaCO_3$ at 4 kb and 750 °C. Geochim Cosmochim Acta 39:1091–1105
Oterdoom WH, Wenk H-R (1983) Ordering and composition of scapolite: field observations and structural interpretations. Contrib Mineral Petrol 83:330–341
Ottolini L, Cámara F, Bigi S (2000) An investigation of matrix effects in the analysis of fluorine in humite-group minerals by EMPA, SIMS, and SREF. Am Mineral 85:89–102
Pan Y, Dong P (2003) Bromine in scapolite-group minerals and sodalite: XRF microprobe analysis, exchange experiments, and application to skarn deposits. Can Mineral 41:529–540
Pan Y, Fleet ME, Ray GE (1994) Scapolite in two Canadian gold deposits: Nickel Plate, British Columbia and Helmo, Ontario. Can Mineral 32:825–837
Pattison DRM (1987) Variations in Mg/(Mg + Fe), F, and (Fe, Mg)Si = 2Al in pelitic minerals in the Ballachulish thermal aureole, Scotland. Am Mineral 72:255–272

Petersen EU, Essene EJ, Peacor DR (1982) Fluorine end-member micas and amphiboles. Am Mineral 67:538–544

Penniston-Dorland SC, Ferry JM (2005) Coupled dichotomies of apatite and fluid composition during contact metamorphism of siliceous carbonate rocks. Am Mineral 90:1606–1618

Piazolo S, Markl G (1999) Humite- and scapolite-bearing assemblages in marbles and calcsilicates of Dronning Maud Land, Antarctica: new data for Gondwana reconstructions. J Metam Geol 17:91–107

Pirajno F (2018) Halogens in hydrothermal fluids and their role in the formation and evolution of hydrothermal mineral systems. In: Harlov DE, Aranovich L (eds) The role of halogens in terrestrial and extraterrestrial geochemical processes: surface, crust, and mantle. Springer, Berlin, pp 759–804

Pitcairn IK, Teagle DAH, Craw D, Olivo GR, Kerrich R, Brewer TS (2006) Sources of metals and fluids in orogenic gold deposits: insights from the Otago and Alpine Schists, New Zealand. Econ Geol 101:1525–1546

Poujol M, Boulvais P, Kosler J (2010) Regional-scale Cretaceous albitization in the Pyrenees: evidence from in situ U–Th–Pb dating of monazite, titanite and zircon. J Geol Soc 167:751–767

Preiss WV (2000) The Adelaide Geosyncline of South Australia and its significance in Neoproterozoic continental reconstruction. Precambr Res 100:21–63

Putnis A (2002) Mineral replacement reactions: from macroscopic observations to microscopic Mechanisms. Mineral Mag 66:689–708

Putnis A (2009) Mineral replacement reactions. Thermodynamics and kinetics of water-rock interaction. Rev Mineral Geochem (Oelkers EH and Schott J editors) 70:87–124

Putnis A, Hinrichs R, Putnis CV, Golla-Schindler U, Collins LG (2007) Hematite in porous red-clouded feldspars: evidence of large-scale crustal fluid–rock interaction. Lithos 95:10–18

Ramseyer K, Boles JR, Lichtner PC (1992) Mechanism of plagioclase albitization. J Sed Petrol 62:349–356

Rapp JF, Klemme S, Butler IB, Harley SL (2010) Extremely high solubility of rutile in chloride and fuoride-bearing metamorphic fuids: an experimental investigation. Geology 38:323–326

Reyes AG, Trompetter WJ (2012) Hydrothermal water-rock interaction and the redistribution of Li, B and Cl in the Taupo Volcanic Zone, New Zealand. Chem Geol 98:228–243

Riley JP, Chester R (1971) Introduction to marine chemistry. Academic Press, London, p 456

Rimstidt JD (1997) Gangue mineral transport and deposition. In: Barnes HL (ed) Geochemistry of hydrothermal ore deposits. Wiley, New York, p 487–516

Rimstidt JD, Barnes HL (1980) The kinetics of silica-water reactions. Geochim Cosmochim Acta 44:1683–1699

Ross M, Smith WL, Ashton WH (1968) Triclinic talc and associated amphiboles from Gouverneur mining district, New York. Am Mineral 53:751–769

Rubenach M (2012) Structural controls of metasomatism on a regional scale. In: Harlov DE, Austrheim H (eds) Metasomatism and the chemical transformation of rock: the role of fluids in terrestrial andextraterrestrial processes, Springer, Berlin, pp 93–140

Rubenach MJ (2005) Relative timing of albitization and chlorine enrichment in biotite in Proterozoic schists, Snake Creek Anticline, Mount Isa Inlier, northeastern Australia. Can Mineral 43:349–366

Rubenach MJ, Foster DRW, Evins PM, Blake KL, Fanning CM (2008) Age constraints on the tectonothermal evolution of the Selwyn Zone, Eastern fold belt, Mount Isa Inlier. Precambr Res 163:81–107

Rumble D (1977) Mineralogy, petrology, and oxygen isotope geochemistry of the Clough Formation, Black Mountain, Western New Hampshire, USA. J Petrol 19:317–340

Ryan CG, Heinrich CA, Mernagh TP (1993) PIXE microanalysis of fluid inclusions and ist application to study ore metal segregation between magmatic brine and vapor. Nucl Instrum Methods Phys Res Sect B 77:463–471

Sallet R (2000) Fluorine as a tool in the petrogenesis of quartz-bearing magmatic associations: applications of an improved F-OH biotite-apatite thermometer grid. Lithos 50:241–253

Sanchez V, Vindel E, Martin-Crespo M, Corbella M, Cardellach E, Banks DA (2009) Sources and composition of fluids associated with fluorite deposits of Asturias (N Spain). Geofluids 9:338–355

Satish-Kumar M, Hermann J, Tsunogae T, Osanai Y (2006) Carbonation of Cl-rich scapolite boudins in Skallen, East Antarctica: evidence for changing fluid condition in the continental crust. J Metamorph Geol 24:241–261

Selverstone J, Sharp ZD (2015) Chlorine isotope behavior during prograde metamorphism of sedimentary rocks. Earth Planet Sci Lett 417:120–131

Sengupta P, Raith MM, Datta A (2004) Stability of fluorite and titanite in a calc–silicate rock from the Vizianagram area, Eastern Ghats Belt, India. J Metamorph Geol 22:345–359

Seo JH, Guillong M, Aerts M, Zajacz Z, Heinrich CA (2011) Microanalysis of S, Cl, and Br in fluid inclusions by LA-ICP-MS. Chem Geol 284:35–44

Seward TM, Barnes HL (1997) Metal transport by hydrothermal ore fluids. In: Barnes HL (ed) Geochemistry of hydrothermal ore deposits, 3rd edn. Wiley, New York, pp 435–486

Shaw DM (1960) The geochemistry of scapolite Part 1. Previous work and general mineralogy. J Petrol 1:218–260

Shmulovich KI, Graham C (2008) Plagioclase-aqueous solution equilibrium: concentration dependence. Petrol 16:177–192

Shmulovich KI, Graham CM, Yardley BWD (2001) Quartz, albite and diopside solubilities in H_2O-NaCl fluids at 0.5–0.9 Gpa. Contrib Mineral Petrol 141:95–108

Shmulovich KI, Graham CM, Yardley BWD (2006) Solubility of quartz in crustal fluids: experiments and general equations for salt solutions and H_2O-CO_2 mixtures at 400–800°C and 0.1–0.9 Gpa. Geofluids 6:154–167

Sisson VB (I987) Halogen geochemistry as an indicator of metamorphic fluid interaction with the Ponder Pluton, Coast Plutonic Complex, British Columbia, Canada. Contrib Mineral Petrol 95:123–131

Sisson VB, Hollister LS (1990) A fluid-inclusion study of metamorphosed pelitic and carbonate rocks, south-central Maine. Am Mineral 75:59–70

Smith MP, Yardley BWD (1999) Fluid evolution during metamorphism of the Otago Schist, New Zealand: (II) Influence of detrital apatite on fluid salinity. J Metam Geol 17:187–193

Sokolova E, Hawthorne FC (2008) The crystal chemistry of the scapolite-group minerals. 1. Crystal structure and long-range order. Can Mineral 46:1527–1554

Spötl C, Kralik M, Kunk MJ (1996) Authigenic feldspar as an indicator of paleo-rock/water intercalations in permian carbonates of the Northern Calcareous Alps, Austria. J Sed Res 66:139–146

Stormer JC, Carmichael ISE (1971) Fluorine-hydroxyl exchange in apatite and biotite: a potential geothermometer. Contrib Mineral Petrol 81:121–131

Stormer JC, Milton JR, Pierson L, Tacker RC (1993) Variation of F and Cl X-ray intensity due to anisotropic diffusion in apatite during electron microprobe analysis. Am Mineral 78:641–648

Symmes GH, Ferry JM (1991) Evidence from mineral assemblages for infiltration of pelitic schists by aqueous fluids during metamorphism. Contrib Mineral Petrol 108:419–438

Tanis EA, Simon AC, Tschauner O, Chow P, Xiao Y, Burnley P, Cline CJ, Hanchar JM, Pettke T, Shen G, Zhao Y (2015) The mobility of Nb in rutile-saturated NaCl- and NaF-bearing aqueous fluids from 1–6.5 GPa and 300–800 °C. Am Mineral 100:1600–1609

Tanis EA, Simon A, Zhang Y, Chow P, Xiao Y, Hanchar JM, Tschauner O, Shen G (2016) Rutile solubility in NaF-NaCl-KCl-bearing aqueous fluids at 0.5–2.79 GPa and 250–650°C. Geochim Cosmochim Acta 177(2016):170–181. http://doi.org/10.1016/j.gca.2016.01.003

Teertstra TK, Sherriff BL (1996) Scapolite cell parameter trends along the solid solution series. Am Mineral 81:169–180

Teertstra TK, Sherriff BL (1997) Substitutional mechanisms, compositional trends and the end-member formulae of scapolite. Chem Geol 136:223–260

Tell I (1974) Hydrothermal studies on fluorine metamorphic reactions in siliceous dolomite. Contrib Mineral Petrol 43:99–110

Torres-Ruiz J, Pesquera A, Gil-Crespo PP, Velilla N (2003) Origin and petrogenetic implications of tourmaline-rich rocks in the Sierra Nevada (Betic Cordillera, southeastern Spain). Chem Geol 197:55–86

Tropper P, Manning CE (2005) Very low solubility of rutile in H_2O at high pressure and temperature, and its implications for Ti mobility in subduction zones. Am Mineral 90:502–505

Tropper P, Manning CE (2007) The solubility of fluorite in H_2O and H_2O-NaCl at high pressure and temperature. Chem Geol 242:299–306

Tropper P, Manning CE, Essene EJ (2002) The substitution of Al and F in titanite at high pressure and temperature: experimental constraints on phase relations and solid solution properties. J Petrol 43:1787–1814

Tropper P, Manning CE, Harlov DE (2011) Solubility of $CePO_4$ monazite and YPO_4 xenotime in H_2O and H_2O–NaCl at 800 °C and 1 GPa: implications for REE and Y transport during high-grade metamorphism. Chem Geol 282:58–66

Tropper P, Manning CE, Harlov DE (2013) Experimental determination of $CePO_4$ and YPO_4 solubilities in H_2O-NaF at 800°C and 1GPa: implications for rare earth element transport in high-grade metamorphic fluids. Geofluids 13:372–380

Trommsdoff V, Skippen G (1986) Vapour loss (“boiling”) as a mechanism for fluid evolution in metamorphic rocks. Contrib Mineral Petrol 94:317–322

Trommsdorff V, Skippen G, Ulmer P (1985) Halite and sylvite as solid inclusions in high-grade metamorphic rocks. Contrib Mineral Petrol 89:24–29

Valley JW, Petersen EU, Essene EJ, Bowman JR (1982) Fluorphlogopite and fluortremolite in Adirondack marbles and calculated C-O-H-F fluid compositons. Am Mineral 67:545–557

Valley JW, Bohlen SR, Essene EJ, Lam W (1990) Metamorphism in the Adirondacks II. The role of fluids. J Petrol 31:555–596

Van den Bleeken G, Corteel C, Van den Haute P (2007) Epigenetic to low-grade tourmaline in the Gdoumont metaconglomerates (Belgium): a sensitive probe of the chemical environment of formation. Lithos 95:165–176

Vanko DA, Bonnin-Mosbah M, Philippot P, Roedder E, Sutton SR (2001) Fluid inclusions in quartz from oceanic hydrothermal specimens and the Bingham, Utah porphyry-Cu deposit: a study with PIXE and SXRF. Chem Geol 173:227–238

Volfinger M, Robert J-L, Vielzeuf D, Neiva AMR (1985) Structural control of the chlorine content of OH-bearing minerals (micas and amphiboles). Geochim Cosmochim Acta 49:37–48

von Knorring O, Kennedy WQ (1958) The mineral paragenesis and metamorphic status of garnet-hornblende-pyroxene-scapolite gneiss from Ghana (Gold Coast). Mineral Mag 31:846–859

Walther JV, Orville PM (1982) Volatile production and transport in regional metamorphism. Contrib Mineral Petrol 79:252–257

Warren JK (1997) Evaporites, brines and base metals: fluids and ’the evaporite that was. Aust J Earth Sci 44:149–183

Warren JK (1999) Evaporites: their evolution and economics. Blackwell Science, Oxford, 438pp

Watson ED, Brenan JM (1987) Fluids in the lithosphere: 1. Experimentally-determined wetting characteristics of CO_2 H_2O fluids and their implications for fluid transport, host-rock physical properties, and fluid inclusion formation. Earth Planet Sci Lett 85:497–515

Wedepohl H (1995) The composition of the continental crust. Geochim Cosmochim Acta 59:1217–1239

Wedepohl KH (1987) The chlorine and sulfur crustal cycle—abundance of evaporites. In: Rodriguez-Clemente R, Tardy YŽ (eds) Geochemistry and mineral formation in the earth surface. Consejo Superior de Investigaciones Cientificas Centre National de la Recherche Scientifique, Madrid, pp 3–27

Williams ML, Jerconovic MJ, Harlov DE, Budzyn B, Hetherington CJ (2011) Resetting monazite ages during fluid-related alteration. Chem Geol 283:218–225

Withnall IW, Hutton LJ (2012) North Australian craton. In: Jell, PA (ed) Geology of Queensland. Queensland Government, Australia, pp 113–224

Worden R (2018) Halogen elements in sedimentary systems and their evolution during diagenesis. In: Harlov DE, Aranovich L (eds) The role of halogens in terrestrial and extraterrestrial geochemical processes: surface, crust, and mantle. Springer, Berlin, pp 185–260
Xie Z, Walther JV (1993) Quartz solubilities in NaCl solutions with and without wollastonite at elevated temperatures and pressures. Geochim Cosmochim Acta 57:1947–1955
Yardley BW (2005) Metal concentrations in crustal fluids and their relationship to ore formation. Econ Geol 100:613–632
Yardley BWD (1996) The evolution of fluids through the metamorphic cycle. In: Jamtveit B, Yardley BWD (eds) Fluid flow and transport in rocks. Chapman & Hall, London, pp 99–121
Yardley BWD (2009) The role of water in crustal evolution. J Geol Soc 166:585–600
Yardley BWD, Bodnar RJ (2014) Fluids in the continental crust. Geochem Perspect 3(1):127
Yardley BWD, Graham JT (2002) Origins of salinity in metamorphic fluids. Geofluids 2:249–256
Zhu C, Sverjensky DA (1991) Partitioning of F-Cl-OH between minerals in hydrothermal fluids. Geochim Cosmochim Acta 55:1837–1858
Zhu C, Sverjensky DA (1992) F-Cl-OH partitioning between biotite and apatite. Geochim Cosmochim Acta 56:3435–3467

Chapter 11
Halogens in High-Grade Metamorphism

Leonid Aranovich and Oleg Safonov

Abstract This chapter reviews factors, which control the distribution of the two major halogens, F and Cl, in high-grade metamorphic rocks; their compositional correlations and partitioning between minerals; experimental data on stability and phase equilibria of the halogen-bearing minerals; the influence of halogens on Fe–Mg exchange reactions; and the means of estimating concentrations/activity of halogen species in the fluid phase ("chlorimetry and fluorimetry") via calculation of equilibrium conditions for mineral assemblages containing halogen-bearing phases. Clear negative correlation between the F content and X_{Fe} = Fe/(Fe + Mg) suggests that natural biotite and amphibole obey the Fe–F avoidance rule. A strong positive correlation exists between K and Cl in amphibole. A scattering of points on the X_{Fe}–Cl and TiO_2–Cl diagrams indicate the possible involvement of an exotic Cl-rich phase (fluid or melt) during the formation of Cl-bearing biotite and amphibole. Fluorine and Cl substituting for OH-groups substantially stabilize minerals relative to dehydration and melting. They should also strongly affect the partitioning of Fe and Mg between biotite, amphibole, and anhydrous minerals. This effect is quantified for Fe–Mg exchange reactions involving biotite (Zhu and Sverjensky 1992), but remains to be evaluated for amphibole. Calculations based on recent thermodynamic systematics show that a relatively Mg-rich, Cl-poor

L. Aranovich (✉)
Institute of Geology of Ore Deposits, Petrography, Mineralogy and Geochemistry RAS, Moscow, Russia
e-mail: lyaranov@igem.ru

L. Aranovich · O. Safonov
Institute of Experimental Mineralogy RAS, Chernogolovka, Moscow region, Russia
e-mail: oleg@iem.ac.ru

O. Safonov
Department of Petrology, Moscow State University, Moscow, Russia

O. Safonov
Department of Geology, University of Johannesburg, Johannesburg, South Africa

D.E. Harlov and L. Aranovich (eds.), *The Role of Halogens in Terrestrial and Extraterrestrial Geochemical Processes*, Springer Geochemistry,
https://doi.org/10.1007/978-3-319-61667-4_11

biotite (for example, X_{Fe} = 0.4 and about 0.2 wt.% Cl) may coexist with a fairly Cl-rich fluid, i.e. total Cl/(Cl + H_2O) ranges from 0.1–0.3, depending on the assemblage, under granulite-facies P–T conditions. Alkali (and Ca) metasomatism, caused by interaction of high grade rocks with halogen-bearing fluids, may have a major impact on the subsolidus phase transformation and melting processes during high-grade metamorphism and anatexis.

11.1 Introduction

There is now abundant evidence for the participation of halogen-bearing solids, fluids, and melts in high-grade metamorphic processes. Fluorine- and Cl-bearing minerals are common in upper amphibolite- and granulite-facies rocks of diverse bulk composition, ranging from metapelite through calc-silicate to meta-ultramafic rocks. Major rock-forming minerals capable of accumulating halogens in their structure are biotite, amphibole, and scapolite. Halogens are also abundant in accessory titanite and apatite. Studies of fluid inclusions in minerals from migmatites and granulites have revealed the presence of variably concentrated alkali and alkali earth chloride solutions, sometimes with salt daughter crystals (e.g., Dolgov et al. 1976; Touret 1995; Touret and Huizenga 2011; Newton et al. 2014 and references therein). Compelling evidence for the involvement of halogens (primarily Cl) in the petrogenesis of the lower crust also comes from the findings of high-temperature intergranular halides in high-grade rocks (Trommsdorff et al. 1985; Markl and Bucher 1998; Markl et al. 1998).

Elevated concentrations of halogen-bearing species have a significant impact on the thermodynamic and transport properties of natural deep-seated fluids; on the dissolution of minerals and metasomatic alteration; on the stability of halogen-bearing minerals; and on melting reactions and the compositions of the resulting magmas. The purpose of this chapter is to discuss some major effects relevant to the action of halogens in the lower and middle crustal environment. Data pertinent to the greenschist- and lower amphibolite-facies conditions are considered in Chap. 10 (Hammerli and Rubenach 2018). Below we review the ranges in halogen content in the major halogen-bearing minerals found in high-grade rocks; the effect of halogens on their stability relations; consider some simple net-transfer reactions between high-grade minerals that can be used to monitor the activity of alkali halides during the formation of the corresponding mineral assemblages; and show that alkali (and Ca) metasomatism caused by the interaction of high grade rocks with halogen-bearing fluids may have a major impact on the subsolidus phase transformation and melting processes during high-grade metamorphism and anatexis.

11.2 Compositional Correlations and Partitioning of Halogens Between Minerals in High-Grade Metamorphic Rocks

Bulk rock composition, metamorphic grade, and fluid activity are the global factors responsible for the re-distribution of halogens in high-grade rocks. However, distribution of Cl and F within specific metamorphic rocks is determined by the compositional characteristics of those minerals that might accommodate halogens in their crystal structures, and, thus, is a function of crystal chemistry. Correlations (or lack thereof) between the halogen content and some other compositional parameters of halogen-bearing minerals serve as a first order indicator of which factors may have exerted major control on the halogen content of a particular metamorphic assemblage.

11.2.1 Compositional Correlations of Halogens in High-Grade Minerals

A strong positive correlation between the F content and X_{Mg} in biotites from amphibolite- and granulite-grade metapelites and intermediate rocks (Fig. 11.1a) reflects a strong crystal-chemical Mg–F affinity (Rosenberg and Foit 1977; Munoz and Ludington 1977; Munoz 1984). Correlation of F with TiO_2 is much less pronounced (Fig. 11.1b), although a positive correlation might be expected since both elements stabilize biotite to higher temperature (Dooley and Patiño Douce 1996; Tareen et al. 1995, 1998). The lack of a clear positive correlation between F and TiO_2 (Fig. 11.4b) might indicate a "Ti–F avoidance rule" (as yet unsupported by experiments) that could counteract the influence of temperature. The scatter can also be due to variations in the chemistry of an external medium (fluid or melt) that equilibrated with the biotite-bearing rocks.

Chlorine, that should obey the Mg–Cl avoidance rule (Rosenberg and Foit 1977; Munoz 1984), and, consequently, negatively correlate with X_{Mg} in biotites, rather shows a large scatter on the Cl–X_{Mg} plot (Fig. 11.2). The reason for this scatter could be a less energetically pronounced Mg–Cl avoidance compared to Mg–F affinity (Munoz 1984; Zhu and Sverjensky 1991). However, as in the case of the Ti–F relations, variations in the activity of Cl-bearing species in a fluid and/or melt phase that interacted with the rocks could also be a reason for the scatter in the Cl–X_{Mg} plot (Fig. 11.2). The positive correlation observed between Cl and Ba in biotite (Kullerud 1996; Zhu et al. 1994) probably indicates an interaction of the rocks with Ba-enriched fluids.

High-grade amphiboles also show a number of important correlations between the Cl and F contents and specific compositional parameters, such as X_{Mg}, A-site occupancy, Si/Al ratio, and K/(K + Na) ratio. A positive correlation between F content and X_{Mg} for granulite pargasites has been reported by Tsunogae et al. (2003) and

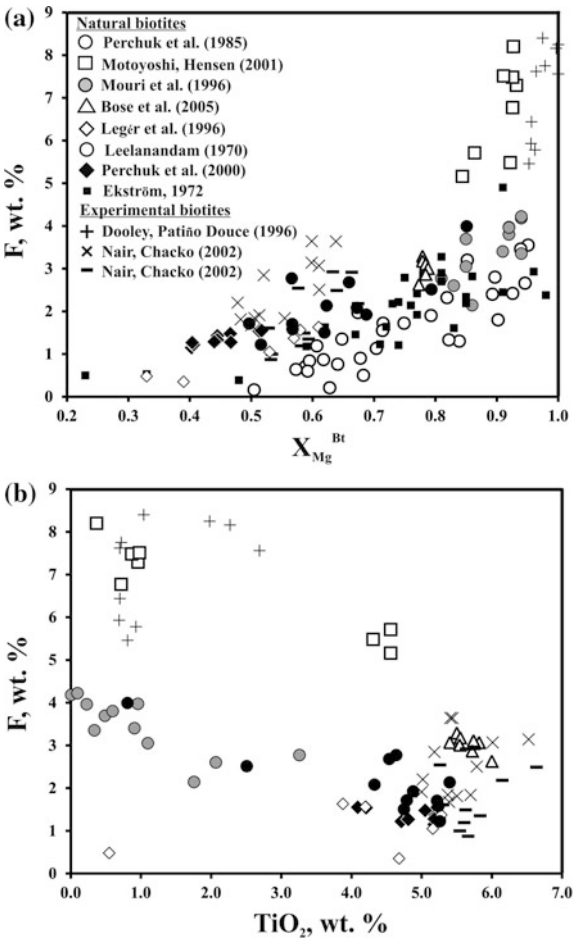

Fig. 11.1 Fluorine content (wt.%) versus X_{Mg} (**a**) and TiO_2 (wt.%) content (**b**) for biotites from various high-grade complexes and experimental products. Natural biotites are from metapelites from the Aldan Shield, Russia (Perchuk et al. 1985); In Quzzal, Algeria (Mouri et al. 1996); the Napier complex, Antarctica (Motoyoshi and Hensen 2001); the Eastern Ghats, India (Bose et al. 2005); amphibole–biotite-two pyroxene gneisses, Black Forest, Hudson Highland, USA (Legér et al. 1996); charnockitic and basic granulites, Kondapalli, India (Leelanandam 1970); biotite–amphibole gneisses and associated arrested charnockites, Kurunegala, Sri Lanka (Perchuk et al. 2000); and iron formations (Ekström 1972). Experimental biotites are taken from the system phlogopite + quartz + rutile (Dooley and Patiño Douce 1996); a biotite–garnet gneiss from Ponmudi, Southern India (Nair and Chacko 2002); and a biotite–garnet gneiss from Kalanjur, southern India (Nair and Chacko 2002)

Sajeev et al. (2009). In contrast, a negative correlation has been observed between the X_{Mg} and the Cl content (see below). However, some studies have noted that the Mg-number could not be the only parameter regulating the Cl content of amphiboles. Morrison (1991) analyzed the degree of Cl incorporation into amphiboles in

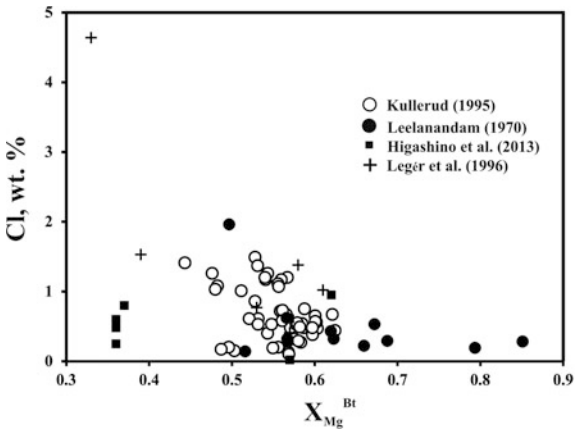

Fig. 11.2 The Cl content (wt.%) versus X_{Mg} for biotites from various high-grade complexes, which include amphibole–biotite-two pyroxene gneisses, Black Forest, Hudson Highland, USA (Legér et al. 1996) and charnockitic and basic granulites, Kondapalli, India (Leelanandam 1970)

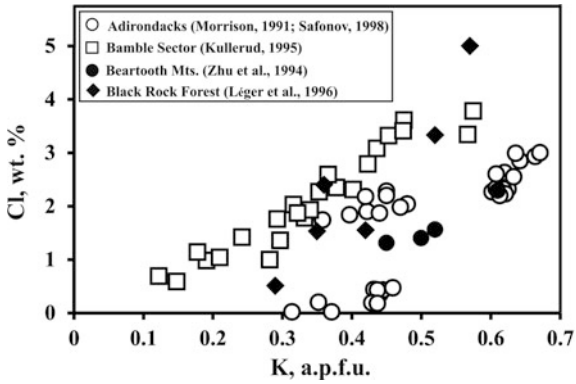

Fig. 11.3 Correlations between the Cl (wt.%) and the K (a.p.f.u.) contents for amphiboles from various granulite- and amphibolite-grade complexes

granulite-facies rocks from the Adirondack Mountains, New York, USA, and recognized two groups of amphiboles: the Cl-rich with 1.84–3 wt.% Cl (chlorferropargasites) and the Cl-poor containing 0.48–0.05 wt.% Cl (ferropargasites). Generally, both types of amphiboles show an inverse correlation between X_{Mg} and the Cl-content. However, Mg–Cl avoidance was found to be much stronger for Cl-poor amphiboles. Morrison (1991) concluded that the weak correlation between X_{Mg} and Cl in the Cl-rich amphiboles suggests that Mg–Cl avoidance was not a dominant control on Cl incorporation in amphiboles with Cl > 1.5 wt.%. Rather there should be other crystal-chemical factors, such as a positive correlation between Cl and K (in the absence of a correlation with Na) (Fig. 11.3) and a negative correlation with A-site vacancies and the Si/(Si + Al) ratio. These observations were further supported by Safonov (1998), who distinguished three compositional groups of amphiboles in the Adirondack rocks: (1) 0–0.5 wt.% Cl, X_{Mg} = 0.12–0.15 and K/(K + Na) = 0.20–0.37; (2) 1.5–2 wt.% Cl, X_{Mg} = 0.07–0.08 and K/(K + Na) = 0.41–0.48; and (3) 2–2.3 wt.% Cl, X_{Mg} = 0.21–0.25 and K/(K + Na) up to 0.57. This sequence clearly shows an increase in the Cl content with K/(K + Na), but the Mg–Cl avoidance

is violated since the more Mg-rich amphiboles in group 3 contain more Cl. Moreover, the amphiboles in the second group show a positive correlation between Cl and X_{Mg}. Safonov (1998) explained these relations as being due to strong compositional variations in the brine fluid (probably KCl-rich) coexisting with the amphiboles of the second and third groups during their growth at the retrograde stage of metamorphism. Negative correlations between Cl and X_{Mg}, Si/Al (and Ti), and a positive correlation with K/(K + Na), as summarized by Morrison (1991) for the Adirondack amphiboles, have been described for other occurrences (Leelanandam 1970; Kullerud 1996; Léger et al. 1996; Suwa et al. 1987).

There are inconsistent reports on the correlation between F and Cl in high-grade amphiboles and biotites. That is because in most cases, F-rich minerals have a low Cl content and, vice versa, such correlations are not distinct. Minerals simultaneously enriched in both halogens are rare (e.g., Leelanandam 1970; Kamineni et al. 1982; Léger et al. 1996; Morrison 1991). For example, F and Cl-enriched biotites and amphiboles reported by Leelanandam (1970), show no correlation between the two halogens, while Morrison (1991) found a negative correlation between F with Cl in both the Cl-rich and Cl-poor amphiboles from the Adirondacks. Léger et al. (1996) showed that there are different negative correlations between Cl and F in biotites variously enriched in the halogens. The F variations in biotites, containing more than 0.4 a.p.f.u. Cl, are restricted between 0.7 and 0.3 a.p.f.u., while in biotites containing less than 0.4 a.p.f.u. Cl, the F variations are much wider, from 0.1 to 0.8 a.p.f.u. Such dependencies could imply that halogen isomorphism in these biotites proceeds mostly by the OH–F substitution, whereas the Cl–F substitution is subordinate. Nevertheless, simultaneous isomorphism of Cl and F into biotites and amphiboles seems to greatly depend on other crystal-chemical parameters.

11.2.2 Distribution of Halogens Between Coexisting Minerals in High-Grade Rocks

Ekström (1972) was, probably, the first who systematically studied the distribution of F between coexisting Ca-amphibole, biotite, apatite, and titanite in samples from iron formations, which differ in metamorphic grade. Distribution coefficient K_D^F (amphibole–biotite) increases from about 0.5 in the low-grade samples to above 1.0 in the higher-grade samples. However, subsequent studies did not support this conclusion. The F-contents in biotite were usually higher than those in coexisting amphibole (e.g., Nijland et al. 1993). Figure 11.4a shows the F distribution between coexisting biotites and hornblendes in rocks in three zones across the transition from the amphibolite-grade zone through the clinopyroxene-rich transition zone to the orthopyroxene-bearing granulite-grade zone in the Shevaroy Block, Tamil Nadu, southern India (Hansen and Harlov 2007). Despite a clear positive correlation between the F concentrations in the minerals, there is no difference between the

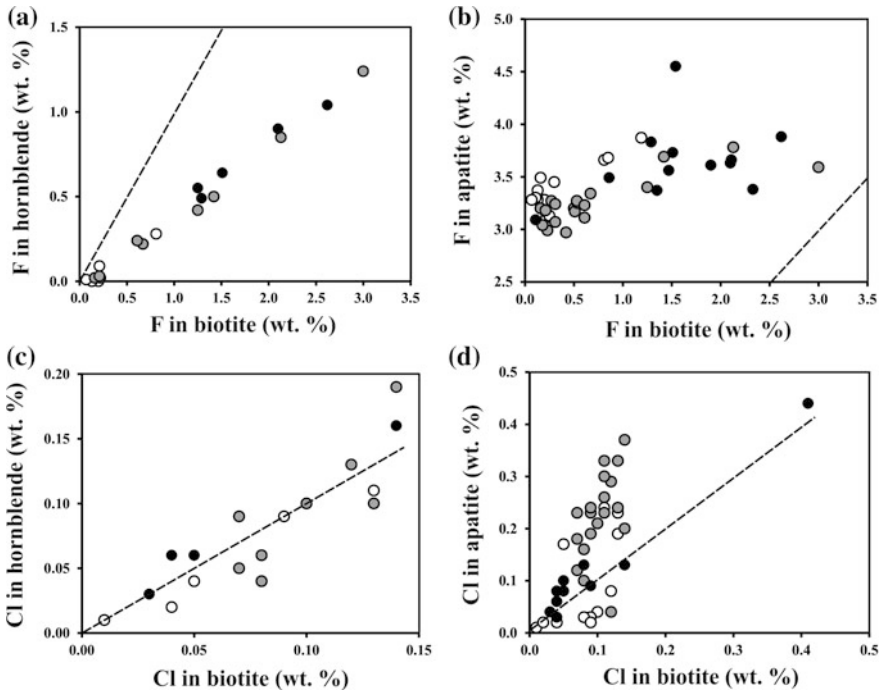

Fig. 11.4 Partitioning of F (**a**, **b**) and Cl (**c**, **d**) between biotite–hornblende (**a**, **c**) and biotite–apatite (**b**, **d**) in rocks from three zones across the transition from biotite–amphibole gneisses to orthopyroxene-bearing gneisses in the Shevaroy Block, Tamil Nadu, southern India (modified after Hansen and Harlov 2007). Abbreviations: northern amphibolite-facies zone, NAF (*white dots*), central clinopyroxene-rich granulite-facies zone, CGF (*gray dots*), and southern (orthopyroxene) granulite-facies zone, SGF (*black dots*). *Dashed lines* show equal halogen partitioning

distribution coefficients for the biotite–hornblende pairs for zones of different metamorphic grade. In all zones, F preferentially partitions into the biotite. Even for the high-temperature (>900 °C) granulites of the Napier Complex (East Antarctica), Tsunogae et al. (2003) found that F preferentially partitioned into biotite relative to pargasite. For tremolite–phlogopite pairs from the Grenville marbles, Valley et al. (1982) found no dependence on the metamorphic grade and suggested that variations in K_D^F(amphibole–biotite) = $[X_F^{Amph}(1-X_F^{Bt})]/[(1-X_F^{Amph})X_F^{Bt})]$ in the range 0.39–0.53 were mainly controlled by the crystal chemistry rather than temperature. Preferential partitioning of F into biotite, characteristic for natural assemblages, is consistent with the available experimental data of Westrich (1981). However, the experiments indicate that the distribution of F depends on the tremolite/pargasite ratio in the amphibole. At constant T and P, the partitioning of F between tremolite and phlogopite is much stronger than between pargasite and phlogopite.

In common metamorphic rocks, apatite is the principal host of F (e.g., Yardley 1985). Usually its F content is directly correlated with the F content of coexisting

amphiboles and biotites (Ekström 1972; Nijland et al. 1993; Harlov and Förster 2002; Tsunogae et al. 2003; Hansen and Harlov 2007; Fig. 11.4b), with the K_D^F (apatite–biotite) and K_D^F (apatite–amphibole) always being greater than 1. Available experimental data and related thermodynamic systematics (e.g., Zhu and Sverjensky 1992 and references therein) show that the extent of the F distribution between apatite and biotite is strongly dependent on temperature and the Fe content of biotite. Increasing the temperature and decreasing the Fe concentration reduce the preference of F for apatite with respect to mica. For example, Fig. 11.4b shows that data points for apatite–biotite pairs from granulite-facies rocks (black dots) from the amphibolite-to-granulite transition terrain of the Shevaroy Block, Tamil Nadu, southern India (Hansen and Harlov 2007) are much closer to the line of the equal F distribution in comparison to those from the lower-temperature amphibolite-grade rocks (white dots). The effects of temperature and Fe content in biotite were subsequently incorporated into the apatite–biotite geothermometer based on the F–OH distribution coefficient between apatite and biotite (Stormer and Carmichael 1971; Luddington 1978; Zhu and Sverjensky 1992; Sallet 2000).

There are no experimental studies on the distribution of F between titanite and coexisting minerals, while data from natural metamorphic assemblages are controversial. Ekström (1972) reported K_D^F (biotite–titanite) to be above 1 independent of the metamorphic grade. However, Nijland et al. (1993) found that the F-content of titanite in granulites from the Bamble Sector (Norway) is comparable to that in biotite and amphibole, but the maximum concentrations tend to be higher in titanite than in the other two minerals.

In amphibolite- and granulite-facies rocks with coexisting amphibole and biotite, Cl partitions preferentially into amphibole and F partitions preferentially into biotite (Kullerud 1996; Léger et al. 1996; Markl and Piazolo 1998). However, there might be exceptions to this rule, especially for low Cl contents in minerals (e.g., Nijland et al. 1993). This conclusion is illustrated by Fig. 11.4c, which shows near-equal distribution of Cl between biotite and hornblende (in contrast to F, Fig. 11.4a) in the rocks from the amphibolite- to granulite-facies transition terrain of the Shevaroy Block, Tamil Nadu, Southern India (Hansen and Harlov 2007), independent of the metamorphic grade.

According to experimental data summarized by Zhu and Sverjensky (1992), Cl is preferentially partitioned into apatite with respect to biotite, but to a much lesser extent than F. Again, this preference depends strongly on temperature and the biotite Fe content. Increasing both the temperature and Fe content in biotite will reduce the preference of Cl for apatite. It is conceivable, therefore, that Cl will be partitioned with no preference for apatite or even preferentially into biotite in high-temperature rocks. As a support for this assumption, Fig. 11.4d shows that Cl partitioning between biotite and apatite in rocks from the granulite-facies portion (black dots) of the amphibolite- to granulite-facies transition of the Shevaroy Block, Tamil Nadu, southern India (Hansen and Harlov 2007) is much closer to unity in comparison to the biotite–apatite pairs from the lower-temperature zones (gray and white dots, respectively).

11.3 Experimental Data on Stability and Phase Equilibria of Halogen-Bearing Phases at High-Grade Conditions

11.3.1 Biotites

Experimental data on the upper temperature stability limit are only available for end member F-phlogopite and F-rich biotites. Shell and Ivey (1969) first reported that melting of end member F-phlogopite, $KMg_3AlSi_3O_{10}F_2$, begins between 1345 and 1390 °C at ambient pressure in contrast to about 905 °C for end member hydroxyl phlogopite (e.g., Wones 1967). A similar effect is observed at higher pressures (Munoz 1984; Foley et al. 1986). Dramatic expansion of the thermal stability field for phlogopite, resulting from the substitution of F for OH, influences the stability of various mineral assemblages involving this phase at amphibolite- and granulite-facies conditions.

Most experimental data on the stability of the F-rich biotites relate to systems with metapelitic compositions. Peterson et al. (1991) found that 60 mol.% of the F substitution for OH in phlogopite stabilizes the phlogopite + quartz assemblage by as much as 125 °C at 8 kbar and 175 °C at 15 kbar relative to enstatite + liquid (Fig. 11.5). Hensen and Osanai (1994) experimentally showed a progressive increase in the phlogopite stability with increasing F-content. According to their experiments, phlogopite with 5–6 wt.% F is stable up to 1045 °C at 9 kbar. Experiments in more complex systems have demonstrated a similar effect. Dooley and Patiño Douce (1996) found that the thermal stability limit of phlogopite with $X_F = 0.43$, co-existing with quartz and rutile, is about 450 °C higher compared to the KMASH system within the pressure interval 7–15 kbar. The F content of biotite progressively increases during partial melting and at 7 kbar it reaches 8.4 wt.% at 1250–1275 °C. These results were further confirmed by Tareen et al. (1995, 1998) who studied the stability of Ti-bearing phlogopite containing 3.57 wt.% F both in the Al-undersaturated and the Al-saturated portions of the KMASH system at 7–12 kbar (Fig. 11.5). In the Al-saturated system, decomposition of biotite to cordierite + liquid (in the H_2O-saturated runs) or to Al-enstatite + liquid (in the H_2O-absent runs) was found to occur 100–140 °C higher than for the reaction phlogopite + quartz = enstatite + sanidine + melt using the F-free phlogopite reported by Vielzeuf and Clemens (1992). These authors concluded that at temperatures above 1000 °C, F- (and Ti-) bearing biotite can coexist with cordierite, sapphirine (+quartz), ossumillite, and Al-rich enstatite, which are indicative of ultra-high temperature (UHT) metamorphism.

Fluorine expands biotite stability during anatexis of natural rocks. This effect has been repeatedly documented in experiments on rocks with different bulk compositions. In pelitic assemblages, F-bearing biotite is found to persist, only melting-out at temperatures above 950 °C and pressures above 7 kbar, which significantly reduces melt productivity (Patiño Douce and Johnston 1991). Nair and Chacko (2002) demonstrated that >1 wt.% F expands the biotite stability field up to 1000 °C at

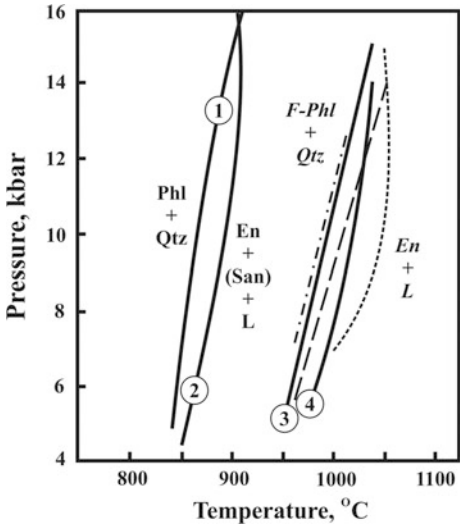

Fig. 11.5 P–T curves for the dehydration melting reaction phlogopite + quartz = enstatite +melt for F-free and F-bearing phlogopites. F-free phlogopite: *1* Vielzeuf and Clemens (1992) and *2* Bohlen et al. (1983). Fluorine-bearing phlogopite: *3* Peterson et al. (1991) and *4* Tareen et al. (1995). Curves from the F-bearing biotite termination, during dehydration melting of natural assemblages, are shown for comparison: *dash-dotted* pelite, i.e. garnet + muscovite + biotite + sillimanite + plagioclase + quartz + ilmenite (Patiño Douce and Johnston 1991); the *short-dashed line* semi-pelite, i.e. garnet + biotite + plagioclase + K-feldspar + quartz (Nair and Chacko 2002); and *long-dashed line* tonalite, i.e. hornblende + biotite + epidote + plagioclase + quartz + apatite (Skjerlie and Johnston 1993). *En* enstatite, *Phl* phlogopite, *Qtz* quartz, *San* sanidine, *L* melt

7–15 kbar during partial melting of a biotite–garnet "semi-pelite" (Fig. 11.5). Skjerlie and Johnston (1993) came to the same conclusion based on experiments, which involved the partial melting of a biotite–amphibole tonalite gneiss. They observed that the F-content of biotite progressively increased with temperature and reached 2.75 wt.%, which is close to the biotite stability limit at 1000 °C. They concluded that substitution of F for OH is the main reason for the high thermal stability of biotite in these experiments.

Experimental data on the stability of F-bearing biotite in basic and calc-silicate systems are absent. Using thermodynamic calculations and an ideal ionic model for the F–OH-biotite, Valley et al. (1982, 1990) estimated that F expands the stability field of biotite in high-grade marbles (as demonstrated by the marbles from the Adirondacks) in assemblages with calcite, tremolite, K-feldspar, diopside, and quartz. However, the degree of stabilization of phlogopite by F in these assemblages depends drastically on the distribution of F between phlogopites and amphiboles, which itself is a function of metamorphic grade.

11.3.2 Amphiboles

Similar to biotites, F significantly expands the stability field of amphiboles to higher temperature. Available experimental data concern only Ca- and Ca–Na amphiboles. Troll and Gilbert (1974) found that fluor-tremolite is stable up to a temperature of about 1150 °C at 1 bar. Gilbert et al. (1982) found that it decomposes at 1190 °C and 5 kbar in contrast to 910 °C for OH-tremolite (Jenkins and Clare 1990). From a comparison of the stability of synthetic tremolite and two natural tremolites, which contained variable concentrations of F, Jenkins and Clare (1990) concluded that increasing the F content of tremolite extends its thermal stability field via the reaction:

$$\text{Tremolite} = 2\ \text{Diopside} + 3\ \text{Enstatite} + \text{Quartz} + H_2O \qquad (11.1)$$

by about 60 °C per 1 wt.% F (Fig. 11.6). According to their data, tremolite, containing 0.5 wt.% F, is stable above 950 °C at pressures of 5–7 kbar. Chernosky et al. (1998) experimentally found that the reactions:

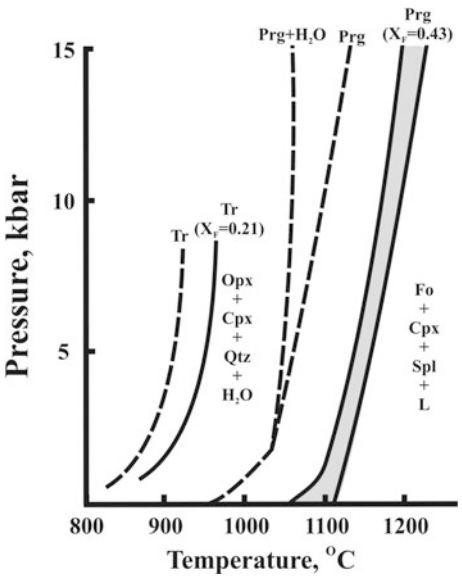

Fig. 11.6 P–T curves illustrating the stability of F-bearing amphiboles with respect to their F-free analogues. Data for the reactions tremolite = clinopyroxene + orthopyroxene + quartz + H_2O are from Jenkins and Clare (1990). Data for the reactions pargasite = forsterite + clinopyroxene + spinel + L are from Holloway and Ford (1975). The *shaded area* shows an interval of the divariant decomposition of F-bearing pargasite, where pargasite, with variable F content, which increases with temperature, coexists with forsterite, clinopyroxene, spinel, and melt. *Cpx* clinopyroxene, *Opx* orthopyroxene, *Prg* pargasite, *Qtz* quartz, *Spl* spinel, *Tr* tremolite, *L* melt

$$\text{Tremolite} + \text{Forsterite} = 2\ \text{Diopside} + 5\ \text{Enstatite} + H_2O \quad (11.2)$$

and

$$\text{Tremolite} + 3\ \text{Calcite} + 2\ \text{Quartz} = 5\ \text{Diopside} + H_2O + 3\ CO_2 \quad (11.3)$$

were displaced to higher temperatures by about 30 and 50 °C, respectively, for the natural Campo Longo tremolite with F/(F + OH) = 0.40 in comparison to a synthetic F-free tremolite. For the second reaction, a stronger effect was observed at 5 kbar than at 1 kbar.

Expansion of the tremolite stability field with increasing F content has been projected to edenite and pargasite. Graham and Navrotsky (1986) synthesized F-bearing varieties of the tremolite–edenite amphiboles at 1000 °C and 2 kbar, i.e. at a temperature, which significantly exceeds the upper stability limit of the hydroxyl end-members. In order to evaluate the effect of F substitution on the upper temperature stability limit of pargasite, Holloway and Ford (1975) studied the fluid-absent melting of pargasite with 43 mol.% F (Fig. 11.6). They found that the amphibole-out boundary occurs at 1060 °C and 1230 °C at 5 and 15 kbar, respectively, and concluded that the F-content of pargasite increases with temperature and, hence, partial melting events could produce F-rich hornblende as residual phases.

11.3.3 Apatite

The standard thermodynamic properties of fluorapatite and chlorapatite, as well as their mixing properties along the binary join, are reliably known from experimental data (Korzhinsky 1981; Zhu and Sverjensky 1991; Dachs et al. 2010; Hovis and Harlov 2010; Schettler et al. 2011). Data on the stability of halogen-bearing apatite at high-grade metamorphic conditions are, however, generally lacking. The strong preference of high-grade apatite for F (e.g., Yardley 1985; Kapustin 1987; Spear and Pyle 2002) implies that this halogen should expand the stability of apatite to high temperatures. This conclusion is consistent with the recent data showing that thermal stability at 1 atm increases from hydroxyapatite through chlorapatite to fluorapatite (Tõnsuaadu et al. 2012). This study showed that the anions along the hexagonal axis were the last to leave the crystal structure of apatite upon heating which ensures the high temperature stability of the mineral. Fluor- and chlorapatites and intermediate members have been successfully synthesized at pressures of 8–12 kbar and temperatures of 640–900 °C (Shaw et al. 1993) indicating stability of these minerals under high-grade metamorphic conditions. At 1 bar, fluor- and chlorapatites (and intermediate members) are commonly synthesized at 1375–1220 °C and 1 bar in molten CaF_2–$CaCl_2$ salt fluxes (cf., Schettler et al. 2011).

When discussing the stability limits of halogen-bearing apatite, its relationship with aluminosilicate melts should be specially noted, since all experiments on the solubility of apatites in granitic liquids have been carried out using fluorapatite as a starting material (e.g., Pichivant et al. 1992; Wolf and London 1994, 1995). The solubility of fluorapatite in silicate liquids is a strong function of the alumina saturation index (molar Al/[Na + K + 2Ca]) in the melt because of the formation of the Al phosphate complex $AlPO_4$. Fluorapatite dissolves incongruently in peraluminous granitic liquids with the formation of REE-rich monazite on its surface (Wolf and London 1995). Similar textures have been reproduced during dissolution of fluorapatite in aqueous, aqueous-carbonic and KCl-brine at temperatures up to 900 °C and 5 and 10 kbar by Harlov and Förster (2003). Inclusions of monazite, both oriented and unoriented, are also characteristic for high-temperature experiments. Similar inclusions form during dissolution-reprecipitation of fluorapatite in the HCl and H_2SO_4 solutions (Harlov et al. 2005). According to Harlov and Förster (2003), the NaCl and $CaCl_2$ brines suppress the formation of monazite. $CaCl_2$ brines additionally promote extensive Cl–F exchange with the conversion of fluorapatite to chlorapatite. However, Antignano and Manning (2008) found that tiny monazite crystals formed on fluorapatite grain surfaces in experiments involving incongruent dissolution of fluorapatite in a series of NaCl-brine concentrations at 700–900 °C and 7–20 kbar. In experiments on the interaction of chlorapatite with aqueous, aqueous-carbonic and $H_2O + CaF_2$ fluids, Harlov et al. (2002) also reproduced monazite and xenotime inclusions along with the exchange-induced formation of F–OH-enriched zones. In contrast, Safonov et al. (2014b) found no evidence for the decomposition of F-bearing apatite in experiments on the partial melting of a biotite-hornblende tonalite gneiss in the presence of H_2O–CO_2–(K, Na)Cl fluids at 5.5 kbar and 750 and 800 °C. The Cl content of the apatite in the experimental products was found to be notably higher than the Cl content in the apatite from the starting gneiss suggesting that the apatite composition is greatly influenced by Cl–OH exchange with chloride-bearing fluids.

11.3.4 Scapolite

Newton and Goldsmith (1976) found that marialite is stable relative to albite + NaCl at T > 800 °C at P = 8–15 kbar. Along with the earlier data by Orville (1975), these results imply a boundary between 750 and 800 °C over a pressure range of 0–8 kbar with a steep Clapeyron slope indicating that Cl-rich scapolite should be stable at upper amphibolite- to granulite-facies metamorphic conditions. The high-temperature stability limit of marialite is probably confined by its incongruent melting at temperatures above 860 °C (e.g., Eugster and Protska 1960). Ellis (1978) found that at 4 kbar and 750 °C, the range of anorthite content, over which scapolite is stable relative to plagioclase, becomes wider (up to a range of An_{25}–An_{87}) with an increasing NaCl/(NaCl + H_2O) ratio in the coexisting fluid. Newton et al. (1998) made a few reconnaissance experiments at 800 °C and

7–10 kbar with a synthetic plagioclase composition of An_{28} in the presence of concentrated NaCl solutions (40–55 mol.% NaCl) and excess quartz, with or without a small admixture of $CaCl_2$ and KCl. All experiments yielded only plagioclase, quartz, and solution, with no scapolite. These authors concluded that concentrated NaCl solutions will not form NaCl-bearing scapolite in quartzofeldspathic rocks at high-grade metamorphic conditions unless some additional components, such as $CaCO_3$ and/or $CaSO_4$, are present. This result appears to contradict those of Ellis (1978) and Vanko and Bishop (1982), who synthesized marialitic scapolite from sodic plagioclase in concentrated NaCl solutions at 750 °C and 1–4 kbar pressure. Newton et al. (1998) explained this apparent discrepancy as being due to a large decrease in the NaCl activity at constant temperature and concentration at pressures above 4 kbar (Aranovich and Newton 1996).

11.3.5 Titanite

Titanite with up to 50 mol.% of the $CaAlSiO_4F$ component occur in HP and UHP metamorphic rocks (Franz and Spear 1985; Sobolev and Shatsky 1991; Carswell et al. 1996; Castelli and Rubatto 2002; Hansen and Harlov 2007). Consequently, earlier studies considered pressure as the dominant factor controlling the $Ti^{4+} + O^{2-} = F^- + Al^{3+}$ substitution in titanite. Smith (1981) examined this substitution at 15–35 kbar and 1000–1200 °C. He found that increasing pressure and decreasing temperature really favor this substitution. However, later studies revealed that titanite, with an Al–F concentration similar to that seen in HP rocks, was also present in medium to low pressure metamorphic rocks (Enami et al. 1993; Markl and Piazolo 1999; Sengupta et al. 2004). This was despite the fact titanite in these rocks tends to show lower F/OH ratios compared to its HP analogues. From a study of titanites in the granulite- to amphibolite-facies calc-silicate rocks in Dronning Maud Land, Antarctica, Markl and Piazolo (1999) came to the conclusion that P and T exert only a partial control on the Al–F-substitution in titanite, whereas the bulk rock and fluid composition are the dominant factors. Later experimental investigations convincingly demonstrated the P–T dependence of the Al–F content in titanite and emphasized the buffering effects of specific mineral assemblages (Troitzsch and Ellis 2002; Tropper et al. 2002).

Tropper et al. (2002) studied phase relations of Al–F titanite in the system $CaSiO_3$-Al_2SiO_5-TiO_2-CaF_2 at 11–40 kbar and 900–1000 °C and found that rutile prevented Al–F incorporation into titanite, while the highest concentrations of the $CaAlSiO_4F$ end-member were observed in assemblages with fluorite and anorthite or kyanite. Tropper et al. (2002) found that the $CaAlSiO_4F$ end-member expands the stability field of Al–F-titanite + kyanite towards lower pressure and higher temperature with respect to anorthite + rutile. The presence of fluorite shifts the stability of Al–F titanite to high pressures and low temperatures. Thermodynamic calculations show that titanite, with up to 50 mol.% of the $CaAlSiO_4F$ end-member, can be formed in equilibrium with anorthite, fluorite, and rutile at T = 900–1000 °C

and P up to 10–11 kbar, i.e. under the conditions of UHT metamorphism. Troitzsch and Ellis (2002) further experimentally demonstrated the dependence of the Al–F content of titanite on pressure, temperature, fluid composition, and mineral assemblage. Titanite in medium-pressure rocks (<8 kbar) can be Al–F-rich if plagioclase and fluorite are the coexisting phases, but Al–F titanite is not stable with sillimanite + fluorite + quartz. This explains the absence of sillimanite and rutile in titanite-bearing plagioclase + fluorite assemblages in the calc-silicate rock described by Sengupta et al. (2004) and the absence of titanite in sillimanite + fluorite-bearing assemblages in the Adirondacks (Bohlen and Essene 1978).

The Al–F content of titanite is vitally dependent on fluid composition (Troitzsch and Ellis 2002). A decrease in the CO_2 activity in the fluid will cause an increase in the Al-content of the titanite in calcite-bearing assemblages at any given P–T. The presence of H_2O destabilizes high concentrations of $CaAlSiO_4F$ with respect to zoisite or grossular-rich garnet, whereas CO_2 assists in the breakdown to calcite-bearing assemblages. Bohlen and Essene (1978) and Markl and Piazolo (1999) suggested that the stability and composition of titanite depend on F and oxygen fugacities. Calculations by Sharova et al. (2012) showed that the content of the $CaAlSiO_4F$ component in titanite in equilibrium with plagioclase, rutile, and quartz directly depended on the activity of F in the fluids.

It should be noted that the problem of Al–F titanite stability is closely related to the question regarding the presence of metamorphic fluorite at high-grade conditions, which is very rare in amphibolite- and granulite-facies rocks (Bohlen and Essene 1978; Valley et al. 1990; Sengupta et al. 2004).

11.3.6 Influence of Halogens on the Fe–Mg Exchange Equilibria in High-Grade Rocks

The Mg–F and Fe–Cl affinities in high-grade biotites and amphiboles point to the strong influence of halogens on the activities of the end-members in the corresponding solid solutions. Perchuk and Aranovich (1984) and Aranovich (1991) estimated a large negative value of ΔG^{int} for the internal reciprocal reaction OH-phlogopite + F-annite = F-phlogopite + OH-annite, which indicated a significant decrease in the phlogopite activity and an increase of the annite activity in the F-bearing biotite solid solution. Such a strong influence of F on the activities of OH-biotite should have a strong influence on the K_d^{Fe-Mg} for the exchange reactions between biotite and other Fe–Mg minerals. Temperatures derived from these reactions as geothermometers will be underestimated if F in biotite is ignored (Aranovich 1983, 1991; Perchuk and Aranovich 1984; Zhu and Sverjensky 1992). Perchuk and Aranovich (1984) found a strong positive correlation between the K_d^{Fe-Mg} of the biotite-garnet Fe–Mg exchange reaction and the F content of biotite. According to the calibration of ΔG^{int} by Zhu and Sverjensky (1992), the temperature correction to the garnet–biotite geothermometer for F in biotite may be up to

100–150 °C for the biotite with an F/(F + OH) ratio of around 0.3–0.5. A similar correction should apply to other Fe–Mg exchange geothermometers involving biotite (e.g., Perchuk et al. 2000).

Chlorine should have an opposite effect on the garnet–biotite exchange equilibrium, but this effect is weaker compared to the effect of F (e.g., Zhu and Sverjensky 1992). In fact, Kullerud (1995) found a clear dependence for the $K_D^{Mg-Fe} = [X_{Mg}^{Bt}(1-X_{Mg}^{Grt})]/[(1-X_{Mg}^{Bt})X_{Mg}^{Grt}]$ between biotite and garnet on the Cl-content in the biotite. Accounting for this dependence in the garnet–biotite geothermometer resulted in lower calculated temperature values but significantly narrowed the calculated temperature scatter (Kullerud 1995). Using biotite–apatite OH–F–Cl experimental exchange data, Zhu and Sverjensky (1992) introduced a combined correction for F and Cl in biotite in the garnet–biotite thermometer. They supported the conclusion that the effects of F and Cl concentrations in biotites on the biotite–garnet geothermometer are of the opposite sign, and the effect of F is about twice as large as that of Cl. Similar corrections should be the case for exchange equilibria involving F- and Cl-bearing amphiboles. However, no such studies have been made, so far.

11.4 Factors Controlling Halogen Abundances in High-Grade Metamorphic Rocks

Three major factors have been suggested to control the amount of F and Cl and their distribution between the halogen-bearing minerals from amphibolite- and granulite-grade rocks: (1) bulk composition of the metamorphic rocks or their protoliths; (2) metamorphic grade and related partial melting; and (3) fluid–rock interaction. This section reviews arguments usually put forth to favor one of the above factors (or their combination), and presents results based on the most recent thermodynamic systematics showing that many of the features of halogen-bearing high-grade assemblages may have been assumed due to fluid–rock interaction.

11.4.1 Bulk Composition of Metamorphic Rocks or Their Protoliths

The presence of halogens in metamorphic rocks, both as components of mineral solid solutions (biotites, amphiboles, scapolites, apatites, etc.) and as saline fluid inclusions, can be a direct consequence of the preservation of the initial halogen content in the protoliths (e.g., Markl et al. 1997; Graham and Yardley 2002). In some amphibolite-facies areas, halogen enrichment is related to metaevaporite sequences, metaexhalites, or salt-bearing sediments (Sharma 1981; Mora and Valley 1989; Oliver et al. 1992; Oen and Lustenhouwer 1992; Gomez-Pugnaire

et al. 1994). Differential enrichment of these rocks in halogens may be related to the initial saline pore brines and authigenic minerals (halite, sylvite, etc.). Significant variations in the halogen content in biotites, amphiboles, and scapolites in such rocks over a scale of centimeters or meters (e.g., Mora and Valley 1989; Oliver et al. 1992) have been interpreted as a consequence of high internal buffering of the rock–fluid systems. This suggests that fluid–rock interaction was limited, such that the halogen activity gradients were not smoothed out by fluids during regional metamorphic event(s).

The participation of the pre-metamorphic halogens in the halogen distribution within high-grade rocks has also been proposed for some metamorphosed igneous rocks. Valley et al. (1990) suggested that the amphiboles containing 1.66–3.24 wt.% Cl, coexisting with the Cl-rich apatites in the meta-anorthosites of the Marcy Complex, Adirondack Highlands, New York, reflect pre-metamorphic, probably magmatic Cl in the rocks. Whereas preservation of high Cl in the metamorphosed rocks is evidence for their fluid-absent metamorphism, since extensive fluid infiltration would have depleted the Cl from the rocks. Bohlen and Essene (1978) described fluorite in the metamangerites from the complex and suggested that it was part of a relic primary magmatic assemblage stable during high-grade metamorphism.

These rocks from the Adirondacks are an instructive example, which illustrates how the rock bulk chemistry controls the distribution of Cl and F. Chlorine-rich amphiboles, biotites, and apatites are characteristic of Fe-rich meta-anorthosites, mangerites, and charnockites from this complex (Valley et al. 1990; Morrison 1991; Safonov 1998). Although F is subordinate, these rocks show evidence for enrichment in F as well. In contrast to orthogneisses, Mg-rich rocks (clinopyroxene + orthopyroxene + biotite + amphibole + plagioclase + quartz), which are considered to be meta-evaporites (Lamb and Valley 1988), contain biotites and amphiboles with up to 0.5–2.0 wt.% and 0.5–1.2 wt.% F, respectively, with Cl concentrations below 0.05 wt.%. Low Cl contents are characteristic for F-rich phlogopites (up to 8.5 wt.% F) and tremolites (1.5–3.8 wt.% F) in the Mg-rich, upper amphibolite-facies siliceous marbles of the Adirondack Lowlands (Valley et al. 1982). These examples clearly demonstrate that high F or Cl contents in minerals from the above rocks are not a consequence of unusually F-rich or Cl-rich environments, but rather reflect a strong Mg–F and Fe–Cl affinity in biotites and amphiboles (see below), whose Mg-number is a function of the bulk rock chemistry.

Other examples, on how the bulk chemistry controls the halogen distribution in metamorphic rocks within a specific complex, include variations in the halogen content in biotites and amphiboles from granulite-facies rocks of the Kondapalli area (India). Leelanandam (1970) concluded that while having widely varying F contents (1.2–3.9 wt.%), biotites from the mafic rocks (orthopyroxene + clinopyroxene + hornblende + biotite + plagioclase + quartz) are more Cl-rich (up to 0.7 wt.% Cl) than the biotites from the associated intermediate rocks (orthopyroxene + garnet + biotite + plagioclase + K-feldspar + quartz) and metapelites (garnet + biotite + sillimanite + K-feldspar + plagioclase + quartz). This

was also the case for amphiboles in mafic rocks, which are Cl-enriched, compared to amphiboles from intermediate rocks. He noted that the Cl-enriched amphiboles (0.6–1.2 wt.%) are also characteristic for the mafic varieties.

11.4.2 Metamorphic Grade and Related Partial Melting

Studies on areas, where the metamorphic grade changes from amphibolite- to granulite-facies, have revealed different trends for variations in the halogen contents for biotites, amphiboles, and apatites. Some of these studies (e.g., De Maesschalck et al. 1991) indicate that granulites generally exhibit higher Cl and F contents than the amphibolite-facies rocks. On the other hand, Nijland et al. (1993) found that amphiboles and biotites in mafic granulites from the Bamble Sector (Norway) did not show systematically higher F and Cl contents than those from their mafic amphibolite-facies counterparts. They suggested that the differences between their data and previous studies (see references in Nijland et al. 1993) are probably related to the different behavior of halogens in mafic and felsic rock types (see also Leelanandam 1970). The study by Hansen and Harlov (2007) focused on variations in the Cl and F contents in biotites, amphiboles, and apatites along a 95 km-long traverse, which works as a gradual transition from biotite–amphibole gneisses to orthopyroxene-bearing gneisses in the Shevaroy Block (Tamil Nadu, southern India). It was found that these minerals are enriched in Cl within a 30 km-wide, clinopyroxene-bearing transition zone in comparison to orthopyroxene-bearing, granulite-facies and amphibolite-facies zones that are located to the south and to the north, respectively. In contrast, F in biotite and apatite decreases from the granulite zone through the transition zone to the amphibolite zone. These same relations have also been described by Harlov and Förster (2002) for a clinopyroxene-rich zone, which straddles the granulite- to amphibolite-facies transition in the Ivrea-Verbano zone (Northern Italy). Here, Cl accumulates in minerals from the clinopyroxene-rich transition zone, while F shows a gradual decrease from the granulite to amphibolite-facies zone.

Enrichment of biotites in F does not always follow metamorphic grade along with an increase of Ti and Al contents in these minerals, as might be expected from experimental studies on the F-bearing biotites (Peterson et al. 1991; Hensen and Osanai 1994; Dooley and Patiño Douce 1996; Tareen et al. 1995, 1998). However, the peak metamorphic high-Mg and Ti-rich biotites with 2–4 wt.% F are reported in Mg–Al rich metapelites from a number of metamorphic terrains around the world (e.g., Mouri et al. 1996; Perchuk et al. 1985; Bose et al. 2005) (Fig. 11.1a). The highest F concentrations in biotites (5–8 wt.%) have been reported from the sapphirine and ossumilite-bearing granulites from the Napier Complex in East Antarctica (Grew 1982; Motoyoshi and Hensen 2001), which were metamorphosed at temperatures up to 1100 °C. Accumulation of F in high-temperature biotites from metapelites can be assisted by partial melting (Dooley and Patiño Douce 1996; Patiño Douce and Johnston 1991; Skjerlie and Johnston 1993; Nair and Chacko

2002), because of the preferential partitioning of F from the granitic melts into the biotite (e.g., Icenhower and London 1997; Chevychelov et al. 2008). For example, Motoyoshi and Hensen (2001) proposed that F-enriched biotites from the sapphirine and ossumilite-bearing granulites of the Napier Complex, East Antarctica, were a product of partial melting in the temperature range 950–1100 °C according to the schematic reactions:

$$\begin{aligned}\text{Biotite} + \text{Sillimanite} + \text{Quartz} = {} & \text{Orthopyroxene} + \text{Osumilite} \\ & + \text{Biotite (enriched in F)} \pm \text{Sapphirine} + \text{Melt}\end{aligned} \tag{11.4}$$

$$\begin{aligned}\text{Biotite} + \text{Quartz} = {} & \text{Garnet} + \text{Orthopyroxene} + \text{Osumilite} \\ & + \text{Biotite (enriched in F)} \pm \text{Sapphirine} + \text{Melt}\end{aligned} \tag{11.5}$$

Bose et al. (2005) related the formation of the F-enriched biotite (up to 3.3 wt.% F) in metapelites from the northern part of the Eastern Ghats (India) to a melting reaction at temperatures above 950 °C:

$$\begin{aligned}\text{Biotite} + \text{Sillimanite} + \text{Quartz} = {} & \text{Sapphirine} + \text{Orthopyroxene} \\ & + \text{Biotite (enriched in F)} \pm \text{Cordierite} \\ & \pm \text{Spinel} + \text{Melt}\end{aligned} \tag{11.6}$$

Reactions (11.4) through (11.6) imply a significant decrease in the total proportion of biotite in the rocks accompanied by the accumulation of F in the residual biotite. However, this is not always the case for the high-grade metapelites. Figure 11.7 demonstrates an example of a metapelite from the Aldan Shield (sample Sut-7, Perchuk et al. 1985), which is composed of the assemblage orthopyroxene + biotite + cordierite + sappherine + sillimanite and where the biotite has an X_{Mg} = 0.9 and 4 wt.% F. The bulk proportion of biotite in the sample is about 25 vol.%, whereas the subhedral shape of the biotite flakes and textural relations (Fig. 11.7) indicate no evidence for its decomposition. Thus, the F-enrichment of biotite in this specific case seems to be related not to a decrease in the mineral content via subsolidus dehydration or partial melting, but to the crystallization of the biotite in the presence of an exotic F-rich medium (fluid or melt).

Amphibole is also expected to preferentially partition F from aluminosilicate melts (e.g., Holloway and Ford 1975). Sajeev et al. (2009) interpreted orthopyroxene–clinopyroxene–plagioclase symplectites around pargasite with X_F up to 0.56 in granulites from the Highland Complex (Sri Lanka) to be products of peak metamorphic dehydration melting at temperatures above 950 °C and pressures of around 10 kbar. The occurrence of F-rich pargasites (with X_F up to 0.43) in syn-metamorphic anatectic pegmatites from the Napier Complex (Grew et al. 2000)

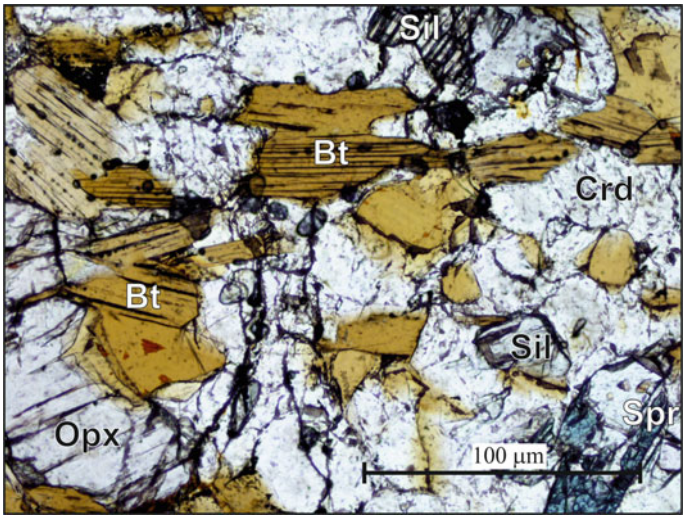

Fig. 11.7 Photomicrograph of sample Sut-7 (Aldan shield; Perchuk et al. 1985) with ubiquitous subhedral F-rich phlogopite grains. See text for discussion. *Bt* biotite, *Crd* cordierite, *Opx* orthopyroxene, *Sil* sillimanite, *Spr* sapphirine

imply that partial melting could be an efficient mechanism for the accumulation of F in high-temperature amphiboles crystallized from F-bearing felsic melts. On the other hand, mafic and ultramafic granulites from the Tonagh Island, Enderby Land, Antarctica, metamorphosed under about the same conditions as the Napier Complex, also contain pargasites with $X_F = 0.12–0.48$ (Tsunogae et al. 2003). Mineral assemblages from these rocks, the ultramafic ones in particular, could hardly form due to partial melting in a closed system, and, thus, require an external (fluid) source to induce the F-enrichment of the pargasites. This conclusion is further supported by a nearly constant $\log(f_{H_2O}/f_{HF})$ calculated for samples with different bulk F contents (Tsunogae et al. 2003).

Because of its high-temperature stability limit (see below), apatite is a common host for halogens at peak metamorphic conditions. Kapustin (1987) was among the first to describe an increase in the apatite F/(F + Cl + OH) ratio with increasing metamorphic grade. In fact, in most amphibolite and granulite-grade metamorphic rocks, accessory apatite is typically fluorapatite with minor Cl and OH (e.g., Harlov and Förster 2002; Harlov et al. 2006; Hansen and Harlov 2007). Spear and Pyle (2002) explained the strong preference of granulite-facies apatite for F over Cl by Rayleigh distillation of Cl accompanying peak-metamorphic dewatering of rocks.

In contrast to F, Cl does not show a prominent dependence on the metamorphic grade. The Cl content in high-temperature, F-rich biotites from metapelites is often at the EMP detection limit. Fluorine-rich biotite (up to 4.2 wt.% F), from the

sapphirine-bearing metapelites of In Ouzzal, Algeria, which contains 0.3–0.6 wt.% Cl (Mouri et al. 1996), is probably the only exception. Examples of peak-metamorphic minerals, enriched in Cl, are rare and exclusively belong to Fe-rich assemblages involving garnet, two pyroxenes, plagioclase, quartz, magnetite, and ilmenite, as well as scapolite, carbonates, and other minerals indicative of metasedimentary origin. Peak-metamorphic (750 °C and 6 kbar) biotites and amphiboles, with up to 2.9 and 2.8 wt.% Cl, respectively, have been described by Zhu et al. (1994) in granulite-facies Fe formation rocks from the Beartooth Mountains (Montana, USA). Léger et al. (1996) reported biotites (0.41–4.6 wt.% Cl and 0.35–1.63 wt.% F) coexisting with amphiboles (0.5–5.1 wt.% Cl and 0.14–0.73 wt.% F), in granulite-facies mafic gneisses from the Black Rock Forest, Hudson Highlands (New York, USA). Peak metamorphic, Cl-rich scapolites are well known in such high-grade metasediments (e.g., Satish-Kumar et al. 2006).

Growth of the Cl-rich minerals has most often been ascribed to the retrograde stage of metamorphism. Coronas of Cl-rich amphiboles around peak-metamorphic pyroxenes and Fe–Ti oxides are well-known in granulite-facies rocks from the anorthosite–mangerite–charnockite–granite suite, Adirondack Mountains, New York, USA (Morrison 1991; Valley et al. 1990; Safonov 1998). Based on textural relations, Morrison (1991) and Safonov (1998) inferred that the amphiboles, which varied widely in their Cl-content, were produced after the peak of metamorphism at 600–700 °C and 6–7 kbar. Kamineni et al. (1982) described the formation of retrograde F–Cl-rich biotite (about 2 wt.% Cl and up to 2.6 wt.% F), amphibole (up to 4.2 wt.% Cl and about 1 wt.% F), and apatite (0.84 wt.% Cl and up to 3 wt.% F) after primary orthopyroxene and garnet in charnockitic rocks from the Eastern Ghats, India. Higashino et al. (2013) recorded Cl-rich biotites (>0.4 wt.% Cl) and apatites (>2 wt.% Cl) included in the outer parts of zoned garnet porphyroblasts in garnet–biotite and garnet–biotite–sillimanite gneisses from the Sør Rondane Mountains (East Antarctica). They inferred that these Cl-rich mineral inclusions were formed due to infiltration of a Cl-rich fluid or melt at near peak metamorphic conditions (about 800 °C and 8 kbar).

11.4.3 Fluid–Rock Interaction

Most of the above studies considered F–Cl enrichment of high-grade minerals as a result of not only metamorphic grade, but also due to the infiltration of the halogen-rich fluids (Kamineni et al. 1982; Morrison 1991; Zhu et al. 1994; Kullerud 1996; Nijland et al. 1993; Safonov 1998; Harlov et al. 1998; Harlov and Förster 2002; Tsunogae et al. 2003; Hansen and Harlov 2007; Higashino et al. 2013; Kusebauch et al. 2015). It should be emphasized that the chemical behavior of F and Cl are very different during fluid–rock interaction since F is preferably partitioned into solid phases or melts, whereas Cl is overwhelmingly partitioned into aqueous fluids (Munoz and Swenson 1981; Volfinger et al. 1985; Zhu and Sverjensky 1991). Thus, the formation of Cl-rich minerals is strong evidence for the

presence of concentrated aqueous low-a_{H_2O} brines (immiscible with CO_2) during the course of metamorphism. In some cases, the action of these brines can be expressed by the formation of specific alkali feldspar reaction micro-veins, along quartz-plagioclase grain boundaries, accompanied by Cl-rich minerals (see Safonov and Aranovich 2014 for a review).

The Cl content of amphiboles is a good monitor of fluid evolution. For example, Morrison (1991) and Safonov (1998) described in detail different generations of amphiboles variously enriched in Cl (from 0.05 up to 3 wt.% Cl) in granulite-facies orthogneisses from the Adirondack Mountains, New York, USA (Fig. 11.8). Taking into account correlations between the Cl content of amphiboles and their X_{Mg}, X_{Si}, and X_K, both authors concluded that the amphiboles seem to be produced at similar retrograde P–T conditions, but probably in equilibrium with fluids of variable salinity. Valley et al. (1990) demonstrated that Cl-rich amphiboles and apatites in meta-anorthosites from the Marcy Complex in the Adirondacks could coexist with fluids with $f_{H_2O}/f_{HCl} = 0.37 - 0.71$, i.e. characteristic for highly-concentrated brines. They doubted that such fluids could infiltrate this large anorthosite massif during metamorphism. Nevertheless, Safonov (1998) found that the Cl-rich minerals in the Adirondack rocks are closely related to K-feldspar micro-veins, which are suggestive of the fluid infiltration along quartz-plagioclase grain boundaries (e.g., Safonov and Aranovich 2014). Figure 11.9 shows another illustrative example of Cl-rich amphibole as an indicator of fluid–rock interaction in an amphibolite from the Southern Marginal Zone of the Limpopo Complex (South Africa) (e.g., Belyanin et al. 2014). Hornblende (Hbl-2), forming after hornblende

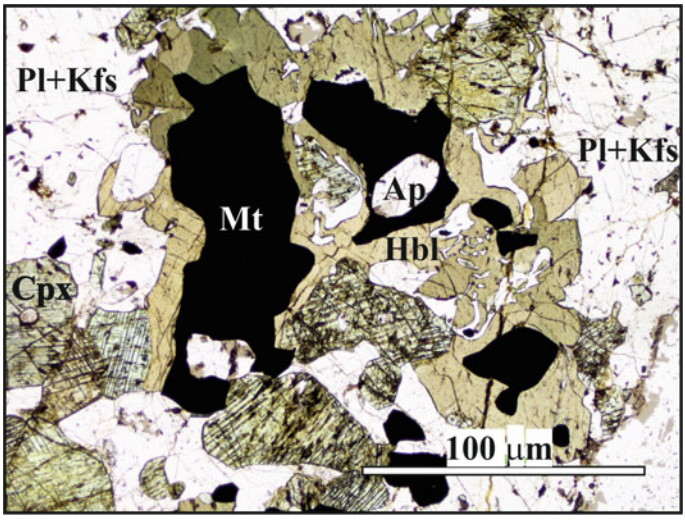

Fig. 11.8 Rims and symplectites of Cl-rich potassic hornblende (Hbl) around clinopyroxene (Cpx) and magnetite (Mt) in a metasyenite from the Adirondack Complex, USA (Morrison 1991; Safonov 1998). *Ap* apatite, *Pl* plagioclase, *Kfs* perthitic K-feldspar

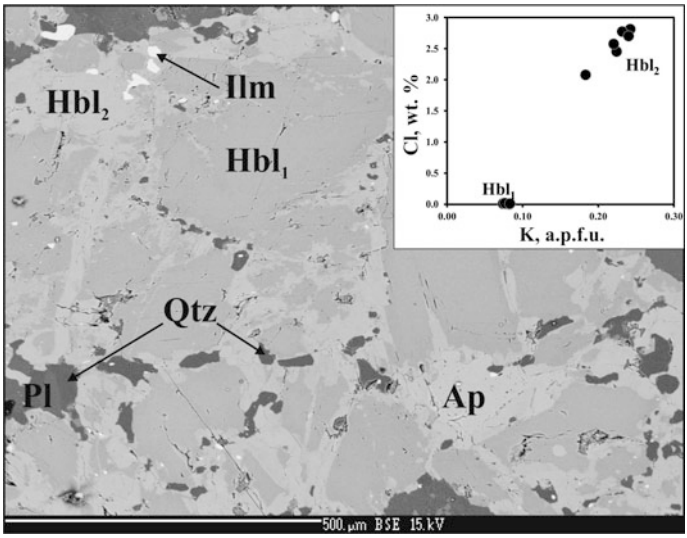

Fig. 11.9 New generation of Cl-rich potassic hornblende Hbl_2, after Cl-free hornblende Hbl_1, from an amphibolite located in the Southern Marginal Zone of the Limpopo Complex, South Africa (e.g., Belyanin et al. 2014). The inset shows differences in the K and Cl contents between Hbl_1 and Hbl_2. Hbl_2 is close to pargasite, whereas Hbl_1 is enriched in the tremolite component (see also Fig. 11.9a in Safonov and Aranovich 2014). The increase of Al in Hbl_2 results in the "exsolution" of quartz (Qtz) and ilmenite (Ilm). BSE image. *Ap* apatite, *Pl* plagioclase

(Hbl-1), shows a notable increase in the K/(K + Na) ratio (0.29–0.35 compared to 0.15–0.16 in Hbl-1) and in the Cl content (2.0–3.4 wt.% Cl in contrast to less than 0.01 wt.% Cl in Hbl-1). These relations suggest interaction with a KCl-rich fluid after the peak of metamorphism.

Since $Cl/(Cl + CO_3)$ in scapolite is controlled by the activity of NaCl in the fluids (e.g., Ellis 1978), this mineral serves as another sensitive monitor of variable fluid salinities during high-grade metamorphism (e.g., Kullerud 1995, 1996; Kullerud and Erambert 1999; Satish-Kumar et al. 2006). The formation of scapolite indicates both the infiltration of halogen-bearing fluids and the leaching of Cl from the rocks interacting with Cl-poor fluids. Satish-Kumar et al. (2006) described zoned scapolite with marialitic cores and meionitic rims in scapolitic boudins within marbles from the Lützow–Holm Complex, East Antarctica. These authors concluded that the cores were equilibrated with an internally buffered, brine-rich fluid, which most likely originated from an evaporate source during prograde to peak metamorphism, while the rims were recrystallized in the presence of an external CO_2-bearing fluid that leached Cl from the mineral. They found additional evidence for Cl leaching in fractures from the fluorapatite, which had been altered to chlorapatite. Thus, in typical regional metamorphic environments, halogen-bearing minerals, such as apatite and/or scapolite, could strongly control the halogen budget of the coexisting fluids. Spear and Pyle (2002) suggested this mechanism for apatite

because of the preferential partitioning of F into apatite and Cl into fluid (Korzhinsky 1981; Yardley 1985; Zhu and Sverjensky 1991). Smith and Yardley (1999) considered the situation in which Cl-rich detrital apatite is present in a rock and suggested that the exchange of Cl with a limited volume of metamorphic fluid could change the concentration of Cl in the fluid by several orders of magnitude. However, this situation can only be applied for low fluid/rock ratios, otherwise the apatite composition would most likely reflect the composition of the infiltrating fluid.

Some studies suggested that enrichment of fluids (and, consequently, coexisting minerals) in halogens (especially in Cl) at least in some metamorphic complexes was not primary, but had resulted from modifications of the fluids via either hydration reactions (desiccation mechanism; Trommsdorff et al. 1985) or immiscibility of the complex H_2O–CO_2-salt ("boiling" mechanism; Trommsdorff and Skippen 1986; Manning and Aranovich 2014). The desiccation mechanism was first suggested by Trommsdorff et al. (1985) and Kullerud (1995, 1996), and later supported by Markl and Bucher (1998) and Markl et al. (1998) to explain the occurrence of brine inclusions in minerals and intergranular high-temperature (K, Na)Cl salts in high-grade metamorphic rocks from Campolungo (Switzerland), Cornone di Blumone (Italy), and Lofoten (Northern Norway). The mechanism is based on the assumption that in a closed system, the Cl-content of the fluid phase (and the ratio a_{NaCl}/a_{H_2O}) will progressively increase as a function of a short-lived series of hydration reactions between the fluid and the rock (Trommsdorff et al. 1985; Kullerud 1995, 1996; Markl and Bucher 1998; Markl et al. 1998). Utilizing this mechanism, Kullerud (1995, 1996) explained several texturally distinct generations of Cl-rich minerals in amphibole–biotite–garnet-plagioclase veins replacing two-pyroxene granulites along narrow shear-zones at Lofoten, North Norway. He concluded that variations in the Cl content of the minerals reflected local variations in the composition of an essentially aqueous CO_2-, Cl-, and Ba-bearing fluid. As a result of desiccation, the latest mineral assemblages, forming in equilibrium with high, Cl-enriched fluids, will be the most Cl-enriched, while low-Cl amphiboles and biotites will occur in domains where the free fluid phase was consumed at an early stage. The "boiling" mechanism proposed by Trommsdorff and Skippen (1986) to explain the occurrence of solid intergranular salts in metamorphic rocks considers fluid evolution in the H_2O–CO_2-salt system in which a CO_2-rich vapor is preferentially removed from the system leaving behind a saline aqueous phase enriched or eventually saturated in dissolved salt components.

Melt generation is yet another factor that influences the Cl concentration in fluids and, in turn, causes redistribution of halogens in the associated rocks. In equilibrium with aluminosilicate melts, Cl, in the form of K, Na, and Ca chlorides, strongly partitions into the coexisting aqueous fluid due to the limited solubility of these chlorides in felsic melts (e.g., Webster 1997; Aranovich et al. 2013). The melts could be either syn-metamorphic intrusions invading host rocks or the products of *in situ* partial melting triggered by fluids. Several studies (Markl and Piazolo 1998; Harlov et al. 2006, 2014; Safonov et al. 2014a) have demonstrated that intruded

magmatic bodies can strongly affect country rocks due to expulsion of Cl-enriched fluids during crystallization. Fluorine in such processes is usually accumulated in melts or successively enters biotites and amphiboles (Markl and Piazolo 1998). The distinct behavior of the two halogens is well-recorded in the f_{H_2O}/f_{HCl} and f_{H_2O}/f_{HF} ratios in both the magmatic rocks and in the surrounding metamorphic rocks (Markl and Piazolo 1998; Harlov et al. 2006, 2014). Fluid assisted partial melting should cause the fluid salinity to increase due to preferential partitioning of H_2O into the melt phase (Shmulovich and Graham 1996; Aranovich et al. 2013, 2014; Manning and Aranovich 2014). This mechanism has been invoked by Safonov et al. (2012) to explain variations in the alkali activity related to chloride-bearing fluids during the evolution of dehydration zones in the Sand River gneisses of the Central Zone of the Limpopo Complex (South Africa), as well as the higher Cl contents in biotites, amphiboles, and apatites (at nearly constant F content) within the dehydration zones in comparison to the host gneiss (e.g., Rajesh et al. 2013, 2014).

11.5 Alkali Halides Activity Estimates

Chlorine and F contents in biotite, amphibole, and apatite have been widely used to estimate the corresponding acid (HCl or HF) to water fugacity ratio in a (hypothetical) coexisting fluid phase. This approach is based on the consideration of equilibrium constants for schematic exchange reactions of the form:

$$A(F \text{ or } Cl)_2 + 2H_2O = A(OH)_2 + 2H(F \text{ or } Cl), \tag{11.7}$$

where A stands for biotite, tremolite, or apatite. As an example, the F–OH exchange between fluid and biotite is expressed as:

$$KMg_3AlSi_3O_{10}(F)_2 + 2H_2O = KMg_3AlSi_3O_{10}(OH)_2 + 2HF, \tag{11.8}$$

$$\ln(f_{H_2O}/f_{HF}) = (\Delta G^0(6)/(2 * RT) + \ln[a(\text{OH-Phl})/a(\text{F-Phl})] \tag{11.9}$$

where a_i is the activity of a component i in a biotite solid solution and f_i is the fugacity of a component i in a fluid.

Using an empirical calibration of the right hand side of equation (11.9), as a function of temperature and biotite composition according to Munoz (1984), Valley et al. (1982, 1990) and Lamb and Valley (1988) deduced a significantly heterogeneous HF fugacity in orthogneisses and marbles from the Adirondacks, New York. They interpreted it as reflecting variable initial F contents in the above rocks from the complex, which locally buffered f_{F2} in the initially F-free fluid interacting with the rocks. More rigorous calculations, based on the thermodynamic systematics by Zhu and Sverjensky (1992), have shown that variations in the halogen content of biotite and amphibole might be caused by variations in the minerals'

Mg/(Mg + Fe) ratio at a more or less constant halogen fugacity in the fluid phase (Zhu et al. 1994), or resulted from the evolution of a single fluid induced by interaction with the host rocks (Kusebauch et al. 2015).

In any event, HF and HCl are expected to be but minor ingredients in the high-grade fluid phase. From a petrogenetic standpoint, it appears that reconstructions of the activity (concentration) of the much more abundant alkali halides, which in large part define the water activity potential for melting, metasomatism, and the homogeneity range of natural deep-seated fluids are much more important (Aranovich and Newton 1996, 1997; Manning and Aranovich 2014). A number of net-transfer reactions, which relate the halogen-bearing end-members of biotite, amphibole, and scapolite with other rock-forming amphibolite- and granulite-facies minerals, have been proposed as a means of estimating the activity of alkali halides in the fluid phase (Zhu et al. 1994; Newton et al. 1998; Markl et al. 1998; Kusebauch et al. 2015).

Korikovskii and Aranovich (2015) described a charnockite assemblage orthopyroxene + biotite + garnet + plagioclase + K-feldspar + quartz containing biotite with up to 1.3 wt.% F (and very low Cl < 0.06 wt.%) from the Lapland granulite belt, Kola Peninsular, Russia (Fig. 11.10). They related the F-phlogopite

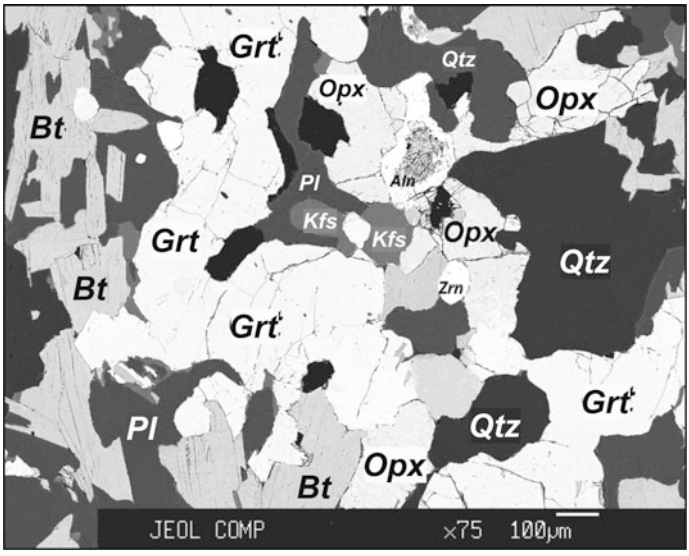

Fig. 11.10 BSE image showing the textural relations between minerals in sample 292-21 (Lapland granulite belt; Korikovskii and Aranovich 2015), which contains biotite with 0.92 wt.% F and X_{Fe} = Fe/(Fe + Mg) = 0.56. *Aln* allanite, *Bt* biotite, *Grt* garnet, *Kfs* K-feldspar, *Opx* orthopyroxene, *Pl* plagioclase, *Qtz* quartz, *Zrn* zircon

in the biotite solid solution with the KF in a (hypothetical) fluid phase (*fl*) via the following reactions:

$$KMg_3AlSi_3O_{10}F_2 + KAlSi_3O_8 = 3MgSiO_3 + Al_2O_3 + 3SiO_2 + 2KF(fl) \quad (11.10)$$

F-phlogopite (in biotite) + K- feldspar
= enstatite (in orthopyroxene) + aluminioOpx (in orthopyroxene) + quartz

$$KMg_3AlSi_3O_{10}F_2 + KAlSi_3O_8 = Mg_3Al_2Si_3O_{12} + 3SiO_2 + 2KF(fl) \quad (11.11)$$

F-phlogopite (in biotite) + K-feldspar = pyrope (in garnet) + quartz

The advantage of using reactions, like (11.10) and (11.11) over (11.8), is that they allow for direct estimates of the alkali halide activity values rather than the $f_{H_2O}/f_{HF(Cl)}$ ratios. Standard thermodynamic properties of the F-phlogopite and F-annite end-members, adjusted from Zhu and Sverjensky (1992) to make them consistent with the Berman et al. (2007) properties for the OH end members and reciprocal solution model for the F-bearing biotite solid solution (Aranovich 1983; Zhu and Sverjensky 1992), were used in the calculations (Korikovskii and Aranovich 2015). Standard thermodynamic properties for molten KF (chosen as the standard state following the approach by Aranovich and Newton (1996, 1997) for alkali chloride solutions) were taken from the National Institute of Standards (NIST) website (http://webbook.nist.gov/cgi/cbook.cgi?Formula=kf). Thermodynamic properties for other phases involved in the reactions (both standard and mixing) were taken from Berman and Aranovich (1996; DEC06 update). Results of these calculations, using the TWQ software (Berman 2007), are shown in Fig. 11.11. At the T–P parameters obtained for this sample (780 °C and 8.7 kbar; Korikovskii and Aranovich 2015), the resulting a_{KF}, (corresponding to the intersection of isopleths in Fig. 11.11), is around 0.002. This value could have been readily converted into the concentration of KF in the fluid if the activity-composition relations of the alkali fluorides in aqueous solutions at high T–P were known.

Reactions similar to (11.10) and (11.11):

$$KFe_3AlSi_3O_{10}Cl_2 + KAlSi_3O_8 = 3FeSiO_3 + Al_2O_3 + 3SiO_2 + 2KCl(fl) \quad (11.12)$$

Cl-annite (in biotite) + K-feldspar = ferrosilite (in orthopyroxene)
+ aluminioOpx (in orthopyroxene) + quartz

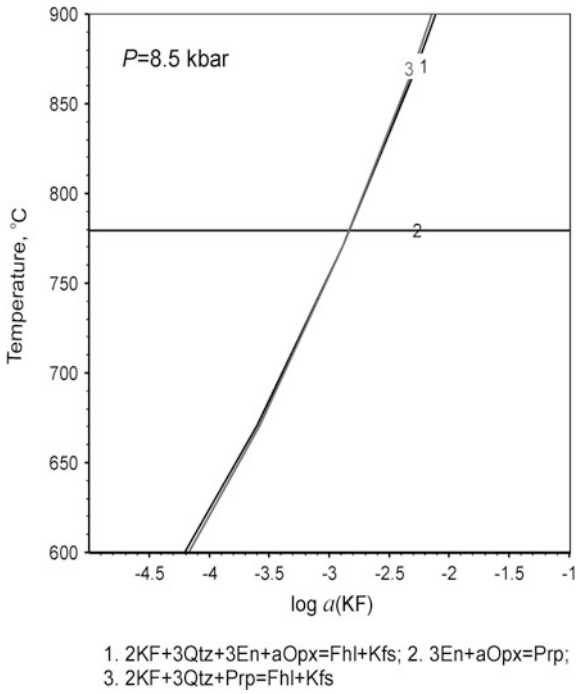

Fig. 11.11 Isobaric temperature versus a_{KF} diagram showing compositional isopleths of minerals in sample 292-21 (Fig. 11.10; Korikovskii and Aranovich 2015), which was calculated using the WinTWQ software (Berman 2007). Intersection of the curves corresponds to equilibrium conditions. Numbered curves correspond to the mineral reactions shown below the diagram. *aOpx* alumino-orthopyroxene end-member (Al_2O_3), *En* enstatite, *Fhl* F-phlogopite, *Kfs* K-feldspar, *Prp* pyrope, *Qtz* quartz

$$KFe_3AlSi_3O_{10}Cl_2 + KAlSi_3O_8 = Fe_3Al_2Si_3O_{12} + 3SiO_2 + 2KCl(fl) \quad (11.13)$$

Cl-annite (in biotite) + K-feldspar = almandine (in garnet) + quartz

have been used (Newton et al. 1998) to evaluate the KCl activity, (relative to the molten KCl standard state, Aranovich and Newton 1997), attained during the formation of a K-feldspar-quartz-plagioclase–orthopyroxene–garnet-biotite granulite from the Shevaroy Hills, northern Tamil Nadu, India (sample 93-F6-X3 from Hansen et al. 1995). According to geothermobarometry estimates, the assemblage equilibrated at around 780 °C, 7.5 kbar, and $a_{H_2O} = 0.5$ (see Fig. 11.6 in Newton et al. 1998). Applying thermodynamic data (both standard and mixing) for Cl-annite from Zhu and Sverjensky (1991), along with the data for the other minerals involved in reactions (11.12) and (11.13) according to Berman and Aranovich (1996) and the measured compositions of the coexisting minerals from Hansen et al. (1995), the calculated a_{KCl} comes out to be 0.036. Assuming that the fluid phase is a H_2O–(Na,K)Cl brine with K/(K + Na) = 0.2, which corresponds to the plagioclase-alkali feldspar equilibrium, the composition of the fluid phase was reconstructed as $X_{H_2O} = 0.66$, $X_{KCl} = 0.07$, and $X_{NaCl} = 0.27$ (Newton et al. 1998)

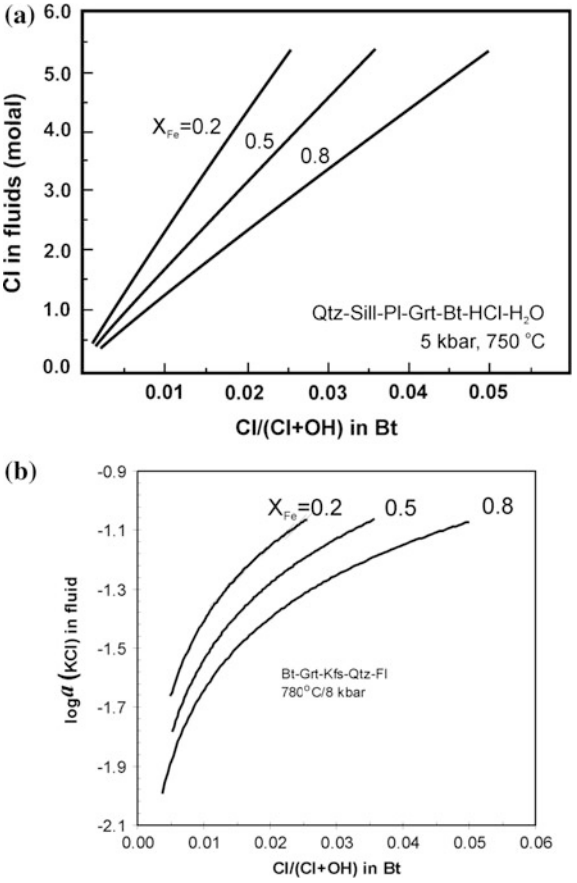

Fig. 11.12 Concentration of Cl (**a**) and KCl activity (**b**) in a fluid phase in equilibrium with biotite, which has variable Cl/(Cl + OH) and X_{Fe} (numbered curves) calculated for the assemblages Qtz–Sil–Pl–Grt–Bt–HCl–H_2O at 5 kbar and 750 °C (**a**) (modified after Zhu et al. 1994) and Bt–Grt–Kfs–Qtz–Fl at 8 kbar and 780 °C (**b**). Analytical data for garnet and K-feldspar in (**b**) after Hansen et al. (1995) (sample 93-F6X3). *Bt* biotite, *Grt* garnet, *Kfs* K-feldspar, *Opx* orthopyroxene, *Pl* plagioclase, *Qtz* quartz, *Sill* sillimanite, *Fl* fluid

based on the activity-composition relations in the H_2O–NaCl–KCl solutions from Aranovich and Newton (1997).

Zhu et al. (1994) employed the thermodynamic systematics by Zhu and Sverjensky (1992) to calculate Cl concentrations in a metamorphic fluid, which could coexist with a representative mineral assemblage from a typical granulite-facies metapelite containing biotite with variable Fe and Cl (Fig. 11.12a). One important point reflected in Fig. 11.12a is that relatively Mg-rich, Cl-poor biotite, with a Cl/(Cl + OH) ratio as low as 0.015, which corresponds to about 0.2 wt.% Cl in biotite, may coexist with a fairly Cl-rich fluid (up to 4 molal, Fig. 11.12a). Calculations for the assemblage relevant to reaction (11.13), (done for illustrative purposes only, as garnet in equilibrium with biotite of variable X_{Fe} at fixed T–P conditions cannot have a constant composition, and hence activity), demonstrate similar (and rather counterintuitive) relationships. That is, relatively high values of a_{KCl} in the fluid phase, which is in equilibrium with the Cl-poor biotite, garnet, K-feldspar, and quartz (Fig. 11.12b). It is worth noting that

phlogopite experimentally equilibrated with a very concentrated KCl solution (X_{KCl} = 0.37–0.39) in the presence of enstatite, sanidine, and quartz at 850 °C and 10 kbar, did not contain more than 0.13 wt.% Cl (Aranovich and Newton 1998).

11.6 Alkali Metasomatism and Granitization Involving Halogen-Bearing Fluids

Fluid inclusions usually containing dissolved NaCl and KCl and, more rarely, NaF and KF as daughter crystals, and intergranular high-temperature (Na, K)Cl phases in granulites (e.g., Markl and Bucher 1998), indicate that Cl and F in the poly-ionic aqueous solutions and brines, which interacted with high-grade metamorphic rocks, are predominantly bound to K and Na (Aranovich and Newton 1996, 1997; Newton et al. 1998; Graham and Yardley 2002; Newton and Manning 2010; Touret and Nijland 2013; Aranovich et al. 2013, 2014; Manning and Aranovich 2014). Common formation of Cl- and F-bearing biotite, amphibole, and mariolitic scapolite, during interaction of metamorphic rocks with fluids, also manifests the affinity of halogens for K and Na in the fluids. Following Korzhinskii's (1946, 1962) concept of "perfect mobility of alkalis during metamorphism and granite formation", the K and Na activities, similar to the conventional intensive variables (e.g., T, P, a_{H_2O}), should also be recorded in the regular changes in mineral assemblages, zoning patterns of minerals, and reaction textures, and, correspondingly, expressed in mineral-fluid reactions controlled by those activities. Korzhinskii (1946, 1962) proposed a number of mineralogical criteria to evaluate the influence of K and Na activities in fluids on mineral assemblages from granitic and syenitic rocks. They have been later supported and supplemented by Perchuk and co-authors (Perchuk and Gerya 1992, 1993; Perchuk et al. 1994, 2000), who related specific textural relations and regular compositional trends in coexisting biotite, orthopyroxene, hornblende, and plagioclase to the development of K-feldspar micro-veins due to fluid–rock interaction in charnockitic gneisses. Subsequently, similar mineral relations have been reported from many high-grade terrains and granulite xenoliths (a compilation of this data can be found in Safonov and Aranovich (2014)). In many cases (although, not always) the reaction textures indicative of K and Na activities are associated with halogen-bearing phases and/or saline fluid inclusions. Thus, specific textures in the rocks, which reflect fluid-mineral reactions controlled by K and Na activities (Safonov and Aranovich 2014), could serve as additional markers for identifying the action of halogen-bearing fluids. For example, reaction rims of Cl-rich hornblende, presented in Figs. 11.8 and 11.9, are associated with the replacement of plagioclase by K-feldspar, which results from a well-known exchange reaction (Iiyama 1965; Orville 1963; Aranovich et al. 2013):

$$\text{Albite} + \text{KCl} = \text{Orthoclase} + \text{NaCl}, \tag{11.14}$$

This reaction may be a part of a more complex set of reactions involving plagioclase:

$$\text{nAnorthite}(1-\text{n})\text{Albite} + \{m\text{KCl}\} = \text{nAnorthite} * (1-n-m)\text{Albite} + m\text{Orthoclase} + \{m\text{NaCl}\} \tag{11.15}$$

$$\text{nAnorthite}(1-\text{n})\text{Albite} + 4\text{nQuartz} + (\text{m} + 2\text{n})\text{KCl} = (1-\text{n} - \text{m})\text{Albite}(\text{m} + 2\text{n})\text{Orthoclase} + \{\text{nCaCl}_2 + \text{mNaCl}\}. \tag{11.16}$$

Reactions (11.14) and (11.15) represent Korzhinskii's (1946) criterion for variations in the K and Na activities in fluids, i.e. the higher the anorthite content of the plagioclase coexisting with K-feldspar, the higher the K activity corresponding to this assemblage. Perchuk and Gerya (1992, 1993) and Perchuk et al. (1994) documented textural and compositional evidence for reaction (11.15) in high-grade metamorphic rocks. Here they observed an increase in the anorthite content of plagioclase in contact with the K-feldspar micro-veins. Reactions (11.15) and (11.16) are a schematic representation of the coupled dissolution/reprecipitation mechanism behind feldspar-chloride fluid reactions. This results in a sharp compositional contact between the initial and new phase; weak compositional zoning in both phases; varying degrees of porosity in the newly formed K-feldspar micro-veins and Ca-enriched plagioclase grain rims (Labotka et al. 2004; Putnis and Austrheim 2013); and the formation of myrmeckitic plagioclase-quartz (Perchuk et al. 2000; Touret and Huizenga 2011; Touret and Nijland 2013; Rajesh et al. 2013) or plagioclase-albite (Harlov and Wirth 2000) intergrowths associated with K-feldspar micro-veins.

Reactions (11.14)–(11.16) constrain the a_{KCl}/a_{NaCl} ratio in the fluids, but do not allow for the comparison of individual activities for mineral assemblages containing alkali feldspars. Such a comparison can be performed using additional net-transfer reactions involving Fe–Mg minerals (see previous paragraph) and two criteria: (1) the more "basic" (i.e. with less polymerized structure) and the "higher the temperature" Fe–Mg (alumino)silicate coexists with K-feldspar (sodic plagioclase), the higher the K (Na) activity corresponding to this assemblage (Korzhinskii 1946); and (2) the lower the Al content in the Fe–Mg mineral coexisting with K-feldspar (sodic plagioclase), the higher the K (Na) activity in the fluid (Perchuk and Gerya 1992). Utilizing these criteria, the "K (Na) activities" can be specified as KCl (KF) and NaCl (NaF) activities for halogen-bearing fluids (Safonov and Aranovich 2014; Korikovskii and Aranovich 2015). Safonov and Aranovich (2014) reviewed

various reactions controlled by the activities of these alkali species in fluids believed to be present in the amphibolite- and granulite-facies rocks. They then used them to estimate variations in alkali activities in specific examples of charnockite formation in gneisses from South Africa, Sri Lanka, and Southern India. Some of these reactions have been reproduced in experiments on the interaction between natural rocks and alkali chloride-bearing fluids (Harlov 2004; Khodorevskaya 2004; Larikova and Zaraisky 2009; Safonov et al. 2014b; Khodorevskaya and Aranovich 2016).

Figure 11.13a shows an example of a clinopyroxene-K-feldspar reaction texture developed in an amphibole–biotite gneiss in the vicinity of charno-enderbite veins at the Causeway locality, Limpopo Complex, South Africa. Based on a fluid inclusion study and Cl variations in biotite and hornblende, Safonov et al. (2012) and Rajesh et al. (2013) explained the formation of this assemblage by reactions of biotite and plagioclase with alkali chloride-bearing H_2O–CO_2 fluids:

$$\begin{aligned}\text{Biotite} + 3\,\text{Anorthite (in Plagioclase)} + 18\,\text{Quartz} + 6\,\text{KCl} + 2\text{H}_2\text{O} \\ = 3\,\text{Clinopyroxene} + 7\,\text{K-feldspar} + 6\,\text{HCl}.\end{aligned} \tag{11.17}$$

As a support for this conclusion, Safonov et al. (2014b) have reproduced the clinopyroxene-K-feldspar reaction textures, accompanied by extensive replacement of plagioclase with K-feldspar, along grain boundaries in experiments, which involve the interaction of the gneiss with H_2O–CO_2–KCl and H_2O–CO_2–(K, Na)Cl fluids at 550 MPa and 750 and 800 °C (Fig. 11.13b). At 800 °C, the clinopyroxene-K-feldspar assemblage is observed only at $X_{chloride}$ above ~0.01 indicating that this assemblage corresponds to the highest activities of KCl in the fluid. Harlov (2004) reported similar relationships in experiments involving the partial dehydration of a tonalite biotite gneiss, which interacted with KCl-bearing fluids at 1000 MPa and 900 °C.

The extraction of Ca from plagioclase can result in the formation of a grossular-rich garnet and K-feldspar after plagioclase (Safonov 1998; Safonov and Aranovich 2014). In the presence of KCl solutions, this reaction can be written as:

$$\begin{aligned}\text{Anorthite (in Plagioclase)} + 3\,\text{Quartz} + 4/3\,\text{KCl} + 2/3\,\text{H}_2\text{O} \\ = 1/3\,\text{Grossular (in Garnet)} + 4/3\,\text{K-feldspar} + 4/3\,\text{HCl}.\end{aligned} \tag{11.18}$$

As an illustration of reaction (11.18), Fig. 11.14a shows the growth of garnet containing up to 30 mol.% grossular in a K-feldspar-apatite vein cross cutting a plagioclase crystal in a meta-anorthosite from the Adirondack Complex, USA (Safonov 1998). Hansen et al. (1995) noted an increase in the grossular content in garnet towards the contact with K-feldspar micro-veins riming the garnet in the

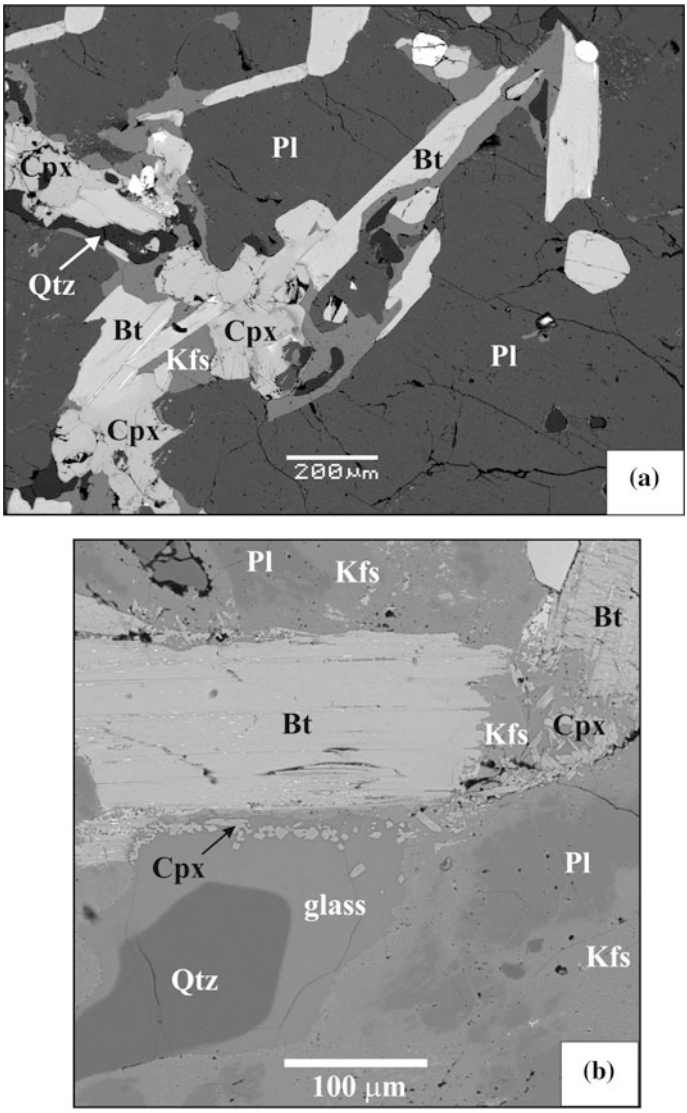

Fig. 11.13 A clinopyroxene-K-feldspar assemblage, formed by the decomposition of biotite interacting with the chloride-rich fluids, which resulted in a high K activity. **a** Clinopyroxene-K-feldspar assemblage in a partially dehydrated, biotite-hornblende gneiss from the Causeway locality, Limpopo Complex, South Africa (Rajesh et al. 2013; Safonov et al. 2012); **b** The experimentally reproduced decomposition of biotite in a biotite-hornblende gneiss from the Causeway locality during its interaction with a H_2O–CO_2–KCl fluid at 550 MPa and 800 °C (Safonov et al. 2014b)

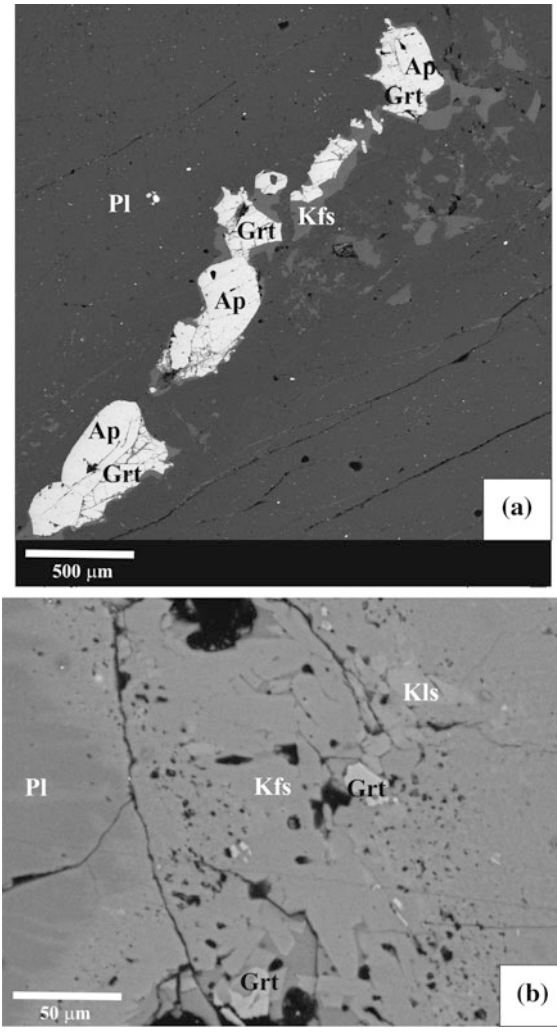

Fig. 11.14 Grossular-rich garnet as a product of plagioclase decomposition, which interacted with chloride-rich fluids. **a** Garnet in the apatite-K-feldspar vein truncating a K-feldspathized plagioclase crystal in a meta-anorthosite from the Adirondack Complex, USA (Safonov 1998). Bright small inclusions in plagioclase are magnetite. **b** Grossular-rich garnet in an assemblage with kalsilite, which formed due to strong K-feldspathization of plagioclase, during interaction with a H_2O–CO_2–KCl fluid at 800 °C and 550 MPa (Safonov et al. 2014b)

Shevaroy Hills charnockites, southern India. It is accompanied by an increase in the anorthite content of the plagioclase and a decrease in the Al content in the coexisting orthopyroxene, which is in accordance with the above criteria by Korzhinskii (1946, 1962) and Perchuk and Gerya (1992, 1993). Safonov et al. (2014b) observed the formation of grossular-rich garnet during strong K-feldspathisation of plagioclase in experiments involving the interaction of a biotite-hornblende gneiss with H_2O–CO_2–KCl fluids at 800 °C and 550 MPa (Fig. 11.14b). Larikova and Zaraisky (2009) observed efficient growth of grossular-rich garnet after plagioclase in the presence of 0.1 M NaCl aqueous solution at 670 and 700 °C and 500 MPa.

The K-feldspar forming reactions are characteristic for plagioclase-dominated assemblages. Biotite becomes a phase indicative of alkali activity (at least K) in peraluminous Mg-rich metapelitic assemblages. Reaction intergrowths of biotite + quartz, (with or without aluminosilicate), after cordierite–garnet -aluminous orthopyroxene assemblages, which initially did not contain K-feldspar, are common in high-grade metapelites. Taking into account the presence of chloride-bearing fluids, these textures can be interpreted in terms of the reaction:

$$\begin{aligned} 3/2\ \text{Cordierite} + 2/3\ \text{KCl} + \text{H}_2\text{O} &= 2/3\ \text{Biotite} + 5/3\ \text{Sillimanite} \\ &\quad + 4/3\ \text{Quartz} + 2/3\ \text{HCl} \end{aligned} \tag{11.19}$$

Figure 11.15 shows biotite (+corundum and a small amount of glass) after cordierite and Al-rich orthopyroxene experimentally produced in a metapelite, which interacted with a H_2O–CO_2–KCl fluid (X_{KCl} = 0.006) at 850 °C and 600 MPa. Even very modest concentrations of KCl in the fluid are sufficient to produce biotite after cordierite. K-feldspar appears in this assemblage approximately at $X_{KCl} > 0.02$. It is interesting to note that the interaction of cordierite with a H_2O–CO_2–NaCl fluid, at similar P–T parameters, results in the formation of Na-bearing biotite (the aspidolite–phlogopite solid solution) in the assemblage with spinel and albite (or glass), whereas reactions of cordierite with orthopyroxene, in the presence

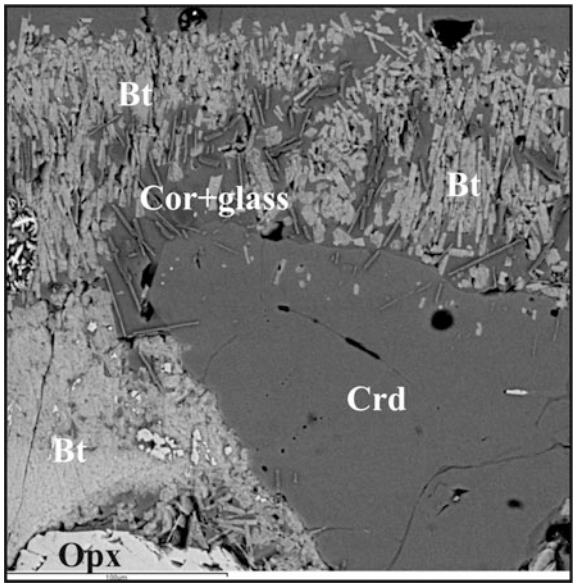

Fig. 11.15 Fringes of biotite (+corundum and a small amount of glass) replacing cordierite and Al-bearing orthopyroxene produced during interaction of a peraluminous metapelite with a H_2O–CO_2–KCl fluid (X_{KCl} = KCl/(KCl + H_2O + CO_2) = 0.0059) at 800 °C and 600 MPa

of this fluid, results in the formation of Na-bearing gedrite (O. Safonov, unpublished data).

Formation of phlogopite, due to an increase in the KCl activity in an aqueous fluid, can also be expected for metaperidotitic assemblages. Safonov and Butvina (2013) experimentally showed that garnet, spinel, and pargasite–edenite amphibole, in association with Al-bearing orthopyroxene, are unstable in the presence of H_2O–KCl fluids, and are replaced by Cl-bearing phlogopite (0.4–1.1 wt.% Cl) at 1900 MPa and 900–1200 °C. For example, for the assemblage orthopyroxene-spinel, which is relevant in meta-ultrabasic rocks, the reactions are as follows:

$$5\ \text{Enstatite} + \text{Mg-Tschermakite} + H_2O + 2KCl = \text{Cl-Phlogopite} + \text{Phlogopite} \quad (11.20)$$

$$\text{Spinel} + 7\ \text{Enstatite} + H_2O + 2KCl = \text{Phlogopite} + \text{Cl-Phlogopite} + \text{Forsterite} \quad (11.21)$$

Although the experiments by Safonov and Butvina (2013) were performed at conditions relevant to the upper mantle, their results could be confidently applied to lower-crustal HT–UHT metamorphic processes.

Reactions (11.14)–(11.18) can also be named "granitization reactions" in the sense of Korzhinskii (1962) as their operation may induce melting under the appropriate $P - T - a_{H_2O}$ conditions with production of granitic melts. In fact, melting accompanies these reactions in the experimental products (Figs. 11.13b, 11.14b, 11.15). For example, a shift of reaction (11.15) to the right due to influx of a fluid with an elevated a_{KCl} (relative to the parental rock), leads to the formation of an alkali feldspar, thus decreasing the melting temperature of the resulting assemblages by 30–100 °C, depending on the final anorthite content of plagioclase (Johannes 1984). Additionally, reactions (11.17)–(11.19) generate HCl in the fluid phase, which is capable of efficiently dissolving Fe–Mg minerals from the host rocks ("leucocratization"), thus further supporting melting (Azimov and Bushmin 2007). It is interesting to note that a shift of reaction (11.16) to the left may also facilitate melting of the originally quartz-free rocks, as the appearance of quartz lowers the melting temperature more significantly than an increase in the anorthite content of plagioclase elevates it (compare curves III and V in Fig. 11.8 of Johannes 1984). Similarly, in the originally quartz- and alkali feldspar-free rocks, granitization can be caused by the influx of a fluid, with a relatively increased a_{CaCl_2}/a_{NaCl} ratio, due to the quartz-forming reaction (Orville 1972; Shmulovich and Graham 2008):

$$2\ \text{Albite} + CaCl_2 = \text{Anorthite} + 4\ \text{Quartz} + 2NaCl \quad (11.22)$$

To illustrate this effect, we have calculated melting curves for plagioclase with and without quartz in the presence of an H_2O–CO_2 fluid with $X_{H_2O} = 0.5$ at 5 kbar (Fig. 11.16). Thermodynamic calculations were done with the mineral thermodynamic data, including solution properties for plagioclase, implemented in the

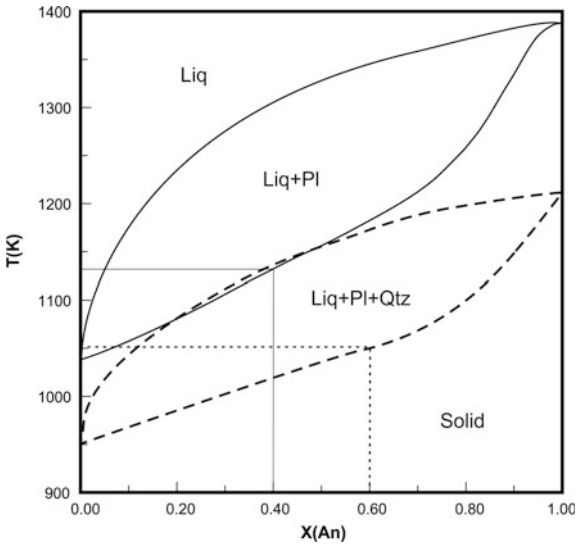

Fig. 11.16 Calculated melting curves of plagiocalse (bold) and plagiocalse + quartz (dashed) at a total pressure of 5 kbar and $X_{H_2O}= H_2O/(H_2O + CO_2) = 0.5$. Melting temperature of the An_{40} composition (*bold straight line*) is about 80° higher than An_{60}+Qtz (*dashed straight line*). See text for discussion

PERPLE_X software by Connolly (2005), and the melt model from White et al. (2007). It can be seen that plagioclase An_{40} melts at a temperature about 80 °C higher than An_{60} in the presence of quartz, which forms via reaction (11.22).

11.7 Concluding Remarks

1. Halogen-bearing minerals are commonly present in high-grade metamorphic rocks whose bulk composition ranges from metapelite to calc-silicate to meta-ultramafics. Halogen substitution for OH-groups significantly expands the stability of hydrous minerals to higher temperatures. Elevated halogen content in some granulite-grade micas and amphiboles has most often been considered to be the result of halogen accumulation, which is accompanied by a continuous decrease in the amount of the corresponding mineral with increasing temperature. This notion, based on the assumption of a closed system style of high grade metamorphism, is, however, at odds with some major compositional correlations, textural relations, and recent thermodynamic calculations that all point to the involvement of an exotic halogen-bearing media (fluids or melts) during high grade rock-forming processes.
2. The partitioning of halogens between biotite and amphibole is almost insensitive to both compositional variations in terms of major oxides and temperature, thus pointing to a small change in enthalpy for the corresponding exchange reactions and very similar mixing properties for the halogen- and OH-bearing species in both minerals. Partitioning of F and Cl between apatite and biotite shows a large

scatter, which reflects its sensitivity to both Fe–Mg compositional variations in biotite (X_{Fe}) and temperature.

3. Existing thermodynamic calibrations allow for at least a semi-quantitative evaluation of the activity (concentration) of halogen-bearing species in the fluid phase from the known amount of halogen(s) in the biotite, given that the appropriate mineral assemblage is present in the rock. Calculations predict that, for some assemblages, the resulting total Cl or KCl concentration in the fluid may be significant, even for low concentrations of Cl in biotite, which emphasizes the importance of analyzing biotite for Cl.
4. Thermodynamic properties of halogen-bearing amphiboles are much less known (with the exception of F-tremolite), and further experimental studies are necessary to include this mineral in a quantitative analysis of halogen behavior during granulite-facies metamorphism. This is particularly true for the K-enriched amphiboles because there appears to be a strong positive K–Cl correlation in amphibole. No thermodynamic model exists for halogen species in aluminosilicate melts, although empirical models, which predict the Cl content of melts as a function of pressure, temperature, and melt composition, have recently been developed (Webster et al. 2015, 2018).
5. Interaction of rocks with halogen-bearing fluids, which contain alkalis and Ca, may cause pronounced metasomatic transformations involving major Fe–Mg and felsic minerals, which may result in melting under appropriate $P-T-a_{H_2O}$ conditions.

Acknowledgments We thank Kostya Podlesskii for providing thin section of the granulite sample from Aldan (Fig. 11.7). The editor D.E. Harlov is thanked for his help and patience. Helpful suggestions and comments by Bill Glassley, Kåre Kullerud and Brian Tattitch helped to improve this chapter. Financial support for this study was provided by Russian Scientific Fund (grant 14-17-00581) and partially by Russian Foundation for Basic Research (grants 15-05-01053 and 16-05-00266).

References

Antignano A, Manning CE (2008) Fluorapatite solubility in H_2O and H_2O–NaCl at 700 to 900 °C and 0.7 to 2.0 GPa. Chem Geol 251:112–119

Aranovich LY (1983) Biotite–garnet equilibria in metapelites: I. Thermodynamics of solid solutions and end-member reactions. In: Zharikov VA (ed) Contributions to physico-chemical petrology, vol 11. Nauka, Moscow, pp 121–136 (in Russian)

Aranovich LY (1991) Mineral equilibria of multicomponent solid solutions. Nauka, Moscow, 253 p (in Russian)

Aranovich LY, Newton RC (1996) H_2O activity in concentrated NaCl solutions at high pressures and temperatures measured by the brucite-periclase equilibrium. Contrib Mineral Petrol 125:200–212

Aranovich LY, Newton RC (1997) H_2O activity in concentrated KCl and KCl–NaC1 solutions at high temperatures and pressures measured by the brucite-periclase equilibrium. Contrib Mineral Petrol 127:261–271

Aranovich LY, Newton RC, Manning CE (2013) Brine-assisted anatexis: experimental melting in the system haplogranite–H_2O–NaCl–KCl at deep-crustal conditions. Earth Planet Sci Lett 374:111–120

Aranovich LY, Makhluf AR, Manning CE et al (2014) Dehydration melting and the relationship between granites and granulites. Precambr Res 253:26–37

Azimov PY, Bushmin SA (2007) Solubility of minerals of metamorphic and metasomatic rocks in hydrothermal solutions of varying acidity: thermodynamic modeling at 400–800 °C and 1–5 kbar. Geochem Int 45:1210–1234

Belyanin GA, Kramers JD, Vorster C et al (2014) The timing of successive fluid events in the Southern Marginal Zone of the Limpopo Complex, South Africa: constraints from ^{40}Ar–^{39}Ar geochronology. Precambr Res 254:169–193

Berman RG (2007) WinTWQ (version 2.3): a software package for performing internally-consistent thermobarometric calculations. Geological Survey of Canada Open File 5462

Berman RG, Aranovich LY (1996) Optimized standard state and solution properties of minerals: I. Model calibration for olivine, orthopyroxene, cordierite, garnet, and ilmenite in the system FeO–MgO–CaO–Al_2O_3–TiO_2–SiO_2. Contrib Mineral Petrol 126:1–22

Berman RG, Aranovich LY, Rancourt P et al (2007) Reversed phase equilibrium constraints on the stability of Mg–Fe–Al biotite. Am Mineral 92:139–150

Bohlen SR, Essene EJ (1978) The significance of metamorphic fluorite in the Adirondacks. Geochim Cosmochim Acta 42:1669–1678

Bohlen SR, Boettcher AL, Wall VI et al (1983) Stability of phlogopite–quartz and sanidine–quartz: A model for melting in the lower crust. Contrib Mineral Petrol 83:270–277

Bose S, Das K, Fukuoka M (2005) Fluorine content of biotite in granulite-grade metapelitic assemblages and its implications for the Eastern Ghats granulites. Eur J Mineral 17:665–674

Carswell DA, Wilson RN, Zhai M (1996) Ultra-high pressure aluminous titanites in carbonate bearing eclogites at Shuanghe in Dabieshan, Central China. Mineral Mag 60:461–471

Castelli D, Rubatto D (2002) Stability of Al- and F-rich titanite in metacarbonate: petrologic and isotopic constraints from a polymetamorphic eclogitic marble of the internal Sesia Zone (Western Alps). Contrib Mineral Petrol 14:627–639

Chernosky JV, Berman RG, Jenkins DM (1998) The stability of tremolite: new experimental data and a thermodynamic assessment. Am Mineral 83:726–739

Chevychelov VY, Botcharnikov RE, Holtz F (2008) Experimental study of fluorine and chlorine contents in mica (biotite) and their partitioning between mica, phonolite melt, and fluid. Geochem Int 46:1081–1089

Connolly JAD (2005) Computation of phase equilibria by linear programming: a tool for geodynamic modeling and its application to subduction zone decarbonation. Earth Planet Sci Lett 236:524–541

Dachs E, Harlov D, Benisek A (2010) Excess heat capacity and entropy of mixing along the chlorapatite–fluorapatite binary join. Phys Chem Mineral 37:665–676

De Maesschalck AA, Touret JLR, Maaskant P, Dahanayake K (1991) Petrology and fluid inclusions in garnetiferous gneisses and charnockites from Weddagala (Ratnapura district, Sri Lanka). J Geol 99:443–456

Dolgov YA, Tomilenko AA, Chupin VP (1976) Inclusions of hydrosaline melts -brines in quartz from deep-seated granites and pegmatites. Doklady AN SSSR 226:938–941 (in Russian)

Dooley DF, Patiño Douce AE (1996) Fluid-absent melting of F-rich phlogopite + rutile + quartz. Am Mineral 81:202–212

Ekström TK (1972) The distribution of fluorine among some coexisting minerals. Contrib Mineral Petrol 34:192–200

Ellis DE (1978) Stability and phase equilibria of chloride and carbonate bearing scapolites at 750 °C and 4000 bar. Geochim Cosmochim Acta 42:1271–1281

Enami M, Suzuki K, Liou JG et al (1993) Al–Fe^{3+} and F–OH substitutions in titanite and constraints on their P–T dependence. Eur J Mineral 5:219–231

Eugster HP, Protska HJ (1960) Synthetic scapolites. Geol Soc Am Bull 71:1859–1860

Foley SF, Taylor WR, Green DH (1986) The effect of fluorine on phase relationships in the system $KAlSiO_4$-Mg_2SiO_4-SiO_2 at 28 kbar and the solution mechanism of fluorine in silicate melts. Contrib Mineral Petrol 93:46–55

Franz G, Spear FS (1985) Aluminous sphene (titanite) from the eclogite Zone, south-central Tauern window, Austria. Chem Geol 50:33–46

Gilbert MC, Helz RT, Popp RK, Spear FL (1982) Experimental studies of amphibole stability. In: Veblen DR, Ribbe PH (eds) Amphibole and other hydrous pyriboles, vol 9B. Mineralogical Society of America, Washington, DC, pp 229–353

Gomez-Pugnaire MT, Franz G, Sanchez-Vizcaino VL (1994) Retrograde formation of NaCl-scapolite in high pressure metaevaporites from Cordilleras Beticas (Spain). Contrib Mineral Petrol 116:448–461

Graham CM, Navrotsky A (1986) Thermochemistry of the tremolite-edenite amphiboles using fluorine analogues, and applications to amphibole-plagioclase-quartz equilibria. Contrib Mineral Petrol 93:18–32

Graham JT, Yardley BWD (2002) The origins of salinity in metamorphic fluids. Geofluids 2:249–256

Grew ES (1982) Osumilite in the sapphirine-quartz terrane of Enderby Land, Antarctica: implications for osumilite petrogenesis in the granulite facies. Am Mineral 67:762–787

Grew ES, Yates MG, Barbier J et al (2000) Granulite-facies beryllium pegmatites in the Napier Complex in Khmara and Amundsen Bays, western Enderby Land, East Antarctica. Polar Geosci 13:1–40

Hammerli J, Rubenach M (2018) The role of halogens during regional and contact metamorphism. In: Harlov DE, Aranovich L (eds) The role of halogens in terrestrial and extraterrestrial geochemical processes: surface, crust, and mantle. Springer, Berlin, pp 649–712

Hansen EC, Harlov DE (2007) Whole-rock, phosphate, and silicate compositional trends across an amphibolite- to granulite-facies transition, Tamil Nadu, India. J Petrol 48:1641–1680

Hansen EC, Newton RC, Janardhan AS et al (1995) Differentiation of late Archean crust in the Eastern Dharwar Craton, South India. J Geol 103:629–651

Harlov DE (2004) Fluid induced dehydration of mafic lower crust from amphibolite to granulite facies: nature and experiment. Am Geophys Union. Fall Meeting, V31A–1409

Harlov DE, Förster H-J (2002) High-grade fluid metasomatism on both a local and regional scale: the Seward Peninsula, Alaska and the Val Strona di Omegna, Ivrea-Verbano Zone, northern Italy. Part I: Petrography and silicate mineral chemistry. J Petrol 43:769–799

Harlov DE, Förster H-J (2003) Fluid-induced nucleation of (Y + REE)-phosphate minerals within apatite: nature and experiment. Part II. Fluorapatite. Am Mineral 88:1209–1229

Harlov DE, Wirth R (2000) K-feldspar-quartz and K-feldspar-plagioclase phase boundary interactions in garnet-orthopyroxene gneisses from the Val Strona di Omegna, Ivrea Verbano Zone, northern Italy. Contrib Mineral Petrol 140:148–162

Harlov DE, Hansen EC, Bigler C (1998) Petrologic evidence for K-feldspar metasomatism in granulite facies rocks. Chem Geol 151:373–386

Harlov DE, Förster H-J, Nijland TG (2002) Fluid-induced nucleation of (Y + REE)-phosphate minerals within apatite: nature and experiment. Part I. Chlorapatite. Am Mineral 87:245–261

Harlov DE, Wirth R, Förster H-J (2005) An experimental study of dissolution–reprecipitation in fluorapatite: fluid infiltration and the formation of monazite. Contrib Mineral Petrol 150:268–286

Harlov DE, Johansson L, Van den Kerkhof A et al (2006) The role of advective fluid flow and diffusion during localized, solid-state dehydration: sondrum Stenhuggeriet, Halmstad, SW Sweden. J Petrol 47:3–33

Harlov DE, Van den Kerkhof A, Johansson L (2014) Localized, solid state dehydration associated with the Varberg charnockite intrusion, SW Sweden. Precambr Res 253:50–62

Hensen BJ, Osanai Y (1994) Experimental study of dehydration melting of F-bearing biotite in model pelitic compositions. Mineral Mag 58A:410–411

Higashino F, Kawakami T, Satish-Kumar M et al (2013) Chlorine-rich fluid or melt activity during granulite facies metamorphism in the Late Proterozoic to Cambrian continental collision zone—an example from the Sør Rondane Mountains, East Antarctica. Precambr Res 234:229–246
Holloway JR, Ford CE (1975) Fluid-absent melting of the fluoro-hydroxy amphibole pargasite to 35 kilobars. Earth Planet Sci Lett 25:44–48
Hovis GL, Harlov DE (2010) Solution calorimetric investigation of fluor-chlorapatite crystalline solutions. Am Mineral 95:946–952
Icenhower JP, London D (1997) Partitioning of fluorine and chlorine between biotite and granitic melt: experimental calibration at 200 MPa H_2O. Contrib Mineral Petrol 127:17–29
Iiyama JT (1965) Influence des anions sur les équilibres d'échange dions Na–K dans les feldspaths alcalins a 600 °C sous une pression de 1000 bars. Bull Soc Franc Minéral Cristallograph 88:618–622
Jenkins DM, Clare AK (1990) Comparison of the high-temperature and high-pressure stability limits of synthetic and natural tremolite. Am Mineral 75:358–366
Johannes W (1984) Beginning of melting in the granite system Qz–Or–Ab–An–H_2O. Contrib Mineral Petrol 86:264–273
Kamineni DC, Bonardi M, Rao AT (1982) Halogen-bearing minerals from Airport Hill, Visakhapatnam, India. Am Mineral 67:1001–1004
Kapustin YL (1987) The composition of apatite from metamorphic rocks. Geochem Int 24:45–51
Khodorevskaya LI (2004) Granitization of amphibolites: 2. Characterization of physical and chemical phenomena related to fluid filtration through a rock. Petrology 12:282–296
Khodorevskaya LI, Aranovich LY (2016) Experimental study of amphibole interaction with H_2O-NaCl fluid at 900 °C, 500 MPa: toward granulite facies melting and mass transfer. Petrology 24(3):215–233
Korzhinskii DS (1946) Principles of alkali mobility during magmatic phenomena. Proc dedicated to Acad. D.S. Belyankin, Izdatel'stvo AN SSSR (in Russian)
Korzhinskii DS (1962) The role of alkalinity in the formation of charnockitic gneisses. trudy Vostochno-Sibirskogo Instituta Academii Nauk SSSR Series of Geology 5:50–61 (in Russian)
Korzhinsky MA (1981) Apatite solid solutions as indicators of the fugacity of HCl and HF in hydrothermal fluids. Geochem Int 3:45–60
Korikovskii SP, Aranovich LY (2015) Charnockitization of feldspar-free orthopyroxene–clinopyroxene-phlogopite meta-ultramafite in the Lapland Granulite Belt, Southern Kola Peninsula: compositional trends of rocks and minerals, P–T parameters, and fluid regime. Petrology 23:211–250
Kullerud K (1995) Chlorine, titanium and barium-rich biotites: factors controlling biotite composition and the implications for garnet–biotite geothermometry. Contrib Mineral Petrol 120:42–59
Kullerud K (1996) Chlorine-rich amphiboles: interplay between amphibole composition and an evolving fluid. Eur J Mineral 8:355–370
Kullerud K, Erambert M (1999) Cl-scapolite, Cl-amphibole, and plagioclase equilibria in ductile shear zones at Nusfjord, Lofoten, Norway: implications for fluid compositional evolution during fluid–mineral interaction in the deep crust. Geochim Cosmochim Acta 63:3829–3844
Kusebauch C, John T, Barnes JD et al (2015) Halogen element and stable chlorine isotope fractionation caused by fluid–rock interaction (Bamble Sector, SE Norway). J Petrol 56 (2):299–324. https://doi.org/10.1093/petrology/egv001
Labotka TC, Cole DR, Fayek M et al (2004) Coupled cation and oxygen-isotope exchange between alkali feldspar and aqueous chloride solution. Am Mineral 89:1822–1825
Lamb WM, Valley JW (1988) Granulite facies amphibole and biotite equilibria, and calculated peak-metamorphic water activities. Contrib Mineral Petrol 100:349–360
Larikova TL, Zaraisky GP (2009) Experimental modeling of corona textures. J Metamorph Geol 27:139–151
Leelanandam C (1970) Chemical mineralogy of hornblendes and biotites from the charnockitic rocks of Kondapalli, India. J Petrol 11:475–505

Léger A, Rebbert C, Webster J (1996) Cl-rich biotite and amphibole from Black Rock Forest, Cornwall, New York. Am Mineral 81:495–504

Luddington S (1978) The biotite-apatite geothermometer revisited. Am Mineral 63:551–553

Manning CE, Aranovich LY (2014) Brines at high pressure and temperature: thermodynamic, petrologic and geochemical effects. Precambr Res 253:6–16

Markl G, Bucher K (1998) Composition of fluids in the lower crust inferred from metamorphic salt in lower crustal rocks. Nature 391:781–783

Markl G, Piazolo S (1998) Halogen-bearing minerals in syenites and high-grade marbles of Dronning Maud Land, Antarctica: monitors of fluid compositional changes during late-magmatic fluid–rock interaction processes. Contrib Mineral Petrol 132:246–268

Markl G, Piazolo S (1999) Stability of high–Al titanite from low-pressure calc-silicates in light of fluid and host rock composition. Am Mineral 84:37–47

Markl G, Musashi M, Bucher K (1997) Chlorine stable isotope composition of granulites from Lofoten, Norway: implications for the Cl isotopic composition and for the source of Cl enrichment in the lower crust. Earth Planet Sci Lett 150:95–102

Markl G, Ferry J, Bucher K (1998) Formation of saline brines and salt in the lower crust by hydration reactions in partially retrogressed granulites from the Lofoten Islands, Norway. Am J Sci 298:705–757

Mora C, Valley JW (1989) Halogen-rich scapolite and biotite: implications for metamorphic fluid–rock interaction. Am Mineral 74:721–737

Morrison J (1991) Compositional constraints on the incorporation of Cl into amphiboles. Am Mineral 76:1920–1930

Motoyoshi Y, Hensen BJ (2001) F-rich phlogopite stability in ultra-high-temperature metapelites from the Napier Complex, East Antarctica. Am Mineral 86:1404–1413

Mouri H, Guiraud M, Hensen BJ (1996) Petrology of phlogopite-sapphirine-bearing Al-Mg granulites from Ihouhaouene, In Ouzzal, Hoggar, Algeria: an example of phlogopite stability at high temperature. J Metamorph Geol 14:725–738

Munoz JL (1984) F–OH and Cl–OH exchange in micas with applications to hydrothermal ore deposits. In: Bailey SW (ed) Micas. Reviews in Mineralogy, vol 13. Mineralogical Society of America, Washington, D.C., pp 469–493

Munoz JL, Ludington SD (1977) Fluorine-hydroxyl exchange in synthetic muscovite and its application to muscovite-biotite assemblages. Am Mineral 62:304–308

Munoz JL, Swenson A (1981) Chloride-hydroxyl exchange in biotite and estimation of relative HC1/HF activities in hydrothermal fluids. Econ Geol 76:2212–2221

Nair R, Chacko T (2002) Phase equilibria and melt productivity in the pelitic system: implications for the origin of peraluminous granitoids and aluminous granulites. J Petrol 43:2121–2142

Newton RC, Goldsmith JR (1976) Stability of the end-member scapolites: $3NaAlSi_3O_8{\cdot}NaCl$, $3CaAl_2Si_2O_8{\cdot}CaCO_3$, $3CaAl_2Si_2O_8{\cdot}CaSO_4$. Z Kristall 143:333–353

Newton RC, Manning CA (2010) Role of saline fluids in deep-crustal and upper-mantle metasomatism: insights from experimental studies. Geofluids 10:58–72

Newton RC, Aranovich LY, Hansen EC et al (1998) Hypersaline fluids in Precambrian deep-crustal metamorphism. Precambr Res 91:41–63

Newton RC, Touret JRL, Aranovich LY (2014) Fluids and H_2O activity at the onset of granulite facies metamorphism. Precambr Res 253:17–25

Nijland TG, Jansen JBH, Maijer C (1993) Halogen geochemistry of fluid during amphibolite–granulite metamorphism as indicated by apatite and hydrous silicates in basic rocks from the Bamble Sector, South Norway. Lithos 30:167–189

Oen IS, Lustenhouwer WJ (1992) Cl-rich biotite, Cl–K hornblende, and Cl-rich scapolite in metaexhalites: Nora, Bergslagen, Sweden. Econ Geol 87:1638–1648

Oliver NHS, Wall VJ, Cartwright I (1992) Internal control of fluid compositions in amphibolite-facies scapolitic calc-silicates, Mary Kathleen, Australia. Contrib Mineral Petrol 111:94–112

Orville PM (1963) Alkali ion exchange between vapor and feldspar phases. Am J Sci 261:201–237

Orville PM (1972) Plagioclase cation exchange equilibria with aqueous chloride solution: results at 700 °C and 2000 bars in the presence of quartz. Am J Sci 272:234–272

Orville PM (1975) Stability of scapolite in the system Ab–An–NaCl–$CaCO_3$ at 4 kbar and 750 °C. Geochim Cosmochim Acta 39:1091–1105

Patiño Douce AE, Johnston AD (1991) Phase equilibria and melt productivity in the pelitic system: implications for the origin of peraluminous granitoids and aluminous granulites. Contrib Mineral Petrol 107:202–218

Perchuk LL, Aranovich LY (1984) Improvement of biotite-garnet thermometer: correction for fluorine content in biotite. Dokl Akad Nauk SSSR 277:131–135 (in Russian)

Perchuk LL, Gerya TV (1992) The fluid regime of metamorphism and the charnockite reaction in granulites: a review. Int Geol Rev 34:1–58

Perchuk LL, Gerya TV (1993) Fluid control of charnockitization. Chem Geol 108:175–186

Perchuk LL, Aranovich LY, Podlesskii KK et al (1985) Precambrian granulites of the Aldan shield, eastern Siberia, USSR. J Metam Geol 3:265–310

Perchuk LL, Gerya TV, Korsman K (1994) A model for charnockitization of gneissic complexes. Petrology 2:451–479

Perchuk LL, Safonov OG, Gerya TV et al (2000) Mobility of components in metasomatic transformation and partial melting of gneisses: an example from Sri-Lanka. Contrib Mineral Petrol 140:212–232

Peterson JW, Chako T, Kuehner SM (1991) The effects of fluorine on the vapor-absent melting of phlogopite + quartz: implications for deep-crustal processes. Am Mineral 76:470–476

Pichavant M, Montel J-M, Richard LR (1992) Apatite solubility in peraluminous liquids: experimental data and an extension of the Harrison-Watson model. Geochim Cosmochim Acta 56:3855–3861

Putnis A, Austrheim H (2013) Mechanism of metasomatism and metamorphism on the local mineral scale: the role of dissolution-precipitation during mineral re-equilibration. In: Harlov DE, Austrheim H (eds) Metasomatism and the chemical transformation of rock. The role of fluids in terrestrial and extraterrestrial processes. Springer, Berlin, pp 141–170

Rajesh HM, Belyanin GA, Safonov OG et al (2013) Fluid-induced dehydration of the paleoarchean Sand River biotite-hornblende gneiss, Central Zone, Limpopo Complex, South Africa. J Petrol 54:41–74

Rajesh HM, Safonov OG, Belyanin GA et al (2014) Monazite-fluorapatite characteristics as evidence for interplay between ~2.04 Ga fluid-induced dehydration and melting of the Sand River gneiss, Limpopo Complex, South Africa. S Afr J Geol 117:237–254

Rosenberg PE, Foit FF Jr (1977) Fe^{2+}-F avoidance in silicates. Geochim Cosmochim Acta 41:345–346

Safonov OG (1998) The role of alkalis in the formation of coronitic textures in metamangerites and meta-anorthosites from the Adirondack Complex, United States. Petrology 6:583–602

Safonov OG, Aranovich LY (2014) Alkali control of high-grade metamorphism and granitization. Geosci Front 5:711–727

Safonov OG, Butvina VG (2013) Interaction of model peridotite with the H_2O–KCl fluid: experiment at pressure 1.9 GPa and its application to the upper mantle metasomatism. Petrology 21:599–615

Safonov OG, Kovaleva EI, Kosova SA et al (2012) Experimental and petrological constraints on local-scale interaction of biotite–amphibole gneiss with H_2O–CO_2–(K, Na)Cl fluids at middle-crustal conditions: example from the Limpopo Complex, South Africa. Geosci Front 3:829–841

Safonov OG, Tatarinova DS, van Reenen DD et al (2014a) Fluid-assisted interaction of peraluminous metapelites with trondhjemitic magma within the Petronella shear-zone, Limpopo Complex, South Africa. Precambr Res 253:114–145

Safonov OG, Kosova SA, van Reenen DD (2014b) Interaction of biotite-amphibole gneiss with the H_2O–CO_2–(K, Na)Cl fluids at 550 MPa and 750 and 800 °C: experimental study and applications to dehydration and partial melting in the middle crust. J Petrol 55:2419–2456

Sajeev K, Osanai Y, Kon Y et al (2009) Stability of pargasite during ultrahigh-temperature metamorphism: a consequence of titanium and REE partitioning? Am Mineral 94:535–545
Sallet R (2000) Fluorine as a tool in the petrogenesis of quartz-bearing magmatic associations: applications of an improved F–OH biotite–apatite thermometer grid. Lithos 50:241–253
Satish-Kumar M, Hermann J, Tsunogae T et al (2006) Carbonation of Cl-rich scapolite boudins in Skallen, East Antarctica: evidence for changing fluid condition in the continental crust. J Metam Geol 24:241–261
Schettler G, Gottschalk M, Harlov DE (2011) A new semi-micro wet chemical method for apatite analysis and its application to the crystal chemistry of fluorapatite–chlorapatite solid solutions. Am Mineral 96:138–152
Sengupta P, Raith MM, Datta A (2004) Stability of fluorite and titanite in a calc-silicate rock from the Vizianagaram area, Eastern Ghats Belt, India. J Metamorph Geol 22:345–359
Sharma RS (1981) Mineralogy of scapolite-bearing rocks from Rajasthan, northwest peninsular India. Lithos 14:165–172
Sharova OI, Chudnenko KV, Avchenko AV et al (2012) Aluminum–fluorine sphene (titanite) as an indicator of fluorine fluid. Dokl Earth Sci 442:126–129
Shaw RK, Venkatesh TL, Gupta AK (1993) Experimental study of the system fluorapatite–chlorapatite under 10 and 12 kbar at 640, 750 and 900 °C. Nat Acad Sci Lett 16:27–35
Shell HR, Ivey KH (1969) Fluorine micas. US Bur Min Bull 647:291
Shmulovich KI, Graham CM (1996) Melting of albite and dehydration of brucite in H_2O–NaCl fluids to 9 kbars and 700–900 °C: implications for partial melting and water activities during high pressure metamorphism. Contrib Mineral Petrol 124:370–382
Shmulovich KI, Graham CM (2008) Plagioclase–aqueous solution equilibrium: concentration dependence. Petrology 16:177–192
Skjerlie KP, Johnston AD (1993) Fluid-absent melting behavior of an F-rich tonalitic gneiss at mid-crustal pressures: implications for the generation of anorogenic granites. J Petrol 34:785–815
Smith DC (1981) The pressure and temperature dependence of Al-solubility in titanite in the system Ti–Al–Ca–Si–O–F. Progress Experiment Petrol Series D 18:193–197
Smith MP, Yardley BWD (1999) Fluid evolution during metamorphism of the Otago Schist, New Zealand; (II), Influence of detrital apatite on fluid salinity. J Metam Geol 17:187–193
Sobolev NV, Shatsky VS (1991) Diamond inclusions in garnets from metamorphic rocks: a new environment for diamond formation. Nature 343:742–746
Spear FS, Pyle JM (2002) Apatite, monazite, and xenotime in metamorphic rocks. Rev Mineral Geochem 48:293–335
Stormer JC, Carmichael SE (1971) Fluorine-hydroxyl exchange in apatite and biotite: a potential igneous geothermometer. Contrib Mineral Petrol 31:121–131
Suwa K, Enami M, Horiuchi T (1987) Chlorine-rich potassium hastingsite from West Ongul Island, Lützow-Holm Bay, East Antarctica. Mineral Mag 51:709–714
Tareen JAK, Keshava Prasad AV, Basavalingu B et al (1995) The effect of fluorine and titanium on the vapor-absent melting of phlogopite and quartz. Mineral Mag 59:566–570
Tareen JAK, Keshava Prasad AV, Basavalingu B et al (1998) Stability of F–Ti-phlogopite in the system phlogopite-sillimanite-quartz: an experimental study of dehydration melting in H_2O-saturated and under saturated conditions. Mineral Mag 62:373–380
Tõnsuaadu K, Gross KA, Pluduma L, Viederma M (2012) A review on the thermal stability of calcium apatites. J Therm Anal Calorim 110:647–659
Touret JRL (1995) Brines in granulites: the other fluid (abstract). ECROFI (European Conference on Fluid Inclusions), Barcelona, June 1995
Touret JLR, Huizenga J-M (2011) Fluids in granulites. Geol Soc Am Memoirs 207:25–37
Touret JLR, Nijland TG (2013) Prograde, peak and retrograde metamorphic fluids and associated metasomatism in upper amphibolite to granulite facies transition zones. In: Harlov DE, Austrheim H (eds) Metasomatism and the chemical transformation of rock. The role of fluids in terrestrial and extraterrestrial processes. Springer, Berlin, pp 415–469

Troitzsch U, Ellis DJ (2002) Thermodynamic properties and stability of AlF-bearing titanite $CaTiSiO_5$-$CaAlFSiO_4$. Contrib Mineral Petrol 142:543–563
Troll G, Gilbert MC (1974) Stability of fluorine tremolite. Trans Am Geophys Union 155:481
Trommsdorff V, Skippen G (1986) Vapor loss ("boiling") as a mechanism for fluid evolution in metamorphic rocks. Contrib Mineral Petrol 94:317–322
Trommsdorff V, Skippen G, Ulmer P (1985) Halite and sylvite solid inclusions in high-grade rocks. Contrib Mineral Petrol 89:24–29
Tropper P, Manning CE, Essene EJ (2002) The substitution of Al and F in titanite at high pressure and temperature: experimental constraints on phase relations and solid solution properties. J Petrol 43:1787–1814
Tsunogae T, Osanai Y, Owada M et al (2003) High fluorine pargasites in ultrahigh temperature granulites from Tonagh Island in the Archean Napier Complex, East Antarctica. Lithos 70:21–38
Valley JW, Petersen EU, Essen EJ, Bowman JR (1982) Fluorphlogopite and fluortremolite in Adirondack marbles and calculated C–Q–H–F fluid compositions. Am Mineral 67:545–557
Valley JW, Bohlen SR, Essene EJ et al (1990) Metamorphism in the Adirondacks: II The role of fluids. J Petrol 31:555–596
Vanko DA, Bishop FC (1982) Occurrence and origin of marialitic scapolite in the Humboldt Lopolith, N.W. Nevada. Contrib Mineral Petrol 81:277–289
Vielzeuf D, Clemens JD (1992) The fluid-absent melting of phlogopite-quartz: experiments and models. Am Mineral 77:1206–1222
Volfinger M, Robert J-L, Vielzeuf D et al (1985) Structural control of the chlorine content of OH-bearing silicates (micas and amphiboles). Geochim Cosmochim Acta 49:37–48
Webster JD (1997) Exsolution of magmatic volatile phases from Cl-enriched mineralizing granitic magmas and applications for ore metal transport. Geochim Cosmochim Acta 61:1017–1029
Webster JD, Vetere F, Botcharnikov RE, Goldoff B, McBirney A, Doherty AL (2015) Experimental and modeled chlorine solubilities in aluminosilicate melts at 1 to 7000 bars and 700 to 1250 °C: applications to magmas of Augustine Volcano, Alaska. Am Mineral 100:522–535
Webster JD, Baker DR, Aiuppa A (2018) Halogens in mafic and intermediate-silica content magmas. In: Harlov DE, Aranovich L (eds) The role of halogens in terrestrial and extraterrestrial geochemical processes: surface, crust, and mantle. Springer, Berlin, pp 307–430
Westrich HR (1981) F–OH exchange equilibria between mica–amphibole mineral pairs. Contrib Mineral Petrol 78:318–323
White RW, Powell R, Holland TJB (2007) Progress relating to calculation of partial melting equilibria for metapelites. J Metamorph Geol 25:511–527
Wolf MB, London D (1994) Apatite dissolution into peraluminous haplogranitic melts: an experimental study of solubilities and mechanisms. Geochim Cosmochim Acta 58:4127–4145
Wolf MB, London D (1995) Incongruent dissolution of REE- and Sr-rich apatite in peraluminous granitic liquids: differential apatite, monazite, and xenotime solubilities during anatexis. Am Mineral 80:765–775
Wones DR (1967) A low pressure investigation of the stability of phlogopite. Geochim Cosmochim Acta 31:2248–2253
Yardley BWD (1985) Apatite composition and fugacities of HF and HCl in metamorphic fluids. Mineral Mag 49:77–79
Zhu C, Sverjensky DA (1991) Partitioning of F–Cl–OH between minerals and hydrothermal fluids. Geochim Cosmochim Acta 55:1837–1858
Zhu C, Sverjensky DA (1992) F–Cl–OH partitioning between biotite and apatite. Geochim Cosmochim Acta 56:3435–3467
Zhu C, Xu H, Ilton ES et al (1994) TEM–AEM observations of Cl-rich amphibole and biotite and possible petrologic implications. Am Mineral 79:909–920

Chapter 12
Halogens in Hydrothermal Fluids and Their Role in the Formation and Evolution of Hydrothermal Mineral Systems

Franco Pirajno

Abstract Halogens (and associated volatiles) in hydrothermal solutions are key elements responsible for the genesis of mineral systems. Chlorine is probably the most common halogen, responsible for complexing metals and transporting them in hydrothermal solutions. The F halogen can be extremely powerful for the transport of metals in some specific mineral systems (e.g., IOCG, carbonatites), in addition to forming their own mineral species, such as fluorites. In this chapter halogen complexes and ligands in hydrothermal solutions are briefly discussed. For the case in point, Cl ligands are considered with regard to their function in the extraction and precipitation of metals and related ores. The progress of halogens during the differentiation of granitic magmas and their role in the development of granitoid-related mineral systems are discussed. The exsolution and near surface venting of halogens in hot springs, geysers, and volcanic complexes in general are treated and examples provided. The function of F in greisen-type mineralisation is discussed, followed by specific examples on fluorite associated with continental porphyry deposits in eastern China and the giant Vergenoeg Fe and fluorite deposit in South Africa. Indeed, fluorite is the one halogen-bearing mineral phase that is abundantly precipitated from hydrothermal fluids, and which commonly constitutes an economically viable ore. Halogens in hydrothermal fluids associated with the formation of skarn deposits are also discussed. Finally, we look at the presence and very important role of halogens in evaporite sequences and their impact in the creation of continental hydrothermal deposits. It is important to note that evaporite sequences may have an active or passive role in supplying halogens to ore-making hydrothermal fluids. The former is exemplified by the sabkah evaporites, which form by direct interaction of basinal fluids with seawater leading to the formation of Copperbelt-type mineral systems. Whereas in the latter case, fluids passively leach and transport halogen-based complexing agents for the epigenetic precipitation of ores. Halogens responsible for the uptake and transport of metals in MVT

F. Pirajno (✉)
Centre for Exploration Targeting, University of Western Australia,
35 Stirling Highway, Crawley, WA 6009, Australia
e-mail: franco.pirajno@uwa.edu.au

D.E. Harlov and L. Aranovich (eds.), *The Role of Halogens in Terrestrial and Extraterrestrial Geochemical Processes*, Springer Geochemistry,
https://doi.org/10.1007/978-3-319-61667-4_12

(Mississippi Valley-type deposits), SEDEX (sedimentary exhalative deposits), IOCG (iron oxide-copper-gold deposits), and orogenic mineral systems conclude this chapter.

12.1 Introduction

In this chapter, the function of halogens in hydrothermal fluids and their role in the making of hydrothermal mineral systems is reviewed and examined. Because of this, it is opportune to present a brief synopsis of hydrothermal solutions, principally for the benefit of the uninitiated. What follows is largely taken from my books (Pirajno 1992, 2009 and references therein) and partly from Pirajno (2013a).

A hydrothermal fluid or solution is defined as a hot ($\sim$50 to >500 °C), aqueous solution, containing Na, K, Ca, Cl as major components, complemented by a variable collection of other elements, which not uncommonly also includes F. Ore-forming fluids may occur as molecular solutions (a solute distributed in a solvent), or colloidal solutions (solid phases dispersed in liquid or gas). Hydrothermal fluids are generally assumed to be liquid solutions in which water is the solvent. Solutions can exist in all three states of matter: gas, solid, or liquid. All gas mixtures are solutions (air, for example), whereas solid solutions are characterized by the substitution or interposing of foreign atoms, or ions, in the lattice sites, or between the lattices of mineral-forming elements. A solution is said to be saturated if it is in equilibrium with the undissolved solute. Therefore, an undersaturated solution is characterized by a lower concentration of solute with respect to the saturated solution. A supersaturated solution, on the other hand, contains more than the equilibrium concentration of solute. This latter type is usually unstable. There are two types of solute in water: non-electrolytes and electrolytes. In non-electrolytic water solutions the solute dissolves as molecules and therefore they do not conduct electric current. Electrolytic solutions conduct electric current through the motion of the dissolved substances which are present as electrically charged ions. The halogenide NaCl is a typical example which, when dissolved in water, dissociates into its constituent ions:

$$\mathrm{NaCl(s)} = \mathrm{Na} + (\mathrm{aq}) + \mathrm{Cl} - (\mathrm{aq}) \tag{12.1}$$

The only direct observation and sample material of hydrothermal solutions come from fluid inclusions and hot springs. Fluid inclusions provide important insights into the physical and chemical environments of ore deposition. They represent samples of hydrothermal fluids, and range in size from a single water molecule up to several millimetres. Details of fluid inclusions are beyond the scope of this chapter and the interested reader is referred to Roedder (1984), Roedder and Bodnar (1997), Shepherd et al. (1985), Wilkinson (2001), and Van den Kerkhof and Hein (2001). Fluid inclusions can provide information on the temperature, pressure, density, and composition of the fluids that originated the mineralisation.

Three types of fluid inclusions are recognised, namely: primary, secondary, and pseudo-secondary (see above cited references for details). Primary inclusions are those that are trapped during the growth of the host mineral and are, therefore, associated with crystallisation features, such as growth zones; or they may occur isolated due to imperfections of the crystal during its growth. Secondary inclusions are those that form after the growth of the host mineral is completed. They cut across growth zones and even crystal boundaries, and may represent infilling of microcracks by late fluids that might be unrelated to the ore-forming event. Pseudosecondary inclusions form during the two stages outlined above and are characterized by their alignment with microcracks that end against a growth zone. Tables of empirical criteria for the identification of the genetic types of fluid inclusions are given in Roedder (1984). A classification scheme can be found in Shepherd et al. (1985). Fluid inclusions normally contain aqueous solution with dissolved ions of Na^+, Cl^-, Ca^{2+}, Mg^{2+}, Fe^{2+}, SO_4^{2-}, HCO_3^{2-}, and CO_3^{2-}. The concentration of the salts in the solutions ranges from less than 1 wt% to greater than 50 wt%. In terms of halogens, NaCl is commonly the dominant salt, but the occurrence of F, Br and I can be quite significant in sedimentary brines. The importance of fluid inclusions studies for the understanding of the nature of ore fluids of hydrothermal mineral deposits is highlighted in a collection of papers edited by Bodnar and Cline (2010) as well as in Chap. 5 (Lecumberri-Sanchez and Bodnar 2018).

12.1.1 The Halogens

The halogens comprise Cl, F, Br, I, and radioactive At. Halogens are important elements that participate to various extents in hydrothermal processes. Fluorine and Cl occur as gases at 25 °C and 1 atm. Bromine is a liquid that boils at 59 °C, while I is a shiny black solid (Masterton et al. 1981). The halogens are very reactive and as such they only occur in nature as halide ions (F^-, Cl^-, Br^-, and I^-). Fluorine and Cl are perhaps the more significant in terms of hydrothermal processes. Fluorine is the most reactive of all elements and mostly found in fluorite and topaz, in addition to some 150 F-bearing other minerals. Chlorine occurs in a number of ionic solids, such as NaCl (halite), KCl (sylvite), carnallite ($KMgCl_3{\cdot}6(H_2O)$), and $MgCl_2$ (chloromagnesite). There are few Br-bearing mineral phases (e.g., bromyrite AgBr, iodobromite Ag(Cl, Br, I)), although Br and I ions tend to be more common in natural brines (see Chap. 3 (Mi and Pan 2018) for a more complete list of halogen-bearing minerals).

Kendrick et al. (2001, 2002a, b, 2006, 2008, 2011) has studied and reported on the role of halogens in mineral systems such as porphyry Cu, Mississippi Valley-type, and sedimentary exhalative (SEDEX) deposits, whereas the works of Agangi et al. (2010) and McPhie et al. (2011a) have examined the specific role of F in iron oxide-copper-gold (IOCG) mineral systems in large igneous provinces (LIP), which mainly are mafic-ultramafic magmatic provinces with an areal extent greater than 100,000 km^2 (Ernst 2014). Halogens are commonly associated with

continental salt lakes, sabkhas, and evaporites in the geological record. The role of halogens in evaporite sequences is highly significant during the formation of basin or rift-related hydrothermal mineral systems (e.g., SEDEX deposits). Details on evaporites, continental brines, and associated mineralisation have been extensively investigated by Warren (1999, 2000, 2006, 2010). This topic is taken up in Sect. 12.8.

The halogen content, as well as that of noble gases (He, Ar, Kr, Xe), and their ratios in inclusion fluids, can be used to characterize different hydrothermal fluids (Wilkinson 2001). Ratios and plots commonly used are Cl/Br versus Na/Br and Cl versus Br, which can provide clues as to the origin of fluids (e.g., seawater and continental brines). Although He and Ar are the more widely used in the study of hydrothermal fluids, isotopes of Kr and Xe, together with key halogens (Cl, Br, I), are also used to fingerprint fluid sources, especially where there is involvement of seawater, evaporites, and organic-rich materials (Ballentine et al. 2002).

Magmatism in tensional zones in plate interiors (rift-related settings) is called anorogenic, where it forms alkaline and superalkaline igneous complexes, characterized by unusual concentrations of non-hydrous volatiles, such as CO_2, B, F, and Cl. The origin of these magmas is by no means certain, except that they are known to form by small degrees of partial melting in regions characterized by a thick lithosphere. It is also envisaged that these magmas may derive from metasomatized parts of subcontinental lithospheric mantle. This metasomatism may be linked with mantle outgassing of CO_2 with high halogen contents (Bailey 1978, 1987). This volatile flux through the lithospheric mantle material lowers the solidus so that liquids would result either from a drop in pressure, or through a local increase in temperature. Mantle plumes and associated lithospheric thinning, accompanied by rifting and pressure release, are the mechanisms invoked (Pirajno 2015). These mechanisms could account for the generation and rise of hydrothermal fluids through conduits that are usually long-lived or re-activated crustal fractures. The enrichment of alkaline magmas in non-hydrous volatiles, such as CO_2 and halogens, leads to the concentration of elements such as Zr, Y, Nb, U, and Th in the residual melts during fractionation (Pirajno 2015). It is generally accepted that systematic differences exist in the F content between convergent, margin-related and anorogenic magmatism, with the latter being enriched in F with respect to Cl (e.g., Aiuppa et al. 2009). Tectonic geothermal systems occur in rift valleys, such as those of the East African Rift System (Fig. 12.1), which are commonly occupied by lakes and where hot mantle material is the primary driving energy source generating high geothermal gradients. Here, deep-circulating meteoric waters will form reservoirs in permeable stratigraphic horizons. Fluids rise along graben faults and may vent as hot and/or as mineral springs at the surface or in lakes. In the East African Rift System, Lake Natron (Tanzania) and Lakes Magadi and Bogoria (Kenya) have hot, saline springs discharging at 40 to 80 °C, which precipitate fluorite, trona, and halite (Renaut and Jones 1997; Renaut et al. 1986, 2002). These are ideal settings for the formation of sedimentary rock-hosted ore systems. Hot springs in Lake Magadi have temperatures of about 86 °C, and are enriched in Na,

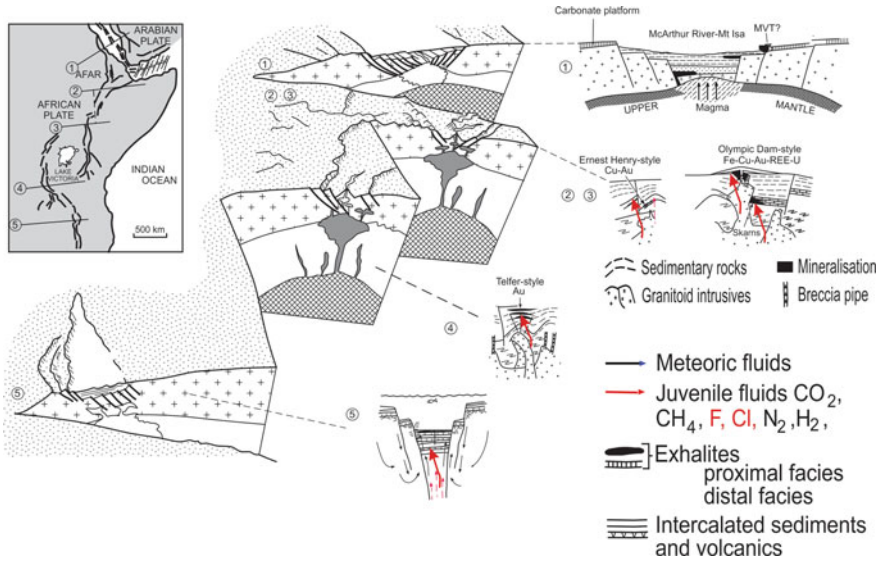

Fig. 12.1 Chlorine and F halogens are common in continental rift systems. This figure shows a schematic illustration of the East African Rift System and hypothetical ore systems that may be associated with it. *1* the advanced Red Sea rift, where oceanic crust is being emplaced and where pools of brines and sulphides are actively forming. *2* and *3* represent a continental rift with anorogenic alkaline magmas at depth, from which magmatic and hydrothermal IOCG style deposits may be forming. The names of the deposits in the figure refer to well-known Australian examples. *4* represents a rift system with a deep lake in which sediments and volcanic materials accumulate together with subaqueous exhalites. *5* is also a rift-lake system, where sediments are organic-rich and where subaqueous hydrothermal venting occurs. Modified after Pirajno (2007, 2009)

HCO_3^-, Cl, K, SO_4, F, SiO_2, P, and B. The environment of Lake Magadi has been compared to some evaporitic sequences in the ancient geological record, such as the HYC shale of the McArthur River ore systems in Australia (Eugster 1986). Renaut et al. (1986) investigated mineralisation in the sediments of Lake Bogoria, a saline and alkaline lake in a deep half-graben from the Kenyan rift. Lake Bogoria is fed by surface waters and approximately 200 hot springs, which are located along its shores and on the floor of the lake. The waters of the lake contain Si, F, Na, HCO_3, and Cl.

The most typical and frequent halogen-bearing mineral phases that are linked to hydrothermal processes are without doubt, halite and fluorite. Fluorite is, although by no means exclusively, associated with alkaline igneous activity in continental rift settings (Fig. 12.1), IOCG, and greisen-type Sn-W deposits. The involvement of NaCl, as testified by fluid inclusions studies, is widespread in porphyry-epithermal systems, volcanogenic massive sulphides deposits, and polymetallic skarn systems. Halogens are also brought to the surface by hot springs, mostly as an expression of larger subsurface hydrothermal convection cells.

12.2 The Role of Halogen Complex Ions and Ligands in Hydrothermal Fluids

A complex ion can be defined as a coordination compound, where a central atom or ion, M, unites with one or more ligands, L, to form a species $ML_iL_jL_k$ (Rickard and Luther 2006). The central ion in a complex is a metal cation, and the neutral molecules or anions bonded to the cation are called ligands. The $Cu(NH_3)_4Cl_2$, for example, is a complex ion balanced by 2 Cl ions. Therefore the complex ion acts in this case as a cation.

Ligands usually contain atoms of the electronegative elements (C, N, O, S, F, Cl, Br, I). The most common ligands are NH_3, H_2O, Cl^-, F^-, OH^- and HS^-. Co-ordination numbers are usually 6, 4, and 2, in that order of frequency. The co-ordination number also determines the geometry of the complex ions. Thus, for complex ions in which the central ion forms only two bonds, the ligands are linear with the bonds directed at 180º (Rickard and Luther 2006). Details on the nature of complex ions and their role in the transport of transitional metals in hydrothermal solutions can be found in Brimhall and Crerar (1987), Crerar et al. (1985), Vigneresse (2009), and Aiuppa et al. (2009).

Metal-ligand interactions are similar to acid-base reactions, with the metal being an electron acceptor and the ligand an electron donor. Metals and ligands can be classified into two important classes: class A, or hard, and class B, or soft. In the former, metals and ligands are highly charged, small and slightly polarizable (Vigneresse 2009). Class B is characterized by species that are large, of low charge, and are highly polarizable. An important aspect of this classification is that soft metals tend to bind with soft ligands, and hard metals with hard ligands. Transition metals show increased hardness at higher temperatures and therefore complexes with intermediate hard ligands such as Cl^- and OH^- become more stable at a given higher temperature (William-Jones et al. 2009). This behavior is corroborated by experimental evidence that indicates the high stability of chloro-complexes at high temperatures. Electronegativity, ionic potential, and the ligand field stabilisation energy (LFSE) or the energy that affects the stability and behavior of transition metal ions in hydrothermal solutions are considered to be important parameters for the behavior of transition metals in hydrothermal solutions (Vigneresse 2009).

Metal solubility in H_2O is very low, so that very large volumes and flow rates of these solutions would be required for the transport and precipitation of these ore metals. However, as pointed out in McPhie et al. (2011a), the presence of OH^-, Cl^-, HS^-, and F^- ligands greatly enhances the capacity of fluids to transport and concentrate metals. Here, F^- is one of the most reactive and powerful ligands for the transport of metal ions in hydrothermal fluids responsible for the generation of IOCG mineral systems, such as Olympic Dam in South Australia. Two other classes of complexes are important for the transport of ore metals in hydrothermal solution, namely sulphide (HS^- and H_2S) and chloride (Cl^-). Both these complexes are capable of transporting large quantities of metals in natural aqueous systems.

A comprehensive review on metal sulphide complexes can be found in Rickard and Luther (2006).

The importance in hydrothermal systems of chloride complexing is indicated by the abundance of NaCl in fluid inclusions. Aqueous species, such as $ZnCl_2$, $CuCl_2^{-3}$, and $AgCl_2^-$, form in chloride-rich solutions. Barnes (1979) and Krauskopf (1979) showed that there is evidence that chloride complexes are more stable than sulphide complexes at higher temperatures (above 350 °C). The predominance of sulphide complexing at lower temperatures and chloride complexing at higher temperatures, and their relationships to certain types of ore deposits, ranging from skarns (high temperature) to hydrothermal veins (low temperature), is illustrated in Fig. 12.2. In the case of Au, its solubility in chloride solutions is defined thus:

$$Au^+ + H^+ + Cl^- = AuCl^{-2} + 1/2\ H_2 \tag{12.2}$$

This type of complexing for the transport of Au is probably valid in the deeper and hotter regions of magmatic and hydrothermal systems, and in hydrothermal fluids originating during metamorphic devolatilization of hydrous silicates. Deposition of sulphides from chloride- complexed metals takes the form:

$$MeCl_2(aq) + H_2S(aq) = MeS + 2H^+ + 2Cl^- \tag{12.3}$$

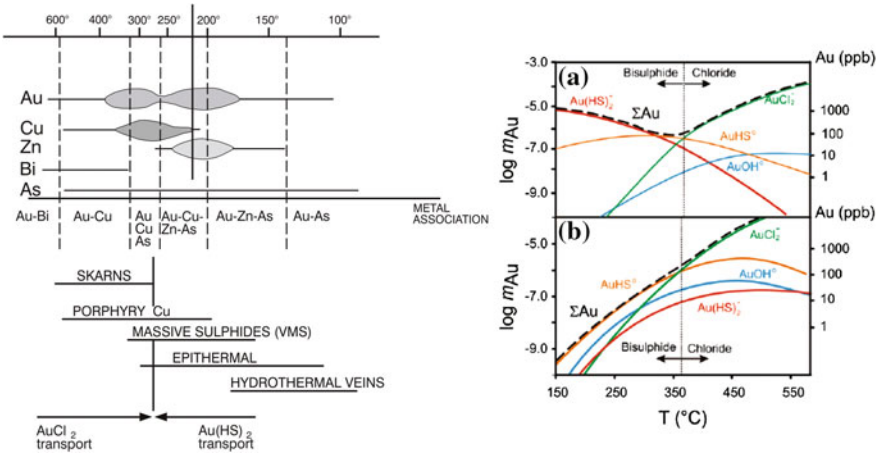

Fig. 12.2 Temperature range of Cl and HS metal transport in mineral systems (Pirajno 2009, based on Huston and Large 1989). The diagram on the *right* (courtesy of Anthony William-Jones; Willliam-Jones et al. 2009) shows Au solubility (molality m and ppb) as a function of temperature in hydrothermal solutions containing 1.5 molal NaCl and KCl. **a** is ΣS (total S) = 0.01 m. fO_2—oxygen fugacity is buffered by the hematite-magnetite assemblage. **b** is ΣS and fO_2 buffered by pyrite-pyrrhotite-magnetite, with a maximum value of ΣS 0.1 m. *Black dashed* line—ΣA—is total solubility of Au. In both **a** and **b**, the temperature limit between Cl and HS complexing is at about 350 °C (see text for more details)

The greater stability of chloride complexes at higher temperatures, with respect to sulphide complexing, is corroborated by modelling studies of Ag/Au ratios in hydrothermal solutions (Cole and Drummond 1986; William-Jones et al. 2009). These studies confirm that $AuCl_2^-$ complexes dominate at temperatures higher than 350 °C and low to moderate pH, thus favoring high Ag/Au ratios in the solution (Fig. 12.2). At temperatures below 350 °C, sulphide complexes more with Au than Ag, which cause lower Ag/Au ratios in the solution. Although experimental modeling seems to indicate that in some cases chloride complexing of Cu, Pb, and Zn for sulphide saturated systems can predominate at lower temperatures over sulphide complexing (Zhong et al. 2015). This is the case for Mississipi Valley-type deposits (MVT, Leach et al. 2005 and see below), in which chloride complexing accounts for the transport of base metals in high salinity basinal brines (Zhong et al. 2015).

Chlorine and F are two major components that form halide ligands for stable metal complexes and are responsible for the transport of metals in solution. Examples of ore deposits related to intrusion-associated hydrothermal systems include greisens, vein systems, mineral systems associated with anorogenic ring complexes, ore systems related to A-type granitic magmas (e.g., Fe oxide-Cu-Au-U), and some breccia pipes and vein deposits that may be peripheral to large intrusions. In some cases, there may be a continuum of spatial, temporal, and genetic relationships with porphyry systems and some epithermal systems. Bodnar and Lecumberri-Sanchez (this book, Chap. 5 (Lecumberri-Sanchez and Bodnar 2018)).

12.2.1 Halogens in Hydrothermal Fluids

12.2.1.1 Chlorine

Chlorine is an ubiquitous halogen in hydrothermal systems. The saline content of fluid inclusions is conventionally measured in terms of NaCl wt% equivalent. Chlorine forms salts from acid solutions of $HClO_2$, $HClO_3$, and $HClO_4$ and occurs in volcanic gases such as HCl. Chlorine can substitute for the hydroxyl ion OH^- in hydrosilicate minerals, leading to a wide range of alteration minerals. Halite (NaCl) is well-known as the most common Cl mineral, and usually occurs in evaporitic sediments. However, in relatively high-temperature hydrothermal fluids, it can also form, either by directly precipitating from hydrothermal fluids or as a replacement of ferromagnesian minerals.

Chlorine is a major ligand component in the solutions, from which ore minerals are precipitated. Aspects of the role attributed to Cl in the formation of hydrothermal ore deposits (forming complex ions with Cu, Ag etc.), and details of the occurrence of Cl-bearing fluids in rocks hosting mineral deposits, can be found in Davison and Kamenetsky (2001) and Kamenetsky et al. (2004). The chloride ion is also a major anion of fluid inclusions in ore deposits and in alteration minerals

from hydrothermal systems. Fluid inclusions typically contain liquid, vapour and solid phases and conbinations thereof. The gaseous and solid species commonly found in inclusion fluids include compounds of halogens, such as NaCl and KCl. The halogen content and their ratios in inclusion fluids is used to characterize hydrothermal fluids (Wilkinson 2001; Cai et al. 2007; Chen et al. 2007, 2009b). Ratios and plots commonly used include Cl/Br, Na/Br, I/Cl, which can provide important clues as to the origin of fluids (e.g., seawater, continental brines), as discussed in more detail below.

12.2.1.2 Fluorine

Fluorine cannot be accommodated to a great extent in differentiating melts, resulting in its accumulation in hydrothermal fluids, from which fluorite veins can form (Fig. 12.3), or during sub-solidus late crystallisation stages that lead to the formation of greisen systems. It is of great significance in silicic volcanics and for

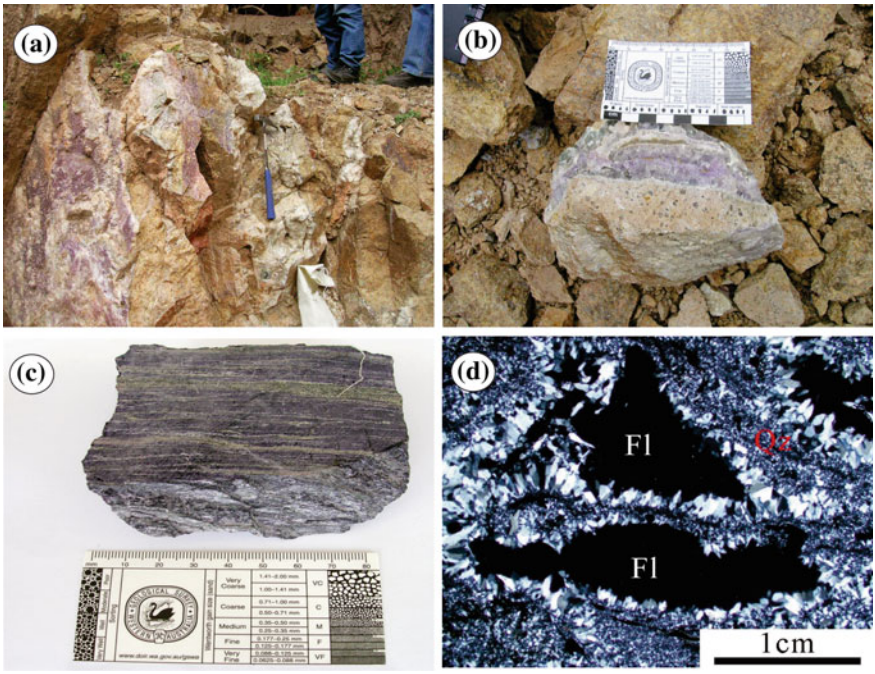

Fig. 12.3 **a** Sheeted fluorite (*purple*) and calcite veins. **b** Fluorite vein cutting quartz-feldspar porphyry. **c** Hand specimen of banded fluorite (*dark bands*), aegirine, and bastnäsite from the Bayan Obo carbonatite (China, after Pirajno 2015). **d** Photomicrograph showing comb quartz and late fluorite in the Yuchiling porphyry Mo deposit (China; after Li et al. 2013). **a** and **b** are fluorite veins associated with an alkaline granite intrusion from the Donggoumen fluorite mine in northern Hebei province (China)

the transport of lithophile elements and of metals, as elaborated further in the sections ahead. Also, hydrothermal fluids can extract F from the country rocks. The mineral fluorite usually occurs in veins of hydrothermal origin generally, but not uniquely, associated with alkaline granitoids (Fig. 12.3). It is sometimes associated with sulphides (see below) or carbonatite systems (Fig. 12.3c). In other cases, fluorite may fill in vesicles, miarolitic cavities, vugs, and microscopic voids (Fig. 12.3d), as exemplified by the Vergenoeg giant fluorite-magnetite deposit in South Africa (Agangi et al. 2010; Li et al. 2013; Graupner et al. 2015). Fluorite can also be a mineral of commercial value with several millions of tonnes being extracted world-wide (Harisch and Eisenhauer 1998). Fluorine also occurs in several economically important REE-bearing mineral phases, such as bastnaesite, parasite, synchysite, and as such F plays a significant role as a ligand for the transport of REE (Migdisov and William-Jones 2014; Stoppa et al. 2016). Fluorite is commonly precipitated from carbonatite-related hydrothermal activity, together with bastanaesite, monazite, xenotime, pyrochlore, and low-temperature feldspar (Mariano 1989; Pirajno 2015). Fluorine in carbonatite-related hydrothermal fluids can also move for long distances with fluorite being precipitated in host rocks that have no relationship with the carbonatites (Pirajno 2015; Stoppa et al. 2016).

12.3 Halogens in Hot Springs, Geysers, Crater Lakes, Fumaroles (Geothermal Fields)

Transfer of heat and dissolved matter through aqueous and gaseous fluids in volcanic areas is manifested at the surface by hot springs, fumaroles, crater lakes, and, less commonly, geysers. This section briefly reviews these surface phenomena. Details may be found in texts on volcanology, such as Sigurdsson et al. (2000), Schminke (2004), Aiuppa et al. (2009), as well as in Chaps. 6 (Webster et al. 2018) and 7 (Dolejs and Zajacz 2018).

Acid-sulphate hot springs are characterized by low pH, due to oxidation of H_2S to H_2SO_4 and are generally low in chlorides, though emanations containing HCl may also be present. Besides H_2S, thermal waters are enriched with other volatiles (Cl, SO_4, HCO_3, F, B, and Br), as well as "volatile" metals like Hg, As, Bi, and Sn. Acid-sulphate thermal waters are generated by condensation of steam and vapors as they rise through cracks and fissures at temperatures below 400 °C (Ellis and Mahon 1977; Pirajno 2009). Alkaline chloride thermal waters are characterized by the presence of Na, K, chlorides, silica, bicarbonates, fluorides, ammonia, As, Li, Rb, Cs, and boric compounds. These hot springs are commonly found in caldera settings, because the convective column is within easy reach of the ground surface (Fig. 12.4). Siliceous sinters (amorphous silica precipitated at the surface by fast flowing hot water) are usually well developed in areas of chloride springs. Here, the dissolved silica is precipitated. Siliceous sinters may take on a variety of bright colours due to Fe oxides and the growth of algae. Their deposits can form spectacular features such as cascades, terraces, and mounds. Alkaline chloride waters

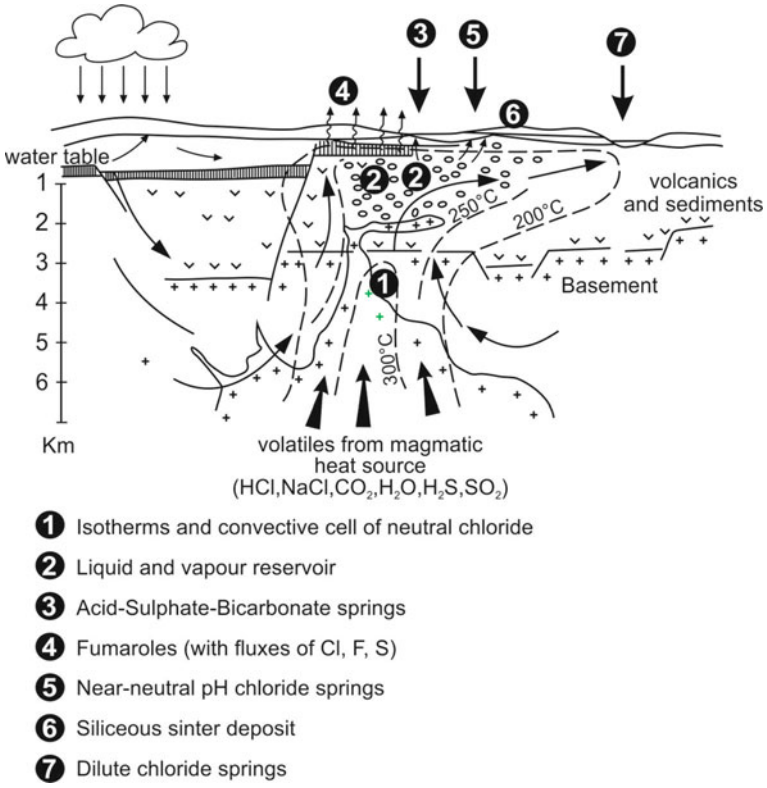

Fig. 12.4 Caldera setting showing convective fluid circulation and the idealised extent of liquid-vapour reservoir from which volatiles and halogens are emitted. (Pirajno 1992, based on Henley and Ellis 1983; see also Hurwitz et al. 2007)

are also associated with geysers. Geysers are abundant in Yellowstone National Park (Fournier et al. 1994), where there are over 200, in New Zealand and in Iceland. They have also been found in Tibet near lake Tengri Nur at 4800 m above sea level, and in the crater of the Socompo volcano in the Atacama region at 6080 m above sea level (Hochstein and Browne 2000).

An example of a geyser field is briefly introduced here. The Geysers-Clear Lake geothermal system, located in the northern Coast Ranges in California, includes active hot springs and recently active epithermal systems that belong to the same geothermal complex. Epithermal deposits of the Geysers-Clear Lake region include the McLaughlin Au-Sb-Hg, Wilbur Springs and the Sulphur Bank S-Hg deposits (Sherlock et al. 1995; Sherlock 2005). The Geysers-Clear Lake region is underlain by the Cretaceous-Jurassic Coast Range ophiolite, the Great Valley sequence, and the Franciscan Complex, the latter being part of an accretionary prism related to the subduction of the Pacific plate beneath North America. These tectonostratigraphic packages are tectonically interleaved and have been affected by thrusting and

strike-slip movements. The Neogene Sonoma Volcanic Suite and the Quaternary Clear Lake Volcanic Suite, which consists of mafic and felsic extrusive and intrusive rocks, were emplaced into the Mesozoic package. The Geysers steam reservoir is contained in greywacke and serpentinite rocks associated with extrusive and intrusive rocks of the Clear Lake Volcanic Suite. The steam field is about 40 km west of the McLaughlin deposit, is vapour-dominated, discharges Hg and hydrocarbons, and is spatially associated with a number of Hg deposits and hot (>60 °C) mineral springs in the general area, all with varying degrees of Au-Hg mineralisation. The surface expression of the Geysers geothermal system is characterized by extensive areas of argillic alteration, small mounds of native S, and boiling mud pools. Calculated temperatures, based on oxygen fractionation between sulphate and water, range from 241 to 249 °C. The distribution of hot and mineral springs in the Geysers-Clear Lake area are all controlled by major northwest-trending fault zones.

The origin of the fluids in the Geysers-Clear Lake geothermal system has long been debated and considered in terms of mixing models between connate, meteoric, and metamorphic fluids. However, Sherlock (2005) suggested that dominantly meteoric fluids evolved into a vapour-dominated system due to decreased permeability of the reservoir rocks, as well as decreased recharge and increased heat flow.

12.3.1 Halogens in Crater Lakes and Fumaroles: Associated Epithermal Systems

Lakes are not uncommon in the craters of dormant volcanoes. The water in these lakes absorbs heat and volatiles emanated from the lake floor. Dissolved volatiles and other components leached from the rocks, including CO_2, HF, HCl, NH_3, SO_2, Ca, Na, Al, Mg, K, Fe, and Si, tend to accumulate between eruptions. Volatile fluxes recorded in the Volcáno Poás acid lake (Costa Rica) include 0.78 Gg/a of F and 15 Gg/a of Cl (Ga/a = Gigagram/per year) (Brantley et al. 1993).

Fumaroles are formed where the influx of groundwater is small and steam readily escapes to the surface. In fact, it is often observed that fumaroles change to acid-sulphate springs, and vice versa, in conjunction with fluctuating groundwater levels. Solfataras are fumaroles with a high H_2S content, but often the terms solfatara and fumaroles are used interchangeably. Ellis and Mahon (1977) defined fumarolic steam as that which derives directly from the magma and has not passed through a hot water body. This type of fumarolic steam would contain HCl, CO_2, H_2S, and SO_2. Solfataric steam is defined by the above authors as steam boiling from an underground geothermal reservoir, as described earlier. Both types may condense in surface waters. The temperature of steam spouts varies from 90 to 300 °C. Mineral encrustations around the orifices and conduits are common, and include sublimates and compounds formed by reaction of the volatiles with the wall rocks. Common products are chlorides of the alkali metals, ferric chloride,

sulphates of the alkali metals and Ca, together with traces of compounds of Cu, Mn, Pb, Zn, As, Hg, and Sn. Fumaroles at Mt.Vesuvius were found to contain $PbCl_2$, $FeCl_3$, and $CuCl_2$, accompanied by galena, hematite, covellite, and even pyrite and chalcopyrite, which had formed by reaction with H_2S and H_2O (Guest et al. 2003; Scandone et al. 2006). Ammonium chloride (NH_4Cl) may locally be so abundant that it can be commercially exploited. The F/Cl ratios in volcanic gases tends to fall with decreasing temperatures, so that Cl is volatilised to a much greater extent than F (Brehler and Fuge 1978).

The Kamchatka region is host to some of the most extensive geothermal areas in the world. One of these is the geothermal system of the Mutnovsky volcano, covering an area of 30 km^2, and investigated by Taran et al. (1992, 1997). A group of steam vents and fumarolic fields are present in this volcano, with vent temperatures of up to 420 °C. Pools of boiling, very acidic water are encrusted with native S (S^0), and locally have domes of S^0, up to 2 m high. The Upper Field fumaroles have temperatures of around 230–320 °C and high concentrations of CH_4 and NH_3, with low $^3He/^4He$ ratios. The Northern Area and Bottom Field fumaroles have abundant S^0, which forms dome structures and small pools of molten S. Intense gas activity was recorded in the Active Funnel, a bowl-shaped structure about 150 m deep and from 100 to 150 m wide. Here, temperatures of up to 600 °C have been measured in fumaroles that discharge more than 200 t/day of SO_2, as well as HCl, HF and H_2.

The Kudriavy volcano, in the north of Iturup Island in the Kuril volcanic arc, has numerous high-temperature (700–940 °C) fumarolic fields covering an area of 2.6 km^2 (Taran et al. 1995; Botcharnikov et al. 2003). The volcano is of basaltic andesite composition and is on the western flank and is part of the Medvezhya caldera, which include rhyolite and dacite domes. The fumaroles are water-rich (92–98 mol%), but also contain varying amounts of gases such as CO_2, SO_2, H_2S, HCl, HF, and CH_4. The low NaCl content of these fumarolic vapours was attributed to separation of hypersaline fluids from the vapour phase at depth. The distribution of the Kudriavy fumaroles and their composition have been interpreted to be related to a stable plumbing system from a convecting and degassing magma conduit in which gases exsolve and ascend to the surface (Taran et al. 1995).

12.3.2 Geothermal Fields of Calderas and Stratovolcanoes

Geothermal fields are commonly found in areas of recent tectonic and igneous activity at plate boundaries. Most geothermal fields are in fact associated with volcanic structures, in particular calderas, at convergent margins (volcanic arcs) and intracontinental rift systems. Figures 12.4 and 12.5 show examples of two volcanic settings, a caldera, and a stratovolcano, respectively, in which hot springs and fumarolic activity are common and are the surface expression of convective circulation associated with shallow magma chambers. The following is taken from Pirajno (1992, 2009 and references therein). There are a number of possible

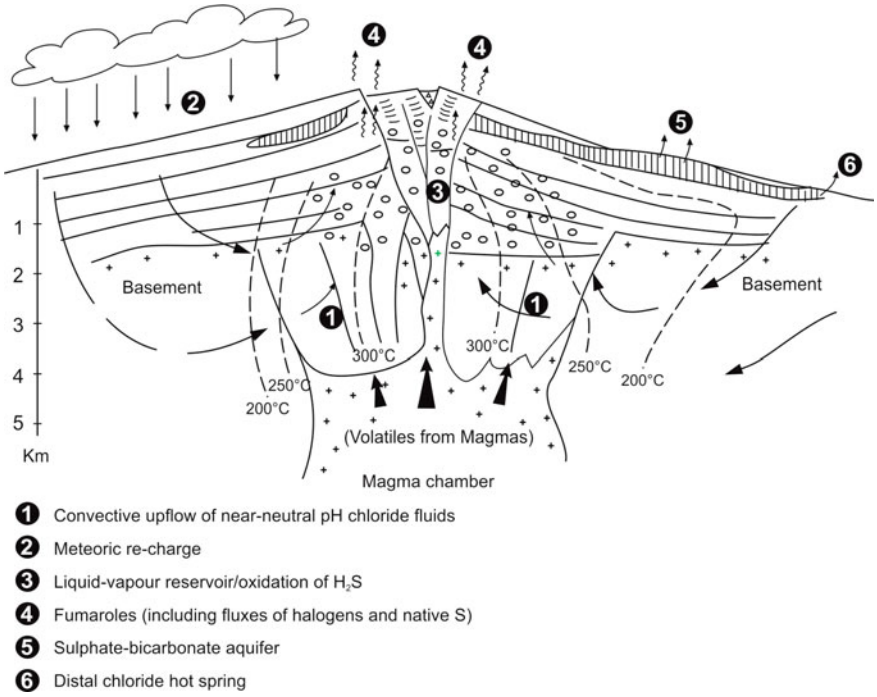

Fig. 12.5 Geothermal features of a stratovolcano showing convective cells with near-neutral pH chloride fluids, fumarolic emissions, hot springs and interaction with meteoric waters (Pirajno 1992, based on Henley and Ellis 1983)

scenarios here for geothermal systems. Four principal settings and associated types of geothermal systems, are: (a) calderas in silicic volcanic terranes; (b) andesitic stratovolcanoes in Andean continental margins; (c) highland monogenetic volcanoes, commonly associated with phreatomagmatic processes; and (d) volcanic islands in the ocean. In a caldera setting (Fig. 12.4), recharge is by meteoric groundwaters, and heat and volatiles, including HCl, CO_2, H_2O, etc., are supplied by a buried magmatic system. A convective cell (1) is formed above the heat source, and consists of near-neutral pH chloride-bearing water. In the upper levels boiling and separation of steam occur, so that a two-phase zone (liquid + steam) is present near the top of the convective column (2). The development of steam and partitioning of the H_2S into the vapour phase results in steam-heated, acid sulphate-bicarbonate waters (3), as well as steaming ground and fumaroles (4) above the two-phase liquid-steam zone. Direct outflow of the near-neutral chloride-bearing waters gives rise to boiling alkaline springs (5), from which siliceous sinter is generally deposited (6). Dilution with groundwaters may result in dilute near-neutral chloride-bearing springs (7), whereas mixing between the deep near-neutral chloride-bearing and the steam-heated acid sulphate waters will produce oxidising Cl-SO_4 waters. A characteristic feature of this particular system is its

situation within a depression formed by the caldera structure, so that water recharge is more or less at the same level as the discharge. In these systems the development of hydrothermal breccias and sinters is very common, a typical example being the Waiotapu geothermal system in the Taupo volcanic zone in New Zealand (Hedenquist and Henley 1985; Hedenquist et al. 1998, 2000).

The precipitation of silica in geothermal systems associated with caldera settings, and particularly the formation of extensive sinters, is probably due to two main factors. One is the solubility of quartz at the temperature of equilibration between the water and the wall rocks (180 °C). Solubility of quartz increases with temperature, and at high temperatures quartz solubility is decreased in chloride solutions and increased in alkaline solutions (Fyfe et al. 1978). Therefore, with a subsurface temperature in excess of 180 °C, and in chloride-bearing waters, the amount of silica may exceed the solubility of quartz, so that precipitation results. The other factor is that the silica-charged waters in these low relief areas readily reach the surface and do not outflow as distal springs, as may be the case for stratovolcanoes where the silica is dispersed en route.

In regions of high relief, such as tall andesitic stratovolcanoes, the features of the associated geothermal system differ as shown in Fig. 12.5 and discussed below. The convective cell is located deep within the volcanic edifice, possibly in its basement (1). The recharge of the system is from areas of low elevation (2). The centrally situated, high relief prevents the discharge of chloride-rich waters in areas above the convective up-flow. Instead, due to boiling and steam separation as well as the presence of H_2S (3), fumaroles and steam-heated aquifers, which produce acid-sulphate fluids, are present high on the volcanic slopes and/or the crater area (4 and 5). Acid-sulphate waters are the principal cause for acid leaching and argillic type alteration. Chloride-bearing springs may be found at considerable distances (up to 20 km) along the outlying regions of the volcanic complex (6) (Henley and Ellis 1983). Here again, silica is likely to be deposited en route to the distal chloride springs, and sinters are unlikely to form in this setting. However, percolation of acid-sulphate waters, and their mixing with the near-neutral reservoir, may deposit silica and anhydrite somewhere above the hydrothermal reservoir.

12.4 Role of Halogens and Other Volatiles in Granitic Magmas and Associated Fluid Phases

The fundamental importance of the role of volatiles in granitic melts is two-fold. First, they modify the physico-chemical behavior of the melt and its crystallisation products. Second, as a result of the volatiles' tendency to partition into the residual fluid phases, they are instrumental in the complexing and transporting of metallic elements, and thus are also important in the understanding of ore genesis processes (Webster 1990, 1997; Webster et al. 1994). The addition of volatiles (B, F, Cl, H_2O) to a mineral assemblage undergoing high-grade metamorphism lowers the

melting temperature of the assemblage (e.g., Zellmer et al. 2015) and the addition of volatiles to a melt phase has the effect of lowering its solidus temperature. The behavior of halogen volatiles (B, F, Cl) in a melt is similar to that of water, in that they react with the "bridging oxygens" of the silicate tetrahedra by breaking the Si-O bridges and depolymerising the melt (Burnham 1979).

Fractionation processes in magmas tend to concentrate volatiles (including halogens) and incompatible elements, such as Sn, W, Mo, Th, U, Zr, Ta, Nb, and Hf, and sometimes also Zn and Pb, in the residual melts (Keppler and Wyllie 1991; Salvi and William-Jones 1996; Thomas et al. 2005). Thus the increase in volatiles not only depolymerises the melt but also provides ligands for complexing trace elements. An increase in the halogen contents in the melt leads to depolymerisation of the magma (Burnham 1979), resulting in the destruction of the Si-O bonds within alumino-silicate tetrahedra due to the activity of F and Cl (and OH). The depolymerised melt develops a range of co-ordination sites capable of readily accepting large, highly charged cations, which do not fit within the depolymerised melt. This halogen-induced depolymerilasation greatly enhances metal enrichment during fractional crystallisation, which leads to enrichment of large highly charged cations, such as Sn, W, Mo, and Ta, in the residual melt (Collins et al. 1982). The effects of this polymerization are greatest in the higher levels of the magma chamber where, in fact, volatiles collect.

Experimental work by Pichavant and Manning (1984) shows that at 1 kbar and near-liquidus temperatures, the addition of B and/or HCl results in a decrease in the Si/alkali and Al/alkali ratios of the melt. Therefore, both B and HCl cause a transfer of alkalies from the melt to the vapour/fluid phase. In the quartz-albite-orthoclase-H_2O system, changes in the melt composition due to the addition of F or B in a source region, undergoing melting, are reflected by the shift of the melt composition towards the quartz-orthoclase side of the ternary system (Sowerby and Kepler 2002). There is also experimental evidence that the solubility of H_2O in magmas may be enhanced in B-rich melts (Pichavant 1981; Sowerby and Keppler 2002), whereas F-rich systems do not appear to have the same effect. The experiments carried out by Pichavant and Manning (1984) indicate that progressive addition of F (between 1 and 4%) and B (between 1 and 4.5%) causes the eutectic composition to shift towards the albite corner. In other words, in the case of magmatic systems, that during fractionation and crystallisation are progressively enriched in B, F and Li, there is a concomitant enrichment in the albite component, while the liquidus temperature is also depressed. Thus, with progressive crystallisation of the volatile-rich melt, Na and Si enter easily into a residual fluid phase. The opposite trend may be observed if the volatiles are removed from the crystallising melt. In this case albite, or peraluminous minerals, crystallises and the residual melt becomes progressively enriched in quartz and orthoclase. The effect of F extraction from the melt would be similar to that of B extraction, resulting in a Na (K)-, Si-, and B(F)-rich aqueous fluid.

Other changes involving increasing amounts of H_2O (H^+ metasomatism) and/or H_2O-absent volatiles include: changing compositions of pyroxenes and amphiboles; growths of tri-octahedral micas, aegirine, and riebeckite; as well as a series of F- or

B-rich mineral assemblages. It must be pointed out that many of the replacement features characteristic of subsolidus changes can also be explained by magmatic crystallisation, or unmixing of solid solutions. However, subsolidus reactions are especially developed in the apical zones of plutons, and along fractures or in pods and lenses.

Topaz-bearing granitoids may contain up to 3% F (Pichavant and Manning 1984). Fluorine preferentially partitions into silicate magmas rather than the co-existing aqueous phases, although F is very mobile during hydrothermal activity (Agangi et al. 2010). For example, F-rich mica and topaz may be replaced by F-poor sericite during the early stages of hydrothermal alteration resulting in the precipitation of fluorite, provided that enough Ca is introduced via aqueous solutions (Pichavant and Manning 1984). Granitic cupolas rich in F, B, and Li are associated with Sn-W greisen style mineral systems. Experimental work shows that in the presence of F, the element W partitions into the melt (Pichavant and Manning 1984). This has been explained in terms of the effect that F and Cl have on the alumina-silicate melt structure. While Cl has relatively little effect on the stability of the alumino-silicate network component of the melt, F reacts with this network by removing the Al causing depolymerization of the network. Consequently, polyatomic W species, being very large in comparison with monoatomic ions, such as Na, cannot be incorporated within the structrure of the melt in Cl-bearing systems. The W species are hence accommodated into the disrupted structure of the F-bearing alumina-silicate melt. These experimental results are very important, because they give an indication of the behavior of incompatible elements in aqueous fluids during the late magmatic stages (Pichavant and Manning 1984). Thus, an increasingly F-rich melt is able to concentrate incompatible elements during the process of differentiation by accommodating them and their complexes within the depolymerized structure of the melt. As soon as an aqueous phase is exsolved, the partitioning of the incompatible elements is controlled by the halogen contents of the aqueous phase. If the aqueous phase is F-rich, or relatively Cl-poor, the partitioning behavior is different allowing for the formation of W-bearing minerals, as discussed below for greisen systems. In a recent study, evidence for the crystallisation of W-Nb-Ta oxides from a F-rich magma, caused by the extraction of F by an immiscible fluoride liquid, which would depress W-Nb-Ta solubility in the silicate melt was reported by Agangi et al. (2014). Webster et al. (2009) and Doherty et al. (2014) have reported on the partitioning of Cl and F in felsic melts at high pressures and temperatures. Considerably more information on the behavior of halogens in magmas can be found in Chaps. 6 (Webster et al. 2018) and 7 (Dolejs and Zajacz 2018).

Experimental data also indicate that W can be mobilised in chloride-bearing hydrothermal solutions. Foster (1977) postulated that molecular hexalides (WCl_6) are probably present at near—magmatic temperatures, but with decreasing temperatures and increasing hydration, W is transported as molecular H_2WO_4. With further decreasing temperatures, the major W species are ionic $(H_3W_6O_{21})^{-3}$; $(HW_6O_{21})^{-5}$, and $(WO_4)^{-2}$. Under these conditions, W transport and deposition are controlled, apart from temperature, by f_{O2}/f_{S2}, the activities of Ca^{2+}, Fe^{2+}, and Mn^{2+}, and the pH of the solution (Foster et al. 1978). The role of F is more

important for Sn than it is for W. However, oxyfluoride complexes may be responsible for the transport of W at low temperatures (±300 °C), in cases where the concentration of F in the solution is high (Foster 1977; Foster et al. 1978). The role of F in the hydrothermal transport and deposition of W may be influenced by the activities of HF and KF, as proposed by Burt (1981). Under conditions of low HF and KF activities, scheelite will form, whereas wolframite occupies a field of higher HF and KF values. This would explain the common association of fluorite and topaz with wolframite mineralisation. Westra and Keith (1981) further substantiated this relationship. They noted that scheelite is common (without cassiterite) in calcic magma series, which have low F, while in F-enriched calc-alkaline magmas wolframite or hubnerite tend to occur together with Mo and Sn.

12.4.1 Fluorine in Greisen Systems

Greisen systems are typically a coarse-grained assemblages of quartz-muscovite with varying amounts of topaz, tourmaline, fluorite, oxides (cassiterite, hematite), wolframite, scheelite, and sulphides of Fe, Cu, Mo, Bi, and Cu-Bi-Pb sulphosalts (Pirajno 2013a; Teiber et al. 2014). In general, greisen alteration is usually preceded by Na metasomatism (albitite), during which H^+ ions are produced, which then initiate the process of greisenisation. This involves the destabilization and destruction of feldspars and biotites to form the assemblage quartz + muscovite. The process may be more complicated in mineralised systems, in which there is the introduction of B, Li and the halogens Cl and F. This will result in new series of reactions that may take place to form topaz, tourmaline, fluorite, and oxide minerals (Pirajno and Bentley 1985; Pirajno and Jacob 1987; Pirajno 1992). Silicification may accompany greisen alteration both during and after, as evidenced by the common quartz flooding of the greisen altered rocks. Muscovite preferentially replaces the biotites, and leads to a release of cations locked in the biotite lattice into the system. These are possibly responsible for the paragenetically later metallic mineralisation. Quartz + muscovite greisens may be followed by progressive stages of F- and/or B-metasomatism. In the latter case the development of tourmaline may be so extensive that quartz-tourmaline assemblages may dominate altogether. Subsequent to greisen alteration, sericitic and argillic metasomatic alteration may follow due to an increase in the H^+ activity (Pirajno 1992).

Teiber et al. (2014) studied the halogen contents of granitic rocks and found that muscovite-bearing granites have higher F contents than Cl, whereas the opposite is observed for amphibole-bearing granitoids. Furthermore, these authors reported that significant amounts of Cl and F tend to be preferentially accommodated in post-magmatic regimes. Although typical skarns are usually associated with porphyry systems, some skarns are spatially and genetically associated with greisen-related systems in which all gradations may be observed, as well-exemplified by the granitic cupola-related Sn-polymetallic mineral deposits in Yunnan Province (SW China) (Cheng et al. 2013). The greisen solutions are

neutralised on contact with the carbonate lithologies, as the anionic species (e.g., F, OH) become fixed by Ca and Al to form fluorite and topaz. Separation of fluids from a residual granitic melt may lead to a concentration of Na in the melt, resulting in the crystallisation of a Na-rich rock, usually with a high F content. The enrichment of the residual melt in Na and F results in post-magmatic albitisation, which is most common in the uppermost zones of the cupolas and along fractures (Pollard 1983). According to Pollard (1983), this may be due to the enhanced F content, and perhaps the influence of CO_2, which lower the solidus. In so doing it allows for an extended period of crystallisation that in turn promotes the exsolution of an aqueous phase to develop and collect in the apical parts of the granitic cupola. Greisenisation follows the stage of Na metasomatism, during which the circulating hydrothermal fluids are characterized by enhanced activities of H^+ and of HF. This results in the wholesale destruction of the granitic mineral components to form greisen assemblages.

Fluid inclusion studies of greisen deposits generally confirm the magmatic origin of the fluids, even though there are cases that have been interpreted as a mixing of magmatic with meteoric waters. According to the type of greisen-related deposit (e.g., endogreisen to exogreisen and quartz veins), the nature of the greisenising fluids varies from high ($\sim$600 to $\sim$400 °C and >40 wt% NaCl equivalent) to low ($\sim$200 °C and 10–15 wt% NaCl equivalent) temperatures and salinities, respectively. Dissolved species include mainly NaCl, KCl and CO_2, but phases such as anhydrite and borax have also been identified (Burt 1982; Pollard 1983; Pirajno 2013a).

The activity of HF in greisen systems determines the stability of scheelite (lower μHF) or wolframite (higher μHF) in the system. At low HF activity, the formation of scheelite occurs, whereas with increasing HF activity, scheelite may convert to wolframite and fluorite (Pollard et al. 1987; Pirajno 2013a).

Increase in the activity of H_2O during cooling of the hydrothermal fluids results in the breakdown of topaz and feldspars, which release large quantities of HF, along with formation of muscovite and quartz. The release of F, together with the muscovitisation and chloritisation of the biotites at depth, results in the leaching of metals and their complexing with F and subsequent transport upward in the evolving system. As previously outlined, F-rich greisen systems are characterized by the presence of fluorite and/or topaz and Li-rich micas (Pirajno 2013a).

Thomas et al. (2005) emphasised the importance of the interplay of H_2O, F, and B in the enrichment of Sn during magma differentiation. Cassiterite is the dominant ore mineral in greisen systems and is commonly associated with fluorite and/or tourmaline, suggesting a cogenetic relationship between these minerals and the transporting hydrothermal fluids. Various mechanisms have been proposed for the dissolution and transport of Sn in hydrothermal solutions. According to Paterson et al. (1981), Sn^{+2} readily complexes with F^-, OH^-, and Cl^-. Tin transport, as a consequence of hydroxyl and hydroxyfluoride complexing, is thought to take place in high temperature, alkaline fluids (Eadington 1983). Fluoride and chloride complexes are more significant for the transport of Sn in hydrothermal solutions. It appears that F is more likely to transport Sn in highly saline solutions. Tin is

considered to be readily transported as a stannous chloride complex ($SnCl^{-}$) under conditions of low pH and low f_{O2} (Paterson et al. 1981). Precipitation of cassiterite, due to the destabilisation of the transporting complexes, would then occur either by f_{O2} increase, an increase in pH, a decrease in temperature, or a combination of these physico-chemical factors. In general, the conditions which cause precipitation of cassiterite are similar to those for wolframite. The metal chloride solutes are converted to oxides and/or sulphides and HCl and H^{+} released (Eugster 1984). The precipitation of cassiterite in carbonate rocks by greisening fluids may be represented as follows (Eugster 1984):

$$SnCl_2 + CaCO_3 + H_2O \rightarrow SnO_2 + CaCl_2 + CO_2 + H_2O. \tag{12.4}$$

In pelitic rocks, the conversion of feldspar and biotite to muscovite may induce precipitation of cassiterite. A possible reaction proposed by Eugster (1984) is:

$$\underset{}{SnCl_2} + \underset{\text{biotite}}{3KFe_3AlSi_3O_{10}(OH)_2} + 2H_2O \rightarrow \underset{}{SnO_2} + \underset{\text{muscovite}}{KAl_3Si_3O_{10}(OH)_2} + 6SiO_2 + 3Fe_3O_4 + 2KCl + H_2 \tag{12.5}$$

As reported in Pirajno (2013a), Burt (1981) demonstrated that the anorthite content of plagioclase and other calcic phases (e.g., titanite) decreases or becomes unstable as the F-content of the system increases, thus making Ca available to form fluorite. In vein-type greisens, the hydrothermal processes are at lower temperatures and there appears to be no evidence of boiling. Thus, in the case of greisenisation without boiling, F-bearing micas and topaz would form at high HF activity. Under conditions of very high F-activity topaz, greisens form as a result of the instability of muscovite in the presence of HF as indicated by the reaction shown below for the topaz-rich greisens of Mount Bischoff (Tasmania) (Wright and Kwak 1989):

$$\underset{\text{muscovite}}{K_2Al_4(Si_6Al_2O_{20})(OH)_4} + 6HF = \underset{\text{topaz}}{3Al_2(SiO_4)(OH,F)_2} + 3SiO_2 + 2K^{+} + 4H^{+} \tag{12.6}$$

An increase in the activity of H_2O, during cooling of the hydrothermal fluids would result in the breakdown of topaz and feldspars to release large quantities of HF, along with the formation of muscovite and quartz. The release of F, together with the muscovitisation and chloritisation of the biotites at depth, would result in the leaching of metals, their complexing with F, and their subsequent transport upward in the evolving system. In low-pressure environments, such as in subvolcanic to volcanic areas, the separation of aqueous phases from F-rich magmas causes low-pressure greisenisation. This results in the formation of greisen mineral assemblages, as indicated by the formation of topaz and fluorite in cavities of rhyolitic volcanics and ash-flow tuffs (Burt 1981). Fluorine-rich greisen systems are

characterized by the presence of fluorite and/or topaz as well as Li-rich micas (e.g., lepidolite or protolithionite). In both F- and B-rich systems, other components, such as CO_2, Cl, and H_2O, assume importance in terms of granitic melt behavior during crystallisation and exsolution of hydrothermal fluids (Pirajno 2013a).

12.5 Fluorine and Fluorite Precipitation in the Porphyry Systems of Eastern China

The porphyry Mo deposits of eastern China exhibit unusual features, particularly in terms of ore-fluid compositions, the common presence of fluorite, and hydrothermal alteration assemblages, which tend to be less hydrous than the porphyries at convergent margins (Pirajno and Zhou 2015). The eastern China porphyry deposits are characterized by generally H_2O-poor wall rock alteration, dominated by K-feldspar, epidote, carbonates, and fluorite and rather weak H_2O-rich alteration minerals, such as sericite and chlorite (e.g., Chen et al. 2009a, b; Han et al. 2013). Fluid inclusion studies (Yang et al. 2012; Li et al. 2012, 2013) have shown that K/Na, CO_2/H_2O, and F/Cl ratios are especially high in these intracontinental porphyry systems. Fluorine has been recognized as being preferentially linked to intracontinental (non-convergent plate margins) settings and having an important role in the transport and concentration of lithophile elements (Agangi et al. 2010). The ore minerals of porphyry deposits in eastern China are molybdenite, pyrite, sphalerite, and galena, accompanied by minor chalcopyrite, pyrrhotite, magnetite, and hematite. The gangue minerals are quartz, K-feldspar, plagioclase, fluorite, sericite, calcite, kaolinite, biotite, chlorite, and epidote.

The *Jiguanshan* porphyry deposit is situated in a Mesozoic rift basin, where ring-type and radial fault structures provided the channel ways for hydrothermal fluids and Mo mineralisation. A north-northwest-trending fault is filled by late fluorite veins cutting through the porphyry and pyroclastic rocks. The *Nannihu* porphyry deposit includes molybdenite, scheelite, pyrite, galena, sphalerite, and chalcopyrite. Hydrothermal alteration consists of potassic alteration with K-feldspar and biotite; widespread silicification associated with the quartz-sulphide stockworks; quartz-sericite overprinting mineral phase of the potassic alteration; and carbonate-fluorite alteration. According to Yang et al. (2012), four stages of alteration-mineralisation, from earliest to late, can be distinguished: (1) K-feldspar + biotite, with minor pyrite and molybdenite; (2) quartz-molybdenite stockworks; (3) quartz and sulphides (pyrite, chalcopyrite, molybdenite, and sphalerite, galena); and (4) veins of carbonate, fluorite, and quartz with little or no sulphides. The *Yuchiling* porphyry Mo deposit typically with stockworks, in which molybdenite is the chief ore mineral, also contains lesser amounts of pyrite, chalcopyrite, digenite, sphalerite, and galena. Li et al. (2012, 2013) recognized five stages of veins, from oldest to younger as follows: (1) early barren quartz ± K-feldspar ± magnetite, generally located in the central

parts of the host granite porphyry; (2) quartz-pyrite ± K-feldspar ± molybdenite ± sericite ± fluorite; (3) quartz-molybdenite veins, with minor pyrite, fluorite, and sericite, account for more than 90% of the ore; (4) quartz-polymetallic veins with a mineral association consisting of pyrite, molybdenite, chalcopyrite, digenite, galena, sphalerite, fluorite, and calcite; and (5) late barren quartz-calcite-fluorite veins. Fluorite is particularly abundant at Yuchiling, especially in the post-ore veins. From these examples and in general, the abundance of fluorite can be considered a diagnostic mineral of intracontinental porphyry systems, typically precipitated in the late stages of the hydrothermal activity.

12.6 Fluorite in the World-Class Vergenoeg Fe Oxides-Fluorite-REE Deposit: The Significance of F in Its Genesis

The Vergenoeg world-class, giant, Fe oxide (hematite, magnetite), fluorite, and REE deposit, is hosted by rhyolitic pyroclastic rocks of the Rooiberg Group and is located almost in the centre of the four lobes of the Bushveld Igneous Complex. The eruption of the Rooiberg rhyolitic rocks took place at about 2.06 Ga, but recent dating of fluorite has yielded a broadly coeval age of 2040 ± 46 Ma (Graupner et al. 2015). The deposit was studied in detail by Crocker (1985) and Borrok et al. (1998), whilst more recent works can be found in Fourie (2000), Goff et al. (2004), and Graupner et al. (2015). Other possibly coeval, and genetically associated deposits in the region, include a fluorite-magnetite-Cu-Au at Slipfontein hosted by Bushveld granite (Bobbejaankop granite), the Buffalo Fluorspar deposit, and the Zwartkloof fluorite-magnetite-fayalite veins, also hosted by the Rooiberg rhyolitic rocks.

The Vergenoeg deposit consists of a volcanic pipe, which formed by a gas-vapor eruption. It has a diameter of about 900 m at the surface, decreasing to about 400 m, at a depth of 600 m (Martini and Hammerback 1998). The pipe contains magnetite, siderite, fayalite, and fluorite, and cuts through the Vergenoeg Pyroclastic Suite (Crocker 1985). The Vergenoeg suite comprises a sedimentary unit, hematite and hematite-fluorite units, and a breccia agglomerate and ignimbrite, which forms a north-south elongate body of about 8–9 km. Hematite-fluorite, magnetite-fluorite, and magnetite-fayalite assemblages make up about 90% of the mineralogy (Fourie 2000). Other ore minerals include apatite, monazite, xenotime, and Fe and Cu sulphides. The fluorite has high P contents, which suggest the presence of xenotime, monazite, and rare-earth fluorocarbonates. Fluorite bodies are locally brecciated with large fluorite crystals in a matrix of fine-grained fluorite, siderite, pyrite, quartz, goethite, and limonite. A plug of massive magnetite is in the centre of the Vergenoeg pipe and is surrounded by a halo of pyrite and fluorite. Fayalite is found in the deepest levels of the pipe.

In the upper parts of the pipe, a porous hematite-goethite gossan, containing up to 20% fluorite, minor cassiterite, apatite, and REE minerals, constituted the main orebody from which fluorite is extracted. The gossan cap grades through a transition zone into the unoxidised ore. Sulphides (pyrite, chalcopyrite, arsenopyrite, and sphalerite) are present in the deeper levels of the pipe. Ore grades ranged from 20 to 40% CaF_2 and 50 to 60% Fe_2O_3 (Martini and Hammerback 1998). Fluorite resources are estimated at about 174 Mt, grading 28% CaF_2 (Fourie 2000; Graupner et al. 2015)

Since the Vergenoeg pipe is a volcanic vent, from which the pyroclastic material was erupted, an apron of fluorite-hematite-rich fragmental rocks (agglomerates, breccias, and epiclastic rocks) surround the pipe. The massive fluorite-hematite unit is interpreted as a lava flow of immiscible Fe-rich magma (Borrok et al. 1998). The breccia and agglomerate rocks contain large fragments of rhyolite and hematite enclosed in a matrix of hematite and fluorite. Also present is a rock that consists of irregular masses of cryptocrystalline silica with inclusions of hematite and fluorite. This rock type can be interpreted as a siliceous sinter deposit. A geological map and schematic section through the Vergenoeg pipe is shown in Fig. 12.6 (Graupner et al. 2015). Borrok et al. (1998) recognized an assemblage of primary minerals in the lower part of the pipe. The primary assemblage consists of fluorite, fayalite, ilmenite, apatite, allanite, and pyrrhotite. Early and late secondary assemblages developed due to alteration of the primary assemblage.

This large-scale, and nearly pervasive Fe enrichment at Vergenoeg, was considered by Crocker (1985) as a general trend of Fe-Ca-F-CO_2 enrichment due to the immiscibility of Fe-oxide-rich magmatic fractions. Exsolution and degassing of HF may have been an important factor, responsible for the pervasive Fe-F alteration in the region. In Crocker's model, HF-rich fluids flowing through an Fe-rich protolith, such as the mafic rocks of the Bushveld Igneous Complex, leach Ca and Fe to form fluorite, Fe-actinolite, and Fe oxides. As the fluids move upward and lose pressure, magnetite, siderite, and fluorite are precipitated. One of the reactions proposed is:

$$\begin{aligned} &4Ca_2Fe_5Si_8O_{22}(OH)(\text{Fe-actinolite}) + 16HF + 6O_2 \\ &\quad \rightarrow 8\,\text{fluorite} + 10\,\text{hematite} + \text{Fe-actinolite} + 32\ \text{quartz} + 10H_2O \end{aligned} \tag{12.7}$$

However, based on fluid inclusion and stable isotope studies, Borrok et al. (1998) dispute Crocker's model of immiscible oxide melts. Instead they suggested that the Vergenoeg mineralisation was formed by Fe-rich, high-temperature and high salinity magmatic hydrothermal fluids. The fluid inclusion assemblages recognized by Borrok et al. (1998) are both primary and pseudosecondary. Primary inclusions are of two types: liquid-rich with halite, Fe chloride, and sylvite daughter crystals, and CO_2-rich vapour with Fe chloride and halite daughter crystals. There are five types of pseudosecondary inclusions: liquid-rich with a single daughter crystal (halite), liquid-vapour, liquid-rich with hematite daughter crystals, liquid-rich with no daughter crystals, and CH_4-rich with no daughter crystals. Primary inclusions are saline (35–68 wt% NaCl equivalent) and have

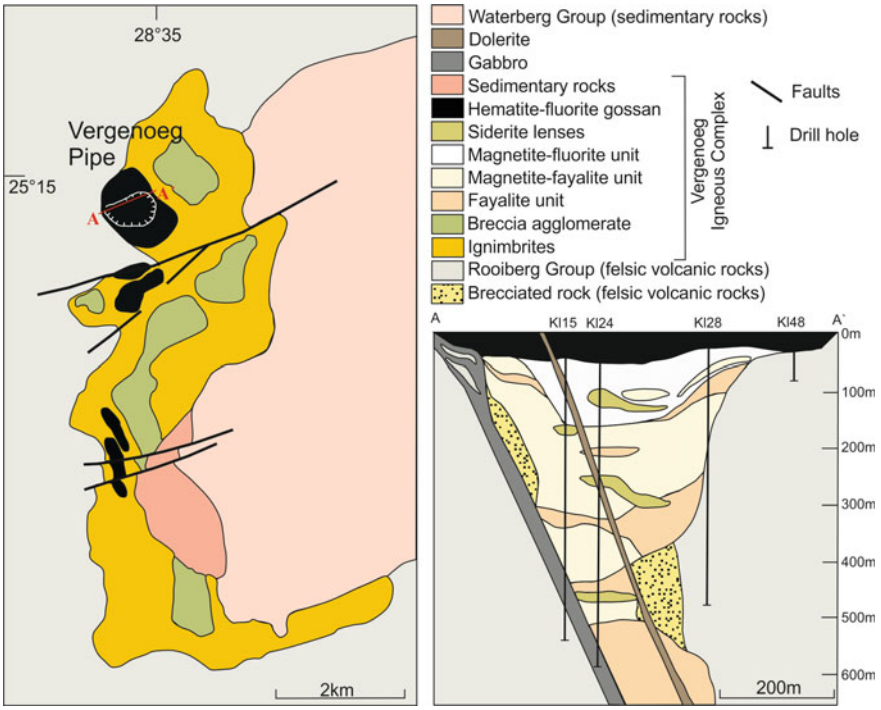

Fig. 12.6 Simplified geological map of the Vergenoeg complex (modified after Goff et al. 2004). On the *right* is a sketch showing a cross-section of the Vergenoeg pipe and lithological units. Figure courtesy of Torsten Graupner (Graupner et al. 2015)

homogenisation temperatures ranging from 482 to 290 °C for type 1 and 485 to 435 °C for the CO_2-rich inclusions. The pseudosecondary inclusions show a range of salinities from as low as 1% (liquid-rich, no daughters) to 29–35% NaCl equivalent for liquid-rich with daughter crystals, and a range of homgenisation temperatures from 120 to 540 °C (Fig. 12.7). Inclusion fluids from fluorite were used to determine the $\delta^{18}O$, δD, and $\delta^{13}C$ compositions. $\delta^{18}O$ values range from −0.9 to −10.8‰, and δD, from −91 to −53‰. The $\delta^{13}C$ compositions, determined from the CH_4 and CO_2-rich fluids, show values of about −28‰ (CH_4) and −12.7 to −1.9‰ (CO_2). Borrok et al. (1998) interpreted the stable isotope data to reflect fluids largely of magmatic origin, although they did not exclude some mixing with oxygenated fluids, probably meteoric. However, the work of Graupner et al. (2015) is in more agreement with the original model proposed by Crocker (1985). Graupner et al. (2015), on the basis of Sm–Nd isotope systematics, proposed that the high-field-strength elements (Y, Nb, REE, and associated minerals, such as fluorocarbonate, samarskite, and fluoroapatite) in the Vergenoeg pipe were derived from a granitic magma (Lebowa Granite, a felsic component of the Bushveld large igneous province; Hill et al. 1996; Ernst 2014). These primary mineral phases were

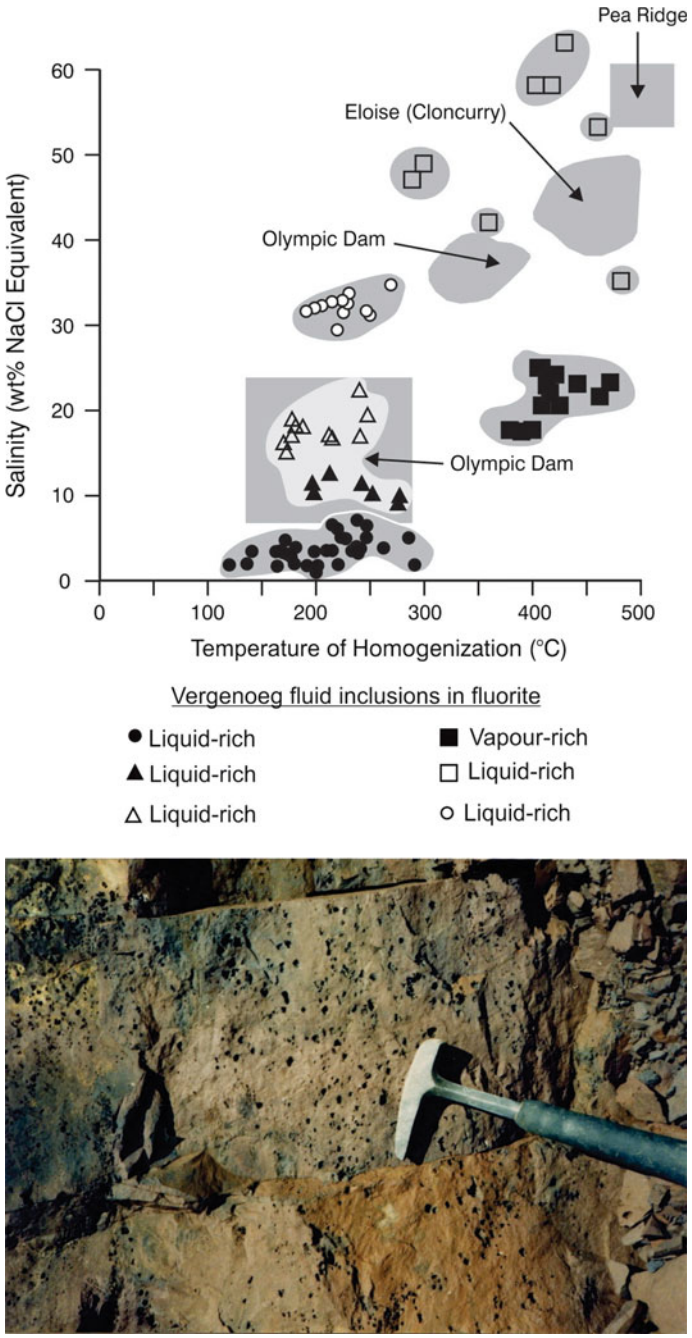

Fig. 12.7 Plot of homogenization temperatures versus salinity of fluid inclusions (wt% NaCl eqv), measured for fluorite in the Vergenoeg deposit, compared with the IOCG Olympic Dam and Cloncurry in Australia and Pea Ridge in the US (*shaded boxes*) (after Borrok et al. 1998). Photograph below shows vugs after fluorite in a hematitic lava flow near the Vergenoeg pipe (Pirajno, unpublished)

remobilised during later hydrothermal activity, resulting in the precipitation of fergusonite and xenotime, fine-grained fluorocarbonate, Ce-monazite, La-monazite, and Y-xenotime. Graupner et al. (2015) citing the fluid inclusions data of Borrok et al. (1998) (Fig. 12.7) emphasised the important role of Fe chlorides in the fluid system, apart from the NaCl component. Furthermore, the breakdown of the early (primary) apatite and fayalite was responsible for the release of Ca, P, F, Cl, and REE, nicely confirmed by cavity fillings of fluorite (Fig. 12.7).

12.7 Halogens in Skarn Deposits

Skarns generally form at the contact between intrusive plutons and the invaded country rocks. The latter generally are carbonates and, less commonly, Ca-rich silicate rocks, involving high-T, low-P metasomatic processes (Pirajno 2013a). Skarn genesis essentially involves isochemical contact metamorphism and metasomatism (prograde skarns), which is entirely due to the transfer of heat, fluids, and metals from the cooling plutonic body to the surrounding wall rocks. Skarns develop at temperatures ranging from between 700 and 200 °C and at pressures of between 3 and 0.3 kbar. The metasomatic fluids have salinities, which range from 10 to about 45 wt% NaCl equivalent.

Skarn alteration systems are typically zoned in response to temperature variations and fluid evolution outwards from the intrusive stock or pluton. This zonation begins from the endoskarn within the intrusion to proximal and distal exoskarns that develop in the country rocks. Retrograde stages of alteration occur during the final stages of cooling, resulting in more intense hydrothermal activity, local mixing with meteoric waters, and precipitation of sulphides and oxides, especially nearer the pluton's contacts, and overprinting of prograde assemblages. Mineral assemblages in retrograde skarns typically include hydrous phases, such as amphibole, biotite, epidote, and chlorite, although, as cautioned by Meinert et al. (2005), the presence of hydrous mineral phases does not necessarily imply retrograde processes. As mentioned above, retrograde minerals reflect the decreasing temperature and salinity of the fluids, leading to a trend from amphibole-epidote → biotite → muscovite-chlorite → sulphides → carbonates (+fluorite or scheelite or powellite).

The role of Cl and F in skarn mineral systems is almost exclusively related to the retrograde hydrous assemblages. There are many skarn systems, which contain fluorite in the retrograde paragenetic sequences. The polymetallic skarn deposits from the Middle-Lower Yangtze River Valley metallogenic province in China provide very good examples (Pirajno 2013b). The Tonglushan deposit is characterized by a massive exoskarn that typically consists of early prograde and a late retrograde skarn assemblages. The prograde skarn assemblage consists of andradite, grossular, diopside, hedenbergite, and scapolite, whereas the retrograde assemblage consists of epidote, actinolite, pargasite, phlogopite, chlorite, fluorite, and quartz. The Tonglushan skarn orebodies are approximately 2100 m long and up to 600 m

wide. The ore minerals are chalcopyrite, magnetite, bornite, and hematite, with minor quantities of chalcocite, cuprite, molybdenite, sphalerite, tetrahedrite, marcasite, and native gold and electrum. As in other skarn deposits, calcic and magnesian skarns occur, depending on the composition of the carbonate rocks (limestone or dolomite). Fluid inclusion data suggest four stages of mineralisation: (1) a skarn stage with homogenisation temperatures ranging from 740 to 426 °C; (2) a magnetite stage with temperatures from 506 to 340 °C; (3) quartz-sulphide precipitation from 360 to 240 °C; and (4) a carbonate stage from 250 to 150 °C.

In the Gascoyne Province of Western Australia are a number of Palaeoproterozoic W skarn occurrences associated with peraluminous granitic rocks (Davies 1998; Pirajno 2004). One of these occurrences is the Kilba Well scheelite prospect, in which skarns are developed in metasedimentary rocks wrapped around a monzogranite intrusion. The Kilba Well skarns consist of discontinuous bodies characterized by complex prograde and fluorite-bearing retrograde zones, which extend from the host marble units to the intrusive stock. The garnet-vesuvianite zone, is characterized by garnets, up to several cm across, and growth-banded vesuvianite. Minor scheelite is present in this zone and is associated with vesuvianite, calcite and feldspar. The garnet-pyroxene zone is present as remnants left from retrograde overprinting, although reconstructions based on drill core data, suggest that this zone was far more extensive. These remnants show coarse poikiloblastic garnet and fine- to medium-grained clinopyroxene, together with minor amounts of calcite, quartz, feldspar, epidote, actinolite, fluorite, and rare scheelite. The pyroxene zone is best developed along the footwall and hanging wall margins and is characterized by an increase in pyroxene and epidote group minerals. The assemblages in this zone occur as fine-grained granoblastic intergrowths of pyroxene with epidote, clinozoisite, and minor vesuvianite, calcite, quartz, albite, scheelite, and pyrrhotite. Zones of retrograde, hydrous alteration, can be separated into an amphibolite, vesuvianite and hydrosilicate zones. The amphibolite zone consists of actinolite laths, accompanied by calcite, phlogopite, clinozoisite, epidote, albite, quartz, titanite, pyyrrhotite and chalcopyrite. The vesuvianite zone is defined by abundant coarse and poikiloblastic vesuvianite with quartz, minor calcite, epidote, clinozoisite, actinolite, pyrrhotite, albite, fluorite, microcline, and apatite. Scheelite is present as inclusions in the vesuvianite or as single grains and is locally associated with fluorite. Hydrosilicate assemblages replace the prograde assemblages and are identified by the presence of hydrous mineral phases, mostly amphibole and phlogopite with varying proportions of quartz, calcite, epidote, vesuvianite, fluorite, scheelite, albite, allanite, titanite, pyrrhotite, chalcopyrite, and sphalerite. The Kilba Well scheelite mineralisation is preferentially sited in the retrograde zones of skarns that are typically Fe-poor. Scheelite solubility in the ore fluids is controlled by their composition and especially Ca concentrations. Hydration of Ca-rich assemblages increases the activity of the Ca^{2+} ions in the ore fluids, thereby enhancing the possibility of scheelite and fluorite precipitation.

12.8 Iodine, Br, and Cl in Evaporite Sequences and Sedimentary Basins

The composition of basinal waters is characteristic of a given sedimentary basin. Salinity increases with depth in sedimentary basins. This is explained by the mechanism of membrane filtration, a process whereby argillaceous sediments allow for the passage of neutral molecules (e.g., H_2O and H_2S), while preventing the migration of anions and cations, resulting in their downward concentration (Fyfe et al. 1978; Warren 2000, 2006). Thus, deeper waters become saltier and enriched in cations and anions. Elements that are usually enriched in formation waters are F, I, and Cl, as well as Pb, Zn, Ba, Br, Sr, and S. Basinal brines are generated by diagenesis and compaction and perhaps heated by a hidden thermal source. The brines move updip along the basin flanks towards the basement highs to form low-temperature Pb-Zn deposits of the Mississippi Valley type (Garven and Raffensperger 1997; Bradley and Leach 2003). During thrusting of various terranes on to a continental margin, saline fluids are expelled from the buried sediments and move towards the foreland (Fig. 12.8). These "tectonic brines" are responsible for Pb-Zn deposits of the Mississippi Valley type in carbonate host rocks (Garven and Raffensperger 1997; Bradley and Leach 2003; Pirajno 2009). Another example of large-scale brine development and movement is that of the northern platform zones of the Damara Orogen, Namibia, where numerous Cu-Pb-Zn-V deposits, including the world-famous Tsumeb, are present. These fluids were expelled and, during the late phases of orogenic compressions, moved along the length of the grabens, forming a mineralising front several hundreds of kilometres in length (Pirajno and Joubert 1993). The fluids moved in response to hydraulic gradients in clastic aquifers, along the grabens, and towards the basin margins, depositing ore minerals in chemically favourable traps constituted by the carbonate rocks of the northern platform of the Damara Orogen (Pirajno 1992). The hydrothermal fluids generated by this episodic dewatering are thought to be moved by tectonic activity such as, for example, the seismic pumping mechanism of Sibson et al. (1975, 2001). A particular mode of sedimentary, diagenetic, metalliferous, circulation of brines in basins was proposed by Jowett (1986) for the Kupferschiefer of central Europe. According to this model, the diagenetic brines form a convective cell which carries the brines downward into the deep parts of the basin, then up along the flanks of the basement highs, and then back down into the basin. Metal deposition occurred below the evaporitic sediments of the Zechstein, which is where the brines turn over for the return flow into the basin. It is acknowledged that many large-scale base metal deposits formed in continental rift basins, due to the fact that these rift basins promote the flow of metallifeorus hydrothermal brines (McKibben and Hardie 1997).

Plimer (1985, 1986) proposed different types of ensialic rifting (failed to successful), mantle degassing, and associated magmatism to explain the development of complex exhalites at Broken Hill and Mt. Isa in Australia. Plimer argued that the Mt. Isa orebodies were formed in an aulacogen-type rift setting where hypersaline

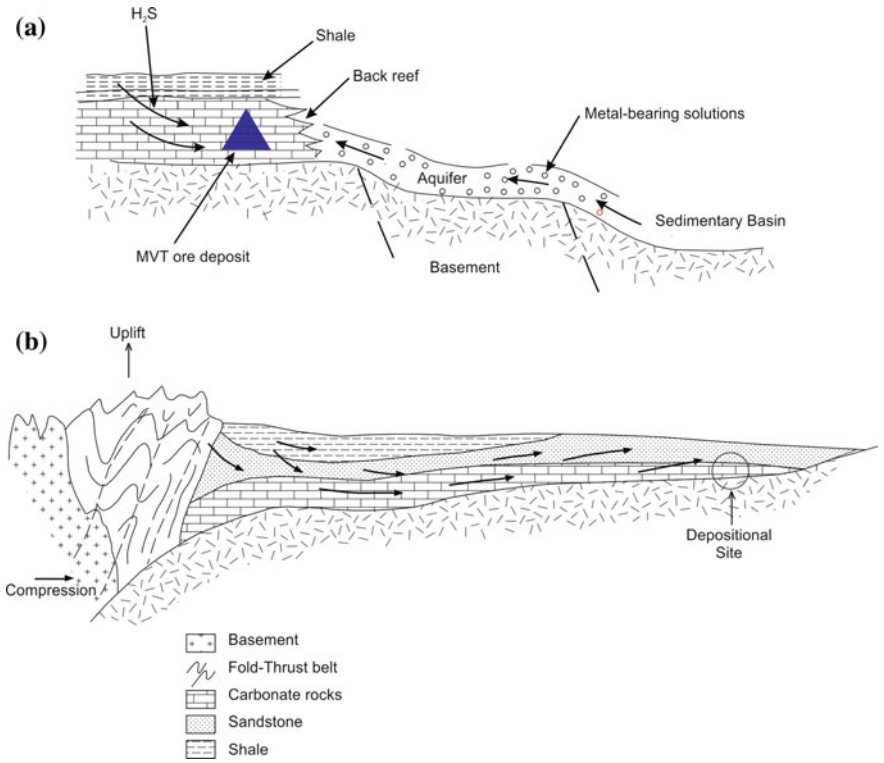

Fig. 12.8 Models to explain the origin of stratabound carbonate rock-hosted ore systems. **a** Basinal brines enriched in F, I, Cl, Pb, Zn, Ba, Br, Sr, and S, migrate from the sedimentary basin towards a carbonate reef where they encounter a reducing environment due to the presence of H_2S in organic matter. Sulphides are precipitated in solution cavities, or along faults and other reef structures (after Sverjensky 1986). **b** Uplift and formation of the Appalachian and Ouachita mountains during the Permian resulted in gravity-driven groundwater flow along regional aquifers across the mid-continent (after Garven and Raffensperger 1997)

(halogen-bearing) brines formed hydrothermal systems that were focused and exhaled into depressions in the deep grabens, with no magmatic component. The brines would have moved along major fractures and faults at high pressure. In contrast, the Broken Hill scenario has an association with bimodal (mafic-felsic) magmatism related to deeper and more successful rifting in a thinner continental crust. Plimer's model assumes mantle fluids, enriched in CO_2, F, Br, I, B, P, Mn, Fe, Pb, Zn, and REE, to have risen along the graben faults and to have locally mixed with sea water.

Worthy of note is the idea that non-magmatic models for the genesis of IOCG systems may include two categories: (1) fluids derived from the surface or a shallow basin or (2) metamorphic fluids passing through Cl-rich rocks or derived from deep basins. Barton and Johnson (1996) proposed that the saline fluids reponsible for these deposits are sourced from evaporites. They cited examples of Holocene

hydrothermal Fe oxides formed from evaporitic sources and the correlation between the Fe oxide-Cu-Au-REE-U of Mesozoic age with zones of low-latitude as revealed by continental reconstructions. The evaporitic source model of Barton and Johnson (1996) suggests that circulation of hydrothermal fluids is caused by magmatic heat, and that the source of the metals is provided by igneous rocks, but that the metal transport is effected by chlorides supplied by evaporitic deposits. An interesting variant on the Barton and Jounson's model was put forward by McPhie et al. (2011b), who suggested that basinal sedimentary rocks may have been involved in the genesis of the Olympic Dam IOCG deposit in South Australia. According to the authors, deep-seated hydrothermal activity and upwelling of related fluids would have interacted with the overlying sedimentary units of a pre-existing sedimentary basin, remnants of which are found as fragmented sedimentary beds in the Olympic Dam Breccia Complex.

Bromine and I ions are very soluble in natural waters and as such exist in several oxidation states, for example Br^-, I^- to BrO_3^- and IO_3^- (Li et al. 2015a). However, these halogen ions do not participate in low temperature exchange reactions nor do they become absorbed onto mineral surfaces, instead they form minerals when halite (NaCl) begins precipitation under extreme evaporation (Li et al. 2015a). These authors also reported that Br has a linear relationship with Cl and that Br/Cl ratios increase with increasing evaporation. Iodine, on the other hand, seems to be closely associated with the decomposition of organic matter. Li et al. (2015a), working on a large potash deposit in China, suggested that the I and I/Cl molar ratios are lower than in modern seawater, oil-field brines, and hydrothermal solutions and that there is no clear relationship between the concentrations of I, Cl, and Br. This could be interpreted to be the result that I remains in residual brines and does not enter crystal lattices, where the concentration of organic carbon is low or where the brines are of continental origin with low I contents.

Evaporites of Triassic age, with their Br-bearing saline brines, have been invoked as the main source of halogens in the fluids that formed the magnetite-apatite deposits in the Middle-Lower Yangtze River Valley (China) by Li et al. (2015b). These authors carried out a detailed fluid inclusions and microthermometric study in apatite, pyroxene, garnet, anhydrite, quartz, and calcite in the Meishan, Luohe, and Nihe magnetite-apatite deposits in the Ningwu and Luzong rift basins. Li et al. (2015b) found hypersaline brine inclusions in pyroxene and garnet, whereas aqueous two-phase inclusions occur in apatite, anhydrite, quartz, and calcite. Li et al. (2015b) also found that Cl/Br ratios in the hypersaline brines are substantially higher than most reference magmatic fluids, with the exception of the ones that have interacted with evaporites. Li et al. (2015b) concluded that the Fe, although in part derived from exsolved magmatic fluids and/or leached out of the igneous rocks, in a far larger amount was likely mobilised by relatively small amounts of hypersaline brines. Importantly, it is also pointed out that magmatic fluids have NaCl salinities of a few wt% and that large volumes of magmas are required to produce the hypersaline brines necessary for the transport of Fe in these magnetite-apatite deposits. However, when the magma is in contact with halite-bearing evaporites, then the resulting fluids can produce something like

20–30 times more brine than when there is no contact/interaction with evaporites. The authors concluded that evaporite assimilation is a powerful means by which large amounts of hypersaline fluids may be generated which in turn greatly enhances the mineralisation potential of the magmas.

Another example of the role of halogens derived from evaporite sequences can be found in the Franklinian Basin succession in northwest Greenland, which is an ideal source of brines as well as complexing ligands, such as Cl^-, for transport of metals and infiltration into the crystalline basement. The idea of external basinal brines causing hydrothermal alteration (and therefore retrogression) and mineralisation has been examined and modelled, in connection with Fe oxide-Cu-Au hydrothermal systems, by Barton and Johnson (2000). They proposed that evaporite-derived brines can cause deep-seated alkali metasomatism, with no magmatic water being necessary. Pirajno et al. (2003) studied Au-Cu and base metal mineralisation in Inglefield Land, NW Greenland and envisaged that external brines, derived from the Franklinian succession, infiltrated the basement via structural channels, provided by shear/mylonitic zones, created during advanced transposition of sandstone-shale layers. On the regional scale, this infiltration was facilitated by the northeast-trending corridor, postulated to be a regional crustal structure spatially associated with the Cu-Au occurrences. A genetic model, which postulates a "passive" role of evaporites in the formation of epigenetic mineralisation, is shown in Fig. 12.9.

12.8.1 Sabkha Evaporites

A sabkha is a coastal evaporite flat bordering a body of water on one side and a desert on the other. It differs from a normal evaporite pan in that the depositional environment is subaerial whereas that of an evaporite pan is subaqueous (Eugster 1986). In a coastal sabkha, groundwater evaporation causes solutes to be deposited at the sabkha surface. This results in a subsurface hydraulic gradient which induces marine water of high pH and low Eh to flow inland towards the sabkha, while meteoric underground water of low pH and high Eh flows seaward. The body of water adjacent to the sabkha is prolific with blue-green algae. These tend to form algal mats which, and upon decay and putrefaction, generate much H_2S, CO_2, and CH_4. The landward flowing marine waters are therefore enriched in these constituents, whereas the terrestrial meteoric waters carry traces of Cu, Ag, Zn, Pb, and Fe. On transgression, the algal facies will onlap the oxygenated desert sediments and at the same time the advancing marine water forces the meteoric waters back towards the land. An incipient sabkha forms when sediment supply and subsidence reach a steady state, causing an evaporite suite (aragonite-gypsum-halite) to rest on desert continental sediments. Magnesium from the sea water brine replaces the aragonite to form dolomite. During regression, the algal mat is over-ridden by the evaporites while the trailing edge is buried by desert sediments. The meteoric groundwaters are drawn towards the surface by the strong evaporation and

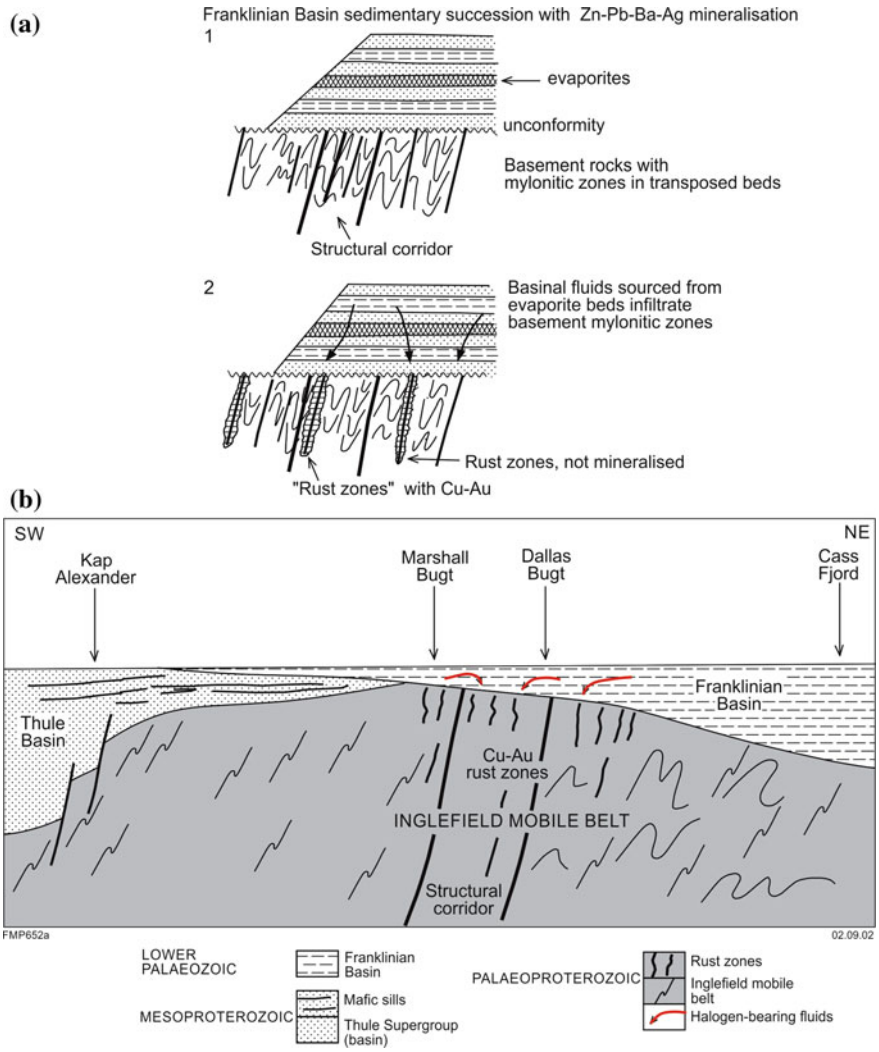

Fig. 12.9 This figure shows an example of the "passive" role of evaporites during the inflow of halogen-bearing hydrothermal fluids. The model purports to explain the origin of Cu–Au mineralisation in fracture zones (informally named rust zones) in basement rocks. Precursor rocks include a succession of sandstones and carbonaceous shales. These were intruded by granitoids and subjected to polyphase deformation and metamorphism up to granulite facies. Pyrrhotite is formed from early diagenetic sulphides, resulting in the transposition of layering parallel to the axial plane of the folds. Late to post tectonic granitoids may have intruded at this stage, with ongoing deformation, ductile shearing, and mylonitisation occurring along limbs of the less competent lithologies, such as carbonaceous shale. Graphite forms from carbonaceous shale. **a** Shows Franklinian sediments deposited in a basin that unconformably overlies the crystalline rocks of the Inglefield mobile belt (*1*). During compaction of the sediments, evaporite-sourced fluids flow downward to the hot basement and infiltrate the mylonitised zones, resulting in remobilisation of sulphides. Precipitation of the ore elements preferentially occurred in the rust zones within a structural corridor (*2*). **b** Is a schematic cross-section across the Inglefield mobile belt, showing the assumed original extent of the overlying Thule and Franklinian Basins (after Pirajno et al. 2003)

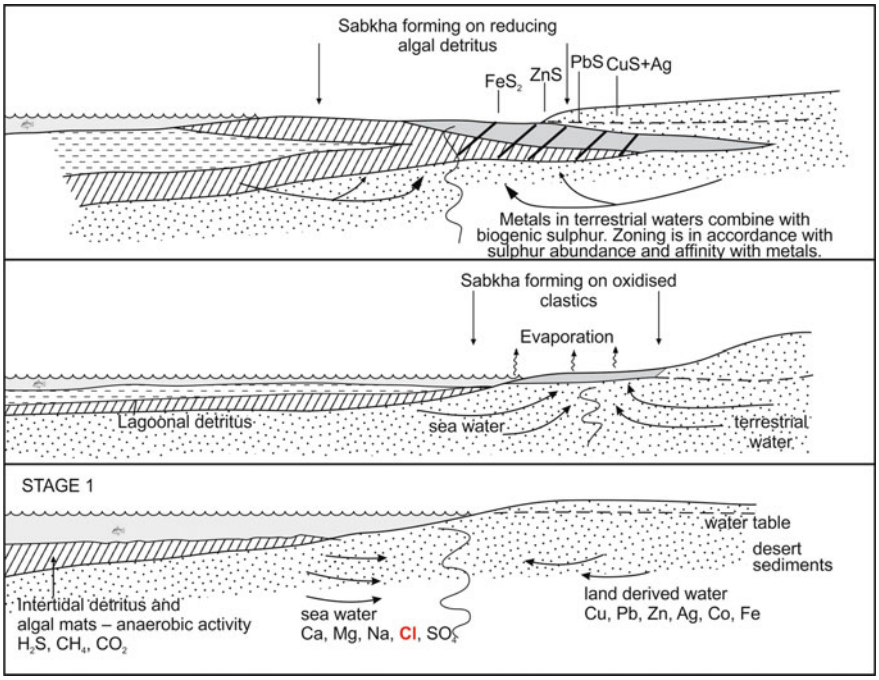

Fig. 12.10 Sabkah model for the genesis of Copperbelt type stratiform mineral systems. Interaction and inflow of halogens from seawater (Renfro 1974; Pirajno 1992). In this model several stages are involved (simplified in the figure), including the formation of the sabkha sequence, which consists mainly of aragonite, gypsum, and halite, overlying algal mats. Meteoric waters then migrate towards the surface due to the strong evaporation and precipitate sulphides when passing through the algal mat, which supplies the necessary H_2S

precipitate sulphides in passing through the decaying algal mat which supplies the necessary H_2S. A sabkha environment, thought to be responsible for the development of stratiform Cu(Co) Copperbelt-style deposits, is shown in Fig. 12.10 (Renfro 1974; Pirajno 1992).

12.9 Halogens in Mississippi Valley-Type, SEDEX, IOCG Mineral Systems and Orogenic (Metamorphogenic) Gold Deposits

The extensive work by Kendrick et al. (2001, 2002a, b, 2006, 2008) has highlighted the role of halogens (and noble gases) in the development, constraints, and evolution of Mississippi Valley-Type deposits (Kendrick et al. 2002a, b), for the Mt. Isa SEDEX deposits, mineral systems (Kendrick et al. 2006, 2008); as well as the influence of evaporitic brines together with hydrocarbons for sediment-hosted

Zn-Pb deposits from the Lennard Shelf in NW Australia. Kendrick and co-authors utilized fluid inclusions to examine the Br/Cl mol and I/Cl mol ratios, which they suggested to be related to interaction with evaporation of seawater and organic matter, respectively. In some cases the salinity of the fluids can reach an average of 22 wt% NaCl eqv, supporting the idea that crustal fluid sources are dominated by basinal brines.

The deposits of the Mississippi Valley have often been considered as classic examples of stratabound carbonate rock-hosted, base metal sulphide deposits, and for this reason are commonly referred to as Mississippi Valley-type, or MVT (Leach et al. 2005). At least three types or styles of MVT have been recognized: deposits of the Viburnun Trend (USA), Alpine-type deposits, and Irish Midland deposits (Pirajno 2009). While these deposits have a wide temporal geological distribution, they are most common in the Devonian to Permian, but also occur in the carbonate sequences of Palaeoproterozoic age, such as those from the Transvaal and Griqualand basins (Transvaal Supergroup) in South Africa (Pirajno 2009). A possible connection between the major Pb-Zn districts and areas containing petroleum and natural gas has been suggested (Sverjensky 1986; Oliver 1986; Eisenlhor et al. 1994). In the USA, areas of MVT Pb-Zn mineralisation occur along basin margins and there is almost a complete lack of overlap with the petroliferous areas. This type of spatial arrangement may reflect differential movement of fluids in the sedimentary basins, with base metal-bearing brines moving over longer distances than the more viscous oils, which require trapping in suitable structures. Mississippi oil-field brines contain appreciable amounts of Pb, Zn, Cu, Ag, Au, Co, and Ni (Saunders and Swann 1990), whereas Sverjensky (1986) showed that fluids with a composition similar to Mississippi oil-field brines could become an ore solution during migration towards the basin margins (Fig. 12.8). Sulphur and Pb isotope systematics and fluid inclusion studies of galenas from the Viburnum Trend corroborate the model that MVT ore-forming brines originated from sedimentary basins and that they have a similar composition to oil-field brines (Crocetti and Holland 1989). On the basis of Br^-, Cl^-, K^+, and Na^+ values of fluid inclusions in cubic and octahedral galenas, respectively, Crocetti and Holland (1989) also showed that the composition of oil-field brines was probably of marine-evaporite origin.

There are a number of conceptual models that attempt to explain the origin of stratabound carbonate rock-hosted base metal deposits. One model looks at the formation of brines during compaction, dewatering, and diagenesis of sediments in an evolving sedimentary basin. The brines include formation or connate waters, which would migrate from the centre towards basin margins in response to hydraulic gradients (Fig. 12.8). Migration of fluids occurs along great distances by mechanisms of tectonic expulsion, following continental collision, resulting in the focusing of the fluids along thrust faults. Another model, which may be more applicable to the Irish deposits, envisages that hydrothermal fluids move along faults and are discharged on the seafloor where they precipitate sulphides, sulphates, and oxides. The origin of the fluids in this case is more problematical, and a geothermal gradient, perhaps enhanced by a magmatic heat source, must be

assumed. The discovery of worm tubes and filamentous fossil bacteria in the Irish deposits confirms the role of bacteriogenic activity.

In all cases, however, it is clear that the carbonate host rocks play a dual role in that they constitute both physical and chemical traps. Features such as basin morphology, palaeotopographic highs, erosional surfaces, and palaeoaquifers are of particular significance for the origin of these deposits. In the case of MVT and Alpine types especially, basement highs play an important role in localising the mineralisation. Thus, the main controlling parameters must include (1) carbonate lithologies, which provide suitable sites for ore deposition, and (2) palaeogeographic features, such as basement highs and unconformities. An important prerequisite for the formation of hydrothermal ore systems is the permeability of the host rocks, which must allow for the passage of the ore fluids. Dissolution, brecciation (karsting), and dolomitisation of the host carbonates are therefore important in this respect. Dolomitisation and silicification are characteristic features of MVT deposits. Evaporite basins, if present, may be important sources of both Mg and S, as well as halogens. Evaporation of sea water causes precipitation of gypsum ($CaSO_4$-$2H_2O$), resulting in the removal of Ca, and thereby increasing the Mg^{2+}/Ca^{2+} ratio and migration of Mg, which may induce dolomitisation. Hydrothermal dolomite, or late dolomite cement (LDC), however, is also thought to form from the migration and effervesence of CO_2-rich basinal fluids interacting with carbonate rocks (Leach et al. 1991). Apart from dolomitisation, other alteration features associated with MVT Pb-Zn deposits are silicification and potassic alteration. The latter has been suggested by Hearn et al. (1987) on the basis of fluid inclusion studies of overgrowths on detrital K-feldspars and quartz grains in unmineralised rocks.Fluid inclusion studies of sphalerite and calcite in MVT deposits indicate that the fluids have temperatures on the order of 50 to 200 °C, more commonly from 95 to 120 °C. The fluids are Na-Ca-Cl sulphur-deficient brines, with salinities of approximately 20–30 wt% NaCl equivalent. Chloride complexing, and pH values less than neutral, were probably important for the transport of Pb and Zn. Other gas components in fluid inclusions are H_2O, CO_2, CH_4, and H_2, with high concentrations of F and Cl. Organic ligands have also been considered, as their presence has been ascertained in brines from oil fields. Metals, possibly contained as adsorbed ions on clay minerals, or even organic matter, could have been released during burial diagenesis and introduced into highly saline, pore fluids that are low in S. The low S content is possibly the result of fixing by Fe to form pyrite or marcasite during diagenesis. Movement of the metal-bearing brines occurs along permeable horizons, such as sandstone units, and up-dip towards the edges of the basin and the topographic highs, against which carbonate reefs are formed (Fig. 12.8). In this environment, there may be an influx of H_2S derived either from organic material in the carbonates or from overlying shales. The H_2S fluids mix with the metalliferous brines to precipitate sulphides in suitable traps within the carbonate lithologies.

With regards to the silica (quartz)-dolomite alteration that is typical of the Mt. Isa giant ore deposit (Queensland, Australia), the molar Br/Cl and I/Cl ratios in fluid inclusions are greater than seawater. It has been proposed that the mineralising fluids were derived from the mixing of metamorphogenic (dehydration of

crystalline basement) and surface-derived bittern brines (brines that form after the separation of NaCl and contain Mg salts, such as chlorides, bromides, and iodides; Warren 1999, 2010). Kendrick et al. (2006) envisaged a genetic model involving fluid mixing in two settings (their Fig. 14): (1) long-lived multiple stages of quartz veining and dolomite, related to asceding metamorphic fluids and subsequent mixing with downward convective bittern brines, and (2) dolomite precipitated from carbonate-rich, bittern brine formation water pore fluids, later mixing, and then overprinted by quartz veining resulting from silica-saturated deep metamorphogenic fluids. Furthermore, Kendrick et al. (2008) also examined fluid inclusions in quartz veins from the eastern Mount Isa Block (Mary Kathleen fold belt and Cloncurry district) in order to characterize the role of halogens (and noble gases) with the regional-scale Na-Ca alteration and its relationship with the IOCG of the Cloncurry district. The Br/Cl and I/Cl values for fluid inclusions from the Mary Kathleen fold belt are higher that those in the Cloncurry district, suggesting that the Na-Ca alteration in the two areas was formed independently and that the fluid inclusion data for Cloncurry indicate a genetic relationship with IOCG mineralisation.

Agangi et al. (2010, 2012) and McPhie et al. (2011a) studied and reported on the role of F in silicic magmas from the ~1590 Ma Gawler large igneous province (South Australia) and the supergiant Olympic Dam IOCG deposit. The Olympic Dam deposit (Laznicka 2010; Pirajno and Hoatson 2012) is hosted by the Olympic Dam Breccia Complex (ODBC) in the ca. 1590 Ma Roxby Downs Granite of the Hiltaba Suite, which is a coarse-granite syenogranite with A-type affinities. The deposit is characterized by a number of large Cu-, Au-, Ag-, U-, and REE-bearing hematite-quartz dyke-like breccia bodies. Copper is present as chalcopyrite, bornite, and chalcocite, Au and Ag form native metals. The main U minerals are coffinite, pitchblende and brannerite. The REE minerals are monazite, xenotime, bastnaesite, and florencite. The abundance of REE correlates with the increasing hematite content of the breccia. The formation of the breccias implies large-scale movements of high-pressure fluids.

The following is summarized from McPhie et al. (2011a). The Olympic Dam deposit is enriched in F. The mineral fluorite is quite common, occurring as disseminations and in veins, with about 2.5 wt% of the total ore mined consisting of fluorite. Furthermore, alteration minerals (sericite, chlorite, apatite) all contain high amounts of F (up to 5.3%). A genetic relationship with the F-rich Gawler Range Volcanics is envisaged, as shown by the presence of fluorite in vesicles and miarolitic cavities. Thus, it is likely that F was exsolved into late magmatic-hydrothermal fluids, which were ultimately responsible for the development of the ore-bearing hematitic breccias, formed by hydraulic fracturing due to fluid overpressure. McPhie and co-authors also suggested an important role for HF, which was able to dissolve the wall rocks of the Roxby Downs Granite, adding to the hematite-rich breccias. Figure 12.11 shows examples of fluorite occurrences in the Gawler Range Volcanics and at Olympic Dam.

Orogenic hydrothermal systems form in all stages of convergent and collisional to post-collision tectonics. These are hydrothermal systems related to devolatisation

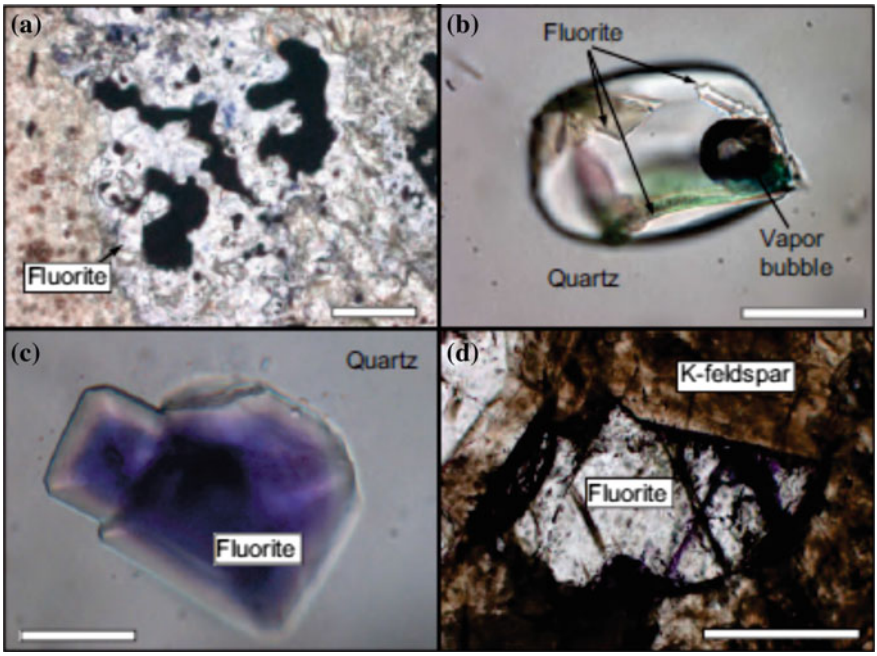

Fig. 12.11 **a** Fluorite intergrown with chalcocite (opaques) at Olympic Dam (scale bar is 100 μm). **b** Fluorite daughter crystals in melt inclusion in quartz from the Gawler Range rhyolitic volcanics (scale bar is 50 μm). **c** Fluorite crystal in quartz from the Gawler rhyolite (scale bar is 20 μm). **d** Fluorite crystal in the Hiltaba granite (scale bar us 500 μm). Figure courtesy of Prof J. McPhie

reactions during prograde regional metamorphism, with some fluids derived from mantle sources and/or magmas (some mixing with meteoric waters can occur). Ore deposition is almost invariably post-peak metamorphism, spanning the ductile, brittle-ductile, to brittle regimes. In some cases there is no obvious temporal and/or spatial relationship with the igneous intrusions. In other cases this relationship with granitic intrusives is inferred but by no means established.

Phillips et al. (1994) examined the role of metamorphic fluids in the formation of metamorphogenic (orogenic) ore deposits. These authors pointed out that the loss of volatiles during metamorphism is related to the metamorphic mineral assemblages, which lose volatiles as the metamorphic grade increases. The generation of fluids during metamorphism is important for metallogenesis, because they dissolve metals from large volumes of rocks and flow through networks of microcracks and fractures, which constitutes giant hydrothermal systems. Metamorphic fluids acquire the capacity of leaching, transporting, and depositing metals in structurally and/or lithologically controlled locales, resulting in a class of metalliferous deposits, commonly labelled metamorphogenic and/or mesothermal. The generation of metamorphic fluids is related to dehydration and decarbonation reactions, which

allow fluid flow, generally in the direction of decreasing temperature (Ferry 1994; Oliver et al. 1998). The dominant species of volatiles that are present in metamorphic environments are H_2O, CO_2, CO, H_2, Cl, F, S, CH_4, NH_3, inert gases, and hydrocarbons.

Finally, it is worth mentioning the work of Altigani et al. (2016), who in their geochemical study of the orogenic gold deposits of the Barberton Greenstone Belt in South Africa, found substantial amounts of Cl, Br, and I in suphides and gold from the Sheba, Fairview, and New Consort mines. Native gold and pyrite showed the highest Cl values. In the New Consort and Sheba Mines, the Cl-Br contents in gold and pyrite display a gap in their concentration, whereas in the Fairview Mine, Cl and Br show a continuous trend. Bromine contents in gold and are higher than in sulphides, whereas Cl concentration is variable within the gold and sulphides. Altigani et al. (2016) also found a positive trend between Hg, and Cl, Br, and I, which was interpreted as possibly due to sub-microscopic inclusions of Hg-containing halogenides (Hg(Cl,I)) (Fig. 12.12a). On the other hand, LA-ICP-MS halogen data indicate two distinct trends in Cl/Br ratios (Fig. 12.12b), and within them are characteristic associations (clusters), which are independent of a specific mineral. This clustering can be seen in the plot for Cluster 2 (pyrite Types 1 and 2 from New Consort, and pyrite Type 2 from Sheba) and Cluster 1 (gold Type 2 from New Consort, and arsenopyrite Type 1 from Fairview).

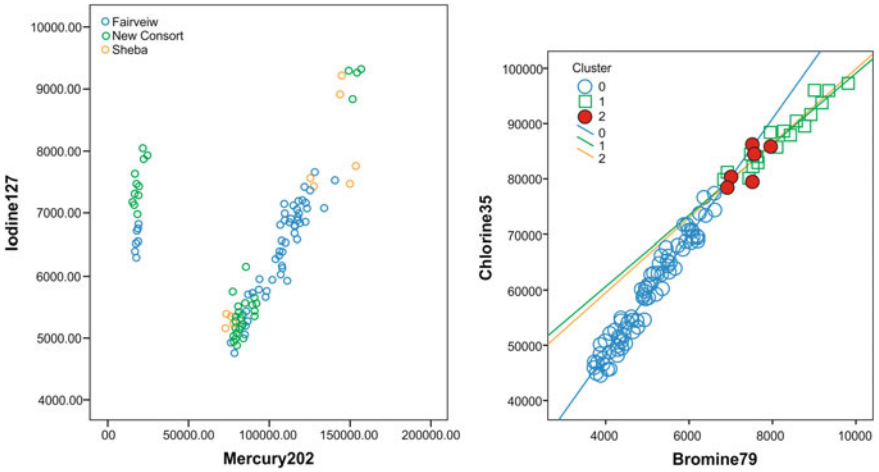

Fig. 12.12 **a** Plot of counts (cps) (LA-ICP-MS) for the range of minerals, from both Type 1 and Type 2, from the Sheba, Fairview, and New Consort mines. There are two distinct I bearing trends. One is without Hg, which could relate to the type of phase occurring as inclusions. This behavior is similar for Cl and Br. **b** Plot of Cl/Br ratios for all mineral phases (of both Types) at all mines. Cluster 2 (Type 1 and 2 pyrite from New Consort, and Type 2 pyrite from Sheba) and Cluster 1 (Type 2 gold from New Consort, and Type 1 arsenopyrite from Fairview) are related, despite the prominent difference in Hg, and are not related to Cluster 0 (the balance of the analysed minerals). Figures courtesy of Roger Dixon (Altigani et al. 2016)

12.10 Concluding Remarks

In this contribution I have reviewed the role of halogens (Cl, F, Br, I) in hydrothermal fluids, using examples of greisen systems, hot springs, geysers, crater lakes, porphyry and skarn deposits, fluids associated with intracontinental evaporite sequences, and Mississippi Valley-type, SEDEX, IOCG, and orogenic/metamorphogenic deposits. The function of halogens in hydrothermal solutions is effectively investigated using fluid and melt inclusions. This brings home the significance of halogens as ligands in complexing metals, whereby allowing their transport in solutions. The high salinity of hydrothermal fluids is largely due to the selective partitioning of halogens into the late stages of magmatic evolution and differentiation, dissolution of evaporite sequences, boiling, etc. There is little doubt that Cl and F are the most important of the halogens as contributors to the formation of hydrothermal mineral deposits. Chlorine is responsible for the complexing of metals at temperatures higher than 350 °C but, unlike F, commonly represented by fluorite, it is rarely found as individual, rock-forming, Cl-mineral phases, such as halite. Apatite, on the other hand, contains both Cl and F. It is interesting to note that the abundance of F is largely confined to specific tectono-thermal settings, such as those of large igneous provinces (Gawler silicic volcanics, Bushveld Igneous Complex) and intracontinental porphyry systems (eastern China). The use of Br/Cl and I/Cl has been proven to be extremely useful for fluid tracing, as well demonstrated through the work of Kendrick and co-workers. The review presented here hardly does justice to the complexity of the halogens in hydrothermal fluids and their evolutionary trends, however in the context of this chapter it is anticipated that some useful information would be gained by the reader.

Acknowledgements I am grateful to Dan Harlov for invitating me to write this contribution. I owe gratitude to Andrea Agangi and two anonymous reviewers for their detailed and insightful comments. These have led to a complete "reconstruction" of the chapter. My neighbour Murray Jones drafted most of the figures in record time; thank you Murray.

References

Agangi A, Kamenetsky VS, McPhie J (2010) The role of fluorine in the concentration and transport of lithophile trace elements in felsic magmas: insights from the Gawler Range Volcanics, South Australia. Chem Geol 273:314–325

Agangi A, Kamenetsky VS, McPhie J (2012) Evolution and emplacement of high fluorine rhyolites in the Mesoproterozoic Gawler silicic large igneous province, South Australia. Precambr Res 208–211:124–144

Agangi A, Kamenetsky VS, Hofmann A, Przybyłowicz W, Vladykin NV (2014) Crystallization of magmatic topaz and implications for Nb-Ta-W mineralization in F-rich silicic melts—the Ary-Bulak ongonite massif. Lithos 202–203:317–330

Aiuppa A, Baker DR, Webster JD (2009) Halogens in volcanic systems. Chem Geol 263:1–18

Altigani MAH, Merkel RKW, Dixon RD (2016) Geochemical identification of episodes of gold mineralization in the Barberton Greenstone Belt, South Africa. Ore Geol Rev 75:186–205

Bailey DK (1978) Mantle metasomatism, continuing chemical changes within the Earth. Nature 296:525–530

Bailey DK (1987) Mantle metasomatism—perspective and prospect. Geol Soc Lond, Spec Publ 30:1–14

Ballentine CJ, Burgess R, Marty B (2002) Tracing fluid origin, transport and interaction in the crust. Geochem Soc Mineral Soc Am, Rev Mineral 47:539–614

Barnes HL (1979) Solubilities of ore minerals. Geochemistry of hydrothermal ore deposits, 2nd edn. Wiley, New York, pp 404–410

Barton MD, Johnson DA (1996) Evaporitic source model for igneous-related Fe oxide-(REE-Cu-Au-U) mineralization. Geology 24:259–262

Barton MD, Johnson DA (2000) Alternative brine sources for Fe-oxide-(Cu-Au) systems: implications for hydrothermal alteration and metals. In: Porter TM (ed) Hydrothermal iron oxide copper-gold & related deposits: a global perspective. Australian Mineral Foundation, Adelaide, pp 43–60

Best MG (1982) Igneous and metamorphic petrology. WH Freeman, New York

Bodnar R, Cline J (2010) A group of papers on fluid inclusion research applied to ore deposits: an introduction. Econ Geol 105:325–327

Borrok DM, Kesler SE, Boer RH, Essene EJ (1998) The Vergenoeg magnetite-fluorite deposit, South Africa: support for a hydrothermal model for massive iron oxide deposits. Econ Geol 93:564–586

Botcharnikov RE, Shmulovich KI, Tkachenko SI, Korzhinsky MA, Rybin AV (2003) Hydrogen isotope geochemistry and heat balance of a fumarolic system: Kudriavy volcanoc, Kuriles. J Volcanol Geotherm Res 124:45–66

Bradley DC, Leach DL (2003) Tectonic controls of Mississippi Valley-type lead-zinc mineralization in orogenic forelands. Mineral Deposita 38:652–667

Brantley SL, Ágútsdóttir AM, Rowe GL (1993) Crater lakes reveal volcanic heat and volatile fluxes. GSA Today 3(7):1, 176–177

Brehler B, Fuge R (1978) Chlorine. In: Wedepohl KH, Correns CW, Shaw DM, Turekian KK, Zemann J (eds) Handbook of geochemistry, vol II-2. Springer, Berlin pp 17-A-1–17-O-1

Brimhall GH, Crerar DA (1987) Ore fluids: magmatic to supergene. In: Carmichael ISE, Eugster HP (eds) Thermodynamics and modelling of geological materials: minerals; fluids and melts. Reviews in mineralogy, vol 17. Mineralogical Society of America, Washington, DC, pp 235–321

Burnham CW (1979) Magmas and hydrothermal fluids. In: Barnes HL (ed) Geochemistry of hydrothermal ore deposits, 2nd edn. Wiley, New York, pp 71–136

Burt DM (1981) Acidity-salinity diagrams—application to greisen and porphyry deposits. Econ Geol 76:832–843

Cai MH, Mao JW, Ting L, Pirajno F, Huilian H (2007) The origin of the Tongken-Changpo tin deposit, Dachang metal district, Guanxi, China: clues from fluid inclusions and He isotope systematics. Mineral Deposita 42:613–626

Chen YJ, Ni P, Fan HR, Pirajno F, Lay Y, Su WC, Zhang H (2007) Diagnostic fluid inclusions of different types hydrothermal gold deposits. Acta Petrol Sinica 23(8):2085–2108 (in Chinese with English Abstract)

Chen YJ, Zhai MG, Jiang SY (2009a) Significant achievements and open issues in the study of orogenesis and metallogenesis surrounding the North China continent. Acta Petrol Sinica 25:2695–2726

Chen YJ, Pirajno F, Li N, Guo DS, Lai Y (2009b) Isotope systematics and fluid inclusion studies of the Qiyugou breccia pipe-hosted gold deposit, Qinling orogeny, Henan Province, China: implications for ore genesis. Ore Geol Rev 35:245–261

Cheng Y, Mao JW, Chang ZS, Pirajno F (2013) The origin of the world class tin-polymetallic deposits in the Gejiu district, SW China: constraints from metal zoning characteristics and 40Ar-39Ar geochronology. Ore Geol Rev 53:50–62

Cole DR, Drummond SE (1986) The effect of transport and boiling on Ag/Au ratios in hydrothermal solutions: a preliminary assessment and possible implications for the formation of epithermal precious metal ore deposits. J Geochem Expl 25:45–79
Collins WJ, Beams SD, White AJR, Chappell (1982) Nature and origin of A-type granites with particular reference to southeastern Australia. Contrib Mineral Petrol 80:189–200
Crerar DA, Wood S, Brantley S, Bocarsly A (1985) Chemical controls on solubility of ore forming minerals in hydrothermal solutions. Can Mineral 23:333–351
Crocetti CA, Holland HD (1989) Sulphur-lead isotope systematics and the composition of fluid inclusions in galena from the ViburnumTrend, Missouri. Econ Geol 84:2196–2216
Crocker IT (1985) Volcanogenic fluorite-hematite deposits and associated pyroclastic rock suite at Vergenoeg, Bushveld Complex. Econ Geol 80:1181–1200
Davidson P, Kamenetsky VS (2001) Immiscibility and continuous felsic melt-fluid evolution within the Rio Blanco porphyry system, Chile: evidence from inclusions in magmatic quartz. Econ Geol 96:1921–1929
Davies BM (1998) Proterozoic zoned tungsten-bearing skarns and associated intrusives of the northwest Gascoyne Complex, Western Australia. Geol Sur West Aus Rpt 53
Doherty AL, Webster JD, Goldoff BA, Piccoli PM (2014) Partitioning behavior of chlorine and fluorine in felsic melt-fluid(s)-apatite systems at 50 MPa and 850–950 °C. Chem Geol 384:94–111
Dolejs D, Zajacz Z (2018) Halogens in silicic magmas and their hydrothermal systems. In: Harlov DE, Aranovich L (eds) The role of halogens in terrestrial and extraterrestrial geochemical processes: surface, crust, and mantle. Springer, Berlin, pp 431–543
Eadington PJ (1983) A fluid inclusion investigation of ore formation in a tin-mineralized granite, New England, New South Wales. Econ Geol 78:1204–1221
Eisenlhor BN, Tompkins LA, Cathles LM, Barley ME, Groves DI (1994) Mississippi Valley-type deposits: products of brine expulsion by eustatically induced hydrocarbon generation? An example from northwestern Australia. Geology 22:315–318
Ellis AJ, Mahon WAJ (1977) Chemistry and geothermal systems. Academic Press, New York, 392pp
Ernst RE (2014) Large igneous provinces. Cambridge Univ Press, Cambridge, p 653
Eugster HP (1984) Granites and hydrothermal ore deposits: a geochemical framework. Mineral Mag 49:7–23
Eugster HP (1986) Lake Magadi Kenya: a model for rift valley hydrochemistry and sedimentation? Geol Soc Lond Spec Publ 25:177–190
Ferry JM (1994) A historical review of metamorphic fluid flow. J Geophys Res 99:15487–15498
Foster RP (1977) Solubility of scheelite in hydrothermal chloride solutions. Chem Geol 20:27–43
Foster RP, Mann AG, Armin T, Burmeister B (1978) Richardson's Kop wolframite deposit: a geochemical model for the behavior of tungsten. In: Verwoerd WJ (ed) Mineralization in metamorphic terranes. Van Schaik, Pretoria, pp 107–128
Fourie PJ (2000) The Vergenoeg fayalite iron oxide fluorite deposit, South Africa: some new aspects. In: Porter TM (ed) Hydrothermal iron oxide copper-gold & related deposits: a global perspective. Australian Mineral Foundation, Adelaide, pp 309–320
Fournier RO, Christainsen RL, Hutchinson RA, Pierce KL (1994) A field-trip guide to the Yellowstone National Park, Wyoming, Montana and Idaho – volcanic, hydrothermal and glacial activity in the region. U.S. Geol Surv Bull 2099
Fyfe WS, Price NJ, Thompson AB (1978) Fluids in the Earth's crust. Elsevier, Amsterdam
Garven G, Raffensperger JP (1997) Hydrogeology and geochemistry of ore genesis in sedimentary basins. In: Barnes HL (ed) Geochemistry of ore deposits, 3rd edn. Wiley, New York, pp 125–189
Goff BH, Weinberg R, Groves DI, Vielreicher NM, Fourie PJ (2004) The giant Vergenoeg fluorite deposit in a magnetite-fluorite-fayalite REE pipe: a hydrothermally altered carbonatite-related pegmatoid? Mineral Petrol 80:173–199

Graupner T, Mühlbach C, Schwarz-Schampera U, Henjes-Kunst F, Melcher F, Terblanche H (2015) Mineralogy of high-field-strength elements (Y, Nb, REE) in the world-class Vergenoeg fluorite deposit, South Africa. Ore Geol Rev 64:583–601

Guest J, Cole P, Duncan A, Chester D (eds) (2003) Volcanoes of Southern Italy. The Geological Society, London, p 284

Han YG, Zhang SH, Pirajno F, Zhou XW, Zhao GC, Qü WJ, Liu SH, Zhang JM, Liang HB, Yang K (2013) U-Pb and Re–Os isotopic systematics and zircon Ce^{4+}/Ce^{3+} ratios in the Shiyaogou Mo deposit in eastern Qinling, central China: insights into the oxidation state of granitoids and Mo (Au) mineralization. Ore Geol Rev 55:29–47

Hearn PP, Sutter JF, Belkin HE (1987) Evidence for Late-Palaeozoic brine migration in Cambrian carbonate rocks of the central and southern Apalachians: implications for Mississippi Valley-type sulfide mineralization. Geochim Cosmochim Acta 51:1323–1334

Hedenquist JW, Henley RW (1985) Hydrothermal eruptions in the Waiotapu geothermal system, New Zealand: origin, breccia deposits and effect on precious metal mineralization. Econ Geol 80:1640–1666

Hedenquist JW, Arribas A, Reynolds TJ (1998) Evolution of an intrusion-centered hydrothermal system: far Southeast-Lepanto porphyry and epithermal Cu-Au deposits, Philipines. Econ Geol 93:373–404

Hedenquist JW, Arribas A, Gonzalez-Urien E (2000) Exploration for epithermal gold deposits. Soc Econ Geol Rev 13:245–277

Henley RW, Ellis AJ (1983) Geothermal systems ancient and modern: a geochemical review. Earth Sci Rev 19:1–50

Hill M, Barker F, Hunter D, Knight R (1996) Geochemical characteristics and origin of the Lebowa Granite Suite, Bushveld Complex. Int Geol Rev 38(3):195–227

Hockstein MP, Browne PRL (2000) Surface manifestations of geothermal systems with volcanic heat sources. In: Sigurdson H (Chief Ed) Encyclopedia of volcanoes. Academic Press, San Diego, pp 835–855

Hurwitz S, Christiansen LB, Hsieh PA (2007) Hydrothermal fluid flow and deformation in large calderas: inferences from numerical simulations. J Geophys Res 112:B02206, p 16. https://doi.org/10.1029/2006JB004689

Huston DL, Large RR (1989) A chemical model for the concentration of gold in volcanogenic massive sulphide deposits. Ore Geol Rev 4:171–200

Jowett EC (1986) Genesis of Kuperfschiefer during Cu-Ag deposits by convective flow of rotliengendes brines during Triassic rifting. Econ Geol 81:1823–1837

Kamenetsky VS, Naumov VB, Davidson P, van Achterbergh E, Ryan CG (2004) Immiscibility between silicate magmas and aqueous fluids: a melt inclusion pursuit into the magmatic-hydrothermal transition in the Omsukchan Granite (NE Russia). Chem Geol 210:73–90

Kendrick MA, Burgess RAD, Pattrick SD, Turner G (2001) Fluid inclusion noble gas and halogen evidence on the origin of Cu- porphyry mineralising fluids. Geochim Cosmochim Acta 65 (16):2651–2668

Kendrick MA, Burgess R, Leach D, Pattrick RAD (2002a) Hydrothermal origins in Mississippi Valley-type ore districts: combined noble gas (He, Ar, Kr) and halogens (Cl, Br, I) analysis of fluid inclusions from the Illinois-Kentucky fluorspar distrit, Viburnum Trend, and Tr-State Districts, Midcontinent United States. Econ Geol 97:453–469

Kendrick MA, Burgess R, Pattrick RAD, Turner G (2002b) Hydrothermal fluid origins in a fluorite-rich MississippiValley-type district: combined noble gas (He, Ar, Kr) and halogen (Cl, Br, I) analyses of fluid inclusions from the South Pennine ore field, United Kingdom. Econ Geol 97(3):435–451

Kendrick MA, Duncan R, Phillips D (2006) Noble gas and halogen constraints on mineralizing fluids of metamorphic versus surficial origin: Mt Isa, Australia. Chem Geol 235:325–351

Kendrick MA, Baker T, Fu B, Phillips D, Williams PJ (2008) Noble gas and halogen constraints on regionally extensive mid-crustalNa-Ca metasomatism, the Proterozoic Eastern Mount Isa Block, Australia. Precambr Res 163:131–150

Kendrick MA, Phillips D, Wallace M, Miller JMcL (2011) Halogens and noble gases in sedimentary formation waters and Zn-Pb deposits: a case study from the Lennard Shelf, Australia. App Geochem 26:2089–2100

Keppler H, Wyllie PJ (1991) Partitioning of Cu, Sn, Mo, W, U and Th between melt and aqueous fluid in the systems haplogranite-H_2O-HCl and aplogranite-H_2O-O-HF. Contrib Mineral Petrol 109:139–150

Krauskopf KB (1979) Introduction to geochemistry, 2nd edn. McGraw-Hill Kogakushu New York, p 617

Laznicka P (2010) Giant metallic deposits; future sources of industrial metals, 2nd edn. Springer, Berlin, pp 960

Leach DL, Plumlee GS, Hofstra AH, Landis GP, Rowan EL, Viets JG (1991) Origin of late dolomite cement by CO_2-saturated deep basin brines: evidence from the Ozark region, central United States. Geology 19:348–351

Leach DL, Sangster DF, Kelley KD, Large RR, Garven G, Allen CR, Gutzmer J, Walters S (2005) Sediment-hosted lead-zinc deposits: a global perspective. Econ Geol 100:561–608

Lecumberri-Sanchez P, Bodnar R (2018) Halogen geochemistry of ore deposits: contributions towards understanding sources and processes. In: Harlov DE, Aranovich L (eds) The role of halogens in terrestrial and extraterrestrial geochemical processes: surface, crust, and mantle. Springer, Berlin, pp 261–305

Li N, Ulrich T, Chen YJ, Thomsen TB, Pease V, Pirajno F (2012) Fluid evolution of the Yuchinling porphyry Mo deposit, East Qinling, China. Ore Geol Rev 48:442–459

Li N, Chen YJ, Pirajno F, Ni ZY (2013) Timing of the Yuchiling giant porphyry Mo system, and implications for ore genesis. Mineral Deposita 48:505–524

Li MG, Yan F, Wang ZR, Liu XM, Fang XM, Li J (2015a) The origins of the Mengye potash deposits in the Lanping-Simao Basin, Yunnan Province, Western China. Ore Geol Rev 69:174–186

Li W, Audédat A, Zhang J (2015b) The role of evaporites in the formation of magnetite-apatite deposits along the Middle and Lower Yangtze River, China: evidence from LA-ICP-MS analysis of fluid inclusions. Ore Geol Rev 67:264–278

Mariano AN (1989) Nature of economic mineralization in carbonatites and related rocks. In: Bell K (ed) Carbonatites, genesis and evolution. Unwin Hyman, London, pp 149–172

Martini JEJ, Hammerback ECI (1998) Fluorspar. In: Wilson MGC, Anhaeusser CR (eds) The mineral resources of South Africa. Council Geoscience Handbook 16, pp 269–279

Masterton WL, Slowinski EJ, Stanitski CL (1981) Chemical principles, Holt-Saunders, 5th edn. Saunders, Philadelphia, p 641

McKibben MA, Hardie LA (1997) Ore-forming brines in active continental rifts. In: Barnes HL (ed) Geochemistry of hydrothermal ore deposits, 3rd edn. Wiley, New York, pp 877–935

McPhie J, Kamenetsky VS, Allen S, Ehrig K, Agangi A, Bath A (2011a) The fluorine link between a supergiant ore deposit and a silicic large igneous province. Geology 39(11):1003–1006

McPhie J, Kamenetsky VS, Chambefort I, Ehrig K, Green N (2011b) Origin of the supergiant Olympic Dam Cu-U-Au-Ag deposit, South Australia: was a sedimentary basin involved? Geology 39(8):795–798

Meinert LD, Dipple GM, Nicolescu S (2005) World skarn deposits. Econ Geol 100(4): 299–336

Mi J-X, Pan Y (2018) Halogen-rich minerals: crystal chemistry and geological significances. In: Harlov DE, Aranovich L (eds) The role of halogens in terrestrial and extraterrestrial geochemical processes: surface, crust, and mantle. Springer, Berlin, pp 123–184

Migdisov AA, William-Jones AE (2014) Hydrothermal transport and deposition of the rare earth elements by fluorine-bearing aqueous liquids. Mineral Deposita 49:987–997

Oliver J (1986) Fluids expelled tectonically from orogenic belts: their role in hydrocarbon migration and other geological phenomena. Geology 14:99–102

Oliver NHS, Rubenach MJ, Valenta RK (1998) Precambrian metamorphism, fluid flow and metallogeny of Australia. AGSO J Geol Geophys 17:31–53

Paterson DJ, Ohmoto H, Solomon M (1981) Geologic setting and genesis of cassiterite-sulfide mineralization at Renison Bell, western Tasmania. Econ Geol 76:393–438

Philips GN, Williams PJ, De Jong G (1994) The nature of metamorphic fluids and significance for metal exploration. Geol Soc Lond, Spec Publ 78:55–68
Pichavant M (1981) An experimental study of the effect of boron on a water saturated haplogranite at 1kbar vapour pressure. Contrib Mineral Petrol 76:430–439
Pichavant M, Manning D (1984) Petrogenesis of tourmaline granites and topaz granites; the contribution of experimental data. Phys Earth Planet Int 35:31–50
Pirajno F (1992) Hydrothermal mineral deposits—principles and fundamental concepts for the exploration geologist. Springer, Berlin, p 708
Pirajno F (2004) Metallogeny in the Capricorn Orogen, Western Australia, the result of multiple ore-forming processes. Precambr Res 128:411–440
Pirajno F (2007) Mantle plumes, associated intraplate tectono-magmatic processes and ore systems. Episodes 30:6–19
Pirajno F (2009) Hydrothermal processes and mineral systems. Springer, p 1250
Pirajno F (2013a) Effects of metasomatism on mineral systems and their host rocks: alkali metasomatism, skarns, greisens, tourmalinites, rodingites, black-wall alteration and listvenites. In: Harlov DE, Austrheim H (eds) Metasomatism and metamorphism: the role of fluids in crustal and upper mantle processes, lecture series in earth science. Springer, Berlin, pp 203–252
Pirajno F (2013b) The geology and tectonic settings of China's mineral deposits. Springer, Dordrecht
Pirajno F (2015) Intracontinental anarogenic alkaline magmatism and carbonatites, associated mineral systems and the mantle plume connection. Gondwana Res 27:1181–1216. https://doi.org/10.1016/j.gr.2014.09.008
Pirajno F, Bentley PN (1985) Greisen-related scheelite, gold and sulphide mineralisation at Kirwans Hill and Bateman Creek, Reefton District, New Zealand. NZ J Geol Geop 28:97–109
Pirajno F, Hoatson DM (2012) A review of Australia's large igneous provinces and associated mineral systems: implications for mantle dynamics through geological time. Ore Gel Rev 48:2–54
Pirajno F, Jacob RE (1987) Sn-W metallogeny in the Damara Orogen, South West Africa/Namibia. S Afr J Geol 90:239–235
Pirajno F, Joubert BD (1993) An overview of carbonate-hosted mineral deposits in the Otavi Mountain Land, Namibia: implications for ore genesis. J Afr Earth Sci 16(3):265–272
Pirajno F, Zhou TF (2015) Intracontinental porphyry and porphyry-skarn mineral systems in eastern China: scrutiny of a special case "made-in-China". Econ Geol 110:603–629
Pirajno F, Thomassen B, Dawes PR (2003) Copper-gold occurrences in the Palaeproteroic Inglefield mobile belt, northwest Greenland: a new mineralisation style? Ore Geol Rev 22:225–249
Plimer IR (1985) Broken Hill Pb-Zn-Ag deposit: a product of mantle metasomatism. Mineral Deposita 20:147–153
Plimer IR (1986) Sediment-hosted exhalative Pb-Zn deposits: products of contrasting ensialic rifting. Trans Geol Soc S Afr 89:57–73
Pollard PJ (1983) Magmatic and postmagmatic processes in the formation of rocks associated with rare element deposits. Trans Inst Min Metall 92:B1–B9
Pollard PJ, Pichavant M, Charoy B (1987) Contrasting evolution of fluorine- and boron-rich tin systems. Mineral Deposita 22:315–321
Renaut RW, Jones B (1997) Controls on aragonite and calcite precipitation in hot spring travertines at Chemurkeu, Lake Bogoria, Kenya. Can J Earth Sci 34:801–818
Renaut RW, Tiercelin JJ, Owen RB (1986) Mineral precipitation and diagenesis in the sediments of Lake Bogoria basin, Kenya rift valley. Geol Soc Lond Spec Publ 25:159–176
Renaut RW, Jones B, Tiercelin JJ, Tarits C (2002) Sublacustrine precipitation of hydrothermal silica in rift lakes: evidence from Lake Baringo, central Kenya Rift Valley. Sed Geol 148:235–257
Renfro AR (1974) Genesis of evaporite-associated stratiform metalliferous deposits—a sabkha process. Econ Geol 15:362–366

Rickard D, Luther GW (2006) Metal sulfide complexes and clusters. Rev Mineral Geochem 61:421–504
Roedder E (1984) Fluid inclusions. Reviews in mineralogy. Mineralogical Society of America 12:644
Roedder E, Bodnar RJ (1997) Fluid inclusion studies of hydrothermal ore deposits. In: Barnes HL (ed) Geochemistry of hydrothermal ore deposits, 3rd edn. Wiley, New York, pp 657–697
Salvi S, William-Jones AE (1996) The role of hydrothermal processes in concentrating high-field strength elements in the Strange Lake peralkaline complex, northeastern Canada. Geochim Cosmochim Acta 60(11):1917–1932
Saunders JA, Swann CT (1990) Trace-metal content of Mississippi oil field brines. J Geochem Explor 37:171–183
Scandone R, Lisetti G, Fattori Speranza F (2006) The volcanological history of the volcanoes of Naples: a review. In: de Vivo B (ed) Volcanism in the Campania Plain: Vesuvius, Campi Flegrei and Ignimbrites. Elsevier, Amsterdam, pp 1–26
Schminke H-U (2004) Volcanism. Springer, Berlin, p 324
Shepherd T, Rankin AH, Alderton DHM (1985) A practical guide to fluid inclusion studies. Chapman & Hall, New York, p 239
Sherlock RL (2005) The relationship between the McLaughlin gold-mercury deposit and active hydrothermal systems in the Geysers-Clear Lake area, northern Coast Ranges, California. Ore Geol Rev 26:349–382
Sherlock RL, Tosdal RM, Lehman NJ, Graney JR, Losh S, Jowett EC, Kesler SE (1995) Origin of the McLaughlin mine sheeted vein complex: metal zoning, fluid inclusion and isotopic evidence. Econ Geol 90:2156–2181
Sibson RH (2001) Seismogenic framework for hydrothermal transport and ore deposition. Rev Econ Geol 14:25–50
Sibson RH, Moore JM, Rankin AH (1975) Seismic pumping: a hydrothermal fluid flow transport mechanism. J Geol Soc London 131:653–659
Sigurdsson H, Houghton BF, McNutt SR, Rymer H, Stix J (eds) (2000) Encyclopedia of volcanoes. Academic Press, New York, p 1417
Sowerby JR, Keppler H (2002) The effect of fluorine, boron and excess sodium on the critical curve in the albite-H_2O system. Contrib Mineral Petrol 143:32–37
Stoppa F, Pirajno F, Schiazza M, Vladykin NV (2016) An overview of Italian carbonatites as a strategic resource. Gondwana Res 37:152–171
Sverjensky DA (1986) Genesis of Mississipi valley-type lead-zinc deposits. Ann Rev Earth Planet Sci 14:177–199
Taran YA, Pilipenko VP, Am Rzhkov, Vakin EA (1992) A geochemical model for fumaroles of the Mutnovsky volcano, Kamchtaka, USSR. J Volcanol Geotherm Res 49:269–283
Taran YA, Hedenquist JW, Korzhinsky MA, Tkachenko SI, Shmulovich KI (1995) Geochemistry of magmatic gases from Kudriavy volcano, Iturup, Kuril Islands. Geochim Cosmochim Acta 59:1749–1761
Taran YA, Pokrovsky BG, Volynets ON (1997) Hydrogen isotopes in hornblendes and biotites from Quaternary volcanic rocks of the Kamchatka-Kurile arc. Geochem J 31:203–221
Teiber H, Marks MAW, Wenzel T, Siebel W, Altherr R, Markl G (2014) The distribution of halogens (F, Cl, Br) in granitoid rocks. Chem Geol 374–375:92–109
Thomas R, Förster H-J, Rickers K, Webster JD (2005) Formation of extremely F-rich hydrous melt fractions and hydrothermal fluids during differentiation of highly evolved tin-granite magmas: a melt/fluid inclusion study. Contrib Mineral Petrol 48:582–601
Van den Kerkhof A, Hein UF (2001) Fluid inclusion petrography. Lithos 55:27–47
Vigneresse JL (2009) Evaluation of the chemical reactivity of the fluid phase through hard-soft acid-base concepts in magmatic intrusions with application to ore generation. Chem Geol 263:69–81
Warren JK (1999) Evaporites: their evolution and economics. Blackwell Scientific, Oxford, p 438
Warren JK (2000) Evaporites, brines and base metals: low-temperature ore emplacement controlled by evaporite diagenesis. Aus J Earth Sci 47:179–208

Warren JK (2006) Evaporites: sediments, resources and hydrocarbons. Springer, Berlin, p 1036
Warren JK (2010) Evaporites through time: tectonic, climatic and eustatic controls in marine and nonmarine deposits. Earth Sci Rev 98:217–268
Webster JD (1990) Partitioning of F between H_2O and CO_2 fluids and topaz rhyolite melt—implications for mineralizing magmatic-hydrothermal fluids in F-rich granitic systems. Contrib Mineral Petrol 104:424–438
Webster JD (1997) Exsolution of magmatic volatile phases from Cl-enriched mineralizing granitic magmas and implications for ore metal transport. Geochim Cosmochim Acta 61:1017–1029
Webster JD, Duffield WA (1994) Extreme halogen abundance in tin-rich magma of the Taylor Creek rhyolite, New Mexico. Econ Geol 89:840–850
Webster JD, Tappen CM, Mandeville CW (2009) Partitioning behavior of chlorine and fluorine in the system apatite-melt-fluid: felsic silicate systems at 200 MPa. Geochim Cosmochim Acta 73:559–581
Webster J, Baker DR, Aiuppa A (2018) Halogens in mafic and intermediate-silica content magmas. In: Harlov DE, Aranovich L (eds) The role of halogens in terrestrial and extraterrestrial geochemical processes: surface, crust, and mantle. Springer, Berlin, pp 307–430
Westra G, Keith SB (1981) Classification and genesis of stockwork molybdenum deposits. Econ Geol 76:844–873
Wilkinson JJ (2001) Fluid inclusions in hydrothermal ore deposits. Lithos 55:229–272
William-Jones AE, Bowell RJ, Migdisov AA (2009) Gold in solution. Elements 5:281–287
Wright JH, Kwak TAP (1989) Tin-bearing greisens of Mount Bischoff, northwestern Tasmania, Australia. Econ Geol 84:551–574
Yang YF, Li N, Chen YJ (2012) Fluid inclusion study of the Nannihu giant porphyry Mo-W deposit, Henan Province, China: implications for the nature of porphyry ore-fluid systems fromed in a continent collision setting. Ore Geol Rev 46:83–94
Zellmer GF, Edmonds M, Straub SM (eds) (2015) The role of volatiles in the genesis, evolution and eruption of arc magmas. Geol Soc Lond Spec Publ 410
Zhong R, Brugger J, Chen YJ, Li WB (2015) Contrasting regimes of Cu, Zn and Pb transport in ore-forming hydrothermal fluids. Chem Geol 395:154–164

Chapter 13
The Role of Halogens in the Lithospheric Mantle

Maria Luce Frezzotti and Simona Ferrando

Abstract The present chapter focuses on the still poorly known sources, distribution and fractionation of halogens in the oceanic and continental lithospheric mantle in intraplate and extensional tectonic settings, and in the deep cratonic sub-continental mantle that hosts diamonds and kimberlites. In the lithospheric mantle, halogens are considered to be mainly stored in volatile-bearing metasomatic minerals, such as apatite, amphibole, and phlogopite. However, recent studies demonstrate that the nominally anhydrous minerals, incorporating measurable amounts of water as hydroxyl, are important storage sites for F, and to a lesser extent Cl. The halogen contents of minerals influence their stability in the lithospheric mantle, and they might be responsible for halogen enrichment and trace element signatures in some primitive basaltic melts. Over the last 20 years a growing body of evidence, based mainly on fluid inclusion data, has confirmed that relatively high amounts of halogens can be dissolved in aqueous-carbonic fluids, which may be locally immiscible, and in hydrous carbonate melts which ascend through the lithospheric mantle in intraplate and extensional settings. Metasomatic halide-bearing fluids are important carriers of incompatible trace elements (e.g., LILE and LREE). The highest halogen concentrations in fluids are observed in inclusions in fibrous and cloudy diamondsfrom the deep cratonic lithosphere. It is now well established that diamond-forming fluids consist of complex silicate-carbonate-Cl-aqueous mixtures formed by mixing of a hydrous-silicic fluid (rich in SiO_2, Al_2O_3, and K_2O), carbonatitic fluid (containing high concentrations of carbonate, CaO, FeO, MgO, and variable Na_2O and K_2O), and saline aqueous fluid (rich in Cl, K, and Na) end-member types. Halogen enrichment in lithospheric mantle fluids, both in the vicinity of, and away from, subduction zones, suggests a dynamic balance in the halogen geochemical cycle, which is ruled by recycling of surface halogens and mantle fractionation processes.

M.L. Frezzotti (✉)
Department of Earth and Environmental Sciences, University Milano-Bicocca,
Piazza della Scienza 4, 20126 Milan, Italy
e-mail: maria.frezzotti@unimib.it

S. Ferrando
Department of Earth Sciences, University of Torino, Via Valperga Caluso, Turin, Italy

D.E. Harlov and L. Aranovich (eds.), *The Role of Halogens in Terrestrial and Extraterrestrial Geochemical Processes*, Springer Geochemistry,
https://doi.org/10.1007/978-3-319-61667-4_13

13.1 Introduction

The Halogens (Cl, F, Br, and I) are volatile elements that are present only in trace amounts in peridotites where F and Cl reach maximum concentrations of tens to hundreds of ppm, and Br and I are present in ultra-low ppb abundances (Table 13.1). Chlorine, and especially F, can substitute for hydroxyl in hydrous and nominally anhydrous mineral phases, since F has an ionic radius similar to that of oxygen (e.g., Faure 1991; Aiuppa et al. 2009).

Despite their very limited abundance, the halogens represent key tracers of volatile fluxes in the mantle, because of their variable degrees of incompatibility and contrasting geochemical behaviour. A large number of studies have confirmed that Cl and F can be fractionated by partial melting processes, by fractional crystallization in magmas, or by partitioning between immiscible fluids and/or melts (e.g., Wyllie 1989; Wyllie and Tuttle 1961, 1964; Koster Van Groos and Wyllie 1968; Webster 1990, 1992; Bureau and Keppler 1999). Very little is known on the behaviour of Br and I, although they are expected to show highly incompatible behaviour because of their larger ionic radii (i.e., Cl < Br < I; Table 13.1; Schilling et al. 1980; Pyle and Mother 2009; John et al. 2011). Halogens are incompatible fluid-mobile elements. Consequently, understanding the distribution of halogens in the Earth's main reservoirs is critical to our knowledge of the Earth's dynamics. In the lithospheric mantle, including the cratonic lithosphere, which hosts diamonds and kimberlites, halogens (e.g., F and Cl) are incorporated mainly in metasomatic

Table 13.1 Halogen chemical properties and distribution in the Earth's mantle

Halogens	F	Cl	Br	I	*Ref.*
Chemical properties					
Atomic number	9	17	35	53	**1, 2, 3**
Atomic mass	18.998	35.453	79.904	126.905	
Radius of ion, $\times 10^{-12}$ m	133	181	195	216	
Stable isotopes	^{19}F	^{35}Cl, ^{37}Cl	^{79}Br, ^{81}Br	^{127}I	
Radiogenic isotopes		^{36}Cl		^{129}I	
Estimated concentrations in the Earth's mantle in ppm[10]					
Primitive mantle	25 (40%)	30 (40%)	0.075 (50%)	0.007	**4**
Primitive mantle	18 (40%)	1.4 (40%)	0.0036 (50%)	0.001	**5**
Depleted mantle	65	7.3	0.02		**6**
Depleted mantle	11	0.51 (18%)			**7**
Depleted mantle	16	1 (50%)			**8**
CI chondrite	58.2 (15%)	698 (15%)	3.5 (10%)	433 (20%)	**9**

Numbers in parentheses indicate the estimated percentage error. 1—Greenwood and Earnshaw (1984); 2—Railsback (2003); 3—Wasson (1985); 4—Palme and Jones (2003); 5—Palme and O'Neill (2003); 6—Lyubetskaya and Korenga (2007); 7—Schilling et al. (1980); 8—Salters and Stracke (2004); 9—Saal et al. (2002); 10—Hofmann (1988). Numbers in parenthesis indicate the estimated percentage error in the value, as quoted by the original source. Modified from Pyle and Mather (2009)

phases, such as apatite, mica, and amphibole, and in nominally anhydrous minerals (e.g., Foley et al. 1986; Dooley and Patiño Douce 1996; Motoyoshi and Hensen 2001; Patiño Douce and Roden 2006; Barnes et al. 2018). An increasing number of fluid inclusion studies confirm that halogen-rich silicate/carbonate melts, or CO_2-brine fluids, are locally present in the lithospheric mantle and can be involved in metasomatic processes, including the genesis of diamonds (e.g., Klein-BenDavid et al. 2007; Kamenetsky et al. 2004, 2007; Frezzotti and Peccerillo 2007, and references therein).

The lithosphere represents the mechanical barrier between asthenospheric fluids or melts and the crust, and for this reason records mass transfer and convective heat processes (i.e. metasomatism). Much recent research has been concentrated on subduction zones, with the perspective of tracing the Earth's halogen cycle, and their effects on upper mantle evolution. In particular, since Cl has a high H_2O fluid-silicate melt partition coefficient, it represents a reliable tracer of H_2O cycling (cf., Barnes and Sharp 2006; Kendrick 2012; Kendrick et al. 2014; Barnes et al. 2018). Up to 70% of the subducted Cl budget is considered by a large part of the scientific community (e.g., Philippot et al. 1998) to be released in the mantle wedge and recycled via arc magmatism as opposed to only 4–6% of the F budget (e.g., Straub and Layne 2003). This suggests that only subordinate amounts of Cl, but relevant amounts of F, may be transported into the convecting mantle.

In the oceanic and continental lithosphere, different halogen concentrations and fractionations are predicted (e.g., higher F/Cl ratios; Table 13.1), although sources and fractionation patterns are still in part obscure. A number of geochemical studies have shown that there are differences in the halogen contents between mid-ocean ridge basalts (MORB) and ocean island basalts (OIB) (e.g., Saal et al. 2002; Salters and Stracke 2004). Remarkable differences in Cl/K ratios are observed in OIBs as a function of radiogenic-isotope signatures. For example, Cl/K ratios are higher in magmas from HIMU-type mantle sources than in those from EM1-, and EM2-type sources (e.g., Stroncik and Haase 2004). These observed differences reflect variable additions of distinct lithospheric components in OIB sources, inducing chemical heterogeneities in the upper mantle (e.g., Hofmann 2003). There is controversy, however, regarding whether substantial amounts of halogens may be attributed to ancient subduction events reactivated by decompression and heating, or whether they testify to the recycling of crustal material in large deep-interior reservoirs (e.g., Philippot et al. 1998; Dixon et al. 2002; Holland and Ballentine 2006; Kendrick et al. 2012).

This chapter focuses on the distribution of halogens in the lithospheric mantle in intraplate, and extensional (e.g., rift) tectonic settings, as well as in deep-cratonic settings. Examples are taken mostly from peridotite and pyroxenite xenoliths from the oceanic and continental lithosphere, diamonds in kimberlites, and peridotite massifs. The main halogen-bearing hydrous and anhydrous mineral phases in peridotites and pyroxenites, including nominally anhydrous minerals, are described, and their utility in understanding halogen geochemistry in the source lithospheric mantle is discussed. Halogen-rich minerals, such as phlogopite, that generally form in the mantle wedge metasomatized by subduction-derived fluids (see Barnes

et al. 2018) are also reported. Estimates of halogen abundance and distribution in the lithospheric mantle are discussed based on the composition of fluid trapped in inclusions in peridotites, pyroxenites, and diamonds. Because of their relatively higher abundances in lithospheric mantle rocks, we focus mainly on reviewing the distribution of Cl and F.

13.2 Halogens in Lithospheric Mantle Minerals

There are two potential categories of mineral hosts for halogens in lithospheric peridodites and pyroxenites. The first one is represented by the volatile-bearing minerals formed during modal metasomatism (O'Reilly and Griffin 2013; Luth 2014). Their compositions, abundance, and microstructural relationships are indirect evidence of the abundance and mobility of halogens and, as a consequence, of fluids and melts in the lithospheric mantle. The second category is represented by the nominally anhydrous minerals, which are able to incorporate measurable amounts of water as hydroxyl. Halogens change the *P-T-X* stability field of metasomatic mantle minerals and nominally anhydrous minerals to an extent that is not in proportion with their low concentration. In addition, halogens are also important for the interpretation of trace element patterns in mantle rocks, and, more generally, for the interpretation of lithospheric mantle chemical, and physical evolution. This chapter presents a review of halogen occurrences, halogen contents, and *P-T-X* evolution (from thermodynamic calculations and/or experiments) of metasomatic minerals hosting halogens in the lithospheric mantle.

13.2.1 Phosphates

13.2.1.1 Apatite

Apatite [$Ca_5(PO_4,CO_3OH, SO_3OH)_3(OH, F, Cl)$] has been shown to be one of the most important halogen-bearing accessory minerals on Earth. In lithospheric mantle rocks, apatite is a common metasomatic phase, typically present only in small amounts (e.g., Smith et al. 1981; O'Reilly and Griffin 2000; Patiño Douce et al. 2011; O'Reilly and Griffin 2013, and references therein). Apatite has also been observed as inclusions in diamonds and in the groundmass of kimberlites and lamproites (e.g., Guthrie et al. 1991; Chalapati Rao et al. 2004). A large number of halogen studies in apatite have shown that almost all metasomatic apatites in the lithospheric mantle incorporate high, although variable, amounts of Cl, F and Br (e.g., Smith et al. 1981, and references therein; O'Reilly et al. 1991; Ionov et al. 1997, 2000; Morishita et al. 2003; O'Reilly and Griffin 2000, and references therein).

Two distinct types of metasomatized, lithospheric mantle apatites were recognized more than 20 years ago (Griffin et al. 1984; O'Reilly et al. 1991; O'Reilly and Griffin 2000, and references therein; Patiño Douce et al. 2011, and references therein). While this classification is not encompassing, it is useful because different halogen concentrations are observed as a function of the metasomatic agents responsible for the mineral formation. The first type is termed metasomatic "lherzolite apatite" (e.g., Smith et al. 1981) or type A (O'Reilly and Griffin 2000) and typically occurs in mantle spinel lherzolites (Type I xenoliths of Frey and Prinz 1978). It is a hydroxy-chlorapatite in which the Cl content ranges from 1 to 3 wt%, and Br from 6 to 50 ppm. The F content is usually below 1.0 wt%. It is commonly associated with amphibole, and can contain abundant fluid inclusions. The highest values of Cl in metasomatic "lherzolite apatite" have been reported in peridotites from the Finero Massif (Italy; Morishita et al. 2003) and in mantle xenoliths from Spitzbergen, Mongolia, and SE Australia (O'Reilly et al. 1991; Ionov et al. 2000; O'Reilly and Griffin 2000). Locally significant CO_2 in the mineral structure, as CO_3OH^{3-} substituting for PO_4^{3-}, has been measured (up to 1.74 wt%; O'Reilly et al. 1991; O'Reilly and Griffin 2000). Usually, these apatites show relatively high Th, U, Sr, and REE contents (O'Reilly et al. 1991; O'Reilly and Griffin 2000).

The second type is a "magmatic mantle apatite" (type B; O'Reilly and Griffin 2000), which commonly occurs in pyroxenitic veins and layers in peridotitic rocks. It represents frozen melts, which show variable degrees of evolution (Type II xenoliths of Frey and Prinz 1978), and as interstitial grains within spinel lherzolites. This type may also occur as discrete megacrysts or be intergrown with other minerals of the "mantle megacryst suite" commonly found as xenocrysts in many alkali basalts. It is a hydroxy-fluor apatite in which Cl ranges from 0.12 to 0.53 wt%, Br from 1–2 ppm, and F from 1.2 to 3.5 wt% (the highest F value is reported from Eifel; O'Reilly and Griffin 2000). CO_2 is either below detection limits, or has, in most cases, not been analyzed.

Thermodynamic calculations presented by Patiño Douce et al. (2011) indicate that both apatite types crystallized from metasomatic fluids (sensu lato), in which the bulk H_2O contents were greater than the F and Cl contents by at least an order of magnitude, and the relative contents of the halogens were variable. This is in agreement with the suggestion of O'Reilly and Griffin (2000) that a carbonate-bearing brine, containing 500–3500 ppm Cl, was the metasomatic fluid responsible for the "lherzolite apatites".

Such relatively Cl-rich, F-poor metasomatic fluids are common in subduction zones (Barnes et al. 2018), though locally they occur in areas of present-day lithospheric extension (Ethiopian plateau; Bullenmerri, Australia; Nunivak, Alaska; Frezzotti et al. 2010; O'Reilly and Griffin 2000; Patiño Douce et al. 2011). In this latter case, a possible origin by crystallization from Cl-rich, aqueous-carbonic metasomatic fluids, related either to ancient subduction events or to deep-seated mantle reservoirs, has been suggested (O'Reilly and Griffin 2000; Frezzotti et al. 2010; Patiño Douce et al. 2011).

However, thermodynamic models suggest that the crystallization of OH- (and Cl-) rich "lherzolite apatites" is enhanced not only by Cl-rich fluids, but also by low crystallization temperatures, and by unusually high P abundances (Patiño Douce et al. 2011). In the lithospheric mantle, apatite can be also derived from C-rich metasomatic fluids/melts. Experiments suggest that these fluids/melts should be Cl-rich, but apatites in carbonatites generally are Cl-free and show extreme enrichment in F (Patiño Douce et al. 2011, and references therein).

Experimental work on apatite stability predicts its presence in cold thermal regimes at $P < 4$–5 GPa (i.e., in the subcontinental lithospheric mantle), but not along an average mantle adiabat (Konzett and Frost 2009; Konzett et al. 2012). There have been several studies on the stability of apatite in complex mantle systems. The solidus for a phlogopite-apatite assemblage in the K_2O–CaO–MgO–Al_2O_3–SiO_2–P_2O_5–H_2O–F system has been experimentally determined at 2 GPa and 1225 °C, for the F-free system, and at 2 GPa and 1260 °C, for the F-bearing system (F/OH = 1) (Vukadinovic and Edgar 1993).

The experimental solidus for the K-richterite + clinopyroxene + phlogopite + ilmenite + apatite assemblage occurs at 1025–1075 °C at 1.5 GPa and at ca. 1300 °C at 5 GPa (Foley et al. 1999). Experiments on Cl-apatite + phlogopite peridotite at 2.5–8.7 GPa and 800–1000 °C reveal that: (i) apatite coexists with Ca-amphibole at 2.5 GPa, with phlogopite at 2.5–5 GPa, and with K-richterite at 7 GPa; (ii) all silicates contain 0.2–0.6 wt% Cl; and (iii) Cl strongly increases the solubility of K in hydrous fluids, and then enhances the breakdown of phlogopite (Konzett et al. 2012). In high-F systems, phlogopite preferentially incorporates F and allows the formation of hydroxy-chloro-apatite (Patiño Douce et al. 2011).

13.2.1.2 Whitlockite

Whitlockite, $Ca_{18}Mg_2(PO_4)_{12}[PO_3(OH)]_2$, is a volatile-poor phosphate (e.g., Hughes et al. 2008) and is the most common accessory phosphate in meteorites and igneous rocks from Mars and the Moon. It also occurs in terrestrial magmatic apatite deposits that probably are mantle-derived (Griffin et al. 1972). Its mantle occurrence has been reported in mantle xenoliths from Siberia (Ionov et al. 2006), where it is associated with F-rich apatite and shows Cl and F contents up to 0.1 wt%, or to 0.2 wt%, respectively. The thermodynamic models by Patiño Douce et al. (2011) reveal that (i) whitlockite usually forms at the expense of apatite due to a decrease in the chemical potential of the volatile components or to an increase in the chemical potential of P_2O_5; (ii) the apatite and whitlockite can coexist at equilibrium only over a relatively restricted *P-T-X* range of chemical potential conditions; and (iii) the equilibrium of the apatite–whitlockite assemblage indicates relatively low water activity conditions and high halogen and P contents.

13.2.2 Hydrous Silicates

13.2.2.1 Amphibole

Amphibole is the dominant hydrous modal metasomatic silicate in the lithospheric mantle (e.g., Dawson and Smith 1982, and references therein; Harte 1987, and references therein; O'Reilly and Griffin 2013, and references therein; Luth 2014, and references therein). In intraplate settings, amphibole occurs as disseminated crystals that are *interstitial*, associated with the spinel, or that surround pyroxenes (Fig. 13.1). It has been reported in peridotites and in pyroxenite veins found as xenoliths in alkali basalts (e.g., Garcia et al. 1980; Smith et al. 1981; Dawson and Smith 1982, and references therein; Witt-Eickschen and Harte 1994; Vannucci et al. 1995; Vaselli et al. 1995; Johnson et al. 1996; Ionov et al. 1997; Moine et al. 2000,

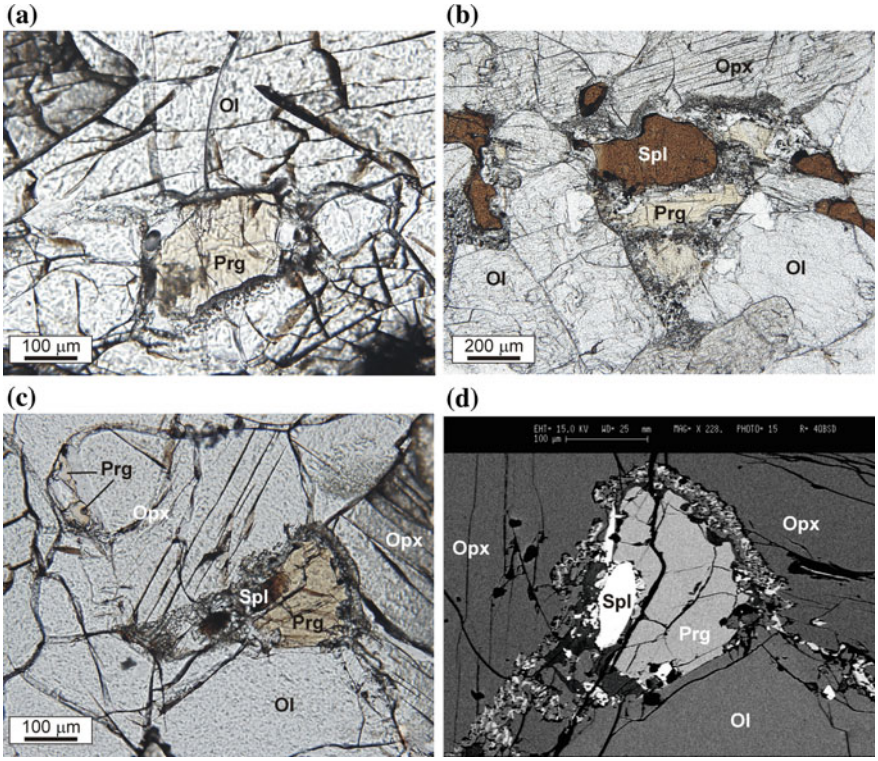

Fig. 13.1 Photomicrographs in plane polarized light (PPL) of amphibole in lherzolite xenolith from Injibara (Ethiopian plateau). **a** Disseminated Ti-pargasite. Sample INJ20. **b** Relict "holly-leaf" spinel partly replaced by Ti-pargasite. A very fine-grained corona grows on it. Modified after Frezzotti et al. (2010). **c, d** Interstitial Ti-pargasite, with a very fine-grained corona grows on it, replacing spinel and orthopyroxene. **c** back-scattered electron (BSE) of image. **d** Mineral abbreviations after Whitney and Evans (2010)

2001; Coltorti et al. 2004, 2007; Ferrando et al. 2008; Touron et al. 2008; Frezzotti et al. 2010; Bonadiman et al. 2014) and in kimberlites (e.g., Aoki 1975; Dawson and Smith 1977; Smith et al. 1981; Erlank et al. 1987; Grégoire et al. 2002); as xenoliths or megacrysts, and in peridotite massifs (e.g., Bodinier et al. 1990; Downes et al. 1991; Agrinier et al. 1993; Vannucci et al. 1995; Zanetti et al. 1996, 1999; Powell et al. 2004; Coltorti et al. 2007; Mazzucchelli et al. 2010; Selverstone and Sharp 2011; El Atrassi et al. 2014). Compositions vary from (Ti- or Cr-) pargasite to edenite, (K-) richterite, and kaersutite, the last mineral phase being present mainly in veins (e.g., Aoki 1975; Dawson and Smith 1982, and references therein; Harte 1987, and references therein; Coltorti et al. 2007; Touron et al. 2008; Mazzucchelli et al. 2010; El Atrassi et al. 2014; Luth 2014, and references therein). The Cl content of mantle amphiboles is generally considered to be low, and most published analyses report values below 1000 ppm (Garcia et al. 1980; Smith et al. 1981; Vannucci et al. 1995; Johnson et al. 1996; Moine et al. 2000, 2001; Bonadiman et al. 2014).

Considerably higher Cl contents (0.33–0.37 wt%) have been measured in Ti-pargasite, which occurs within spinel-peridotite xenoliths from the Ethiopian plateau (Ferrando et al. 2008), and in peridotites from Zabargad Island in the Red Sea (Cl up to 0.55 wt%; Agrinier et al. 1993). Geochemical studies of the East African rift system metasomatic amphiboles suggest that low Cl-amphiboles occur in peridotites that interacted with hydrous silicate melts, whereas high-Cl amphiboles occur in peridotites metasomatized by Pb-LILE-Cl-rich aqueous fluids exsolved (through immiscibility) from a former Cl-rich CO_2-H_2O fluid phase (Frezzotti et al. 2010).

Relatively high Cl contents of 0.27–0.40 wt% and F contents up to 0.19 wt% were measured in the rare amphiboles present in massive, coarse-grained, phlogopite segregations and veins from the Finero Massif in the Italian Alps (Smith et al. 1981; Vannucci et al. 1995; Selverstone and Sharp 2011), which may have experienced subduction metasomatism followed by metasomatism in an extensional intraplate setting (Selverstone and Sharp 2011). More rarely, relatively high F contents of 0.22–0.40 wt% are reported in metasomatic amphiboles crystallized from volatile-bearing melts (Dish Hill, California and Eifel; Dreiser Weiher, Eifel, Johnson et al. 1996; Baker Rocks, Northern Victoria Land, Antarctica, Bonadiman et al. 2014).

Experiments in the N_2O-CaO-MgO-Al_2O_3-SiO_2-H_2O system indicate that pargasite is the stable amphibole in the lithospheric mantle at *ca.* 880–1060 °C for P = 0.1–0.6 GPa, at *ca.* 820–1060 °C for P = 0.6–1.0 GPa, and at *ca.* 740–1060 °C for $P > 1.0$ GPa (Fig. 13.2), because small amounts of Na are able to stabilize Ca-amphiboles to higher P and/or T (Jenkins 1983). Other experiments in the same system performed by Fumagalli et al. (2009) indicated that Mg-hornblende can be stable up to 1.5–1.8 GPa and 800–850 °C and, at higher temperatures, it is replaced by pargasite, which is stable up to 2.5 GPa and 1000 °C. Both compositions show an increase in the richterite component with pressure. Also in K-rich peridotites, that are thought to represent portions of the mantle wedge above subduction zones, the alkali content controls the HP stability of pargasite, which breaks down between 2.2 and

3.0 GPa at 1000 °C (Wallace and Green 1991; Mengel and Green 1989; Conceição and Green 2004). Other experiments in the K_2O-Na_2O-CaO-FeO-MgO-Al_2O_3-SiO_2-H_2O system indicate that K-richterite is stable from 6.5 GPa and 1100 °C to 8.0 GPa and 1200–1300 °C (Konzett and Ulmer 1999) and that edenitic amphibole is stable up to 3.2 GPa at 900 °C and up to 3.0 GPa at 1000 °C (Fumagalli et al. 2009). Under fluid-present conditions, amphibole-out reactions proposed by experiments are:

$$\text{Amphibole} + \text{Orthopyroxene} = \text{Clinopyroxene} + \text{Garnet} + \text{Olivine} + H_2O \quad (13.1)$$

in K-poor peridotite (Niida and Green 1999), and:

$$\text{Amphibole} + \text{Orthopyroxene} + \text{Phlogopite1} = \text{Clinopyroxene} + \text{Garnet} + \text{Olivine} + \text{Phlogopite2} \quad (13.2)$$

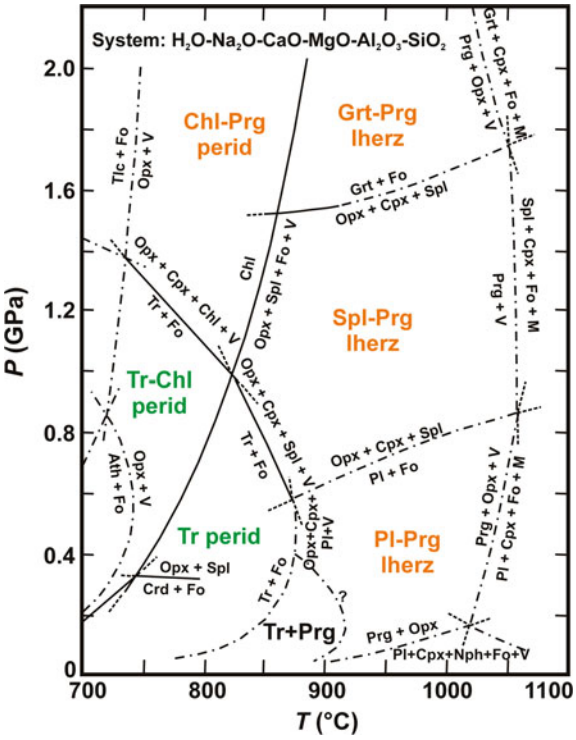

Fig. 13.2 Schematic phase relations for ultramafic rocks modelled in the system H_2O-Na_2O-CaO-MgO-Al_2O_3-SiO_2 with excess H_2O and Mg_2SiO_4. *Solid lines* are experimentally determined. *Dashed lines* are metastable extensions. *Dashed-dotted lines* are approximated. Abbreviations: *V* aqueous vapour; *M* silicate melt; *perid* peridotite; *lherz* lherzolite. Modified after Jenkins (1983)

(i.e., without fluid release) in K-bearing peridotite (Fumagalli et al. 2009). Experiments in the presence of a C-O-H fluid by Tumiati et al. (2013) show that at 900–1050 °C pargasite is stable with dolomite below 1.9 GPa, with dolomite + magnesite between 1.9 GPa and 2.4 GPa (at 900 °C) or 2.7 GPa (at 1050 °C), and with magnesite at $P > 2.4$ GPa (at 900 °C) or 2.7 GPa (at 1050 °C). The pargasite-out reaction:

$$\text{Amphibole} + \text{Orthopyroxene} = \text{Clinopyroxene} + \text{Garnet} + \text{Olivine} + \text{Phlogopite} + H_2O \quad (13.3)$$

occurs at 3.1 GPa and 900 °C and at 2.7 GPa and 1050 °C. It is interesting to note that, to our knowledge, the role of halogens in the stability of mantle amphiboles has still not been investigated experimentally. Only Condamine and Médard (2014) report an increase in the F content from 0.2 to 0.4 wt% in a pargasitic amphibole with increasing temperature from a spinel lherzolite metasomatized by adding 10 wt% of phlogopite with up to 0.71 wt% of F (see following Sect. 13.2.2.2).

13.2.2.2 Phlogopite

Phlogopite-rich mica typically occurs in mafic and peridotitic xenoliths found in kimberlites (e.g., Aoki 1975; Matson et al. 1986; Erlank et al. 1987; Grégoire et al. 2002; Bell et al. 2005; Sobolev et al. 2009b; O'Reilly and Griffin 2013, and references therein), and, more rarely, in mantle xenoliths from alkaline lavas (e.g., Ionov and Hofmann 1995; Johnson et al. 1996; Shaw and Klügel 2002; Scribano et al. 2009) and in peridotite massifs (e.g., Exley et al. 1982; Zanetti et al. 1999; Morishita et al. 2003; Zaccarini et al. 2004; Selverstone and Sharp 2011; El Atrassi et al. 2014). It is also often present in multiphase kelephitic rims surrounding garnet in garnet-bearing xenoliths (Carswell 1975; Bonadiman et al. 1999). It occurs as disseminated crystals, which locally define the anisotropy in deformed mantle (e.g., in orogenic peridotite massifs), or in veins. It can be interstitial, or can partly replace spinel or amphibole (Fig. 13.3). Disseminated phlogopite in type I peridotites (Frey and Prinz 1978) has an Mg# [i.e., 100*(Mg/(Mg + Fe))] of around 90, is usually poor in TiO_2 (0.1–1.4 wt%), and rich in Cr_2O_3 (1.0–1.7 wt%) and Na_2O (1.2–1.6 wt%), relative to phlogopite in type II veins and pyroxenites (Mg# < 90; TiO_2: 3.9–7.4 wt%; Cr_2O_3: 0.1–0.8 wt%; Na_2O: 0.2–0.6 wt%; e.g., Ferreira et al. 1995; Grégoire et al. 2002; Shaw and Klügel 2002; Morishita et al. 2003; El Atrassi et al. 2014). Exceptions to this rule have been reported in Eifel lherzolites, Germany (Johnson et al. 1996) and Hyblean xenoliths, Sicily (Scribano et al. 2009).

The Cl and F contents of phlogopite are rarely reported in the literature. The highest Cl contents, so far reported, are up to 0.55 wt%. The highest Cl values are from South African kimberlites and from inclusions in diamonds (Matson et al. 1986; Bell et al. 2005; Sobolev et al. 2009a, b). Fluorine contents in phlogopite range from 0.02 to 3.4 wt%. The highest values are from Phl-pyroxenite xenoliths

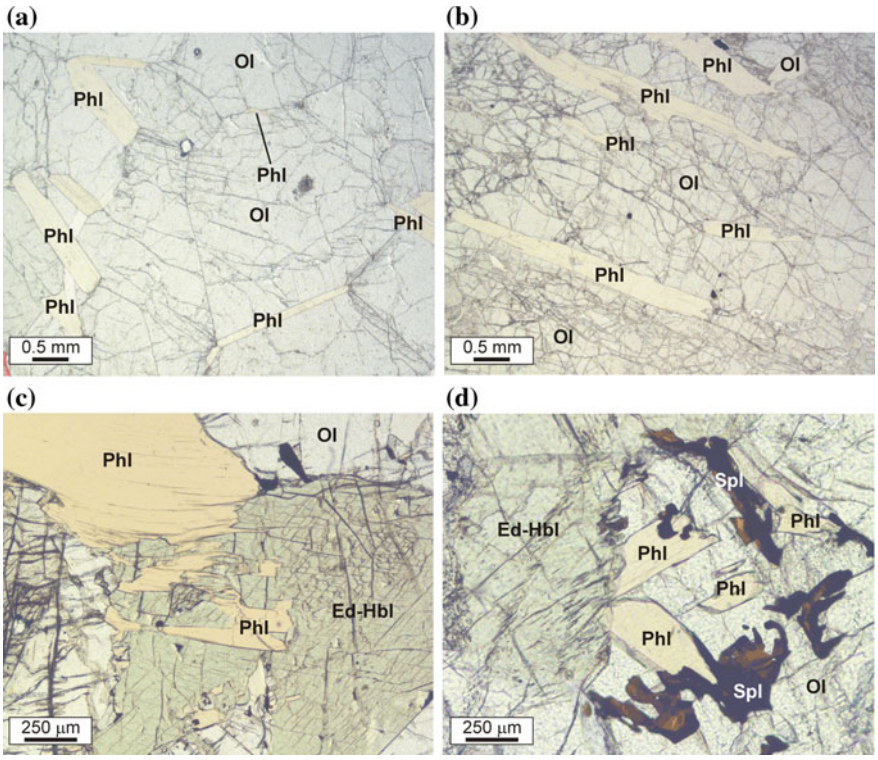

Fig. 13.3 Photomicrographs (PPL) of phlogopite in peridotite from the Finero Massif (western Alps). **a** Disseminated granoblastic phlogopite with local triple joins boundaries with olivine in coarse-grained dunite. **b** Disseminated oriented phlogopite in coarse-grained dunite. **c** Phlogopite partly replacing edenitic-hornblende in harzburgite. **d** Phlogopite partly replacing spinel and edenitic-hornblende in lherzolite

from NE Brazil (Ferreira et al. 1995). They occur in alkali feldspar syenites emplaced along shear zones and are interpreted as having been derived from the mantle source metasomatized by CO_2-saturated fluids/melts, possibly derived from the subduction of continental crust (Ferreira et al. 1995).

In the Finero Massif, the three main populations of metasomatic phlogopite show different halogens contents and ratios. The first population is represented by phlogopite inclusions in massive chromitite (Zaccarini et al. 2004) and disseminated phlogopite (Fig. 13.3a; Exley et al. 1982). This phlogopite has Ti up to 4.5 wt%, Cl from 0.02 to 0.29 wt%, and F from 0.10 to 1.92 wt%. Population I is interpreted as having been produced by a carbonatite-type liquid and related hydrous fluids, during continental rifting (Zaccarini et al. 2004). The second population corresponds to disseminated phlogopite with low Ti, Cl < 0.10 wt%, and F < 0.03 wt%, which may have been derived by infiltration of subduction-related "hydrous clinopyroxenite silicate" melts (Fig. 13.3b; Selverstone and Sharp 2011). The third population

is represented by massive, coarse-grained, phlogopite segregations and veins in which phlogopite contains Cl from 0.20 to 0.45 wt%, and F < 0.23 wt%. It has been interpreted as having been produced by the infiltration of subduction-related brines enriched in alkalis, LILE, HFSE, and Cr (Selverstone and Sharp 2011). Interestingly, similarly high halogen contents (Cl from 0.31 to 0.38 wt%; F from 0.25 to 0.81 wt%) were measured in metasomatic phlogopites in from (garnet)-spinel peridotite xenoliths from the Ethiopian rift, equilibrated at 2.2–2.4 GPa and about 950 °C (Casagli et al. 2017).

Crystallization of phlogopite and Al-rich enstatite, produced by breakdown of phengite in the presence of olivine and enstatite, has been used to experimentally simulate metasomatism at the slab-mantle interface (e.g., Wunder and Melzer 2003). Phlogopite can coexist with amphibole at low pressures and it is stable to higher pressures than amphibole. Experiments in the K-rich peridotite system (Fumagalli et al. 2009) show that phlogopite can coexist with Ca-amphibole up to 3.2 GPa and 900 °C and that a significant amount of a talc/10Å-phase component is incorporated into phlogopite at 5.5 GPa and 680 °C. K-richterite replaces phlogopite at 6–7 GPa and 1150 °C in lherzolite experimentally doped with phlogopite + K-richterite (Konzett and Ulmer 1999; Luth 1997; Sudo and Tatsumi 1990).

At 1 GPa, phlogopite breakdown has been experimentally achieved at 1050 °C at both water-saturated and undersaturated conditions (Fig. 13.4) in a depleted spinel lherzolite metasomatized by addition of 1.5 wt% of phlogopite (Conceição and Green 2004), and at 1150–1200 °C at fluid-absent conditions in a fertile spinel lherzolite metasomatized by adding 10 wt% of phlogopite (Condamine and Médard 2014). The incongruent melting reaction is:

$$\text{Phlogopite} + \text{Orthopyroxene} + \text{Spinel} \pm \text{Clinopyroxene} = \text{Olivine} + \text{melt}. \quad (13.4)$$

The F content in phlogopite increases with temperature from 0.3 to 0.8 wt% and the presence of F and Ti increase the temperature of phlogopite breakdown (Condamine and Médard 2014).

In the presence of a C-O-H fluid phase, phlogopite is stable at 1.6–3.2 GPa and 900–1050 °C (Tumiati et al. 2013). At 4–7 GPa, phlogopite is stable with magnesite and pyrope. The assemblage phlogopite + magnesite breakdowns to produce Olivine + Enstatite + Pyrope + melt at 1150–1250 °C (Enggist et al. 2012).

13.2.3 Nominally Anhydrous Minerals (NAMs)

Measurable (ppm) amounts of 'water' have been detected in mantle-derived, nominally anhydrous minerals (NAMs), mainly by Fourier transform infrared spectroscopy (FT-IR) and secondary ion mass spectrometry (SIMS) (Keppler and Smyth 2006; Peslier 2010; Luth 2014, and references therein). For this reason, NAMs potentially might represent the largest water reservoir in the mantle (Bell and Rossmann 1992; Pearson et al. 2014).

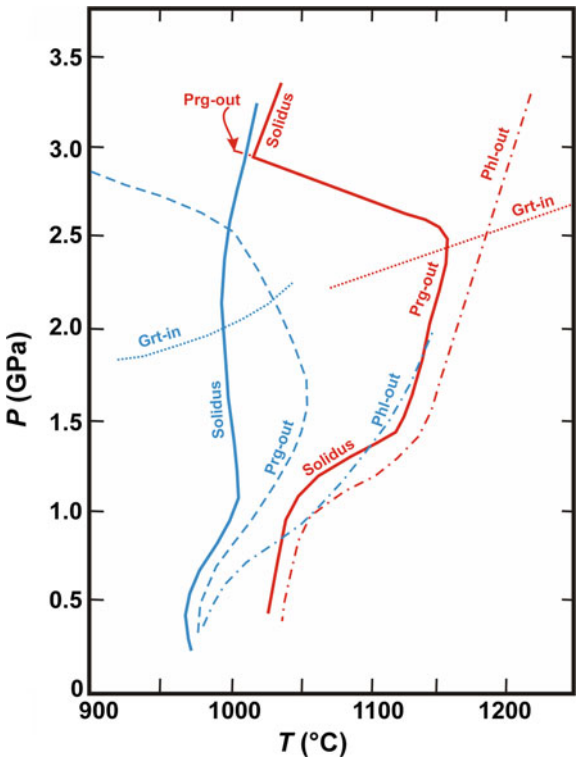

Fig. 13.4 *PT*-diagram showing experimental determination of the solidus, and related above-solidus stabilities of pargasite and phlogopite, for water-saturated (in *blue*) and water-undersaturated (0.35–0.4% H_2O at solidus; in *red*) melting of a metasomatized depleted lherzolite in which 60% of the olivine has been subtracted. Modified after Conceição and Green (2004)

The storage of halogens in NAMs may occur because of the tendency of F and, to a much lesser extent Cl, to substitute for OH^- in the crystal structure. An experimental study in the system Mg_2SiO_4–MgF_2 produced olivine with up to 0.45 wt% F (Bromiley and Kohn 2007). Concentrations measured in natural samples are considerably lower and correspond to 30–100 ppm of F in olivine megacrysts from South African kimberlites (Hervig and Bell 2005), and a maximum of 14 ppm of F in olivine from upper mantle xenoliths (Guggino et al. 2007). Data on olivine and orthopyroxene from distinct tectonic settings, as measured by Mosenfelder and Rossman (2013a), reveal very low F contents (≤ 3 ppm) for upper granulite-facies crustal rocks from Myanmar, India, and Tanzania, relative to those (up to 47 ppm in olivine and up to 17 ppm in orthopyroxene) from mantle xenoliths in volcanic rocks from New Mexico (USA), and kimberlites from Namibia and South Africa. Similarly, F contents up to 46 ppm have been measured in clinopyroxene from mantle xenoliths in volcanic rocks from New Mexico and Arizona (USA), and in kimberlites from Namibia and South Africa, whereas the highest F concentrations (up to 214 ppm) have been found in diopside from high-temperature crustal granulites from Tanzania and Adirondack Mountains (USA) (Mosenfelder and Rossman 2013b). Comparable values (2.9–30.3 ppm of F and 5.0–6.3 ppm of Cl in olivine and 12–28 ppm of F in orthopyroxene) were measured by Beyer et al. (2012) in peridotite xenoliths from kimberlites from

South Africa and United States, and in basaltic lavas from the Eifel region, Germany, and Mt. Leura, Australia.

A cautionary note by Mosenfelder et al. (2011) points out that some heterogeneity in the F content can be produced by the presence of sub-micrometre to micrometre hydrous phases (Fig. 13.5). Similarly, halides and hydrous silicate minerals can form within fluid inclusions (i.e., halite, sylvite, gypsum, talc, clinochlore, and/or serpentine) during cooling, either by post-trapping reactions between residual H_2O fluids in the inclusions and the surrounding minerals, or by solute supersaturation.

Complementary, though indirect, evidence for possible enrichment of halogens, in particular Cl, by interaction between hydrous fluids and mantle minerals on the micron-scale, has been obtained by synchrotron Fourier transform infrared spectroscopy (FT-IR) maps of H_2O distribution in olivine, orthopyroxene, and clinopyroxene from mantle peridotite xenoliths in alkaline basalts. Such maps (Fig. 13.6) reveal gradients in the distribution of H_2O in NAMs, with considerable enrichment along intragranular microfractures and around fluid inclusions (Frezzotti et al. 2010; Hidas et al. 2010). Whereas microstructural evidence is indicative of fluid-rock interaction during fluid percolation, the symmetrical haloes of water

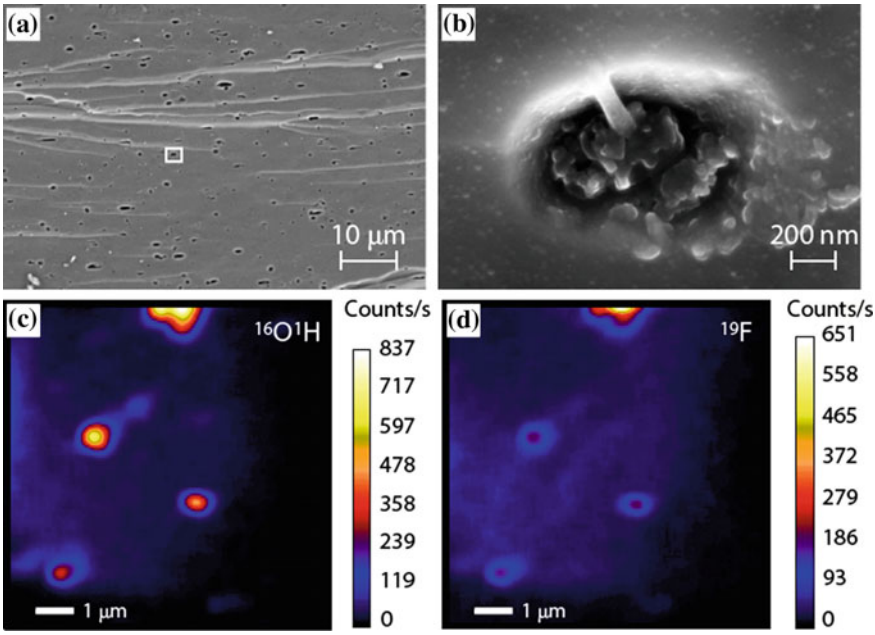

Fig. 13.5 **a** Scanning electron microscope (SEM) image of open primary fluid inclusions in olivine. The *square* indicates the area in Fig. 13.5b. **b** SEM magnified view at 200 000 × (InLens detector) of an open fluid inclusion showing nanoparticles, believed to be precipitates of $Mg(OH,F)_2$ brucite. **c, d** Nano-secondary ion mass spectrometry (SIMS) maps of $^{16}O^1H$ (**c**) and ^{19}F (**d**) distribution in olivine. The spots corresponds to fluid inclusions. Color scale is in counts/s. (Modified from Mosenfelder et al. 2011; courtesy of J.L. Mosenfelder)

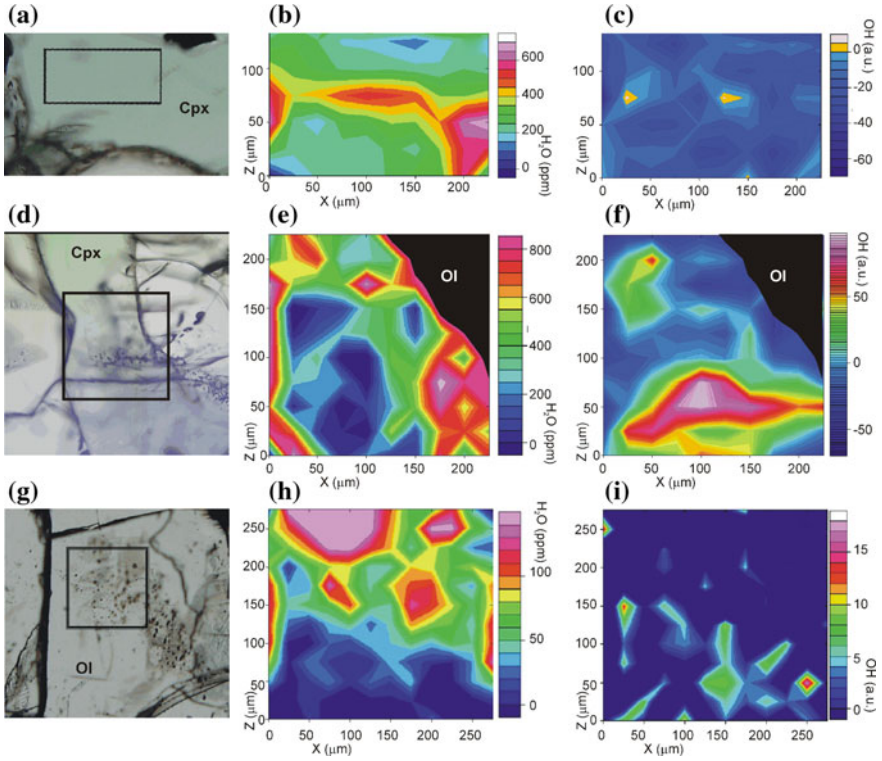

Fig. 13.6 Synchrotron Fourier-transform infrared (FT-IR) imaging of the water distribution in clinopyroxene and olivine from the Injibara spinel lherzolites (Ethiopian plateau). Each set of maps includes a microscopic image in plane-polarized light, and relative infrared maps in selected absorbance regions. **a** Clinopyroxene not containing fluid inclusions (PPL). **b** Absorbance map in the 3000–3800 cm^{-1} region and relative calculated water contents in clinopyroxene (ppm). **c** Qualitative OH absorbance map in the 3600–3800 cm^{-1} region relative to the distribution of amphibole inclusions. **d** Clinopyroxene containing a trail of fluid inclusions, PPL. **e** Absorbance map in the 3000–3800 cm^{-1} region and the relative calculated water contents in clinopyroxene (ppm). **f** Qualitative OH absorbance distribution map in the 3600–3800 cm^{-1} region relative to the distribution of amphibole inclusions. **g** Olivine containing several fluid inclusions. **h** Absorbance map in the 3000–3600 cm^{-1} region and relative calculated water contents in olivine (ppm). **i** Qualitative OH absorbance distribution map in the 3600–3800 cm^{-1} region relative to the distribution of talc and serpentine inclusions. Sizes of investigated areas are in microns. Measured water contents are drawn with a precision of 10's of ppm. Abbreviations: *a.u.* arbitrary units. Modified after Frezzotti et al. (2010, 2012)

enrichment around fluid inclusions, as revealed by FT-IR mapping, indicate hydrogen diffusion into the host mineral. Local hydration of the host mineral can form talc inclusions in olivine, and Cl-rich pargasite inclusions (or phlogopite) in clinopyroxene (Fig. 13.7; Frezzotti et al. 2012). All these processes may in part contribute to the heterogeneities in the halogen contents measured around fluid inclusions in NAMs (Fig. 13.5; Mosenfelder et al. 2011).

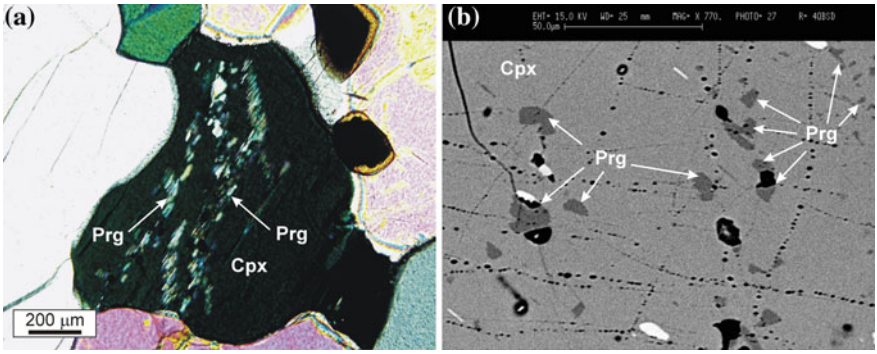

Fig. 13.7 Microstructural relationships between fluid inclusions and amphibole in clinopyroxene from the Injibara hydrous spinel lherzolite xenoliths (Ethiopian plateau). **a** Photomicrographs showing trailbound fluid inclusions and pargasite in clinopyroxene. (PPL) **b** BSE image showing the pargasite distribution around trails of fluid inclusions (*black*) in clinopyroxene. Spinel inclusions are also visible (*white*). Modified after Frezzotti et al. (2010)

Experiments on the partitioning of F between olivine, orthopyroxene, and basaltic melts up to 2.5 GPa and 1285–1445 °C indicate that: (i) F is more compatible than H_2 in both olivine and orthopyroxene; (ii) F is more compatible in orthopyroxene than in olivine; and (iii) the incorporation of F into the olivine structure is balanced by defects on the oxygen site (Beyer et al. 2012). The partitioning of F and Cl between lherzolite and basaltic melt at pressures of 0.8–2.5 GPa and temperatures of 1265–1430 °C has been experimentally studied by Dalou et al. (2012). These authors observe that: (i) the F contents are 16–626 ppm in clinopyroxene, 2–520 ppm in orthopyroxene, 73 ppm in garnet, <19 ppm in olivine, and 15 ppm in plagioclase, respectively; (ii) the Cl contents are 2–77 ppm in clinopyroxene, 4–43 ppm in orthopyroxene, 13 ppm in garnet, <19 ppm in olivine, and 3 ppm in plagioclase; (iii) the relative compatibility of both F and Cl is Clinopyroxene > Orthopyroxene > Garnet > Olivine > Plagioclase; (iv) in each mineral, F is more compatible than Cl; (v) the Cl content in ortho- and clinopyroxene increases with the jadeite and Ca-Tschermak components, respectively; (vi) the F partition coefficients in pyroxenes show a positive correlation with melt viscosity; and (vii) the incorporation of F and Cl into orthopyroxene shows negative correlation with crystallographic sites M1 and M2, respectively.

Other experiments on the partitioning of halogens between forsterite, enstatite (±pyrope) and aqueous fluids, such as Bernini et al. (2013) and Fabbrizio et al. (2013), allow for the definition of Cl/F fractionation. The experiments of Bernini et al. (2013) were performed at 2.6 GPa and 1100 °C in the system forsterite-enstatite-pyrope-H_2O-$MgCl_2$-MgF_2 with the fluid salinity ranging from 0.3 to 30 wt% Cl, whereas those of Fabbrizio et al. (2013) were performed at 2.0 GPa and 900–1300 °C in the system MgO-SiO_2-H_2O-NaCl-BaO-C ± $CaCl_2$ ± TiO_2 ± Al_2O_3 ± F with a molar ratio of $Cl/(Cl + H_2O)$ = 0.01–0.26. These experiments reveal that: (i) Cl strongly fractionates into the fluid phase

(Bernini et al. 2013; Fabbrizio et al. 2013); (ii) Cl solubility in NAMs is very low (2.1–3.9 ppm in forsterite; 2.9–3.5 in enstatite; 4.0–11.4 ppm in pyrope; Bernini et al. 2013); (iii) F solubility in NAMs is higher than that of Cl (170–336 ppm in enstatite; 510–1110 ppm in pyrope; Bernini et al. 2013); (iv) Cl and F solubility in enstatite and pyrope are not related to the salinity of the coexisting fluid (Bernini et al. 2013; Fabbrizio et al. 2013); (v) if Al, Ca, or F are present in the fluid phase, the Cl solubility can increase up to 133 ppm in forsterite and up to 119 ppm in enstatite (Fabbrizio et al. 2013); and (vi) F contents in forsterite are 1750–1900 ppm for a fluid salinity of 1.6 wt% F; at higher F contents in the system, forsterite is replaced by humite (Bernini et al. 2013).

13.2.4 Halides (Halite-Sylvite)

Although halide minerals are not reported in lithospheric peridotites (possibly due to sample preparation techniques, which utilize water, Manning and Aranovich 2014), halide ± carbonate nodules of variable sizes, from a few cm to more than 1 m across (Fig. 13.8), have been described in the deep levels of the diamantiferous East Udachnaya pipe, Yakutia (Kamenetsky et al. 2007, 2009a, b, and references therein). Nodules are chloride-rich, and contain bluish halite (Fig. 13.8) with included round grains of sylvite, along with from 1 to 30 vol.% of fine-grained silicate-carbonate-halide aggregates or silicate-sulfate-halide aggregates. Halide phases include djerfisherite [$K_6(Na,Cu)(Fe,Ni,Cu)_{24}S_{26}Cl$], northupite [$Na_3Mg(CO_3)_2Cl$], zoned "nyerereite" [$Na_2Ca(CO_3)_2$], shortite [$Na_2Ca_2(CO_3)_3$], calcite, and sodalite [$Na_8(Al_6Si_6O_{24})Cl_2$]. Nodules have sharp contacts with the host kimberlite (Fig. 13.8), consisting of thin (<1 mm) aggregates of olivine, calcite,

Fig. 13.8 Photograph of a halide (*bluish*) ± carbonate nodule in diamantiferous Yakutian kimberlites (East Udachnaya pipe); picture courtesy of V.S. Kamenetsky

sodalite, traferriphlogopite, humite-clinohumite, Fe–Mg carbonates, perovskite, apatite, and magnetite (Maas et al. 2005; Kamentsky et al. 2007, 2009a, b, and references therein). According to these authors, both halite and sylvite nodules, and Na-K-chlorides present in the groundmass, are mantle-derived, and crystallized from residual, dry, non-silicate melts, preserved in an extremely fresh kimberlite free of post-magmatic hydration (i.e., leaching of Cl and alkalis).

These results are extremely relevant for kimberlite petrogenesis, since they suggest that primary kimberlite melts are essentially alkaline (e.g., Na/K) carbonatitic melts, evolving toward carbonate–silicate compositions (up to 20 wt% SiO_2) on ascent (e.g., Kamenetsky et al. 2009a, b, 2012; Sharygin et al. 2014, and references therein). In this hypothesis, the parental kimberlite melt should be an alumino-silicate-poor Na–Ca-rich carbonate melt that is virtually anhydrous, but enriched in LILE, halogens, and sulfur. This is consistent with the presence of relatively high Cl contents in the mineral inclusions (e.g., phlogopite) and fluid inclusions present in diamonds (cf., next Sect. 13.3.2). Nevertheless, the mantle origin of halide-rich nodules, at depths >200 km, is not unanimously accepted. Doubt has been shed on the exceptionally fresh nature of the East Udachnaya kimberlite. According to Kjarsgaard et al. (2009), a Cl-rich kimberlite magma should induce crystallization of Cl-rich phlogopite and hydroxy-chloro-apatite. However, in the kimberlite groundmass these phases are Cl-poor (Cl lower than 0.08 wt% in phlogopite, and 0.1 wt% in apatite). More recently, Kopylova et al. (2013) have argued that the halide ± carbonate nodules are derived from within the shallow crust, and reflect syn-eruptive assimilation by ascending kimberlite melts of evaporite-bearing carbonate sediments saturated with brines, which are present in the Siberian platform.

13.3 Halogens in Metasomatic Fluids and Melts

At lithospheric mantle depths, the mobile metasomatic phases generally consist of C-O-H fluids (dominated by CO_2 and/or H_2O), and melts, such as silicate- or carbonate-rich, with significant amounts of dissolved volatiles. Both of them contain variable amounts of C–O–H–Cl–S–F–N volatile components. As Cl and F are soluble in aqueous fluids and silicate melts, respectively, strong partitioning between fluid and mantle phases is expected during metasomatic processes (e.g., Webster 1990, 1992; Bureau and Keppler 1999; Webster et al. 2018; Dolejs and Zajacz 2018). Direct evidence of halogen migration in the lithospheric mantle is preserved in fluid phases trapped as inclusions in peridotite and pyroxenites, as well as in diamonds. As fluid phases have different properties at increasing pressure and temperature conditions, it is helpful to consider fluids in ultramafic rocks and in diamonds separately.

13.3.1 Sub-Continental and Oceanic Lithosphere

Over the long history of fluid inclusion studies in mantle xenoliths, many sets of fluid compositional data have accumulated, and not all are consistent with each other (cf., for review, Roedder 1965, 1984; Murk et al. 1978; Pasteris 1987; Andersen and Neumann 2001; Frezzotti et al. 2012; Frezzotti and Touret 2014, and references therein). Even though halogen-bearing aqueous fluids are well documented by inclusions of brines in spinel and garnet peridotites from subduction zones (i.e., fluid inclusions containing liquid water and solid salts; Trial et al. 1984; Scambelluri et al. 1997; McInnes et al. 2001; Hidas et al. 2010; Kawamoto et al. 2013; Barnes et al. 2018), saline aqueous fluids have been mostly ignored in peridotite xenoliths from intraplate and extensional settings, where fluid inclusions have been generally found to be CO_2-rich (e.g., Roedder 1965; Andersen and Neumann 2001; Luth 2014, references therein). As a consequence, CO_2 (and minor N_2, CO, SO_2, and noble gases) have been considered the dominant fluid phases in the lithospheric mantle at depths < of 80–90 km.

Nevertheless, thermodynamic calculations indicate that H_2O should also be a major component in carbon-undersaturated C-O-H fluids at lithospheric mantle *P-T-*f_{O2} conditions (T = 800–1000 °C; *P* = 2 GPa; $f_{O2} \geq$ QFM buffer; Huizenga 2001, 2005). Moreover, the presence of a saline aqueous component in the lithospheric mantle fluids is suggested by indirect evidence, such as the halogen contents of the modal metasomatic minerals (see Sect. 13.2), and the chemistry of gases contained in, or discharged from, some basaltic magmas (e.g., Marty and Zimmermann 1999; Aiuppa et al. 2009).

The earliest report of halogens in lithospheric mantle fluids from extensional tectonic settings was made more than 30 years ago. Andersen et al. (1984) first proposed that CO_2 inclusions in spinel peridotites and garnet pyroxenites from Bullenmeri maar (Victoria, SE Australia) must have contained both H_2O and Cl, F, as well as alkalis, before the growth of secondary amphibole on the walls of the cavities. O'Reilly et al. (1990), supplied more data on these inclusions and argued for the coexistence of silicate melt, sulphide melt and a CO_2-H_2O fluid containing Cl and F.

Firm observation of brines in fluid inclusions has so far been reported only in hydrous (Cl-rich pargasite) spinel peridotite xenoliths beneath the Ethiopian plateau area (Frezzotti et al. 2010). Here the orthopyroxene in lherzolites preserves Cl-rich H_2O–CO_2 fluid inclusions (Fig. 13.9) including, a generally very rare, possible halide cube (Fig. 13.9b, c). The presence of subordinate H_2O and halides, i.e., Cl, is confirmed by microthermometric measurements (i.e., the melting temperature of CO_2-H_2O clathrates) and by Raman analysis (Fig. 13.9d). The high fluid density, calculated in the inclusions, corresponds to minimum trapping pressures of 1.4–1.5 GPa or to a 50–54 km depth (at *T* = 950 °C). The resulting calculated composition in molar fractions for the metasomatic, halide-bearing fluid is: $X_{CO2} = 0.64$, $X_{H2O} = 0.33$, $X_{Na} = 0.006$, $X_{Mg} = 0.006$, $X_{Cl} = 0.018$, with a resulting $a_{H2O} = 0.2$ at trapping *P-T* conditions (cf., Frezzotti et al. 2010).

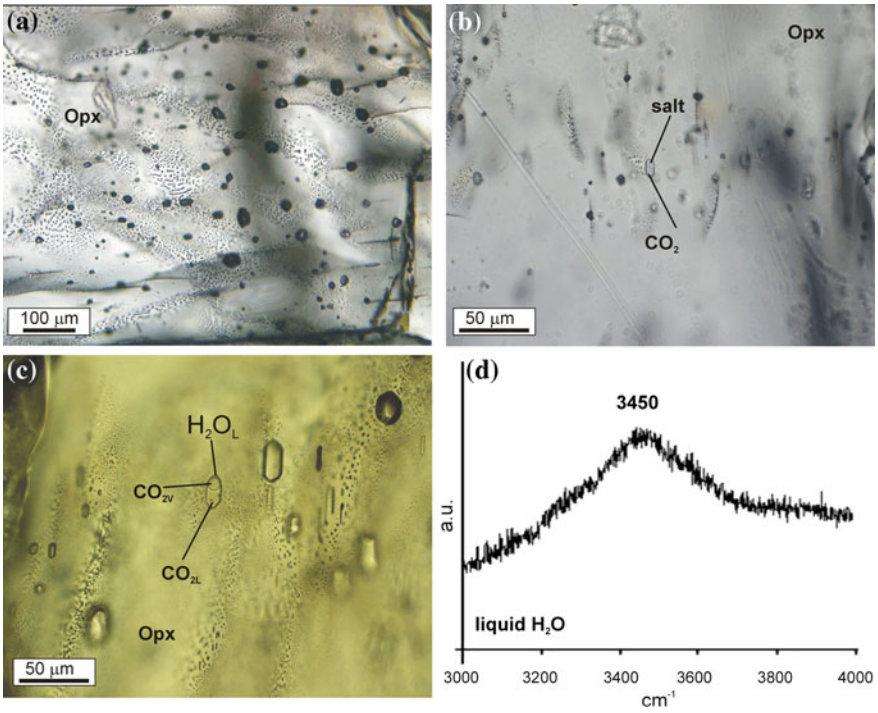

Fig. 13.9 Photomicrographs of H_2O–CO_2 fluid inclusions in orthopyroxene from hydrous lherzolite xenoliths (Ethiopian plateau). **a** CO_2-rich fluid inclusions in orthopyroxene. (PPL) **b** Fluid inclusion consisting of CO_2 and an isotropic cube phase that is not Raman active (i.e., likely a salt). (PPL) **c** A large inclusion containing CO_2 (liquid + vapor) and liquid H_2O at the cavity rim (see Raman spectrum in Fig. 13.9d). (PPL) **d** Raman spectrum of liquid H_2O rimming CO_2 in the fluid inclusion in Fig. 13.9c. *a.u.* arbitrary unit

The aqueous component of the supercritical fluid phase has a minimum salinity of 14–10 NaCl eq. wt%, and contains 4–5 mol% Cl. Calculated trace-element fractionation patterns in clinopyroxene, in equilibrium with a 5 molar NaCl solution (Fig. 13.10; Keppler 1996; Ayers 1998), suggest that halide-bearing fluids were important metasomatic carriers of LILE and Pb in these lithospheric peridotites.

The availability of improved analytical approaches [e.g., Raman microspectroscopy; Scanning Electron Microscopy with X-ray microanalysis (SEM-EDS); Fourier transform infrared spectroscopy (FT-IR)] in the study of fluid inclusions has provided further evidence, though indirect, for the former presence of halide-bearing fluids in CO_2-rich inclusions from both oceanic and continental peridotites and pyroxenites from several key localities, including Hawaii, the Canary Islands, and Sardinia (Andersen et al. 1984; De Vivo et al. 1988; Frezzotti and Peccerillo 2007; Frezzotti et al. 1992, 2002a, b, 2012). As an example, the former presence of halogens in fluids can be revealed by the occurrence of K, Na, and Cl in the EDS/EDAX spectra from opened fluid inclusion cavities (Fig. 13.11).

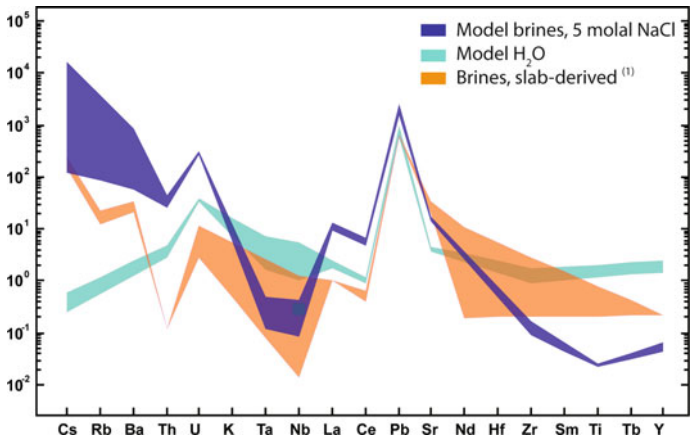

Fig. 13.10 Trace-element composition of model aqueous fluids (5 molar NaCl and pure H_2O) in equilibrium with clinopyroxene from Ethiopian plateau spinel lherzolites (Keppler 1996; Ayers 1998). Comparison of model brines with Cl-rich slab-derived brines generated by antigorite breakdown (cf., Scambelluri et al. 2002). Modified from Frezzotti et al. (2010)

Detection of subordinate amounts of brines in CO_2-rich fluid inclusions is hampered by many factors, explaining why they have been long overlooked. The small size (<5–10 μm) and the regular shapes typical of most mantle fluid inclusions strongly limit the optical resolution, especially in dense and coloured peridotite minerals (cf., Roedder 1965). In other cases, brines could have reacted with the surrounding host mineral to form a coat of step-daughter minerals, i.e. minerals formed by reaction of the fluid inclusion with the host minerals (Svensen et al. 1999), distributed along the fluid inclusion rims (Andersen et al. 1984; Frezzotti et al. 2002a; Hidas et al. 2010). Types and amounts of stepdaughter silicate minerals, detected by Raman micro-spectroscopy and SEM-EDS analyses, seem to depend on the nature of the host mineral in the peridotite. Fluid inclusions within olivine are filled by hydrous Mg-rich silicates (talc or Mg-chlorite), chlorides (halite), and carbonates (magnesite), whereas those in orthopyroxene and clinopyroxene mainly contain carbonates (magnesite and dolomite, respectively), Cl-rich amphibole, and, locally, apatite (Andersen et al. 1984; Frezzotti et al. 1992, 2002a, b, 2010).

Diffusion of molecular H_2O from the fluid inclusions into the host mineral may potentially have the effect of increasing the halide content of the fluid inclusions due to the selective loss of H_2O (Fig. 13.6, and Sect. 13.2.3). Natural examples (Mackwell and Kohlstedt 1990; Viti and Frezzotti 2000, 2001) and experiments (Sterner and Bodnar 1989; Wanamaker and Evans 1989; Hollister 1990; Bakker and Jansen 1991) demonstrated that this process might result in the total loss of molecular water from these micro-cavities. Fluid inclusion "desiccation" can occur very quickly during rock decompression. It is driven both by H_2O fugacity gradients and by the formation of micro-cracks, dislocations, and lattice defects in mantle minerals induced by differential pressures.

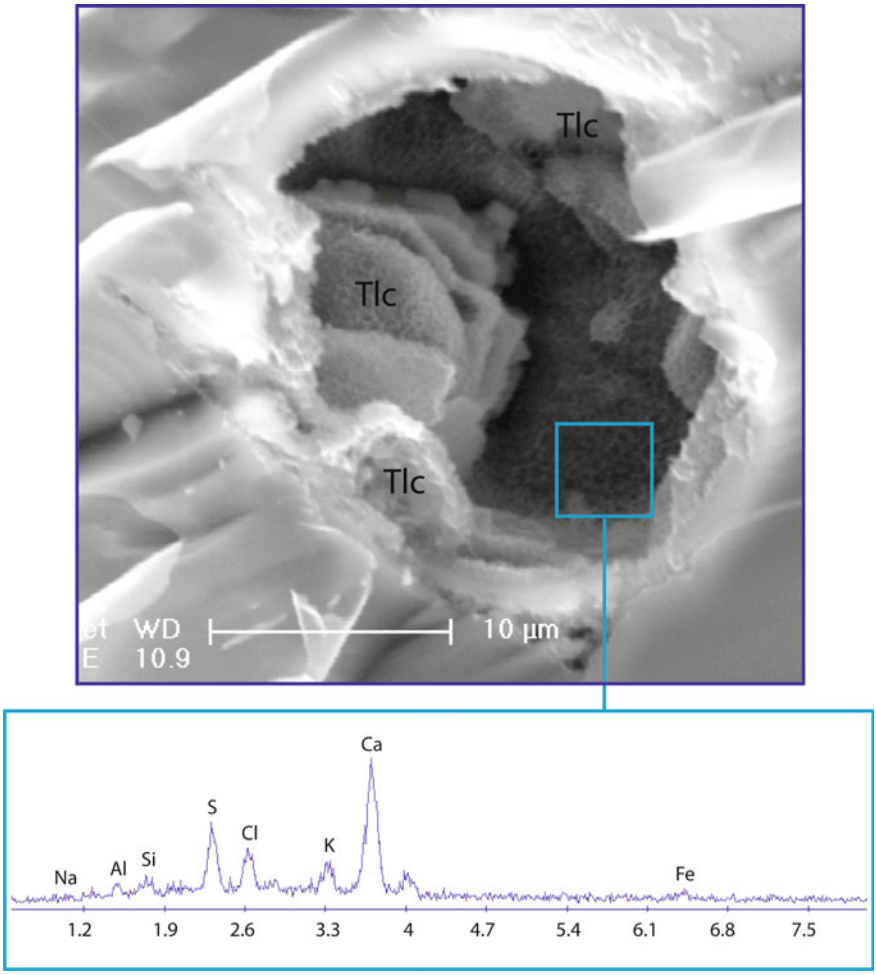

Fig. 13.11 Electron microphotograph of an open fluid inclusion in orthopyroxene. Talc (Tlc) coats the inclusion walls. On the talc crystals, a thin microcrystalline coating of gypsum, KCl, SiO_2, and Fe-Al oxides is revealed by qualitative EDS-EDAX chemical analysis in the inset image area. Microstructures clearly indicate that relatively large magnesite and talc crystals are stepdaughter minerals that formed through reaction with the hosting mineral, while chlorides, sulfates, and silica are precipitated from the fluid as tiny aggregates during cooling and decompression. Modified after Frezzotti et al. (2012)

Because of the above-mentioned processes, inclusions still preserving the original fluid compositions are extremely rare, which prevents a firm estimate of the original Cl-content of lithospheric fluids. One set of measurements in peridotites, equilibrated at depths of 60–70 km in the East African sub-continental lithospheric mantle, corresponds to 10–14 wt% NaCl equivalent (Frezzotti et al. 2010). These fluid inclusion data are consistent with estimates of the 3.5–9 wt% NaCl equivalent

(or 2–5 wt% Cl) predicted for mantle fluids (Burgess and Turner 1995), and with the amount of solutes calculated in H_2O-rich subduction fluids at 1–2 GPa (6–10 wt%; Manning 2004).

The total content of halogens and other solutes does not need to be extreme in order to permit the occurrence of a single supercritical CO_2–H_2O–NaCl fluid phase under most lithospheric *P*–*T* conditions. Because of the presence of a large two-phase field in the CO_2–H_2O–NaCl ternary system, fluids of higher salinity than those measured in the natural examples discussed above would imply the coexistence of immiscible CO_2 and brines, with halogens concentrated in the aqueous fluid phase (Fig. 13.12; Heinrich 2007; Aranovich et al. 2010; Newton and Manning 2010).

A number of studies have previously proposed two-phase fluid conditions at lower crustal and upper mantle depths (e.g., Skippen and Trommsdorff 1986; Trommsdorff and Skippen 1986; Newton et al. 1998; Heinrich et al. 2004; Newton and Manning 2010). Unquestionable microstructural features, such as the coexistence of CO_2 and brine inclusions, have not yet been described in mantle rocks. However, the association of coeval CO_2-rich fluid inclusions and Cl-pargasite (Fig. 13.7), or phlogopite inclusions, of similar sizes in some hydrous peridotites suggest the distinct trapping of immiscible CO_2 and brines, with the latter reacting with the surrounding mantle minerals to form Cl-enriched hydrous phases. Different wetting angles and densities would allow for the migration of saline brines separately from carbonic fluids in the lithospheric mantle (Johnson 1991; Heinrich 2007; Touret and Huizenga 2012). The different wetting behaviour between the "immobile" CO_2, which is trapped as fluid inclusions, and the "mobile" brine, which can migrate and react with peridotites (Watson and Brenan 1987; Gibert et al. 1998; Newton and Manning 2010), might induce large-scale metasomatic effects in the lithospheric mantle.

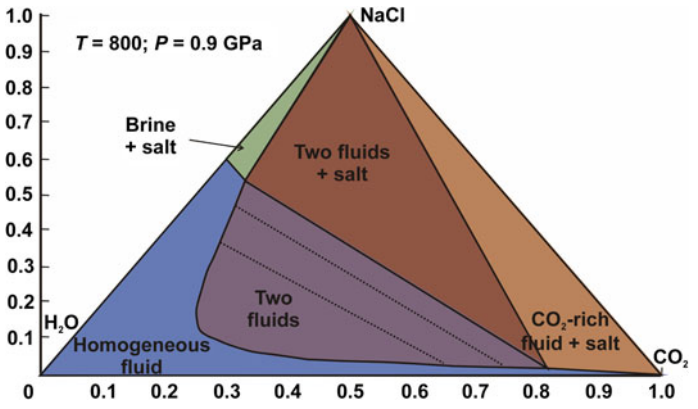

Fig. 13.12 Phase diagram for the ternary system H_2O–CO_2–NaCl (heavy continuous lines in the compositional triangle) at 800 °C and 0.9 GPa. *Dashed lines* show tie lines of coexisting immiscible fluids. Redrawn and modified from Aranovich et al. (2010)

13.3.2 Deep Cratonic Sub-Continental Lithosphere

In deep cratonic sub-continental lithosphere, diamonds represent metasomatic phases formed by redox reactions between peridotites and a mobile C-rich volatile phase, often referred to as a fluid phase. Thus, nanometre and micrometre-sized fluid inclusions in diamonds (Fig. 13.13a) are direct evidence of deep metasomatic fluids infiltrating the sub-continental cratonic lithosphere. With a few exceptions (Smith et al. 2014, 2015), extensive chemical analyses have been performed on fluid inclusions in fibrous diamonds, or on fluid inclusions in cloudy coats on octahedral diamond mono-crystals (Fig. 13.13a), which are supposed to have crystallized from metasomatic fluid phases related to host kimberlite magma petrogenesis (cf., Boyd et al. 1987, 1994; Navon et al. 1988; Izraeli et al. 2004; Klein-BenDavid et al. 2007; Safonov et al. 2007; Rege et al. 2010; Zedgenizov et al. 2007; Weiss et al. 2009).

Fluids trapped during the fast growth of fibrous and cloudy diamonds consist of complex silicate-carbonate-Cl-aqueous mixtures, which are generally assigned to three chemical end-member types (Fig. 13.13b), that are present in variable amounts (e.g., Klein-BenDavid et al. 2007; Weiss et al. 2009 and references therein). These include: (I) hydrous-silicic fluids rich in SiO_2, Al_2O_3, as well as K2O; (II) carbonatitic fluids (both high Mg and low Mg); and (III) saline aqueous fluids rich in Cl, K, and Na (brines). These fluids have a high density, and the volatile contents appear to be lower than 50 mol%. Since diamond formation in the subcontinental lithospheric mantle requires pressure conditions greater than 4.5 or 5 GPa (>130–150 km depth), fluids and melts cannot be distinguished from each

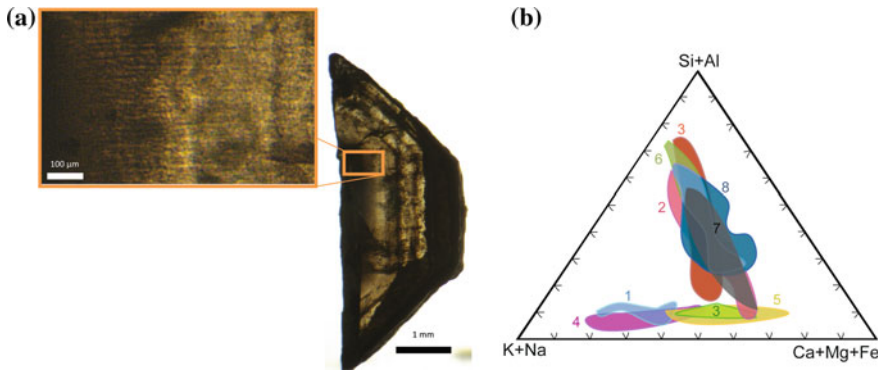

Fig. 13.13 Halogens in fibrous diamonds. **a** Photomicrograph of nanometric fluid inclusions in fibrous diamond; picture courtesy E.M. Smith. **b** Ternary diagram of averaged (Si + Al)-(Ca + Mg + Fe)-(Na + K) mol% in diamond fluid inclusions from different localities: *1* Koffiefontein, *2* Kankan, *3* Yakutia, *4* Diavik, *5* Panda, *6* Botswana, *7* Brazil, and *8* Democratic Republic of Congo. Data *1–7* are from Klein-BenDavid et al. (2009), *8* from Kopylova et al. (2010). Modified from Kopylova et al. (2010); plot courtesy of M.G. Kopylova

other, as the *P-T* conditions are beyond or close to the critical end-point of the *solidus* in a peridotite-H_2O-(CO_2) system (e.g., Wyllie and Ryabchikov 2000; Stachel and Harris 2009).

The presence of aqueous-halide-carbonate fluids was first reported in cloudy diamonds from South Africa (Koffiefontein; Izraeli et al. 2001), and later confirmed in both peridotitic and eclogitic diamonds worldwide (e.g., Klein-BenDavid et al. 2004, 2006, 2007; Tomlinson et al. 2006; Smith et al. 2012). Overall, brines enclosed in diamonds can contain high Cl-contents (up to 30–40 wt%). Bromine also shows variable, but significant, enrichments. Schrauder et al. (1996) analyzed the Br content of fluid inclusions in African diamonds and found that concentrations range from 14 to 470 ppm. Among the cations, K is a characteristic component, which is dominant over Na, Fe, Ca, and Mg. Carbonates are also present in relevant amounts, while silica is subordinate. Micro-FT-IR-based model compositions, calculated for aqueous-chloride-carbonate fluids in South African diamonds by Izraeli et al. (2001), correspond to about 19–22 wt% Cl, 14–17 wt% K and Na, 30–42% H_2O, 22–25% Fe-Ca-Mg-carbonates, and 3–4% SiO_2. Chlorine-enriched (bulk salinity 6–32 mass%) aqueous fluid inclusions have similarly been reported in the clinopyroxene, zircon, and K-richterite from composite MARID-metasomatized (mica–amphibole–rutile–ilmenite–diopside) peridotite xenoliths (P = 3 GPa; T = 800–1100 °C; Waters and Erlank 1986) from kimberlites of the central Kaapvaal Craton (South Africa). The authors found the predicted mantle Cl-enrichment pattern in the sample, namely $Cl_{ap} \gg Cl_{phl} \gg Cl_{Kr}$.

Brines from fluid inclusions in diamonds imply halogen-rich fluids in the cratonic subcontinental lithosphere. The compositional trends of the fluid inclusions in fibrous diamonds reveal that, under the P-T conditions present in the subcontinental lithosphere, full miscibility exists between carbonatitic fluid and saline aqueous fluid end-members, and between hydrous-silicic and carbonatitic fluid end-members (Fig. 13.13b; cf., Navon et al. 1988; Schrauder and Navon 1994; Shiryaev et al. 2005; Klein-BenDavid et al. 2006, 2007; Weiss et al. 2015). Conversely, saline aqueous fluids and hydro-silicic fluids appear more as distinct fluid phases (Fig. 13.13b; Perchuk et al. 2002; Navon et al. 2003; Klein-BenDavid et al. 2004, 2006, 2007).

The processes leading to the origin of the brine fluid inclusions in diamonds are only partly understood. The relatively low abundance of intermediate compositions between saline aqueous fluid and hydro-silicic fluid end members has been interpreted as evidence for fluid immiscibility at upper mantle P-T conditions by many authors (Perchuk et al. 2002; Navon et al. 2003; Klein-BenDavid et al. 2007, 2009; Safonov et al. 2009, 2011). In particular, Klein-BenDavid et al. (2007) suggested that, at high temperature, immiscibility between brines and hydrous-silicic end-members could originate following carbonate fractionation from a parental Cl-bearing, carbonate-rich fluid. On the other hand, experimental studies ($P \geq 4.5$ GPa; Safonov et al. 2007, 2009) have shown that partial melting of carbonate- and chloride-bearing peridotite and eclogite during interaction with

silica-poor, alkali-rich, chloride-carbonate fluids could generate all the compositional trends observed in fluid inclusions in diamonds. Finally, Weiss et al. (2015) have recognized a continuous compositional change in fluid composition from saline to high-Mg carbonatitic in diamond growth zones. Therefore, they emphasized that brines can be the parental fluids from which both hydro-silicic and carbonatitic fluids formed by fluid-rock interaction and local mantle melting processes.

Brines in diamonds are enriched in incompatible elements and show fractionated patterns. They generally have high LREE/HREE, with a positive Ba, U, Th, and Sr anomaly, but a negative Nb and Ta anomaly (cf., Rege et al. 2010; Weiss et al. 2015, and references therein). According to a comprehensive study on fibrous diamonds worldwide (Rege et al. 2010), trace element fractionation should result from immiscibility between hydro-silicic and carbonate-halide fluid end members. Recently, Weiss et al. (2015) found that saline fluids have positive Eu and Sr anomalies and pronounced light-REE/medium-REE and Th/U ratios, while hydro-silicic fluids show no Eu anomaly, a negative Sr anomaly, and less pronounced light-REE/medium-REE and Th/U ratios, which are suggestive of distinct sources.

The recognition of variable degrees of enrichment, and chemical fractionation in halogen (e.g., Br/Cl and I/Cl) ratios, even in diamonds from the same locality, is of special interest for understanding the ultimate source for halide-rich fluids. In diamonds from the Panda kimberlite (Slave Craton, Canada), halogen concentrations are 10 to 50 times higher than in diamonds from other localities, with Br/Cl and I/Cl ratios that are distinct from seawater (Cartigny et al. 2009). Although not fully understood, different processes may contribute to the chemical fractionation of halogens in diamond fluids. These include recycling of crustal halogens, variable mixing trends between distinct end-member fluids, crystallization of Cl-bearing minerals such as mica and apatite, and/or fluid unmixing processes (Johnson et al. 2000; Izraeli et al. 2001; Burgess et al. 2002; Klein-BenDavid et al. 2007; Cartigny et al. 2009). As an example, Fig. 13.14 (data from Johnson et al. 2000; Burgess et al. 2009) illustrates the extreme differences in Br/Cl and I/Cl molar ratios in diamond-hosted brines. Diamonds from some localities form an array overlapping the range of marine pore fluids, while diamonds from other localities form a distinct fractionation trend, with ratios similar to the highest values measured in crustal fluids (Burgess et al. 2002).

Geochemical data discussed above suggest that recycled halogens represent an important component in diamond fluids, but that the amounts derived directly from subducted lithosphere, vs. the amounts recycled in the deep convecting mantle are disputed (cf., Burgess et al. 2002). In particular, recent independent research by Weiss et al. (2015), based on Sr isotopic compositions and incompatible element fractionation of brines in diamonds from the Slave craton, Canada, has provided firm evidence that halogen-rich fluids were directly released from a subducting Mesozoic plate under western North America.

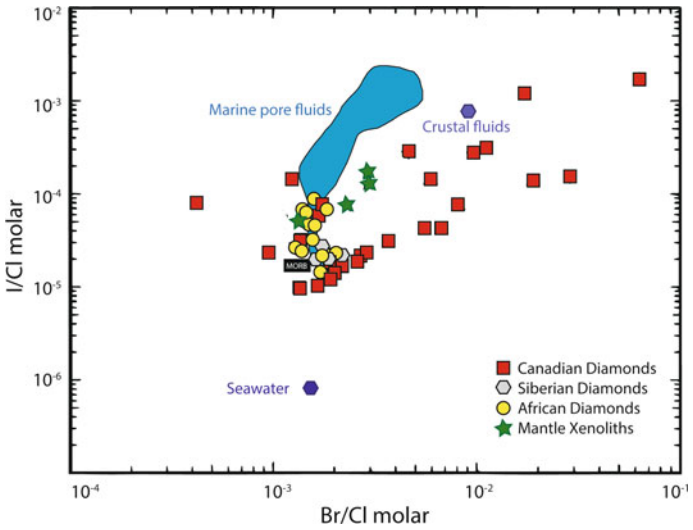

Fig. 13.14 Br/Cl versus I/Cl (molar) for brines in fluid inclusions in diamonds from Canada (Panda, Fox, Grizzly, Koala, and Leslie kimberlites), Africa (Jwaneng kimberlite, Botswana and Democratic Republic of Congo), and Siberia (Aikhal). Compositions of marine pore fluids from Martin et al. (1993) and Mahn and Gieskes (2001). Redrawn based on data plot from Johnson et al. (2000) and Burgess et al. (2002, 2009)

13.4 Implications for Halogens in the Lithospheric Mantle

Our knowledge of halogens in the lithospheric mantle has increased considerably over the last 10–20 years, along with improvements in analytical techniques and theoretical studies. First recognized in metasomatic hydrous phases, the halogens (particularly F) have also been measured in recently nominally anhydrous minerals and in fluid inclusions, suggesting that the lithospheric mantle represents an important halogen reservoir on Earth.

Chlorine appears to be the principal halogen present in the aqueous component of lithospheric subduction-zone fluids, which are expected to be rich in recycled Cl. The Cl contents of fluid inclusions from subduction settings are generally high, up to 50 wt% NaCl equivalent (i.e., saline brines; e.g., Scambelluri and Philippot 2001). However, halogen enrichment in lithospheric aqueous fluids is more widespread than generally accepted. Significant amounts of Cl have been measured recently in hydrous metasomatic phases (e.g., amphibole and phlogopite) , and in H_2O-CO_2 fluid inclusions in minerals from peridotites and pyroxenites from the oceanic and continental lithosphere. Remarkably, high Cl concentrations also characterize deeper, halide-bearing alkali carbonate-rich fluids in the deep cratonic continental lithosphere, which are responsible for mantle metasomatic processes related to diamond genesis. Another piece of relevant information, arising from studies in mantle rocks and in diamonds, is that halide-bearing aqueous fluids are

complex solutions, dominated by alkali- (e.g., K), and Ca-rich chlorides, but also containing measurable amounts of dissolved silica, carbonates, sulfates, and probably fluorides.

Brines in fluid inclusions, and Cl in hydrous metasomatic mineral phases in peridotite and pyroxenites xenoliths, suggest that significant amounts of halogens are present in C-O-H fluids associated with regions of OIB magmatism within the lithospheric mantle, which were not previously widely recognized. For example, at Hawaii and the Azores, Cl-enrichment in melt inclusions in OIB has been interpreted by many authors to reflect shallow interaction with seawater or with deep-crustal brines (e.g., Stolper et al. 2004; Seaman et al. 2004; Le Roux et al. 2006). These mechanisms for Cl enrichment are considered as unlikely in peridotites from regions of continental flood basalts and rifting (e.g., Ethiopian Plateau and Southern Main Ethiopian rift). Here, halogen enrichment in minerals and fluids testifies to fluxes of supercritical CO_2-H_2O fluids, rich in halogens and other incompatible elements, which infiltrate the lithospheric mantle, and are probably related to the geodynamic evolution of the area (Frezzotti et al. 2010, 2012).

These results indicate that halogens play a major role in the geochemical and petrological evolution of the lithospheric mantle globally. Halide-bearing C-O-H fluids present in peridotites, which equilibrated at depths <80 km in intraplate and extensional geodynamic settings, show broad compositional similarities with deeper halogen-bearing carbonate melts/fluids generated at greater depths in the lithospheric mantle, or in the asthenosphere (e.g., Frezzotti and Touret 2014).

Carbonate-rich (i.e., dolomitic) melts are produced by low-degree partial melting of carbonated peridotite at the *P–T* conditions of the kimberlitic-magma source (Wallace and Green 1988; Dalton and Presnall 1998; Gudfinnsson and Presnall 2005; Dasgupta et al. 2007; Dasgupta and Hirshmann 2010). Small fractions of carbonate-rich melts have very low viscosity and low dihedral angles with respect to mantle olivine grains, and can segregate from source regions and percolate very rapidly through the lithospheric mantle (e.g., Hammouda and Laporte 2000). At pressures below 2.4–2.6 GPa, metasomatic melts would decarbonate on reactions with mantle minerals. As a result of metasomatic reactions, such as:

$$\mathrm{CaMg(CO_3)_2melt} + 4\mathrm{MgSiO_3} = \mathrm{CaMgSi_2O_6} + 2\mathrm{Mg_2SiO_4} + 2\mathrm{CO_2}, \qquad (13.5)$$

one mole of reacting dolomitic melt can produce two moles of CO_2, and, as a consequence, large fluxes of CO_2-bearing fluids, containing significant H_2O and halides, might be degassed into the lithospheric mantle. Regardless of the original halogen budget for hydrous carbonate-rich melts, the released CO_2-H_2O-fluids would be enriched in Cl, since melt/fluid partitioning of F and Cl between a carbonatitic melt and a fluid is similar to that in the silicate melt–fluid system (O'Reilly and Griffin 2000; Patino Douce et al. 2011).

Halide-enriched, aqueous fluids and hydrous carbonate melts represent effective metasomatic agents, since high halogen concentrations influence the capacity for mass transfer and the density of aqueous fluids. Under lithospheric mantle conditions, even at moderate halide concentrations, brines are capable of dissolving and

transporting chemical species, even those generally considered immobile (e.g., Keppler 1996; Rege et al. 2010; Bali et al. 2011). As in the example shown in Fig. 13.10, the calculated trace-element fractionation, by metasomatic Cl-rich fluid phases in equilibrium with clinopyroxene, shows increasingly higher abundances of incompatible elements associated with prominent positive Pb and Sr anomalies, and negative HFSE anomalies. These are similar to the pattern measured in slab-derived mantle brines, and distinct from pure H_2O or hydrous metasomatic silicate melts.

Significant amounts of halogens in mantle fluids also variably influence the petrological evolution of lithospheric peridotites. The effect of halogens on the onset of volatile-present peridotite melting, even though not extensively studied, might be different, depending on halogen solubility in silicate melts. At lithospheric depths, and in the presence of aqueous fluids, high levels of Cl have the effect of increasing the peridotite hydrous solidus, since Cl lowers the H_2O activity of the fluid, given the square root dependence of water solubility on water fugacity at high P-T (Aranovich and Newton 1996, 1997). On the contrary, halogens, particularly Cl, may strongly decrease the solidus temperature of carbonated mantle rocks, without reducing the temperature interval for the transition from carbonate- to silicate-dominated melts. The experiments of Safonov et al. (2011) demonstrated that melting phase relations in carbonated peridotites show a gradual transition from a carbonatitic melt (5–7 wt% SiO_2, MgO/CaO = 0.5–0.6, $\sim$2 wt% Cl) at 1000–1100 °C, through to a Cl-rich carbonate–silicate melt (12–15 wt% SiO_2, MgO/CaO = 0.6, and up to 14 wt% Cl) with increasing temperature (1360–1400 °C), and lastly to a Cl-bearing ultrabasic carbonate–silicate melt, i.e. kimberlite-like (26–29 wt% SiO_2, MgO/CaO = 1.5–2.8, and 6–4 wt% Cl), at 1500–1600 °C. Metasomatism and, eventually, mantle melting, control the transfer of halogens from upper-mantle depths to the exosphere. Data on the cycling of halogens, published so far, still leave some large areas of uncertainty, notably regarding the mechanisms that control the distribution of halogens among the Earth's different reservoirs, including recycling by subduction, and mantle degassing. Significant amounts of recycled halogens in lithospheric fluids globally suggests that there may be a dynamic balance in the halogen geochemical cycle, controlled both by subduction and by mantle fractionation processes.

Probably the most demanding question is whether recycled halogen budgets are derived from ancient subducted lithosphere at depths not exceeding about 200–300 km (Ito et al. 1983; Dixon et al. 2002). This would imply a relatively shallow Cl-cycle, or that only part of the halogens, extracted from subducted slabs, are recycled by arc magmas, and that substantial amounts may be returned to large deep convecting mantle reservoirs (Philippot 1993; Magenheim et al. 1995; Sobolev et al. 2011). Both hypotheses are broadly consistent with high halogen abundances and variable chemical fractionation among the halogens (i.e., Br/Cl and I/Cl) measured in mantle fluids in fibrous and cloudy diamonds from the deep cratonic lithosphere. Currently, very little data on the chemical composition and fractionation of halogens in mantle peridotites exist. Further research on halogens in fluids in tectonically active regions is necessary to better constrain the origin of halogen fluxes in the lithospheric mantle, and the extent of halogen heterogeneity in

upper mantle. It is only with these data that we will be able to recognize if halogens, and more general volatile components, can be efficiently returned to the deep convective Earth's mantle.

Acknowledgements We thank Daniel Harlov for his patience, and his thoughtful editorial handling of the manuscript. We are extremely grateful to W. Griffin, J. Konzett, and an anonymous reviewer for thoughtful comments which have considerably improved the manuscript. We thank D. Kamenetsky, M.G. Kopylova, J.L. Mosenfelder, and E.M. Smith for making illustrations available for this chapter. This work was supported by the Italian PRIN grant 2010PMKZX7.

References

Agrinier P, Mével C, Bosch D, Javoy M (1993) Metasomatic hydrous fluids in amphibole peridotites from Zabargad Island (Red Sea). Earth Planet Sci Lett 120:187–205

Aiuppa A, Baker DR, Webster JD (2009) Halogens in volcanic systems. Chem Geol 263:1–18

Andersen T, Neumann ER (2001) Fluid inclusions in mantle xenoliths. Lithos 55:301–320

Andersen T, O'Reilly SY, Griffin WL (1984) The trapped fluid phase in upper mantle xenoliths from Victoria, Australia: implications for mantle metasomatism. Contrib Mineral Petrol 88:72–85

Aoki K (1975) Origin of phlogopite and potassic-richterite bearing peridotite xenoliths from South Africa. Contrib Mineral Petrol 53:145–156

Aranovich LY, Newton RC (1996) H_2O activity in concentrated NaCl solutions at high pressures and temperatures measured by the brucite-periclase equilibrium. Contrib Mineral Petrol 125:200–212

Aranovich LY, Newton RC (1997) H_2O activity in concentrated NaCl solutions at high pressures and temperatures measured by the brucite-periclase equilibrium. Contrib Mineral Petrol 127:261–271

Aranovich LY, Zakirov IV, Sretenskaya NG, Gerya TV (2010) Ternary system H_2O–CO_2–NaCl at high T-P parameters: an empirical mixing model. Geochem Int 48:446–455

Ayers J (1998) Trace element modeling of aqueous fluid–peridotite interaction in the mantle wedge of subduction zones. Contrib Mineral Petrol 132:390–404

Bakker RJ, Jansen JBH (1991) Experimental post-entrapment water loss from synthetic CO_2-H_2O inclusions in natural quartz. Geochim Cosmochim Acta 55:2215–2230

Bali E, Audetat A, Keppler H (2011) The mobility of U and Th in subduction zone fluids: an indicator of oxygen fugacity and fluid salinity. Contrib Mineral Petrol 161:597–613

Barnes JD, Sharp ZD (2006) A chlorine isotope study of DSDP/ODP serpentinized ultra-mafic rocks: insights into the serpentinization process. Chem Geol 228:246–265

Barnes JD, Manning C, Scambelluri M, Selverstone J (2018) The behavior of halogens during subduction-zone processes. In: Harlov DE, Aranovich L (eds) The role of halogens in terrestrial and extraterrestrial geochemical processes: surface, crust, and mantle. Springer, Berlin, pp 545–590

Bell DR, Rossman GR (1992) Water in Earth's mantle: the role of nominally anhydrous minerals. Science 255:1391–1397

Bell DR, Grégoire M, Grove TL, Chatterjee N, Carlson RW, Buseck PR (2005) Silica and volatile-element metasomatism of Archean mantle: a xenolith-scale example from the Kaapvaal Craton. Contrib Mineral Petrol 150:251–267

Bernini D, Wiedenbeck M, Dolejš D, Keppler H (2013) Partitioning of halogens between mantle minerals and aqueous fluids: implications for the fluid flow regime in subduction zones. Contrib Mineral Petrol 165:117–128

Beyer C, Klemme S, Wiedenbeck M, Stracke A, Vollmer C (2012) Fluorine in nominally fluorine-free mantle minerals: experimental partitioning of F between olivine, orthopyroxene and silicate melts with implications for magmatic processes. Earth Planet Sci Lett 337–338:1–9

Bodinier JL, Vasseur G, Vernieres J, Dupuy C, Fabries J (1990) Mechanism of mantle metasomatism: geochemical evidence from the Lherz orogenic peridotite. J Petrol 31:597–628

Bonadiman C, Coltorti M, D'Ambrosi F, Salvini L, Stiefenhofer J, Sweeney RJ, Zanetti A (1999) Enrichment processes in garnet-bearing mantle xenoliths from Kimberley pipes (South Africa). Ophioliti 24:70–71

Bonadiman C, Nazzareni S, Coltorti M, Comodi P, Giuli G, Faccini B (2014) Crystal chemistry of amphiboles: implications for oxygen fugacity and water activity in lithospheric mantle beneath Victoria Land, Antarctica. Contrib Mineral Petrol 167:984–1001

Boyd SR, Mattey DP, Pillinger CT, Milledge HJ, Mendelssohn M, Seal M (1987) Multiple growth events during diamond genesis: an integrated study of carbon and nitrogen isotopes and nitrogen aggregation state in coated stones. Earth Planet Sci Lett 86:341–353

Boyd SR, Pineau F, Javoy M (1994) Modelling the growth of natural diamonds. Chem Geol 116:29–42

Bromiley DW, Kohn SC (2007) Comparisons between fluoride and hydroxide incorporation in nominally anhydrous and fluorine-free mantle minerals. Geochim Cosmochim Acta 71:A124

Bureau H, Keppler H (1999) Complete miscibility between silicate melts and hydrous fluids in the upper mantle: experimental evidence and geochemical implications. Earth Planet Sci Lett 165:187–196

Burgess R, Turner G (1995) Halogen geochemistry of mantle fluids in diamonds. In: Farley KA (ed) Volatiles in the earth and solar system. AIP conference proceedings, vol 341. pp 91–98

Burgess R, Layzelle E, Turner G, Harris JW (2002) Constraints on the age and halogen composition of mantle fluids in Siberian coated diamonds. Earth Planet Sci Lett 197:193–203

Burgess R, Cartigny P, Harrison D, Hobson E, Harris JW (2009) Volatile composition of microinclusions in diamonds from the Panda kimberlite, Canada: implications for chemical and isotopic heterogeneity in the mantle. Geochim Cosmochim Acta 73:1779–1794

Carswell DA (1975) Primary and secondary phlogopites and clinopyroxenes in garnet lherzolite xenoliths. Phys Chem Earth 9:417–429

Cartigny P, Farquhar J, Harris JW, Thomassot E, Wing B, Masterson A, McKeegan K, Stachel TS (2009) A mantle origin for Paleoarchean peridotitic diamonds from the Panda kimberlite, Slave craton: evidence from 13C-, 15 N- and 33, 34S- stable isotope systematics. Lithos 67:234–246

Casagli A, Frezzotti ML, Peccerillo A, Tiepolo M, De Astis G (2017) (Garnet)-spinel peridotite xenoliths from Mega (Ethiopia): evidence for rejuvenation and dynamic thinning of the lithosphere beneath the southern Main Ethiopian Rift. Chem Geol 455:231–248

Chalapati Rao NV, Gibson SA, Pyle DM, Dickin AP (2004) Petrogenesis of Proterozoic lamproites and kimberlites from the Cuddapah Basin and Dharwar Craton, Southern India. J Petrol 45:907–948

Coltorti M, Beccaluva L, Bonadiman C, Faccini B, Ntaflos T, Siena F (2004) Amphibole genesis via metasomatic reaction with clinopyroxene in mantle xenoliths from Victoria Land, Antarctica. Lithos 75:115–139

Coltorti M, Bonadiman C, Faccini B, Grégoire M, O'Reilly SY, Powell W (2007) Amphiboles from suprasubduction and intraplate lithospheric mantle. Lithos 99:68–84

Conceição RV, Green DH (2004) Derivation of potassic (shoshonitic) magmas by decompression melting of phlogopite + pargasite lherzolite. Lithos 72:209–229

Condamine P, Médard E (2014) Experimental melting of phlogopite-bearing mantle at 1 GPa: implications for potassic magmatism. Earth Planet Sci Lett 397:80–92

Dalou C, Koga KT, Shimizu N, Boulon J, Devidal JL (2012) Experimental determination of F and Cl partitioning between lherzolite and basaltic melt. Contrib Mineral Petrol 163:591–609

Dalton JA, Presnall DC (1998) The continuum of primary carbonatitic–kimberlitic melt compositions in equilibrium with lherzolite: data from the system $CaO–MgO–Al_2O_3–SiO_2–CO_2$ at 6 GPa. J Petrol 39:1953–1964

Dasgupta R, Hirschmann MM (2010) The deep carbon cycle and melting in Earth's interior. Earth Planet Sci Lett 298:1–13

Dasgupta R, Hirschmann MM, Smith ND (2007) Partial melting experiments of peridotite + CO_2 at 3 GPa and genesis of alkalic ocean island basalts. J Petrol 48:2093–2124

Dawson JB, Smith JV (1977) The MARID (mica–amphibole–rutile–ilmenite–diopside) suite of xenoliths in kimberlite. Geochim Cosmochim Acta 41:309–323

Dawson JB, Smith JV (1982) Upper-mantle amphiboles: a review. Mineral Mag 45:35–46

De Vivo B, Frezzotti ML, Lima A (1988) Spinel lherzolite nodules from Oahu Island (Hawaii): a fluid inclusion study. Bull Minéral 111:307–319

Dixon JE, Leist L, Langmuir C, Schilling JG (2002) Recycled dehydrated lithosphere observed in plume-influenced mid-ocean-ridge basalt. Nature 420:385–389

Dolejs D, Zajacz Z (2018) Halogens in silicic magmas and their hydrothermal systems. In: Harlov DE, Aranovich L (eds) The role of halogens in terrestrial and extraterrestrial geochemical processes: surface, crust, and mantle. Springer, Berlin, pp 431–543

Dooley DF, Patiño Douce AE (1996) Fluid-absent melting of F-rich phlogopite + rutile + quartz. Am Mineral 81:202–212

Downes H, Bodinier JL, Thirlwall MF, Lorand JP, Fabriès J (1991) REE and Sr-Nd isotopic geochemistry of Eastern Pyrenean peridotite massifs: sub-continental lithospheric mantle modified by continental magmatism. J Petrol, Spec Vol Orogenic Lherzolites and Mantle Processes: 97–115

El Atrassi F, Chazot G, Brunet F, Chopin C, Bouybaouene M (2014) Amphibole genesis in pyroxenites from the Beni Bousera peridotite massif (Rif, Morocco): evidence for two different metasomatic episodes. Lithos 208–209:67–80

Enggist A, Chu L, Luth RW (2012) Phase relations of phlogopite with magnesite from 4 to 8 GPa. Contrib Mineral Petrol 163:467–481

Erlank AJ, Waters FG, Hawkesworth CJ, Haggerty SE, Allsopp HL, Rickard RS, Menzies M (1987) Evidence for mantle metasomatism in peridotite nodules from the Kimberley pipes, South Africa. In: Menzies M, Hawkesworth CJ (eds) Mantle metasomatism. Academic Press, London, pp 221–309

Exley RA, Sills JD, Smith JV (1982) Geochemistry of micas from the Finero spinel-lherzolite, Italian Alps. Contrib Mineral Petrol 81:59–63

Fabbrizio A, Stalder R, Hametner K, Günther D (2013) Experimental chlorine partitioning between forsterite, enstatite and aqueous fluid at upper mantle conditions. Geochim Cosmochim Acta 121:684–700

Faure G (1991) Principles and applications of geochemistry, 2nd edn. Prentice Hall, Upper Saddle River, NJ

Ferrando S, Frezzotti ML, Neumann ER, De Astis G, Peccerillo A, Dereje A, Gezahegn Y, Teklewold A (2008) Composition and thermal structure of the lithosphere beneath the Ethiopian plateau: evidence from mantle xenoliths in basanites, Injibara, Lake Tana Province. Mineral Petrol 93:47–78

Ferreira VP, Sial AN, Cruz MJM (1995) Mineral chemistry of mica-pyroxenite xenoliths in NeoProterozoic ultrapotassic syenitic magmas, NE Brazil. Anais Acad Bras Ciên 67:307–319

Foley SF, Taylor WR, Green DH (1986) The effect of fluorine on phase relationships in the system $KAlSiO_4$-Mg_2SiO_4-SiO_2 at 28 kbar and the solution mechanism of fluorine in silicate melts. Contrib Mineral Petrol 93:46–55

Foley SF, Musselwhite DS, Van der Laan SR (1999) Melt compositions from ultramafic vein assemblages in the lithospheric mantle: a comparison of cratonic and non-cratonic settings. In: Gurney JJ, Gurney JL, Pascoe MD, Richardson SH (eds) The J. B. Dawson volume: Proceedings of the VIIth international kimberlite conference, Cape Town, pp 238–246

Frey FA, Prinz M (1978) Ultramafic inclusions from San Carlos, Arizona: petrologic and geochemical data bearing on their petrogenesis. Earth Planet Sci Lett 38:129–176

Frezzotti ML, Peccerillo A (2007) Diamond-bearing C-O-H-S fluids in the mantle beneath Hawaii. Earth Planet Sci Lett 262:273–283

Frezzotti ML, Touret JLR (2014) CO_2, carbonate-rich melts, and brines in the mantle. Geosci Front 5:697–710

Frezzotti ML, Burke EAJ, De Vivo B, Stefanini B, Villa IM (1992) Mantle fluids in pyroxenite nodules from Salt Lake Crater (Oahu, Hawaii). Eur J Mineral 4:1137–1153

Frezzotti ML, Andersen T, Neumann ER, Simonsen SL (2002a) Carbonatite melt-CO_2 inclusions in mantle xenoliths from Tenerife, Canary Islands: a story of trapping, immiscibility and fluid-rock interaction in the upper mantle. Lithos 64:77–96

Frezzotti ML, Neumann ER, Touret JLR (2002b) Ephemeral carbonate melts in the upper mantle: carbonate silicate immiscibility in microveins and inclusions within spinel peridotite xenoliths, La Gomera, Canary Islands. Eur J Mineral 14:891–904

Frezzotti ML, Ferrando S, Peccerillo A, Petrelli M, Tecce F (2010) Chlorine-rich metasomatic H_2O-CO_2 fluids in amphibole-bearing peridotites from Injibara (Lake Tana region, Ethiopian plateau): nature and evolution of volatiles in the mantle of a region of continental flood basalts. Geochim Cosmochim Acta 74:3023–3039

Frezzotti ML, Ferrando S, Tecce F, Castelli D (2012) Water content and nature of solutes in shallow-mantle fluids from fluid inclusions. Earth Planet Sci Lett 351–352:70–83

Fumagalli P, Zanchetta S, Poli S (2009) Alkali in phlogopite and amphibole and their effects on phase relations in metasomatized peridotites: a high-pressure study. Contrib Mineral Petrol 158:723–737

Garcia MO, Muenow DW, Liu NWK (1980) Volatiles in Ti-rich amphibole megacrysts, southwest USA. Am Mineral 65:306–312

Gibert F, Guillaume D, Laporte D (1998) Importance of fluid immiscibility in the H_2O-CO_2-NaCl system and selective CO_2 entrapment in granulites: experimental phase diagram at 5–7 kbar, 900 °C and wetting textures. Eur J Mineral 10:1109–1123

Greenwood NN, Earnshaw A (1984) Chemistry of the elements. Pergamon, Oxford, p 567

Grégoire M, Bell DR, Le Roex AP (2002) Trace element geochemistry of phlogopite-rich mafic mantle xenoliths: their classification and their relationship to phlogopite-bearing peridotites and kimberlites revisited. Contrib Mineral Petrol 142:603–625

Griffin WL, Åmli R, Heier KS (1972) Whitlockite and apatite from lunar rock 14310 and from Ödegården, Norway. Earth Planet Sci Lett 15:53–57

Griffin WL, Wass SY, Hollis JD (1984) Ultramafic xenoliths from Bullenmerri and Gnotuk maars, Victoria, Australia: petrology of a subcontinental crust-mantle transition. J Petrol 25:53–87

Gudfinnsson GH, Presnall DC (2005) Continuous gradations among primary carbonatitic, kimberlitic, melilititic, basaltic, picritic, and komatiitic melts in equilibrium with garnet lherzolite at 3–8 GPa. J Petrol 46:1645–1659

Guggino SN, Hervig RL, Bell DR (2007) Fluorine in olivines from plutonic, extrusive, and hypabyssal suites. EOS transations, vol 88. American Geophysical Union, V41B-0609

Guthrie GD, Veblen DR, Navon O, Rossman GR (1991) Submicrometer fluid inclusions in turbid-diamond coats. Earth Planet Sci Lett 105:1–12

Hammouda T, Laporte D (2000) Ultrafast mantle impregnation by carbonatite melts. Geology 28:283–285

Harte B (1987) Metasomatic events recorded in mantle xenoliths: an overview. In: Nixon PH (ed) Mantle xenoliths. Wiley, pp 625–640

Heinrich W (2007) Fluid immiscibility in metamorphic rocks. In: Liebscher A, Heinrich CA (eds) Fluid-fluid interactions, vol 65. Reviews in Mineralogy and Geochemistry. Mineralogical Society of America, Washington, DC, pp 389–430

Heinrich W, Churakov SS, Gottschalk M (2004) Mineral-fluid equilibria in the system CaO-MgO-SiO_2-H_2O-CO_2-NaCl and the record of reactive fluid flow in contact metamorphic aureoles. Contrib Mineral Petrol 148:131–149

Hervig RL, Bell DR (2005) Fluorine and hydrogen in mantle megacrysts. EOS Transations, vol 86. American Geophysical Union, V41A-1426

Hidas K, Guzmics T, Szabó C, Kovács I, Bodnar RJ, Zajacz Z, Nédli Z, Vaccari L, Perucchi A (2010) Coexisting silicate melt inclusions and H_2O-bearing, CO_2-rich fluid inclusions in mantle peridotite xenoliths from the Carpathian-Pannonian region (central Hungary). Chem Geol 274:1–18

Hofmann AW (1988) Chemical differentiation of the Earth: the relationship between mantle, continental crust and oceanic crust. Earth Planet Sci Lett 90:297–314

Hofmann AW (2003) Sampling mantle heterogeneity through oceanic basalts: isotopes and trace elements. In: Carlson RW (ed) The mantle and core, vol 2. Treatise on geochemistry. Elsevier, Oxford, pp 61–101

Holland G, Ballentine CJ (2006) Seawater subduction controls the heavy noble gas composition of the mantle. Nature 441:186–191

Hollister LS (1990) Enrichment of CO_2 in fluid inclusions in quartz by removal of H_2O during crystal-plastic deformation. J Struct Geol 12:895–901

Hughes JM, Jolliff BL, Rakovan J (2008) The crystal chemistry of whitlockite and merrillite and the dehydrogenation of whitlockite to merrillite. Am Mineral 93:1300–1305

Huizenga JM (2001) Thermodynamic modelling of C-O-H fluids. Lithos 55:101–114

Huizenga JM (2005) C-O-H, an Excel spread sheet for composition calculations in the C-O-H fluid system. Comp Geosci 31:797–800

Ionov DA, Hofmann AW (1995) Nb-Ta-rich mantle amphiboles and micas: implications for subduction-related metasomatic trace element fractionations. Earth Planet Sci Lett 131:341–356

Ionov DA, Griffin WL, O'Reilly SY (1997) Volatile-bearing minerals and lithophile trace elements in the upper mantle. Chem Geol 141:153–184

Ionov DA, Bodinier J-L, Mukasa SB, Zanetti A (2000) Mechanisms and sources of mantle metasomatism: major and trace element compositions of peridotite xenoliths from Spitsbergen in the context of numerical modelling. J Petrol 43:2219–2259

Ionov DA, Hofmann AW, Merlet C, Gurenko AA, Hellebrand E, Montagnac G, Gillet P, Prikhodko VS (2006) Discovery of whitlockite in mantle xenoliths: inferences for water-and halogen-poor fluids and trace element residence in the terrestrial upper mantle. Earth Planet Sci Lett 244:201–217

Ito E, Harris DM, Anderson AT (1983) Alteration of oceanic crust and geologic cycling of chlorine and water. Geochim Cosmochim Acta 47:1613–1624

Izraeli ES, Harris JW, Navon O (2001) Brine inclusions in diamonds: a new upper mantle fluid. Earth Planet Sci Lett 187:323–332

Izraeli ES, Harris JW, Navon O (2004) Fluid and mineral inclusions in cloudy diamonds from Koffiefontein, South Africa. Geochim Cosmochim Acta 68:2561–2575

Jenkins DM (1983) Stability and composition relations of calcic amphiboles in ultramafic rocks. Contrib Mineral Petrol 83:375–384

John T, Scambelluri M, Frische M, Barnes JD, Bach W (2011) Dehydration of subducting serpentinite: implications for halogen mobility in subduction zones and the deep halogen cycle. Earth Planet Sci Lett 308:65–76

Johnson EL (1991) Experimentally determined limits for H_2O-CO_2-NaCl immiscibility in granulites. Geology 19:925–928

Johnson KE, Davis AM, Bryndzia LT (1996) Contrasting styles of hydrous metasomatism in the upper mantle: an ion microprobe investigation. Geochim Cosmochim Acta 60:1367–1385

Johnson LH, Burgess R, Turner G, Harris JH, Milledge HJ (2000) Noble gas and halogen geochemistry of mantle fluids in diamond: comparison of African and Canadian stones. Geochim Cosmochim Acta 64:717–732

Kamenetsky MB, Sobolev AV, Kamenetsky VS, Maas R, Danyushevsky LV, Thomas R, Pokhilenko NP, Sobolev NV (2004) Kimberlite melts rich in alkali chlorides and carbonates: a potent metasomatic agent in the mantle. Geology 32:845–848

Kamenetsky VS, Kamenetsky MB, Sharygin VV, Faure K, Golovin AV (2007) Chloride and carbonate immiscible liquids at the closure of the kimberlite magma evolution (Udachnaya East Kimberlite, Siberia). Chem Geol 237:384–400

Kamenetsky VS, Kamenetsky MB, Weiss Y, Navon O, Nielsen TFD, Mernagh TP (2009a) How unique is the Udachnaya-East kimberlite? Comparison with kimberlites from the Slave Craton (Canada) and SW Greenland. Lithos 112:334–346

Kamenetsky VS, Maas R, Kamenetsky MB, Paton C, Phillips D, Golovin AV, Gornova MA (2009b) Chlorine from the mantle: magmatic halides in the Udachnaya-East kimberlite, Siberia. Earth Planet Sci Lett 285:96–104

Kamenetsky VS, Kamenetsky MB, Golovin AV, Sharygin VV, Maas R (2012) Ultrafresh salty kimberlite of the Udachnaya-East pipe (Yakutia, Russia): a petrological oddity or fortuitous discovery? Lithos 152:173–186

Kawamoto T, Yoshikawa M, Kumagai Y, Mirabueno MHT, Okuno M, Kobayashi T (2013) Mantle wedge infiltrated with saline fluids from dehydration and decarbonation of subducting slab. Proc Natl Acad Sci 110:9663–9668

Kendrick MA (2012) High precision Cl, Br and I determinations in mineral standards using the noble gas method. Chem Geol 292–293:116–126

Kendrick MA, Kamenetsky VS, Phillips D, Honda M (2012) Halogen (Cl, Br, I) systematics of mid-ocean ridge basalts: a Macquarie Island case study. Geochim Cosmochim Acta 81:82–93

Kendrick MA, Arculus RJ, Danyushevsky LV, Kamenetsky VS, Woodhead JD, Honda M (2014) Subduction-related halogen (Cl, Br and I) and H_2O in magmatic glasses from Southwest Pacific Backarc Basins. Earth Planet Sci Lett 400:165–176

Keppler H (1996) Constraints from partitioning experiments on the composition of subduction-zone fluids. Nature 380:237–240

Keppler H, Smyth JR (2006) Water in nominally anhydrous minerals. Reviews in mineralogy and geochemistry. Mineralogical Society of America, Washington, DC, p 62

Kjarsgaard BA, Pearson DG, Tappe S, Nowell GM, Dowall DP (2009) Geochemistry of hypabyssal kimberlites from Lac de Gras, Canada; comparisons to a global data base and applications to the parent magma problem. Lithos 112:236–248

Klein-BenDavid O, Izraeli I, Hauri E, Navon O (2004) Mantle fluid evolution—a tale of one diamond. Lithos 77:243–253

Klein-BenDavid O, Wirth R, Navon O (2006) TEM imaging and analysis of microinclusions in diamonds: a close look at diamond-growing fluids. Am Mineral 91:353–365

Klein-BenDavid O, Izraeli ES, Hauri E, Navon O (2007) Fluid inclusions in diamonds from the Diavik mine, Canada and the evolution of diamond-forming fluids. Geochim Cosmochim Acta 71:723–744

Klein-BenDavid O, Logvinova AM, Schrauder M, Spetius ZV, Weiss Y, Hauri EH, Kaminsky FV, Sobolev NV, Navon O (2009) High-Mg carbonatitic microinclusions in some Yakutian diamonds—a new type of diamond-forming fluid. Lithos 112:648–659

Konzett J, Frost DJ (2009) The high P-T stability of hydroxyl-apatite in natural and simplified MORB—an experimental study to 15 GPa with implications for transport and storage of phosphorus and halogens in subduction zones. J Petrol 50:2043–2062

Konzett J, Ulmer P (1999) The stability of hydrous potassic phases in lherzolitic mantle—an experimental study to 9·5 GPa in simplified and natural bulk compositions. J Petrol 40:629–652

Konzett J, Rhede D, Frost DJ (2012) The high PT stability of apatite and Cl partitioning between apatite and hydrous potassic phases in peridotite: an experimental study to 19 GPa with implications for the transport of P, Cl and K in the upper mantle. Contrib Mineral Petrol 163:277–296

Kopylova M, Navon O, Dubrovinsky L, Khachatryan G (2010) Carbonatitic mineralogy of natural diamond-forming fluids. Earth Planet Sci Lett 291:126–137

Kopylova MG, Kostrovitsky SI, Egorov KN (2013) Salts in southern Yakutian kimberlites and the problem of primary alkali kimberlite melts. Earth Sci Rev 119:1–16

Koster Van Groos AF, Wyllie PJ (1968) Liquid immiscibility in the join $NaAlSi_3O_8$-Na_2CO_3-H_2O and its bearing on the genesis of carbonatites. Am J Sci 266:932–967

Le Roux PJ, Shirey SB, Hauri EH, Perfit MR, Bender JF (2006) The effects of variable sources, processes and contaminants on the composition of northern EPR MORB (8–108 N and 12–148 N): evidence from volatiles (H_2O, CO_2, S) and halogens (F, Cl). Earth Planet Sci Lett 251:209–231

Luth RW (1997) Experimental study of the system phlogopite-diopside from 3.5 to 17 GPa. Am Mineral 82:1198–1209

Luth RW (2014) Volatiles in Earth's mantle. In: Carlson RW (ed) The mantle and core, vol 3. Treatise on geochemistry. Elsevier, Oxford, pp 355–391

Lyubetskaya T, Korenaga J (2007) Chemical composition of Earth's primitive mantle and its variance: 1. Method and results. J Geophys Res-Solid Earth 112:B03211

Maas R, Kamenetsky MB, Sobolev AV, Kamenetsky VS, Sobolev NV (2005) Sr, Nd, and Pb isotope evidence for a mantle origin of alkali chlorides and carbonates in the Udachnaya Kimberlite, Siberia. Geology 33:549–552

Mackwell SJ, Kohlstedr DL (1990) Diffusion of hydrogen in olivine: implications for water in the mantle. J Geophys Res 95:5079–5088

Magenheim AJ, Spivack AJ, Michael PJ, Gieskes JM (1995) Chlorine stable-isotope composition of the oceanic-crust—implications for Earths distribution of chlorine. Earth Planet Sci Lett 131:427–432

Mahn CL, Gieskes JM (2001) Halide systematics in comparison with nutrient distributions in sites 1033B and 1034B, Saanich Inlet: ODP Leg 169S. Mar Geol 174:323–339

Manning CE (2004) The chemistry of subduction-zone fluids. Earth Planet Sci Lett 223:1–16

Manning CE, Aranovich LY (2014) Brines at high pressure and temperature: thermodynamic, petrologic and geochemical effects. Precambr Res 253:6–16

Martin JB, Gieskes JM, Torres M, Kastner M (1993) Bromine and iodine in Peru margin sediments and pore fluids—implications for fluid origins. Geochim Cosmochim Acta 57:4377–4389

Marty B, Zimmermann L (1999) Volatiles (He, C, N, Ar) in mid-ocean ridge basalts: assessment of shallow-level fractionation and characterization of source composition. Geochim Cosmochim Acta 63:3619–3633

Matson DW, Muenow DW, Garcia MO (1986) Volatile contents of phlogopite micas from South African kimberlite. Contrib Mineral Petrol 93:399–408

Mazzucchelli M, Zanetti A, Rivalenti G, Vannucci R, Teixeira Correia C, Gaeta Tassinari CC (2010) Age and geochemistry of mantle peridotites and diorite dykes from the Baldissero body: insights into the Paleozoic-Mesozoic evolution of the Southern Alps. Lithos 119:485–500

McInnes BIA, Gregoire M, Binns RA, Herzig PM, Hannington MD (2001) Hydrous metasomatism of oceanic sub-arc mantle, Lihir, Papua New Guinea: petrology and geochemistry of fluid-metasomatised mantle wedge xenoliths. Earth Planet Sci Lett 188:169–183

Mengel K, Green DH (1989) Stability of amphibole and phlogopite in metasomatized peridotite under water-saturated and water-undersaturated conditions. In: Kimberlites and related rocks. Geol Soc Aust Spec Pub 14:571–581

Moine BN, Cottin JY, Sheppard SMF, Grégoire M, O'Reilly SY, Giret A (2000) Incompatible trace element and isotopic (D/H) characteristics of amphibole- and phlogopite-bearing ultramafic to mafic xenoliths from Kerguelen Islands (TAAF, South Indian Ocean). Eur J Mineral 12:761–777

Moine BN, Grégoire DC, O'Reilly SY, Sheppard SMF, Cottin JY (2001) High field strength element fractionation in the upper mantle: evidence from amphibole-rich composite mantle xenoliths from the Kerguelen Islands (Indian Ocean). J Petrol 42:2145–2167

Morishita T, Arai S, Tamura A (2003) Petrology of an apatite-rich layer in the Finero phlogopite–peridotite, Italian Western Alps; implications for evolution of a metasomatising agent. Lithos 69:37–49

Mosenfelder JL, Rossman GR (2013a) Analysis of hydrogen and fluorine in pyroxenes: I Orthopyroxene. Am Mineral 98:1026–1041
Mosenfelder JL, Rossman GR (2013b) Analysis of hydrogen and fluorine in pyroxenes: II Clinopyroxene. Am Mineral 98:1054–1942
Mosenfelder JL, Le Voyer M, Rossman GR, Guan Y, Bell DR, Asimov PD, Eiler JM (2011) Analysis of hydrogen in olivine by SIMS: evaluation of standards and protocol. Am Mineral 96:1725–1741
Motoyoshi Y, Hensen BJ (2001) F-rich phlogopite stability in ultra-high-temperature metapelites from the Napier Complex, East Antarctica. Am Mineral 86:1404–1413
Murck BW, Burruss RC, Hollister LS (1978) Phase equilibria in fluid inclusions in ultramafic xenoliths. Am Mineral 63:40–46
Navon O, Hutcheon ID, Rossman GR, Wasserburg GJ (1988) Mantle-derived fluids in diamond micro-inclusions. Nature 335:784–789
Navon O, Izraeli ES, Klein-BenDavid O (2003) Fluid inclusions in diamonds—the carbonatitic connection. In: Proceedings of the 8th international kimberlite conference, vol 107, Victoria, Canada, pp 1–5
Newton RC, Manning CE (2010) Role of saline fluids in deep-crustal and upper-mantle metasomatism: insight from experimental studies. Geofluids 10:57–72
Newton RC, Aranovich LY, Hansen EC, Vandenheuvel BA (1998) Hypersaline fluids in Precambrian deep-crustal metamorphism. Precambr Res 91:41–63
Niida K, Green DH (1999) Stability and chemical composition of pargasitic amphibole in MORB pyrolite under upper mantle conditions. Contrib Mineral Petrol 135:18–40
O'Reilly SY, Griffin WL (2000) Apatite in the mantle: implications for metasomatic processes and high heat production in Phanerozoic mantle. Lithos 53:217–232
O'Reilly SY, Griffin WL (2013) Mantle Metasomatism. In: Harlov DE, Austrheim H (eds) Metasomatism and the chemical transformation of rock. Lecture notes in earth system sciences. Springer, Berlin, pp 471–533
O'Reilly SY, Griffin WL, Segalstad TV (1990) The nature and role of fluids in the upper mantle: evidence in xenoliths from Victoria, Australia. In: Herbert HK, Ho EH (eds) Stable isotopes and fluid processes in mineralization, vol 23. Geology Department and University Extension, The University of Western Australia, pp 315–323
O'Reilly SY, Griffin WL, Ryan CG (1991) Residence of trace elements in metasomatized spinel lherzolite xenoliths: a proton-microprobe study. Contrib Mineral Petrol 109:98–113
Palme H, Jones A (2003) Solar system abundances of the elements. Treatise Geochem 1:41–61. In: Davis AM (ed) Meteorites, comets, and planets. treatise on geochemistry, vol 1. Elsevier, Oxford, pp 41–61
Palme H, O'Neill HSTC (2003) Cosmochemical estimates of mantle composition. In: Carlson RW (ed) The mantle and core, vol 2. Treatise on geochemistry. Elsevier, Oxford, pp 1–38
Pasteris JD (1987) Fluid inclusions in mantle xenoliths. In: Nixon PH (ed) Mantle xenoliths. Wiley, New York, pp 691–708
Patiño Douce AE, Roden M (2006) Apatite as a probe of halogen and water fugacities in the terrestrial planets. Geochim Cosmochim Acta 70:3173–3196
Patiño Douce AE, Roden MF, Chaumba J, Fleisher C, Yogodzinski G (2011) Compositional variability of terrestrial mantle apatites, thermodynamic modeling of apatite volatile contents, and the halogen and water budgets of planetary mantles. Chem Geol 288:14–31
Pearson DG, Brenker FE, Nestola F, McNeill J, Nasdala L, Hutchison MT, Matveev S, Mather K, Silversmit G, Schmitz S, Vakemans B, Vincze L (2014) Hydrous mantle transition zone indicated by ringwoodite included within diamond. Nature 507:221–224
Perchuk LL, Safonov OG, Yapaskurt VO, Barton JM (2002) Crystal-melt equilibria involving potassium-bearing clinopyroxene as indicator of mantle-derived ultrahigh potassic liquids: an analytical review. Lithos 60:89–111
Peslier AH (2010) A review of water contents of nominally anhydrous natural minerals in the mantles of Earth, Mars and the Moon. J Volcanol Geoth Res 197:239–258

Philippot P (1993) Fluid-melt-rock interaction in mafic eclogites and coesite-bearing metasediments: constraints on volatile recycling during subduction. Chem Geol 108:93–112
Philippot P, Agrinier P, Scambelluri M (1998) Chlorine cycling in the subducted oceanic lithosphere. Earth Planet Sci Lett 161:33–44
Powell W, Zhang M, O'Reilly SY, Tiepolo M (2004) Mantle amphibole trace-element and isotopic signatures trace multiple metasomatic episodes in lithospheric mantle, western Victoria, Australia. Lithos 75:141–171
Pyle DM, Mather TA (2009) Halogens in igneous systems. Chem Geol 263:110–121
Railsback B (2003) An earth scientist's periodic table of the elements and their ions. Geology 31:737–740
Rege S, Griffin WL, Pearson NJ, Araujo D, Zedgenizov D, O'Reilly SY (2010) Trace element patterns of fibrous and monocrystalline diamonds: insights into mantle fluids. Lithos 118:313–337
Roedder E (1965) Liquid CO_2 inclusions in olivine-bearing nodules and phenocrysts from basalts. Am Mineral 50:1746–1782
Roedder E (1984) Fluid inclusions. Reviews in mineralogy and geochemistry, vol 12. Mineralogical Society of America, Washington, DC
Saal AE, Hauri EH, Langmuir CH, Perfit MR (2002) Vapour undersaturation in primitive mid-ocean-ridge basalt and the volatile content of Earth's upper mantle. Nature 419:451–455
Safonov OG, Perchuk LL, Litvin YA (2007) Melting relations in the chloride-carbonate-silicate systems at high pressure and the model for formation of alkalic diamond-forming liquids in the upper mantle. Earth Planet Sci Lett 253:112–128
Safonov OG, Chertkova NV, Perchuk LL, Litvin YA (2009) Experimental model for alkalic chloride-rich liquids in the upper mantle. Lithos 112:260–273
Safonov OG, Kamenetsky VS, Perchuk LL (2011) Links between carbonatite and kimberlite melts in chloride-carbonate-silicate systems; experiments and application to natural assemblages. J Petrol 52:1307–1331
Salters VJM, Stracke A (2004) Composition of the depleted mantle. Geochem Geophys Geosys 5: Q05004
Scambelluri M, Philippot P (2001) Deep fluids in subduction zones. Lithos 55:213–227
Scambelluri M, Piccardo GB, Philippot P, Robbiano A, Negretti L (1997) High salinity fluid inclusions formed from recycled seawater in deeply subducted alpine serpentinite. Earth Planet Sci Lett 148:485–499
Scambelluri M, Bottazzi P, Trommsdorff V, Vannucci R, Hermann J, Gomez-Pugnaire MT, Lopez-Sanchez Vizcaıno V (2002) Incompatible element-rich fluids released by antigorite breakdown in deeply subducted mantle. Earth Planet Sci Lett 192:457–470
Schilling JG, Bergeron MB, Evans R (1980) Halogens in the mantle beneath the North Atlantic. Philos Trans R Soc Lond A297:147–178
Schrauder M, Navon O (1994) Hydrous and carbonatitic mantle fluids in fibrous diamonds from Jwaneng, Botswana. Geochim Cosmochim Acta 58:761–771
Schrauder M, Koeberl C, Navon O (1996) Trace element analyses of fluid-bearing diamonds from Jwaneng, Botswana. Geochim Cosmochim Acta 60:4711–4724
Scribano V, Viccaro M, Cristofolini R, Ottolini L (2009) Metasomatic events recorded in ultramafic xenoliths from the Hyblean area (Southeastern Sicily, Italy). Mineral Petrol 95:235–250
Seaman C, Sherman SB, Garcia MO, Baker MB, Balta B, Stolper E (2004) Volatiles in glasses from the HSDP2 drill core. Geochem Geophys Geosyst 5:Q09G16
Selverstone J, Sharp ZD (2011) Chlorine isotope evidence for multicomponent mantle metasomatism in the Ivrea Zone. Earth Planet Sci Lett 310:429–440
Sharygin IS, Litasov KD, Shatskiy A, Golovin AV, Ohtani E, Pokhilenko NP (2014) Melting phase relations of the Udachnaya-East Group-I kimberlite at 3.0–6.5 GPa: experimental evidence for alkali-carbonatite composition of primary kimberlite melts and implications for mantle plumes. Gondwana Res 28:1391–1414

Shaw CSJ, Kleugel A (2002) The pressure and temperature conditions and timing of glass formation in mantle-derived xenoliths from Baarley, West Eifel, Germany: the case for amphibole breakdown, lava infiltration and mineral–melt reaction. Mineral Petrol 74:163–187
Shiryaev AA, Izraeli ES, Hauri EH, Zakharchenko OD, Navon O (2005) Chemical, optical and isotopic investigation of fibrous diamonds from Brazil. Russ Geol Geophys 46:1185–1201
Skippen G, Trommsdorff V (1986) The influence of NaCl and KCl on phase relations in metamorphosed carbonate rocks. Am J Sci 286:81–104
Smith EM, Kopylova MG, Nowell GM, Pearson D, Ryder J (2012) Archean mantle fluids preserved in diamonds from Wawa, Superior Craton. Geology 40:1071–1074
Smith EM, Kopylova MG, Frezzotti ML, Afanasiev VP (2014) N-rich fluid inclusions in octahedrally-grown diamond. Earth Planet Sci Lett 393:39–48
Smith EM, Kopylova MG, Frezzotti ML, Afanasiev VP (2015) Fluid inclusions in Ebelyakh diamonds: evidence of CO_2 liberation in eclogite and the effect of H_2O on diamond habit. Lithos 216:106–117
Smith JV, Delaney JS, Hervig RL, Dawson JB (1981) Storage of F and Cl in the upper mantle: geochemical implications. Lithos 14:133–147
Sobolev NV, Logvinova AM, Efimova ES (2009a) Syngenetic phlogopite inclusions in kimberlite-hosted diamonds: implications for role of volatiles in diamond formation. Russian Geol Geophys 50:1234–1248
Sobolev NV, Logvinova AM, Zedgenizov DA, Pokhilenko NP, Malygina EV, Kuzmin DV, Sobolev AV (2009b) Petrogenetic significance of minor elements in olivines from diamonds and peridotite xenoliths from kimberlites of Yakutia. Lithos 112S:701–713
Sobolev SV, Sobolev AV, Kuzmin DV et al (2011) Linking mantle plumes, large igneous provinces and environmental catastrophes. Nature 477:312–316
Stachel T, Harris JW (2009) Formation of diamond in the Earth's mantle. J Phys Condens Mat 21:364206
Sterner SM, Bodnar RJ (1989) Synthetic fluid inclusions. VII. Re-equilibration of fluid inclusions in quartz during laboratory-simulated metamorphic burial and uplift. J Metamorph Geol 7:243–260
Stolper E, Sherman S, Garcia MO, Baker MB, Seaman C (2004) Glass in the submarine section of the HSDP2 drill core, Hilo, Hawaii. Geochem Geophys Geosyst 5:Q07G15
Straub SM, Layne GD (2003) The systematics of chlorine, fluorine and water in Izu arc front volcanic rocks: implications for volatile recycling in subduction zones. Geochim Cosmochim Acta 67:4179–4203
Stroncik NA, Haase KM (2004) Chlorine in oceanic intraplate basalts: constraints on mantle sources and recycling processes. Geology 32:945–948
Sudo A, Tatsumi Y (1990) Phlogopite and K-amphibole in the upper mantle: implication for magma genesis in subduction zones. Geophys Res Lett 17:29–32
Svensen H, Jamtveit B, Yardley BWD, Engvik AK, Austrheim H, Broman C (1999) Lead and bromine enrichment in eclogite-facies fluids: extreme fractionation during lower-crustal hydration. Geology 27:467–470
Tomlinson EL, Jones AP, Harris JW (2006) Co-existing fluid and silicate inclusions in mantle diamond. Earth Planet Sci Lett 250:581–595
Touret JLR, Huizenga JM (2012) Fluid-assisted granulite metamorphism: a continental journey. Gondwana Res 22:224–235
Touron S, Renac C, O'Reilly SY, Cottin JY, Griffin WL (2008) Characterization of the metasomatic agent in mantle xenoliths from Deve's, Massif Central (France) using coupled in situ trace-element and O, Sr and Nd isotopic compositions. Geol Soc London Spec Publ 293:177–196
Trial AF, Rudnick RL, Ashwal LD, Henry DJ, Bergman SC (1984) Fluid inclusions in mantle xenoliths from Ichinomegata, Japan: evidence for subducted H_2O. EOS Transations. Am Geophys Union 65:306
Trommsdorff V, Skippen G (1986) Vapour loss ("boiling") as a mechanism for fluid evolution in metamorphic rocks. Contrib Mineral Petrol 94:317–322

Tumiati S, Fumagalli P, Tiraboschi C, Poli S (2013) An experimental study on COH-bearing peridotite up to 3.2 GPa and implications for crust-mantle recycling. J Petrol 54:453–479

Vannucci R, Piccardo GB, Rivalenti G, Zanetti A, Rampone E, Ottolini L, Oberti R, Mazzucchelli M, Bottazzi P (1995) Origin of LREE-depleted amphiboles in the subcontinental mantle. Geochim Cosmochim Acta 59:1763–1771

Vaselli O, Downes H, Thirwall M, Dobosi G, Coradossi N, Seghedi I, Szakacs A, Vannucci R (1995) Ultramafic xenoliths in Plio-Pleistocene alkali basalts from the eastern Transylvanian Basin: depleted mantle enriched by vein metasomatism. J Petrol 36:23–53

Viti C, Frezzotti ML (2000) Re-equilibration of glass and CO_2 inclusions in xenolith olivine: a TEM study. Am Mineral 2000:1390–1396

Viti C, Frezzotti ML (2001) Transmission electron microscopy applied to fluid inclusion investigations. Lithos 55:125–138

Vukadinovic D, Edgar AD (1993) Phase relations in the phlogopite-apatite system at 20 kbar: implications for the role of fluorine in mantle melting. Contrib Mineral Petrol 114:247–254

Wallace ME, Green DH (1988) An experimental determination of primary carbonatite magma composition. Nature 335:343–345

Wallace ME, Green DH (1991) The effect of bulk rock composition on the stability of amphibole in the Upper Mantle. Mineral Petrol 44:1–19

Wanamaker BJ, Evans B (1989) Mechanical re-equilibration of fluid inclusions in San Carlos olivine by power law creep. Contrib Mineral Petrol 102:102–111

Wasson JT (1985) Meteorites, their record of early solar-system history. WH Freeman, New York

Waters FG, Erlank AJ (1986) Isotopic evidence for an ancient component in metasomatised peridotites and MARID rocks from Kimberley kimberlites, South Africa. Terra Cognita 6:242

Watson EB, Brenan JM (1987) Fluids in the lithosphere. 1. Experimentally determined wetting characteristics of CO_2-H_2O fluids and their implications for fluid transport, host-rock physical properties, and fluid inclusion formation. Earth Planet Sci Let 85:594–615

Webster JD (1990) Partitioning of F between $H_2O \pm CO_2$ fluids and topaz rhyolite melt: implications for mineralizing magmatic-hydrothermal fluids in F-rich granitic systems. Contrib Mineral Petrol 104:424–438

Webster JD (1992) Fluid-melt interactions involving Cl-rich granites: experimental study from 2 to 8 kbar. Geochim Cosmochim Acta 56:679–687

Webster JD, Baker DR, Aiuppa A (2018) Halogens in mafic and intermediate-silica content magmas. In: Harlov DE, Aranovich L (eds) The role of halogens in terrestrial and extraterrestrial geochemical processes: surface, crust, and mantle. Springer, Berlin, pp 307–430

Weiss Y, Kessel R, Griffin WL, Kiflawi I, Klein-BenDavid O, Bell DR, Harris J, Navon O (2009) A new model for the evolution of diamond forming fluids: evidence from microinclusion-bearing diamonds from Kankan, Guinea. Lithos 112:660–674

Weiss Y, McNeill J, Pearson G, Nowell GM, Ottley CJ (2015) Highly saline fluids from a subducting slab as the source for fluid-rich diamonds. Nature 524:339–345

Whitney DL, Evans BW (2010) Abbreviations for names of rock-forming minerals. Am Mineral 95:185–187

Witt-Eickschen G, Harte B (1994) Distribution of trace elements between amphibole and clinopyroxene from mantle peridotites of the Eifel (Western Germany): an ion-microprobe study. Chem Geol 117:235–250

Wunder B, Melzer S (2003) Experimental evidence on phlogopitic mantle metasomatism induced by phengite dehydration. Eur J Mineral 15:641–647

Wyllie PJ (1989) Origin of carbonatites: evidence from phase equilibrium studies. In: Bell K (ed) Carbonatites: genesis and evolution. Unwin Hyman, Boston, pp 500–545

Wyllie PJ, Ryabchikov ID (2000) Volatile components, magmas, and critical fluids in upwelling mantle. J Petrol 41:1195–1206

Wyllie PJ, Tuttle OF (1961) Experimental investigation of silicate systems containing two volatile components: Pt. II. The effects of NH_3 and HF, in addition to H_2O on the melting temperatures of albite and granite. Am J Sci 259:128–143

Wyllie PJ, Tuttle OF (1964) Experimental investigations of silicate systems containing two volatile components: Part III. The effects of SO_3, P_2O_5, HCl and Li_2O, in addition to H_2O, on the melting temperatures of albite and granite. Am J Sci 262:930–939

Zaccarini F, Stumpfl EF, Garuti G (2004) Zirconolite and Zr-Th-U minerals in chromitites of the Finero Complex, Western Alps, Italy: evidence for carbonatite-type metasomatism in a subcontinental mantle plume. Can Mineral 42:1825–1845

Zanetti A, Vannucci R, Bottazzi P, Oberti R, Ottolini L (1996) Infiltration metasomatism at Lherz as monitored by systematic ion-microprobe investigations close to an hornblendite vein. Chem Geol 134:113–133

Zanetti A, Mazzucchelli M, Rivalenti G, Vannucci R (1999) The Finero phlogopite-peridotite massif: an example of subduction-related metasomatism. Contrib Mineral Petrol 134:107–122

Zedgenizov DA, Rege S, Griffin WL, Kagi H, Shatsky VS (2007) Compositional variations of micro-inclusions in fluid-bearing diamonds from Udachnaya kimberlite pipe as revealed by LA-ICP-MS. Chem Geol 240:151–162

Chapter 14
Halogens in the Earth's Mantle: What We Know and What We Don't

Stephan Klemme and Roland Stalder

Abstract The Earth's mantle is known to contain significant amounts of volatile elements, such as hydrogen (H), carbon (C) and halogens. In the past decades our knowledge about the storage of H and C in mantle minerals, and their behavior during melting of mantle peridotite has improved considerably. In contrast, the behavior of other volatile elements, such as the halogens (Cl, F, I or Br) in the mantle is not so well constrained. Here we review the available experimental, analytical and theoretical data on halogen storage in mantle rocks and minerals, halogen concentrations in nominally halogen free minerals, and halogen partitioning during magmatic processes.

14.1 Introduction

Volatile elements (H, C, N, S, and the halogens) are known to have a profound influence on almost all processes in the Earth's interior (e.g., Bell and Rossman 1992; Fumagalli and Klemme 2015; Luth 2013). We know that H_2O, probably the most important volatile phase on Earth, plays an enormous role in magmatic processes, as it is known to lower melting temperatures of rocks dramatically. Moreover, water has also profound influence on the rheological properties of mantle rocks (Hirth and Kohlstedt 1996; Karato et al. 1986). Numerous experimental and analytical studies showed that the Earth's upper mantle can store up to several hundreds μg/g H_2O and analytical studies of mantle rocks show that mantle olivines and pyroxenes indeed contain significant amounts of water (10–100 μg/g H_2O). As mentioned above, there is a wealth of information on the storage potential of water

S. Klemme
Institut für Mineralogie, Universität Münster, Corrensstrasse 24, 48149 Münster, Germany
e-mail: stephan.klemme@uni-muenster.de

R. Stalder (✉)
Institut für Mineralogie und Petrographie, Universität Innsbruck, Innrain 52f, 6020 Innsbruck, Austria
e-mail: roland.stalder@uibk.ac.at

D.E. Harlov and L. Aranovich (eds.), *The Role of Halogens in Terrestrial and Extraterrestrial Geochemical Processes*, Springer Geochemistry,
https://doi.org/10.1007/978-3-319-61667-4_14

in the mantle (Bolfan-Casanova 2005; Keppler and Smyth 2006) and somewhat less data on actual measured water concentration in mantle rocks. However, much less attention has been paid to the other volatile elements such as S, C, N and the halogens in the mantle.

The aim of this chapter is to review the available experimental, analytical, and theoretical data on halogen storage in mantle rocks and minerals, halogen concentrations in nominally halogen free minerals, and halogen partitioning during magmatic processes. This chapter is short as the data set needed to address the aforementioned issues is only limited. Nevertheless, the future work section at the bottom of this chapter lists important questions, which need addressing in the near future.

14.1.1 Bulk Halogen Concentrations in Mantle Rocks

With this in mind, the first step is to consider bulk chemical constraints on halogen contents of the Earth's mantle. As the halogens are highly volatile elements (with the exception of F and Cl which are classified as moderately volatile) their concentrations in the bulk silicate Earth (BSE), i.e. the crust and mantle, are much lower than elements with similar incompatibility but less volatility (Lodders 2003; Palme and O'Neill 2014). Note that the heavy halogens (Cl, Br and I) are far more depleted than expected from their condensation temperatures (Fig. 14.1).

One common approach to estimate bulk halogen concentrations in the depleted upper mantle is based on trace element ratios in mid ocean ridge basalts (MORB) (Salters and Stracke 2004). As F and P are of similar incompatibility, the F of the depleted MORB mantle was estimated based on F/P ratios. Using a similar approach, different mantle reservoir concentrations of F, Cl, and the other halogens were estimated (Table 14.1). We would like to refer the interested reader to several excellent reviews and original publications (Aiuppa et al. 2009; le Roux et al. 2006; McDonough and Sun 1995; Newsom 1995; Palme and O'Neill 2014; Pyle and Mather 2009; Salters and Stracke 2004; Workman et al. 2006).

Note that the above arguments for estimating the bulk concentrations of F and Cl in mantle reservoirs are based on similar incompatibilities of e.g., F and P (Salters and Stracke 2004) or Cl and K (Workman et al. 2006). Whilst there are lots of data on the geochemical behavior of K, there were no (or very few) partition coefficients published for either P, Cl or F when the above papers were published. It is difficult to estimate uncertainties for the values given in Table 14.1 but we assume that the uncertainties are rather high. However, in a recent paper Beyer et al. (2012) calculated depleted MORB mantle compositions using published F contents of primary basalts and experimentally derived F partition coefficients between olivine and pyroxene. They calculated some 6–15 μg/g F for the source of MORB and 8–31 μg/g F in the source peridotite for a typical ocean island basalt, which is in excellent agreement with previous estimates for the MORB mantle source (e.g., Salters and Stracke 2004). The bulk reservoir estimates for Br and I are based on

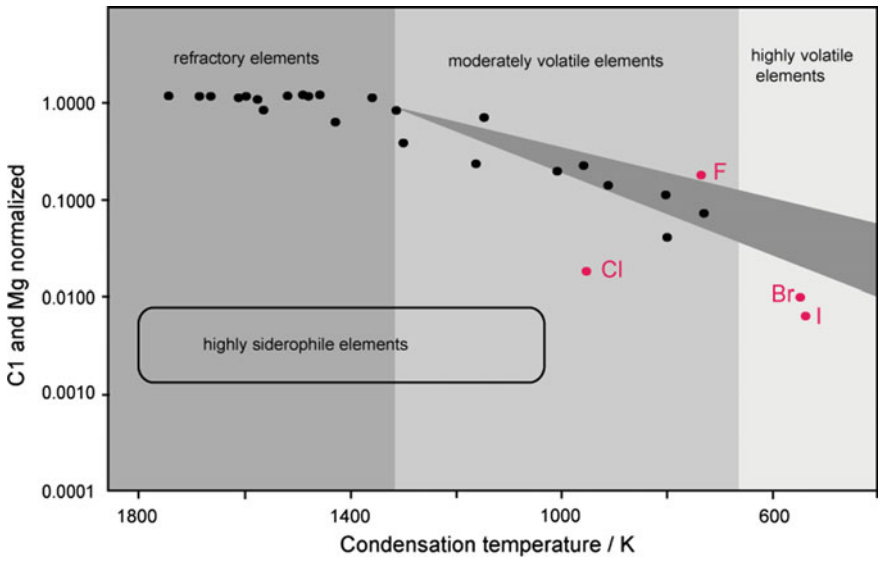

Fig. 14.1 C1-Chondrite and Mg-normalized element concentrations in the Earth's mantle plotted against their condensation temperatures (Lodders 2003; Palme and O'Neill 2014). Only lithophile elements (*circles*) are depicted. The field for highly siderophile elements is shown for comparison. Note that only F follows the Earth depletion trend. The heavy halogens Cl, Br and I exhibit much lower concentrations in the mantle than expected from their volatility. It is unclear what causes this deviation but we surmise that the database for heavy halogens in mantle rocks in basalts is just too thin (see text)

Table 14.1 Bulk halogen concentrations in different mantle reservoirs

	F	Cl	Br	I
Chondrite (C1)	58.2 [PON14]	1000 [J95]	3.7 [J95]	0.53 [PON14]
Depleted MORB Mantle (DMM)	11 [S&S] 16 [S]	0.5 [S&S] 1 [S]	0.008 [SBE]	0.0008 [DDJ]
Bulk silicate Earth (BSE)	15 [BMD]	17 [BMD]	0.3 [BMD]	0.05 [BMD]
Primitive mantle (PM)	25 [PON14] 18 [L&K]	35 [J95] 1.4 [L&K]	0.088 [J95] 0.0036 [L&K]	0.007 [PON14] 0.001 [L&K]

All concentrations in µg/g, data sources: J95 (Jambon et al. 1995), BMD (McDonough 2004), SBE (Schilling et al. 1980), PON14 (Palme and O'Neill 2014), S&S (Salters and Stracke 2004), DDJ (Deruelle et al. 1992), S (Saal et al. 2002), L&K (Lyubetskaya and Korenaga 2007). Reviews over halogen concentrations in different reservoirs are given in Pyle and Mather (2009) and Sharp and Draper (2013)

analyses of basalts (e.g., Deruelle et al. 1992) and the assumption of perfect incompatibility during partial melting.

As the Earth's mantle is known to be heterogeneous, indirect information sources are needed for the determination of the chemical composition of different reservoirs that serve as recent sources for mantle melting. Important study objects in

this context are melt inclusions in early crystallizing minerals such as olivine (Churikova et al. 2007; Kovalenko et al. 2007a; Portnyagin et al. 2007; Saal et al. 2002; Straub and Layne 2003b), where primitive, un-degassed melt is preserved. Systematic variations of Cl/K and F/P in these melts were used as geochemical proxies to estimate the halogen content of different mantle sources. In this way, the average source for ocean island basalts (OIB) is estimated to contain 21 μg/g Cl and 55 μg/g F (Kovalenko et al. 2007b), and estimates for the MORB (mid ocean ridge basalt) source plot around 1 μg/g Cl and 16 μg/g F (Saal et al. 2002; see Fig. 14.2), the latter one in good agreement with the Beyer et al. (2012) data. Subduction zone basalt seems to be rather different, as the Cl concentrations in melt inclusions from subduction zones are generally higher than their OIB counterparts, which is probably related to the enrichment of incompatible halogens such as Cl, I, and Br by slab fluids (Bernini et al. 2013; Fabbrizio et al. 2013a, b; Wu and Koga 2013). The Cl content of the subducted slab is progressively released to the mantle wedge during subduction and breakdown of serpentine, chlorite, and Ti-clinohumite (Debret et al. 2014; Scambelluri et al. 2004). In this way, most of the subducted Cl, but only minor fractions of the subducted F, are recycled to the mantle wedge by slab fluids (Straub and Layne 2003a) and finally are transported to the surface by arc volcanism. This will not be discussed further since other chapters in this volume focus on the role of halogens in basalts (Webster et al. 2018), subduction zones

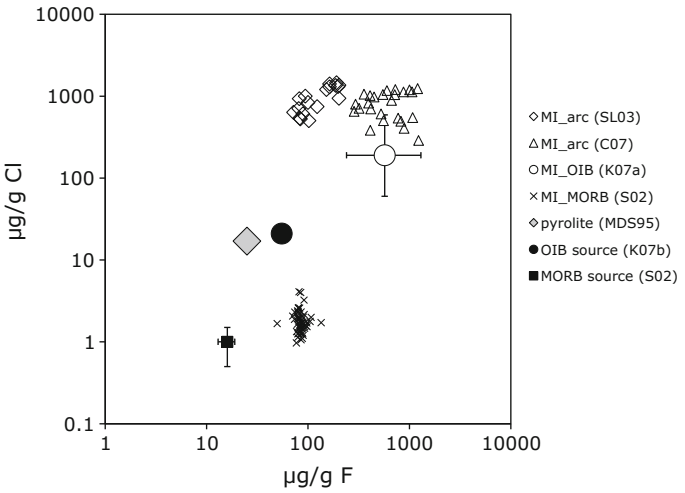

Fig. 14.2 Halogen contents in different mantle sources and melt inclusions from different geodynamic settings. MI = melt inclusion, OIB = ocean island basalt, MORB = mid ocean ridge basalt, SL03 = Straub and Layne (2003b), C07 = Churikova et al. (2007), K07a,b = Kovalenko et al. (2007a, b), S02 = Saal et al. (2002), and MDS95 = McDonough and Sun (1995). Melt inclusions from Straub and Layne (2003a) only represent normal group glasses. Note that the database from melt inclusions and basaltic glasses is much larger and growing rapidly. Chapters 6 (Webster et al. 2018) and 8 (Barnes et al. 2018) deal with these issues in much greater detail

(Barnes et al. 2018), and the metasomatized upper (lithospheric) mantle (Frezzotti and Ferrando 2018).

The average compositions of different mantle reservoirs are certainly helpful for constraining planetary differentiation processes or melting of well-mixed asthenospheric mantle. However, when it comes to the lithospheric mantle, which has been, at least in parts, extensively melted, metasomatized and re-fertilized, the aforementioned methods of estimating bulk compositions are less useful. To establish the halogen concentrations of upper mantle rocks from the continental lithosphere, measurements of actual mantle rocks are needed. However, as we will report later, there are very few actual measurements of F and other halogens in mantle rocks. However, over the last few years the number of halogen analyses from basalts, both MORB and OIB, and subduction zone basalts, and melt inclusions in basalts and related rocks, have increased (Bouvier et al. 2008, 2010; Elburg et al. 2006; Kendrick et al. 2012b, 2014; Koleszar et al. 2009; Le Voyer et al. 2010, 2014; Metrich and Wallace 2008; Portnyagin et al. 2007; Rose-Koga et al. 2012, 2014; Vigouroux et al. 2012; Wallace 2005; Wysoczanski et al. 2006). Thorough discussion of these data can be found in Chap. 6 (Webster et al. 2018), Chap. 7 (Dolejs and Zajacz 2018) and Chap. 8 (Barnes et al. 2018). Combined with halogen partitioning coefficients, this is certainly the way forward to better our understanding of halogen behavior in the upper mantle.

After having established bulk halogen concentrations in the upper mantle, the next questions are concerned with the storage of halogens in the mantle. Which mineral or fluid phases can store halogens in typical mantle rocks? How much F, Cl, I, and Br can be stored in mantle minerals and what happens to the halogens when these phases break down, melt or react with other phases? How much F, Cl, I, and Br do 'normal' mantle minerals contain? Will the halogens be fractionated during these processes and how do they partition between minerals, fluids, and melts? In the following paragraphs we will briefly review the available data to partially address these issues. However, we would like to stress that there is only scant data and, therefore, the paragraph "future work" is probably the most interesting part to read in this article.

14.2 Halogen Storage in Mantle Rocks

14.2.1 Hydrous Mantle Minerals: Stability and Natural Occurrences in the Lithospheric Mantle and Subducted Slab

Apart from volatiles in volcanic melts and gases, the presence of volatiles in the Earth's mantle is obvious from the occurrence of volatile-bearing minerals in mantle xenoliths and mantle nodules. Apatite, amphibole, and mica host significant amounts of water and halogens (Fig. 14.3). Of these, apatite is considered as the major host for Cl in the mantle (Ionov et al. 1997; Smith 1981; Smith et al. 1981).

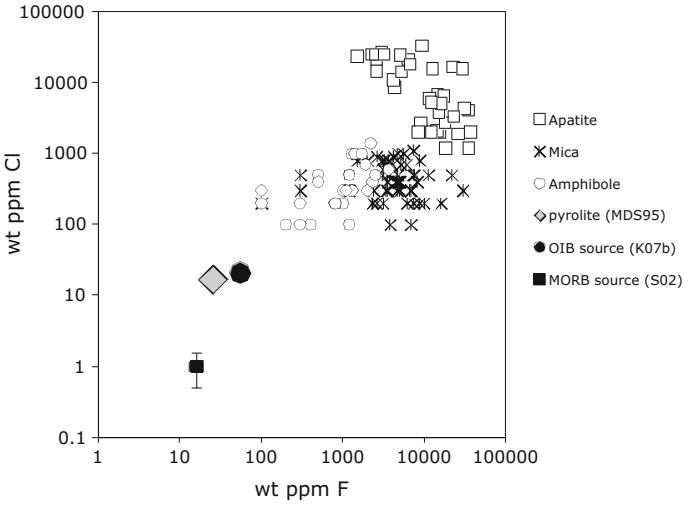

Fig. 14.3 Halogen contents in volatile-bearing mantle minerals such as amphibole, mica, or apatite found in magmatic megacrysts, nodules and peridotite xenoliths. Data from Boettcher and O'Neil (1980), Smith (1981), Irving and Frey (1984), Ionov et al. (1997), O'Reilly and Griffin (2000), Douce et al. (2011), and Bonadiman et al. (2014)

For the correlation between F and P in kimberlites (Smith 1981) and in tholeiitic melts from Iceland (Stecher 1998), apatite melting at the source was suggested as the controlling factor. Likewise, the correlation between F and K in basaltic melts was interpreted to be due to the melting of phlogopite and amphibole in the mantle (Aoki et al. 1981). Recent models, however, show that variations in trace element ratios, such as F/K, can be well explained by the melting of phlogopite- and amphibole-free mantle peridotites (e.g., Salters and Stracke 2004). Furthermore, members from the humite group of minerals, such as Ti-clinohumite and Ti-chondrodite, have been observed in mantle xenoliths from kimberlites (Aoki et al. 1976; McGetchin et al. 1970).

In contrast, the occurrence of other volatile-bearing phases such as serpentine and chlorite is limited to the lithospheric mantle in or close to subduction zones, where temperatures are low compared to the average mantle geotherm. With increasing temperature, volatile-bearing minerals tend to decompose successively to volatile-poorer minerals and a fluid phase. Results from high-pressure experiments show that at realistic mantle compositions, serpentine is stable up to 700 °C/2 GPa and 600 °C/6 GPa (Ulmer and Trommsdorff 1995), chlorite up to 900 °C/2 GPa and 700 °C/5 GPa (Fockenberg 1995; Staudigel and Schreyer 1977), phlogopite up to 1100 °C/6 GPa (Konzett and Ulmer 1999), amphibole (K-richterite) up to 1300 °C (Konzett and Ulmer 1999) and apatite up to 1100 °C between 6 and 8 GPa (Konzett et al. 2012). It is important to stress that all the aforementioned volatile-bearing minerals are only stable at temperatures below the average current mantle adiabat (ACMA). Hence all these phases should not be stable in the 'normal' asthenospheric

mantle but they are certainly stable and could be important halogen storing phases in the colder lithospheric mantle and certainly in the mantle above subduction zones.

A few studies show that F-end member minerals (e.g., mica and amphibole) are characterized by a strongly enhanced thermal stability compared to their hydroxyl counterparts (e.g., Edgar et al. 1994, 1996; Edgar and Pizzolato 1995; Foley 1991; Stalder and Ulmer 2001), underlining the role of halogens for the stabilization of mica and amphibole minerals in the mantle. The incorporation behavior of F and Cl in minerals is closely connected to the Mg/Fe molar ratio due to an avoidance of Fe^{2+} and F in silicate structures (Rosenberg and Foit 1977). This leads to a positive correlation between Mg and F in hydrous mantle minerals such as amphibole and mica (Volfinger et al. 1985).

14.2.2 Halogen Incorporation in Nominally Anhydrous Minerals (NAM)

14.2.2.1 Incorporation Mechanisms

In the last two decades, a large amount of data has emerged on the stability and volatile storage potential of nominally anhydrous minerals—often abbreviated as "NAMs"—(e.g., see the "Reviews in Mineralogy" issue on nominally anhydrous minerals (Keppler and Smyth 2006) for excellent review articles). Numerous publications report that even nominally anhydrous minerals (e.g., olivine, pyroxene or garnet) are able to incorporate small quantities (generally up to several hundreds of μg/g) of water as OH-defects. As halogens and OH are usually incorporated on the same structural sites in silicate minerals, nominally anhydrous silicates in the mantle may, consequently, also serve as host for minor amounts of halogens.

Generally, two major types of defects have to be considered: point defects and planar defects. Point defects are often generated by charge compensations (such as $Si^{4+} = 4\ H^{+}$, the hydro-garnet substitution or coupled substitutions) on a local scale, and usually do not account for high impurity concentrations. A more efficient way to incorporate large quantities of volatiles in NAMs is in the form of planar defects, where monolayers of a hydrous phase are formed. An example of planar defects in minerals from the Earth's mantle was the observation of humite-type lamellae in olivine by transmission electron microscopy (TEM) (Drury 1991; Kitamura et al. 1987). Later, the appearance of humite-type planar defects have been linked to the breakdown sequence Ti-Clinohumite → humite-type defects in olivine → Ti-related point defects in olivine with increasing temperature (Hermann et al. 2007). Important chemical parameters for the stabilization and survival of clinohumite are Ti and F (Evans and Trommsdorff 1983), which has significant implications for the occurrence of humite-type defects and halogen incorporation in olivine. Most recently, an experimental study (Crepisson et al. 2014) has suggested

the occurrence of clumped fluoride-hydroxyl defects in olivine. This may well explain the high F concentrations in mantle minerals via a point defect mechanism.

14.2.2.2 Halogen Storage Potential in Nominally Anhydrous and Halogen-Free Mantle Minerals: Experimental Constraints

Unfortunately, there is scant experimental data available for the storage potential of halogens in nominally halogen free minerals. In an abstract, Bromiley and Kohn (2007) show that forsteritic olivine may contain up to 0.45 wt% F. This is probably the maximum amount of F, as their data is based on experiments in which forsterite crystals were equilibrated with fluorides and humite-type phases. Recent work by Grützner et al. (2017), confirms this. Therefore, olivine is capable of storing much more F than water (Bolfan-Casanova 2005). There is only one paper on F incorporation in other deep mantle mineral phases, named "super-fluorous" phase B (Hazen et al. 1997). Additionally, the incorporation of F^- for OH^- has also been reported for garnet and zircon (Caruba et al. 1985; Visser 1993). To our knowledge, there is no data for other mineral phases, yet, but we expect that in the deep mantle and transition zone, wadsleyite and ringwoodite may contain several wt% of F, even higher than the reported water contents (Bolfan-Casanova 2005).

In Table 14.2 we show the published F-concentrations in NAMs from high-pressure experiments, which span a wide range over several orders of magnitude (Table 14.2, Fig. 14.4a), which further indicate the high F-storage potential of olivine and pyroxenes. In contrast, Cl-concentrations exhibit much smaller variations and median values plot interestingly very close to the primitive mantle values (Fig. 14.4b). This may indicate that nominally anhydrous and halogen free mantle minerals may be saturated in terms of Cl so that a free fluid phase, if present in the mantle, may contain significant amounts of Cl. In another series of experiments, a positive correlation between Al and halogen incorporation has been observed (Beyer et al. 2012; Fabbrizio et al. 2013b; O'Leary et al. 2010) and a coupled substitution $Al^{3+} + F^- = Si^{4+} + O^{2-}$ has been proposed (Beyer et al. 2012).

14.2.2.3 Halogens in Naturally Occurring Nominally Anhydrous and Halogen-Free Mantle Minerals

The database concerning halogens in nominally anhydrous and halogen-free minerals found in naturally occurring mantle rocks, mantle xenoliths, is rather thin (Beyer et al. 2012; Debret et al. 2014; Mosenfelder and Rossman 2013a, b; Scambelluri et al. 2004). This is probably related to the fact that the standard in-house analytical methods (e.g., ICP-MS, EMPA) cannot be employed to routinely analyze low-levels of halogens in silicates. However, secondary ion mass spectrometry (SIMS) methods have recently been developed for the accurate analysis of low level (low μg/g) halogen trace concentrations (e.g., Beyer et al. 2012; Hauri

Table 14.2 Halogen concentrations in NAMs from high pressure experiments

Mineral	Reference	F (μg/g)	Cl (μg/g)
Olivine	Hauri et al. (2006)	0–13	
Olivine	Bromiley and Kohn (2007)	4500–5000	
Olivine	Beyer et al. (2012)	6–14	
Olivine	Dalou et al. (2012, 2014)	1–33	1–20
Olivine	O'Leary et al. (2010)	0.04	
Olivine	Bernini et al. (2013)	1750–1900	2–4
Olivine	Fabbrizio et al. (2013a)		11–133
Olivine	Fabbrizio et al. (2013b)	1–900	14–170
Orthopyroxene	Hauri et al. (2006)	3–88	
Orthopyroxene	Stalder et al. (2008)		22–71
Orthopyroxene	Beyer et al. (2012)	55–432	
Orthopyroxene	Dalou et al. (2012, 2014)	2–2001	4–148
Orthopyroxene	Bernini et al. (2013)	170–336	3–4
Orthopyroxene	Fabbrizio et al. (2013a)		8–119
Orthopyroxene	Fabbrizio et al. (2013b)		19–34
Clinopyroxene	Hauri et al. (2006)	8–138	
Clinopyroxene	Dalou et al. (2012, 2014)	16–2319	2–77
Clinopyroxene	O'Leary et al. (2010)	0.9–11	
Garnet	Hauri et al. (2006)	2–16	
Garnet	Dalou et al. (2012, 2014)	73–986	13–229
Garnet	Bernini et al. (2013)	790–1110	4–11

NAM: Nominally anhydrous mineral, in this case olivine, pyroxene and garnets

et al. 2011; Hoskin 1999; Mosenfelder et al. 2011; Mosenfelder and Rossman 2013a, b; Ottolini and Le Fevre 2007) in nominally halogen-free minerals. Other groups (Crepisson et al. 2014) use particle induced gamma-ray emission (PIGE). It is important to note that at the present time, there are no well-established matrix-matched standards for F in NAM. As noted by Mosenfelder et al. (2011, 2013a, b), most SIMS groups use reference material glasses, e.g., NIST glasses or MPI-DING glasses for SIMS analyses (Dalou et al. 2012; Hauri et al. 2006, 2011; Le Voyer et al. 2014; Mosenfelder et al. 2011; Mosenfelder and Rossman 2013a, b). However, it has been shown that individual shards of these glasses are sometimes heterogeneous (perhaps zoned) with respect to F (and Cl) concentrations (Hinton et al. 1995; Mosenfelder et al. 2011; Mosenfelder and Rossman 2013a, b). Other groups (Bernini et al. 2013; Beyer et al. 2012) chose F-implanted reference materials as standards during SIMS analysis, perhaps also not ideal as the structure of the mineral standard is at least on the surface severely altered during implantation itself. Both standardization methods clearly need improvement. We suspect that some of the scatter for F in the reported NAMs data may have resulted from the different analytical methods used.

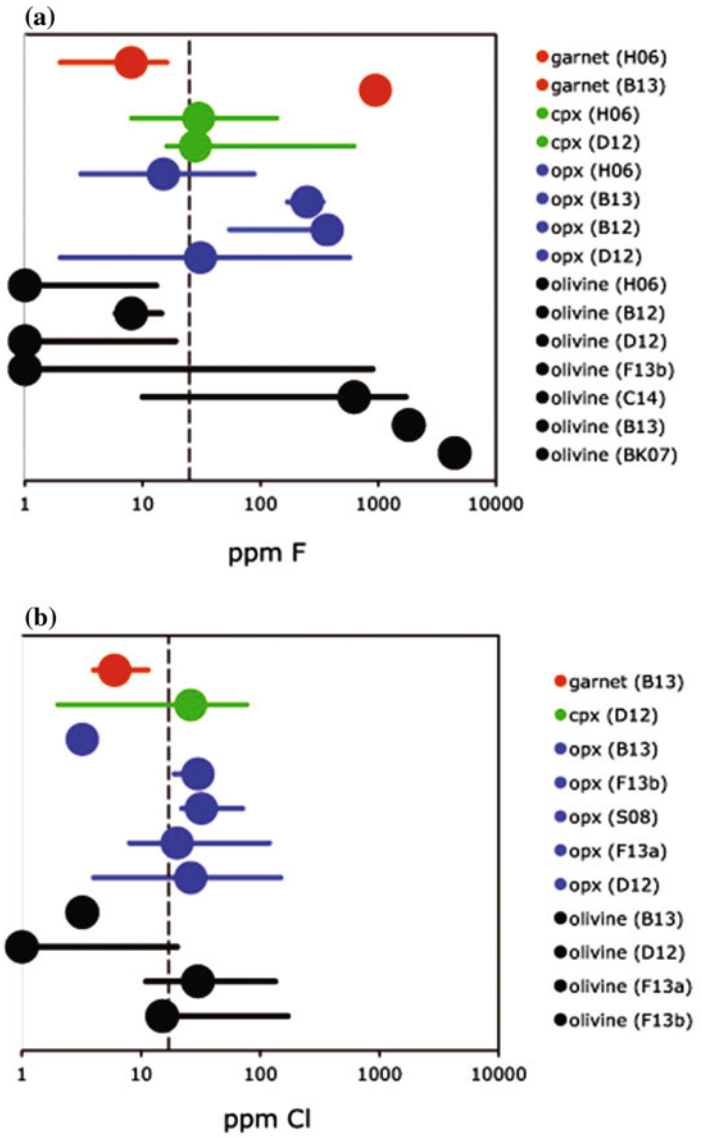

Fig. 14.4 Range of F-contents **a** and Cl-contents **b** in nominally anhydrous minerals from high-pressure experiments. The median value of each study is shown as a *filled circle* and the range as a *bar*. *Vertical broken lines* represent the halogen content of the primitive mantle (McDonough and Sun 1995). H06 = Hauri et al. (2006), BK07 = Bromiley and Kohn (2007), S08 = Stalder et al. (2008), B12 = Beyer et al. (2012), D12 = Dalou et al. (2012), B13 = Bernini et al. (2013), F13a,b = Fabbrizio et al. (2013a, b), and C14 = Crepisson et al. (2014). Halogen concentrations were determined by electron microprobe with high beam currents and long counting times in BK07, S08, F13a,b, and by SIMS in all other studies

The first SIMS measurements on olivines from deep mantle xenoliths (Hervig and Bell 2005) reported F concentrations in olivine between 50 and 240 μg/g at equally high (and variable) H_2O concentrations (80–250 μg/g). More recent measurements indicate mean F-concentrations in olivine of 8 ± 1 μg/g from a variety of basalt-hosted spinel lherzolites, 30 μg/g F in olivine from a deep garnet lherzolite, and 20 ± 8 μg/g F in orthopyroxene from spinel lherzolites (Table 14.3). Similarly, very low F concentrations (a few μg/g) in olivine and pyroxene xenocrysts have been reported from the Colorado Plateau (USA), compared to substantially higher F in olivine and pyroxenes from kimberlite-hosted mantle megacrysts (Mosenfelder and Rossman 2013a, b). Recent data by J. Mosenfelder and co-workers (Mosenfelder et al. 2011; Mosenfelder and Rossman 2013a, b) also clearly show that F concentrations in NAM differ rather strongly between different mantle reservoirs. The database is still very thin, but it seems that the shallow lithospheric mantle is not significantly enriched in F but rather the deeper lithospheric roots in the old lithosphere that seem to be significantly enriched in F. This agrees well with previous data on F enrichment in mica and amphiboles from the metasomatically enriched sub-continental lithosphere sampled by South African kimberlites (e.g., Edgar and Arima 1985; Edgar et al. 1994).

Chlorine concentrations in olivine from spinel and garnet lherzolites plot in a very narrow range centered around 5.8 ± 0.5 μg/g Cl (Beyer et al. 2012). However, the breakdown products from oceanic serpentinites exhibit higher and more variable concentrations, with 20–120, 25, and 20–420 μg/g Cl for olivine, orthopyroxene and clinopyroxene, respectively (Debret et al. 2014; Orberger et al. 1999; Scambelluri et al. 2004). In metasomatized mantle rocks, Cl zonation is an important issue as shown in the case of orthopyroxene, where Cl is very low (<<10 μg/g) in the core of the crystals and strongly enriched towards the rim (Ottolini and Le Fevre 2007).

14.2.3 Halogen Partitioning Between Minerals, Melt and Fluid

In this section we present the few available data sets that address the behavior of F and Cl during partial melting or fluid interaction in the mantle. Cl^- is a much larger anion than F^-, which makes Cl much more incompatible during mantle melting or fluid/mineral interaction in the mantle. In addition, while there is no partitioning data on the behavior of I^- and Br^-, it is probably safe to assume that both elements are nearly perfectly incompatible (i.e. D_{Br} and D_I <<< 1) during mantle melting due to their even larger ionic radii compared to Cl^- (Table 14.4).

Table 14.3 Halogen concentrations in naturally occurring mantle minerals

	F/μ g/g	Reference	Cl/μg/g	Reference
Ol in mantle xenoliths	70–240	Hervig and Bell (2005)		
Ol in spl lhz xenoliths	2.9–9.2	Beyer et al. (2012)	5.7 ± 0.5	Beyer et al. (2012)
Ol in gar lhz xenoliths	30	Beyer et al. (2012)		
Opx in spl lhz xenoliths	12–28	Beyer et al. (2012)		
Ol and opx xenocrysts Colorado Plateau	<3	Mosenfelder and Rossman (2013a)		
Ol megacrysts, Kimberlite, Southern Africa	6–47	Mosenfelder and Rossman (2013a)		
Opx megacrysts, Kimberlite, Southern Africa	12–17	Mosenfelder and Rossman (2013a)		
Cpx megacrysts, Kilborne Hole, USA	46	Mosenfelder and Rossman (2013b)		
Cpx megacrysts, Kimberlite, Southern Africa	up to 29	Mosenfelder and Rossman (2013b)		
Ol in subduction zones			20–120	Scambelluri et al. (2004)
Opx in subduction zones			25	Scambelluri et al. (2004)
Cpx in subduction zones			20–420	(Scambelluri et al. 2004)

Note that, to our knowledge, no data are available for I and Br in mantle minerals. spl = spinel. lhz = lherzolite, gar = garnet, ol = olivine. Refer to the original papers for details

14.2.3.1 Mineral/Melt Partitioning

Recently, O'Leary et al. (2010), Beyer et al. (2012), Dalou et al. (2012, 2014), and Rosenthal et al. (2015) have reported experimentally determined F (and Cl) partition coefficients (D = c mineral/c melt (or fluid)) for olivine, orthopyroxene, and garnet. Dalou et al. (2012) show convincingly that Cl is much more incompatible than F, i.e. the D_F crystal/melt ratio is much higher than the corresponding D_{Cl}. While their pyroxene partition coefficients agree rather well with the Beyer et al. (2012) data, there is some discrepancy between the F partition coefficients for olivine. The only data point for olivine (D_F = 0.1164) published in Dalou et al. (2012) published is much higher than the data by Beyer et al. (2012). However, this data point was later revised (Dalou et al. 2014) and now gives a much lower D_F for olivine, which is in much better agreement with the Beyer et al. (2012) data. Hauri et al. (2006) also measured F in olivines and orthopyroxenes, which were

experimentally equilibrated with silicate melts, and their partition coefficients D_F (Ol/melt) = 0.0012–0.0047 and D_F (Opx/melt) = 0.015–0.0448 agree well with the Beyer et al. (2012) data. A paper by O'Leary et al. (2010), which focused on the incorporation of OH^- in pyroxenes, contains some data on D_F for olivine and clinopyroxene. Their D_F for olivine are in excellent agreement with the Beyer et al. (2012) data, the D_F data on clinopyroxene agree well with the data points by Dalou et al. (2012). Most recently, Rosenthal et al. (2015) have published D_F (min/melt) values for orthopyroxene, clinopyroxene, and garnet. Their data agree very well with the partition coefficients determined by Beyer et al. (2012), O'Leary et al. (2010), and Hauri et al. (2006) (Table 14.4 and Fig. 14.5)

Olivine/melt partition coefficients for Cl have been reported by (or can be calculated from) Dalou et al. (2012) and Hauri et al. (2006). They are generally very low (D_{Cl} Ol/melt < 0.0002 (Hauri et al. 2006)), though slightly higher for Dalou et al. (2012) (D_{Cl} Ol/melt < 0.0043). More recent data from Dalou et al. (2014) have confirmed their earlier measurements. The available mineral/melt partition coefficients are given in Table 14.4. Available partitioning data for F and Cl are depicted in Fig. 14.5a. Overall, Cl is very incompatible during melting. Fluorine is also incompatible but much less incompatible than Cl.

14.2.3.2 Mineral/Fluid Partitioning

Several recent studies investigated the partitioning of Cl and F between olivine, orthopyroxene, clinopyroxene, and hydrous fluids (Table 14.4) (Bernini et al. 2013; Fabbrizio et al. 2013a, b; Stalder et al. 2008). Chlorine is always very incompatible in olivine and pyroxenes and F is only moderately incompatible (and sometimes even compatible) in olivine, owing to an efficient incorporation mechanism (see previous section). However, a general problem for the determination of mineral/fluid partition coefficients arises from the observation that the halogen content in NAMs from high-pressure experiments in simple synthetic systems seem to be independent of the salinity of the coexisting fluid, especially with respect to Cl partitioning (Bernini et al. 2013; Fabbrizio et al. 2013a, b; Stalder et al. 2008), such that at high salinities the system can be considered to be outside Henry's law behavior.

14.2.3.3 Summary of Halogen Partitioning

In summary, the partition coefficients show convincingly, that all halogens are incompatible during mantle melting. However, it is obvious that F is much less incompatible than Cl. By analogy, though despite an absence of data, Br and I can be argued to be even more incompatible due their even larger ionic radii.

Table 14.4 Mineral/melt and mineral/fluid partition coefficients

Mineral	$-\log D_F$	$-\log D_F$	$-\log D_{Cl}$	$-\log D_{Cl}$	Reference
	Mineral/melt	Mineral/fluid	Mineral/melt	Mineral/fluid	
Olivine	2.3–2.8				Hauri et al. (2006)
Olivine	2.5–3.2				Beyer et al. (2012)
Olivine	0.9–2.7		2.5–3.0		Dalou et al. (2012, 2014)
Olivine	3.3–3.6				O'Leary et al. (2010)
Olivine		0.1–1.0		3.8–4.7	Bernini et al. (2013)
Olivine				2.2–4.0	Fabbrizio et al. (2013a)
Olivine				3.8–4.7	Fabbrizio et al. (2013b)
Opx	1.3–1.8				Hauri et al. (2006)
Opx	1.4–1.5				Beyer et al. (2012)
Opx	0.7–1.8		1.2–2.7		Dalou et al. (2012, 2014)
Opx	1.4–1.7				Rosenthal et al. (2015)
Opx		0.9–2.7		3.9–4.7	Bernini et al. (2013)
Opx				2.3–4.3	Fabbrizio et al. (2013a)
Opx				3.4–3.8	Fabbrizio et al. (2013b)
Cpx	1.2–1.9				Hauri et al. (2006)
Cpx	0.8–2.4		1.5–2.7		Dalou et al. (2012, 2014)
Cpx	1.3–1.85				O'Leary et al. (2010)
Cpx	1.3–1.5				Rosenthal et al. (2015)
Cpx				3.7–3.9	Fabbrizio et al. (2013b)
Garnet	2.4–2.8				Hauri et al. (2006)
Garnet	0.8–2.0		1.1–2.6		Dalou et al. (2012, 2014)
Garnet	2.4–2.7				Rosenthal et al. (2015)
Garnet		0.6–1.9		2.9–4.9	Bernini et al. (2013)

cpx = clinopyroxene, opx = orthopyroxene. Note that the experiments were run at different pressures, temperatures and bulk compositions. To select appropriate partition coefficients for geochemical modeling, the reader is referred to the original publications

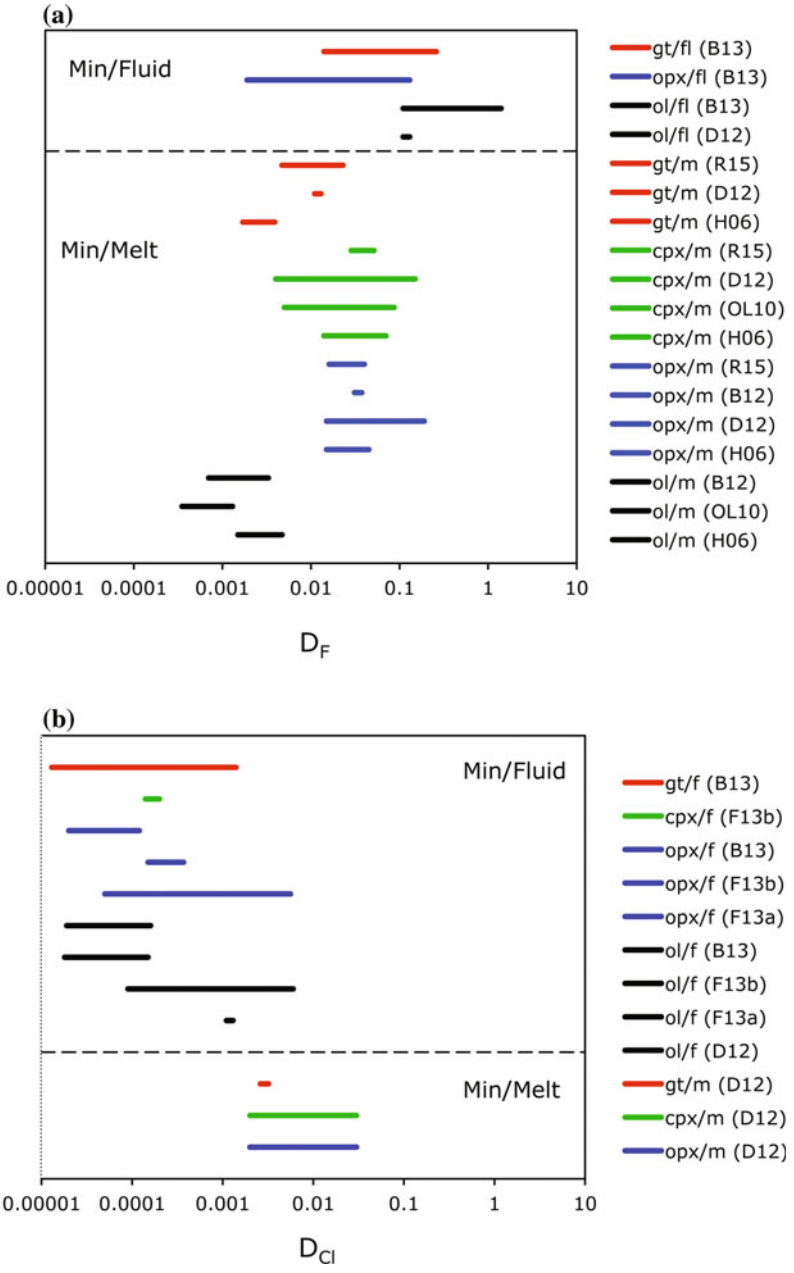

Fig. 14.5 Partition coefficients mineral/melt and mineral/fluid for F (**a**) and Cl (**b**). OL10 = O'Leary et al. (2010), R15 = Rosenthal et al. (2015). For all other references see captions Fig. 14.4

Clinopyroxene, closely followed by orthopyroxene, has the highest affinity for F and D_F (mineral/melt) are the highest for the pyroxenes, followed by garnet and olivine.

14.3 Future Work

To better understand the storage of halogens in the mantle and the geochemical cycles of halogens within and out of the mantle, we critically need both more analyses of halogens in different Earth reservoirs. At the same time we also need more experimental constraints on how halogens are incorporated into mantle minerals, and how halogens behave during partial melting of peridotite and fractional crystallization of melts. A very important aspect will be the extension of experimental partitioning data to a wider p-T-range. As very recently suggested, Cl and F seem to become more compatible at elevated temperatures and D_F and D_{Cl} may reach values around 0.1 for orthopyroxene and olivine at 1600 °C (Joachim et al. 2015), but this needs further investigation.

To this end, we present a somewhat subjective list below of what next needs to be done in the near future.

14.3.1 Chemical Analysis of Halogens in Bulk Rocks, Minerals and Quenched Melts

Bulk chemical analysis of halogens are complicated due to the fact that most silicate rocks are usually dissolved in HF-rich acids. However, accurate bulk rock analyses are possible using alternative analytical techniques such as pyrohydrolysis (e.g., Dreibus et al. 1979) followed by ion chromatography (e.g., Balcone-Boissard et al. 2009; John et al. 2011). Heavier halogens can be analyzed using highly sensitive ICP-MS techniques (e.g., Bu et al. 2003). Furthermore, there is a noble gas technique (e.g., Johnson et al. 2000), which has been used in several recent studies to determine very low concentrations of the heavy halogens (i.e. Cl, Br and I) in basalts from mid-ocean ridges and ocean islands (Kendrick 2012; Kendrick et al. 2012a, b, 2013; Ruzie et al. 2012).

As noted above, new reference materials are needed to better enable in situ chemical analysis of halogens in minerals at low concentrations. This is especially important as secondary ion mass spectrometry (SIMS), which is the method of choice for the analysis of low concentrations (i.e. <500 μg/g) of halogens in silicate and oxide minerals or melt inclusions, requires well-characterized matrix matched reference materials. In this context, both well characterized implanted reference materials and synthetic or natural glasses are urgently needed.

14.3.2 Storage of Halogens in the Mantle and Partitioning of Halogens Between Minerals, Melts and Fluids

To investigate the storage potential of halogens in "nominally halogen-free minerals" we need experimental studies designed to saturate olivines, pyroxenes, and garnets in F-rich silicate melt or fluids. F-solubility in olivine is expected to depend on temperature, pressure, and F-activity in melts. The experiments should therefore be performed in different bulk compositions at different temperatures and pressures, ideally up to pressures well within the transition zone. Particular attention should be paid to the thermal stability of nominally OH- and halogen-bearing phases that are able to survive as planar defects above their breakdown temperature, enabling much more efficient halogen incorporation other than by mechanisms such as point defects. Based on the few experimental results hitherto reported, we expect several thousands μg/g F concentrations in olivine and pyroxene at saturation level.

The Cl concentration of olivine and pyroxene in natural systems is unknown at saturation but should also be explored in a similar manner. Furthermore, more specifically designed experiments are also needed to investigate the substitution mechanism by which F and Cl are incorporated into the olivine, pyroxene and garnet structure. As to partition coefficients, the most recent experimental data consist of partition coefficients for olivine and pyroxenes in melt systems, and for pyroxene and garnet in fluid-bearing systems. Future experiments should focus on the effects of temperature, pressure, or bulk composition on D_F and D_{Cl}. It would also be desirable to measure Br and I partition coefficients at similar conditions.

14.3.3 Influence of Halogens (F, Cl) on Mantle Melting

Little is known about the effect of halogens on melting relations in the mantle. Whilst there are several studies on the effect of F on melting in bulk compositions related to the origin of granite in the crust (e.g., Manning 1981; Wyllie and Tuttle 1961; see also Dolejs and Zajacz 2018), there are, to our knowledge, only two studies (Filiberto et al. 2012; Luth 1988), which investigated the effect of F on melting relations in the mantle. If F has an effect on melting relations (e.g., liquidus/solidus depression, etc.) similar to that of H_2O, we urgently need more detailed experiments to investigate these matters. Correspondingly, the effect of Cl on mantle melting is also only poorly constrained (Chu et al. 2011; Filiberto et al. 2014; Filiberto and Treiman 2009) again requiring considerably more experimental data before its effect on melting can be resolved.

Acknowledgements We would like to thank T. John for many helpful and inspiring discussions on an early version of the manuscript. Our thanks also go to four reviewers for constructive and helpful comments and editors D. E. Harlov and L. Aranovich.

References

Aiuppa A, Baker DR, Webster JD (2009) Halogens in volcanic systems. Chem Geol 263:1–18

Aoki K, Fujino K, Akaogi M (1976) Titanochondrodite and titanoclinohumite derived from upper mantle in Buell Park kimberlite, Arizona, USA. Contrib Mineral Petrol 56:243–253

Aoki K, Ishiwaka K, Kanisawa S (1981) Fluorine geochemistry of basaltic rocks from continental and oceanic regions and petrogenetic application. Contrib Mineral Petrol 76:53–59

Balcone-Boissard H, Michel A, Villemant B (2009) Simultaneous determination of Fluorine, Chlorine, Bromine and Iodine in six geochemical reference materials using pyrohydrolysis, ion chromatography and inductively coupled plasma-mass spectrometry. Geostand Geoanal Res 33:477–485

Barnes JD, Manning C, Scambelluri Selverstone J (2018) The behavior of halogens during subduction-zone processes. In: Harlov DE, Aranovich L (eds) The role of halogens in terrestrial and extraterrestrial geochemical processes: surface, crust, and mantle. Springer, Berlin, pp 545–590

Bell DR, Rossman GR (1992) Water in Earth's mantle—the role of nominally anhydrous minerals. Science 255:1391–1397

Bernini D, Wiedenbeck M, Dolejs D, Keppler H (2013) Partitioning of halogens between mantle minerals and aqueous fluids: implications for the fluid flow regime in subduction zones. Contrib Mineral Petrol 165:117–128

Beyer C, Klemme S, Wiedenbeck M, Stracke A, Vollmer C (2012) Fluorine in nominally fluorine-free mantle minerals: experimental partitioning of F between olivine, orthopyroxene and silicate melts with implications for magmatic processes. Earth Planet Sci Lett 337:1–9

Boettcher AL, O'Neil JR (1980) Stable isotope, chemical, and petrographic studies of high-pressure amphiboles and micas—evidence for metasomatism in the mantle source regions of alkali basalts and kimberlites. Am J Sci 280:594–621

Bolfan-Casanova N (2005) Water in the Earth's mantle. Mineral Mag 69:229–257

Bonadiman C, Nazzareni S, Coltorti M, Comodi P, Giuli G, Faccini B (2014) Crystal chemistry of amphiboles: implications for oxygen fugacity and water activity in lithospheric mantle beneath Victoria Land, Antarctica. Contrib Mineral Petrol 167:1–17

Bouvier AS, Metrich N, Deloule E (2008) Slab-derived fluids in the magma sources of St. Vincent (Lesser Antilles arc): volatile and light element imprints. J Petrol 49:1427–1448

Bouvier AS, Metrich N, Deloule E (2010) Light elements, volatiles, and stable isotopes in basaltic melt inclusions from Grenada, Lesser Antilles: inferences for magma genesis. Geochem Geophyss Geosyst 11:Q09004

Bromiley DW, Kohn SC (2007) Comparisons between fluoride and hydroxide incorporation in nominally anhydrous and fluorine-free mantle minerals. In: VM Goldschmidt Conference, Köln, Germany, vol 71. Geochim Cosmochim Acta: A124

Bu X, Wang T, Hall G (2003) Determination of halogens in organic compounds by high resolution inductively coupled plasma mass spectrometry (HR-ICP-MS). J Anal At Spectrom 18:1443–1451

Caruba R, Baumer A, Ganteaume M, Iacconi P (1985) An experimental-study of hydroxyl-groups and water in synthetic and natural zircons—a model of the metamict state. Am Mineral 70:1224–1231

Chu L, Enggist A, Luth RW (2011) Effect of KCl on melting in the Mg_2SiO_4-$MgSiO_3$-H_2O system at 5 GPa. Contrib Mineral Petrol 162:565–571

Churikova T, Woerner G, Mironov N, Kronz A (2007) Volatile (S, Cl and F) and fluid mobile trace element compositions in melt inclusions: implications for variable fluid sources across the Kamchatka arc. Contrib Mineral Petrol 154:217–239

Crepisson C, Blanchard M, Bureau H, Sanloup C, Withers AC, Khodja H, Surble S, Raepsaet C, Beneut K, Leroy C, Giura P, Balan E (2014) Clumped fluoride-hydroxyl defects in forsterite: implications for the upper-mantle. Earth Planet Sci Lett 390:287–295

Dalou C, Koga KT, Shimizu N, Boulon J, Devidal J-L (2012) Experimental determination of F and Cl partitioning between lherzolite and basaltic melt. Contrib Mineral Petrol 163:591–609
Dalou C, Koga KT, Le Voyer M, Shimizu N (2014) Contrasting partition behavior of F and Cl during hydrous mantle melting: implications for Cl/F signature in arc magmas. Prog Earth Planet Sci 1:26
Debret B, Koga KT, Nicollet C, Andreani M, Schwartz S (2014) F, Cl and S input via serpentinite in subduction zones: implications for the nature of the fluid released at depth. Terra Nova 26:96–101
Deruelle B, Dreibus G, Jambon A (1992) Iodine abundances in oceanic basalts—implications for earth dynamics. Earth Planet Sci Lett 108:217–227
Dolejs D, Zajacz Z (2018) Halogens in silicic magmas and their hydrothermal systems. In: Harlov DE, Aranovich L (eds) The role of halogens in terrestrial and extraterrestrial geochemical processes: surface, crust, and mantle. Springer, Berlin, pp 431–543
Douce AEP, Roden MF, Chaumba J, Fleisher C, Yogodzinski G (2011) Compositional variability of terrestrial mantle apatites, thermodynamic modeling of apatite volatile contents, and the halogen and water budgets of planetary mantles. Chem Geol 288:14–31
Dreibus C, Spettel B, Wänke H (1979) Halogens in meteorites and their primordial abundances. In: Ahrens LH (ed) Origin and distribution of the elements, vol 34. Pergamon, Oxford, pp 33–38
Drury MR (1991) Hydration-induced climb dissociation of dislocations in naturally deformed mantle olivine. Phys Chem Mineral 18:106–116
Edgar AD, Arima M (1985) Fluorine and chlorine contents of phlogopites crystallized from ultrapotassic rock compositions in high-pressure experiments—implication for halogen reservoirs in source regions. Am Mineral 70:529–536
Edgar AD, Pizzolato LA (1995) An experimental-study of partitioning of fluorine between K-richterite, apatite, phlogopite, and melt at 20 kbar. Contrib Mineral Petrol 121:247–257
Edgar AD, Lloyd FE, Vukadinovic D (1994) The role of fluorine in the evolution of ultrapotassic magmas. Mineral Petrol 51:173–193
Edgar AD, Pizzolato LA, Sheen J (1996) Fluorine in igneous rocks and minerals with emphasis on ultrapotassic mafic and ultramafic magmas and their mantle source regions. Mineral Mag 60:243–257
Elburg M, Kamenetsky VS, Nikogosian I, Foden J, Sobolev AV (2006) Coexisting high- and low-calcium melts identified by mineral and melt inclusion studies of a subduction-influenced syncollisional magma from South Sulawesi, Indonesia. J Petrol 47:2433–2462
Evans B, Trommsdorff V (1983) Fluorine hydroxyl titanium clinohumite in alpine recrystallized garnet peridotite: compositional controls and petrologic significance. Am J Sci 283:355–369
Fabbrizio A, Stalder R, Hametner K, Günther D (2013a) Experimental chlorine partitioning between forsterite, enstatite and aqueous fluid at upper mantle conditions. Geochim Cosmochim Acta 121:384–700
Fabbrizio A, Stalder R, Hametner K, Günther D, Marquardt K (2013b) Experimental partitioning of halogens and other trace elements between olivine, pyroxenes, amphibole and aqueous fluid at 2 GPa and 900–1,300 degrees C. Contrib Mineral Petrol 166:639–653
Filiberto J, Treiman AH (2009) The effect of chlorine on the liquidus of basalt: first results and implications for basalt genesis on Mars and Earth. Chem Geol 263:60–68
Filiberto J, Wood J, Dasgupta R, Shimizu N, Le L, Treiman A (2012) Effect of fluorine on near-liquidus phase equilibria of an Fe-Mg rich basalt. Chem Geol 312–313:118–126
Filiberto J, Dasgupta R, Gross J, Treiman AH (2014) Effect of chlorine on near-liquidus phase equilibria of an Fe–Mg-rich tholeiitic basalt. Contrib Mineral Petrol 168:1027–1034
Fockenberg T (1995) Synthesis and chemical variability of Mg-staurolite in the system MgO-Al_2O_3-SiO_2-H_2O as a function of water pressure. Eur J Mineral 7:1373–1380
Foley S (1991) High-pressure stability of the fluor-endmembers and hydroxy-endmembers of pargasite and K-richterite. Geochim Cosmochim Acta 55:2689–2694

Frezzotti M-L, Ferrando S (2018) The role of halogens in the lithospheric mantle. In: Harlov DE, Aranovich L (eds) The role of halogens in terrestrial and extraterrestrial geochemical processes: surface, crust, and mantle. Springer, Berlin, pp 805–845

Fumagalli P, Klemme S (2015) Mineralogy of the Earth: phase transitions and mineralogy of the upper mantle. In: Schubert G (ed) Treatise on geophysics, vol 2. Elsevier, Oxford, pp 7–31

Grützner T, Kohn SC, Bromiley DW, Rohrbach A, Berndt J, Klemme S (2017) The storage capacity of fluorine in olivine and pyroxene under upper mantle conditions. Geochim Cosmochim Acta 208:160–170

Hauri EH, Gaetani GA, Green TH (2006) Partitioning of water during melting of the Earth's upper mantle at H_2O-undersaturated conditions. Earth Planet Sci Let 248:715–734

Hauri EH, Weinreich T, Saal AE, Rutherford MC, Van Orman JA (2011) High pre-eruptive water contents preserved in lunar melt inclusions. Science 333:213–215

Hazen RM, Yang H, Prewitt CT, Gasparik T (1997) Crystal chemistry of superfluorous phase B ($Mg_{10}Si_3O_{14}F_4$): implications for the role of fluorine in the mantle. Am Mineral 82:647–650

Hermann J, Fitz Gerald JD, Malaspina N, Berry AJ, Scambelluri M (2007) OH-bearing planar defects in olivine produced by the breakdown of Ti-rich humite minerals from Dabie Shan (China). Contrib Mineral Petrol 153:417–428

Hervig RL, Bell DR (2005) Fluorine and hydrogen in mantle megacrysts. AGU Fall Meeting, pp V41A-1426

Hinton RW, Harte B, Witt-Eickschen G (1995) Ion probe measurements of national-institute-of-standards-and-technology standard reference material SRM-610 glass, trace-elements. Analyst 120:1315–1319

Hirth G, Kohlstedt DL (1996) Water in the oceanic upper mantle: implications for rheology, melt extraction and the evolution of the lithosphere. Earth Planet Sci Lett 144:93–108

Hoskin PWO (1999) SIMS determination of µg/g-level fluorine in geological samples and its concentration in NIST SRM 610. Geostand Newsl 23:69–76

Ionov DA, Griffin WL, Oreilly SY (1997) Volatile-bearing minerals and lithophile trace elements in the upper mantle. Chem Geol 141:153–184

Irving AJ, Frey FA (1984) Trace-element abundances in megacrysts and their host basalts—constraints on partition-coefficients and megacryst genesis. Geochim Cosmochim Acta 48:1201–1221

Jambon A, Deruelle B, Dreibus G, Pineau F (1995) Chlorine and bromine abundance in MORB: the contrasting behaviour of the Mid-Atlantic Ridge and East Pacific Rise and implications for chlorine geodynamic cycle. Chem Geol 126:101–117

Joachim B, Pawley A, Lyon IC, Marquardt K, Henkel T, Clay PL, Ruzie L, Burgess R, Ballentine CJ (2015) Experimental partitioning of F and Cl between olivine, orthopyroxene and silicate melt at Earth's mantle conditions. Chem Geol 416:65–78

John T, Scambelluri M, Frische M, Barnes JD, Bach W (2011) Dehydration of subducting serpentinite: implications for halogen mobility in subduction zones and the deep halogen cycle. Earth Planet Sci Lett 308:65–76

Johnson LH, Burgess R, Turner G, Harris JH, Milledge HJ (2000) Noble gas and halogen geochemistry of mantle fluids in diamond: comparison of African and Canadian stones. Geochim Cosmochim Acta 64:717–732

Karato SI, Paterson MS, Fitz Gerald JD (1986) Rheology of synthetic olivine aggregates—influence of grain-size and water. J Geophys Res-Solid Earth Planets 91:8151–8176

Kendrick MA (2012) High precision Cl, Br and I determinations in mineral standards using the noble gas method. Chem Geol 292:116–126

Kendrick MA, Kamenetsky VS, Phillips D, Honda M (2012a) Halogen systematics (Cl, Br, I) in Mid-Ocean Ridge Basalts: a Macquarie Island case study. Geochim Cosmochim Acta 81:82–93

Kendrick MA, Woodhead JD, Kamenetsky VS (2012b) Tracking halogens through the subduction cycle. Geology 40:1075–1078

Kendrick MA, Arculus R, Burnard P, Honda M (2013) Quantifying brine assimilation by submarine magmas: examples from the Galapagos Spreading Centre and Lau Basin. Geochim Cosmochim Acta 123:150–165

Kendrick MA, Arculus RJ, Danyushevsky LV, Kamenetsky VS, Woodhead JD, Honda M (2014) Subduction-related halogens (Cl, Br and I) and H_2O in magmatic glasses from Southwest Pacific Backarc Basins. Earth Planet Sci Lett 400:165–176

Keppler H, Smyth JR (2006) Water in nominally anhydrous minerals. In: Rosso JJ (ed) Reviews in mineralogy, vol 62. Mineralogical Society of America, Chantilly, p 478

Kitamura M, Kondoh S, Morimoto N, Miller GH, Rossman GR, Putnis A (1987) Planar OH-bearing defects in mantle olivine. Nature 328:143–145

Koleszar AM, Saal AE, Hauri EH, Nagle AN, Liang Y, Kurz MD (2009) The volatile contents of the Galapagos plume; evidence for H_2O and F open system behavior in melt inclusions. Earth Planet Sci Lett 287:442–452

Konzett J, Ulmer P (1999) The stability of hydrous potassic phases in lherzolitic mantle—an experimental study to 9.5 GPa in simplified and natural bulk compositions. J Petrol 40:629–652

Konzett J, Rhede D, Frost DJ (2012) The high PT stability of apatite and Cl partitioning between apatite and hydrous potassic phases in peridotite: an experimental study to 19 GPa with implications for the transport of P, Cl and K in the upper mantle. Contrib Mineral Petrol 163:277–296

Kovalenko VI, Naumov VB, Girnis AV, Dorofeeva VA, Yarmolyuk VV (2007a) Average compositions of magmas and mantle sources of mid-ocean ridges and intraplate oceanic and continental settings estimated from the data on melt inclusions and quenched glasses of basalts. Petrology 15:335–368

Kovalenko VI, Naumov VB, Girnis AV, Dorofeeva VA, Yarmolyuk VV (2007b) Volatiles in basaltic magmas of ocean islands and their mantle sources: II. Estimation of contents in mantle reservoirs. Geochem Int 45:313–326

le Roux PJ, Shirey SB, Hauri EH, Perfit MR, Bender JF (2006) The effects of variable sources, processes and contaminants on the composition of northern EPR MORB (8-10 degrees N and 12-14 degrees N): evidence from volatiles (H_2O, CO_2, S) and halogens (F, Cl). Earth Planet Sci Lett 251:209–231

Le Voyer M, Rose-Koga EF, Shimizu N, Grove TL, Schiano P (2010) Two contrasting H_2O-rich components in primary melt inclusions from Mount Shasta. J Petrol 51:1571–1595

Le Voyer M, Asimow PD, Mosenfelder JL, Guan Y, Wallace PJ, Schiano P, Stolper EM, Eiler JM (2014) Zonation of H_2O and F concentrations around melt inclusions in olivines. J Petrol 55:685–707

Lodders K (2003) Solar system abundances and condensation temperatures of the elements. Astrophys J 591:1220–1247

Luth RW (1988) Effects of F on phase equilibria and liquid structure in the system $NaAlSiO_4$-$CaMgSi_2O_6$-SiO_2. Am Mineral 73:306–312

Luth RW (2013) Volatiles in Earth's mantle. In: Holland HD, Turekian KK (eds) Treatise on geochemistry, vol 3. Elsevier, Amsterdam, pp 319–361

Lyubetskaya T, Korenaga J (2007) Chemical composition of Earth's primitive mantle and its variance: 1. Method and results. J Geophys Res-Solid Earth 112:B03212

Manning DAC (1981) The effect of fluorine on liquidus phase relationships in the system Qz-Ab-Or with excess water at I kb. Contrib Mineral Petrol 76:206–215

McDonough WF (2004) Compositional model for the Earth's core. In: Holland HD, Turrekian KK (eds) Treatise on geochemistry, vol 2. Elsevier, Amsterdam, pp 547–568

McDonough WF, Sun SS (1995) The composition of the Earth. Chem Geol 120:223–253

McGetchin T, Silver LT, Chodos AA (1970) Titanoclinohumite—a possible mineralogical site for water in upper mantle. J Geophys Res 75:255–259

Metrich N, Wallace PJ (2008) Volatile abundances in basaltic magmas and their degassing paths tracked by melt inclusions. In: Putirka KD, Tepley FJ (eds) Minerals, inclusions and volcanic processes, vol 69. American Mineralogical Society, Washington, pp 363–402

Mosenfelder JL, Le Voyer M, Rossman GR, Guan Y, Bell DR, Asimow PD, Eiler JM (2011) Analysis of hydrogen in olivine by SIMS: evaluation of standards and protocol. Am Mineral 96:1725–1741

Mosenfelder JL, Rossman GR (2013a) Analysis of hydrogen and fluorine in pyroxenes: I. Orthopyroxene. Am Mineral 98:1026–1041

Mosenfelder JL, Rossman GR (2013b) Analysis of hydrogen and fluorine in pyroxenes: II. Clinopyroxene. Am Mineral 98:1042–1054

Newsom HE (1995) Composition of the solar system, planets, meteorites, and major terrestrial reservoirs. In: Ahrens TJ (ed) Global earth physics. A handbook of physical constants. American Geophysical Union, Washington, DC, pp 159–189

O'Leary JA, Gaetani GA, Hauri EH (2010) The effect of tetrahedral Al3 + on the partitioning of water between clinopyroxene and silicate melt. Earth Planet Sci Lett 297:111–120

O'Reilly SY, Griffin WL (2000) Apatite in the mantle: implications for metasomatic processes and high heat production in Phanerozoic mantle. Lithos 53:217–232

Orberger B, Metrich N, Mosbah M, Mevel C, Fouquet Y (1999) Nuclear microprobe analysis of serpentine from the mid-Atlantic ridge. Nucl Instrum Methods Phys Res B 158:575–581

Ottolini LP, Le Fevre B (2007) SIMS analysis of chlorine in metasomatised upper-mantle rocks. Microchim Acta 161:329–339

Palme H, O'Neill HSC (2014) Cosmochemical estimates of mantle composition. In: Holland HD, Turekian KK (eds) Treatise on geochemistry, vol 3. Elsevier, Amsterdam, pp 1–39

Portnyagin M, Hoernle K, Plechov P, Mironov N, Khubunaya S (2007) Constraints on mantle melting and composition and nature of slab components in volcanic arcs from volatiles (H_2O, S, Cl, F) and trace elements in melt inclusions from the Kamchatka Arc. Earth Planet Sci Lett 255:53–69

Pyle DM, Mather TA (2009) Halogens in igneous processes and their fluxes to the atmosphere and oceans from volcanic activity: a review. Chem Geol 263:110–121

Rose-Koga EF, Koga KT, Schiano P, Le Voyer M, Shimizu N, Whitehouse MJ, Clocchiatti R (2012) Mantle source heterogeneity for South Tyrrhenian magmas revealed by Pb isotopes and halogen contents of olivine-hosted melt inclusions. Chem Geol 334:266–279

Rose-Koga EF, Koga KT, Hamada M, Helouis T, Whitehouse MJ, Shimizu N (2014) Volatile (F and Cl) concentrations in Iwate olivine-hosted melt inclusions indicating low-temperature subduction. Earth Planets Space 66:81

Rosenberg PE, Foit FF (1977) Fe^{2+}-F avoidance in silicate. Geochim Cosmochim Acta 41:345–346

Rosenthal A, Hauri EH, Hirschmanna MM (2015) Experimental determination of C, F, and H partitioning between mantle minerals and carbonated basalt, CO_2/Ba and CO_2/Nb systematics of partial melting, and the CO_2 contents of basaltic source regions. Earth Planet Sci Lett 412:77–87

Ruzie L, Moreira M, Crispi O (2012) Noble gas isotopes in hydrothermal volcanic fluids of La Soufriere volcano, Guadeloupe, Lesser Antilles arc. Chem Geol 304:158–165

Saal AE, Hauri EH, Langmuir CH, Perfit MR (2002) Vapour undersaturation in primitive mid-ocean-ridge basalt and the volatile content of Earth's upper mantle. Nature 419:451–455

Salters VJM, Stracke A (2004) Composition of the depleted mantle. Geochem Geophys Geosyst 5: Q05004

Scambelluri M, Fiebig J, Malaspina N, Müntener O, Pettke T (2004) Serpentinite subduction: implications for fluid processes and trace-element recycling. Int Geol Rev 46:595–613

Schilling JG, Bergeron MB, Evans R (1980) Halogens in the mantle beneath the north-atlantic. Philos Trans Roy Soc A 297:147–178

Sharp ZD, Draper DS (2013) The chlorine abundance of Earth: implications for a habitable planet. Earth Planet Sci Lett 369:71–77

Smith JV (1981) Halogen and phosphorus storage in the Earth. Nature 289:762–765

Smith JV, Delaney JS, Hervig RL, Dawson JB (1981) Storage of F and Cl in the upper mantle—geochemical implications. Lithos 14:133–147

Stalder R, Ulmer P (2001) Phase relations of a serpentine composition between 5 and 14 GPa: significance of clinohumite and phase E as water carriers into the transition zone. Contrib Mineral Petrol 140:670–679

Stalder R, Kronz A, Simon K (2008) Hydrogen incorporation in enstatite in the system MgO-SiO_2-H_2O-NaCl. Contrib Mineral Petrol 156:653–659

Staudigel H, Schreyer W (1977) Upper thermal-stability of clinochlore, $Mg_5AlSi_3O_{10}(OH)_8$, at 10-35 kb pH_2O. Contrib Mineral Petrol 61:187–198

Stecher O (1998) Fluorine geochemistry in volcanic rock series: examples from Iceland and Jan Mayen. Geochim Cosmochim Acta 62:3117–3130

Straub SM, Layne GD (2003a) Decoupling of fluids and fluid-mobile elements during shallow subduction: evidence from halogen-rich andesite melt inclusions from the Izu arc volcanic front. Geochem Geophys Geosyst 4:9003

Straub SM, Layne GD (2003b) The systematics of chlorine, fluorine, and water in Izu arc front volcanic rocks: implications for volatile recycling in subduction zones. Geochim Cosmochim Acta 67:4179–4203

Ulmer P, Trommsdorff V (1995) Serpentine stability to mantle depths and subduction-related magmatism. Science 268:858–861

Vigouroux N, Wallace PJ, Williams-Jones G, Kelley K, Kent AJR, Williams-Jones AE (2012) The sources of volatile and fluid-mobile elements in the Sunda arc: a melt inclusion study from Kawah Ijen and Tambora volcanoes, Indonesia. Geochem Geophy Geosyst 13:Q090

Visser D (1993) Fluorine-bearing hydrogarnets from Blengsvatn, Bamble sector, South Norway. Mineral Petrol 47:209–218

Volfinger M, Robert JL, Vielzeuf D, Neiva AMR (1985) Structural control of the chlorine content of OH-bearing silicates (micas and amphiboles). Geochim Cosmochim Acta 49:37–48

Wallace PJ (2005) Volatiles in subduction zone magmas: concentrations and fluxes based on melt inclusion and volcanic gas data. J Volcanol Geotherm Res 140:217–240

Webster JD, Baker DR, Aiuppa A (2018) Halogens in mafic and intermediate-silica content magmas. In: Harlov DE, Aranovich L (eds) The role of halogens in terrestrial and extraterrestrial geochemical processes: surface, crust, and mantle. Springer, Berlin, pp 307–430

Workman RK, Hauri E, Hart SR, Wang J, Blusztajn J (2006) Volatile and trace elements in basaltic glasses from Samoa: Implications for water distribution in the mantle. Earth Planet Sci Lett 241:932–951

Wu J, Koga KT (2013) Fluorine partitioning between hydrous minerals and aqueous fluid at 1 GPa and 770–947 degrees C: a new constraint on slab flux. Geochim Cosmochim Acta 119:77–92

Wyllie PJ, Tuttle OF (1961) Experimental investigation of silicate liquids containing two volatile components Part II. The effects of NH_3 and HF in addition to H_2O on the melting temperatures of albite and granite. Am J Sci 259:128–143

Wysoczanski RJ, Wright IC, Gamble JA, Hauri EH, Luhr JF, Eggins SM, Handler MR (2006) Volatile contents of Kermadec Arc-Havre Trough pillow glasses: fingerprinting slab-derived aqueous fluids in the mantle sources of arc and back-arc lavas. J Volcanol Geotherm Res 152:51–73

Chapter 15
Halogens in Chondritic Meteorites

Adrian J. Brearley and Rhian H. Jones

Abstract We review the abundances, distributions and isotopic compositions of halogens in chondritic meteorites and discuss formation of the mineral and other carriers of these elements. Halogens provide tracers of processes that occurred in circumstellar and interstellar environments, within the solar nebula, and after accretion within asteroidal meteorite parent bodies. Knowledge of the halogen abundances in chondrites is fundamental to understanding the halogen contents of the Earth and other terrestrial planets. However, the full potential of halogens to constrain processes in the solar nebula and the chondrite parent bodies has not yet been realized due to both analytical challenges and uncertainties in halogen condensation temperatures. Analytical challenges make robust determinations of absolute halogen abundances extremely difficult, and some large uncertainties remain. Halogens in chondritic meteorites are present in both soluble (water extractable) and insoluble fractions, and they are therefore highly susceptible to alteration by weathering. Potential contamination from terrestrial sources is a perennial problem, even for meteorite falls. However, although there are significant variations in the analytical data, even within individual chondrite groups, it is clear that there are distinct, but complex differences between the three main classes of chondrites, carbonaceous, ordinary, and enstatite. In most chondrites, the abundances of the halogens are controlled by their cosmochemical volatility, and the halogens are depleted in most of the chondrite groups relative to CI chondrites. Measurements of halogen isotope compositions in chondrites are somewhat limited. In general, bulk $\delta^{37}Cl$ values show little deviation from the terrestrial standard ($-0.3 \pm 0.3‰$ relative to SMOW), although there are some notable exceptions with more negative values down to –4‰ that are possibly related to either the initial

A.J. Brearley (✉)
Department of Earth and Planetary Sciences, MSC03-2040,
University of New Mexico, Albuquerque, NM 87131, USA
e-mail: brearley@unm.edu

R.H. Jones
School of Earth and Environmental Sciences,
University of Manchester, Manchester, UK
e-mail: rhian.jones-2@manchester.ac.uk

D.E. Harlov and L. Aranovich (eds.), *The Role of Halogens in Terrestrial and Extraterrestrial Geochemical Processes*, Springer Geochemistry,
https://doi.org/10.1007/978-3-319-61667-4_15

condensation of ices, or to parent body fluid interactions. In addition, ^{129}Xe and ^{36}S excesses in individual components of chondritic meteorites indicate that the short-lived radioisotopes, ^{129}I and ^{36}Cl, were present in the early solar system. The ^{129}I-^{129}Xe system is well established as an important chronometer for constraining the early chronology of solar system materials, but the chlorine-S system has not yet been used widely as a chronometer because of uncertainties in the initial ^{36}Cl/^{35}Cl ratio. Distinct halogen-bearing phases are generally rare in chondritic meteorites, but include silicates, silicate glasses, aluminates, sulfides, halides, phosphates, and oxides. With the exception of the enstatite chondrites, where chlorine (and possibly other halogens) are present in djerfisherite and chlorine-enriched chondrule glass, the primary (nebular) mineralogical carriers of the halogens in the most pristine (low petrologic type 3) carbonaceous and ordinary chondrites are poorly constrained. In type 1 and 2 carbonaceous chondrites that have been affected by interaction with aqueous fluids at low temperatures, such as the CI, CM, and CR chondrites, the mineralogical carriers of the halogens are also highly uncertain. In contrast, the redistribution and concentration of halogens into discrete minerals, particularly chlorine-rich phases, has occurred in essentially all carbonaceous and ordinary chondrites that have been affected by even moderate degrees of metamorphism, sometimes in the presence of aqueous fluids. Fluorine-bearing chlorapatite occurs typically as the major halogen-bearing phase in type 4–6 ordinary chondrites, as well as CK and other metamorphosed carbonaceous chondrites. Extensive metasomatic effects observed in the Allende subgroup of the oxidized CV chondrites (CV_{OxA}) have resulted in the formation of sodalite, wadalite, and the rare aluminates chlormayenite and adrianite, most typically in CAIs, although sodalite also occurs in chondrules and matrices. Evidence for limited development of sodalite and rare scapolite is also present in chondrules in some petrologic type 3 ordinary chondrites and in CAIs in CO3 chondrites. Rare occurrences of fluor-richerite and fluorphlogopite have been reported as crystallization products of impact melts in enstatite chondrites, and fluorine- and chlorine-bearing biotite also occurs in some high petrologic type R chondrites.

15.1 Introduction

Chondritic meteorites are a remarkably diverse suite of asteroidal samples that are a unique source of information about processes and conditions during the earliest stages of the formation of our solar system. Chondrites contain the oldest known materials in the solar system, and also have primitive compositions, with elemental abundances that match closely with those of the solar photosphere. They represent materials that may have been the fundamental building blocks of the inner terrestrial planets and, hence, provide important constraints on their bulk compositions. Unlike other meteorite groups, chondrites have escaped wholesale melting and differentiation, although many chondrites have been affected by secondary processes, such as aqueous alteration, thermal metamorphism, and metasomatism that

occurred after asteroid accretion (Brearley 2006, 2014; Huss et al. 2006; Zolensky et al. 2008; Brearley and Krot 2013). These processes have principally modified the textural and mineralogical characteristics of the primary components of chondrites, but have generally not changed their bulk compositions to any significant degree.

Chondrites are accretionary rocks that contain a diverse array of components that formed under different physico-chemical conditions in the solar protoplanetary disk (solar nebula) during the first few million years of solar system history. They therefore provide a remarkable record of the evolution of the protoplanetary disk prior to and during the accretion of planetesimals and planets, as well as geologic processes in asteroids that post-date accretion. The major primary nebular components of chondrites are chondrules (millimeter-sized, ultramafic, silicate spherules), refractory inclusions (Ca–Al-rich inclusions, or CAIs, and ameboid olivine aggregates, or AOAs), fine-grained matrix, Fe,Ni metal, and iron sulfides, each of which formed at different times and under different conditions within the solar nebula. Organic materials are also an important component of chondritic meteorites. Organic materials consist of a complex mixture of compounds that appear to have formed in a wide range of different environments including the interstellar medium, the solar nebula, and within asteroidal parent bodies (Kerridge 1993; Alexander et al. 2010; Gilmour 2014).

Compositionally, the CI carbonaceous chondrites are the most primitive group of meteorites known, with elemental abundances that are a close match to the abundances of the rock-forming elements measured in the solar photosphere by spectroscopic techniques (Anders and Grevesse 1989; Asplund et al. 2009; Palme et al. 2014). All other chondrites from the carbonaceous, ordinary, and enstatite chondrite groups are chemically fractionated from the bulk CI carbonaceous chondrite composition, as a result of chemical processes within the solar nebula such as condensation and evaporation. For most chondrites, these processes have resulted in a depletion in volatile elements and an enrichment in refractory elements, relative to CI chondrites, which imparted unique chemical signatures that are used to distinguish between the different groups of chondrites.

Cosmochemically, the halogens are all considered to be volatile elements and to have highly variable abundances in chondritic meteorites that were most likely established primarily in the solar nebula. However, because the halogens are highly mobile in aqueous fluids, they act as important recorders and tracers of the interaction of aqueous fluids with chondritic materials. In addition, short-lived radioisotopes of chlorine and I are also of cosmochemical significance because they provide important chronological constraints on early solar system processes. In this chapter, we discuss the current state of knowledge of the halogen cosmochemistry of chondritic meteorites, potential carriers of halogens in primary nebular components, and their redistribution as a result of parent body asteroidal processes such as aqueous alteration and thermal metamorphism. As will become apparent, our understanding of many aspects of the behavior of halogens in chondrites is still in its infancy and there are many fundamental questions that remain to be addressed.

15.2 Halogen Behavior in Chondrites—Cosmochemical Versus Geochemical Behavior

Chondritic meteorites have experienced complex histories, from the formation of their individual components in the solar nebula, through accretion into asteroidal parent bodies and subsequent processing within asteroids as a result of aqueous alteration, and/or thermal and shock metamorphism (see summary of chondrite classification, Table 15.1). The bulk chemical compositions of chondrites and the distribution of elements within different mineral phases therefore depend strongly on the history of each individual chondrite. For the earliest primary processes that occurred within the protoplanetary disk, such as condensation and evaporation, the behavior of the halogens must be considered according to the cosmochemical classification of the elements (Larimer 1988; Palme and Jones 2003; Palme et al. 2014) that classifies the elements according to their thermodynamically-estimated relative volatilities into three groups: refractory, moderately volatile, and highly volatile. Fluorine is considered to be moderately volatile with a 50% condensation temperature above 640 K, and Br and I are highly volatile elements, condensing below 640 K. There is some disagreement about the condensation temperature of chlorine, which has been viewed as both a moderately volatile (Lodders 2003) and a highly volatile element (Palme and Jones 2003). This issue is discussed in more detail below. In contrast to this volatility-related classification, when evaluating the behavior of the halogens within an asteroidal environment, a geochemical interpretation, such as mineral-fluid partitioning behavior, is much more relevant. However, under some conditions, such as the effects of shock, which may cause volatile loss, a consideration of the elements in terms of their cosmochemical behavior may be more appropriate.

15.2.1 Cosmochemical Behavior of Halogens

The primary controls on the bulk concentrations of halogens in chondrites are related to their cosmochemical volatilities, and are generally considered to have been established in the solar nebula (e.g., Fegley and Lewis 1980; Lodders 2003). The cosmochemical behavior of the elements is based on the calculated temperature at which 50% of the element in question has condensed under canonical solar nebular conditions from a gas of solar composition (Lodders 2003; Wasson 1974). For many rock-forming elements, the 50% condensation temperature is well constrained by thermodynamical models. However, as pointed out by Lodders (2003), the 50% condensation temperatures for the halogens are among the least well constrained. Fegley and Lewis (1980) carried out detailed equilibrium thermodynamic

Table 15.1 Chondrite classification: classes, groups and petrologic types

Class and group[1]	Meaning of group name[2]	Petrologic types[3]						Notes[4]
		1	2	3	4	5	6	
Carbonaceous - C		Some C chondrites are carbon-rich, up to a few wt% C						
CI	Ivuna	■						
CM	Mighei	▒	■					Type 2 is subdivided
CO	Ornans			■				Type 3 is subdivided
CR	Renazzo	▒	■					Type 2 is subdivided
CV	Vigarano		▒	■				Type 3 is subdivided
CK	Karoonda			▒	■	■	■	
CH	ALH85085 (high metal)			■				
CB	Bencubbin			■				
Ordinary - O		Ordinary chondrites are the most common class of meteorite falls and finds						
H	High abundance iron metal			■	■	■	■	Type 3 is subdivided
L	Low abundance iron metal			■	■	■	■	Type 3 is subdivided
LL	Low iron metal, low total iron			■	■	■	■	Type 3 is subdivided
Enstatite - E		Enstatite chondrites are highly reduced and contain a high abundance of enstatite						
EH	High abundance total iron			■	■	■		
EL	Low abundance total iron			■	■	■	■	
Other								
K	Kakangari			■				
R	Rumuruti			■	■	■	■	Many are R3-6 regolith breccias

[1]Chondrite classes C, O, E are divided into groups e.g., CI, CM etc.

[2]Group names for C, K and R chondrites are derived from typical chondrites of that group (mostly observed falls)

[3]Petrologic types describe the degree of alteration of a chondrite. Petrologic type 3.0 represents the most pristine material that is unaltered since its formation in the solar nebula. Petrologic types 3.0 to 2 to 1 represent a sequence of increasing aqueous alteration. Petrologic types 3.0 to 4 to 5 to 6 represent a sequence of increasing thermal metamorphism (equilibration). The dominant petrologic type(s) for each chondrite group are indicated as *black boxes* and less abundant petrologic types are indicated with *grey boxes*

[4]Subdivision of a petrologic type into subtypes has been made in order to describe detailed changes with either aqueous alteration or thermal metamorphism. Petrologic subtypes in type 2 represent increasing aqueous alteration from 3.0 to 2.9, 2.8, 2.7, etc. Petrologic subtypes in type 3 represent increasing thermal metamorphism from 3.0 to 3.1, 3.2, 3.3 etc. The most unaltered CO and O chondrites are divided further into 3.00, 3.01, 3.02 etc.

Further details of chondrite classification can be found in Scott and Krot (2014) and Krot et al. (2014)

calculations to constrain the condensation of Na, K, F, chlorine, Br, and P in the solar nebula under two different model conditions. In the first case, chemical equilibrium is maintained between the gas and solid condensates, and F, chlorine, and Br condense into apatite and sodalite. In the second case, an element is removed from further reactions as soon as it condenses. In this case, F condenses in NaF while chlorine and Br go into ammonium halides. Determination of the condensation temperatures of Br and I requires a significant number of assumptions that were discussed by Lodders (2003), involving the incorporation of these elements into fluorapatite, which condenses at 739 K. In order to calculate the condensation

temperature of Br and I, it is assumed that these elements substitute for F in the CaF_2 component of apatite as $CaBr_2$ and CaI_2. This assumption is required because there are no thermodynamic data available for Br- or I-apatite. Lodders (2003) reported 50% condensation temperatures for F, chlorine, Br, and I to be 739 K, 948 K, 546 K, and 535 K, respectively, with F condensing into fluorapatite, chlorine condensing into sodalite, and Br and I into fluorapatite. Prior to the Lodders (2003) calculations the condensation temperatures of these latter two elements were either unknown or highly uncertain.

Based on evidence that Br and I may be present in troilite (Allen and Mason 1973; Mason and Graham 1970), Lodders (2003) also explored the possibility that these elements could condense in troilite, but found that the solubility of $FeBr_2$ and FeI_2 in FeS is negligible and therefore the sulfide is not a viable host for these halogens.

The Lodders (2003) calculations are the best current estimates for halogen condensation temperatures, but create a significant paradox that has no simple resolution at this point. As pointed out by Fegley and Lewis (1980) and followed by Lodders (2003), sodalite and F- and chlorine-bearing apatite are all present in chondrites, favoring the equilibrium condensation model, whereas fluorides and ammonium halides are not. However, as discussed in Sect. 15.8, there is no evidence for F- and chlorine-bearing apatite in the most pristine (low petrologic type 3—see Table 15.1) chondrites. Instead, chlorapatite clearly formed during the chemical and textural equilibration resulting from parent body metamorphism. Phosphorus is largely contained within Fe–Ni metal in the most pristine, low petrologic type 3 chondrites (Zanda et al. 1994; Kimura et al. 2008), rather than in primary phosphates. The P diffuses out of the metal to form secondary phosphates as metamorphic grade increases (Jones et al. 2014). Similarly, chlorine is also concentrated in sodalite ($Na_4[Al_3Si_3O_{12}]Cl$) in some CV3, CO3, and petrologic type 3 ordinary chondrites, but the textural occurrences of the sodalite suggest very strongly that it is not a primary nebular phase and that it is likely the product of metasomatic reactions (Brearley and Krot 2013). Therefore, even the condensation temperatures of F and chlorine may not be as well constrained as desired, because of this discrepancy between the predicted theoretical and observational data for the host phases of the halogens in chondrites.

More recently, Zolotov and Mironenko (2007) explored the behavior of chlorine under solar nebular conditions and proposed a very different mechanism for the incorporation of chlorine into chondritic meteorites based on their thermodynamic calculations. In the solar nebula, rather than condensing into phases such as sodalite or apatite, Zolotov and Mironenko (2007) have suggested that chlorine was dominantly present as gaseous HCl, particularly after the condensation of water ice at $\sim$180 K. Formation of halides is possible, but is likely to have been limited due to the very low partial pressure of nebular HCl ($P_{HCl} = 10^{-12.4}$ bar at a total nebular pressure of 10^{-6} bars). Although some HCl may have been trapped during the condensation of water ice, at $\sim$160–140 K, all remaining HCl in the gas phase

would have condensed as $HCl{\cdot}3H_2O$, onto the surfaces of mineral grains and water ice particles. If this model is correct, then the estimated 50% condensation temperature of 948 K for chlorine may be significantly in error, an issue that is explored further below. Chlorine should then be considered to be a volatile rather than moderately volatile element (Lodders 2003) in terms of its cosmochemical behavior.

15.2.2 Geochemical Behavior of Halogens in Chondrites

Following accretion of the different primary components of chondrites into asteroids, a variety of processes on parent bodies modified the original mineralogy and distribution of the elements. These processes include aqueous alteration, thermal metamorphism, metasomatism and shock metamorphism. The behavior of elements, including the halogens, during these processes is largely governed by their geochemical behavior rather than their cosmochemical behavior. With the exception of F, which forms insoluble fluoride salts, the halogens chlorine, I, and Br are highly soluble in aqueous fluids (Eggenkamp 2014). Therefore, during aqueous alteration they are transported in solution and incorporated into secondary minerals, particularly soluble salts. In many meteorites, this process has resulted in the halogens being concentrated into specific mineral phases, as discussed later, which were not present in the primary nebular mineral assemblages. The bulk concentrations of the halogens in chondrites cover three orders of magnitude, with chlorine being the most abundant, reaching a few hundred parts per million (ppm) in the CI chondrites (see Sect. 15.4). Therefore, the process of concentration of the halogens into specific phases by geochemical processes only produces rare grains of chlorine-rich phases in chondrites.

In the past, thermal metamorphism in chondritic meteorites was generally considered to have occurred under fluid-absent conditions. However, as discussed later for individual chondrite groups, there is an increasing body of evidence that metamorphism occurred in many chondrites in the presence of fluids. This is certainly the case for chondrites that show significant evidence for localized metasomatism. Therefore, under fluid-present conditions, halogens are redistributed into metamorphic phases, such as apatite, and their concentrations are controlled by mineral-fluid partition coefficients.

Evidence for the interaction of aqueous fluids with chondritic meteorites, over a range of temperatures and time intervals, has become increasingly apparent, particularly over the last 20 years (see Brearley 2006a, 2014; Zolensky et al. 2008; Brearley and Krot 2013 for recent reviews). However, definitive evidence demonstrating that bulk chondrite concentrations of fluid-soluble halogens have been modified by mineral-fluid interactions is ambiguous at best, as discussed in detail below, and remains a significant question in cosmochemistry.

15.3 Solar System Abundances of Halogens

The abundances of halogens in the Sun are not well constrained. Only F and chlorine abundances have been measured by spectroscopic techniques; no measurements are available for Br and I. In detail, there are no atomic lines for F and chlorine in the solar spectrum, i.e. in the solar photosphere, but measureable lines are present in sunspot spectra (Hall and Noyes 1969, 1972). There are large uncertainties in these abundances, as discussed by Anders and Grevesse (1989). Fluorine and chlorine are in a group of 20 elements that are considered to be poorly determined in the solar photosphere. Despite the large errors in the measurements and the fact that they are from sunspots, the agreement with the CI chondrite abundances is actually relatively good. Presented relative to hydrogen [$A_{El} = \log(N_{El}/N_H) + 12.00$], F abundances in the solar photosphere and CI chondrites are 4.56 (±0.3) and 4.48 (±0.06), respectively and chlorine abundances are 5.5 (±0.3) and 5.27 (±0.06), respectively (Anders and Grevesse 1989). The most recent summaries of solar system abundances by Asplund et al. (2009) and Palme et al. (2014) report exactly the same values. Given the analytical uncertainties in both measurements, as well as possible sample heterogeneity for the CI chondrites (see below), the relatively good agreement suggests that the CI

Table 15.2 Halogen concentrations in the different chondrite groups, compared with abundances in the bulk solar system

	F (ppm)		Cl (ppm)		Br (ppm)		I (ppm)	
	W&K	L&F	W&K	L&F	W&K	L&F	W&K	L&F
CI	64	60	680	700	3.6	3.5	0.5	0.43
CM	38	38	160	430	2.6	3.0	0.425	0.27
CV	24	24	210	250	1.5	1.6	0.2	0.16
CO	30	30	240	280	1.3	1.4	0.188	0.2
CK		20		260		0.6		0.2
CR						1.0		
CH						1.4		
H	32	125	80	140	0.5	0.1–1.0	0.068	0.06
L	41	100	76	270	0.8	0.05–2.0	0.053	0.07
LL	63	70	130	200	0.6	1.0		
R				<100		0.55		
EH	238	155	660	570	2.4	2.7	0.15	0.21
EL	180	140	210	230	0.8	0.8	0.053	0.08
	A&G	P/L	A&G	P/L	A&G	P/L	A&G	P/L
Solar System	60.7	58.2	704	698	3.57	3.26	0.433	0.53

W&K: Bulk compositions of individual chondrite groups from Wasson and Kallemeyn (1988)
L&F: Bulk compositions of individual chondrite groups from Lodders and Fegley (1998)
A&G: Mean solar system abundances by mass (ppm), given by Anders and Grevesse (1989). Data are calculated from solar abundances and relative to the mass of Si in CI chondrites (see text)
P/L: Mean solar system abundances by mass (ppm), based on CI chondrites, given by Palme et al. (2014): data are updated from Lodders (2009)

chondrite measurements are reasonably robust. Normalized to 10^6 atoms of Si, the respective revised solar system abundances for F and chlorine reported by Palme et al. (2014) are both slightly lower than the values given by Anders and Grevesse (1989), i.e. 804 vs. 843 (F) and 5.17×10^3 vs. 5.24×10^3 (chlorine). In Table 15.2, we give solar system abundances for the halogens by mass, based on two independent sources. Anders and Grevesse (1989) calculated mass abundances from the solar photosphere composition, by calculating masses of elements relative to Si = 10.46 wt% (the value in CI chondrites). The data from Palme et al. (2014) are solar system abundances based on CI chondrites, using data updated from Lodders (2009). There is close agreement between these two sources: 60.7 vs. 58.2 ppm for F and 704 vs. 698 ppm for chlorine, from Anders and Grevesse (1989) and Palme et al. (2014), respectively.

Due to the lack of any spectroscopic analyses for Br and I in the Sun, the solar photospheric abundances are derived solely from the meteoritic abundances and are therefore highly reliant on the quality of the analytical data for the CI chondrites (see below for a detailed discussion). Anders and Ebihara (1982) and Anders and Grevesse (1989) used CI chondrite analytical data and elemental ratios to calculate solar photospheric abundances for Br and I. The value for Br was determined using In and Cd concentrations in CI chondrites and making the assumption that CI chondrites have similar Br/In and Br/Cd ratios to CV, CO, and EH chondrites. Iodine was constrained using the ratios I/F, I/Br, I/In, and I/Cd. However, as pointed out by Lodders (2003), the solar photospheric Br and I abundances determined using this approach have uncertainties that are no better than those obtained from direct measurements of Br and I in CI chondrites. Lodders (2003), instead, relied solely on the directly measured CI chondrite data to derive solar system abundances for Br and I of $A_{El} = 2.59 \pm 0.09$ (Br) and 1.54 ± 0.12 (I). Asplund et al. (2009) and Palme et al. (2014) report revised CI chondrite-derived Br A_{El} values of 2.54 ± 0.06 and 2.56 ± 0.06, respectively and A_{El} for I of 1.55 ± 0.08 and 1.57 ± 0.08, respectively. Normalized to 10^6 atoms of Si, the respective revised solar system abundances for Br and I reported by Palme et al. (2014) and Anders and Grevesse (1989) are 10.7 vs. 11.8 (Br) and 1.05 vs. 0.9 (I). Solar system abundances by mass given by Palme et al. (2014) and Anders and Grevesse (1989) are 3.26 vs. 3.57 (Br) and 0.53 vs. 0.433 (I), respectively (Table 15.2: see explanation of these values above).

15.4 Bulk Halogen Compositions of Chondrites

Halogen concentrations in chondritic meteorites have considerable cosmochemical importance. The abundances of these elements, and their relative ratios, can provide important constraints on processes that occurred in the solar nebula, such as volatility-controlled fractionation, as well as processes in asteroidal parent bodies, such as mobilization by aqueous fluids. In addition, such data are also of fundamental importance for understanding the geochemical evolution of the Earth and

other terrestrial planets. Unfortunately, determination of bulk halogen concentrations for chondritic meteorites is beset with analytical problems, which we summarize below before discussing the data available for different chondrite groups.

15.4.1 Measurement of Halogen Abundances in Chondrites: Analytical Considerations

Halogen concentrations in chondritic meteorites have been measured using a variety of different analytical methods including spectroscopy, neutron activation, nuclear reaction, and pyrolysis techniques (Allen and Clark 1977; Clarke et al. 1967; Dreibus et al. 1979; Garrison et al. 2000; Goles et al. 1967; Greenland and Lovering 1965; Kallemeyn and Wasson 1981; Sharp et al. 2013). Data from these different studies show considerable disagreement that result from the different analytical approaches, as well as the fact that there is significant heterogeneity within individual meteorites. Analytical uncertainties result from counting statistics and incomplete yields, as well as sample contamination (e.g., Dreibus et al. 1979). For many of the analytical techniques that have been used, the errors are considerable, as summarized by Rubin and Choi (2009). Although preferred values for the concentration of the halogens in chondrites have emerged, based on careful evaluation of the available analytical data (Wasson and Kallemeyn 1988; Lodders and Fegley 1998), there are still major gaps in our knowledge, particularly for chondrite groups that have only been recognized relatively recently, such as the CR, CK, CH, and R groups (Table 15.1). Uncertainties in their concentrations are further exacerbated by the fact that halogens are demonstrably enhanced in meteoritic finds as a result of terrestrial contamination caused by weathering (Dreibus and Wänke 1983; Heumann et al. 1987, 1990; Shinonaga et al. 1994; Kato et al. 2000; Noll et al. 2003). Terrestrial contamination may also be a problem for falls, depending on how a meteorite has been handled and curated since it fell. Nevertheless, the determination of reliable bulk halogen concentrations should, wherever possible, only be carried out on falls. However, there may even be significant problems with some terrestrial falls, because it is known that chlorine, for example, is present in both soluble and insoluble forms (e.g., Bonifacie et al. 2007; Sharp et al. 2013). Even during curation, soluble salts may be mobilized and leached from the chondrite, particularly if samples are stored under humid conditions. This phenomenon has been documented for the CI chondrite fall Orgueil, which has exhibited notable evidence of efflorescence during its curation history (Gounelle and Zolensky 2001). This behavior may have modified its halogen concentrations and contributed to the apparent heterogeneity that is observed in different samples of this chondrite.

Analysis of bulk F concentrations is far from routine. Studies in the 1960s and 1970s measured F concentrations in chondrites using several different analytical techniques, including activation analysis (Reed 1964), emission spectroscopy (Greenland and Lovering 1965), resonant nuclear reaction (Allen and Clark 1977; Goldberg et al. 1974), and specific ion electrode analysis (Dreibus et al. 1979).

The relative precision of the F measurements reported by Reed (1964), Green and Lovering (1965), and Allan and Clark (1977) are between 10 and 20% depending on the study. Dreibus et al. (1979) is generally regarded as one of the most definitive of these studies, based on their careful comparison of their analytical data with a variety of known standards, and reported an analytical precision of 10%. However, there is still a paucity of reliable F measurements for all the chondrite groups.

Chlorine is by far the most abundant halogen in chondritic meteorites, in the range of hundreds of ppm. There are a large number of independent determinations of bulk chlorine contents in chondritic meteorites of all classes and groups. Chlorine has been determined by a variety of techniques. Neutron activation analysis is the most commonly used technique (Greenland and Lovering 1965; von Gunten et al. 1965; Reed and Allen 1966; Goles et al. 1967; Quijano-Rico and Wänke 1969; Dreibus et al. 1979). Several of these studies required post-irradiation extraction of chlorine using a complex, multistep procedure, whereas Dreibus et al. (1979) employed a pre-irradiation extraction into an aqueous phase with a reported precision of 5%. More recently other techniques have been used for chlorine determinations, including the nuclear reaction $^{37}Cl\ (n,\gamma)\ ^{38}Ar$ used for ^{39}Ar–^{40}Ar dating (Garrison et al. 2000; Clay et al. 2013), a pyrohydrolysis-mass spectrometric technique to extract chlorine into an aqueous phase, followed by conversion to CH_3Cl (Sharp et al. 2013), or pyrohydrolysis followed by analysis using ion chromatography (Ménard et al. 2013). These techniques have typical analytical precisions of 10–15%, but errors may be higher for cases when chlorine is in low concentrations (<100 ppm; Sharp et al. 2013).

A major challenge for the determination of chlorine, as well as Br and I, concentrations is that these elements are present in both water-soluble and insoluble (structurally-bound) fractions, which have not been determined separately in most studies. The study of Sharp et al. (2013) is the only one that systematically analyzed water-soluble and insoluble chlorine fractions in a suite of chondrite falls. This study showed that, in some cases, the water-soluble fraction can be almost 50% of the total chlorine in the meteorite, although it is generally <20%. As discussed in Sect. 15.8, the carriers of water-soluble chlorine are very poorly constrained, except in a few rare cases. Therefore, it is not clear to what extent the variability in bulk chlorine concentration is the result of terrestrial contamination, even for chondrite falls. Contamination could result from handling during and post collection, as well as inadequate sample curation to prevent contamination. There does appear to be clear evidence that carbonaceous and ordinary chondrite finds from Antarctica are significantly contaminated with terrestrial chlorine (see Sect. 15.4.2). Ménard et al. (2013) have reported chlorine data for several Antarctic CM chondrites, most of which show elevated chlorine concentrations ranging from 448 to 1116 ppm. In comparison, bulk chlorine contents for CM chondrite falls range from 190 to 510 ppm.

Although some variability in bulk chlorine concentrations could result from contamination, there is, nevertheless, clear evidence that this cannot be the only contributing factor. Sharp et al. (2013) found that in some samples, where they carried out duplicate or triplicate analyses, the structurally-bound chlorine also showed significant variability. For example, replicate analyses of the LL6 fall Saint

Séverin gave values of 70, 70, and 130 ppm structurally-bound chlorine, variability, which does not appear to be the result of contamination and is probably related to the heterogeneous distribution of chlorine-bearing minerals. Sample sizes ranged from around 0.2–1 g, i.e. typical samples are in the size range of a few mm^3. Heterogeneity in the apatite distribution at this scale has been discussed by Jones et al. (2014).

The issue of potential chlorine contamination has also been addressed by Garrison et al. (2000) in their analytical study of chlorine concentrations using the nuclear reaction ^{37}Cl (n,γ) ^{38}Ar technique developed for ^{39}Ar–^{40}Ar dating. Garrison et al. (2000) identified low- and high-temperature chlorine components, based on the release of ^{38}Ar during stepwise heating. They suggested that the low-temperature component, which was higher for finds than falls, may be terrestrial contamination. Although the concentrations of chlorine in this component are typically <40 ppm, some meteorites contain a significantly higher fraction of this lower temperature component.

The low-temperature chlorine component identified by Garrison et al. (2000), does not necessarily correspond completely to the water-soluble fraction identified by Sharp et al. (2013). For example, water soluble alkali halides would not be released at low temperatures during stepwise heating, although they may of course have formed at low temperatures by precipitation from an aqueous fluid. Instead, the low temperature component may be chlorine that is adsorbed onto the surfaces of minerals in low concentrations, rather than being in a distinct phase. The water-soluble component likely consists of chlorine that is weakly bonded to mineral surfaces as well as chlorine in soluble halides.

Of all the halogens, Br concentrations in chondrites are the best constrained, largely as a result of the extensive systematic analyses of different chondrite groups using INAA techniques by Kallemeyn and Wasson (Kallemeyn 1988; Kallemeyn and Wasson 1981, 1982, 1986; Kallemeyn et al. 1989, 1991, 1994, 1996; Sears et al. 1982). A limited number of analyses of a few meteorites from the major chondrite groups have also been reported in several other studies (Reed and Allen 1966; Dreibus et al. 1979; Goles et al. 1967; Krähenbühl et al. 1973). Analytical precision for Br determinations are typically ∼5% or less (Dreibus et al. 1979; Kallemeyn and Wasson 1981).

Iodine is present in low concentrations in chondrites, typically <0.5 ppm, decreasing progressively from CC to EC to OCs. Bulk I data for chondrites comes from several different studies, mainly using INAA (Goles and Anders 1961, 1962; Reed and Ralph 1966; Clarke et al. 1967; Goles et al. 1967; Dreibus et al. 1979) with an analytical precision of ∼10%.

15.4.2 Bulk Halogen Concentrations in the Different Chondrite Groups

Because of the analytical complexities discussed above, the precise determination of bulk halogen concentrations in chondrites remains a significant problem in cosmochemistry. Wide ranges of concentrations of all the halogen elements have

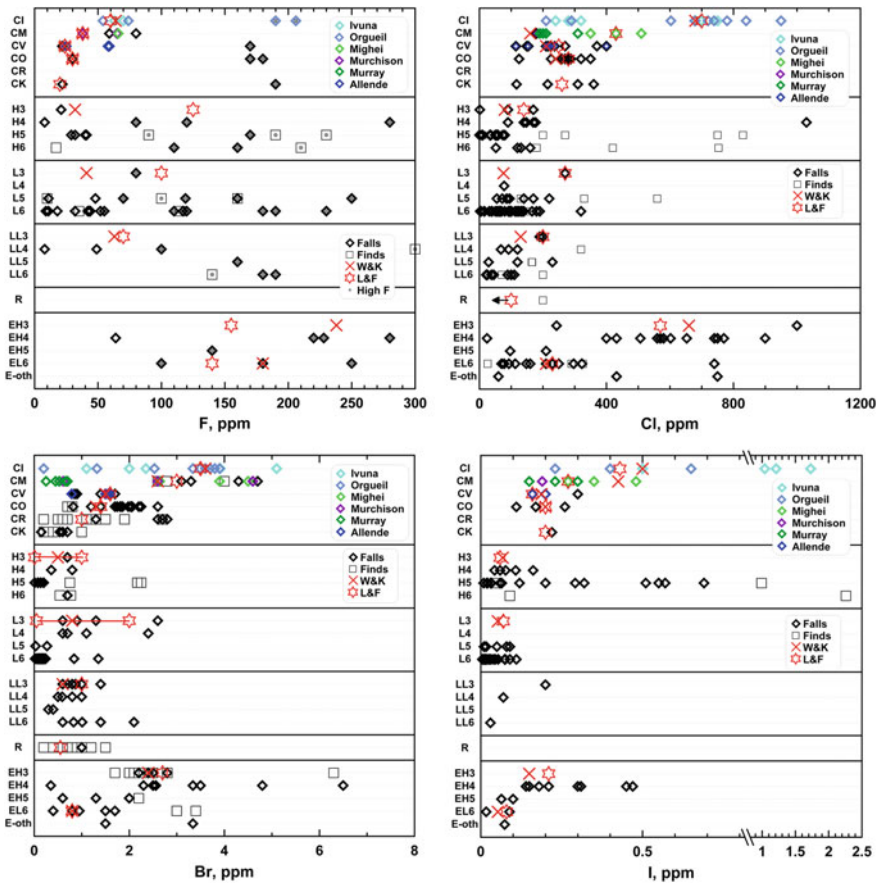

Fig. 15.1 Halogen concentrations in chondrites. Chondrite groups represented include carbonaceous chondrites (C prefix), ordinary chondrites (H, L and LL groups), Rumuruti (R) group chondrites, and enstatite chondrites (EH and EL groups). Ordinary and enstatite chondrites are divided into petrologic type, where type 3 is the most primitive material and type 4, 5, and 6 indicate progressively higher degrees of metamorphism. "E-oth" refers to other enstatite chondrites including petrologic type 7 and impact melt (see text). *Diamond symbols* represent meteorite falls, and open squares are finds. For carbonaceous chondrites, *colored symbols* indicate individual meteorites. For F, analyses from Reed (1964) and Greenland and Lovering (1965) with high F values are indicated by "•" superimposed on the diamond or square symbol. Bulk chondrite values, given by Wasson and Kallemeyn (1988) and Lodders and Fegley (1998), are indicated by a *red X* and *open star symbols*, respectively. For the ordinary and enstatite chondrites, bulk chondrite values are given on the petrologic type 3 lines of the plot but represent average values for the entire group. Bromine concentrations in H and L chondrites, given by Lodders and Fegley (1998), are ranges of values, indicated by a *solid line*. The chlorine concentration in R chondrites, given by Lodders and Fegley (1998), is a maximum, indicated by an *arrow*. For individual chondrites, F data are from Reed (1964), Greenland and Lovering (1965), Allen and Clark (1967), Goldberg et al. (1974), and Dreibus et al. (1979). Chlorine data are from Reed (1964), Greenland and Lovering (1965), Reed and Allen (1966), Goles et al. (1967), Dreibus et al. (1979), Garrison et al. (2000), and Sharp et al. (2013). Bromine data are from Reed and Allen (1966), Goles et al. (1967), Krähenbühl et al. (1973), Dreibus et al. (1979), Kallemeyn and Wasson (1981, 1982), and Kallemeyn et al. (1989, 1991, 1994, 1996). Iodine data are from Reed (1964), Reed and Allen (1966), Goles et al. (1967), and Dreibus et al. (1979)

been reported for most chondrite groups, and there are few systematic trends (Fig. 15.1). Estimates of the best values of bulk halogen concentrations for different groups of chondritic meteorites, compiled by Wasson and Kallemeyn (1988) and Lodders and Fegley (1998) (hereafter referred to as W&K and L&F), are compared in Table 15.2 and indicated in Fig. 15.1. For most meteorite groups, the two compilations are in good agreement, but there are some notable exceptions that are discussed in more detail below. For the W&K compilation, Rubin and Choi (2009) reported uncertainties in the average values of 25% for F, ~50% for chlorine, ~20% for Br, and ~40% for I.

15.4.2.1 Carbonaceous Chondrites

The currently accepted bulk F concentrations for the carbonaceous chondrites decrease in the sequence CI > CM > CO > CV > CK, with a relatively restricted range from 60 ppm (CI) to 20 ppm (CK) (Fig. 15.1a). Compilations by W&K (1988) and L&F (1998) (Table 15.2) are in good agreement, and are very close to the values of Dreibus et al. (1979). The most significant datasets for carbonaceous chondrite falls are the work of Goldberg et al. (1974) and Dreibus et al. (1979), with some additional measurements reported by Reed (1964), Greenland and Lovering (1965), and Allen and Clark (1977). The Dreibus et al. (1979) values are systematically lower than the data reported by Goldberg et al. (1974) and are a factor of 4–10 lower than those of other studies. All data for carbonaceous chondrites, above 100 ppm in Fig. 15.1a, are from the studies of Reed (1964) and Greenland and Lovering (1965). Additional F data for Antarctic CM finds, reported by Ménard et al. (2013), are in the range 70–140 ppm, which overlaps with, but is significantly higher, than the range of data for CM chondrite falls. The measured bulk F value for the CI chondrites is in reasonable agreement with the spectroscopic measurement for the Sun (Anders and Grevesse 1989; Lodders 2003; Palme et al. 2014: Table 15.2), although there is considerable uncertainty in the solar value (Sect. 15.3).

In general, the carbonaceous chondrites have high chlorine concentrations, up to ~950 ppm in the CI chondrites (Fig. 15.1b). Analytical data for CI chondrites are quite variable and show a distinct bimodal distribution with most of the early analytical studies yielding chlorine concentrations between ~250–320 ppm (Reed et al. 1966; Greenland et al. 1965), and later studies generally showing much higher concentrations that lie between 600 and 950 ppm (Goles et al. 1967; Dreibus et al. 1979; Sharp et al. 2007, 2013). Given the important evidence that the CI chondrite Orgueil has experienced efflorescence since its recovery and subsequent storage (Gounelle and Zolensky 2001), it is possible that some variability in the CI chondrites could be the result of mobilization and redistribution of soluble chloride salts. However, despite intrasample variability, there is a consensus in the literature that analyses that yield low chlorine concentrations are probably not reliable. For example, the bulk CI chondrite chlorine concentrations reported by W&K (1988) and L&F (1998) are in good agreement, at 680 and 700 ppm, respectively

(Table 15.2). These values are consistent with chlorine concentrations measured in the Sun by spectroscopic techniques (Anders and Grevesse 1989; Table 15.2).

For some of the other carbonaceous chondrite groups, there is disagreement between the values reported by W&K (1988) and L&F (1998). The two compilations differ significantly for the CM chondrites by almost a factor of 3: 160 vs. 430 ppm, respectively. As discussed below (Sect. 15.5.1), the CI normalized chlorine abundances in CM chondrites reported by W&K (1988) fall significantly below the volatility trends defined by the 50% condensation temperatures. The W&K value is also at the low end of all analyses of CM chondrite falls (Fig. 15.1b). In contrast, the value reported by L&F (1998) is consistent with the volatility trend. However, the justification for using this high value is questionable, given that only one CM chondrite fall analyzed to date, Mighei, contains such high concentrations of chlorine (350–510 ppm) (Fig. 15.1b). The only other two CM chondrite falls for which chlorine data are available, Murchison and Murray, have chlorine concentrations between 180 and 310 ppm (Fig. 15.1b). These differences may reflect real heterogeneity in the chlorine concentrations between CM chondrite falls that needs to be more thoroughly investigated.

For the CV and CO chondrites, W&K (1988) give lower concentrations of chlorine than L&F (1998) (Table 15.2). For the CV chondrites these values are 210 and 250 ppm, respectively, and for the CO chondrites, 240 and 280 ppm, respectively. Unfortunately, data are only available for three CV chondrite falls (Allende, Mokoia, and Vigarano) and most of these analyses are from Allende (Fig. 15.1b). The Allende data reported in the literature vary from 216 ppm to 400 pm, but most analyses lie in the range 216–237 ppm. The two analyses from Vigarano report chlorine concentrations of 170 and 270 ppm, and for Mokoia, 370 ppm, covering a wider range. In comparison, data for six different CO chondrite falls are generally more consistent, lying between 226 and 350 ppm, with one exception, an analysis of Lancé by Reed et al. (1966) that is anomalously low. For the CO chondrites, the value reported by L&F (1998) of 280 ppm appears to best represent the average bulk chlorine composition (Fig. 15.1b). Chlorine data are only available for one CK chondrite fall, Karoonda, with four separate measurements that range between 117 and 360 ppm. The lowest value is from Reed et al. (1966). Lodders and Fegley (1998) report a mean bulk chlorine content for CK chondrites of 260 ppm, the only available estimate in the literature.

For the carbonaceous chondrites, all measured Br concentrations are low, <5 ppm, and there is good agreement between the bulk Br contents reported by W&K (1988) and L&F (1998) (Table 15.2, Fig. 15.1c). Bulk Br concentrations in the carbonaceous chondrites decrease in the progression CI > CM > CV > CO > CR > CK, with a total range from 3.6 ppm (CI) to 0.6 ppm (CK) (Fig. 15.1c).

Measurements of I concentrations in CI chondrites show significant variability, probably as a result of the sample variability discussed earlier. Compilations of W&K (1988) and L&F (1998) report similar average CI chondrite I contents of 0.5 and 0.43 ppm, respectively, both of which are intermediate values within the range of analyses available (Fig. 15.1d). Bulk I abundances in the carbonaceous chondrites decrease in the progression CI > CM > CO > CV > CK, with a total range

from 0.43 ppm (CI) to 0.16 ppm (CK). There are currently no I determinations for the CR chondrites.

15.4.2.2 Ordinary Chondrites

The most comprehensive data set for F concentrations in ordinary chondrites is that of Allen and Clark (1977), who also made comparisons of their analytical technique with well-known standards. Unfortunately, only one of the ordinary chondrites they analyzed was also analyzed by Dreibus et al. (1979), so comparisons between separate studies are limited. For the L6 fall, Bruderheim, the Allen and Clark (1977) data are a factor of three higher than the determination of Dreibus et al. (1979) (32 vs. 11 ppm, respectively), but it is impossible to determine whether this is at least partly because of sample heterogeneity. The F concentrations measured by Reed (1964) and Greenland and Lovering (1965) are significantly higher than other studies, mostly >50 ppm (Fig. 15.1a). Dreibus et al. (1979) argued that these data are inaccurate. Overall, the current state of knowledge of the concentrations of F in ordinary chondrites is quite poor.

The preferred bulk F values for ordinary chondrites reported by W&K and L&F (Table 15.2, Fig. 15.1) are in significant disagreement. The F concentrations for the H and L chondrites determined by the two studies differ by a factor of almost four for the H chondrite (32 vs. 125 ppm) and by a factor of 2.5 for the L chondrites (41 vs. 100 ppm). The lower W&K values are weighted to the analyses of Dreibus et al. (1979) and Allen and Clark (1977). The higher L&F values appear to represent an average that includes analyses from Greenland and Lovering (1965), despite the fact that data from that study are not given significance for the carbonaceous chondrite preferred values. The averages of the two compilations are in better agreement for the LL chondrites (63 vs. 70 ppm), although the large spread in measured bulk F concentrations (9–190 ppm) and small number of meteorite analyses (only six falls and two finds) clearly introduces considerable uncertainty into these values.

Chlorine concentrations in the ordinary chondrites have been reported by numerous authors for both falls and finds, and for all petrologic types that represent the sequence of metamorphism from type 3 to type 6 (Table 15.1; Fig. 15.1b). Although there is considerable variation in the chlorine concentrations for both falls and finds, the values for falls are much more restricted, almost invariably <200 ppm. Analyses of ordinary chondrites with anomalously high chlorine contents are, with one exception, from finds, suggesting that terrestrial weathering introduces chlorine into the meteorites, rather than leaches it out. This problem has been demonstrated to be particularly acute for Antarctic meteorites where chlorine and other halogen concentrations have been shown to increase towards the fusion crust (Kato et al. 2000; Langenauer and Krähenbühl 1993). Chlorine is likely incorporated into the mineral akaganéite, a common weathering product of Fe–Ni metal in the Antarctic environment (Bland et al. 2006). In Antarctica, the elevated chlorine concentrations have been attributed to chloride-rich aerosols derived from

surrounding oceanic waters as sea spray that are transported into the Antarctic interior by prevailing winds (Langenauer and Krähenbühl 1993). The halogen contamination is not related to the visible degree of weathering, but the duration of residence of the meteorites on the Antarctic ice.

A few ordinary chondrites have been analyzed for chlorine multiple times, by different authors or, in rare cases, the same study, providing some useful insights into analytical variability and sample heterogeneity for this chondrite group. The L6 fall Bruderheim, in particular, has been analyzed in at least five different studies, including multiple analyses reported by Goles et al. (1967), which range from 66 to 130 ppm, in good agreement with the entire range found by all the studies (67–137 ppm: Dreibus et al. 1979; Garrison et al. 2000). These data for a single chondrite suggest that there is significant internal variability in the distribution of chlorine within ordinary chondrites and that multiple analyses are necessary to accurately determine the bulk chlorine content of any given ordinary chondrite.

As for the carbonaceous chondrites, there are significant differences between the average bulk chlorine contents reported by W&K (1988) and L&F (1998) for the H, L, and LL chondrites (Table 15.2; Fig. 15.1b). L&F (1998) report abundances that bring the chlorine abundances into line with their condensation temperatures relative to other elements, and are higher than the values reported by W&K (1988). This is most extreme for the L chondrites, where the L&F (1998) concentration (270 ppm) is a factor of three higher than the W&K (1988) value (76 ppm). This elevated value is not consistent with the analytical data for L chondrite falls, which are mostly less than 200 ppm. The differences for H (80 vs. 140 ppm) and LL (130 vs. 200 ppm) groups are smaller, but place the L&F (1998) values at the high end of the data distribution for both groups of meteorites.

Bulk Br contents for the H, L, and LL chondrites show a significant range, although less variation than for the carbonaceous chondrites (Fig. 15.1c). Most analyses of Br in ordinary chondrites lie in the range of $\sim$0.5 to $\sim$2.5 ppm. However, there are also a significant number of measurements for H, L, and LL chondrite falls where Br concentrations are below the detection limit of INAA analysis, <0.01 ppm: these are not plotted in Fig. 15.1c. This is particularly the case for the H chondrites where the vast majority of the data fall close to or below detection limits. There is a suggestion that Br contents may, at least in part, be related to metamorphic grade. For all the chondrite groups, all the type 3, and many type 4 chondrites, have Br contents >0.5 ppm. In contrast, for petrologic types 5 and 6, almost all H and LL chondrites have Br contents <0.5 ppm with most analyses <0.2 ppm or below INAA detection limits.

Wasson and Kallemeyn (1988) reported bulk H, L, and LL chondrite Br contents of 0.5, 0.8, and 0.6 ppm, respectively (Fig. 15.1c). In contrast, L&F (1998) chose to give ranges of values for H (0.1–1.0 ppm) and L (0.05–2 ppm) and a value of 1 ppm for LL chondrites (Fig. 15.1c). Neither of these compilations appears to take into account the large amount of data that lies below INAA detection limits, and hence they are skewed towards measurable, higher values, although they may

also be considered as representative of petrologic type 3. Choosing a specific value of bulk Br concentration for the ordinary chondrites is therefore not straightforward.

Reliable bulk I data are only available for the H and L chondrites. For the LL chondrites, there are very few data and there is currently no accepted bulk I value. Iodine concentrations in ordinary chondrites are typically <0.5 ppm. The H chondrites show a range of I contents (Fig. 15.1d), and the bulk I contents for the H chondrites reported by W&K (1988) and L&F (1998) are in close agreement, 0.068 and 0.07 ppm, respectively. Two analyses above 1 ppm are for finds, and the highest value of 2.26 ppm is for the Antarctic H chondrite, Y-74014, that clearly shows Antarctic contamination (Kato et al. 2000). Bulk I determinations for the L chondrites are all low, mostly less than 0.1 ppm, and many <0.02 ppm, although the preferred bulk I values for the L chondrites are only slightly lower than those for the H chondrites at 0.053 ppm (W&K) and 0.07 ppm (L&F).

15.4.2.3 Enstatite Chondrites

Halogen concentrations have been measured in a variety of enstatite chondrites. For the EH group, the data include petrologic types from 3 to 5, but for the ELs the data are only from EL6 and EL7 chondrites. Petrologic type 7 is used rather inconsistently in the chondrite literature, to identify chondrites that are highly recrystallized with little evidence of chondrules. In Fig. 15.1, we plot several enstatite chondrites as "other" (E-oth). These include Ilafegh 09, EL7; Happy Canyon, EL6/7 (i.e., it is either type 6 or type 7); Itqiy, classified as EL7-an (an = anomalous), which probably experienced partial melting (Patzer et al. 2001); and an impact melt clast and an EL6 clast from the EH4 impact melt breccia, Abee.

Fluorine concentrations have been reported for three EL and three EH chondrites, including the impact melt breccia, Abee (EH4) (Reed 1964; Dreibus et al. 1979; Greenland and Lovering 1965). Measured F concentrations range from 64 to 280 ppm for the EH and from 100 to 250 ppm for the EL groups (Fig. 15.1a). In comparison with most other chondrite groups, it appears that the distribution of F concentrations is skewed to higher values in enstatite chondrites, with no values <50 ppm. However, this is because most of the data are from the studies of Greenland and Lovering (1965) and Reed (1964). As discussed above, Dreibus et al. (1979) argued that the high values from those studies are incorrect. Dreibus et al. analyzed only one E chondrite, Abee, for which their F concentration, 64 ppm, is more consistent with the ranges of O and C chondrites. Bulk F values for enstatite chondrites reported by W&K (1988) and L&F (1998) differ significantly (Table 15.2). The respective values for the EH and EL chondrites are 238 vs. 155 ppm and 180 vs. 140 ppm, respectively. The higher values are weighted to the higher F concentrations of the Greenland and Lovering (1965) and Reed (1964) studies, and are therefore likely to be significantly higher than the true values.

Accurate F concentrations of enstatite chondrites should be regarded as essentially unknown at present.

There is a substantial body of analytical data for chlorine in EH and EL chondrite falls. Although the ranges of chlorine concentrations in EH and EL chondrites overlap, the EHs consistently have higher concentrations of chlorine, up to 1000 ppm, with the EH3 fall Qingzhen having the highest chlorine concentration of any meteorite measured to date (Sharp et al. 2013). For the EL chondrites, the range is 60–740 ppm but only Eagle (EL6) has a concentration above 326 ppm. The unusual EH4 impact melt breccia, Abee, has been analyzed multiple times (Reed and Allen 1966; Goles et al. 1967; Garrison et al. 2000; Sharp et al. 2013). Measured chlorine concentrations range between 432 and 750 ppm in these different studies, emphasizing again the issues of determining chlorine concentrations precisely, even in a single meteorite.

W&K (1988) reported average bulk chlorine concentrations of 660 and 210 ppm for the EH and EL chondrites (Table 15.2), respectively, whereas L&F (1998) give values of 570 and 230 ppm (Table 15.2; see also Fig. 15.1b). Although these values are somewhat in agreement, the wide variation in chlorine abundances determined for the enstatite chondrites suggest that there is still uncertainty in the mean bulk chlorine concentration in these meteorites. Nevertheless, it is clear that chlorine concentrations in the EH chondrites are much higher than any of the other chondrite groups, with the exception of CI chondrites. Chlorine concentrations in the EL group appear to be comparable to the ordinary and carbonaceous chondrites.

Bromine concentrations in E chondrites are low, generally <5 ppm (Fig. 15.1c). Like chlorine, Br concentrations are higher in the EH chondrites than the EL chondrites (Fig. 15.1c). There is good agreement between the bulk Br contents reported by W&K (1988) and L&F (1998): 2.7 ppm for EH and 0.8 ppm for EL (Table 15.2; Fig. 15.1c).

Figure 15.1d shows the reported I concentrations in a number of enstatite chondrites. Determinations for EH chondrites show significant variability, with a range from <0.01 to 0.45 ppm. Iodine concentrations for only one EL chondrite, Hvittis (EL6), have been reported in the literature, so the bulk value for the EL chondrites is not well constrained. W&K (1988) and L&F (1998) report similar average bulk I contents for the EH chondrites, 0.15 and 0.21 ppm, respectively, and for the EL chondrites, 0.053 and 0.08 ppm, respectively.

15.4.3 Halogen Ratios in Chondrites

Figure 15.2 shows the halogen ratios, F/Cl, Br/Cl, and I/Cl for carbonaceous, ordinary, and enstatite chondrites. These figures show the same data as for Fig. 15.1, but data points are limited to instances where both relevant elements were measured in the same analysis. The data represented are all from the studies of Reed and Allen (1966), Goles et al. (1967), Greenland and Lovering (1965), and

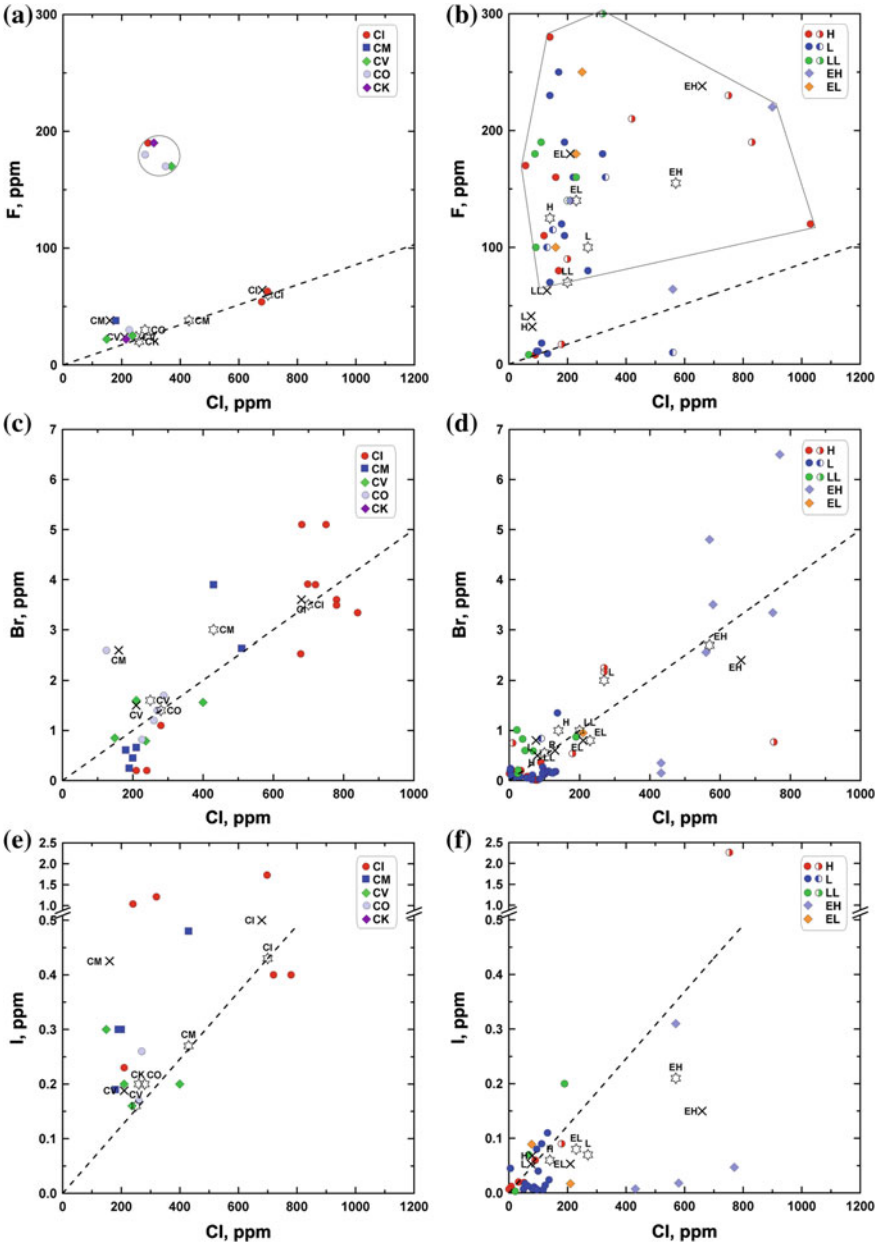
(a)
F, ppm
Cl, ppm
CI
CM
CV
CO
CK
(b)
F, ppm
Cl, ppm
H
L
LL
EH
EL
(c)
Br, ppm
Cl, ppm
CI
CM
CV
CO
CK
(d)
Br, ppm
Cl, ppm
H
L
LL
EH
EL
(e)
I, ppm
Cl, ppm
CI
CM
CV
CO
CK
(f)
I, ppm
Cl, ppm
H
L
LL
EH
EL

◂**Fig. 15.2** Halogen ratios in chondrites: F/Cl, Br/Cl, and I/Cl. Carbonaceous chondrites are illustrated in (**a**), (**c**) and (**e**), and ordinary and enstatite chondrites in (**b**), (**d**), and (**f**). *Colored symbols* show individual chondrite groups according to the legend. Bulk chondrite values, given by Wasson and Kallemeyn (1988) and Lodders and Fegley (1998), are indicated as *X* and *open star symbols*, respectively, with labels identifying the different chondrite groups. *Dashed lines* show the CI ratio, defined by the CI concentrations of Lodders and Fegley (1998), which is considered to be the solar ratio. Data are the same as those shown in Fig. 15.1, but limited to studies where chlorine and the other relevant halogen was measured. All data are from Reed and Allen (1966), Goles et al. (1967), Greenland and Lovering (1965), and Dreibus et al. (1979). The *grey ellipse* in (**a**) and *polygon* in (**b**) indicate analyses with high F from Greenland and Lovering (1965)

Dreibus et al. (1979). In all the plots, the dashed lines show the halogen ratios for CI chondrites defined by Lodders and Fegley (1998), which are taken to be equivalent to the solar values. For all the halogens, the L&F values are in fairly close agreement with the W&K values for CI chondrites (Fig. 15.1).

The two plots of F/Cl (Fig. 15.2a, b) show a bimodal distribution of data for all chondrite groups. One group of data lies close to the F/Cl ratio for CI chondrites. The second group has much higher F/Cl ratios. These are predominantly data from the study of Greenland and Lovering (1965), which have been suggested to have erroneously high F concentrations (Dreibus et al. 1979). The data that lie close to the CI chondrite line are probably more reliable, indicating that all chondrite groups may record a similar bulk F/Cl ratio. Comparison of Fig. 15.2a and b highlights the complexities associated with the W&K (1988) and L&F (1998) compilations of bulk chondrite halogen concentrations, as discussed above. For carbonaceous chondrites, even though F and chlorine concentrations vary, the F/Cl ratios for the different chondrite groups are all close to solar. In contrast, both W&K and L&F give much higher F/Cl ratios for ordinary and enstatite chondrites, favoring the values with high F, such that the two studies disagree significantly.

For the carbonaceous chondrites, there is a strong correlation between Br and chlorine, such that the data lie close to the CI ratio (Fig. 15.2c). Most of the data for ordinary and enstatite chondrites also cluster around the same ratio (Fig. 15.2d), although several analyses of H and L chondrites, with low chlorine contents (<100 ppm), deviate from the trend. In addition, most of the W&K and L&F bulk values for different chondrite groups lie close to the solar ratio. As noted above, there are many analyses of Br concentrations in ordinary chondrites that lie below INAA detection limits, <0.01 ppm. None of these data have corresponding chlorine analyses, so they cannot be plotted on this figure.

In the I/Cl plots (Fig. 15.2e, f), the data show quite a lot of scatter, although many analyses lie close to the CI chondrite ratio line. For the carbonaceous and ordinary chondrites, most W&K and L&F bulk chondrite values also lie close to the solar ratio. The W&K values give a high I/Cl ratio for the CM group. W&K and L&F values for EH chondrites differ from each other and from the solar ratio, reflecting the large amount of scatter in the data for the EH group. The L chondrite fall Y-74014, which shows Antarctic contamination of halogens (Kato et al. 2000: see above), lies far from the CI chondrite ratio line (2.26 ppm I).

Fig. 15.3 Comparison of abundances of moderately volatile and volatile elements, normalized to Si and CI chondrite values versus 50% condensation temperature (at 10^{-5} atm) for carbonaceous chondrites using concentration data from W&K and L&F. Data for the halogen elements are shown in color with chlorine (*green*), F (*red*), Br (*blue*), and I (*yellow*). **a–c** Plots using data from W&K for the CM, CV, and CO carbonaceous chondrites. Data for the halogen elements are shown in color with chlorine (*green*), F (*red*), Br (*blue*), and I (*yellow*). **d–f** Plots using data from L&F for the CM, CV, and CO carbonaceous chondrites. Condensation temperatures are from Lodders (2003). The plots illustrate that, with the exception of the CM chondrites, F, Br, and I fall quite consistently on the condensation trend. However, for chlorine the W&F dataset consistently show significant underabundances for chlorine, particularly for the CM and CV chondrites compared with the 50% condensation trend. This underabundance is also apparent in the L&F dataset, but is much less pronounced for chlorine in the CM chondrites. Bromine in the L&F dataset appears anomalous, falling above the condensation trend ▶

Although there is a certain amount of scatter on most of the plots in Fig. 15.2, the overall picture that emerges is that halogen ratios in chondrites from all classes and groups appear to show general trends similar to CI chondrite, or solar values. If this is true, it is a significant relationship for the interpretation of halogen abundances and behavior in the inner solar system during the period of evolution of the protoplanetary disk, as well as for the bulk halogen contents of the terrestrial planets.

15.5 Halogen Abundances in Chondrites: Cosmochemical Trends

Recognizing that there are uncertainties in the halogen concentrations for some meteorite groups, as well as halogen condensation temperatures, we now consider halogen abundances in the different chondrite groups relative to abundances of other moderately volatile and volatile elements in CI chondrites. This comparison gives insights into the cosmochemical processes that may have controlled halogen behavior during early solar system evolution. Figures 15.3, 15.4, and 15.5 show volatility trends for elements plotted as element abundances relative to CI and Si abundances (e.g., $(El_{CM}/Si_{CM})/(El_{CI}/Si/_{CI})$). For each group of chondrites, the abundances and condensation temperatures taken from the compilations of W&K (1988) and L&F (1998) are shown on the left and right hand sides of the figures, respectively.

15.5.1 Carbonaceous Chondrites

The abundances of moderately volatile and volatile elements in carbonaceous chondrites, normalized to CI chondrite and Si, are shown in Fig. 15.3. The diagrams illustrate the general, well-established trends of decreasing abundances of the moderately volatile and volatile elements with decreasing condensation

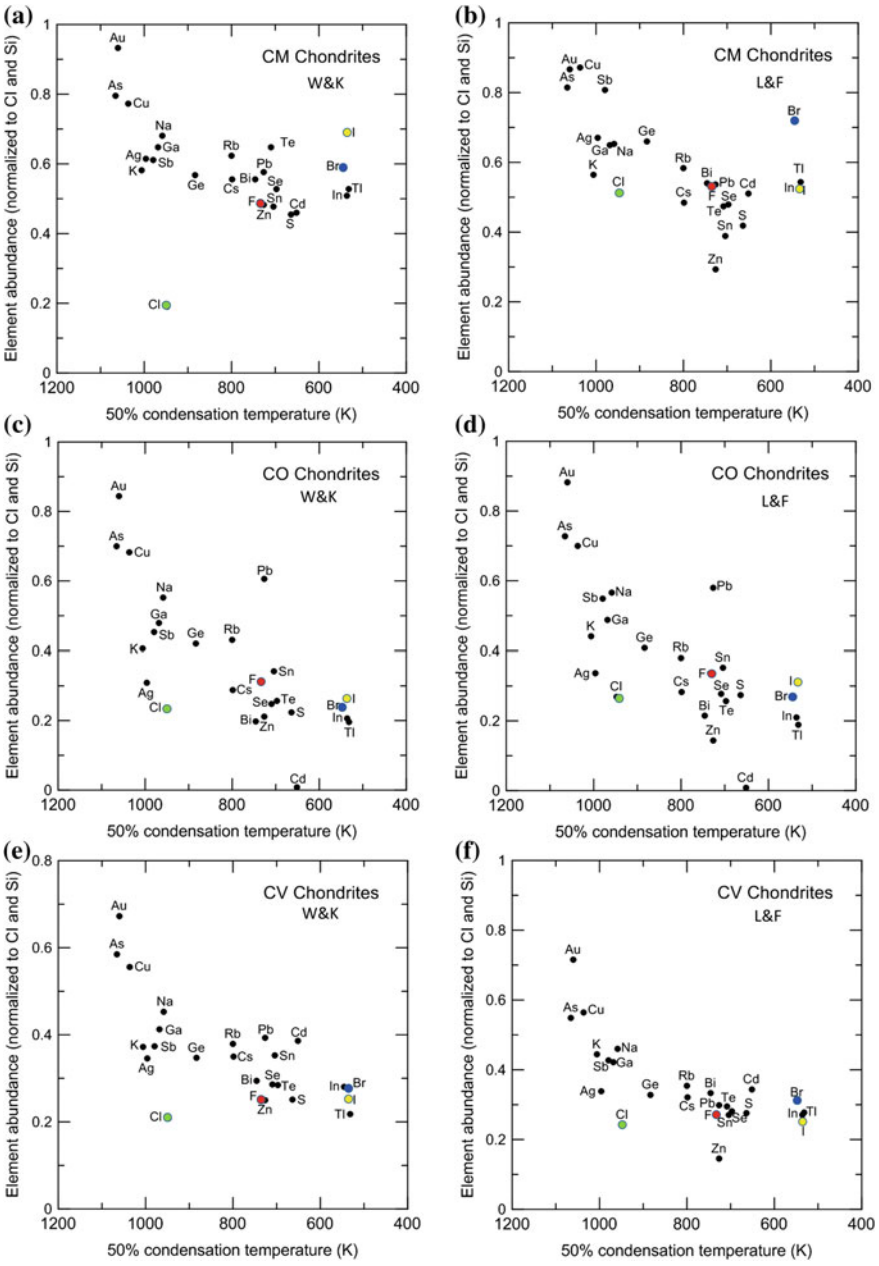
(a)
CM Chondrites
W&K
(b)
CM Chondrites
L&F
(c)
CO Chondrites
W&K
(d)
CO Chondrites
L&F
(e)
CV Chondrites
W&K
(f)
CV Chondrites
L&F
Element abundance (normalized to CI and Si)
50% condensation temperature (K)

Fig. 15.4 Comparison of abundances of moderately volatile and volatile elements, normalized to Si and CI chondrite values versus 50% condensation temperature (at 10^{-5} atm) for H, L, and LL ordinary chondrites using concentration data from W&K and L&F. Data for the halogen elements are shown in color with chlorine (*green*), F (*red*), Br (*blue*), and I (*yellow*). **a–c** Plots using data from W&K for the H, L and LL ordinary chondrites. **d–f** Plots using data from L&F for the H, L, and LL ordinary chondrites. Unlike the carbonaceous chondrites, the ordinary chondrites show more complex relationships between their elemental abundances and 50% condensation temperature. Although there is a general decrease in abundance with condensation temperature, there are major differences between the depletions in the lithophile elements versus the chalcophile and siderophile elements. Chlorine falls slightly below the condensation trend using both datasets, with some small variations from the H to the LL chondrites. Fluorine shows some major differences between the two datasets, falling well above the condensation trend using the L&F compilation and, to a lesser degree for the L and LL chondrites, using the W&K data. Bromine and I data, where available, are generally quite consistent with the condensation trend ▶

temperature, and depletions of all these elements relative to CI chondrite and Si. There are several notable features of the behavior of the halogens on these plots, and some significant differences between the W&K and L&F datasets.

For the W&K data (Fig. 15.3a, c, e), irrespective of the volatile element trends of the bulk chondrite, the depletion of chlorine in the CM, CO, and CV chondrites is very similar. In all three cases, the chlorine abundances lie distinctly off the progressive depletion trend. Normalized to CI chondrite and Si, the chlorine depletions are remarkably similar, ~ 0.2. In contrast, the remaining halogens all show consistent behavior and generally lie on the volatility trend defined by the other elements, with the exception of I in the CM chondrites that appears to be slightly over-abundant (Fig. 15.3a). Chlorine in CM chondrites is especially anomalous, being significantly more depleted than any other volatile or moderately volatile element (Fig. 15.3a).

The low relative abundance of chlorine in CM chondrites given by W&K (Fig. 15.3a), could be attributable to several possible causes. These include analytical error, an underestimation of the condensation temperature of chlorine, or real depletions caused by processes such as mobilization due to aqueous alteration. From the above discussion, it seems reasonable to assume that although there is heterogeneity among the CM chondrite analyses, the data are quite robust. The halogens are certainly mobile in aqueous solutions, but if chlorine has been leached from CM chondrites, we would expect the other halogens (except F) to show similar behavior, which they apparently do not. Bromine and I depletions in CM chondrites are quite consistent with their estimated condensation temperatures. It is possible that there is a significant error in the condensation temperature for chlorine, as discussed in Sect. 15.2.1. If the arguments of Zolotov and Mironenko (2007) that chlorine actually condenses as $HCl{\cdot}3H_2O$, and not sodalite, are correct, the condensation temperature of chlorine would be several hundred degrees lower, and the chlorine abundance in CM chondrites would be more consistent with the volatility trend. As discussed in Sect. 15.4.2.1, the preferred chlorine concentration in CM chondrites of 160 ppm reported by W&K may be too low, because it actually lies outside the range of any of the chlorine measurements reported in the literature, as shown in Fig. 15.1a. Note that increasing the value of the chlorine concentration by

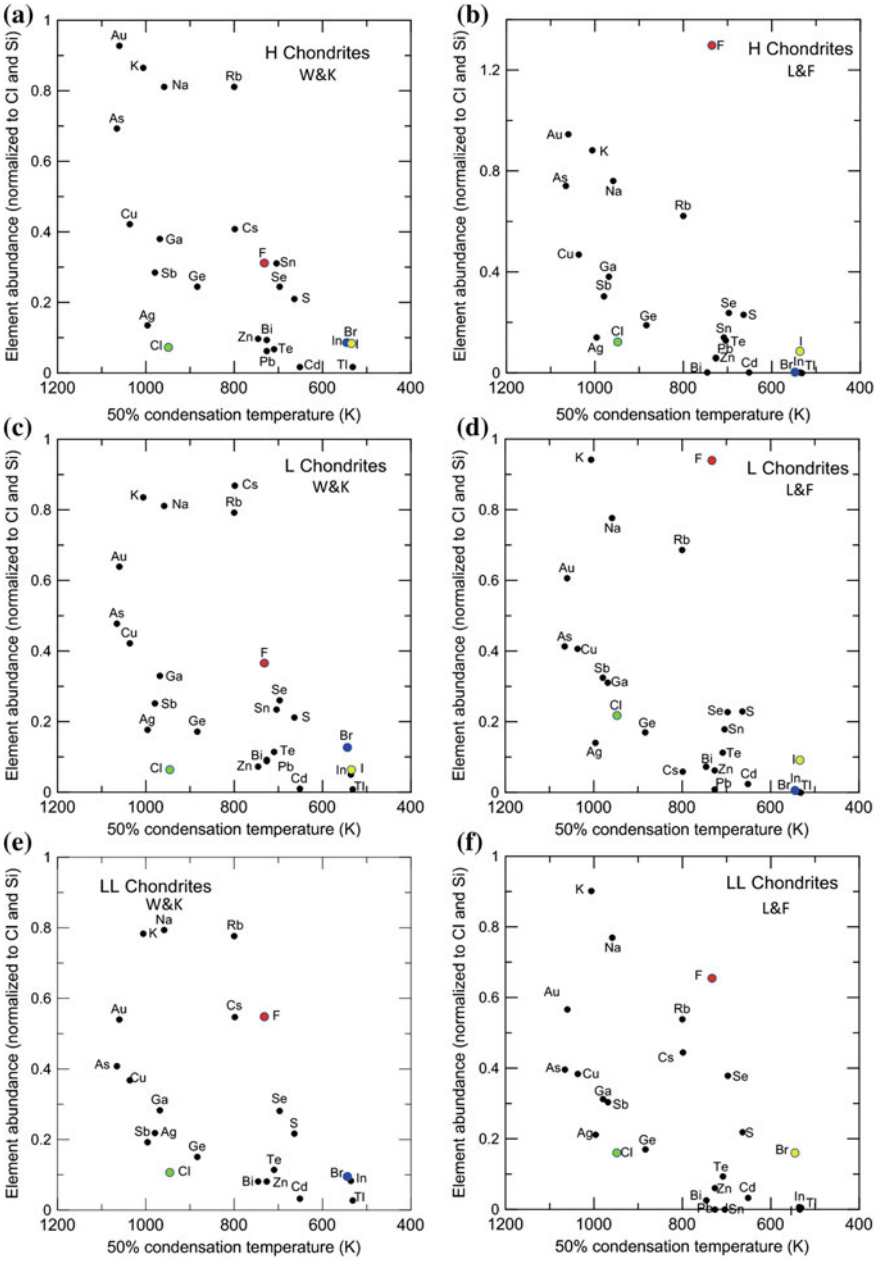
(a)
H Chondrites
W&K
(b)
H Chondrites
L&F
(c)
L Chondrites
W&K
(d)
L Chondrites
L&F
(e)
LL Chondrites
W&K
(f)
LL Chondrites
L&F
Element abundance (normalized to CI and Si)
50% condensation temperature (K)

a factor of two has the effect of increasing the abundance value on the plot in Fig. 15.3a by a factor of two. The anomalous location of chlorine in Fig. 15.3a could thus be attributable to multiple factors.

For the L&F plots (Fig. 15.3b, d, f), all of the halogens show more consistent behavior, and generally lie on volatility trends defined by other elements. An exception is Br in CM chondrites that is over-abundant (Fig. 15.3b). The higher value for chlorine in CM chondrites (430 ppm) reported by L&F (in comparison to the W&K value) is also outside the range of most values determined analytically (Fig. 15.1a) and can only be justified on the grounds that this value brings the abundance of chlorine close to the condensation trend (Fig. 15.3b). However, this is predicated on the assumption that the high chlorine condensation temperature

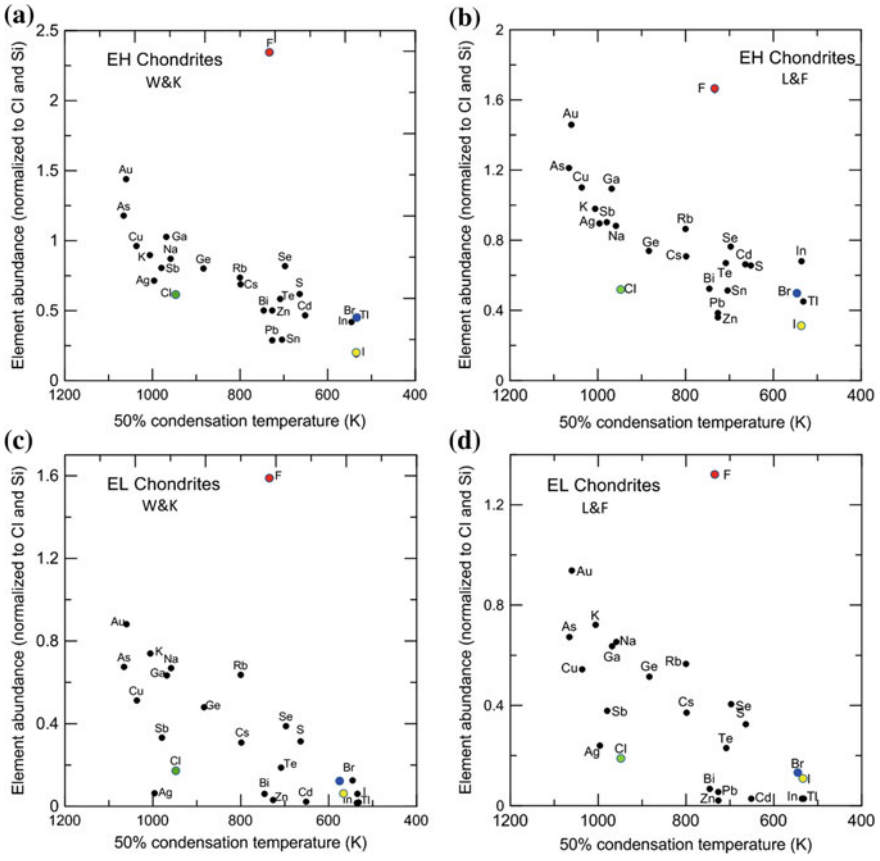

Fig. 15.5 Comparison of abundances of moderately volatile and volatile elements, normalized to Si and CI chondrite values versus 50% condensation temperature (at 10^{-5} atm) for EH and EL chondrites using concentration data from W&K and L&F. Data for the halogen elements are shown in color with chlorine (*green*), F (*red*), Br (*blue*), and I (*yellow*). **a–b** Plots using data from W&K for the EH and EL chondrites. **d–f** Plots using data from L&F for the EH and EL chondrites. Chlorine falls below the condensation trend to varying degrees for the EH and EL chondrites in both datasets, whereas Br and I show good agreement. Fluorine is highly overabundant to different degrees in both datasets, a phenomenon that has been attributed to the extreme electronegativity of F (Rubin and Choi 2009)

(948 K) is correct, an assumption that may not be justified, as discussed above. Chlorine abundances in CO and CV chondrites are also more consistent with a lower condensation temperature (Fig. 15.3d, f). However, for the CO and CV chondrite data plotted in Fig. 15.3, one might argue that the halogens actually show no volatility-related trend, and that all halogen abundances relative to CI chondrite and Si are in fact comparable, i.e. the trend is flat. A reevaluation of the bulk concentration of chlorine in CM chondrites, as well as the condensation temperature of chlorine, is clearly needed to resolve the interpretation of the volatility-related dependence of halogen abundances.

Rubin and Choi (2009) have pointed out that in the enstatite and, to a lesser extent, the ordinary chondrites, there is a correlation between the abundance of the halogens and their electronegativity (see enstatite chondrites below). However, no such correlation exists for the carbonaceous chondrites. Rubin and Choi (2009) suggested that the difference between ordinary and carbonaceous chondrites is because carbonaceous chondrites generally formed under more oxidizing conditions, with the result that chlorine (and other halogens) did not form simple binary compounds, but stayed longer in the nebular gas phase. However, the oxidation states of different components of carbonaceous chondrites are actually highly variable, and in detail it is not clear how this mechanism would operate. Retention of halogens in the gas phase would be consistent with the proposal of Zolotov and Mironenko (2007) that chlorine condenses at low temperatures as HCl hydrate ($HCl{\cdot}3H_2O$). However, if HCl did accrete as a hydrate, a correlation would be expected between the bulk water content of the carbonaceous chondrites and their chlorine content. Such a relationship does not appear to exist, with the CM, CO, and CV chondrites all having very different initial water contents, but very similar ranges of bulk chlorine contents (Fig. 15.1b). However, several factors prevent a reliable analysis of the relationship between chlorine and water contents in carbonaceous chondrites. These include the significant variation in bulk water contents even within members of an individual chondrite group (Alexander et al. 2013), the lack of bulk chlorine data for many carbonaceous chondrites, and the fact that an indeterminate amount of the original accreted water may have been lost to space by degassing.

15.5.2 Ordinary Chondrites

As shown in Fig. 15.4, volatility depletion trends for the ordinary chondrites are not as well defined as for the carbonaceous chondrites. According to the data of W&K (Fig. 15.4a, c, e), chlorine, Br and I are all highly depleted (relative to CI and Si) by about the same amount in all the ordinary chondrite groups. Chlorine lies off the general volatility trend, particularly for the H and L chondrites. This behavior again suggests that the condensation temperature for chlorine may need to be reevaluated, although chlorine lies closer to the condensation trends in the L&F plots (Fig. 15.4b, d, f). The depletions of Br and I, on the other hand, are very consistent

with the volatility trend for both sets of data. The behavior of F is somewhat different, showing a higher abundance compared to the other halogens that increases progressively from the H group to the LL group. This is more pronounced in the L&F plots than in the W&K plots. Based on data for the enstatite chondrites (Sect. 15.5.3), Rubin and Choi (2009) have suggested that enrichment in F, relative to the other halogens in the ordinary chondrites, may be due to accretion of a simple metal fluoride that formed under reducing conditions. This conclusion is based on the fact that there is a correlation between the concentration of the halogens and their electronegativity, an effect that is less strong in ordinary chondrites than for the enstatite chondrites. However, as discussed above and illustrated in Fig. 15.1a, F concentrations given by both L&F and, to a lesser extent, W&K, may be overestimated because they are weighted to early studies that reported high values.

15.5.3 Enstatite Chondrites

One of the notable characteristics of the enstatite chondrites is that their CI chondrite normalized volatile and moderately volatile element abundances are significantly higher than for any other chondrite group (Fig. 15.5). In general, the halogens also reflect this trend, but there are some complexities in the behavior of the halogens compared with the other chondrite groups. The EH chondrites are significantly richer in halogens than the ELs (Table 15.2, Fig. 15.1), although only data for EL6-7 chondrites are available, whereas for EH chondrites, the data span petrologic types 3–5. In general, EL chondrites have chlorine, Br and I abundances that are comparable to those in the ordinary, CO, and CV carbonaceous chondrite groups. Only chlorine in the EH chondrites is consistently higher than in the other groups (Fig. 15.1b) and is comparable to the range in CI chondrites. Fluorine abundances in both the EH and EL groups are notably higher than the ordinary and carbonaceous chondrites (3.71 and 2.81 $\times$ CI, respectively), and F abundances in Fig. 15.5 fall a long way from the volatility trends. Similar to the ordinary chondrites, F concentrations given by both L&F and W&K may be significantly overestimated because they are weighted to early studies that reported high values (Fig. 15.1a).

Rubin and Choi (2009) discussed the possible cosmochemical controls on the abundances of halogens in enstatite chondrites. Based on the 50% condensation temperatures, which as discussed earlier have large uncertainties associated with them, halogen abundances in enstatite chondrites are not correlated with their volatility (Fig. 15.5), assuming chlorine condensed at high temperature. On these grounds, Rubin and Choi (2009) argued that the halogen abundances could not be the result of either accretion of chondritic components, prior to complete condensation of the halogens, or of volatile loss due to heating of enstatite-chondrite materials, perhaps during chondrule formation or post-accretion thermal or shock metamorphism. However, a caveat to this conclusion is that the condensation temperatures of the halogens, calculated for canonical solar nebular conditions, may

not be applicable to the highly reducing conditions of formation for the enstatite chondrites (e.g., Grossman et al. 2009). Rubin and Choi (2009) found, instead, that halogen abundances in both groups of enstatite chondrites show a strong correlation with electronegativity, with abundances decreasing in order of decreasing electronegativity. Under the reducing conditions of formation of the enstatite chondrites, the highly reactive halogens in the gas phase may have reacted to form simple metal halides, such as $FeCl_2$, MgF_2, $FeBr_2$, and MgI_2 that were then incorporated along with other nebular components into the enstatite chondrite parent bodies. Only $FeCl_2$, occurring as the mineral lawrencite, has been observed in enstatite chondrites (Keil 1968), but redistribution of primary halides by parent-body processing may have occurred to eradicate evidence of primary halide phases.

15.6 Halogen Stable Isotopic Compositions of Chondrites —Bulk Chondrites and Individual Phases

Fractionations in stable isotope compositions of a given element can be used to investigate a range of cosmochemical and geochemical processes. For the halogens, stable isotope studies are somewhat restricted in scope. Fluorine and I each have only one stable isotope, ^{19}F and ^{127}I, so stable isotope studies of these elements are not possible. Bromine has two stable isotopes, ^{79}Br and ^{81}Br, with natural relative abundances of 51% and 49%, respectively. A recent effort to measure Br isotope compositions in ordinary chondrites does not report any data (Schaefer 2012, 2013).

The main focus of halogen stable isotope work has been on chlorine isotopes. The two stable isotopes of chlorine, ^{35}Cl and ^{37}Cl, have relative abundances of 76% and 24%, respectively. The relative mass difference of 5.7% means that chlorine isotopes fractionate significantly and can be used as tracers of a variety of processes. Variations in chlorine isotope composition are expressed as:

$$\delta^{37}\mathrm{Cl}(‰) = \left[\left(^{37}\mathrm{Cl}/^{35}\mathrm{Cl}\right)_{\mathrm{sample}} \Big/ \left(\left(^{37}\mathrm{Cl}/^{35}\mathrm{Cl}\right)_{\mathrm{seawater}} - 1\right)\right] \times 1000.$$

The $\delta^{37}Cl$ value of the bulk Earth is −0.2‰ (Sharp et al. 2013). In chondrites, variations in chlorine isotopes may arise from isotopic heterogeneity in the solar nebula, fractionation during events such as chondrule formation, and/or processes that took place after accretion, into the chondrite parent bodies. This means that the chlorine isotopes are potentially important recorders of cosmochemical processes, but it also means that contributions to the measured isotopic ratios from different processes are difficult to disentangle. The picture is further complicated by the spectre of terrestrial contamination.

Chlorine isotope compositions have been measured on bulk chondrites and individual minerals using different analytical methods, including thermal ionization

mass spectrometry (TIMS), secondary ion mass spectrometry (SIMS), and gas source isotope ratio mass spectrometry (IRMS). TIMS measurements of bulk chondrites show a wide range of δ^{37}Cl values, which range from −4.6‰ to +5.0‰ for ordinary chondrites, −0.6‰ to +4.4‰ for carbonaceous chondrites, and +2.6‰ to +5.2‰ for enstatite chondrites (Nakamura et al. 2007; Magenheim et al. 1995). In contrast, IRMS measurements show a much more limited range, with most analyses between −2‰ and +1‰ for bulk chondrites from O, C, and E groups (Sharp et al. 2007, 2013; Bonifacie et al. 2007). The large ranges reported by TIMS studies are now considered to be attributable to analytical errors (Bonifacie et al. 2008; Sharp and Barnes 2008; Nakamura et al. 2011; Sharp et al. 2013).

Sharp et al. (2013) measured chlorine isotope compositions in chondrites from different chondrite groups that showed differing degrees of both aqueous alteration and metamorphism. They also distinguished between insoluble, structurally-bound chloride, and water-soluble chloride fractions. Structurally-bound chlorine is considered to reside primarily in apatite, sodalite, and glass. Water soluble chlorine is expected to be hosted by salts such as NaCl, KCl, and $FeCl_2$. Bulk isotope compositions of six petrologic type 3 chondrites, from CV, CO, H, and EH groups, all have remarkably similar δ^{37}Cl values, with the average for six meteorites −0.3 ± 0.3‰, and the average structurally-bound chlorine also −0.3 ± 0.3‰. This constant value for δ^{37}Cl indicates the presence of a single, homogeneous chlorine isotope reservoir in the inner solar nebula, which contrasts with the isotopic heterogeneity observed in O and N stable isotopes among chondrite groups (Kung and Clayton 1978; Kerridge 1993; Robert and Epstein 1982; Clayton 1993; Clayton and Mayeda 1999; Sephton et al. 2003; Franchi 2008). A notable exception to the constant δ^{37}Cl value of −0.3‰ is the LL3.6 chondrite Parnallee, which has considerably lighter average δ^{37}Cl values of −4.1‰ for structurally-bound chlorine and −1.4‰ for water-soluble chlorine. The origin of this difference is unclear. Parnallee has undergone mild metamorphism (to petrologic subtype 3.6), but is not considered to have undergone aqueous alteration. However, it does contain chondrules with Na- and chlorine-rich mesostasis (Bridges et al. 1997; Sharp et al. 2013) and feldspar in chondrules shows nephelinization (Lewis and Jones 2014), indicating that it experienced metasomatism on its parent body. However, due to the very limited amount of data for chlorine concentrations in LL3 ordinary chondrites (Chainpur—190 ppm—Goles et al. 1967; and Parnallee—200 ppm—Sharp et al. 2013), it is not possible to establish whether the bulk chlorine concentration of Parnallee is anomalously high. One possible explanation for the low δ^{37}Cl values is that condensation of NaCl in the solar nebula was kinetically impeded. A fraction of the HCl hydrate, then forming in a cold region of the nebula at ∼140–160 K, would be highly fractionated (Schauble and Sharp 2011). If this hydrate was removed from the system, it would leave a residual HCl gas that was depleted in ^{37}Cl and could have been incorporated into Parnallee components. An alternative is that the Parnallee parent body contained light pore waters similar to those that have been measured on Earth, as a result of preferential incorporation of ^{37}Cl into early formed phyllosilicates (Ransom et al. 1995; Godon et al. 2004). However, neither of these explanations is completely satisfactory.

Carbonaceous chondrites that have undergone aqueous alteration, including Orgueil (CI1) and Murray (CM2), show a wider range of δ^{37}Cl values and internal heterogeneity compared with the type 3 chondrites. Sharp et al. (2013) attributed this to variable pore water isotopic compositions, although terrestrial contamination, especially in Orgueil, cannot be ruled out. Metamorphosed ordinary chondrites, i.e. petrologic types 4–6, show no systematic variations. An increase in δ^{37}Cl of $\sim$1‰ between EH3 Qingzhen and two EL6 chondrites, Eagle and Yilmia, could be interpreted as preferential degassing of the lighter isotope during metamorphic heating (Sharp et al. 2013). However, overall it appears that neither aqueous alteration nor metamorphism affected δ^{37}Cl values of bulk chondrites significantly. The Zag H3-6 regolith breccia is unusual in that it contains extraterrestrial halite. Thermal ionization mass spectrometry analyses of chlorine isotopes in halite and water-soluble extracts from Zag showed light values of δ^{37}Cl, −1.4‰ to −2.8‰ (Bridges et al. 2004). Bulk chondrite values for Zag of structurally-bound chlorine (−0.71‰) and water-soluble chlorine (−1.75‰) are consistent with these measurements (Sharp et al. 2013). The halite is probably clastic and possibly exogenous. Proposed exogenous sources could be from comets or ancient cryovolcanoes on, for example, asteroid 1 Ceres (Fries et al. 2013; Zolensky 2015), similar to those that occur today on the Saturnian moon Enceladus (Bridges et al. 2004; Zolensky et al. 2013; Yurimoto et al. 2014; see Chap. 17 (Hand 2018)).

A few SIMS measurements of chlorine isotopes have been made on individual mineral grains in chondrites. Sharp et al. (2007) analyzed sodalite in the Allende CV3 chondrite and measured an average δ^{37}Cl value of -1.3 ± 0.6‰, significantly lighter than average bulk chondrites, which they suggested to be the result of equilibrium fractionation between sodalite and NaCl when sodalite formed in the CV parent body. SIMS measurements of δ^{37}Cl in apatite show considerable variability. The reason for this is not clear. δ^{37}Cl in apatite from the Chelyabinsk LL5 chondrite ranges from −4‰ to +7‰, although the lower values are suspected to reflect contamination (Taylor et al. 2014).

15.7 Halogen Short-Lived Radioisotopes—Radiometric Dating of Early Solar System Processes

The halogens I and chlorine play a key role in two different short-lived radioisotope decay systems that are important for dating early solar system processes. The I–Xe system is a well-established method for dating processes ranging from the formation of chondrules to secondary alteration processes on asteroidal parent bodies (Swindle and Podosek 1988; Brazzle et al. 1999; Gilmour et al. 2006). The chlorine-S system has only relatively recently become an isotopic system of interest for understanding early solar system processes and has been applied in a limited number of studies to date (Lin et al. 2005; Turner et al. 2013).

15.7.1 I–Xe System as an Early Solar System Chronometer

Among the many short-lived radioisotope systems that have been used for the dating of early solar system processes, the I–Xe system is one of the most well established (Jeffery and Reynolds 1961; Reynolds 1963; Swindle and Podosek 1988; Gilmour et al. 2006) and has been applied successfully to a number of important cosmochemical problems. Live ^{129}I, with a half-life of 15.7 million years, formed in supernovae and was incorporated into solid materials that formed in a variety of early solar system environments. As a result of the β-decay of ^{129}I, the stable daughter isotope ^{129}Xe is produced in I-bearing sites. Assuming that no Xe was lost after isotopic closure of the system, the amount of excess radiogenic ^{129}Xe (^{129}Xe*) is used to determine the initial ^{129}I/^{127}I ratio when isotopic closure occurred. The ratio of the parent to daughter isotopes is preserved in both whole rock samples and in mineral separates from meteorites. The measured values of the initial I isotopic ratios in different meteorite samples form the basis of I–Xe dating.

Details of the I–Xe dating technique are provided in Swindle and Podosek (1988) and Gilmour et al. (2006). To determine the (^{129}I/^{127}I) ratio, samples are irradiated by neutrons in a reactor, together with a meteorite sample of known age (Nichols et al. 1994). This process converts a fraction of the ^{127}I to ^{128}Xe [^{127}I (n, $\gamma\beta$) $\rightarrow$ ^{128}Xe]. After irradiation, stepwise pyrolysis is used to release correlated quantities of two I-derived Xe isotopes (^{129}Xe* and ^{128*}Xe*) that are measured by ion counting mass spectrometry (Hohenberg 1980). A comparison of the slopes of the isochrons with the sample of known age (usually the Shallowater aubrite or Bjurböle L4 ordinary chondrite) provides the relative I–Xe age. Isochron diagrams are typically plotted using the ratio of ^{129}Xe to a Xe isotope, such as ^{130}Xe or ^{132}Xe, that is not produced in the irradiation, against the ratio of ^{128}Xe to that same isotope. The data points will define an I–Xe isochron (a straight line) if the ^{128}Xe* and ^{129}Xe* are both derived from I of a uniform isotopic composition. The slope of the isochron is proportional to the ^{129}I/^{127}I ratio at the last time the Xe isotopes were in equilibrium (Swindle and Podosek 1988). The I–Xe isochron represents a two-component mixture of trapped and I-derived Xe, with the trapped Xe component, typically of "planetary" composition, constrained to the lower end of this isochron (Lavielle and Marti 1992). The differences in isochron slopes between (^{129}Xe*/^{128}Xe*)$_{\text{sample}}$ and that of the standard (^{129}Xe*/^{128*}Xe*)$_{\text{standard}}$ are used to calculate the age of the sample. The Shallowater aubrite or Bjurböle L4 ordinary chondrite are typically used as the reference standards, with Bjurböle being 460,000 years older than Shallowater (Brazzle et al. 1999). Using the Shallowater standard:

$$\Delta t_{\text{sample}-\text{Shallowater}}(\text{Ma}) = 1/\lambda \times \ln\left[\left(^{129}\text{I}/^{127}\text{I}\right)_{\text{Shallowater}} \Big/ \left(^{129}\text{I}/^{127}\text{I}\right)_{\text{sample}}\right]$$

where $\lambda = \ln 2/15.7$ is the ^{129}I decay constant. Negative values correspond to older ages than Shallowater, and positive values to younger ages.

Petrologic evidence from chondrites (e.g., Sect. 15.8.1.4) suggests that most discrete halogen-bearing phases were formed by secondary alteration processes that typically involved an aqueous fluid (see Krot et al. 2006 for a recent review; see also Brearley and Krot 2013). These processes appear to concentrate halogens, which are present in low abundances in chondrites, into specific phases due to their mobility in fluids. For example, the major carrier phase for I in CV chondrites is secondary sodalite. Iodine–Xe chronometry has been used with some success to date secondary alteration events in chondrites with a resolution of a few hundred thousand years between the closure times of different mineral phases from the same meteorite (e.g., Swindle 1998; Brazzle et al. 1999; Pravdivtseva et al. 2001, 2003a, b). However, as discussed by Krot et al. (2006), successful I–Xe dating of secondary alteration events requires careful sample selection and preparation, combined with detailed petrologic analysis (e.g., Krot et al. 1999) so that the exact phases that are being dated are properly constrained.

15.7.2 *Decay of Short-Lived ^{36}Cl as an Early Solar System Chronometer*

The short-lived radioisotope ^{36}Cl has a half-life of 3×10^5 years and undergoes decay to ^{36}Ar (98%) and ^{36}S (2%). The presence of ^{36}Cl in early solar system materials at their time of formation can be inferred by a correlation between the chlorine content of the host phases and the presence of excess ^{36}Ar or ^{36}S in them. Several studies, using high precision ion microprobe analyses, have measured excess ^{36}Cl in sodalite ($Na_8Al_6Si_6O_{24}Cl_2$) and wadalite ($Ca_6Al_5Si_2O_{16}Cl_3$) from CAIs and chondrules in the Allende (CV3) and Ningqiang (anomalous carbonaceous) chondrites (Lin et al. 2005; Hsu et al. 2006; Ushikubo et al. 2007; Jacobsen et al. 2009, 2011; Wasserburg et al. 2011). Measurement of excess ^{36}Ar has been more elusive, but Turner et al. (2013) demonstrated the presence of ^{36}Ar, unambiguously derived from ^{36}Cl, in sodalite within the "Pink Angel" refractory inclusion in Allende. There is general agreement from these studies that sodalite and wadalite (see Sect. "Sodalite") formed about 3–7 million years after the solidification of the host CAIs, during a period of fluid mobility on the chondrite parent bodies.

Although the ^{36}Cl isotopic system has the potential as a chronometer to date the formation of chlorine-rich phases, this system has not been used extensively, because only a limited number of studies have shown correlations between excess ^{36}S and ^{35}Cl/^{34}S, and the calculated initial ^{36}Cl/^{35}Cl ratios vary widely. Decoupling of ^{36}Cl–^{36}S abundances from ^{26}Al–^{26}Mg systematics indicates different production mechanisms for the two short-lived radioisotopes, ^{36}Cl and ^{26}Al. The mechanism for production of ^{36}Cl is inferred to be neutron irradiation of a chlorine-rich fluid on the chondrite parent body, in an optically thin region of the protoplanetary disk, and while the Sun was in its T-Tauri stage (Wasserburg et al. 2011; Jacobsen et al. 2011; Turner et al. 2013).

15.8 Carriers of Halogens in Chondritic Meteorites and Formation Mechanisms

Numerous studies of chondritic meteorites have identified a limited number of distinct halogen-bearing phases, particularly F- and chlorine-bearing minerals. The carriers of the less abundant halogens, Br and I, are more poorly constrained, but are assumed, in some cases, to be the same as the carriers of chlorine and F. A tabulation of halogen-bearing phases reported in chondritic meteorites is presented in Table 15.3, and includes silicates (sodalite, wadalite, adrianite, scapolite, fluor-richterite, fluorphlogopite), aluminates (mayenite), phosphates (apatite), halides (halite, sylvite), sulfides (djerfisherite), and oxides (akaganéite) (see also Mi and Pan 2018). In addition, halogens, notably chlorine, are also found in the glass component of chondrules in some chondrites, particularly the enstatite chondrites. As discussed earlier, chlorine is by far the most abundant halogen in chondritic

Table 15.3 Compilation of halogen-bearing minerals in chondritic meteorites

Mineral	Formula	Meteorite group
Silicates with halogens as major elements		
Sodalite	$Na_4Al_3Si_3O_{12}Cl$	CV, CO, OC
Wadalite	$Ca_6Al_5Si_2O_{16}Cl_3$	CV
Adrianite	$Ca_{12}(Al_4Mg_3Si_7)O_{32}Cl_6$	CV
Scapolite	$Na_4A1_3Si_9O_{24}Cl$	OC
Fluor-richterite	$Na_2Ca(Mg,Fe)_5Si_8O_{22}F_2$	EC
Fluorphlogopite	$KMg_3(Si_3Al)O_{10}F_2$	EC
Chlorine-bearing chondrule glass		EC
Silicates with halogens as minor elements		
Magnesian edenite	$NaCa_2Mg_5(Si_7Al)O_{22}(F,Cl,OH)_2$	R
Ferri-magnesiohornblende	$Ca_2Mg_4Al_{0.75}Fe^{3+}_{0.25}(Si_7Al)O_{22}(F,Cl,OH)_2$	R
Phlogopite	$KMg_3(Si_3Al)O_{10}(OH,Cl,F)_2$	R
Smectite*	$(Na_{1.2}K_{0.2}Ca_{0.2})(Mg_{1.5}Fe_{0.8}Al_{0.5})(Si_{7.3}Al_{0.7})O_{22}(OH,Cl)_4$	OC
Aluminates		
Chlormayenite	$Ca_{12}Al_{14}O_{32}Cl_2$	CV
Sulfides		
Djerfisherite	$K_6Na_9(Fe,Cu)_{24}S_{26}Cl$	EC
Phosphates		
Apatite	$Ca_5(PO_4)_3(F,Cl,OH)$	CO
Halides		
Halite	NaCl	CM, OC
Lawrencite	$FeCl_2$	EC
Sylvite	KCl	CM, OC

Notes: *approximate composition based on analytical TEM analysis of smectite from Bishunpur reported by Alexander et al. (2007)

meteorites, but it is still only present at levels of tens to hundreds of ppm in bulk samples. Therefore, chlorine-rich phases are at best accessory or trace phases in chondrites. In the case of water-soluble halides, the rarity of descriptions of these minerals in chondrites may also be partially attributable to the common practice of preparing petrographic polished thin sections using water. In addition, as noted earlier, dissolution and loss of chlorides during extended curation under less than ideal conditions (i.e., humid atmosphere) may also have occurred. Therefore, the dearth of chlorides in most chondrites may not be a true reflection of their preterrestrial occurrence and distribution.

In addition to these specific, identifiable halogen-rich minerals in chondritic meteorites, halogens are also clearly present at low concentrations in several other phases, for example in presolar grains and organic matter (soluble and insoluble) that are distributed in variable concentrations throughout the different chondrite groups. Below we discuss the known mineralogical carriers of halogens in each of the chondrite groups, and finally discuss evidence for carriers of halogens that may be common to all the different groups, including presolar grains and organic material. We note here that this summary is not intended to be an exhaustive overview of halogen measurements of all the different components of chondrites, but just focuses on identified mineralogical carriers of halogens. There are also measurements of halogen contents in chondrules and fine-grained rims in ordinary chondrites (e.g., Grossman and Wasson 1987; Swindle et al. 1991; Grossman et al. 2000), for example, which we do not discuss.

15.8.1 Halogen-Bearing Minerals in Carbonaceous Chondrites

Carbonaceous chondrites represent a wide range of alteration conditions, covering the entire scale of the petrologic type classification scheme from type 1 to type 6 (Table 15.1: Van Schmus and Wood 1967; Huss et al. 2006). Within this scheme, type 3.0 chondrites represent the most primitive, unaltered, solar nebular material. Types 3.0 to 2 to 1 represent progressive aqueous alteration, and types 3.0 to 4 to 5 to 6 represent progressive thermal metamorphism. Within type 3 chondrites, progressive metamorphism is indicated by subtypes 3.1, 3.2, 3.3 etc. for the CO and CV groups. The CI carbonaceous chondrites are the most chemically primitive of all known meteorites, with elemental abundances that closely match those of the solar photosphere. Paradoxically, they have also experienced the most extensive aqueous alteration of all chondrites and consequently have the highest water contents (e.g., Cloëz 1864; Pisani 1864; Wiik 1956; Alexander et al. 2013). All CI chondrites are petrologic type 1, which represents essentially complete aqueous alteration of original anhydrous phases. The CM and CR chondrite groups are mostly type 2, with some members classified as type 1. These have experienced significant aqueous alteration that has modified the primary mineralogical

characteristics to varying degrees. Halogen-bearing phases in type 1 and 2 carbonaceous chondrites are discussed below in Sects. 15.8.1.1–15.8.1.4.

The type 3 meteorites, represented by the CO, CV, and rare CK chondrites, have experienced varying degrees of aqueous alteration at low temperatures, as well as mild to moderate thermal metamorphism, and interaction with aqueous fluids (metasomatism) (see Huss et al. 2006; Brearley 2014; Brearley and Krot 2013). Most members of the CK chondrite group show the effects of metamorphism and are petrologic type 4, 5, and 6. Even though the carbonaceous chondrites represent a wide range of alteration conditions, including a high degree of aqueous activity, it is surprising that they contain a limited range of halogen-bearing minerals (with the exception of the CV group). The halogen-bearing mineralogy of type 3 and higher petrologic type carbonaceous chondrites is presented in Sects. 15.8.2.1–15.8.2.5.

15.8.1.1 CI Carbonaceous Chondrites

The first known member of the CI chondrite group, Alais, was recognized and described more than 200 years ago (Monge et al. 1806; Thénard 1806). The presence of hydrated minerals was first described in the CI chondrite Orgueil in 1864 (Pisani 1864). CI chondrites represent the archetypal petrologic type 1 meteorites, because they exhibit the most advanced stage of aqueous alteration of any chondrite. They contain almost no evidence of primary anhydrous mineral phases, consisting instead of a variety of minerals including phyllosilicates, oxides, carbonates, sulfates, etc. that are the product of aqueous alteration (Zolensky and McSween 1988; Brearley 2006a). Although these highly-altered meteorites are relatively rare, they can be distinguished from type 1 CM and CR chondrites, based on their mineralogy, chemistry, and O-isotopic composition.

Despite the fact that the CI chondrites contain the highest chlorine contents of any chondrite group (see Sect. 15.4.2.1), there is no reported evidence of any halides or other chlorine-rich phases in any CI chondrite. This is surprising given that CI chondrites contain significant concentrations of soluble salts, particularly sulfates, such as gypsum, epsomite, and bloedite (e.g., DuFresne and Anders 1962; Boström and Fredriksson 1966; Bass 1971; Fredriksson and Kerridge 1988). The carrier phases of chlorine in CI chondrites are, therefore, currently unconstrained, but chlorine could be present in low concentrations in phyllosilicate phases, substituting for hydroxyl.

15.8.1.2 CM Carbonaceous Chondrites

CM carbonaceous chondrites are a complex group of breccias that have experienced variable degrees of aqueous alteration. Most CM chondrites are petrologic type 2 meteorites, which have hydrated fine-grained matrices, as well as limited to extensive replacement of chondrules and CAIs (Zolensky and McSween 1988; Brearley 2006a). However, a significant number of type 1 CM chondrites have also

been recognized whose primary mineralogy has been entirely replaced by secondary alteration phases (Zolensky et al. 1997). The sequence of progressive alteration exhibited by the CM chondrites has been well described in a number of different studies (Browning et al. 1996; Rubin et al. 2007; Howard et al. 2011, 2015). This alteration has resulted in the formation of a range of secondary phases, including phyllosilicates, carbonates, oxides, sulfates, sulfides, and oxysulfides (e.g., tochilinite) (Zolensky and McSween 1988; Brearley 2006a; Howard et al. 2009, 2011).

To date, the only documented occurrence of chlorine-rich phases in CM chondrites is the presence of rare halite and sylvite as small grains ($\sim$0.2 μm) identified by TEM in the matrix of the Murchison CM2 chondrite (Barber 1981). As discussed earlier, the apparent absence of halides in CM chondrites may be related to the low chlorine concentration (compared with CI chondrites) that is apparent in bulk analyses. It seems unlikely that this difference is a depletion in CM chondrites due to leaching by aqueous alteration, because the more highly-altered CI chondrites have bulk chlorine abundances that appear to match reasonably well with measurements from the Sun. As noted earlier, there is a dearth of good chlorine measurements for CM chondrites, so it is difficult to evaluate if there is evidence of a correlation between the degree of alteration and the bulk chlorine concentration that might indicate mobilization of chlorine during aqueous alteration. It is impossible at this point to constrain whether halides are the only carrier of chlorine in CM chondrites, or whether chlorine is also disseminated at low concentrations within the matrix, perhaps substituting for hydroxyl in phyllosilicates.

15.8.1.3 CR Carbonaceous Chondrites

The CR carbonaceous chondrite group includes some members that carry an extremely pristine record of early solar system processes (Weisberg et al. 1993; Krot et al. 2002). Other members of the group have experienced variable degrees of aqueous alteration, from very minimal to complete hydration (Weisberg et al. 1993; Weisberg and Huber 2007; Abreu and Brearley 2010; Schrader et al. 2011; Alexander et al. 2013; Harju et al. 2014; Howard et al. 2015). Most CR chondrites are petrologic type 2, although Abreu and Brearley (2010) suggested that some may actually be petrologic type 3.0 meteorites, with limited evidence of aqueous alteration. However, this view has been challenged by more recent studies which demonstrate that, despite retaining a very pristine record of solar system processes, these type 3.0 meteorites have a water content that is comparable to that of CR chondrites, which show more extensive evidence of aqueous alteration (Bonal et al. 2013; Alexander et al. 2013; Le Guillou and Brearley 2014; Howard et al. 2015). Rare, completely altered, petrologic type 1 members of the CR group have also been identified (Weisberg and Huber 2007).

There is a dearth of evidence of distinct halogen-bearing phases or halogen-enriched components, such as chondrule mesostasis in CR chondrites. Calcium phosphates have been described forming as a result of alteration of

phosphorus-bearing chondrule glass, but these phosphates appear to be F and chlorine-free (Burger and Brearley 2005; Brearley and Burger 2009).

15.8.1.4 Possible Role of Chlorine-Rich Fluids in the Aqueous Alteration of CI, CM, and CR Chondrites

The CI, CM, and CR chondrites have experienced interaction with a water-rich fluid at relatively low temperatures (0–150 °C) (see Zolensky et al. 1993; Brearley 2006a), a process which has resulted in the formation of variable amounts of phyllosilicates, as the dominant alteration products. We, therefore, consider the possible role of chlorine-bearing fluids for these meteorites together. Although the occurrence of distinct chlorine-rich phases in CI, CM, and CR chondrites is extremely rare, chloride-bearing fluids may, nevertheless, have played a role in the aqueous alteration of these meteorites. As discussed in Sect. 15.2.1, Zolotov and Mironenko (2007) have suggested that chlorine may have been accreted into the parent bodies of the carbonaceous chondrites as $HCl{\cdot}3H_2O$. Following accretion, temperatures progressively increased as a result of heat that was released from the decay of short-lived radionuclides, particularly ^{26}Al. The H_2O–HCl eutectic occurs at ~186 K and, although the amount of the eutectic solution is limited, it is concentrated and so will be reactive with minerals. Observations from CM chondrites suggest that the initial conditions of alteration, particularly inside chondrules, were acidic (Brearley 2006b) and resulted in the early alteration of a SiO_2-rich chondrule mesostasis glass by these low pH fluids. However, as temperatures rose, and more ice melted, the pH would have decreased as the solutions became more diluted, and as amorphous materials in matrices reacted and neutralized the solutions, by absorbtion of hydrogen ions. Hence, the solutions would move progressively to more alkaline conditions that favored precipitation of carbonates that occur widely in CI, CM, and CR chondrites (e.g., Fredriksson and Kerridge 1988; Johnson and Prinz 1993; Benedix et al. 2003). The extreme rarity of discrete chlorine-rich phases in these chondrites indicates that chlorine is distributed at low concentrations among the alteration products. One possibility is that chlorine is hosted in phyllosilicates, such as serpentine and saponite, which are the most common alteration products in these meteorites. Serpentine does not seem to readily accommodate high levels of chlorine by substitution for OH^-, but incorporation of low concentrations is certainly viable (Miura et al. 1981; Anselmi et al. 2000). Alternatively, as demonstrated by Brearley et al. (2007) for terrestrial ocean floor serpentinites, chlorine can be readily incorporated into the cores of chrysotile nanotubes. Chrysotile occurs commonly in the matrices of CM chondrites (e.g., Barber 1981; Mackinnon 1980; Zega et al. 2006), and so is certainly a potential carrier of chlorine in these meteorites. However, the concentrations are clearly too low to detect by conventional analytical electron microscopy techniques.

The presence of minor halite and sylvite in CM chondrites indicates that at late stages in the alteration of these meteorites, concentration of halogens in the fluid

phase occurred resulting in the formation of brines, at least locally. This is consistent with trace element analyses of carbonates (calcite and dolomite) in CI and CM chondrites using the ion microprobe (Riciputi et al. 1994), which show that the carbonates precipitated from brines with elevated concentrations of trace elements. This process presumably happened during the waning stages of aqueous alteration as water was consumed by reactions producing hydrous phases from primary anhydrous silicates.

15.8.2 Halogen-Bearing Minerals in CV, CO, CK and Other Carbonaceous Chondrites

15.8.2.1 Halogen-Bearing Minerals in CV Chondrites

The CV chondrites consist of two major groups, the reduced (CV_R) and the oxidized (CV_{Ox}) groups, which are distinguished by their modal metal/magnetite ratios and Ni contents of metal and sulfides (McSween 1977a). In the reduced CV chondrites, metallic Fe,Ni metal is the common opaque phase, whereas in the oxidized CV chondrites, magnetite dominates. The oxidized CV chondrites are further divided into two subgroups (Weisberg et al. 1997), the Allende (CV_{OxA}) subgroup and the Bali (CV_{OxB}) subgroup, which differ in the degree of secondary alteration that they have experienced. The effects of secondary alteration in these two subgroups have been recently reviewed by Brearley and Krot (2013) and will not be discussed in detail here. Mineralogically, CV_R and CV_{OxB} chondrites contain only minor abundances of distinct halogen-bearing phases, whereas the CV_{OxA} chondrites exhibit the most diverse range of halogen-bearing minerals of any of the chondrite groups. The CV_{OxB} chondrites (e.g., Kaba, Bali) experienced moderate degrees of alteration and minor thermal metamorphism. This diversity can be attributed to the action of metasomatic processes that have affected the components of these meteorites to different degrees (see Brearley and Krot 2013 for a detailed overview).

The CV_{OxA} subgroup of the oxidized CV chondrites have experienced extensive alkali-Fe-halogen metasomatism that affected all the primary components (CAIs, chondrules, matrix) to different degrees (Krot et al. 1995). The exact location and nature of these metasomatic processes remains a subject of considerable debate; both nebular and asteroidal locations have been proposed (Krot et al. 1995; Brearley 2014). However, there is an increasing body of evidence that supports the view that the alteration occurred after accretion within a parent body environment and involved an aqueous fluid phase that catalyzed alteration reactions and acted as a mass transport agent. The conditions under which the metasomatic alteration occurred are not fully constrained, but are generally considered to have taken place in the temperature range $\sim$400–600 °C at pressures of a few tens of bars.

Sodalite

The most widely recognized and documented halogen-bearing phase formed by secondary alteration processes in the CV_{OxA} chondrites is the feldspathoid, sodalite ($Na_4Al_3Si_3O_{12}Cl$), commonly associated with a wide variety of other secondary alteration minerals (see Brearley and Krot 2013 for details). This includes the rarer Ca-endmember equivalent of sodalite, wadalite ($Ca_6Al_5Si_2O_{16}Cl_3$). The development of sodalite is most commonly observed in CAIs and has been documented in a large number of studies, particularly in the heavily-studied CV3 chondrite Allende. These studies have demonstrated that the degree of alteration of CAIs is variable and depends on the primary mineralogy, texture, and size of the inclusions. Summaries of the classification and characteristics of different types of CAIs in carbonaceous chondrites, including CV chondrites, are reviewed in Brearley and Jones (1998) and MacPherson (2014) and will not be discussed in detail here. Fine-grained inclusions in Allende are typically completely replaced by secondary alteration products, whereas type A and type B inclusions show variable degrees of replacement. Fluffy type A inclusions, that consist of aggregates of nodules, often show quite extensive replacement, whereas compact type A inclusions are typically less altered, probably because they are less porous. Coarse-grained, large type B CAIs generally show the lowest degrees of secondary alteration with replacement by secondary phases occurring dominantly on the periphery of the inclusions with more limited evidence of alteration in inclusion interiors.

A zoned distribution of Na- and chlorine-bearing minerals is a common feature of CAIs in $CV3_{OxA}$ chondrites and has been described in type A and B inclusions and in fine-grained inclusions. In general, in CAIs that show the lowest degrees of alteration (Fig. 15.6), sodalite occurs associated with nepheline in just the outer part of the inclusions. At more advanced stages of alteration, the zone of nepheline and sodalite increases progressively in width (Fig. 15.7). In heavily-altered inclusions, nepheline and sodalite occur throughout the inclusions.

Evidence for direct replacement of primary CAI phases by sodalite is rare. Instead, textural evidence indicates that the formation of sodalite is a complex process that involves several intermediate reaction steps and probably represents the final stage of alteration of CAIs. Sodalite typically occurs as irregularly-shaped grains, ranging from <10 μm to ~50 μm in size, that are intergrown commonly with nepheline, but also with other secondary minerals, such as grossular, and relict primary CAI minerals (Fig. 15.8). In type A CAIs, whose primary mineralogy is dominated by melilite (Åk-rich), Al–Ti diopside, and spinel, the formation of sodalite and nepheline results from the breakdown of melilite by a sequence of reactions that initially forms a rim of grossular adjacent to melilite, which is replaced by dmisteinbergite (hexagonal anorthite) (Fig. 15.8b–d) (Fintor et al. 2014; Brearley et al. 2014). The final stage of alteration is the replacement of dmisteinbergite by a complex intergrowth of nepheline and sodalite. Textural evidence in CAIs suggests that sodalite is probably the last phase to form based on the fact that it infills cracks and typically embays grains of nepheline, suggesting that it may actually be a replacement product of nepheline.

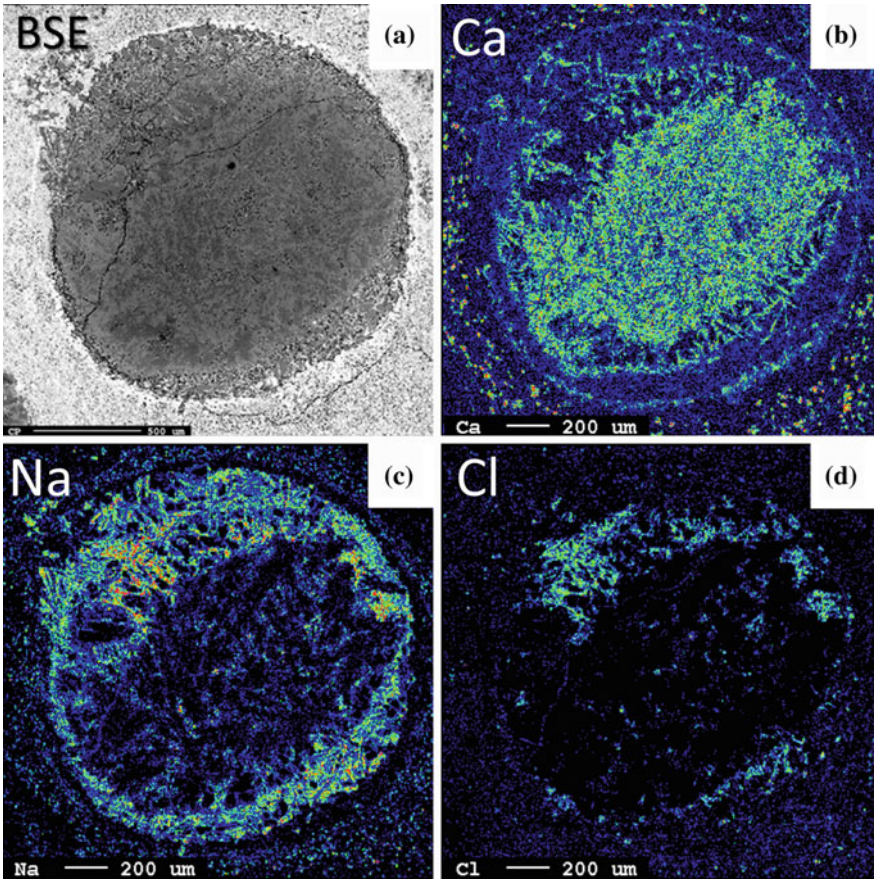

Fig. 15.6 Backscattered electron (BSE) image and X-ray maps of a moderately-altered type B inclusion from the Allende CV_{OxA} chondrite. The inclusion is somewhat unusual because it contains aluminous enstatite, rather than diopside around its peripheral region. **a** BSE image of type B inclusion, consisting of melilite, anorthite, Al-rich enstatite, and spinel that has undergone alteration around its periphery to a mixture of fine-grained reaction products, including nepheline and sodalite. **b** Calcium X-ray map showing that in the altered region of the CAI, Ca has been lost as a result of extensive replacement of melilite and anorthite (laths along the lower right side of the altered inclusion). However, in the interior of the inclusion unaltered melilite is still present. Nodules of Ca–Fe pyroxenes and andradite are present in the matrix around the inclusion. **c** Sodium X-ray maps showing that the altered regions of the inclusion are highly enriched in Na, due to the presence of fine-grained nepheline and sodalite. **d** Chlorine X-ray maps showing that enrichment in Na is also locally correlated with higher chlorine contents due to the presence of sodalite. Development of sodalite is, however, much more localized than nepheline. Rare, small grains of sodalite are also present in the matrix surrounding the altered inclusion, but are much less common than nepheline (**c**)

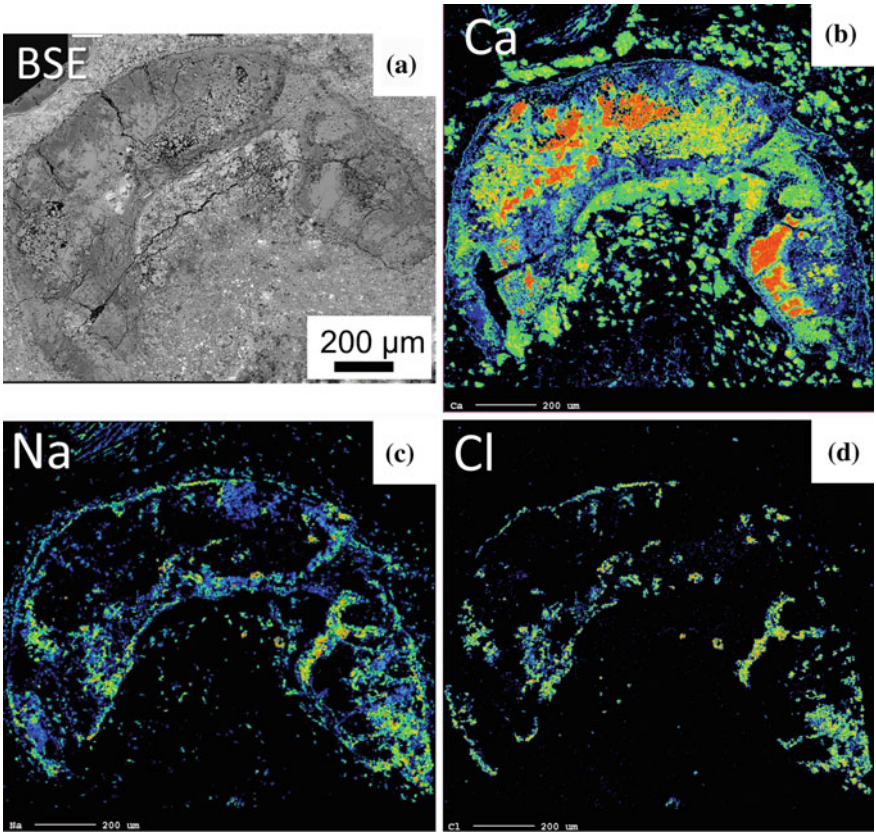

Fig. 15.7 Backscattered electron image and X-ray maps of a heavily-altered, arcuate, compact type A inclusion from the Allende CV_{OxA} chondrite. **a** BSE image of compact type A inclusion, consisting of melilite, Al–Ti pyroxene, and spinel, that has undergone heavy alteration around its periphery and along fractures through the inclusion. Melilite in the inclusion has undergone extensive alteration to a mixture of fine-grained reaction products including grossular, dmisteinbergite, nepheline, and sodalite. **b** Ca X-ray map showing that extensive redistribution of Ca has occurred in the alteration process. In the inclusion, unaltered melilite is *bright red* and the *bright green* regions are unaltered regions of Al–Ti diopside. The *green* regions outside the inclusion are nodules of secondary Ca–Fe pyroxenes and andradite formed by Ca that has been leached from the inclusion. The *blue mottled* regions on the exterior of the inclusion are regions of secondary alteration products, dominantly fine-grained nepheline and sodalite intergrown with secondary grossular, dmisteinbergite, and relict primary melilite, Al–Ti diopside, and spinel. **c** Sodium X-ray maps showing that the altered regions of the inclusion along the periphery, and along fractures, are highly enriched in Na, due to the presence of fine-grained nepheline and sodalite. **d** Chlorine X-ray maps showing that enrichment in Na is also correlated with higher chlorine contents due to the presence of sodalite. Development of sodalite is much more extensive than in the type B inclusion shown in Fig. 15.6. Rare, small grains of sodalite are also present in the matrix surrounding the altered inclusion, but are much less common than nepheline (**c**). Image courtesy of Rena Ford

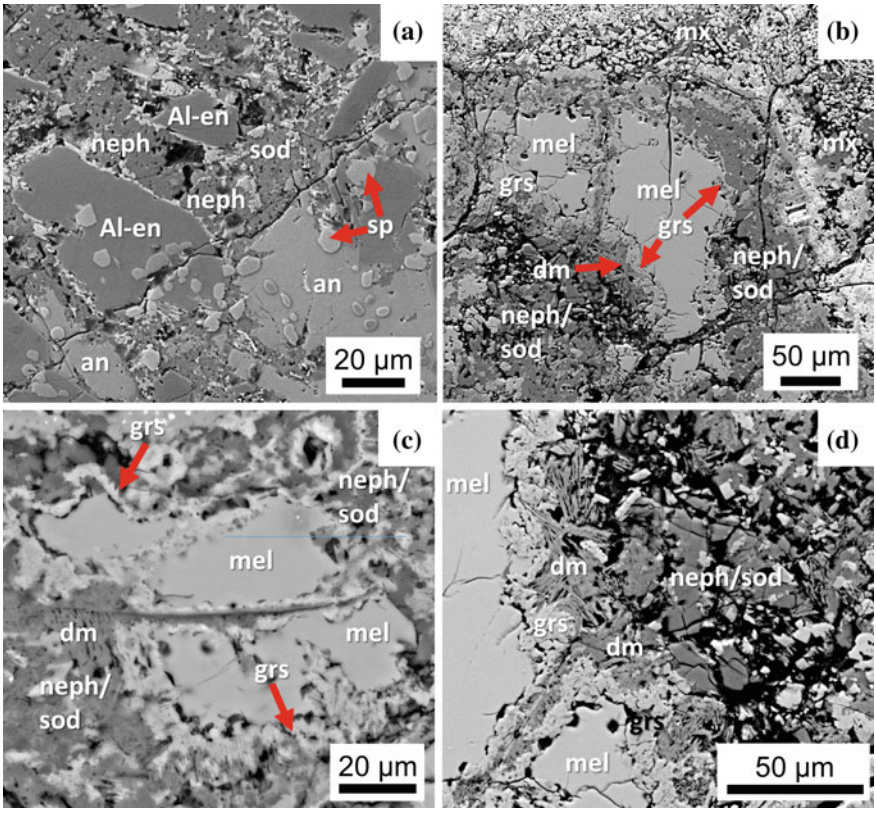

Fig. 15.8 Backscattered electron images showing the occurrence of sodalite in a type B and compact type A inclusion from the Allende CV_{OxA} chondrite. **a** Region of fine-grained alteration from the Allende type B inclusion shown in Fig. 15.6. Porous, fine-grained nepheline (neph) occurs intergrown with sodalite that has replaced anorthite (an). Aluminous enstatite (Al-en) and spinel (sp) are also present. **b** Closeup of alteration of melilite to sodalite in the compact type A inclusion shown in Fig. 15.7. Corroded relict islands of melilite (mel) are rimmed by a thin layer of grossular (grs—*arrowed*) that is overgrown locally by dmisteinbergite (dm—*arrowed*). The outer part of the melilite grains is replaced by a fine-grained intergrowth of porous nepheline and sodalite (neph/sod). The matrix (mx) outside the CAI consists of elongate, ferroan olivine intergrown locally with nepheline, rare sodalite, Ca–Fe pyroxenes (Hd–Di), and andradite garnet. **c** Closeup BSE image showing sequential replacement of melilite (mel) by a grossular (grs) rim, which is overgrown by fibrous dmisteinbergite (dm) and finally a porous, fine-grained intergrowth of nepheline and sodalite. **d** Closeup BSE image of melilite being replaced by grossular (grs), fibrous dmisteinbergite (dm), and finally intergrown nepheline and sodalite (neph/sodalite) on the outer part of the primary melilite grain

Sodalite is the only chlorine-bearing phase that has been identified in chondrules in CV chondrites. It occurs exclusively in CV_{OxA} meteorites and has been extensively documented in chondrules in Allende by Lumpkin (1980) and Kimura and Ikeda (1995). Glassy mesostasis and plagioclase have been largely replaced by fine-grained (≤ 10 μm) nepheline and sodalite (Kimura and Ikeda 1995), with

nepheline being the dominant phase in most chondrules. Nepheline associated with sodalite is present in 90% of the chondrules studied by Kimura and Ikeda (1995) with the remainder containing just nepheline as the Na-bearing phase. Several other minor phases occur intergrown with the nepheline and sodalite, including hedenbergite, andradite, grossular, kirschsteinite, and wollastonite.

In Allende, the degree of alteration of glassy chondrule mesostasis by secondary phases is variable, ranging from partial, where unaltered mesostasis is only present in the core of the chondrules, to complete, where all the primary mesostasis has been replaced. Kimura and Ikeda (1995) attributed this variability to differences in the primary mineralogy, texture, and chemical composition of mesostasis in different chondrules. In some chondrules, Na and Ca show a zoned distribution, with Na typically concentrated in the outer parts of the chondrules and Ca in the interior, similar to the distribution of these elements in altered CAIs in Allende. Compositionally, the alteration of chondrule mesostasis involved the introduction of Na, K, Fe, and chlorine into, and the removal of Si and Ca, from the chondrules (Ikeda and Kimura 1995; Krot et al. 1998b). CV_{OxA} clasts with characteristics similar to those in Allende occur in the Mokoia $CV_{OxA/OxB}$ breccia in which chondrule mesostasis has been replaced by nepheline and sodalite. In Mokoia, this alteration has been overprinted by a second phase of alteration where phyllosilicates have replaced nepheline and sodalite (Kimura and Ikeda 1995).

An extreme example of Na-chlorine halogen metasomatism in a chondrule in Allende has been described by Wasserburg et al. (2011). This chondrule, Al3509, is a large (8 mm diameter) radially-zoned object (Fig. 15.9) that consists of a core and mantle, which each have several mineralogically- and chemically-distinct zones. None of the primary mineralogy of the object has been preserved. The core of the object has a spherulitic texture and is highly enriched in Na and chlorine contained in abundant sodalite that occurs interstitially to elongated ferroan Al-diopside or ferroan olivine (Fig. 15.10a, b). Several other zones also occur in the core and mantle that are less enriched in Na and chlorine and contain lower abundances of sodalite intergrown with a range of different secondary alteration phases. Wasserburg et al. (2011) concluded that this chondrule had undergone Fe-alkali-halogen metasomatism as a result of interaction with a fluid with the same O-isotopic composition as that which modified CAIs and other chondrules in Allende.

Sodalite is found in the matrix of Allende-like CV carbonaceous chondrites, but is comparatively rare; nepheline is the major Na-bearing phase. In Allende, for example, sodalite occurs as irregularly-shaped grains up to tens of microns in size intergrown with platy ferroan olivine grains that are the dominant constituent of the matrix.

Sodalite also occurs in so-called dark inclusions in Allende (Kurat et al. 1989; Buchanan et al. 1997; Krot et al. 1995). Dark inclusions are clasts of distinct, typically fine-grained lithologies that occur widely in both CV_{Ox} and CV_{R} chondrites and also record similar alteration processes to the host chondrite. However, in many cases, they exhibit more extensive evidence of metasomatic alteration than the host chondrites (Krot et al. 1995). In Allende, dark inclusions show evidence of at least two stages of alteration resulting from interaction with an aqueous fluid after

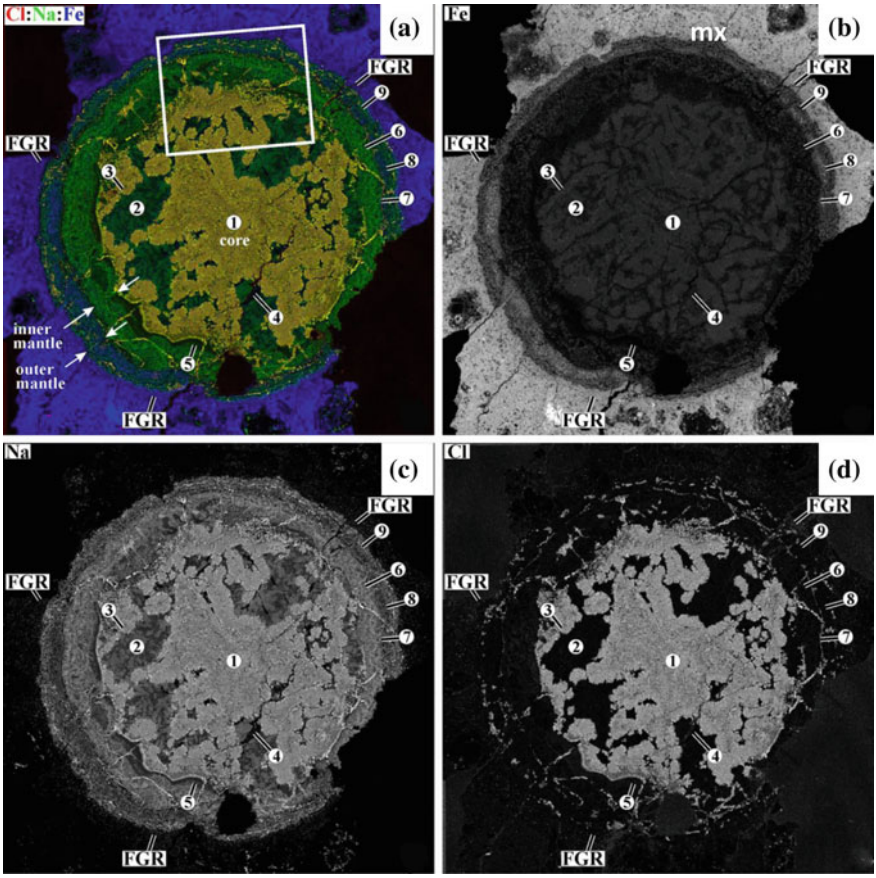

Fig. 15.9 X-ray maps of heavily metasomatized Al-rich chondrule Al3509 from the Allende CV_{OxA} chondrite (Wasserburg et al. 2011). **a** Composite chlorine (*red*), Na (*green*), and Fe (*blue*) X-ray map of Al3509, showing the significant enrichment of Na and chlorine in the object and low Fe content compared to the surrounding Allende matrix. The altered chondrule is surrounded by a fine-grained rim (FGR) and has an inner and outer mantle. Nine distinct zones of alteration with different mineral assemblages are present. The *yellow* and *green* regions of the inclusion correspond to sodalite and nepheline, respectively, demonstrating that the core of the inclusion is highly enriched in sodalite, whereas the nepheline is in the outer region of the chondrule. **b** Iron X-ray map of the chondrule demonstrating that only the mantle of the inclusions show any significant Fe content. **c** Sodium X-ray map showing the extensive enrichment in Na throughout the inclusion, particularly in the core, where sodalite is present. **d** Chlorine X-ray map showing that enrichment of chlorine is constrained to the core region of the inclusion where sodalite is present, except for some narrow veins of sodalite that extend through the mantle of the inclusion to the chondrule core

lithification and aggregation (Krot et al. 2001). Sodalite and nepheline, among other alteration phases, occur replacing primary chondrule minerals, a process that appears to have occurred in one of the alteration stages. A second alteration stage occurred after the dark inclusion was emplaced within the host Allende material,

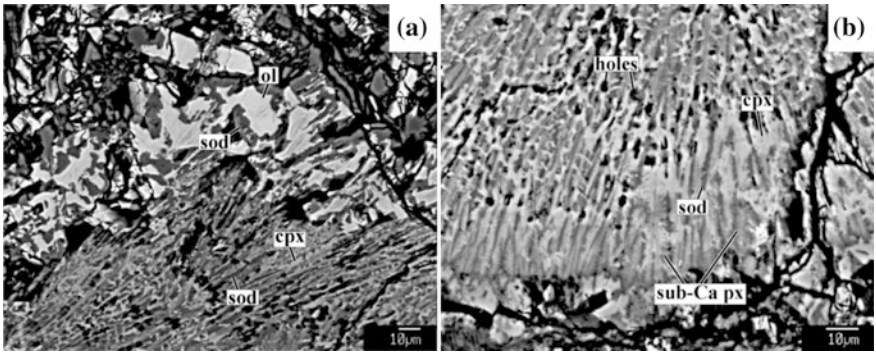

Fig. 15.10 Back-scattered electron images showing different occurrences of sodalite in metasomatized Al-rich chondrules Al3509. **a** Region of the object with a radial texture indicative of quenching that consists of skeletal crystals of sub-Ca pyroxene that has been partially replaced by ferroan Al-diopside (cpx) and interstitial sodalite. **b** Intergrowth of ferroan olivine and nepheline that have pseudomorphed the primary minerals, probably Ca pyroxene

but was dominated by the formation of Ca-bearing minerals around the periphery of the dark inclusions rather than chlorine-bearing phases (Krot et al. 2001).

Sodalite has been described in all the components of the unique carbonaceous chondrite, Ningqiang, which has affinities to the CV3 carbonaceous chondrites (Rubin et al. 1988; Lin et al. 2005; Sugita et al. 2009; Wang and Hsu 2009; Matsumoto et al. 2014). The occurrences of sodalite bear close similarities to those in the Allende CV3 chondrite. It is found replacing mesostasis in chondrules and is associated with nepheline replacing melilite in CAIs. However, the abundance of sodalite appears to be generally minor in CAIs compared with Allende (Sugita et al. 2009). Matsumoto et al. (2014) also documented the presence of sodalite in the matrix of Ningqiang, but argued that these grains did not form in situ. Instead, they suggested that the matrix sodalite originates from CAIs and chondrules that had experienced parent body metasomatic alteration, but were subsequently fragmented, disaggregated, and mixed into the matrix, probably as a result of brecciation.

Wadalite

Wadalite ($Ca_6Al_5Si_2O_{16}Cl_3$), a member of the mayenite-type ($Ca_{12}Al_{14}O_{33}$) family, has only been described relatively recently (Ishii et al. 2010) in CAIs in the Allende CV3 chondrite. Although sodalite occurs in both type A and B inclusions, wadalite appears to occur exclusively as a replacement product of primary minerals in coarse-grained, igneous type B CAIs (Fig. 15.11a, b). Mineralogically, type B inclusions are dominated by primary anorthite, Al–Ti diopside, melilite, and spinel, but only melilite and anorthite show evidence of replacement by wadalite in different textural occurrences. Wadalite, with typical grain sizes of $\sim$15 μm, coexists with secondary grossular and monticellite in regions of porous alteration at the

boundaries between anorthite and melilite grains (Fig. 15.11c). Ishii et al. (2010) also described irregular grains of wadalite intergrown with melilite and in cross-cutting veins of grossular, monticellite, and wollastonite (Fig. 15.11d). Minor amounts of nepheline and sodalite are also present in the regions of secondary alteration. However, coexisting wadalite and sodalite are very rare.

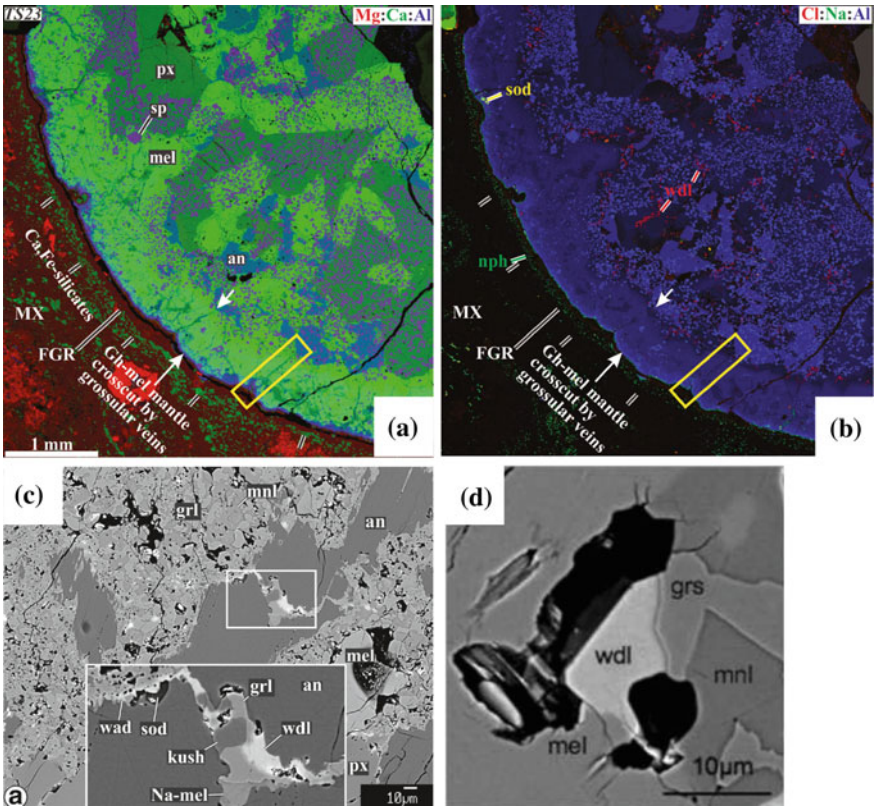

Fig. 15.11 X-ray maps and BSE images showing an example of a type B CAI TS23 from Allende. **a** A composite Mg (*red*), Ca (*blue*), and Al (*green*) X-ray map showing part of TS23 and associated matrix. The inclusion has a mantle of gehlenitic melilite that is free of other phases except minor spinel. The interior of the inclusion consists of primary melilite (mel), anorthite (an), Al–Ti diopside (px), and spinel (sp). The inclusion is surrounded by a fine-grained rim (FGR) and matrix (MX) further away from the inclusion. Ca–Fe silicates are distributed in the matrix around the inclusion and the mantle of the melilite is crosscut by veins of secondary grossular. **b** A chlorine (*red*), Na (*green*), and Al (*blue*) composite X-ray map of the same region of the inclusion. Wadalite (wdl—*red* grains) occurs exclusively in the interior of the inclusion, whereas minor sodalite (*yellow*) occurs only at the periphery of the grain. Small grains of nepheline are present within the matrix. **c** A region of secondary alteration in TS23 where melilite (mel) and anorthite (an) have been replaced by grossular (grl) and monticellite (mnl). Enlargement of the boxed region (*white*) in the lower center shows a vein of secondary wadalite (wdl), grossular, kushiroite (kush), and Na-melilite crosscutting primary anorthite (an). Minor sodalite occurs at the edge of the anorthite, associated with a small grain of wadalite. **d** A high magnification image of a region of altered melilite containing a grain of wadalite (wdl), coexisting with grossular (grs) and monticellite (mnl). **a–c** from Brearley and Krot (2013) and **d** from Ishii et al. (2010)

The distribution of Na- and chlorine-bearing minerals (nepheline, sodalite, wadalite, and Na-melilite) in Allende Type B1 CAIs appears to be strongly controlled by the composition of primary melilite. Ishii et al. (2010) found that wadalite is mainly restricted to the cores of the CAIs and replaces åkermanitic melilite and anorthite, whereas nepheline and sodalite occur dominantly in the outer regions of the CAIs replacing gehlenitic melilite and primary anorthite (Fig. 15.11a, b).

Adrianite

Adrianite, a new Si-rich mayenite-group mineral ($Ca_{12}Al_4Mg_3Si_7O_{32}Cl_6$) with the wadalite structure, has recently been described as a rare, secondary alteration phase in a CAI in Allende (Ma and Krot 2014a, b). To date, it has only been described in one igneous Type B1 inclusion in regions of fine-grained alteration in cracks between primary melilite, spinel, and Al–Ti diopside (Fig. 15.12a). The adrianite grains are small (2–6 μm) and are associated with secondary grossular, monticellite, wadalite, and hutcheonite. Like wadalite, adrianite is proposed to have formed by reaction of chlorine-rich fluids with primary anorthite, melilite, and Al–Ti diopside.

Chlormayenite

The mayenite group mineral, chlormayenite ($Ca_{12}Al_{14}O_{32}Cl_2$), occurs in an unusual krotite ($CaAl_2O_4$) rich CAI in the Northwest Africa (NWA) 1934 meteorite (Ma et al. 2011). The chlormayenite was originally named brearleyite, a name that is now discredited, following the revision of the Mayenite Supergroup in 2013. Chlormayenite is found as aggregates of very fine-grained (80–300 nm) grains that occur in veins within the krotite and is associated with gehlenitic melilite, hercynitic spinel, and perovskite (Fig. 15.12b).

Apatite

Occurrences of phosphates as potential carriers of halogens have been documented in some CV chondrites (Ebihara and Honda 1987; Rubin and Grossman 1985; Keller et al. 1994; Martin et al. 2013). However, details of their chemistry have not been investigated thoroughly, because they are typically fine-grained (<5 μm) and hard to analyze. Most occurrences of phosphates in CV3 chondrites appear to be the halogen-free phosphate, merrillite, as reported by Rubin and Grossman (1985) in the CV3 chondrites Allende and Vigarano. Merrillite is associated with secondary sulfide assemblages in these meteorites. Apatite, which appears to be halogen-free, also occurs in the CV3 chondrite Bali. Only recently has halogen-bearing apatite been reported coexisting with merrillite in Allende (Dyl et al. 2014), where it is also associated with sulfides. Ion microprobe measurements of grains of apatite show that it is F, chlorine, and OH bearing with 1.2–1.4 wt% H_2O, 6000–10,000 ppm F,

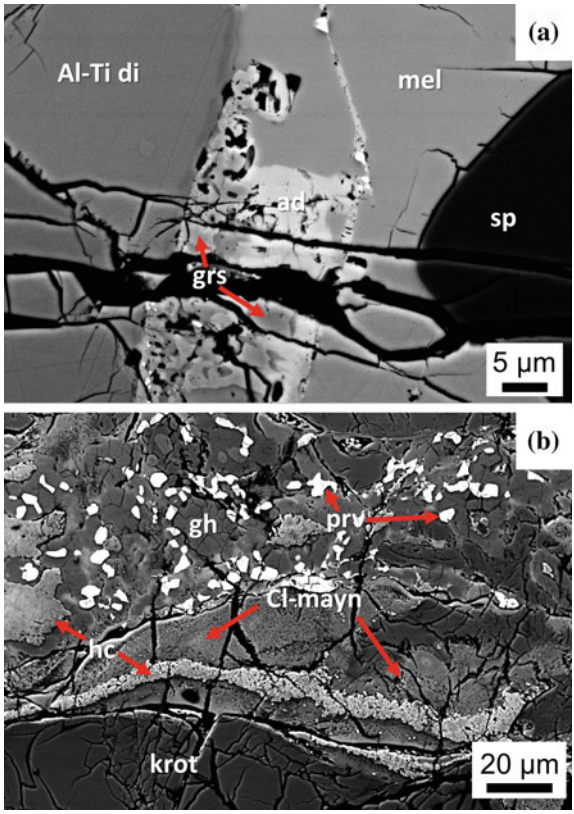

Fig. 15.12 Backscattered electron images of secondary chlorine-rich phases in CAIs in CV3 chondrites. **a** Occurrence of adrianite (ad) coexisting with grossular (grs) that are both replacing melilite. Al–Ti-diopside (Al–Ti di) and spinel (sp) show no evidence of alteration. Image courtesy of Chi Ma. Copyright California Institute of Technology. **b** BSE image showing the occurrence of chlormayenite (formerly brearleyite) in an unusual krotite-rich CAI from the NWA 1934 CV3 chondrite. Chlormayenite occurs as fine-grained masses replacing krotite (krot) in an inclusion that also contains gehlenitic melilite (gh), perovskite (pv), and hercynitic spinel (hc). Image courtesy of Chi Ma, California Institute of Technology, modified from Ma et al. (2011)

and 900–3000 ppm chlorine, corresponding to $X_{H_2O} \approx 0.7$, $X_F \approx 0.25$, $X_{Cl} \approx 0.05$, where X is the fractional occupancy of the anion site.

Origin of Halogen-Bearing Phases in CV Chondrites

Several lines of evidence have been used to constrain the origins of the chlorine-bearing phases in oxidized CV chondrites, including textural observations, O-isotopic data for individual mineral phases, and chronological data obtained from short-lived radioisotope chronometers such as the I–Xe and chlorine-S systems. Texturally, it is clear that the chlorine-bearing phases, discussed above, are

secondary replacement products of the primary constituents of CAIs, and that they occur with a diverse array of other secondary phases, typically Ca and Ca–Fe silicate phases, as well as fayalitic olivine and magnetite. The primary questions that have been addressed by studies of these assemblages are where, when, and under what conditions this secondary replacement occurred. All of these questions are closely related and have primarily focused on two different scenarios, the first being formation as a result of gas-solid interactions in the solar nebula prior to accretion, and the second being fluid-solid interaction that occurred post accretion within an asteroidal environment. Although interaction with a nebular gas, to produce the secondary alteration observed in CV chondrites, was the favored scenario of alteration for a number of years (e.g., Wark 1986; Hashimoto and Grossman 1987; Peck and Wood 1987; Weinbruch et al. 1990; Kimura and Ikeda 1995), a significant body of recent research has favored an asteroidal environment for the majority of the secondary alteration effects. This does not completely rule out a nebular environment for some alteration, but has refocused the discussion much more towards post-accretionary, mineral-fluid interactions. Details of the arguments for and against these two scenarios have been summarized in Krot et al. (1995), Brearley (2014), and Brearley and Krot (2013), and will only be reviewed briefly here.

The fall of the Allende CV3 chondrite in 1969 revolutionized research on CAIs in carbonaceous chondrites, because it provided a very significant mass of material for a variety of different analytical studies. Numerous early studies, focusing on Allende CAIs, recognized evidence of secondary alteration of the primary CAI minerals (e.g., Marvin et al. 1970; Allen et al. 1978; Grossman et al. 1975; MacPherson and Grossman 1984; Kornacki and Wood 1985). Further studies recognized significant effects of secondary alteration in chondrules and other components (e.g., Housley and Cirlin 1983; Peck and Wood 1987; Kimura and Ikeda 1995). Hashimoto and Grossman (1987) and McGuire and Hashimoto (1989) recognized that alteration of fine-grained CAIs in Allende must have occurred in an open system and proposed that elemental exchange occurred between CAIs and a hot nebular gas. The proposed nebular alteration scenario of the CV_{OxA} component involves evaporation at high temperatures (>1450 K) within regions of the solar nebula that have high silicate dust + water ice/gas ratios, followed by condensation (e.g., Weinbruch et al. 1990; Dohmen et al. 1998). On the other hand, asteroidal alteration of the components of CV_{OxA} chondrites to produce chlorine-bearing phases is considered to be the result of the interaction of aqueous fluids with chondritic components in situ at moderate (300–600 °C) metamorphic temperatures. A significant body of data has been presented in the recent literature to support the latter scenario, as summarized in Brearley and Krot (2013) and Brearley (2014).

Although there are still significant questions to be addressed regarding the asteroidal formation of chlorine-bearing phases, such as sodalite, wadalite, chlormayenite, and adrianite in CV chondrites, there is general agreement that these minerals formed as a result of the interaction of chlorine-bearing aqueous fluids (either gases or liquids) with primary CAI minerals, under metamorphic conditions (Brearley and Krot 2013; Ishii et al. 2010; Ma et al. 2011; Ma and Krot 2014a, b).

This conclusion is supported by the high water content of apatite in the Allende CV3 chondrite reported by Dyl et al. (2014). The specific phases that formed appear to have been controlled largely by the composition of the primary phases in the CAIs, as demonstrated by the zoned sequence of wadalite and sodalite in Allende type B CAIs described above (Fig. 15.11a–c). The reaction pathways also appear to be different for different phases. For example, in the case of sodalite in type A CAIs in Allende, formation by direct replacement of primary CAI phases is uncommon. Instead, sodalite appears to be the final alteration product in a sequence of reactions that commenced with the replacement of melilite by grossular, which is then replaced by dmisteinbergite, nepheline, and, ultimately, sodalite.

The textural occurrences of wadalite in type B CAIs provide useful constraints on the genesis of this phase and suggest that there were several different episodes of alteration involving fluids of different compositions. In at least some cases, wadalite appears to have formed directly from the primary CAI phases, anorthite and åkermanitic melilite, in a fluid-mediated metamorphic reaction. Ishii et al. (2010) proposed that some wadalite may have crystallized from the fluid at the interface between reactant melilite and anorthite, along with other fine-grained secondary phases such as grossular and anorthite. However, the presence of alteration veins in melilite, that contain just grossular and secondary anorthite, also suggest that some wadalite could have formed by reaction of grossular with a later-stage, chlorine-bearing metamorphic fluid (Ishii et al. 2010). The porosity generated by the metasomatic reactions provides effective pathways for fluid infiltration into the interiors of CAIs to allow alteration by later generations of fluids. Although much rarer, adrianite, that occurs associated with wadalite in one Allende Type B1 CAI, appears to have formed by similar processes (Ma and Krot 2014a).

The formation of chlormayenite (formerly brearleyite), coexisting with hercynitic spinel in the CV3 chondrite NWA 1934, may have also formed by reactions between hot chlorine-bearing gases or fluids (Ma et al. 2011), probably within a parent body environment. However, the exact mechanisms and conditions of formation are not fully constrained. Chlormayenite has only been reported in a unique CAI that consists largely of the unusual aluminate phase krotite, $CaAl_2O_4$. Ma et al. (2011) considered different possible mechanisms for the formation of chlormayenite and argued that the most likely scenario involved the breakdown of krotite by interaction with a chlorine-bearing vapor to form chlormayenite and corundum. Later reaction with a FeO-bearing gas converted the corundum to hercynitic spinel. Alternatively, the formation of hercynite from krotite may have occurred in a single reaction event that evolved progressively from corundum as the initial reaction product towards hercynitic spinel. As is the case for wadalite, the formation of chlormayenite demonstrates the strong control of the precursor phase on the reaction products in metasomatic reactions in CV chondrites. The conditions of formation of chlormayenite from krotite are essentially unconstrained, although Ma and Krot (2014) argued that the transformation of corundum to hercynite required temperatures in excess of 400 °C, due to the likely sluggish kinetics of this reaction.

Oxygen Isotopic Constraints on the Environment of Formation of Secondary Alteration Phases in CV Chondrites

The O-isotopic compositions of secondary chlorine-bearing and associated phases is one of the major lines of evidence to support a parent body environment for alteration in the oxidized CV chondrites. On an O three-isotope diagram, the primary isotopic compositions of minerals in CAIs and chondrules, measured by ion microprobe, define a well-constrained line with a slope of ~1, the so-called Carbonaceous Chondrite Anhydrous Mineral (CCAM) line. The origin of the slope of this line is still under discussion, but could be the result of mixing between two different O-isotopic reservoirs or mass-independent fractionation (e.g., Yurimoto et al. 2008). The O-isotopic composition of secondary alteration phases, such as Ca, Fe-pyroxenes, andradite, and wollastonite in Allende CAIs, matrix, and in dark inclusions, is one of the major lines of evidence to support a parent body formation environment. These phases all have O-isotopic compositions that lie on a mass-dependent fractionation line (slope of 0.52) with a large (~20‰) range in $\delta^{18}O$ that indicates a low temperature of formation from an aqueous fluid. The range of $\delta^{18}O$ values is comparable to the range found in magnetites and fayalites in the CV_{OxB} chondrites (Choi et al. 2000), which also have the same $\Delta^{17}O$ value (vertical offset from the terrestrial fractionation line) within the uncertainty of the SIMS measurements (Cosarinsky et al. 2008). This scenario is also compatible with other petrologic and thermodynamic lines of evidence summarized by Brearley and Krot (2013). Although the O-isotopic compositions of chlorine-rich bearing phases, such as sodalite and wadalite, have not yet been measured, the frequent association of these phases with Ca–Fe-rich pyroxenes and garnets suggests that they share a common origin and are therefore also likely to be the products of fluid-rock interaction with an isotopically-heavy, ^{16}O-poor reservoir on the CV chondrite parent body (Brearley and Krot 2013).

The origin of the chlorine-bearing fluid, proposed as the reacting agent for the formation of the secondary chlorine-bearing phases, is not fully constrained. There is inadequate bulk chlorine data to determine whether the oxidized CV chondrites show an enrichment in chlorine compared with the reduced CV chondrites. This would help to constrain whether the fluids were derived from an external source. However, data from other elements, such as Na, Mn, Fe, and Br, provide some evidence that an externally-derived fluid may have been involved. The CV chondrites are recognized to be one of the most compositionally heterogeneous chondrite groups (Palme et al. 1988). Notably, the oxidized and reduced CV chondrite subgroups are compositionally distinct, with Fe and Mn contents typically 10% higher in the oxidized subgroups and Na, K, and Br factors of 2–3 higher (Palme et al. 1988). As noted by Krot et al. (1995), however, the fact that only one reduced CV chondrite fall, Vigarano, exists makes detailed comparison between the subgroups challenging and prone to uncertainty. Nevertheless, the data indicate that some fluid-mobile elements, such as Na and chlorine, are enriched in the oxidized CV chondrites, suggesting that they may have been derived externally (Krot et al. 1998). In particular, the enrichment observed in Br suggests, by implication, that

chlorine may also be enhanced in the oxidized CV chondrites from an externally-derived fluid, i.e. a fluid from another part of the CV3 chondrite parent body.

However, although the bulk compositional data indicate that chlorine and Br are enriched, relative to the CV_R, there are difficulties in arguing for an externally-derived fluid for these elevated concentrations in the CV_{OxA} chondrites. For example, multiple analyses of multiple samples of Allende (cubes ~5–6 mm on edge) by Stracke et al. (2012) show remarkable compositional homogeneity for a variety of elements that have very different geochemical behaviors (Mg, Si, Fe, Mn, Cr, Ni, Co, P, Zn, and Pb). These data suggest that, despite the fact that Allende (and other chondrites) is a mixture of several different components with different solar nebular histories, these elements were accreted uniformly at the subcentimeter scale. The preserved compositional uniformity at this scale excludes elemental redistribution during parent body aqueous alteration or thermal metamorphism above a scale of a few millimeters (Stracke et al. 2012). Based on this evidence, alteration appears to have been effectively isochemical and did not involve the addition of fluid-soluble elements from an external source.

In addition, MacPherson and Krot (2014) have pointed out that although the permeability of Allende (10^{-15} to 10^{-16} m^2) is the highest of any of the CV3 chondrites (Corrigan et al. 1997), fluids could only have traveled on the order of several meters over a time scale of 1 My. These distances appear to be insufficient to allow significant influx of externally-derived fluids, and instead argue for isochemical alteration, as proposed by Bland et al. (2009). MacPherson and Krot (2014) have argued that the elevated Na concentrations in the CV_{OxA} chondrites may reflect the amount of interstitial and granular ices that were trapped during accretion of the CV_{OxA} chondrites, although the exact carriers of the Na are unclear in this scenario. In the case of chlorine, however, such a scenario appears to be more viable assuming that chlorine was trapped with water ices as HCl hydrate (Zolotov and Mirenenko 2007). However, this model does not readily explain the elevated concentrations of Fe and Mn in the CV_{OxA} chondrites compared with the CV_R chondrites. It is also inconsistent with the arguments presented by Wasserburg et al. (2011) that the metasomatic fluids that affected chondrules and CAIs in Allende were derived from the asteroid interior and transported outwards towards the outer regions of the parent body.

Even if an external fluid was involved in the alteration of Allende and other CV_{OxA} chondrites, redistribution of indigenous chlorine within the oxidized chondrites must also have taken place. However, as discussed earlier, exactly what the precursor hosts of chlorine in the accreted nebular materials were remains speculative. Based on current observations, it appears that chlorine was not concentrated in any specific phase, but was probably distributed at low concentrations within a variety of different phases or was adsorbed on the surfaces of mineral grains, particularly the fine-grained matrix components. Alternatively, the bulk of the chlorine could have been associated with HCl hydrate as discussed earlier.

The development of chlorine- and alkali-rich secondary phases is evidently most common in CAIs in CV3 chondrites, but they also occur replacing chondrule glass

and less commonly as grains in the matrix. As discussed by Brearley and Krot (2013), the major constraint on the formation of these phases appears to be the local bulk composition. Sodium and chlorine both have large ionic radii and are accommodated effectively into framework silicates such as feldspathoids or aluminates. Aluminum, unlike Si, appears to be essentially immobile during alteration of CAIs and chondrules, constraining the formation of phases such as sodalite and wadalite as replacement products of high-Al phases such as anorthite, melilite, and chondrule glass. Numerous studies have demonstrated that these three phases are the most susceptible to alteration under the conditions experienced by the CV_{OxA} chondrites (and the CO chondrites—see Sect. 15.8.2.2). This observation also holds true for type 3 ordinary chondrites that show evidence for the development of chlorine-rich phases that are restricted to Al-rich chondrules (Sect. 15.8.3). The relatively low abundances of sodalite in the matrices of CV_{OxA} can reasonably be attributed to the fact that the bulk Al_2O_3 content of this material is consistently low (<5 wt%).

Timing of Formation of Chlorine-Bearing Phases in CV3 Carbonaceous Chondrites

Data from the short-lived radioisotope systems ^{26}Al–^{26}Mg and ^{129}I–^{129}Xe provide useful constraints on the possible formation environments of chlorine-bearing phases in CV carbonaceous chondrites. In essence, old formation ages within the first 2–3 million years of the first solids forming in CAIs are considered to be indicative of formation within a solar nebular environment, whereas younger ages of ~2–5 Ma or more after the first CAI solids, are more likely to be the result of processes that occurred post-accretion of asteroidal parent bodies (Krot et al. 2006; Brearley and Krot 2013).

In situ decay of the short-lived radioisotope ^{26}Al, with a half-life of ~0.72 My, results in the presence of an excess of the stable daughter isotope ^{26}Mg ($^{26}Mg^*$) within Al-rich minerals, which can be detected by SIMS or ICP–MS techniques. In situ decay is indicated by a correlation of the $^{26}Mg^*$ with the Al/Mg ratio of the specific mineral. An Al–Mg isochron is defined by plotting $\delta^{26}Mg$ (‰ deviation from the terrestrial $^{26}Mg/^{24}Mg$ ratio of 0.13932) against the $^{27}Al/^{24}Mg$ ratio for individual phases, resulting in a straight line with a slope that is proportional to the $^{26}Al/^{27}Al$ ratio at the time of system closure. The relative formation age of the sample corresponds to the difference in the initial $^{26}Al/^{27}Al$ ratios between the unknown sample and the canonical $^{26}Al/^{27}Al$ ratio ($^{26}Al/^{27}Al$ ratio of the oldest dated solar system solids: Amelin et al. 2002, 2010) measured in CAIs.

Secondary minerals, such as nepheline, sodalite, anorthite, and grossular, that form from the alteration of primary CAI minerals, are well suited to Al–Mg studies because they have high Al/Mg ratios and, therefore, potential large values of $^{26}Mg^*$. Several different ion microprobe studies have found that in most coarse-grained CAIs from CV_{OxA} chondrites, these phases show no evidence of any $^{26}Mg^*$ (e.g., Hutcheon and Newton 1981; Hsu et al. 2006; Fagan et al. 2007;

Jacobsen et al. 2008), unlike primary CAI phases that typically yield initial $^{26}Al/^{27}Al$ ratios that are close to the canonical value. The absence of $^{26}Mg^*$ in secondary minerals, including sodalite, indicates that they formed, at minimum, several half-lives of ^{26}Al after crystallization of the primary minerals in the host CAIs. However, in some CAIs, nepheline and sodalite that replace melilite and anorthite show variable excesses of ^{26}Mg, indicating earlier formation of these phases that commenced in the solar nebula, and continued later after accretion into an asteroidal environment. However, Krot et al. (2010) have argued that in these cases, the secondary replacement phases have inherited their Mg-isotopic compositions from the precursor primary CAI melilite and actually formed after significant decay of ^{26}Al had occurred, perhaps ~ 3 Ma after formation of the CAI minerals in the solar nebula. If this hypothesis is correct then alteration within an asteroidal environment is more likely, which is consistent with most of the Al–Mg data for secondary alteration phases.

Iodine–Xe dating has been applied to constrain the timing of metasomatic alteration of CV_{OxA} and CV_{OxB} chondrites, and the dark inclusions that they contain. As summarized above, and in Krot et al. (2006) and Brearley and Krot (2013), there is a significant body of evidence that the major halogen-bearing phase in CV chondrites, sodalite, formed as a result of secondary metasomatic alteration. A similar origin has also been proposed for the formation of wadalite that has only been recognized relatively recently (Ishii et al. 2010). Although there are no direct measurements of I concentrations in either of these phases, Kirschbaum (1988) reported a strong correlation between I and chlorine in two fine-grained CAIs in Allende. This correlation has been used to infer that sodalite is the major carrier phase of I in CAIs and, by implication, it is also probable that wadalite could be a carrier of I as well. Therefore I–Xe dating of CV_{OxA} chondrites and dark inclusions is likely to date the age of the alteration event(s) that affected the primary mineralogical constituents of these meteorites.

Results of I–Xe dating of CV_{OxA} chondrites and dark inclusions have been summarized in Krot et al. (2006). Iodine–Xe ages for CAIs in Allende, which show evidence of iron-alkali metasomatism, indicate a spread of ages of ≥ 10 Ma (Swindle et al. 1988). This range of ages is generally considered to extend beyond the expected lifetime of the solar nebula, a few million years (e.g., Boss and Goswami 2006) and is therefore thought to be consistent with alteration within an asteroidal environment.

Iodine–Xe measurements of Allende dark inclusions performed by Pravdivtseva et al. (2003a) yield well-defined isochrons with a range of ages from 0.5 ± 0.3 Ma to 2.8 ± 0.3 Ma older than the standard Shallowater. The release profiles from each inclusion all show two major peaks that may be due to the presence of two different I carriers, possibly sodalite and wadalite (Brearley and Krot 2013), although this has yet to be proven. These young I–Xe ages probably represent the age of the alteration event that occurred elsewhere on the Allende parent body prior to excavation and incorporation of the dark inclusions into the Allende host as a result of impact processes. In comparison, the dark inclusions from CV_R chondrites, reported by Swindle et al. (1998), Krot et al. (1999), and Pravdivtseva et al.

(2003b), show a wide range of I–Xe ages, but are typically younger than Allende dark inclusions with a range of ages from −4.9 ± 1.8 Ma (older) to 9.5 ± 2.3 Ma (younger) relative to Shallowater. However, compared with the Allende dark inclusions, the potential carrier phase of the I has not been identified, because no chlorine-bearing phases are present. Collectively, the I–Xe ages for dark inclusions in CV chondrites suggest that there was extended metasomatic alteration and thermal metamorphism covering a period of ∼14 Ma, within the CV chondrite parent asteroid.

15.8.2.2 CO Carbonaceous Chondrites

The CO chondrite group is characterized by a well-defined metamorphic sequence that exemplifies the effects of relatively low degrees of metamorphism. The details of metamorphism in this group have been reviewed recently by Huss et al. (2006) and Brearley and Krot (2013). All known CO chondrites are petrologic type 3, and the metamorphic sequence extends from type 3.0 to type 3.7 or 3.8 depending on the specific study (McSween 1977b; Rubin et al. 1985; Scott and Jones 1990; Sears et al. 1991; Chizmadia et al. 2002; Grossman and Brearley 2005; Greenwood and Franchi 2004; Bonal et al. 2007; Kimura et al. 2008). There is a consensus in the literature that this metamorphic sequence is produced by progressive thermal metamorphism resulting from internal radioactive heating of the CO parent asteroid.

Although it has commonly been accepted that metamorphism of the CO chondrites occurred under fluid absent conditions, it is now apparent that fluids played a role in producing the observed mineralogical and textural characteristics of this group of meteorites. In addition to the thermal effects of metamorphism, such as grain growth and equilibration of mineral compositions with increasing metamorphic grade, there is significant evidence for the replacement of primary mineral phases by secondary alteration products. These effects are especially prevalent in CAIs and ameboid olivine aggregates (Chizmadia et al. 2002), but also occur to a lesser extent in chondrules. The recognition that these secondary alteration effects are strongly correlated with increasing degrees of thermal metamorphism has led to a model of fluid-assisted metamorphism for the CO chondrites, as first proposed by Rubin (1998) and extended by Wasson et al. (2001) and Chizmadia et al. (2002). In the case of CAIs and chondrules, the alteration effects can be considered to be a highly localized form of metasomatism that involved the introduction of alkalis (Na and K) and Fe into CAIs and chondrules, and the loss of Ca from primary phases such as anorthite and melilite (Russell et al. 1998; Kojima et al. 1995).

At present, there is very little known about the behavior of halogens in the CO chondrites, and reports of the occurrence of distinct halogen-bearing phases are extremely rare. Nevertheless, the CO chondrites represent a potential opportunity to understand both the primary nebular carriers of the halogens, as well as their redistribution as a result of fluid-assisted asteroidal metamorphism. An important aspect of the CO chondrite group is that it contains a few members that are classified as having a very low petrologic type and could provide the opportunity to

understand the distribution of halogens in some of the least metamorphosed asteroidal samples in our collections. However, it is unfortunate that all the lowest petrologic type CO chondrites, such as Colony, ALH A77307 (3.03), and Y-81020 (3.05), are terrestrial finds whose preterrestrial halogen contents, distributions, and mineralogies are likely to have been modified to varying degrees by terrestrial weathering.

In contrast, there are a significant number of CO chondrite falls that span the range of petrologic types, providing the potential to study the evolution of halogen distributions and mineralogies as a function of increasing fluid-assisted metamorphism. Based on the evidence from the CV and unequilibrated (petrologic type 3) ordinary chondrites, the involvement of fluids during the metamorphic processing of the CO chondrites might have caused significant halogen mobility and resulted in the formation of halogen-rich, particularly chlorine-bearing, phases. However, evidence for the mobility of halogens in the CO chondrites is remarkably limited, although there is clear evidence of Na, K, and Fe metasomatism. Alteration effects have been reported in CAIs, AOAs, and chondrules (Ikeda 1982; Fahey et al. 1994; Holmberg and Hashimoto 1992; Tomeoka et al. 1992; Kojima et al. 1995; Russell et al. 1998; Wasson et al. 2001; Itoh et al. 2004). However, in comparison with the extremely detailed studies of these components in CV3 chondrites, the documentation of alteration effects in CO3 chondrites is much less detailed. This is at least partially because the components in CO3 chondrites are much finer-grained than in the CVs. Also, alteration is much less extensive than in the CV chondrites, except in higher petrologic types where, for example, all the primary components of the CAIs have either been replaced or had their compositions modified (e.g., Russell et al. 1998). In comparison with the CV chondrites, metasomatism of the CO chondrites is dominated by Na–K–Fe metasomatism with much less evidence for transport and redistribution of halogens.

In CAIs from CO chondrites, primary melilite is typically replaced by fine-grained nepheline, pyroxene, and troilite, not sodalite or wadalite as occurs in CAIs in the CV chondrites (Sect. 15.8.2.1). Nevertheless, microbeam studies of CAIs in CO3 chondrites do indicate the presence of minor amounts of chlorine correlated with Na in regions of fine-grained alteration products. For example, electron microprobe analyses of regions of fine-grained nepheline in CAIs in Y-791717 (Tomeoka et al. 1992) and Y-82050 (CO3.1) (Kojima et al. 1995) contain low concentrations of chlorine, suggesting that sodalite may be intergrown as a minor phase at the micron to submicron scale. Fahey et al. (1994) also reported the presence of minor sodalite associated with nepheline that occurs in voids in the ultrarefractory CAI HH-l from Lancé. X-ray maps of CAIs from CO chondrites, ranging from petrologic type 3.3 (Felix) to petrologic type 3.8 (Isna), show local enrichments in chlorine correlated with Na (Fig. 15.13) indicative of the presence of sodalite (Brearley and Krot 2013). The degree of alteration of CAIs in CO chondrites generally shows an increase with increasing petrologic type, with melilite being progressively replaced by nepheline and very minor sodalite. The amount of sodalite shows no clear correlation with the degree of alteration and is

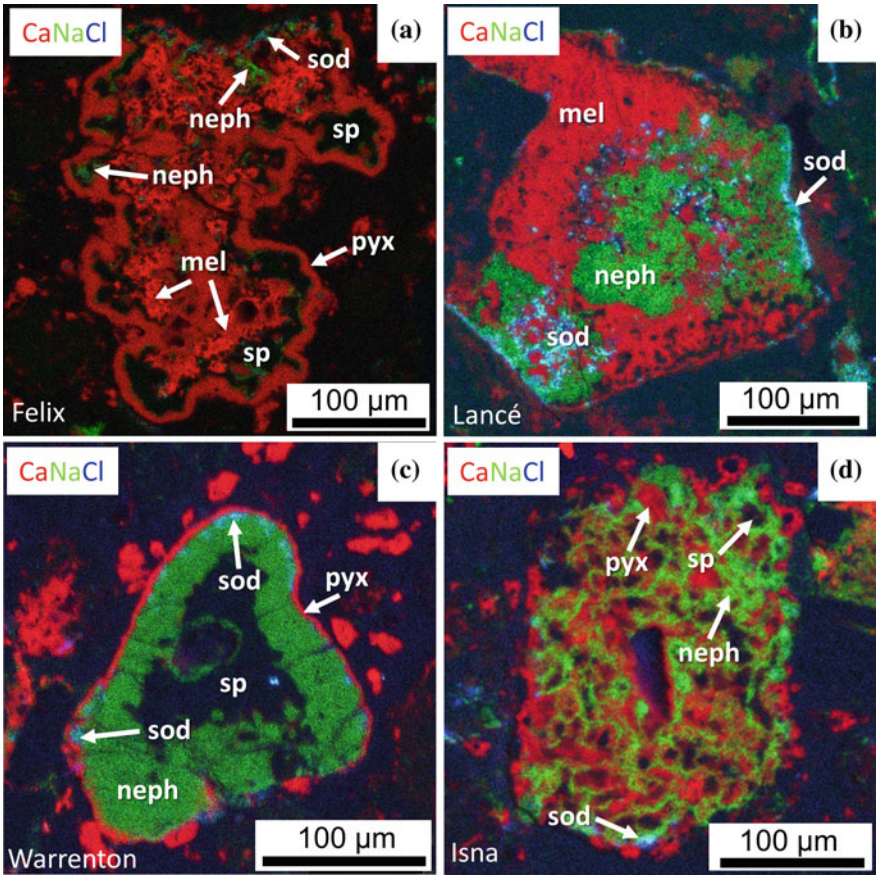

Fig. 15.13 Composite Ca (*red*), Na (*green*), and chlorine (*blue*) X-ray maps of CAIs from CO3 chondrites showing variable degrees of development of sodalite. **a** A map of a nodular melilite-spinel bearing inclusion from the CO3 chondrite Felix (type 3.3). The CAI consists of nodules of spinel (sp) associated with melilite (mel). The object is rimmed by Al-diopside (pyx) and diopside is also present on the interior of the object. Minor nepheline (*green*) (neph) is present locally within the inclusions, but sodalite (sod—*light blue*) is extremely rare and only occurs at the upper edge of the inclusion as extremely small grains. **b** A map of a melilite-rich inclusions from the CO3 chondrite Lancé (type 3.5). In this inclusion, melilite (mel) has been extensively replaced by nepheline (neph) that occurs through an extensive region of the central part of the inclusion. Sodalite (sod) is developed quite extensively in this inclusion and occurs locally along the rim of the inclusion and as patches within regions of nepheline. Small grains of sodalite also occur locally within altered patches of melilite. **c** A map of an extensively altered melilite-spinel-bearing CAI from the CO3 chondrite Warrenton (type 3.7). The core of the inclusion consists of spinel (sp—*black*) that is surrounded by a thick layer of nepheline (*green*) that has completely replaced melilite. The whole inclusion is rimmed by a layer of diopside (pyx). Small patches of sodalite (sod—*light blue*) are developed locally along the interface between the nepheline and pyroxene, but is quite rare. **d** A map of a very altered spinel-pyroxene inclusion from the CO3 chondrite Isna (type 3.8). Spinel grains (sp—*black*) and Al–Ti diopside (pyx) have not been replaced, but melilite has been entirely replaced throughout the inclusion by nepheline (neph—*green*). Despite the high degree of alteration in this inclusion, sodalite is extremely rare and is only present as one grain (sod—*light blue*) at the lower edge of the inclusion

generally only an extremely minor phase in comparison with CAI alteration in the CV3 chondrites.

The studies discussed above show that the style of metasomatic effects in the different components of CO3 chondrites, i.e., chondrules, AOAs, and CAIs, are all basically similar. All these studies show that the principle type of metasomatism involved is the introduction of Na into these objects that has promoted alteration of Ca-bearing phases (melilite, anorthite, and chondrule mesostasis) to form nepheline. However, compared with the CV3 chondrites, there is minimal evidence of halogen metasomatism as indicated by the rarity of sodalite as a metasomatic alteration product in the CO3 chondrites.

Apatite, as a potential carrier of halogens, does occur in CO3 chondrites (Kurat 1975), but very little is known about its crystal chemistry, so it is unclear whether it is chlorine- and/or F-bearing.

15.8.2.3 CK Carbonaceous Chondrites

The CK carbonaceous chondrites are the only group of carbonaceous chondrites that exhibit the full range of petrologic types from type 3 to type 6. They appear to have strong affinities to the CV chondrites and some workers have proposed that the two groups represent a continuum of meteorites (Greenwood et al. 2010). Like the ordinary chondrites, the only halogen-bearing phase reported in the CK chondrites is apatite, but details of its occurrence and crystal chemistry are sparse. Some studies (e.g., Scott and Taylor 1985; Rubin 1993; Noguchi 1993) did not report apatite in CK chondrites, but several more recent studies have documented the presence of both apatite and chlorapatite (Keller et al. 1992; Ivanova et al. 2000; Kurat et al. 2002; Tomeoka et al. 2001, 2005; Greenwood et al. 2010; Martin et al. 2013). Chlorapatite appears to be present in at least some type 3 CK chondrites (e.g., NWA 5956; Martin et al. 2013) and is also present in higher petrologic types as well. Only Kurat et al. (2002) have reported any compositional data for chloroapatite in CK chondrites. Unfortunately, this is in an unusual occurrence within a CAI in the Maralinga CK4 chondrite that contains 4.5 wt% chlorine. It is not clear if this is representative of chloroapatite in the meteorite as a whole. There are also no data on the F contents of apatites in CK chondrites. Although details are lacking, it appears that during thermal metamorphism, as is the case for the ordinary chondrites, chlorine, and possibly F, were redistributed into apatite as the major halogen-bearing phase.

15.8.2.4 Unique Carbonaceous Chondrites and K Chondrites

There are a number of important and unusual chondrites, such as the complex microbreccia Kaidun (Zolensky and Ivanova 2003), the very low petrologic type 3 ungrouped carbonaceous chondrite Acfer 094 (Newton et al. 1995), and the ungrouped C2 chondrite Tagish Lake (Zolensky et al. 2002; Blinova et al. 2014a,

b), that have been studied in considerable detail. However, there are very few reports of halogen-bearing phases in these meteorites. Rare fluorapatite has been reported in two unusual alkali-rich clasts in the Kaidun microbreccia (Zolensky and Ivanova 2003). Blinova et al. (2014a) described phosphate minerals in Tagish Lake but the mineral phase was not determined and it is not clear whether it is halogen-bearing. Four different Br analyses for Tagish Lake range from 0.37 to 4.0 ppm (Blinova et al. 2014b), consistent with data from other C chondrites shown in Fig. 15.1. (These data are not included in Fig. 15.1 because Tagish Lake is ungrouped.) Other halogens were not reported. In addition, Berlin et al. (2007) found chlorapatite associated with ferrihydrite replacing kamacite in matrix and chondrules in the K chondrite, Kakangari. However, details of the chemistry of apatite in these occurrences are not currently available.

15.8.2.5 Other Metamorphosed Carbonaceous Chondrites

A significant number of unique carbonaceous chondrites have been recognized that appear to have experienced an episode of aqueous alteration that was followed by thermal metamorphism (Tomeoka et al. 1989a, b; Tomeoka 1990; Ikeda et al. 1992; Noguchi 1994; Tonui et al. 2003). Some of these chondrites show clear evidence of dehydration of phyllosilicate phases (Akai 1988, 1990) and have affinities to both CI and CM chondrites (Ikeda 1991; Tomeoka et al. 1989a, b, c; Tonui et al. 2003). A number of these meteorites have been studied in detail, but only limited evidence is available about any halogen-bearing phases, which appear to be exclusively F- and chlorine-bearing apatite (e.g., Y-82104; Nakamura 1993; Y-82162, Ikeda 1992). Ikeda (1991) found that apatite in Y-82162 contains variable F contents. Apatite has also been described in several other metamorphosed carbonaceous chondrites, such as Coolidge (Noguchi 1994), Y-86720 (Ikeda et al. 1992), Y-86789 (Matsuoka et al. 1996), and Belgica 7904 (Tomeoka 1990; Kimura and Ikeda 1992), but no information is available on their halogen contents, suggesting that they may be hydroxyl-apatite. Development of apatite in these meteorites can reasonably be attributed to metamorphic redistribution of halogens during parent body heating.

15.8.3 Halogen-Bearing Minerals in Ordinary Chondrites

All three ordinary chondrite groups exhibit the full range of secondary metamorphic effects, with increasing degrees of thermal metamorphism from the least-altered petrologic type 3.00, to highly recrystallized petrologic type 6. For ordinary chondrites, the type 3 classification in the 3-4-5-6 petrologic type scheme of Van Schmus and Wood (1967) is further broken down into subtypes 3.00, 3.01, 3.02, etc., up to 3.9 (Grossman and Brearley 2005). There is also considerable evidence for fluid-rock reactions over a range of temperatures, the effects of which are

notably recorded by halogen-bearing minerals. Since most, if not all, observed halogen-bearing minerals are secondary, there is considerable uncertainty about the phases in which halogens were initially incorporated into primary ordinary chondrite components. Possibilities include glassy mesostasis in chondrules, and ices that were mixed with the ordinary chondrite matrix when the ordinary chondrite parent bodies accreted. However, there is currently little direct evidence for primary halogens in ordinary chondrite chondrule glass. Chondrule mesostases in LL3.4 Chainpur and LL3.6 Parnallee contain up to 4.6 wt% chlorine (Bridges et al. 1997), but it is not clear whether these high abundances are primary. Zolotov and Mironenko (2007) suggested that during condensation, chlorine remains in the gas phase as $HCl_{(g)}$ until it condenses to solid $HCl{\cdot}3H_2O$ (HCl hydrate) at extremely low temperatures, around 140–160 K. Fine-grained matrix in one of the least altered (i.e. highly unequilibrated) ordinary chondrites, Bishunpur (LL3.15), contains smectite with up to 0.3 wt% chlorine, as well as chlorapatite and scapolite (Alexander et al. 1987, 1989), which is consistent with incorporation of chlorine in ices that melted to form some of the earliest parent-body fluids. The primary carriers of Br and I in ordinary chondrites are not well understood. Iodine may reside in pyroxene, mesostasis, and troilite in the LL3.00 chondrite Semarkona (Goswami et al. 1998).

In some petrologic type 3 ordinary chondrites, a record of chlorine- and F-rich fluids is preserved in the secondary halogen-bearing minerals scapolite, sodalite, and apatite, as well as effects observed in the glassy mesostasis of the chondrules. The relationship between the degree of metasomatism and the petrologic (sub)type is currently not well established, and the effects of metasomatism are very heterogeneous. The effects of metasomatism in type 3 ordinary chondrites are generally subtle and not widely developed. Key indicators of metasomatism are the presence of the feldspathoids, nepheline, and sodalite, and rarer scapolite ($Na_4A1_3Si_9O_{24}Cl$). Chondrules and clasts from Chainpur (LL3.4) and Parnallee (LL3.6) contain rare to minor microcrystalline nepheline, sodalite, and scapolite (Bridges et al. 1997; Lewis and Jones 2014). Aluminum-rich chondrules in Bo Xian (LL3.9) contain a mixed nepheline-anorthite composition with ≤ 4 wt% chlorine and localized chlorine-bearing glass (Li et al. 2000). These secondary phases appear to replace anorthite and/or chondrule glass. Chlorine-bearing phases, tentatively identified as sodalite and scapolite, also occur in Semarkona (LL3.00) and Bishunpur (LL3.15) (J. Lewis, personal communication: Fig. 15.14a).

The H3 chondrite, Tieschitz (H3.6), shows significant evidence for metasomatism, including a "white matrix", which consists of a feldspathic nepheline- or albite-like phase and Ca-rich pyroxene (Christophe Michel-Lévy 1976; Ashworth 1981; Hutchison et al. 1979; Alexander et al. 1989; Dobrică and Brearley 2014), and mesostasis at the edge of the chondrules that has a blocky appearance on the scale of ~ 10 μm. Blocky mesostasis is enriched in chlorine and F, from 5–47× and 2–56× the abundances in unaltered mesostasis, and has low analytical totals (81–89 wt%) due to the presence of voids, and possibly the presence of unanalyzed water (Hutchison et al. 1998). However, the mineralogy of this material is poorly constrained. Chondrules in Tieschitz also exhibit effects such as the widespread

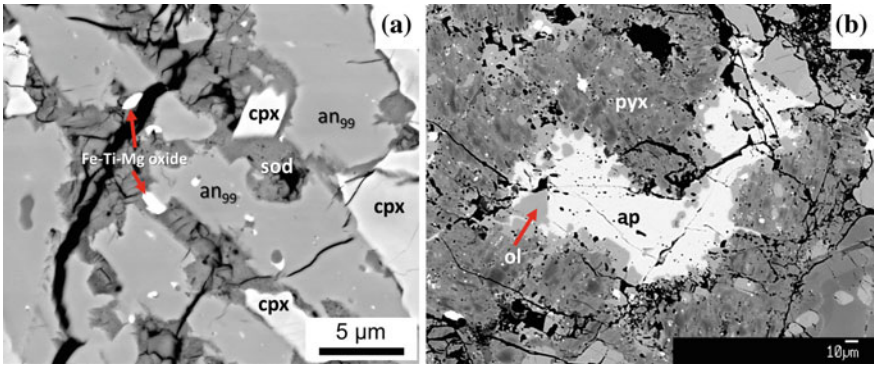

Fig. 15.14 Occurences of halogen-bearing phases in ordinary chondrites. **a** A BSE image of porous, fine-grained sodalite (sod) that has probably formed by replacement of mesostasis glass and/or anorthite (An_{99}) in a chondrule from the LL3.15 chondrite Bishunpur. The anorthite is a primary crystallization product in the chondrule. The region also contains Ca-rich pyroxene (cpx) grains and a Fe–Ti–Mg oxide phase. Image courtesy of J. Lewis (University of New Mexico). **b** A BSE image of an irregularly-shaped, porous chlorapatite from the LL3.9 chondrite Bo Xian. In this example, the chlorapatite (ap) is surrounded by olivine (ol) that overgrows low-Ca pyroxene (pyx). Modified from Jones et al. (2014)

occurrence of voids, ranging in size from a few tens to several hundreds of microns, which have been attributed to the leaching of mesostasis glass by an aqueous metasomatic fluid (Kurat 1969; Christophe Michel-Lévy 1976; Hutchison et al. 1998).

Lin et al. (2006) described 24 CAIs in L3, H3, and H4 chondrites, all of which were highly altered from their original melilite-spinel assemblages. The predominant alteration product of melilite is fine-grained nepheline, with sodalite indicated by the presence of chlorine.

In several ordinary chondrites of petrologic type 3 and 4, anorthitic feldspar commonly shows the effects of pervasive metasomatic alteration (Jones and Brearley 2010a, b; Lewis and Jones 2015). In Bo Xian (LL3.9), primary anorthitic plagioclase in chondrules shows the development of submicron lamellae of a phase composed of an amorphous Si,Al-rich material that is locally highly enriched in chlorine (Jones and Brearley 2010a). Calcium has been leached completely from these lamellae; however, no evidence of hydrous phases is present. The same texture has been described in Bjurböle (L/LL4), Saratov (L4), and Avanhandava (H4) (Jones and Brearley 2010b; Lewis and Jones 2015). Although no chlorine-bearing minerals have been identified in these assemblages, the evidence for metasomatic alteration by chlorine-bearing fluids is important for the interpretation of the overall alteration environment.

The dominant carrier of F and chlorine in ordinary chondrites is fluor-chlor- apatite, $Ca_5(PO_4)_3(F,Cl,OH)$ (hereafter apatite), which commonly occurs in association with a second phosphate mineral, merrillite, $Na_2(Mg,Fe^{2+})_4Ca_{18}(PO_4)_{14}$ (Fig. 15.14b) (Van Schmus and Ribbe 1969; Brearley and Jones 1998). The abundances of these two

minerals are typically around 0.2 vol.% and 0.3 vol.%, respectively, in ordinary chondrites, although their absolute and relative abundances can vary widely. Apatite in all ordinary chondrites is chlorine-rich and shows a general textural development from petrologic type 4–6 ordinary chondrites. In the LL group (Jones et al. 2014), apatite forms initially in petrologic type 4, in fine-grained assemblages with merrillite, olivine, and albite, most likely as a result of reactions between merrillite and halogen-bearing fluids. In petrologic types 5 and 6, apatite development occurs in response to diffusional equilibration during metamorphism, accompanied by interface-coupled dissolution–reprecipitation reactions during metasomatism. Apatite grains become coarser, up to around 300 μm, and some show porosity and evidence for replacement of merrillite even in petrologic type 6. Apatite shows a similar sequence of development in H and L chondrites (Lewis and Jones 2016). Apatite in ordinary chondrites has very low H_2O contents (Jones et al. 2014), indicating that the latest stage fluids that it records were halogen-rich and very dry. These fluids could have been derived by degassing of melts, produced either by partially melting in the interior of the ordinary chondrite parent bodies, or as a result of impact melting (Jones et al. 2014). U–Pb ages of apatite in ordinary chondrites span a wide range from 4563 Ma to 4452 Ma (Göpel et al. 1994; Bouvier et al. 2007; Yin et al. 2014).

The F/Cl ratio in apatite varies among different chondrites and among chondrite groups, with lower F/Cl ratios in H than in L and LL groups (Lewis and Jones 2016). For all OCs, the F/Cl ratios in apatite are significantly lower than the average F/Cl ratios of the bulk ordinary chondrites using concentrations given by Lodders and Fegley (1998), and more similar to F/Cl ratios of CI chondrites (Lewis and Jones 2016). As discussed above (Sect. 15.4.2.2; Figs. 15.1 and 15.2), there are significant uncertainties relating to the bulk F concentrations of ordinary chondrites. It is possible that halogens in apatite may provide a useful means to determine the bulk F/Cl ratio, although this is an avenue for future research. In the Zag H4-6 regolith breccia, apatite shows a range of compositions in different lithologies, from 5.9 wt% chlorine and 0.03 wt% F in H4 material to 3.3 wt% chlorine, 2.0 wt% F in H6 material (Jones et al. 2016). This significant heterogeneity means that formation of apatite must predate brecciation.

Zag and the H5 chondrite, "Monahans (1998)", are important ordinary chondrite falls in that they contain dark blue/purple mm-sized aggregates of demonstrably extraterrestrial halides (Zolensky et al. 1999; Whitby et al. 2000; Rubin et al. 2002; Bridges et al. 2004). Zag contains only halite, whereas halides in Monahans consist of a mixture of halite and sylvite (KCl). Iodine is concentrated in the sylvite, with overall I contents in the Monahans halides of around 400 ppb (Busfield et al. 2004). Halite in both chondrites contains low-temperature (<100 °C) aqueous fluid inclusions and is considered to result from evaporation of brines. For models in which halite forms on the H chondrite parent body, various sources for the water have been proposed. These include exogenous water delivered to the parent body by cometary or asteroidal ice fragments (Zolensky et al. 1999; Bridges et al. 2004),

dehydration of the asteroid interior (Whitby et al. 2000), or impact heating of phyllosilicates (Rubin et al. 2002). Alternatively, it has been argued that halite occurs as a clastic component, delivered to the H chondrite parent body either by impacts (Zolensky et al. 1999; Whitby et al. 2000; Bridges et al. 2004) or ancient cryovolcanism that took place on a nearby large, icy body, possibly Ceres (Zolensky et al. 2013; Yurimoto et al. 2014).

15.8.4 Halogen-Bearing Minerals in R Chondrites—Rumurutiites

The rumurutiites, or R chondrites, have affinities to the ordinary chondrites, but are significantly more oxidized and characterized by high abundances of magnetite, the absence of Fe,Ni metal, and O-isotopic compositions that are distinct from those of other non-carbonaceous chondrite groups (Bischoff et al. 1994; Rubin and Kallemeyn 1994; Schulze et al. 1994; Kallemeyn et al. 1996; Bischoff 2000). The rumurutiites exhibit a petrologic sequence from type 3 to type 6 and also contain many members that are regolith breccias consisting of fragments of different petrologic types. Among the rumurutiites, two members, LAP 04840 and MIL 11207, have been recognized as unique, because they contain a significant volume of OH-rich amphibole and minor biotite that are unknown in other rumurutiites and any of the other chondrite groups (McCanta et al. 2008; Gross et al. 2013). These phases are also chlorine- and F-bearing as discussed below.

Amphiboles

The R chondrite LAP 04840 contains ~13 vol.% ferri-magnesiohornblende that occurs as euhedral to subhedral grains, several hundred microns across that are distributed throughout the sample (McCanta et al. 2008). The amphibole occurs in chondrules, in chondrule fragments, and in the matrix. Based on electron microprobe and ion microprobe analyses of the hornblende, it is OH-rich, but contains low average F and chlorine concentrations of 0.03 wt% and 0.04 wt%, respectively. A second R chondrite, MIL 11207, also contains amphibole (Gross et al. 2013), but in this case the amphibole is magnesian edenite. Like LAP 04840, the amphibole is hydroxyl-rich with only minor contents of F (0.02 structural formula units (sfu) F) and chlorine (0.02 sfu) (based on 22 oxygens).

Phlogopite

Phlogopite in LAP 04840 is much less abundant than amphibole (0.2–0.5 vol.%) and occurs as small (<100 μm), anhedral to subhedral grains (McCanta et al. 2008). The phlogopite contains an average of 0.04 wt% F and 0.08 wt% chlorine. Hydroxyl-rich phlogopite also occurs in MIL 11207 with minor concentrations of F (0.06 sfu) and chlorine (0.02 sfu) (based on 20 oxygens) (Gross et al. 2013).

Apatite
Chlorapatite is present in rumurutiites at modal abundances of 0.2–1%, based on measurements from several different R chondrites, as summarized by McCanta et al. (2008). There are very few analyses of apatite in rumurutiites in the literature, but McCanta et al. (2008) reported extremely chlorine-rich apatite in LAP 04840 with an average composition of 1.99 wt% chlorine and 0.03 wt% F. Gross et al. (2013) reported apatite in MIL 11207, which is significantly more hydroxyl-rich than in LAP 04840, with up to 0.72 sfu OH, 0.14 sfu F and 0.35 sfu chlorine.

The formation of amphibole and phlogopite in LAP 04840 appears to have required hydration of the host rock at elevated temperatures, a process that was widespread and pervasive given the high abundance of amphibole in the rock. McCanta et al. (2008) concluded that the rock was infiltrated by an oxidizing fluid at temperatures of 670 ± 60 °C and $P\mathrm{H_2O}$ between 250 and 500 bars at $f\mathrm{O_2}$ = QFM + 0.5. The source of the fluid remains unconstrained, but elevated D/H ratios of water in the amphibole suggest that the fluid may have been derived from oxidation of insoluble organic matter. Alternatively, the amphibole may have formed from residual water resulting from the oxidation of metal, as proposed by Alexander et al. (2010) to explain elevated D/H ratios in organic materials in ordinary chondrites.

15.8.5 Halogen-Bearing Minerals in Enstatite Chondrites

Details of the halogen cosmochemistry and mineralogy of the enstatite chondrites are reported by Rubin and Choi (2009); only a brief summary is presented here. The enstatite chondrites, comprised of the EH (high total Fe) and EL (low total Fe) groups, represent the chondrite class that formed under the most reducing conditions in the solar nebula, in regions characterized by high C/O and/or $P\mathrm{H_2}/P\mathrm{H_2O}$ ratios (Larimer and Bartholomay 1979; Grossman et al. 2009; Ebel and Alexander 2011). Their very reduced formation conditions have resulted in a highly unusual mineralogy, which consists of very low oxidized Fe contents in their silicate minerals (dominantly enstatite), the presence of graphite and Si-rich metallic Fe, a high modal abundance of kamacite, and abundant sulfides including several unusual sulfides such as oldhamite (CaS), niningerite (Mg,Fe)S, and ferroan alabandite (Mn, Fe)S (Brearley and Jones 1998).

Given the high abundances of halogens in the enstatite chondrites, it is perhaps not surprising that they exhibit one of the most diverse suites of halogen-bearing minerals of any chondrite group. Rubin and Choi (2009) listed five different specific occurrences of halogen-bearing carriers in enstatite chondrites, including minerals and quenched glasses in chondrules that were once melts. Only the concentrations of F and/or chlorine have been measured in these phases. No data are currently available on the hosts of I or Br.

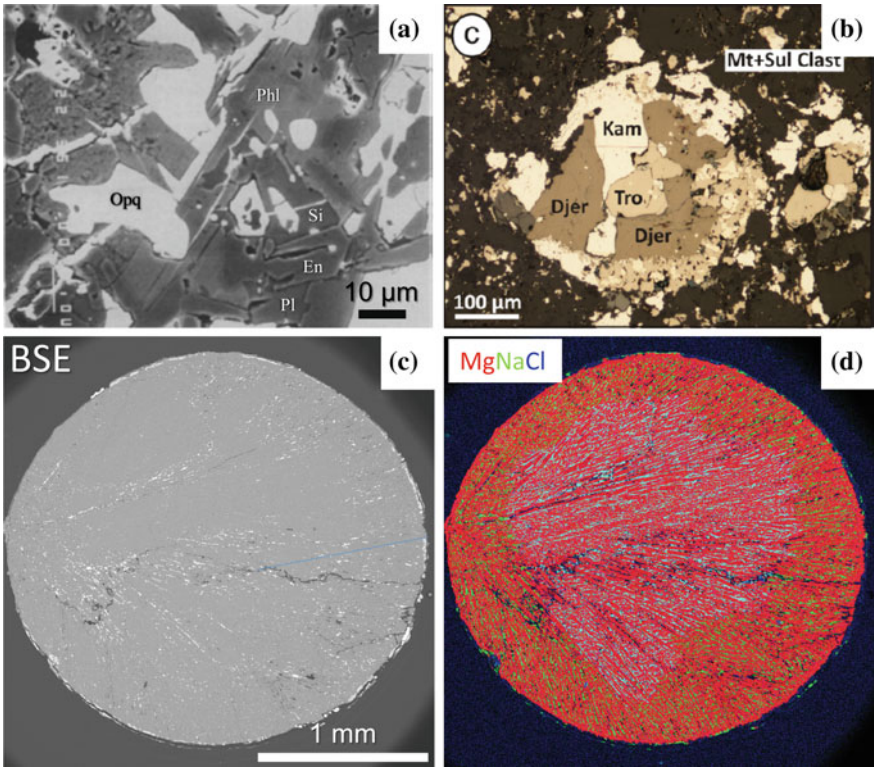

Fig. 15.15 Occurrences of chlorine-bearing minerals in enstatite chondrites. **a** BSE image of grains of fluorphlogopite within a region of impact melt within the EH chondrite impact melt rock Y-82189. Image from Lin and Kimura (1998). **b** Reflected light microscope image of a clast containing a nodular opaque assemblage from the EH3 chondrite ALH 77295 showing an assemblage of djerfisherite (Djer), troilite (Tro), and kamacite. **c** BSE image of a radiating pyroxene (enstatite) chondrule from the Qingzhen EH3 chondrite. In addition to enstatite, small grains of the Ca sulfide oldhamite occur between the pyroxene laths and as a rim along the outside of the inclusion. Image from Clay et al. (2014). **d** Composite Mg(*red*)-Na(*green*)-chlorine(*blue*) X-ray map of the same chondrule showing a zoned distribution of chlorine within interstitial chondrule glass. The irregular core of the chondrule has elevated chlorine concentrations and appears as *light blue* regions, due to the presence of both Na and chlorine in the glass. The outer part of the chondrule contains much lower chlorine concentrations and appears *green* due to the presence of Na and much lower concentrations of chlorine

Fluor-richterite ($Na_2Ca(Mg,Fe)_5Si_8O_{22}F_2$)

Acicular grains of the F-bearing amphibole, fluor-richterite, rarely up to 3.5 mm in length, have been described by Douglas and Plant (1969) and Olsen et al. (1973) in the matrix of the EH impact melt breccia Abee. The fluor-richterite is fully fluorinated with no hydroxyl. Rubin (1983) also reported fluor-richterite in the EH5 St Sauveur, where it occurs as subhedral grains ~40 μm × 100 μm in size. Fluorine contents in these amphiboles range from ~4.0–4.5 wt% F.

Fluorphlogopite ($KMg_3(Si_3Al)O_{10}F_2$)
Lin and Kimura (1998) reported the occurrence of rare crystals of the trioctahedral mica, fluorphlogopite with an average F content of 5.1 wt% in the EH impact-melt rock Y-82189 (Fig. 15.15a). The grains occur as subhedral grains, 10–30 μm in size, associated with enstatite, silica, and albite.

Djerfisherite ($K_6Na_9(Fe,Cu)_{24}S_{26}Cl$)
The highly unusual alkali, Cu–Fe sulfide, djerfisherite was first described by Fuchs (1966) as an accessory phase (0.1–0.5 vol.%) in the Kota-Kota (EH3) and St Mark's (EH5) chondrites (see also El Goresy et al. 1971), but was not found in several other enstatite chondrites. It has since been recognized in several additional EH chondrites, including the EH3s Qingzhen, Y-691 (El Goresy et al. 1988; Lin and El Goresy 2002), ALHA 77295, and Sahara 97096 (Clay et al. 2014), and contains ~1.5 wt% chlorine. Djerfisherite occurs only as a minor phase in EL chondrites (MAC 88136; Lin et al. 1991). Djerfisherite occurs almost exclusively in the matrix of the EH3 chondrites and only rarely in chondrules (Fig. 15.15b). Djerfisherite in Qingzhen is notable, because it occurs only as sulfide-rich, millimeter-sized clasts and veins in the matrix. In addition, El Goresy et al. (1988) found that in Qingzhen and Y-691, djerfisherite exhibited evidence of decomposition by the so-called Qingzhen reaction to very fine-grained, porous troilite, covellite, idaite, bornite, and various other unidentified phases, including an unknown K-rich mineral. The fate of chlorine released during the reaction is unknown. In addition, the decomposition temperature of djerfisherite in EH3 chondrites is currently not constrained, because it is dependent on the djerfisherite composition. For example, the substitution of Cu into djerfisherite increases its stability down to temperatures well below 473 K, but as emphasized by Ebel and Sack (2013), the temperature of the reaction needs to be determined experimentally.

Djerfisherite has been proposed as a potential carrier of I in St. Mark's based on the correlated release of radiogenic $^{129}Xe^*$ and $^{40}Ar^*$ derived from in situ decay of ^{129}I and ^{40}K, respectively (Busemann et al. 2002a, b). However, based on stepwise heating, two carrier phases are implied (Clay et al. 2014), one of which is highly likely to be djerfisherite. In addition to I, djerfisherite in Qingzhen also contains Br (170 ppm), based on PIXE analyses by Woolum et al. (1984). Note that Grossman et al. (1985) stated incorrectly that Br and chlorine were present in caswellsilverite in Qingzhen, which was not actually analyzed by Woolum et al. (1984).

Chlorine-bearing chondrule glass
Elevated concentrations of chlorine-bearing glass have been found in the Qingzhen EH3 (Fig. 15.15c, d) (Grossman et al. 1985; El Goresy et al. 1988) and MAC 88136 EL3 (Lin et al. 1991) chondrites. In Qingzhen, chlorine concentrations as high at 4.4 wt% have been reported, but elevated chlorine concentrations are only present in glass in some chondrules. No measurements of other halogens in these glasses have been made to date. However, Grossman et al. (1985) did perform INAA analyses of a suite of chondrules separated from Qingzhen and found a positive correlation between chlorine and Br in the bulk chondrule compositions, suggesting that in many chondrules, Br is also in the mesostasis with chlorine. A comparison of the average

chondrule composition with the bulk EH composition shows that the two are very similar with abundances close to CI, indicating that Br and chlorine in the bulk chondrite are mostly contained within mesostasis in chondrules.

Lawrencite ($FeCl_2$)
Keil (1968) found thin rims of lawrencite around silica grains in the EH4 fall, Indarch, in addition to inclusions within kamacite and troilite and as isolated grains in the matrix with enstatite. Reports of extraterrestrial lawrencite in meteorites have been questioned by Buchwald and Clarke (1989), who suggest that it may be the product of terrestrial corrosion of Fe metal. However, the occurrences of lawrencite in Indarch do not appear to be readily explained as alteration products.

15.8.5.1 Origin of Chlorine-Bearing Assemblages E Chondrites

As discussed in Sect. 15.4.2.3, enstatite chondrites, especially the EH chondrites, have among the highest halogen contents of any of the chondrite groups. It is, therefore, reasonable that these meteorites should contain a diverse assemblage of halogen-bearing phases. In addition, the highly reducing conditions of the enstatite chondrites favor the formation of unusual phases, such as djerfisherite.

Fluorine appears to be particularly enriched in EH chondrites, although most of the data for bulk F concentrations is questionable (see Sect. 15.4.2.3). There is no evidence of discrete F-rich phases in type 3 enstatite chondrites to constrain the primary nebular carrier of F in these meteorites. As suggested by Rubin and Choi (2009), F may have condensed as simple fluorides such as MgF_2, but there is no direct evidence of this phase in any enstatite chondrite. Instead, the phases that show significant enrichment in F, i.e., fluor-richterite and fluorphlogopite, typically occur in highly modified enstatite chondrites, such as the impact melt rocks Y-82189 and Abee. Both these phases have been interpreted as crystallization products from an impact melt that is enriched in F (Lin and Kimura 1998). However, it is not clear whether the formation of F-bearing amphibole or phlogopite requires an enrichment in F in the bulk meteorite, or whether F is in typical EH concentrations in these rocks, but is highly incompatible and is concentrated in the last melt fraction from which fluor-richterite or fluorphlogopite crystallize. The petrologic context of the fluor-richterite in St. Sauveur (EH5) was not discussed by Rubin (1983), so the possible origin of this phase is unconstrained at this point.

The occurrence of djerfisherite in the unequilibrated EH3 chondrites Qingzhen and Y-691, provides clear evidence that this unusual mineral is a primary nebular phase and not the product of thermal metamorphism. El Goresy et al. (1988) argued that that djerfisherite represents a primary condensate phase that, based on the fine-grained stratigraphy of metal-sulfide clasts that contain it, condensed from the solar nebular gas, after the sulfide minerals oldhamite, niningerite, and caswellsilverite, and after chondrule formation. A similar conclusion was also reached by Clay et al. (2014). Thermodynamic analysis of the stability of djerfisherite (Ebel and Sack 2013) has provided significant constraints on its formation conditions,

placing it as a primary nebular condensate that forms at temperatures above 1000 K. Djerfisherite is stable in a solar composition gas that is enriched >500× in a component comparable to anhydrous chondritic interplanetary dust (C-IDPs). Under these conditions, elements such as S, K, and chlorine that are generally considered to be moderately volatile in more typical oxidizing nebular conditions, are more refractory (Ebel and Sack 2013) and may be incorporated into the solid phase at higher temperatures.

Alternatively, instead of being a primary condensate, some recent models have argued that the sulfides and reduced silicates in enstatite chondrites formed by sulfidization of Mg–Fe silicates at high temperatures (1400–1600 K) during a secondary nebular reheating event in a H-depleted, S-rich nebular gas reservoir (Lehner et al. 2013). Under such conditions, the formation of Mg-rich niningerite, resulting from sulfidization of enstatite, causes an increase in the volatility of Mg, which is lost into the gas phase, whereas typical volatile elements, such as K, Na, chlorine etc., become more refractory and may be incorporated into sulfides such as djerfisherite.

Evidence of decomposition of djerfisherite in Qingzhen—the so called "Qingzhen reaction" (El Goresy et al. 1988), indicates that it undergoes a devolatilization reaction that results in the loss of chlorine. The observed breakdown of djerfisherite may be the result of a short thermal event resulting from a late impact onto the EH parent body (Torigoye and Shima 1993). Ebel and Sack (2013) stated that djerfisherite is not present in petrologic type 4 and 5 chondrites, with the implication that it may undergo thermal decomposition during parent body metamorphism. However, although it is true that djerfisherite is not present in most EH4 and EH5 chondrites, it does occur in the EH5 chondrite St. Mark's, one of the first documented occurrences of djerfisherite (Fuchs 1966) in enstatite chondrites. On the other hand, the absence of djerfisherite in other type 4 and 5 enstatite chondrites does support the view that it is generally unstable under metamorphic conditions. Its presence in St. Mark's is therefore anomalous.

The occurrence of chondrule mesostasis in EH3 chondrites, such as Qingzhen and MAC 88136 EL3, that is significantly enriched in chlorine, in some cases at the several weight percent level, has been noted in several studies. The general interpretation of these data is that chlorine was present in the precursor dust of the chondrules and was, therefore, present as a nebular condensate phase. Djerfisherite might potentially be a precursor candidate as a carrier of chlorine in nebular dust prior to chondrule formation. However, El Goresy et al. (1988) argued that djerfisherite condensed after chondrule formation, based on the common occurrence of niningerite in chondrules that condensed at higher temperatures than djerfisherite. In addition, the chlorine content of djerfisherite is only ∼1.5 wt%, requiring a significant amount of it to produce the elevated concentrations of chlorine in chondrule mesostases. If djerfisherite decomposed during chondrule melting, evidence of residual Cu would be expected as a reaction product, but is not observed.

15.8.6 Other Potential Carriers of Halogens in Chondritic Meteorites—Presolar Grains and Organic Matter

15.8.6.1 Organic Matter

Organic matter is present in essentially all the different chondrite groups, but is most abundant in the carbonaceous chondrites (Alexander et al. 2007). The dominant component is an insoluble macromolecular material that constitutes ~70% of the total organic material (Gilmour 2014), representing as much as 2.25 wt% C in the CI chondrites to around 0.2–0.3 wt% in the ordinary and enstatite chondrites (Alexander et al. 2007). The remainder consists of a wide range of soluble organic compounds that have been documented in detail in a number of different studies (Botta and Bada 2002; Gilmour 2014). Several studies have documented evidence that organohalogens are present in chondritic organic material, but the details of their occurrence and characteristics are limited in comparison with other types of organic compounds. Mueller (1953) reported 5.89% halogens in the insoluble macromolecular carbon in the CM chondrite Cold Bokkeveld, of which most is assumed to be chlorine. However, the possibility that this high chlorine content is the result of contamination from the solvent tricholomethane used in the extraction was not considered (Schöler et al. 2005). We are not aware of any, more recent bulk analyses that have determined chlorine in macromolecular carbon. Kuehner et al. (2007) have reported C-rich objects, up to 50 μm in size, in the NWA 3340 CM2 chondrite, which contains elevated concentrations of chlorine (up to 17 wt%). They suggested that this was some kind of halogenated carbonaceous material. However, it is unclear exactly what this material is or whether it has any affinities to macromolecular carbon. More recently, Le Guillou and Brearley (2014) have reported that individual, distinct grains of organic material, within the CR2 chondrite MET 00426, frequently contain low, but detectable concentrations of chlorine associated with Na. This observation suggests that chlorine may be present as a minor functional group within macromolecular organic carbon in this meteorite. To date, however, this is the only reported occurrence of organic material in CR chondrites with detectable chlorine concentrations.

Several different volatile chlorinated organic compounds have been detected in low concentrations in carbonaceous chondrites. These include alkyl chlorides (C12–C18) in Orgueil (CI) and Cold Bokkeveld (CM) (Studier et al. 1965), chlorinated benzenes and alkanes in Murray (CM) (Hayes and Biemann 1968; Studier et al. 1968), and chlorinated benzoic acids in several CM chondrites and Orgueil (Schöler et al. 2005). In addition to chlorinated organics, Schöler et al. (2005) also reported F- and Br-bearing organic halogens in different extracts from Cold Bokkeveld.

These limited data indicate that a small component of the halogens in chondrites, particularly in carbonaceous chondrites, may be present in organic materials, but it is an extremely small fraction, which remains comparatively poorly understood.

15.8.6.2 Presolar Grains

Investigations of noble gas anomalies in chondrites have been instrumental in identifying the presence of presolar grains in chondritic meteorites (Anders and Zinner 1993). The painstaking analysis of different fractions of residues extracted from meteorites has resulted in a remarkable inventory of different types of presolar grains including diamond, silicon carbide, and graphite (Bernatowicz et al. 2006; Meyer and Zinner 2006; Zinner 2014). Xenon isotopic anomalies were one of the first types of noble gas isotopic anomalies to be recognized in meteorites. It is now known that nanodiamonds are the carrier of the so-called Xe–HL signature, which is a result of r- and p-process nucleosynthesis (neutron capture on a rapid time scale and proton capture or photonuclear reactions) in supernovae. On the other hand, the Xe–S signature is the product of the s-process (neutron capture on a slow time scale) and is carried by silicon carbide. In addition to Xe that clearly originates from nucleosynthetic processes, nanodiamonds also carry a ^{129}Xe* excess that is produced from in situ decay of the short-lived radioisotope ^{129}I, demonstrating that nanodiamonds host a very minor component of the I that is present in chondrites (Huss and Lewis 1995; Gilmour et al. 2005).

15.9 Future Research

Although there has been significant progress towards understanding many different aspects of the cosmochemistry of halogens, this overview of the current state-of-knowledge of the role of halogens in chondritic meteorites demonstrates that there are many unresolved issues and questions to be addressed. First and foremost is the issue of reliable analyses of halogens in chondritic meteorites in order to provide a high quality database of abundances. The analysis of halogens is challenging and no single technique has established itself as being the gold standard. Efforts to carry out comparative analyses using different techniques in different laboratories would be highly beneficial in this regard. Having reliable data is essential to addressing very fundamental questions, such as the cosmochemical behavior of halogens in different chondrite groups, determining if and to what extent halogens are distributed heterogeneously within chondritic meteorites and at what scale, as well as the major issue of terrestrial contamination. The issue of terrestrial contamination, even in meteoritic falls, cannot be overstated given the ubiquitous presence of halite in the terrestrial environment. An important first step would be to ensure the routine measurement of both soluble and insoluble halogen contents in meteorites, as performed by Sharp et al. (2013). It is reasonable to assume that any terrestrial contamination will be solely within the soluble fraction. Therefore, it is possible to at least determine halogen heterogeneity in the insoluble fraction of chondrites on different scales, using this approach. Efforts to perform

analyses of the soluble fraction would be best carried out on meteorites that have low permeabilities and porosities in order to minimize the possibility of migration of saline solutions into the interior of the samples that might be the result of, for example, inappropriate handling and storage in high humidity environments. Better control on the locations of the samples from individual stones, even falls, could also be important to provide constraints on whether contamination is more prevalent close to the surface of the stone vs the interior, as has been done for Antarctic meteorites.

There remain significant uncertainties in the accepted bulk halogen concentrations for several chondrite groups, and for some groups no data are available at all. In particular, F remains highly uncertain, because the most extensive analytical studies of F in chondrites, dating from the 1960s, yielded significantly higher values than more recent studies. Resolution of these issues, by careful studies of well-chosen, interior samples of well-curated falls, are essential to resolving these issues. In addition, analysis of halogens in new falls should be a high priority and protocols to minimize terrestrial contamination, similar to those utilized to minimize organic contaminants, should be utilized routinely for at least a subsample of recovered stones. This approach would enable much better constraints to be placed on the relative proportions of soluble and insoluble halogens within chondrites, as well as addressing more thoroughly the issue of the scale of heterogeneity in the distribution of halogens in chondrites. Such data are essential for constraining the scales of halogen mobility on chondritic parent bodies and helping address whether the evidence of metasomatic processes in some CV, CO, and ordinary chondrites is the result of an influx of fluid from external sources or simply a redistribution of indigeneous halogens that only occurred on a localized scale.

High quality analytical data are the key to constraining the cosmochemical processes that have fractionated halogens in chondritic meteorites. However, further efforts to evaluate and refine the condensation temperatures of the halogens are also essential. There have been considerable and important efforts to determine these values, but there still remains a significant disconnect between the equilibrium thermodynamic condensation calculations and the actual halogen-bearing phases that occur in chondrites. It is apparent that halogens, with the exception of the enstatite chondrites, become concentrated into a specific phase in chondrites, almost entirely as a result of secondary processes. Therefore, the halogen mineralogy of chondrites should generally not be used as a constraint on potential condensate phases in equilibrium condensation calculations. Although the halogen-bearing phases, predicted to condense by Fegley and Lewis (1980), may not be observed in chondrites, it may be that these phases are highly sensitive to even the slightest parent body processing and are not preserved in even the most unequilibrated petrologic type 3 chondrites. This would certainly be the case for chlorine, if the major carrier is HCl hydrate as hypothesized by Zolotov and Mironenko (2007).

Continued efforts to constrain the mineralogical and other halogen carriers in chondritic meteorites are necessary to establish a more complete understanding of

their primary carriers and how they are redistributed during aqueous alteration and thermal metamorphism/metasomatism. There are several meteorite classes where there is almost nothing known about the hosts of the halogens. For meteorites that have experienced aqueous alteration, the possibility that chlorine and other halogens may be hosted in soluble halides needs more detailed investigation. However, such efforts clearly need to be carried out on samples that are known to have been handled and processed under entirely water-absent conditions, certainly a significant challenge. Routine analysis of the surface of freshly-broken chondrite falls would certainly be appropriate, as indicated by the discovery of halite in the Monahans (1999) H5 fall (Zolensky et al. 1999). Such efforts are key to constraining the carriers of the water-soluble fraction of halogens, which are a major component of the halogen inventory in most chondrites.

A significant gap in our understanding of the distribution of halogens in chondrites is the lack of high spatial resolution trace element analyses for these elements. Our knowledge of the occurrence of chlorine and, to some extent, F, which can occur as major and minor elements in some minerals (e.g., sodalite, apatite), is reasonable. However, there are major gaps in our understanding of the distribution of these elements as trace elements, a problem that is particularly acute for I and Br. It is commonly assumed that these elements are incorporated into the same phases as chlorine and F (e.g., Kirschbaum 1988), but this has not yet been fully demonstrated in most cases, with the exception of, for example, analysis of halite and sylvite in the H5 chondrite Monahans (1998) (Busfield et al. 2004), which confirmed the presence of I in sylvite. There have been only limited efforts to measure I and Br in situ in minerals using SIMS and PIXE techniques (e.g., Goswami et al. 1998; Woolum et al. 1984), so there is clearly much to be done. This work is of particular significance for providing important constraints on the carriers of I when carrying out I–Xe studies to establish the chronology of, for example, secondary alteration on asteroidal parent bodies (Krot et al. 2006). Enhanced efforts to develop and improve analytical techniques for high spatial resolution analyses of halogens at trace concentrations could potentially answer key questions, such as the carriers of these elements in the most pristine solar system materials, as well as constraining how these elements may be mobilized and redistributed by low temperature aqueous alteration.

In summary, there are significant opportunities in cosmochemistry for exciting and innovative research into the many different aspects of the role of halogens in the evolution of early solar system materials. Several aspects of halogen cosmochemistry are of first order importance and are currently areas of considerable uncertainty that must be resolved in order to advance our understanding of processes within the protoplanetary disk and asteroidal parent bodies where halogens were fractionated. Since our understanding of the halogen budget of the Earth, and its different reservoirs, depends on our knowledge of halogen behavior in the early solar system, a better grasp of the halogen content of chondrites is of fundamental importance for geochemistry as well as cosmochemistry.

References

Abreu NM, Brearley AJ (2010) Early solar system processes recorded in the matrices of two highly pristine CR3 carbonaceous chondrites, MET 00426 and QUE 99177. Geochim Cosmochim Acta 74(3):1146–1171

Akai J (1988) Incompletely transformed serpentine-type phyllosilicates in the matrix of Antarctic CM chondrites. Geochim Cosmochim Acta 52:1593–1599

Akai J (1990) Mineralogical evidence of heating events in Antarctic carbonaceous chondrites, Y-86720 and Y-82162. Proc NIPR Symp Antarct Meteor 3:55–68

Alexander CMO'D, Hutchison RH, Graham AL, Yabuki H (1987) Discovery of scapolite in the Bishunpur (LL3) chondritic meteorite. Mineral Mag 51:733–735

Alexander CMO'D, Barber DJ, Hutchison R (1989) The microstructure of Semarkona and Bishunpur. Geochim Cosmochim Acta 53:3045–3057

Alexander CMO'D, Fogel M, Yabuta H, Cody GD (2007) The origin and evolution of chondrites recorded in the elemental and isotopic compositions of their macromolecular organic matter. Geochim Cosmochim Acta 71:4380–4403

Alexander CMO'D, Newsome SD, Fogel ML, Nittler LR, Busemann H, Cody GD (2010) Deuterium enrichments in chondritic macromolecular materials: implications for the origin and evolution of organics, water and asteroids. Geochim Cosmochim Acta 74:4417–4437

Alexander CMO'D, Howard KT, Bowden R, Fogel ML (2013) The classification of CM and CR chondrites using bulk H, C and N abundances and isotopic compositions. Geochim Cosmochim Acta 123:244–260

Allen RO, Clark PJ (1977) Fluorine in meteorites. Geochim Cosmochim Acta 41:581–585

Allen RO, Mason B (1973) Minor and trace elements in some meteoritic minerals. Geochim Cosmochim Acta 37:1435–1456

Allen JM, Grossman L, Davis AM, Hutcheon ID (1978) Mineralogy, textures and mode of formation of a hibonite-bearing Allende inclusion. Proc Lunar Planet Sci Conf 9th:1209–1233

Anders E, Ebihara M (1982) Solar system abundances of the elements. Geochim Cosmochim Acta 46:2363–2380

Anders E, Grevesse N (1989) Abundances of the elements: meteoritic and solar. Geochim Cosmochim Acta 53:197–214

Anders E, Zinner E (1993) Interstellar grains in primitive meteorites: diamond, silicon carbide, and graphite. Meteoritics 28:490–514

Anselmi B, Mellini M, Viti C (2000) Chlorine in the Elba, Monti Livornesi and Murlo serpentines: evidence for sea-water interaction. Eur J Mineral 121:137–146

Ashworth JR (1981) Fine structure in H-group chondrites. Proc R Soc Lond A374:179–194

Asplund M, Grevesse N, Sauval J, Scott P (2009) The chemical composition of the Sun. Ann Rev Astron Astrophys 47:481–522

Barber DJ (1981) Matrix phyllosilicates and associated minerals in C2M carbonaceous chondrites. Geochim Cosmochim Acta 95:3945–3970

Bass MN (1971) Montmorillonite and serpentine in Orgueil meteorite. Geochim Cosmochim Acta 35:139–148

Benedix SA, Leshin LA, Farquhar J, Jackson TL, Thiemens MH (2003) Carbonates in CM chondrites: Constraints on alteration conditions from oxygen isotopic compositions and petrographic observations. Geochim Cosmochim Acta 67:1577–1588

Berlin J, Jones RH, Brearley AJ (2007) A closer look at chondrules and matrix in Kakangari: evidence for widespread reduction and sulfurization (abstract). Lunar Planet Sci 38:2395

Bernatowicz T, Groat TK, Daulton TL (2006) Origin and evolution of carbonaceous presolar grains in stellar environments. In: Lauretta DS, McSween HY Jr (eds) Meteorites and the early solar system II. University of Arizona Press, Tucson, pp 109–126

Bischoff A (2000) Mineralogical characterization of primitive, type-3 lithologies in Rumuruti chondrites. Meteor Planet Sci 35:699–706

Bischoff A, Geiger T, Palme H, Spettel B, Schultz L, Scherer P, Bland P, Clayton RN, Mayeda TK, Herpers U, Michel R, Dittrich-Hannen B (1994) Acfer 217- a new member of the Rumuruti chondrite group (R). Meteoritics 29:264–274

Bland PA, Zolensky ME, Benedix GK, Sephton MA (2006) Weathering of chondritic meteorites. In: Lauretta DS, McSween HY Jr (eds) Meteorites and the early solar system. University of Arizona Press, Tucson, AZ, pp 853–867

Bland PA, Jackson MD, Coker RF, Cohen BA, Webber JBW, Lee MR, Duffy CM, Chater RJ, Ardakani MG, McPhail DS, McComb DW, Benedix GK (2009) Why aqueous alteration in asteroids was isochemical: high porosity [not equal to] high permeability. Earth Planet Sci Lett 287:559–568

Blinova AI, Zega TJ, Herd CD, Stroud RM (2014a) Testing variations within the Tagish Lake meteorite—I: mineralogy and petrology of pristine samples. Meteor Planet Sci 49:473–502

Blinova AI, Herd CD, Duke MJ (2014b) Testing variations within the Tagish Lake meteorite—II: whole-rock geochemistry of pristine samples. Meteor Planet Sci 49:1100–1118

Bonal L, Bourot-Denise M, Quirico E, Montagnac G, Lewin E (2007) Organic matter and metamorphic history of CO chondrites. Geochim Cosmochim Acta 71:1605–1623

Bonal L, Alexander CMOD, Huss GR, Nagashima K, Quirico E, Beck P (2013) Hydrogen isotopic composition of the water in CR chondrites. Geochim Cosmochim Acta 106:111–133

Bonifacie M, Jendrzejewski N, Agrinier P, Coleman ML, Pineau F, Javoy M (2007) Pyrohydrolysis-IRMS determination of silicate chlorine stable isotope compositions: application to oceanic crust and meteorite samples. Chem Geol 242:187–201

Bonifacie M, Jendrzejewski N, Agrinier P, Humler E, Coleman M, Javoy M (2008) The chlorine isotope composition of earth's mantle. Science 319:1518–1520

Boss AP, Goswami JN (2006) Presolar cloud collapse and the formation and early evolution of the solar nebula. In: Lauretta DS, McSween HY Jr (eds) Meteorites and the early solar system II. University of Arizona Press, Tucson, pp 171–186

Boström K, Fredriksson K (1966) Surface conditions of the Orgueil meteorite parent body as indicated by mineral associations. Smithson Misc Coll 151:1–39

Botta O, Bada JL (2002) Extraterrestrial organic compounds in meteorites. Surv Geophys 23:411–467

Bouvier A, Blichert-Toft J, Moynier F, Vervoort JD, Albarède F (2007) Pb–Pb dating constraints on the accretion and cooling history of chondrites. Geochim Cosmochim Acta 71:1583–1604

Brazzle RH, Pravdivtseva OV, Meshik AP, Hohenberg CM (1999) Verification and interpretation of the I–Xe chronometer. Geochim Cosmochim Acta 63:739–760

Brearley AJ (2006a) The action of water. In: Lauretta DS, McSween Jr HY (eds) Meteorites and the early solar system II. University of Arizona Press, Tucson, AZ, pp 587–624

Brearley AJ (2006b) The role of microchemical environments in the alteration of CM carbonaceous chondrites. Lunar Planet Sci XXXVII.CDROM abstract #2074

Brearley AJ (2014) Nebular vs parent body processing of chondritic meteorites. In: Davis AM (ed) Meteorites, comets and planets, vol 1. Elsevier, Cambridge, pp 309–334

Brearley AJ, Burger PV (2009) Mechanisms of aqueous alteration of type IIA chondrule glass in the CR chondrite EET 92105: insights from FIB/TEM analysis (abstract). Meteor Planet Sci 44:A39

Brearley AJ, Jones RH (1998) Chondritic meteorites. In: Papike JJ (ed) Planetary materials, reviews in mineralogy, vol 36. Mineralogical Society of America, Washington, DC, p 398

Brearley AJ, Krot AN (2013) Metasomatism in chondritic meteorites. In: Harlov DE, Austrheim H (eds) Metasomatism and the chemical transformation of rock: the role of fluids in terrestrial and extraterrestrial processes. Springer, Berlin, pp 653–782

Brearley AJ, Barnes JD, Sharp ZD (2007) Chrysotile nanotubes: potential host of insoluble chlorine in serpentinitized oceanic crust (abstract). American Geophysical Union, Fall Meeting 2007:V11E-04

Brearley AJ, Fagan TJ, Washio M, MacPherson GJ (2014) FIB-TEM characterization of dmisteinbergite with intergrown biopyriboles in Allende Ca–Al-rich inclusions: Evidence for alteration in the presence of aqueous fluid (abstract). Lunar Planet Sci 45:2287

Bridges JC, Alexander CMO, Hutchison R, Franchi IA, Pillinger CT (1997) Sodium-, chlorine-rich mesostases in Chainpur (LL3) and Parnallee (LL3) chondrules. Meteor Planet Sci 32:555–565

Bridges JC, Banks DA, Smith M, Grady MM (2004) Halite and stable chlorine isotopes in the Zag H3-6 breccia. Meteor Planet Sci 39:657–666

Browning LB, McSween HY Jr, Zolensky ME (1996) Correlated alteration effects in CM carbonaceous chondrites. Geochim Cosmochim Acta 60:2621–2633

Buchanan PC, Zolensky ME, Reid AM (1997) Petrology of Allende dark inclusions. Geochim Cosmochim Acta 61:1733–1743

Buchwald VF, Clarke RS Jr (1989) Corrosion of Fe–Ni alloys by Cl-containing akaganéite (beta-FeOOH): the Antarctic meteorite case. Am Mineral 74:656–667

Burger PV, Brearley AJ (2005) Localized chemical redistribution during aqueous alteration in CR2 carbonaceous chondrites EET87770 and EET92105 (abstract). Lunar Planet Sci 26:2288

Busemann H, Baur H, Wieler R (2002a) On line etching of bulk EH5 St. Mark's—radiogenic and subsolar noble gases (abstract). Meteor Planet Sci 37:A28

Busemann H, Baur H, Wieler R (2002b) Noble gas characteristics of the E chondrite St. Mark's (abstract). Goldschmidt Conf Abstr:A112

Busfield A, Gilmour JD, Whitby JA, Turner G (2004) Iodine-xenon analysis of ordinary chondrite halide: implications for early solar system water. Geochim Cosmochim Acta 68:195–202

Chizmadia L, Rubin A, Wasson J (2002) Mineralogy and petrology of amoeboid olivine inclusions in CO_3 chondrites: relationship to parent-body aqueous alteration. Meteor Planet Sci 37:1781–1796

Choi B-G, Krot AN, Wasson JT (2000) Oxygen-isotopes in magnetite and fayalite in CV chondrites Kaba and Mokoia. Meteor Planet Sci 35:1239–1249

Christophe Michel-Lévy M (1976) La matrice noire et blanche de la chondrite de Tieschitz. Earth Planet Sci Lett 30:143–150

Clarke RSJ, Rowe MW, Ganapathy R, Kuroda PK (1967) Iodine, uranium and tellurium contents in meteorites. Geochim Cosmochim Acta 31:1605–1613

Clay P, Burgess R, Busemann H, Ruzie L, Joachim B, Ballentine C (2013) Halogen (Cl, Br and I) inventory of the primitive meteorites (abstract). Mineral Mag 77:896

Clay PL, O'Driscoll B, Upton BGJ, Busemann H (2014) Characteristics of djerfisherite from fluid-rich, metasomatized alkaline intrusive environments and anhydrous enstatite chondrites and achondrites. Am Mineral 99:1683–1693

Clayton RN (1993) Oxygen isotopes in meteorites. Ann Rev Earth Planet Sci 21:115–149

Clayton RN, Mayeda TK (1999) Oxygen isotope studies of carbonaceous chondrites. Geochim Cosmochim Acta 63:2089–2104

Cloëz S (1864) Analyse chimique de la pierre météoritique d'Orgueil. Comp Rend Acad Sci, Paris 59:37–38

Corrigan CM, Zolensky ME, Dahl J, Long M, Weir J, Sapp C, Burkett PJ (1997) The porosity and permeability of chondritic meteorites and interplanetary dust particles. Meteor Planet Sci 32:509–515

Cosarinsky M, Leshin LA, MacPherson GJ, Guan YB, Krot AN (2008) Chemical and oxygen isotopic compositions of accretionary rim and matrix olivine in CV chondrites: constraints on the evolution of nebular dust. Geochim Cosmochim Acta 72:1887–1913

Dobrică E, Brearley AJ (2014) Widespread hydrothermal alteration minerals in the fine-grained matrices of the Tieschitz unequilibrated ordinary chondrite. Meteor Planet Sci 49:1323–1349

Dohmen R, Chakraborty S, Palme H, Rammensee W (1998) Solid-solid reactions mediated by a gas phase: an experimental study of reaction progress and the role of surfaces in the system olivine-iron metal. Am Mineral 83:970–984

Douglas JAV, Plant AG (1969) Amphibole: first occurrence in an enstatite chondrite (abstract). Meteoritics 4:166

Dreibus G, Wänke H (1983) Halogens in Antarctic meteorites (abstract). Meteoritics 18:291–292
Dreibus G, Spettel B, Wänke H (1979) Halogens in meteorites and their primordial abundances. Phys Chem Earth 11:33–38
DuFresne ER, Anders E (1962) On the chemical evolution of the carbonaceous chondrites. Geochim Cosmochim Acta 26:1085–1114
Dyl KA, Boyce JW, Guan Y, Bland PA, Eiler JM (2014) Characterizing early solar system fluids on the Allende (CV3) parent body: NanoSIMS study of phosphate volatile contents (abstract). Meteor Planet Sci Supp 49:A454
Ebel DS, Alexander CMO'D (2011) Equilibrium condensation from chondritic porous IDP enriched vapor: implications for mercury and enstatite chondrite origins. Planet Space Sci 59:1888–1894
Ebel DS, Sack RO (2013) Djerfisherite: nebular source of refractory potassium. Contrib Mineral Petrol 166:923–934
Ebihara M, Honda M (1987) Rare earth elements in Ca-phosphates of Allende carbonaceous chondrite. Meteoritics 22:179–190
Eggenkamp H (2014) The halogen elements. In: Eggenkamp H (ed) The geochemistry of stable chlorine and bromine isotopes. Springer, Heidelberg, pp 3–13
El Goresy A, Grögler N, Ottermann J (1971) Djerfisherite composition in Bishopville, Pena Blanca Springs, St. Marks and Toluca meteorites. Chem Erde 30:77–82
El Goresy A, Yabuki H, Ehlers K, Woolum D, Pernicka E (1988) Qingzhen and Yamato-691: a tentative alphabet for the EH chondrites. Proc NIPR Symp Antarct Meteor 1:65–101
Fagan TJ, Guan Y, MacPherson GJ (2007) Al–Mg isotopic evidence for episodic alteration of Ca–Al-rich inclusions from Allende. Meteor Planet Sci 42:1221–1240
Fahey AJ, Zinner E, Kurat K, Kracher A (1994) Hibonite-hercynite inclusion HH-1 from the Lance (CO3) meteorite: the history of an ultrarefractory CAI. Geochim Cosmochim Acta 58:4779–4793
Fegley B Jr, Lewis JS (1980) Volatile element chemistry in the solar nebula—Na, K, F, Cl, Br, and P. Icarus 41:439–445
Fintor K, Park C, Nagy S, Pál-Molnár E, Krot AN (2014) Hydrothermal origin of hexagonal $CaAl_2Si_2O_8$ (dmisteinbergite) in a compact type A CAI from the Northwest Africa 2086 CV3 chondrite. Meteor Planet Sci 49:812–823
Franchi IA (2008) Oxygen isotopes in asteroidal materials. In: MacPherson GJ (ed) Oxygen in the solar system, vol 68. Mineralogical Society of America, Chantilly, VA, pp 345–398
Fredriksson K, Kerridge JF (1988) Carbonates and sulfates in Cl chondrites: formation by aqueous activity on the parent body. Meteoritics 23:35–44
Fries M, Messenger S, Steele A. and Zolensky M (2013) Do we already have samples of Ceres? H chondrite halites and the Ceres-Hebe link (abstr). 76th Annual Meteoritical Society #5266
Fuchs LH (1966) Djerfisherite, alkali copper-iron sulfide: a new mineral from enstatite chondrites. Science 153:166–167
Garrison D, Hamlin S, Bogard D (2000) Chlorine abundances in meteorites. Meteor Planet Sci 35:419–429
Gilmour I (2014) Structural and isotopic analysis of organic matter in carbonaceous chondrites. In: Davis AM (ed) Meteorites, comets and planets, vol 1. Elsevier, Cambridge, pp 215–233
Gilmour JD, Verchovsky AB, Fisenko AV, Holland G, Turner G (2005) Xenon isotopes in size separated nanodiamonds from Efremovka: ^{129}Xe*, Xe-P3, and Xe-P6. Geochim Cosmochim Acta 69:4133–4148
Gilmour JD, Pravdivtseva OV, Busfield A, Hohenberg CM (2006) The I–Xe chronometer and the early solar system. Meteor Planet Sci 41:19–31
Godon A, Jendrzejewski N, Castrec-Rouelle M, Dia A, Pineau F, Boulégue J, Javoy M (2004) Origin and evolution of fluids from mud volcanos in the Barbados accretionary complex. Geochim Cosmochim Acta 68:2153–2165
Goldberg RH, Burnett DS, Furst MJ, Tombrellot A (1974) Fluorine concentrations in carbonaceous chondrites. Meteoritics 9:347

Goles GG, Anders E (1961) On the geochemical character of iodine in meteorites. J Geophys Res 66:3075–3077
Goles GG, Anders E (1962) Abundances of iodine, tellurium and uranium in meteorites. Geochim Cosmochim Acta 26:723–737
Goles GG, Greenland LP, Jerome DJ (1967) Abundances of chlorine, bromine and iodine in meteorites. Geochim Cosmochim Acta 31:1771–1787
Göpel C, Manhes G, Allegre CJ (1994) U–Pb systematics of phosphates from equilibrated ordinary chondrites. Earth Planet Sci Lett 121:153–171
Goswami JN, Sahijpal S, Kehm K, Hohenberg CM, Swindle T, Grossman JN (1998) In situ determination of iodine content and iodine–xenon systematics in silicates and troilite phases in chondrules from the LL3 chondrite Semarkona. Meteor Planet Sci 33:527–534
Gounelle M, Zolensky ME (2001) A terrestrial origin for sulfate veins in CI1 chondrites. Meteor Planet Sci 35:1321–1329
Greenland L, Lovering JF (1965) Minor and trace element abundances in chondritic meteorites. Geochim Cosmochim Acta 29:821–858
Greenwood RC, Franchi IA (2004) Alteration and metamorphism of CO3 chondrites: evidence from oxygen and carbon isotopes. Meteor Planet Sci 39:1823–1838
Greenwood RC, Franchi IA, Kearsley AT, Alard O (2010) The relationship between CK and CV chondrites. Geochim Cosmochim Acta 74:1684–1705
Gross J, Treiman AH, Connolly Jr. HC (2013) A new subgroup of amphibole-bearing R-chondrites: evidence from the new R chondrite, MIL 11207 (abstract). 44th Lunar Planet Sci 44:2212
Grossman JN, Brearley AJ (2005) On the onset of metamorphism in ordinary and carbonaceous chondrites. Meteor Planet Sci 40:87–122
Grossman JN, Wasson JT (1987) Compositional evidence regarding the origin of rims on Semarkona chondrules. Geochim Cosmochim Acta 51:3003–3011
Grossman L, Fruland RM, McKay DS (1975) Scanning electron microscopy of a pink inclusion from the Allende meteorite. Geophys Res Lett 2:37–40
Grossman JN, Rubin AE, Rambaldi ER, Rajan RS, Wasson JT (1985) Chondrules in the Qingzhen type-3 enstatite chondrite: possible precursor components and comparison to ordinary chondrite chondrules. Geochim Cosmochim Acta 49:1781–1795
Grossman JN, Alexander CMO, Wang JH, Brearley AJ (2000) Bleached chondrules: evidence for widespread aqueous processes on the parent asteroids of ordinary chondrites. Meteor Planet Sci 35:467–486
Grossman L, Beckett JR, Fedkin AV, Simon SB and Ciesla FJ (2009) Redox conditions in the solar nebula: observational, experimental, and theoretical constraints. In: MacPherson GJ (ed) Oxygen in the solar system. Reviews in mineralogy and geochemistry, vol 68. Mineralogical Society of America, Chantilly, pp 93–140
Hall DNB, Noyes RW (1969) Observation of hydrogen fluoride in sunspots and the determination of the solar fluorine abundance. Astrophys J 4:L143–L148
Hall DNB, Noyes RW (1972) The identification of the 1-0 and 2-1 bands of HCI in the infrared sunspot spectrum. Astrophys J 175:L95–L97
Hand KP (2018) Halogens on and within the ocean worlds of the outer solar system. In: Harlov DE, Aranovitch L (eds) The role of halogens in terrestrial and extraterrestrial geochemical processes: surface, crust, and mantle. Springer, Berlin, pp 997–1016
Harju ER, Rubin AE, Ahn I, Choi B-G, Ziegler K, Wasson JT (2014) Progressive aqueous alteration of CR carbonaceous chondrites. Geochim Cosmochim Acta 139:267–292
Hashimoto A, Grossman L (1987) Alteration of Al-rich inclusions inside ameboid olivine aggregates in the Allende meteorite. Geochim Cosmochim Acta 51:1685–1704
Hayes JM, Biemann K (1968) High resolution mass spectrometric investigations of the organic constituents of the Murray and Holbrook chondrites. Geochim Cosmochim Acta 32:239–267
Heumann KG, Gall M, Weiss HM (1987) Geochemical investigations to explain iodine-overabundances in Antarctic meteorites. Geochim Cosmochim Acta 51:2541–2547

Heumann KG, Neubauer J, Reifenhäuser W (1990) Iodine overabundances measured in the surface layers of an antarctic stony and iron meteorite. Geochim Cosmochim Acta 54:2503–2506

Hohenberg CM (1980) High sensitivity pulse-counting massspectrometer system for noble gas analysis. Rev Sci Instrum 51:1075–1082

Holmberg AA, Hashimoto A (1992) A unique, (almost) unaltered spinel-rich fine-grained inclusion in Kainsaz. Meteoritics 27:149–153

Housley RM, Cirlin EH (1983) On the alteration of Allende chondrules and the formation of matrix. In: King EA (ed) Chondrules and their origins. Lunar and Planetary Institute, Houston, pp 145–161

Howard KT, Benedix GK, Bland PA, Cressey G (2009) Modal mineralogy of CM2 chondrites by X-ray diffraction (PSD-XRD). Part 1: total phyllosilicate abundance and the degree of aqueous alteration. Geochim Cosmochim Acta 73:4576–4589

Howard KT, Benedix GK, Bland PA, Cressey G (2011) Modal mineralogy of CM chondrites by X-ray diffraction (PSD-XRD). Part 2: degree, nature and settings of aqueous alteration. Geochim Cosmochim Acta 75:2735–2751

Howard KT, Alexander CMO'D, Schrader DL, Dyl KA (2015) Classification of hydrous meteorites (CR, CM and C2 ungrouped) by phyllosilicate fraction: PSD-XRD modal mineralogy and planetesimal environments. Geochim Cosmochim Acta 149:206–222

Hsu W, Guan Y, Leshin LA, Ushikubo T, Wasserburg GJ (2006) A late episode of irradiation in the early solar system: evidence from extinct ^{36}Cl and ^{26}Al in meteorites. Astrophys J 640:525–529

Huss GR, Lewis RS (1995) Presolar diamond, SiC, and graphite in primitive chondrites: abundances as a function of meteorite class and petrologic type. Geochim Cosmochim Acta 59:115–160

Huss GR, Rubin AE, Grossman JN (2006) Thermal metamorphism in chondrites. In: Lauretta DS, McSween HY Jr (eds) Meteorites and the early solar system II. University of Arizona Press, Tucson, AZ, pp 567–586

Hutcheon ID, Newton RC (1981) Mg isotopes, mineralogy and mode of formation of secondary phases in C3 refractory inclusions (abstract). Lunar Planet Sci 12:491–493

Hutchison R, Bevan AWR, Agrell SO, Ashworth JR (1979) Accretion temperature of Tieschitz H3, chondritic meteorite. Nature 280:116–119

Hutchison R, Alexander CMOD, Bridges JC (1998) Elemental redistribution in Tieschitz and the origin of white matrix. Meteor Planet Sci 33:1169–1180

Ikeda Y (1982) Petrology of the ALH-77003 chondrite (C3). Proceedings of the Seventh Symposium on Antarctic meteorites. Mem Natl Inst Polar Res Spec Issue 25:34–65

Ikeda Y (1991) Petrology and mineralogy of the Yamato-82162 chondrite (CI). Proc NIPR Symp Antarct Meteor 4:187–225

Ikeda Y, Kimura M (1995) Anhydrous alteration of Allende chondrules in the solar nebula I: description and alteration of chondrules with known oxygen-isotopic compositions. Proc NIPR Symp Antarct Meteor 8:97–122

Ikeda Y, Noguchi T, Kimura M (1992) Petrology and mineralogy of the Yamato-86720 carbonaceous chondrite. Proc NIPR Symp Antarct Meteor 5:136–154

Ishii HA, Krot AN, Bradley JP, Keil K, Nagashima K, Teslich N, Jacobsen B, Yin Q-Z (2010) Discovery, mineral paragenesis, and origin of wadalite in a meteorite. Am Mineral 95:440–448

Itoh S, Kojima H, Yurimoto H (2004) Petrography and oxygen isotopic compositions in refractory inclusions from CO chondrites. Geochim Cosmochim Acta 68:183–194

Ivanova MA, Nazarov MA, Kononkova NN, Taylor LA, Patchen AD, Clayton RN (2000) Dhofar 015, a new CK chondrite: a record of nebular processes (abstract). Meteor Planet Sci 35:A83

Jacobsen B, Yin Q-Z, Moynier F, Amelin Y, Krot AN, Nagashima K, Hutcheon ID, Palme H (2008) ^{26}Al–^{26}Mg and ^{207}Pb–^{206}Pb systematics of Allende CAIs: Canonical solar initial ^{26}Al/^{27}Al ratio reinstated. Earth Planet Sci Lett 272:353–364

Jacobsen B, Matzel J, Hutcheon ID, Ramon E, Krot AN, Ishii HA, Nagashima K, Yin QZ (2009) The ^{36}Cl-^{36}S systematics of wadalite from the Allende meteorite (abstract). Lunar Planet Sci 40:2553–2554

Jacobsen B, Matzel J, Hutcheon ID, Krot AN, Yin QZ, Nagashima K, Ramon EC, Weber PK, Ishii HA, Ciesla FJ (2011) Formation of the short-lived radionuclide ^{36}Cl in the protoplanetary disk during late-stage irradiation of a volatile-rich reservoir. Astrophys J Lett 731:L28–L34

Jeffery PM, Reynolds JH (1961) Origin of excess Xe129 in stone meteorites. J Geophys Res 66:3582–3583

Johnson CA, Prinz M (1993) Carbonate compositions in CM and CI chondrites and implications for aqueous alteration. Geochim Cosmochim Acta 57:2843–2852

Jones RH, Brearley AJ (2010a) Late-stage fluids on the LL chondrite parent body: evidence from feldspar in the LL4 chondrites Bo Xian and Bjurböle (abstract). Lunar Planet Sci 41:2133

Jones RH, Brearley AJ (2010b) Fluids on the LL chondrite parent body: evidence from the Bo Xian chondrite (abstract). Meteor Planet Sci 45:5276

Jones RH, McCubbin FM, Dreeland L, Guan Y, Burger PV, Shearer CK (2014) Phosphate minerals in LL chondrites: a record of the presence and action of fluids during metamorphism on asteroids. Geochim Cosmochim Acta 132:120–140

Jones RH, McCubbin FM, Guan Y (2016) Phosphate minerals in the H group of ordinary chondrites, and fluid activity recorded by apatite heterogeneity in the Zag H3-6 regolith breccia. Am Mineral 101:2452

Kallemeyn GW (1988) Compositional study of carbonaceous chondrites with CI–CM affinities. Proc NIPR Symp Antarct Meteor 13:132–134

Kallemeyn GW, Wasson JT (1981) The compositional classification of chondrites-I. The carbonaceous chondrite groups. Geochim Cosmochim Acta 45:1217–1230

Kallemeyn GW, Wasson JT (1982) The compositional classification of chondrites: III. Ungrouped carbonaceous chondrites. Geochim Cosmochim Acta 46:2217–2228

Kallemeyn GW, Wasson JT (1986) Compositions of enstatite (EH3, EH4,5 and EL6) chondrites: implications regarding their formation. Geochim Cosmochim Acta 46:597–608

Kallemeyn GW, Rubin AE, Wang D, Wasson JT (1989) Ordinary chondrites: bulk compositions, classification, lithophile-element fractionations and composition-petrographic type relationships. Geochim Cosmochim Acta 53:2747–2767

Kallemeyn GW, Rubin AE, Wasson JT (1991) The compositional classification of chondrites: V. The Karoonda (CK) group of carbonaceous chondrites. Geochim Cosmochim Acta 55:881–892

Kallemeyn GW, Rubin AE, Wasson JT (1994) The compositional classification of chondrites: VI. The CR carbonaceous chondrite group. Geochim Cosmochim Acta 58:2873–2888

Kallemeyn GW, Rubin AE, Wasson JT (1996) The compositional classification of chondrites: VII. The R chondrite group. Geochim Cosmochim Acta 60:2243–2256

Kato F, Ozaka H, Ebihara M (2000) Distribution of halogens in an Antarctic ordinary chondrite Y-79014. Antarct Meteor Res 13:121–134

Keil K (1968) Mineralogical and chemical relationships among enstatite chondrites. J Geophys Res 73:6945–6976

Keller LP, Clark JC, Lewis CF, Moore CB (1992) Maralinga, a metamorphosed carbonaceous chondrite found in Australia. Meteoritics 27:87–91

Keller LP, Thomas KL, Clayton RN, Mayeda TK, DeHart JM, McKay DS (1994) Aqueous alteration of the Bali CV3 chondrite: evidence from mineralogy, mineral chemistry, and oxygen isotopic compositions. Geochim Cosmochim Acta 58:5589–5598

Kerridge JF (1993) Origins of organic matter in meteorites. Proc NIPR Symp Antarct Meteor 6:293–303

Kimura M, Ikeda Y (1992) Mineralogy and petrology of an unusual Belgica-7904 carbonaceous chondrite: genetic relationships among the components. Proc NIPR Symp Antarct Meteor 5:74–119

Kimura M, Ikeda Y (1995) Anhydrous alteration of Allende chondrules in the solar nebula: Alkali-Ca exchange reactions and the formation of nepheline, sodalite and Ca-rich phases in chondrules. Proc NIPR Symp Antarct Meteor 8:123–138

Kimura M, Grossman JN, Weisberg MK (2008) Fe–Ni metal in primitive chondrites: indicators of classification and metamorphic conditions for ordinary and CO chondrites. Meteor Planet Sci 43:1161–1177

Kirschbaum C (1988) Carrier phases for iodine in the Allende meteorite and their associated $^{129}Xe_r/^{129}I$ ratios; a laser microprobe study. Geochim Cosmochim Acta 52:679–699

Kojima T, Yada S, Tomeoka K (1995) Ca–Al-rich inclusion in three Antarctic CO_3 chondrites, Yamato 81020, Yamato-82050 and Yamato-790992: record of low temperature alteration processes. Proc NIPR Symp Antarct Meteor 8:79–86

Kornacki AS, Wood JA (1985) Mineral chemistry and origin of spinel-rich inclusions in the Allende CV3 chondrite. Geochim Cosmochim Acta 49:1219–1237

Krähenbühl U, Morgan JW, Ganapathy R, Anders E (1973) Abundance of 17 trace elements in carbonaceous chondrites. Geochim Cosmochim Acta 37:1353–1370

Krot AN, Scott ERD, Zolensky ME (1995) Mineralogical and chemical modification of components in CV3 chondrites: Nebular or asteroidal processing? Meteoritics 30:748–775

Krot AN, Petaev MI, Zolensky ME, Keil K, Scott ERD, Nakamura K (1998) Secondary calcium-iron minerals in the Bali-like and and Allende-like oxidized CV3 chondrites and Allende inclusions. Meteor Planet Sci 33:623–645

Krot AN, Brearley AJ, Ulyanov AA, Biryukov VV, Swindle TD, Keil K, Mittlefehldt DW, Scott ERD, Clayton RN, Mayeda TK (1999) Mineralogy, petrography and bulk chemical, I–Xe, and oxygen isotopic compositions of dark incusions in the reduced CV3 chondrite Efremovka. Meteor Planet Sci 34:67–90

Krot AN, Petaev MI, Meibom A, Keil K (2001) In situ growth of Ca-rich rims around Allende dark inclusions. Geochem Int 38:S351–S368

Krot AN, Meibom A, Weisberg MK, Keil K (2002) The CR chondrite clan: implications for early solar system processes. Meteor Planet Sci 37:1451–1490

Krot A, Hutcheon ID, Brearley AJ, Pravdivtseva OV, Petaev MI, Hohenberg CM (2006) Timescales for secondary alteration of chondritic meteorites. In: Lauretta D, McSween HY Jr (eds) Meteorites and the early solar system II. University of Arizona Press, Tucson, AZ, pp 525–555

Krot AN, Nagashima K, Hutcheon ID, Ishii HA, Jacobsen B, Yin Q-Z, Davis AM, Simon SB (2010) Mineralogy, petrography, oxygen and magnesium isotopic compositions and formation age of grossular-bearing assemblages in the Allende CAIs (abstract). Lunar Planet Sci 41:1441

Krot AN, Keil K, Scott ER, Goodrich CA, Weisberg MK (2014) Classification of meteorites and their genetic relationships. In: Davis AM (ed) Meteorites and cosmochemical processes, vol. 1 of Treatise on geochemistry, 2nd edn. Elsevier, Oxford, pp 1–63

Kuehner SM, Irving AJ, Rumble D III, Sipera PP (2007) Chlorine-rich carbonaeous compound in anomalous CM2 chondrites Northwest Africa 3340 (abstract). Meteor Planet Sci 42:5131

Kung C-C, Clayton RN (1978) Nitrogen abundances and isotopic compositions in stony meteorites. Earth Planet Sci Lett 38:421–435

Kurat G (1969) The formation of chondrules and chondrites and some observations on chondrules from the Tieschitz meteorite. In: Millman PM (ed) Meteorite research. Springer, Dordrecht, pp 185–190

Kurat G (1975) De kohlige Chondrit Lance: Eine petrologische Analyse der komplexen Genese eines Chondriten. Tschermaks Mineral Petrogr Mitt 22:38–78

Kurat G, Palme H, Brandstatter F, Huth J (1989) Allende Xenolith AF: Undisturbed record of condensation and aggregation of matter in the Solar Nebula. Z Naturforsch 44a:988–1004

Kurat G, Zinner E, Brandstätter F (2002) A plagioclase–olivine–spinel–magnetite inclusion from Maralinga (CK): evidence for sequential condensation and solid–gas exchange. Geochim Cosmochim Acta 66:2959–2979

Langenauer M, Krähenbühl U (1993) Halogen contamination in Antarctic H5 and H6 chondrites and relation to sites of recovery. Earth Planet Sci Lett 120:431–442

Larimer JW (1988) The cosmochemical classification of the elements. In: Kerridge JF, Matthews MS (eds) Meteorites and the early solar system. University of Arizona Press, Tucson, AZ, pp 375–389

Larimer JW, Bartholomay M (1979) The role of carbon and oxygen in cosmic gases: some applications to the chemistry and mineralogy of enstatite chondrites. Geochim Cosmochim Acta 43:1455–1466

Lavielle B, Marti K (1992) Trapped xenon in ordinary chondrites. J Geochem Res 97:875–881

Le Guillou C, Brearley A (2014) Relationships between organics, water and early stages of aqueous alteration in the pristine CR3.0 chondrite MET 00426. Geochim Cosmochim Acta 131:344–367

Lehner SW, Petaev MI, Zolotov MY, Buseck PR (2013) Formation of niningerite by silicate sulfidation in EH3 enstatite chondrites. Geochim Cosmochim Acta 101:34–56

Lewis JA, Jones RH (2014) Nephelinization and metasomatism in the ordinary chondrite Parnallee (LL3.6) (abstract). Lunar Planet Sci 45:1661

Lewis JA, Jones RH (2015) Microtextural study of feldspar in petrologic type 4 ordinary chondrites: contrasting records of parent body metasomatism (abstract). Lunar Planet Sci 45:5119

Lewis JA, Jones RH (2016) Phosphate and feldspar mineralogy of equilibrated L ordinary chondrites: the record of metasomatism during metamorphism in ordinary chondrite parent bodies. Meteor Planet Sci 51:1886

Li CL, Bridges JC, Hutchison R, Franchi IA, Sexton AS, Ouyang ZY, Pillinger CT (2000) Bo Xian (LL3.9): Oxygen-isotopic and mineralogical characterisation of separated chondrules. Meteor Planet Sci 35:561–568

Lin Y, El Goresy A (2002) A comparative study of opaque phases in Qingzhen (EH3) and MacAlpine Hills 88136 (EL3): representatives of EH and EL parent bodies. Meteor Planet Sci 37:577–599

Lin Y, Kimura M (1998) Petrographic and mineralogical study of new EH melt rocks and a new enstatite chondrite grouplet. Meteor Planet Sci 33:501

Lin YT, Nagel H-J, Lundberg LL, El Goresy A (1991) MAC88136- The first EL3 chondrite (abstract). Lunar Planet Sci 22:811–812

Lin Y, Guan Y, Leshin LA, Ouyang Z, Wang D (2005) Short-lived chlorine-36 in a Ca- and Al-rich inclusion from the Ningqiang carbonaceous chondrite. Proc Natl Acad Sci 102:1306–1311

Lin Y, Kimura M, Miao B, Dai D, Monoi A (2006) Petrographic comparison of refractory inclusions from different chemical groups of chondrites. Meteor Planet Sci 41:67–81

Lodders K (2003) Solar system abundances and condensation temperatures of the elements. Astrophys J 591:1220–1247

Lodders K, Fegley BJ (1998) The planetary scientist's companion. Oxford University Press, Oxford

Lodders K, Palme H, Gail HP (2009) Abundances of the elements in the solar system. In: Trümper JE (ed) Landolt-Börnstein, new series, VI/4B. Springer, Berlin, pp 560–598

Lumpkin GR (1980) Nepheline and sodalite in a barred olivine chondrule from the Allende meteorite. Meteoritics 15:139–145

Ma C, Krot AN (2014a) Discovery of a new Cl-rich silicate mineral, $Ca_{12}(Al_2Mg_3Si_7)O_{32}Cl_6$: an alteration phase in Allende (abstract). Meteor Planet Sci Supp 49:5432

Ma C, Krot AN (2014b) Adrianite, IMA 2014-028. CNMNC Newsletter No 21, August 2014, page 801. Mineral Mag 78:797–804

Ma C, Connolly Jr HC, Becket JR, Tschauner O, Rossman GR, Kampf AR, Zega TJ, Sweeney Smith SA, Schrader DL (2011) Brearleyite, $Ca_{12}Al_{14}O_{32}Cl_2$, a new alteration mineral from the NWA 1934 meteorite. Am Mineral 96:1199–1206

Mackinnon IDR (1980) Structures and textures of the Murchison and Mighei carbonaceous chondrite matrices. Proc 11th Lunar Planet Sci Conf:839–852

MacPherson GJ (2014) Calcium–aluminum-rich inclusions in chondritic meteorites. In: Davis AM (ed) Meteorites and Cosmochemical Processes, vol 1. Elsevier, Oxford, pp 139–179

MacPherson GJ, Grossman L (1984) "Fluffy" Type A Ca,-Al-rich inclusions in the Allende meteorite. Geochim Cosmochim Acta 48:29–46
MacPherson GJ, Krot AN (2014) The formation of Ca-, Fe-rich silicates in reduced and oxidized CV chondrites: the roles of impact-modified porosity and permeability, and heterogeneous distribution of water ices. Meteor Planet Sci 49:1250–1270
Magenheim AJ, Spivack AJ, Michael PJ, Gieskes JM (1995) Chlorine stable isotope composition of the oceanic crust: implications for Earth's distribution of chlorine. Earth Planet Sci Lett 131:427–432
Martin C, Debaille V, Lanari P, Goderis S, Vandendael I, Vanhaecke F, Vidal O, Claeys P (2013) REE and Hf distribution among mineral phases in the CV–CK clan: a way to explain present-day Hf isotopic variations in chondrites. Geochim Cosmochim Acta 12:496–513
Marvin UB, Wood JA, Dickey JS (1970) Ca–Al rich phases in the Allende meteorite. Earth Planet Sci Lett 7:346–350
Mason B, Graham AL (1970) Minor and trace elements in meteoritic minerals. Smithsonian Contrib Earth Sci 3:1–17
Matsumoto M, Tomeoka K, Seto Y, Miyake A, Sugita M (2014) Nepheline and sodalite in the matrix of the Ningqiang carbonaceous chondrite: implications for formation through parent-body processes. Geochim Cosmochim Acta 126:441–454
Matsuoka K, Nakamura T, Nakamuta Y (1996) Yamato-86789: a heated CM-like carbonaceous chondrite. Proc NIPR Symp Antarct Meteor 9:20–36
McCanta MC, Treiman AH, Dyar MD, Alexander CMOD, Rumble D III, Essene EJ (2008) The LaPaz Icefield 04840 meteorite: mineralogy, metamorphism, and origin of an amphibole- and biotite-bearing R chondrite. Geochim Cosmochim Acta 72:5757–5780
McGuire AV, Hashimoto A (1989) Origin of zoned fine-grained inclusions in the Allende meteorite. Geochim Cosmochim Acta 53:1123–1133
McSween HY Jr (1977a) Petrographic variations among carbonaceous chondrites of the Vigarano type. Geochim Cosmochim Acta 41:1777–1790
McSween HY Jr (1977b) Carbonaceous chondrites of the Ornans type: a metamorphic sequence. Geochim Cosmochim Acta 44:477–491
Ménard JM, Caron B, Jambon A, Michel A, Villemant B (2013) Halogens in CM chondrites (abstract). Lunar Planet Sci 44:2375
Meyer BS, Zinner E (2006) Nucleosynthesis. In: Lauretta DS, McSween HY Jr (eds) Meteorites and the early solar system II. University of Arizona Press, Tucson, AZ, pp 69–108
Mi J-X, Pan Y (2018) Halogen-rich minerals: crystal chemistry and geological significances. In: Harlov DE, Aranovich L (eds) The role of halogens in terrestrial and extraterrestrial geochemical processes: surface, crust, and mantle. Springer, Berlin, pp 123–184
Miura Y, Rucklidge J, Nord GL (1981) The occurrence of chlorine in serpentine minerals. Contrib Miner Petrol 76:17–23
Monge G, Fourcroy A, Berthollet C (1806) Extrait du proces-verbal de la seance de 1'Institut national, du 23 juin 1806. Ann Chim 59:35–40
Mueller G (1953) The properties and theory of genesis of the carbonaceous complex within the Cold Bokkeveld meteorite. Geochim Cosmochim Acta 4:1–10
Nakamura T, Tomeoka K, Takeda H (1993) Mineralogy and petrology of the CK chondrites Yamato-82104, -693 and a Carlisle Lakes-type chondrite Yamato-82002. Proc NIPR Symp Antarct Meteor 6:171–185
Nakamura N, Fujitani T, Kimura M (2007) A new isotope tracer for the early solar system processes: stable chlorine isotopes and distribution of Cl-bearing phases in chondrites (abstract). Lunar Planet Sci 38:1707
Nakamura N, Nyquist LE, Reese Y, Shih C-Y, Fujitani T, Okano O (2011) Stable chlorine isotopes and elemental chlorine by thermal ionization mass spectrometry and ion chromatography: martian meteorites, carbonaceous chondrites, and standard rocks (abstract). Lunar Planet Sci Conf 42:2513
Newton J, Bischoff A, Arden JW, Franchi IA, Geiger T, Greshake A, Pillinger CT (1995) Acfer 094, a uniquely primitive carbonaceous chondrite from the Sahara. Meteoritics 30:47–56

Nichols RH Jr, Hohenberg CM, Kehm K, Kim Y, Marti K (1994) I–Xe studies of the Acapulco meteorite: absolute I–Xe ages of individual phosphate grains and the Bjurböle standard. Geochim Cosmochim Acta 58:2553–2561

Noguchi T (1993) Petrology and mineralogy of CK chondrites: implications for the metamorphism of the CK chondrite parent body. Proc NIPR Symp Antarct Meteor 6:204–233

Noguchi T (1994) Petrology and mineralogy of the Coolidge meteorite (CV4). Proc NIPR Symp Antarct Meteor 7:42–72

Noll K, Döbeli M, Krähenbühl U, Grambole D, Herrmann F, Koeberl C (2003) Detection of terrestrial fluorine by proton induced gamma emission (PIGE): a rapid quantification for Antarctic meteorites. Meteor Planet Sci 38:759–765

Olsen E, Huebner JS, Douglas JA, Plant AG (1973) Meteoritic amphiboles. Am Mineral 58:869–872

Palme H, Jones A (2003) Solar system abundances of the elements. In: Davis AM (ed) Meteorites, comets and planets. Treatise on geochemistry, vol 1. Elsevier, Oxford, pp 41–61

Palme H, Larimer JW, Lipschutz ME (1988) Moderately volatile elements. In: Kerridge JF, Matthews MS (eds) Meteorites and the early solar system. University of Arizona Press, Tucson, pp 436–461

Palme H, Lodders K, Jones A (2014) Solar system abundances of the elements. In: Davis AM (ed) Planets, asteroids, comets and the solar system. Treatise on geochemistry, vol 2. Elsevier, Oxford, pp 15–36

Patzer A, Hill DH, Boynton WV (2001) Itqiy: a metal-rich enstatite meteorite with achondritic texture. Meteor Planet Sci 36:1495–1505

Peck JA, Wood JA (1987) The origin of ferrous zoning in Allende chondrule olivine. Geochim Cosmochim Acta 51:1503–1510

Pisani F (1864) Etude chimique et analyse de l'aerolithe d'Orgueil. Compt Rend 59:132–135

Pravdivtseva OV, Hohenberg CM, Meshik AP, Krot AN (2001) I–Xe ages of different mineral fractions from Bali and Kaba (CV3) (abstract). Meteor Planet Sci 36:A168

Pravdivtseva OV, Hohenberg CM, Meshik AP (2003a) The I–Xe age of Orgueil magnetite: new results (abstract). Lunar Planet Sci 24:1863

Pravdivtseva OV, Krot AN, Hohenberg CM, Meshik AM, Weisberg MK, Keil K (2003b) The I–Xe record of alteration in the Allende CV chondrite. Geochim Cosmochim Acta 67:5011–5026

Quijano-Rico M, Wănke H (1969) Determination of boron, lithium and chlorine in meteorites. In: Millman PM (ed) Meteorite research, vol D. Reidel, Dordrecht, pp 132–145

Ransom B, Spivack AJ, Kastner M (1995) Stable Cl isotopes in subduction-zone pore waters: implications for fluid-rock reaction and the cycling of chlorine. Geology 23:715–718

Reed GW (1964) Fluorine in stone meteorites. Geochim Cosmochim Acta 28:1729–1743

Reed GW, Allen RO (1966) Halogens in chondrites. Geochim Cosmochim Acta 30:779–800

Reed GW, Ralph OA (1966) Halogens in chondrites. Geochim Cosmochim Acta 30:779–800

Reynolds JH (1963) Xenology. J Geophys Res 68:2939–2956

Riciputi LR, McSween HY Jr, Johnson CA, Prinz M (1994) Minor and trace element concentrations in carbonates of carbonaceous chondrites, and implications for the compositions of coexisting fluids. Geochim Cosmochim Acta 58:1343–1351

Robert F, Epstein S (1982) The concentration and isotopic composition of hydrogen, carbon and nitrogen in carbonaceous meteorites. Geochim Cosmochim Acta 46:81–95

Rubin AE (1983) The Adhi Kot breccia and implications for the origin of chondrites and silica-rich clasts in enstatite chondrites. Earth Planet Sci Lett 64:201–212

Rubin AE (1993) Magnetite-sulfide chondrules and nodules in CK carbonaceous chondrites: implications for the timing of CK oxidation. Meteoritics 28:130–135

Rubin AE (1998) Correlated petrologic and geochemical characteristics of CO3 chondrites. Met and Planet Sci 33:383–391

Rubin AE, Choi BG (2009) Origin of halogens and nitrogen in enstatite chondrites. Earth Moon Planet 105:41–53

Rubin AE, Grossman JN (1985) Phosphate-sulfide assemblages and Al/Ca ratios in type 3 chondrites. Meteoritics 20:479–489

Rubin AE, Kallemeyn GW (1994) Pecora Escarpment 91002: a member of the new Rumuruti (R) chondrite group. Meteoritics 29:255–264
Rubin AE, James JA, Keck BD, Weeks KS, Sears DWG, Jarosewich E (1985) The Colony meteorite and variations in CO3 chondrite properties. Meteoritics 20:175–196
Rubin AE, Wang D, Kallemeyn GW, Wasson JT (1988) The Ningqiang meteorite: classification and petrology of an anomalous CV chondrite. Meteoritics 23:13–23
Rubin AE, Zolensky ME, Bodnar RJ (2002) The halite-bearing Zag and Monahans (1998) meteorite breccias: shock metamorphism, thermal metamorphism and aqueous alteration on the H-chondrite parent body. Meteor Planet Sci 37:125–141
Rubin AE, Trigo-Rodríguez JM, Huber H, Wasson JT (2007) Progressive aqueous alteration of CM carbonaceous chondrites. Geochim Cosmochim Acta 71:2361–2382
Russell SS, Huss GR, Fahey AJ, Greenwood RC, Hutchison R, Wasserburg GJ (1998) An isotopic and petrologic study of calcium-aluminum-rich inclusions from CO3 chondrites. Geochim Cosmochim Acta 62:689–714
Schaefer BF (2012) Br isotope signatures in ordinary chondrites (abstract). Meteor Planet Sci Suppl 47:5166
Schaefer BF (2013) A pilot Br isotopic study of arid playa lakes and ordinary chondrites. Mineral Mag 77:2147
Schauble EA, Sharp ZD (2011) Modeling isotopic signatures of nebular chlorine condensation (abstract). Mineral Mag 75:1810
Schöler HF, Nkusi G, Niedan VW, Müller G, Spitthoff B (2005) Screening of organic halogens and identification of chlorinated benzoic acids in carbonaceous meteorites. Chemosphere 60:1505–1512
Schrader DL, Franchi IA, Connolly HC Jr, Greenwood RC, Lauretta DS, Gibson JM (2011) The formation and alteration of the Renazzo-like carbonaceous chondrites I: implications of bulk-oxygen isotopic composition. Geochim Cosmochim Acta 75:308–325
Schulze H, Bischoff A, Palme A, Spettel B, Dreibus G, Otto J (1994) Mineralogy and chemistry of Rumuruti: the first meteorite fall of the new R chondrite group. Meteoritics 29:275–286
Scott ERD, Jones RH (1990) Disentangling nebular and asteroidal features of CO3 carbonaceous chondrites. Geochim Cosmochim Acta 54:2485–2502
Scott ERD, Krot AN (2014) Chondrites and their components. In Davis AM (ed) Meteorites and cosmochemical processes. Treatise on geochemistry, vol 1, 2nd edn. Elsevier, Oxford, pp 65–137
Scott ERD, Taylor GJ (1985) Petrology of types 4 to 6 carbonaceous chondrites. Proc Lunar Planet Sci Conf 15th:C699–C709
Sears DW, Kallemeyn GW, Wasson JT (1982) The chemical classification of chondrites II: the enstatite chondrites. Geochim Cosmochim Acta 46:597–608
Sears DWG, Batchelor DJ, Lu J, Keck BD (1991) Metamorphism of CO and CO-like chondrites and comparisons with type 3 ordinary chondrites. Proc NIPR Symp Antarct Meteor 4:319–343
Sephton M, Verchovsky A, Bland P, Gilmour I, Grady M, Wright I (2003) Investigating the variations in carbon and nitrogen isotopes in carbonaceous chondrites. Geochim Cosmochim Acta 67:2093–2108
Sharp ZD, Barnes JD (2008) Comment to "Chlorine stable isotopes and halogen concentrations in convergent margins with implications for the Cl isotopes cycle in the ocean" by Wei et al.: a review of the Cl isotope composition of serpentinites and the global chlorine cycle. Earth Planet Sci Lett 274:531–534
Sharp ZD, Barnes JD, Brearley AJ, Fischer T, Chaussidon M, Kamenetsky VS (2007) Chlorine isotope homogeneity of the crust, mantle and carbonaceous chondrites. Nature 446:1062–1065
Sharp ZD, Mercer JA, Jones RH, Brearley AJ, Selverstone J, Bekker A, Stachel T (2013) The chlorine isotope composition of chondrites and earth. Geochim Cosmochim Acta 107:189–204
Shinonaga T, Endo K, Ebihara M, Heumann KG, Nakahara H (1994) Weathering of Antarctic meteorites investigated from contents of Fe^{3+}, chlorine, and iodine. Geochim Cosmochim Acta 58:3735–3740

Stracke A, Palme H, Gellissen M, Münker C, Kleine T, Birbaum K, Günther D, Bourdon B, Zipfel J (2012) Refractory element fractionation in the Allende meteorite: implications for solar nebula condensation and the chondritic composition of planetary bodies. Geochim Cosmochim Acta 85:114–141

Studier MH, Hayatsu R, Anders E (1965) Organic compounds in carbonaceous chondrites. Science 149:1455–1459

Studier MH, Hayatsu R, Anders E (1968) Origin of organic matter in early solar system-I. Hydrocarbons. Geochim Cosmochim Acta 32:151–173

Sugita M, Tomeoka K, Seto Y (2009) Sodium-metasomatism of Ca–Al-rich inclusions in the anomalous carbonaceous chondrite Ningqiang. J Mineral Petrol Sci 104:296–300

Swindle T (1998) Implications of iodine–xenon studies for the timing and location of secondary alteration. Meteor Planet Sci 33:1147–1156

Swindle TD, Podosek FA (1988) Iodine-xenon dating. In: Kerridge JF, Matthews MS (eds) Meteorites and the early solar system. The University of Arizona Press, Tucson, pp 1127–1146

Swindle TD, Caffee MW, Hohenberg CM, Lindstrom MM, Taylor GJ (1991) Iodine–xenon and other studies of individual Chainpur chondrules. Geochim Cosmochim Acta 55:861–880

Swindle TD, Cohen B, Li B, Olson E, Krot AN, Birjukov VV, Ulyanov AA (1998) Iodine–xenon studies of separated components of the Efremovka (CV3) meteorite (abstract). Lunar Planet Sci 29:1005

Taylor LA, Liu Y, Guan Y, Day JMD, Ma C, Hiroi T, Corder CA, Assayag N, Rumble D, Cartigny P, Chen Y, Hand KP, Pieters CM, Eiler JM, Pokhilenko NP, Podgornykh NM (2014) Metamorphism in the Chelyabinsk meteorite (abstract). Lunar Planet Sci 45:2346

Thénard LJ (1806) Analyse d'un aerolithe tombe dans l'arrondissement d'Alais, le 15 mars 1806. Ann Chim 59:103–110

Tomeoka K (1990) Mineralogy and Petrology of Belgica-7904: a new kind of carbonaceous chondrite from Antarctica. Proc NIPR Symp Antarct Meteor 3:40–54

Tomeoka K, Kojima H, Yanai K (1989a) Yamato-82162: a new kind of CI carbonaceous chondrite found in Antarctica. Proc NIPR Symp Antarct Meteor 2:36–54

Tomeoka K, Kojima H, Yanai K (1989b) Yamato-86720: a CM carbonaceous chondrite having experienced extensive aqueous alteration and thermal metamorphism. Proc NIPR Symp Antarct Meteor 2:55–74

Tomeoka K, McSween HY Jr, Buseck PR (1989c) Mineralogical alteration of CM carbonaceous chondrites: a review. Proc NIPR Symp Antarct Meteor 2:221–234

Tomeoka K, Nomura K, Takeda H (1992) Na-bearing Ca–Al-rich inclusions in the Yamato-791717 CO carbonaceous chondrite. Meteoritics 27:136–143

Tomeoka K, Ohnishi I, Nakamura N (2001) Silicate darkening in the Kobe CK chondrite: evidence for shock metamorphism at high temperature. Meteorit Planet Sci 36:1535–1545

Tomeoka K, Kojima H, Ohnishi I, Ishii Y, Nakamura N (2005) The Kobe CK carbonaceous chondrite: petrography, mineralogy and metamorphism. J Mineral Petrol Sci 100:116–125

Tonui EK, Zolensky ME, Lipschutz ME, Wang M-S, Nakamura T (2003) Yamato-86029: aqueously altered and thermally metamorphosed CI chondrite with unusual textures. Meteor Planet Sci 38:269–292

Torigoye N, Shima M (1993) Evidence for a late thermal event of unequilibrated enstatite chondrites: a Rb–Sr study of Qingzhen and Yamato 6901 (EH3) and Khairpur (EL6). Meteoritics 28:515–527

Turner G, Crowther SA, Burgess R, Gilmour JD, Kelley SP, Wasserburg GJ (2013) Short lived ^{36}Cl and its decay products ^{36}Ar and ^{36}S in the early solar system. Geochim Cosmochim Acta 123:358–367

Ushikubo T, Guan Y, Hiyagon H, Sugiura N, Leshin LA (2007) 36Cl, 26Al, and O isotopes in an Allende type B2 CAI: implications for multiple secondary alteration events in the early solar system. Meteor Planet Sci 42:1267–1279

Van Schmus WR, Ribbe PH (1969) Composition of phosphate minerals in ordinary chondrites. Geochim Cosmochim Acta 33:637–640

Van Schmus WR, Wood JA (1967) A chemical-petrological classification for the chondritic meteorites. Geochim Cosmochim Acta 31:747–765
von Gunten HR, Wyttenbach A, Scherle W (1965) Determination of chlorine in stony meteorites by neutron activation analysis. Geochim Cosmochim Acta 29:475–480
Wang Y, Hsu W (2009) Petrology and mineralogy of the Ningqiang carbonaceous chondrite. Meteor Planet Sci 44:763–780
Wark DA (1986) Evidence for successive episodes of condensation at high temperatures in a part of the solar nebula. Earth Planet Sci Lett 77:129–148
Wasserburg GJ, Hutcheon ID, Aléon J, Ramon EC, Krot AN, Nagashima K, Brearley AJ (2011) Extremely Na- and Cl-rich chondrule from the CV3 carbonaceous chondrite Allende. Geochim Cosmochim Acta 75:4752–4770
Wasson JT (1974) Meteorites: classification and properties. Springer, Berlin
Wasson JT, Kallemeyn GW (1988) Composition of chondrites. Phil Trans R Soc Lond A 325:535–544
Wasson JT, Yurimoto H, Russell SS (2001) O-16-rich melilite in CO3.0 chondrites: possible formation of common, O-16-poor melilite by aqueous alteration. Geochim Cosmochim Acta 65:4539–4549
Weinbruch S, Palme H, Muller WF, El Goresy A (1990) FeO-rich rims and veins in Allende forsterite: evidence for high temperature condensation at oxidizing conditions. Meteoritics 25:115–125
Weisberg MK, Huber H (2007) The GRO 95577 CR1 chondrite and hydration of the CR parent body. Meteorit Planet Sci 42(1495–1503):1495–1503
Weisberg MK, Prinz M, Clayton RN, Mayeda TK (1993) The CR (Renazzo-type) carbonaceous chondrite group and its implications. Geochim Cosmochim Acta 57:1567–1586
Weisberg MK, Prinz M, Clayton RN, Mayeda TK (1997) CV3 chondrites: three subgroups, not two (abstract). Meteorit Planet Sci 32(Suppl):A138–A139
Whitby JA, Burgess R, Turner G, Gilmour JD, Bridges JC (2000) Extinct ^{126}I in halite from a primitive meteorite: evidence for evaporite formation in the early solar system. Science 208:1819–1821
Wiik HB (1956) The chemical composition of some stony meteorites. Geochim Cosmochim Acta 9:279–289
Woolum DS, Cochrane RB, Joyce D, El Goresy A, Benjamin TM, Rogers PSZ, Maggiore CM, Duffy CJ (1984) Trace element PIXE studies of Qingzhen (EH3) metal and sulfides (abstract). Lunar Planet Sci XV:935–936
Yin Q-Z, Zhou Q, Li Q-L, Li X-H, Liu Y, Tang G-Q, Krot AN, Jenniskens P (2014) Records of the moon-forming impact and the 470 Ma disruption of the L chondrite parent body. Meteor Planet Sci 49:1426–1439
Yurimoto H, Krot AN, Choi BG, Aleon J, Kunihiro T, Brearley AJ (2008) Oxygen isotopes of chondritic components. In: Macpherson GJ (ed) Oxygen in the solar system, vol 68. Mineralogical Society of America, Washington DC, pp 141–186
Yurimoto H, Itoh S, Zolensky ME, Kusakabe M, Karens A, Bodnar R (2014) Isotopic compositions of asteroidal liquid water trapped in fluid inclusions of chondrites. Geochem J 48:549–560
Zanda B, Bourot-Denise M, Perron C, Hewins RH (1994) Origin and metamorphic redistribution of silicon, chromium, and phosphorus in the metal of chondrites. Science 265:1846–1849
Zega TJ, Garvie LAJ, Dódony I, Friedrich H, Stroud RM, Buseck PR (2006) Polyhedral serpentine grains in CM chondrites. Meteor Planet Sci 41:681–688
Zinner E (2014) Presolar grains. In: Davis AM (ed) Meteorites and cosmochemical processes. Treatise on geochemistry, vol 1. Elsevier, Oxford, pp 181–213
Zolensky ME, Ivanov A (2003) The Kaidun microbreccia meteorites: a harvest from the inner and outer asteroid belt. Chem Erde 63:185–246
Zolensky ME, McSween HY, Jr. (1988) Aqueous alteration. In: Kerridge JF, Matthews MS (eds) Meteorites and the early solar system. University of Arizona Press, Tucson, pp 114–143

Zolensky ME, Barrett T, Browning L (1993) Mineralogy and composition of matrix and chondrule rims in carbonaceous chondrites. Geochim Cosmochim Acta 57:3123–3148

Zolensky ME, Mittlefehldt DW, Lipschutz ME, Wang M-S, Clayton RN, Mayeda TK, Grady MM, Pillinger C, Barber D (1997) CM chondrites exhibit the complete petrologic range from type 2 to 1. Geochim Cosmochim Acta 61:5099–5115

Zolensky ME, Bodnar RJ, Gibson EKJ, Nyquist LE, Reese Y, Shih C-Y, Wiesmann H (1999) Asteroidal water within fluid inclusion-bearing halite in an H5 chondrite, Monahans (1998). Science 285:1377–1379

Zolensky ME, Nakamura K, Gounelle M, Mikouchi T, Kasama T, Tachikawa O, Tonui EK (2002) Mineralogy of Tagish Lake: an ungrouped type 2 carbonaceous chondrite. Meteor Planet Sci 37:737–761

Zolensky ME, Krot AN, Benedix G (2008) Record of low-temperature alteration in asteroids. Oxyg Sol Syst 68:429–462

Zolensky ME, Fries M, Bodnar R, Yurimoto H, Itoh S, Steele A, Mikouchi T, Hagiya K, Ohsumi K, Le L, Rahman Z (2013) Early solar system cryovolcanics in the laboratory (abstract). Meteor Planet Sci 48:5200

Zolensky ME, Fries M, Chan QH-S, Kebukawa Y, Steele A, Bodnar RJ (2015) The mineralogy of Ceres* (*or something an awful lot like it) (abst). 78th Annual Meteoritical Society Meeting (#5270)

Zolotov MY, Mironenko MV (2007) Hydrogen chloride as a source of acid fluids in parent bodies of chondrites (abstract). Lunar Planet Sci 38:234

Chapter 16
The Role of Halogens During Fluid and Magmatic Processes on Mars

Elizabeth B. Rampe, Julia A. Cartwright, Francis M. McCubbin and Mikki M. Osterloo

Abstract The geochemistry of halogens on Mars gives insight into the composition of the martian mantle, igneous evolution of the martian crust, aqueous processes on the martian surface, and the overall habitability of the planet. Halogen abundances have been measured from martian meteorites, in situ by landers and rovers, and from orbital missions around Mars. The bulk rock abundances of halogens have been determined for many martian meteorite samples including all petrological five types (nakhlites, chassignites, shergottites, orthopyroxenites, and regolith breccias). Measurements of basaltic martian meteorites (i.e., shergottites and regolith breccias) provide important insights into halogen abundances in mantle and crustal reservoirs. Fluorine, Cl, Br, and I have been detected in silicate, phosphate, sulfate, oxide, and halide group minerals in martian meteorites. These halogen-bearing minerals are found in melt inclusions, as secondary hydrothermal or aqueous alteration products, or in the interstices between cumulus igneous silicates. Measurements from meteorites and from martian missions indicate that Cl is the most abundant halogen on and in Mars. Measurements from landed missions suggest that Cl is commonly present in oxychlorine compounds (e.g., perchlorate and chlorate salts), whereas measurements from orbit have identified both oxychlorine minerals and halite. Halite is constrained to local depressions in the ancient southern highlands, suggesting precipitation from

E.B. Rampe (✉) · F.M. McCubbin
NASA Johnson Space Center, Mail Code XI3,
2101 NASA Parkway, Houston, TX 77058, USA
e-mail: elizabeth.b.rampe@nasa.gov

F.M. McCubbin
e-mail: francis.m.mccubbin@nasa.gov

J.A. Cartwright
Department of Geological Sciences, Bevill Building,
The University of Alabama, Tuscaloosa, AL 35487, USA
e-mail: jacartwright@ua.edu

M.M. Osterloo
Laboratory for Atmospheric and Space Physics, University of Colorado,
3665 Discovery Dr, Boulder, CO 80303, USA
e-mail: Mikki.Osterloo@lasp.colorado.edu

D.E. Harlov and L. Aranovich (eds.), *The Role of Halogens in Terrestrial and Extraterrestrial Geochemical Processes*, Springer Geochemistry,
DOI 10.1007/978-3-319-61667-4_16

the evaporation of water in closed basins at ~3.5–4 Ga. The presence of oxychlorine minerals on the martian surface has important implications for the habitability of present day Mars because oxychlorine minerals may deliquesce to create seasonal deposits of liquid water. Furthermore, oxychlorine compounds are considered both a resource and potential hazard to the eventual human exploration of Mars.

16.1 Introduction

Other than the Earth and the Moon, Mars may be the best-studied object in the Solar System. Geological and geochemical data have been collected by orbiters and landers, and a wealth of knowledge has been gained through the study of martian meteorites. Mars' early history may have mimicked that of the Earth, including significant volcanism and an active hydrological cycle. There is abundant geomorphological and mineralogical evidence for surface or near-surface water early in Mars' history (e.g., Carr 1995; Ehlmann et al. 2011). Life as we know it on Earth requires liquid water, and the relative proximity of Mars to Earth makes it a high-priority target for answering the question: "Are we alone in the universe?"

Mars, however, differs in many ways from the Earth. There is little evidence for plate tectonics, and, as such, there may not have been a planet-wide process to recycle the crust and create evolved magmas. Regarding magnetism, Mars lost its dynamic magnetic field ~4 billion years ago (Ga) following the termination of an internal dynamo (e.g., Acuña et al. 1999). As a result, the atmosphere was gradually stripped by solar-wind-induced sputtering and photochemical escape (e.g., Jakosky et al. 1994), causing the loss of much of Mars' surface water. The noble gas signature of the martian atmosphere hints at a significant loss early in its history, leading to elevations in certain noble gas isotope abundances (e.g., Jakosky et al. 1994; Jakosky and Jones 1997). Mars is also geochemically different from Earth because it accreted from a more volatile-rich portion of the protoplanetary disk. The silicate portion of Mars is more enriched in FeO, MnO, alkalis, and halogens and is depleted in siderophile and chalcophile elements (Longhi et al. 1992). Mars also has an iron-nickel-sulfur (Fe-Ni-S) core (Longhi et al. 1992), compared to Earth's core, which is mostly dominated by Fe and Ni.

Many details surrounding Mars' early history remain a mystery. Halogens, however, can give us an insight into martian mantle composition, igneous evolution, aqueous processes, and climatic history. In this chapter, we review both the abundance and mineralogy of halogens in martian meteorites and discuss the significance of these measurements for the martian interior and crust. We then review the detection of halogens on the surface from landed and orbital missions and consider the speciation of halogens and the implications for climate and habitability.

16.2 Halogens in Martian Meteorites

The halogens—fluorine (F), chlorine (Cl), bromine (Br), and iodine (I) make up group 7 of the periodic table and are considered to be moderately to highly volatile. Early studies of martian meteorites highlighted that Mars is a volatile-rich planet (Dreibus and Wanke 1985). The bulk rock abundances of halogens in martian meteorites have been determined for a number of samples across all five martian meteorite types (i.e., nakhlites, chassignites, shergottites, orthopyroxenites, and regolith breccias). Bulk rock and mineral separate/chemical aliquot abundances for halogens within martian meteorites are shown in Table 16.1, and plotted in Fig. 16.1. The overall martian halogen abundances indicate that, in general, Cl is more abundant than F, and both are more abundant than Br and I, which is in-keeping with the relative abundances of halogens in CI chondrites (Lodders 2003). As bulk rock compositions of cumulate rocks do not represent magmatic liquids, halogen bulk rock abundances of martian cumulate rocks, like the

Table 16.1 Summary of halogen data for martian meteorites

Meteorite	F (ppm)	Cl (ppm)	Br (ppb)	I (ppb)	Reference
Shergottites					
ALHA 77005	22	14	69	1720	Dreibus and Wänke (1987)
DaG 476	–	840	–	–	Zipfel et al. (2000)
Dho 019		22	–	–	Williams et al. (2016)
EET 79001 Lith A	39	26	189	100	Dreibus and Wänke (1987)
EET 79001 Lith A		180	–	–	Williams et al. (2016)
EET 79001 Lith B	31	48	287	960	Dreibus and Wänke (1987)
EET 79001 Lith B		42			Williams et al. (2016)
EET 79001 Lith C		35	378	12	Dreibus and Wänke (1987)
LEW 88516	27	29	–	–	Lodders (1998)
Los Angeles		115	–	–	Williams et al. (2016)
NWA 1068	–	13	–	–	Bogard et al. (2010)
NWA 2975		24	–	–	Williams et al. (2016)
NWA 6234	–	59	–	–	Burgess et al. (2013)
QUE 94201	40	91	–	–	Dreibus et al. (1996)
RBT 04262-Ol/Pyx	–	14 ± 2	–	–	Cartwright et al. (2009)
RBT 04262-Maskelynite	–	47 ± 1	–	–	Cartwright et al. (2009)
RBT 04262-Accessory	–	175 ± 52	–	–	Cartwright et al. (2009)
Shergotty	41.6	108	890	36	Dreibus and Wänke (1987)
Shergotty		108	–	–	Williams et al. (2016)
SaU 005	56	143	–	–	Dreibus et al. (2000)
Tissint-Bulk		22	–	–	Williams et al. (2016)

(continued)

Table 16.1 (continued)

Meteorite	F (ppm)	Cl (ppm)	Br (ppb)	I (ppb)	Reference
Tissint-Glass		69	–	–	Williams et al. (2016)
Tissint-Igneous		30	–	–	Williams et al. (2016)
Y-980459	86	60.7	–	–	Dreibus et al. (2003)
Zagami	41	145	760	4	Dreibus and Wänke (1987)
Zagami		49	–	–	Williams et al. (2016)
Nakhlites					
Lafayette		101 ± 5	590 ± 30	54 ± 3	Dreibus et al. (2006)
Lafayette Iddingsite		3600	9000 ± 3000	–	Treiman and Lindstrom (1997)
MIL 03346		248 ± 12	450 ± 23	1590 ± 80	Dreibus et al. (2006)
MIL 03346		163.7 ± 0.9	411.8 ± 2.2	15.1 ± 0.6	Cartwright et al. (2013)
Nakhla		563	3410	24	Dreibus and Wänke (1987)
"Nakhla E"		1890 ± 95	3460 ± 173	17 ± 1	Dreibus et al. (2006)
"Nakhla K"		1145 ± 57	4300 ± 215	10 ± 1	Dreibus et al. (2006)
"Nakhla G"		876 ± 44	8450 ± 423	26 ± 1	Dreibus et al. (2006)
Nakhla Vein		7700 ± 900	151000 ± 49000	–	Rao et al. (2005)
Nakhla–Bulk Crush		104.5 ± 4.9	952.7 ± 5.3	11.8 ± 0.5	Cartwright et al. (2013)
Nakhla–Olivine Crush		14.2 ± 0.3	557.9 ± 2.0	20.0 ± 0.4	Cartwright et al. (2013)
Nakhla–Pyroxene Crush		59.2 ± 4.5	722.2 ± 1.6	12.3 ± 0.3	Cartwright et al. (2013)
Nakhla–Mesostasis		75.7 ± 2.1	–	–	Cartwright et al. (2013)
Nakhla–Pyroxene		40.5 ± 1.1	–	–	Cartwright et al. (2013)
Nakhla–Olivine		17.8 ± 0.6	–	–	Cartwright et al. (2013)
Nakhla–Bulk1		56.4 ± 3.5	–	–	Cartwright et al. (2013)
Nakhla–Bulk2		45.0 ± 0.9	–	–	Cartwright et al. (2013)
Nakhla–Bulk Acid-Etched		5.7 ± 0.2	–	–	Cartwright et al. (2013)
Nakhla–Bulk Water-Etched		35.3 ± 0.9	–	–	Cartwright et al. (2013)

(continued)

Table 16.1 (continued)

Meteorite	F (ppm)	Cl (ppm)	Br (ppb)	I (ppb)	Reference
NWA 817		117	–	–	Williams et al. (2016)
NWA 998		127 ± 6	180 ± 9	281 ± 14	Dreibus et al. (2006)
NWA 998–Feldspar		55.4 ± 1.7	–	–	Cartwright et al. (2013)
NWA 998–Pyx1		11.1 ± 0.3	–	–	Cartwright et al. (2013)
NWA 998–Pyx2		15.4 ± 0.2	–	–	Cartwright et al. (2013)
NWA 998–Pyx3		48.2 ± 1.3	85.6 ± 1.0	66.1 ± 1.4	Cartwright et al. (2013)
NWA 998–Pyx-4		35.5 ± 4.1	47.5 ± 2.2	105.6 ± 4.9	Cartwright et al. (2013)
NWA 998–Olivine		62.8 ± 8.8	45.7 ± 1.9	9.5 ± 1.1	Cartwright et al. (2013)
NWA 5790		72	–	–	Williams et al. (2016)
Y-000593		101 ± 5	80 ± 4	378 ± 19	Dreibus et al. (2006)
Y-000749		73 ± 4	60 ± 3	682 ± 34	Dreibus et al. (2006)
Chassigny	14.7	34	97	10	Dreibus and Wänke (1987)
NWA 7034		2200	–	–	Williams et al. (2016)

Analytical uncertainties are shown, where reported

chassignites, nakhlites, and orthopyroxenite (Allan Hills 84001), provide little insight into the halogen abundances of the martian interior. However, basaltic rocks, like the shergottites, and highly mixed sedimentary rocks like the regolith breccia Northwest Africa 7034 and its pairings, could provide important insights into halogen abundances in mantle and crustal reservoirs.

One important point to make at this stage is that halogens can occur within meteoritic samples as either a primary component that was incorporated into the sample on formation, or they can become incorporated later due to secondary processes such as aqueous alteration. Bulk analyses are thus useful in giving an idea of the overall abundances present, but mineral separate analyses allow us to better characterize the processes leading to halogen occurrence within materials. There is some additional complexity to using bulk rock halogen abundances as a proxy for interior values. Volatile elements, in particular Cl, are susceptible to degassing (e.g., Aiuppa et al. 2009), which can result in underestimates of halogen abundances in parental magmas and magmatic source regions. In particular, studies by McCubbin and colleagues (2013–2016) have suggested that H and Cl degassing in martian samples is highly likely due to the fact that: (1) the bulk rock abundances of H_2O and Cl are much lower than expected from reconstructing the abundances of H and Cl

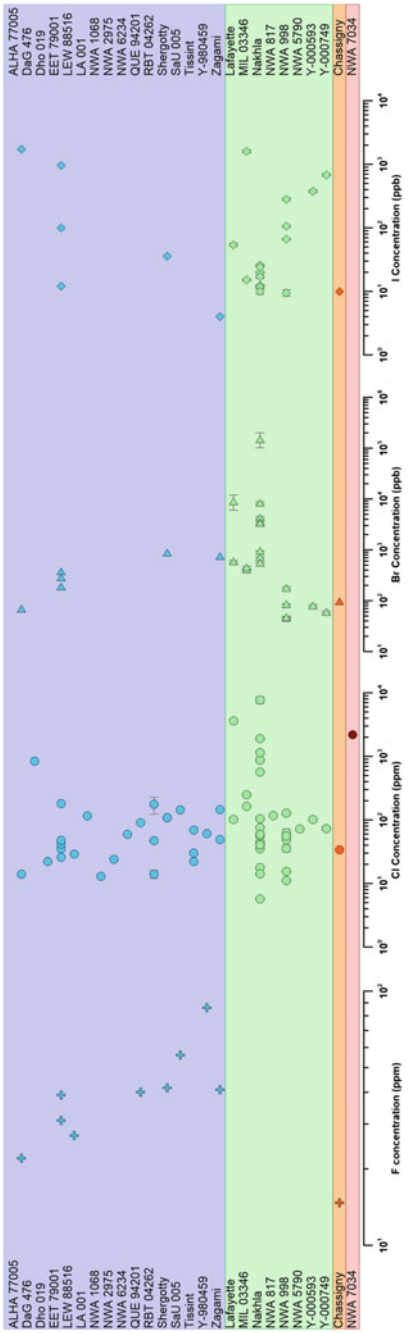

Fig. 16.1 A plot showing the halogen abundances for F (ppm), Cl (ppm), Br (ppb), and I (ppb) determined from analyses of martian meteorites, as bulk values, mineral separates, and other chemical aliquots, as shown in Table 16.1. For references, see Table 16.1

from mineral-melt partitioning relationships; (2) measurements of F and Cl in some magmatic apatite grains demonstrate that F has been concentrated; and (3) the Cl/F ratios in the martian mantle calculated from bulk rock measurements are less than terrestrial Cl/F ratios (McCubbin et al. 2013, 2015, 2016; McCubbin and Jones 2015; Filliberto et al. 2016).

While the abundances of halogens within meteorites are important, so too are the actual minerals that host them. Martian meteorites contain a diverse array of mineral phases that have halogens as essential structural constituents, commonly substituting for OH^- groups in mineral structures. For the majority of minerals, halogens are present as F and/or Cl members, though Br and I can occur in trace abundances. These minerals include silicates, phosphates, sulfates, oxides, and halides (Bunch and Reid 1975; Floran et al. 1977; Johnson et al. 1991; McSween and Harvey 1993; Watson et al. 1994; McSween and Treiman 1998; Leshin 2000; Righter et al. 2002; Boctor et al. 2003; Sautter et al. 2006; McCubbin and Nekvasil 2008; Greenwood et al. 2008; Filiberto and Treiman 2009a; McCubbin et al. 2009, 2010, 2012, 2013, 2016; Gross et al. 2013; Filiberto et al. 2014, 2016; Muttik et al. 2014; Santos et al. 2015). Understanding the origin of these halogen-bearing minerals is important for understanding both the petrogenesis of the martian meteorites and the behavior of halogens in martian magmatic, hydrothermal, and aqueous systems. Furthermore, they are important for constraining the abundances of halogens in the martian mantle and crust. In the following text, we will review the halogen-bearing minerals that have been identified in each of the distinct martian meteorite types, focusing on the distribution of F, Cl, and OH in the monovalent anion sites within each of the minerals that accept halogen elements as essential structural constituents.

Given that both the bulk rock abundances of halogens and halogen mineralogy are of critical importance for understanding the halogen budget of the martian interior, we have summarized the bulk rock and mineral data for each of the five martian meteorite groups below. These data will be discussed later in the chapter in order to understand the roles that halogens play in geologic processes in the martian interior and to place constraints on the halogen abundances in the martian crust and mantle.

16.2.1 Shergottites

The shergottite meteorites are the most abundant group of materials from Mars and are generally basaltic in composition. At the time of writing, there are 154 separate stones that constitute the shergottite meteorite group, though many of these are paired (they are genetically related, and likely split during impact). They are basaltic rocks that display a range of compositional and textural features relating to martian melt compositions with varying degrees of partial accumulation and/or fractionation. The shergottites are commonly grouped based on their abundances of incompatible trace elements and compositions with respect to Sm-Nd and Rb-Sr isotopic systems into three distinct groups, including enriched, intermediate, and

depleted (Borg and Draper 2003). In addition, some studies have suggested that they may be genetically related to substantial volcanic systems (Symes et al. 2008). However, the bulk rock abundances of halogens do not correlate strongly with these geochemical groupings (Table 16.1; Filiberto et al. 2016). Of the major minerals present in shergottites, apatite—$Ca_5(PO_4)_3(OH,F,Cl)$—(Fig. 16.2) is the only phase that is suitably halogen-bearing (McCubbin et al. 2016). Previous work has reported on the occurrence of kaersutitic amphibole (a Ti-rich variety of calcic amphibole) in some melt inclusions within shergottites (Treiman 1986), though these reports have not been confirmed by analysis of halogen or OH abundances. The apatites present in shergottites span a wide range of compositions that encompass fluorapatite, chlorapatite, and hydroxyapatite (Fig. 16.3). The occurrence of these minerals is important because the mineral compositions, bulk-rock abundances of F, and mineral-melt partitioning relationships can be used to quantify pre-eruptive (pre-degassing) water and Cl abundances in martian magmas, which have been used, in part, to constrain the halogen and water abundances of the martian mantle in previous studies (e.g., Gross et al. 2013; McCubbin et al. 2016).

16.2.2 Nakhlites

The nakhlite meteorites are clinopyroxenite cumulates that consist of ~19 separate stones, believed to have comprised a single cumulate pile or thick lava flow on Mars. As discussed above, the bulk rock halogen abundances of cumulate rocks cannot be used to constrain the halogen abundances of their parental magmas because their bulk compositions do not represent magmatic liquids. However, the halogen mineralogy in the whole rock can be used to understand the role that halogens have played during both high-T and low-T processes, depending on the textural context in which the minerals occur. Halogen-bearing mineral phases have been shown to occur in three distinct petrographic contexts in nakhlites: (1) discrete phases within partially crystallized, olivine- or clinopyroxene-hosted melt inclusions; (2) igneous textured apatite that are interstitial to the cumulus olivine and clinopyroxene; and (3) secondary, low-temperature, hydrothermal- or aqueous-alteration products purported to be of martian origin. The partially crystallized melt inclusions host a number of halogen-bearing phases, including apatite, Cl-rich amphibole, and Cl-bearing jarosite (Treiman 1986, 1990, 1993; Harvey and McSween 1992; Aoudjehane et al. 2006; Sautter et al. 2006; McCubbin et al. 2009, 2013). However, not all of these phases are present in every inclusion, and some of the melt-inclusion minerals are specific to individual meteorites. Compositional information relating to the amphibole and apatite phases found in nakhlite melt inclusions is shown in Fig. 16.3. Halogen analyses of mineral separates following crushing also revealed elevations in halogen abundances, and are thought to represent components released from fluid inclusions (Cartwright et al. 2013). Apatite is the only primary, igneous, halogen-bearing mineral phase that occurs interstitial to the cumulus clinopyroxene and olivine. The intercumulus apatite compositions are displayed in Fig. 16.3. The nakhlites also have low-temperature,

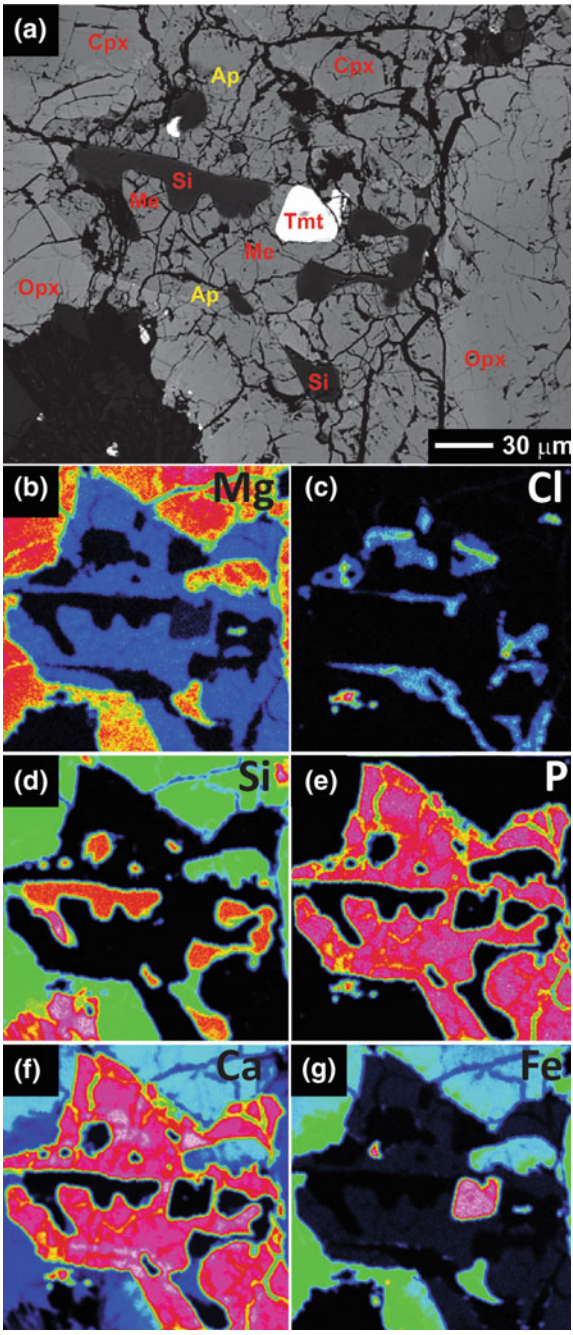

Fig. 16.2 Back scattered electron (BSE) and elemental X-ray maps of apatite–merrillite intergrowth in Zagami. **a** BSE image of Zagami. All phases present are identified, and the phase abbreviations are indicated as follows: *Ap* apatite, *Cpx* clinopyroxene, *Me* merrillite, *Msk* maskelynite, *Opx* orthopyroxene, *Si* silica, and *Tmt* titanomagnetite. **b** Mg X-ray map, **c** Cl X-ray map, **d** Si X-ray map, **e** P X-ray map, **f** Ca X-ray map, and **g** Fe X-ray map

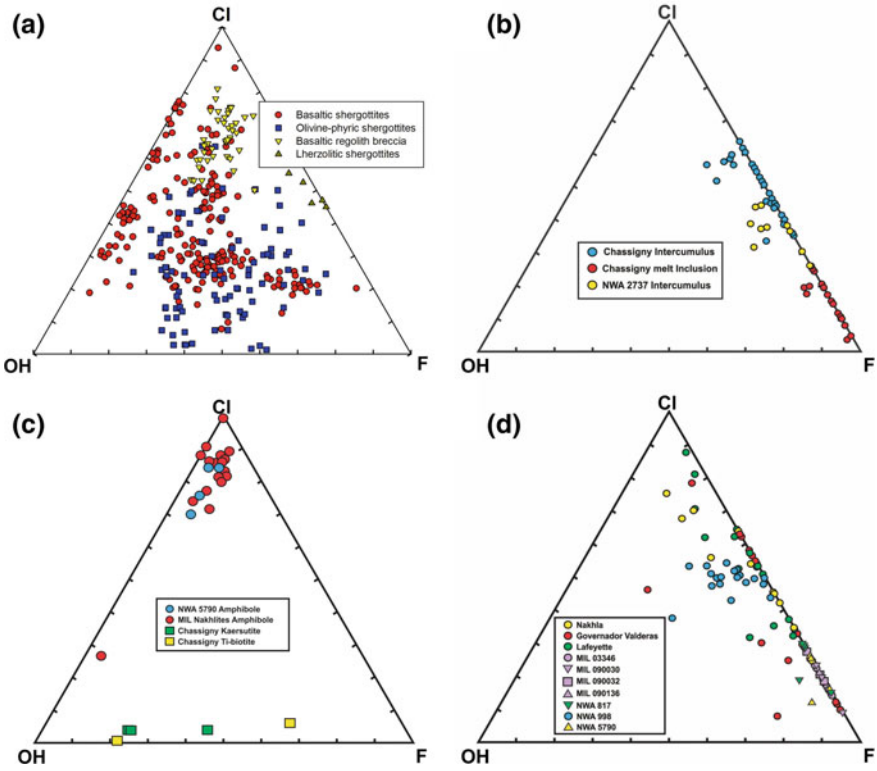

Fig. 16.3 Ternary plots of halogen-site occupancy (expressed as mol% of the halogen site) in apatite, amphibole, and biotite from martian meteorites. For apatite analyses where OH was not directly measured, it was calculated assuming 1–F–Cl = OH. For the amphiboles that do not commonly have oxy-components in the O(3) site (NWA 5790 and MIL nakhlites), OH was not directly measured, so we assumed that 2–F–Cl = OH, whereas kaersutite and Ti-biotite within Chassigny were only plotted if OH was measured directly because of the likelihood of O^{2-} substitution in the O(3) site. To plot within the F-Cl-OH ternary, we normalized the molar sums of F, Cl, and OH from the SIMS analyses to one. **a** Apatites from shergottites and regolith breccia NWA 7034, **b** Apatites from chassignites, **c** Amphiboles and biotite from chassignites and nakhlites, and **d** Apatites from nakhlites. Data within these plots are compiled from McCubbin et al. (2013, 2016)

halogen-bearing, alteration phases that are likely martian in origin. These minerals include Cl-poor smectite, Cl-bearing iddingsite, and halite (Bridges and Grady 1999, 2000; Bridges et al. 2001; Treiman 2005; Bridges and Schwenzer 2012).

16.2.3 Chassignites

The three chassignite meteorites (Chassigny, NWA 2737, and NWA 8694) are dunites, and may originate from the same cumulate pile as the nakhlites.

Halogen-bearing mineral phases occur in two distinct petrographic contexts in chassignites: (1) as discrete phases within crystallized, olivine-hosted melt inclusions; and (2) igneous textured apatite that is interstitial to the cumulus olivine. The crystallized melt inclusions have mineral assemblages that include kaersutitic amphibole, Ti-rich biotite, apatite, and Cl-OH-bearing shock-vitrified plagioclase (maskelynite) (Johnson et al. 1991; Watson et al. 1994; McCubbin and Nekvasil 2008; McCubbin et al. 2010, 2013). The amphibole, biotite, and apatite compositions from the olivine-hosted melt inclusions in the chassignites are shown in Fig. 16.3. The intercumulus regions of the chassignite meteorites host only apatite as a volatile-bearing mineral phase. The compositions of intercumulus apatites, shown in Fig. 16.3, have higher abundances of Cl than the apatites hosted by melt inclusions. This observation is reported to be the result of interactions between intercumulus melt in the chassignites and Cl-rich crustal fluids on Mars at the time of their formation (McCubbin and Nekvasil 2008; McCubbin et al. 2013).

16.2.4 Orthopyroxenite (Allan Hills 84001)

The single orthopyroxenite meteorite—Allan Hills 84001 (ALH 84001), has been shown to contain apatite phases that are interstitial to the cumulus orthopyroxenes (Boctor et al. 2003; Greenwood et al. 2008). A single study measured the light halogen abundances of these apatites, showing that they are Cl-rich with 3.42 wt.% Cl and 1.29 wt.% F (Boctor et al. 2003). Hydroxyl (OH) abundances have also been determined by secondary ion mass spectrometry (SIMS), yielding approximately 0.08–0.22 wt.% H_2O (Boctor et al. 2003; Greenwood et al. 2008). As OH is a standard substitution site for Cl and other halogens, these data indicate that the apatites are predominantly halogen-rich, and similar in composition to apatites in the nakhlites and chassignites.

16.2.5 Regolith Breccia

Until recently, we had no non-igneous martian meteorites within our inventory, and thus no samples that could represent the crust. However, in 2011, a martian regolith breccia—NWA 7034—was recovered, and since this discovery, at least eight additional paired stones have been reported. This sample-set is considered to be the most representative of martian crust to-date. A bulk Cl content of 2200 ppm was determined for NWA 7034, which is similar to values reported for the martian crust from gamma ray spectroscopy, ranging from 350–4200 ppm (Taylor et al. 2010; Taylor 2013). The only halogen-rich phase within this regolith breccia is Cl-rich apatite, which is hosted in three distinct petrographic contexts: (1) as mineral clasts within the bulk matrix of the breccia (Agee et al. 2013; Humayun et al. 2013); (2) within igneous clasts that appear to be primary crystallization products (Santos et al. 2015);

and (3) as submicron apatites that constitute the thermally annealed granoblastic groundmass of the breccia (Muttik et al. 2014). Apatite compositions from each of the petrographic domains are available in Fig. 16.3. The occurrence of these phases is important because apatite has been shown to account for the entire Cl budget of NWA 7034, so it provides us with at least one data point on the mineralogical hosts for Cl in the martian regolith. Although bulk rock F abundances have not been determined for NWA 7034, the abundance is estimated to be ~316 ppm from the average F/Cl ratio of the apatites throughout NWA 7034 (McCubbin et al. 2016), and the bulk rock abundance of Cl, which can be entirely attributed to Cl in apatite.

16.3 Significance of Halogens in Martian Meteorites

The study of halogens within martian meteorites has important implications for igneous, atmospheric, and aqueous processes on Mars, as well as representing an important analogue with which to quantify the budget of halogens in the martian interior. Some studies have highlighted the importance of Cl in lowering the basalt liquidus, which acts to reduce pressure or temperature parameters for crystallization and melting in the martian interior (Filiberto and Treiman 2009a, b; see also Webster et al. 2018). They suggested that Cl may have had a larger impact than H_2O on basalt formation within the martian mantle, and thus the formation of martian rocks and soils, which may explain the elevated halogen concentrations observed in such materials compared to terrestrial basalts (see below). Later studies found that many martian meteorites have been affected by contamination from martian crustal material and, therefore, could not be used to reliably estimate volatile abundances in the martian mantle (McCubbin et al. 2016; Williams et al. 2016). Recently constrained volatile abundances show that the source region for martian meteorites is similar to the terrestrial Mid-Ocean-Ridge Mantle source, and melting of this source would produce magmas with roughly equivalent abundances of H_2O and Cl (Filiberto et al. 2016; McCubbin et al. 2016).

The Cl and F abundances of the martian mantle and crust have been estimated and modeled from shergottites and regolith breccia samples, respectively, in a number of studies through methods that combine halogen mineral chemistry, bulk rock abundances of F, bulk rock abundances of incompatible-refractory-lithophile elements, and mineral-melt partitioning relationships (McCubbin et al. 2012, 2016; Gross et al. 2013; Filiberto et al. 2016). These models first determine the pre-degassing abundances of Cl in the parental liquids of the shergottites, and then ratio the F and Cl values for the parental liquids to the bulk rock abundances of incompatible-refractory-lithophile elements. These are used to calculate the F and Cl abundances of the source, where the abundances of incompatible refractory lithophile elements for bulk silicate Mars are constrained relatively well based on their chondritic abundances (Dreibus and Wanke 1985; McDonough and Sun 1995; Taylor 2013). The abundances of refractory, incompatible, lithophile elements are useful for estimating the abundances of volatile, incompatible, lithophile elements

because they both exhibit similar behavior during magmatic processes. Based on these methods, it is estimated that the depleted shergottite source has 1.6–4.2 ppm Cl and 1.0–1.6 ppm F, and that the enriched shergottite source has 12–23 ppm Cl and 3.6–5.4 ppm F (McCubbin et al. 2016). In addition, the martian crust has 450 ppm Cl and 106 ppm F (McCubbin et al. 2016). Combined, these estimates imply that the bulk silicate composition of Mars is approximately 44 ppm Cl and 10 ppm F (McCubbin et al. 2016).

Recent work by Williams et al. (2016) and Sharp et al. (2016) assessed the Cl isotopic abundance in a number of martian meteorites and determined a range in ^{37}Cl, where the martian mantle (olivine-phyric shergottites) is depleted at −3.8‰ (i.e., the difference in isotopic composition from standard mean ocean Cl in per mil, or parts per thousand), while the crust (NWA 7034) is enriched at up to 8.6‰. They conclude that the enrichment on the surface was likely caused by preferential loss of ^{35}Cl to space, while the low ^{37}Cl value likely relates to the primordial bulk composition of Mars, inherited during accretion.

A study by Cartwright et al. (2013) on nakhlites Nakhla, NWA 998, and MIL 03346 found evidence for a trapped fluid component enriched in Cl, which correlates with excess ^{40}Ar (excess $^{40}Ar = {}^{40}Ar_{measured} - {}^{40}Ar_{radiogenic}$, thus leaving the composition of the trapped fluid component), consistent with the martian atmosphere. The range of I/Cl and Br/Cl ratios for the mineral separates studied was similar to that observed on the Earth, which was surprising given the lack of crustal recycling processes, organic activity, and evident fluid activity on Mars. The authors also concluded that the halogen components are likely dispersed within minor phases in the nakhlites, and that the fluid observed had a low salinity, suggesting that it may have originated as a shallow sub-surface fluid within the nakhlite cumulate pile. A similar Cl-rich component was also observed in halogen analyses of shergottite RBT 04262 (Cartwright and Burgess 2011).

Earlier work by Bridges et al. (2000, 2001) studied the formation of alteration assemblages in the nakhlite suite and suggested that brines with a seawater-like composition could have percolated through the crust and deposited evaporite assemblages within the nakhlites under low temperature conditions. An additional source of fluid interaction could be through impact-induced heating. Later studies have suggested that impacts on the surface produced sufficient heat sources to drive hydrothermal activity at impact sites and the surrounding areas, leading to volatile formation in the crust, and alteration phases in the surface that include phyllosilicates and S-rich phases (Newsom 1980; Abramov and Kring 2005; Schwenzer and Kring 2009, 2010). A study by Changela and Bridges (2010) on alteration phases within nakhlites led the authors to conclude that the assemblages may result from the formation of an impact-induced 'hydrothermal cell', where a stratigraphic variation in alteration phase abundance was caused by fluid flow from the base to the top of the pile rather than top-to-bottom. Later work by Bridges and Schwenzer (2012) further modeled this hydrothermally driven fluid, determined that it was likely impact-generated, and that it had an alkaline pH. Additional studies have also modeled the flow of hydrothermal fluids following an impact on Mars and found

clear processes of interaction with the martian surface (Abramov and Kring 2005; Schwenzer and Kring 2009).

An additional observation for martian meteorites is that elevated I/Cl ratios are observed in finds compared to falls, especially for those recovered from Antarctica (Cartwright et al. 2013). This is consistent with the findings of Langenauer and Krähenbühl (1993) who studied terrestrial halogen contamination in chondrites from Antarctica, and found some abundance patterns based on distance from the Antarctic coast. While falls are less likely to experience terrestrial weathering due to their shorter exposure time as a result of fast recovery in the field, some variation was observed in sub-samples of Nakhla (E, K, G—which relate to the museum/collection that they were provided from—Table 16.1). This was explained as either a result of contamination by salts from terrestrial brines prior to recovery, or the result of heterogeneous martian weathering (Dreibus et al. 2006). Here, Nakhla G is considered to be the most 'pristine' sample, and shows higher I/Cl ratios compared to E and K (Dreibus et al. 2006). While small-scale terrestrial contamination within Nakhla may be possible, it is also plausible that martian weathering is a factor. In fact, Greenwood (2008) suggested that Antarctic weathering may be a good analogue for martian weathering, where elevated halogen contents should be expected in martian weathering products.

16.4 In Situ Detections of Halogens on the Martian Surface

Halogens have been detected on the martian surface by all landed missions (Fig. 16.4, Table 16.2). Chlorine has been detected in all landed missions to date, whereas Br has only been measured in more recent missions, and F was recently measured by the *Curiosity* rover (Table 16.3). Iodine has not yet been measured on the martian surface, likely because of low abundances and instrument detection limits. Overall, surface rocks and soils have higher concentrations of halogens than martian meteorites. The type and the abundance of halogens and their speciation have important implications for ancient and modern environments on Mars. Here, we review the types of halogens that have been detected in situ by rovers and landers and the phases in which these halogens may reside. We discuss the variability and mobility of halogens on the surface and the processes that control this variability. Finally, we discuss the implications that the discovery of Cl in the form of perchlorate has for the modern habitability of the martian surface and the preservation of organics.

The NASA Viking Landers, VL1 and VL2, landed in 1976 in Chryse and Utopia Planitiae, respectively. The X ray Fluorescence Spectrometers (XRFS), mounted within the body of both landers, used a ^{55}Fe and ^{109}Cd sources and had the ability to detect fluorescent emissions of elements between the mass ranges of Mg and U, as long as they were above the limit of detection (Clark et al. 1977). The only

Table 16.2 Largest halogen abundances measured at each landing site

Mission	Landing site	Cl (wt.%)	Br (ppm)
Viking L1	Chryse Planitiae	0.9 + 1.5/−0.5* (C-5 & C-13)	–
Viking L2	Utopia Planitiae	0.6 + 1.5/−0.5* (U-2 & U-5)	–
Pathfinder	Ares Vallis	1.2 ± 0.3† (A-9)	–
MER—Opportunity	Meridiani Planum	2.13 ± 0.03‡ (Dorsal_new)	1232 ± 38‡ (Ellesmere_Barbeau)
MER—Spirit	Gusev Crater	2.62 ± 0.03§ (Uchben_Chiikbes_brush)	1543 ± 28§ (Temples_dwarf_asis)
Phoenix	Northern Plains	0.6 mM Cl^-; 2.6 mM ClO_4^- ‖ (Rosy Red)	<100 ppm¶
MSL—Curiosity	Gale Crater	3.44 ± 0.09‡ (Stephen_Raster2)	1978 ± 60‡ (Windjana_center_postDRT)

Targets of the measurements are in parentheses

*From XRFS data (Clark et al. 1982). Total uncertainty includes uncertainty with instrument precision, calibration, and soil matrix effects

†From APXS (Foley et al. 2003). Error includes the statistical and laboratory combined error at 1σ

‡Values from the Planetary Data System. Absolute statistical 2σ errors are derived from peak area errors and do not include calibration uncertainties

§From APXS data (Gellert et al. 2006). Absolute statistical 2σ errors are derived from peak area errors and do not include calibration uncertainties

‖From WCL data (Hecht et al. 2009). Concentration error = ±20%

¶Br^- and I^- were not detected in solution, indicating they must be present in abundances below the WCL sensor's limits of detection (Kounaves et al. 2010)

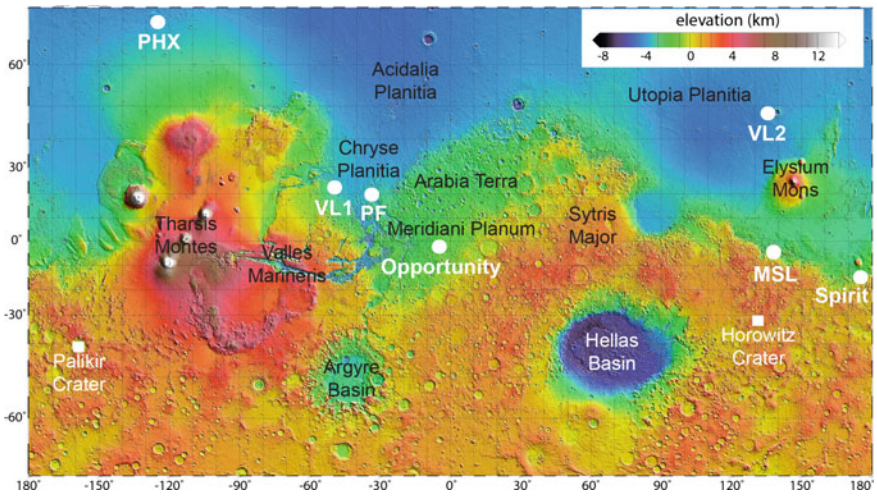

Fig. 16.4 Topographic map of Mars from the Mars Orbiter Laser Altimeter showing the landing sites of landers and rovers, important features, and locations discussed in the text. *Image credit* MOLA Science Team

Table 16.3 Halogen abundances measured by APXS on *Curiosity* of drilled and scooped samples

Location	Sample	Lithology	Sol	Cl (wt.%)	Br (ppm)
Near landing site	Rocknest	Aeolian Sand	102	0.88 ± 0.05	65 ± 10
Yellowknife Bay	Cumberland	Mudstone	487	1.19 ± 0.04	65 ± 10
Kimberley	Windjana	Sandstone	704	0.57 ± 0.01	122 ± 5
Pahrump Hills	Confidence Hills	Mudstone	767	0.35 ± 0.01	38 ± 5
Pahrump Hills	Mojave2	Mudstone	888	0.46 ± 0.02	57 ± 5
Pahrump Hills	Telegraph Peak	Mudstone	922	0.34 ± 0.01	93 ± 5
Marias Pass	Buckskin	Mudstone	1065	0.28 ± 0.01	60 ± 5
Bridger Basin	Big Sky	Sandstone	1126	0.84 ± 0.02	300 ± 10
Bridger Basin	Greenhorn	Sandstone	1143	0.49 ± 0.01	219 ± 10
Bagnold Dunes	Gobabeb	Aeolian Sand	1223	0.50 ± 0.01	37 ± 5
Naukluft Plateau	Lubango	Sandstone	1326	0.32 ± 0.01	60 ± 5
Naukluft Plateau	Okoruso	Sandstone	1339	0.61 ± 0.01	115 ± 5
Murray Buttes	Oudam	Mudstone	1368	0.35 ± 0.01	24 ± 5

Measurements from rocks (i.e., mudstone and sandstone) were made on drilled fines prior to sieving, except for the measurement from Telegraph Peak, which is on drill tailings. Values are from the Planetary Data System

halogen detected by the XRFS on VL1 and VL2 was Cl with a detection limit of ~0.3 wt.% (Clark and Baird 1973).

The NASA Mars Pathfinder mission featured the first rover, *Sojourner*, which landed in Ares Vallis in 1997. The alpha proton X-ray spectrometer (APXS) mounted on the back of the rover used a ^{244}Cm source and operated in three separate modes (alpha backscattering, proton emission, and X-ray emission) to measure a different range of elements (from C to Zr) than the Viking XRFS (Rieder et al. 1997; Foley et al. 2003). A deployment mechanism allowed the instrument to investigate both rocks and soils (Rieder et al. 1997). Like the XRFS instruments on VL1 and VL2, the APXS on Pathfinder only detected Cl in martian rocks and soils at Ares Vallis.

The NASA Mars Exploration Rovers (MER), *Opportunity* and *Spirit*, landed in Meridiani Planum and Gusev crater, respectively, in 2004. *Opportunity* continues to rove the martian surface today. Both rovers had an updated APXS instrument mounted on the turret of a robotic arm. Upgrades from the Pathfinder-APXS included an improved X-ray detector, which gave higher energy resolution and sensitivity (Rieder et al. 2003; Gellert et al. 2006). The APXS instruments on both rovers detected Cl and made the first detections of Br on the martian surface (e.g., Rieder et al. 2004; Gellert et al. 2006).

The NASA *Phoenix* lander landed in 2008 in Vastitas Borealis in the northern plains of Mars (at 68.22°N). The Wet Chemistry Laboratory (WCL) on *Phoenix* had the capability to detect Cl^-, Br^-, and I^- anions in solution and indeed detected

Cl^- in soil solutions (Hecht et al. 2009). The Thermal and Evolved Gas Analyzer (TEGA) on *Phoenix* showed that the Cl was present in oxychlorine compounds (Boynton et al. 2009; Hecht et al. 2009).

The NASA Mars Science Laboratory (MSL) *Curiosity* rover landed in Gale crater in 2012, and the mission is in its second Extended Mission at the time of this writing. An APXS instrument mounted on the turret of the arm has detected Cl and Br in nearly every measurement to date (e.g., Mangold et al. 2017; Thompson et al. 2016, 2017), and the Sample Analysis at Mars (SAM) instrument has confirmed the presence of oxychlorine compounds from evolved gas analysis (EGA) of most drilled rock samples and scooped sand samples measured to date (e.g., Glavin et al. 2013; Leshin et al. 2013; Archer et al. 2014, 2016; McAdam et al. 2014; Sutter et al. 2016, 2017; Stern et al. 2017). *Curiosity* has made the first in situ measurement of F by laser induced breakdown spectroscopy (LIBS) using the ChemCam instrument (Forni et al. 2015). This technique is currently being developed to quantify Cl abundances (Thomas et al. 2017).

16.4.1 Chlorine

Chlorine is the most abundant halogen detected on the martian surface by landers and rovers (Table 16.3 and Fig. 16.4). Early detections of Cl by the Viking landers and MER were generally proposed to be in the form of chloride salts (e.g., Clark and Baird 1979; Clark et al. 2005; Knoll et al. 2008). Enrichments in both Na and Cl in rinds on rocks in Meridiani measured by *Opportunity* suggest the presence of halite on rock surfaces, which may have formed by transient thin films of liquid water (Knoll et al. 2008). *Curiosity* is ascending the lower slopes of Mount Sharp in Gale crater to study progressively younger sedimentary strata (Fig. 16.5), which were deposited in lacustrine, fluvial, deltaic, and aeolian environments at ~3.6 Ga. *Curiosity* is currently investigating the Murray formation (Fig. 16.5b), which is dominated by lacustrine mudstone in the lower Murray formation in Pahrump Hills and Marias Pass, but is made up of lacustrine, fluvial, and aeolian deposits in the upper Murray formation south of the Murray Buttes. Association of Cl with Na and a greater abundance of Cl have been observed in the upper Murray formation compared to the lower Murray formation (Thomas et al. 2017). This indication of halite, along with the presence of Ca-sulfate minerals, hematite, and desiccation cracks, suggests that this mudstone was deposited in an evaporative lake environment (Stein et al. 2017; Vaniman et al. 2017). This is in contrast to the perennial lake environment inferred from finely laminated mudstone investigated at the Pahrump Hills and Marias Pass (Rampe et al. 2017).

Clark et al. (2005) noted that Cl on the martian surface could be present in oxidized compounds, including chlorites, chlorates, and perchlorates. Data from TEGA on *Phoenix* and SAM on *Curiosity* indeed indicate that much of the Cl detected in samples measured from the northern plains and Gale crater is in the form of oxychlorine compounds chlorate (ClO_3^-) and/or perchlorate (ClO_4^-) (e.g., Boynton et al.

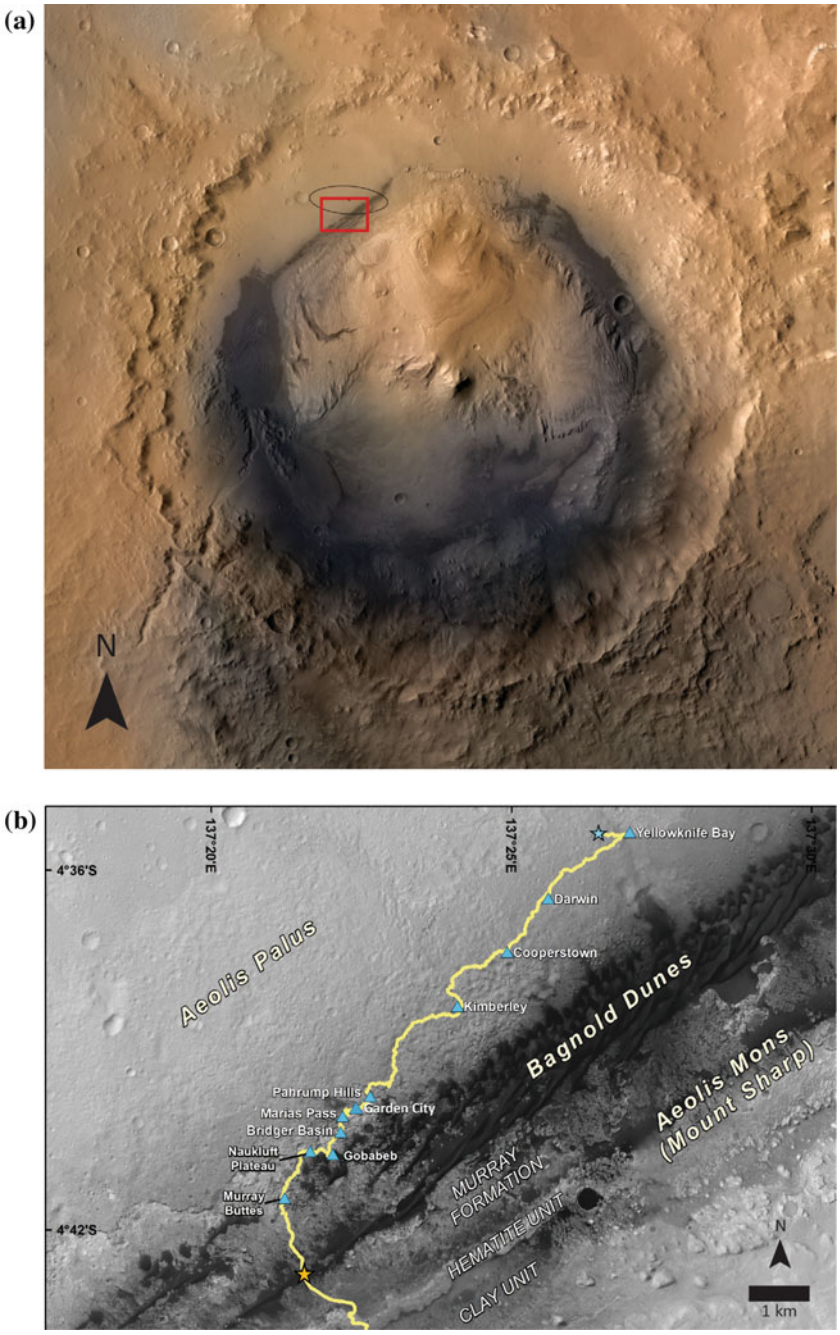

Fig. 16.5 **a** View of Gale crater from a combination of data from three Mars orbiters. The crater is 154 km in diameter, and the landing ellipse is in *black*. Location of Fig. 16.5b is outlined in *red*. *Image credit* NASA/JPL-Caltech/ESA/DLR/FU Berlin/MSSS. **b** *Curiosity* rover traverse, showing the important waypoints through Sol 1500. At the time of writing, *Curiosity* is located at the *gold star*. *Image credit* NASA/JPL-Caltech/Univ. of Arizona

2009; Archer et al. 2014; Sutter et al. 2016, 2017; Stern et al. 2017). The identification of oxychlorine compounds is based on O_2 gas releases from ~100–600 °C in EGA data. The position of this release can help differentiate between chlorate and perchlorate and can help identify the cation associated with the oxychlorine (Sutter et al. 2015; Archer et al. 2016). The presence of perchlorate was inferred at the Viking landing sites based on the detection of chloromethane and dichloromethane in the Viking Gas Chromatograph Mass Spectrometer (Navarro-González et al. 2010). Oxychlorine compounds in modern aeolian sediments and ancient sedimentary rocks in Gale crater are generally much more abundant than in terrestrial soils (10^6–10^7 μg/kg vs. 10^{-1}–10^5 μg/kg, respectively; Stern et al. 2017), though similar abundances have been identified in soils from the Atacama Desert (Catling et al. 2010). Wilson et al. (2016) and Stern et al. (2017) suggested that this discrepancy may give us insight into the mechanisms by which oxychlorine compounds form on Mars.

Oxychlorine compounds have been hypothesized to form by a variety of processes on Mars, including oxidation on mineral surfaces, radiolysis by ionizing radiation, and/or UV irradiation. Recent laboratory studies and in situ measurements on Mars point toward radiolysis by ionizing and/or UV radiation as an important process for forming and destroying oxychlorine compounds on Mars (e.g., Quinn et al. 2013; Carrier and Kounaves 2015; Wilson et al. 2016; Stern et al. 2017). Wilson et al. (2016) proposed a mechanism for the production of perchlorate through radiolysis of the martian surface by galactic cosmic rays from which Cl oxides sublimate into the atmosphere and form perchloric acid ($HClO_4$). Perchloric acid is then deposited onto the surface and crystalizes to form perchlorate salts. The similarity in oxychlorine abundances in rocks from the early Hesperian period (~3.7–3.4 Ga) rocks and in modern sediments as measured by SAM in Gale crater suggests ionizing radiation may play a role in both the formation and destruction of oxychlorine compounds to maintain a steady surface concentration (Stern et al. 2017). UV radiation may also add to the concentration of oxychlorine compounds on the martian surface. This has been demonstrated by Carrier and Kounaves (2015), whom exposed grains of halite and silica to UV radiation resulting in the oxidation of Cl.

Mudstone sampled from the Yellowknife Bay sampling site in Gale crater and sandstone sampled from the Kimberley outcrop measured by SAM on *Curiosity* have light and highly variable $\delta^{37}Cl$ values (Farley et al. 2016). The isotopic composition of Cl was measured from thermally evolved HCl. The $\delta^{37}Cl$ values range from $-1 \pm 25‰$ to $-51 \pm 5‰$. The mineral phase in which the Cl resides has important implications for the reasons behind the isotopically light Cl. If the Cl is in oxychlorine compounds, then atmospheric chemical reactions may be responsible for the light Cl. Similar reactions create isotopically light Cl in Atacama Desert soils (e.g., Jackson et al. 2010). Alternatively, if the Cl is in chloride salts, then partial reduction of isotopically normal perchlorate could fractionate and produce isotopically light chloride. The CheMin X-ray diffractometer on *Curiosity* did not definitively detect oxychlorine compounds or chloride salts in any of these samples, suggesting they are below the instrument's detection limits of ~1–2 wt.% (Blake et al. 2012). Although it is not certain whether the Cl in the evolved HCl was from an oxychlorine or chloride source, the low-temperature evolution of O_2 with

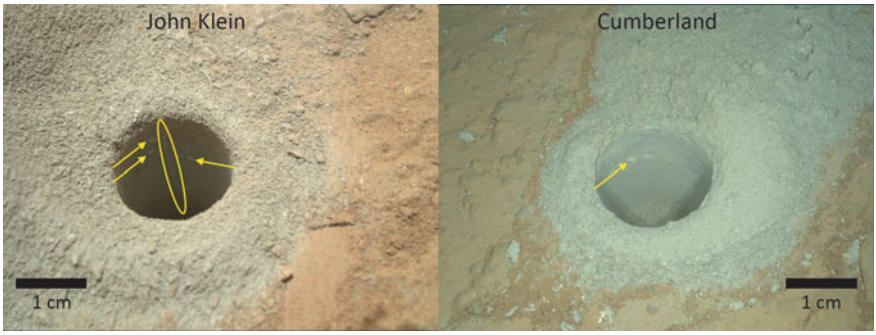

Fig. 16.6 Mars Hand Lens Imager (MAHLI) images of the John Klein and Cumberland drill holes, taken on sols 270 and 293, respectively. For scale, the drill holes are 1.6 cm in diameter. Note the fine, bright veins in the walls of the John Klein drill hole (highlighted in *yellow*) and the relative paucity of veins in the walls of the Cumberland drill hole. The late-stage fluids in these fractures could have mobilized oxychlorine compounds in the mudstone on a local scale. *Image credit* NASA/JPL-Caltech/MSSS

the concomitant release of HCl implicates oxychlorine (e.g., Glavin et al. 2013; Leshin et al. 2013; Archer et al. 2014; Ming et al. 2014).

Whatever its mechanism of formation, the discovery of oxychlorine in areas of the martian surface so-far- sampled demonstrates the paucity of liquid water since its deposition. Oxychlorine compounds are extremely soluble in liquid water and will persist in soils as long as there is no water to mobilize them (e.g., Catling et al. 2010). The samples measured by SAM are sourced from ~5–6 cm depth, so the discovery of oxychlorine compounds in these ancient rocks (~3.6 Ga) suggests either that the oxychlorine compounds are ancient or that late-stage diagenetic fluids have affected their concentrations and mobilized them from elsewhere in the crater. Indeed, in two samples drilled from mudstone at Yellowknife Bay, there was a marked difference between the oxychlorine abundance in the two samples, named Cumberland and John Klein, drilled only a few meters apart. The ClO_4 abundances in the Cumberland drill sample were an order of magnitude greater than those in the John Klein sample (10.5 ± 4.5 vs. 0.87 ± 0.39 g/kg, respectively; e.g., Ming et al. 2014; Stern et al. 2017). Images of the John Klein drill hole (Fig. 16.6) and geochemical measurements of the walls by ChemCam showed hairline fractures filled with Ca-sulfate cement (Vaniman et al. 2014), suggesting that later stage fluids removed a majority of the oxychlorine compounds from that part of the mudstone.

16.4.2 Bromine

Bromine is present in almost all APXS measurements by MER (*Opportunity* and *Spirit*) and MSL (*Curiosity*). Bromine concentrations on Mars are much higher than on Earth, on the order of 1–10% of Cl concentrations, whereas Br concentrations in seawater on Earth are 0.35% of Cl (e.g., Gellert et al. 2006; Marion et al. 2009).

On Earth, Br typically substitutes for Cl in halite, rather than precipitating as a discrete bromide mineral. To evaluate the phases in which Br may precipitate on Mars, Marion et al. (2009) investigated the partitioning of Br in chloride minerals in the Burns formation (a 7 m exposed stratigraphic section in Meridiani Planum) using an equilibrium chemical thermodynamic model, FREZCHEM. They found that the mineral bischofite ($MgCl_2 \cdot 6H_2O$) may be a more important sink for Br than halite on Mars. Jarosite ($(K,Na,H_3O)Fe_3(SO_4)_2(OH)_6$) has been unequivocally identified by rovers in Meridiani Planum and Gale crater (e.g., Klingelhöfer et al. 2004; Rampe et al. 2017). Laboratory experiments of jarosite precipitation in Br- and Cl-bearing solutions demonstrate that jarosite may be another mineral host for Br (Zhao et al. 2014). Others have speculated that Br is present in oxidized forms, as bromates and perbromates (Clark et al. 2005).

Many studies have noted extremely variable Br concentrations, particularly in Meridiani and Gusev. Concentrations of Br at the surface of Meridiani and Gusev soils are typically less than 50 ppm, but these concentrations are elevated by factors of 2–30 in subsurface soils, grains armoring sedimentary bedforms, and low-lying rocks (Yen et al. 2005). Enrichments in Br and Cl are decoupled from one another in these soil profiles, where APXS measurements show a relative loss of Br compared to Cl at the surface (Clark et al. 2005; Karunatillake et al. 2013). Initially, this variability was attributed to the presence of liquid water and the high solubility of bromide in solution. It was hypothesized that thin films of liquid water could form from the sublimation of frost, and cycles of diurnal or seasonal thin films of liquid water could mobilize Br^- and concentrate it in the subsurface and local depressions (Yen et al. 2005). Bromine concentrations, however, show no obvious relationship with other highly soluble salts (Clark et al. 2005). More recent studies have suggested that UV photolysis and the subsequent oxidation of Br may explain the lower concentrations of Br in soil surfaces (Karunatillake et al. 2013). In this scenario, Br is converted to gas phases (e.g., BrO) by UV photolysis. In fact, depletion of Br from salt flats in Abu Dhabi and from terrestrial polar sea ice is observed and attributed to UV photochemical reactions and the formation of Br in the vapor phase (Simpson et al. 2007; Wood and Sanford 2007).

16.4.3 Fluorine

Fluorine was recently measured in Gale crater with ChemCam (*Curiosity*), marking the first in situ measurement of F on Mars. Atomic or ionic emission lines from F in laser induced breakdown spectra (LIBS) from MSL-ChemCam have a detection limit of $\sim$5 wt.% because of atmospheric absorption, laser coupling, and detector sensitivity (Forni et al. 2015). However, F can be detected by ChemCam with a detection limit of $\sim$0.2 wt.% by observing CaF molecular bands. As of early 2017, F had been identified in 600+ targets (Forni et al. 2017). The highest concentration was found in the Alvord Mountain target at 10 wt.% F in the lower Murray formation in a location with a complex series of veins called Garden City

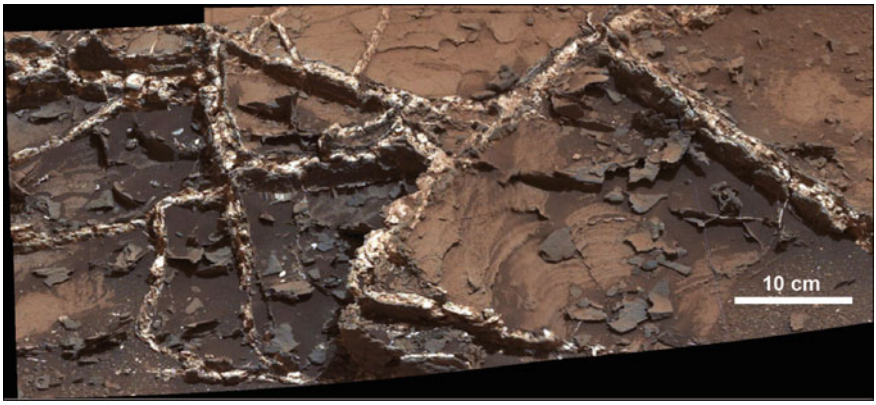

Fig. 16.7 *Curiosity* Mastcam image of complex series of veins at the Garden City site. *Image credit* NASA/JPL-Caltech/MSSS

(Figs. 16.5b, 16.7). Fluorine has been identified in a variety of targets, suggesting multiple sources and formation mechanisms. It has been identified (1) in conglomerates where the F-bearing phase is an aluminosilicate, (2) in conglomerates where the F-bearing phase is high in Ca (e.g., fluorapatite or fluorite), (3) associated with Si at the base of the Pahrump Hills outcrop, (4) in dark veins in Garden city and fracture fills in aeolian sandstone where the F-bearing phase is high in Ca, and (5) in correlation with Ca near the unconformity between lacustrine mudstone and aeolian sandstone (Forni et al. 2015, 2016, 2017). The detection of F, associated with Al and/or Si, may indicate that F is in the phyllosilicates. The association of F with Ca suggests the presence of fluorapatite and/or fluorite. Fluorapatite was detected by the CheMin X-ray diffractometer in abundances of ~1–2 wt.% in mudstone samples from the Pahrump Hills (Rampe et al. 2017). The prevalence of Ca-F minerals in veins and along unconformities suggests they precipitated from late-stage, low-temperature diagenetic fluids (Forni et al. 2015, 2016, 2017).

16.5 Orbital Detections of Halogens on the Martian Surface

Halogens have been detected on a global scale by orbiting spectrometers, providing clues to past and present geologic environments and processes.

16.5.1 Chlorine

The first measurements of Cl from orbit were made from the 2001 NASA Mars Odyssey Gamma Ray Spectrometer (GRS). Keller at al. (2006) determined a mean concentration of 0.49 wt.% Cl from the summation of the GRS spectra collected

over the planet. Consistent with lander measurements and the meteorite isotope work performed at the time (Rao et al. 2002), Cl is enriched significantly within the upper few tens of centimeters of the surface relative to the martian meteorites and the estimate for the bulk composition of the planet. However, Cl is not homogenously distributed over the martian surface and varies by a factor of ~4. Only regional variations can be investigated by GRS due to the instrument's relatively large footprint (~600 km diameter). Keller et al. (2006) observed that the Medusae Fossae formation west of the Tharsis volcanic complex shows significantly elevated Cl, whereas distinctly low Cl values are observed in the southern highlands and in a region north of Syrtis Major extending into Utopia Planitia. Furthermore, measurable differences from the global mean are observed around the outflow channels of Chryse and Acidalia Planitiae and Arabia Terra. Chlorine appears to be positively linked with H and negatively associated with Si and thermal inertia (Keller et al. 2006).

Genetic relationships between Cl enrichment and depletion are likely due to many factors. The strong spatial overlap between the Cl-rich region west of Tharsis and the previously mapped Medusae Fossae formation suggest enrichments through volcanic outgassing given the proximity to Tharsis. The denudation of volcanic ignimbrite deposits enriched in Cl through reactions of acid-fog or acid precipitation, in addition to possible aqueous activity, could result in Cl enrichment in the region (Keller et al. 2006). However, movement of Cl in ground or surface water could have depleted Cl in some regions, such as the ancient southern highlands, through leaching and erosion and deposition in other regions through evaporitic processes (e.g., Kargel 2004). Because of weak correlations with surface dust, Cl distribution is also likely the result of aeolian processes resulting in the deposition of Cl-rich fines. The Cl-bearing species in the dust have not been determined because the physical nature of the fine-grained surface dust makes it difficult to decipher the composition from orbiting visible/near-infrared (VNIR) and mid-infrared (MIR) spectrometers.

16.5.2 Halite-Bearing Materials

The Thermal Emission Imaging System (THEMIS) onboard NASA's Mars Odyssey provided the first orbital evidence for chloride salts on the surface (Osterloo et al. 2008). The chloride salt deposits were discovered based on their spectral distinctiveness in false-color THEMIS images. The materials exhibit featureless sloping emissivity spectra in THEMIS (~672–1475 cm^{-1} or ~14.88–6.78 μm) and NASA's Mars Global Surveyor (MGS) Thermal Emission Spectrometer (TES) data (~300–1300 cm^{-1} or ~33.33–7.70 μm). The observed spectral slope is due to an erroneous assumption of unit emissivity (i.e., maximum emissivity of one over the wavelength range) in the conversion of measured radiance to emissivity (e.g., Ruff et al. 1997; Osterloo et al. 2008, 2010). Very few geological materials exhibit relatively featureless spectra over this region as well as non-unit emissivity

with the exception of some anhydrous chloride salts, such as halite (NaCl). VNIR spectral data obtained by the NASA Mars Reconnaissance Orbiter (MRO) Compact Reconnaissance Imaging Spectrometer for Mars (CRISM) (Murchie et al. 2009) as well as the European Space Agency (ESA) Mars Express Observatoire pour la Minéralogie, l'Eau, les Glaces et l'Activité (OMEGA) (Ruesch et al. 2012) indicate that the chloride salts are distinctively brighter when compared to the typical background soils. Ratio reflectance data over the deposits exhibit featureless red slopes over the 1–2.5 μm region and an inverted 3 μm feature, indicating that these deposits are desiccated compared to the surrounding regolith. Although halite does not contain strong spectral features over the VNIR-MIR wavelength range, a combination of laboratory (Jensen and Glotch 2011), theoretical studies (Glotch et al. 2016), and geological arguments (e.g., Osterloo et al. 2008, 2010; Glotch et al. 2010), strongly suggest that it is the most likely candidate for the chloride salt phase present on Mars. Halite abundance is constrained to 5–20 wt.% for most deposits (Jensen and Glotch 2011). Furthermore, although phyllosilicates have been observed in close proximity to some deposits (Glotch et al. 2010; Ruesch et al. 2012), there appear to be no hydrated or additional evaporite phases intermixed with the chloride salts.

Based on THEMIS detections, the number of halite-bearing deposits ranges into the hundreds, dispersed primarily in the most ancient (i.e., Noachian-aged) terrains in the southern highlands (Fig. 16.8). The deposits occur in a variety of geologic settings but commonly occur in local depressions on plains units, including filling craters and channels (Osterloo et al. 2010; Osterloo and Hynek 2015; Hynek et al. 2015). Based on these observations, the most likely depositional scenario for halogens includes precipitation from evaporating surface waters in closed basins. Cross cutting relationships with phyllosilicates in close proximity to the deposits indicate that the halite-bearing materials are likely the products of late stage aqueous activity and are unlikely to be geologically related to the older phyllosilicates (e.g., Glotch et al. 2010). The lack of observed sulfates, carbonates, silica, phyllosilicates, and other expected authigenic phases, intermixed with the chloride salts, are problematic for drawing a clear link to a long-lived lacustrine depositional setting.

The geologic setting, geomorphological observations, and relative ages of the halite-bearing surfaces indicate that they may represent the last surge of major surface water activity on Mars (Osterloo and Hynek 2015). Halite crystals have been shown to provide information about the precursory liquid compositions entrapped in inclusions and clues to the depositional environment and climate at the time of formation (Lowenstein et al. 1999; Roedder 1984). As such, these materials likely hold important clues regarding the paleoclimate and environment of this intriguing and dynamic time period of martian geologic history. Furthermore, terrestrial salt deposits contain microbial fossils (e.g., Huval and Vreeland 1991), cellulose fibers (e.g., Griffith et al. 2008), and microscopic prokaryotes, including both haloarchaea and halobacteria biomarkers (e.g., Fredrickson et al. 1997; McGenity et al. 2000; Barbieri et al. 2006; Schubert et al. 2009). In addition, fluid inclusions in halite have been shown to be a favorable refuge for the short to long term (possibly hundreds of millions of years) survival of halophilic microorganisms

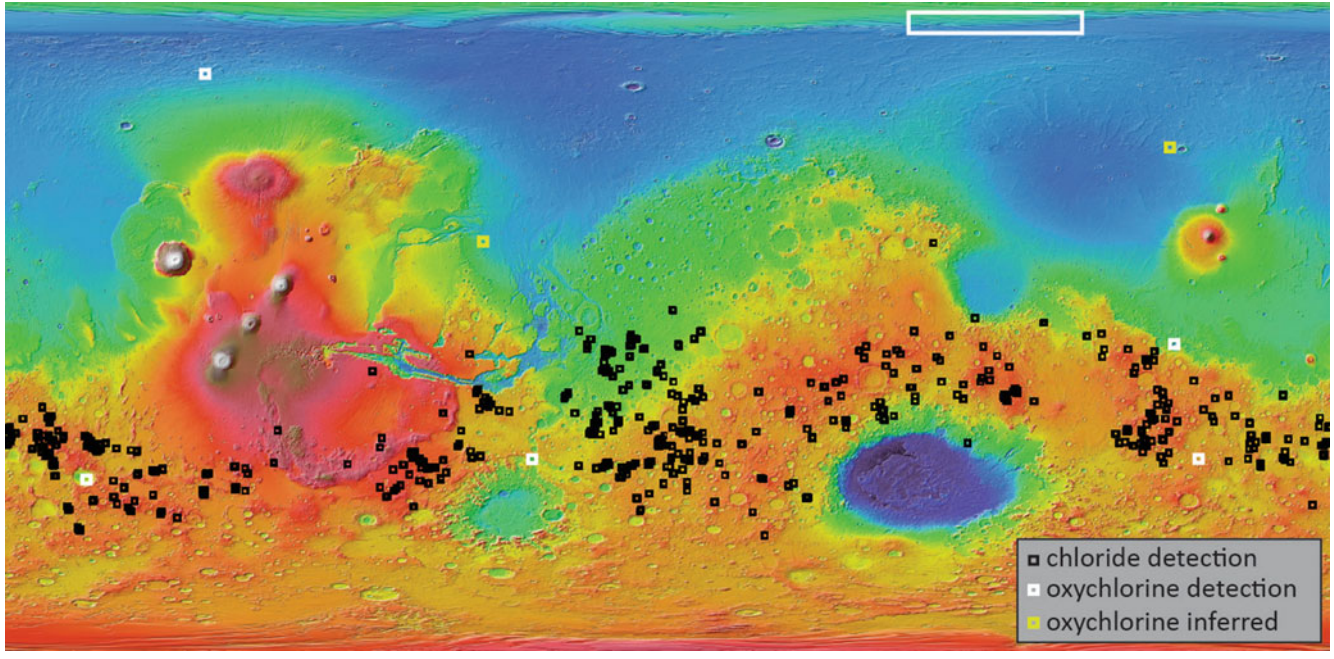

Fig. 16.8 Topographic map of Mars from the Mars Orbiter Laser Altimeter showing the locations where halide minerals have been detected by thermal infrared spectroscopy (*black squares*), oxychlorine phases have been detected by both near-infrared spectroscopy on orbiters and evolved gas analysis on *Phoenix* and *Curiosity* (*white squares*), and oxychlorine phases have been inferred at the VL1 and VL2 landing sites (*yellow squares*). *Image credit* MOLA Science Team

(e.g., Norton and Grant 1988; Javor 1989; Norton et al. 1993; Vreeland et al. 2000; Fish et al. 2002; Satterfield et al. 2005; Schubert et al. 2009). One of the primary goals of martian exploration is to determine whether life ever existed on the planet. Considering the ability of salts to both preserve and harbor microbial life, these halite deposits should be considered for future sample return missions.

16.5.3 Perchlorates

A limited number of detections of perchlorate and chlorate salts have been made from orbit (Fig. 16.8). Like halite, anhydrous oxychlorine salts do not have any strong features in the VNIR (Hanley et al. 2015). VNIR spectra of hydrated oxychlorine salts have many bands near 1.4 and 1.9 μm to allow their detection by orbital spectroscopy (Hanley et al. 2015). However, the VNIR spectra of hydrated oxychlorine salts are similar to some hydrated sulfate salts (Hanley et al. 2015). VNIR observations from OMEGA and CRISM demonstrate that hydrated sulfates are widespread across the surface of Mars (e.g., Bibring et al. 2006; Carter et al. 2013). As such, some detections of hydrated sulfates may actually be hydrated oxychlorine salts and vice versa (Hanley et al. 2015).

Data from MRO-CRISM provide evidence for perchlorates and chlorates over recurring slope lineae (RSL) in some locales (Ojha et al. 2015). RSL are narrow, low-reflectance features that form on present-day Mars (McEwen et al. 2011). These features are thought to form from either transient flow of liquid water or from granular flow of material (McEwen et al. 2011, 2014; Chevrier and Rivera-Valentin 2012). RSL extend incrementally downslope on steep, relatively warm slopes, fade when inactive, and reappear annually over multiple Mars years (Fig. 16.9) (McEwen et al. 2011, 2014; Ojha et al. 2014). Generally, RSL range from a few meters in length (<5 m), down to the detection limit for the High Resolution Imaging Science Experiment (HiRISE) camera ($\sim$0.25 m/pixel). The coarse spatial sampling of CRISM ($\sim$18 m/pixel), compared to HiRISE, limit the number of RSL that can be investigated with VNIR spectroscopy. However, Ojha et al. (2015) identified a few locations that were sufficient in size and/or number to undertake compositional studies using CRISM.

CRISM pixels measured over a densely packed area of RSL in Palikir crater (Fig. 16.9) contained absorption features consistent with the presence of oxychlorine compounds. Pixels closest to the RSL exhibited features near $\sim$1.48, 1.91, and $\sim$3 μm, whereas pixels farther away only had features at $\sim$1.91 and $\sim$3 μm. The $\sim$1.4 μm feature weakens with dehydration and disappears more rapidly than the 1.91 and 3 μm absorption bands suggesting higher hydration states in areas closest to the center of the RSL. Ojha et al. (2015) found that the wavelength position of the observed 1.4 μm absorption band is longer than is typical for perchlorates, suggesting the presence of an additional mineral. The absorptions observed are too narrow to be explained by liquid water and instead are hypothesized to be consistent with hydrated salts. A linear spectral mixture of martian soil with magnesium

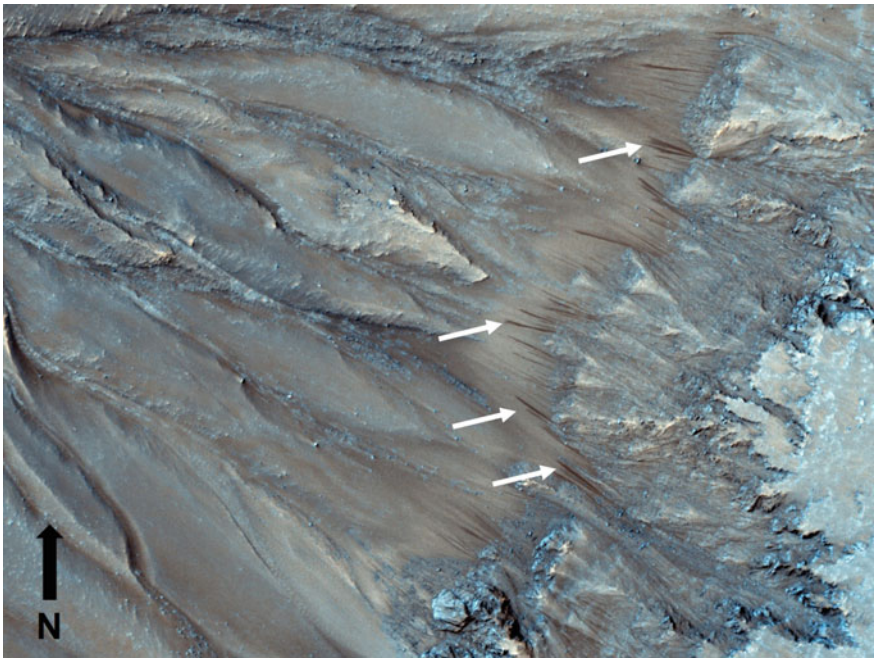

Fig. 16.9 Image of RSL in Palikir crater taken by HiRISE. RSL appear as dark streaks on northwest-facing slopes (highlighted by *white arrows*). *Image credit* NASA/JPL/University of Arizona

perchlorate, chlorate, and chloride salts provides the closest spectral match to what was observed in Palikir crater with CRISM (Ojha et al. 2015). A similar mixture of Mg-oxychlorine and chloride minerals was inferred from CRISM spectra of RSL in Hale crater (Ojha et al. 2015). Further evidence of hydrated salts comes from RSL on two central peaks in Horowitz crater, which show spectra best modeled by a linear mixture of martian soil and sodium perchlorate. RSL are abundant in Coprates Chasma, but spectra over these features only exhibited 1.9 μm absorptions, which limited assignment of a particular salt mineralogy (Ojha et al. 2015). Another notable detection of perchlorate from orbit using CRISM, although not from a region with RSL, is in dune sediments and sublimation tills surrounding the martian North Polar Cap (Massé et al. 2012). This perchlorate is associated with gypsum and may form by sublimation of the polar ice cap.

The origin of the water forming the RSL is not well understood (McEwen et al. 2011, 2014; Ojha et al. 2014). However, despite the uncertainty in formation mechanisms, hydrated salts likely play a role. Sodium perchlorate can lower the freezing point of water by up to 40 K, whereas magnesium perchlorate and magnesium chlorate can depress the freeing point even more by up to 70 K (Chevrier et al. 2009; Hanley et al. 2012). The presence of perchlorates and chlorates support the hypothesis that the RSL are formed from brine-enriched liquids on contemporary Mars. In the Atacama Desert on Earth, deliquescence of hygroscopic salts is

a refuge for microbial communities (Davila et al. 2008, 2013b) and halophylic prokaryotes (Aharonson et al. 2014). This would suggest that if the RSL provide transiently wet conditions near the surface, they may have astrobiological significance, although the water activity in perchlorate solutions may be too low to support known terrestrial life (Rummel et al. 2014).

16.6 Oxychlorine Compounds and Implications for the Habitability and Exploration of the Martian Surface

The presence of oxychlorine compounds on Mars has important implications for the detection and preservation of organic molecules, habitability of the modern martian surface, and for eventual human exploration of the martian surface. Although perchlorate is a strong oxidizing agent, it is typically inert under Mars ambient conditions (Catling et al. 2010; Kounaves et al. 2014). The pathways by which perchlorate is generated, however, produce intermediates (e.g., hypochlorite (ClO^-), chlorite (ClO_2^-), chlorate (ClO_3^-), and their associated radicals) that could oxidize all but the most refractory organic molecules (Kounaves et al. 2014). Trace abundances of native martian organic molecules have been detected on the martian surface by SAM (e.g., Freissinet et al. 2015), but it is important to consider the role oxychlorine compounds may have played in forming the assemblage of organic molecules on the surface today. By comparison, the presence of oxychlorine compounds may enhance the microbial habitability of the modern surface by providing liquid water. Perchlorate can depress the freezing point of water to between 206 and 273 K, depending on salt concentration and relative humidity (Chevrier et al. 2009; Gough et al. 2011; Hanley et al. 2012).

Perchlorate has been discussed as both a resource and a potential hazard to the human exploration of Mars (e.g., Davila et al. 2013a). It could provide oxygen for life-support and fuel, yet it could be a hazard to humans if ingested, because it can inhibit the uptake of I ions by the thyroid, therefore resulting in thyroid hyperplasia, goiter, and reduced metabolism (e.g., Smith 2006; Davila et al. 2013a). Astronauts could be exposed to perchlorate through inhalation of dust, consumption of food grown in soils containing perchlorate, and in drinking water. The reference dose for perchlorate equates to 24.5 μg/l in drinking water (Brown and Gu 2006; Davila et al. 2013a). Davila et al. (2013a) suggest a biochemical pathway to remove O_2 from perchlorate in the soil, where enzymes separate ClO_4^- to $O_{2(g)}$ and Cl^-. They suggest that this process would not violate planetary protection requirements because terrestrial microbes would not be necessary, and the resulting perchlorate-free soil could be used to grow crops.

16.7 Potential Measurements by Future Mars Missions

Many future orbital and landed missions to Mars are planned over the next 3–5 years, and this phase of Mars exploration will involve countries from around the world. NASA has two lander missions planned: InSight, which will have geophysical instruments to examine the interior, and the Mars 2020 rover, which will continue in *Curiosity's* tire treads to examine the habitability of the martian surface. Both ESA and the Russian Federal Space Agency will collaborate to send the ExoMars rover in 2020 to search for biomarkers. Three additional missions are also planned for 2020: India plans to send a lander and a rover to follow on to its Mars Orbiter Mission; China plans to send an orbiter, a lander, and a small rover; and the United Arab Emirates plans to send an orbiter.

A few of the instruments on ExoMars and Mars 2020 will have the capability to identify some halogens or halogen-bearing minerals in situ. The MicrOmega infrared spectrometer will cover the spectral range from 0.5–3.5 μm, and the Infrared Spectrometer for ExoMars (ISEM) will cover the spectral range from 1.15–3.3 μm, both allowing for the detection of oxychlorine salts. Both ExoMars and Mars 2020 will have Raman spectrometers (the Raman Laser Spectrometer (RLS) on ExoMars, and the Scanning Habitable Environments with Raman and Luminescence for Organics and Chemicals (SHERLOC) and SuperCam instruments on Mars 2020). Although halite does not have any first-order Raman modes (e.g., Kieffer 1979), oxychlorine compounds are detectable by Raman (e.g., Wu et al. 2015). Like ChemCam on *Curiosity*, SuperCam on Mars 2020 will have a LIBS instrument capable of detecting Cl and F. There will not be an APXS instrument on Mars 2020, but the Planetary Instrument for X-ray Lithochemistry (PIXL) will determine bulk chemistry though X-ray fluorescence. PIXL will be able to detect Cl and Br directly, and scanning the beam may be able to put halogen geochemistry into a spatial context (e.g., identify whether halogens are present in veins, individual grains, or cements).

In addition to its science payload, Mars 2020 will have the ability to collect samples and cache them on the surface for a future sample return mission. With returned samples, the halogen geochemistry and speciation of these elements can be determined with greater precision using the high-powered instruments we have in terrestrial labs. As a word of caution: many of the mineral phases in which halogens reside are hydrated and can be hygroscopic. If the temperature and relative humidity in the sample tubes do not mimic those of the near subsurface, the halogen-bearing minerals could experience phase changes so that these minerals, when they're analyzed on Earth, are not the same as those actually present on Mars. Curating the returned samples under cold temperatures will also be important for preventing further phase changes.

References

Abramov O, Kring DA (2005) Impact-induced hydrothermal activity on early Mars. J Geophys Res 110(E12). https://doi.org/10.1029/2005JE002453

Acuña MH, Connerney JEP, Ness NF et al (1999) Global distribution of crustal magnetization discovered by the Mars Global Surveyor MAG/ER experiment. Science 284:790–793

Agee CB, Wilson NV, McCubbin FM et al (2013) Unique meteorite from early Amazonian Mars: water-rich basaltic Breccia Northwest Africa 7034. Science 339:780–785

Aharonson O, Bardavid RE, Mana L (2014) Perchlorate and halophilic prokaryotes; Implications for possible halophilic life on Mars. Extremophiles 18:75–80

Aiuppa A, Baker DR, Webster JD (2009) Halogens in volcanic systems. Chem Geol 263:1–18

Aoudjehane HC, Jambon A, Boudouma O (2006) A cathodoluminescence study of cristobalite and K-feldspar in the nakhlite Mil 03346. Meteorit Planet Sci 41(8):A37

Archer PD Jr, Franz HB, Sutter B et al (2014) Abundances and implications of volatile-bearing species from evolved gas analysis of the Rocknest aeolian deposit, Gale Crater, Mars. J Geophys Res Planets 119:237–254. https://doi.org/10.1002/2013JE004493

Archer PD Jr, Ming DW, Sutter B et al (2016) Oxychlorine species on Mars: implications from Gale crater samples. Paper presented at the 47th lunar and planetary science conference, The Woodlands, TX, 21–25 March 2016

Barbieri R, Stivaletta N, Marinangeli L, Ori GG (2006) Microbial signatures in sabkha evaporate deposits of Chott el Gharsa (Tunisia) and their astrobiological implications. Planet Space Sci 54:726–736. https://doi.org/10.1016/j.pss.2006.04.003

Bibring J-P, Langevin Y, Mustard JF et al (2006) Global mineralogical and aqueous Mars history derived from OMEGA/Mars Express data. Science 312(5772):400–404

Blake DF, Vaniman D, Achilles C et al (2012) Characterization and calibration of the CheMin mineralogical instrument on Mars Science Laboratory. Space Sci Rev 170:341–399

Boctor NZ, Alexander CMO, Wang J, Hauri E (2003) The sources of water in martian meteorites: clues from hydrogen isotopes. Geochim Cosmochim Acta 67:3971–3989

Bogard DD, Garrison DH, Park J (2010) Chlorine abundances in martian meteorites. Paper presented at the 41st lunar and planetary science conference, The Woodlands, TX, 1–5 March 2010

Borg LE, Draper DS (2003) A petrogenetic model for the origin and compositional variation of the martian basaltic meteorites. Meteorit Planet Sci 38:1713–1731

Boynton WV, Ming DW, Kounaves SP et al (2009) Detection of perchlorate and the soluble chemistry of martian soil at the Phoenix lander site. Science 325:61–64. https://doi.org/10.1126/science.1172768

Bridges JC, Grady MM (1999) A halite-siderite-anhydrite-chlorapatite assemblage in Nakhla: mineralogical evidence for evaporites on Mars. Meteorit Planet Sci 34(3):407–415

Bridges JC, Grady MM (2000) Evaporite mineral assemblages in the nakhlite (martian) meteorites. Earth Planet Sci Lett 176:267–279

Bridges JC, Schwenzer SP (2012) The nakhlite hydrothermal brine on Mars. Earth Planet Sci Lett 359–360:117–123

Bridges JC, Catling DC, Saxton JM et al (2001) Alteration assemblages in Martian meteorites: implications for near-surface processes. Space Sci Rev 96:365–392

Brown GM, Gu B (2006) The chemistry of perchlorate in the environment. In: Gu B, Coates JD (eds) Perchlorate, environmental occurrence, interactions and treatment. Springer, New York, pp 17–47

Bunch TE, Reid AM (1975) The Nakhlites, part 1. Petrography and mineral chemistry. Meteoritics 10:303–315

Burgess R, Cartwright JA, Filiberto J (2013) Halogen abundances of the martian mantle. Geochim Cosmochim Acta 77:793

Carr MH (1995) The Martian drainage system and the origin of valley networks and fretted channels. J Geophys Res 100(E4):7479–7507. https://doi.org/10.1029/95JE00260

Carrier BL, Kounaves SP (2015) The origins of perchlorate in the Martian soil. Geophys Res Lett 42:3739–3745. https://doi.org/10.1002/2015GL064290
Carter J, Poulet F, Bibring J-P et al (2013) Hydrous minerals on Mars as seen by the CRISM and OMEGA imaging spectrometers: updated global view. J Geophys Res Planets 118(4):831–858
Cartwright JA, Burgess R (2011) Ar-Ar crystallisation ages of shergottite RBT 04262 mineral separates. Paper presented at the 74th annual meeting of the Meteoritical Society, London, UK, 8–12 August 2011
Cartwright JA, Gilmour JD, Burgess R (2009) Halogens in Martian Shergottite RBT 04262. Paper presented at the 40th lunar and planetary science conference, The Woodlands, TX, 23–27 March 2009
Cartwright JA, Gilmour JD, Burgess R (2013) Martian fluid and Martian weathering signatures identified in Nakhla, NWA 998 and MIL 03346 by halogen and noble gas analysis. Geochim Cosmochim Acta 105:255–293
Catling DC, Claire MW, Zahnle KJ et al (2010) Atmospheric origins of perchlorate on Mars and the Atacama. J Geophys Res Planets 115(E1). https://doi.org/10.1029/2009JE003425
Changela HG, Bridges JC (2010) Secondary minerals in the nakhlites formed at varying depth in an impact hydrothermal cell. Paper presented at the 41st lunar and planetary science conference, The Woodlands, TX, 1–5 March 2010
Chevrier VF, Rivera-Valentin EG (2012) Formation of recurring slope lineae by liquid brines on present-day Mars. Geophys Res Lett 39(21). https://doi.org/10.1029/2012GL054119
Chevrier VF, Hanley J, Altheide TS (2009) Stability of perchlorate hydrates and their liquid solutions at the Phoenix landing site, Mars. Geophys Res Lett 36(10). https://doi.org/10.1029/2009GL037497
Clark BC, Baird AK (1973) Martian regolith X-ray analyzer: test results of geochemical performance. Geology 1:15–18. https://doi.org/10.1130/0091-7613(1973)1<15:MRXATR>2.0.CO;2
Clark BC, Baird AK (1979) Is the martian lithosphere Sulfur rich? Geophys Res Lett 84:8395–8403
Clark BC, Baird AK, Rose HJ Jr et al (1977) The Viking X ray fluorescence experiment: analytical methods and early results. J Geophys Res 82:4577–4594
Clark BC, Baird AK, Weldon J et al (1982) Chemical composition of martian fines. J Geophys Res 87:10059–10067. https://doi.org/10.1029/JB087iB12p10059
Clark BC, Morris RV, McLennan SM et al (2005) Chemistry and mineralogy of outcrops at Meridiani Planum. Earth Planet Sci Lett 240(1):73–94. https://doi.org/10.1016/j.epsl.2005.09.040
Davila AF, Gómez-Silva B, de Los Rios A et al (2008) Facilitation of endolithic microbial survival in the hyperarid core of the Atacama Desert by mineral deliquescence. J Geophys Res 113:2005–2012
Davila AF, Wilson D, Coates JD, McKay CP (2013a) Perchlorate on Mars: a chemical hazard and a resource for humans. Int J Astrobio 12:321–325. https://doi.org/10.1017/S1473550413000189
Davila AF, Hawes I, Ascaso C, Wierzchos J (2013b) Salt deliquescence drives photosynthesis in hyperarid Atacama Desert. Environ Microbiol Rep 5:583–587
Dreibus G, Wänke H (1985) Mars, a volatile-rich planet. Meteoritics 20:367–381
Dreibus G, Wänke H (1987) Volatiles on Earth and Mars: a comparison. Icarus 71:225–240
Dreibus G, Spettel B, Wlotzka F et al (1996) QUE94201: an unusual martian basalt. Meteorit Planet Sci 31:A39–A40
Dreibus G, Spettel B, Haubold R et al (2000) Chemistry of a new shergottite: Sayh al Uhaymir 005. Meteorit Planet Sci 35:A49
Dreibus G, Haubold R, Huisl W, Spettel B (2003) Comparison of the chemistry of Yamato 980459 with DaG 476 and SaU 005. In: International symposium, evolution of solar system materials: a new perspective from Antarctic meteorites. National Institute of Polar Research (NIPR), Tokyo, pp 19–20
Dreibus G, Huisl W, Spettel B, Haubold R (2006) Halogens in nakhlites: studies of pre-terrestrial and terrestrial weathering processes. Paper presented at the 37th lunar and planetary science conference, League City, TX, 13–17 March 2006
Ehlmann BL, Mustard JF, Murchie SL et al (2011) Subsurface water and clay mineral formation during the early history of Mars. Nature 479:53–60. https://doi.org/10.1038/nature10582

Farley KA, Martin P, Archer PD Jr et al (2016) Light and variable $^{37}Cl/^{35}Cl$ ratios in rocks from Gale crater, Mars: possible signature of perchlorate. Earth Planet Sci Lett 438:14–24. https://doi.org/10.1016/j.epsl.2015.12.013

Filiberto J, Treiman AH (2009a) Martian magmas contained abundant chlorine, but little water. Geology 37:1087–1090

Filiberto J, Treiman AH (2009b) The effect of chlorine on the liquidus of basalt: first results and implications for basalt genesis on Mars and Earth. Chem Geol 263:60–68

Filiberto J, Treiman AH, Giesting PA et al (2014) High-temperature chlorine-rich fluid in the martian crust: a precursor to habitability. Earth Planet Sci Lett 401:110–115

Filiberto J, Gross J, McCubbin FM (2016) Constraints on the water, chlorine, and fluorine content of the Martian mantle. Meteorit Planet Sci 51:2023–2035

Fish SA, Shepherd TJ, McGenity TJ, Grant WD (2002) Recovery of ^{16}S ribosomal RNA gene fragments of ancient halite. Nature 417:432–436. https://doi.org/10.1038/417432a

Floran RJ, Prinz M, Hlava PF et al (1977) Chassigny meteorite—cumulate dunite with hydrous amphibole-bearing melt inclusions. Meteoritics 12:225

Foley CN, Economou T, Clayton RN (2003) Final chemical results from the Mars Pathfinder alpha proton X-ray spectrometer. J Geophys Res 108(E12). https://doi.org/10.1029/2002JE002019

Forni O, Gaft M, Toplis MJ et al (2015) First detection of fluorine on Mars: implications for Gale crater's geochemistry. Geophys Res Lett 42(4):1020–1028. https://doi.org/10.1002/2014GL062742

Forni O, Nachon M, Mangold N et al (2016) Fluorine in the Pahrump outcrop, Gale crater: implications for fluid circulation and alteration. Paper presented at the 47th lunar and planetary science conference, The Woodlands, TX, 21–25 March 2016

Forni O, Meslin P-Y, L'Haridon J et al (2017) Detection of fluorine-rich phases, phosphates and halite in the Stimson-Murray units, Gale crater, Mars. Paper presented at the 48th lunar and planetary science conference, The Woodlands, TX, 20–24 March 2017

Fredrickson JK, Chandler DP, Onstott TC (1997) Potential for preservation of halobacterial and their macromolecular constituents in bring inclusions from bedded salt deposits. In: Optical science, engineering and instrumentation '97. International Society for Optics and Photonics, pp 318–329

Fressinet C, Glavin DP, Mahaffy PR et al (2015) Organic molecules in the Sheepbed mudstone, Gale crater, Mars. J Geophys Res Planets 120(3):495–514. https://doi.org/10.1002/2014JE004737

Gellert R, Rieder R, Brückner J et al (2006) Alpha Particle X-Ray Spectrometer (APXS): results from Gusev crater and calibration report. J Geophys Res 111(E2). https://doi.org/10.1029/2005JE002555

Glavin DP, Freissinet C, Miller KE et al (2013) Evidence for perchlorates and the origin of chlorinated hydrocarbons detected by SAM at the Rocknest aeolian deposit in Gale Crater. J Geophys Res Planets 118(10):1955–1973. https://doi.org/10.1002/jgre.20144

Glotch TD, Bandfield JL, Tornabene LL et al (2010) Distribution and formation of chlorides and phyllosilicates in Terra Sirenum, Mars. Geophys Res Lett 37(16). https://doi.org/10.1029/2010GL044557

Glotch TD, Bandfield JL, Wolff MJ et al (2016) Constraints on the composition and particle size of chloride salt-bearing deposits on Mars. J Geophys Res 121(3):454–471. https://doi.org/10.1002/2015JE004921

Gough RV, Chevrier VF, Baustian KJ et al (2011) Laboratory studies of perchlorate phase transitions: support for metastable aqueous perchlorate solutions on Mars. Earth Planet Sci Lett 312(3–4):371–377. https://doi.org/10.1016/j.epsl.2011210.026

Greenwood JP (2008) Gypsum and jarosite in Roberts Massif 04262: Antarctic(?) weathering as a proxy for Martian weathering. Paper presented at the 39th lunar and planetary science conference, League City, TX, 10–14 March 2008

Greenwood JP, Itoh S, Sakamoto N et al (2008) Hydrogen isotope evidence for loss of water from Mars through time. Geophys Res Lett 35(5). https://doi.org/10.1029/2007GL032721

Griffith JD, Wilcox S, Powers DW et al (2008) Discovery of abundant cellulose microfibers encased in 250 Ma Permian halite: a macromolecular target in the search for life on other planets. Astrobiology 8(2):215–228

Gross J, Filiberto J, Bell AS (2013) Water in the martian interior: evidence for terrestrial MORB mantle-like volatile contents from hydroxyl-rich apatite in olivine–phyric shergottite NWA 6234. Earth Planet Sci Lett 369–370:120–128

Hanley J, Chevrier VF, Berget DJ, Adams RD (2012) Chlorate salts and solutions on Mars. Geophys Res Lett 39(8). https://doi.org/10.1029/2012GL051239

Hanley J, Chevrier VF, Barrows RS et al (2015) Near- and mid-infrared reflectance spectra of hydrated oxychlorine salts with implications for Mars. J Geophys Res Planets 120(8):1415–1426

Harvey RP, McSween HY (1992) The parent magma of the nakhlite meteorite: clues from melt inclusions. Earth Planet Sci Lett 111(2–4):467–482

Hecht MH, Kounaves SP, Quinn RC et al (2009) Detection of perchlorate and the soluble chemistry of martian soil at the Phoenix Lander site. Science 325:64–67. https://doi.org/10.1126/science.1172466

Humayun M, Nemchin A, Zanda B et al (2013) Origin and age of the earliest Martian crust from meteorite NWA 7533. Nature 503:513–516

Huval JH, Vreeland RH (1991) Taxonomy and halophilic bacteria from underground saline waters and salt formations. In: Rodriguez-Valera F (ed) General and applied aspects of Halophilic bacteria. Plenum, New York, pp 53–60

Hynek BM, Osterloo MK, Kierein-Young KS (2015) Late-stage formation of Martian chloride salts through ponding and evaporation. Geology 43(9):787–790

Jackson WA, Bohlke JK, Gu BH et al (2010) Isotopic composition and origin of indigenous natural perchlorate and co-occurring nitrate in the southwestern United States. Environ Sci Technol 44(13):4869–4876

Jakosky BM, Jones JH (1997) The history of Martian volatiles. Rev Geophys 35:1–16. https://doi.org/10.1029/96RG02903

Jakosky BM, Pepin RO, Johnson RE, Fox JL (1994) Mars atmospheric loss and isotopic fractionation by solar-wind-induced sputtering and photochemical escape. Icarus 111:271–288. https://doi.org/10.1006/icar.1994.1145

Javor B (1989) Hypersaline environments. Springer, New York

Jensen HB, Glotch TD (2011) Investigation of the near-infrared spectral character of putative Martian chloride deposits. J Geophys Res 116, E00J03. https://doi.org/10.1029/2011JE003887

Johnson MC, Rutherford MJ, Hess PC (1991) Chassigny petrogenesis—melt compositions, intensive parameters, and water contents of martian (questionable) magmas. Geochim Cosmochim Acta 55(1):349–366

Kargel JS (2004) Proof of water, hints of life? Nature 436:66–99

Karunatillake S, Zhao Y-YS, McLennan SM et al (2013) Does martian soil release reactive halogens to the atmosphere? Icarus 226(2):1438–1446. https://doi.org/10.1016/j.icarus.2013.08.018

Keller JM, Boynton WV, Karunatillake S et al (2006) Equatorial and midlatitude distribution of chlorine measured by Mars Odyssey GRS. J Geophys Res 111(E3). https://doi.org/10.1029/2006JE002679

Kieffer SW (1979) Thermodynamics and lattice vibrations of minerals: 2. Vibrational characteristics of silicates. Rev Geophys 17:20–34. https://doi.org/10.1029/RG017i001p00020

Klingelhöfer G, Morris RV, Bernhardt B et al (2004) Jarosite and hematite at Meridiani Planum from Opportunity's Mössbauer spectrometer. Science 306:1740–1745. https://doi.org/10.1126/science.1104653

Knoll AH, Joliff BL, Farrand WH et al (2008) Veneers, rinds, and fracture fills: relatively late alteration of sedimentary rocks at Meridiani Planum, Mars. J Geophys Res 113(E6). https://doi.org/10.1029/2007JE002949

Kounaves SP, Hecht MH, Kapit J et al (2010) Wet chemistry experiments on the 2007 Phoenix Mars Scout Lander mission: data analysis and results. J Geophys Res 115(E1). https://doi.org/10.1029/2009JE003424

Kounaves SP, Carrier BL, O'Neil GD et al (2014) Evidence of martian perchlorate, chlorate, and nitrate in Mars meteorite EETA79001: implications for oxidants and organics. Icarus 229:206–213. https://doi.org/10.1016/j.icarus.2013.11.012

Langenauer M, Krähenbühl U (1993) Halogen contamination in Antarctic H5 and H6 chondrites and relation to sites of recovery. Earth Planet Sci Lett 120:431–442
Leshin LA (2000) Insights into martian water reservoirs from analyses of martian meteorite QUE94201. Geophys Res Lett 27:2017–2020
Leshin LA, Mahaffy PR, Webster CR et al (2013) Volatile, isotope, and organic analysis of martian fines with the Mars Curiosity Rover. Science 341(6153):1238937. https://doi.org/10.1126/science.1238937
Lodders K (1998) A survey of shergottite, nakhlite and chassigny meteorites whole-rock compositions. Meteorit Planet Sci 33(S4):A183–A190. https://doi.org/10.1111/j.1945-5100.1998.tb01331.x
Lodders K (2003) Solar system abundances and condensation temperatures of the elements. Astrophys J 591:1220–1247
Longhi J, Knittle E, Wänke H (1992) The bulk composition, mineralogy and internal structure of Mars. In: Kieffer HH, Jakosky BM, Snyder CW, Matthews, MS (ed) Mars. The University of Arizona Press, Tucson, pp 184–208
Lowenstein TK, Li J, Brown C et al (1999) 200 ky paleoclimate record from Death Valley salt core. Geology 27:3–6. https://doi.org/10.1130/0091-7613
Mangold N, Thompson LM, Forni O et al (2017) Composition of conglomerates analyzed by the Curiosity rover: implications for Gale Crater crust and sediment sources. J Geophys Res 121:353–387. https://doi.org/10.1002/2015JE004977
Marion GM, Catling DC, Kargel JS (2009) Br/Cl partitioning in chloride minerals in the Burns formation on Mars. Icarus 200:436–445. https://doi.org/10.1016/j.icarus.2008.12.004
Massé M, Bourgeois O, Le Mouélic S et al (2012) Martian polar and circum-polar sulfate-bearing deposits: sublimation tills derived from the North Polar Cap. Icarus 209(2):424–451
McAdam AC, Franz HB, Sutter B et al (2014) Sulfur-bearing phases detected by evolved gas analysis of the Rocknest aeolian deposit, Gale Crater, Mars. J Geophys Res Planets 119:373–393. https://doi.org/10.1002/2013JE004518
McCubbin FM, Jones RH (2015) Extraterrestrial apatite: planetary geochemistry to astrobiology. Elements 11:183–188
McCubbin FM, Nekvasil H (2008) Maskelynite-hosted apatite in the Chassigny meteorite: insights into late-stage magmatic volatile evolution in martian magmas. Am Mineral 93:676–684
McCubbin FM, Tosca NJ, Smirnov A et al (2009) Hydrothermal jarosite and hematite in a pyroxene-hosted melt inclusion in martian meteorite Miller Range (MIL) 03346: implications for magmatic-hydrothermal fluids on Mars. Geochim Cosmochim Acta 73:4907–4917
McCubbin FM, Smirnov A, Nekvasil H et al (2010) Hydrous magmatism on Mars: a source of water for the surface and subsurface during the Amazonian. Earth Planet Sci Lett 292:132–138
McCubbin FM, Hauri EH, Elardo SM et al (2012) Hydrous melting of the martian mantle produced both depleted and enriched shergottites. Geology 40:683–686
McCubbin FM, Elardo SM, Shearer CK et al (2013) A petrogenetic model for the co-magmatic origin of chassignites and nakhlites: inferences from chlorine-rich minerals, petrology, and geochemistry. Meteorit Planet Sci 48:819–853
McCubbin FM, Vander Kaaden KE, Tartèse R et al (2015) Experimental investigation of F, Cl, and OH partitioning between apatite and Fe-rich basaltic melt at 1.0–1.2 GPa and 950–1000 °C. Am Mineral 100:1790–1802
McCubbin FM, Boyce JW, Srinivasan P et al (2016) Heterogeneous distribution of H_2O in the martian interior: implications for the abundance of H_2O in depleted and enriched mantle sources. Meteorit Planet Sci 51:2036–2060
McDonough WF, Sun SS (1995) The composition of the Earth. Chem Geol 120:223–253
McEwen AS, Ojha L, Dundas CM et al (2011) Seasonal flows on warm Martian slopes. Science 333:740–743
McEwen AS, Dundas CM, Mattson SS et al (2014) Recurring slope linear in equatorial regions of Mars. Nat Geosci 7:53–58
McGenity TJ, Gemmell RT, Grant WD, Stan-Lotter H (2000) Origins of halophilic microorganisms in ancient salt deposits. Environ Microbiol 2:243–250. https://doi.org/10.1046/j.1462-290.2000.00105.x

McSween HY, Harvey RP (1993) Outgassed water on Mars—constraints from melt inclusions in SNC meteorites. Science 259:1890–1892
McSween HY, Treiman AH (1998) Martian meteorites. Reviews in Mineralogy and Geochemistry 36:6-1
Ming DW, Archer PD Jr, Glavin DP et al (2014) Volatile and organic compositions of sedimentary rocks in Yellowknife Bay, Gale crater. Mars. Science 343(6169):1245267. https://doi.org/10.1126/science.1245267
Murchie SL, Mustard JF, Ehlmann BL et al (2009) A synthesis of Martian aqueous mineralogy after 1 Mars year of observations from the Mars Reconnaissance Orbiter. J Geophys Res 114 (E2). https://doi.org/10.1029/2008JE003342
Muttik N, McCubbin FM, Keller LP et al (2014) Inventory of H_2O in the ancient Martian regolith from Northwest Africa 7034: the important role of Fe oxides. Geophys Res Lett 41:8235–8244
Navarro-González R, Vargas E, de la Rosa J et al (2010) Reanalysis of the Viking results suggest perchlorate and organics at midlatitudes on Mars. J Geophys Res 115(E12). https://doi.org/10.1029/2010JE003599
Newsom HE (1980) Hydrothermal alteration of impact melt sheets with implications for Mars. Icarus 44:207–216
Norton CR, Grant WD (1988) Survival of halobacteria within fluids inclusions in salt crystals. J Gen Microbiol 134:1365–1373
Norton CF, McGenity TJ, Grant WD (1993) Archaeal halophiles (halobacteria) from two British salt mines. J Gen Microbiol 139:1077–1081
Ojha L, McEwan A, Dundas C et al (2014) HiRISE observations of recurring slope lineae (RSL) during southern summer on Mars. Icarus 231:365–376
Ojha L, Wilhelm MB, Murchie SL et al (2015) Spectral evidence for hydrated salts in recurring slope lineae on Mars. Nat Geosci 8:829–832. https://doi.org/10.1038/Ngeo2546
Osterloo MM, Hynek BM (2015) Martian chloride deposits: the last gasps of widespread surface water. Paper presented at the 46th lunar and planetary science conference, The Woodlands, TX, 16–20 March 2015
Osterloo MM, Hamilton VE, Bandfield JL et al (2008) Chloride-bearing materials in the southern highlands of Mars. Science 319:1651–1654. https://doi.org/10.1126/science.1150690
Osterloo MM, Anderson FS, Hamilton VE, Hynek BM (2010) Geologic context of proposed chloride-bearing materials on Mars. J Geophys Res 115(E10): https://doi.org/10.1029/2010JE003613
Quinn RC, Martucci HFH, Miller SR et al (2013) Perchlorate radiolysis on Mars and the origin of Martian soil reactivity. Astrobiology 13(6):515–520. https://doi.org/10.1089/ast.2013.0999
Rampe EB, Ming DW, Blake DF et al (2017) Mineralogy of an ancient lacustrine mudstone succession from the Murray formation, Gale crater, Mars. Earth Planet Sci Lett (in press). https://doi.org/10.1016/j.epsl.2017.04.021
Rao MN, Bogard DD, Nyquist LE et al (2002) Neutron capture isotopes in the Martian regolith and implications for Martian atmospheric noble gases. Icarus 156:352–372
Rao MN, Sutton SR, McKay DS, Dreibus G (2005) Clues to Martian brines based on halogens in salts from nakhlites and MER samples. J Geophys Res 110(E12). https://doi.org/10.1029/2005JE002470
Rieder R, Wänke H, Economou T, Turkevich A (1997) Determination of the chemical composition of martian soils and rocks: the alpha proton X ray spectrometer. J Geophys Res 102:4027–4044
Rieder R, Gellert R, Brückner J et al (2003) The new Athena alpha particle X-ray spectrometer for the Mars Exploration Rovers. J Geophys Res 108(E12). https://doi.org/10.1029/2003JE002150
Rieder R, Gellert R, Anderson RC et al (2004) Chemistry of Rocks and Soils at Meridiani Planum from the Alpha Particle X-ray Spectrometer. Science 306(5702):1746–1749
Righter K, Dyar MD, Delaney JS et al (2002) Correlations of octahedral cations with OH^-, O^{2-}, Cl^-, and F^- in biotite from volcanic rocks and xenoliths. Am Mineral 87:142–153
Roedder E (1984) The fluids in salts. Am Mineral 69:413–439

Ruesch O, Poulet F, Vincendon M et al (2012) Compositional investigation of the proposed chloride-bearing materials on Mars using near-infrared orbital data from OMEGA/MEx. J Geophys Res 117(E11). https://doi.org/10.1029/2012JE004108

Ruff SW, Christensen PR, Barbera PW, Anderson DL (1997) Quantitative thermal emission spectroscopy of minerals: a laboratory technique for measurement and calibration. J Geophys Res 102:14899–14913. https://doi.org/10.1029/97JB00593

Rummel JD, Beaty DW, Jones MA et al (2014) A new analysis of Mars "Special Regions": findings of the second MEPAG Special Regions Science Analysis Group (SR-SAG2). Astrobiology 14:887–968

Santos AR, Agee CB, McCubbin FM et al (2015) Petrology of igneous clasts in Northwest Africa 7034: implications for the petrologic diversity of the martian crust. Geochim Cosmochim Acta 157:56–85

Satterfield CL, Lowenstein TK, Vreeland RH et al (2005) New evidence for 250 Ma age of halotolerant bacterium from a Permian salt crystal. Geology 33(4):265–268. https://doi.org/10.1130/G21106.1

Sautter V, Jambon A, Boudouma O (2006) Cl-amphibole in the nakhlite MIL 03346: evidence for sediment contamination in a Martian meteorite. Earth Planet Sci Lett 252:45–55

Schubert BA, Lowenstein TK, Timofeeff MN, Parker MA (2009) How do prokaryotes survive in fluids inclusions in halite for 30 k.y.? Geology 37:1059–1062. https://doi.org/10.1130/G30448A.1

Schwenzer SP, Kring DA (2009) Impact-generated hydrothermal systems capable of forming phyllosilicates on Noachian Mars. Geology 37:1091–1094

Schwenzer SP, Kring DA (2010) Evaluating the effect of sulfur on alteration assemblages in impact cratered terrains on Mars. Paper presented at the 41st lunar and planetary science conference, The Woodlands, TX, 1–5 March 2010

Sharp Z, Williams J, Shearer C et al (2016) The chlorine isotope composition of Martian meteorites 2. Implications for the early solar system and the formation of Mars. Meteorit Planet Sci 51(11):2111–2126

Simpson WR, Carlson D, Hönninger et al (2007) First-year seas-ice contact predicts bromine monoxide (BrO) levels at Barrow, Alaska better than potential frost flower contact. Atmos Chem Phys 7:4375–4418

Smith PN (2006) The ecotoxicology of perchlorate in the environment. In: Gu B, Coates JD (eds) Perchlorate, environmental occurrence, interactions and treatment. Springer, New York, pp 153–168

Stein N, Grotzinger JP, Schieber J et al (2017) Candidate desiccation cracks in the upper Murray formation, Gale crater, Mars. Paper presented at the 48th lunar and planetary science conference, The Woodlands, TX, 20–24 March 2017

Stern JC, Sutter B, Jackson WA et al (2017) The nitrate/(per)chlorate relationship on Mars. Geophys Res Lett 44(6):2643–2651. https://doi.org/10.1002/2016GL072199

Sutter B, Heil E, Morris RV et al (2015) The investigation of perchlorate/iron phase mixtures as a possible source of oxygen detected by the Sample Analysis at Mars (SAM) instrument in Gale Crater, Mars. Paper presented at the 46th lunar and planetary science conference, The Woodlands, TX, 16–20 March 2015

Sutter B, McAdam AC, Rampe EB et al (2016) Evolved gas analysis of sedimentary materials in Gale crater, Mars: results from the Curiosity rover's Sample Analysis at Mars (SAM) instrument from Yellowknife Bay to the Stimson formation. Paper presented at the 47th lunar and planetary science conference, The Woodlands, TX, 21–25 March 1990

Sutter B, McAdam AC, Rampe EB et al (2017) Evolved gas analysis of the Murray formation in Gale crater, Mars: results of the Curiosity rover's Sample Analysis at Mars (SAM) instrument. Paper presented at the 48th lunar and planetary science conference, The Woodlands, TX, 20–24 March 2017

Symes SJK, Borg LE, Shearer CK, Irving AJ (2008) The age of the martian meteorite Northwest Africa 1195 and the differentiation history of shergottites. Geochim Cosmochim Acta 72:1696–1710

Taylor GJ (2013) The bulk composition of Mars. Chem Erde-Geochem 73(4):401–420

Taylor GJ, Boynton WV, McLennan SM, Martel LMV (2010) K and Cl concentrations on the martian surface determined by the Mars Odyssey Gamma Ray Spectrometer: implications for bulk halogen abundances in Mars. Geophys Res Lett 37(12). https://doi.org/10.1029/2010GL043528

Thomas NH, Ehlmann BL, Anderson DE et al (2017) ChemCam survey of volatile elements in the Murray formation, Gale crater, Mars. Paper presented at the 48th lunar and planetary science conference, The Woodlands, TX, 20–24 March 2017

Thompson LM, Schmidt ME, Gellert R et al (2016) APXS compositional trends along Curiosity's traverse, Gale crater, Mars: implications for crustal composition, sedimentary provenance, diagenesis and alteration. Paper presented at the 47th lunar and planetary science conference, The Woodlands, TX, 21–25 March 2016

Thompson LM, the MSL APXS and Science Teams (2017) Compositional characteristics and trends identified by APXS within the Murray formation, Gale crater, Mars: implications for provenance, diagenesis and alteration. Paper presented at the 48th lunar and planetary science conference, The Woodlands, TX, 20–24 March 2017

Treiman AH (1986) The parental magma of the Nakhla achondrite: ultrabasic volcanism on the shergottite parent body. Geochim Cosmochim Acta 50(6):1061–1070

Treiman AH (1990) Complex petrogenesis of the Nakhla (SNC) meteorite: evidence from petrography and mineral chemistry. Paper presented at the 20th lunar and planetary science conference, Houston, TX, 13–17 March 1990

Treiman AH (1993) The parent magma of the Nakhla (SNC) meteorite, inferred from magmatic intrusions. Geochim Cosmochim Acta 57(19):4753–4767

Treiman AH (2005) The nakhlite meteorites: augite-rich igneous rocks from Mars. Chem Erde-Geochem 65(3):203–270

Treiman AH, Lindstrom DJ (1997) Trace element geochemistry of Martian iddingsite in the Lafayette meteorite. J Geophys Res 102:9153–9161

Vaniman DT, Bish DL, Ming DW et al (2014) Mineralogy of a mudstone at Yellowknife Bay, Gale crater, Mars. Science 343(6169):1243480. https://doi.org/10.1126/science.1243480

Vaniman DT, Martínez GM, Rampe EB et al (2017) Calcium sulfates at Gale crater and limitations on gypsum stability. Paper presented at the 48th lunar and planetary science conference, The Woodlands, TX, 20–24 March 2017

Vreeland RH, Rosenzweig WD, Powers DW (2000) Isolation of a 250 million-year-old halotolerant bacterium from a primary sat crystal. Nature 407:897–900. https://doi.org/10.1028/35038060

Watson LL, Hutcheon ID, Epstein S, Stolper EM (1994) Water on Mars: clues from deuterium/hydrogen and water contents of hydrous phases in SNC meteorites. Science 265:86–90

Webster J, Baker DR, Aiuppa A (2018) Halogens in mafic and intermediate-silica content magmas. In: Harlov DE, Aranovich L (eds) The role of halogens in terrestrial and extraterrestrial geochemical processes: surface, crust, and mantle. Springer, Berlin, pp 307–430

Williams JT, Shearer CK, Sharp ZD et al (2016) The chlorine isotopic composition of Martian meteorites 1: chlorine isotope composition of Martian mantle and crustal reservoirs and their interactions. Meteorit Planet Sci 51(11):2092–2110

Wilson EH, Atreya SK, Kaiser RI, Mahaffy PR (2016) Perchlorate formation on Mars through surface radiolysis-initiated atmospheric chemistry: a potential mechanism. J Geophys Res Planets 121:1472–1487. https://doi.org/10.1002/2016JE005078

Wood WW, Sanford WE (2007) Atmospheric bromine flux from the coastal Abu Dhabi sabkhat: a ground-water mass-balance investigation. Geophys Res Lett 34(14). https://doi.org/10.1029/GL029922

Wu Z, Wang A, Li Z et al (2015) Identification and detection limits of perchlorate-chlorate in mixtures by vibrational spectroscopy. Paper presented at the 46th lunar and planetary science conference, The Woodlands, TX, 16–20 March 2015

Yen AS, Gellert R, Schröder C et al (2005) An integrated view of the chemistry and mineralogy of martian soils. Nature 436:49–54. https://doi.org/10.1038/nature03637

Zhao Y-YS, McLennan SM, Schoonon MAA (2014) Behavior of Br, Cl, and phosphate during low-temperature aqueous Fe(II) oxidation processes on Mars. J Geophys Res Planets 119:998–1012. https://doi.org/10.1002/2013JE004417

Zipfel J, Scherer P, Spettel B et al (2000) Petrology and chemistry of the new shergottite Dar al Gani 476. Meteorit Planet Sci 35:95–106. https://doi.org/10.1111/j.1945-5100.2000.tb01977.x

Chapter 17
Halogens on and Within the Ocean Worlds of the Outer Solar System

Kevin P. Hand

Abstract Life as we know it requires liquid water, a suite of approximately fifty-four elements from the periodic table, and some form of light or chemical energy to power life. The search for liquid water in our solar system has revealed that several moons of the outer solar system harbor oceans beneath their icy shells. Halogen salts serve as a key indicator of whether or not these liquid water environments could satisfy the latter two requirements for life. The presence of salts within these oceans is, and can be, an indicator of water-rock interactions between liquid water and silicate, halogen-rich, seafloors. In some cases, seafloor cycling within these moons may be sufficient to drive low-, or possibly even high-temperature hydrothermalism. Here I review the current state of knowledge of these oceans beyond Earth and provide both empirical and modelling constraints on halogens within these environments. Past, present, and future spacecraft missions to these worlds are described, and the implications for future discoveries of astrobiological importance is discussed.

17.1 Introduction

The halogens derive their name from the fact that they form salts, and few geochemical environments offer more interesting and ubiquitous salt chemistry than our ocean. But Earth's ocean is just one of many oceans that exist today within our solar system. There are five moons of the outer solar system (i.e. beyond the asteroid belt) for which we have strong evidence of subsurface oceans (Fig. 17.1). These include Jupiter's moons Europa, Ganymede, and Callisto, and Saturn's moons Enceladus and Titan (Kivelson et al. 2000; Porco et al. 2006; Khurana et al. 2007; Lorenz et al. 2008; Postberg et al. 2011; Iess et al. 2014; Saur et al. 2015). In addition, several more moons, such as Neptune's Triton and Saturn's Mimas, offer hints of possible subsurface liquid water environments (McKinnon 1984;

K.P. Hand (✉)
Jet Propulsion Laboratory, M/S 183-601, 4800 Oak Grove Drive, Pasadena, CA 91109, USA
e-mail: khand@jpl.nasa.gov

D.E. Harlov and L. Aranovich (eds.), *The Role of Halogens in Terrestrial and Extraterrestrial Geochemical Processes*, Springer Geochemistry,
https://doi.org/10.1007/978-3-319-61667-4_17

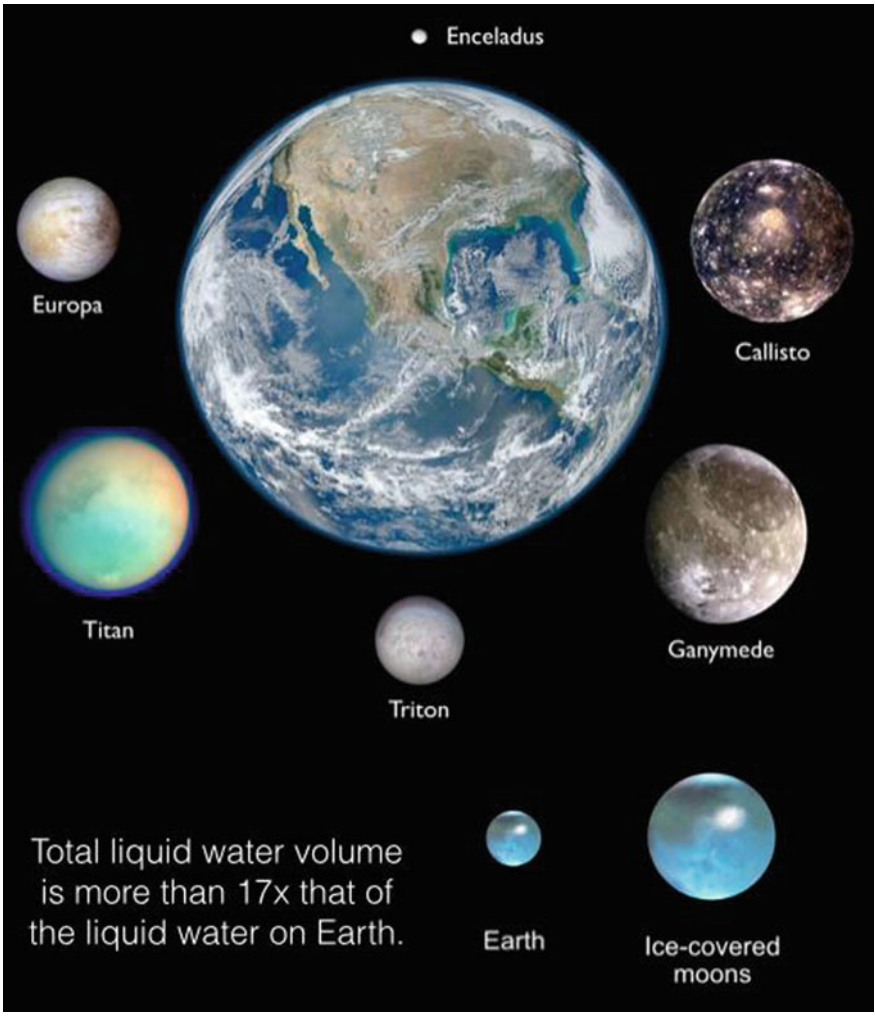

Fig. 17.1 Several candidate ocean worlds of our solar system, shown to scale with Earth. Jupiter's moons Europa, Ganymede, and Callisto; Saturn's Enceladus and Titan; and possibly even Neptune's moon Triton may harbor liquid water oceans beneath their icy crusts. Europa and Enceladus may also have rocky seafloors that permit hydrothermal geochemistry. At bottom is shown the volume of Earth's ocean water relative to the size of the Earth and to a conservative estimate for the total volume of water contained within moons of the outer solar system (Note, the volume of water shown for the Earth does not include water trapped in the mantle.). *Image credits* NASA/JPL/Caltech/SwRI/WHOI

McKinnon and Mueller 1989; Kirk et al. 1995; Tajeddine et al. 2014), and it may be that several of the, as yet to be explored, moons of Uranus could harbor subsurface liquid water, or have harbored it in the past (Hussmann et al. 2006). Figures 17.2 and 17.3 detail some of these ocean worlds of the outer solar system. Finally, it may

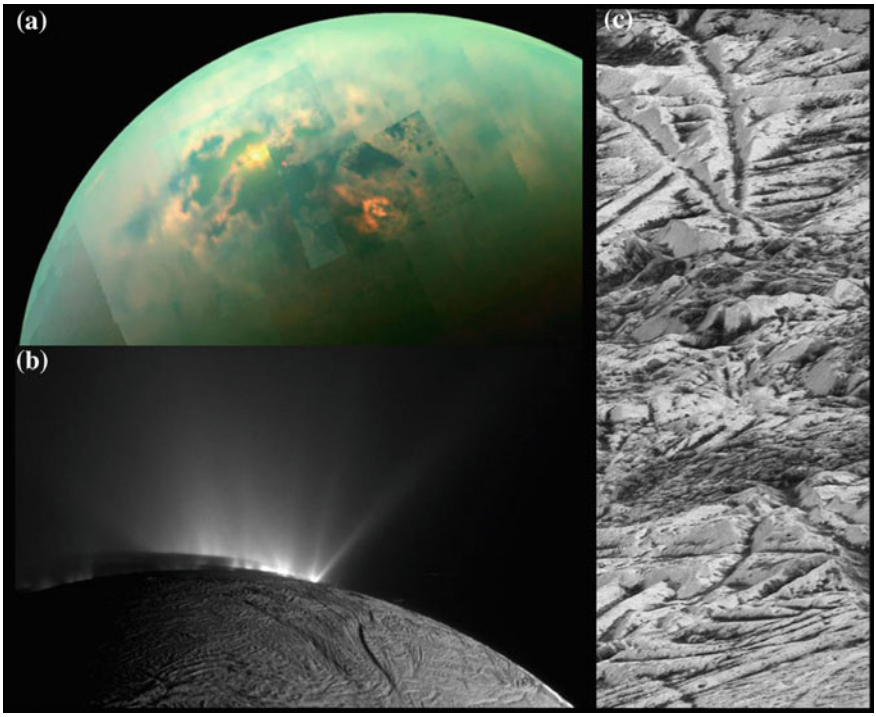

Fig. 17.2 Spacecraft images of Titan, Enceladus, and Europa. **a** Specular reflectance off of Titan's liquid hydrocarbon seas can be seen near the center of this mosaic from the *Cassini* spacecraft. **b** Enceladus' erupting water-rich plumes rise above the South Polar terrain and 'tiger stripes' in this image from *Cassini*. The shadow of the limb of Enceladus can be seen projected onto the plumes beyond the terminator. **c** A high-resolution ($\sim$6 m per pixel) greyscale image of Europa's surface, as captured by the *Galileo* spacecraft. The white ridges and terrain is water ice. The dark material is likely a mixture of sulfuric acid, produced as ions of sulfur bombard Europa's surface, and salts from the liquid water ocean below. *Image credits* NASA/JPL/Caltech/SwRI

be that the largest object in the asteroid belt, Ceres, also contains, or may have contained at some point in the past, a subsurface liquid water region (Kuppers et al. 2014). These oceans are maintained either through tidal energy interactions with their primary planet (e.g., Jupiter) or through radiogenic decay, or a combination of both. In all cases, the liquid water environment—be it a global ocean or localized sea—is sheltered from the space environment (or atmosphere, as is the case for Titan, the only moon with an atmosphere) by ice lithospheres of several to many 10–100's of kilometers in ice thickness (Zimmer et al. 2000; Hussmann et al. 2006; Iess et al. 2014; Mitri et al. 2014; Vance et al. 2014).

These ocean worlds are exciting targets for future solar system exploration in large part due to their astrobiological potential. NASA's mantra in the search for life elsewhere has long been 'follow the water' and these worlds likely host vast quantities of liquid water. Conservative estimates for the collective volume of liquid

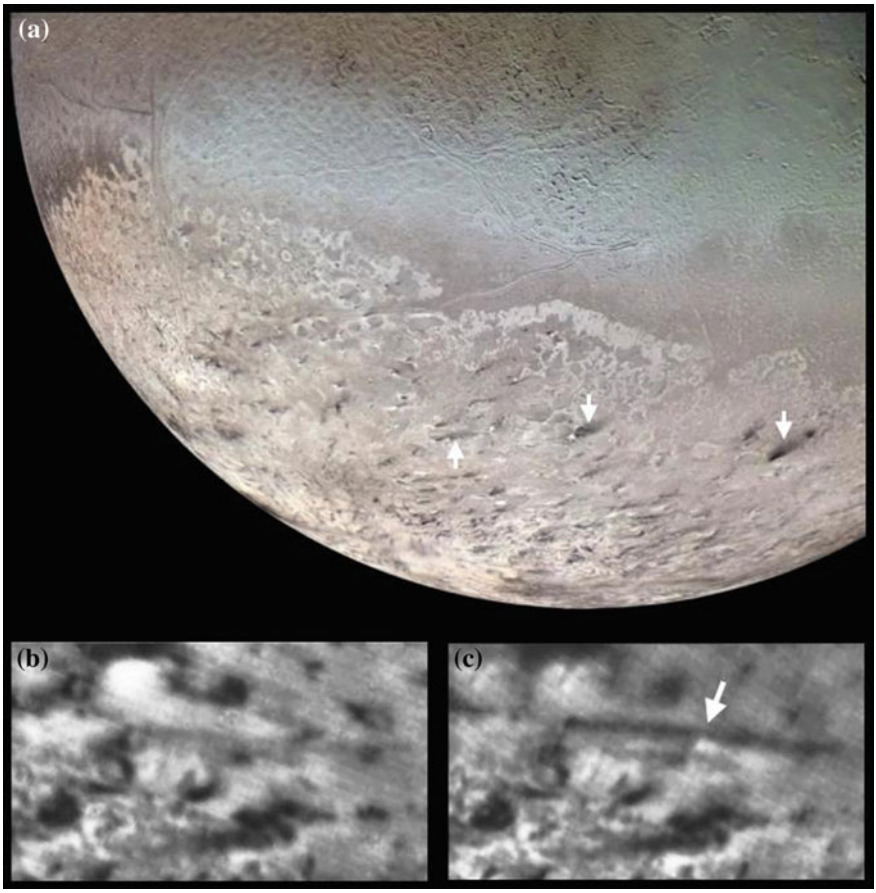

Fig. 17.3 Neptune's moon Triton as imaged by the Voyager 2 spacecraft in 1989. **a** The dichotomy between the 'cantaloupe' terrain (*upper half*) and the plume-rich terrain (*lower half*) can be seen in this hemisphere-scale image. Several candidate plumes are indicated by the *arrows*. **b** and **c** were taken 90 min apart and show an active plume, as indicated by the *arrow* in (**c**). The plume height was measured to be approximately 8 km and the plume cloud extends for approximately 150 km. *Image credit* NASA/JPL/Caltech

water in the worlds listed above leads to a volume some 20–40× that of all the liquid water on Earth.

But liquid water is of course not enough for providing and sustaining a habitable environment. Life as we know it also requires access to the elements needed to build life (e.g., C, N, P, S, and various quantities of some 54 elements from the periodic table (Wackett et al. 2004)), and life requires some form of light or chemical energy to power metabolism. Key to the 'elements' and 'energy' requirements is having liquid water in contact with, and reacting with, silicate rocks. Salts, and in particular the halogen salts, provide one of the clearest indicators of water-rock interactions. Consequently, as we have explored—and

continue to explore—these ocean worlds, the detection and characterization of salts is a high priority science task. In this review on halogens in these ocean worlds I focus largely on Cl since this is the halogen of greatest significance, and likely abundance, within these extraterrestrial oceans.

17.2 Formation Models and Initial Compositions

The large moons of Jupiter, and most of the larger moons of Saturn, likely formed within their respective circumplanetary accretion disks during the late stages of gas accretion onto the planet (Canup and Ward 2002). These accretion disks—sometimes referred to as 'gas-starved' disks because models indicate much lower densities of gases relative to older subnebula models (Pollack and Consolmagno 1984; Pollack et al. 1991; Canup and Ward 2002)—carved out gaps in the solar nebula and provided a slow flux of gas and solids for the formation of icy moons at relatively low temperatures ($<10^3$ K).

Consequently, the abundance of the halogens in these worlds was set by the available gas and chondritic material in each region, and the respective condensation temperatures for halogens. For Jupiter the disk was sufficiently cold so as to retain water and a variety of volatiles associated with sulfur (e.g., H_2S, SO_2) and possibly some carbon (e.g., CO_2, CH_4). For Saturn temperatures were sufficiently lower such that a significant carbon volatile inventory was retained, along with possibly some nitrogen volatiles (N_2, NH_3).

Within the solar nebula Cl was present at 698 ppm, however the condensation temperatures for the halogens remain uncertain (Lodders and Fegley 1998; Lodders 2010). As discussed by Allen and Mason (1973) and Mason and Graham (1970), halogens in meteorites are concentrated largely in chlorapatite and fluorapatite ($Ca_5(PO_4)_3(Cl, F)$), the latter of which condenses at 739 K (Lodders 2003), with troilite also hosting Br and I (see Chap. 15, (Brearley and Jones 2018)). Sodalite ($Na_4(Al_3Si_3O_{12})Cl$) serves as an additional significant halogen-bearing mineral in chondrites with a condensation temperature higher than (i.e. before) apatite (i.e. 984 K).

There is sparse data on Br- and I-apatite condensation profiles (Lodders 2003, 2010). They are therefore modeled as a substitution for Cl and F in corresponding Ca bromide and iodides. Those workers find Br and I to have 50% condensation temperatures of 546 and 535 K, respectively.

Significantly, Zolotov (2012) argues that high temperature condensation in the solar nebula does not work for halogens and that phosphates and sodalite are not initial condensates but rather secondary products. Phosphates, they argue, cannot form in the redox conditions of the nebula and sodalite is a metamorphic trace mineral in CV3 chondrites. For moons of the outer solar system Zolotov and Mironenko (2007) hypothesize that halogens were largely derived from hydrates such as $HCl{\cdot}3H_2O$.

The net result of condensation and subsequent accretion and evolution into moons yields initial conditions for these worlds in which halogens are available as

minor elements in the bulk silicate inventory. Subsequent differentiation and aqueous leaching, as discussed below, then determines the relative partitioning of these elements in the solid or aqueous phase. Importantly, the moons formed in the disks are compositionally distinct from moons captured from the Kuiper or asteroid belts (which may be the case for Saturn's Hyperion and Neptune's Triton (Farinella et al. 1990; Buratti et al. 2005; Agnor and Hamilton 2006). Kuiper belt objects likely contain larger fractions of volatiles such as ammonia, nitrogen, methane, carbon dioxide, and possibly even carbon monoxide (Prinn and Fegley 1981; Kargel 1992; Marion et al. 2012; Fortes and Choukroun 2010). Salts leached into solution from silicates in Kuiper Belt Objects (KBOs) might thus undergo a significantly different chemistry than typical water-rock interactions.

In the sections below I consider the two moons for which we have the most compelling evidence for salty subsurface oceans—Europa and Enceladus—and I then provide a brief context for additional moons that may harbor halogen-rich oceans.

17.3 Europa

Evidence for a global subsurface ocean of roughly 100 km in thickness beneath a ~10 km thick icy crust on Europa is strong and well-established. Spectroscopy through the 1950–1970s established the water ice surface of Europa (Moroz 1966; Kuiper 1957; Pilcher et al. 1972) and subsequent imagery from the *Voyager* and *Galileo* missions determined that its ice lithosphere is geologically young (<100 Ma). Gravity data established a low-density (~1 g/cc) outer shell of 80–170 km thickness, which is best explained by water in either liquid or solid phase (Anderson et al. 1998). The determination of a liquid water layer comes largely from *Galileo* measurements of an induced magnetic field around Europa—a field induced by the time-varying component of Jupiter's primary field (Kivelson et al. 2000; Zimmer et al. 2000). The best explanation for the strong observed induced field—as first predicted by Kargel and Consolmagno (1996) shortly before *Galileo* flew by Europa—is a near-surface conducting layer, which when combined with the spectroscopy and gravity data leads to a global salty liquid water ocean.

Spectroscopy of Europa's surface using the Galileo Near-Infrared Mapping Spectrometer (NIMS) has led some workers to argue that Europa's dark non-ice surface material is a hydrated sulfate salt such as a Mg or Na sulfate hydrate (McCord et al. 1999; Dalton et al. 2005). Others have argued that the spectroscopic data does not require an endogenous salt and can be sufficiently explained by radiation processing of S from volcanism on Jupiter's innermost large moon Io (Carlson et al. 1999; Brown and Hand 2013). The spectroscopic challenge is that chloride salts such as NaCl, KCl, and $MgCl_2$ lack significant features across much of the visible to near-infrared range and thus elude detection with remote sensing instruments.

Recently, using ground based telescopic data, Brown and Hand (2013) proposed that a newly observed spectroscopic feature at 2.07 μm is best explained by Mg sulfate. However, based on the geographic distribution of the 2.07 μm feature, they argue that the Mg sulfate is not the endogenous salt from Europa's ocean. In their model Europa's ocean is dominated by Na, K, and Mg chloride salts, for reasons similar to the residence times and water-rock interactions that take place in Earth's ocean (Elderfield and Schultz 1996; Mottl and Wheat 1994). On Earth, much of the oceanic Mg comes from continental weathering, a source term that is not relevant to Europa. Furthermore, hydrothermal cycling on Earth draws down magnesium but has little effect on Na and Cl. Thus for Europa, where no continents exist but where hydrothermal activity might be vigorous, Cl salts with Na, K, and limited Mg should be expected. When exposed to Europa's surface radiation environment and the water and S on the surface, however, Brown and Hand (2013) argue that the endogenous Mg chloride is at least partially processed into Mg sulfate. The key observational constraint was that the 2.07 μm Mg sulfate feature was observed only on Europa's trailing hemisphere, which is the hemisphere that receives the most irradiation from charged particles, and it also receives the most S from Io. Thus, on much of Europa's surface, Brown and Hand (2013) postulate that endogenous $MgCl_2$ is present at low levels (due to a low concentration in the ocean water (Zolotov and Kargel 2009)), but it is primarily on the trailing hemisphere that radiation processing transforms some of the $MgCl_2$ to $MgSO_4$ hydrate. This leads to a radiolytic salt cycle on Europa's surface, as illustrated in Fig. 17.4. In this model the magnesium of the $MgSO_4$ is from the ocean, the S is from Io, and the oxygen is derived from water molecules on Europa's surface. The fate of the Cl is uncertain, but some may be sputtered into space and some may be processed into chlorates and perchlorates.

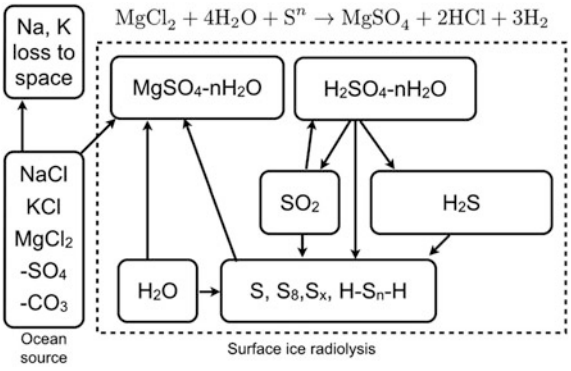

Fig. 17.4 Proposed radiolytic salt cycle for Europa, based on the observations and model from Brown and Hand (2013). In this model, the $MgSO_4$ hydrate observed on Europa's trailing hemisphere is created via radiation processing of endogenous $MgCl_2$, sulfur from volcanism on Io, and water from ice on Europa's surface. Europa's trailing hemisphere receives most of the particle irradiation and S implantation, thereby accounting for the observed dichotomy. The 'n' with the S on the left-hand side of the chemical equation indicates that sulfur from Io can impact Europa's surface as a charged ion or neutral

Interestingly, theoretical models of water-rock interactions and leaching of chondritic material (a reasonable assumption for Europa's initial composition) have long favored a sulfate ocean, in large part due to the initial interpretation of the spectroscopic data and the abundance of Mg and S in chondrites (Fanale et al. 2001; Kargel et al. 2000). For a global ocean in contact with, and cycling through a reduced silicate seafloor crust, however, the residence time of magnesium sulfate is too short to sustain a salty ocean over billions of years; halides are much stronger candidate for long-lived salty oceans.

Europa formed in the jovian disk and subsequently underwent differentiation into at least three layers, including a $\sim$600 km metal core, a $\sim$800 km silicate mantle, and a $\sim$70–180 km water layer (of which $\sim$100 km is liquid) (Anderson et al. 1998). Halogens would have preferentially been sequestered into the upper part of the mantle and crust (Zolotov and Kargel 2009), permitting leaching and accumulation into the ocean layer. Table 17.1 provides a summary of halogens in chondrites, Earth, and in chemical models for Europa's ocean. The models shown (K0, K1, K2, K1a) correspond to different extraction factors for the elements from the bulk Earth scaled to Europa. Model K0 is the fraction extracted into the core, the upper continental crust, the ocean, and lost to space. This extraction factor provides a reasonable upper limit for extraction during differentiation and leaching. Model K1 corresponds to extraction only into the Earth's upper continental crust and ocean, and brackets a possible scenario for Europa's ocean since terrestrial-type evaporitic processes do not exist on Europa. Thus this fraction might be expected to reside in the ocean. Model K2 is strictly the extraction factor from the bulk silicate Earth into the Earth's ocean, and sets a reasonable low-end estimate. Finally, in their K1a model, Zolotov and Shock (2001) use the K1 extraction and then decrease the K concentration to correspond to the measured value of Na/K in Europa's tenuous exosphere (Brown 2001; Johnson et al. 2002). This decreases other salts below saturation levels in order to achieve charge balance.

Zolotov and Shock (2001) find that relative to the Earth's ocean, Europa should be depleted in Cl and Br, even for cases of complete leaching of a chondritic mantle. The basis for this observation results from the fact that the available mass of mantle rock on Europa is in contact with an ocean, whose mass is some two to three times that of Earth's ocean mass. As noted by Zolotov and Kargel (2009) and Zolotov and Shock (2001), the total extraction of Na and Cl into the ocean would lead to a maximum salinity of only $\sim$70 g/kg. Where Cl the limiting component, the salinity drops to $\sim$5–26 g/kg (Zolotov 2008). Their equilibrium and mass balance models (K1a) yield a concentration of 2.087×10^{-2} mol/(kg H_2O)$^{-1}$ for Cl.

In an effort to constrain the total salinity, Hand and Chyba (2007) used the *Galileo* magnetometer data and modeled the induced field amplitude response as a function of ice shell thickness, ionospheric conductivity, ocean salinity and depth, and mantle and core conductivity. They found that the induced magnetic field signature observed by *Galileo* requires salt concentrations of several grams to hundreds of grams (saturation) of sea salt per kg of water in order to achieve the necessary conductivity.

Table 17.1 Mass abundances of halogens in chondrites, Earth, and models for a Europa ocean based on a chondrite formation and leaching model from Zolotov and Shock (2001)

	Chondritic abundances (g/kg)				Earth (g/kg)		Europa ocean Zolotov and Shock (2001) models (g/kg water)			
	H	CV	CM	CI	Bulk Silicate Earth	Earth seawater	K0	K1	K2	K1a
F	16	0.31	0.049	0.77	0.27	1.3×10^{-3}	0.058	0.026	6.6×10^{-6}	–
Cl	1.8	3.2	5.5	9.0	0.47	19	3.0	0.74	0.58	0.74
Br	6.4×10^{-3}	0.021	0.039	0.045	4.5×10^{-4}	0.067	0.02	0.016	0.013	–
I	7.7×10^{-4}	2.1×10^{-3}	3.5×10^{-3}	5.5×10^{-3}	1.4×10^{-4}	6.0×10^{-5}	1.8×10^{-3}	7.6×10^{-4}	3.9×10^{-6}	–

Values for F, Br, and I in model K1a of Zolotov and Shock (2001) were not reported

Is there a better way to constrain the salinity and halogen abundance on and within Europa? A future mission to Europa will carry numerous instruments capable of probing Europa's conductivity and composition, but in the near-term our observations might be aided by a curious attribute of alkali halides. Europa's irradiated surface is bombarded by $\sim$125 mW/m^2 of charged particles (electron, protons, and ions), which drives considerable radiolytic chemistry on the surface (Cooper et al. 2001). Any alkali halides, such as NaCl and KCl, exposed to this environment will accumulate trapped electrons, forming the so-called color centers, or F- and M-centers (Weerkamp et al. 1994; Seinen et al. 1994). Recently, Hand and Carlson (2015) have demonstrated the production of these color centers in salts under temperature, pressure, and radiation conditions comparable to Europa. They found strong absorption features in the visible part of the spectrum that could be used to map and quantify these compounds on Europa with ground based telescopes or future spacecraft. Furthermore, they find a decent match of these broad absorption features, using color filter wheel measurements on the *Galileo* spacecraft camera, with similar absorption features from geologically young regions on Europa. These irradiation induced spectral features may prove to be the most effective way for measuring halide salts on Europa, short of going down to the surface with a landed spacecraft.

17.4 Enceladus

Saturn's small moon Enceladus (504 km diameter) harbors a liquid water sea beneath its ice shell. The initial evidence came from Cassini's magnetometer (Khurana et al. 2007) with corroboration by imagery (Porco et al. 2006), mass spectrometry (Waite et al. 2009; Postberg et al. 2011; Hsu et al. 2015), and gravity data (Iess et al. 2014). Debate persists regarding the full extent of the ocean and whether it is constrained to the south polar region or covers the full globe. The most recent interpretation of the *Cassini* gravity data indicates a localized ocean beneath the south polar region (southward of approximately 60° south latitude) (Iess et al. 2014). Debate also persists as to the magnitude of tidal heating within Enceladus. Early models based on *Voyager* results calculated a flux of $\sim$5 mW m^{-2} (Ross and Schubert 1989; Poirier et al. 1983; Squyres et al. 1983), but *Cassini* thermal mapping results indicate $\sim$10 GW from the south polar region alone (Howett et al. 2011).

The 'smoking gun' for the subsurface ocean of Enceladus is the set of over 100 jets emanating >200 kg/s of water vapor and ice grains from fractures in the ice of the south polar region (Porco et al. 2006, 2014). Though heavily debated, these fractures—the largest four of which are referred to as the 'tiger stripes'—may experience a tidal opening and closing that modulates the jet activity as Enceladus orbits Saturn on its 1.37 day, slightly eccentric (0.005 eccentricity) orbit (Hedman et al. 2013).

The detection of halogens—specifically Cl—in the material ejected from Enceladus' plumes provides key evidence that the water in the plumes is derived from a liquid water region in contact with silicate rocks, i.e. an ocean with a rocky seafloor. The plume material was initially characterized by the Ion and Neutral Mass Spectrometer (INMS) on board *Cassini* during a 2005 flyby that brought the spacecraft to within 168 km of Enceladus' south polar region. The INMS is a mass spectrometer capable of detecting ion neutral species over a mass range of 1–99 atomic mass units (amu), with a resolution of 100 (Waite et al. 2004). The plume material is >90% water, with CO_2 at $\sim$1500 molecules cm^{-3} and N_2 or CO (which both correspond to the 28 amu peak in the mass spectrometer, and thus differentiating these species is difficult) at 2100 molecules cm^{-3} (Waite et al. 2006, 2009; Bouquet et al. 2015).

This composition alone is not unlike that of a comet, but Cassini's Cosmic Dust Analyzer (CDA) measured the presence of salts in ice grains from the plumes. Postberg et al. (2009, 2011) reported that within these grains there is 0.05–0.2 mol NaCl kg^{-1}, and between 0.02 and 0.1 mol kg^{-1} of Na-carbonates. They conclude that Enceladus' ocean should have a pH of between 8.5 and 9. Subsequent work by Postberg et al. (2011) revealed that more than 70% of the grains (>0.2 μm in diameter) are salt-rich, leading to a 99% mass flux of salt-rich grains. Glein et al. (2015) used data from the Cosmic Dust Analyzer and Ion & Neutrals Mass Spectrometer on *Cassini* to update earlier models concerning the geochemistry of the ocean (Glein et al. 2008; Glein and Shock 2010). Using the measured CO_2/H_2O ratio of 0.006 for the plume gas, those workers find that the abundance of carbon dioxide and carbonates in the plume data indicates an ocean with a pH between 10.8 and 13.5, and with a total Cl abundance of 0.2 mol/kg of ocean water.

To understand how the ice grain measurements connect to the ocean composition it is critical to understand the physics of the plume. The jet-like plumes of Enceladus are not analogous to geysers on Earth, or even to a pressurized water source, such as a hose. Rather the material that forms the jets is largely derived from gases that evaporate or liquids that boil at the ice-water interface when fractures expose the liquid water to low pressures (Schmidt et al. 2008; Brilliantov et al. 2008; Postberg et al. 2009, 2011). Some ice grains (generally salt-poor) form as gas is compressed during its journey through the several tens of kilometers of ice shell (30–40 km, Iess et al. 2014). Salts, such as NaCl, solvate out of the ocean into the gas phase and are entrained into the gas mixture. Nucleation into salt-rich grains proceeds as gas compression and interactions with the ice walls take place during the migration of the material upward through the fracture channels. Other ice grains (the salt-rich grains) form from oceanic 'spray' and boiling near the site where the ice shell fracture reaches the ocean. In this scenario, material is ejected directly from the ocean but it has a low initial velocity relative to the gas-phase and therefore does not escape far out into space as part of the plume (Brilliantov et al. 2008; Postberg et al. 2011). The plume chemistry that ultimately results from these processes is one in which the grains that are most representative of the ocean composition are likely those that are heaviest and ejected from Enceladus' surface at lower velocities.

These grains are harder to capture with the *Cassini* spacecraft since they only rise a few to perhaps a few tens of kilometers above the surface.

Interestingly, the *Cassini* INMS and CDA measurements of the salts match well with theoretical models for ocean chemistry, which produce a Na chloride and Na bicarbonate/carbonate ocean (Zolotov 2007). Using a chemical equilibrium model, which balances both mass and charge, Zolotov (2007) found that an early global ocean within Enceladus should contain a total of 3–8 g kg^{-1} of salt, with a corresponding pH between 8 and 11. This value may be a good lower limit for Enceldaus' present day ocean salinity. This value is well below terrestrial salinity but still indicates significant water-rock interaction between a rocky seafloor on Enceladus and its liquid water ocean.

17.5 Other Moons

Here I present a brief summary of other worlds that may have oceans or seas, and that consequently may have halogens in solution.

17.5.1 Ganymede & Callisto

Jupiter's Ganymede and Callisto likely share an initial composition not unlike that of Europa and their oceans may also be rich in salts, however the bulk density of Ganymede (1.9 g cm^{-3}) and Callisto (1.8 g cm^{-3}) is significantly lower than that of Europa (3.0 g cm^{-3}), perhaps indicative of reduced water-rock interactions. An added key compositional difference for these moons may be that the seafloors of the oceans in Ganymede and Callisto are made of higher pressure, denser phases of water ice, not silicates. As a result the water-rock interaction and leaching may be more limited, leading to lower concentrations of dissolved solutes such as halogen salts. Nevertheless, the surfaces of these worlds both display significant non-ice components, some of which have been attributed to sulfate and carbonate salts on Ganymede (McCord et al. 2001), and possibly organics on Callisto (McCord et al. 1997). Furthermore, depending on the degree of differentiation and resulting salinities, these moons may be multi-layered with ice phases III, V, and VI possibly separating high-salinity, dense liquid water regions (Vance et al. 2014).

17.5.2 Io

Io, Jupiter's innermost large satellite, is our solar system's most volcanically active world. Tidal energy dissipation yields a total power output from Io of in excess of 10^{14} W, which if taken to be a global average results in 2.5 W m^{-2}

(Veeder et al. 1994; Geissler 2003). This is significantly larger than Earth's 4×10^{13} W (78 mW m^{-2} average). Based on Io's induced magnetic field signature Khurana et al. (2011) conclude that an ultramafic magma ocean must exist beneath Io's crust. This is consistent with observed surface temperatures of 1800 K for magma flows on Io (McEwen et al. 1998), and the resulting tidal amplitude for the crust would be approximately 90 m as Io orbits Jupiter every 1.77 days (Geissler 2003). High-temperature volcanism and ultramafic lava flows on Io have led some to make comparisons to early komatiitic flows on a Precambrian Earth (Williams et al. 2000; Geissler 2003). The dark colors on, and spectroscopy of, Io's surface are consistent with such silicates, but much of the bright red, yellow and white is attributed to sulfur in oxidized, elemental, and polymer forms (Geissler 2003), with possible contributions from Fe sulfides and S-rich materials containing Te, Se, and As (Carlson et al. 2010). Kargel et al. (1999) also hypothesized that some of Io's surface composition, including chlorides, may have initially been derived from a primordial evaporitic ocean. Halogen chemistry, in the form of NaCl, has been confirmed and observed in the volcanic outgassing from Io (Lellouch et al. 2003). Observations of the 1.3 and 2.1 mm NaCl gas phase rotational transitions indicate a total outgassing flux of NaCl of 1.7×10^{24}–8×10^{25} NaCl molecules s^{-1}, with an additional 1.7×10^{25}–1.6×10^{27} Na and Cl atoms s^{-1} (Lellouch et al. 2003). Though Nelson and Nash (1979) examined their ground-based spectra for signs of the alkali halide color centers mentioned in the Europa section, they found no compelling evidence for such absorptions. Future observations with improved instrumentation may reveal these radiation-processed halides on Io's surface.

17.5.3 Titan

Titan's surface is dotted with methane and ethane lakes in the high latitude regions and it likely has a salty liquid water ocean beneath its water icy crust (Mitri et al. 2007; Lunine and Lorenz 2009; Baland et al. 2014). The thickness of Titan's ice shell is still highly uncertain but models for a conductive shell in thermal equilibrium indicate a global average of $\sim$70 km (Mitri et al. 2014; Baland et al. 2014). The novel organic-rich chemical environment of Titan's surface presents what is perhaps the solar system's best prospect for testing 'weird life' evolutionary scenarios (Chyba and Hand 2005). Titan is the only moon with a significant atmosphere. The surface pressure is $\sim$1.5$\times$ that of the Earth. The atmosphere consists largely of N_2 with 1.4% methane in the stratosphere and 4.9% methane near Titan's surface (Niemann et al. 2005). Photolysis of methane yields ethane and larger hydrocarbons that form large seas and lakes on Titan's $\sim$95 K surface. These liquid hydrocarbon environments are very intriguing from an astrobiology perspective. If it is possible for life to form from a non-polar solvent such as ethane and methane, then the environment of Titan could be host to such ecosystems.

Interestingly, one limitation may be the extent to which these hydrocarbon seas permit dissolution of salts and silicates needed for building life (the 'elements').

A key problem is that 'like dissolves like', i.e. the halogen salts and other polar compounds will not readily dissolve into these non-polar systems (Cordier et al. 2009; Tan et al. 2013, 2015). Furthermore, Titan, as with Ganymede and Callisto, likely has a seafloor of high-pressure water ice phases and thus its ocean may be chemically limited by the available water-rock interaction. Even if Titan's lithosphere permits cryovolcanism (Lopes et al. 2007, 2013), it is uncertain whether the resulting ice flows would contain a significant fraction of dissolved components. Models using Titan's gravity field data (Baland et al. 2014), however, indicate a dense, solute-rich, subsurface ocean, perhaps containing dissolved ammonium and magnesium sulfates. Much remains to be discovered about Titan's unique geochemical environment and though the Cassini mission will continue to make Titan flybys until 2017, no missions are currently funded to explore Titan once the *Cassini* mission concludes.

17.5.4 Mimas

Only recently has any consideration been given to Saturn's moon Mimas as a possible candidate for harboring a subsurface sea beneath a $\sim$30 km ice shell. The data are tenuous at best and consist of observations of surface librations as Mimas orbits Saturn on its slightly elliptical 0.94 day orbit (Tajeddine et al. 2014). If Mimas were found to have a subsurface ocean it would, at $\sim$200 km radius, be the smallest world within our solar system to harbor liquid water.

17.6 Astrobiological Considerations

Though the halogens serve as a hallmark of water-rock interactions that are likely critical to the astrobiological potential of ocean worlds, there are additional ways in which salts may impact the habitability of these worlds. Microbial life on Earth is capable of living in even the most saline of natural salt environments (Oren 1994, 2001). However, the evolution of these so-called 'halophiles' on Earth likely came from a long sequence of selection and adaptation. Just because an environment is habitable does not require that it be conducive to the origin of life. On this latter point Monnard et al. (2002) showed that concentrations of Na chloride as low as 1.46 g per kg of water impeded oligomerization of biomolecules such as nucleobases, with further reduction as salinity increased. Such experiments support a popular view that life on Earth may have arisen in a freshwater environment, and thus salty oceans such as those of Europa and Enceladus could be problematic for the chemistry that leads to life. Within ocean worlds such as Europa and Enceladus, microenvironments may persist within the ice shell or in hydrothermal systems that could be advantageous to 'origin of life chemistry' (Hand et al. 2009; Priscu and Hand 2012). Some have even postulated that a freshwater oceanic 'stratosphere'

could persist at the base of Europa's ice shell, serving as the buoyant interface between the ice shell and a salty ocean (Melosh et al. 2004).

17.7 Future Missions and Measurements

The *Cassini* mission will continue to collect data on the Saturnian system until September of 2017. The final flybys of Enceladus occurred in late 2015 and no more data will be returned concerning the composition of Enceladus' plumes. The *Cassini* mission culminates with a series of 'proximal', or high inclination, orbits that will enable polar observations of Saturn and top-down views of the rings. The spacecraft periapse will gradually move to the region between the rings and Saturn, with the final orbit sending the spacecraft into Saturn's atmosphere, where it may make a few atmospheric measurements before contact is lost. Once the Cassini spacecraft is lost to Saturn the saturnian system will go dark for at least a decade—no follow-on missions are in production or approved at this point in time. The next chance for a mission to Enceladus or Titan is within the competed mission class known as *New Frontiers*, where these moons are being presented as key targets in our exploration of 'ocean worlds' within our solar system.

As *Cassini* begins the last stage of its mission, the *Juno* spacecraft will be arriving at Jupiter (July, 2016) and entering into a polar orbit. This mission will not study Jupiter's moons directly, but it will reveal much about the origin, structure, and composition of Jupiter, thereby leading to a better understanding of the jovian accretion disk from which the moons formed. *Juno's* infrared and ultraviolet spectrometers will be used to determine the composition of Jupiter's atmosphere, down to about 7 bars into the atmosphere.

For direct spacecraft observations of Europa, Ganymede, and Callisto, the next approved mission is the European Space Agency's Jupiter Icy Moons Explorer mission (JUICE). This mission will make two flybys of Europa and several flybys of Callisto before going into orbit around Ganymede. Launch of this mission is planned for 2022, with arrival at Jupiter in 2030.

NASA has long studied mission options for Europa, the most recent of which is the Europa Clipper, a Jupiter-orbiting spacecraft that would make upwards of 45 flybys of Europa. This mission, now being referred to as the Europa Multiple Flyby Mission, is now approved and in Phase A with a projected launch date between 2022 and 2024. This mission includes cameras, spectrometers, and an ice-penetrating radar to map ice-water boundaries. The primary science objective will be to assess the habitability of Europa and perform reconnaissance for a future lander. Arrival at Jupiter will be in the timeframe of 2026–2031, depending on the launch vehicle and corresponding trajectory out to Jupiter.

Finally, it is well worth noting that the recent magnificent *New Horizon*'s spacecraft flyby of Pluto has revealed a surprisingly young and dynamic surface on this bizarre world of ice. The *New Horizon*'s spacecraft flew by Pluto on July 14, 2015 and over the course of the past year the data has been slowly downlinked to

reveal a new and exciting world. Pluto's surface geology reveals a paucity of craters and landscapes of water, methane, and nitrogen ices yielding mountains and flowing plains of volatile ices breathing into and condensing out of Pluto's variable atmosphere (Stern et al. 2015; Grundy et al. 2016). Little has been reported regarding heavier non-volatile components on Pluto's surface (such as salts), but much work remains to be done with the new data set. Interior models do however report the possibility of a past, if not possibly present, ocean of liquid water (possibly with some ammonia fraction), which could then leach with the limited silicate fraction within Pluto's interior (Robuchon and Nimmo 2011; Moore et al. 2016). Unfortunately, the *New Horizon*'s spacecraft was limited to just one flyby of Pluto and it is now onto its next destination, a Kuiper Belt object that it will flyby on January 1st of 2019.

Acknowledgements The author acknowledges support from the Jet Propulsion Laboratory, California Institute of Technology, under a contract with the National Aeronautics and Space Administration and funded in part through the internal Research and Technology Development program. He would also like to thank Jeff Kargel, Christopher Glein, and Mischa Zolotov for very useful reviews.

References

Agnor CB, Hamilton DP (2006) Neptune's capture of its moon Triton in a binary-planet gravitational encounter. Nature 441(7090):192–194

Allen RO, Mason B (1973) Minor and trace elements in some meteoritic minerals. Geochim Cosmochim Acta 37(6):1435–1456

Anderson JD, Schubert G, Jacobson RA et al (1998) Europa's differentiated internal structure: inferences from four Galileo encounters. Science 281(5385):2019–2022

Baland RM, Tobie G, Lefèvre A, Van Hoolst T (2014) Titan's internal structure inferred from its gravity field, shape, and rotation state. Icarus 237:29–41

Bouquet A, Mousis O, Waite JH, Picaud S (2015) Possible evidence for a methane source in Enceladus' ocean. Geophys Res Lett 42(5):1334–1339

Brearley AJ, Jones RH (2018) Halogens in chondritic meteorites. In: Harlov DE, Aranovitch L (eds) The role of halogens in terrestrial and extraterrestrial geochemical processes: surface, crust, and mantle. Springer, pp 871–958

Brilliantov NV, Schmidt J, Spahn F (2008) Geysers of Enceladus: quantitative analysis of qualitative models. Planet Space Sci 56(12):1596–1606

Brown ME (2001) Potassium in Europa's atmosphere. Icarus 151(2):190–195

Brown ME, Hand KP (2013) Salts and radiation products on the surface of Europa. Astron J 145:110 (7 pp)

Buratti BJ, Hicks MD, Davies A (2005) Spectrophotometry of the small satellites of Saturn and their relationship to Iapetus, Phoebe, and Hyperion. Icarus 175(2):490–495

Canup RM, Ward WR (2002) Formation of the Galilean satellites: conditions of accretion. Astron J 124(6):3404–3423

Carlson RW, Johnson R, Anderson M (1999) Sulfuric acid on europa and the radiolytic sulfur cycle. Science 286:97–99

Carlson RW, Kargel JS, Doute S, Soderblom LA, Dalton JB (2010) Io's surface composition. In: Lopes RC, Spencer JR (eds) Io after Galileo. Praxis-Springer, Berlin, pp 193–229

Chyba CF, Hand KP (2005) Astrobiology: the study of the living universe. Ann Rev Astron Astrophys 43:31–74
Cooper JF, Johnson RE, Mauk BH et al (2001) Energetic ion and electron irradiation of the icy Galilean satellites. Icarus 149(1):133–159
Cordier D, Mousis O, Lunine JI et al (2009) An estimate of the chemical composition of Titan's lakes. Astrophys J Lett 707(2):L128
Dalton JB, Prieto-Ballesteros O, Kargel JS et al (2005) Spectral comparison of heavily hydrated salts with disrupted terrains on Europa. Icarus 177(2):472–490
Elderfield H, Schultz A (1996) Mid-ocean ridge hydrothermal fluxes and the chemical composition of the ocean. Ann Rev Earth Planet Sci 24:191–224
Fanale FP, Li YH, De Carlo E et al (2001) An experimental estimate of Europa's "ocean" composition independent of Galileo orbital remote sensing. J Geophys Res 106:14595–14600
Farinella P, Paolicchi P, Strom RG et al (1990) The fate of Hyperion fragments. Icarus 83:186–204
Fortes AD, Choukroun M (2010) Phase behavior of ices and hydrates. Space Sci Rev 153:185–218
Geissler PE (2003) Volcanic activity on Io during the Galileo era. Ann Rev Earth Planet Sci 31 (1):175–211
Glein CR, Shock EL (2010) Sodium chloride as a geophysical probe of a subsurface ocean on Enceladus. Geophys Res Lett 37:L09204. https://doi.org/10.1029/2010GL042446
Glein CR, Zolotov MY, Shock EL (2008) The oxidation state of hydrothermal systems on early Enceladus. Icarus 197:157–163
Glein CR, Baross JA, Waite JH (2015) The pH of Enceladus' ocean. Geochim Cosmochim Acta 162:202–219
Grundy WM, Binzel RP, Buratti BJ et al (2016) Surface compositions across Pluto and Charon. Science 351(6279):aad9189
Hand KP, Chyba CF (2007) Empirical constraints on the salinity of the Europan ocean and implications for a thin ice shell. Icarus 189(2):424–438
Hand KP, Carlson RW (2015) Europa's surface color indicates an ocean rich with sodium chloride. Geophys Res Lett 42:3174–3178
Hand KP, Chyba CF, Priscu JC et al (2009) Astrobiology and the potential for life on Europa. In: Pappalardo RT, McKinnon WB, Khurana KK (eds) Europa. University of Arizona Press, Tucson, p 589
Hedman MM, Gosmeyer CM, Nicholson PD et al (2013) An observed correlation between plume activity and tidal stresses on Enceladus. Nature 500(7461):182–184
Howett CJA, Spencer JR, Pearl J, Segura M (2011) High heat flow from Enceladus' south polar region measured using 10–600 cm^{-1} Cassini/CIRS data. J Geophys Res: Planets 116(E3)
Hsu HW, Postberg F, Sekine Y et al (2015) Ongoing hydrothermal activities within Enceladus. Nature 519(7542):207–210
Hussmann H, Sohl F, Spohn T (2006) Subsurface oceans and deep interiors of medium-sized outer planet satellites and large trans-neptunian objects. Icarus 185(1):258–273
Iess L, Stevenson DJ, Parisi M et al (2014) The gravity field and interior structure of Enceladus. Science 344(6179):78–80
Johnson RE, Leblanc F, Yakshinskiy BV, Madey TE (2002) Energy distributions for desorption of sodium and potassium from ice: the Na/K ratio at Europa. Icarus 156(1):136–142
Kargel JS (1992) Ammonia-water volcanism on icy satellites: phase relations at 1 atmosphere. Icarus 100:556–574
Kargel JS, Consolmagno GJ (1996) Magnetic fields and the detectability of brine oceans in Jupiter's icy satellites. Paper presented at lunar and planetary science XXVII, Houston, 643–644
Kargel JS, Delmelle P, Nash DB (1999) Volcanogenic sulfur on Earth and Io: composition and spectroscopy. Icarus 142:249–280
Kargel JS, Kaye JZ, Head JWI et al (2000) Europa's crust and ocean: origin, composition, and the prospects for life. Icarus 148:226–265
Khurana KK, Dougherty M, Russell C, Leisner J (2007) Mass loading of Saturn's magnetosphere near Enceladus. J Geophys Res 112:A08203. https://doi.org/10.1029/2006JA012110

Khurana KK, Jia X, Kivelson MG et al (2011) Evidence of a global magma ocean in Io's interior. Science 332(6034):1186–1189
Kirk RL, Soderblom LA, Brown RH et al (1995) Triton's plumes: discovery, characteristics, and models. In: Cruikshank DP, Matthews MS, Schumann AM (eds) Neptune and Triton, vol 1. University of Arizona Press, Tucson, pp 949–989
Kivelson MG, Khurana KK, Russell CT et al (2000) Galileo magnetometer measurements: a stronger case for a subsurface ocean at Europa. Science 289(5483):1340–1343
Kuiper GP (1957) Infrared observations of planets and satellites. Astron J 62:245–245
Küppers M, O'Rourke L, Bockelée-Morvan D et al (2014) Localized sources of water vapour on the dwarf planet Ceres. Nature 505(7484):525–527
Lellouch E, Paubert G, Moses JI et al (2003) Volcanically emitted sodium chloride as a source for Io's neutral clouds and plasma torus. Nature 421(6918):45–47
Lodders K (2003) Solar system abundances and condensation temperatures of the elements. Astrophys J 591(2):1220–1247
Lodders K (2010) Solar system abundances of the elements. Principles and perspectives in cosmochemistry. Springer, Berlin, pp 379–417
Lodders K, Fegley B Jr (1998) The planetary scientist's companion. Oxford University Press, New York, p 371
Lopes RC, Mitchell KL, Stofan ER et al (2007) Cryovolcanic features on Titan's surface as revealed by the Cassini Titan Radar Mapper. Icarus 186(2):395–412
Lopes RC, Kirk RL, Mitchell KL et al (2013) Cryovolcanism on Titan: new results from Cassini RADAR and VIMS. J Geophys Res: Planets 118:1–20
Lorenz RD, Stiles BW, Kirk RL et al (2008) Titan's rotation reveals an internal ocean and changing zonal winds. Science 319:1649–1651
Lunine JI, Lorenz RD (2009) Rivers, lakes, dunes, and rain: crustal processes in Titan's methane cycle. Ann Rev Earth Planet Sci 37:299–320
Mason B, Graham AL (1970) Minor and trace elements in meteoritic minerals. Smithsonian Contrib Earth Sci 3:1–17
McCord TA, Carlson RW, Smythe WD, Hansen GB, Clark RN, Hibbitts CA, Fanale FP, Granahan JC, Segura M, Matson DL, Johnson TV (1997) Organics and other molecules in the surfaces of Callisto and Ganymede. Science 278(5336): 271–275
McCord TB, Hansen GB, Matson DL et al (1999) Hydrated salt minerals on Europa's surface from the Galileo near-infrared mapping spectrometer (NIMS) investigation. J Geophys Res 104:11827–11851
McCord TB, Hansen GB, Hibbitts CA (2001) Hydrated salt minerals on Ganymede's surface: evidence of an ocean below. Science 292(5521):1523–1525
McEwen AS, Keszthelyi L, Spencer JR et al (1998) High-temperature silicate volcanism on Jupiter's moon Io. Science 281(5373):87–90
McKinnon WB (1984) On the origin of Triton and Pluto. Nature 311:355–358
McKinnon WB, Mueller S (1989) The density of Triton: a prediction. Geophys Res Lett 16 (6):591–594
Marion G, Kargel JS, Catling DC, Lunine JI (2012) Modelling ammonia-ammonium aqueous chemistries in the Solar System's icy bodies. Icarus 22:932–946
Melosh HJ, Ekholm AG, Showman AP, Lorenz RD (2004) The temperature of Europa's subsurface water ocean. Icarus 168(2):498–502
Mitri G, Showman AP, Lunine JI, Lorenz RD (2007) Hydrocarbon lakes on Titan. Icarus 186 (2):385–394
Mitri G, Meriggiola R, Hayes A et al (2014) Shape, topography, gravity anomalies and tidal deformation of Titan. Icarus 236:169–177
Monnard P-A, Apel CL, Kanavarioti A, Deamer DW (2002) Influence of ionic solutes on self-assembly and polymerization processes related to early forms of life: implications for a prebiotic aqueous medium. Astrobiology 2:213–219
Moore JM, McKinnon WB, Spencer JR et al (2016) The geology of Pluto and Charon through the eyes of New Horizons. Science 351(6279):1284–1293

Moroz VI (1966) Infrared spectrophotometry of the Moon and the Galilean satellites of Jupiter. Soviet Astron 9:999
Mottl MJ, Wheat CG (1994) Hydrothermal circulation through mid-ocean ridge flanks: fluxes of heat and magnesium. Geochim Cosmochim Acta 58(10):2225–2237
Nelson RM, Nash DB (1979) Spectral reflectance change and luminescence of selected salts during 2–10 KeV proton bombardment: implications for Io. Icarus 39(2):277–285
Niemann HB, Atreya SK, Bauer SJ et al (2005) The abundances of constituents of Titan's atmosphere from the GCMS instrument on the Huygens probe. Nature 438(7069):779–784
Oren A (1994) The ecology of the extremely halophilic archea. FEMS Microbiol Rev 13:415–440
Oren A (2001) The bioenergetic basis for the decrease in metabolic diversity at increasing salt concentrations: implications for the functioning of salt lake ecosystems. Hydrobiologia 466:61–72
Pilcher CB, Ridgway ST, McCord TB (1972) Galilean satellites: identification of water frost. Science 178(4065):1087–1089
Poirier JP, Boloh L, Chambon P (1983) Tidal dissipation in small viscoelastic ice moons: the case of Enceladus. Icarus 55(2): 218–230
Pollack JB, Consolmagno G (1984) Origin and evolution of the Saturn system. In: Gehrels T, Matthews MS (eds) Saturn. University of Arizona Press, Tucson, p 811
Pollack JB, Lunine JI, Tittemore WC (1991) Origin of the Uranian satellites. In: Bergstralh JT, Miner ED, Matthews MS (eds) Uranus. University of Arizona Press, Tucson, p 469
Porco C, Helfenstein P, Thomas PC et al (2006) Cassini observes the active south pole of Enceladus. Science 311(5766):1393–1401. https://doi.org/10.1126/science.1123013
Porco C, DiNino D, Nimmo F (2014) How the Geysers, tidal stresses, and thermal emission across the South Polar Terrain of Enceladus are related. Astron J 148(3):45
Postberg F, Kempf S, Schmidt J et al (2009) Sodium salts in E-ring ice grains from an ocean below the surface of Enceladus. Nature 459(7250):1098–1101
Postberg F, Schmidt J, Hillier J, Kempf S, Srama R (2011) A salt-water reservoir as the source of a compositionally stratified plume on Enceladus. Nature 474(7353):620–622
Prinn RG, Fegley B (1981) Kinetic inhibition of CO and N_2 reduction in circumplanetary nebulae: implications for satellite composition. Astrophys J 249:308–317
Priscu JC, Hand KP (2012) Microbial habitability of icy worlds. Microbe 7(4):167–172
Robuchon G, Nimmo F (2011) Thermal evolution of Pluto and implications for surface tectonics and a subsurface ocean. Icarus 216(2):426–439
Ross MN, Schubert G (1989) Viscoelastic models of tidal heating in Enceladus. Icarus 78 (1):90–101
Saur J, Duling S, Roth L et al (2015) The search for a subsurface ocean in Ganymede with Hubble Space Telescope observations of its auroral ovals. J Geophys Res Space Phys 120 (3):1715–1737
Schmidt J, Brilliantov N, Spahn F, Kempf S (2008) Slow dust in Enceladus' plume from condensation and wall collisions in tiger stripe fractures. Nature 451(7179):685–688
Seinen J, Groote JC, Weerkamp JR et al (1994) Radiation damage in NaCl. II. The early stage of F-center aggregation. Phys Rev B 50(14):9787
Squyres SW, Reynolds RT, Cassen PM, Peale SJ (1983) The evolution of Enceladus. Icarus 53 (2):319–331
Stern SA, Bagenal F, Ennico K et al (2015) The Pluto system: initial results from its exploration by New Horizons. Science 350(6258):aad1815
Tajeddine R, Rambaux N, Lainey V et al (2014) Constraints on Mimas' interior from Cassini ISS libration measurements. Science 346(6207):322–324
Tan SP, Adidharma H, Kargel JS, Marion GM (2013) Equation of state for solid solution–liquid–vapor equilibria at cryogenic conditions. Fluid Phase Equilib 360:320–331
Tan SP, Kargel JS, Jennings DE et al (2015) Titan's liquids: exotic behavior and its implications on global fluid circulation. Icarus 250:64–75
Vance S, Bouffard M, Choukroun M, Sotin C (2014) Ganymede's internal structure including thermodynamics of magnesium sulfate oceans in contact with ice. Planet Space Sci 96:62–70

Veeder GJ, Matson DL, Johnson TV et al (1994) Io's heat flow from infrared radiometry: 1983–1993. J Geophys Res Planet 99(E8):17095–17162

Wackett LP, Dodge AG, Ellis LB (2004) Microbial genomics and the periodic table. Am Soc Microbiol 70(2):647–655

Waite JH, Lewis WS, Kasprzak WT, Anicich VG, Block BP, Cravens TE, Fletcher GG, Ip W-H, Luhmann JG, Mcnutt RL, Niemann HB, Parejko JK, Richards JE, Thorpe RL, Walter EM, Yelle RV (2004) The Cassini ion and neutral mass spectrometer (INMS) investigation. Space Sci Rev 114(1):113–231

Waite JH Jr, Combi MR, Ip WH et al (2006) Cassini ion and neutral mass spectrometer: Enceladus plume composition and structure. Science 311(5766):1419–1422

Waite JH Jr, Lewis WS, Magee BA et al (2009) Liquid water on Enceladus from observations of ammonia and ^{40}Ar in the plume. Nature 460(7254):487–490

Weerkamp JRW, Groote JC, Seinen J, Den Hartog HW (1994) Radiation damage in NaCl. I. Optical-absorption experiments on heavily irradiated samples. Phys Rev B 50(14):9781

Williams DA, Wilson AH, Greeley R (2000) A komatiite analog to potential ultramafic materials on Io. J Geophys Res Planet 105(E1):1671–1684

Zimmer C, Khurana KK, Kivelson MG (2000) Subsurface oceans on Europa and Callisto: constraints from Galileo magnetometer observations. Icarus 147:329–347

Zolotov MY (2007) An oceanic composition on early and today's Enceladus. Geophys Res Lett 34:L23203

Zolotov MY (2008) Oceanic composition on Europa: constraints from mineral solubilities. Paper presented at lunar and planetary science XXXIX, Houston, 39:2349

Zolotov MY (2012) Aqueous fluid composition in CI chondritic materials: chemical equilibrium assessments in closed systems. Icarus 220(2):713–729

Zolotov MY, Kargel JS (2009) On the chemical composition of Europa's icy shell, ocean, and underlying rocks. In: Pappalardo RT, McKinnon WB, Khurana KK (eds) Europa. University of Arizona Press, Tucson, pp 431–458

Zolotov MY, Mironenko MV (2007) Hydrogen chloride as a source of acid fluids in parent bodies of chondrites. Lunar and planetary science conference, vol 38

Zolotov MY, Shock EL (2001) Composition and stability of salts on the surface of Europa and their oceanic origin. J Geophys Res 106:32815–32827

Index

D.E. Harlov and L. Aranovich (eds.), *The Role of Halogens in Terrestrial and Extraterrestrial Geochemical Processes*, Springer Geochemistry,
DOI 10.1007/978-3-319-61667-4

N

Q

R

T